DFI 41st Annual Conference on Deep Foundations

DEEP FOUNDATIONS INSTITUTE

DFI

International Conference on Deep Foundations, Seepage Control and Remediation



2016 Proceedings

Deep Foundations

DFI 41st Annual Conference on Deep Foundations

International Conference on Deep Foundations, Seepage Control and Remediation

New York Marriott Marquis | October 12-15, 2016



CONFERENCE PROCEEDINGS

- DEEP FOUNDATIONS -

2016

New York, New York | USA

Deep Foundations Institute
326 Lafayette Avenue
Hawthorne, New Jersey 07506 USA
Tel: (973) 423-4030
Fax: (973) 423-4031
staff@dfi.org
www.dfi.org

Table of Contents

Addressing and Resolving Issues facing an Ever Changing Industry

Applications of Known Concepts for Management of Construction Vibrations; *Mark R. Svinkin …. 1*

Ethical and Risk Aspects of Deep Foundation Subcontracts; *Alexander Filotti, M.B.A., P.E. and Richard Kalson, Esq. …….. 11*

Execution of Diaphragm and Cut-Off-Walls in Rock – Applications, Performance and Limits; *Franz-Werner Gerressen, Albert Neumann, P.E. and Giancarlo Santarelli ……. 21*

Strength and Deformations of Piles Supporting Transient Pipe Anchors in Heavy Industrial Pipelines; *Konstantin G. Ashkinadze …….. 31*

Data Integration & Management to Improve Design, Lower Risk & Improve Products

Ground Disturbance Due to Static Pressure Driving of Opened-Ended PHC Piles; *Guowei Li, Andrew C. Amenuvor, Xiaocen Lu, Jiantao Wu and Thang N. Nguyen ……. 41*

Performance Monitoring for Deep Excavations; *Alexi J. Neill, P.E. …….. 55*

Deep Foundations and Earth Retention used in Urban Construction

"Trevi-Calatore": Innovation in Cut and Cover and Tunneling for the Installation of Plunge Columns Aimed to Excavate Underground Structures through the Top-Down Method; *Alessandro Bertero, Vincenzo Tirozzi and Manuel Toniolo ……. 67*

A Case Study, Design Change from Spread Footing to Drilled Shafts; *Mohammad Ayub Iqbal, Ph.D, P.E., Drew M. Kurtz, P.E., Sara F. Frailey, P.E. and Jeff L. Rai, P.E. ……. 77*

A Comparative Study on Behavior of Bucket Pile in Sand According to Installation Methods; *Juhyung Lee, Jinung Do and Sung-Ryul Kim …….. 85*

A Decade of Experience with Drilled Foundations in Honolulu; *James W. Niehoff, MSCE, P.E. … 91*

A Study on Bearing Capacity of Waveform Micropiles Using Centrifuge Test; *Young-Eun Jang, Jin-Tae Han and Chengcan Wang ……. 101*

A Tall Slender Tower Rises on Secant Piles and Drilled Shafts; *Sitotaw Y. Fantaye, T. C. Michael Law, Renzo D. Verastegui and Alfredas Daugiala …….. 111*

Accumulated Rotations of Bucket Foundations under Long-Term Cyclic Loads in Sandy Ground; *Sung-Ryul Kim, Si-Hoon Lee, Woong-Jong Park and Juhyung Lee …… 123*

ACIP Pile Performance and Installation in the Northeastern United States; *W. Morgan NeSmith Jr., P.E. …… 129*

An Alternative Approach for Estimating the Vertical Capacity of L-Shaped Segmental Underpinning Systems in Urban Basement Construction; *Abid O. Adekunte, David Hilton and David Greentree …… 139*

Applications of Diaphragm Wall Technology for Deep Foundations and Permanent Underground Structures for the Transbay Transit Center and the Transbay Developments; *Mikael Calando and Thomas Joussellin …… 157*

Behavior of Settlement Reducing Piles under Static and Seismic Loadings; *Alaa A. Ata, Faculty of Eng. and Marwa Nabil, Faculty of Eng. …… 167*

Construction of a Deep Soil Mixed Cut-Off and Retaining Wall in Richmond BC; *Keith MacKay, Fernando Faminia, David Siddle and John Carter …… 179*

Design Issues for Mini-Caissons in the NYC Area; *Nidal M. AbiSaab, P.E., M.ASCE and Joseph J. Caciola Jr., P.E., M.ASCE …… 189*

Drilled Displacement Pile in the Northeastern United States; *W. Morgan NeSmith Jr., P.E …… 197*

Driven Pile Foundation Design and Construction Issues for a High-Rise Building in Manhattan; *Sandy Larimer, P.E., Satyajit Vaidya, P.E. and Rudolph Frizzi, P.E., G.E., D.GE. …… 207*

Full Scale Uplift Load Testing of Micropiles in Cohessionless Soil; *Maged A. Abdlrahem and M. Hesham El Naggar …… 217*

Ground Improvement by Dry Concrete Columns; *Tatiana Tronda …… 225*

High Capacity Drilled Piles in Brooklyn; *Frederick C. Rhyner, P.E., Steven R. Lowe, P.E. and Ahmed Elmekati, Ph.D., P.E. …… 233*

High Capacity Grouted Helical Piles; *Mohamed A. Mansour, Ahmed M. Soliman and M. H. El-Naggar …… 241*

Innovative Deep Foundation Support Using Ductile Iron Piles; *Doug LeDo, P.E., Thomas Billups, P.E., David Carchedi, Ph.D., P.E. and Brendan FitzPatrick, P.E. …… 249*

Innovative SSP Design and Construction for a Complex Soil Remediation Project; *Mark C. Spence, P. Eng. and Matthew C. Janes, M. E. Sc., P. Eng. …… 259*

Installation of Secant Pile Wall in Rock Adjacent to Fragile Building; *Chu E. Ho, Alfredas Daugiala and Nicola Ebanks …… 271*

Micropiles in an Urban Setting - TBTA Verrazano Narrows Bridge HOV/Bus Ramps, Brooklyn, NY and the NYSDOT Kosciuszko Bridge Replacement, Brooklyn, NY; *Brian T. Felber and M. D. Riegel …… 281*

Piled-Raft Foundations in Belarus; *V. A. Sernov …… 291*

Prediction of Axial Geotechnical Resistance of Base Grouted Drilled Shafts; *Ehab S. Shatnawi, Ph.D., P.E. and Emad Farouz, P.E. …… 301*

Removal of the Former San Francisco-Oakland Bay Bridge Foundation Caisson E3 by Mechanical Means and Explosives; *Michael Gebman, Ph.D., P.E. and Jack Gerwick, P.E. …… 313*

Replacement of the Kosciuszko Bridge Brooklyn Connector: An Integrated Design and Construction Approach; *Britain A. Materek, M. D. Riegel, P. B. Pizzimenti and E. M. Zamiskie ….. 323*

Rock Socketed Drilled Shafts for the Goethals Bridge Replacement; *John P. Turner, Steven S. Dapp and Dan A. Brown …… 337*

Screw and Straight Pile Behavior under Cyclic Compressive Loading in Dense Sand; *Adnan A. Malik, Jiro Kuwano, Shinya Tachibana and Tadashi Maejima …… 347*

Silver Star Motors "Tackles" Brownfield Site and Adjacent NYCT Subway; *Michael J. Chow, P.E., Senior Consultant and Dharmil Patel, EIT, Engineer I …… 355*

TBM Recovery Shaft Construction- SR-99 Tunnel; *John Starcevich, P.E., Lance Rasband and Rick Hanke, Peng …… 365*

UB Digs Deep and Builds over Adjacent Subway for New Medical Building Hub; *Walter E. Kaeck, Lisa R. Papandrea, P.E. and David Chen, P.E. …… 375*

Use of APG Piles for Support of New Hospital Replacement Wing in a Site Susceptible to Excessive Ground Settlement - Ventura, California; *Justin Ray, P.E., Maria Flessas, P.E., GE, Danielle Steinmetz, P.E. and Brian Zuckerman, P.E. …… 387*

Deep Foundations and Earth Retention used in Urban Construction

Bored Pile Construction Challenges in Highly Variable Limestone for a Supertall Building; *Seth K. Martin, Alan R. Poeppel, Konstantinos Syngros and Tony Nichlany …… 397*

Buttressing Berms for Stability of Cantilever Sheet Piles – Limit Equilibrium and Finite Element Approaches; *Meena L. Viswanath, Mustafa B. Erten, Ph.D., P.E., Ali Ebrahimi, Ph.D., P.E., Ming Zhu, Ph.D., P.E. and John F. Beech, Ph.D., P.E. …… 409*

Deep Foundation Support for the Iconic New York Wheel; *Quadri Owokoniran, Satyajit Vaidya, P.E. and Rudolph Frizzi, P.E., GE, D.GE. …… 419*

Design, Construction Challenges and Quality Control of a Deep Soil Mixing System for Waterfront Slope Stabilization; *Yan Lap J. Kan, GE, CEG …… 431*

Settlement Evaluation of Large Water Storage Tanks under Challenging Conditions; *Yogesh Prashar and Ben M. Lewis …… 441*

Fraser Heights Bridge – Comparison between PDA Tests and Pile Capacity Estimation Methods; *Ali Azizian and Brian Hall …… 453*

Goethals Bridge Replacement Foundation Design Modifications Due to Field Conditions; *Bobby Daita, P.E., John P. Turner and Mark Jen, Ph.D., P.E. …… 465*

Goethals Bridge Replacement Project - Performance-Based Design of the Drilled Shaft Foundations; *Chunli Wei, Mark Jen and Xiaojun Wang …… 477*

Inclusion of Overburden Soils Resistance into Shaft Nominal Capacity for Significant Economic Savings – An Osterberg Cell Load Test Case Study; *Aditya Ayithi, Ph.D., P.E., Dean Herbst, P.E. and William G. Ryan …… 487*

Influence of Surface Replacement Layer on Behavior of Laterally Loaded Large Bored Piles in Soft Clay: Pile Load Tests and Numerical Investigation; *Mamdouh M. Hamza, Marawan M. Shahien, Hayel M. El-Naggar and Mohamed Sobhi …… 497*

Innovative Earth Retention Project for a Parking Garage; *Andreas Brandner, Dipl.-Ing …… 507*

Jet Grouted Foundation for 57-Story Tower; *Robert Alperstein, P.E., D.GE, L.M.ASCE, Consultant, Nidal AbiSaab, P.E., M.ASCE, Partner and Joe Pastore, Vice President …… 519*

Kosciuszko Bridge Main Pylon Foundation Deep Foundation Solution; *D. Coleman and A. Daugiala …… 529*

Lateral Pressure-Relief by Geotextile Encased Columns (GECs) at Piled Bridge Abutments: Two Case Studies; *Dimiter Alexiew, Lilma Schimmel and Sven Schröer …… 541*

Load Tests on Drilled Shafts at Goethals Bridge Replacement; *Steven S. Dapp, John P. Turner and Dan A. Brown …… 551*

Physical Modeling and Development of Design Criteria for Maintainable Drains for Earth Retention Systems; *Andrew Z. Boeckmann and J. Erik Loehr …….. 561*

Practical Construction Considerations for Runway Extension and Taxiway Expansion over Soft/Organic Soil Using a Column-Supported Load Transfer Platform; *Brian T. Nereson, P.E. and Michael C. Penney, P.E. …….. 571*

Pressure-Grouting Improves Performance of Helical Piles: A Production Case History, Static Load Test Results, and Comparisons to Predicted Lateral Deflection and Axial Resistance; *Karen J. Dawson, P.E. and Francisco Johnson …….. 583*

Protection of Waterfront Properties by Pressed-In Sheet Pile Seawalls; *Ian Vaz, Rafael Holcombe, Takefumi Takuma and Chris DellAringa …….. 593*

Risk Assessment and Quality Control on Grouted Water-Retaining Layers by Observational Engineering; *Bartho J. Admiraal and Falco A. van Dijck …….. 603*

Rock Excavation and Underpinning below a 19-Story Building; *Steven C. Highfill, P.E. and Kevin P. Gleckler …….. 613*

Slope Repairs in a Tight Footprint: Slope Stabilization Using Multiple Technologies; *Dan Mahrt, P.E. …….. 625*

Turning the Valley of Ashes into a Tennis Haven: The Development History of the USTA Site in Queens, NY; *Alfred H. Brand, Sissy Nikolaou, Pablo V. Lopez, Athena C. Denivo and Michael McMaster …….. 637*

Washington Avenue Tunnel Project: Fortifying Aging Underground Infrastructure; *Andrew R. Klaetsch and Peter W. Deming …….. 649*

Resiliency and Sustainability – Protecting our Cities and Support Structures

A Resilience Approach for Design of Earth Retaining Systems with Application on MSE Walls; *Rallis Kourkoulis, Fani Gelagoti, Irene Georgiou, Sissy Nikolaou and George Gazetas …….. 657*

Challenging Ground Conditions during Flooding Leads to Innovative Deep Foundation Design Process and Load Test Evaluation; *James F. Mehnert, P.E. and Glen M. Bellew, P.E. …….. 667*

Experimental Evaluation of Building Settlements Founded on Liquefiable Soils; *Joseph A. W. Toth, Ramin Motamed and Farshid Ghazavi …….. 677*

Use of Alternative Project Delivery for Deep Foundations Projects: What, Why & How

Design Build of the New NY Bridge Foundations; *Chris J. Leykam, PE and Scott A. Jacobs, PE .. 689*

Sheikh Jaber Al-Ahmad Causeway Project in Kuwait - A Case Study; *Paolo Cavalcoli, Marco Chiarabelli and Federico Pagliacci …… 701*

Value-Engineering of H-Pile Foundations in Karstic Geology; *Daniel J. Woeste, Rachael M. Fischer and Terence P. Holman …… 721*

Use of Emerging Technologies in Planning, Design, Construction & QC/QA

A Case Study of Multichannel Analysis of Surface Waves (MASW) As a Tool to Characterize Unknown Foundations; *Siavash Mahvelati, Joseph T. Coe and Philip Asabere …… 731*

A Comparison of Non-Destructive Integrity Tests on Experimental Drilled Shafts; *Armin W. Stuedlein, Qiang Li, Jim Zammataro, Daniel Belardo, Bernie Hertlein and Antonio Marinucci …… 741*

Analysis of Structural Capacity and Stiffness of Drilled Shafts with Construction Defects and Repairs; *Benjamin J. Turner and John P. Turner …… 751*

Comparison of the Pre-Construction and Production QC Test Results for the SELA-22 Elliptical Jet Grouting Project (New Orleans, LA); *Filippo Maria Leoni, Gianluca Pianezze and Alessandro Bertero …… 763*

Design, Installation, and Testing of Hollow Bar Tiebacks Used as Excavation Support; *Marco D. Boscardin, Ph.D., P.E., D.GE, Kenneth A. Pidgeon, P.E. and Adriane G. Boscardin, Ph.D. …… 775*

Drilled Shaft Acceptance Criteria Based upon Thermal Integrity Profiling; *George Piscsalko, Garland Likins and Gray Mullins …… 785*

PREFACE

On behalf of Deep Foundations Institute (DFI) and the 2016 Conference Organizing Committee, we extend our thanks and gratitude to all attendees, exhibitors, underwriters, invited speakers, and presenters who helped make the DFI International Conference on Deep Foundations, Seepage Control and Remediation (41st Annual Conference) a success. The Conference was held in New York City from October 12-15, 2016.

As we prepared to host this conference in the The Big Apple for the first time since 2008, it was remarkable to witness just how much it has changed and reshaped itself since September 11, 2001. Moreover, we were reminded how integral DFI members were, and still are, in the history of the construction of some of the world's most famous landmarks. During the 1960s, DFI members served on design and construction teams for the diaphragm wall systems, underground garages, and tunnels under and adjacent to the original World Trade Center towers. During the 2000s, other members provided design and construction expertise to support the existing substructures and transit lines during the recovery, then expansion and renewal process. DFI members have a rich, laudable history in Manhattan, the outer boroughs, and metropolitan region where they have designed and built foundations for skyscrapers, incredible underground facilities, new tunnels to transit system capacity, and retrofit systems for increasing the longevity of existing structures. More recently, key DFI members became involved with urban sustainability efforts in the city, which are critical in the aftermath of Hurricane Sandy's destruction of the region in 2012.

The DFI 41st Annual Conference featured two concurrent technical tracks focused on (1) deep foundations and earth retention, and (2) seepage control and remediation. Together these sessions provided an international forum for a wide range of geo-professionals to gather together and present, discuss, and debate all aspects and current challenges pertaining to the advancement of the deep foundation, earth retention, and seepage control and remediation industries. This conference stressed the importance of the work performed, the quality thereof, and the key role DFI members have throughout the process. We kept to the conference goals of analyzing the present to better prepare for the future and its uncertainties, while recognizing and striving to develop areas for improvement and innovation.

More than 90 technical presentations were delivered and discussed by industry experts from more than 12 countries including the U.S.A., Canada, U.K., Australia, Germany, Italy, Austria, Sweden, Belarus, Albania, Egypt, India, and China. The deep foundations track focused on planning and mitigation, design and construction, project delivery, communication and training, incorporation of emerging technology, data management, risk and liability, and advancements for deep foundation and earth retention systems. The seepage control and remediation track focused on cutting-edge information on technologies for ground improvement and seepage remediation, dam and levee design and construction guidance for controlling seepage, best practices in dam and levee safety risk assessment and management, and the latest research on internal erosion and piping mechanisms. The seepage control and remediation track was developed to concentrate attention on the importance of water, as we consider it the most precious and most feared natural resource; there is no life without water and, simultaneously, lives are taken away by water's power if it is not contained. Worldwide, human tragedies and the economic damages produced by scarcity of unstoppable flooding water are incalculable. This publication contains the peer-reviewed technical papers pertaining to the session topics described above and as selected by the Conference Organizing Committee for 2016.

We were honored to host four keynote presenters this year. Dr. Satoru Ueda, leader specialist at the World Bank, was this year's Conference Keynote Lecturer. He shared the crucial role of the World Bank's involvement, strategy, policy, and lessons learned while supporting worldwide projects and programs. George J. Pierson, president and CEO of Kleinfelder, was this year's Deep Foundation Keynote Lecturer. He spoke about his career and his expertise in risk management, mitigation, and resolution. James C. Dalton, P.E., director of civil works for the U.S. Army Corps of Engineers, was this year's Seepage Control and Remediation Keynote Lecturer. He delivered a presentation on the incredible challenges to remediate the Mosul Dam (Iraq), which is considered the most unstable and seepage related problematic dam in the world. Notably, Dr. Mae Jemison, former NASA Astronaut, delivered this year's Hal Hunt Lecture entitled "Exploring the Frontiers of Science and Human Potential." She addressed the

achievements and obstacles she faced throughout her life as a NASA astronaut, Peace Corps volunteer, and principal of the 100 Year Starship Project.

This year's conference included networking and social opportunities for attendees including DFI's Annual Awards Reception and Banquet, Women in Deep Foundations Reception, a business meeting luncheon, welcome reception and more. Members of DFI's 21 technical committees and working groups also gathered to discuss, debate, and offer solutions to the various challenges affecting the deep foundations industry. In addition, more than 125 exhibits were featured and showcased by member companies with innovative products, highly technical methods, their latest materials, and professional services.

Undoubtedly, without the hard work and dedication of all those involved, this Annual Conference would not have been possible. We, especially, would like to express our sincerest gratitude to the conference organizing committee, session chairs and moderators, authors, reviewers, underwriters, exhibitors, and volunteers. As we have come to expect and appreciate, t DFI has done an amazing job organizing, preparing, guiding, supporting, corralling, and gently prodding to ensure the Conference was executed flawlessly. We would be remiss if we did not acknowledge specifically the efforts of DFI Executive Director Theresa Engler, Events Manager Lauren Nance, and Technical Activities Manager Mary Ellen Bruce Large, P.E., D.GE-, and all staff at DFI for making this event possible.

In closing, we express our appreciation for the opportunity to be a part of the DFI 41st Annual Conference on Deep Foundations, Seepage Control and Remediation. We look forward to next year's event in New Orleans, Louisiana!

Conference Co-Chairs, Deep Foundations

Dr. Antonio Marinucci, M.B.A., P.E.
Independent Consultant; Research Professor at NYU

Silas C. Nichols, P.E.
Federal Highway Administration

Conference Co-Chairs, Seepage Control and Remediation

David Paul, P.E.
U.S. Army Corps of Engineers

Gianfranco Di Cicco
GDConsulting, LLC

APPLICATIONS OF KNOWN CONCEPTS FOR MANAGEMENT OF CONSTRUCTION VIBRATIONS

Mark R. Svinkin, VIBRACONSULT, Cleveland, Ohio, USA, 216-531-2547

ABSTRACT

Construction equipment and operations usually produce soil and structural vibrations which may harmfully affect various structures and also the content of buildings and houses. The level of structural vibrations depends on a number of factors such as characterized sources of vibrations, soil conditions, and susceptibility of structures. There are certain knowledge and experience for managing the effects of construction vibrations which require implementation of condition survey of structures, information on construction dynamic sources and soil conditions at a site, evaluation of possible vibration effects on structure, calculation of ground vibrations before construction, use mitigation measures to decrease vibrations, and a choice of appropriate vibration limits. The paper presents the application of known concepts for assessment of vibration effects on structures from bridge constructions.

Keywords: pile driving, dynamic compaction, construction vibrations, settlement, condition surveys, peaks particle velocity, vibration limits

INTRODUCTION

Vibrations producing by construction activities such as pile driving, dynamic compaction of loose soils, demolition work, heavy construction equipment and trucks can affect adjacent and remote structures. Vibration effects on structures, sensitive devices and processes may create significant practical problems. Legal actions are often required for solutions of vibration consequences.

The level of construction vibrations depends on dynamic sources, soil conditions at a site in particularly availability of soils with settlement potential, distances from the sources, parameters of waves propagating at a site and susceptibility rating of adjacent and remote structures. It is likely that intolerable structural vibrations from direct vibration effects of impact pile driving and resonant floor vibrations from vibratory pile driving may be induced in adjacent structures to construction sites.

Foundation settlements resulting from soil vibrations in loose soils usually occur in the proximity of dynamic sources, but it is important that dynamic settlement may happen at various distances from the source. There are such examples. First, Kaminetzky (1991) mentioned a case history of building settlements developed at a distance of about 305 m (1000 ft) away from a pile driving site. Foundations of the buildings were underpinned on piles down to the tip elevation of the new driven piles to prevent building settlements. Second, Lacy and Gould (1985) shows that the peak particle velocity (PPV) of 2.5 mm/s (0.1 in/s) of ground vibrations could trigger dynamic settlements at distances up to 30.5 m (100 ft) from driven piles.

Engineering analysis of expected vibrations at the site includes evaluation of local construction experience and clarification of soil conditions on a subject of possible dynamic settlement; condition survey of structures; evaluation of possible direct vibration effects and resonance structural vibrations; assessment of construction dynamic sources and their dynamic characteristics; assessment of expected ground vibrations; use preventive measures to decrease vibrations; and a choice of appropriate vibration limits, Svinkin (2013).

Condition surveys are very useful for analysis of the causes of the existing damage to structures and the following analysis of vibration effects on structures, Svinkin (2012). Knowledge of a local experience of

© 2016 Deep Foundations Institute

construction effects on environment can be beneficial for assessment of expected vibration outcomes of new construction.

The existing knowledge of construction vibration effects was applied and FDOT field data were utilized for preparation of "Specifications for the Control of Ground and Structural Vibrations from Roadway and Bridge Construction" for Florida DOT.

EXPERIENCE OF CONSTRUCTION VIBRATION EFFECTS IN FLORIDA

There are several publications with the results of vibration effects from pile driving and other construction operations on the existing structures.

Lynch (1960) reported installation of 30 cm (12 in) pipe piles and 36 cm (14 in.) or 41 cm (16 in) shells by a Vulcan OR hammer with the rated energy of 41 kJ at Port Everglades. The soil at the site consisted of sand fill, organic silt (muck), loose to medium dense sand, limestone, and compact sand. Piles were driven to the average depth of 21 m (70 ft) because all strata below this elevation were so compact that no appreciable settlements would occur as a result of their consolidation under loads. However, telltale measurements of the test piles indicated downdrag loading of the pile tip caused by organic and sand layers compaction that settled previously driven piles up to 17.8 cm (7 in). Those piles were driven to practical refusal and settlement happened, before placing loads on piles, because of the effect of other pile installation.

Hesham et al. (2003) evaluated how construction-related vibrations may affect existing structures proximate to the areas of a large construction site in Palm Beach County, Florida. Based upon a simplified equation in which PPV depends on a distance and the coefficients 'n' and 'k', the conservative allowable vibration level of 5 mm/s (0.2 in/s) was determined at distances between 80-125 m (262-410 ft) for the Delmag D30 and Delmag D46 hammers and also the sheetpile vibratory drivers.

Heung et al. (2007) present the results of vibration monitoring studies conducted during pile driving operations on Florida's Turnpike Enterprise projects in central and south Florida. Most of the available data were derived from installation of 455 mm (18 in) PPC piles. The study underlined the importance of predrilling to penetrate through a shallow medium dense layer and recommended the use of correlations with a scaled horizontal distance.

Svinkin and Saxena (2004) performed a study of vibration effects of stormwater treatment construction on residential houses. In addition, special vibration tests were made at a staging area. During tests, ground vibrations were measured from various vibration sources: driving of two sheet piles in parallel; driving of two perpendicular sheet piles; dropping a heavy weight on the ground; moving a vibratory compactor and a loader; and a moving loader and excavation. It was concluded that environmental forces and aging processes in house materials appear to be the actual causes of the damages to houses.

The demonstrated case histories brought attention to possible dynamic settlements and downdrag forces in collapsing soils triggered by pile driving, importance of predrilling to penetrate a shallow medium dense layer and the necessity of condition surveys of structures before and after construction.

CONDITION SURVEYS OF STRUCTURES

A preconstruction condition survey of structures before the beginning of construction activities is necessary for evaluation of construction vibration effects on integrity and serviceability of adjacent and remote structures. This survey has to be implemented prior to the start of any other activities on the site including the test pile program. The survey will include all buildings within a radius of about 50-80 m

© 2016 Deep Foundations Institute

from construction operations with adjustment to local conditions. The preconstruction condition survey should be particularly performed at locations susceptible to dynamic settlement and for historic structures in the area with a radius of approximately 400 m. Dowding (1996) also underlined the importance of condition surveys for the contractor protection from unfounded complaints and possible litigations.

The objective of this survey is to determine the conditions of structures including the house and building susceptibility to vibration effects from construction operations, possible dynamic settlement hazard and vibration background. This survey can detect possible disruptions of businesses from construction activities which include cosmetic cracking and other damage on surrounding houses and building and also impacts on sensitive devices and equipment.

Goals of Preconstruction Condition Surveys

Surveys should include observation and documentation of existing cracks and other damage of foundations, exterior and interior walls, ceilings, floors and roofs. Cracks and other damage should be detailed by videotapes and photographs. Notes and sketches should be made to highlight, supplement, or enhance the photographic evidence. According to Siskind (2000), it is necessary to distinguish different types of cracking in structures such as cosmetic cracking, architectural or minor damage and structural cracking or major damage.

A preconstruction condition survey of structures is important for the determining of possible causes of the existing damage because environmental forces, geotechnical hazards and dynamic forces from construction operations can be the cause of similar structural damage, and such damage can exist before the beginning of construction. Verification of dynamic settlement risk should be done because dynamic settlement can be a cause of major damage to structures from construction operations, Svinkin (2008; 2013).

Inspected houses and buildings should be classified into three different categories as a function of building's susceptibility to cracking during pile driving: high, moderate, or low susceptibility, Dowding (1996). Historic buildings usually have high susceptibility rating.

Measurements of existing vibration background should be made to obtain information regarding effects of existing vibration sources. Moreover, the presence of sensitive devices and operations such as electronics, medical facilities, optical and computerized systems placed usually on the floors requires measurement of floor vibrations.

Condition surveys performed after the completion of construction operations and sometimes during construction operations are significant for analysis of possible causes of damage to structures. Such surveys contain complete information on structural responses and damage from vibration excitations. Each construction site is unique and even similarity of soil strata does not mean the same development of dynamic settlements. Physical evidences of damage to structures from dynamic sources are very important. It is typical that crack widths may vary in time. If crack widths increase without increasing crack lengths, it is a safe situation. However, if variation in crack widths trigger increasing crack lengths, it becomes dangerous for structures. Therefore, it is necessary to measure crack widths together with an assessment of crack length enlargements.

STRUCTURAL RESPONSES TO GROUND VIBRATIONS

Assessment of construction vibrations is a complicated problem. There is a considerable diversity of buildings and underground facilities. These structures and their parts, for instance, floors, external and internal walls etc., have different responses to the same ground vibrations. The structural responses to

© 2016 Deep Foundations Institute

ground vibrations depend on parameters of forced vibrations, soil-structure interaction and soil conditions under structures. Ground vibrations can produce direct vibration effects on structures and trigger resonant structural vibrations of adjacent and remote structures. Moreover, vibratory pile driving may trigger resonant soil layer vibrations. Soil-structure interaction will be different for soil failure. Thus the structural response to ground excitation depends on soil deformations triggered by wave propagated from the source and soil structure interaction, Svinkin (2004; 2008).

Direct Vibration Effects

Direct damage to structure happens as a result of soil-structure interaction when frequencies of ground vibrations do not match natural frequencies of structures. Such damage may be expected within a distance of about one pile length from pile driving. This distance can be substantially larger for susceptible structures. Structures have significant resistance to direct vibration effects. According to available experience in the blasting industry (Siskind, 2000), direct minor and major structural damage to 1-2 story residential houses without resonant structural responses were observed in the velocity range of 33-191 mm/s (1.3-7.5 in/s) for frequencies of 2 to 5 Hz and in the velocity range of 102-254 mm/s (4-10 in/s) for frequencies of 60 to 450 Hz, Svinkin (2006).

Resonant Structural Vibrations

The proximity of the dominant frequency of ground vibrations to one of building's natural frequency can amplify structural vibrations and even generate the condition of resonance. If ground vibrations have only a few cycles with the dominant frequency equal to one of building's natural frequency, resonant vibrations do not develop. The resonant structural vibrations are independent of the structure stiffness being limited only by damping.

Vibratory drivers with various operating frequencies may produce resonant floor vibrations because the natural frequencies of vertical floor vibrations range between 8-30 Hz. These vibrations may affect precise and sensitive devices installed on the floors.

Resonant low-frequency structural vibrations at large distances from blasts are typical for coal surface mining and quarry blasting operations. However, pile driving is much less powerful source of vibrations than blasting, and consequently probability of triggering resonant structural vibrations by impact hammer during pile driving is very low. At the best of the writer knowledge, there are no case histories of low-frequency resonant structural vibrations generated at large distances from impact pile driving. It is reasonable to not consider such effects for practical goals, Svinkin (2015).

Resonant Soil Layer Vibrations

A coincidence of the dominant frequency of propagated waves with the frequency of a soil layer can create the condition of resonance and generate large soil vibrations. In such situation, it is necessary to stop pile driving and change the vibratory frequency.

Dynamic Settlement

Diverse case histories available in numerous publications demonstrate devastating effects of dynamic settlement on structures, for example, Swiger (1948), Lynch (1960), Horn (1966), D'Appolonia (1971), Clough and Chameau (1980), Lacy and Gould (1985), Feld and Carper (1997), Svinkin (2006) and other. It is extremely important to evaluate possible dynamic settlement in collapsing soils because small ground vibrations from construction operations cannot be the cause of direct vibration effects and resonant

© 2016 Deep Foundations Institute

structural vibrations, but these small ground vibrations may trigger significant dynamic settlement and damage structures.

Kaminetzky (1991) reported a case history of serious damage to structures from pile installation by heavy impact hammers at a site with uniform medium dense sands. Street pavements cracked and settled as much as 406 mm (16 in) after only one-fourth the piles had been driven. Therefore, sheet piles were installed to prevent additional settlement and damage to sewer and water pipelines. After the contractor substituted impact hammers for vibratory drivers, damage became even worse. High-rise neighboring buildings as tall as 19 stories were so severe damaged that eventually all buildings within a radius of 122 m (400 ft) were denounced as unsafe and had to be demolished. Also, Kaminetzky (1991) mentioned an interesting case with building settlement developed at a distance of about 305 m (1000 ft) away from a pile driving site. Foundations of the buildings were underpinned on piles down to the tip elevation of the new driven piles to prevent building settlements.

Movements of adjacent buildings during pile installation can be an important problem if clay susceptible to the dynamic loading-induced settlement is present at a construction site. Effects of pile driving in soft to medium clay on the surrounding area should be expected at distances from the pile installation equal to about the thickness of the clay layer being penetrated, D'Appolonia (1971). Also, it is necessary to say that there are case histories of pile driving in sands without dynamic settlements, for example, Ashraf et al. (2002) and Svinkin (2013).

Additional Cause of Damage

It is necessary to take into account the accumulated effect of repeated dynamic loads from production pile driving. This approach is especially important for historic and old buildings.

ASSESSMENT OF EXPECTED GROUND VIBRATIONS

For practical goals, it is important to assess the maximum PPV of ground vibrations expected during construction operations prior to the beginning of construction operations. Wiss (1981) applied the scaled-distance (SD) approach for construction sources of vibrations and proposed the following equation to calculate the peak particle velocity of ground vibrations

$$v = k[D/\sqrt{W_r}]^{-n} \quad (1)$$

where k = value of velocity at one unit of distance, n = attenuation coefficient. The attenuation rate represented by the coefficient 'n' is a conventional combination of mostly material damping and partially geometric one. This is a so-called pseudo-attenuation coefficient. The value of 'n' yields a slope of amplitude attenuation for all tested soils in the 1-2 narrow range on a log-log chart, and this coefficient is independent of the soil type, the source energy, and the energy level. Coefficient n=1 means lower attenuation of ground vibrations and consequently higher PPV of ground vibrations.

The energy transferred to driven piles can be substantially less than the hammer rated energy because hammer efficiency changes in 0.9-0.15 limits. Therefore, it is reasonable to replace the rated energy, W_r, with the transferred energy, W_t, Svinkin (2008)

$$v = k[D/\sqrt{W_t}]^{-n} \quad (2)$$

Equation (2) provides very rough assessment of ground vibrations as a function of the source energy and a distance from the source. Also, Equation (2) does not take into account the soil conditions, the pile

© 2016 Deep Foundations Institute

penetration depth, the soil resistance to pile penetration, the soil heterogeneity and uncertainty, the soil-structure interaction, and has no connections with structural vibrations, dynamic settlements, and vibration effects on sensitive equipment. However, Equation (2) adjusted for site soil conditions and pile types with field pile testing provides relatively better calculation results than other empirical equations for assessment of the upper limits of expected ground vibrations, Svinkin (2013).

For receiving good practical results, preliminary conditions should be employed to determine variables of equation (2). Distance D. For any location on the ground surface, slope distances in comparison with horizontal ones yield smaller PPV, but due to soil heterogeneity and uncertainty, measured ground vibrations may be even larger than those calculated with horizontal distances. Therefore, horizontal distances should be used in calculations. Energy W_t. The hammer energy transferred to piles can be calculated as the product of the rated energy and efficiency. An existing experience provides information about efficiency of different hammer models. Coefficient 'n'. This coefficient represents the attenuation rate (slope of an attenuation line) of ground vibrations. Lower attenuation (n=1) and consequently higher PPV of ground vibration should be chosen. Values of 'k'. This coefficient can be found out from a local experience or pile testing performed at a site.

An example of determination of an appropriate scaled-distance equation for calculation of expected ground vibrations PPV at a construction site is shown in Figure 1. The coefficient k=5.4 was determined on the basis of ground vibration measurements from pile installation and back analysis of a scaled-distance equation. Then the extreme values of the scaled-distance equation graph were found for scaled distances of 0.1 and 300 using the following equation

$$v = k/SD \qquad (3)$$

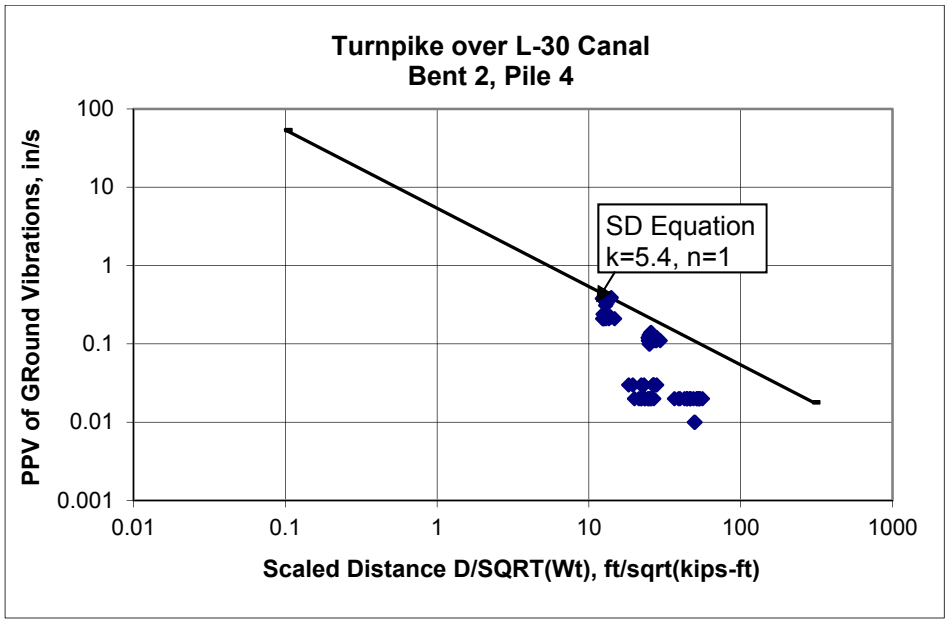


Figure 1. Scaled distance equation for driving of 18" PSC pile

The same approach was applied for vibratory drivers used for sheet pile installation and vibratory rollers employed for soil compaction, Svinkin (2008). Coefficients 'k' determined from field data are presented in Table 1.

© 2016 Deep Foundations Institute

Table 1. The Coefficient 'k' determined from field data

Equipment	Transferred Energy ft-lbs	Number of Piles, or Vibratory Rollers	Pile Types	Coefficient 'k'
Impact Pile Driving				
ICE 120-S, ICE 100-S, ICE 80-S, ICE I-19 APE D30-22, APE D36-32 Delmag D46-32, D36-32, D30-02 Bergminghammer B5505	5,000 – 30,000	40	PSC 18"x18" PSC 24"x24" HP 14x89	5.6
		10		8.0
		5[1]		6.4
		4		3.4
		6		1.7
Vibratory Pile Driving				
Vibratory Driver/Extractor Power 150 kW, Frequency 26.67 Hz, Amplitude 1 inch	1,400[2]	4[1]	AZ-18	19.0
		5[1]		14.9
Vibratory Rollers				
Bomag, Sakai, Hamm 120, Hamm HD 110, Ingersol Rand	64[2]	5	N/A	43.0

[1]Sheet piles.

[2]The maximum energy transferred to a vibratory driven pile per a cycle of driving is a product of the maximum power, the period of pile vibrations and efficiency, Svinkin (2008). A similar approach was used to determine the energy transferred from a vibratory roller on the ground.

It can be seen from Table 1 that the coefficient 'k' increases with a reduction of the energy of dynamic sources.

REDUCTION OF VIBRATION EFFECTS

Mitigation measures depend on the vibration effects produced by construction operations, Svinkin (2006).

Direct Vibration effects on Structures

For mitigation of vibrations generated by installation of driven piles, a few factors should be considered. First, installation of non-displacement piles instead of displacement piles can reduce ground and structure vibrations. Second, hard pile driving to a depth about 10 m from the ground surface may increase ground vibrations but hard pile driving at a greater penetration depth does not affect ground vibrations. Predrilling may be helpful for overcoming high penetration resistance in the upper soil layers. However, predrilling or jetting in sand should be done with caution. Third, substantial decrease of the hammer energy can be helpful; however, slight reduction of the hammer energy will have a small effect because PPV of ground vibrations depends on the square root of the hammer energy. Fourth, vibratory hammers may trigger resonant vibrations of soil layers, but hammers with variable frequency can eliminate these phenomena. Fifth, according to D'Appolonia (1971), pile driving operations should start nearby the existing structures and continue away from the structures because previously driven piles act as a shield and soil movements are greater in the direction away from the stiffer zone around the driven piles. Sixth, criteria for vibration monitoring and control should be included in pile driving specifications. Examples of such specifications are available in Dowding (1996) and Woods (1997). Since pile impedance is sometimes mentioned as a factor which can influence ground vibrations, it is necessary to point out that pile impedance affects force and velocity at the pile head in opposite ways. Therefore, the pile impedance effect on the intensity of ground vibrations is not obvious, Svinkin et al. (2000).

© 2016 Deep Foundations Institute

Soil Settlement in Sand Soils from Pile Driving

Some measures can be considered for mitigating pile driving effects on settlements in sand soils. First, reduce the level of ground vibrations as much as possible. Second, use preboring holes for pile installation or use jetting to install piles. Third, choose a light hammer. Fourth, monitor and control vibrations and structure settlements at a site.

VIBRATION LIMITS

Different vibration criteria should be used for proper assessment of vibration effects of construction vibrations on structures.

Structures have the relatively high resistance to direct vibration effects from construction operations, and they can withstand ground vibrations up to 25 mm/s (1.0 in/s) without damage. The application of the frequency-independent safe limit of 51 mm/s (2 in/s) for measured structural vibrations can help to determine unacceptable vibrations of various structures: low-rise houses, multi-story residential, commercial and industrial buildings. This criterion automatically takes into account soil-structure interaction for the whole building frequency range, Svinkin (2004; 2013; 2015). For a more comprehensive assessment of structural vibrations from construction sources, ANSI (1990) should be used.

Dynamic settlement can be a cause of major damage to structures from construction vibrations. Ground and foundation settlements as a result of relatively small ground vibrations in diverse sand soils may occur at various distances from the source for account of soil densification. This phenomenon is quite different from liquefaction because liquefaction can be triggered by relatively high ground vibrations with PPV of about 10 cm/s (4 in/s), but ground vibrations with PPV about 2.5 mm/s (0.1 in/s) may be the cause of soil densification and dynamic settlements in vulnerable sandy soils, Lacy and Gould (1985). Siskind (2000) paid attention that the low vibration amplitude of 0.5-1.5 mm/s (0.02 – 0.06 in/s) in loess soils may be the cause of dynamic settlement. Such soil deformations may occur at adjacent and remote locations.

CONCLUSIONS

An available knowledge and experience in the field of construction vibrations provides an opportunity to successfully manage construction vibration effects on structures.

Preconstruction condition surveys are very important for a proper assessment of vibration effects on structures. Surveys of structures should be performed before, during, and after the completion of construction operations, and these surveys should be used in a combination of evaluation of expected maximum ground vibrations from construction sources and prevention of possible damage to structures.

Calculation of the peak particle velocity (PPV) of ground vibrations is imperative to evaluate ground vibrations prior to the beginning of pile driving operations conducted in urban areas because such vibrations can affect sensitive devices and processes, disturb people and even damage structures. A scaled-distance equation is mostly used for calculation of expected PPV of ground vibrations prior to pile installation. This equation adjusted for site soil conditions and pile types with field pile testing provides relatively better calculation results than other empirical equations for assessment of the upper limits of expected ground vibrations.

© 2016 Deep Foundations Institute

The limit of 25 mm/s (1.0 in/s) would be reasonable for ground vibrations which cannot damage residential structures due to only direct vibration effects on structures. This criterion is not accepted for resonance structural vibrations and dynamic settlement.

There are no case histories of resonant low frequency structural vibrations generated by impact pile driving.

The limit of 2.5 mm/s (0.1 in/s) should be used as the threshold of possible significant settlement at vulnerable sandy sites.

Preventive measures should be used to mitigate construction vibration effects. A set of such measures depends on soil deformation (elastic or plastic) under vibration excitation and soil-structure interaction.

ACKNOWLEDGEMENT

This research was supported by the Florida DOT under contract No. BDK80 977-22. In addition, thanks to Mr. Wing Heung of Florida Turnpike and Mr. Brian Bixler of FDOT for sharing field data of construction operations and measurements of ground vibrations performed for FDOT projects. The contents of this paper reflect the view of the author who is responsible for analysis, discussions and interpretations presented herein.

REFERENCES

ANSI S2.47-1990. American National Standard. Vibration of Buildings – Guidelines for the Measurement of Vibrations and Evaluation of Their Effects on Buildings, Accredited Standards Committee S2, Mechanical Shock and Vibration, Standard Secretariat c/o Acoustical Society of America, New York.

Ashraf, S., Jayakumaran, S. and Chen, L. 2002. Case history: pile driving and vibration monitoring for Avenue P Bridge in Brooklyn, New York, Deep Foundations 2002, Geotechnical Special Publication No. 116, V. One, ASCE, pp. 500-509.

Clough, G.W. and Chameau, J-L. 1980. “Measured effects of vibratory sheetpile driving.” Journal of Geotechnical Engineering Division, 106 (GT10), pp. 1081-1099.

Feld, J. and Carper, K.L. 1997. Construction Failure. John Wiley and Sons, New York, 512 p.

D’Appolonia, D.J. 1971. Effects of foundation construction on nearby structures. Proceedings, 4th Panamerican Conference on Soil Mechanics and Foundation Engineering, Puerto Rico, ASCE, New York, V. 2, pp. 189-235.

Dowding, C.H. 1996. Construction Vibrations. Prentice Hall, Upper Saddle River, 610 p.

Hesham, A., Castellanos, J., Hart, D., and Nukunya, B. 2003. Real-time measurement of the impact of pile driving vibrations on adjacent property during construction. TRB 2003 Annual Meeting, CD-ROM.

Heung, W. Morgan, K, Yoon, Y.H., Gobin, R., Gollamudi, S. 2007. Vibration due to driving concrete piles using open-ended Diesel hammer in Central and South Florida. Proceedings of the Seventh International Symposium on Field Measurement in Geomechanics, Boston, Massachusetts, CD-ROM.

Horn, H.M. 1966. Influence of pile driving and pile characteristics on pile foundation performance. Lecture Notes, New York Metropolitan Section, ASCE, Soil Mechanics and Foundation Group.

© 2016 Deep Foundations Institute

Kaminetzky D. 1991. Design and Construction Failures – Lessons from Forensic Investigations, McGraw-Hill, Inc., New York, 600 p.

Lacy H.S. & Gould J.P. 1985. Settlement from pile driving in sand, Proceedings of Symposium on Vibration Problems in Geotechnical Engineering, Gazetas G. & Selig E.T. (eds.), ASCE, New York, pp. 152-173.

Lynch, T.J. 1960. Pile driving experience at Port Everglades. Journal of Soil Mechanics and Foundation Division, 85(SM2), pp. 41-62.

Siskind D.E. 2000. Vibration from Blasting. International Society of Explosives Engineers, Cleveland, Ohio, 120 p.

Svinkin, M.R., Roth, B.C., and Hannen, W.R., D. 2000. The effect of pile impedance on energy transfer to pile and ground vibrations. Proceedings, Sixth International Conference on the Application of Stress-Wave Theory to Piles, Sao Paulo, Brazil, 11-13 September, pp. 503-510.

Svinkin, M. R. 2004. Minimizing construction vibration effects. Practice Periodical on Structural Design and Construction, ASCE, 9(2), pp. 108-115.

Svinkin, M.R. 2006. Mitigation of soil movement from pile driving. Practice Periodical on Structural Design and Construction, ASCE, 9(2), 108-115.

Svinkin, M.R. 2008. Soil and structure vibrations from construction and industrial sources. OSP8, Proceedings, Sixth International Conference on Case Histories in Geotechnical Engineering, OmniPress, Arlington, Virginia, 14 p.

Svinkin, M.R. 2012. The necessity of condition surveys for structural protection against pile driving effects. Proceedings, 9th International Conference on Testing and Design Methods for Deep Foundations, Kanazawa, Japan, 18-20 September 2012, pp. 429-439.

Svinkin, M.R. 2013. Forensic engineering of construction vibrations. Forensic Engineering, ICE, 166(FE2), 81-93.

Svinkin, M.R. 2015. Tolerable limits of construction vibrations. Journal of Structural Design and Construction, ASCE, 20(2), pp. 1-7.

Svinkin, M.R. and Saxena, D.S. 2004. Vibration Monitoring, Data Evaluation, and Engineering Consultation Services Report, Conducted on: Existing Residences of 20 Claimants Seville Drive Stormwater Treatment/Enhancement Project (Clark Site), Pensacola, Escambia County, Florida, 46 p.

Swiger, W.F. 1948. Effect of vibration on piles in loose sand. Proceedings, 2nd International Conference on Soil mechanics and Foundation Engineering, V. II, Rotterdam.

Wiss, J.F. 1981. Construction vibrations: State-of-the-art. Journal of Geotechnical Engineering Division, ASCE, 107(2), pp. 167-181.

Woods, R.D., 1997. Dynamic Effects of Pile Installations on Adjacent Structures, NCHRP Synthesis 253. Transportation Research Board, National Research Council, Washington, D.C., 86 p.

© 2016 Deep Foundations Institute

ETHICAL AND RISK ASPECTS OF DEEP FOUNDATION SUBCONTRACTS

Alexander Filotti, M.B.A., P.E., Underpinning and Foundation Skanska, Inc., Maspeth, NY, USA, 718-340-1021, alex.filotti@skanska.com
Richard Kalson, Esq. Partner- Benesch, Friedlander, Coplan & Aronoff LLP, Pittsburgh, PA, USA, 614.223.9380, RKalson@beneschlaw.com

ABSTRACT:
In the last decade, the construction industry has witnessed significant changes in the project delivery systems and contractual relationships between the general contractors (GC) and Deep Foundation Specialty Contractors. The Deep Foundation industry, especially including industry specialty subcontractors, have experienced a significant increase in requests that project risks be transferred through contract documents to subcontractors and suppliers with a decrease in margins for the industry. GCs regularly revise their form subcontracts to take into account recent experiences/contractual trends and newly issued judicial precedent, an exercise that is less frequently undertaken by subcontractors and suppliers. These contradictory trends are at the base of the ethical analysis of subcontracts that comprises the subject matter of this paper. Using contracts as a risk management tool in order to mitigate the general contractor's risks in the context of dynamic changes in the legislative environment will also be addressed. Furthermore, another possibility for risk mitigation for the industry is to actively promote the introduction of the latest technical developments into the contract documents.

Keywords: contracts, ethics, risk management, deep foundation industry

CONTRACTS' ETHICS

For thousands of years, ethics have been a constant presence in our lives and have been debated by different branches of philosophy. In modern times, ethics in business started to be an imperative for the success of a globalized economy.

"Ethics are standards by which one should act based on values. Values are code beliefs such as duty, honor, and integrity that motivate attitudes and actions." (Rumbaugh 2004). Some of these values and actions have been carved in legislation in general and in business legislation in particular. More and more, unethical business practices (e.g., corruption) are identified as the root cause of poverty, underdevelopment, and war around the world. In the context of contract ethics, three aspects are of interest:

- Ethics of contract construction
- Ethics of contracting processes
- Ethics of risk allocation in contracts

The ethical construction of contracts is the obligation of legal professionals who write the contracts, and how ethical principles are applied to the contract construction is the subject of vast legal literature and

© 2016 Deep Foundations Institute

case law and it is out of the scope of this paper. For our industry's contract professionals (i.e. contract managers, risk managers etc.) the following construction contract issues are of interest:

- Clauses on the edge of validity
- Invalid or illegal clauses
- Ambiguous language which could lead to different interpretations

All of the three aforementioned types of clauses should be identified and eliminated from contracts by subcontractors, as their mere presence is at least unethical if not illegal. A significant possibility of unfavorable consequences exists when these provisions are imposed upon and accepted by a less sophisticated Subcontractor who does not possess substantial legal knowledge and may have limited access to legal counsel.

The contracting process presents the following ethical or unethical practices:

- Delaying the execution of the subcontract until the job has to start or even after the mobilization of the Subcontractor's equipment, at which point the bargaining power of the GC increases exponentially. Therefore, no material should be released, no equipment should be mobilized, and no submittals released by a Deep Foundation Subcontractor without an executed subcontract.

- Lately, it is customary for most subcontracts to incorporate the prime contract between the Owner and the GC by reference as part of the subcontract. Many times, the prime contract is not transmitted to the Deep Foundation Subcontractor for analysis, and in many cases is not executed at the time of the negotiation of the subcontract. This practice makes it very difficult to appreciate the impact of flow-downs from the prime contract relative to the scope of work and the legal obligations and remedies of the subcontract. It is the duty of the Deep Foundation Subcontractor to communicate clearly and unequivocally that a subcontract will not be executed and no work will take place without the Subcontractor having access to and time to study all documents listed in the subcontract. It is the only way for Subcontractors to have a complete picture of their scope of work, the risk transferred to Subcontractors by the contract documents, and make an educated assessment of the final price of the subcontract. It is very common for the flow-down provisions of the prime contract, plus the boilerplate subcontract, to add scope of work items and risks to the Subcontractor's obligations, which were not present in the bid documents. This scope creep is one of the causes of reduced profit margins witnessed lately in the deep foundation industry.

- Another aspect of the contracting process detrimental to Deep Foundation Subcontractors is the consolidation of the general contracting and geotechnical engineering industries, which have resulted in powerful organizations generating contracts and subcontracts of a complexity that could be overwhelming for the organization and business of some Deep Foundation Subcontractors. For example, fifteen years ago, our company was driving piles based on a purchase order from the general contractor (GC). Now, for the same type of job, we may receive a one hundred and thirty-page contract. The complexity of such contracts represents a huge risk for the Subcontractor, especially if the contract lands in a court of law for a dispute resolution.

© 2016 Deep Foundations Institute

To mitigate the complexity of these contracts, good practice is to thoughtfully negotiate the scope of work and insist on a clause in the subcontract that the scope of work governs in the event of a conflict between the contract documents and the subcontract.

The ethics of risk allocation in contracts is the aspect that this paper will look into a more detail, particularly in connection with contract delivery systems and the utilization of contracts as a risk management tool. The most controversial allocations of risk are: no compensation for delays, overreaching indemnification clauses, unrealistic payment terms and conditions, uncompensated schedule alteration, outdated technical conditions, unfair conflict resolution clauses, unrealistic notification time-frames, and unethical and illegal waiving of rights.

CONTRACTS AS A RISK MANAGEMENT TOOL

Ideally, contracts should be a fair risk allocation tool where the risks are allocated to the party that has the best ability to manage or assume a specific risk. For example, the GC should bear the risks of trades coordination and possible associated delays to the project, because the GC controls the trade subcontracts. The Subcontractor should only bear the risk of means and methods in the execution of its work, because the Subcontractor has the best knowledge and expertise in this instance.

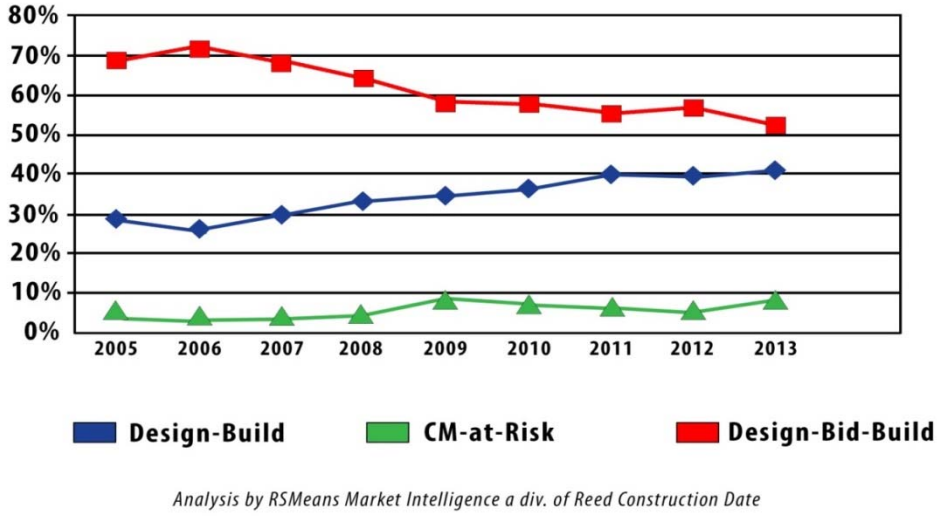


Fig. 1. Project delivery method market share for non-residential construction

Misallocating contractual risks is not only unethical, but is also detrimental to the project schedule, quality, and commercial success. It is unconscionable how many contracts put the responsibility of trade coordination on the Subcontractors, who not only lack the knowledge and staff to perform trade coordination, but also, most importantly, the legal right to perform this task due to the absence of obligations between Subcontractors. Fortunately, a new contract philosophy has started emerging lately, a

© 2016 Deep Foundations Institute

philosophy that places cooperation between parts above coercion (Karr, 2016). While contracts have always had the power of producing legal obligations and enforcing promises, new dynamics in project delivery systems such as Design-Build and Public-Private-Partnership (P3) advocate for a more cooperative environment between GC and specialty Subcontractors, cooperation that should be established based on professional respect and knowledge. The Design-Build contract delivery system approaches the value of contracts with that of the Design-Bid-Build system, the traditional project delivery system for the US (figure 1 tracks the trends of the two systems for non-residential construction).

Contracts should evolve in terms of better cooperation and partnership methods to better confront the increased complexity of the construction projects and the increased risk of the design builders and the removal of the owners from any construction risk.

RISK AND ETHICAL ISSUES WITH DESIGN-BID-BUILD PROJECT DELIVERY METHOD

The contract relationship between the Design-Bid-Build team members is exhibited in Figure 2. Please note how many contractual obligations are flowing to the Specialty Deep Foundation Contractor (shown in red in Figure 2) and how little recourse the subcontract provides to the Specialty Deep Foundation Contractors.

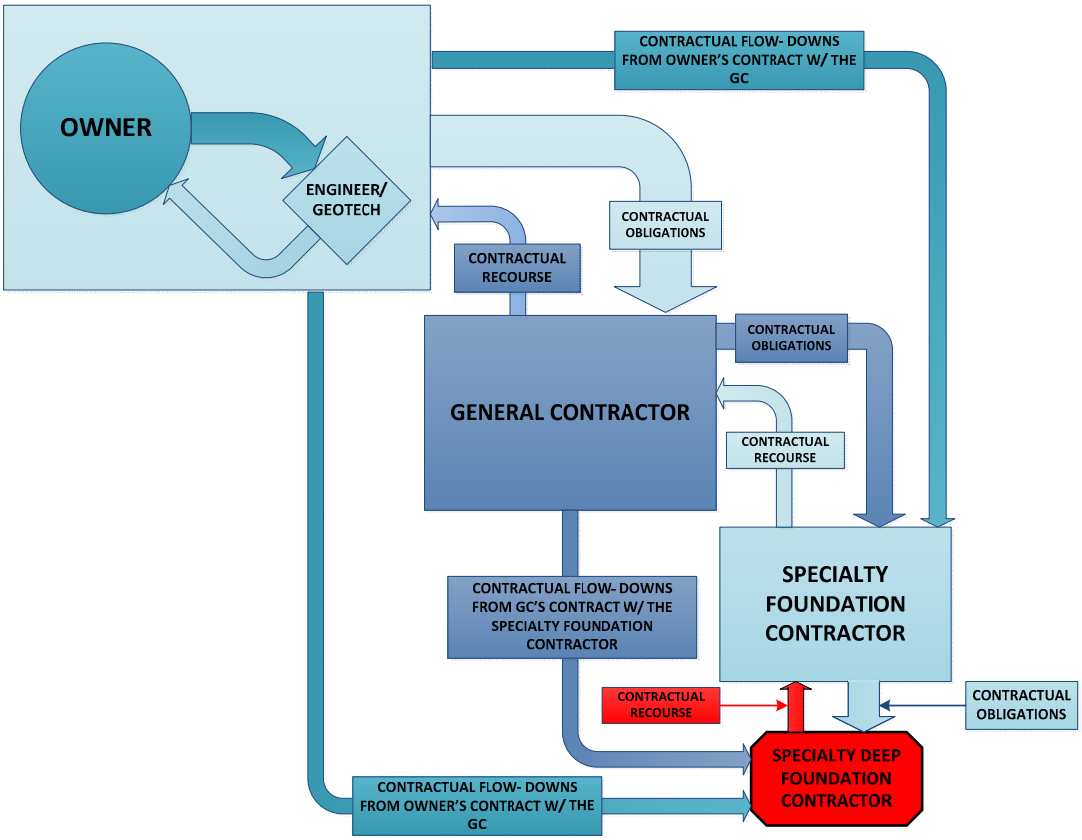


Fig. 2. Contract relationship between the Design-Bid-Build team members.

© 2016 Deep Foundations Institute

Occasionally, the General Contractor fulfills the tasks of the Specialty Foundation Contractor (i.e. the contractor responsible for the delivery of the complete underground concrete structure of the building), alleviating to some degree, the flow downs for the Specialty Deep Foundation Contractor.

In the Design-Bid-Build contract delivery system, the Owner and the Engineer are formed into a unit that retains the risk of design, differing site conditions, payment, and Owner-Engineer generated delays. All the parts of the project downstream have significant risks and obligations transferred by contract from the Owner, directly or indirectly, and at the same time, they have recourse against the Owner for the risks retained by the Owner-Engineer team. The division of risks between the GC and Owner has created an environment where the payment risks and profitability risks are a constant source of complaint for the Specialty Deep Foundation Subcontractors. Slow payment (see Figure 3), combined with change order related delays and non-payment at the end of a contract, are some of the major contributors to the decline of profitability of the Specialty Deep Foundation Subcontractors. Unfortunately, this decrease of profitability comes at the same time as a general decrease in profitability of the overall heavy construction industry (see Figure 4).

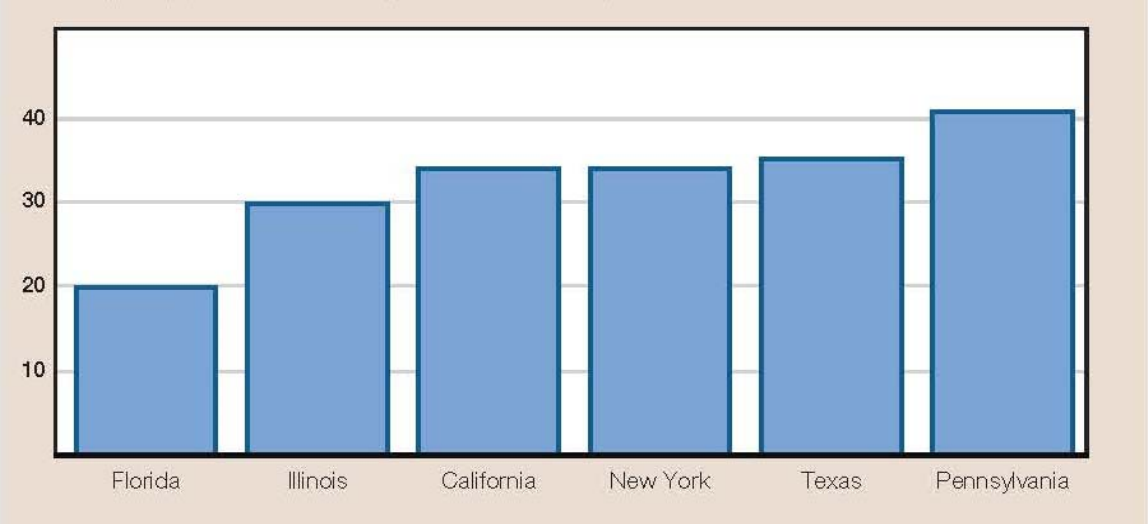


Fig. 3. Slow-Pay Misery- Average day past due reported by subcontractors in key states. Source: ENR Top 600 Specialty Contractors survey, October 2015; minimum 30 firms per state.

Figure 4 clearly shows how, after the 2008 financial crisis, the heavy construction industry has experienced a constant decline in profitability averaging under 2% in 2013. Such a decline in profitability is normally explained by an increase in prices of labor and material and a decrease of the market value, none of which materialized in the subject period to explain such a sharp decrease in the profitability of the industry.

© 2016 Deep Foundations Institute

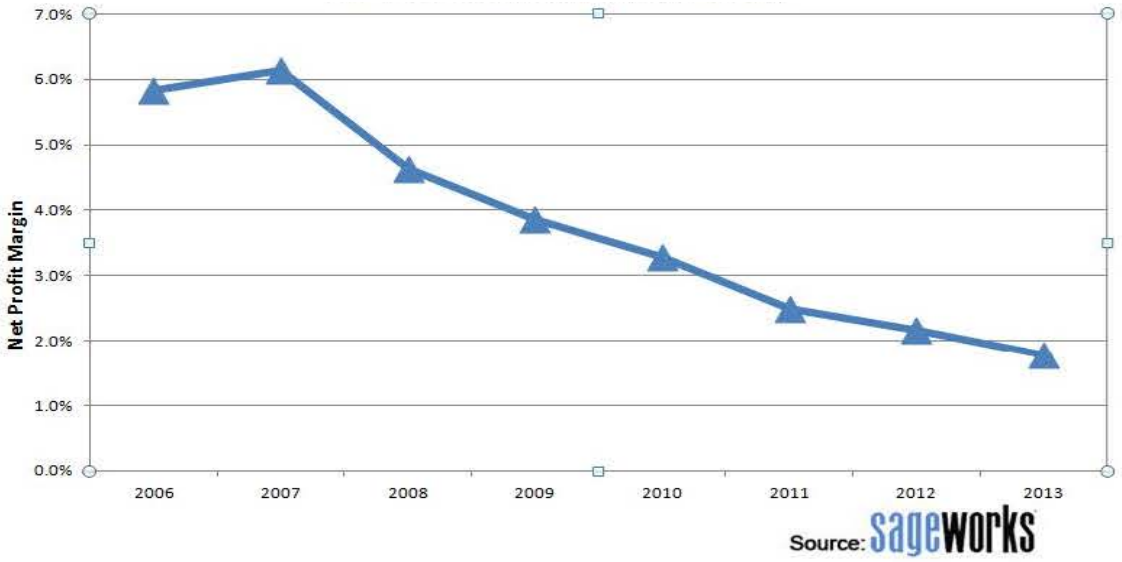


Fig. 4. Profitability trends for privately held highway, street and bridge construction firms (NAICS 2373)

The 2008 financial crisis generated a risk adverse business community that is considered the fundamental cause of the amplification in the tendency of transferring risks from the Owner and GC toward specialty Subcontractors in general, and Deep Foundation Subcontractors in particular. This pronounced contractual trend has resulted in diminished professional collaboration between the project participants and an increase of contract-mandated activities with negative impacts on profitability for subcontractors.

Contract mandated obligations such as indirect flow-downs, unrealistic notification times, and an abusive waiving of various rights of the Subcontractor; create a legal maze that makes each claim against the GC and the Owner a lengthy and costly affair with minimal chances of adjudication in favor of the Subcontractor. In order to secure a future for the industry, this trend has to be reversed, and the allocation of risks in contracts needs to become fair and ethical. This goal has to become a priority for our industry and national organizations.

RISK AND ETHICAL ISSUES WITH DESIGN-BUILD PROJECT DELIVERY METHOD

The contract relationships for a design-build delivery system are shown in Figure 5. As mentioned in the previous section, occasionally, the General Contractor fulfills the tasks of the Specialty Foundation Contractor, alleviating to some degree the flow downs for the Specialty Deep Foundation Contractor (shown in red in Figure 5). In this type of project delivery, the Owner is removed from most of the construction and land ownership risks, and these risks are transferred to the design-build team formed by the GC and its Engineer.

The Design-Build contractual relationship has the advantage of advancing the design and the construction of the project at the same time, lowering the general cost, and reducing the delivery time of the project.

© 2016 Deep Foundations Institute

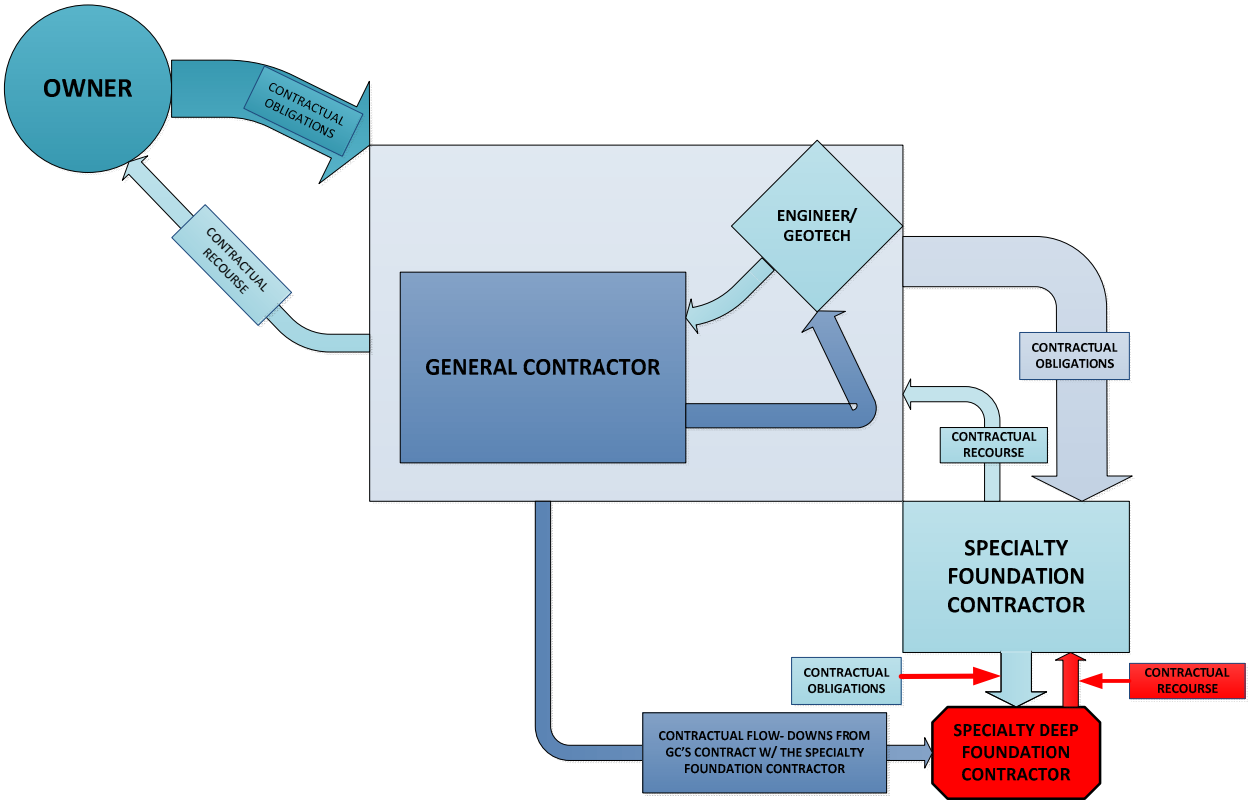


Fig. 5. Contract relationship between the Design-Build team members.

Having the project management and the design under the same roof improves the overall efficiency of the design, but at the same time, creates a bigger risk for the Deep Foundation Specialty Contractors such as:

- Because the construction progresses simultaneously with the design, the probability of changes in the Subcontractor's scope of work increases substantially. On the other hand, the fact that these changes are generated at the Design-Build level, which is not the source of money of the project (the Owner is), the chances of fair compensation of the Subcontractor for the changes in its scope of work are very dim.

- The geotechnical investigation is shared by the Design-Build team, with the Owner creating a blurred boundary of responsibility for differing site conditions (DSC). This situation will accentuate the payment risk for DSCs that are encountered by the Deep Foundation Subcontractor. In order to mitigate this risk, the contract between the Design-Build and Deep Foundation Subcontractor must clearly assign the DSC risk and cost.

- The lack of standardized subcontracts for the Design Build project delivery method causes the use of traditional subcontracts (i.e. subcontracts specific to the Design-Bid-Build project delivery) that unethically assign design responsibilities to the Specialty Deep Foundation Contractor.

© 2016 Deep Foundations Institute

UNETHICAL ALLOCATION OF RISKS IN SUBCONTRACTS

An unethical allocation of risks refers to contract provisions that allocate a risk to the party less able to manage and assume that specific risk. The following is a list of risks unethically allocated in deep foundation subcontracts:

1. Non-Payment for Owner and/or GC Generated Delays.
   While most subcontracts recognize the right of the Subcontractor to pursue a delay claim against the Owner, they deny the right of a Subcontractor to pursue any delay/claim against the GC. Accepting such a clause exposes the Subcontractor to potential catastrophic losses.

2. Pay if Paid or Pay when Paid.
   In many states, New York included, pay if paid clauses are considered to be against public policy. For the states where this clause is legal, the Subcontractor should transfer the risk of an owner payment failure to the GC, especially where the subcontract contains a *Pay if Paid* clause.

3. Excess Flow-Downs.
   The Subcontractor should minimize the extent of the flow-down provisions from the general contract to its specific scope of work. Any flow-downs that could create contractual obligations outside its scope of work (i.e. design obligations, coordination obligations, etc.) and result in the waiver of contractual remedies and their imposition of additional obligations upon the Subcontract should be rejected.

4. Site Inspections
   Many subcontracts state that by inspecting the project site, the Subcontractor accepts all site related risks related to its scope of work; the hidden meaning is that the Deep Foundation Subcontractor is responsible for all underground and above ground risks. The Subcontractor should carefully weigh accepting such risks, try to negotiate the same, and make commercial contingencies if it is forced to accept the risk of unknown underground conditions.

5. Notifications
   The Subcontractor should fight any unreasonable time limits for notifications of claims and delays and should make the GC similarly responsible for time notifications for back-charges to subcontractors.

6. Liquidated Damages
   Liquidated damages and other damages should only be accepted if they are properly related to the Subcontractor's scope of work, milestones related to the Subcontractor's scope of work, and limited to an equitable amount. Consequential damages should never be accepted.

7. Waiving of Lien Rights
   In many states, it is against public policy to request a Subcontractor to waive its lien rights. As a general rule of thumb, no lien or any other legal rights of the Subcontractor should be waived in the subcontract.

© 2016 Deep Foundations Institute

8. Unrealistic Schedule
   Lately, more and more GCs are using the schedule as a tool for back-charges and damage claims against the Subcontractor. Therefore, indifferent to the general schedule of the project, the schedule for the scope of work of the subcontract has to be mutually agreed between the GC and the Deep Foundation Subcontractor and aligned with the reality of the field conditions. The GC should not have the contractual right to direct overtime work or accelerated work without compensation. The Deep Foundation Subcontractor needs to be alert to any Owner/GC generated delay, stoppage, or interruption of work, and must immediately notify the GC and request an extension of time. Unfortunately, doing the proper work does not necessarily guarantee commercial success for the Subcontractor. The Subcontractor has also to win the paperwork game imposed by the subcontract.

9. Indemnification
   Subcontractors are requested to indemnify a GC for the GC's exclusive or partial negligence and for counsel fees in instances of breach of contract.

Other risks wrongly allocated to Subcontractors are improper coordination requests, acceptance of work outside of the scope of the project without compensation, acceptance of acceleration, and work interruption or stoppages without compensation.

DEEP FOUNDATION SUBCONTRACTOR RISK MITIGATION TOOLBOX

To combat the unethical risks allocation in subcontracts, the Deep Foundation Subcontractor has be educated and retain legal counsel when necessary, and understand and properly assign contingencies for all contractual risks. Hence, reading, thoroughly understanding and properly negotiating subcontracts is one of the most important tools the Subcontractor has to preserve profitability. If the Subcontractor finds that after the negotiation of the subcontract with the GC, the contract still holds unacceptable risks, the Subcontractor should walk away from the job rather than hope that those risks will not materialize. Another tool is the negotiation of what the Deep Foundation Subcontractor knows best: a detailed scope of work. Many times, the GCs formulate subcontracts with a very general scope of work referencing all contract documents. This type of scope of work should not be accepted. A detailed scope of work, usually the one presented by Subcontractor in its proposal, should be specifically included in the subcontract.

Redesigning the scope of work by its own forces or by a Subcontractor's consultant places the Subcontractor in a position of cooperation with and membership in the Design-Build team or with the Owner, reducing the level of risk for the Subcontractor. Last, but not least, industry knowledge within national organizations, primarily the DFI, can be used to mitigate contractual risks and improve profitability.

Subcontractors have a duty to contribute to shaping public policy. Political activism in the industry has resulted in major legislative actions at the federal, state, and local levels to improve the fairness of contracts. For example, starting in 2008, the New York City General Construction Contract recognizes the right of compensation for justified delays. In addition, many states have passed payment legislation for GCs and Subcontractors. Unfortunately, the acceptance conditions for specialty Subcontractors for payments are so convoluted that the law is practically inapplicable.

© 2016 Deep Foundations Institute

FUTURE WORK AND RESEARCH

This opinion paper should be continued by a national survey of the DFI members regarding the unethical allocation of risks in Deep Foundation subcontracts. The result of this national survey should be the cornerstone of a new ethical policy in contracts of the DFI as an organization and for its members.

REFERENCES

Rumbaugh, M. G. (2004). Ethical Decision-Making: Issues for Contract Managers and Educators. Contract Management. April, pg. 34-35.

Kar, R. B. (2016). Contracts as Empowerment. University of Chicago Law Review. 82(2)-759.

Jackson, Barbara, PhD, DBIA. (2007). Making the Transition from Designer to Design-Builder. AIA Best Practices 09.05.01.

Moodley, K, Smith N, & Preece, N. C. (2008). Stakeholder matrix for ethical relationships in the construction industry. Construction Management and Economics. 26, 625–632.

Duhl, G. M. (2010). The ethics of contract drafting. Lewis & Clark Law Review, Vol 14(3).

Wood, G., McDermott P., and Swan W. (2002). The ethical benefits of trust-based partnering: the example of the construction industry. Business Ethics: A European Review. Volume 11 (1).

Biery, M. E. (2014). Highway and bridge construction firms' profitability declining. Forbes/ Entrepreneurs. http://www.forbes.com/sites/sageworks/2014/04/07/highway-and-bridge-construction-firms-profitability-declining. Accessed 5-8-2016.

Kunz, Christina L. (2006). The Ethics of Invalid and 'Iffy' Contract Clauses, in Symposium: Contracting Out of the Uniform Commercial Code. Faculty Scholarship. Paper 126. http://open.mitchellhamline.edu/facsch/126. Accessed 4-25-2016

© 2016 Deep Foundations Institute

EXECUTION OF DIAPHRAGM AND CUT-OFF-WALLS IN ROCK – APPLICATIONS, PERFORMANCE AND LIMITS

Franz-Werner Gerressen, BAUER Maschinen GmbH, Germany
Albert Neumann, P.E & Giancarlo Santarelli, Bencor Global Inc., United States

ABSTRACT

Diaphragm walls are known as underground structural elements commonly used for retention systems and permanent foundation walls or elements. In addition they are also quite often used as deep groundwater barriers, named Cut-Off-Walls (COW). Due to the requirements of each particular job site, e.g. the need for carrying high loads or as seepage barriers, there is an increasing industry demand for efficiently cutting into rock. Besides the removal of boulders, cutting through rock, is always the most difficult part of the excavation process of a diaphragm wall or COW.
There are a number of influencing factors which have an impact on the rock cutting performance. Besides the influence of the rock characteristics itself, which is not always the same, there are other factors related to equipment, tooling as well as the operating staff. In addition to RQD, the most commonly available rock property found in geotechnical reports is the Unconfined Compressive Strength (UCS) value. There are however some other related properties, such as weathering, bedding, inclination, abrasiveness, etc., which can have a major impact on the achievable cutting performance.
This paper will discuss the various parameters, and how they can be considered for performance estimation. Based on experiences gained on over 100 projects, a performance estimation chart was developed to allow for a better approach to these kinds of projects. This paper also explains the general installation process in as well as some specific features related to specific site conditions. In addition, some job site references will give more detailed information about such type of site conditions and how to deal with them.

Keywords: Diaphragm wall, Cut-Off-Wall, Trench Cutter, Rock

INTRODUCTION

Diaphragm walls are known as underground structural elements commonly used as retention systems for excavation pits, shafts, permanent foundation walls and load bearing elements.
It can be anticipated that, with the increasing trend of utilizing more and more underground space to accommodate environmental considerations and urban/suburban development, there will be an increasing requirement for diaphragm wall usage in even more difficult conditions.
In addition diaphragm walls can also be used as deep groundwater barriers (Cut-Off-Walls). This market has demonstrated that the demand for these types of walls is reaching ever more difficult soil conditions and greater depths which are surpassing the current industry standards. The trench cutter is the most important tool for performing this type of work.

The trench cutter itself is a reverse circulation excavation tool. It consists of a heavy steel frame with two drive gears attached to its bottom end, which rotate in opposite directions around a horizontal axis. Cutter wheels are mounted onto the drive gears. As they rotate, the soil beneath the cutter is continuously being broken up, removed, mixed with the bentonite slurry in the trench and moved towards the opening of the pump suction box. The slurry loaded with soil and rock particles is pumped up to the surface by a centrifugal pump which is located right above the cutter wheels, up through a hose system up to a desanding plant where the slurry is cleaned and returned into the trench.
The torque of the cutter wheels combined with the weight of the cutter is strong enough to cut into hard soils, crush rock to a certain size and to overcut into the concrete of adjacent panels.
Depending on the soil type, different types of cutter wheel configurations and teeth can be deployed, ranging from aggressive teeth for cutting fine-grained soil to percussive teeth for crushing boulders.

© 2016 Deep Foundations Institute

Changing the cutter wheels to suit different types of rock can be readily accomplished in the field. Experiences exist for cutters being able to cut rock with strengths up to 250 MPa. This paper's focus is especially on cutting performance in rock.

THE WORKING PRINCIPLE

Working sequence

The typical working sequence for the construction of a diaphragm wall as shown in figure 1 comprises the following key steps:

- Site preparation,
- Guide wall construction
- Trench pre-excavation
- Panel excavation
- Panel cleaning (desanding)
- Reinforcement installation (for retaining walls)
- Concreting

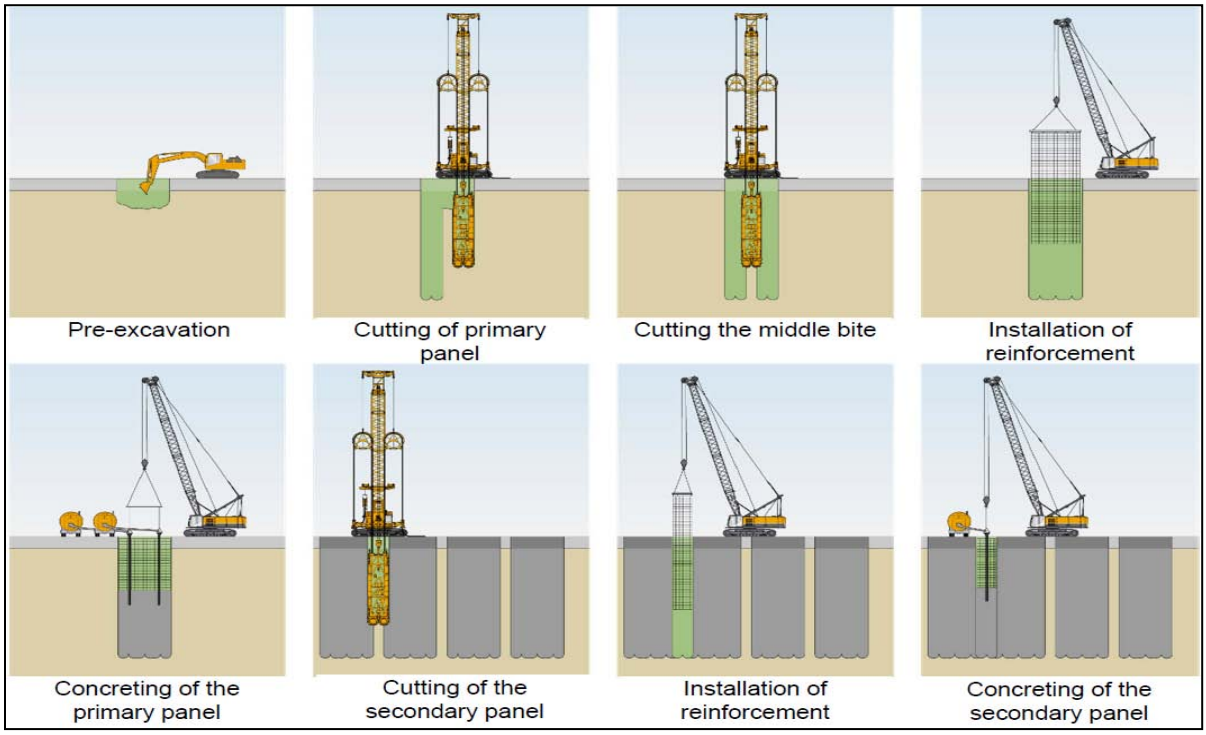


Figure 1: Construction process, exemplary for Diaphragm wall process

FACTORS OF INFLUENCE

There are a number of influencing factors which have an impact on the rock cutting performance. Besides the influence of the rock characteristics itself there are also other factors related to equipment, tooling and the operating staff (figure 2).
The estimation of these parameters and characteristics for a specific rock type might have a major impact in the cost structure of a job. It can also bear a high risk of increased costs. Therefore, accurate prediction would be highly desirable.

© 2016 Deep Foundations Institute

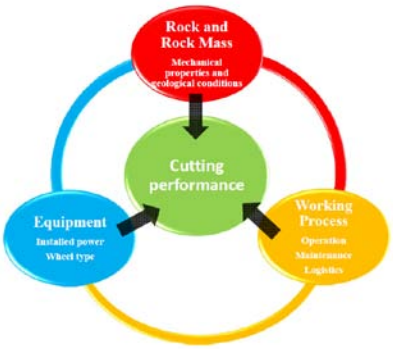


Figure 2: Conceptual overview of the main parameter influencing the cutting performance

ROCK CHARACTERISTICS

A rock mass is usually made up of the rock material or rock substance and the discontinuities. The presence of these discontinuities and the effects of weathering have significant influence on the mechanical properties and behaviour of a rock mass. These characteristics can also have major impact on the achievable performance of rock cutting.
Unfortunately, most relevant data is often not available for evaluation and estimation. In addition to RQD, the most commonly available rock property found in geotechnical reports is the UCS value. But there are some other related characteristics which should be described in a bit more detail to explain their importance. At this stage it must be mentioned, that the categorization of various properties can differ from each other depending on the region in the world, which makes it even more difficult to give a definitive overall guideline.

Weathering

"Weathering is the process of alteration and breakdown of rock and soil materials at and near the Earth's surface by chemical decomposition and physical disintegration." (Geological Society Engineering Group Working Party Report, 1995). Weathering can occur either due to physical (e.g. thermal, frost, erosion…) or biogeochemical (e.g. carbonation, hydration…)

Table 1: Scale of Rock Mass Weathering according to "field description of soil and rock" NZ geotechnical society

Term	Grade	Abbreviation	Description
Un-weathered (fresh)	I	UW	Rock mass shows no loss of strength, discolouration or other effects due to weathering. There may be slight discolouration on major rock mass defect surfaces or on clasts.
Slightly Weathered	II	SW	The rock mass is not significantly weaker than when un-weathered. Rock may be discoloured along defects, some of which may have been opened slightly.
Moderately Weathered	III	MW	The rock mass is significantly weaker than the fresh rock and part of the rock mass may have been changed to a soil. Rock material may be discoloured, and defect and clast surfaces will have a greater discolouration, which also penetrates slightly into the rock material. Increase in density of defects due to physical disintegration process such as slaking, stress relief, thermal expansion/contraction and freeze/thaw.
Highly Weathered	IV	HW	Most of the original rock mass strength is lost. Material is discoloured and more than half the mass is changed to a soil by chemical decomposition or disintegration (increase in density of defects/fractures). Decomposition adjacent to defects and at the surface of clasts penetrates deeply into the rock material. Lithorelicts or cores tones of un-weathered or slightly weathered rock may be present.
Completely Weathered	V	CW	Original rock strength is lost and the rock mass changed to a soil either by chemical decomposition (with some rock fabric preserved) or by physical disintegration.
Residual Soil	VI	RS	Rock is completely changed to a soil with the original fabric destroyed

Based on the descriptions of weathering effects and products, the rock mass can be classified according to a weathering scale as shown in Table 1.

© 2016 Deep Foundations Institute

The Oregon Department of Transportation, Highway Division, distinguishes in their Soil and Rock classification manual only 5 different grades of weathering, starting from fresh, continuing with “slightly” and “moderately” weathered to “predominantly“ decomposed and decomposed.

Discontinuities

Discontinuities such as joints, bedding and cleavage should be described where applicable in terms of their spacing, persistence, orientation, separation, tightness and roughness.
For instance, it is well known that cutting/drilling into a rock with horizontal bedding is much more efficient than cutting/drilling into vertical or steeply inclined rock bedding.
Thuro describes in his “habilitation treatise” detailed from experiences made during the use of a TBM in various rock conditions (see figure 3). It can be seen, that the difference in cutting/penetration performance could be at least in a range of approx. 40% depending on the relative angle to the bedding.

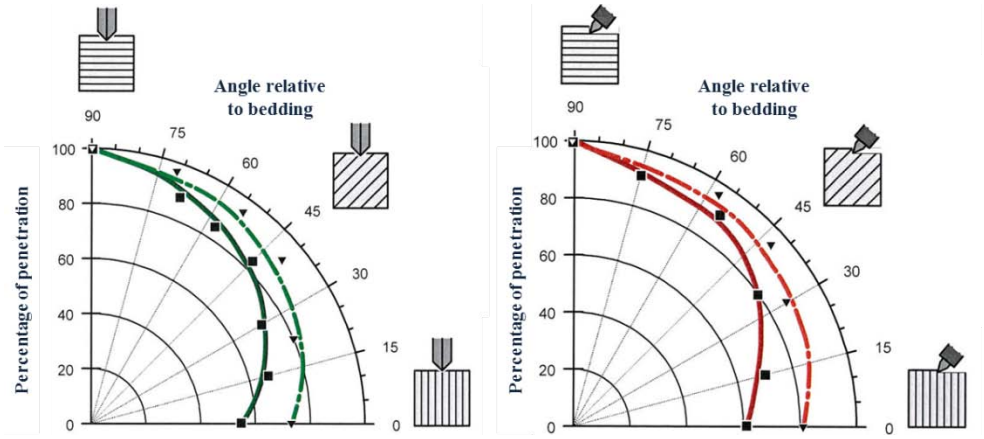


Figure 3: specific penetration in phyllite and phyillite/schist (left), specific cutting in clay shale and silty slate

Strength

The strength term is based on a range of the uniaxial compressive strength (UCS) of the intact rock material comprising the rock mass. The means by which the strength term is selected in the field is given in Table 2, according to the Soil and Rock classification manual of the Oregon DOT.

Table 2: Scale of relative rock hardness (Oregon DOT)

Term	Hardness Designation	Field Identification	Approximate Unconfined Compressive Strength (psi)
Extremely Soft	R0	Can be indented with difficulty by thumbnail. Maybe moldable or friable with finger pressure	<100
Very Soft	R1	Crumbles after firm blows with point of geology pick. Can be peeled by a pocket knife. Scratched with finger nail.	100-1,000
Soft	R2	Can be peeled by a pocket knife with difficulty. Cannot be scratched with finger nail. Shallow indentation made by firm blow of geology pick.	1,000-4,000
Medium Hard	R3	Can be scratched be knife or pick. Specimen can be fractured with a single firm blow of hammer/geology pick.	4,000-8,000
Hard	R4	Can be scratched with knife or pick only with difficulty. Several hard hammer blows required to fracture specimen.	8,000-16,000
Very Hard	R5	Cannot be scratched by knife or sharp pick. Specimen requires many blows of hammer to fracture or chip. Hammer rebounds after impact.	>16,000

The description of rock material strength using the terms ‘strong’ and ‘weak’ is also common in various countries and may also cover rock strength of more than 250 MPa (Approx. 36,000 psi).

© 2016 Deep Foundations Institute

Commonly, rocks with Qu values in excess of 50 MPa (7,250 psi) are informally referred to as 'hard' rocks and those less than 20 MPa (2,900 psi) (especially < 10 MPa (1450 psi)) as 'soft' rocks.

Abrasiveness

The test most often used to verify the abrasiveness of rock is the so called Cerchar Test. The Cerchar Abrasiveness Test was introduced in the 1970s by the Centre d'Etudes et Recherches des Charbonages (CERCHAR) de France for abrasiveness testing in coal bearing rocks. The test layout is described in Cerchar (1986) and in the French standard NF P94-430-1 in general. The testing principle is based on a steel pin with defined geometry and hardness that scratches the surface of a rough rock sample over a distance of 10 mm under static load of 70 N (see figure 3).

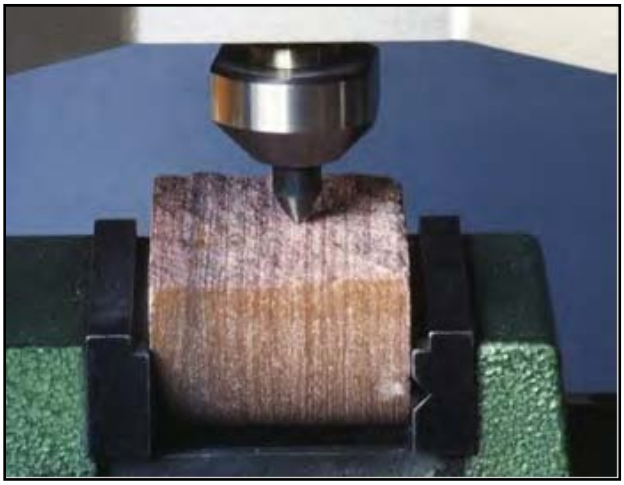


Figure 3: Cerchar test set-up

The Cerchar-Abrasivity-Index (CAI) is then calculated from the measured diameter of the resulting wear flat on the pin:

$$CAI = 10 \times d/c \qquad [1]$$

Where CAI = Cerchar-Abrasivity-Index (-); d = diameter of wear flat (mm); c = unit correction factor (c=1mm).

The classification of the CAI can be seen in table 3.

Table 3: Abrasiveness classification chart according to Thuro

CAI	Abrasiveness classification	Examples
0.0 - 0.3	not abrasive	organic material
0.3 - 0.5	not very abrasive	mudstone, marl
0.5 - 1.0	slightly abrasive	slate, limestone
1.0 - 2.0	(medium) abrasive	schist, sandstone
2.0 - 4.0	very abrasive	basalt, quarzitic sandstone
4.0 - 6.0	extremely abrasive	amphibolite, quartzite

The rock abrasiveness has a big influence on tool consumption regarding wear and tear, which directly affects the cutting process and resulting costs.

© 2016 Deep Foundations Institute

EQUIPMENT AND TOOLS

Wheels and teeth

Use of the most appropriate cutting wheels and teeth is one of the main keys to optimized productivity. Trench cutters are typically fitted with one of three types of wheels and teeth. Commonly they differ for the range of rock strength, where they usually are used. Figure 4 shows the three types of wheels.



Figure 4: Standard Cutter Wheel (left), Round shank chisel cutter wheel (centre), Roller bit cutter wheel (right)

The “Standard Cutter Wheels” are usually used in all types of soils with various types of teeth but is also able to cut into weak to moderately strong rock conditions. Obviously, there is no strict borderline but starting with rock strengths approximately in the range of 50 MPa (7,250 psi), which means dealing with strong/hard rock, a more aggressive wheel like the “Full Face Cutter Wheel (or Round shank chisel cutter wheel (RSC) Cutter Wheel)”, equipped with special round shank teeth, will provide a better cutting performance. At the upper end of the scale, when dealing with rock strengths exceeding 120 MPa (17,400 psi), there may be a need to consider using the “Roller bit cutter wheel”. Usually, when using the Roller bit cutter wheels, the cutter with higher weight is required, as each Roller bit requires a load of at least 4-8 metric tons for a reasonable functionality.

Functionality of flipper teeth

The Flipper teeth are special teeth which ensure the cutting of the soil underneath the gear shield in the space between the cutter wheels. Especially in soil/rock conditions where the remaining soil/rock material will be stable enough to resist underneath the gear shield, and active cutting is required. Therefore, the existence and functionality of the flipper teeth are essential for cutting progress. Regularly checking for wear and tear and its functionality is mandatory. Figure 5 shows the positioning and the function of the flipper teeth.

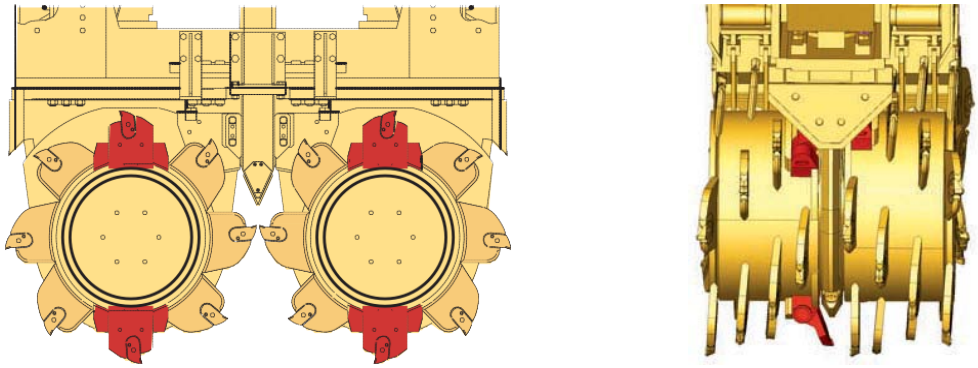


Figure 5: Position of flipper teeth (red)

© 2016 Deep Foundations Institute

Wear and tear on wheels and teeth

Teeth which are worn out, were the pockets broke or RSC teeth which are not turning anymore are not able to provide the function of cutting and/or breaking the rock. These teeth must be changed to maintain optimal cutting performance.
There is always a challenge to find the right balance between continuing cutting without changing teeth to save costs which decreases performance or the decision to change teeth more frequently to increase performance. This challenge is a function of experience either gained on the particular jobsite or due to the long experience of the operators.

OPERATOR

Operator experience can become a major factor in the performance of cutter works in rock. As mentioned before, the experienced operator will recognize the moment when it is the best time to control and change the teeth. Since this has a major influence on the overall performance, the operator plays an important role in the matrix of influencing factors.

Summary about the factors of influence:

It can be seen that the number of influencing factors is nearly endless. A lot of variables, with various importance, interact during the construction process. Some of these factors are measurable, but not provided on a regular base. Some of them are not measurable, like the human factor, but is also very important. This leads to a situation, were reliable performance estimation is nearly impossible. Nevertheless, everybody expects to get the best possible estimation, however given all the variables, this condition can never be guaranteed.

PERFORMANCE ESTIMATION

Based on experiences made on over 100 projects, a performance estimate chart has been developed to provide a better approach to these kinds of jobsites.
As already stated, due to the availability of relevant data, the chart just shows generalized performance data based on experienced gained on these projects. Utilizing at least one factor as a guide, the most commonly provided information is the unconfined compressive strength UCS. Therefore, the performance is displayed as a function of the UCS values.

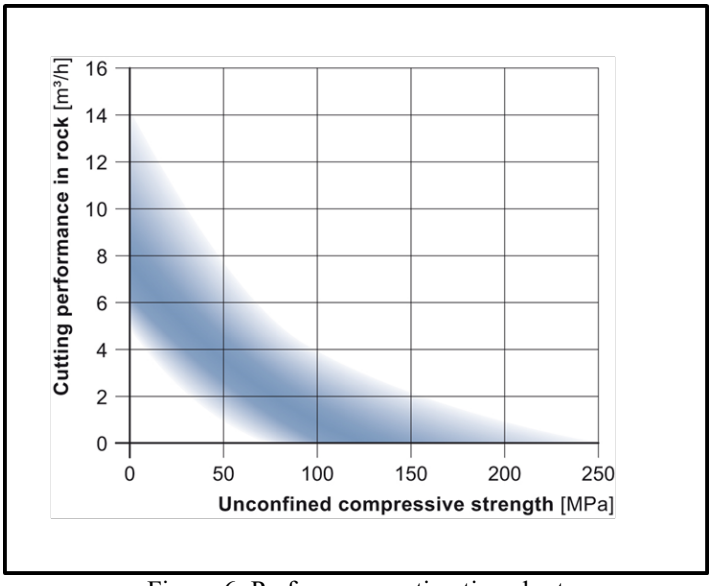


Figure 6: Performance estimation chart

© 2016 Deep Foundations Institute

As the diagram is based on experiences gained from a limited number of completed projects, these values do not represent any legally binding assurance or warranty for future projects. The final selection has to be made by the end-user, based on the type and weight of the cutter, the type of cutter wheels and above all on the detailed knowledge of ground conditions as described before.

JOB SITE EXPERIENCE

Clearwater Lake Dam, USACE Little Rock District, Piedmont, MO

Project Description

Clearwater Dam was started in 1940 and completed in 1948 for flood control, recreation, and fish and wildlife conservation. As originally designed, seepage was allowable and estimated at that time to be relatively minor and of no significant long term effect. Shortly after completion, seepage was detected and in 1950 became more pronounced than expected.
Since that time the US Army Corps has attempted to remediate the seepage problems using various methods, including installation of two under-drainage systems, installation and ongoing monitoring with 73 piezometers, continual O&M studies and technical investigations, construction of a seepage control berm at the base and recently performed the largest dam grouting program. In spite of these efforts, seepage problems continued and became worse over time.
The Corp's Final Remediation Plan consisted of a concrete cut off wall for the entire length of the dam. The cut-off wall extends deep into bedrock under the dam and through the impervious core of the dam to prevent seepage and migration both through and under the dam.

Geology

Clearwater dam was built on sandy alluvial deposits underlain by karstic limestone. The site is located on the Salem Plateau of the Ozark Plateau Province just west of the Mississippi Embayment. Rock at the dam vicinity consists of dolomite, with significant karstic solution features and thin chert beds. The two formations exposed at the dam site are the Eminence and Potosi formation, both of Cambrian age.
The Potosi underlies the reservoir, most of the dam and the largest part of the lake rim. The Potosi is a massive, fine to medium-grained dolomite deposited in thick beds. The overlying Eminence makes up the rest of the lake rim and in the upper parts of the abutments. The Eminence is a coarse to medium-grained dolomite rock found in massive beds. The dolomite is brown to grey in color. Both the Eminence and Potosi are carbonates and are subject to dissolution by water producing many solution cavities and extremely weathered joints.



Figure 7: Dolomite sampling and testing

The dolomite limestone rock at the Clearwater Lake Dam ranged from 3,000 psi (20 MPa) to well over 32,000 psi (220 MPa). Biggest challenge on this project was cutting over 235,000 ft^2 (21.830 m^2) of hard limestone rock area totaling 26,000 ft^3 (18.000 m^3) and maintaining the schedule.

© 2016 Deep Foundations Institute

Execution

Bencor decided to utilize 5 cutters (2 as backup) to install the deep cut-off wall. The work platform was designed for efficient operation for all of the large equipment and safety of the crews (see figure 8). In addition, also a cable grab was utilized for starting trench excavations ahead of the cutter.



Figure 8: Cutter and working platform

Based on the nature of the dolomite limestone rock, Bencor chose to use bullet type teeth with various wheel configurations to optimize rock cutting performance. The hard rock required frequent changing of worn teeth and hard facing cutter wheels (see figure 9). Bencor utilized various cutter wheel and teeth arrangements to achieve rock cutting rates between 1 to 6 m^3/hr depending on local rock conditions.



Figure 9: Round shank chisel cutter wheels, hard facing

The operator uses the cutter's built in electronics and B-Tronic system to steer the decent to within very accurate vertical tolerances of less than 0.1%. In addition, Koden measurements were used to check vertical accuracy and panel dimensions. After the cut-off wall concrete cured, verification holes were drilled to confirm the quality of the joints between panels. Red stained secondary panel concrete was poured next to regular primary panel concrete to distinguish the clean panel joints (see figure 10).



Figure 10: Verification of joints

© 2016 Deep Foundations Institute

The right choice of equipment and tooling setup as well as using experiences operators along with accurate instrumentation lead to a successful project as documented in the as-built profile, especially showing the rock quantity.

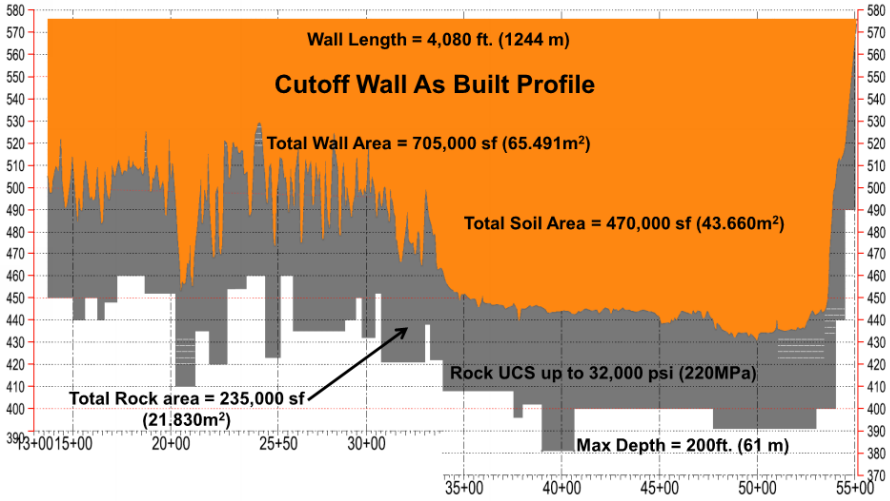


Figure 11: Cut-off wall as build profile

SUMMARY

As there are a number of influencing factors which have an impact on the rock cutting performance, there is a need to get more information about those, especially with regards to the rock characteristics, to enable a better estimation for the executing companies. More investigation and research needs to be done at least to achieve better performance and to save money.
So far, the most commonly available rock property, the Unconfined Compressive Strength (UCS) value allows a first approach, as shown in the estimation chart, but this can only be seen as a guide.
This information is helpful, however a close look at the details of all relevant data enables experienced staff to choose the most suitable equipment and tooling configuration, to successfully face the geological challenges as shown in these references.

REFERENCES

Deere, D. U.; Deere, D.W. 1988. The Rock Quality Designation (RQD) Index in Practice. Rock Classification Systems for Engineering Purposes. ASTM STP, Louis Kirkaldie, Ed., American Society for Testing and Materials, Philadelphia, S.91-101

NZ GEOTECHNICAL SOCIETY INC, December 2005
FIELD DESCRIPTION OF SOIL AND ROCK, GUIDELINE FOR THE FIELD CLASSIFICATION AND DESCRIPTION OF SOIL AND ROCK FOR ENGINEERING PURPOSES

Oregon Department of Transportation, Highway Division, 1987. Soil and Rock classification manual

Käsling, H. & Thuro, K., 2010: Determining rock abrasivity in the laboratory. - In: Proceedings of the European Rock Mechanics Symposium EUROCK 2010, Lausanne, Switzerland, 15-18 June 2010, 4 S.

Thuro, K.. habilitation treatise, 2002. Geologisch-felsmechanische Grundlagen der Gebirgslösung im Tunnelbau

Cerchar-Centre d'Etudes et des Recherches des Charbonages de France. 1986. The Cerchar abrasiviness index.

© 2016 Deep Foundations Institute

STRENGTH AND DEFORMATIONS OF PILES SUPPORTING TRANSIENT PIPE ANCHORS IN HEAVY INDUSTRIAL PIPELINES

Konstantin G. Ashkinadze, Consulting Engineer, Edmonton, AB, Canada, Ph. 780-945-9746, email@k-the-eng.com

ABSTRACT

The paper considers performance of piles supporting transient pipe anchors in heavy industrial pipelines. Events such as pump trips or opening and closing of large valves produce short-term dynamic pulses in the pipeline with variable spectral characteristics. Their magnitude is large enough to cause major damage to the pipeline and its anchors, which face horizontal impact loads amounting to hundreds of kN. Design of pile foundations supporting these anchors is often governed by limitation of deflection of the support to prevent overstressing pipeline connections and equipment nozzles. The maximum deflection does not always correspond to the largest load because the stiffness of the soil surrounding the piles heavily depends on the rate of loading. Faster actions encounter stiffer soil response while loads of smaller magnitude applied slowly may be more critical for the deflection time history of the anchor. A typical transient action has both high- and low-frequency harmonics, which makes the response complex. Using load rate-dependent *p-y* curves published in literature, the paper develops methods of analysis of pile foundations for transient anchors. Pile displacement amplitude – input frequency – natural frequency correlations and time histories of pile response are constructed for typical profiles of transient actions, considering nonlinear soil response to large horizontal loads.

Keywords: Anchor, dynamic, foundation, frequency, nonlinear, pile, pipeline, response, soil springs, time history, transient event.

INTRODUCTION: TRANSIENT EVENTS

Transient mitigation has become a major business in pipeline industry in the recent years because it directly addresses pipeline safety. Pump trips or opening-closing of large valves cause pressure buildup in the pipeline that needs to be relieved. When the relief valve is opened, the pipeline sustains a short-term dynamic loading (a hydraulic hammer) that propagates at the speed of sound in the pumped liquid. The horizontal load on pipe anchors reaches its maximum value (measured in hundreds of kN) in a matter of 0.1 seconds or less and then decays more slowly.

Derivation of load time histories of the transient events is a three-step process (Wilcox and Walters 2012). First, a pressure time history is constructed by means of a pipeline hydraulic computer simulation. This load history is derived in coordinates *P-t* (pressure vs. time). Next, a dynamic analysis of the piping system is performed using a suitable pipe stress analysis program with dynamic analysis capability, using the *P-t* time history as an input. The response time history is expressed in R_{anc} - t coordinates (reaction at the anchor vs. time). Finally, on the third step of the procedure the R_{anc} - t time history is used as an input for a dynamic analysis of the structure and the piles.

A typical time history of a transient event is shown in Fig. 1. The Hydraulic time history starts when the pump trips and the station check valve closes, which leads to pressure build-up in the pipe. When it reaches the set pressure of the surge relief valve, the valve opens and the transient event occurs. As long as the process remains hydrostatic, due to Pascal's law the pressures in the relief line are balanced and the net force in the anchor is zero. The hydrodynamic regime sets in when the pressure wave front arrives. At this point, the R_{anc} - t time history starts. As the pressure wave travels along the relief line, the pressure behind its front drops and the one before the front increases, which causes a net force to appear at the anchor.

© 2016 Deep Foundations Institute

At the end of the transient event, the pressure has dropped to normal but the valve is still open, there is still flow in the system, so there is a residual net force in the anchor. Relief valves usually close slowly to avoid a second transient event, but eventually after some surges the valve becomes fully closed, the flow velocity reduces to zero and the hydrostatic condition re-establishes itself, therefore the force in the anchor returns to zero.

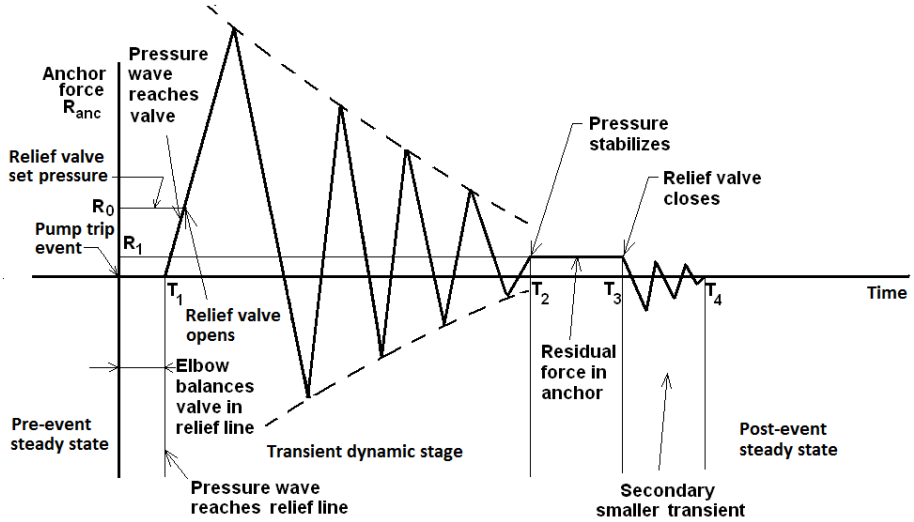


Fig. 1. Transient anchor load time history – hydraulic and structural.

FREQUENCY DEPENDENCE AND NONLINEARITY OF PILE REACTION

Since the soil stiffness is heavily dependent on the rate of loading, the largest loads during the transient dynamic event may not be the most critical. If significant loads are sustained quasi-statically at the end of the event, the soil may respond more softly and the anchor deflection may increase even though the load decreases. This may be critical for piping tees and flanges.

For a pile vibrating in soil, the elementary spring constant for the soil in the horizontal direction is given by the following formula (Novak 1974):

$$K = G_s\left(S_{u1} + iS_{u2}\right) \qquad [1]$$

In this formula, K[MPa] = q/y = [N/mm] lineal load / [mm] displacement; S_{u1} and S_{u2} are coefficients graphed by Novak as a function of frequency. The dependence of the factors S_{u1} and S_{u2} on frequency is rather weak for single piles but may be more significant if the piles are used in groups (El Naggar).

G_s in Eq. 1 is the dynamic soil shear modulus. It is greater than the static one because in a short-term loading, grain slippage, consolidation, or plastic flow in the soil mass do not have time to develop. The conventionally termed "dynamic soil shear modulus", G_{max}, is suitable for strains in the order of 10^{-6}. However, in transient impact problems, the strains and stresses are not small, and may exceed the shear strength of the soil. El Naggar suggested to use $G_s \approx 0.8\text{-}0.9\ G_{max}$, estimating the shear strain in transient events as 10^{-4}. Several researchers (Abbas et al. 2009, Brown et al. 2001) have shown that the initial stiffness of the soil at the small strain is identical for all rates of loading. However, nonlinearity and the shear failure of the soil occur at different load levels depending on the frequency (see Fig. 2), hence the apparent frequency-dependence of the secant value of G_s.

© 2016 Deep Foundations Institute

CONSTITUTIVE EQUATION FOR ELEMENTARY SPRINGS

Bentley and El Naggar (Bentley 1999, Brown et al. 2001) have studied frequency dependence and nonlinearity of the response of the soil surrounding a dynamically loaded pile, using a representation of a flat slice of soil surrounding the pile as a chain of two springs: near-field and far-field. The far-field is a linear massive spring of infinite dimension that can propagate elastic waves. The near-field spring is a massless, nonlinear element that can represent degradation of the soil stiffness for larger amplitudes, slippage, gapping etc.

In the following derivation, we used Bentley and El Naggar's graph for the reaction of soil surrounding piles for one specific example (Case C1). The pile was a straight shaft driven steel pipe, 0.25 m in diameter × 9 mm thick wall and 10 m long, surrounded by clayey soil with undrained shear strength C_u = 25 kPa. The soil elastic modulus variation with depth was parabolic. This pile size is smaller than the usual pile sizes for transient anchors, so the parameters of the action were adjusted to suit this reduction.

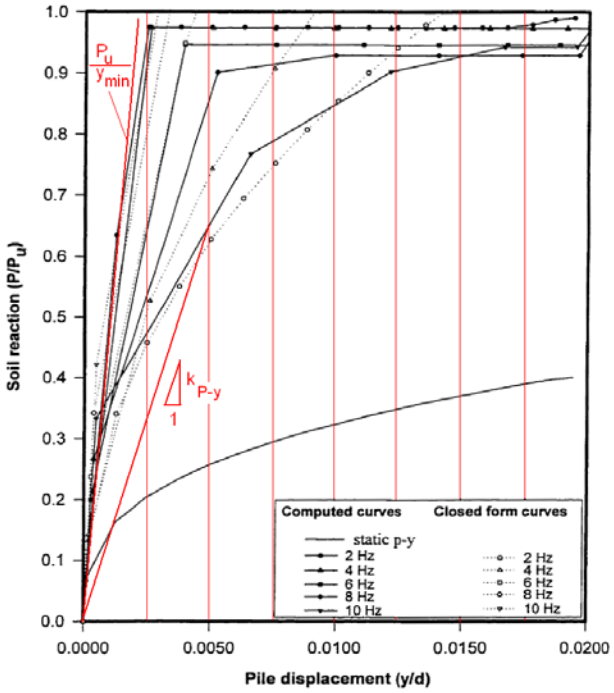


Fig. 2. Interpolated elementary soil spring stiffness as a function of input frequency and amplitude of displacement (Case C1 by Bentley 1999): P_u = lateral load-bearing capacity, d = pile diameter.

The stiffness of each elementary spring as determined by Fig. 2 is, after non-dimensionalizing:

$$k_{P-y} = \frac{P}{y} = \frac{P/P_u}{y/y_{\min}} \frac{P_u}{y_{\min}} \equiv \kappa_{rel} \frac{P_u}{y_{\min}} \qquad [2]$$

As seen from Fig. 2, the ratio $P_u/y_{\min}$ is an analog of the "initial", "small-strain" soil shear modulus, G_s. In Bentley and El Naggar's Case C1, it equals $P_u/y_{\min}$ = 90 MPa. The parameter κ_{rel} has been scaled off Fig. 2 as shown. In Fig. 3, this parameter is plotted against the frequency of excitation, u, for different amplitudes of displacement, y/y_{min}. A fairly close representation of this function can be obtained by the following bilinear approximation:

© 2016 Deep Foundations Institute

$$\kappa_{rel}(u) = \min\left(\kappa_0 + \frac{\kappa_2 - \kappa_0}{2\ \text{Hz}} u, \kappa_{10} \right) \quad [3]$$

where κ_0, κ_2 and κ_{10} are κ values for u = 0 Hz (static case), 2 Hz and 10 Hz, respectively. In Fig. 4, these parameters are plotted against y/y_{min}. These hyperbolic correlations can be interpolated as

$$\kappa_{0,2,10} = \frac{C}{(y/y_{\min})^{\beta}} \quad [4]$$

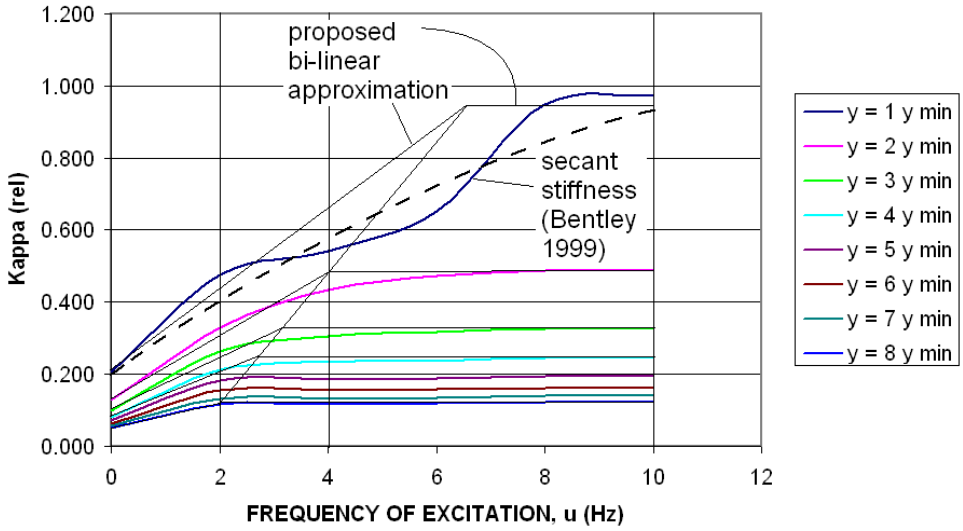


Fig. 3. Relative stiffness of elementary soil springs as a function of the rate of loading (input frequency).

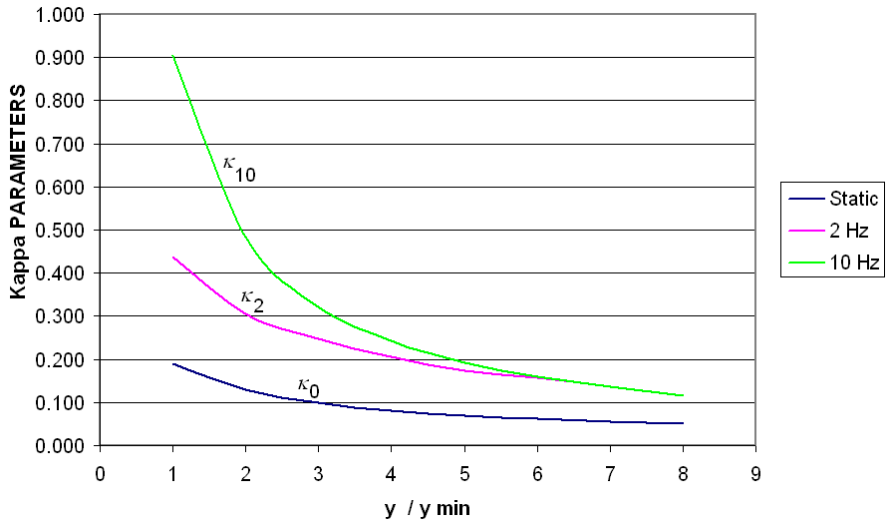


Fig. 4. Relative stiffness of elementary soil springs at input frequency 0 Hz (static), 2 Hz and 10 Hz as a function of displacement amplitude.

Parameters C and β have been calibrated using least squares method. The results are presented in Table 1.

© 2016 Deep Foundations Institute

Table 1. Parameters of interpolation in Eq. 4.

u, Hz	C	β
0 (static)	0.192	0.621
2	0.444	0.580
10	0.911	0.956

PILE ANALYSIS

The next step is to determine the natural frequency of the pile laterally restrained by the above-formulated springs. The method of pile analysis used in this paper is based on analytical solution of the differential equation of pile motion:

$$EIy^{IV} + \rho A y + k_{P-y}(1 + 2i\gamma_x)y = 0 \qquad [5]$$

by method of weighted residuals (Gallagher 1975). In Eq. 5, EI is the flexural stiffness of the pile and ρA is the distributed mass per unit length of pile. γ_x is the combined geometric + material damping, which can be omitted for natural frequencies calculation. Consider the case of a fixed-headed pile, assuming that the resistance of the rigid anchor superstructure will effectively prevent the pile rotation at the ground level. Approximating the pile deflection $y(z, t)$ as a function (satisfying the boundary conditions):

$$y(z,t) = Ae^{-\alpha z}(\sin \alpha z + \cos \alpha z)\sin \omega t \qquad [6]$$

where A is the amplitude and α is an unknown parameter, and integrating along the length of the pile (considered infinite), find that a non-trivial solution of Eq. 5 may exist if

$$\omega = \sqrt{\frac{-4\alpha^4 EI + k_r}{\rho A}} \qquad [7]$$

where $k_r(u, A)$ is the equivalent modulus of lateral subgrade reaction:

$$k_r = \frac{\int_0^\infty k_{P-y}(z) y_0^2 dz}{\int_0^\infty y_0^2 dz} = \frac{4\alpha}{3}\int_0^\infty \frac{P_u}{y_{\min}}(z)\kappa_{rel}(u, Ay_0(z))y_0^2(z)dz\,; \quad y_0(z) = e^{-\alpha z}(\sin \alpha z + \cos \alpha z) \qquad [8]$$

Equation 7 is one resolvent equation of the natural frequency problem. The second equation results from the boundary condition of dynamic equilibrium for horizontal translation: the shear force at the top of the pile must equal the inertia force of the tributary supported mass in horizontal motion, hence

$$V(0) = -EIy'''(0,t) = My(0,t) \qquad [9]$$

where M is the *tributary* mass of the support and the piping per one pile (taken as 5000 kg in this example). For the assumed function $y(z, t)$,

$$EI \times 4\alpha^3 = M\omega^2 \qquad [10]$$

© 2016 Deep Foundations Institute

From Eqs. 7 and 10, the two unknown parameters α and $\omega = \omega_0$ – the natural frequency of the support can be computed using Solver add-on program to the spreadsheet application. The resulting correlations of ω_0 with the input frequency u and the amplitude of displacement y are presented graphically in Figs. 5 and 6. The natural frequency of the pile varies by about 2 times from the stiffest to the softest response within the range considered. This corresponds to the variation of the pile stiffness and the top displacement by 4 times. Using the least squares method, the following expression was fitted to the graphs of Figs. 5 and 6:

$$\omega_0(u, y) = \omega_0^* \frac{1.000 - 0.309e^{-0.503u[\mathrm{Hz}]}}{(y/y_{\min})^{0.189}} \qquad [11]$$

where ω_0* is the linear frequency-independent value of ω_0, equalling 56.1 rad/s in this case.

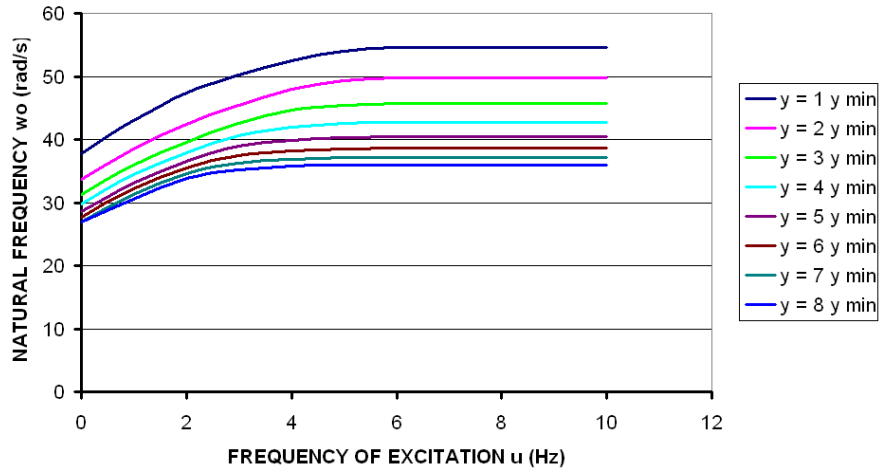


Fig. 5. Pile natural frequency as a function of input frequency for different amplitude.

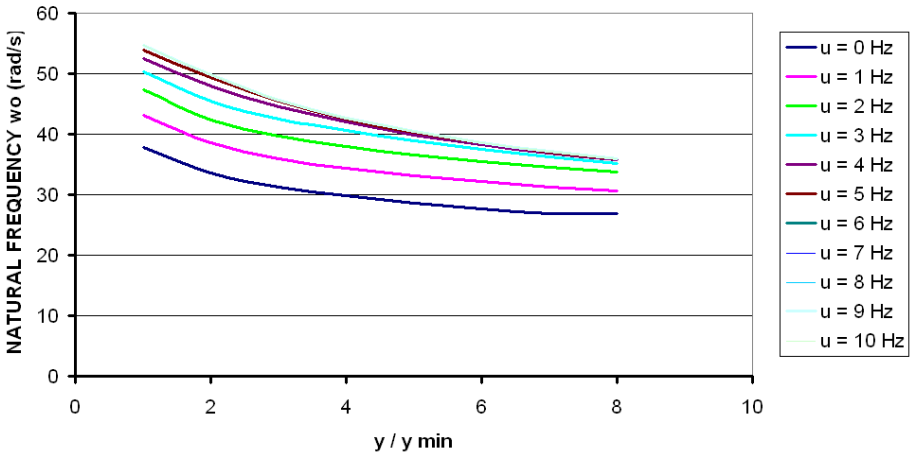


Fig. 6. Pile natural frequency as a function of amplitude for different input frequency.

LOAD HISTORY AND ITS FOURIER SPECTRUM

From consideration of transient event physics (see above), the following generalized load history has been assumed for the study:

© 2016 Deep Foundations Institute

– At $T_1 \le t \le T_2$, $R(t) = R_1\left(1 - e^{-\delta\varphi(t-T_1)}\cos\varphi(t-T_1)\right)$
– At $T_2 < t \le T_3$, $R(t) = R_1 = \text{const}$ [12]
– At $T_3 < t < \infty$, $R(t) = R_1 e^{-\delta\varphi(t-T_3)}\cos\varphi(t-T_3)$

The graph of the adopted time history approximates the diagram in Fig. 1. The median value of the load was taken as R_1 = 80 kN; the maximum load magnitude is 152 kN. In the following, the origin of the time history has been shifted to exclude prehistory, so $t = T_1$ became $t = 0$.

The sine-Fourier spectrum of the assumed action was constructed by analytical integration as follows:

$$R(t) = \frac{2}{\pi}\int_0^\infty \rho(u)\sin utdu \quad \text{, where} \quad [13]$$

$$\rho(u) = R_1\left[\frac{1-\cos u\tau_3}{u} + \frac{1}{2}\left(\frac{(\varphi-u)(1-\cos u\tau_3)+\delta\varphi\sin u\tau_3}{(1+\delta^2)\varphi^2 - 2\varphi u + u^2} - \frac{(\varphi+u)(1-\cos u\tau_3)-\delta\varphi\sin u\tau_3}{(1+\delta^2)\varphi^2 + 2\varphi u + u^2}\right)\right] \quad [14]$$

where $\tau_3 \equiv t - T_3$; the terms with τ_2 have vanished from the expression. The resulting load spectrum $\rho(u)$ is shown in Fig. 7. It has two dominant harmonics: the very low frequency component (u = 0.4 Hz) and the components near u = 8 Hz which correspond to the set frequency of excitation (φ = 50 rad/s = 8 Hz). The first one of these underscores the importance of low-pace, quasi-static regimes of loading.

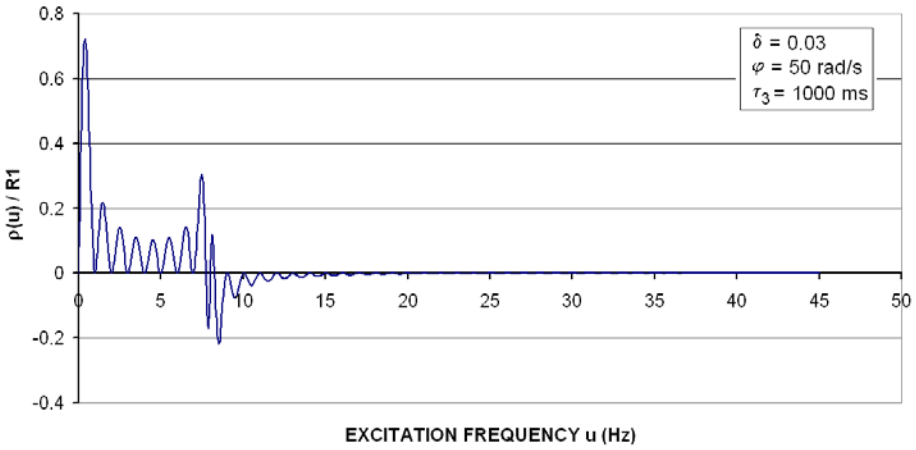


Fig. 7. Transient load spectrum.

RESPONSE TIME HISTORIES IN TERMS OF DISPLACEMENT

If a single-degree-of-freedom oscillator is linear and the load is represented by its sine-Fourier spectrum, then the time history of displacement is given by the Duhamel integral (Clough and Penzien 2003). With consideration of the free vibration component, which is significant in short-term loadings, obtain:

$$y(t) = e^{-\gamma\omega_0 t}\left(C_1\sin\omega_0 t + C_2\cos\omega_0 t\right) + \frac{2}{\pi}\int_0^\infty \frac{\rho(u)/M \times du}{\left(\omega_0^2 - u^2\right)^2 + \left(2\gamma\omega_0 u\right)^2}\left[\left(\omega_0^2 - u^2\right)\sin ut - 2\gamma\omega_0 u\cos ut\right] \quad [15]$$

Here in, C_1 and C_2 are arbitrary constants, determined from the initial conditions of motion. Assuming that the system starts its motion from the condition of rest ($y(0) = y(0) = 0$), find:

© 2016 Deep Foundations Institute

$$y(t)=\frac{2}{\pi}\int_0^{\infty}H(u)\Pi(u,t)du \qquad \text{where} \qquad [16]$$

$$H(u)=\frac{\rho(u)/M}{\left(\omega_0^2-u^2\right)^2+\left(2\gamma\omega_0 u\right)^2}\ , \qquad [17]$$

$$\Pi(u,t)=\frac{u}{\omega_0}\left(u^2-\left(1-2\gamma^2\right)\omega_0^2\right)e^{-\gamma\omega_0 t}\sin\omega_0 t+\left(\omega_0^2-u^2\right)\sin ut+2\gamma\omega_0 u\left(e^{-\gamma\omega_0 t}\cos\omega_0 t-\cos ut\right) \qquad [18]$$

The integral form of Eq. 16 allows ω_0 to be a function of u, which accounts for frequency dependence of the dynamic soil reaction. As for the nonlinearity (i.e. the dependence of ω_0 on y), the following algorithm is proposed based on the simple iteration (trial and error) procedure:

– Assuming $y = y_{min}$, calculate $\omega_0(u)$ for each u of the mesh, and construct the response history $y_0(t)$.

– Assume $y(t) = \chi\, y_0(t)$, calculate $\omega_0(u, y(t))$ for each u and each t of the discretization mesh, and construct the response history $y_1(t)$. Since $y_1(t) > y_0(t)$ due to nonlinearity (softening) of the response, χ should be picked sufficiently large so that $\chi\, y_0(t) > y_1(t)$. If the trial is successful, then the solution is localized and can be refined by adjusting the χ value within the interval.

– Assume $y(t) = \chi\, y_1(t)$ and continue (by eye or collocation method) until χ on consecutive iterations is sufficiently close to 1. In the example considered, the process converged almost perfectly after 3 trials.

RESPONSE TIME HISTORIES IN TERMS OF RESTITUTION FORCE

The restitution force, which equals the lateral force at the top of the pile, is calculated as $F(t)=ky(t)$. Noting that $k = M\omega_0^2$, obtain

$$F(t)=\frac{2}{\pi}\int_0^{\infty}S(u)\Pi(u,t)du \qquad \text{where} \qquad [19]$$

$$S(u)=\frac{\rho(u)\times\omega_0^2(u)}{\left(\omega_0^2-u^2\right)^2+\left(2\gamma\omega_0 u\right)^2}\ ,\Pi(u, t) \text{ as per Eq. 18.} \qquad [20]$$

If the system is linear and frequency-independent, then $\omega_0(u) = const$ and $F(t)$ will be proportional to $y(t)$. With frequency dependence and especially nonlinearity, $\omega_0(u)$ reduces when the force increases, which causes the restitution force time history to lag behind the displacement time history.

RESULTS

As a result of the numerical simulations, the following facts have been established (see Figs. 8, 9):

– In the *linear frequency-independent* case, the maximum displacement and reaction is achieved at the beginning of the load history and reduces towards the end of it, together with the load intensity.

– In the *linear frequency-dependent* case, the maximum displacement and reaction are also achieved at the beginning of the loading history, and are just marginally different than in the frequency-independent case. However, as the rate of loading reduces towards the end of the transient event, the amplitude starts

© 2016 Deep Foundations Institute

to increase compared to the linear frequency-independent case. This is due to reduction of the pile-surrounding soil stiffness for slower loadings. For installations where components of the piping system may be damaged by yielding of the anchor, this fact may be critical.

- In the *nonlinear frequency-dependent* case, the behaviour is similar to the linear frequency-dependent case but the scale of the events increases significantly. In the example considered, the displacement was 3 times greater than in the linear case. Also the frequency of response reduces greatly in the nonlinear case, by 2 times initially, by 3 times closer to the end of the load history. At the end of the load history, the deflections remain large despite reducing load but the reactive force in the pile continues to diminish, due to degradation of the pile stiffness for slow loadings. The maximum force in the pile in the nonlinear case is smaller than in the linear case, despite the large displacement.

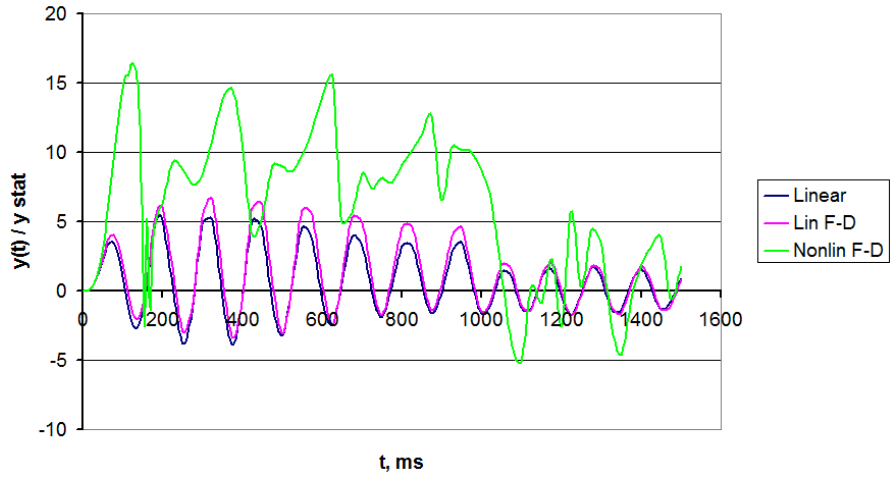


Fig. 8. Displacement response history in linear frequency-independent, linear frequency-dependent, and nonlinear frequency-dependent case.

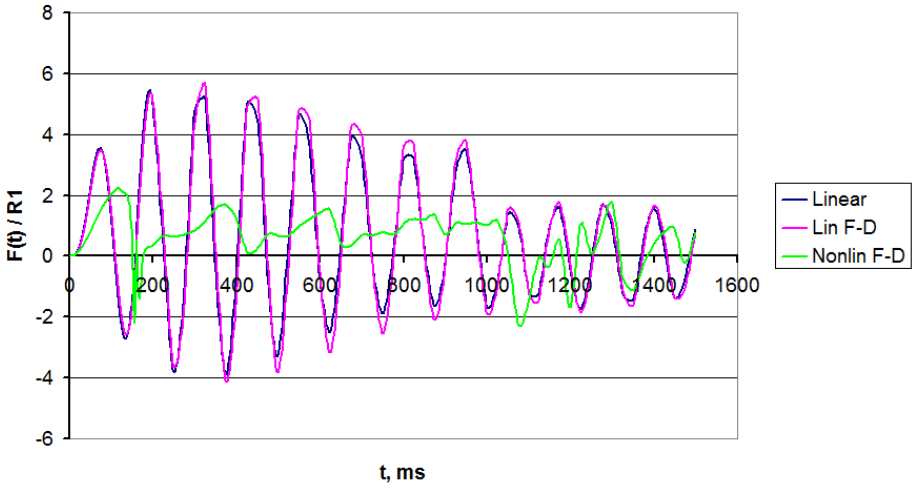


Fig. 9. Response history of restutition force.

SUMMARY

Transient mitigation is a rapidly developing field in pipeline industry safety assurance. Events such as pump trips or opening and closing of large valves produce short-term pressure pulses in the pipeline, which can cause horizontal impact forces on pipeline anchors amounting to hundreds of kN. Design of

© 2016 Deep Foundations Institute

piles supporting these anchors is often governed by limitation of support deflection to prevent overstressing pipeline connections and equipment nozzles. The maximum deflection does not always correspond to the largest load because dynamic pile stiffness increases with the rate of loading. A typical transient action has both high- and low-frequency harmonics, which makes the response complex.

Using load rate-dependent *p-y* curves published in literature, pile displacement amplitude – input frequency – natural frequency correlations have been developed and time histories of pile response constructed for typical profiles of transient actions. It is shown that in the *linear frequency-independent* case, the maximum reaction and displacement is achieved at the beginning of the load history and reduces afterwards. In the *linear frequency-dependent* case, the maximum displacement and reaction are also achieved at the beginning of the loading history; however, as the rate of loading reduces towards the end of the transient event, the amplitude starts to increase compared to the linear frequency-independent case, due to reduction of the pile stiffness for slower loadings. In the *nonlinear frequency-dependent* case, the behaviour is similar to the linear frequency-dependent case except the displacement is much larger than in the linear case, and the frequency of response is significantly smaller. The reactive force in the pile reduces towards the end of the load history due to stiffness degradation, despite the large displacement.

The proposed methodology allows performing the analysis and design of pile-supported transient anchors simply, using no other software than a spreadsheet application. The correlations developed ($\omega_0(u, y)$ and others) are not deemed universally applicable to all piles and all soils; however, they provide an insightful illustration of the dynamic reaction of pile-supported transient anchors to high intensity loads of variable spectral content.

REFERENCES

Abbas, J.M., Chik, Z.H., Taha, M.R., and Shafiqu, Q.S.M., 2009. Analysis of time dependent laterally loaded pile in clay. Electronic Journal of Geotechnical Engineering, 14(N), online at: <www.ejge.com /2009/Ppr09115/Ppr09115.pdf> (accessed April 8, 2016).

Bentley, K.J., 1999. Lateral response of piles under extreme events, M. Sc. thesis, University of Western Ontario, London, ON, online at <http://citeseerx.ist.psu.edu/viewdoc/download?doi=10.1.1.470.4934 &rep=rep1&type=pdf> (accessed April 8, 2016).

Brown, D.A., O'Neill, M.W., Hoit, M., McVay, M., El Naggar, M.H., and Chakraborty S., 2001. Static and dynamic lateral loading of pile groups. National Cooperative Highway Research Program (NCHRP), Report 461, Appendix B: Dynamic response of piles to earthquake loading – analytical, online at <http://onlinepubs.trb.org/onlinepubs/nchrp/nchrp_rpt_461-c.pdf> (accessed April 8, 2016).

Clough, R.W. and Penzien, J., 2003. Dynamics of structures, 3rd edition, Computers & Structures: Berkeley, CA, 2003.

El Naggar, M.H. Design of foundations for dynamic loads, University of Western Ontario, London, ON.

Gallagher, R.H., 1975. Finite element analysis – fundamentals, Prentice-Hall Inc., Englewood Cliffs, NJ.

Novak, M. 1974. Dynamic stiffness and damping of piles. Canadian Geotechnical Journal, 11, 574-598.

Wilcox, J. and Walters, T. 2012. Evaluating dynamic loads in piping systems caused by waterhammer, online at: <http://www.accutech2000.com.au/AFT/AFT%20Brochures/AFT-Evaluating-Pipe-Dynamic-Loads-Caused-by-Waterhammer.pdf> (accessed April 8, 2016).

© 2016 Deep Foundations Institute

GROUND DISTURBANCE DUE TO STATIC PRESSURE DRIVING OF OPENED-ENDED PHC PILES

Guowei Li, Key Laboratory of Ministry of Education for Geotechnique and Embankment Engineering Hohai University，Nanjing，Jiangsu，China. Phone: +86 13805162119, Email: lgwnj@163.com

Andrew C. Amenuvor, Geotechnical Research Institute，Hohai University，Nanjing，Jiangsu，China, Phone: +86 13645177311, Email: ac.amenuvor@gmail.com

Xiaocen Lu, Geotechnical Research Institute，Hohai University，Nanjing，Jiangsu，China, Phone: +86 18666698360, China Email: luxiaocen@hhu.edu.cn

Jiantao Wu, Highway and Railway Research Institute，Hohai University，Nanjing，Jiangsu，China, +86 13915975806, Email: jiantao.wu@hhu.edu.cn

Thang N. Nguyen Geotechnical Research Institute，Hohai University，Nanjing，Jiangsu，China, Phone: +86 15895986781, Email: thangnn@tlu.edu.vn

ABSTRACT

This paper investigates the effect of driving a group of 52 open-ended Prestressed High Strength Concrete (PHC) piles on an existing highway embankment based on field measurements of excess pore pressure and lateral soil displacement. Excess pore pressure due to pile driving increased with depth and decreased with increasing distance from the pile, influencing a distance of 43 pile diameters. For pile groups, the rate of dissipation of excess pore pressure decreased with increasing depth and averaged 79% in 20 days, during which maximum ultimate bearing capacity was not yet attained. Lateral soil displacement continued to increase for a period of time after the end of pile driving and this could have resulted in significant inclination of piles if pile installation was too quick and pile spacing was too small. Lateral soil displacement due to pile group decreased with decreasing distance to the existing embankment as a result of high soil density produced by the embankment loading. The results also indicate that the effect of pile group installation on the existing embankment is negligible.

Keywords: Existing embankment widening; PHC pile; Pile driving; Excess pore pressure; Lateral displacement

INTRODUCTION

Pile driving can cause excessive lateral displacement of soil and heaving of the ground surface, which may adversely affect nearby structures. In addition, lateral deformation and excess pore water pressure resulting from pile driving can exert lateral pressures and vertical forces on the piles, and impact negatively on the project and its surroundings. Therefore, it is important to evaluate the influence of pile driving on the nearby structures as well as the project itself when expansion works are carried out.

Recent years have seen some development in the application of field tests for studying soil disturbance due to piles, and these tests usually involves pore water pressure and lateral soil displacement monitoring during pile driving. Results of field experiments performed by Reese and Seed (1957) in San Francisco Bay Mud with instrumented piles showed that pile installation generated large pore water pressures at the pile surface, with only slight increase at a distance of 15 pile diameters away. The measurements indicated that the increase in pore water pressures can exceed the initial total overburden pressure. Holtz and Lowitz (1965) reported a decrease in undrained shear strength immediately after pile installation, which was largely recovered after full pore pressure dissipation for field measurements within 1.5–2 pile

© 2016 Deep Foundations Institute

diameters from the pile surface. Hwang et al. (2001) presented results of large scale pile driving tests where maximum excess pore water pressure generated decreased rapidly with increasing distance from pile. The excess pore water pressure became negligible at 15 pile diameters from the pile. Their results also showed that lateral displacement of the ground decreased with increasing distance from the pile. Pestana et al. (2002) carried out full-scale closed ended pile tests in the Young Bay Mud deposit. Higher excess pore pressures were observed for points closer to the pile, which decreased with increasing distance from the pile wall. Exponential decay of excess pore pressure with time was also noted. An 80% dissipation of excess pore pressure was achieved for soils more than one pile diameter away from the pile wall between 50 to 80 days. Lateral deformation generally decreased with increasing distance from pile wall, whilst varying erratically with depth. Bozozuk et al. (1978) reported on soil disturbance due to driving of 116 concrete piles in sensitive marine clays in a construction project. Maximum pore water pressures after pile driving within the group, and 6m (20 pile diameters) from the group were over 35-40% of the total overburden pressures, and the influence of pile driving on pore water pressure at 20m away from the group was very small. Cooke and Price (1973) studied a 168-mm-diameter instrumented pile jacked into over consolidated London clay. Outward lateral displacements ranging from 10 to 20mm were recorded, depending on initial distance from the pile.

Most of the previous studies focused mainly on soil disturbance resulting from single pile, with less consideration given to pile group and pile driving order. Therefore, it is imperative to systemically study the influence of pile group and pile driving sequence on the disturbance of soil. This paper presents a study of the influence of driving open-ended PHC piles on an existing highway embankment based on field measurements of pore pressure and lateral soil displacement along the K55+ 630 - 660 section of the Guangqing Highway Expansion Project in China.

TEST SITE DESCRIPTION

The Guangqing Highway lies mainly in the quaternary flood plains made of organic clay, silt and other organic soils, which are widely distributed in the plains and valleys. The geology of the project site comprises, from top to bottom, silty clay, organic clay, and highly weathered limestone. The distribution and index properties of the soil at the test site are shown in Table 1. Also present around the construction site is the fill of the existing embankment, the properties of which were determined in addition to that of the natural soil.

PILE LAYOUT AND INSTRUMENTATION

Pile Installation

The piles were driven through the soil at an average rate of 50mm/s with their tips embedded in the highly weathered limestone layer. The piles, of the type PHC-C70-A300, have design length and pipe wall thickness of 11m and 7cm, respectively. . A total of 52 piles were installed in a square pattern, 2.6m apart as shown in Fig.1, where the arrows indicate the installation order of the piles, and the circles with vertical or horizontal lines indicating piles driven on alternate days. Dates are also shown beside the first pile driven each day. The installation of pile began from pile #4-8 on December 9, 2011, and ended on December 13, 2011. The pile identity is expressed as #row number-column number, so pile #4-8 indicates the pile in the 4th row and 8th column.

© 2016 Deep Foundations Institute

Table 1 Index properties of soil

Soil category	Average thickness/m	Moisture content/%	Unit (kN·m-3)	Void ratio	Compression index	Cohesion /kPa	Internal friction angle / (°)	Plastic limit	Liquid limit
filling of the existing road	6	20.3	17.93	0.78	0.15	1.5	12.39		
silty clay	2	20.3	16.86	0.89	0.23	16.67	22.6	26.0	40
organic clay	3	46	17.35	0.9	0.36	0	26.9	32.8	48.6
organic clay	4	42.5	17.79	1.6	0.34	12.57	32.32	33.3	52.6

Inclinometer Instrumentation

In-place inclinometers with automatic data collection system, which provides real time continuous measurement during construction, was used to record changes in soil displacement during and after pile driving. The coordinate was set with the X-axis parallel to the road foundation, while the Y-axis was perpendicular to the road foundation, with its positive direction pointing away from the existing road (or embankment). Four inclinometer casings designated as C1, C2, C3 and C4, were installed to measure the lateral deformation of the soil. The elevation of the existing road is 6m higher than that of the construction ground. One of the inclinometer casings, C1 was installed on the shoulder of the existing road, whose elevation is 6m higher than the construction ground, to the depth of 19m. C2 was installed on the shoulder of the road under construction to a depth of 15m. C3 was installed at the slope toe of the existing road to a depth of 12m, while C4 was installed at the slope toe of the embankment under construction to a depth of 11.2m. Detailed layout of inclinometers is shown in Fig. 1.

Piezometer Instrumentation

Pore water pressure measurements were obtained with nine vibrating wire piezometers installed in four different boreholes K1, K2, K3, and K4. At K1, measurements were taken by piezometers K1-9.5 and K1-14.5 at depths of 9.5m and 14.5m relative to the existing road, respectively. At K2, piezometers K2-3.5 and K2-5.5 took measurements at depths of 3.5m and 5.5m relative to the road under construction, respectively. Instrumentation at K3 and K4 is similar to that of K2, but K3 obtained additional measurements at 7m depth. Fig. 1 shows the instrumentation in detail. Considering the instantaneity and dynamic nature of pore pressure in the soil during pile driving process, pore pressure data collection was automated to continually record changes in pore water pressure.

© 2016 Deep Foundations Institute

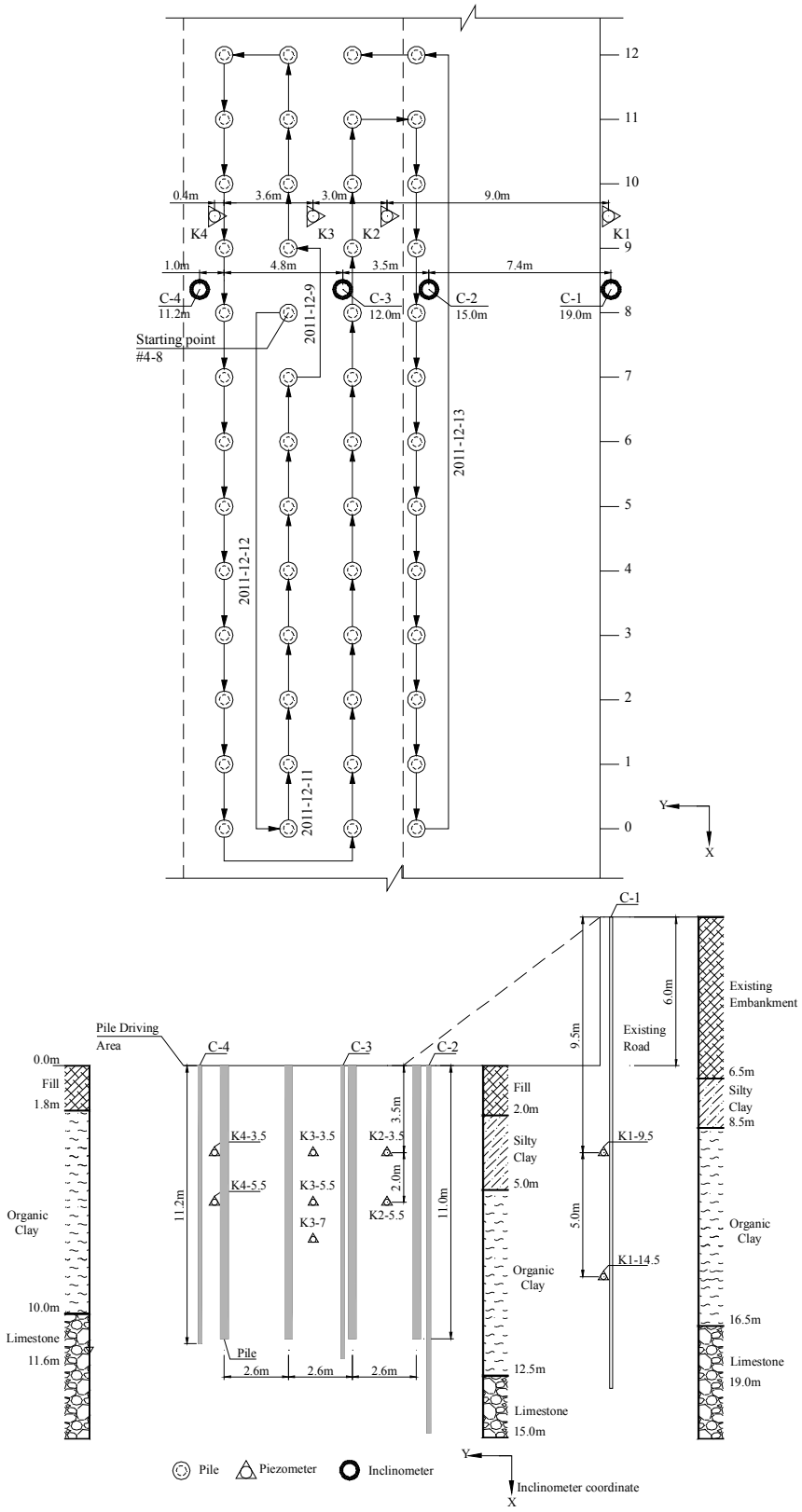


Fig. 1 Layout of piles and instrumentation

© 2016 Deep Foundations Institute

RESULTS AND DISCUSSION

Pore water pressure

Figure 2 shows the variation of excess pore water pressure with distance from single pile #4-8, for pore pressure piezometers K1-9.5, K2-3.5, K3-3.5 and K4-3.5 at the depth of 3.5m relative to the construction ground. Excess pore water pressure decreased linearly with increasing distance from the pile. The reduction of excess pore water pressure with distance from pile was also observed by Seed and Reese (1957), Roy et al. (1980), and Pestana et al (2002).

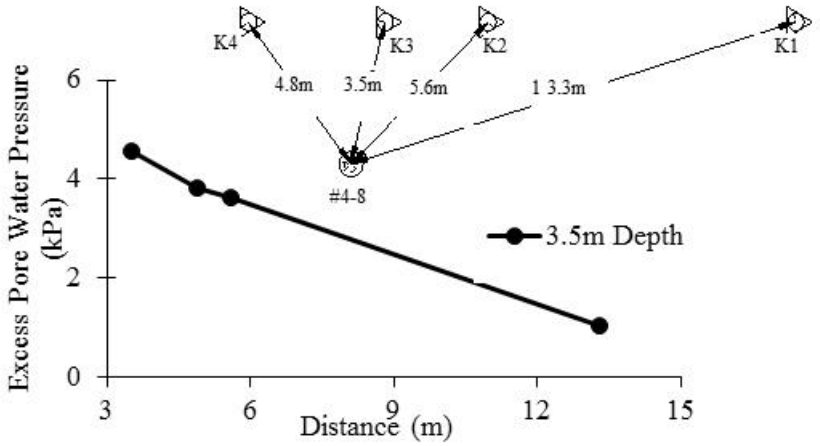


Fig.2 Variation of excess pore water pressure with distance

Figure 3 shows the variation of excess pore pressure with time, due to pile group installation, for the various borings over a period of more than 86 hours. It is evident that piezometers within the pile driving area experienced faster and higher pore water pressure increments as compared to those outside the pile driving area. Piezometers K2-5.5, K3-5.5 and K4-5.5 (shown in Figs. 3(b), 3(c) and 3(d), respectively), which are within the pile driving area, recorded maximum pore water pressure values of over 40kPa, while piezometer K1-14.5 (shown in Fig 3(a)), 7.5m away from the area, recorded pore water pressure values mostly less than 10kPa, with a maximum of just 14kPa. This suggests the distance beyond which the excess pore water pressure induced by pile driving becomes insignificant. The influence of pile driving on the existing embankment can therefore be considered to be very weak. In addition, the excess pore water pressure generally increased with time, with occasional oscillations, with the troughs indicating the periods of dissipation at night after pile driving in the day. Pile installation was carried out within three days, only during day time. However, the excess pore water pressure dissipated only slightly at night after construction in daytime. The slow dissipation is due to the clayey soil type in the area. During pile driving, pore water pressure at all piezometers increased with depth, with Fig. 3(a) in particular, showing a significant difference between pore water pressure values at the depths of 3.5m and 5.5m.

Figure 4 shows the variation of excess pore water pressure with depth for the pile group, at piezometer K3 on December 11 at various times.

Pore water pressure increment can be calculated according to Henkel's equation:

$$\Delta u = \beta \Delta \sigma_{OCT} + \alpha_f \Delta \tau_{OCT} \quad [1]$$

Where $\Delta\sigma_{OCT}$ is octahedral normal stress increment; $\Delta\tau_{OCT}$ is octahedral shear stress increment; and β and α_f are Henkel's pore water pressure coefficients. β=1 for saturated soils.

The soil is assumed as an ideal elasto-plastic material, obeying Mohr-Coulomb failure criterion, and it is in a state of limit equilibrium (e.g. Yao Xiaoqing et al 1997). Two soil elements are taken from the depths of h_1 and h_2 for a homogeneous soil layer whose initial stress state is K_0 state, and radial stresses $\Delta\sigma_{r1}$ and $\Delta\sigma_{r2}$ are separately applied to the soil at the depth of h_1 and h_2.

© 2016 Deep Foundations Institute

According to earth pressure theory, when the soil is in the state of limit equilibrium, the following deductions can be made.

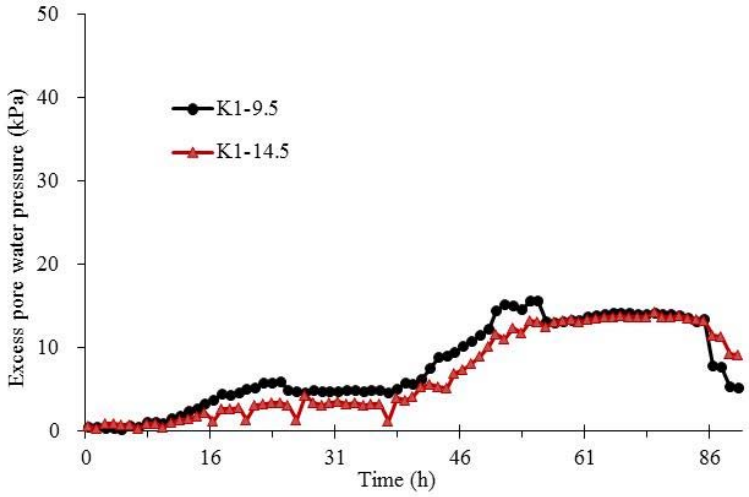
$$K_0 r h_1 + \Delta\sigma_{r1} = r h_1 \tan^2\left(45^\circ + \frac{\varphi}{2}\right) + 2C\tan\left(45^\circ + \frac{\varphi}{2}\right) \quad [2]$$

$$K_0 r h_2 + \Delta\sigma_{r2} = r h_2 \tan^2\left(45^\circ + \frac{\varphi}{2}\right) + 2C\tan\left(45^\circ + \frac{\varphi}{2}\right) \quad [3]$$

$$\frac{\Delta\sigma_{r2} - \Delta\sigma_{r1}}{h_2 - h_1} = r\left[\tan^2\left(45^\circ + \frac{\varphi}{2}\right) - K_0\right] \quad [4]$$

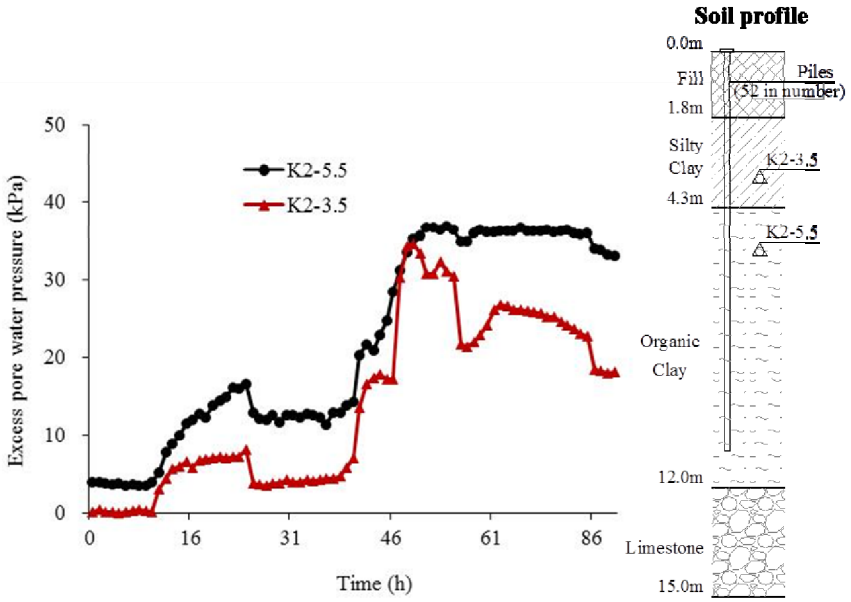
Where $\tan^2(45^\circ + \varphi/2) = K_p$ is the coefficient of passive earth pressure.

From pile driving with hammer, the coefficient of passive earth pressure K_p of the soil is found to be the upper bound of the coefficient of earth pressure at rest for over-consolidated soils (e.g. Duncan et al 1986; Luo et al 2010), which implies $K_p - K_0 > 0$. According to the analysis above, it can be concluded that the radial stress applied to the soil increases with increasing depth. Since shear stress and normal stress are positively correlated, then according to Henkel's equation, it can be concluded that excess pore water pressure increases with depth. The measured data in Fig. 4 indicates that excess pore water pressure generated by pile driving increases with depth, and it is essentially linear. The measured data is consistent with the above theoretical equation and analysis.

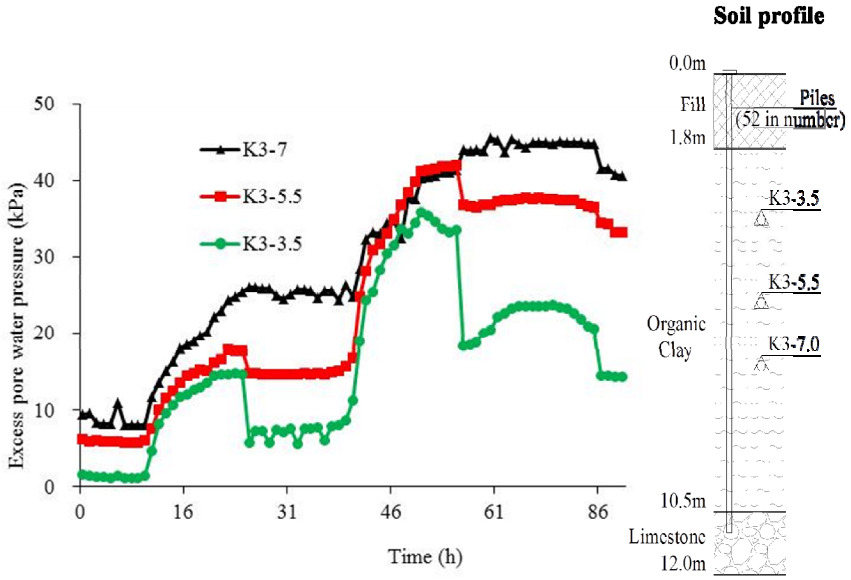


(a)

© 2016 Deep Foundations Institute

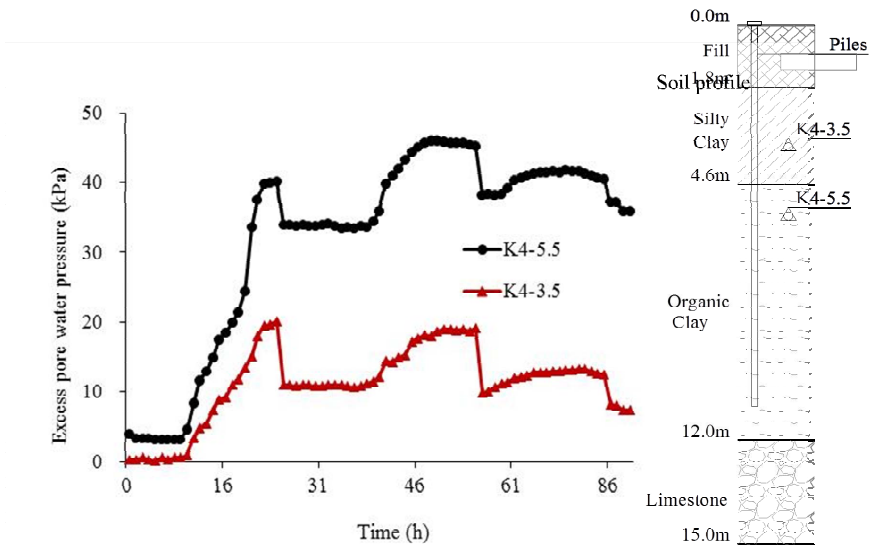


(b)



(c)

© 2016 Deep Foundations Institute



(d)

Fig. 3 Pile group pore water pressure histories: (a) K1; (b) K2; (c) K3; (d) K4

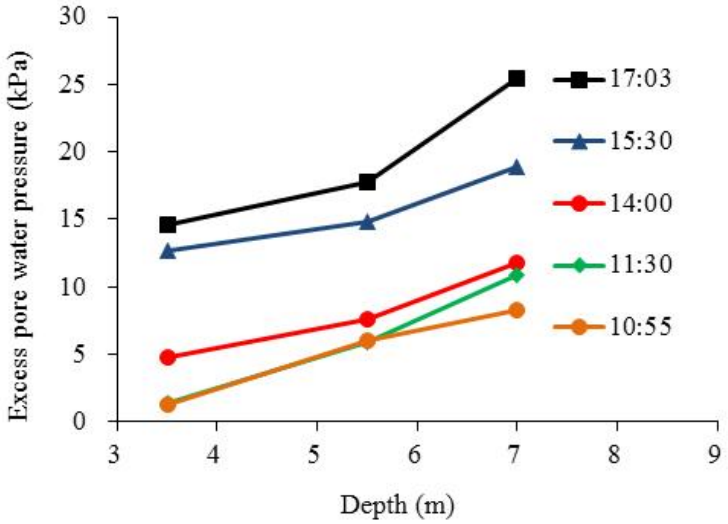


Fig. 4 Variation of excess pore water pressure with depth at K3

A summary of the development and dissipation of excess pore water pressure at each piezometer location is shown in Table 2. The ratio, in percentage, of the maximum excess pore water pressure to overburden pressure of the piezometers located in the pile driving area averages 85. At piezometer K1, the maximum value of excess pore water pressure and the ratio of excess pore water pressure to overburden pressure are low. This indicates that the influence of pile driving on the shoulder of the existing 7.5m away from the pile driving area is small; thus, the test pile driving site is at a safe distance from the existing road. Excess pore water pressure built up dissipated to an average of 79% over a period of 20 days.

© 2016 Deep Foundations Institute

Table 2 Summary of excess pore water pressure for pile group

Piezoemeter		Depth/m	Layer	Effective overburden pressure σ'/kPa	Maximum excess pore pressure u_{max} /kPa	p_{hp}/p_o/%	Excess pore pressure after 20 days/kPa	Percentage dissipation after 20 days (/%)
K1	K1-9.5	9.5	Organic clay	73.4	15.67	21.3		
	K1-14.5	14.5	Organic clay	107.7	14.35	13.3		
K2	K2-3.5	3.5	Organic clay	25.8	34.59	134.1	1.67	95.17
	K2-5.5	5.5	Organic clay	36.3	36.80	101.4	7.44	79.78
K3	K3-3.5	3.5	Silty clay	27.9	35.91	128.7	2.46	93.14
	K3-5.5	5.5	Organic clay	41.7	42.05	100.8	13.55	67.77
	K3-7	7	Organic clay	51.9	45.49	87.6	21.01	53.81
K4	K4-3.5	3.5	Organic clay	27.9	20.11	72.1	0.42	97.89
	K4-5.5	5.5	Organic clay	41.7	46.08	110.5	14.36	68.84

Lateral Displacement of Soil due to Single Pile and Pile Group Installation

Huang et al. (2000) proposed Equation 5 to predict the soil displacement caused by pile driving. The soil is assumed to be homogeneous, isotropic, and saturated infinite medium. The effect of pile driving is equivalent to that of a series of penetrating globoids. It is an axisymmetric motion, so only X-Z coordinate plane is considered.

$$S_{xs} = \frac{d_0^2}{16}\left[\frac{z+L_0}{x\sqrt{x^2+(z+L_0)^2}} - \frac{z-L_0}{x\sqrt{x^2+(z-L_0)^2}}\right] \quad [5]$$

Where, S_{xs} is the lateral displacement of the soil, d_0 is the pile diameter, L_0 is the pile length, x is the distance to the axis of the pile, and z is the depth.

Taking the derivative of Equation 5 with respect to the variable z results Equation 6:

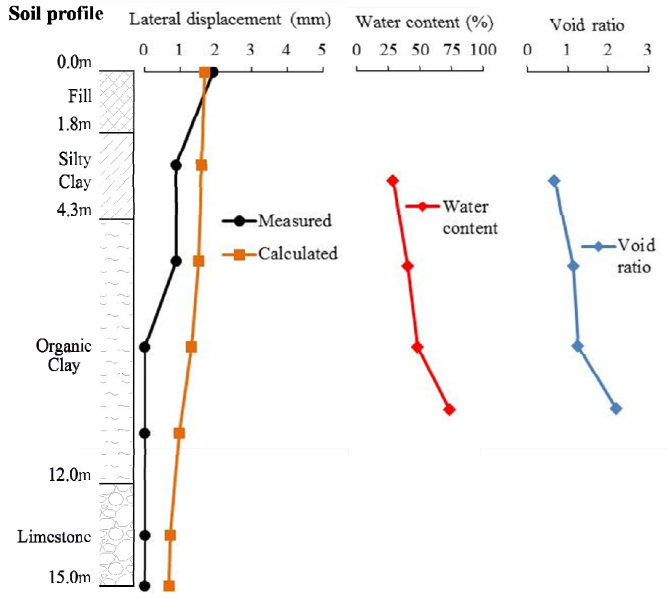
$$S_{xs}' = \frac{d_0^2 x}{16}\left[\frac{1}{\left(\sqrt{x^2+(z+L_0)^2}\right)^{\frac{3}{2}}} - \frac{1}{\left(\sqrt{x^2+(z-L_0)^2}\right)^{\frac{3}{2}}}\right] \quad [6]$$

Where S_{xs}' is less than 0, so the lateral displacement decreases with increasing depth, but the rate of decrement is small. The slope of the displacement-depth curve changes sharply at the tip of the pile, indicating a decrease in lateral displacement. According to Equation 5, lateral displacement decreases exponentially with increasing distance along the X-axis.

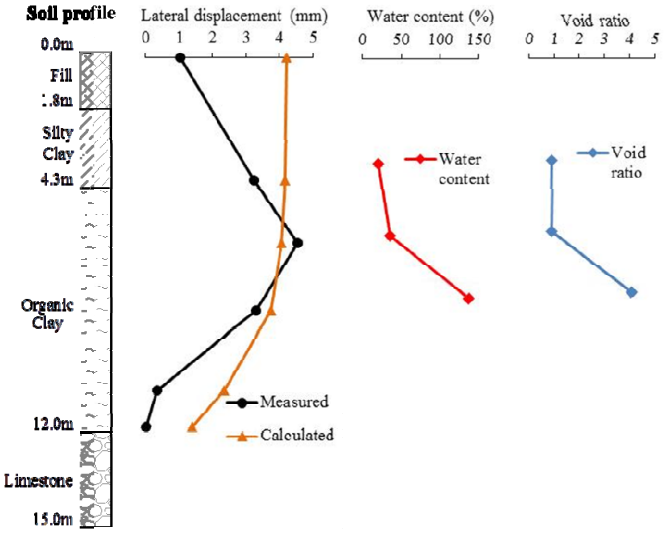
Figure 5 shows the variation of measured and calculated (Huang et al. 2000) lateral displacement at inclinometer C2 and C3 with depth due to single pile driving (pile #4-8). A plot of void ratio and water content has been added to the lateral displacement plot to help explain the observed phenomena. The displacement recorded at C3 is generally higher than that at C2 since C3 is closer to the pile than C2. C2 is closer to the existing road, where the upper soil layer has higher degree of compaction compared to the lower layer. This factor coupled with its farther distance from the pile resulted in the generally low measured and calculated displacement obtained as shown in Fig 5a. Also, the trend of the measured displacement above the 6m depth agrees fairly with that of the calculated displacement. However, there is some discrepancy in the displacement below 6m depth (i.e., the measured displacement became zero), and this is due to the embedment of the inclinometer casing in the relatively stable limestone layer. In Fig. 5b the displacement measured at C3 increased with depth to 4.5mm at a depth of 6m before decreasing sharply to zero. The trend of measured lateral displacement seems to be dependent on the void ratio and water content of the soil – both water content and void ratio increased with depth. The 4.5mm displacement occurs within the organic clay layer which has significantly high void ratio and water

© 2016 Deep Foundations Institute

content of 4 and 135.9%, respectively. The displacement measured at the ground surface is significantly small since the ground surface is composed of compacted fill with low void ratio. Thus, high void ratio and water content probably made the soil more deformable resulting in higher lateral displacement and vice versa.



(a)



(b)

Fig. 5 Lateral displacement due to pile #4-8: (a) C2; (b) C3

The trend of lateral deformation during installation of the pile group is very complex. Figure 6 shows the variation of lateral displacement with depth at C3 during installation of piles in row 4. Piles #4-3 to #4-7 are located on the same side of the inclinometer. All the curves show a similar trend, conforming to that of a single pile since piles of this row were driven first and were not influenced by piles driven subsequently. Three of the piles #4-3, #4-4 and #4-5 which were at different distances beyond three pile spacing (7.8m) away from C3 have their displacement curves almost coinciding. This indicates that the soil displacement due to pile driving is negligible around a distance of 7.8m and beyond. It is also apparent that the soil displacement decreased with increasing distance from the inclinometer. For example, Pile #4-7 is more than one pile spacing from C3, and its resulting lateral deformation is about 3mm.

© 2016 Deep Foundations Institute

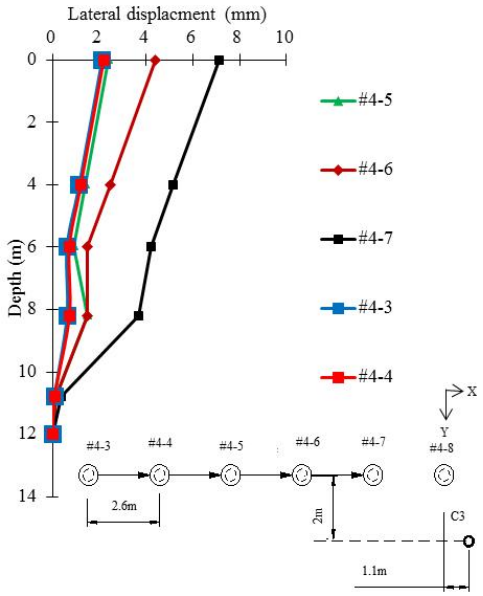


Fig. 6 Variation of lateral displacement with depth about C3

Figure 7 shows the variation of lateral displacement with depth at C2 during installation of piles in row 2. Pile #2-9 is on one side of the inclinometer whilst the other three are on the opposite side. Both the trend and magnitude of displacement significantly changed for piles driven after Pile #2-9. Pile #2-6 and Pile #2-7 are on the same side with Pile #2-8 and their induced displacements are just a little higher than of that of Pile #2-8 while their trend is essentially the same. It can be seen that the lateral displacement induced by Pile #2-6 is higher than that of Pile #2-7, and this was unexpected since Pile #2-6 is farther from the inclinometer than Pile #2-7. The displacement measured for Pile #2-6 might not be due solely to this pile, but might have been contributed partly by previously driven piles. And this might be an indication that the soil displacement is not instantaneous, but is delayed and occurred sometime after the pile had been driven. The displacement-depth curves for the pile group do not conform to the theoretical curves for single piles, and this could be attributed to the displacement been influenced by piles driven earlier in other rows.

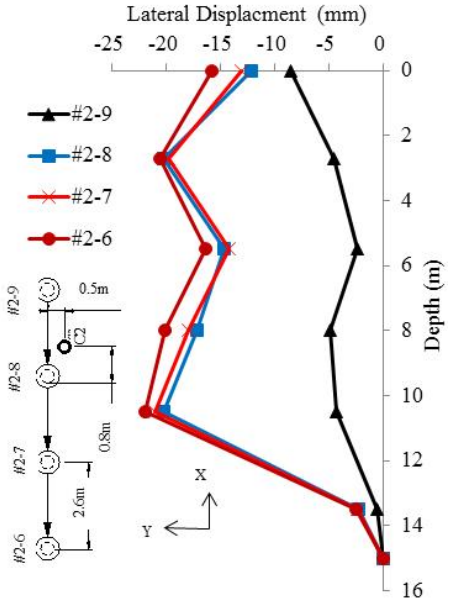


Fig. 7 Variation of lateral displacement with depth about C2

© 2016 Deep Foundations Institute

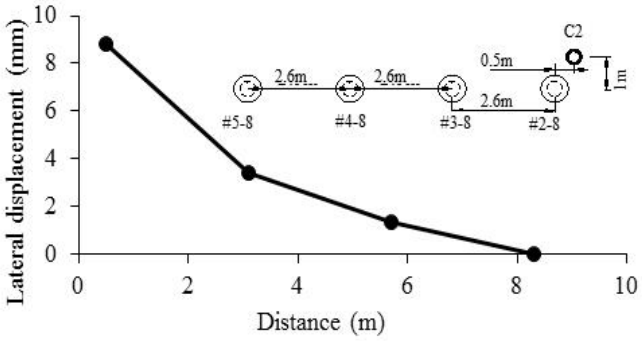


Fig. 8 Variation of lateral displacement with distance about C2

Figure 8 shows the variation of Y-axis lateral displacement at the ground surface with distance from C2. It can be seen that the lateral displacement induced by pile driving decreased with distance from the inclinometer and becomes zero at a distance of 8.3m, which is equivalent to 3.2 pile spacing.

It can be concluded that the lateral displacement induced by pile driving decreases with distance, though, the point of measurement and the direction of the displacement are different. And there is a distance beyond which the influence of pile driving on lateral displacement becomes very small. This distance may be up to three times the pile spacing. Also, the soil disturbance induced by driving of the earlier driven piles is delayed. In other words, the displacement induced by piles driven earlier may be accumulated and reflected in the displacement due to subsequently driven piles. Thus, attention should be paid to the order and timing of pile driving in order to avoid intensive accumulation and release of displacement.

Effect of pile driving on the existing road foundation

Figure 9 shows the relationship between lateral displacement and depth at C1, which is located on the shoulder of the existing road. The displacements recorded by C1 due to the installation of some piles in row 2 and row 3 differ only slightly. The difference in displacement is less than 1mm, and the displacement curves almost coincide. After the installation of all the 52 piles, the accumulated displacement measured by C1 is less than 100mm, which indicates that the effect of the pile group installation on the existing road is negligible. Figure 10 shows the variation of lateral displacement with depth at the end of pile driving at C2 and C4, which are located separately at opposite sides of test pile area.

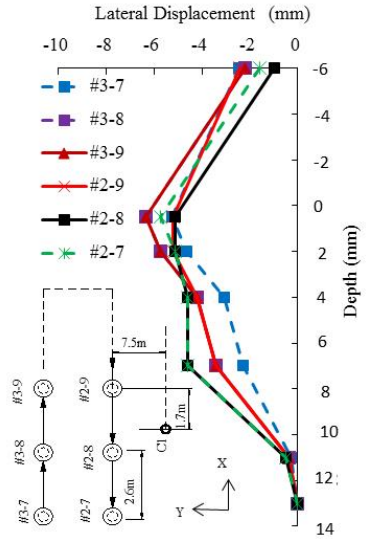


Fig. 9 Variation of lateral displacement with depth about C1

© 2016 Deep Foundations Institute

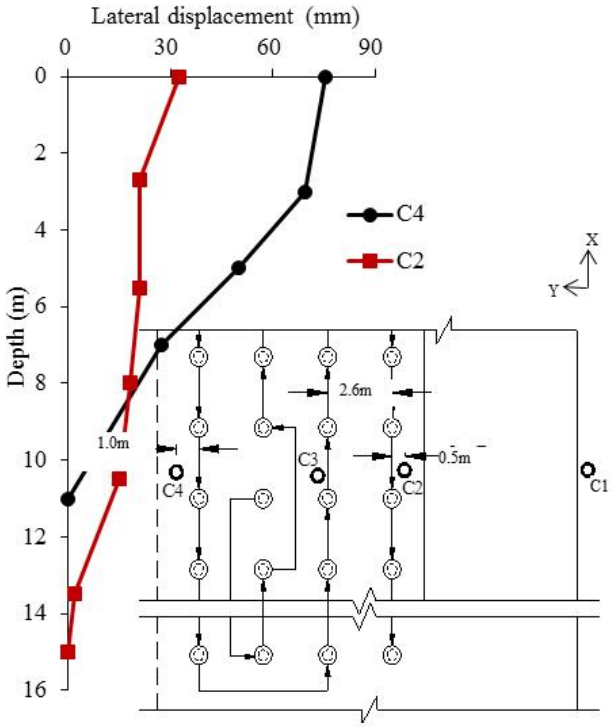


Fig.10 Variation of lateral displacement with depth about C2 and C4

C2 is located along the slope of the existing road, 0.5m away from the outer edge of test pile area, while C4 is located on the opposite side, 1.0m away from the outer edge of the test pile area, under natural soil conditions. The maximum displacement measured by C2 is 32mm, while that measured by C4 is 75mm. Though C2 is closer to the test pile area, its measured lateral displacement is smaller than that of C4. The reason for the above phenomenon is that the load of the existing road increased the stress on the foundation soil, thereby increasing its degree of consolidation, and consequently decreasing its displacement.

SUMMARY AND CONCLUSIONS

Pore water pressure and lateral soil displacement measurements were made during and after driving some 52 opened-ended PHC piles in order to assess the extent of soil disturbance resulting from the pile installation. The results are summarized as follows:

Excess pore water pressure decreased linearly with increasing distance from the pile group, while increasing with depth in an approximately linear fashion. The excess pore water pressure dissipated averagely, 79%, over a period of 20 days.

The lateral displacement resulting from pile driving decreased with depth, and its magnitude seem to depend on the properties of the soil (i.e., void ratio and water content). Higher void ratio and water content made the soil more deformable, resulting in higher lateral displacement and vice versa. The rate of decrease of lateral displacement with depth is slower at shallower depths (in the clayey layers), but faster at deeper depths. Lateral displacement decreased rapidly with increasing distance, and became zero beyond a certain range. Also, there seem to be a delay in lateral displacement during pile group installation resulting in accumulation of lateral displacement. And this could result in movement or inclination of piles if pile driving is too quick.

© 2016 Deep Foundations Institute

Pile driving had little influence on the foundation of the existing road during the expansion process. However, the soil properties have some influence on ground disturbance due to pile driving. The embankment of the existing road has restricted to some extent, lateral displacement perpendicular to the embankment. The shoulder of the existing road, which is 7.5 m away from the pile driving area, recorded less than 10mm lateral displacement due to driving of the two closest rows of piles, while the accumulated lateral displacement due to all the 52 piles recorded in the same direction at 1m away from the edge of the pile driving area is 75mm. Therefore, the pile driving has negligible influence on the existing road.

REFERENCES

Bozozuk, M., Fellenius B.H., and Samson L. (1978). "Soil disturbance from pile driving in sensitive clay." *Canadian Geotechnical Journal*, 15(3), 346 – 361.

Cooke, R.W., and Price, G. (1973). ''Strains and displacements around friction piles.'' Proc., 8th Int. Conf. Soil Mechanics Foundation Engineering, Moscow, 3(9), 53– 60.

Duncan, J.M, and Seed, RB. (1986). "Compaction-induced earth pressures under K0-conditions." Journal of Geotechnical Engineering, 112(1), 1-22.

Holtz, W.G., and Lowitz, C.A. (1965). ''Effects of driving displacement piles in lean clay.'' *J. Soil Mech. Found. Div., Am. Soc. Civ. Eng.,* 91(SM5), 1-13.

Huang, Y.-X., Xu, Q.-X., and Hu, Z.-X. (2000). "Soil's displacemnet due to driving pile in saturated clay." J. Industrial Construction, 30(7), 15-19, (in Chinese)).

Hwang, J.-H., Liang, N. & Chen, C.-H. (2001). "Ground response during pile driving." J. Geotech. Geoenviron. Eng., 10.1061/(ASCE)1090-0241(2001)127:11(939), 939–949.

Pestana, J.M., Hunt, C. E., and Bray J. D. (2002). "Soil deformation and excess pore pressure field around a closed-ended pile." J. Geotech. Geoenviron. Eng., 10.1061/(ASCE)1090-0241(2002)128:1(1), 1-12.

Luo, Y.-W., Ling, D.-S., Chen, Y.-M., and Hu, Q. (2010). "The change in horizontal stress of soils during K0 loading-unloading". J. Industrial Construction, 40(7), 56-58 (in Chinese).

Roy, M., Blanchet, R., Tavenas, F., and Rochelle, P.L. (1980). "Behaviour of a sensitive clay during pile driving". *Canadian Geotechnical Journal*, 18(1), 67-85.

Seed, H.B., and Reese, L. C. (1957). ''The action of soft clay along friction piles.'' Trans. Am. Soc. Civ. Eng., 122, 731–754.

Yao, X.-Q， and Hu, Z.-X. Saturated soft soil pile-sinking caused by the pore water pressure estimation[J]. Rock and soil mechanics, 1997, 18（4）：30-35. (in Chinese).

© 2016 Deep Foundations Institute

PERFORMANCE MONITORING FOR DEEP EXCAVATIONS

Alexi J Neill, P.E., Geocomp Corporation, Atlanta, GA, 770-217-5388, aneill@geocomp.com

ABSTRACT

This presentation will showcase two challenging projects with deep excavation support systems in the Atlanta area where state-of-the-art instrumentation and monitoring systems were used to manage risk by confirming design performance requirements / calculations during construction. The instrumentation and monitoring system successfully reduced risk by recording real-time data on a project website while simultaneously sending email alarms to key site personnel when data exceeded pre-determined alarm thresholds. The monitoring data revealed unexpected performance at an early enough stage so that contingency plans could be engaged and remedial efforts devised in order to limit the consequences. Finite element analysis was used to model deformations, analyze the unexpected performance, and prepare the remedial design.

INTRODUCTION

Construction in densely populated urban areas is becoming more common in order to keep up with the increasing infrastructure demands of our growing population. America's big cities continue to outpace the overall nation in population growth. The city of Atlanta, the nation's ninth largest city based on metropolitan population, is a prime example of this. The population has grown at a rate of 6.6% between 2010 and 2013, nearly triple the overall growth rate of the United States during the same period (SustainAtlanta, 2015).

As a result of increasing infrastructure demands in Atlanta, developers are now constructing larger buildings on smaller properties. In addition, developers are attempting to maximize space on their selected properties, often by designing underground parking garages to accommodate as many cars as possible on these compact sites. In some cases the selected sites are adjacent to buildings, utilities, and other existing structures. The risk associated with construction increases during underground work that requires a support of excavation system, particularly on confined sites adjacent to existing structures. There is a risk posed to people, property, and the environment that the project team should monitor when constructing in these conditions.

ROLE OF INSTRUMENTATION AND MONITORING

A good instrumentation and monitoring system reduces risk during construction and beyond by helping to eliminate unknowns. Geotechnical engineering relies on a number of assumptions that are based on representative borehole samples and known geological conditions in the area. One thing that these assumptions cannot account for are anomalies underground. They also cannot account for means and methods of the Contractor, which may differ from the assumptions used to prepare the predictive models during the design phase. Loading conditions and resulting movement from existing structures whose foundations are disturbed during construction are also difficult to predict.

Instrumentation installed at key locations prior to construction to measure performance of the support of excavation system and/or existing structures within the zone of influence reduces the risks described above. Real time data collected via monitoring is used to analyze the performance as construction progresses. The frequency of monitoring intervals is especially important in order to correlate the impact of construction activities and environmental conditions to construction activities. Real-time alarms are sent to key personnel whenever instrumentation readings exceed predicted levels or whenever readings approach levels

© 2016 Deep Foundations Institute

that jeopardize the structural integrity of the structure being monitoring. This advanced warning then allows the project team to implement contingency measures before endangering human life and property.

COX TOWER CASE STUDY

The Cox Tower project in Atlanta, GA is an example of a project where instrumentation and monitoring played a pivotal role in reducing and actively managing risk on a construction project. Two 12-story towers required 390 feet long by 420 feet wide by 35 feet deep excavations through saturated residual soils for construction of an underground parking garage. The support of excavation walls consisted of soldier piles with timber lagging held in place with 3 rows of tieback anchors. Shotcrete was used to finish the wall. Dewatering wells behind the shoring wall were used to draw the water table down as the site was excavated in approximately 5 feet increments. Figure 1 shows the first of the two towers under construction while the support of excavation is constructed to the West of the tower.



Fig. 1 – Overview photograph of the construction site

The initial scope of work was the installation of instrumentation and to provide real-time monitoring services of the shoring walls and an existing parking deck adjacent to the excavation. Instrumentation consisted of an automated motorized total station (AMTS) to monitor lateral movements and settlement of 65 survey prisms attached to the top and middle of every fifth soldier pile. The AMTS used for the project was a Leica Model TCA 1201, 1 second instrument, with an accuracy of plus or minus 1 millimeter (0.04 inch) as shown in Figure 2.

© 2016 Deep Foundations Institute



Fig. 2 – AMTS monitoring the construction site

Two vibrating wire piezometers, Geokon Model 4500S, were also installed inside of two monitoring wells located within the excavation in order to monitor the groundwater level as the site was dewatered. The piezometer data was recorded once every hour by Geocomp iSite vibrating wire data loggers and the AMTS recorded data once every 2 hours using Leica Geomos software. IP Phones were used to communicate all data wirelessly and in real-time to the Geocomp iSiteCentral website and a permanent record of the data was stored in the database. The website automatically processed the instrumentation data into engineering units and displayed the data in graphical format. Alarms were set at 3 different levels (yellow, orange, and red) determined by the shoring wall designer. Yellow alarms were a caution state where performance was outside the range expected in the design, or anomalous behavior not anticipated in the design was occurring. Orange alarms indicated that undesirable performance was occurring at an increasing rate and approaching the limit value. Red alarms (limit value) represented performance in a range where safety of the facility was in question, or performance was deteriorating and not controllable. Generally, the red alarms were set at a value of 0.5 percent of the retained depth, yellow alarms were set at half of red alarm value, and orange alarms were set half way between the red and yellow alarm values.

© 2016 Deep Foundations Institute

During construction, excessive vertical and horizontal deformations triggered an alarm on one of the soldier piles, Pile 74, after a tower crane pad was over excavated near the toe of the shoring wall. Construction activities leading up the alarm and following the alarm were as follows. The wall between Piles 69 and 78 was excavated to elevation 998 feet on November 9, 2010. The tower crane excavation was sloped at about 1(H) to 1(V) from the shoring wall down to the top of footing at about elevation 989. The tower crane excavation was cut with vertical sides to the bottom at about elevation 984.5 feet on November 10, 2010. An inspector recommended undercutting of soft soils at the bottom of the pit on November 13, 2010 and an alarm triggered that same day. This area of the shoring wall was supporting an existing major roadway behind the wall and small cracks were first noticed in the road on November 15, 2010. Figure 3 below shows the location of cracks in the roadway behind the wall.



Fig. 3 – Roadway cracks

Personnel were brought to the site to take remedial measures in order to stabilize the movement and the tower crane footing was backfilled on November 16. A fourth row of tiebacks were installed near the bottom of the shoring wall and the tiebacks were stressed on November 20, 2010. The tower crane was excavated a second time on November 22, 2010 and concrete placement for the tower crane was completed on November 24, 2010. Figure 4 shows the location of Pile 74 in relation to the tower crane.

© 2016 Deep Foundations Institute



Fig. 4 – Pile 74 photograph with tower crane pad

An analysis of the wall was performed in order to determine the cause of the movement and recommend remedial actions. The analysis was challenging because of the groundwater draw down during the construction and the soils were still consolidating from the changes in effective stress during the excavation. Finite element analyses were performed using Plaxis software to evaluate the deformations and factors of safety for various stages of the construction process. The analysis considered the partially drained behavior of the soils by modeling the time rate of groundwater drawn down and the effective stress changes. The results indicated that about 3 to 4 inches of horizontal and vertical movement would have occurred at the site due to the excavation as designed which is consistent with where the limit value was set. The factor of safety against global instability was computed to be 1.3 prior to the tower crane pad excavation and was most likely reduced by activities associated with the tower crane excavation to very close to 1. The factor of safety against global instability was raised to 1.4 with the additional row of tiebacks. The results of the analysis suggested that the factor of safety would be further increased by adding a row of auger cast piles at the toe of wall outside of the area that had been stabilized with the fourth row of tiebacks. The auger cast pile solution was beneficial to the project cost and schedule because equipment was already on-site installing auger cast piles for the building. The factor of safety would increase again to 1.5 when final grading was completed and additional wall movements would not exceed 1 inch over the design life of the facility.

© 2016 Deep Foundations Institute

It was concluded that over excavation of the crane pit and leaving it open for several days was a major factor for causing movements much larger than expected. Other factors that may have contributed to the large movement included heavy rainfall and fill that was added outside of the wall along with positioning a heavy crane over the fill during the same time. Figure 5 shows the data chart for Pile 74 from the project website along with comments at the top of the chart indicating key factors related to the movement; 74-1 was the prism installed at the top of the soldier pile and 74-2 was the prism installed near the middle of the soldier pile.

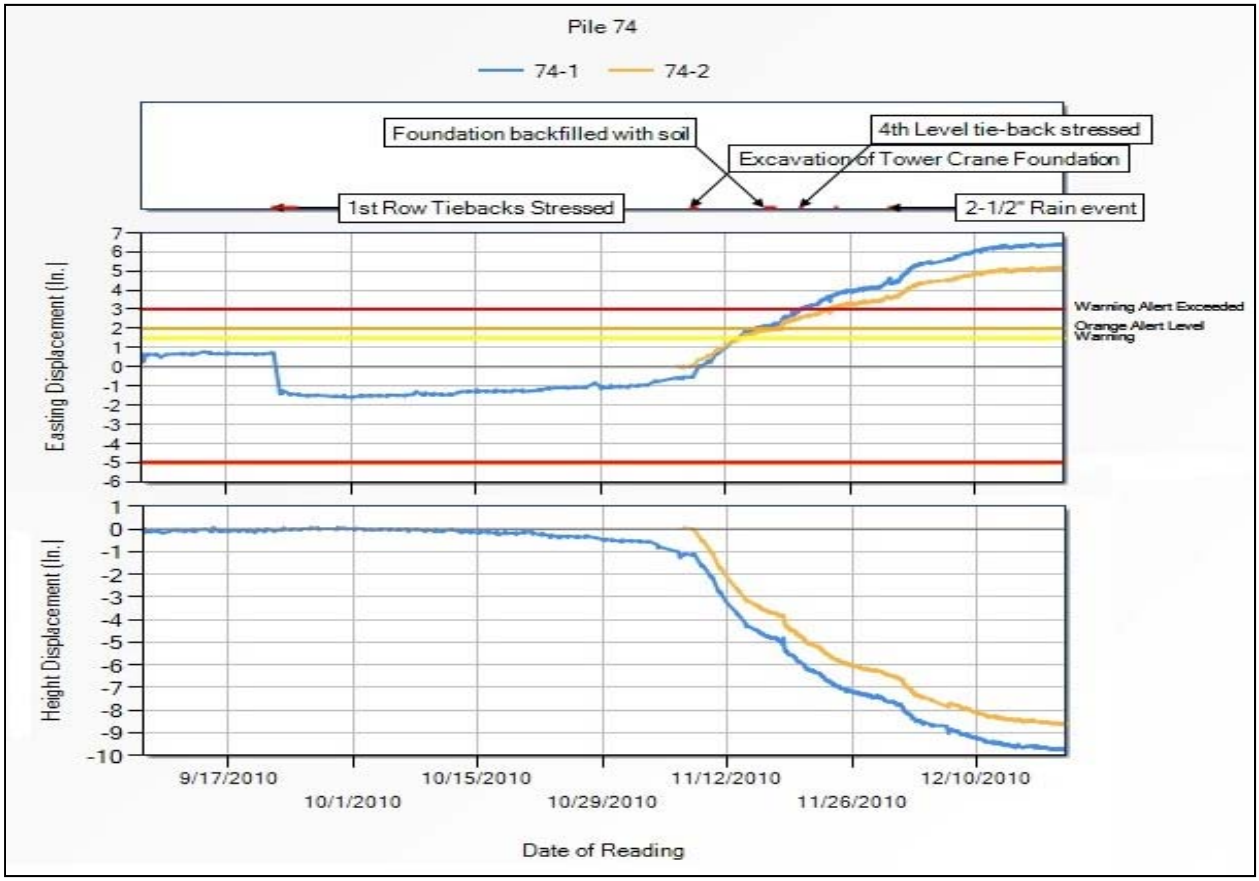


Fig. 5 – Pile 74 data chart

Cracking of the ground surface behind the wall that developed between November 27 and December 4 may have indicated the onset of global instability. The real-time instrumentation and monitoring system alerted the project team immediately when unexpected performance occurred and allowed the team to react quickly in order to implement a solution prior to potential failure of the wall. The reduced level of accuracy and reading frequency typically used by traditional manual survey methods as well as the additional time involved to manually process and communicate the data and results might not have identified the problem in enough time to save the wall from possible failure.

© 2016 Deep Foundations Institute

COX TOWER II CASE STUDY

The Cox Tower II project was an expansion on the property that included construction of a 20-story tower building with an adjacent 7-level underground parking garage. Construction of the parking deck required a 75 feet deep excavation and a dewatering system to lower the water table by 40 feet. The support of excavation system consisted of soldier piles with shotcrete lagging held in place with up to 5 rows of tiebacks. The risk was even greater on this project compared to the previous project on the property due to the deeper soil cut that required blasting of rock in order to excavate down to finished grade. In addition, there were several structures within the zone of influence of the parking deck excavation, including the new tower building, an existing building, existing generator pad, existing parking deck, and existing roadway.

The expected performance of the shoring wall design was predicted using Plaxis software prior to construction because of both the elevated construction risk and also the unexpected movement that occurred on the first tower project on the same property. An instrumentation and real-time monitoring system was installed to monitor performance of the shoring wall during construction. The instrumentation consisted of two AMTS units, Leica Model TM-30, 1 second instruments, with accuracies of plus or minus 1 millimeter (0.04 inch) to measure horizontal and lateral movements of 80 survey prisms. The survey prisms were installed on the top of soldier piles, on ground settlement points behind the wall, and on existing structures within the zone of influence of the excavation. Four in-place-inclinometers, Geokon Model 6150 biaxial sensors, were installed within Slope Indicator inclinometer casing. The casing was attached to selected soldier piles as shown in Figure 6 to measure lateral movements of the wall at predetermined depths and create a vertical profile of the shoring wall.



Fig. 6 – Slope Indicator casing attached to soldier pile

© 2016 Deep Foundations Institute

Four vibrating wire piezometers were installed inside of four monitoring wells located within the excavation to monitor the groundwater level as the site was dewatered. Instrumentation data was recorded at least once every 2 hours and displayed on real-time charts on a project website. Alarms were set at levels determined by the shoring wall designer according to the predictive analysis results.

A finite element model performed on the shoring wall section at Wall H where the deepest cut was required revealed a maximum predicted displacement of approximately 3.7 inches. Figure 7 below is a graph of the predicted output generated by the finite element analysis program that shows both the displacement profile of the wall and the maximum displacement.

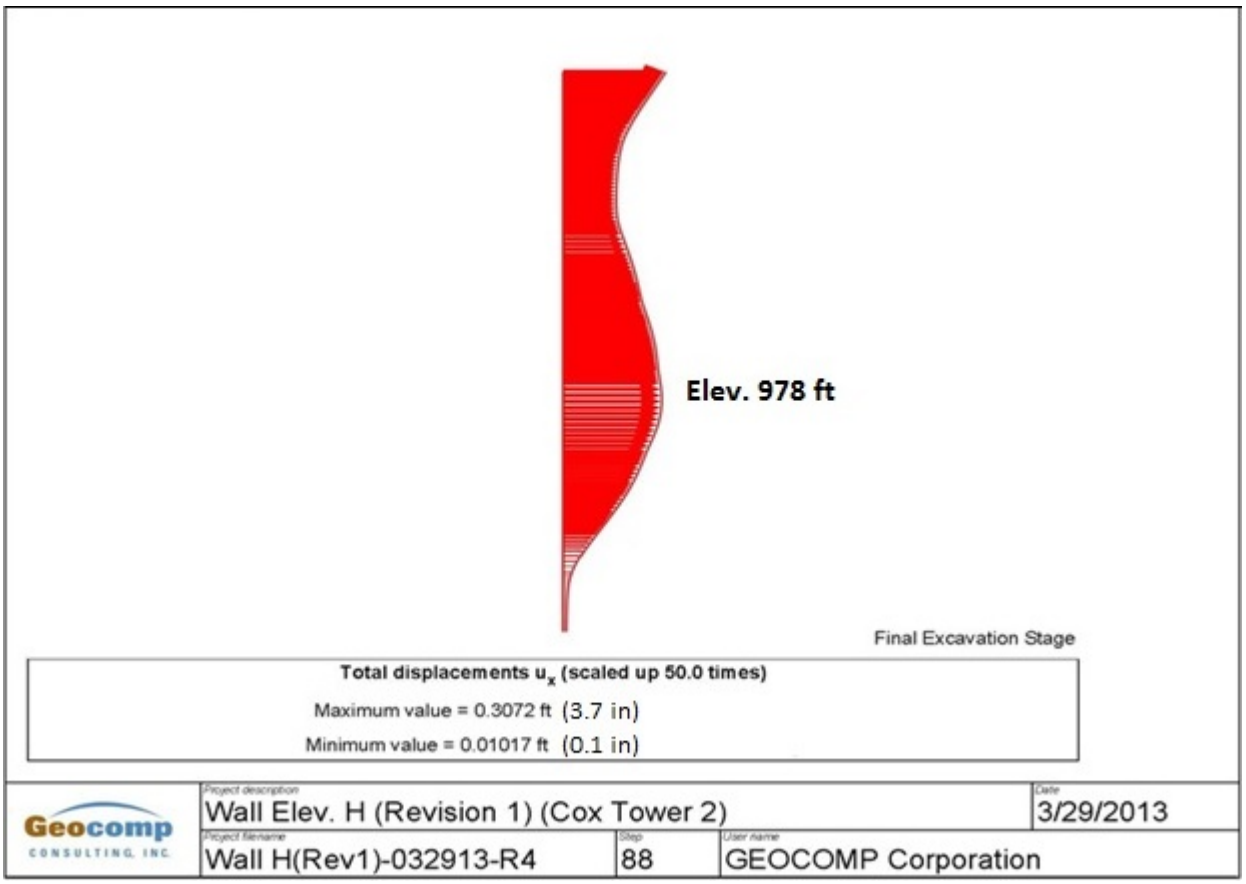


Fig. 7 – Predicted displacement at Wall H

An in-place-inclinometer was installed at Wall H in order to measure field performance of the wall during construction. The maximum displacement measured during construction was 3.6 inches. This demonstrates the high level of accuracy of instrumentation monitoring devices when construction goes as planned. Figure 8 below displays a graph of the measured displacement which shows a similar shape when compared to the predicted graph and also shows the maximum displacement at nearly the same elevation.

© 2016 Deep Foundations Institute

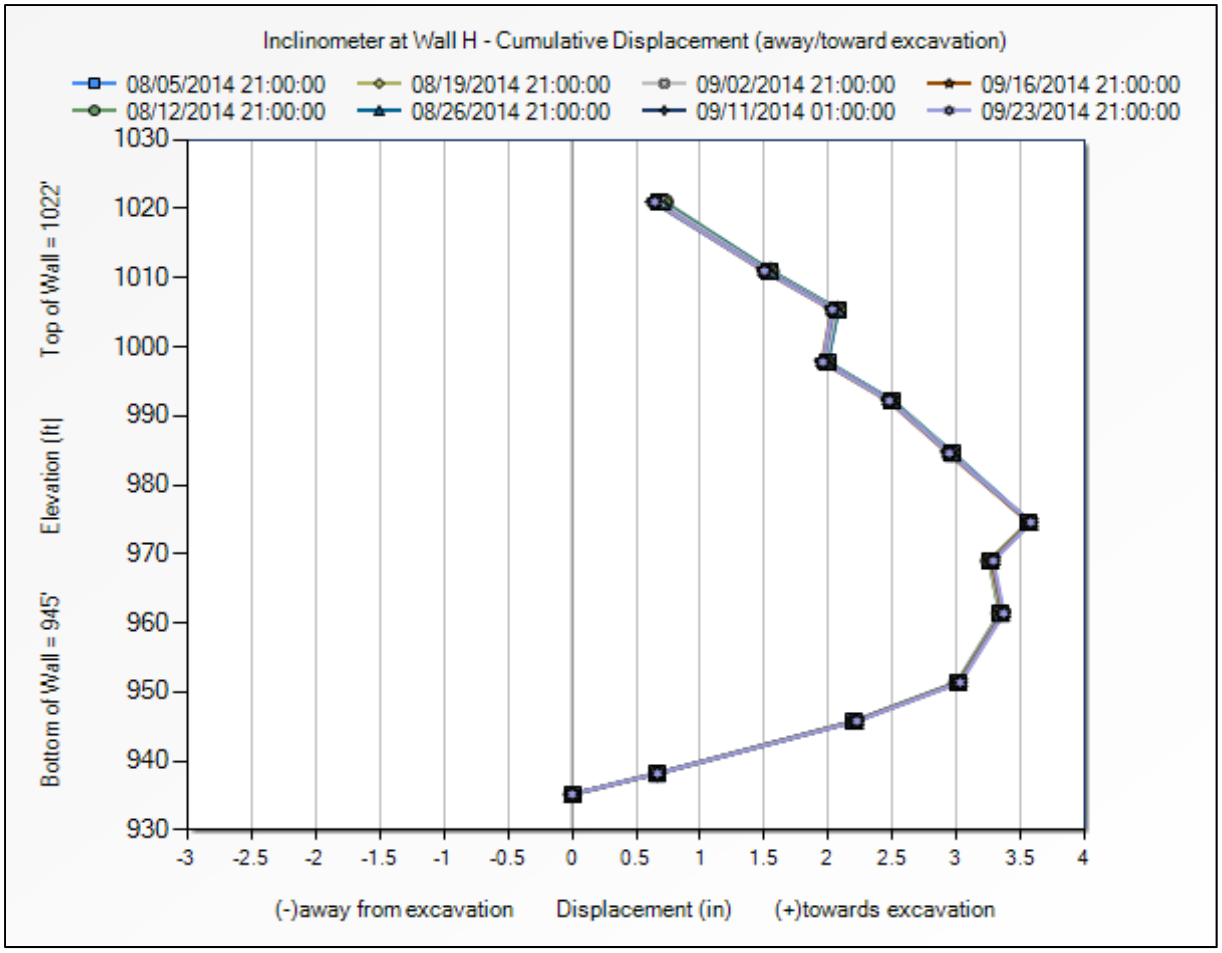


Fig. 8 – Measured displacement at Wall H

There was a location at the site where prisms on an existing building triggered an alarm indicating that the building was beginning to settle beyond the anticipated level. The building was located very close to the excavation, approximately 10 feet behind the shoring wall. One corner of the building at the existing loading dock was of particular concern where settlement was the greatest. A meeting at the site was scheduled immediately with the project team in order to perform a visual inspection of the existing building to determine if any damage occurred and to determine other factors causing the excess settlement. During the site visit, cracks were observed in the bottom floor and basement walls of the building. Manual crack gages were installed to monitor the larger cracks. It was also noted on site that there was a large unanticipated stockpile of soil placed inside of the loading dock area. The dimensions of the stockpile were approximately 50 feet long by 20 feet wide by 8 feet tall and the load was estimated to weigh approximately one million pounds.

© 2016 Deep Foundations Institute

After the site visit it was determined that cosmetic cracks of the building were not of major concern because the construction scope of work included future renovation the basement of the existing building. The major concern was ensuring that building was not settling to a point where a structural failure might occur. However, it was also determined that the soil stockpile staged in the loading dock area was an additional load on the building and adjacent shoring wall that was not part of the original design and construction plan. It was recommended that the additional soil load be removed immediately to prevent accelerating the settlement during further excavation activities adjacent to the building. The soil was removed and the prism on the corner of the building indicated a small heave afterward. Figure 9 shows a graph from the project website of the height displacement of the survey prism on the corner of the building next to the loading dock.

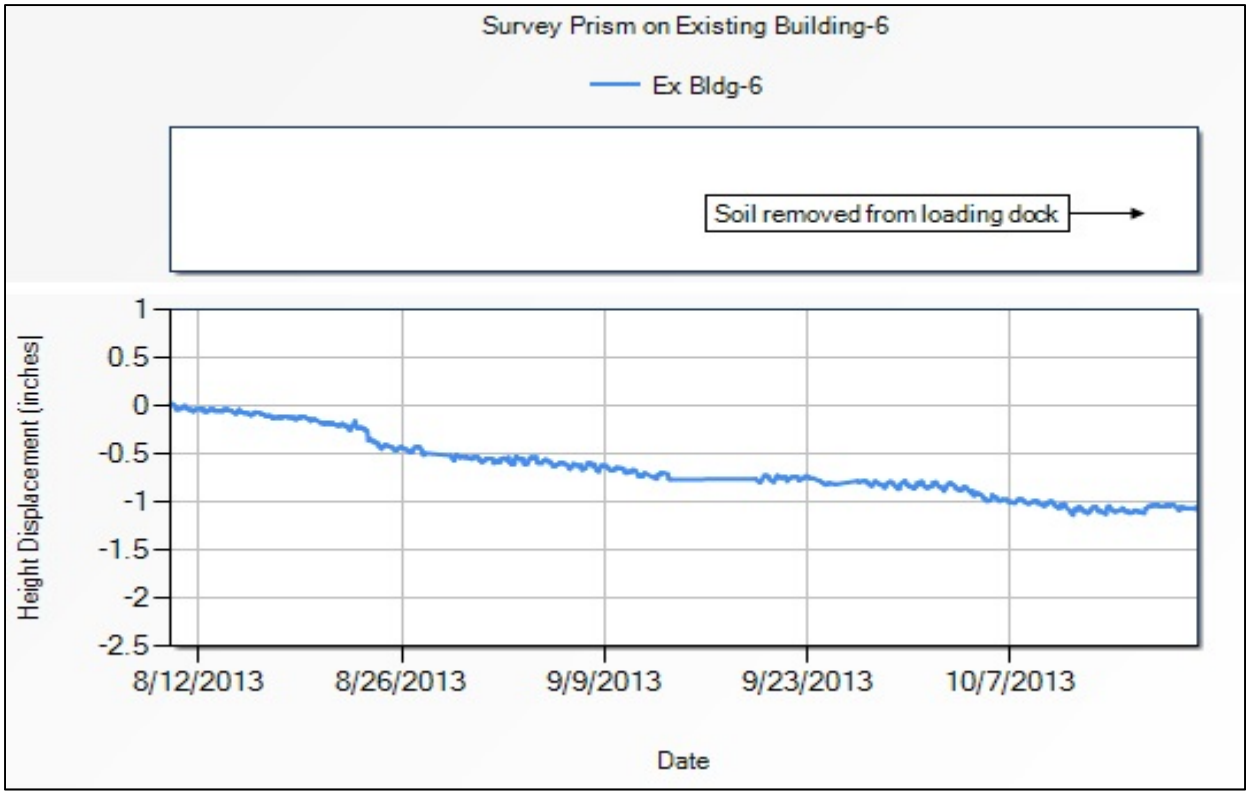


Fig. 9 – Prism data chart (Height Displacement)

The real-time monitoring and alarming system allowed the project team to closely monitor the existing building and monitor any additional movement. Monitoring continued after the excavation had reached the deepest point and during construction of the new parking deck in order to confirm that movement had stabilized.

© 2016 Deep Foundations Institute

SUMMARY AND CONCLUSIONS

Increasing population in large urban areas goes hand in hand with constructing new resources to support human growth. These construction projects often come with more risk associated with building next to existing structures and property, particularly when underground construction is required. The Cox Tower and Cox Tower II projects both demonstrated the importance of a real-time monitoring system to protect both people and existing infrastructure. Real-time alarms alerted the project team about unforeseen conditions with enough time to develop and implement remedial measures and prevent major problems from occurring. The real-time monitoring system allowed the project team to react quickly, which reduced delays and minimized additional costs to the project. Predictive modeling when combined with real-time monitoring was very effective in order to clearly define expected conditions or movements of structures in advance of construction.

ACKNOWLEDGMENTS

The author thanks ABE Enterprises, Inc. and Berkel & Company Contractors, Inc. for their contributions to this paper.

REFERENCES

SustainAtlanta, 2015. Atlanta Joins America's Largest Cities in Rapid Population Growth. https://sustainableatlantaga.com/2015/03/05.

© 2016 Deep Foundations Institute

This page left intentionally blank

© 2016 Deep Foundations Institute

"TREVI-CALATORE": INNOVATION IN CUT AND COVER AND TUNNELING FOR THE INSTALLATION OF PLUNGE COLUMNS AIMED TO EXCAVATE UNDERGROUND STRUCTURES THROUGH THE TOP-DOWN METHOD

Alessandro Bertero, Trevi S.p.A, Italy, ++390547319111, abertero@trevispa.com
Vincenzo Tirozzi, Trevi S.p.A, Italy, ++390547319111, vtirozzi@trevispa.com
Manuel Toniolo, Treviicos, MA, USA, 617-7889885, mtoniolo@treviicos.com

ABSTRACT

The installation of foundation elements (large-diameter Bored Piles or Diaphragm Walls) for the execution of underground works to be performed through the "Top Down" Technique (Stations, Car Parks, Subways, Artificial Tunnels) often requires the insertion, with pinpoint accuracy, of steel or prefabricated elements within the foundation system, to provide temporary and/or permanent support to the whole structure.
The future high-speed railway station of Florence Belfiore (Italy) is a perfect example; the new station will be built in the Northwest area of Florence, about two kilometers far from the existing station of Santa Maria Novella. The project envisages installation of about 500 bored piles (1200-1500-2100 mm diameter), with lengths ranging between 50 and 70 m. In the upper inner part of 250 piles, a steel pipe (weight: 15-20 tons, length: 22-25 mt.) has to be inserted with pinpoint accuracy.
The "TREVI-CALATORE" system allows to install the plunge columns and adjust their position and verticality.

Keywords: Top-down method, plunge columns, bored piles, verticality

INTRODUCTION

The execution of underground works via the "Top Down" technique, train or tube underground stations, parking shafts, tunnels, often implies the need to carefully insert steel or prefabricated structures, serving as provisional/definitive pillars, into the foundation elements.
The future high-speed railway station of Florence Belfiore is a perfect example; the new station will be built in the Northwest area of Florence, located about two kilometers far from the existing station of Santa Maria Novella.
The new Belfiore Station is part of the new European high-speed railway network. The works related to Florence urban penetration include (figure 1):

- a 6.5 km. twin tunnel excavated via TBM/EPB, that will run beneath Florence in a north-east direction, passing under more than 150 buildings, many of which can be considered historic buildings, with a soil coverage ranging from 6 m to 20 m;
- a North portal in Rifredi area, Firenze Castello Station;
- a South portal near Campo di Marte Station (which is also the launch shaft of the TBM)
- the new Underground Station in Belfiore area.

© 2016 Deep Foundations Institute

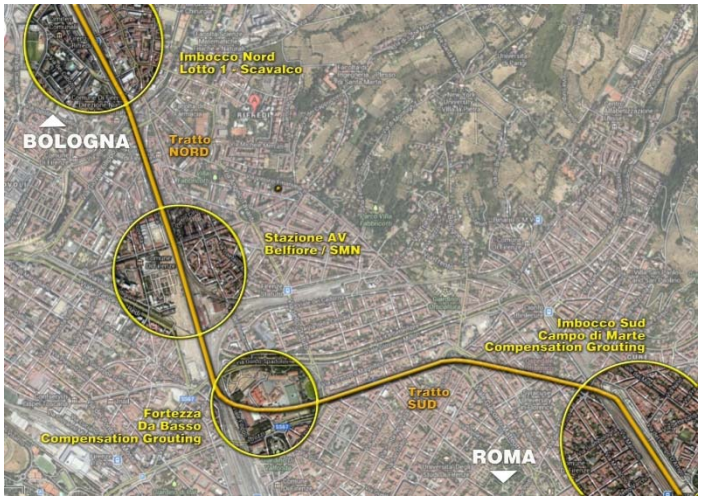


Figure 1. Map of the new high speed railway line, Florence, Italy

The construction project was awarded to Nodavia JV, while Trevi Group was involved in the special foundation activities which mainly included:

- Diaphragm walls;
- Bored and CFA (continuous flight auger) piles;
- Micropiles;
- Ground anchors;
- Soil improvement by means of soil mixing (Turbojet), jet-grouting and AGF (artificial ground freezing)
- Compensation grouting

THE NEW HIGH SPEED BELFIORE RAILWAY STATION

The architectural design of the new Belfiore station is by Norman Foster (figure 2), while the engineering design is by Arup. The project involves construction of a facility that will occupy an area of about 45,000 square meters with a vertical distribution up to 25 meters below street level. The supporting roof structure will be made entirely of glass, which lets the light get in at the trains' level; the underground levels will be accessible via elevators and escalators.

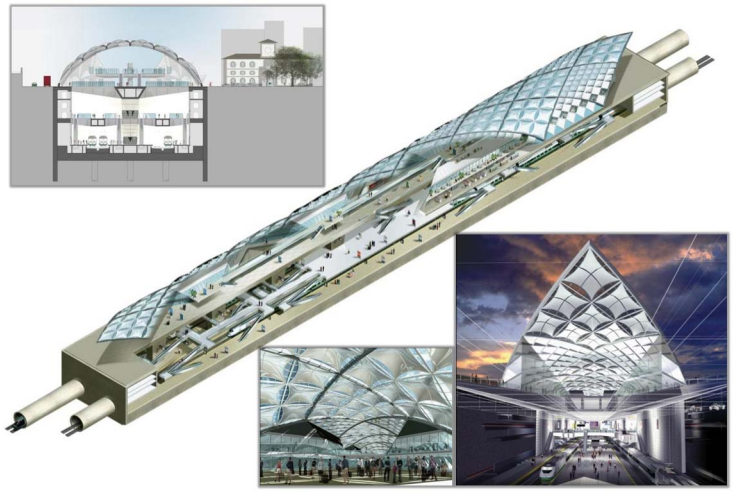


Figure 2. 3D view of the new Belfiore Station, Florence, Italy

© 2016 Deep Foundations Institute

Construction sequence and methods

The construction procedure involves the use of the top-down system, with the following phases:
Phase 1: preliminary mitigation works and realization of the external supporting structure by means of 41,000 square meters of 1.6 m thick, 40 m deep reinforced concrete diaphragm walls.
Phase 2: execution of 500 bored piles within the station footprint, with a diam. of 1200-1500-2100 mm and a depth ranging from 50 to 70 m. This foundation system will support the loads exerted by internal structures and by the roof structure (figure 3). Inside half of the piles, a heavy steel column (up to 20 tons each) will be installed in the blind part (about 20-25 meters), acting as a pillar to support the temporary struts during stage excavation. About 2.5 million kilograms of steel will be used to produce the plunge columns. In order to accomplish this task, a special device named "TREVICALATORE" was specially designed, developed and employed to insert - with high accuracy - the heavy steel columns inside the bored piles. This innovative system will be described in the following paragraphs.

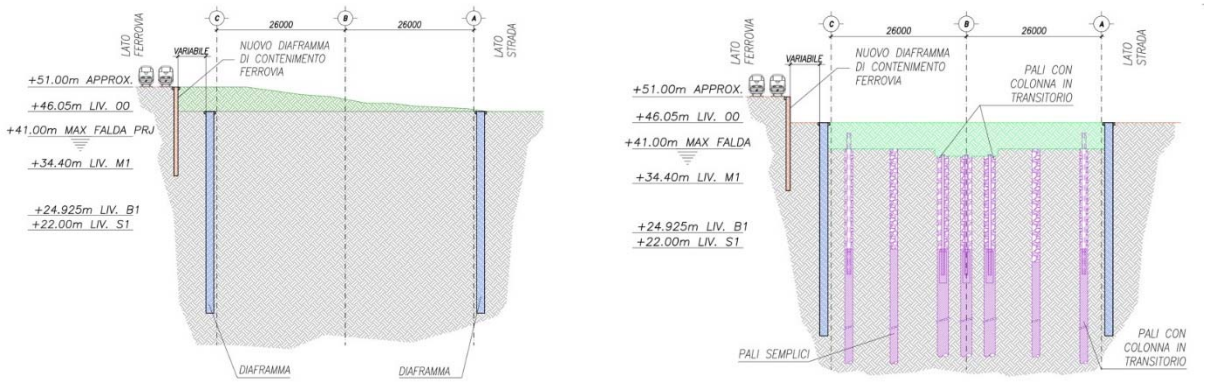


Figure 3. Phase 1 – mitigation works and DW execution; Phase 2 - Bored piles execution.

Phase 3: first stage of excavation, permanent and temporary struts installation, supported by the plunge columns, beams and slabs construction (figure 4). During this phase, the first TBM will run through the station, before excavation reaches the final level.
Phase 4: second stage of excavation up to the final level and temporary struts' installation supported by the plunge columns.

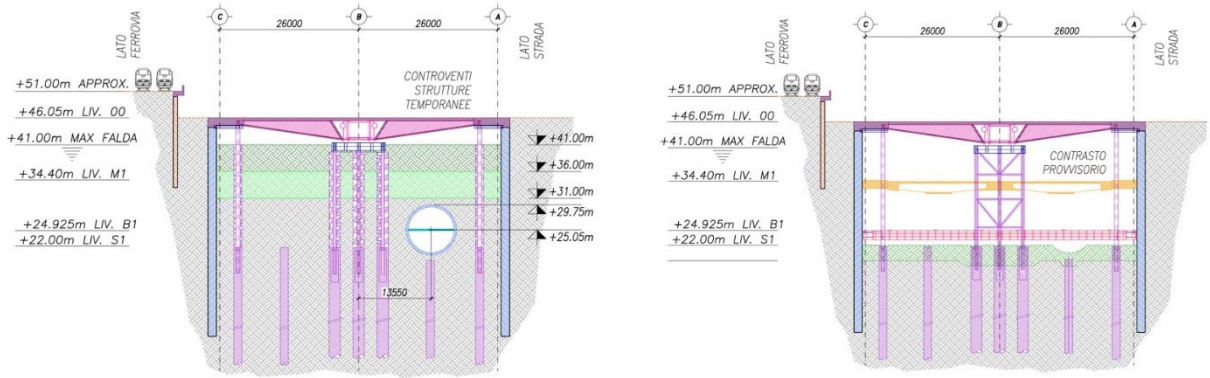


Figure 4. First stage of excavation, struts installation, beams and slabs realization; Second stage of excavation, temporary struts installation, beams and slabs realization.

© 2016 Deep Foundations Institute

Phase 5: execution of the bottom slab, temporary struts' removal and construction of a saddle to support the TBM movement inside the station (figure 6).
Phase 6: completion of the internal structures, finishing facilities and installation of the glass roof.

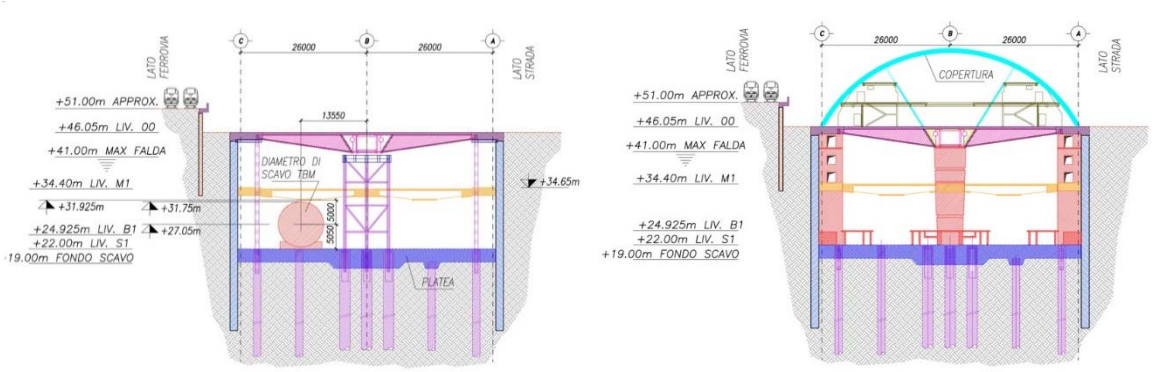


Figure 6. bottom slab realization, temporary struts removal and realization of the TBM saddle; internal structures completion, finishing facilities and the glass roof installation.

"TREVI-CALATORE"

Installing steel heavy columns within the foundation bored piles with pinpoint accuracy and keeping them in the right position (planimetric + vertical), implies the need to study and develop an innovative device named "TREVI-CALATORE".
The state of the art provides devices that utilize support and contrast guide systems placed inside the hole and/or require the use of heavy and bulky prefabricated concrete or steel platforms.
In order to vary the position and the inclination of the column pillar, these systems require the planimetric and vertical positioning of the entire structure which carries the pillar column, rigidly fixed to the structure itself. As a consequence, the positioning structure has to be very heavy and rigid, capable of moving pillar columns of considerable weight, i.e. over 20 tons .
The new system allows to install and adjust the pillars'position and their verticality; it consists of two lightweight frames (base frame and leveling frame), not bulky, that can be quickly installed just by means of a small service crane.
The main feature of the system is that the horizontal setup is initially performed by moving the upper leveling frame, while the base frame is positioned and fixed to the drilling casing. Once the leveling frame has been accurately positioned, the heavy steel column is lowered and suspended in the proper position, while tilt adjustments are performed. In this way, there is no need to move the heavy column, hence the base and leveling frames can be considerably lighter.

Advantages and innovation features

The "TREVI-CALATORE" has the following advantages and innovation features:

- The system uses a steel casing, previously inserted into the ground, as a support and contrast for the base frame;
- All the supporting and adjusting devices of the system are located out of the excavation, hence it is easy to access and control;
- The system consists of lightweight, flexible, easy-to-handle steel frames;
- The system allows to install and adjust the pillar column's position regardless of the steel cage previously laid inside the pile; in this way, the system allows to separate the verticality tolerances of the pillar elements (<0.4%) from those of the bored pile (generally < 1.5%);
- The system allows the use of pillar columns or elements with different shape or dimensions.

© 2016 Deep Foundations Institute

Working sequence

The working sequence involves the following steps:
Construction of a lean concrete slab for the planimetric centering of the drilling casing (figure 7).



Figure 7. Lean concrete slab for the planimetric centering of the drilling casing.

Installation of a steel casing (figure 8); the casing can be installed by means of either a vibrator or a rotary rig.

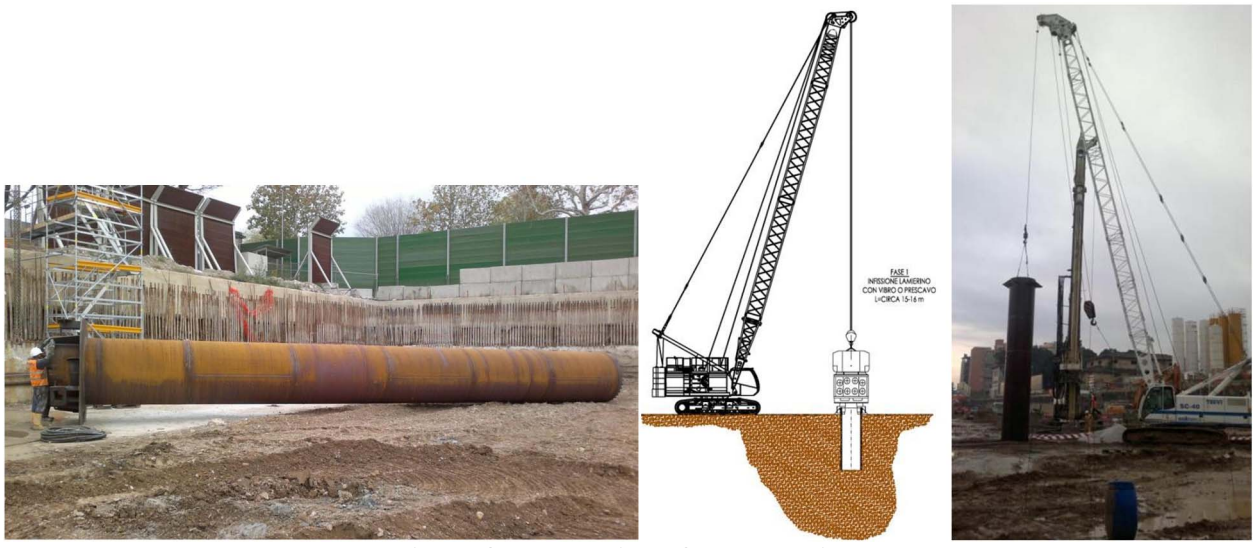


Figure 8. Installation of a steel casing.

© 2016 Deep Foundations Institute

Bored pile execution (figure 9).



Figure 9. Bored pile execution.

De-sanding and insertion of the steel reinforcement cage (figure 10).

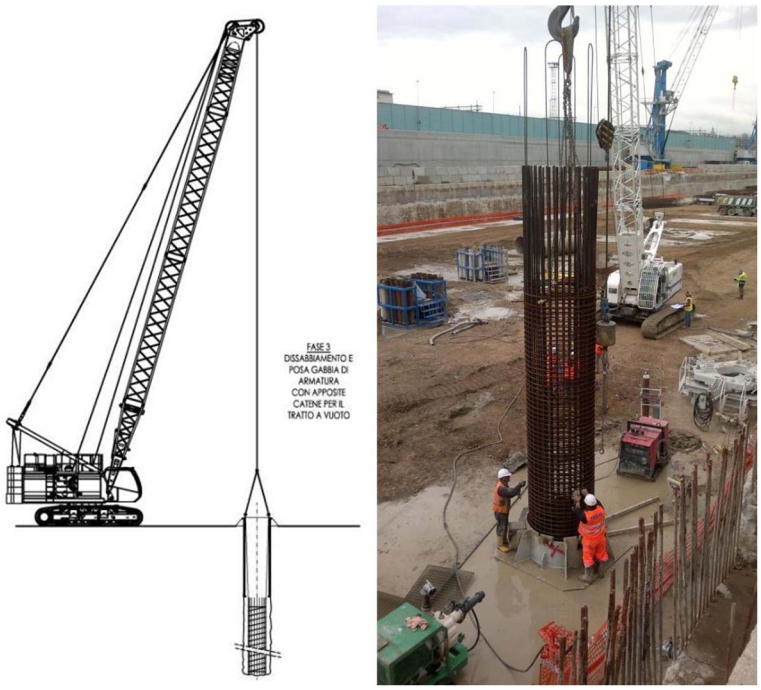


Figure 10. De-sanding and insertion of the steel reinforcement cage.

Positioning of the "TREVI-CALATORE"

- positioning of the support base frame, equipped with screw bars to adjust the plan position of the upper leveling frame; the three screw bars are arranged at 120 °; the support base frame is linked to the drilling casing by means of special “pockets” created in the casing head itself (figure 11).
- planimetric positioning of the upper leveling frame, which is kept suspended by means of a service crane, through a topographic control and by using the above-mentioned 3 adjusting screw bars of the base support frame;

© 2016 Deep Foundations Institute



Figure 11. Positioning of base support frame; positioning of leveling frame.

Positioning of the pillar column, pre- assembled on the ground and fitted with a positioning head rigidly connected to the pillar itself by means of a bolting system (figure 12). The positioning head will be disconnected and reused at the end of the cycle for another installation.



Figure 12. Positioning head with bolt connectors; Steel column pillar positioning

Positioning of the pillar column exactly at the center of the leveling frame, by means of rigid metallic centering devices (figure 13); the pillar column head's inclination can be subsequently adjusted by means of three screw jacks with spherical bearings having vertical contrast on the base support frame; an inclinometer provides real-time monitoring of the pillar column head's inclination.

© 2016 Deep Foundations Institute



Figure 13. Metallic centering devices; inclinometer fixed to the column head.

Positioning of a pouring platform, specially designed to be installed on top of the “TREVI-CALATORE”, with railings and stairs for an easy access and for running the pouring phases safely (figure 14). Concrete pouring is carried out by means of a concrete pump, using the contractor system with the tremie pipe within the pillar column; generally, the concrete cut-off is fixed with reasonable tolerance above the final pile’s cut-off level, leaving the blind boring stretch full of drilling mud.



Figure 14. Special platform for pouring operations.

Removal of the "TREVI-CALATORE" system soon after the required curing time, while the pillar column is kept centered and fixed to the steel drilling casing through a system of screws (figure 15); then, the blind boring stretch can be filled with lean concrete or coarse material (sand or gravel).

© 2016 Deep Foundations Institute



Figure 21. Screw system to keep the column head fixed during backfilling of the blind boring stretch.

Disconnection and removal of the pillar column's positioning head; the drilling steel casing can be extracted by means of a vibrator.
Backfilling of the inner area of the column with grout or concrete.

CONCLUSIONS

The "TREVI-CALATORE" system allowed to successfully complete the installation 0f 250 plunge columns within design tolerances and also according to the work schedule. This system can be employed in the future for similar top-down structures.

ACKNOWLEDGEMENTS

The Authors wish to express their appreciation to Mr. Danilo Fusaroli and Mr. Maurizio Anelli who worked hard in the jobsite to ensure the project's success; special thanks also to Mr. Terzo Turci, Mr Michele Allegra and Mr Davide Delmonte who contributed to the system's design.

© 2016 Deep Foundations Institute

This page left intentionally blank

© 2016 Deep Foundations Institute

A CASE STUDY, DESIGN CHANGE FROM SPREAD FOOTING TO DRILLED SHAFTS

Mohammad Ayub Iqbal, Ph.D, P.E., Applied Geoscience & Engineering, Inc., Reading, PA, USA, Phone: (610) 777-5027 x111, ayub_iqbal@appliedgeoscience.com
Drew M. Kurtz, P.E., Applied Geoscience & Engineering, Inc., Reading, PA, USA, Phone: (610) 777-5027 x118, dkurtz@appliedgeoscience.com
Sara F. Frailey, P.E., Gannett Fleming, Inc., Camp Hill, PA, USA, Phone: (717) 763-7212 x2543, sfrailey@gfnet.com
Jeff L. Rai, P.E., Pennsylvania Department of Transportation, Engineering District 5-0, Allentown, PA, USA, Phone: (610) 871-4523, jrai@pa.gov

ABSTRACT

This paper presents the foundation changes made for a five-span bridge over the Lehigh River constructed as a design-build project. During excavation within the cofferdam at Pier 2 for the construction of a spread footing to bear on rock, it proved extremely difficult to control the water entering the excavation as the sheet pile tips were variable due to the bedrock pinnacles and a weathered rock zone above the top of rock allowing water to pass below the sheeting. Water also entered from the bottom of the excavation, possibly due to the presence of solution openings within the dolomite bedrock. After repeated failures to achieve subgrade elevation and maintain a dry excavation, a design change to drilled shafts was made. Additional borings were performed for each of the shaft locations to explore the area underlain by karstic dolomite rock. A seal consisting of tremie concrete with adequate weight was placed to counter the differential head of water and the three drilled shafts (with minimum 25 feet [7.62 meter] rock sockets) were installed. A detailed construction sequence was followed and advanced quality control testing was performed. The construction of Pier 2 was completed successfully.

1. INTRODUCTION

This paper presents the description of the design change made from spread footing to drilled shafts as a result of site conditions encountered during the excavation for the spread footing for a bridge pier in the Lehigh River in Allentown, Pennsylvania. The bridge is located in an area underlain with dolomite rock, presenting karstic conditions including irregular top of rock and solution openings that provided high hydraulic conductivity below the top of rock. Also, the presence of a zone of weathered rock and pinnacle rock prevented the advancement of sheet piles when constructing the cofferdam. Thus, the difficulties of advancing the excavation to the desired spread footing level resulted in the design change to drilled shafts during construction. Since the project was Design-Build, the design could be changed by a collaborative process through the efforts of the Contractor, its geotechnical and structural engineers, and the State's (owner's) geotechnical and structural engineers and construction management staff.

1.1. Location of the Bridge

The location of the bridge (**Fig. 1**) is in the City of Allentown, Lehigh County, Pennsylvania, and it carries the American Parkway over the Lehigh River, the Norfolk Southern Railroad, and Dauphin Street (State Route 1007). The five (5) span continuous composite pre-stressed concrete bulb-tee beam bridge is 705 feet (214.88 meter) long between the centerlines of abutment bearings. The structure accommodates four 12-foot (3.66-meter) traffic lanes and one five-foot sidewalk.

© 2016 Deep Foundations Institute

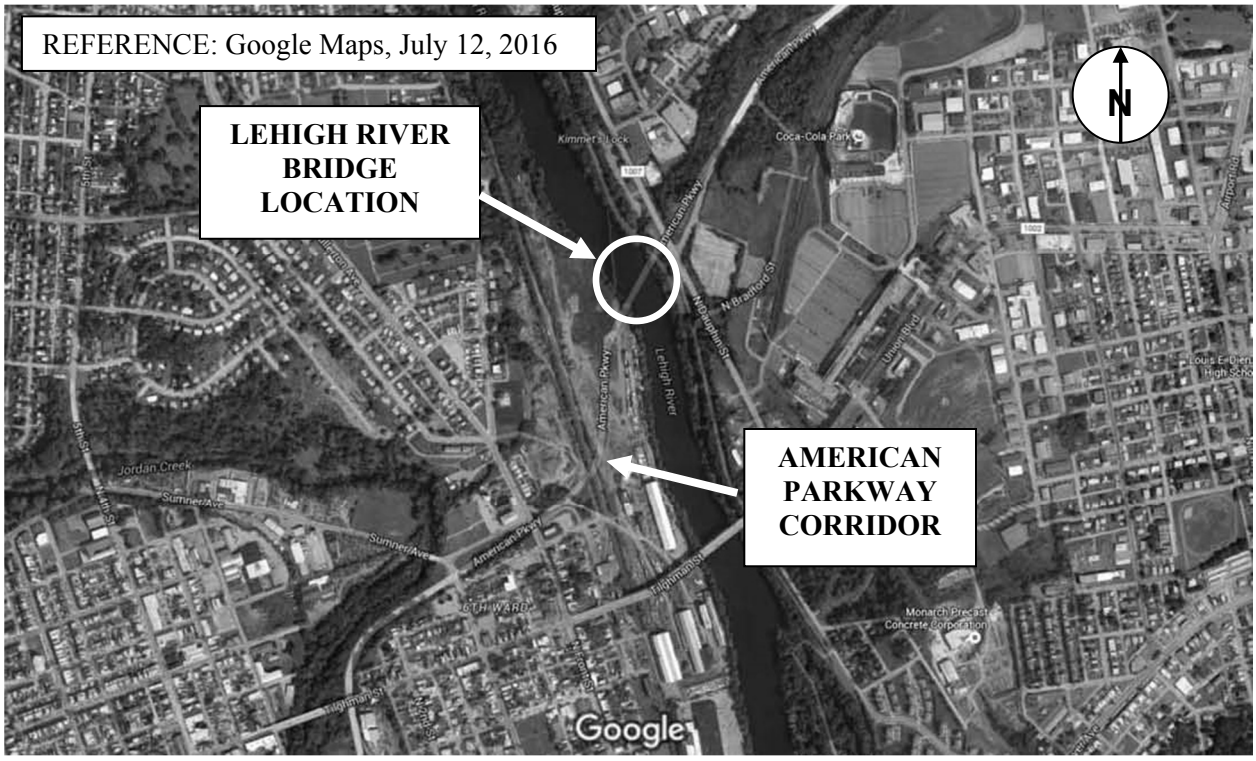


FIGURE 1: Site Location Map - City of Allentown, Lehigh County, Pennsylvania

1.2. Preliminary Design

A total of twenty (20) soil and rock borings were taken during the conceptual design of the five-span bridge, including four borings for the initial conceptual design and sixteen borings for the final conceptual design (four borings for each abutment, and two borings for each of the four piers. Soil profiles were prepared. Preliminary design included all of the subsurface information, along with the preliminary recommended foundation. Also, alternative foundations were discussed in the No As-Designed Foundation Design Guidance Report prepared by Applied Geoscience & Engineering, Inc. (2012).

1.3. Final Design

As this was a design-build project, the contractor's geotechnical engineer prepared the final foundation report. The final foundation report was based on the soil boring and profile information presented in the preliminary foundation report.

Because of the varied subsurface conditions characterized by underlying dolomite bedrock (Karst area) and the geometry of the bridge, the types of foundations used for abutments and piers varied. For both abutments and Pier 4, steel piles (HP 14x102) were designed. For Piers 1, 2, and 3, spread footings were designed. All piles were designed to be driven to Absolute Refusal requirements on dolomite bedrock. All spread footings were designed to be placed on competent dolomite bedrock below the 500-year flood scour elevation. The design team anticipated that tremie concrete might be needed to help dewater the excavations at Piers 1, 2, and 3 for the placement of spread footings.

© 2016 Deep Foundations Institute

Except for Piers 1 and 2, all of the other structure foundations were constructed as designed, including the spread footing foundation in the river at Pier 3, although there were challenges in dewatering the Pier 3 excavation.

2. CONSTUCTION OF PIER 2 AND DESIGN CHANGE

2.1. As-Designed Pier 2 Spread Footing Construction Effort

For the construction of the as-designed spread footing for Pier 2, the sheet piles for the cofferdam were intended to be driven into rock to provide a seal against the flow of water; however, the presence of a zone of weathered rock and pinnacles in the top of rock resulted in variable sheet pile tip elevations and prevented the sheet piles from gaining a good seal in the rock. In addition, solution channels and fractures within the rock permitted water to flow in through the base of the excavation. Water flowed into the cofferdam in greater quantities than could be effectively pumped out to maintain a dry excavation. As the depth of excavation increased, keeping up with the water inflow became more difficult, until it was determined that a safe excavation could not be maintained for the inspection of the rock at the footing subgrade and during the placement of the footing reinforcement.

The decision was made in the meetings participated by representatives from all design and construction personnel that a drilled shaft foundation redesign option be explored in order to circumvent the construction issues of the as-designed spread footing foundation.

The Contractor's geotechnical engineer recommended a drilled shaft foundation to reduce the required excavation depth and maintain a dry excavation. Because of the Karstic geology and anticipated depth of the shafts, additional borings were required to determine the rock condition at the location of the drilled shaft foundation.

2.2. Additional Soil and Rock Borings

A boring plan was developed for the drilled shaft redesign, which would supplement the information from the previous borings performed for the spread footing foundation. A total of seven (7) borings were proposed, each to extend 50 feet (15.24 meters) into the bedrock. This was intended to allow the borings to extend 20 feet (6.10 meters) beyond the bottom of the proposed 15-foot (minimum) (4.57-meter) rock socket, and provide some additional drilling in the top of rock in the event that voids, weathered rock, and/or soil seams were encountered. Borings for Pier 2 were performed in the dead of winter under unfavorable weather conditions on a barge within the cofferdam.

2.3. Design of Drilled Shafts (Reference 2)

A drilled shaft design was performed for both Pier 2 and Pier 1 in the Structure Foundation Geotechnical Report prepared by Gannett Fleming, Inc. (2014). This paper describes the design for Pier 2. The foundation configuration needed to accommodate the construction of a solid pier stem for a consistent appearance with the other substructures; a sunburst pattern aesthetic treatment was applied to all substructures. A grade beam at the top of the drilled shafts was used to provide a construction platform for the pier stem.

The design involved a coordinated approach between the structure and geotechnical designers. Loads at the top of the drilled shafts were determined by the structural designers using a Structural Analysis and Design (STAAD) analysis. The geotechnical designers evaluated the axial and lateral drilled shaft

© 2016 Deep Foundations Institute

capacities. Three drilled shafts were required at each pier. The salient features of the drilled shaft design are indicated below and in **TABLE 1**:

2.3.1. The drilled shafts were designed conservatively using only skin friction (tip resistance was neglected).

2.3.2. If a void or soil seam was encountered in the rock socket, the design geotechnical engineer was informed for further advice. However, all the shafts were advanced to a minimum of 25 feet (7.62 meters).

TABLE 1: SUMMARY OF REDESIGN DRILLED SHAFT DESIGN FEATURES

Approx. Streambed Elevation at Pier 2, ft (m)	239 (72.85)	
Approx. Normal River Water Elevation, ft (m)	248 (75.59)	
Bottom of Grade Beam Elevation, ft (m)	239.0 (72.85)	
Recovery Range (Avg), (%)	30-100 (93)	
RQD Range (Avg), (%)	0-75 (26)	
Top of Rock Elevation, ft (m)	Varies from 225 (68.58) to 228 (69.49)	
Drilled Shaft Rock Socket Diameter (min), ft (m)	5.0 (1.52)	
Drilled Shaft Rock Socket Length (min), ft (m)	25 (7.62)	
Bearing Stratum	Dolomite Bedrock	
Recommended Shaft Tip Elevation, ft (m)	200 (60.96)	
Axial Shaft Resistance, kips (kg)	Strength Limit	2,358 (1,069,571)
	Service Limit	1,759 (797,869)
Lateral Shaft Resistance, kips / kips-ft (kg / kg-m)	Strength Limit Shear/Moment	154 / 4,875 (69,853 / 673,993)
	Service Limit Shear/Moment	70 / 4,567 (31,751 / 631,410)
Expected Settlement, inch (mm)	< 0.5 (< 12.7)	

2.4. Construction of the Redesign Pier 2 Drilled Shaft Foundation

A detailed construction sequence was provided on the construction plans that reflected the collaboration between the designers and the contractors. Construction of the drilled shafts (**Fig. 2**) took place as listed below:

2.4.1. Inside of the cofferdam was excavated to approximate Elevation 225.00 feet (68.58 m).

2.4.2. A tremie concrete seal, approximately 14.0 feet (4.27 m) thick, was placed inside the cofferdam from Elevation 239.00 feet (72.85 m) to Elevation 225.00 feet (68.58 m) to resist uplift forces during dewatering operations.

2.4.3. A temporary 96-inch (2,438 mm) diameter casing was set at each drilled shaft location.

© 2016 Deep Foundations Institute

2.4.4. An aggregate fill was placed on top of the tremie concrete seal in the cofferdam to support the temporary casings that were used to construct the drilled shafts and provide a working area.

2.4.5. The temporary 96-inch (2,438 mm) diameter casing was filled with water. The water level was maintained at Elevation 252.00 (76.81 m) prior to drilling the shafts and until the drilled shaft concrete had set.

2.4.6. A 60-inch (1,524 cm) diameter rock socket was drilled through the tremie concrete seal and underlying rock to the bottom of the proposed rock sockets at Elevation 200.00 feet (60.96 m).

2.4.7. After the drilled rock socket was cleaned out, a mini-SID digital video camera was used to ensure 50 percent of the base of each rock socket had less than 0.5 inch (1.27 cm) of sediment and the maximum thickness of sediment/loose materials did not exceed 1 inch (2.54 cm).

2.4.8. Steel reinforcement, with six Crosshole Sonic Logging (CSL) tubes attached at 60° equal spacing in a circular manner, was placed inside the rock socket.

2.4.9. Using the tremie method, self-consolidating concrete (SCC) was placed in the drilled shaft underwater.

2.4.10. CSL testing was performed to determine if any anomalies were apparent in the drilled shaft concrete. After all CSL testing was completed, the CSL tubes were filled with 4,000 psi non-shrink grout.

2.4.11. The aggregate fill and 96-inch (2,438 mm) diameter casing was removed.

2.4.12. The cofferdam was dewatered to allow construction of the 5 feet (1.52 m) thick grade beam connecting the 3 drilled shafts on top of the tremie concrete seal.

2.5. Quality Assurance/Quality Control for drilled shaft construction

All three shafts were constructed successfully and met all quality control criteria.

2.5.1. Mini-SID Inspection (see 2.4.7 above).

2.5.2. Concrete was tested prior to placement as required by the approved special provisions.

2.5.2.1. Slump Flow Test (ASTM C 1611): 20" to 30" measured horizontally at the time of placement. No segregation of the mixture may occur. The Visual Stability Index (VSI) of the concrete, at the time of placement in the shaft, is to be 1.5 or less.

2.5.2.2. J-Ring Test (ASTM C 1621): Values to be within 2" of slump flow

2.5.2.3. Air Content (ASTM C 231): 2%, ± 1.5% (in field)

2.5.2.4. Temperature (ASTM C 1064)

2.5.2.5. Concrete Test Specimens (ASTM C 31): 4,500 psi compressive strength in 28 days

2.5.3. CSL testing (see 2.4.10 above).

© 2016 Deep Foundations Institute

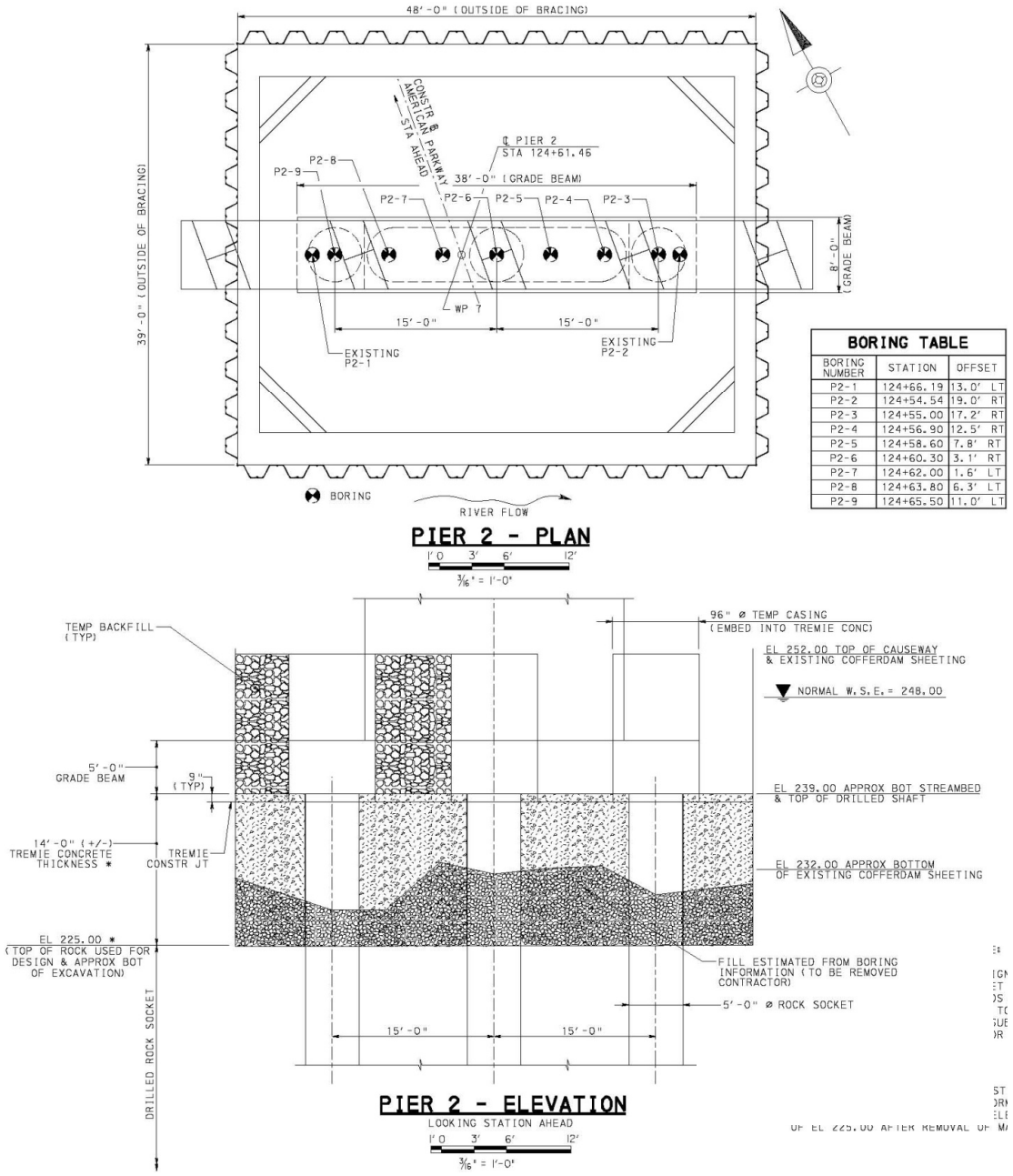


Figure 2: Drilled Shaft Foundation Redesign Plan and Elevation

2.5.3.1. C 231): 2%, ± 1.5% (in field)

2.5.3.2. Temperature (ASTM C 1064)

2.5.3.3. Concrete Test Specimens (ASTM C 31): 4,500 psi compressive strength in 28 days

2.5.4. CSL testing (see 2.4.10 above).

© 2016 Deep Foundations Institute

3. CONCLUSIONS / LESSONS LEARNED

3.1. With this project being a Design-Build project, the redesign of the foundation at Pier 2 was streamlined with representatives from the Contractor and the State (owner) working together. The designers were able to consider and take advantage of the Contractor's capabilities and the Owner's designers and construction management personnel were involved as the design evolved.

3.2. Even though spread footings appeared to be the cheapest and most feasible option during the design, the karstic nature of this site resulted in issues that impeded the construction of spread footing. The possibility of the various issues that may arise during construction should be discussed in design work when spread footings are recommended in a stream/river course underlain by karst features.

3.3. Specifications should include provisions that provide possible remediation in the event karst features are encountered during construction.

4. REFERENCES

1. Applied Geoscience & Engineering, Inc. (June 14, 2012). No As-Designed Foundation Design Guidance Report. S.R. 96216, Section PRK - American Parkway Lehigh River Bridge.

2. Gannett Fleming. (May, 2014). Structure Foundation Geotechnical Report. Pier 2 Foundation Redesign.

© 2016 Deep Foundations Institute

This page left intentionally blank

© 2016 Deep Foundations Institute

A COMPARATIVE STUDY ON BEHAVIOR OF BUCKET PILE IN SAND ACCORDING TO INSTALLATION METHODS

Juhyung Lee, Korea Institute of Civil Engineering and Building Technology, Gyeonggi-do, Korea, +82-10-2912-7736, leejh73@kict.re.kr
Jinung Do, North Carolina State University, NC, USA, jdo@ncsu.edu
Sung-Ryul Kim, Dong-A University, Pusan, Korea, sungryul@dau.ac.kr

ABSTRACT

Model tests have been performed to investigate the vertical, horizontal and cone tip resistances of bucket pile embedded in sand by different installation methods; suction force by pump and jacking force by actuator. Micro-cone penetrometer is used to evaluate the variation of the effective stress inside and outside of the pile after installation. As a result of vertical pull-out test, the jacked pile shows 3 times larger resistance than the suction-installed pile. For horizontal pull-out test, the ultimate horizontal capacity and the slope of load-displacement curve on the suction-installed pile decreases by 22% and 40%, respectively, compared to the jacked pile. In cone penetration test, inside cone tip resistance of the suction-installed pile is about 40% smaller than the jacked pile, which indicates that the effective stress is reduced due to upward seepage of bucket pile in sand by suction force. Therefore, installation methods can affect the behavior of the bucket pile significantly.

Keywords: bucket pile, jacking installation, suction installation, pull-out test, micro-cone penetrometer

INTRODUCTION

A suction force occurred when bucket pile penetrates into sandy soils induces seepage flow into the bucket pile so downward seepage near the outside of bucket pile causes to increases the effective stress, while upward seepage inside the bucket pile decreases the effective stress (Mahn, 2005; Fig. 1). The effect of induced seepage causes to reduce the penetration resistance during installation. On the other hand, reduced effective stress can decrease the horizontal and vertical capacities of bucket pile by significant disturbance at the tip of the bucket pile due to the flow net. Due to the complexity and difficulty considering the effects of suction installation, many previous researchers generally have neglected the effect of suction installation in their experiments. Therefore in this study, the effects of suction installation on resistance of bucket pile is examined.

TEST METHODS

The model pile is installed by suction force and jacking force, respectively. For the pile installed by jacking force (jacked pile), model pile is installed into the model ground by actuator. For the pile installed by suction force (suction-installed pile), model pile is installed by applying suction force using venturi pump. The size of model pile, penetrating depth and velocity are controlled equally for both tests. The model piles are fabricated by aluminum pipe with 1.2 mm thickness, 60 mm diameter and 180 mm length. The size of the soil chamber is 1 m width, 1 m length and 2 m height. *Joomoonjin* sand from the East Sea of Korea is used in this study (Table 1); where G_s is specific gravity, C_u and C_c are the uniformity coefficient and the coefficient of gradation, e_{min} and e_{max} are minimum and maximum void ratio, USCS and SP are Unified Soil Classification System and poorly graded sands, respectively.

© 2016 Deep Foundations Institute

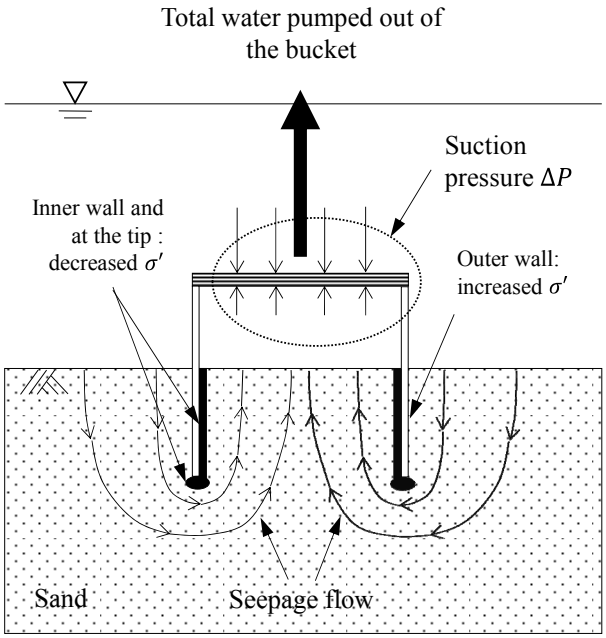


Fig. 1. Effect of seepage gradient on effective stress of soil (Mahn, 2005)

Table 1. Engineering properties of the test sands

G_s	C_u	C_c	e_{min}	e_{max}	USCS
2.62	1.43	0.9	0.93	0.62	SP

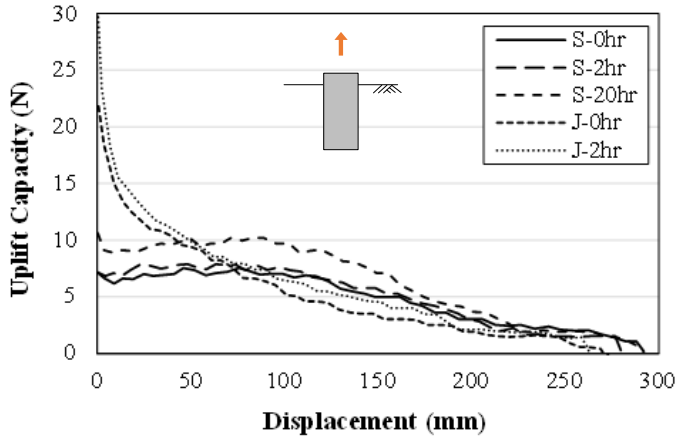
A miniature cone penetration test (micro-cone penetrometer) is conducted to evaluate the changed soil conditions inside and outside of the bucket pile. The cone penetrometer used in this study consists of 5 mm diameter at lower part and a 12 mm diameter at upper part with micro strain gauge.
Vertical pull-out test, the horizontal pull-out test and micro-cone penetration test inside and outside of the bucket pile are conducted to assess the effect of the installation methods.

TEST RESULTS

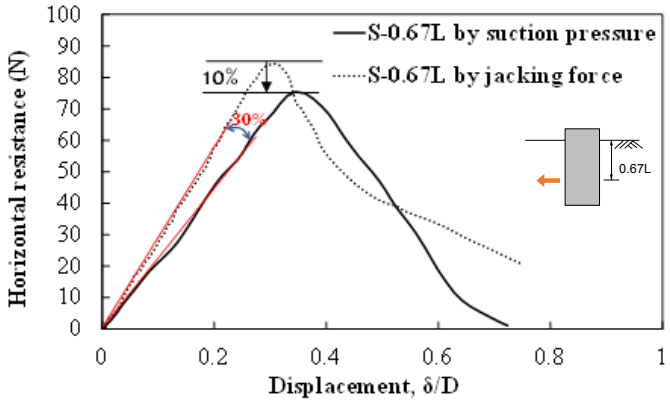
VERTICAL PULL-OUT TEST

The model ground is formed with a 30% relative density (D_r) to simulate a loose ground condition. After the model pile is installed by jack and suction, the vertical pull-out test is performed by using a hydraulic cylinder. A displacement rate is maintained as 100 mm/min (Bang, 2011; Coffman et al., 2004). To evaluate the set-up effect of the sand, vertical pull-out tests are performed in 0 hour, 2 hours and 20 hours after installation
Vertical pull-out test results are shown in Fig. 2a. In general, the uplift capacity of the jacked pile reaches the peak at the zero displacement and then decreases gradually. However, the uplift capacity of the suction-installed pile is maintained till 0.56L (*i.e.*, 100 mm of L 180 mm) which then decreases gradually. In addition, the results show that the jacked piles have initial uplift resistance (*i.e.*, capacity) three times greater than suction-installed piles. It indicates that the instant suction force causes the

© 2016 Deep Foundations Institute



(a)



(b)

Fig. 2. Results of pull-out tests; Vertical (a) and horizontal (b)

significant reduction of the uplift resistance of the bucket pile.

Besides, most of the results show similar uplift capacities after 75 mm displacement. On the contrast, suction-installed pile in 20 hours shows higher uplift resistance than other results which implies that although applied suction can cause the reducing resistance, the some portion of the resistance can be recovered by relaxation (*i.e.*, aging) because of a creep.

HORIZONTAL PULL-OUT TEST

The horizontal pull-out tests were conducted to evaluate the horizontal resistance of the bucket pile since bucket foundation is also widely used as an anchor. Fig. 2b shows experimental comparison of horizontally-loaded model bucket pile installed by suction force and by jacking force, respectively. The model ground is formed with D_r 70%. Loading location of model pile is 67% of the embedded pile length (*i.e.*, L) with no inclination. The horizontal load is applied using a wire.

In general, the behaviors of the bucket piles show a *short pile* which indicates rigid body motion (Broms, 1965). As shown in Fig. 3b, the ultimate horizontal capacity and gradient (*i.e.*, stiffness) of horizontal resistance-displacement curve of suction-installed pile indicate approximately 10% and 30% lower than jacked pile. It indicates that the effect of suction also affect horizontally, not only vertically. Thus, cone

© 2016 Deep Foundations Institute

penetration test is conducted to estimate the change of the effective stress outside of the bucket pile and inside of the bucket pile.

CONE PENETRATION TEST

Due to difficulties to measure engineering properties inside of the pile, a specially contrived micro-cone penetrometer is used to examine the small model bucket pile. As shown in Fig. 3a, cone tip resistance of jacked pile shows approximately 50% larger than suction-installed pile (*e.g.*, 5 MPa to 3 MPa). In addition, the cone tip resistance of jacked pile increase at the penetration depth 180 mm (expressed as 'D'), while those of suction-installed pile show the decrease or constant values.

To elaborate the resisting mechanism of cone penetration over depth, a detailed scheme is provided (Fig. 3b). Before the micro cone escapes from the tip of the pile, the cone tip resistance was increased (Fig. 6a-b 'A'; 0 - 150 mm). But near the tip of the pile, the cone tip suffers extremely high confining pressure due to the pile wall till penetration depth 150 mm (Fig. 6a-b 'B'; 150 mm). Sequentially, after escaping from the tip of the pile, the cone tip resistance rapidly decreases due to stress release from the high confining pressure (Fig. 6a-b 'C'; 150 - 180 mm). Lastly, after penetrating further, the cone tip resistance increases again due to the confining stress of original model ground (Fig. 6a-b 'D'; 180 mm -).

As aforementioned, the cone tip resistance on suction-installed pile shows almost same pattern with jacked installed pile (phase 'A' to 'C'), but the increase of cone tip resistance at phase 'D' remains unclear. Therefore, it is clear that the tip zone of the bucket pile is disturbed by suction force so that the cone tip resistance of suction-installed pile could be lower than those of undisturbed ground.

Fig. 4 represents the additional CPT results inside and the outside of the bucket piles to further verify the effect of the installation methods. The significant difference in CPT results inside and outside of the bucket pile results from the higher cone tip resistance due to the higher confinement inside of the pile wall.

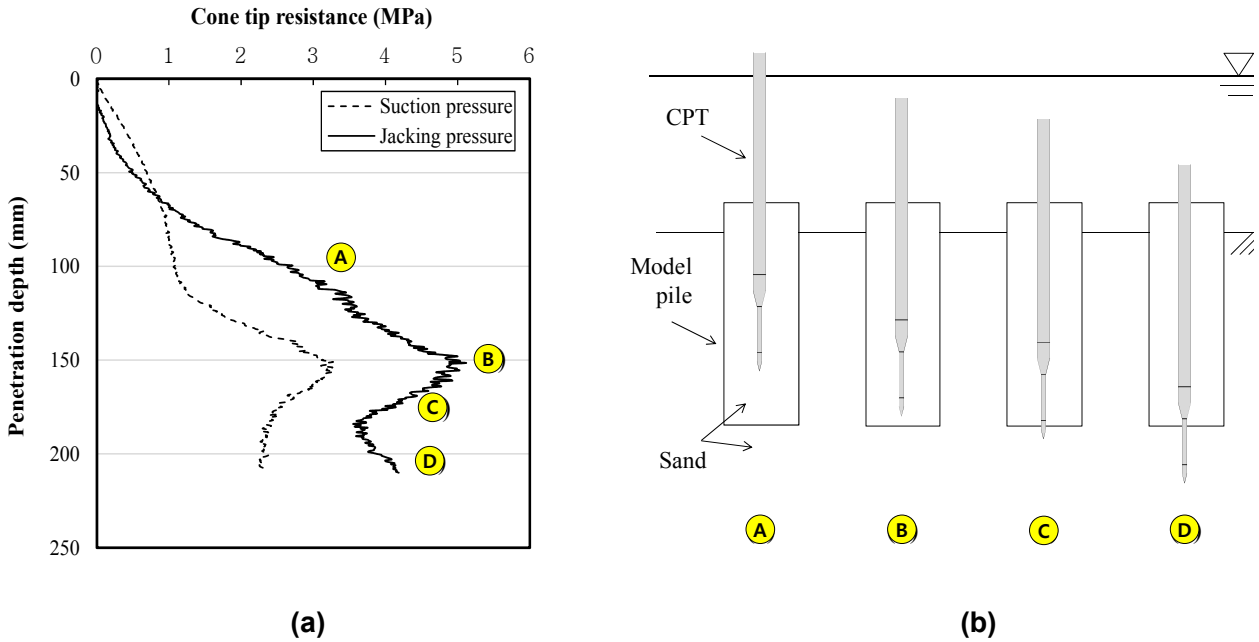


Fig. 3. Results of cone penetration tests; results (a) and resisting mechanism over depth (b)

© 2016 Deep Foundations Institute

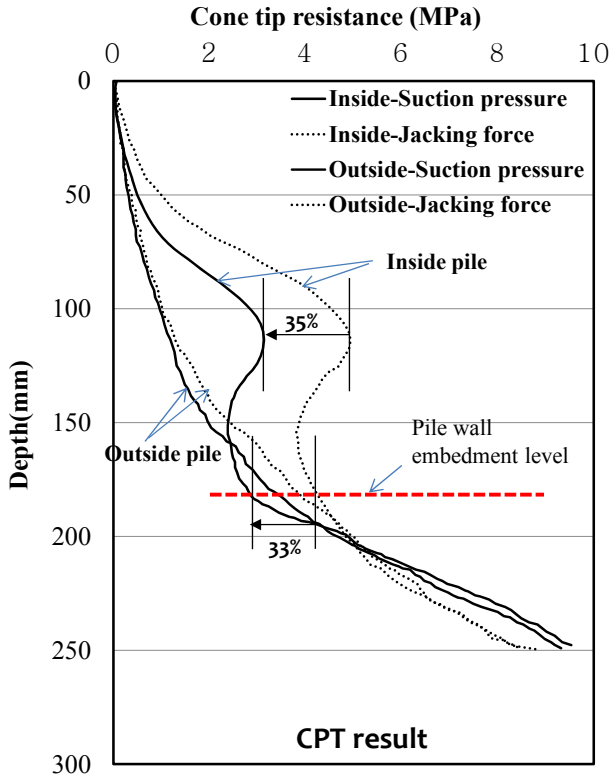


Fig. 4. CPT results inside and outside of the bucket pile by different installations

The effect of the suction installation of the cone tip resistance inside of the bucket pile is much greater than those outside of the pile. The outside of the bucket pile indicate that the cone resistances at depths of 100 mm and 200 mm for the jacked pile are 2% - 15% higher than those of the suction-installed pile. As mentioned by Mahn (2005), downward seepage from the outside of the bucket pile within dense sand (relative density approximately equal to 70%) may not increase the effective stress significantly. Contrarily, the cone resistance inside the suction-installed pile was 35% lower than that inside the jacked pile. Lower cone resistance inside the suction-installed pile may result from the decreased effective stress induced by the upward seepage (Mahn, 2005).

Cone resistance of the suction-installed pile tip is approximately 33% less than that the jacked pile tip. It ‘s estimated that the lower cone resistance of suction-installed pile compared to jacked pile at any depth contributes to the lower horizontal capacity (about 10% difference as shown in Fig. 2b) of the bucket pile. However, more precise and extensive future research is required to identify the lower horizontal capacity for suction-installed pile.

CONCLUSION

In this study, effect of installation methods on bucket pile is analyzed experimentally. As a result, the resistances on bucket pile installed by suction force and jacking force show the difference substantially from vertical and horizontal pull-out test. Moreover, the cone tip resistance also supports the differences of the jacked pile and suction-installed pile. This can be caused by seepage flow from the outside to the inside of the pile, thus the effective stress decreases. In addition, the difference in the resistances may be attributable to compounding effect of the reduced density and the effective stress of the sand. Thus,

© 2016 Deep Foundations Institute

it’s obvious that the installation methods affect the bucket pile capacity substantially. To further verify the effect of the installation methods, more diverse conditions, such as relative density, loading location and cone penetrating location should be tested.
In summary, to evaluate the in situ behavior of bucket pile in sand, suction effect on vertical and horizontal behavior of bucket pile plays an important role. Therefore, the effect of the suction should be considered importantly in designing the bucket pile.

ACKNOWLDEGEMENTS

The research presented in this paper was conducted by the fund from the project entitled "Horizontal Drilling and Stabilization Technologies for Urban Search and Rescue (US&R) Operations" at Korea Institute of Civil Engineering and Building Technology. The authors acknowledge the financial support from the institution.

REFERENCES

Bang, S., Jones, K.D., and Kim, K.O., 2011. Inclined loading capacity of bucket piles in sand. Ocean Engineering, 38(1) 915-924.

Broms, B.B., 1965. Design of laterally loaded piles. Journal of the soil mechanics and foundations division, ASCE, 91(SM3) 79-99.

Coffman, R.A., and Fugro-McClelland Marine Geosciences, Inc.; El-Sherbiny, R.M., Rauch, A.F., Olson, R.E., 2004. Measured Horizontal Capacity of Suction Caissons. Offshore Technology Conference, Houston, Texas, U.S.A., OTC 16161.

Manh, N.T., 2005. Installation of Suction Caisson in Dense Sand and the Influence of Silt and Cemented Layers. Ph.D. Thesis, The University of Sydney. Australia.

© 2016 Deep Foundations Institute

A DECADE OF EXPERIENCE WITH DRILLED FOUNDATIONS IN HONOLULU

James W. Niehoff, MSCE, PE, GEI Consultants, Inc., Denver, Colorado, USA, (303) 704-8390, jniehoff@geiconsultants.com

ABSTRACT

Prior to 2003, most high rise structures in Honolulu, Hawaii were supported on driven pile foundations, extending through shallow coral strata and bearing in competent formations at depths of 100 ft (30 m) or greater. In 2003, the 40-story Hokua Tower became the first building in Hawaii to use continuous flight auger (CFA) piles for support. These piles derived most of their capacity from side shear in the shallow coral formations, which reduced their required lengths to less than 100 ft (30 m) sand significantly increased their capacity. Not only did CFA piles prove to be more efficient and cost-effective than driven piles, but the reduced noise and vibration associated with their installation made them and drilled piers the foundations of choice for most mid- to high-rise projects going forward. Because drilled foundations were new to Hawaii, it was necessary to develop effective design parameters for the unique soil and rock conditions found within this urban area. While drilled foundations were found to have many advantages over driven piles, construction techniques had to be modified to compensate for extensive voids in the coral formations. This paper presents a compendium of the data derived from numerous full scale, instrumented load tests conducted during the past decade and provides guidance for the design and installation of CFA and drilled pier foundation systems in areas having geologic settings and history similar to that of Honolulu.

Keywords: drilled, piles, piers, foundations, Hawaii

INTRODUCTION

The State of Hawaii is one of the most remote areas in the world, lying nearly 2400 miles (3800 km) from the nearest continental land mass. In spite of this vast distance, the population of the islands has grown to over 1 million people, the majority of whom live within and in close proximity to the City of Honolulu on the Island of Oahu. The city is densely populated with over 400 high rise apartments, condominiums, hotels and office buildings located within 5 miles (8 km) of the city center (Fig.1). Nearly all of these buildings have been constructed within the past 50 years.



Fig 1. Waikiki area of Honolulu

© 2016 Deep Foundations Institute

GEOLOGIC SETTING

Hawaii consists of a chain of islands situated in the central part of the Pacific Ocean. They were, and continue to be formed by volcanic activity associated with a "hot spot" located within the central portion of the Pacific Crustal Plate. This plate moves westward relative to the hot spot and has created a long series of islands extending over 1600 miles (2600 km) from the west to the east. The Island of Oahu is located within the eastern portion of the chain to the east of the island of Kauai and to the west of Molokai. Oahu was formed by two major volcanoes. The Waianae Volcano, which formed the western part of the island, broke the surface of the Pacific Ocean first, about 10 million years ago, follow by the Koolau Volcano to the east about 9 million years ago. These two extinct volcanoes formed two elongated mountain ranges, separated by a southeast to northwestern trending central valley.

As a result of sea level changes over time, a series of coral reefs formed at elevations both above and below the current level of the Pacific Ocean around the periphery of the island. During periods of low sea level elevations, these coral reefs were periodically exposed and were eroded in some locations as a result of stream flows. In these areas, clayey and silty alluvial soils, eroded from residual soils at higher elevations were deposited. These alluvial materials were typically interbedded with cobbles, gravel, and volcanic cinders. Many of the deeper, older, alluvial materials present in these incised channels experienced drying and became desiccated during periods when sea levels dropped. These older alluvial soils are typically dense and overconsolidated.

In most near-coastal locations on the Island of Oahu, the coral formations and older alluvial soils have been blanketed with soft, loose lagoonal deposits, consisting of coral gravel and silty and clayey sand materials. These soils are typically 10 to 30 ft (3 to 9 m) in thickness in the metropolitan Honolulu area.

EARLY DEVELOPMENT

What is now the City of Honolulu was originally settled by Polynesians as early as the 11th Century. However, significant permanent development did not occur in the area until the mid-1800's when Honolulu was established as the capital of the Kingdom of Hawaii by King Kamehameha III. Over time, the city expanded to the west, north and east from the original settlement, as agricultural lands were converted to residential properties. The Waikiki area, located about 2 miles (3 km) to the east of the original city center, originally consisted of a sand bar, separated from the rest of the island by a swamp. This area was drained and filled in the late 1920s, opening the area to the construction of the first tourist hotels.

Most development in Hawaii consisted of low to mid-rise buildings through the first half of the 20th Century. However, following the end of the Second World War and the establishment of statehood in 1959, the City of Honolulu experienced an explosion in high rise construction that continues to the current day.

DRIVEN PILE FOUNDATIONS

The presence of weak lagoonal deposits in much of the greater Honolulu area generally precluded the use of shallow foundations for support of high rise construction, except near the city center, where coral bedrock is relatively shallow (Fig. 2). To provide adequate support in other near-shoreline areas, driven precast concrete pile foundations were used almost exclusively for support of mid to high rise buildings. The shallow coral formations were difficult to penetrate with the concrete piles and loose materials above the coral did not provide adequate lateral resistance. To overcome these issues, contractors employed predrilling to penetrate the upper coral formations prior to pile driving. Piles were driven through the upper coral and into lower coral reef formations to derive adequate support. To achieve capacities of 100 tons (900 kN) or greater piles were typically driven to depths in excess of 100 ft (30 m).

© 2016 Deep Foundations Institute



Fig 2. Shallow coral in the downtown Honolulu area

While driven pile foundations were found to be relatively inexpensive on a per foot basis, predrilling through the upper coral formations required piles to be driven to significant depths and were thus relatively inefficient from a geotechnical support standpoint. Further, driving piles generated significant noise and vibrations in the densely populated urban setting.

While drilled foundation systems had been used on some larger transportation projects in Hawaii prior to the year 2000, few had been used on significant commercial developments due to the shortage of local equipment and contractors as well as a general lack of experience with such foundations within the geotechnical community.

DRILLED FOUNDATION DESIGN

Drilled piers and continuous flight auger (CFA) piles derive support from side shear generated between the foundation concrete/grout and the surrounding soil and rock, as well as by end bearing. For piles and piers extending through soils, side shear can be estimated by the following relationships:

For cohesive soils: $f_s = \alpha S_u$ [1]

For granular soils: $f_s = K \sigma_v' \tan \phi$ [2]

Where:

f_s = ultimate side shear in ksf
α = a factor ranging from 0.55 for softer soils to 0.45 for stiffer materials
S_u = shear strength of cohesive materials
K = lateral pressure coefficient

© 2016 Deep Foundations Institute

σ_v' = effective overburden pressure
ϕ = angle of internal friction

For rock socketed piles and piers, side shear capacity can be estimated by the general formula:

$$F_{max} = \mu\, q_{ui}^{0.5} \qquad [3]$$

Where:

μ = a factor relating to the roughness of the pier sidewall
q_{ui} = the unconfined compressive strength of the rock in ksf

The μ factor has been found to vary from less than 1 for smooth wall drilled foundations to almost 3 for very rough side walls. The coralline limestone common to Hawaii excavates to a very rough surface and contains small vugs as well as small to moderate cavities. In the State of Florida, which is underlain by coralline limestone similar in character to that found in coastal areas of Hawaii, the μ factor has been correlated to the rock core recovery as well as the split tensile strength of the bedrock in the following manner:

$$\mu = \tfrac{1}{2} * CR * q_t^{\,0.5} \qquad [4]$$

Where:

CR = rock core recovery expressed as a fraction
q_t = split tensile strength of rock in ksf

The relationship between the compressive strength and spilt tensile strength varies significantly. However, the follow graph presents a generalized trend of these two parameters for weak to moderately strong coralline limestone.

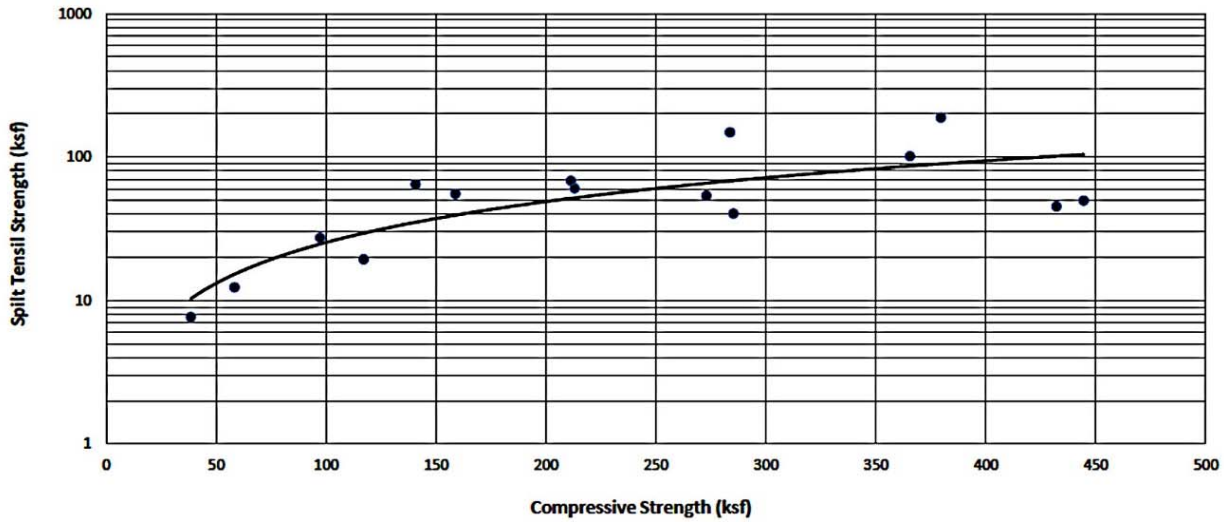


Fig 3. Typical relationship between compressive strength and spilt tensile strength of coralline limestone

For hard, intact coral, with a compressive strength of 150 ksf (7200 kPa) and a rock core recovery of 80%, the resulting μ factor would be approximately 2.5. This yields an estimated ultimate side shear value of

© 2016 Deep Foundations Institute

about 30 ksf (1400 kPa). For a more typical, weaker coral having a compressive strength of 75 ksf (3600 kPa) and a core recovery of 70%, the μ factor drops to 1.5. The resulting estimated ultimate side shear value would be about 13 ksf (600 kPa).

In general, only movements on the order of 1/10 to 1/4 in (0.25 to 0.6 cm) are required to generate the majority of side shear in drilled foundations. Conversely, drilled piles and piers typically must deflect downward more than 1/2 in (1.3 cm) to yield substantial end bearing. Deep foundations installed within the Hawaiian coastal plains generally extend below the groundwater table, making it difficult to clean or inspect the bearing materials. Consequently, the design of drilled pier and pile foundations generally neglect the contribution of end bearing to the overall compressive capacity in Hawaii.

HOKUA TOWER

In 2003, a new high-rise condominium was planned for the Kakaako area of Honolulu, a short distance to the west of Waikiki. The Hokua Tower was to be a 40-story residential building with a detached 4-story parking deck. The subsurface conditions within this site were found to consist of surficial fill, followed by soft lagoonal deposits extending to depths of about 15 to 30 ft (4.5 to 9 m). These deposits are underlain by a coralline limestone stratum varying from about 25 to 50 ft (7.5 to 9 m) in thickness. This upper coral stratum is underlain by medium dense sand and coral materials to a depth of about 80 ft (24 m), then by another stratum of coral (Fig.4).

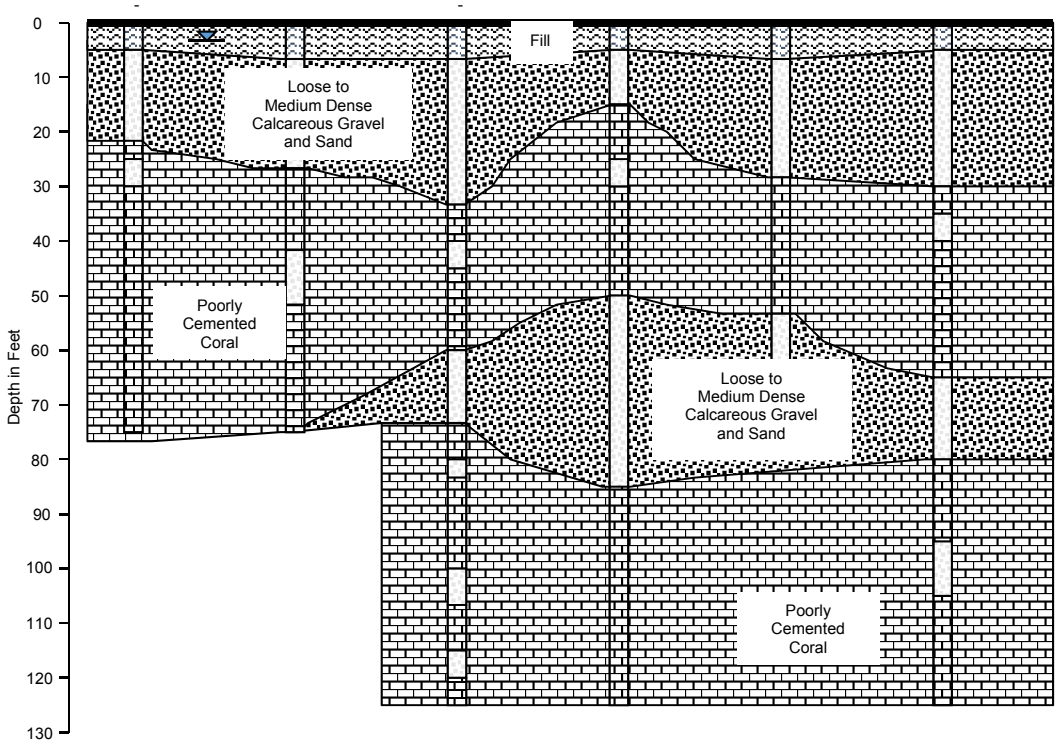


Fig 4. Subsurface profile at the Hokua Tower

The upper soils were too soft and compressible to support either of the structures on shallow foundations. However, we considered the moderately hard coralline limestone strata present at shallow to moderate depths suitable for the use of continuous flight auger (CFA) piles. For the tower structure, calculations suggested that 18-in (46-cm) diameter piles could be designed to support allowable axial compressive loads of 200 tons (1800 kN) each. While the full capacity could be generated in the upper coral formation, there

© 2016 Deep Foundations Institute

was concern that the zone of medium dense soils between the upper and lower coral formations would compress excessively under the cumulative load of the structure bearing within the upper coral stratum. Consequently, the piles were designed to extend through the intermediate soil layer and at least 10 ft (3 m) into the lower coral formation. For the low-rise parking structure, the magnitude of deflection of the upper coral was considered tolerable. The piles for this structure were designed to extend to a total depth of about 60 ft (18 m) and support compressive loads of 150 tons (1350 kN) each. The CFA piles were considered to be substantially more cost effective than driven piles as they would be significantly shorter and support a much higher load per pile.

As this was the first CFA pile project to be constructed in Honolulu, the city permitting department expressed concerns as to the ability of this foundation system to support the design loads. As no local contractors had the equipment to install CFA piles at the time, an experienced contractor was mobilized from the mainland to install test piles at the site, and later to install production piles. Neither the 60 ft (18 m) nor 90 ft (27 m) long test piles experienced failure when loaded to twice their design capacities (Fig 5).

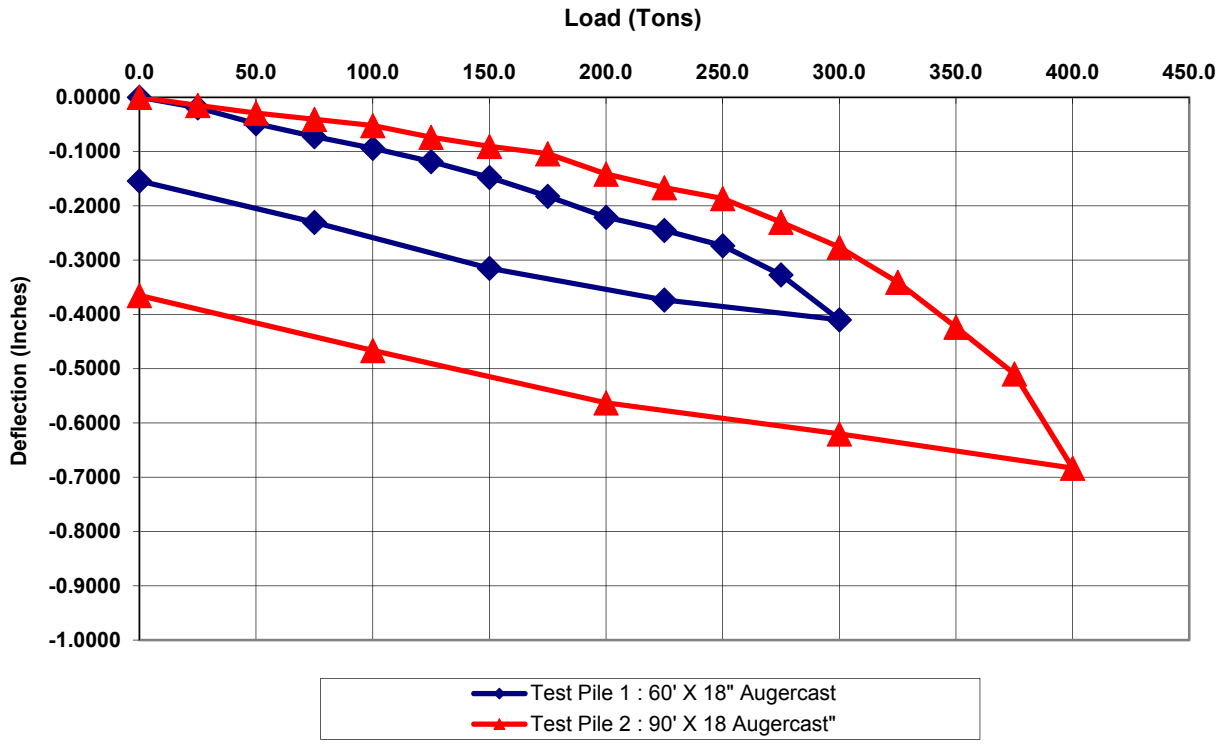


Fig 5. Load – deflection curves for test piles at the Hokua Tower project

No adverse issues occurred during the foundation installation process, and neighboring developments appreciated the low levels of noise and vibration. Overall, it was estimated that the use of CFA piles resulted in a cost savings of nearly 30 percent over the cost of a conventional driven pile system. The Hokua Tower was successfully completed in 2006.

DRILLED FOUNDATION SIDE SHEAR PARAMETERS

Following the successful completion of the Hokua Tower, CFA piles gained local acceptance and were used to support the majority of the high rise structures constructed during the following 5 years. Subsequently, drilled shaft foundations also began to find widespread use. Drilled shafts having diameters

© 2016 Deep Foundations Institute

ranging from 36 to 60 in (90 to 150 cm) penetrating coral strata, and stiff alluvial soils were found to be capable of supporting loads of up to 5000 kips (22,000 kN) each.

For most of the major drilled foundation projects constructed in Honolulu, load tests are employed to assess side shear resistance. For this purpose, Osterberg Cells (O-Cells) are typically embedded within test foundations to confirm or modify design side shear parameters. In this type of test, an instrumented hydraulic jack is attached to the central portion of a test frame or reinforcing cage. The jack exerts an upward load on the upper portion of the pile or pier and an equal downward force on the lower part of the foundation. In so doing, the test applies a force equivalent to twice the jack load to the pier as a whole. Strain gauges and tell-tales attached to the reinforcing cage assist in the assessment of load transfer along the length of the foundation (Fig. 6).

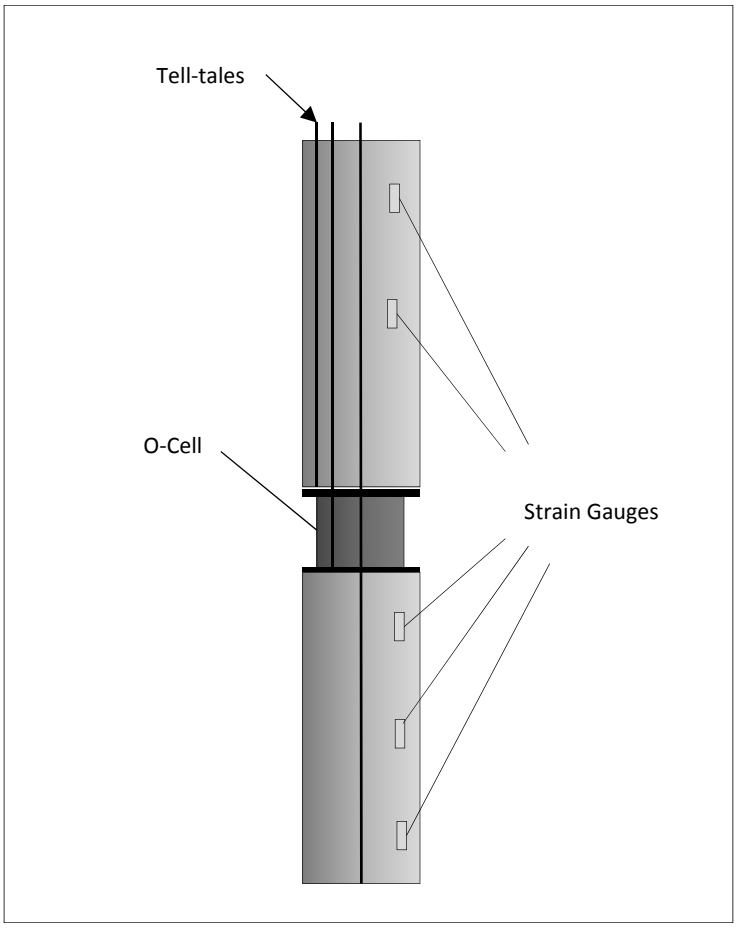


Fig 6. Typical instrumented test pile/pier with O-Cell

Through work on over a dozen high rise buildings in the Honolulu area, the author has compiled a database of load test results for piles and piers penetrating loose soils, stiff cohesive alluvial materials, and weak and more intact coralline limestone. The following figure presents composite results of load test data to illustrate the typical side shear vs. foundation movement for a range of materials encountered in the area (Fig. 7).

© 2016 Deep Foundations Institute

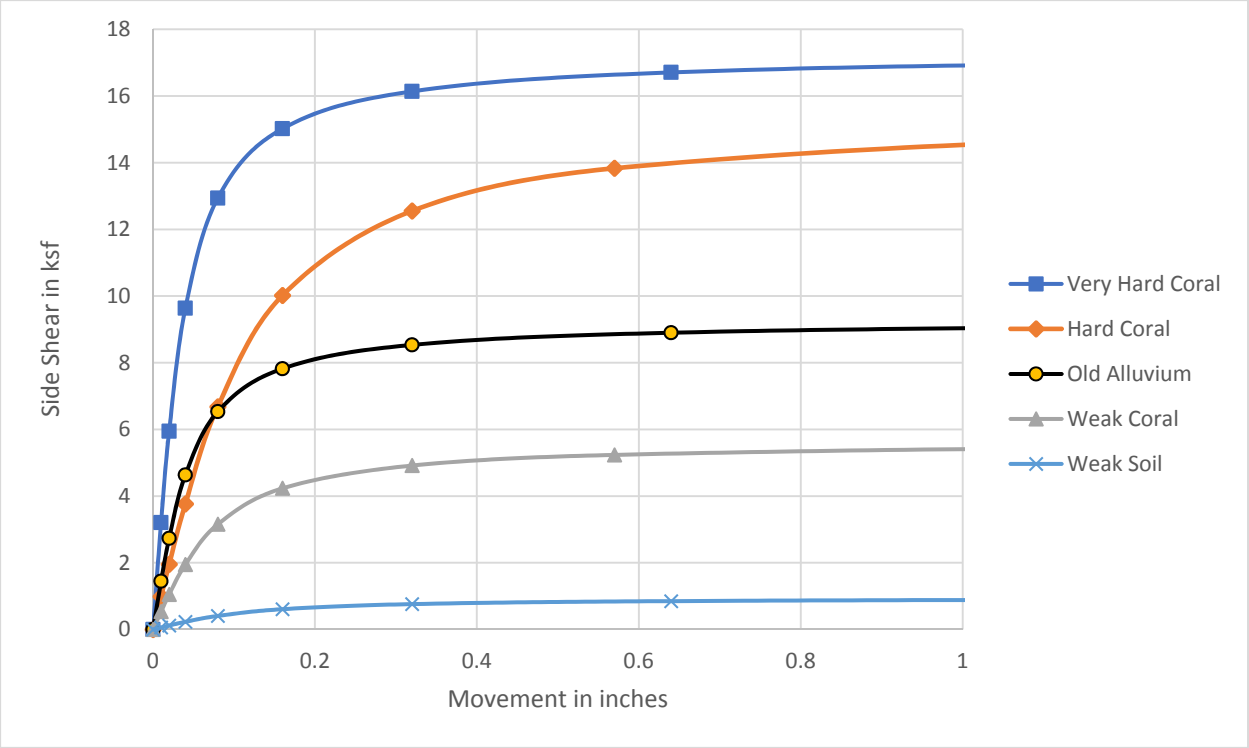


Fig 7. Typical side shear vs. foundation movements for common soil and rock types in the Honolulu area

The ultimate side shear values measured in the coralline limestone have been found to be consistent with values obtained in similar formations in Florida and correlate well with the analysis methods developed by the Florida Department of Transportation referenced previously.

CONSTRUCTION ISSUES

CFA piles and drilled pier foundations are currently the preferred and predominant foundation system for high-rise construction in the Honolulu area. While cost-effective, problems have arisen on some sites due to the presence of voids within and below the coral limestone formations. For CFA piles, grout take ratios (actual/theoretical volume) are typically in the range of 1.6 to 1.8 in this porous material, but can be substantially higher. When constructing CFA piles, grout pressures must be monitored continuously during installation and the level of grout must be observed for an extended period of time after construction to confirm that voids have been filled. On one early CFA project, the general contractor employed a target grout factor of only 1.4, and covered the newly cast piles with plywood immediately after construction to protect workers. Overnight, the grout dropped over 6 ft (2 m) in some pile locations allowing soils to cave into the open hole and causing contamination of the upper part of the grout and deformation of the reinforcing cages (Fig 8). These piles required replacement at significant cost.

© 2016 Deep Foundations Institute



Fig 8: Damage to top of CFA pile due to grout infiltration into subsurface voids

With the availability and use of digital CFA pile installation monitoring equipment, voids and grout loss can often now be detected and compensated for during construction. However, even with this equipment, 10 to 20 percent of piles may require redrilling and regrouting when significant voids are penetrated.

Drilled pier foundations also experience a loss of concrete into voids, although to a lesser extent than CFA piles. In general, concrete overage factors of 60 percent or more are anticipated in drilled pier construction. All piers are installed using slurry drilling procedures as groundwater is typically less than 10 ft (3 m) in depth. If the subsurface profile includes sand and clay strata, it is critical that piers are drilled and poured on the same day to avoid sloughing and softening of the sidewalls. Concrete is introduced by tremie into the pier base, and pours are continued until the slurry is displaced and contaminated concrete is flushed out of the top of the pier.

SUMMARY AND CONCLUSIONS

In summary, the introduction of CFA piles and drilled piers to the Honolulu area of Hawaii has had a significant impact on high rise building construction during the past 10 years. Drilled foundations are particularly well suited to the local geologic conditions, which include interbedded vuggy coral, medium dense sands and gravels and stiff alluvial deposits. Such foundations represent an efficient and cost-effective alternative to driven pile foundations used almost exclusively in the past. These drilled foundation systems should find wider use in other areas having similar geologic conditions, provided that the effects of voids are considered, and subsurface materials are properly characterized. Methods of analyses developed for the assessment of side shear capacity in porous coral formations have been verified through a substantial number of load tests and are recommended for continued use in foundation design.

© 2016 Deep Foundations Institute

This page left intentionally blank

© 2016 Deep Foundations Institute

A STUDY ON BEARING CAPACITY OF WAVEFORM MICROPILES USING CENTRIFUGE TEST

Young-Eun Jang, University of Science and Technology, Deajeon, South Korea, 82) 31-910-0237, yejang@kict.re.kr
Jin-Tae Han, Korea Institute of Civil Engineering and Building Technology, Goyang, South Koera, 82) 31-910-0259, jimmyhan@kict.re.kr
Chengcan Wang, University of Science and Technology, Deajeon, South Korea, 82) 31-910-0237, wangchengcan@kict.re.kr

ABSTRACT

The waveform micropile is a newly developed foundation type for increasing the bearing capacity with the created shear keys on the pile's shaft. Analyzing the increment of resistance at the shear key zone is a crucial factor in the design of the waveform micropile. Hence, centrifuge tests were carried out employing six different models, including a waveform micropile in the axial loading condition. The analysis results of the load-settlement curves showed that the waveform micropile achieved a higher bearing capacity compared to the micropile without shear keys. In addition, the test results revealed that the load-settlement relationship was affected not only by the pile shape but also by the locations of the shear keys

INTRODUCTION

A micropile is a small-diameter pile, typically constructed with a less than 300 mm diameter. Generally, the micropile's construction involves drilling, grouting, and insertion of a reinforcement material, such as a thread bar. The micopile can be utilized in a variety of fields for reinforcing the foundations of existing structures. It also has advantages for accessing challenging areas like limited-access construction sites, including those with a low headroom space and adjacent structures, due to the small size of the construction equipment. Thus, since it was introduced in 1950 in Italy, the micropile has become one of the preferred solutions when other deep-foundation methods are not applicable to the site.

Federal Highway Administration (FHWA) gives the micropile design implementation guideline of neglecting the end bearing due to its small diameter but considering the frictional resistance if the bond zone of the pile is in the soil or on a weak rock. The bearing capacity is considered primarily only if the micropile is founded on a high-quality sound rock (FHWA, 2005). Micropile design in South Korea is currently being performed based on the FHWA manual and taking into consideration the frictional resistance for the design as the pile generally sockets into a weak rock or soft rock. Moreover, the frictional resistance within the soil layer has usually been ignored, considering only the shaft resistance of the rock-socketed length in the conservative design. The design concept excluding the frictional resistance in the soil layer, however, may lead to an extension of the pile socket length, which will increase the construction cost. Hence, many researches have attempted to provide better design and construction methods to increase the bearing capacity in a cost-effective way (Juran et al. 2001; Sadek and Isam 2004; Tsukada et al. 2006; Finno 2002; Gomez et al. 2003; Seo et al. 2013).

The use of the waveform micropile is also suggested for improving the frictional resistance with the soil layers compared to the conventional micropile (Jang and Han 2015). It can be achieved by changing the construction process and the shape of the pile shaft using the soil jet grouting method. The results of the numerical analysis, field, and model tests showed that the bearing capacity of the waveform micropile was improved much more than the conventional micropile.

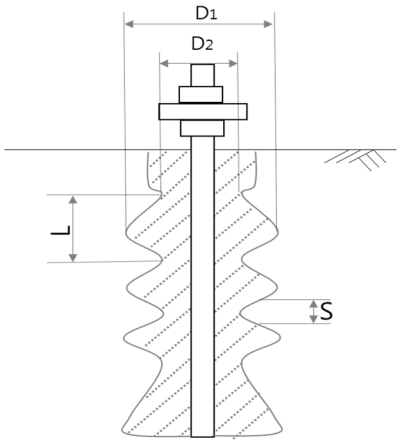
The waveform micropile consists of one or more pitched shear keys, as illustrated in Fig. 1. The shear key length and the separation distance between the keys are considered crucial factors in improving the bearing capacity. It is expected that the pile capacity can be improved through both the shaft friction and the end bearing because the pile tip has an enlarged diameter compared with the conventional micropile.

© 2016 Deep Foundations Institute

The shape of waveform micropile consisted of two parts; a shear key zone with 500 mm (D_1) in diameter, and none shear key zone of 300 mm (D_2). Moreover, it is expected that the waveform micropile will present different types of failure mechanism depends on the shear key length (L) and spacing between shear keys (S).

The waveform micropile can be installed through a process of drilling, grouting and installation of reinforcing bar without casing. Grouting work is a significant part of the installation of the waveform mocripile as the primary purpose of grouting is to strengthen the soil layer by making shear keys on the pile shaft. The grouting construction process employs the soil jet grouting method, which is a well-known pressure grouting method.

For the design of the waveform micropile, it is necessary to have a better understanding of the performance characteristics and capacity of the bonded area between the shear key and the soil. Therefore, this study was conducted for evaluating the behaviors of waveform micropile with a single shear key in the different depths and with multiple shear keys by centrifuge test.



D_1: max. diameter of shear key zone
D_2: diameter of none shear key zone
L: length of shear key
S: spacing between shear keys

Figure 1. Concept of waveform micropile

CENTRIFUGE TESTS

A geotechnical centrifuge was used for the model tests that were performed to study the axial behavior of the waveform micropile. The centrifuge test is an advanced model test for investigating the various geotechnical problems. Ever since it was recognized as a cost- and time-effective tool compared to the field test to solve the complex soil and foundation problems, many researchers have tried to set up centrifuge test facilities in their laboratory (Ng, 2014). In 2009, Korea Advanced Institute of Science and Technology (KAIST) constructed the centrifuge test facilities that were utilized in this study as shown in Fig. 2 (Kim et al. 2013). The geotechnical centrifuge produces the maximum centrifugal acceleration of 130 g for simulating the behavior of the 1/n scaled model. The small-scale model represents the state of the prototype model through the recreation of the stress condition during the test. For the test, the small-scale models were manufactured using scaling factors for the centrifuge test proposed by Ko (1988).

© 2016 Deep Foundations Institute



Figure 2. KOCED Geo-centrifuge, KAIST

MODEL PILE PREPARATION

Six different models were selected to represent the different types of micropile. The test models were a waveform micropile, a conventional micropile, a jet-grouted micropile, and the three other model types that were manufactured with a single shear key located in three different depth levels. The models with a single shear key were chosen to examine the contribution of a shear key to the frictional resistance increment. The jet-grouted micropile is a pile without shear keys and with the same construction process as the waveform micropile. The jet-grouted micropile was selected to study the shape effect of the waveform grout body more precisely. All the test models were scaled down to about 1/40 and were made with polyvinyl chloride (PVC; Young's modulus E = 2,900 MPa) which has a smaller elastic modulus than the prototype model that composited with concrete and steel (Alnuaim et al. 2015). The geometric dimensions of the small-scale models were decided using equations [1] and [2] to ensure the accurate model axial rigidity (EA) and dimension of the prototype models, respectively.

$$\frac{E_p A_p}{E_m A_m} = n^2, \quad [1]$$

Where $E_p A_p$ is the axial rigidity of the prototype model, $E_m A_m$ is the axial rigidity of the small-scale model, and n is the scaling factor.

$$L_m = \frac{L_p}{n}, \quad [2]$$

Where L_p is the length of the prototype model and L_m is the length of the small-scale model.

Figure. 3 presents the dimensions of the prototype and test models. The pile length was made 300 mm while 250 mm (10 m in the prototype model) was embedded in the soil the shear keys were idealized with a triangular shape in the picture. To measure the axial forces, 10 strain gauges (GFLA-6-50) were evenly attached to each micropile.

© 2016 Deep Foundations Institute

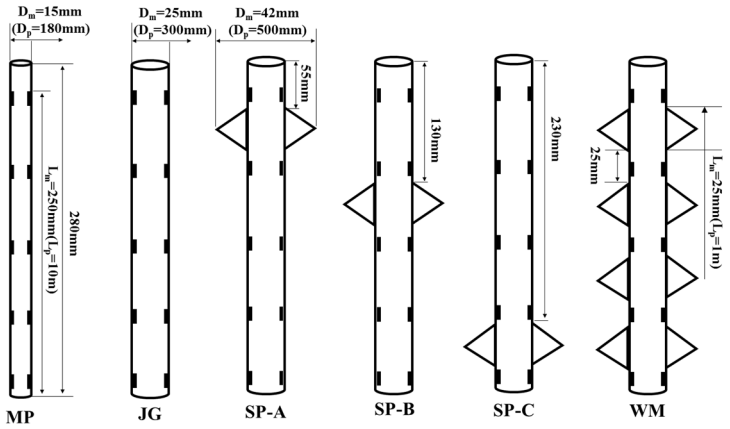


Figure 3. Configuration of test models

MODEL PILE INSTALLATION AND LOAD TESTING

The centrifuge tests were performed on the micropiles installed in silica sand. Silica sand is poorly graded soil that classified as SP by USCS (Unified Soil Classification System). The physical properties of the sand are presented in Table 1: γ_{dmax} and γ_{dmin}: dry unit weight; C_u: uniformity coefficient; and C_c: coefficient of curvature.

Table 1. Parameters of silica sand

Soil type	USCS	γ_{dmax} (kN/m^3)	γ_{dmin} (kN/m^3)	C_U	C_C
Silica sand	SP	15.8	12.5	1.77	1.16

To enable the piles to be installed vertically and aligned with the loading system, the model piles were placed in two steps. First, silica sand was air-pluviated into the soil container (d=0.9 m; h=0.7 m) until its thickness reached 250 mm, followed by the penetration of the pile only up to 100 mm. Second, the soil layer was air-pluviated on its top, leading to a total height of 400 mm, with a relative density (D_r) of around 70%. Then the soil container was placed in the centrifuge system, and the test pile was connected to the instrumentation system. A layer of sand coating was applied to all the models for simulating a rough surface due to the injection of high grouting pressure in the prototype model. Figure. 4 presents the procedure for setting up the pile and soil for the test.



(a) 1st sand air-pluviation (h=250mm) (b) Pile tip installation (c) 2nd sand air-pluviation (h=400mm) (d) View of instrumentation system

Figure 4. Centrifuge test procedure

© 2016 Deep Foundations Institute

Eventually, a 250-mm-long pile was made in the soil out of the total depth of 400 mm. The instrumentation systems were used for measuring the axial forces from the strain gauges and the axial movement from the two LVDTs and a load cell during the load test. Figure. 5 illustrates a schematic for the setup used in the testing program. To prevent damage to the strain gauge wire with the increment of the applied loading pressure, the wire cables were connected to the channel passing through the inside of the pile. In this paper, only the results of the load-settlement relationship measured from the LVDTs and the load cell are presented. The testing was conducted under the displacement control method with the loading rate of 0.05 mm/sec and maximum displacement of 5.0 mm (200 mm in prototype)

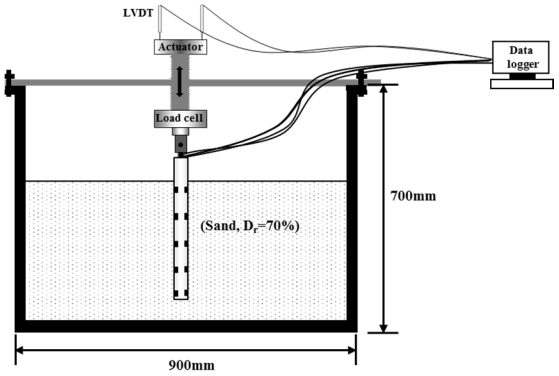


Figure 5. Schematic diagram of instrumentation system

TEST RESUTLS AND DISCUSSION

DESIGN LOAD ESTIMATION OF TEST MODELS

In this chapter, the design load of each pile was calculated to have an idea of the failure point. The design load was estimated with the consideration of the prototype piles constructed in the sand under the same conditions in the centrifuge test. The soil profile of each layer was determined from the cone penetration resistance q_c obtained in the CPT test which was conducted in the silica sand by Kim et al (2015) as presented in Fig. 6(b). The characteristics of each soil layer of the pile bond length 10 m (250 mm in the small-scale model) were classified by referring to Table 2. From the table, it is assumed that the soil layer is multi-layered, composed of a loose-sand layer (0-2.7 m), a medium-dense-sand layer (2.7-7.3 m), and a dense sand layer (7.3-10 m).

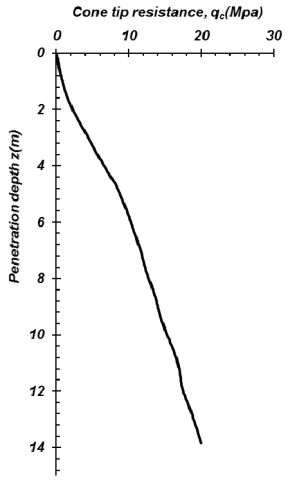


Figure 6. Con tip resistance profile of silica sand at D_r=65%

© 2016 Deep Foundations Institute

Table 2. Relationship between q_c and other soil parameters (Meyerhof, 1956)

Consistency	Relative density (D_r)	N value	Internal friction (ϕ)	Cone resistance (q_c, MPa)
Very loose	<0.2	<4	<30	<2
Loose	0.2~0.4	4~10	30~35	2~4
Compact	0.4~0.6	10~30	35~40	4~12
Dense	0.6~0.8	30~50	40~45	12~20
Very dense	>0.8	>50	>45	>20

Following the FHWA micropile design guideline, equation [3] was used to predict the design loads of the micropiles in this study. FHWA gives the ranges of the design parameter α_{bond} (grout-to-ground ultimate bond strength) for various soil types, and four methods of grouting, including gravity grouting and pressure grouting. In this case, the ultimate capacity was calculated for micropile type B considering the specified soil conditions. Then the allowable loads for the conventional micropile and the jet-grouted micropile were defined with a 2.5 factor of safety as 323.0 and 538.3 kN, respectively. Here, it is assumed that the micropiles with a single shear key and those with multiple shear keys behave under the same design load with the jet-grouted micropile due to the design process considering that the shape of waveform micropiles has not yet been proposed.

$$Q_a = \frac{\alpha_{bond}}{\text{F.S}} \times \pi \times D_{bond} \times L_b, \quad [3]$$

Where α_{bond} is the grout-to-ground ultimate bond strength, D_{bond} is the diameter of the drill hole, L_b is the bond length, and FS is the factor of safety applied to the ultimate bond strength.

LOAD-SETTLEMENT RELATIONSHIP

Figure. 7 presents the load-settlement curves for all the test piles in proto scale. As the diameter of the jet-grouted micropile was enlarged to 300 mm, it shows higher load resistance compared to the conventional micropile, as expected. The micropiles with a single shear key generally displayed reduced settlement compared to the jet-grouted micropile under the same loading condition. In addition, the micropiles with a single shear key showed a different response based on the location of the shear key. This result indicates that not only the addition of a shear key but also the shear key's surrounding ground condition can affect the behavior of micropiles. It was also observed that there was no obvious capacity increase in the waveform micropile with multiple shear keys compared to the piles with a single shear key (SP-B and SP-C). In terms of the increase rate, it can be said that the pile may not show significant difference if the shear key is constructed below the center of pile.

To examine the pile behavior more precisely in terms of the failure state, the ultimate capacities of the piles corresponding to the allowable settlement were determined. There already exist several approaches to estimate the ultimate loads of piles based on the load-settlement relationship. For example, Eurocode 7 (EN1997-1) proposed that the failure load corresponding to the displacement of the pile head settlement is equal to 10% of the pile diameter (0.1D). In addition, p-s curve and Davisson's method suggested that the maximum curvature point load can be defined as a failure load. FHWA defines the ultimate loads when the settlement rate meets with a slope of 0.15 mm/kN for micropile design.

For a comparison of the bearing capacities of the micropiles in this study, the failure point was estimated corresponding to the pile head settlement of 25.4 mm (Terzaghi and Peck, 1967). However, it was considered that the load-settlement curve obtained from the jet-grouted micropile and the other waveform micropiles with the shear key were not fully mobilized at the 25.4 mm settlement from Fig. 7. Therefore, the ultimate loads corresponding to 10% of the settlement for the jet-grouted micropile, the waveform

© 2016 Deep Foundations Institute

micropiles were also estimated. Accordingly, the failure point of 0.1D=30 mm was drawn on the graph considering the diameters of all the micropiles, excluding the conventional micropile. At the same time, the diameter of the waveform micropile was considered to have an average value of 400 mm as the waveform micropile has multiple shear key diameters (300 mm, D_1; 500 mm, D_2). The ultimate load capacities of all the micropiles are shown in Fig. 7, and the allowable capacities are defined with a 2.5 factor of safety as FHWA suggested.

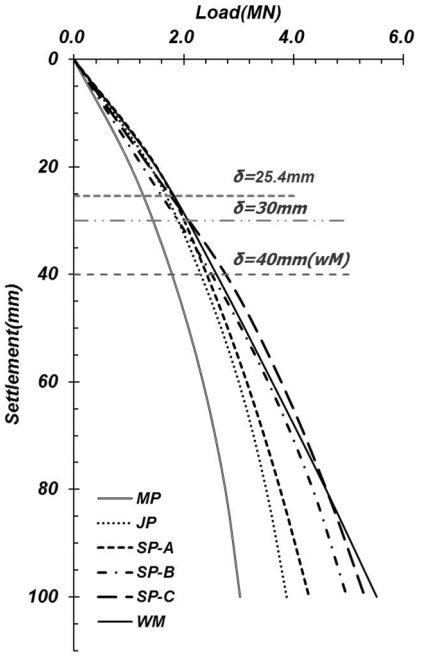


Figure 7. Load-settlement curve of test models (prototype scale)

Table 3 shows a comparison of the calculated and estimated allowable loads of all the test piles. It is clearly shown that the estimated load values are much higher than the calculated results. This indicates that the equation for the micropile design proposed by FHWA cannot accurately reflect the ground condition and the shape effect of waveform micropiles. Based on the estimation results obtained using the existing methods, the waveform micropile with multiple shear keys had the highest capacity, followed by the waveform micropile with a single shear key, the jet-grouted micropile, and the conventional micropile. The waveform micropiles with a single shear key (SP-A, SP-B, SP-C), however, and the waveform micropile (WM) models showed different trends depending on the load estimation methods that were used.

Even though a higher bearing capacity was observed in the micropiles with a single shear key, the bearing capacity should be examined in a more reasonable way to more specifically analyze the load-bearing behavior of the waveform micropile. For this, a comparative study was conducted with normalized estimated values, as presented in Fig. 8.

Table 3. Allowable bearing capacities of piles corresponding to different settlement

		MP	JP	SP-A	SP-B	SP-C	WM
Design load (kN)		323.0	538.3				
Estimated load (kN)	S=25.4 mm	524.3	711.2	747.3	695.7	765.2	765.9
	S=0.1D	-	790.6	821.6	805.1	873.2	854.6 (0.1D=30 mm)
							1073.4 (0.1D=40 mm)

© 2016 Deep Foundations Institute

Figure. 8 shows a direct comparison of the normalized allowable load values for both estimated criteria: (a) 25.4 mm; and (b) 0.1D. Here, the normalized values in graph (a) were obtained from the conventional micropile ($P_{pile}/P_{mp_25.4mm}$) while those in graph (b) were obtained from the jet-grouted micropile ($P_{pile}/P_{jp_0.1D}$).

In curve (a), it is shown that the jet-grouted micropile had an about 36% higher value compared to the conventional micropile. As discussed earlier, it is considered that there was increase in the bearing capacity affected by the enlarged diameter of the jet-grouted micropile. The waveform micropiles with a single shear key and the waveform micropile with multiple shear keys presented a maximum bearing capacity increase of 46% (in SP-C, WM) and a minimum bearing capacity increase of 33% (in SP=B) compared with the conventional micropile. In the observation of the load gap between the jet-grouted micropile and the waveform micropiles with a single shear key, the shear key micropiles were found to have 10% higher resistance on average compared to the jet-grouted micropile. A decreased value was obtained, however, in the SP-B pile, which had a shear key in the middle of the shaft.

For more details, the bearing capacity of the piles, excluding the conventional micropile, are also discussed herein based on curve (b), which was obtained using the s=0.1D criteria. Curve (b) displays the results of two cases considering that the two waveform micropile (WM) diameters corresponding to s=0.1D (D=300 and 400 mm). As discussed above, the overall behavior of the waveform micropiles with a single shear key indicate that the bearing capacity increased, but there were differences among the values according to the shear key location and shape. Among the micropiles with a single shear key, those with the highest load values were SP-C (10%), SP-A (4%), and SP-B (2%), showing a tendency similar to that of curve (a): s=25.4 mm. This observation implies that the existence of a shear key clearly contributes to the advancement of the axial behavior, but the shear key location should be carefully decided because a higher bearing capacity occurs based on the surrounding ground condition and the confining pressure. When the 300 mm waveform micropile diameter was considered, the pile showed about 8% increase in the bearing capacity compared to the jet-grouted micropile whereas the waveform micropile achieved about 36% higher resistance with the value corresponding to 10% of the settlement to the 400 mm diameter. Based on the results, it was clearly shown that the bearing capacity of the waveform micropile with added shear keys increased. In addition, the bearing capacities of the waveform micropiles vary with not only the estimation method used but also the pile diameter corresponding to the allowable settlement, which reflects the failure state of the pile.

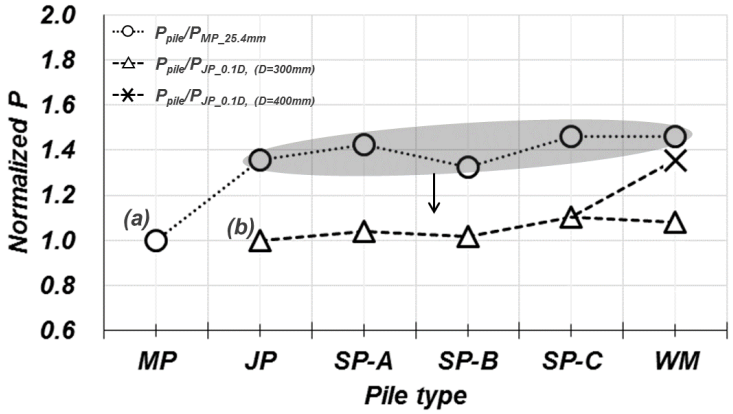


Figure 8. Comparison of the normalized pile load

CONCLUSION

A series of centrifuge tests was carried out to investigate the axial behavior of the waveform micropile. The

© 2016 Deep Foundations Institute

test models were a waveform micropile, a conventional micropile, and a jet-grouted micropile without shear keys and with the same construction process as the waveform micropile. Other models were manufactured with a single shear key located at three different depth levels to estimate the contribution of the shear key to the bearing capacity improvement. All the test models were scaled down to about 1/40 and were made with PVC. Based on the centrifuge tests performed using six different models, the conclusions below can be drawn.

(1) From the tests, the load-settlement relationship was determined, which made it possible to clearly observe the increase in the bearing capacity at least by 33% in the waveform micropile with shear key compared to the conventional micropile.
(2) The ultimate pile capacity was determined according to the given pile settlement, which were s=25.4 mm criteria and s=10% of the pile diameter criteria, and the estimated bearing capacity showed different values based on the estimation method. Especially, the waveform micropile showed an increase in the bearing capacity by 7% compared to the jet-grouted micropile with s=25.4mm criteria, while the bearing capacity increased by 36% with s=0.1D criteria.
(3) Such results emphasized that a reasonable procedure for determining the ultimate load should be suggested based on the study of the failure mechanism of the waveform micropile. Moreover, as the analysis data showed that factors like the location of a shear key and the shape of the waveform affect the bearing capacity of waveform micropile, the failure mechanism will be analyzed considering the various configurations of the shear key and ground conditions.

ACKNOWLEDGEMENT

This research was supported by a grant from “Design and construction of artificial ground with the vertical spaces above existing urban infrastructure” which is funded by the Korea Institute of Civil Engineering and Building Technology (KICT).

REFERENCES

EN 1997-1, 2004. Eurocode 7: Geotechnical design – Part 1: General rules, EN 1997-1:2004(E), European Committee for Standardization (CEN), Brussels, November, 168 p.

FHWA, 2005. Micropile Design and Construction: Reference Manual. FHWA-NHI-05-039, Federal Highway Administration, 1(1), pp. 7-28.

Finno, R.J., 2002. Evaluation of capacity of micropiles embedded in dolomite. Final Rep. of Infrastructure Technology Institute, Northwestern Univ., Evanston, IL.

Gomez, J., Cadden, A., and Bruce, D.A., 2003. Micropiles founded in rock: Development and evolution of bond stresses under repeated loading. Proc. of the 12th Pan-American Conferemce on Soil Mechanics and Geotechnical Engineering(Soil Rock America 2003), VGE, Essen, Germany, pp. 1911-1916.

Jang, Y.E., and Han, J.T., 2015. Study of load capacity of waveform micropile by centrifuge test. Proc. Of the 25th International Offshore and Polar Engineering Conference. International Society of Offshore and Polar Engineers, pp. 700-706.

Juran, I., Benslimane, A., and Hanna, S., 2001. Engineering analysis of dynamic behavior of micropile systems. Transportation Research Record No. 1772: Soil Mechanics, pp. 91–106.

Kim, D.S., Kim, N.R., Choo, Y.W., and Cho, G.C., 2013. A newly developed state-of-the-art geotechnical centrifuge in Korea. Journal of Korean Society of Civil Engineering, 17(1), pp. 77-84.

Kim, J.H., Choo, Y.W., Kim, D.J., and Kim, D.S., 2015. Miniature Cone Tip Resistance on Sand in a

© 2016 Deep Foundations Institute

Centrifuge. Journal of Geotechnical and Geoenvironmental Engineering, 142(3), 04015090 p.

Ko, H.Y., 1988. Summary of the state-ofthe-art in centrifuge model testing. Centrifuge in Soil Mechanics, pp. 11-28.

Mayerhof, G.G., 1956. Penetration test and bearing capacity of cohesionless soils. Proc. Of the ASCE, Journal of the Soil Mech. and Found. Div., 82(1), 866 p.

Ng, C.W.W., 2014. The state-of-the-art centrifuge modelling of geotechnical problems at HKUST. Journal of Zhejiang University SCIENCE A, 15(1), pp. 1-21.

Sadek, M. and Isam, S., 2004. Three-dimensional finite element analysis of the seismic behavior of inclined micropiles. Soil Dynamics and Earthquake Engineering, 24(6), pp. 473-485.

Seo, H., Prezzi, M., and Salgado, R., 2013. Instrumented Static Load Test on Rock-Socketed Micropile. Journal of Geotechnical and Geoenvironmental Engineering, 139(12), pp. 2037-2047.

Terzaghi, K. and Peck, R.B., 1967. Soil Mechanics in Engineering Practice. 2nd ed, John Wiley and Sons, New York, pp. 346-352.

Tsukada, K., Miura, Y., Tsubokawa, Y. and Otani, G.L., 2006. Mechanism of bearing capacity of spread footings reinforced with micropiles. Journal of soils and foundations, 46(3), pp. 367-376.

© 2016 Deep Foundations Institute

A TALL SLENDER TOWER RISES ON SECANT PILES AND DRILLED SHAFTS

Sitotaw Y. Fantaye, Mueser Rutledge Consulting Engineers, New York, NY, USA, sfantaye@mrce.com
T.C. Michael Law, Mueser Rutledge Consulting Engineers, New York, NY, USA, mlaw@mrce.com
Renzo D. Verastegui, Mueser Rutledge Consulting Engineers, New York, NY, USA, rverastegui@mrce.com
Alfredas Daugiala, Underpinning & Foundations Skanska, Maspeth, NY, USA, alfredas.daugiala@skanska.com

ABSTRACT

When completed, 520 Park Avenue will amend the Manhattan skyline and be one of the most prestigious high rise towers in New York City. The 52-story condominium building is located on a 60 by 100 feet lot on East 60th Street between Park and Madison Avenues. The geographically complex site is bounded by two fragile 5-story masonry buildings on the east and west, a mid-rise building on the north, and a New York City subway tunnel on the south. To add to this complexity, the ambitious development required 70 to 80 feet of excavation, mostly below groundwater level in highly permeable rock, to accommodate four levels of cellars. The new building also cantilevers 24 feet over a five-story historic building on the east. The limited footprint of the building coupled with large compressive and tensile axial loads, considerable base shear and over-turning moments, and the required deep excavation, presented unique foundation challenges. This paper describes how the challenges were solved with an innovative combination of permanent secant pile walls and drilled shafts.

Keywords: deep excavation, subway, groundwater, foundation construction, secant pile walls, drilled shafts

INTRODUCTION

The project site is located at 45 East 60th Street, on the block bounded by East 61st Street to the north, East 60th Street to the south, Park Avenue to the east, and Madison Avenue to the west. As shown in Fig. 1, the site is surrounded on three sides by buildings sensitive to differential settlement. In addition, a NYCT underground subway structure lies below East 60th Street approximately 13 feet south of the site. The base of the subway structure is approximately 42 feet below the street.

The project consisted of constructing a 52-story tall building. A portion of the superstructure cantilevers 24 feet over an adjacent five-story historic building. The underground construction for the new building involved a four-level basement, extending about 60 feet below ground surface. The excavation subgrade is much deeper than both the subway structure and the adjacent shallowly-founded building foundations.

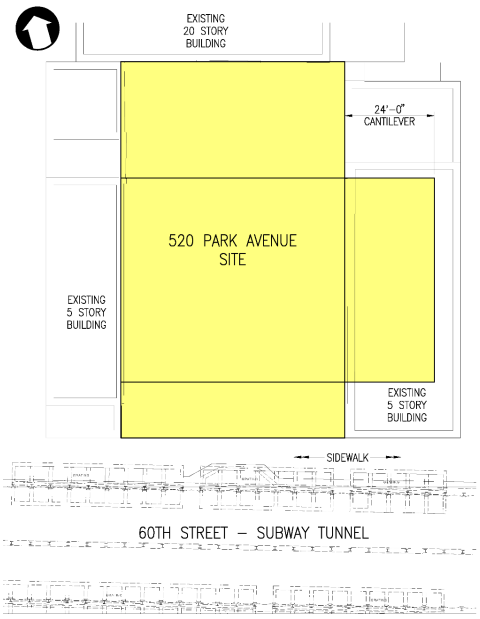


Fig. 1. Site plan

SITE GEOLOGY

Figure 2 is a section of the 1865 Viele Map showing site topographic conditions prior to area development. The map indicates that the site was at the eastern edge of a historic marshland, which was approximately west of Park Avenue and north of 58th Street. An historic stream which ran alongside the eastern edge of the site was part of a larger stream network that traversed the surrounding area. This stream network is also visible in the map. In addition, the bedrock underlying the site lies in a highly weathered zone due to a couple of ancient faulted zones that transect the site. These indicate that a zone of highly weathered rock is expected.

© 2016 Deep Foundations Institute



Fig. 2. 1865 Viele map

SUBSURFACE CONDITIONS

Two subsurface investigations were performed at the site, one in 2012 and another in 2013. The initial investigation, performed by another firm, consisted of seven borings. At that time the site was occupied by a five-story masonry structure with one basement level and five out of the seven borings were made within the basement using a low headroom, portable electric rig, which is not efficient. The remaining two borings were located outside the property line within the sidewalk; these borings were performed with a regular truck-mounted rig. Based on the foundation load demands of the new design and the foundations and excavation support systems envisioned for it, coupled with a review of the rock cores from the initial investigation, it was decided that an additional comprehensive investigation was required. The excavation for the new design would extend well into the bedrock and the foundations very likely needed to be high capacity deep foundations to resist the large compressive and tensile forces from the shear walls. Of particular interest in the supplemental investigation was the characteristic of the bedrock, since the rock cores from the initial investigation exhibited extensive weathering that did not improve with depth.

In 2013, after the existing building was demolished and the site was backfilled to street level, a supplemental investigation consisting of 12 borings was performed to further investigate the strength and permeability of the weathered rock. All additional borings were performed at proposed foundation locations. Borings were advanced 15 to 75 feet into bedrock, the depth extending at least as deep as the assumed socket length of the deep foundations.

This investigation confirmed that, in general, the subsurface conditions at the site consist of surficial fill over compressible clay, underlain by sand and silt, glacial till, and decomposed rock overlying bedrock. Bedrock exhibits a profile of weathering that does not improve with depth.

© 2016 Deep Foundations Institute

Bedrock Quality

Rock core samples recovered in the 2013 investigation indicate that the quality of bedrock is highly varied. It is generally described as slightly to highly weathered gray schistose gneiss with occasional pink pegmatite intrusions, closely jointed to broken, with weathered and occasionally soil-filled joints. Rock core recoveries range from 0 to 100 percent, averaging 69 percent. The Rock Quality Designation (RQD) ranges from 0 to 88 percent, averaging only 12 percent. Rock core recoveries and RQD did not increase with depth as is typically encountered.

As indicated in the historical maps, the bedrock underlying the site lies in a highly weathered zone due to a couple of ancient faulted zones that transect the site. The bedrock underlying Manhattan commonly has faulted and jointed zones, likely dating back to the Mesozoic Era, that trend in a North-West direction. A NW trending fault that runs below the site has been offset along another faulted zone with a North-East trend. This offset creates a deep "crisscrossing" fault pattern across the site. The faulting has created deep zones of fracturing within the bedrock that can be seen in the rock core photo in Fig. 3.

Historic streams ran along these fractured zones and further weathered the rock; the effect of this intense weathering can be seen in the sometimes soil-like consistency of the rock. Veins of intrusive rock are present in the rock, including pegmatite, a very hard igneous rock. The intrusions can be seen in the sporadic light pink colored zones in some of the rock cores. As rock tends to weather more at the contact zone between two different rock types, it is apparent from the rock cores that it has helped create deep interconnecting weak zones within the bedrock.



Fig. 3. Representative rock core photo

Bedrock Permeability

Packer permeability tests were planned in isolated zones of the bedrock for permeability testing. However, due to the poor quality of rock encountered, variable head permeability tests (both falling and rising head tests) using piezometers screened and sealed in the rock were performed instead. The tests indicated that the permeability of rock at the site is between 1 x 10-4 and 1 x 10-5 cm/sec.

© 2016 Deep Foundations Institute

DESIGN CHALLENGES

Due to the geographical constraints, difficult subsurface conditions, and the nature and sensitivity of the adjacent structures, the foundation and excavation support system design posed several challenges. The design team collaborated closely to implement an effective solution that considered schedule, cost, and constructability.

High Foundation Demand

The new condominium tower was designed to occupy the entire lot, rising over 750 feet into the New York City skyline and dwarfing all other structures in its immediate vicinity. It features full floor residences, with floors cantilevering approximately 24 feet over the 5-story historic building to the east. Considering that the site is only 60 feet wide in the east-west direction and the cantilevered portion of the building is 24 feet wide, the eccentric gravity loading, coupled with external forces such as wind, seismic, and live loads, produce substantial forces that must be transferred to the building's foundation and ultimately into the bedrock, as shown in Fig. 4.

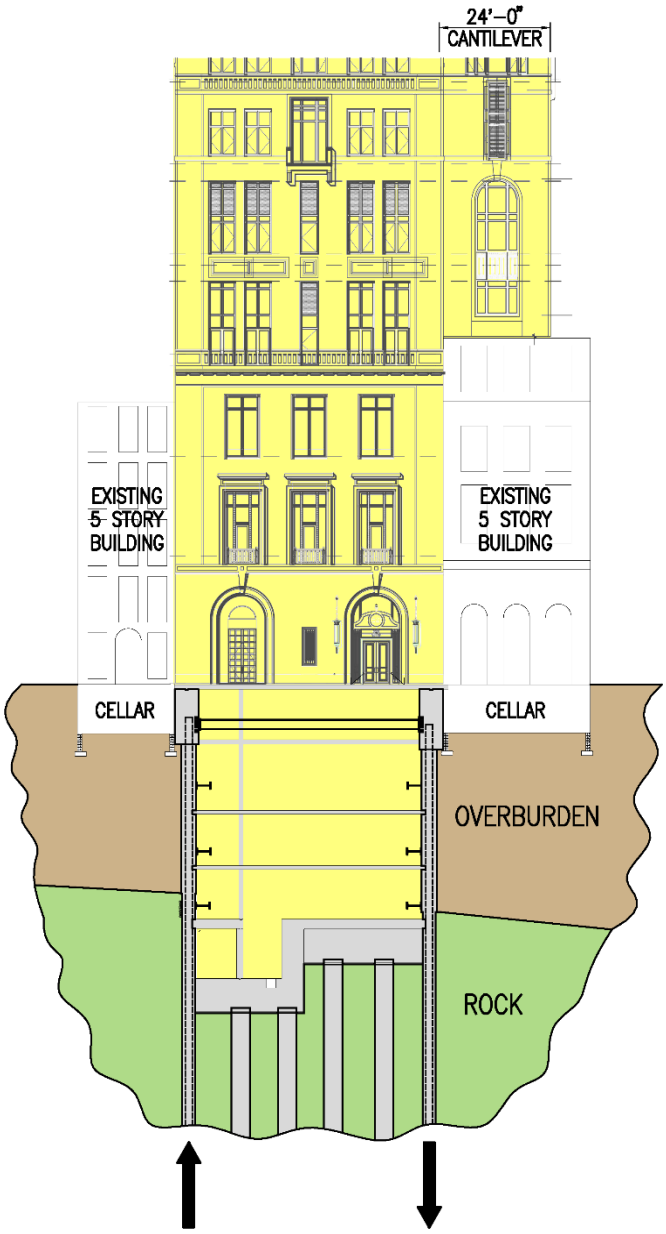


Fig 4. High tension-compression foundation

To efficiently counterbalance the building's eccentric loads, the structural engineers designed a series of shear walls in the east-west and north-south directions. Shear walls in the north-south direction are strategically located at the perimeters of the building to maximize the usable space within the basement. In addition, their location along the full length of the eastern and western perimeters of the building maximized the tension-compression coupled resistance to counteract the overturning forces. This arrangement reduced the foundation demand on individual elements. Maximizing utilization of basement space through the efficient use of shear walls led to the concentration of significant loads at the shear walls adjacent to neighboring buildings founded on shallow rubble stone foundations.

Deep Excavation

Some of the amenities for this high-end tower include a swimming pool, wine cellar, and storage spaces which consume considerable amounts of space. Locating such amenities above the ground floor would erode the profitability of the development. In the heart of Manhattan, where land is a very scarce resource, the basement becomes the ideal place for such amenities. To accommodate this, the building's basement comprises of four cellar levels. This required an excavation that reached 70 to 80 feet below the street

© 2016 Deep Foundations Institute

elevation. This ambitiously deep excavation, combined with a high groundwater table producing up to 45 feet of head, the presence of sensitive neighboring shallow foundations, an adjoining NYCT subway within close proximity, and significant perimeter foundation demands, meant that an integrated solution needed to be implemented.

DESIGN SOLUTIONS

Integrated Support of Excavation and Foundation

The support of excavation and foundation system needed to efficiently address the following critical items:

- Soft rock conditions
- High foundation demands concentrated at the perimeter of the building
- Deep excavation
- Movement of neighboring buildings founded on sensitive shallow ruble stone foundations
- Protection of NYCT tunnel structure
- High groundwater table
- Meeting construction cost and schedule constraints

During the initial phase of design, several schemes were studied and evaluated by the design team. Pros and cons and cost-to-benefit studies were performed to ensure that the most efficient combination was selected. One of the schematic designs included the use of grouped large caissons tied together with pile caps and tie beams, and conventional underpinning piers underneath adjacent shallow foundations to transmit the loads to the bedrock. However, due to installation clearance restrictions, the caissons at the perimeter of the building were eccentric to the foundation shear walls located at the site boundaries, further exacerbating the foundation demands. In addition, constructing approximately 25 to 40 feet tall underpinning piers below a high groundwater table in soils with high silt content can cause unacceptable building settlements. Further, excavation below the underpinning piers would be followed by an additional 20 feet of rock removal to reach final subgrade. As quality of the rock and the degree of weathering in the rock at the site do not improve with depth, exposure of the soft rock, as excavation advances, created challenges in maintaining rock face stability during construction. The stabilization measures would include installation of rock bolts, and protection of the exposed rock face with welded-wire reinforced shotcrete with weep holes to relieve hydrostatic pressures.

Considering the degree of difficulty in implementing such a system, the risk of causing unacceptable adjacent building settlements and the enormous demand on caisson foundations placed eccentric to high concentrated loads, it was decided that this scheme would not be suitable. Instead, the design team devised an integrated system using rigid secant pile walls which served as support of excavation during foundation construction and provided permanent support to the perimeter shear walls.

Secant pile walls are formed by drilling overlapping primary and secondary holes, with the secondary holes typically reinforced with wide flange core beams. In this arrangement, the wall primarily derives its rigidity and ability to resist lateral and axial loads from the composite action of the concrete and reinforcing steel of the secondary piles, while the primary piles filled with plain concrete serve as lagging between the secondary piles. Lateral load from the primary to the secondary piles is transmitted through the arching action of the concrete between the stiffer secondary piles (Megson 2009).

The secant pile wall system was used on all four sides of the site, with the north, east and west walls located directly below the shear walls and integrated into the permanent structure. The south secant pile wall was placed outside of the property line within the sidewalk, and served as a temporary rigid support of excavation (SOE) wall to protect the NYCT subway tunnel. A cast-in place concrete foundation wall with waterproofing

© 2016 Deep Foundations Institute

was constructed along the south property line and tied at each end to the east and west secant pile walls.

The secant pile walls supporting the shear walls were essentially designed as an extension of the shear walls to bring forces directly down to the soft bedrock. The axial capacity of the secant pile wall was developed in the rock socket below final subgrade by bond friction between the rock and the secondary piles.

Lateral Bracing

Temporary lateral bracing of the secant pile walls was provided by a rigid internal bracing system consisting of wales, corner bracing, and cross lot struts, as shown in Fig. 5. Permanent lateral bracing was provided by the cellar floor slabs. The design of the secant pile wall and lateral bracing system, estimation of wall movements, and settlement of adjacent buildings, was performed using conventional and soil-structure analytical methods. The initial secant pile wall analysis was performed using the "Continuous Beam Method" (CBM), which included calculating lateral pressures and performing staged analyses to obtain the internal forces (moments and shears) in the wall and line load reactions at the supports. Using these results, the thickness of the wall, compressive strength of concrete, size of core beam and bracing members were estimated. This method assumes the secant pile wall acts as a continuous beam, with the soil, water, and surcharge pressures applied outside the wall and the internal bracing and passive soil pressure resisting the applied loads. Rankine active and passive soil and at-rest pressures were used in the initial CBM analyses.

Soil-structure interaction analysis was then performed using the finite element program, Plaxis 2D, with wall and bracing parameters derived from the initial CBM analysis (Brinkgreve et al. 2006). The refined analysis was to estimate the movement of the wall and settlement of the adjacent structures, and in turn refine the secant pile wall and bracing member properties. The wall movements and settlement of adjacent shallow foundations were limited to an acceptable risk tolerance by determining pre-stressing loads for the bracing. In construction, the strut pre-loading were implemented using flat jacks between the struts and the wales.

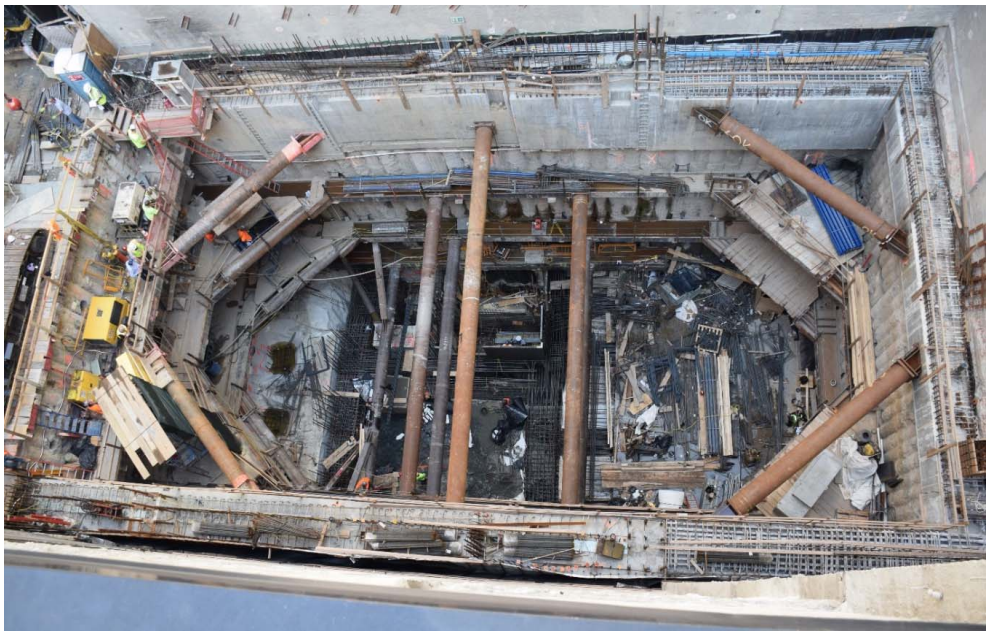


Fig. 5. Temporary lateral bracing to secant pile wall system

Groundwater Control

Groundwater control and cut-off was a significant challenge. As revealed in the subsurface investigations, the permeability of the bedrock is quite high, consistent with the permeability of sand with some fines.

© 2016 Deep Foundations Institute

However, the permeability could be even higher if the rock is excavated and left exposed due to the highly fractured and decomposed nature of the bedrock. In addition, during the subsurface investigation it was observed that the permeability of rock is high enough that there was communication between the boreholes, indicating that the joints and fractures can extend over a significant distance. If the rock is excavated and left exposed, confinement will be lost and if the rock face is left unprotected, the water pressure from outside of the SOE system could slowly wash out the decomposed rock from within the rock fractures into the excavation, significantly affecting the stability of the rock mass, and negatively impacting the foundation construction. Groundwater cut-off was provided by extending the secant pile wall, including the primary secant piles, into the bedrock and below the final subgrade.

OSTERBERG LOAD TEST

The selected foundation system consisted of four feet nominal diameter drilled shaft with rock sockets. To help optimize the drilled shaft, and the load bearing perimeter secant pile wall's rock socket design, an Osterberg load test was performed in late 2013. The load test shown in Fig. 6 was designed such that 12 feet of highly weathered bedrock was tested. The average mobilized unit side shear of about 170 psi was measured at the maximum load at about two inches of upward movement. In addition, about 60 tsf of end bearing was mobilized at about 0.6 inches of settlement.

Based on the test results, the allowable unit side shear of 67psi and 30 tsf end bearing were selected for the design. The initial design of the secant pile wall and drilled shaft rock socket lengths were based on assumed rock-to-shaft side friction (bond stress) allowable capacity of 100 psi; the rock socket lengths were revised based on the results of the load test.



Fig. 6. Osterberg load test

CONSTRUCTION

Secant pile wall construction method

The site previously was occupied by a five-story building that was demolished and its basement backfilled to street level with clean crushed concrete and brick rubble. The construction of a secant pile wall through building remnants, obstructions, and inconsistent materials poses challenges during drilling and can have negative impacts on the alignment, verticality and overall quality of the wall. To mitigate the negative impacts, pre-trenching along the wall position to clear obstructions was performed.

As illustrated in Fig. 7, a reinforced concrete guide wall was then constructed along the alignment of the secant pile wall using scalloped Styrofoam block-outs that served as a template for the secant drilled holes.



Fig 7. Guide wall construction

The guide wall is an essential starting point for the construction of a secant pile wall and serves the following functions:

- Provides drill tool alignment and a second rigid point of contact at grade level.

© 2016 Deep Foundations Institute

- Assists in maintaining proper secant pile overcutting at the beginning of pile installation.
- Assists in drill casing extraction effort and reaction block.
- Assists in the core beam installation into the secondary piles and where required splicing of the core beam.

Secant pile construction involved advancing the temporary double-wall segmental Bauer Casing through overburden soils and seating it into competent bedrock. The drilling then continued through the rock to the required tip elevation. The double-wall casing provided adequate axial stiffness and flexural rigidity for advancement through the overburden, while making casing extraction efforts efficient due to its lighter weight when compared to a single-wall casing of equivalent stiffness. Soil was removed from within the casing with tools consisting of augers and digging buckets. Decomposed, weathered, and competent rock was removed with rock augers and core barrels. A percussion hammer was also available in case hard rock formation was encountered.

CONSTRUCTION CHALLENGES AND SOLUTIONS

Spatial Constraints

The spatial constraints of this urban site posed the greatest construction challenges to the contractor due to the limited available space. The secant pile wall drilling was performed with one hydraulic rotary drill rig, a Liebherr LB36. A Berming Hammer drilling unit was on standby in case the drilling production rates slowed below anticipated targets due to the unexpected presence of hard rock. A crawler crane and two excavators were used to handle the spoils and loading to dump trucks. As the wall construction progressed, core beams and other supplies were constantly moved around the site, to make room for the drill rig and other equipment.



Fig 8. Installing secant piles in close proximity to the neighboring structure

Secant pile length / drilling depth

The maximum primary secant pile length was 70 feet. However, secondary secant pile lengths extended up to 150 feet below the construction grade, with rock sockets as deep as 75 feet. The challenge of the secant pile wall construction was drilling to such substantial depths while maintaining out-of-plumb tolerance to achieve proper overcut between primary and secondary piles for the length of the wall. One of the challenges involved an incident where a special extractor tool had to be used for casing withdrawal operations because the casing was skewed beyond the verticality tolerance and could not be withdrawn due to the drill rig pull capacity limitation and proximity of the adjacent building to the drill rig, as shown in Fig. 8.

Secondary pile core sections

Secondary secant pile holes were outfitted with wide-flange core beam sections. Core beam sizes on the permanent secant pile walls were typically W18x211. However, larger sizes up to W14x500 were required

© 2016 Deep Foundations Institute

at certain locations where load demand was greatest. Most core beam lengths were in excess of the single piece standard mill and NYC delivery limitations. Therefore, field splicing designed by the contractor was often required. As splicing of large sections by welding would be cost prohibitive and require significant quality control and assurance procedures, the contractor selected bolted splice connections. The splice connections illustrated in Fig. 9 were designed for moments, shears, and axial forces provided by the designers following AISC provisions for slip critical bolted connection using twist off bolts to provide controlled bolt installation torque and verify proper installation (AISC 2005).

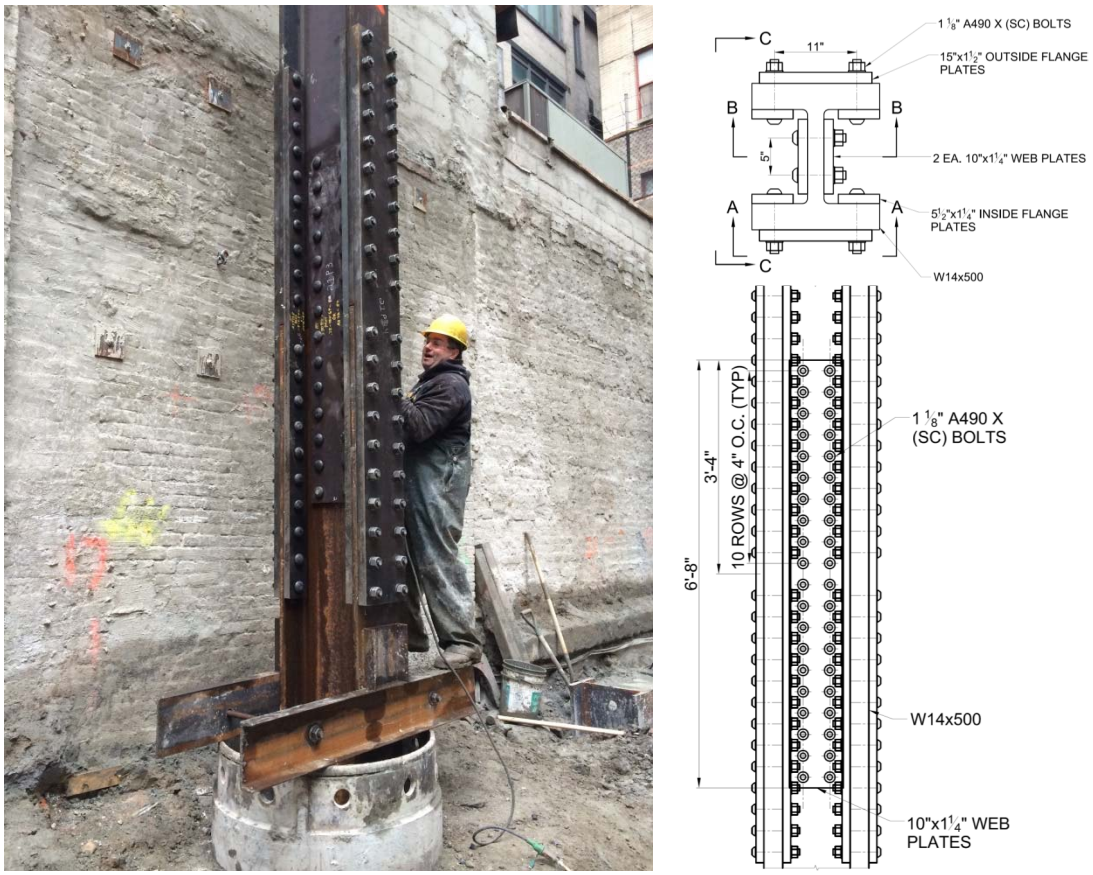


Fig 9. Bolted splice connection details

Concrete Mix Design

A proper mix design is critical to the overall quality of the secant pile wall. During the first concrete pours at the north secant pile wall, the special inspector observed the sensitivity of the mix to the tremie concrete placement method. Between intervals of tremie pipe removal and in-situ concrete sounding using a weighted tape, the inspector noted that unacceptable levels of laitance accumulated. Laitance is a milky, watery deposit on the surface of the concrete, usually occurring at the end of a tremie pour. It is caused by bleeding of the concrete where a mixture of water and cement is continuously pushed to the top as fresh concrete is added via the tremie pipe to the column of concrete rising within the hole. The accumulation of unacceptable levels of laitance is an indication of concrete segregation, an undesirable situation where the concrete aggregate separates from the cement when in contact with the water within the hole. This required significant over-pour at the end of the tremie placement in an attempt to displace the accumulated laitance.

Following the engineer's direction, the contractor investigated, re-evaluated the mix design, and provided

© 2016 Deep Foundations Institute

an adjusted mix with properties following mix stability guidelines, utilizing 50% coarse and 50% fine aggregate fraction in general conformance with the FHWA-NHI-10-016 and ACI 237R-07 (USDOT 2010).

In summary, it is essential to recognize that the secant pile mix requires particular parameters that address mix placement, extended workability, post placement mix stability, and bleed control. In addition, having an experienced engineer present to observe drilling, installation, and tremie concrete placement is important to ensure proper quality control of the secant pile wall. Commonly, concrete suppliers have readily available concrete mixes that meet the specialized applications for strength, slump and water-to-cement ratios. However, for the deep secant pile walls such as were used on this project, the concrete mix design properties and parameters should be carefully weighed and properly designed.

Remedial work items

When excessive laitance was observed at two locations along the north secant pile wall, the contractor implemented remedial actions per the engineer's request. These involved coring of the concrete using an NX core barrel to retrieve cores at five foot intervals at both locations. Visual inspection of the retrieved cores and core compressive strength evaluation was then performed. The test results indicated that the majority of the concrete met the minimum acceptable standards, but that there were limited concrete anomalies at certain depths. In general, the compressive strengths at these locations were lower than at other locations.

Due to the limited nature of the anomalies, it was decided that backfilling the core hole with high strength grout would be sufficient, with additional grouting from within the site if required. As excavation to the observed depths of the anomalies was reached, each secant pile was visually inspected and no additional measures were required.

Excavation and Bracing installation

Prior to excavation and advancing the excavation to the next staged level, it is imperative to follow the excavation limits, procedures, and installation of bracing, including pre-loading of struts. These measures were implemented and verified through the presence an experienced field engineer. All instrumentation required to monitor the movement of adjacent buildings and structures, such as the Automated Motorized Total Station, seismographs, and tilt meters were installed and activated prior to guide wall construction. Remaining instrumentation such as inclinometers within the secant pile walls and the optical prisms at the top of the walls were installed and baselined ahead of the excavation.

Water infiltration and management

Because a secant pile wall is comprised of many vertical construction joints which run along the full length the piles, and these joints are sensitive to wall movement that could exacerbate water infiltration into the basement, potential excessive wall movement is a concern. Wall movement was minimized by providing adequate wall and bracing stiffness and proper implementation of the staged excavation sequence. The specification for the secant pile wall allowed formation of damp spots, but with no active water infiltration through the wall. Upon wall excavation, several damp spots were noted and some with active water infiltration. These locations of water infiltration were successfully treated with chemical grouting. To mitigate any minor leaks that may develop overtime, the wall was outfitted with a leakage collection system at each floor.

© 2016 Deep Foundations Institute

CONCLUSIONS

Many challenges were faced during the design and construction of the 520 Park Avenue project. They included geographical constraints, difficult subsurface conditions, and sensitivity of the surrounding adjacent structures. These challenges were solved with innovative design approaches, attention to details, implementation of sound construction techniques, enforcement of good quality assurance measures, and above all, through outstanding communication and cooperation between all members of the Design, Engineering and Construction team.

ACKNOWLEDGMENTS

The authors would like to acknowledge the developer, Zeckendorf; the foundation general contractor, The L'Aquila Group; the secant pile wall subcontractor, Underpinning and Foundation Skanska; the construction management team, LendLease; the Architects, Robert M. Stern, and SLCE; the structural engineers, WSP; and the geotechnical and foundation engineers, Mueser Rutledge Consulting Engineers.

REFERENCES

American Institute of Steel Construction Inc. (AISC), 2005, Thirteenth Edition. Steel Construction Manual, pp. 16.1-70 - 16.1-113.

Brinkgreve, R.B. J., Broere, W., and Waterman, D., 2006, Plaxis 2D, Version 8, User's Manual, Plaxis b.v., Delft, NL.

Megson, T.H.G., 2009, Second Edition. Structural and Stress Analysis, Elsevier Ltd, pp. 133-149.

U.S. Department of Transportation Federal Highway Administration: Drilled Shafts Manual, 2010: Construction Procedures and LRFD Design Methods. Publication No. FHWA-NHI-10-016, pp. 9-1 - 10-17.

© 2016 Deep Foundations Institute

This page left intentionally blank

© 2016 Deep Foundations Institute

ACCUMULATED ROTATIONS OF BUCKET FOUNDATIONS UNDER LONG-TERM CYCLIC LOADS IN SANDY GROUND

Sung-Ryul Kim, Department of Civil Engineering, Dong-A University, Busan, South Korea, +82-51-200-7622, sungryul@dau.ac.kr
Si-Hoon Lee, Rhehwa Engineering Co. Ltd., Busan, South Korea, white2sh@gmail.com
Woong-Jong Park, Design Team, Nambu Construction District Department, Korea Electric Power Corporation, Busan, South Korea, escape22@kepco.co.kr
Juhyung Lee, Geotechnical Engineering Research Institute, Korea Institute of Civil Engineering and Building Technology, Gyeonggi-do, South Korea, leejh73@kict.re.kr

ABSTRACT

A bucket foundation has been considered to be a potential foundation technology for offshore wind turbines. In this study, a series of 1-g model tests were performed to analyze the accumulated rotation of suction bucket foundations under long-term cyclic horizontal loads. The model suction buckets were made to have the embedment ratios of 0.5 and 1. The dry model ground was prepared to have two different soil densities by air-pluviation method. A horizontal cyclic load over 10^4 cycles was applied varying the loading amplitude. Test results showed that the accumulated rotation of the bucket foundation increased with the increase in the number of cycles and load magnitudes. Based on the model test results, a new equation was proposed to evaluate the accumulated rotation of the bucket foundations in sandy ground under long-term cyclic horizontal loads.

Keywords: model test, bucket foundation, accumulated rotation

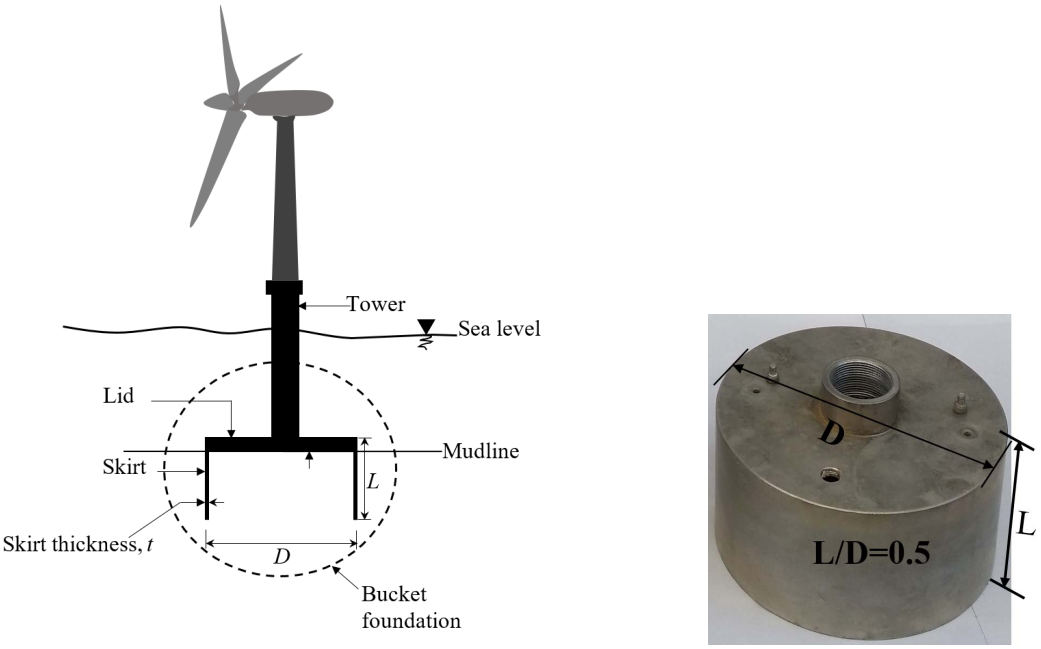
INTRODUCTION

Recently, a bucket foundation has been considered to be a potential foundation technology for offshore wind turbines. In terms of economy, a bucket foundation has been considered to be an economical foundation type at sea beds where ground condition is clay or medium dense sand.

A bucket foundation resembling a bucket is a kind of suction-installed foundation units. It is a skirted steel foundation which is open at the lower end and closed at the upper end by a lid. The embedment depth ratio (L/D) of a bucket foundation is usually less than one. Figure 1 shows an example of a bucket foundation. Offshore wind turbines are subjected to long-term cyclic loading by wind or currents. A bucket foundation is installed in soil grounds, so the long-term cyclic loading may induce the accumulation of soil deformation.

In this study, the accumulated rotations of the bucket foundations in sandy ground were investigated under long term cyclic horizontal load. The number of cycles up to 10^4 cycles was applied varying load magnitude. The accumulated rotations of the bucket foundations in sandy ground were analyzed based on the test results.

© 2016 Deep Foundations Institute



(a) Bucket foundation features (b) Bucket model

Fig. 1. Example of bucket foundation showing (a) basic features (b) bucket model

MODEL TESTS

Figure 2 shows a schematic diagram of the test equipment used in this study. A loading equipment, which is similar to that presented in the works of LeBlanc et al. (2010), was designed and manufactured. The working mechanism of the equipment is described as follows: the weight m_2 is equal to the total weight of the driving motor, the load lever and the small steel frame. When the driving motor is rotated, the moment load due to weight m_1 induces a sinusoidal load to the wire connected to the bucket. The amplitude of the cyclic load is controlled by adjusting the weight m_1. The loading frequency used in this study was 0.25Hz.

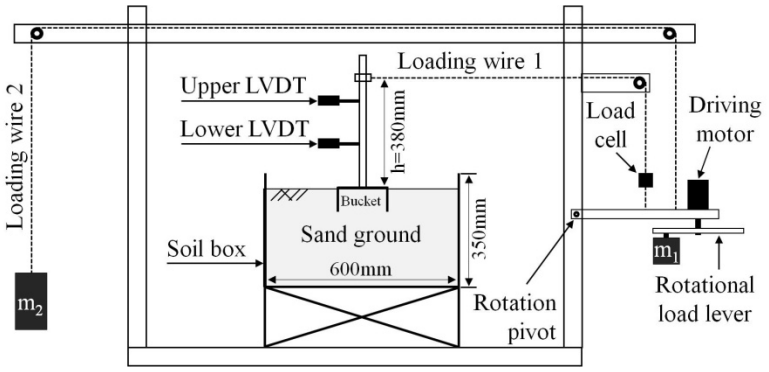


Fig. 2. Schematic diagram of the test equipment

The model bucket was made of aluminum and had a diameter, *D* of 150mm and a skirt thickness, *t* of 1mm. The lengths, *L* of the bucket, were 75mm for *L/D*=0.5 and 150mm for *L/D*=1.0. The model bucket was designed to have a length scale of 1:100. The scaling law was adopted from Wood (2004).

© 2016 Deep Foundations Institute

A dry model ground was prepared to have two different soil densities by air-pluviation method. The sand was dropped into the soil box from the sieve and when the sand layer reached 50mm thickness, the sieve was raised up 50mm to maintain constant drop height. Model grounds of Dr=18% and 25% were made by applying the constant drop heights of 350mm and 550mm, respectively.

The bucket was pushed into the prepared sand ground by using an automatic jacking system. The penetration rate of the bucket was 0.5 mm/s until the bucket lid touched the sand ground.

The rotation of the tower and foundation system was calculated basing on the differential displacement between LVDT1 and LVDT2, and the distance between these two LVDTs. The load-cell was attached to the loading wire for measuring the cyclic load.

The horizontal cyclic load was applied as shown in Figure 3. Up to 10^4 cycles were considered. Figure 3 shows an example of a typical variation of cyclic load with number of cycles, N. The amplitude of the cyclic load is indicated as H_c, which was determined to have a certain ratio, $R_c = H_c/H_0$. H_0 refers to the static failure load.

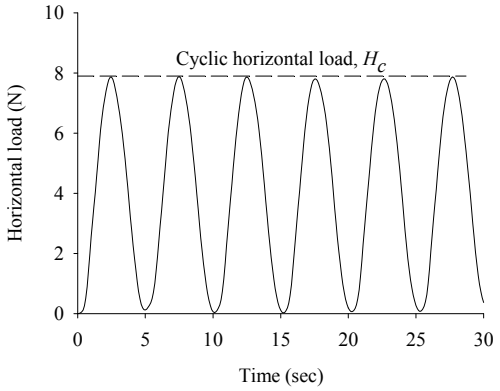


Fig. 3. Typical cyclic load applied to the bucket

TEST RESULTS

A Total of 16 tests were performed; four static loading tests and twelve cyclic loading tests with varying R_c values.

Figure 4 shows the load-bucket rotation curves of the static loading tests. To obtain the horizontal failure load, the tower was pulled horizontally at a constant rate of 0.5mm/s. The horizontal failure load was defined by using a tangential intersection method. The method plots two tangential lines along the initial and later portions of the load-rotation curve, and the load corresponding to the intersections point of these two lines is taken as the failure load (H_0) (Villalobos, 2006; Hung and Kim, 2014). The failure load was 7.60N for L/D=0.5 and 17.66N for L/D=1.0 at Dr=18%, and H_0 was 9.42N for L/D=0.5 and 20.60N for L/D=1.0 at Dr=25%. The failure load increased with the increase of Dr and L/D ratio.

© 2016 Deep Foundations Institute

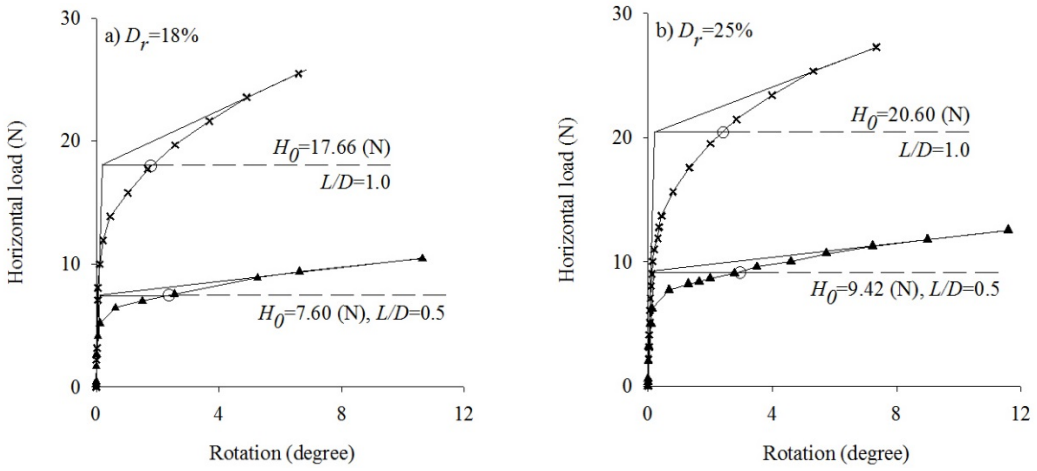


Fig. 4. Horizontal static loading tests and determination of failure load

Figure 5 shows a typical result of the cyclic loading tests. The horizontal displacement of the tower continuously increased with the number of cycles. The displacement rapidly increased at initial cycles and the increasing rate became smaller and constant with the number of cycle.

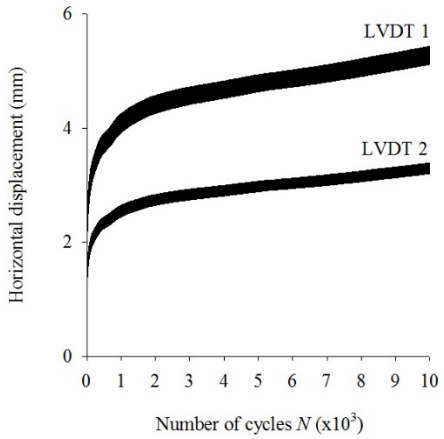


Fig. 5. Horizontal accumulated displacement under cyclic loading

Figures 6 and 7 show the normalized rotation of the bucket. The bucket rotation was normalized dividing (θ_N-θ_0) by θ_0, in which θ_N is the rotation angle at N^{th} cycle and θ_0 is the rotation at the first cycle. The normalized rotation increased with an increase in the number of cycles and R_c ratio.

© 2016 Deep Foundations Institute

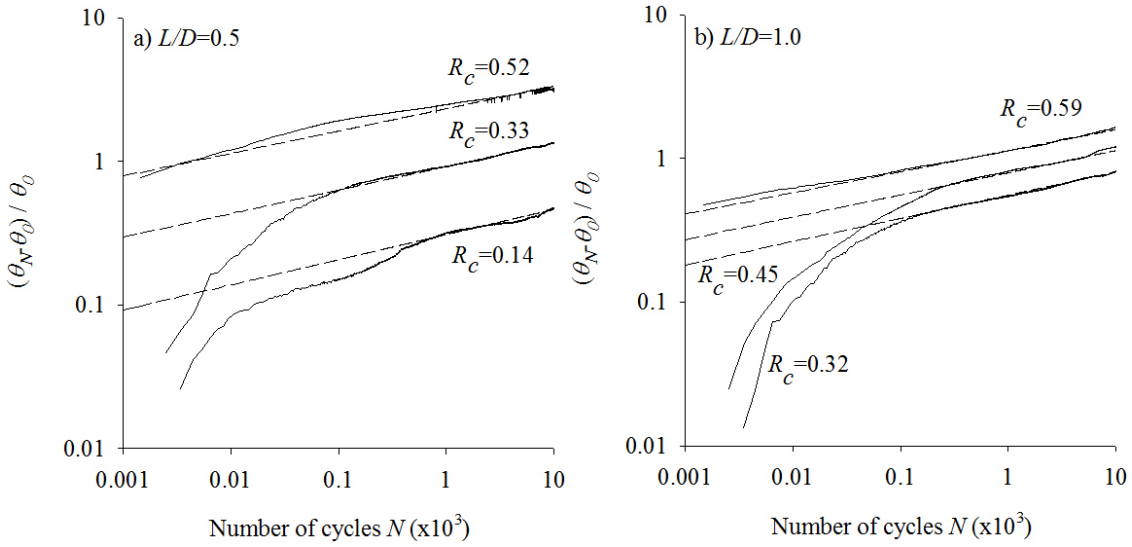


Fig. 6. Accumulated rotation of bucket with various R_c (Dr=18%)

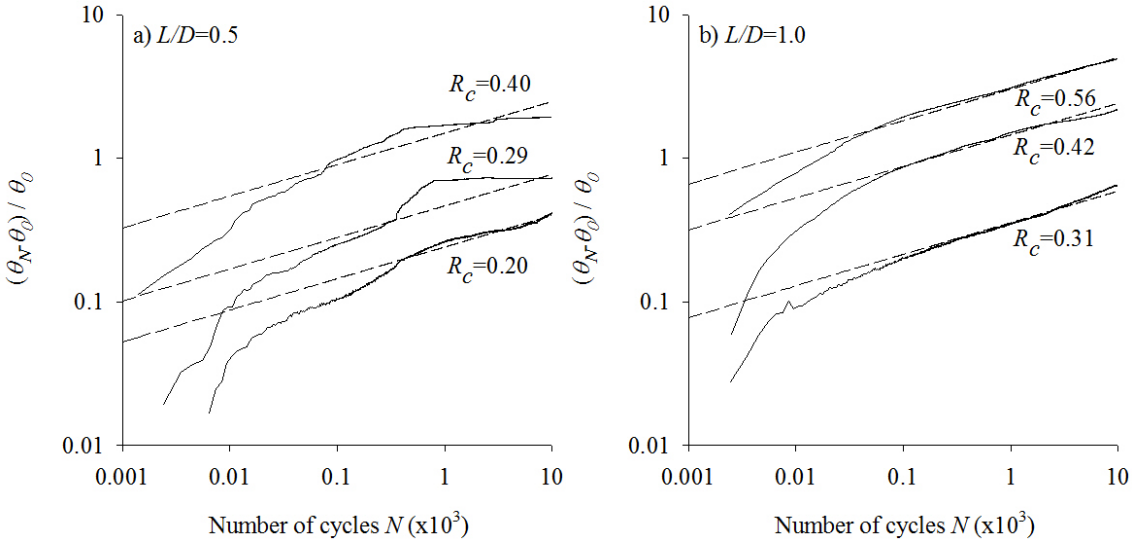


Fig. 7. Accumulated rotation of bucket with various R_c (Dr=25%)

Based on the test results, empirical equations were introduced to evaluate the accumulated rotation of the bucket foundations in sandy ground. The input parameters are the number of cycle N, L/D and R_c ratio. The form of the proposed equation was mainly derived by referring to those proposed by other works for monopiles in sand (i.e. LeBlanc et al., 2010), and for bucket foundations in sand (i.e. Zhu et al., 2013). The accumulated rotation is expressed as shown in Eq.[1].

$$\frac{\theta_N-\theta_0}{\theta_0} = T_b \times N^{\alpha} \times \beta \qquad [1]$$

Where θ_N is the accumulated rotation after N cycles, θ_0 is the rotation obtained from the first cycles or from the static load-rotation curve at the same load magnitude. The α and β parameters are the factors to take

© 2016 Deep Foundations Institute

into account the effect of the number of cycles N and L/D ratios, respectively. T_b was suggested to consider the R_c ratios.

Least-square regression analyses were carried out to determine the α, β and T_b parameters. Based on these analyses, α=0.14, β=1.8(for L/D=0.5), β=0.9(for L/D=1.0) for Dr=18% and α=0.22, β=1.3(for L/D=0.5), β=1.0(for L/D=1.0) for Dr=25% were obtained. The T_b parameter can be expressed as a function of R_c as shown in Eqs. [2] and [3].

$$T_b = 1.06 \times R_c^{1.421} \text{ at } Dr=18\% \quad [2]$$

$$T_b = 3.72 \times R_c^{2.961} \text{ at } Dr=25\% \quad [3]$$

CONCLUSIONS

1-g model tests were performed to analyze the accumulated rotation of a bucket subjected to long-term horizontal cyclic load. The accumulated rotations of the bucket foundation increased with the increasing number of cycles and cyclic load amplitude. Based on the results, equations that can evaluate the accumulated rotation of the bucket foundation in sand ground, were proposed. The equations consider the effect of number of cycles N, the embedment ratio L/D, and the cyclic horizontal load ratio, R_c. The proposed equation properly defined the accumulated rotation of the bucket foundation in comparison with the model test results.

ACKNOWLEDGEMENT

This research was supported by Basic Science Research Program through the National Research Foundation of Korea(NRF) funded by the Ministry of Education (2014R1A1A2055858 and 2016R1A6A1A03012812).

REFERENCES

Hung, L. C. and Kim, S. R. (2014), "Evaluation of undrained bearing capacities of bucket foundations under combined loads", Marine Georesources and Geotechnology 32, pp. 76-92.

LeBlanc, C., Houlsby, G. T. and Byrne, B. (2010), "Response of stiff piles in sand to long-term cyclic lateral loading", Geotechnique, Vol. 60, No. 2, pp. 79-90.

Wood, D. M. (2004), Geotechnical Modelling, Spon Press, New york, USA.

Villalobos, F. A., (2006), "Model testing of foundations for offshore wind turbines", PhD dissertation, Keble College, University of Oxford.

Zhu, B., Byrne, B. W. and Houlsby, G. T.(2013), "Long-term lateral cyclic response of suction caisson foundations in sand", Journal of Geotechnical and Geoenvironmental Engineering, ASCE, Vol. 139, No. 1, pp. 73-83.

© 2016 Deep Foundations Institute

ACIP PILE PERFORMANCE AND INSTALLATION IN THE NORTHEASTERN UNITED STATES

W. Morgan NeSmith, Jr, PE Berkel & Company Contractors, Inc. Austell GA. USA, 770.941.5100, mnesmith@berkelapg.com

ABSTRACT

Augered-cast-in-place (ACIP) pile installation technology has matured extensively since the first auger, pressure grouted pile was patented in 1959. The current technology allows for successful pile installation across a variety of stratigraphies to meet various project load resistance requirements. This paper presents an overview of current ACIP techniques by comparing a number of case histories in a variety of geologic settings from Eastern Pennsylvania, New York City and New Jersey to demonstrate ACIP pile constructability in soft soils as well as the penetration, and resulting significant loads resisted, of ACIP piles in dense soils and intermediate geo-materials. Geologic settings that will be discussed include the Piedmont and Coastal Plain geologic provinces as well as glacial till deposits.

Keywords: Deep Foundations, Piles, Augercast, Augered-cast-in-place, Auger pressure grouted, ACIP, APG

INTRODUCTION

The author, along with two colleagues, published an article in Deep Foundations magazine (NeSmith et al, 2013) which described a number of the advances in equipment, techniques, installation monitoring and post-construction testing that have expanded the geologies in which Augered Cast-in-place (ACIP) piles are installed as well as increasing their efficiency in some traditional ACIP pile geologies. The author uses the term efficiency to refer to the load resisted by a pile of a certain diameter and the increased efficiency noted refers to increased allowable loads over those traditionally resisted by piles of certain diameter (or a reduction in pile diameter from that which was traditionally used to support a certain design load). The performance and installation of ACIP piles in a variety of geologies in the Northeastern U.S. are discussed herein.

PIEDMONT PHYSIGRAPHIC PROVINCE

The Piedmont physiographic province stretches from Alabama to the east through Georgia and up the east coast, just west of the Coastal Plain to Pennsylvania and New York (Brown, 2002). It generally consists of soils weathered in place from the underlying bedrock, which is typically a combination of granite, schist and gneiss depending on the location within the province. The author's experience in the Northeastern US has been on sites where alluvial or coastal plain soils overly the residual soils and partially weathered or intact rock of the Piedmont. The example presented here, from a site on Walnut St in Philadelphia PA, is representative of these projects.

A log of boring with the representative stratigraphy at the site is presented in Figure 1. The stratigraphy includes urban fill and four layers of alluvial soils over residual soil (referred to as weathered rock) with SPT N-values of 80 to 100. Not shown are the underlying weathered rock with N-values > 100 (a drillable intermediate geo-material often referred to as Partially Weathered Rock, PWR) and auger refusal on bedrock.

Project requirements called for piles to be installed from a basement level approximately 25-ft below boring level. The resulting test pile (with applied compressive load vs pile-head deflection shown in Figure 2) was approximately 60-ft long. It can be seen that there is a small change in slope of the load-deflection plot at a load of about140 tons, after which the relationship is fairly liner to the maximum applied load of 500 tons (the design load of the piles was 200 tons).

© 2016 Deep Foundations Institute

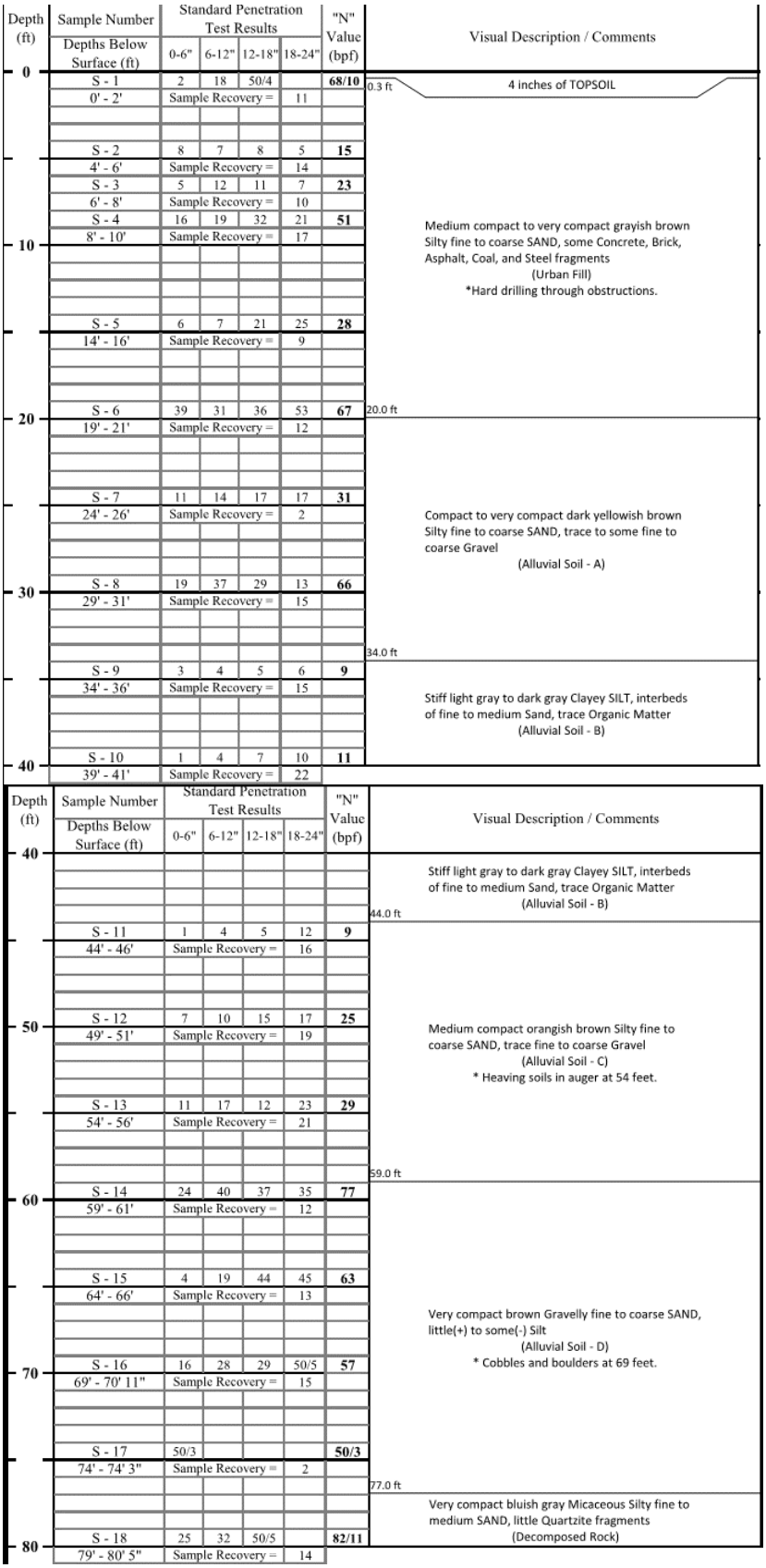


Figure 1 – Boring showing Alluvial Soil Over Weathered Rock of Piedmont

© 2016 Deep Foundations Institute

In the author's experience, these results are typical where modern techniques are employed to ensure auger penetration through the PWR to refusal on the underlying bedrock. These include using a gearbox with appropriate torque, an auger tip with teeth conducive to penetrating the very densely packed PWR, and often introducing compressed air to force the PWR up the auger flights. The allowable load on an ACIP pile so installed is typically limited by structural code limitations rather than geotechnical capacities. Thus, rather large compression loads (e.g. over 200 tons on a single 18-in diameter pile or 500 tons on a single 24-in diameter pile) can be resisted. ACIP piles can then be very efficient due to the speed at which they can be installed (typically one drill down and one withdrawal as the pile is cast) as well as the cost of grout compared to the cost of steel for an equivalently loaded driven pile. In urban areas, such as the subject site, the relative reduction in noise and vibrations compared to driven piles is also advantageous. It should be noted that if insufficient equipment or techniques are used and refusal is encountered at or within the PWR, the geotechnical capacity may govern and the pile may not perform as efficiently as it could have. Also, where the underlying bedrock of the Piedmont is very shallow or very large axial or lateral loads are to be resisted (particularly within a small footprint), large diameter drilled shafts may be more efficient than large groups of ACIP piles.

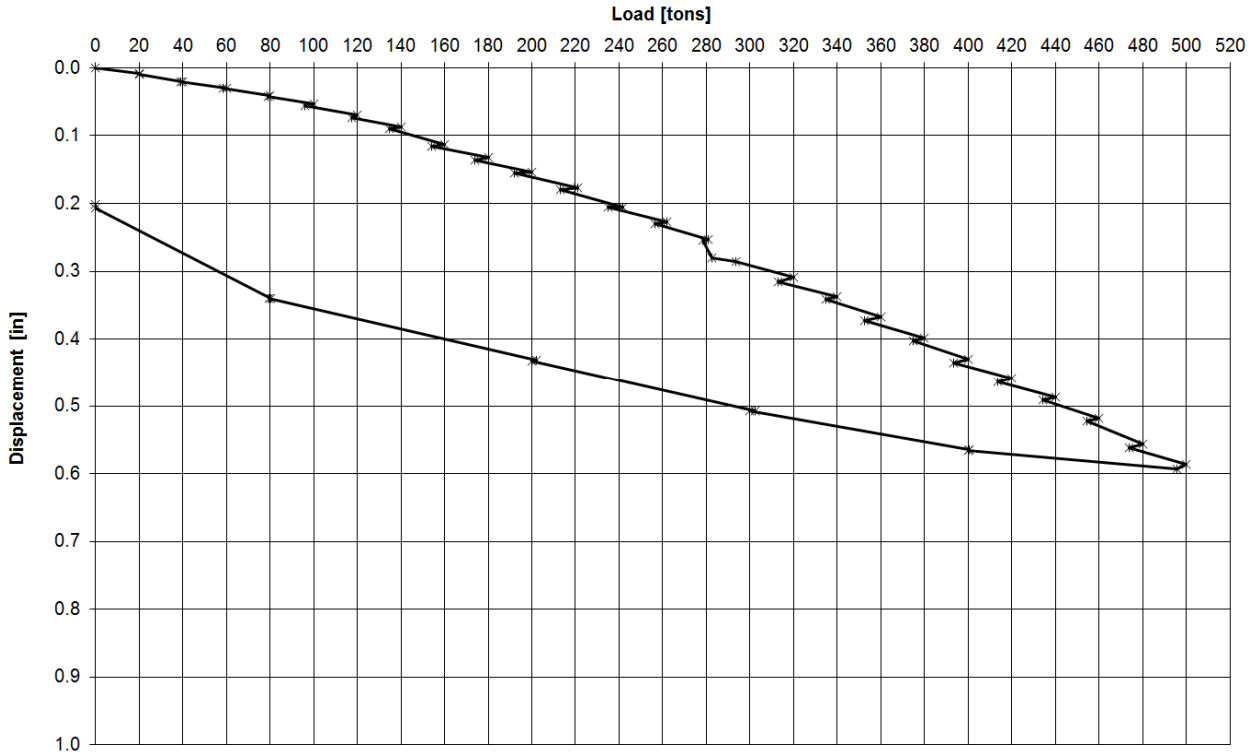


Figure 2 – Applied Compressive Load vs. Pile-head Displacement – 18-in dia. ACIP Pile x 59-ft

SOFT ALLUVIAL SOILS

In contrast to the previous example, soft soils are easily penetrated by augering, however, constructability and pile shaft integrity may be questioned without appropriate monitoring and post-construction verification testing. The following example is from an industrial/utility site adjacent to the Raritan River in Sayreville NJ. The site included existing facilities in close quarters. The proposed expansion was within the footprint of existing facilities. Because of this, the owner/designer preferred a drilled and grouted system to reduce noise and vibrations during installation.

© 2016 Deep Foundations Institute

Design compression loads were 60 tons per pile an although a 12-in diameter bored pile would have been suitable based on structural code limitations, due to the presence of very soft alluvial deposits, 14-in diameter piles were proposed to provide excess pile diameter beyond the structural requirements.

The results of a Cone Penetrometer Test (CPT) are shown in Figure 3 and results of a Dilatometer Test (DMT), performed due to the very low qt values recorded during the CPT, are shown in Figure 4. Based on the interpreted shear strengths from the DMT, it was considered that the 14-in piles could be successfully installed into the lower dense alluvial sand to the underlying bedrock (see refusal level in Figure 3).

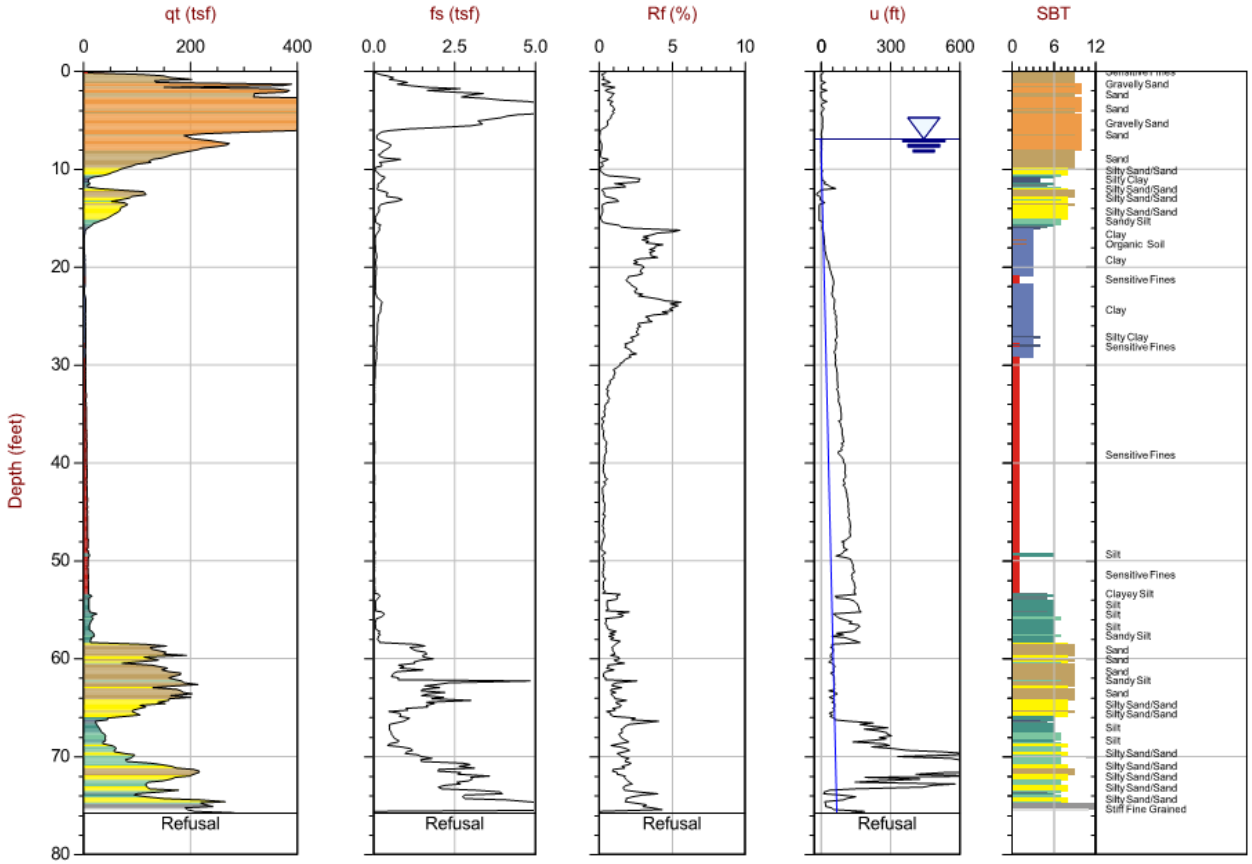


Figure 3 – CPT Result from Soft Alluvial Site

Shaft integrity of the piles was verified by using Thermal Integrity Profiling. In this method, a wire with temperature sensors located at 1-ft intervals is attached to the center bar inserted into the pile and temperature along the entire length of the pile is automatically recorded through the peak heat of hydration (typically for 24 to 36 hours). There is also a method where a PVC tube is attached to the center bar and a temperature probe is lowered through the tube to measure temperature along the length of the pile, however the wire method was used for the subject project. The temperature at the peak heat of hydration is plotted with depth and the diameter of the pile is then estimated from the temperature vs. depth readings along with the volume of grout placed in the pile.

For the subject project, the test pile and twenty percent of production piles were profiled. Temperature vs. depth and the corresponding estimated pile radius of the compression test pile at the subject site are presented in Figure 5. It can be observed that the estimated pile radius increased in the very soft soils until such depth as the shear strength of the soils increases to a level as to prevent this increase and keep the pile radius closer to plan.

© 2016 Deep Foundations Institute

The pile radius in the dense alluvial soils is also much closer to plan, as would be expected. For this project, assuring the grouted piles had the appropriate diameter when completed was more important than the particular installation equipment selected. This relatively new method of evaluating the diameter of cast-in-place piles allowed for the use of ACIP piles, which could be installed more quickly than other cast-in-place methods, used less expensive materials than driven steel piles, and avoided vibration issues with the new facilities being situated directly between and next to existing facilities.

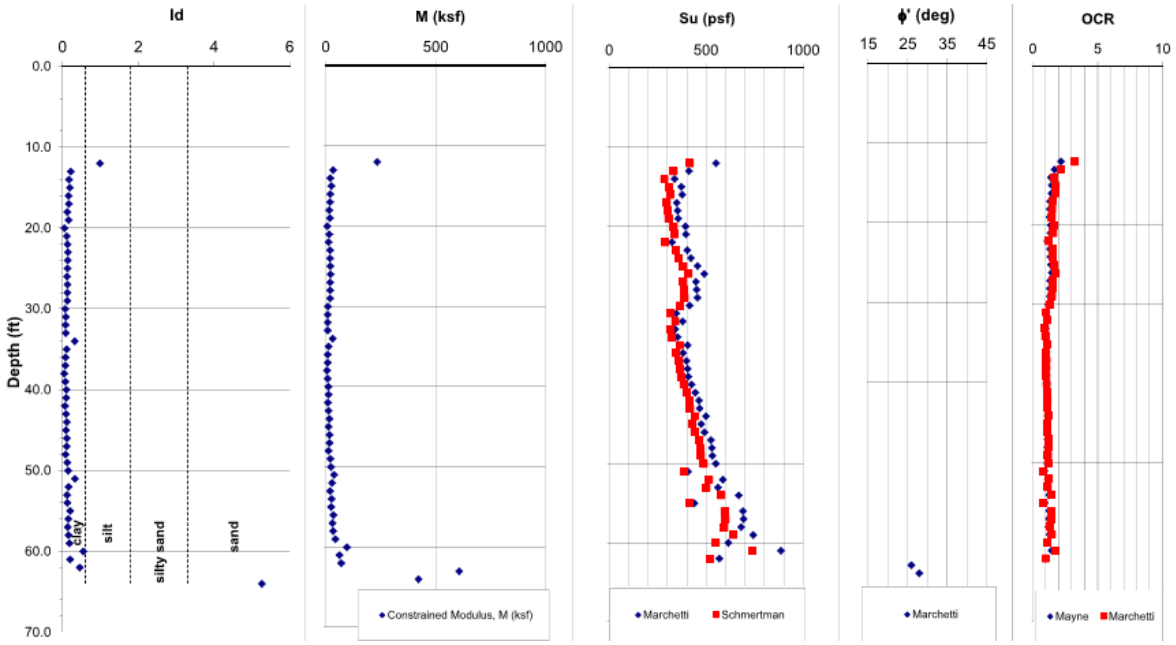


Figure 4 – Dilatometer Results from Soft Alluvial Site

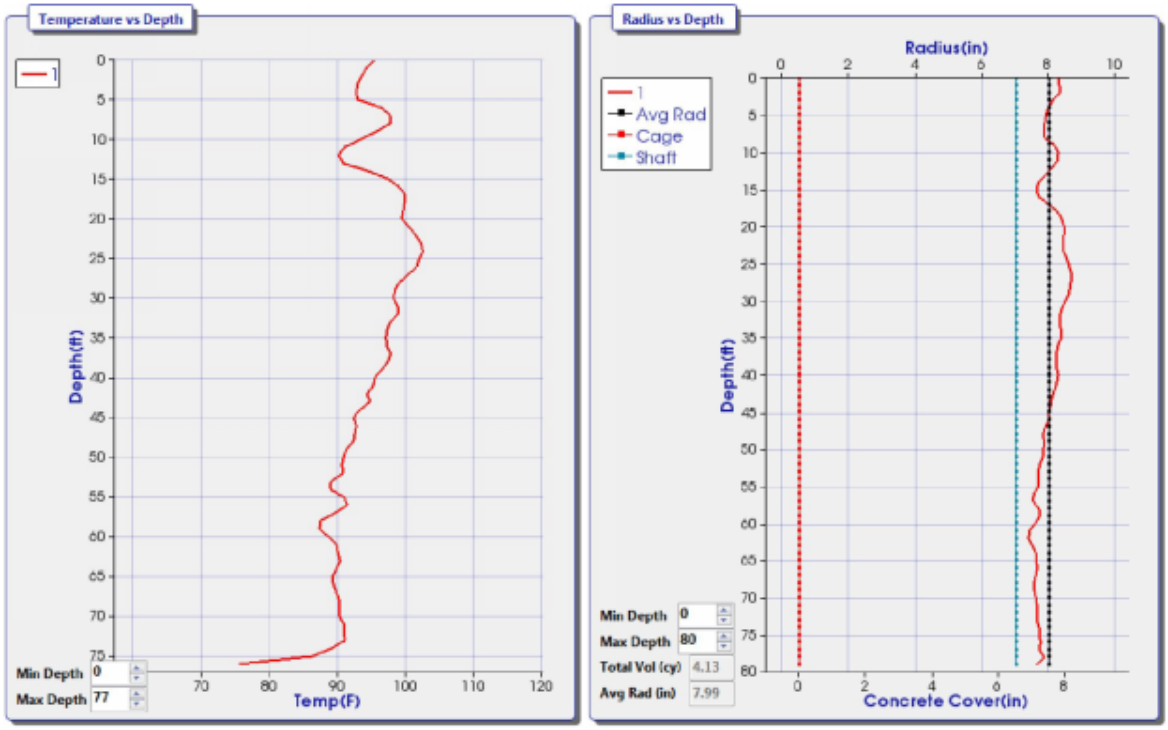


Figure 5 – Thermal Integrity Profiling of 14-in dia. x 76-ft ACIP Pile

© 2016 Deep Foundations Institute

SOFT TO STIFF COASTAL PLAIN SOILS

Coastal Plain soils in the Northeastern US often consist of interbedded layers of various density and soil make-up from the deposition (and often subsequent partial erosion) of these soils during different historic geological events. Figure 6 is a CPT result from a typical site in Mercer County NJ and is an excellent example of this. Fill soils and medium dense sands overly firm fine-grained soils, below which are a layer of dense sand followed by a heavily overconsolidated fine-grained deposit. ACIP piles were proposed to resist 200-ton design compression loads. Based on available design methods for coarse and fine-grained soils, 18-in diameter ACIP piles to a depth of 80-ft below boring level were proposed.

In this example, it is important for an ACIP pile to quickly penetrate the dense sands from 40-ft to 55-ft depth, as well as the stiff to hard fine-grained soils below, so as not to over-excavate any sandy soil layers. This requires a gearbox with significant torque and in this example, the potential introduction of compressed air in the lower fine-grained stratum to aid in moving these stiff to hard soils up the auger flights.

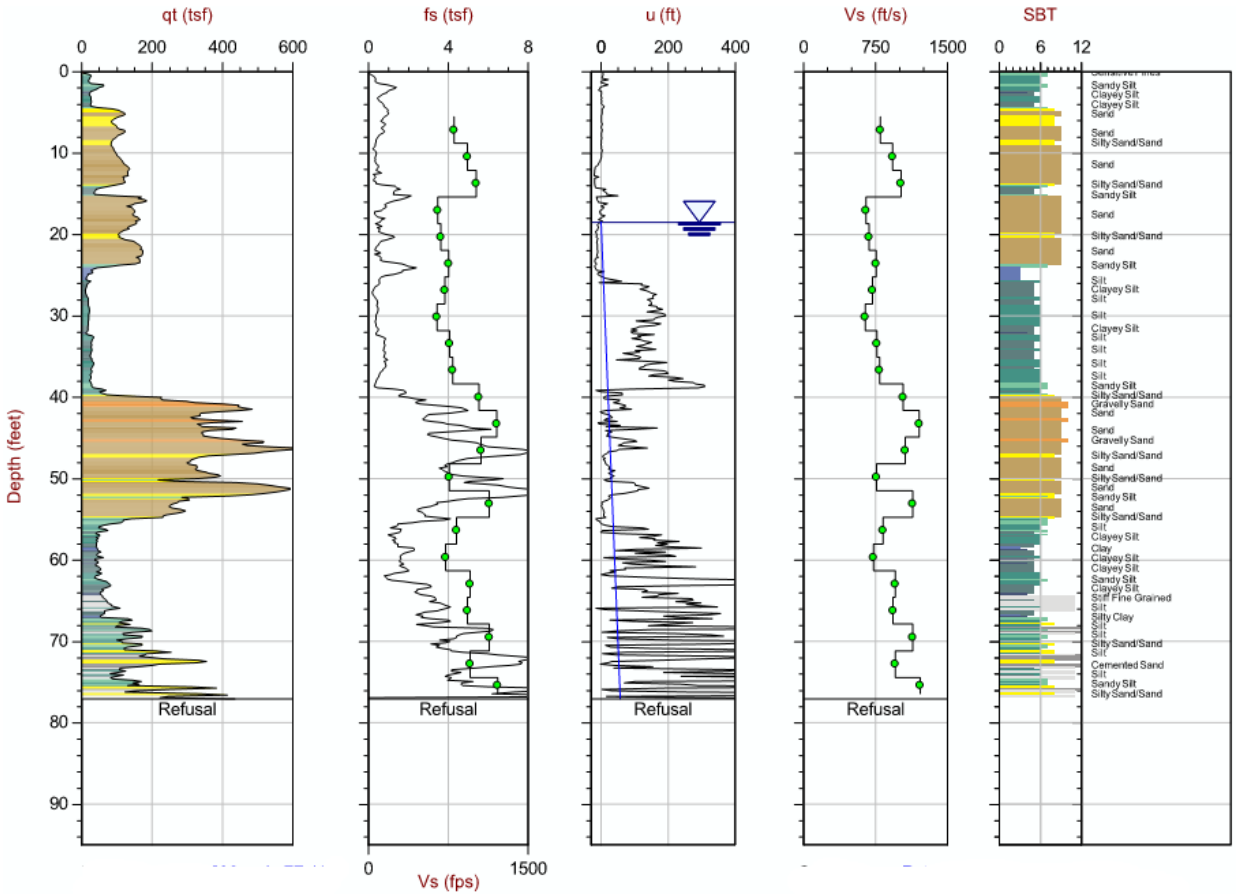


Figure 6 – CPT of Interbedded Coastal Plain Soils

A plot of applied compression load vs. pile-head deflection is presented in Figure 7. The plot unfortunately includes the estimation of ultimate load as per the Davison Offset Limit (by others), which the author considers inappropriate for the estimation of ultimate load of ACIP piles (NeSmith and Siegel, 2009; Studlien et al, 2013). Regardless, it is clear that the pile-head deflection does not reach a level to apply any of the methods listed in the International Building Code (IBC, 2015) and that the ultimate load is in excess of the maximum applied load.

© 2016 Deep Foundations Institute

In turn, it is also well in excess of the predicted performance by available design methods. The successful installation of ACIP piles into a stratum where the code-based structural limits of the allowable load are reached before geotechnical failure made the ACIP piles very efficient due to the speed at which they are installed compared to other bored and cast-in-place methods as well as material costs.

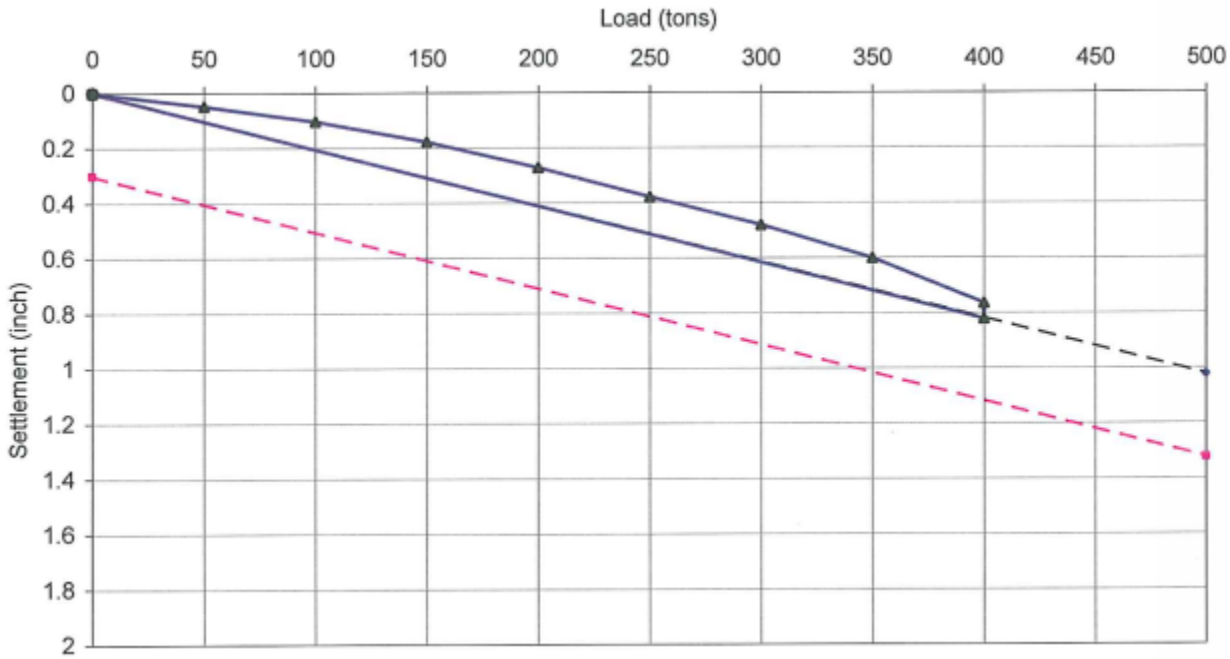


Figure 7 – Applied Compression Load vs Pile-head Deflection of 18-in dia. X 80-ft ACIP Pile

COARSE-GRAINED GLACIAL TILL

The final example included is a site near the water at a New York City municipal facility in the northern section of Queens which consisted of a series of sites with facilities that required pile support. The general stratigraphy is shown in Figure 8 and is representative of the various separate locations. SPT N-values are typically shown at 5-ft intervals with corresponding soil descriptions. Generally, below up to 10-ft of urban fill, typically dense to very dense sandy till was present, however, a portion of the site included significant stiff to very stiff clay till was present.

ACIP piles, 16-in in diameter, were proposed to resist 150-ton to 160-ton design compression loads, depending on the location within the project extents. Figure 10 shows the applied load vs. pile-head deflection for the test pile installed in the predominantly clay till portion of the site (2nd boring profile from right in Figure 8) while Figure 11 shows the same results for the test pile installed in a predominately coarse-grained till portion of the site (in this case, near the boring profile shown on the far right of Figure 8). The successful application of ACIP piles required, again, a high-torque gear box and appropriate auger-tips (cutting teeth) depending on the predominant soil type at each discrete facility location.

The test pile in Figure 10 is probably about at its interpreted ultimate load according to the Butler-Hoy method (Studlein et al, 2013) at its maximum applied load of about 375 tons. The test pile in Figure 11 did not have enough pile-head deflection to estimate ultimate load, however, it is clear that the ultimate load is well in excess of the maximum applied load of 300 tons. In both cases, the ultimate load of the test piles was in excess of that which would be predicted by currently available design methods. Historically similar facilities have been supported on driven piles or other cased and bored-piles. The high-torque equipment and development of more specific cutting-teeth for different predominant soil types allowed ACIP piles to be installed to a level to provide a more economical foundation in this case.

© 2016 Deep Foundations Institute

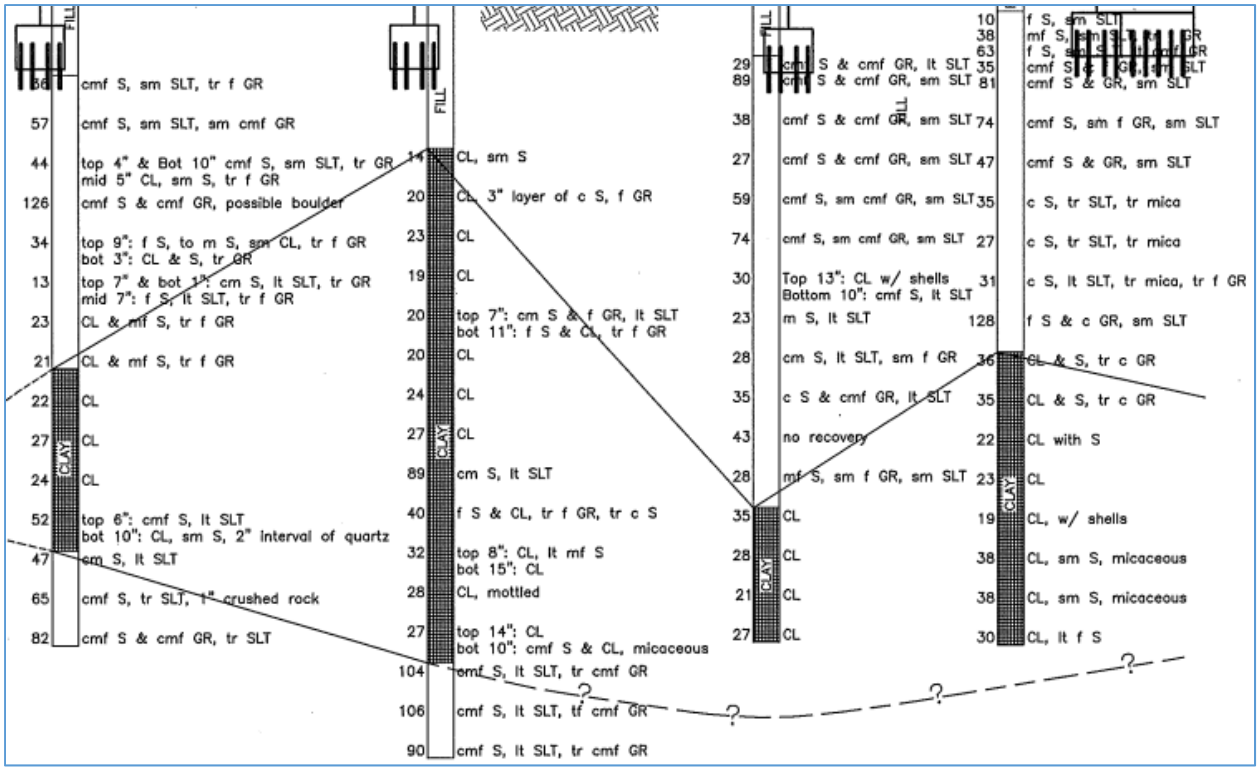


Figure 8 – N-values and Soil Descriptions of Glacial Till in Queens NY


Figure 9 – Boulders Removed in the Upper 25-ft of Queens NY Site to Facilitate ACIP Pile Installation

© 2016 Deep Foundations Institute

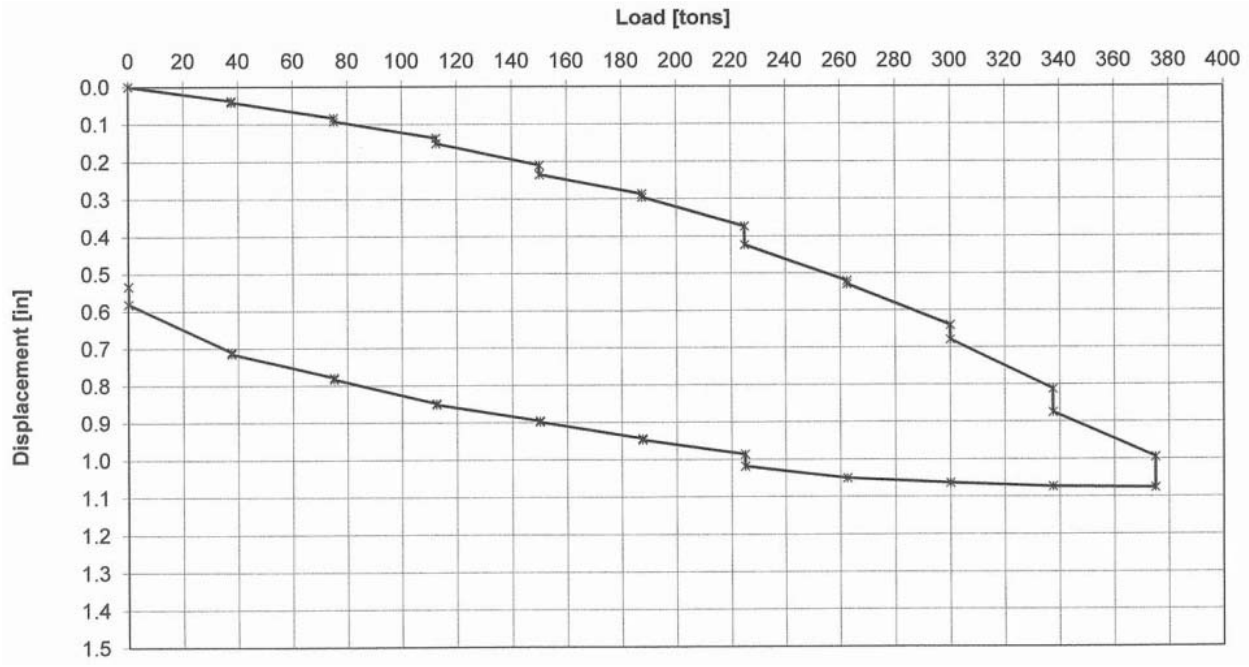


FIGURE 10 – 16-in ACIP Pile x 82-ft in Predominantly Clay Profile

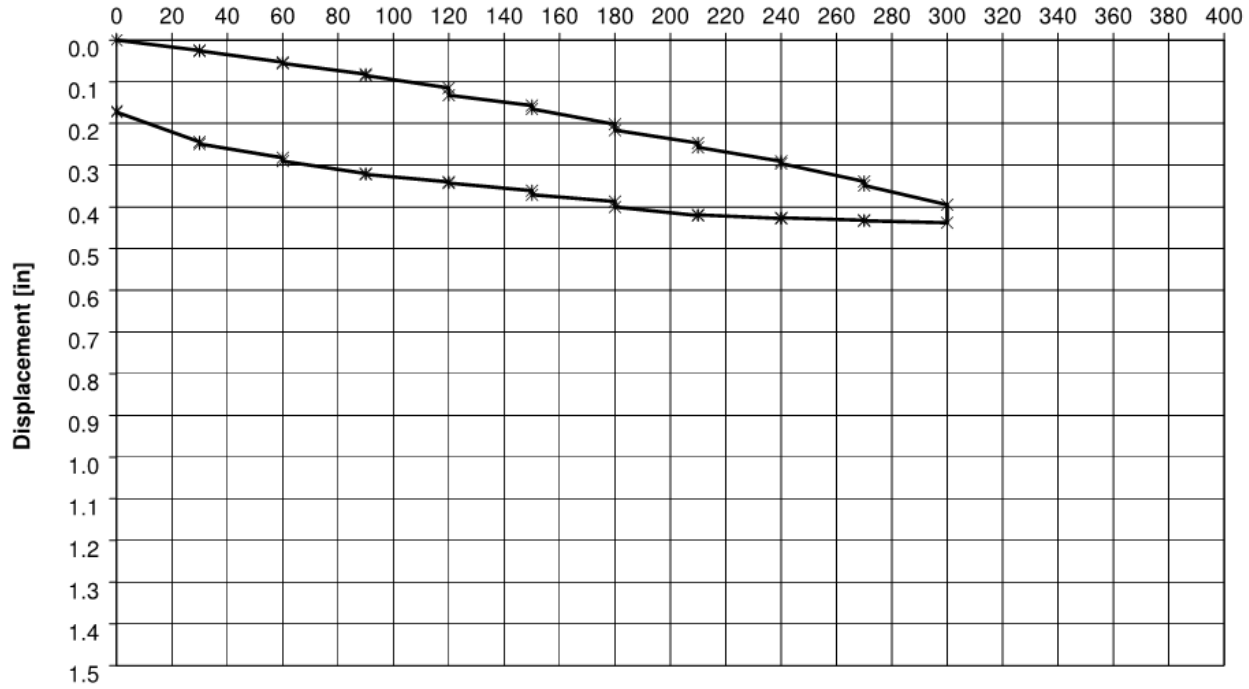


FIGURE 11 – 16-in ACIP Pile x 77-ft in Predominantly Sand Profile

© 2016 Deep Foundations Institute

CONCLUSIONS

When they can be properly installed, ACIP piles offer an efficient foundation option due to their speed of installation compared to other bored, cast-in-place piles as well as the cost of materials compared to driven piles. ACIP pile equipment and installation technology has advanced to a point where piles are being successfully installed in geologies which, in previous generations, they might not have been, often resulting in higher loads being resisted by these piles than were previously available. Additionally, post-construction verification technology has advanced to a level where successful construction of ACIP piles can be verified on very soft, potentially problematic soils. These advances have expanded both the geographic areas in which ACIP piles can be installed as well as the projects on which they may offer some efficiencies (more heavily loaded than moderately loaded structures).

In very dense coarse grained soil, as well as stiff to hard fine-grained soils, recent measured ACIP pile performance is often greater than would be predicted by available models/methods. The same phenomenon has been observed for ACIP piles installed in fine and coarse grained till and, in particular, in intermediate geo-materials (including the PWR used as an example here) where unit shaft resistances are SIGNIFICANTLY higher than dense or hard soil model would predict. So while industry advances have expanded the range of materials into which ACIP piles can be installed and increased the maximum loads these piles can support, current design models should only be considered a potentially lower-bound guide to ACIP pile performance in these materials.

REFERENCES

Brown, D.A. (2002). “Effects of Construction on Axial Capacity of Drilled Foundations in Piedmont Soils”. Journal of Geotechnical and Geoenvironmental Engineering. Volume 128. No. 12. ASCE. Pp. 967-973.

International Code Council (2015). International Building Code, Chapter 18 Soils and Foundations. 30 May 2014 (last printing October 2015).

NeSmith, W.M. and Siegel, T. (2009). Shortcomings of the Davisson Offset Limit Applied to Axial Compressive Load Tests on Cast-in-Place Piles. Contemporary Topics in Deep Foundations. Selected Papers from the 2009 IFCEE. GSP 185, pp. 568 – 574. Orlando FL, 15 – 19 March 2009.

Studlein, A.W., Reddy, S.C., Evans, T.M. (2014). “Interpretation of Augered Cast in Place Pile Capacity Using Static Loading Tests”. The Journal of the Deep Foundations Institute. Vol 8, No. 1, pp. 39 – 47. 09 June 2014.

© 2016 Deep Foundations Institute

AN ALTERNATIVE APPROACH FOR ESTIMATING THE VERTICAL CAPACITY OF L-SHAPED SEGMENTAL UNDERPINNING SYSTEMS IN URBAN BASEMENT CONSTRUCTION

Abid O. Adekunte, Geobond (UK) Limited, Farnborough, Hampshire, U.K, +44 1252 515 168, abida@geobond.co.uk
David Hilton, ABTECH Basement Systems Limited, Farnborough, Hampshire, U.K, +44 1252 515 168, sales@abtechbasements.co.uk
David Greentree, Geobond (UK) Limited, Farnborough, Hampshire, U.K, +44 1252 515 168, engineers@geobond.co.uk

ABSTRACT

The construction industry is witnessing an upsurge in demand by property developers to have basements incorporated into their residential and commercial development schemes. This is attributable to perceived improvement to aesthetic and commercial values of buildings by underground space, amongst property owners. This trend is compelling more owners of buildings with no basements to explore the possibility of creating underground additional space beneath their existing buildings. The creation of a basement beneath an existing building entails the installation of a reinforced concrete (RC) underpinning system, temporary works, bulk excavation to basement formation level and construction of the basement structure, with associated aesthetic finishes.

The L-shaped segmental RC underpins are a common system of choice for such underpinning works. They are multi-functional; providing vertical support to the existing superstructure, providing lateral support to earth and groundwater, supporting temporary and permanent surcharge loads from adjacent structures and services, whilst also forming part of the basement slab. This paper focuses on the first function of the L-shaped RC underpins; capacity under vertical compressive loading from the superstructure. The most common industry approach for the prediction of vertical capacities of L-shaped underpins is the old-fashioned Meyerhof's (1953, 1963) effective width method, which is based on the traditional bearing capacity theory, whilst accounting for correction factors for eccentricity and foundation depth.

The traditional bearing capacity formula is surrounded by a significant degree of uncertainty; estimates are highly user-dependent, as capacity prediction is sensitive to the chosen angle of shearing resistance (ϕ), while there are difficulties in accurately measuring the in-situ ϕ value of cohesionless soils. In addition, the effective width approach has been shown to be very conservative by many research workers. The segmental RC underpins presented in this paper have been designed with an alternative less conservative method, which involves the use of a recently proposed consistent work-hardening plasticity model calibrated with field-based tests on footings of various aspect ratios and relative embedment in sand. The paper highlights the principles behind underpinning works for urban basement construction, the design of L-shaped RC underpins with the recently proposed plasticity model and the advantages of the method over traditional bearing capacity solutions and pre-existing plasticity models.

Keywords: underpinning, basements, eccentric loading, bearing capacity, moment, plasticity models.

INTRODUCTION

L-shaped segmental underpins are often used to enable the construction of basements underneath existing buildings. As illustrated in Fig. 1, they are subject to a combination of vertical compressive loading from the existing superstructure and lateral loading from the retained earth and groundwater. Because of the geometry of the underpins, the compressive loading from the existing building is transferred to the underpin

© 2016 Deep Foundations Institute

base as vertical eccentric loading. The design of footings to support vertical eccentric loading is a more complex problem when compared with centrally loaded footings. Designers of L-shaped underpins typically adopt the Meyerhof's (1953 & 1963) effective width approach or Vesic's (1973) extension to the method. Both are essentially based on the traditional bearing capacity formula (see equation 1), but modified with correction factors to account for load eccentricity, load inclination and foundation depth;

$$V_u = [½\gamma B N_\gamma S_\gamma + c N_c S_c + q N_q S_q] \,.\, A_{footing} \quad \text{---------- [1]}$$

In equation 1, V_u is the ultimate vertical loading that can be supported by the foundation, B is foundation width, $A_{footing}$ is foundation area, c is unit soil cohesion, γ is the effective unit weight of the soil beneath foundation within the failure zone, q is the effective overburden pressure at foundation depth, N_c, N_γ & N_q are dimensionless bearing capacity factors, S_c, S_γ & S_q are dimensionless shape factors.

Foundation design with equation 1 is an approach surrounded by a great deal of uncertainty. The equation is very sensitive to the angle of shearing resistance ϕ of the bearing stratum e.g. bearing capacity factor N_γ increases by five-fold when ϕ increases from 30° to 40°, while there is difficulty in accurately measuring the in-situ ϕ value of cohesionless soils. Also, there are marked differences between bearing capacity factors recommended by different workers as illustrated in Fig. 2; particularly for $\phi > 40°$. The main implication of these is that predictions based on the traditional bearing capacity formula tend to be highly user-dependent. Ingra & Baecher (1983) showed that for small uncertainty in soil properties, variation in predicted bearing capacity using the traditional bearing capacity equation ranges between 20%-30%. In addition, Sieffert & Bay-Gress (2000) showed predictions based on the traditional bearing capacity approach to be conservative, when compared with experimental measurements.

Based on traditional bearing capacity solution, Meyerhof (1953) proposed that the bearing capacity of an eccentrically loaded footing may be calculated with the equation;

$$q_{ue} = q_u . R_e \quad \text{---------- [2]}$$

In equation 2, q_u is the ultimate capacity of a centrally loaded footing estimated with equation 1, ignoring bending moments. R_e is a reduction factor accounting for load eccentricity.

For cohesive soils, R_e is given by;

$$R_e = 1 - 2.e/B \quad \text{---------- [3]}$$

where B and e are footing width and load eccentricity respectively. For cohesionless soils with $0 < e/B < 0.3$, R_e is given by;

$$R_e = 1 - (e/B)^{0.5} \quad \text{---------- [4]}$$

While Meyerhof's (1953) solution is based on the traditional bearing capacity theory that has already been described as flawed for a number of reasons, the approach has also been shown to produce very conservative estimates by many workers e.g. Gourvenec & Randolph (2003), Okamura et al. (2002), Ukritchon et al. (1998). The method has also been regarded as old-fashioned by other workers e.g. Houlsby & Byrne (2001) and as an alternative, they have recommended the use of work-hardening plasticity models, which express the interaction between vertical loads (V) and overturning moments (M) with a yield surface in V-M space, similar to the one shown in Fig. 3. Any point on the yield surface corresponds to the load combination (vertical loading & moment) that would result in the failure of a footing. In Fig. 3, V is applied vertical loading, V_u is ultimate vertical capacity if footing is centrally loaded, M is overturning moment and B is

© 2016 Deep Foundations Institute

footing width. Generally, yield loci in V-M space assume parabolic cross-sections, with maximum overturning moment corresponding to $V/V_u = 0.5$.

In recent years, a number of plasticity models have been proposed by workers e.g. Georgeadis & Butterfield (1988), Nova & Montrasio (1991), Gottardi et al. (1995 & 1999), Bransby & Randolph (1998), Byrne & Houlsby (1999), Okamura et al. (2002), Zdravkovic et al. (2002). Most of these have been calibrated with laboratory-based experimental works on surface scale footings in test tanks and centrifuges. As each model has been calibrated with a single surficial footing, these plasticity models fail to account for the influence of aspect ratio/geometry and relative embedment on footing capacity. In addition, data obtained from laboratory-based test tank experiments are often affected by modelling difficulties, which include; boundary conditions and control of soil properties, scale effects due to low stress levels and dimensional considerations. Therefore, many of these plasticity models are hardly relevant to practical engineering applications.

As a development over pre-existing plasticity models, Adekunte (2011) proposed and validated a new plasticity model for eccentrically loaded footings, which accounts for the influence of both aspect ratio and relative embedment. Adekunte's (2011) plasticity model was proposed in the form of an analytical equation, which gives an approximate fit to the shape of the yield loci. This is presented in equation 5 below:

$$M/BV_u = f\,\alpha\,\varphi\,r\,(1 - r) \quad \text{---------- [5]}$$

In equation 5, M is overturning moment, V_u is ultimate vertical capacity of footing if loaded centrally, B is footing width, f is a dimensionless factor that accounts for the influence of footing embedment on the size of the failure envelope, which is expressed as;

$$f = 1 + 0.1\,(d/B) \quad \text{---------- [6]}$$

α is a dimensionless factor accounting for the influence of aspect ratio on size of the failure envelope and this is expressed as;

$$\alpha = (A_s)^{-0.205} \quad \text{---------- [7]}$$

where A_s is aspect ratio. φ is a dimensionless parameter, which defines the size of the failure envelope.

Also, in equation 5, r is expressed as;

$$r = V/V_u \quad \text{---------- [8]}$$

where V is applied vertical load.

Adekunte's (2011) plasticity model was calibrated with a series of scale footings of various aspect ratios, tested in the field at various relative embedment below ground. Its main advantage over pre-existing plasticity models is its consistency regardless of footing geometry/aspect ratio and relative embedment.

This paper presents the design and construction of basements underneath existing buildings on two recently completed project sites in England. The paper focuses on the design of the L-shaped underpinning systems on both sites, with special interest on their capacities to support vertical compressive loading. Vertical capacity designs for both schemes were based on Adekunte's (2011) work-hardening plasticity model. Designs are compared with parallel predictions of existing traditional bearing capacity solutions and pre-existing plasticity models.

© 2016 Deep Foundations Institute

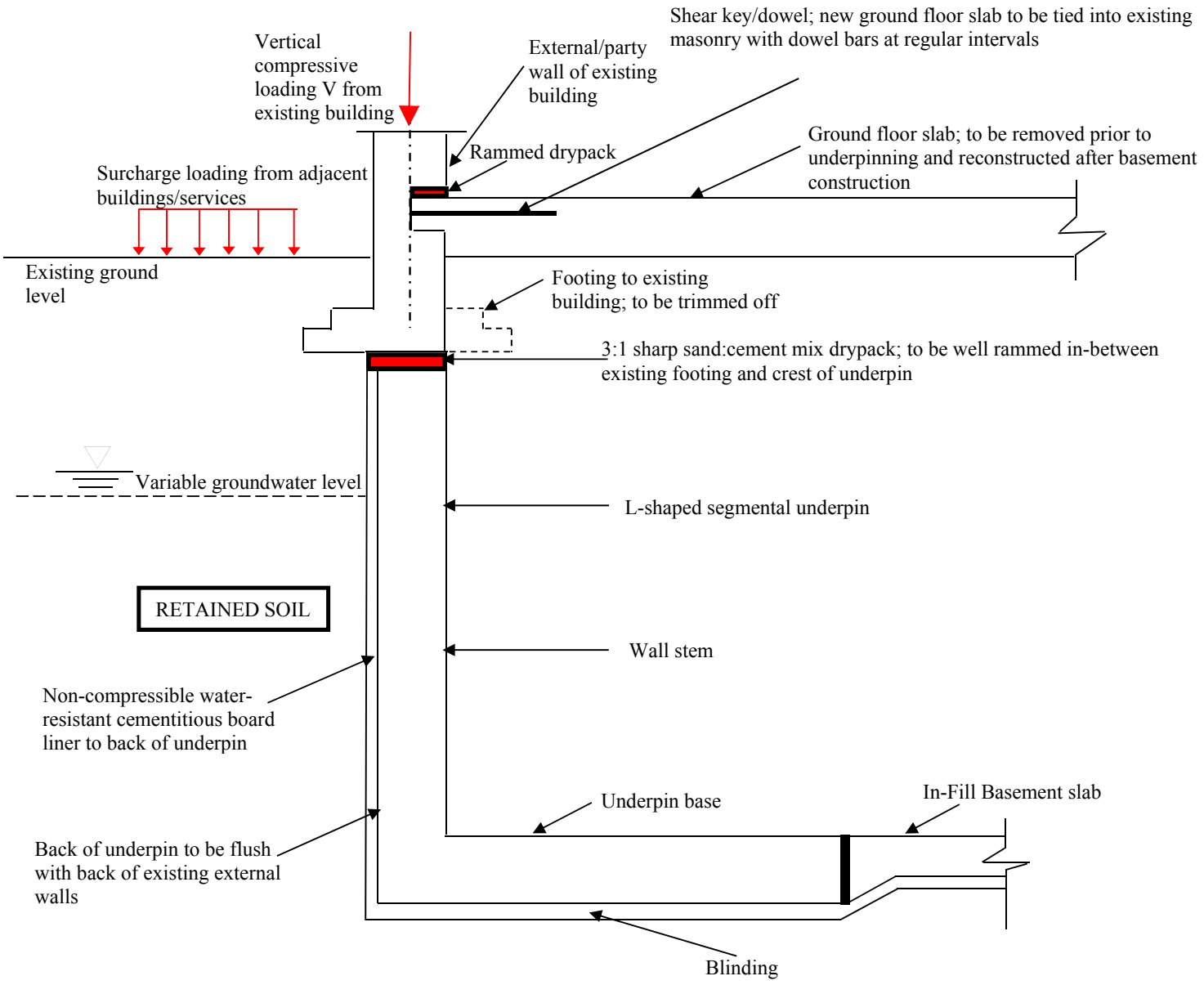


Fig. 1. Typical L-shaped underpinning system

© 2016 Deep Foundations Institute

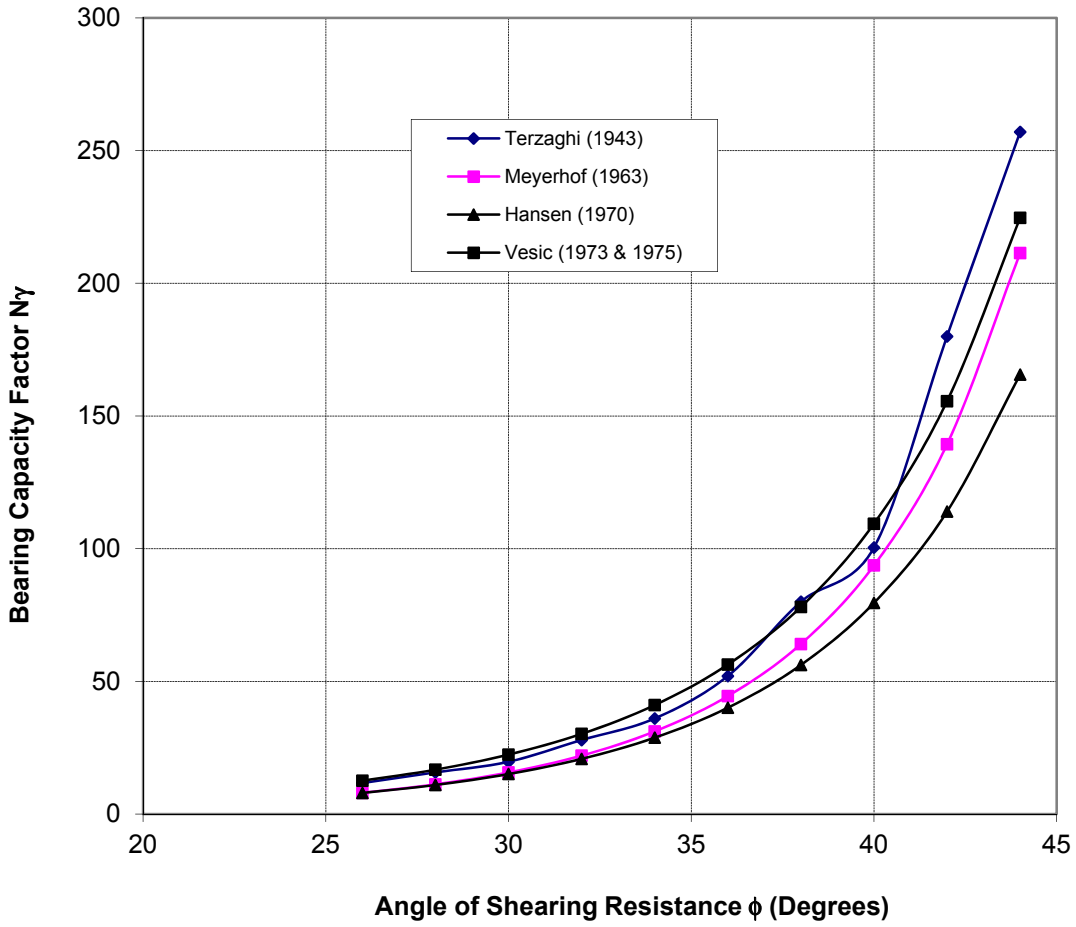


Fig. 2. Discrepancies in recommended bearing capacity factors.

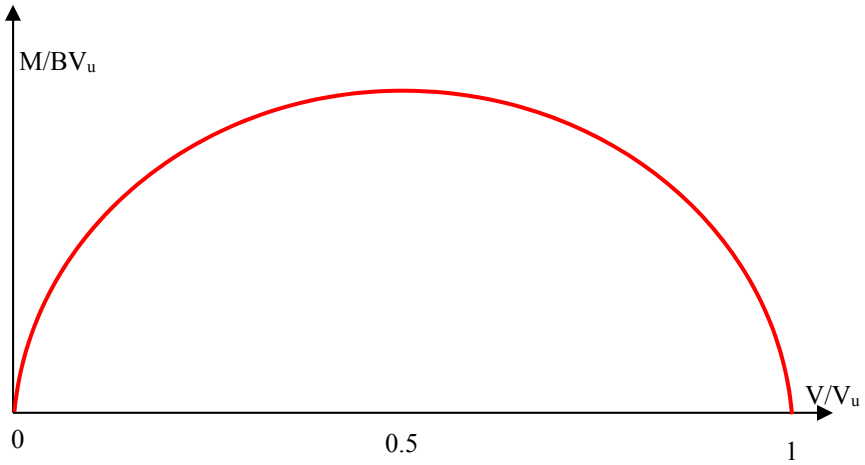


Fig. 3. Typical cross-section of a yield surface in normalised moment-vertical load space.

© 2016 Deep Foundations Institute

LOCAL GEOLOGY OF SITES & GROUND MODELLING

This study focuses on two separate sites; site 1, which is located in Kensington, West London and site 2, which is located in Oxford. Stratigraphy on site 1 comprises of 3m thick made ground underlain by a 2.5m thick layer of dense to very dense river terrace deposit, which in turn overlies a stiff to very stiff to hard London clay stratum that extends down to the limit of ground investigation at 20m depth.

The river terrace deposit is chiefly made up of pebble-gravel and sand. These were deposited 500,000 years ago when the River Thames was diverted from its original course to its current channel. The London clay stratum is essentially an overconsolidated material of low permeability and high plasticity, with measured plasticity indices ranging between 40%-50%. Monitored highest static groundwater level over the winter months was 2.5m below ground level (bgl).

Stratigraphy on site 2 comprises of 2m of non-compact fill overlying a layer of medium dense silty sand and gravel, which is underlain by stiff Oxford clay down to the limit of ground investigation at 15m depth. Oxford clay is a heavily overconsolidated material, with strong lamination in the horizontal direction and it chiefly originates from marine sedimentary rocks formed over 145 million years ago. Measured liquid limit of Oxford clay sampled on site 2 ranges between 52%-70%. Average measured plasticity index and optimum moisture content are 19.8% and 24% respectively. Measured overconsolidation ratio (OCR) reduces from 100 at 6m depth to 40 at 14m depth. Measured coefficient of earth pressure K_o varies between 1.5-2.5.

In order to allow for the influence of stress relief and remoulding during excavation and basement construction, coefficients of earth pressure K_o for the overconsolidated materials were limited to 1.0, in accordance with the recommendations of the CIRIA report No. C580 (2003). All soil layers were conservatively assumed to exhibit drained behaviour and thus modelled with effective stress parameters accordingly. Coefficients of active and passive pressure K_a and K_p were deduced from Caquot & Kensel's (1984) chart. Effective wall friction angle δ on the passive side was generally taken to be $0.5\phi'$ (where ϕ' is the effective angle of shearing resistance). However, as the wall is subject to permanent vertical compressive loading from the existing superstructure, angle of wall friction on the active side was assumed to be zero in numerical modelling.

PROPOSED DEVELOPMENTS

The project on site 1 was centred on the construction of a single level basement beneath an existing 3 storey-building on a site at Russell Garden Mews, Kensington, London. The site is bounded on two sides by existing 3 storey-neighbouring properties. An active railway line runs behind the site, while the front end of the building is adjacent to the street. To enable the construction of the new basement, it was primarily required to install reinforced concrete (RC) L-shaped segmental underpinning units beneath the existing building, to form a continuous retaining wall round the building perimeter, below ground level.

Essentially, the underpinning system was required to provide both temporary and permanent lateral retention to soil and groundwater, as well as vertical support to the existing 3 storey-structure. Maximum retained height is 3.2m. A typical section of the underpinning system is shown in Fig. 4.

The project on site 2 was centred on the underground rear and side extension to an existing substantial Victorian 4 floor-villa with an existing basement, to create some additional underground space and sunken terrace. The site is bounded on two sides by existing buildings. The underground extension required the installation of an L-shaped reinforced concrete underpinning system for lateral earth support and vertical support to existing masonry boundary walls and proposed reinforced concrete roof slab at ground level. Maximum retained height is 2.2m.

© 2016 Deep Foundations Institute

CONSTRUCTION PROCEDURE

The construction sequence followed on both sites is outlined below:

- Install temporary steel beams at ground/upper floor levels to support internal walls and floors, whilst cutting-in padstones and beam supports into external/party walls.
- Remove existing ground floor.
- Excavate for bases of individual underpinning units in 1m wide-bays, following a hit and miss sequence; 1, 3, 5, 2, 4, whilst ensuring that no two adjacent bays are excavated simultaneously. The hit and miss sequence adopted on site 1 is illustrated in Fig. 5.
- Provide trench sheets as earthwork support to the sides of the excavation in each bay, whilst supporting the exposed face with plywood sheeting and propping back directly to the face of the unexcavated central soil mound.
- Install steel reinforcement and construct the base and stem of underpinning unit, providing a minimum cover of 75mm to reinforcement and terminating concrete approximately 75mm from underside of existing foundation. The base and stem of each underpinning unit was dowelled into the adjacent underpinning unit at 300mm vertical intervals using proprietary fixing resin.
- After 24 hours, clean and regularise the underside of the existing foundation and ram 75mm drypack (3:1 sharp sand-cement mix) in-between crest of underpinning unit and underside of existing foundation, ensuring that all voids are filled.
- Back-fill underpinning bay to ground floor level once concrete achieves sufficient strength (minimum of 48 hours).
- Upon completion of all segmental underpins, a continuous perimeter retaining wall was achieved.

  It should be noted that all phase 1 underpinning bays were constructed and back-filled first. Thereafter, same underpinning operation was repeated for phase 2 bays. These were logically followed by repetitions for phases 3, 4 & 5 underpins.

- Carry out mechanical bulk excavation to 2m depth.
- Install temporary steel waling beams and flying struts at 1.5m depth.
- Continue mechanical bulk excavation to top of underpin bases.
- Complete excavation to final basement formation level in phases by hand.
- Construct in-fill basement slab in front of underpin bases at formation level and connect to bases of underpinning units.
- Remove temporary waling beams and flying struts at 1.5m depth.
- Construct new ground floor slab.

Figure 6 shows steel reinforcement installed within an underpinning bay on Site 2 (Oxford), prior to concreting. Figure 7a shows bulk excavation on site 1, while Fig. 7b shows finished underpinning works on site 1, prior to the construction of the in-fill basement slab in front of the underpin bases.

Based on the construction methodology described above, which involved the segmental installation of wall units in adequately supported/braced isolated 1m wide-bays, ground movement during underpinning was virtually negligible. In addition, the installation of temporary props at 1.5m depth limited wall displacement and structural movement of neighbouring buildings to a maximum of 3mm during bulk excavation. No additional noticeable movement was recorded after the construction of the in-fill basement slab.

© 2016 Deep Foundations Institute

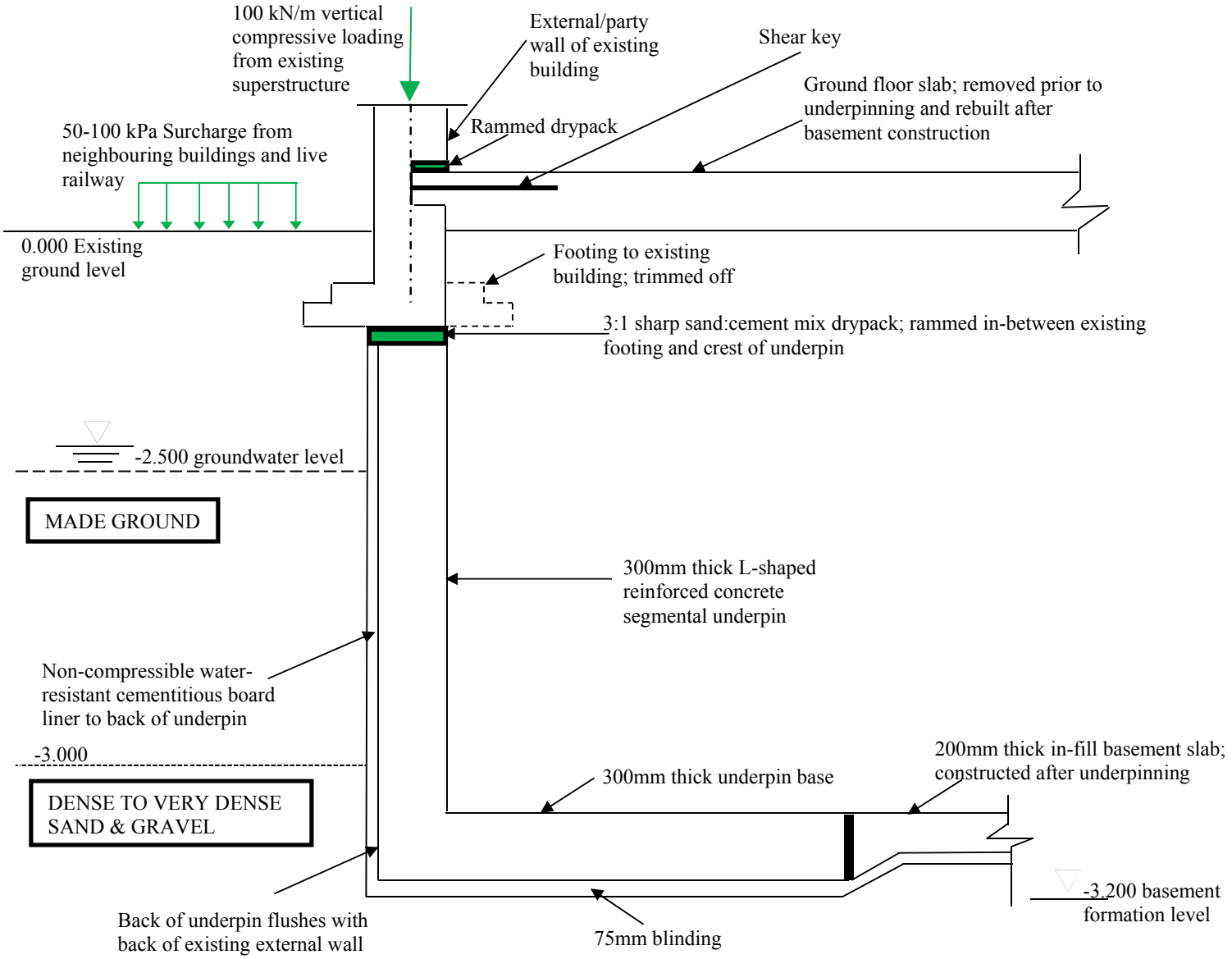


Fig. 4. Typical section of underpinning works on Site 1 (Kensington, West London).

© 2016 Deep Foundations Institute

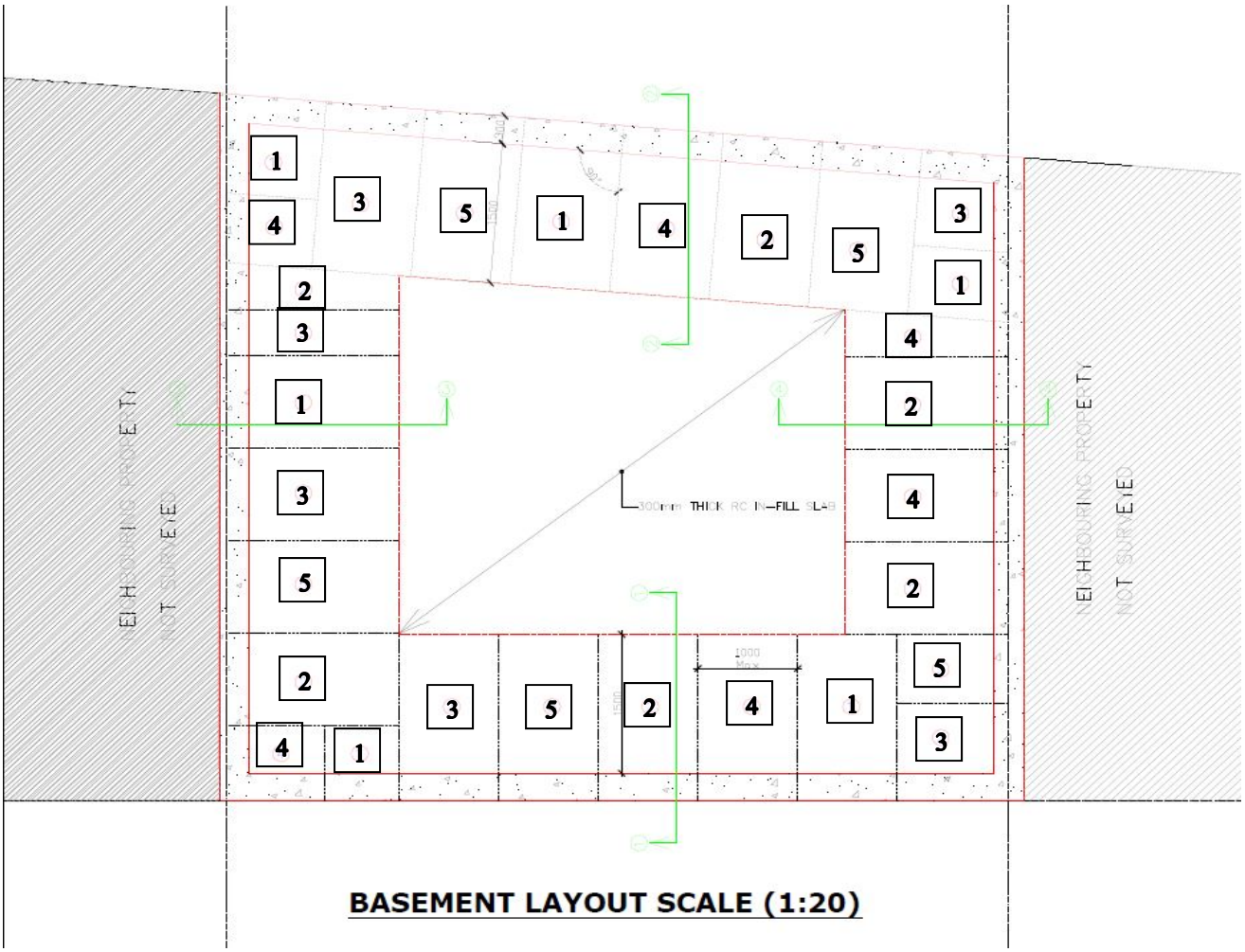


Fig. 5. An illustration of the hit and miss underpinning sequence followed on Site 1 (Kensington, West London).

DESIGN METHODOLOGY & COMPARISON WITH TRADITIONAL APPROACHES

For simplicity, the design methodology adopted on both sites, will be illustrated with the case of site 1 only. Design for the underpinning system involved a combination of structural design for the underpin to support axial forces, bending moments and shear forces induced by the retained soil/groundwater and the existing superstructure/foundation, as well as the geotechnical design for the wall to support same set of loads. However, this paper mainly focuses on the geotechnical design of the underpinning system to support axial forces in the wall stem.

© 2016 Deep Foundations Institute



Fig. 6. Installation of steel reinforcement within an underpinning bay on site 2 (Oxford).



Fig. 7a. Bulk excavation on site 1 (Kensington, West London).

© 2016 Deep Foundations Institute



Fig. 7b. Finished underpinning works on site 1 (Kensington, West London), prior to the construction of the in-fill basement slab in front of the underpin bases.

Axial loading on the underpinning wall stem comprises of 2 main components; vertical loading from the existing superstructure foundation and axial force induced by the lateral loading on wall stem by the retained soil and groundwater. The first component (superstructure loading) was estimated by load take-down, based on the recommendations of the BS 6399-1 (1996). Approximate estimated service load from the superstructure was 100 kN/m.

The combined effect of the first and second components was estimated by finite element (FE) modelling with PLAXIS 2D 2012 soil-structure interaction modelling programme. The FE model is shown in Fig. 8a, while the computer output file for the axial forces generated in the wall stem is shown in Fig. 8b. Figure 8b shows the estimated maximum axial force in the wall stem to be 130 kN/m run of wall. This load acts at an eccentricity of 0.9m from the centreline of the underpin base, as illustrated in Fig. 9.

The design for the underpin base to support vertical eccentric loading was based on the consistent plasticity model proposed by Adekunte (2011). The vertical capacity of the underpin base under vertical central loading was not estimated with the conventional bearing capacity equation, which is shrouded in uncertainty, but by correlations with in-situ measurements of static cone penetration resistance on the site.

In recent years, new CPT-based design methods have been developed for estimating the vertical central capacities of foundations. Experimental works backing-up these methods show that ultimate bearing capacity q_u under vertical central loading corresponds to normalised foundation settlement s/B = 5% or

© 2016 Deep Foundations Institute

10%, where B is foundation width and s is measured vertical displacement. Based on deep plate tests in calibration chambers, Ghionna et al. (1994) proposed that at normalised settlements of 5% and 10%, normalised ultimate vertical capacity q_u/q_c of a foundation (where q_c is cone penetration resistance and q_u is ultimate bearing capacity) equals 0.1–0.16 and 0.13–0.21 respectively. Similar deep plate tests in calibration chambers by Jamiolkowski & Sarri (2000) showed q_u/q_c at normalised settlements of 5% and 10% to be 0.13 and 0.18 respectively.

With reference to the above correlations, the ultimate bearing capacity q_u of the underpin base on site 1 was estimated with a moderately conservative correlation given by;

$$\frac{qu}{qc} = 0.13 \qquad \text{---------- [9]}$$

The founding layer of the underpinning system on site 1 was dense sand and gravel, with an average measured q_c value of 35 MPa. With equation 9, estimated ultimate bearing capacity q_u of the underpin base on site 1 under vertical central loading was estimated as;

$q_u = 0.13q_c = 0.13 * 35$ MPa = 4.5 MPa
≡ 4550 kPa

Base width is 1.8m. Considering a metre strip of the wall base, ultimate vertical capacity V_u under vertical central loading was estimated to be;

$V_u = 4550 * 1.8 * 1.0 = 8190$ KN.

Adopting Adekunte's (2011) plasticity model for eccentrically loaded footings (equation 5), which is rewritten below;

$$M/BV_u = f\ \alpha\ \varphi\ r\ (1 - r) \qquad \text{---------- [10]}$$

In equation 10;

V_u = 8190 KN (as shown above)

B = underpin base width = 1.8m

f = dimensionless factor accounting for the influence of embedment on base capacity. f is a function of normalised footing embedment d/B (where d is depth of base and B is base width);

$$f = 1 + 0.1\ (d/B) \qquad \text{---------- [11]}$$
(Adekunte, 2011)

The formation level of underpin is 3.2m bgl and base of underpin is 1.8m wide. Hence d/B = 3.2/1.8 ≅ 1.8.

$\therefore f = 1 + 0.1\ (1.8) = 1.2$
α = dimensionless factor accounting for the influence of aspect ratio on base capacity;

$$\alpha = [A_s]^{-0.2} \qquad \text{---------- [12]}$$
(Adekunte, 2011)

© 2016 Deep Foundations Institute

where A_s is aspect ratio L/B (L is length of footing strip under consideration = 1m and B is base width = 1.8m).
$\therefore A_s = 1.0/1.8 = 0.56$

$\alpha = [0.56]^{-0.2} = 1.13$

φ = dimensionless parameter, which defines the size of the yield envelope. This can be taken as $\varphi = 0.55$ (Adekunte, 2011).

$r = V/V_u$ ---------- [13]

where V is the estimated vertical axial load in the wall stem = 130 kN/m (as shown earlier) and V_u is the vertical capacity of the underpin base if loaded centrally = 8190 KN (as shown earlier).

$\therefore r = 130/8190 \cong 0.02$

Rearranging equation 10 and substituting the above values in the equation, allowable overturning moment M on the underpin base is given by;

$M = f\ \alpha\ \varphi\ r\ (1 - r)\ B\ V_u$ ---------- [14]

$M = 1.2 * 1.13 * 0.55 * 0.02\ (1 - 0.02) * 1.8 * 8190$

$\therefore M = 215$ kNm

Service overturning moment M_s on base due to applied vertical eccentric loading is calculated as;

$M_s = V\ .\ e$ ---------- [15]

where V is applied vertical eccentric loading and e is load eccentricity.

$\therefore M_s = 130$ KN * 0.9m = 117 kNm

$\therefore M > M_s$; 215 kNm > 117 kNm (O.K.).

It must be noted that no factor of safety has been directly applied in calculations as the plasticity model is based on normalised load effects.

Based on the design approach presented above, the normalised failure envelope for the underpin base on site 1 is presented in M-V space in Fig. 10. For the same normalised vertical loading $V/V_u = 0.02$, normalised allowable overturning moment predictions (M/BV_u) of the traditional bearing capacity solutions of Meyerhof (1993) and Vesic (1970), as well as the plasticity models of Okamura et al. (2002), Lesny & Richwien (2002) and Smith-Pardo & Borbet (2007) are presented within same envelope for comparison. In addition, raw predictions of allowable overturning moment (in kNm) on the underpinning base by the same solutions are presented in Fig. 11.

Essentially, Figs. 10-11 show the design model for site 1 to be less conservative than other pre-existing solutions. Meyerhof's (1953) and Vesic's (1970) traditional bearing capacity solutions are seen to be the most conservative. Meyerhof's (1953) solution had already been shown to produce very conservative

© 2016 Deep Foundations Institute

predictions by a number of workers e.g. Ukritchon et al. (1998), Okamura et al. (2002) and Gourvenec & Randolph (2003).

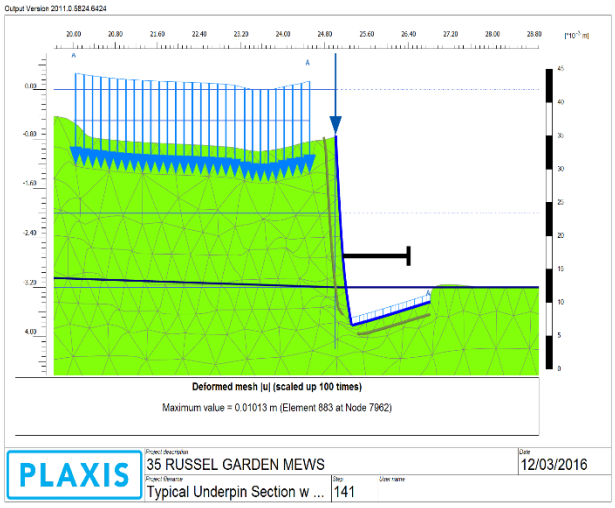


Fig. 8a. Deformed FE mesh; temporarily propped L-shaped underpin after completion of bulk excavation.

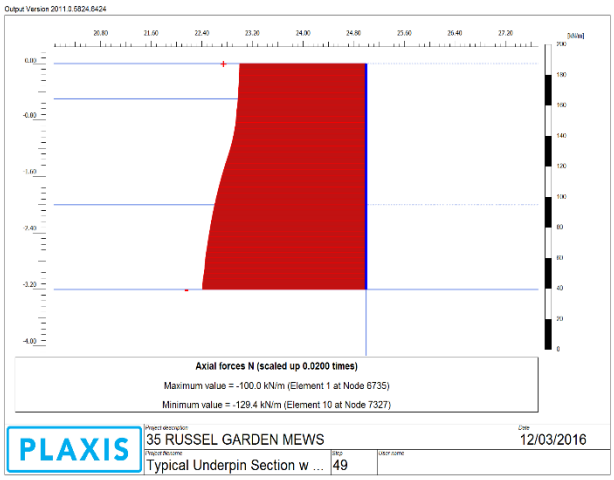


Fig. 8b. FE analysis output; distribution of axial force in underpin stem.

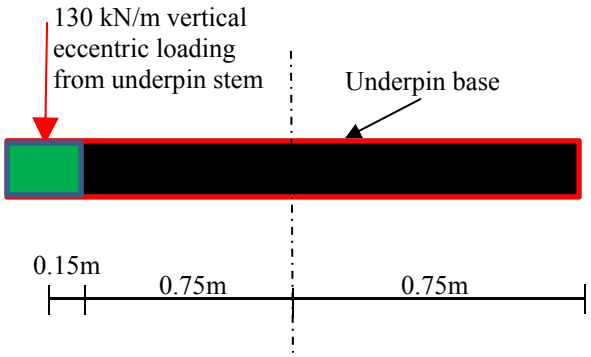


Fig. 9. An illustration of the vertical eccentric loading on the underpin base.

© 2016 Deep Foundations Institute

The work-hardening plasticity models of Smith-Pardo & Borbet (2007), Lesny & Richwien (2002) and Okamura et al. (2002) produce estimates that are relatively closer to site 1's design overturning moment. However, while Lesny & Richwien's (2002) model accounts for the influence of footing relative embedment on size of the failure envelope, it does not account for the influence of geometry/aspect ratio; Gourvenec & Randolph (2003), Nova & Montrasio (1997) and Okamura et al. (2002) had shown size of a failure envelope to vary with geometry/aspect ratio.

Okamura et al.'s (2002) model does not account for the influence of footing embedment on yield surface, as the model had been calibrated with surface footings in a centrifuge. Smith-Pardo & Bobet's (2007) model was calibrated with laboratory-based tests on square footings only; Okamura et al. (2002) had shown footing capacity under vertical eccentric loading to increase with increasing aspect ratio, such that a plasticity models calibrated with square footing(s) may under-estimate the capacities of strip footings.

The underpin base on site 1 was designed with Adekunte's (2011) plasticity model, which was calibrated with a series of field-based tests on footings of various aspect ratios, at various relative embedment depths. Therefore, the model accounts for the effects of both aspect ratio and footing embedment on capacity; this allows for a reasonable level of consistency in capacity predictions irrespective of geometry or embedment, unlike many pre-existing models. In addition, it is believed that testing in the field overcomes the difficulties with boundary conditions, scale effect and control of soil properties typically associated with laboratory-based tests. These could be the reason behind the relatively lower level of conservatism shown by the model in Figs. 10-11.

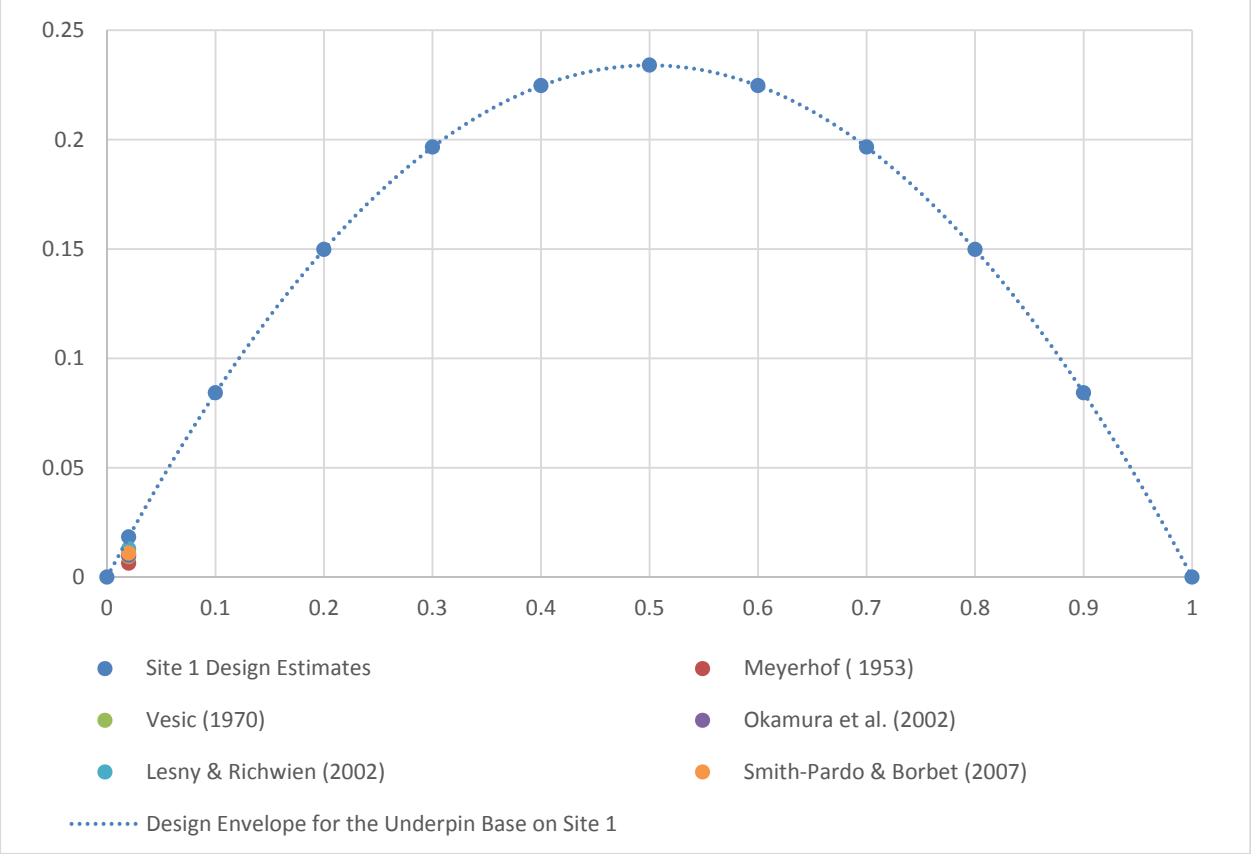


Fig. 10. Normalised failure envelope for the underpin base on site 1 and comparison with predictions of pre-existing solutions, for normalised applied vertical loading $V/V_u = 0.02$.

© 2016 Deep Foundations Institute

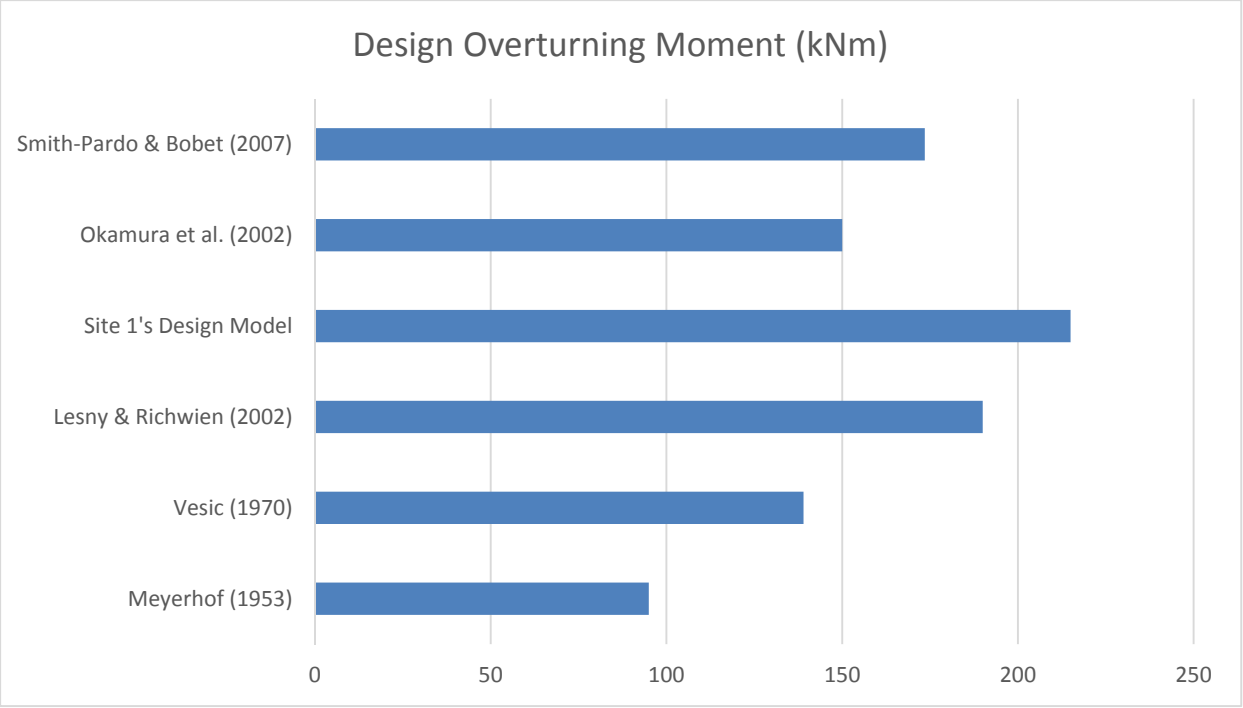


Fig. 11. Design overturning moment for underpin base on site 1 compared with predictions of pre-existing solutions.

Therefore, the model accounts for the effects of both aspect ratio and footing embedment on capacity; this allows for a reasonable level of consistency in capacity predictions irrespective of geometry or embedment, unlike many pre-existing models. In addition, it is believed that testing in the field overcomes the difficulties with boundary conditions, scale effect and control of soil properties typically associated with laboratory-based tests. These could be the reason behind the relatively lower level of conservatism shown by the model in Figs. 10-11.

SUMMARY & CONCLUSIONS

The design and construction of L-shaped segmental underpinning systems on two separate basement schemes (site 1 & site 2) have been presented. Emphasis has been placed on the design of the underpin bases to support vertical eccentric loading. The paper highlights the inadequacies and uncertainties surrounding existing conventional bearing capacity approaches, which are the most commonly used methods amongst designers across the industry.

The underpin bases in the current study were designed with an alternative work-hardening plasticity model proposed by Adekunte (2011). The procedure involved in the application of the model has been carefully laid out, with particular reference to the design of the L-shaped underpins on site 1. The design estimates are compared with the predictions of traditional bearing capacity solutions and a number of pre-existing plasticity models.

Comparison has shown the traditional bearing capacity methods to be quite conservative, while the pre-existing plasticity models have been found to produce closer capacity estimates to the design model. The design model is shown to be the least conservative. Deficiencies and inconsistencies in the pre-existing plasticity models are discussed, while the advantages of the design model over pre-existing plasticity models have also been highlighted.

© 2016 Deep Foundations Institute

REFERENCES

ADEKUNTE, A., 2011. The behaviour of spread footings for onshore wind turbine towers. PhD thesis, UCD College of Engineering & Architecture, University College Dublin.

BRANSBY, M.F., and RANDOLPH, M.F., 1998. Combined loading of skirted foundations. Geotechnique, 1998, 48(5), pp. 637-655.

BRITISH STANDARDS INSTITUTION., 1996. BS 6399-1: 1996 – Loading for buildings. Code of practice for dead and imposed loads. BSI, London, 1996.

BYRNE, B.W., and HOULSBY, G.T., 1999. Drained behaviour of suction caisson foundations on very dense sand. Proceedings of the Offshore Technology Conference, Houston Texas, 1999.

CAQUOT, A. and KERISEL, J., 1948. Tables for the calculation of passive pressure, active pressure and bearing capacity of foundations. Gauthier-Villars, Paris, 1948.

CONSTRUCTION INDUSTRY RESEARCH AND INFORMATION ASSOCIATION., 2003. Report No. C580 – Embedded Retaining Walls – Guidance for Economic Design, CIRIA, London, 2003.

GEORGEADIS, M., and BUTTERFIELD, R., 1988. Displacements of footings on sand under eccentric and inclined loads. Canadian Geotechnical Journal, 1988, Vol. 25, pp. 199-212.

GHIONNA, V.N., JAMIOLKOWSKI, M.B., PEDRONI S., and SANGADO, R., 1994. Tip displacement of drilled shafts in sand. In Vertical and Horizontal Deformations of Foundations and Embankments, ASCE, GSP40, New York, Vol. 2, pp. 1039-1057.

GOTTARDI, G., HOULSBY, G.T., and BUTTERFIELD, R., 1995. The displacement of a model rigid surface footing on dense sand under general planar loading. Soils and Foundations, 1995, 35(3), pp. 71-82.

GOTTARDI, G., HOULSBY, G.T., and BUTTERFIELD, R., 1999. Plastic response of circular footings on sand under general planar loading. Geotechnique, 1999, 49(4), pp. 453-469.

GOURVENEC, S., and RANDOLPH, M., 2003. Failure of shallow foundations under general combined loading. Proceeding of the 13th ECSMGE, Prague, 2003, pp 583-588.

HANSEN, J.B., 1970. General formula for bearing capacity. Bulletin of the Danish Technical Institute, No. 11, pp. 38-46.

HOULSBY, G.T., and BYRNE, B.W., 2001. Suction caisson foundations for offshore wind turbines and anemometer masts. Wind Engineering, 2001, 24(4), pp. 249-255.

INGRA, T.S., and BAECHER, G.B., 1983. Uncertainty in bearing capacity of sands. ASCE Journal of Geotechnical Engineering, 1983, 109(7), pp. 899-914.

JAMIOLKOWSKI, M.B., and SARRI, H., 2000. On axial load capacity of drilled shafts in coarse grained soils. Libro Homenaje on Jose Antonio Jimenes Salas, Ministero de Fomento, Cedex, Madrid, 2000, pp. 111-128.

LESNY, K., and RICHWIEN, W., 2002. A consistent failure model for single footings embedded in sand. Proceedings of the International Workshop on Foundation Design Codes, Tokyo, 2002, pp. 159-165.

© 2016 Deep Foundations Institute

MEYERHOF, G.G., 1953. The bearing capacity of foundations under eccentric and inclined loads. Proc. 3rd ICSMFE, 1953, pp. 440-445.

MEYERHOF, G.G., 1963. Some recent research on bearing capacity of foundations. Canadian Geotechnical Journal, 1963, Vol. 1, pp. 16-26.

NOVA, R., and MONTRASIO, L., 1991. Settlements of shallow foundations on sand. Geotechnique, 1991, 41(2), pp. 243-256.

NOVA, R., and MONTRASIO, L., 1997. Settlements of shallow foundations on sand; geometrical effects. Geotechnique, 1997, 47(1), pp. 49-60.

OKAMURA, M., MIHARA, J., TAKEMURA J., and KUWANO, J., 2002. Effects of footing size and aspect ratio on the bearing capacity of sand subjected to eccentric loading. Soils and Foundations, 2002, 42(4), pp. 43-56.

SIEFFERT, J.G., and BAY-GRESS, Ch., 2000. Comparison of European bearing capacity calculation methods for shallow foundations. Proceeding of the Institution of Civil Engineers, Geotechnical Engineering, 2000, Vol. 143, pp. 65-74.

SMITH-PARDO, J.P., and BOBET, A., 2007. Behaviour of rigid footings on gravel under axial load and moment. ASCE Journal of Geotechnical & Geoenvironmental Engineering, 133(10), pp. 1203-1215.

TERZAGHI, K., 1943. Theoretical soil mechanics. Wiley Publ., New York, 1943.

UKRICHTON, B., WHITTLE, A.J., and SLOAN, S.W., 1998. Undrained limit analysis for combined loading of strip footings on clay. Journal of Geotechnical and Geoenvironmental Engineering, 1998, 129(6), pp. 468-474.

VESIC, A.S., 1973. Analysis of ultimate loads of shallow foundations. Proc. ASCE, Vol. 99, SM1, pp. 45-73.

VESIC, A.S., 1975. Bearing capacity of shallow foundations. In Foundation Engineering Handbook, Van Nostrand Reinhold Publ., New York, pp. 121-147.

ZDRAVKOVIC, L., NG, P.M., and POTTS, D.M., 2002. Bearing capacity of surface foundations on sand subjected to combined loading. Proceedings of the International Conference on Numerical Methods in Geotechnical Engineering, NUMGE V, 2002, pp. 323-330.

ACKNOWLEDGEMENTS

The first author would like to dedicate this paper to my daughter; Omojadesola Adebimpe Aduke, her mum Adedoyin, every child in Yewaland Southwest Nigeria and every member of the Young Yewa Professionals Foundation; a non-profit youth-led organisation committed to the improvement of the standard of education and the overall standard of living in the community. The first author is also grateful to Dr. Kenneth Gavin of the University College Dublin, for supervising the PhD research that forms the basis of the designs presented in this paper. Appreciation also goes to Sustainable Energy Ireland, Enterprise Ireland, ESB International Ireland and the Geotechnical Trust Fund of the Institution of Engineers of Ireland, for providing the funds for the research. Finally, the hard work put into the management of both projects presented in this paper by Gary Winter, Rob Easton, David Bond and Andrew Rideout is acknowledged and well appreciated.

© 2016 Deep Foundations Institute

APPLICATIONS OF DIAPHRAGM WALL TECHNOLOGY FOR DEEP FOUNDATIONS AND PERMANENT UNDERGROUND STRUCTURES FOR THE TRANSBAY TRANSIT CENTER AND THE TRANSBAY DEVELOPMENTS

Mikael CALANDO, Nicholson Construction
Thomas JOUSSELLIN, Nicholson Construction

Abstract

San Francisco's rapid growth has caused the city to plan for the Transbay Transit Center Project, a visionary transportation and housing project, that will transform downtown San Francisco and the San Francisco Bay Area's regional transportation system by creating a "Grand Central Station of the West" in the heart of a new transit-friendly neighborhood that will be home to more than 20 new towers rising a high a 1,070 ft. This paper describes the specificities of using advanced diaphragm wall technology, tooling, equipment and installation practices for deep foundation and permanent underground structures. In particular, this paper will emphasize on the urban constraints, geotechnical conditions, and the novel approaches adopted for the construction challenges of the Transbay Transit Center's Load Bearing Elements, or Barrette Piles

Paper

The Transbay Transit Center Project consists of the construction of a new multimodal, five-story Transit Center located in the South of Market neighborhood near the Financial District in San Francisco. The future Transit Center will incorporate nearly 83,000 square feet of retail, a 5.4-acre rooftop park, an extensive public arts program and bus ramps that will connect the Transit Center to a new off-site bus storage facility and the San Francisco–Oakland Bay Bridge. The new facility will accommodate more than 100,000 passengers each weekday and up to 45 million per year. Additionally, the new Transbay Transit Center will replace the since-demolished San Francisco Transbay Terminal, and nearly 20 towers, such as Salesforce Tower, will take advantage of the height increases allowed through the Transit Center District Plan.

The approximately $4.5 billion project features a new five-story structure (including two underground stories) and new bus ramps which include a cable-stay bridge. The deep foundations for the pylon of the bridge (Pylon 9) consist of two each 21 ft x 5 ft barrettes (also called Load Bearing Elements in the US) extending more than 180 feet below grade and 10 feet into the bedrock. The barrettes were chosen because of the combination of high loads, significant depth and small footprint. The barrettes are installed using the Diaphragm Wall technology. Nicholson Construction was contracted by Shimmick Construction to install the cable-stay bridge's foundation elements.

© 2016 Deep Foundations Institute



Figure 1 - Rendering of the Bus Ramps Cable-Stayed Structure

© 2016 Deep Foundations Institute

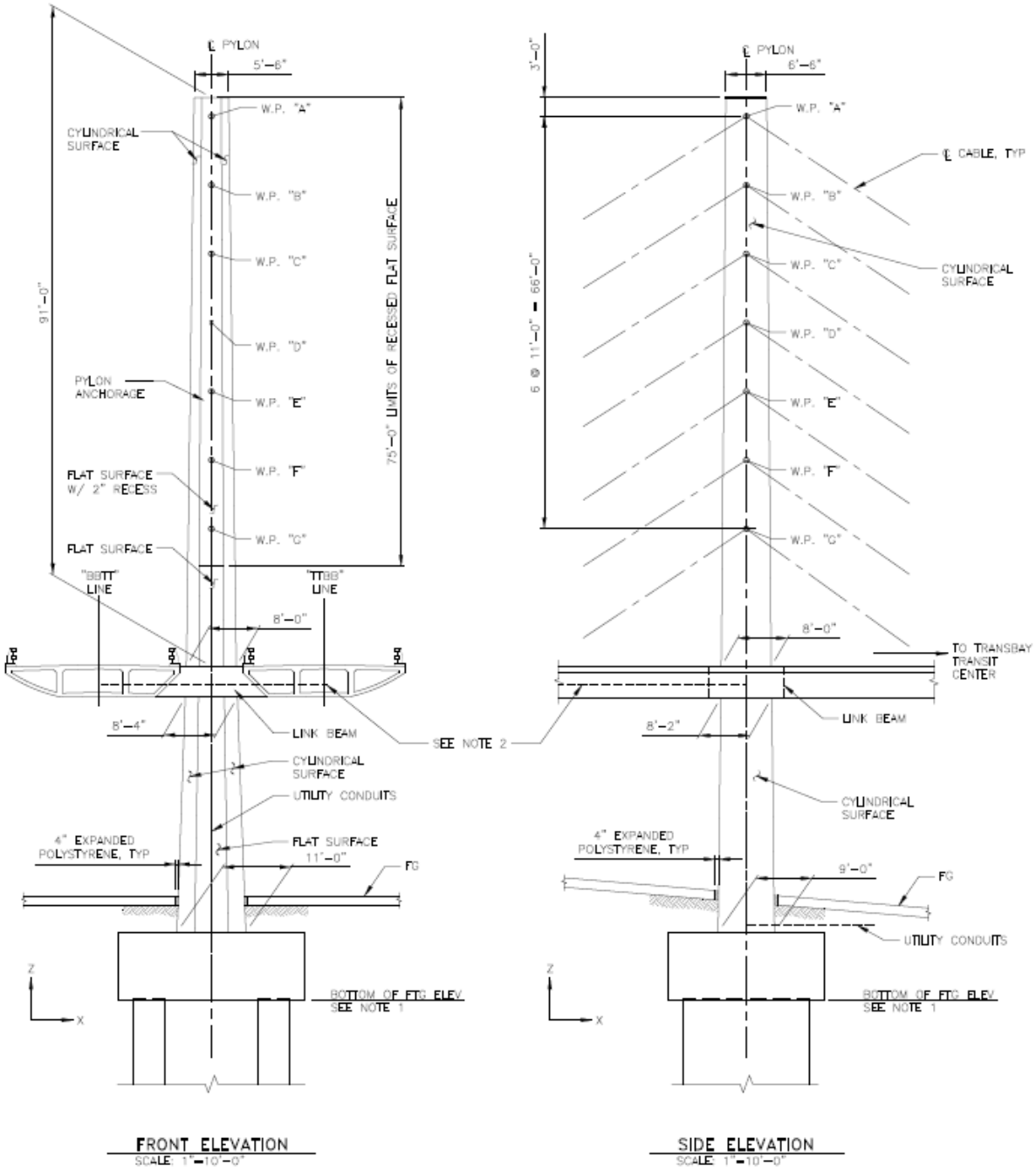


Figure 2: Pylon of the cable-stay structure

© 2016 Deep Foundations Institute

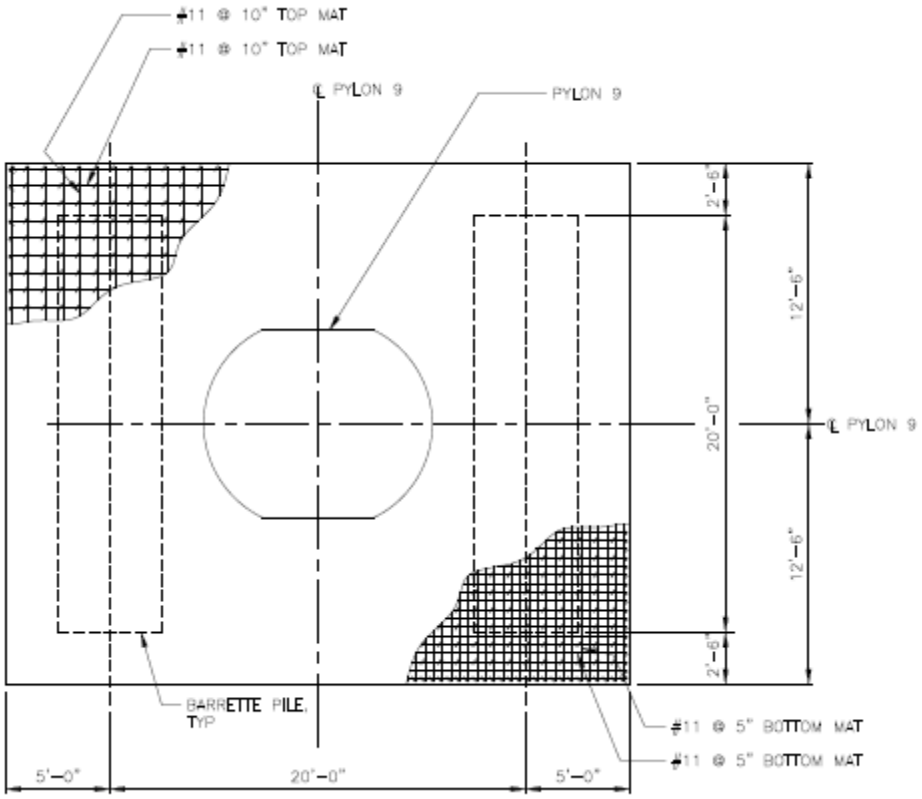


Figure 3: Footing of the pylon

The project's geotechnical conditions consisted of fill, dense to very dense Colma formation, stiff old bay clay and the San Franciscan complex bedrock.

© 2016 Deep Foundations Institute

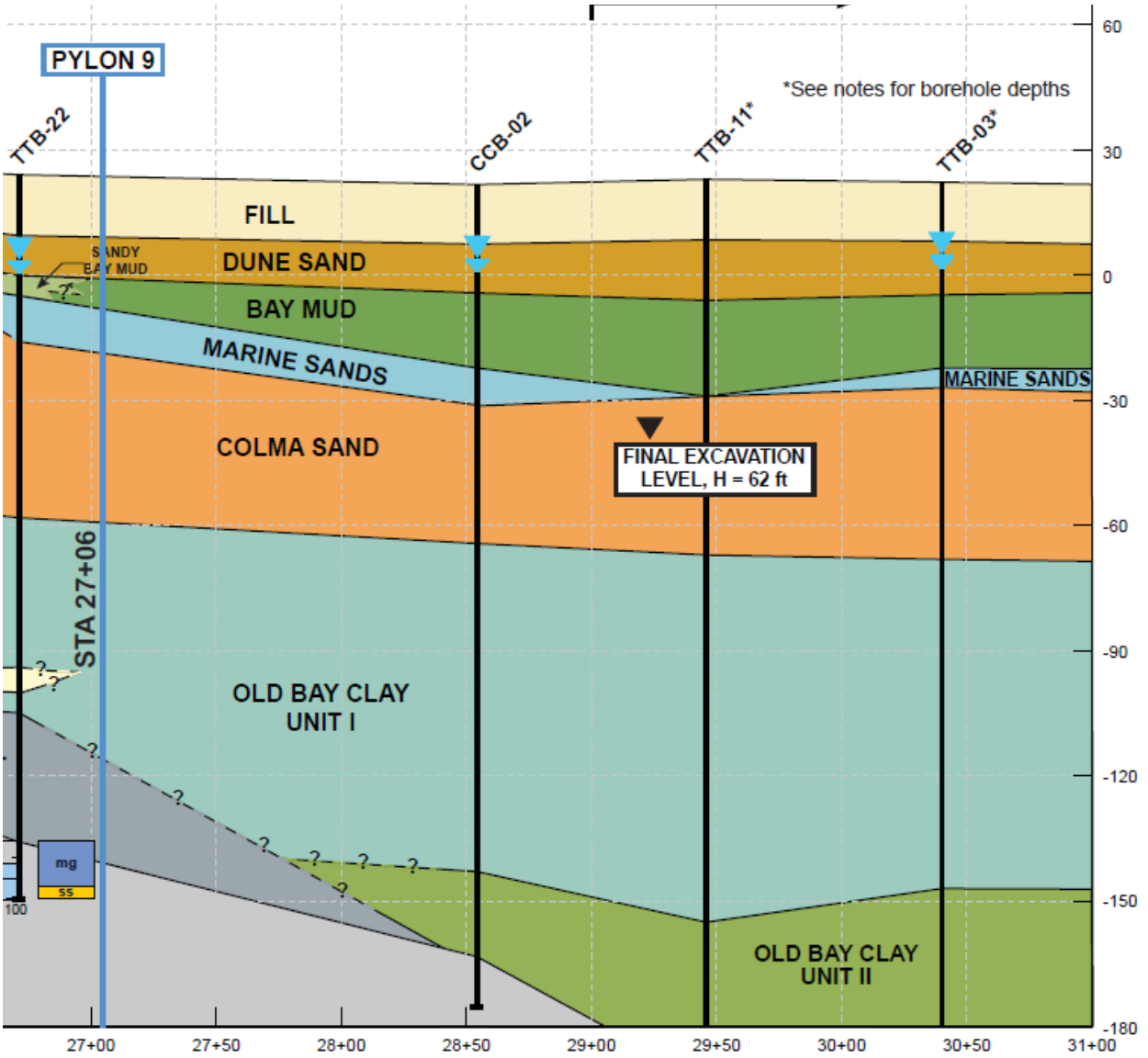


Figure 4: Geology at Pylon 9

Due to the seismic design requirements, the reinforcement cage of the Barrettes was dense with a center to center spacing of stirrups of 9” horizontal and 6” vertical. During the pre-construction stage, Nicholson worked efficiently with the structural Engineer of Record to optimize the design of the barrettes’ reinforcing cage. The optimization process generally consisted in increasing the bar size diameter in order to increase the clear space between bars while keeping an equivalent steel section. After redesign, the center to center spacing of the stirrups was 18” horizontal and 11” vertical. This allowed for sufficient space to install the tremie pipes in the cage and enough clear space to facilitate the flow of the concrete throughout the cage. All design was done according to reference standards of the project.

© 2016 Deep Foundations Institute

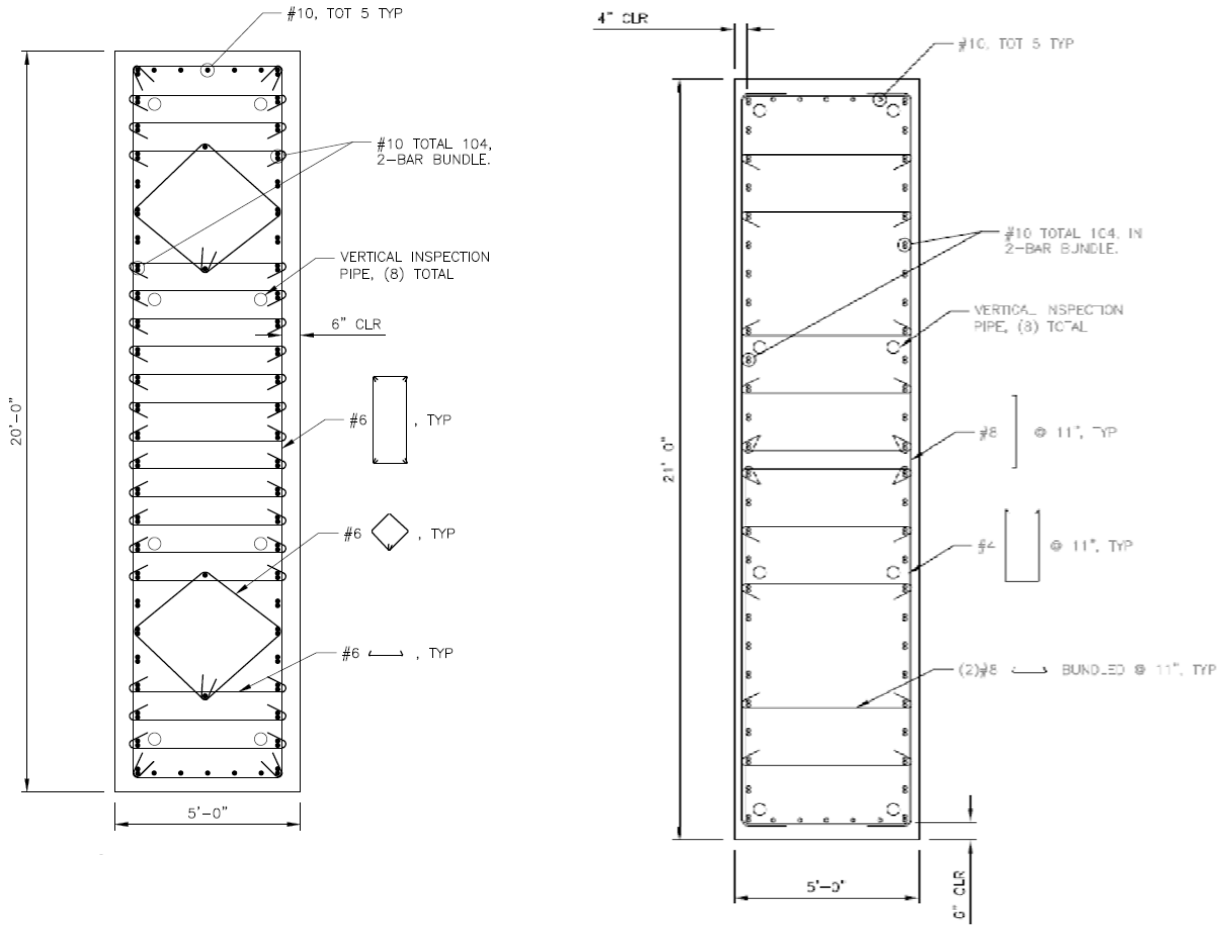


Figure 5 - Original Design Optimized design

In addition, Nicholson carried out an extensive pre-production concrete mix design test phase, with the support of the materials department of the parent company Soletanche Bachy. This department is amongst other things, focused on the development of recommendations and tests for concrete design mixes for big tremie pours. The volume of concrete for each barrette was in excess of 700 cubic yards, and each pour was an uninterrupted operation of roughly 12 hours. This requires the concrete set to be retarded so that the concrete keeps flowing during the pour (workability). This also requires the mix to retain its water as it is still in its fluid state and submitted to the pressure of the concrete (stability). No less than four different batches were tested both at the supplier's lab and on site until the mix meeting the contract requirements and the internal recommendations was found.

Two different excavation equipment were mobilized on site for the excavation of the barrettes:

- the hydraulic grab, featuring clamshell buckets
- the hydromill featuring 2 cutting wheels and a pump to evacuate the spoils

The excavation typically starts with the hydraulic grab, and is carried on at least deep enough to submerge the pump of the hydromill in the bentonite slurry. The hydromill then carries on with the excavation of the trench through the remaining overburden and the rock. The excavation with the grab is sometimes carried out deeper with the hydraulic grab to make sure both equipment are fully utilized.

© 2016 Deep Foundations Institute



Figure 6: the hydromill

One additional challenge on the project was the overall logistics. Due to its location and the fact that the construction of the main Terminal was ongoing during the bus ramps foundation construction, the project available construction area was extremely limited. The excavation equipment was squeezed-in between the excavation of the Terminal and the very busy Howard St. The laydown area was across Howard St (lot G). Consequently each 60 ton cage was fabricated in the rebar supplier yard in 6 different pieces: two (2) 10ft wide by three (3) 60ft long sections approximately. The pieces were then delivered on site and assembled 2 by 2 to form 20' wide sections. Nicholson then loaded each 20' section on a custom-made trailer and moved the cage from Lot G to Pylon 9 for placement in the trench. The 20' sections were spliced together as they were lowered in the trench.

© 2016 Deep Foundations Institute



Figure 7: 20’ section transported across Howard St on custom-made trailer

A detailed lifting plan was developed to ensure stability of the cranes and structural integrity of the reinforcement cages during each step of the installation of the cages. The forces in each 20’ wide section was analyzed using a 3D structural software.

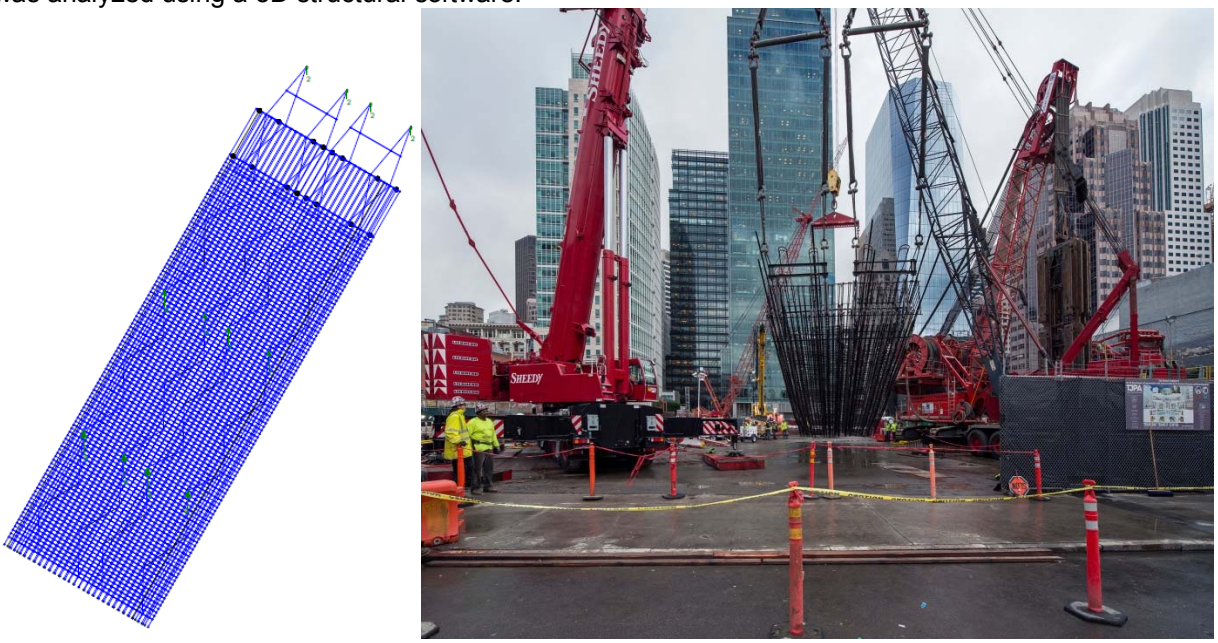


Figure 8: Tilting the cage, theory and practice

© 2016 Deep Foundations Institute

All this upfront work in the preparation of the job led to an uneventful operation. Nicholson completed the project and both barrettes successfully passed the cross-sonic hole tests.



Figure 9. Overview of the construction of the barrettes

This project demonstrates that barrettes are a viable option to drilled shafts. In the US, large diameter drilled shafts have historically been used as the deep foundations solution. With the introduction of the diaphragm wall technology, Barrettes are more and more considered as an alternate for very deep and highly loaded foundations, which is typically the case with high-rise towers. A significant number of high-rise towers in Europe and Asia were built on barrettes. In other countries, such as the UK and US, drilled shafts are more common.

Besides the asymmetrical nature of the rectangular piles versus drilled shafts, which can be useful when loads are asymmetrical themselves, there is no major technical difference between the two techniques. From a design stand point there have been recent studies on how the allowable skin friction on Barrettes compares with that of drilled shafts. Depending on the country/region, some contractors and engineers tend to find drilled shafts more attractive when depths are relatively shallow (200 ft range) and Barrettes more attractive when the loads require the element to go deeper (300 ft+).

Both techniques are perfectly viable for deep foundations, however, non rational factors might play a role in preferring a system over another and the preferred system tend to be more cost-effective with time due to increased competition, technical and operational knowledge. The barrette technique provides another valid and cost effective option for deep foundations that should be part of the standard toolbox of both the Structural and Geotechnical Engineer of every Project.

References

EFFC/DFI Best Practice Guide to Tremie Concrete for Deep Foundations, 1st edition 2016
EN 1538:2010 Execution of special geotechnical works — Diaphragm walls, September 2010

© 2016 Deep Foundations Institute

This page left intentionally blank

© 2016 Deep Foundations Institute

BEHAVIOR OF SETTLEMENT REDUCING PILES UNDER STATIC AND SEISMIC LOADINGS

Alaa A. Ata, Faculty of Eng., Zagazig University, Egypt, aata@aucegypt.edu
Marwa Nabil, Faculty of Eng., Zagazig University, Egypt, marwa_nabil_amin@yahoo.com

ABSTRACT

Recent developments in the analysis of piled rafts has incorporated the load sharing of the raft and the piles to support the superstructure. In the piled-raft system, piles are cast monolithically with the raft and the load is partly transmitted by the raft to the soil directly below it, and partly by the piles to more competent deep soil. While these piles are effective in increasing the bearing capacity and reducing the settlements, they often lead to significant straining actions at the pile head-raft connection which may constitute the weakest link. An attempt to provide a more economical solution, that at the same time overcomes this weak link, is to disconnect the pile heads from the raft and introduce an intermediate cushion of compacted fill. In this case, the piles are considered as reinforcement to the subsoil and will also act as settlement reducers. This paper investigates the load transfers mechanism of the unconnected piled raft with cushion using ABAQUS finite elements Program. The main objective is to provide an in depth analysis of the raft–soil–pile interactions in multi-layered soil under static and seismic loads. The investigated system provides an economical alternative for traditional connected piled raft foundation, where there is no need to reinforce the piles, no need for pile head demolition or expensive waterproofing of the pile head connection. Cost analyses of unconnected versus connected piled raft systems confirmed a cost savings in the construction that may reach from 50 to 70 percent.

Keywords: piled raft, settlement reducing piles, unconnected piled raft.

INTRODUCTION

Designers around the world have gained more confidence to use the piled-raft as a more realistic system where the raft and the piles share transferring the superstructure loads to shallow and deep soil layers. A further advancement is to use unconnected piled rafts as another practical and economical alternative to the traditional piled rafts. Unconnected piled raft is also synonymous to settlement reducing piles; or simply, soil improvement piles. Liang et al. (2003) has extended the concept of pile-raft-foundation to a new type of foundation called composite piled raft foundation or unconnected piled raft foundation. The foundation is composed of a sand/gravel cushion sandwiched between the raft and piles. The piles group may contain short and long piles. The short piles are constructed of flexible materials such as soil-cement columns or sand-gravel columns, and are used mainly to improve the bearing capacity of shallow soft soil; the long piles, which are made of relatively rigid materials such as concrete, and their main function is to reduce settlements. The cushion plays an important role in mobilizing the bearing capacity of the subsoil and in modifying the load transfer mechanism of the piles. In Shanghai, China, this system of unconnected piled raft has proved to be quite suitable and effective in coastal areas, where deep soft soil deposits exist.

Fioravante and Giretti (2010) performed a centrifuge test on piled raft foundation in sandy soil. They found that contact piles act as settlement reducers by diffusing the load applied to their heads to greater and deeper volumes of soil. They also observed that the load sharing mechanism depends on both properties of the piles as well as the stiffness of the soil cushion underneath raft. Providing a deformable layer between the raft and the pile heads might not insure compatibility of displacements, and the pressure in the cushion is partly transmitted to the pile heads and partly to the soil between the piles, which may cause a downdrag force on the upper part of the piles. The unconnected piles act mainly as soil

© 2016 Deep Foundations Institute

reinforcement. The presence of a flexible gravel/sand cushion between pile heads and raft minimizes the differential settlements between pile heads and soil underneath the raft.

Song and Wu (2009) studied the use of an unconnected piled raft with cushion using rigid composite piles composed of cement-fly-ash-gravel (CFG) or concrete piles without reinforcement. They investigated the seismic behavior of these unconnected piles using both shaking table tests and seismic finite elements analysis. They explained that this composite system is widely used in northern China, especially in the surrounding regions of Beijing. They added that the system is proven to be a technically and economically feasible alternative to connected piled raft, specifically for buildings that are less than 30 stories and subject to earthquakes. Siegel (2011) proposed a simplified model for shallow foundation on composite ground where the foundations settlement is estimated as the sum of the downward movement of the piles and the downward movement of the shallow foundation relative to the pile head. Siegel (2011) concluded that although the model has been applied to two examples of shallow square foundations, it should be validated before final design by an acceptable large-scale load test.

Baziar and Azizkandi (2012) studied the behavior of connected and unconnected piled raft systems under seismic loading using ABAQUS finite elements software. They concluded that the unconnected piled raft has provided better performance compared to the connected piled raft under static and seismic loads. They stated that the bending moments along the unconnected piles have decreased significantly, while the horizontal displacement has increased slightly. Sharma et al. (2012) studied the behavior of composite piled raft foundation, with and without intermediate cushion, in layered soil under seismic forces. They also concluded that the unconnected piled raft with intermediate cushion is effective in decreasing bending moments and axial stresses at the pile head than when no cushion is considered.

FINITE ELEMENTS MODEL

Soil Data

Site investigation geotechnical data are collected from the Lake Mariout area, west of Alexandria city, on the Mediterranean Sea coast in Egypt, where large industrial and residential developments have been recently planned for construction. In general, the subsoil at the site consists of four distinct layers. The first is medium dense sand having an average thickness of 4 m. The second layer is a soft to very soft silty clay, extending down to a depth of 10 m. The soft clay is followed by a stiff-to-very stiff clay layer extending down to a depth of 15 m. The fourth layer is dense sand and extends down to a depth of 22 m. The ground water table is at the ground surface. The soil parameters are summarized in Table 1.

Model Description

A three-dimensional finite element commercial software (ABAQUS) is used in the analysis. The superstructure, raft, cushion and piles are elements in a finite region and are modeled as elastic materials. These elements are modeled by an eight-node linear brick element with reduced integration and hourglass control (C3D8R).The soil is divided into two sub-domains: the near-field region (finite region) and free far-field region. The near field region is modeled with elastic ideally plastic constitutive model. The soft clay layer is modeled by using the modified cam clay plasticity model. The other soil layers are modeled by elastic ideal plastic constitutive model following Mohr-Coulomb yield criterion. Soil mass is described by an eight-node brick, tri-linear displacement and tri-linear pore pressure element (C3D8P). The far-field region is modeled by an eight-node three-dimensional infinite element (CIN3D8). The CIN3D8 infinite element is considered in this study to represent the energy absorption by the far-field soil to avoid reflection of dilatational and shear wave energy back into the finite element model (Chu and Truman (2003)). The infinite elements are assumed to have linear behavior. Infinite elements are defined as which connected nodes to finite model and nodes of infinite side are open which it provides support fixed conditions in far field. The horizontal boundary conditions are chosen to be infinite element and bottom boundary is constrained against vertical directions by fixed support.

© 2016 Deep Foundations Institute

Three-dimensional 10-storys-space structure of square typical floors resting on non-homogeneous soil medium is analyzed nonlinearly considering the soil-structure interaction. The model has two bays and the distance between the column centers is 4.5 m. The heights of ground and typical floors are assumed to be 3.0 m. The structural system of all roofs is assumed to be a 20-cm-thick flat slab.

Table 1. Soil parameters used in modeling

Material		Raft	Cushion	Pile	Medium sand	Soft clay	Stiff clay	Dense sand
Model		Elastic	Elastic	Elastic	Mohr-Coulomb	Modified Cam-clay	Mohr-Coulomb	Mohr-Coulomb
E, (MPa)		3.4E4	40	2.1E4	40	1.25	20	70
Poisson ratio		0.20	0.25	0.20	0.3	0.45	0.35	0.25
s_u, kPa		---	----	----	-----	12.5	120	------
ϕ, degrees		----	----	----	35	----	5.0	38
λ-factor		--	--	--	-	0.25	-	-
κ-factor		--	--	--	-	0.028	-	-
Void ratio		--	--	--	0.6	1.4	0.7	0.5
γ_{sat},(kN/m^3)		25.0	20	25	18.0	16.0	18.0	18.0
K, (m/sec.)		--	----	----	0.0001	1×10-8	1×10-7	0.0001
k_o		--	----	----	---------	1.00	1.00	---------
M		--	----	----	-------	1.00	1.00	---------
Elevation(m)		0.8	0.3	12	0-4	4-10	10-15	15-22
ξ		2%	5%	2%	5%	5%	5%	5%
Damping	α	0.024	0.436	0.024	0.436	0.088	0.318	0.705
	ß	0.0167	0.0057	0.017	0.0057	0.028	0.0078	0.0035

where: E = Young's modulus, s_u = undrained shear strength, ϕ = angle of shearing resistance, λ = slope of the normal compression line, κ = slope of a swelling line, γ_{sat} = Saturated unit weight, K =Coefficient of permeability, k_o = Coefficient of lateral pressure at rest, M =Slope of the critical-state line, ξ = damping ratio, α and ß= Rayleigh damping coefficients.

Columns dimensions are 0.6 × 0.6 m. The thickness of the raft is 0.8 m and the cushion thickness is 0.3 m, the pile diameter is 0.6 m and the pile length is 12 m. Fig. 1 shows modeling and meshing of piled raft foundation in the ABAQUS software. Additional details and verification of the numerical model are in Ata et al. (2015).

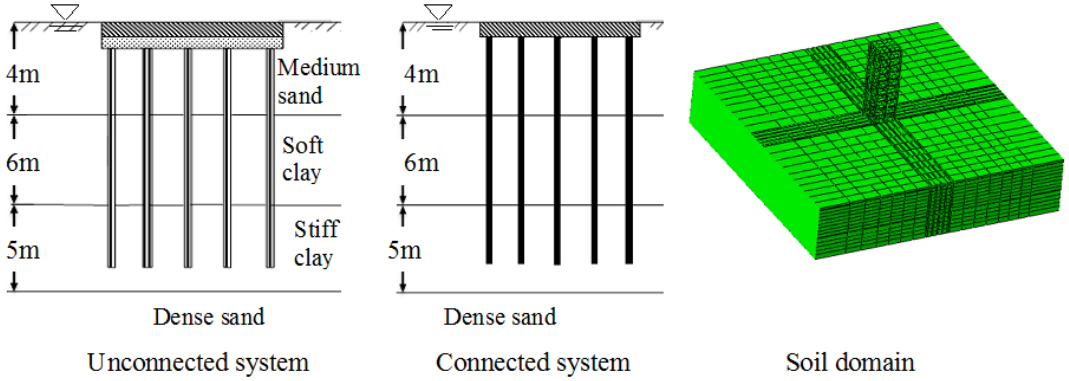


Fig. 1. Models and meshing for unconnected and connected pile rafts

© 2016 Deep Foundations Institute

The load is applied in four steps. In the first step, the initial condition is applied to the soil with geostatic command. The effective body forces are calculated to account for geostatic equilibrium before the loads are applied; next (static load), the slab and raft are subjected to a uniformly distributed load of 21.5 kN/m^2. Therefore, the estimated total load on the square raft is 21.5 MN. The third step is the consolidation step which takes up to 10.0 years. In the last step, seismic loading is applied at the base level of the soil domain in the horizontal direction only as acceleration time history. Time history analysis of El-Centro 1940 earthquake is used in this study. The Imperial Valley or El-Centro 1940 earthquake, southern California, USA had a moment magnitude of 7.1. The time history of the earthquake is scaled to an acceleration of 0.2 g and is presented in Fig. 2.

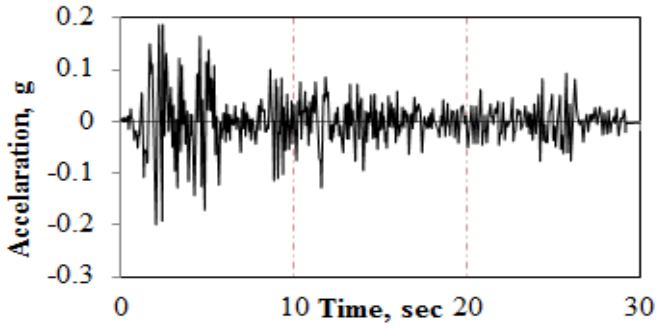
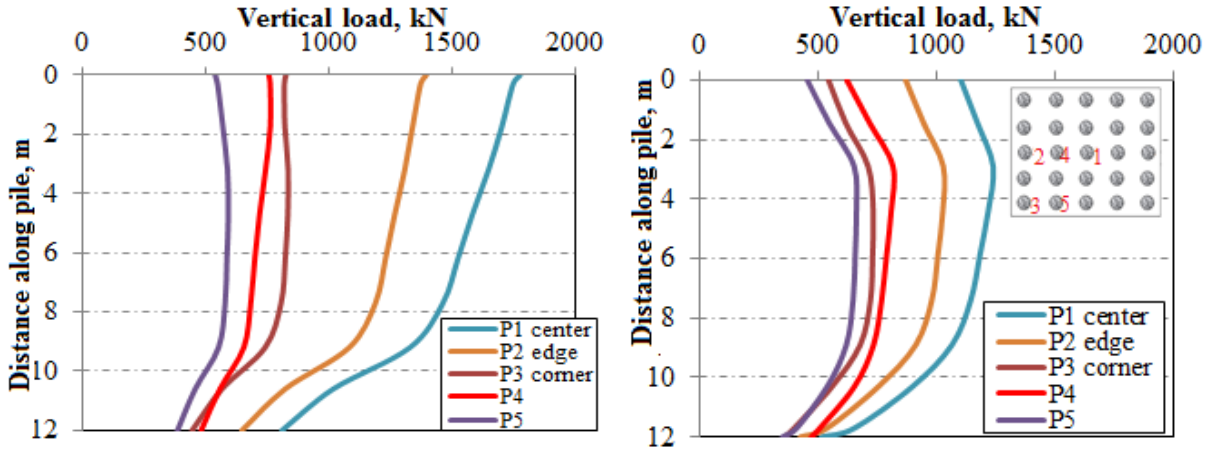


Fig. 2. Acceleration time history of the El-Centro 1940 earthquake

RESULTS AND DISCUSSION

Results for vertical loads along piles, shear stresses, and bending moments are compared for the two cases of connected and unconnected piled rafts. In addition, the vertical and horizontal displacements at foundation level and at the top of the structure are also compared for both systems. The distribution of the vertical loads along the pile length for selected piles under static loading for the connected and unconnected systems, are shown in Figs.3a and 3b, respectively. The layout of the piles is shown in Fig. 3b, where the centers of piles Nos. 1, 2, and 3 coincide with the columns centers.



a) Connected b) Unconnected

Fig. 3. Vertical load distribution along pile length under static load

For the case of connected piles, Fig. 3a, the piles that are directly under the columns, carry most of the axial column load and are also greater than the loads on any other piles located away from the columns. The maximum vertical loads at pile number 4, which is located away from columns, is less than the pile number 1, under the column center, by about 57%. The vertical load along the pile length in the

© 2016 Deep Foundations Institute

unconnected system is significantly smaller than that in the connected system, especially at piles immediately under the columns. Moreover, in the case of unconnected piled raft, the loads are almost equally distributed on all piles, regardless of proximity to columns. The maximum vertical load in the connected system occurs at the pile head, and then decreases along the length of the pile. However, in the unconnected system, the location of maximum vertical load is shifted downwards to a certain depth below the pile head. In the unconnected system, the static vertical loads at the pile heads are less than that of the connected system by about 38%.

Fig. 4 presents the vertical dynamic load time history at the pile head of the center pile in the connected and unconnected systems. From this figure it is again confirmed that the vertical load in the unconnected system is smaller than that in the connected system under seismic load. These differences between the connected and unconnected are due to the existence of the cushion under the raft. In the unconnected system, the maximum vertical load at the pile head is reduced by 43%.

Fig. 5 shows the bending moment distribution along the pile length which is calculated from the vertical stresses along the side of the central pile for connected and unconnected systems. The bending moment is calculated by using the equation,

$$M = \frac{(\sigma_l - \sigma_r)}{y} I \qquad [1]$$

Where M is the bending moment, σ_l and σ_r are the normal stress at the left and right sides of the pile, respectively, y is the distance between the left side and right side and I is the moment of inertia of the pile. Fig. 5 shows that at a time of 4.33 sec, the bending moment value at the pile head in the unconnected system is smaller than that in the connected system by about 100%.

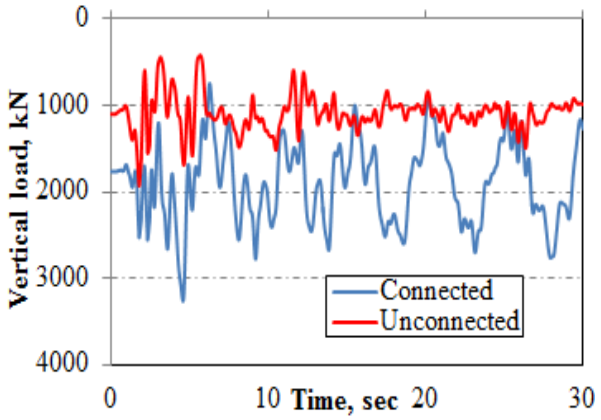


Fig. 4. Vertical load at the head of the center pile

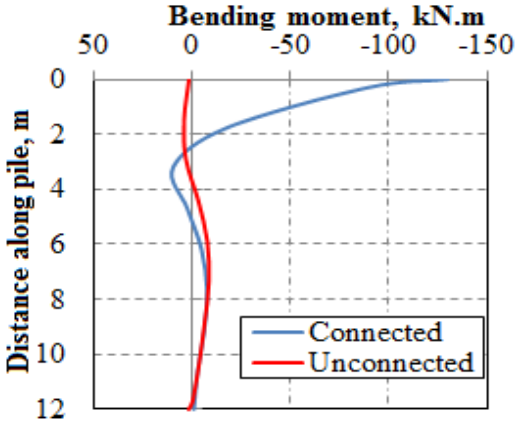


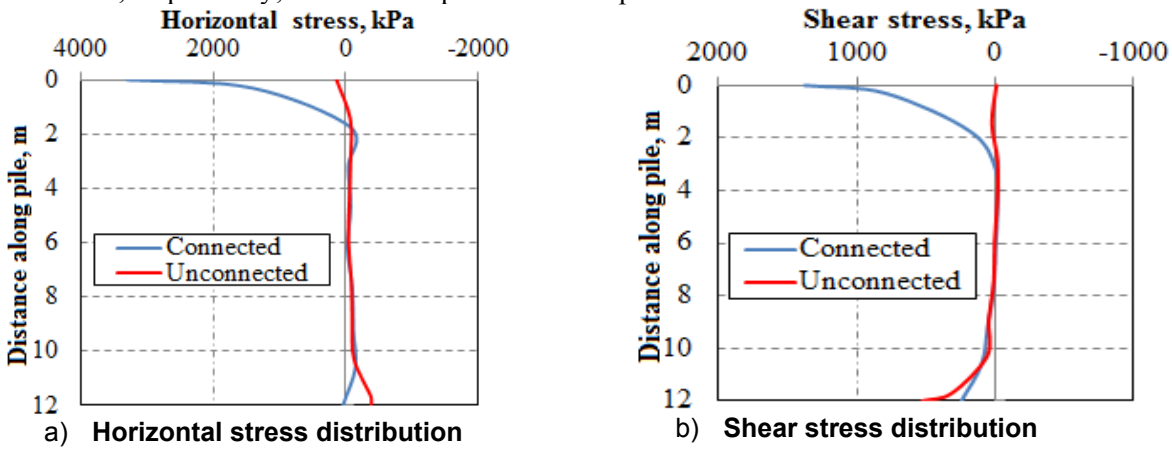
Fig. 5. Bending moment distribution along center pile at 4.33 seconds

Fig. 6a shows the horizontal stress distribution along the pile length for connected and unconnected systems at the central pile. Fig. 6b shows the shear stress distribution along the length of pile for connected and unconnected systems at the central pile. The figures show that for the connected system, the maximum horizontal and shear occurs at the pile head due to the connection between raft and pile, and then decreases along the pile length. However, in the unconnected system; these stresses values totally diminish at the pile head due to the presence of the cushion. So it is clear that the cushion has the effect of shock absorption.

Fig. 7 shows the lateral displacement at the top level of structure and at the base of the soil domain, at the center of top surface of raft in the unconnected system. The results indicate that the lateral displacement at the top level of the structure is generally higher when compared to that computed at the base of the soil domain. The lateral displacement at the top level of structure is greater than the lateral displacement at the raft surface. In addition, the location of the peak lateral displacement at the base of the soil domain does not coincide with the location of the peak lateral displacement at the top of structure. The value of the

© 2016 Deep Foundations Institute

maximum lateral displacement at the raft surface and at the top of the structure is approximately 120 mm and 324 mm, respectively; which corresponds to an amplification of 268%.



a) **Horizontal stress distribution** b) **Shear stress distribution**

Fig. 6. Stress distribution along pile

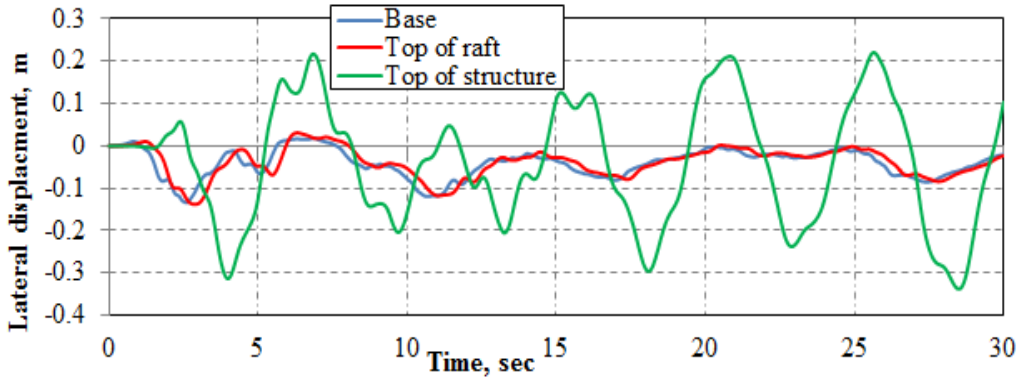


Fig. 7. Lateral displacement under seismic load for unconnected piled raft system

Fig. 8 shows the vertical displacement at the center of the top surface of raft for unconnected and connected systems under seismic loads only. From the figure, it can be seen that the final settlement of the unconnected system is only 1-mm greater than that of the connected system. This slight difference in settlement is attributed to the settlements that took place within the cushion body itself.

From this analysis it is confirmed that, for the studied cases, the performance of the unconnected system is better than connected system as stresses generated in the unconnected system are smaller, while the settlements in both cases are similar.

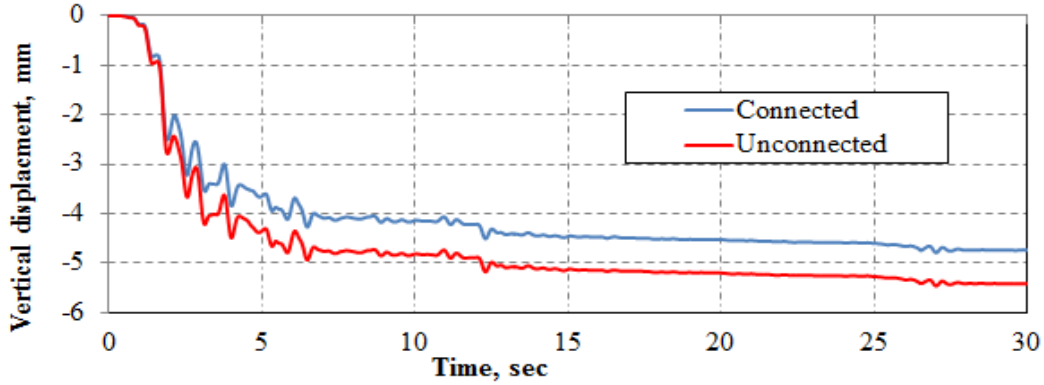


Fig. 8. Overall displacement under seismic load for connected and unconnected systems

© 2016 Deep Foundations Institute

ECONOMIC FEASIBILITY CASE STUDY

In order to assess the economic feasibility of the unconnected system, a case study of an existing 14-story residential building is investigated. The actual building is founded on a connected piled raft resting on stratified soil deposits. The groundwater level is at 2.5 m below the ground surface. Table 2 presents the soil parameters at the selected site.

Structures Geometry

The structure of the case study is summarized as follows:
Building height = 42.0 m, footprint area = 16.88 m x 13.56 m, number of shear walls = 13 walls, shear wall dimensions = 0.3 m x 2.0 m, length of piles = 12.0 m, diameter of piles = 600 mm, number of piles = 81, thickness of raft = 1400 mm, bottom level of raft = 2.4 m below the ground surface. Total applied load on the raft = 200 kPa. Allowable capacity of pile = 850 kPa.

ANALYSIS AND RESULTS

The selected project was originally designed and constructed as a pile group system, where the entire load is supported by 81 piles each extending down to 12 m. A finite element model has been developed for the three cases of raft, connected piled raft and unconnected piled raft with cushion and all are supported on the same number of piles (81 piles).

Table 2. Soil parameters at the site of the case study

Material	Silty clay	Clayey silt	Medium Dense sand	Very dense sand	Raft	Cushion	Pile
Model	Mohr-Coulomb	Mohr-Coulomb	Mohr-Coulomb	Mohr-Coulomb	Elastic	Elastic	Elastic
E, (Mpa)	10.0	4.0	110	150	3.4E4	20	2.1E4
Poisson ratio	0.35	0.4	0.25	0.25	0.20	0.25	0.20
γ,(kN/m^3)	18	16	18	18	25.0	18	25
Void ratio	0.8	1.2	0.7	0.5	--	--	--
ϕ, ^{o}	5.0	5.0	35	40	----	----	----
s_u, kPa	100	30	1	1	---	----	----
ψ	0	0	5	10	--	----	----
Depth (m)	2.2	3.3	2.5	27.0	1.4	0.3	12.0

Fig. 9 presents a comparison of the settlements of the raft, connected piled raft and unconnected piled raft systems with cushion. The cushion is 0.3 m thick, and is assumed to be composed of compacted sand having a Young's modulus of 20 MPa. From Fig. 9, it can be seen that the maximum settlement of raft foundation is much greater than the allowable settlement. Therefore, deep foundation piles should be employed underneath the raft to increase the bearing capacity and minimize the settlements. It can be also observed that, compared to the case of raft without piles, the maximum settlement of the connected piled raft has decreased markedly by 90.4 %, while the maximum settlement of the unconnected piled raft has also decreased by a close value of 85.2%.
Fig. 10 summarizes the pile loading ratio for the three cases of pile group, connected piled raft and unconnected piled raft. It is observed that for the case of pile group, the entire load is carried by the piles. However, for the case of the connected system, the pile load share has reduced to 86% of the total load. For the case of the unconnected system, the pile load share has been further reduced to 79% of the total load.

© 2016 Deep Foundations Institute

Fig. 11 shows the axial load distribution in the piles, for the two cases of connected and unconnected systems. From this figure, it can be seen that for the connected piled raft the axial load is maximum at the top of the pile (at the raft-pile connection), and then decreases with depth down to be a minimum at the tip of the pile. The maximum axial stress in the case of connected system is greater than that in the case of unconnected system.

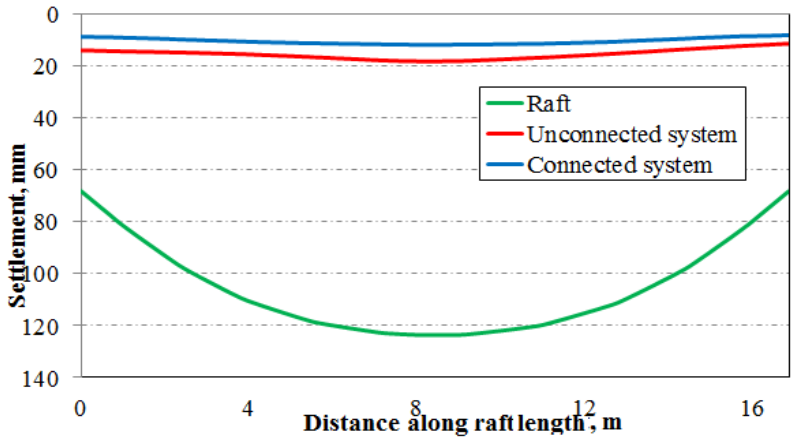


Fig. 9. Overall settlement of the raft, unconnected and connected systems

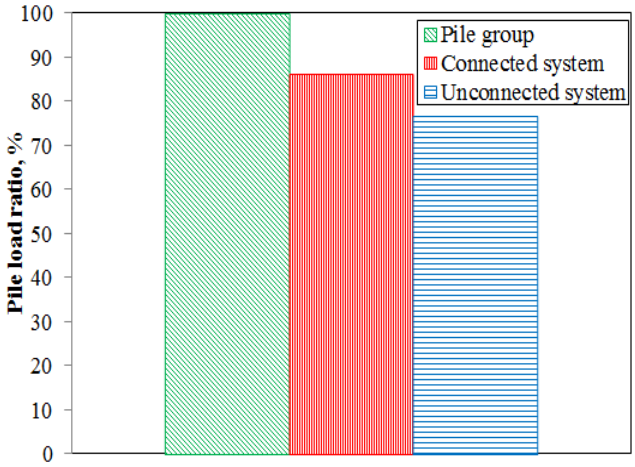


Fig. 10. Pile loading ratio for pile group, connected and unconnected systems

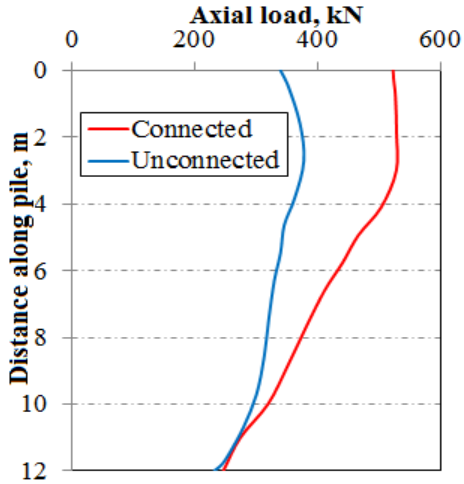


Fig. 11. Axial load along pile for connected and unconnected systems

A further attempt to optimize the number and length of piles (for the case study) to reach a more economical design, provided that settlements are limited to values specified by the Egyptian Code of Practice for soil mechanics and foundations (2003). New runs were performed to compare the settlements of the unconnected system for the following four cases:

- Case 1: n= 81 and L= 12 m,
- Case 2: n= 81 and L= 10 m,
- Case 3: n= 47 and L= 12 m, and
- Case 4: n= 81, L= 12 m and the pile material is sand cement.

Fig.12 shows that for all the four cases, the maximum settlement of foundation is smaller than the allowable value of 150 mm prescribed by the Egyptian Code for rafts on clayey soil. It is also observed that compared to the case of raft without piles, the maximum settlement of the unconnected piled raft for Case 1 has decreased by 85.2%, while the maximum settlement for Case 2 has decreased by 84%, and the

© 2016 Deep Foundations Institute

maximum settlement for Case 3 has decreased by 80% and the maximum settlement for Case 4 has also decreased by 79%.

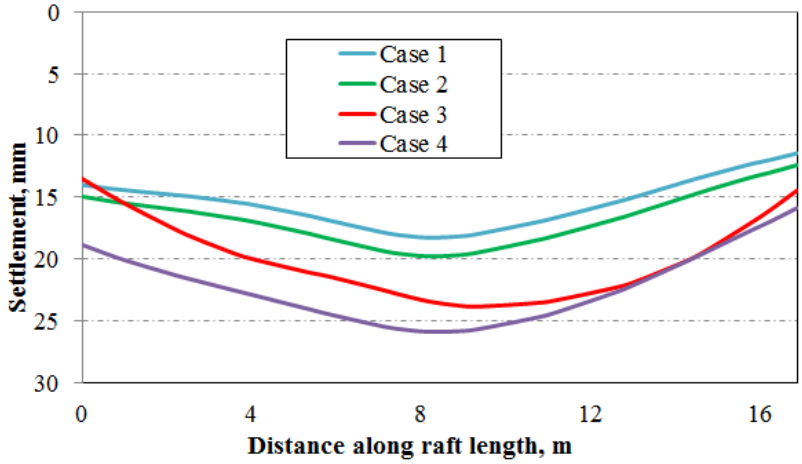


Fig. 12. Overall settlement at top of foundation for Cases 1 through 4

COST ANALYSIS

This section presents an attempt to quantify the economic advantage of using unconnected in lieu to connected piled raft. Table 3 presents the estimated construction cost of the case of pile group foundation. Table 4 shows the estimated construction cost of case 1 of the unconnected system (where n= 81 and L= 12m). The estimated construction costs are in Egyptian pounds as of the year 2014-2015. From Tables 3 and 4, it is clear that the alternative of unconnected piled raft (case 1, using the same number and length of piles) has resulted in a savings of 57.8 % in the cost of piles; which correspond to the savings in the estimated cost of steel reinforcement and pile head demolition.

Tables 5 and 6 present the construction cost analyses for cases 2 and 3, where attempt is made to consider additional saving by decreasing the length and the number of piles, respectively. From Table 5, the unconnected system allows for reducing the pile lengths from 12 m to only 10 m, while keeping settlements within acceptable limits. For this case, the cost savings is increased to 63.7%. For case 3, the number of piles is reduced to 47 instead of 81 and again while keeping settlements at the allowable limits and the cost savings has increased to 72.5%.

Table 3. Construction cost for the case of pile group foundation

Item No.	Description	Quantity	Unit	Rate (L.E)	Cost ((L.E)
1	Pile	972	m	270	262440
2	Pile head demolition	81	No.	300	24300
3	Plain concrete	45.77	m^3	400	18311
	Total cost	----	---	----	305051

Table 4. Construction cost for case 1 of unconnected system (n= 81 and L= 12m)

Item No.	Description	Quantity	Unit	Rate (L.E)	Cost (L.E)	Cost reduction, percentage
1	Pile	972	m	110	106920	60 %
2	Pile head demolition	-----	No.	300	----	100 %
3	Plain concrete	45.77	m^3	400	18311	0 %
4	Cushion	68.66	m^3	50	3433	0 %
	Total cost	----	---	----	128664	57.8 %

© 2016 Deep Foundations Institute

Table 5. Construction cost for case 2 of unconnected system (n= 81 and L= 10m).

Item No.	Description	Quantity	Unit	Rate (L.E)	Cost (L.E)	Cost Reduction percentage
1	Pile	810	m	110	89100	66 %
2	Pile head demolition	-----	No.	300	----	100 %
3	Plain concrete	45.77	m^3	400	18311	0 %
4	Cushion	68.66	m^3	50	3433	0 %
	Total cost	----	---	----	110844	63.7 %

Table 6. Construction cost for case 3 of unconnected system (n= 47 and L= 12m).

Item No.	Description	Quantity	Unit	Rate (L.E)	Cost (L.E)	Cost reduction percentage
1	Pile	564	m	110	62040	76 %
2	Pile head demolition	-----	No.	300	----	100 %
3	Plain concrete	45.77	m^3	400	18311	0 %
4	Cushion	68.66	m^3	50	3433	0 %
	Total cost	----	---	----	83784	72.5 %

SUMMARY AND CONCLUSIONS

In general, the proposed alternative of an unconnected piled raft is confirmed to be technically and economical feasible, where the piles are not designed as structural members but as soil reinforcing elements. The following are the specific conclusions from the parametric study under seismic load for soil profiles uses in the study:

1- In the connected piled raft, the maximum axial load occurs at the pile head, while in the unconnected piled raft, the location of maximum axial stress is shifted downwards to a certain depth below the pile head.
2- The maximum horizontal stress and shear stress in the connected system occurs at the pile head, and then decreases along the length of the pile. However, in the unconnected case; these values totally diminish at the pile head due to the presence of the cushion. So it is clear that the cushion has the effect of shock absorption for the straining action.
3- The maximum vertical load at the pile head is reduced by 43% for the unconnected system under seismic load, and the maximum bending moment at the pile head is reduced by 50% to 100% for the unconnected system.
4- In unconnected piled raft there is no need to reinforce the piles, no need for pile head demolition nor for expensive waterproofing of pile-head-raft connection. Furthermore, the horizontal force can be resisted directly by the raft-soil cushion interface, and by the passive pressures mobilized by basement underground walls.
5- There are no appreciable differences in the lateral displacement of the connected and unconnected systems under lateral seismic loads. Therefore, the maximum lateral displacement is only affected by the structural system and stiffness of the superstructure, rather than whether the raft is connected or disconnected from the piles.
6- Cost analyses of unconnected versus connected piled raft systems confirmed a construction cost savings that may reach from 50 to 70 percent.

© 2016 Deep Foundations Institute

REFERENCES

Alaa Ata, Essam Badrawi and Marwa Nabil, 2015. Numerical analysis of unconnected piled raft with cushion. Ain Shams Engineering Journal, ASEJ, Vol. 6, Issue 2, June 2015, Pages 421-428.

Baziar, M.H. and Azizkandi, A.S., 2012. Response of Piled Raft Foundation Under Seismic Load; Connected And Non-Connected Systems. PEER Report. Seismic Performance of Structural Systems, pp. 303-312.

Chu, D. and Truman, K. Z., 2003. Modeling Of Unbounded Domain in Seismic Soil-Pile-Structure Interaction. Proceedings of the 6th Technical Council on Lifeline Earthquake Engineering, Long Beach, CA.

Egyptian Code for Soil Mechanics and the Design and Construction of Foundations, 2003, Code 202, Vol. 4, Deep Foundations.

Fioravante, V. and Giretti, D., 2010. Contact versus Noncontact Piled Raft Foundations. Canadian Geotechnical Journal, 47(11) 1271-1287.

Liang, F.Y., Chen, L.Z., and Shi, X.G., 2003. Numerical Analysis of Composite Piled Raft With Cushion Subjected To Vertical Load. Computers and Geotechnics, Vol. 30, pp. 443-453.

Sharma, V.J, Vasanvala, S.A. and Solanki, C.H., 2012 Behavior of Composite Piled Raft Foundation With Intermediate Cushion In Layered Soil Under Seismic Forces. International Journal of Applied Engineering and Technology, 2(3) 36-48.

Siegel, T.C., 2011. Simplified Settlement Model for a Shallow Foundation Composite Ground with Rigid Piles. DFI Journal, Vol. 5, No. 1, pp. 68-72.

Song, E. and Wu, S., 2009. Seismic Analysis of Rigid Pile Composite Ground. Advances in ground improvement: research to practice in the United States and China: proceedings of the US-China Workshop on Ground Improvement Technologies, Orlando, Florida, pp. 189-197.

© 2016 Deep Foundations Institute

This page left intentionally blank

© 2016 Deep Foundations Institute

CONSTRUCTION OF A DEEP SOIL MIXED CUT-OFF AND RETAINING WALL IN RICHMOND BC

Keith MacKay, Golder Associates, Vancouver, BC, Canada, 604 345 5797, KMacKay@golder.com
Fernando Faminia, Golder Associates, Vancouver, BC, Canada, 604 354 1429, FFamania@golder.com
David Siddle, Golder Associates, Vancouver, BC, Canada, 604 296 2893, DSiddle@golder.com
John Carter, GeoPacific Consultants Ltd., Vancouver, BC, Canada, 604-439-0922, Carter@geopacific.ca

ABSTRACT

The River Green Residential development, is located in the municipality of Richmond, BC adjacent to the Fraser River. Ground conditions at the site consisted of medium to fine grained alluvial sands and a high groundwater elevation. A temporary low permeability retaining wall was required in order to facilitate the construction of an underground parking structure without inducing settlement of adjacent structures, which include the Richmond Olympic Oval; part of the legacy of the Vancouver 2010 Winter Olympics. Golder Associates Ltd. and GeoPacific Consultants Ltd. utilized Cutter Soil Mixing (CSM) technology to enable construction of a continuous combined low permeability cut-off and retaining wall around the perimeter of the property. The 350m long wall was keyed into marine clay at a depth of 28m below ground surface, and contained H-Pile reinforcement installed at regular intervals. The CSM technology provided many benefits for this project, allowing the combined cut-off and retaining wall to be constructed within a very narrow footprint (650mm width). The low noise impact and near vibration free construction of the CSM equipment provided minimal inconvenience to nearby stakeholders during construction. To reduce dewatering volumes during excavation and prevent significant water-table drawdown the Hydraulic Conductivity requirements for the wall were 1 x 10-7 cm/s or less. Project specifications called for a different strength requirement for upper and lower portions of the wall. The top 13 meters of the wall required an Unconfined Compressive Strength (UCS) of 4MPa to act as a retaining and cut-off wall, whereas the bottom 15 meters of the wall required a UCS of only 0.5 MPa to act only as a cut-off wall. Wet-grab and core samples were obtained from the panels to confirm the UCS and Hydraulic Conductivity specifications were met.

Keywords: Cutter Soil Mixing, Seepage Control, Deep Mixing, Quality Control and Assurance

INTRODUCTION

Golder Construction Inc. and GeoPacific Consultants Ltd. conducted the design and construction of a deep soil mixed cut-off and retaining wall system. The “dry-box” solution was used to surround the excavation of an underground parkade and prevent flows of groundwater into the excavation.

Cutter Soil Mixing (CSM) is a form of the deep mixing method developed by BAUER and Soletanche. CSM consists of two cutter wheels, rotating around a horizontal axis, penetrating the ground while cement or bentonite slurry is injected out of a nozzle located between the two wheels. In this application, CSM was used to cut into natural soils, inject bentonite and cement slurries, and mix the resulting combination into a soil cement material. The CSM operator controls the penetration rate of the cutter wheels and flow rate of slurry injection in order to reach a target “injection rate” (or target volume of slurry per meter depth of panel). The operator also controls the speed and direction of rotation of the two cutter wheels in order to optimize the mixing of the soil cement material and deviation of the final soil cement element. An example of the CSM cutter head and process is presented in Figure 1 on the following page.

© 2016 Deep Foundations Institute

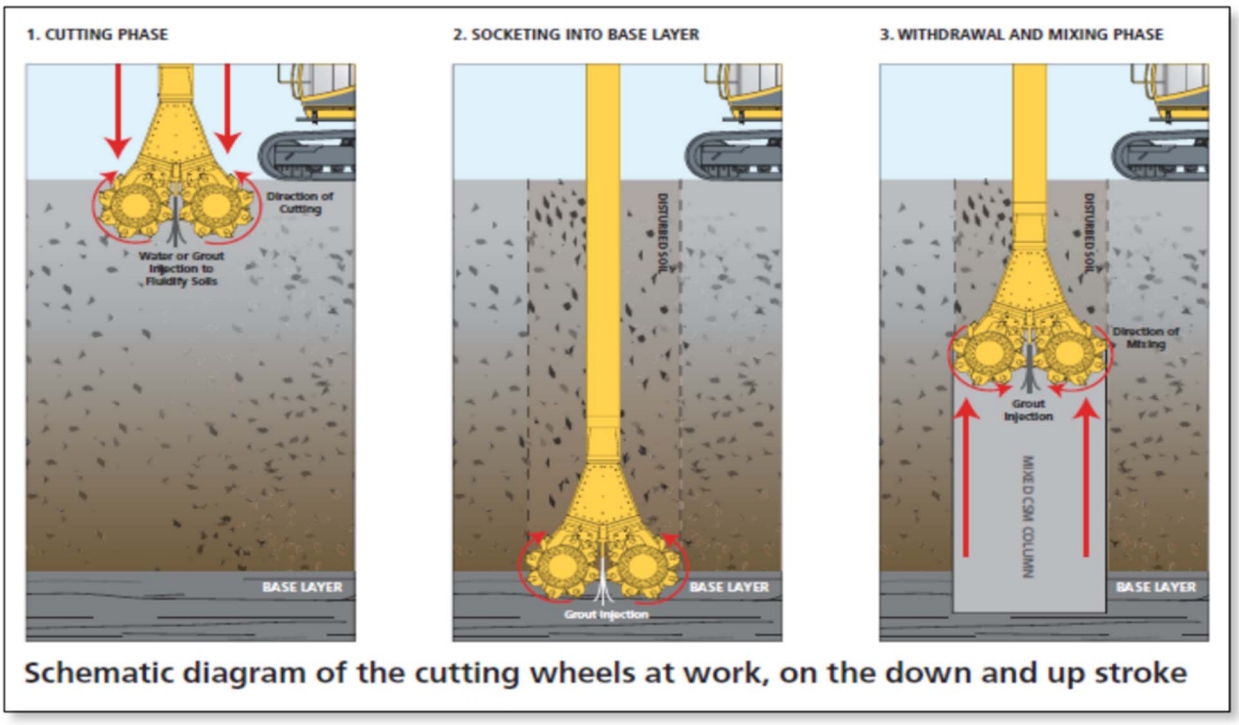


Figure 1: The CSM panel production procedure. A form of the deep mixing method. (Bauer 2007)

SITE LAYOUT AND LOCATION

The proposed development is located in the City of Richmond, BC atop the Fraser River delta, and adjacent to the Fraser River and the Richmond Olympic Oval as shown in Figure 2 of the following page. The area where the site was located had historically been used for commercial purposes, but is slowly changing to residential – with several planned developments nearby. The ground conditions of the City, namely high water tables and coarser grained permeable soils, make deep excavations difficult. The City has a chronic shortage of parking spots, and hesitates to issue building permits to developments without sufficient parking. As such, an underground parkade was required in order to comply with the city by-law.

The design of the cut-off and retaining wall consisted of 139 soil cement panels with I-beam reinforcement arranged in a hexagon surrounding the boundaries of the proposed excavation. The Northeast, Southeast and Southwest corners of the site were bounded at 90 degree angles, whereas the Northwest corner of the site deviated inwards. This layout is pictured in Figure 3 on the following page.

© 2016 Deep Foundations Institute



Figure 2: A view of the site, highlighted in red, adjacent to the Fraser River and the Richmond Olympic Oval. (Google Earth 2016)

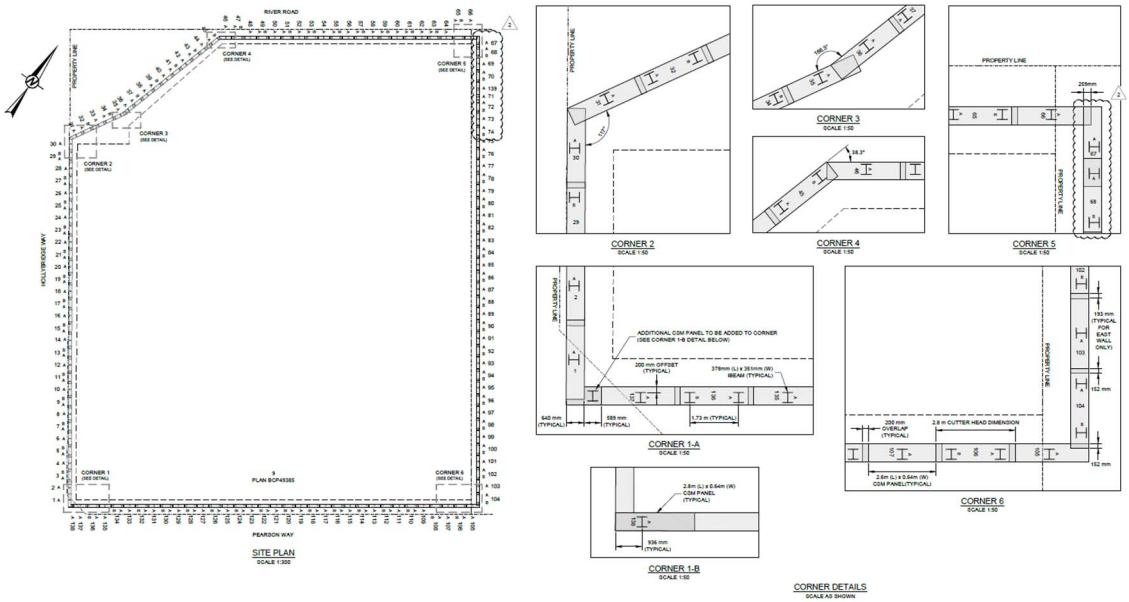


Figure 3: The layout of the deep mixing panels and imbedded H-piles. (Golder Associates, 2014)

© 2016 Deep Foundations Institute

SITE INVESTIGATIONS

Detailed site investigations were conducted by GeoPacific Consultants Ltd in 2010, 2011, 2013 and 2014. The site investigations included four solid stem auger test holes of depths up to 7.6m below ground surface, seven cone penetration tests of depths up to 48.3m below ground surface, and five sonic dill holes of depths up to 19.8m below ground surface. Several piezometers were located around the site, and it was determined that the groundwater elevation was both close to surface and variable with the tides.(GeoPacific, 2013)

SITE GEOLOGY & GROUND CONDITIONS

The site consisted of a fine to medium grain sands, with varying amounts of silt down to approximately 27m depth where a marine clay unit was located. The sand and silt material was expected to have quite high permeability, which would cause issues of water inflow during the proposed 7m deep excavation. During one of the site's previous uses, gravel columns had been installed at an approximate 2.4m spacing.

LABORATORY TRIAL

In order to determine which binder type, binder content, and mix parameters were to be used in construction of field trial panels, a soil-cement laboratory trial was conducted. Samples of material were collected from site, brought to Golder Associates' testing laboratory, and mixed with varying contents of bentonite, cement, GGBS (Ground Granulated Blast Slag), magnesia, and lime. Fifteen unique batches of soil-cement were prepared in the laboratory and tested for Unconfined Compressive Strength (UCS) and permeability. A range of target water contents was chosen to prepare the samples to, based on data from wet grab soil cement samples previously obtained from a site with similar soil and groundwater conditions. The water to cement ratio of each samples was found to be a great determiner of the strength of the soil cement panels, whereas GGBS content was found to decrease the permeability. Results of the laboratory trial testing are presented in Figure 4 below.

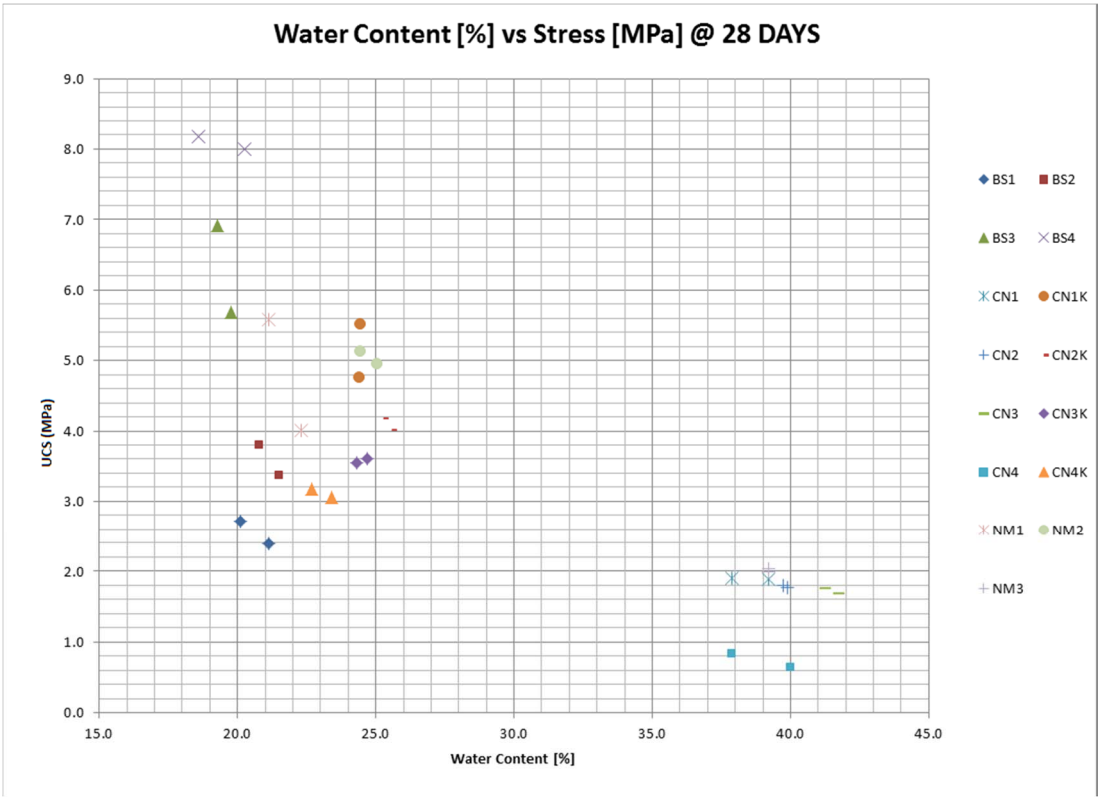


Figure 4: Laboratory trial results.

© 2016 Deep Foundations Institute

FIELD TRIAL

In order to confirm the soil cement samples constituted in the lab were an accurate representation of the in-situ CSM production process, a field trial program was initiated. The field trial consisted of 11 interlocking panels of 1 meter thickness installed in the middle of the site as displayed in Figure 5 below. The panels were constructed to varying depths, with only one penetrating to the full 28m required of the production panels. In the upper portion of the panels, where a UCS of 4MPa was required, a higher cement slurry injection rate was used to achieve a higher cement content, whereas in the lower portion of the panels, where a UCS of only 0.5 MPa was required, a lower cement slurry injection rate was used. Wet-grab and core samples were retrieved from various depths of each panel, and tested for UCS and permeability.

There were several important findings resulting from the field trials, which were fed into the standard operating procedure and final mix design for production panel installation. It was determined that using bentonite slurry as a cutting fluid, in replacement of water, results in faster penetration rates and less abrasion to the CSM cutter wheels. A Portland Cement and GGBS mix was found to provide the most suitable results for strength and permeability. Panels cut through gravel columns were found to have slower penetration rates. In general, panels were found to have a stratigraphy that matched that expected; with higher strengths found at the depths with higher injection rates, and lower strengths found at the depths with lower injection rates. Panels cut through gravel columns were found to lack this stratigraphy and have samples with generally a higher moisture content; indicated that the wet soil-cement mixture had "flipped" after cement slurry injection (ie. the high inject rate material at the top of the panel had sunk below the low injection rate more buoyant material at the bottom of the panel). The mix design chosen for production panels met project requirements in both native ground and gravel columns. UCS results from a field trial panel are presented in Figure 6 on the following page.



Figure 5: Field Trial Panels exposed to ensure interlocking connection.

© 2016 Deep Foundations Institute

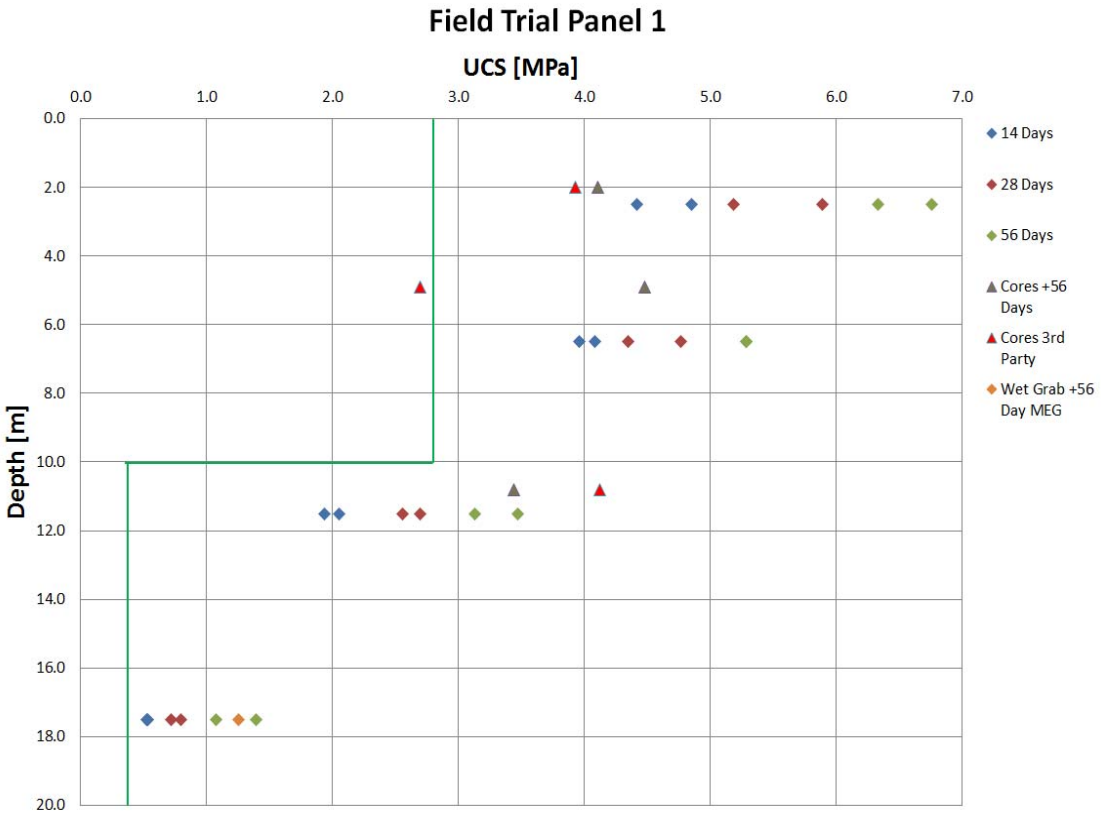


Figure 6: UCS results from a Field Trial Panel.

CONSTRUCTION METHODOLOGY

Equipment and Logistics

A Bauer RG25S CSM rig was mobilized to site for soil cement panel installation. Due to the space-constraints of the project, 650mm width wheels were imported for production panels. It was found that the smaller footprint of the wheels, afforded slightly faster panel production than had been experienced during field trial panel production. A high-shear mixer was brought to site, in order to combine the bentonite with water and ensure it was properly sheared prior to hydration. Two 80,000 liter tanks, with agitators were placed onsite to store the bentonite while it was being hydrated. A MAT SCC 30K batchplant was used to batch cement slurry, and could produce over 30,000L of slurry per hour at full operating speed. The batch plant was fed by two cement silos, one at 90mT containing GGBS-portland cement blend and one at 50 mT containing pure portland cement. The batch plant fed into an agitator tank which could store over 5,000L of cement slurry prior to it being injected into the ground during CSM production. Due to the setup time of the cement slurry, batching would start only once the CSM panel penetration had reached a certain depth. This was to ensure there would be enough time for wet-grab sampling and H-Pile installation into the fresh soil cement panels once CSM production was complete. H-Piles were typically installed within 2 hours of completing each panel, and no major issues were encountered. The batching area was covered by a larger tent, in order to protect batching activities from the heavy rains associated with the area.

© 2016 Deep Foundations Institute



Figure 7: RG25S installing CSM panels on the western edge of site.

Quality Assurance and Quality Control

The production of CSM panels contains many stages of quality control and assurance. A detailed Inspection and Test Plan was created, summarizing all of the quality steps for the soil mixing process. Water samples were retained from groundwater at the site and tested for contaminants which could potentially affect the curing of the soil cement. Shipments of cement and bentonite arriving onsite were tracked in an onsite log, and reconciled with quality documentation received from the suppliers. When bentonite slurry is batched as cutting fluid, it is tested by an onsite quality control technician for specific gravity, marsh viscosity and temperature, prior to being injected; to ensure it is mixed to the correct consistency and properly hydrated. When cement slurry was batched, it was tested for specific gravity prior to being injected, and batching proportions are recorded by the mixing computer.

During panel construction, the CSM's onboard computer measured and recorded cutter-head depth, injection volume per depth, cutter wheel rotation speed, cutterhead verticality in the X-Y plane, cutterwheel rotation speed, cutterwheel pressure, and other relevant panel construction parameters. After panel construction is complete – a specialized wet grab sampling device was lowered by crane into the fresh soil cement, and "wet-grab" samples were retrieved. The sampling device consisted of a steel capsule with a hydraulically actuated gate which can be open and closed at the desired depth to retrieve a sample of the wet soil cement. Once retrieved to surface, the wet grab samples were cast into 50mm by 100mm sample cylinders and tested for UCS and permeability at various curing times. UCS tests were conducted to ASTM D1633 and permeability was tested to ASTM D5084-10. Samples were cured onsite in a temperature and humidity controlled environment prior to testing. The temperature of the curing room was documented at regular intervals, to confirm the soil cement samples were curing in consistent conditions. An onsite laboratory conducted UCS testing in order to reduce the risks of damage to the samples at an offsite facility. Samples tested for permeability were transported to a nearby 3rd party lab for testing. At three intervals during the project, a mud rotary coring drill rig was mobilized to site, and cured soil cement panels were cored in order to retrieve soil cement samples which had been cured in-situ. The cored soil cement samples were tested for UCS and permeability.

© 2016 Deep Foundations Institute

Adjacent Sites Monitoring and Construction Vibrations

The Richmond Olympic Oval, located directly adjacent to the site, was constructed between 2006 and 2008, and is part of the legacy of the Vancouver 2010 Winter Olympics. The glass located on the windows of the Oval structure was susceptible to damage from construction induced vibrations. The excavation method employed by CSM results in minimal vibrations, especially when compared with conventional shoring techniques such as sheet pile driving. This made CSM a particularly attractive option, as it could complete work in close proximity to the adjacent structure, with minimal risk of damage to the adjacent structure. A MiniMate Plus Vibration Monitor and Geophone unit was used to measure vibrations adjacent to the CSM panel installation area. Peak Particle Velocities of less than 10 mm/s were recorded at a location approximately 2m away from the Cut-Off Wall alignment during CSM production.

Another concern was lowering the groundwater table below the foundations of the Richmond Olympic Oval during the excavation of the parking lot. A piezometer was installed to the west of the site, in order to confirm there was no change in the groundwater elevation due to activities inside the Cut-Off Wall footprint.

RESULTS

At the end of the project, the average UCS for all specimens tested, was 5.3 MPa. The average permeability of the bentonite-soil-cement samples tested was 8.8 x 10^{-8} cm/s. Some inconsistent core results were reported from one of the panels, but following excavation the core results were found to be unrepresentative. The project was completed to specification and ahead of schedule; the excavation was completed and tie-back anchors were installed as per the design and pictured in Figure 8 below. Tie-back anchors were tensioned against a strip of shotcrete placed ontop of the soil cement material of the wall.



Figure 8: The completed soil-cement wall, with a first row of tie-back anchors installed.

© 2016 Deep Foundations Institute

CONCLUSION

The proceeding was a synopsis of a cutting edge construction technique used to overcome an engineering challenge. Lessons learned include the following:

- CSM and the deep mixing method, in conjunction with tie-back anchors, can be used to construct a robust impermeable box around a proposed excavation; isolating the groundwater inside the excavation and providing sidewall support so that the excavation can be safely completed without affecting the groundwater elevation outside of the box.
- The deep mixing method, allows for different portions of a soil cement element to be constructed for different applications. In this case the top of each panel was constructed to act as a Cut-Off and Retaining Wall, whereas the bottom was constructed as only a Cut-Off Wall.
- Contractor involvement from an early stage can improve several aspects of a deep mixing project. Laboratory trials, field trials, and design can be constructive when they occur with contractor involvement and thereby produce opportunities for improving project costs, quality and schedule.
- CSM construction produces minimal vibration, reducing risk of damage to adjacent structures in urban areas, and improving stakeholder relations.

ACKNOWLEDGEMENTS

The River Green Cutter Soil Mixing project was an exciting project, with many different stakeholders working towards it success. The authors would like to thank all those who were a part of its successful completion, specifically the design team, site personnel, the City of Richmond, and the owner.

REFERENCES

BAUER Maschinen GmbH, 2007, *Cutter Soil Mixing Technical Information Pamphlet*. Schrobenhausen, Germany

GeoPacific Consultants Ltd., 2013, *6527-F: River Green Parcel 9: DSM and Shoring Plan*. Vancouver, BC, Canada

Golder Associates Ltd., 2013, *River Green Cutter Soil Mixing Production Layout*. Vancouver, BC.

Google Earth, 2015. Accessed February 2, 2016.

© 2016 Deep Foundations Institute

This page left intentionally blank

© 2016 Deep Foundations Institute

DESIGN ISSUES FOR MINI-CAISSONS IN THE NYC AREA

Nidal M. AbiSaab, P.E., M.ASCE, Partner, RA Consultants LLC New York, NY, USA (646) 484-3250, nidal@racllc.com

Joseph J. Caciola Jr., P.E., M.ASCE, Senior Design Engineer, RA Consultants LLC, New York, NY, USA (646) 484-3250, joe@racllc.com

ABSTRACT

Thanks in great part to the geology of the New York City Metropolitan area, mini-caissons are a popular choice for deep foundations. These drilled elements are readily available, easy to install with minimal impact on adjacent structures, and can be designed with large compressive and tensile capacities. Despite the frequency with which they are employed, the engineering design community is divided over several of the underlying principles governing the design of mini-caissons. This paper seeks to draw attention to several of these issues in an effort to encourage further research and discussion, namely: (1) how the allowable stresses have changed for the NYC Building Code over time, (2) the inconsistent load transfer mechanisms considered for geotechnical capacity, and (3) the role of the permanent steel casing towards structural capacities of mini-caissons.

Keywords: mini-caisson, foundations, New York City Building Code

INTRODUCTION

In the local construction nomenclature, mini-caissons are drilled deep foundation elements which derive their capacity from a socket in rock. A permanent steel casing (commonly between 7- and 24-inches in diameter) aides the drilling through overburden soils to the top of bedrock. Afterwards, an uncased rock socket is drilled into the bedrock and the inside of the casing and rock socket is inspected by means of portable video equipment. After inspection, the interior of the socket and casing is filled with steel reinforcement and concrete or grout. The casing-soil interface is generally ignored for axial design purposes and the full geotechnical compressive or tensile capacity is assumed to be generated in the rock socket. Figure 1 shows a typical mini-caisson cross section.

Mini-caissons have been used for decades in the New York City area for a number of reasons. They have historically been proven to develop high axial capacities in the city's metamorphic rock (Tamaro et. al. 2000), often exceeding 300- to 500-tons. Additionally, their method of installation (drilling) is generally able to bypass layers of dense Glacial Till, boulders, and manmade fill which would interfere with the installation of other pile types (e.g. driven piles, auger cast piles). Further they are able to extend to depths exceeding 50-ft to reach bedrock underlying a site, making them a useful tool in areas where rock is relatively deep or varied in elevation. Drilled casing installation also results in fewer vibrations and disturbances to adjacent structures and can occur in areas of restricted access (a constant concern for any project in a dense urban environment such as NYC).

© 2016 Deep Foundations Institute

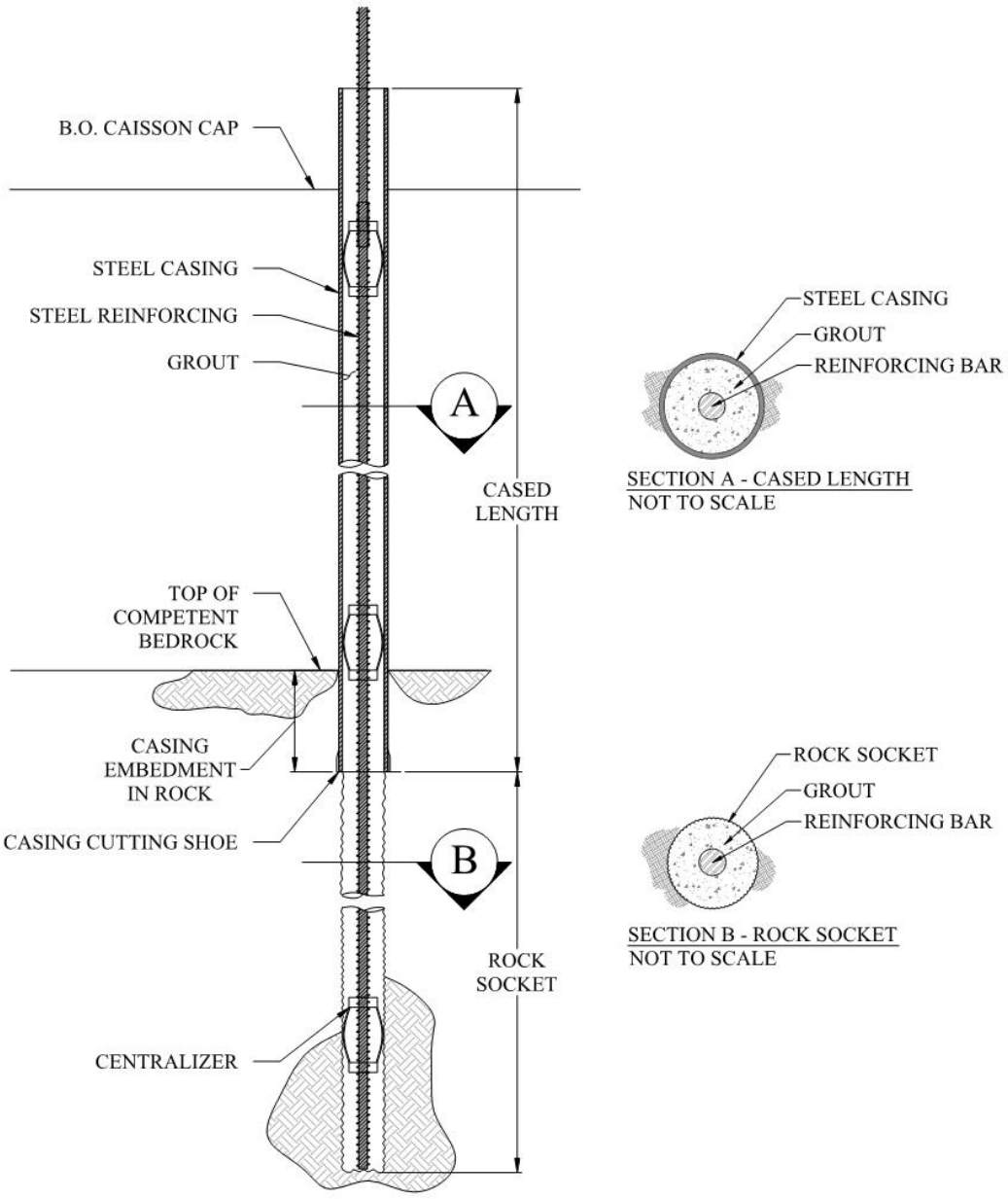


Figure 1: Typical Mini-Caisson Cross Section

Despite their popularity amongst design professionals and contractors, the body of knowledge around certain aspects of mini-caissons remains limited. Many local engineers disagree on several fundamental principles and governing codes and design manuals don't always agree or provide clear direction on some of the finer design details (NCHRP 2006). This paper seeks to explore some of these issues and in turn summarize the current state of practice for mini-caisson design in the New York City Metropolitan Area.

BUILDING CODE REQUIREMENTS: ALLOWABLE STRESSES

The current governing building code for the area is the 2014 New York City Building Code. Although the current code, as well as its preceding versions from 1968 and 2008, explicitly cover requirements for

© 2016 Deep Foundations Institute

caisson construction[1] they do not provide specific design methodologies for mini-caissons. However, the codes do provide factors for the allowable stresses of the main structural components of a mini-caisson: the permanent steel casing, the reinforcing steel, and the interior grout.

The allowable stresses have changed with each iteration of the building code, however not as expected. Refer to Table-1 below for a summary of the allowable stresses.

Table 1 –Allowable Stresses on Mini-Caisson Components

Source	*Compression*						*Tension*	
	Concrete		Reinforcing		Casing		Reinforcing	
	α_c	Max. f_c' (ksi)	α_{sc}	Max. F_{sc} (ksi)	α_{pc}	Max. F_{pc} (ksi)	α_{sc}	Max. F_{sc} (ksi)
2014 NYCBC	0.33[2]	n/a	0.4[2]	30[2]	0.35[2]	16[2]	0.5[2]	24
2008 NYCBC	0.33[3]	n/a	0.5[3]	48.5[4]	0.35[3]	n/a	0.6	n/a
1968 NYCBC	0.25[5]	n/a	0.4[5]	36[5]	0.35[5]	36[5]	0.6	n/a

Despite the advancement in quality control of the construction of mini-caissons over the past 5 decades, the current code in fact provides the most conservative design parameters since 1968. The impact on the allowable structural capacity of mini-caissons is further illustrated in Figures 2, 3, and 4. The following typical designs are for comparison purposes and utilize Grade 75 steel reinforcement assuming no reduction due to corrosion.

[1] As an aside, the term caisson itself refers to a system for deep foundation construction dating back to at least the 19th century. The system traditionally consisted of hand excavating within a large diameter box that was continuously lowered as the excavated soil was removed. The process was used to bypass unsuitable soils and reach a higher capacity bearing material such as bedrock. Mini-caissons derive their name from this parent foundation system as they accomplish the same result as caissons within a much smaller footprint.
[2] Source: 2014 New York City Building Code Table 1808.8
[3] Source: 2008 New York City Building Code Section 1810.7.5
[4] At the time that the 2008 New York City Building Code was in effect, the highest grade steel approved for use by the Department of Buildings was 97-ksi. Therefore, despite the commercial availability of higher grade steel, the maximum effective steel grade was 48.5-ksi.
[5] Source: 1968 New York City Building Code Table 11-3

© 2016 Deep Foundations Institute

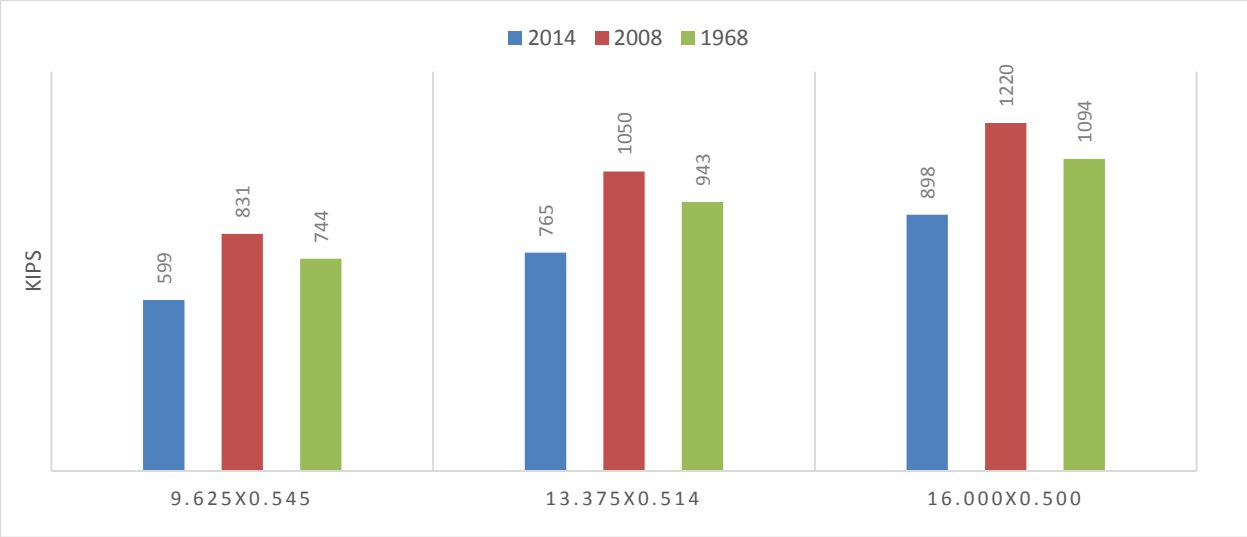


Figure 2: Total Allowable Compressive Loads for Typical Mini-Caisson Designs Based on Various Versions of the NYCBC

Figure 2 above shows how the total allowable load for the same mini-caisson increases between 1968 and 2008 NYCBC and decreases between 1968 and 2014 and between 2008 and 2014 NYCBC for three typical mini-caissons designs:

- 9.625”O.D.x0.545” Steel Casing with (1) #28 Grade 75 Reinforcing Bar & 4-ksi Grout
- 13.375”O.D.x0.514” Steel Casing with (1) #28 Grade 75 Reinforcing Bar & 4-ksi Grout
- 16”O.D.x0.500” Steel Casing with (1) #28 Grade 75 Reinforcing Bar & 4-ksi Grout

The total pile capacity based on the 2008 building code is approximately 12% more than that of the 1968 code. The total pile capacity based on the 2014 building code is approximately 19% less than that of the 1968 code and 28% less than that of the 2008 code.

Figure 3 below shows the effect of neglecting the contribution of the permanent steel casing in the compressive capacities of the mini-caissons. Interestingly, the 2014 version of the code is similar to the 1968 Code but less than 2008 Code. This reflects a trend of discrediting the contribution of the steel casing (discussed in further detail below).

© 2016 Deep Foundations Institute

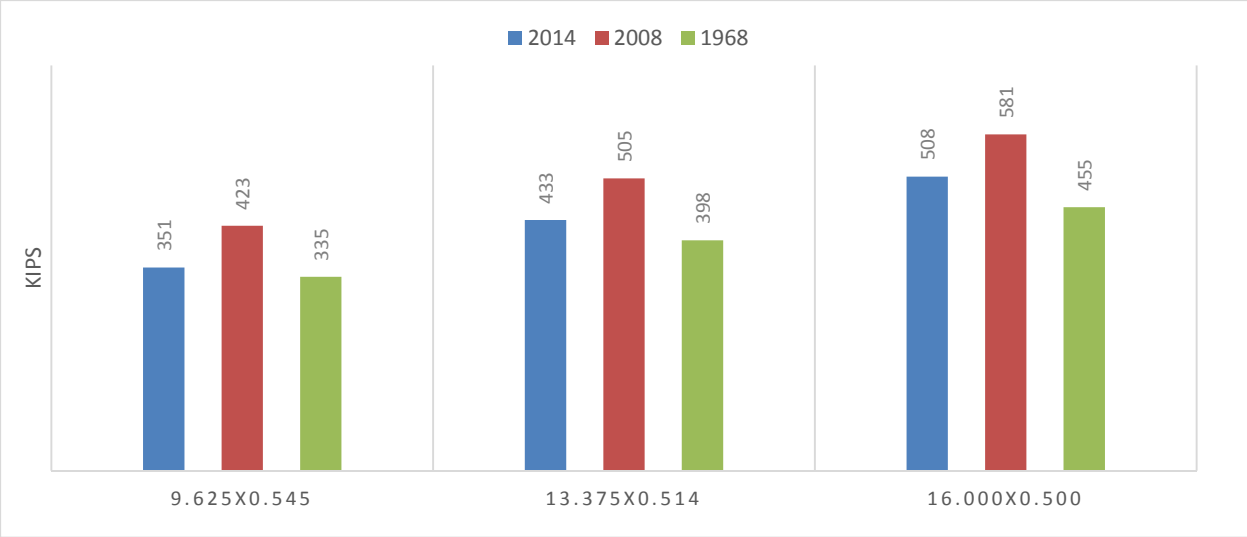


Figure 3: Total Allowable Compressive Loads for Typical Mini-Caisson Designs Based on Various Versions of the NYCBC Neglecting Permanent Steel Casing

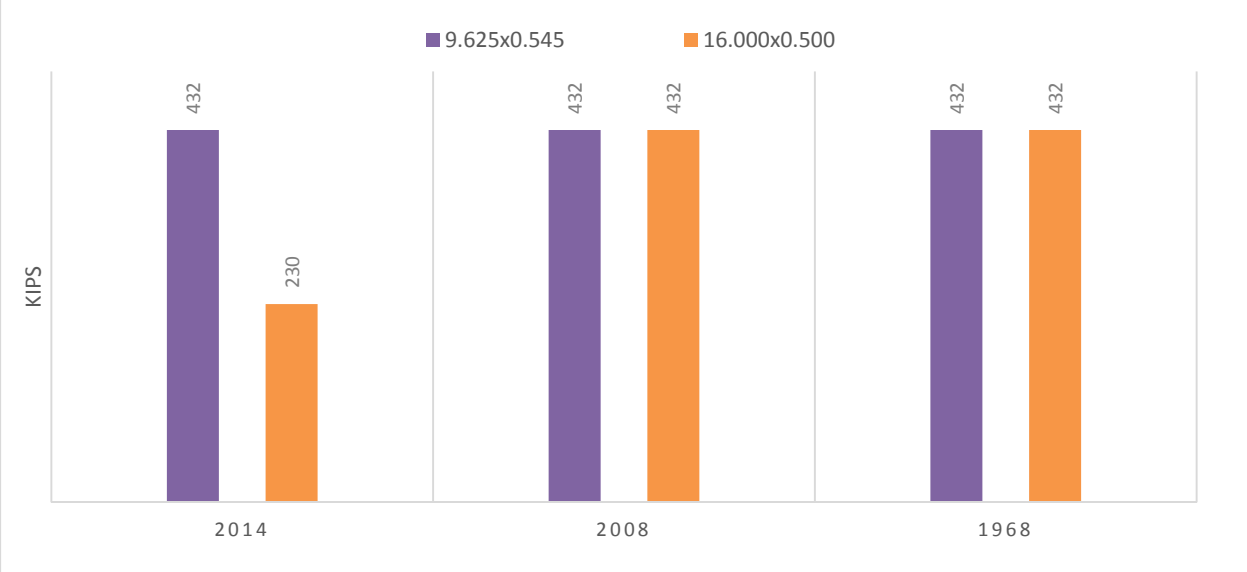


Figure 4: Allowable Tensile Loads for Two Different Mini-Caisson Designs Based on Various Versions of the NYCBC Neglecting Permanent Steel Casing

Additionally, a new stipulation in the 2014 New York City Building Code limits the tensile capacity of steel reinforcing for mini-caissons with diameters greater than 14-in^2. The effect of this requirement is quite pronounced when comparing the different versions of the code for two identical mini-caissons as shown in Figure 4.

In Figure 4, a 9.625" and 16" mini-caisson are designed with the same reinforcement: a single #28 bar. Over the years, the allowable tensile capacity of the smaller mini-caisson remains unchanged. Since the tensile capacity of a mini-caisson is solely dependent on the reinforcement, the larger diameter mini-caisson unsurprisingly also results in the same allowable tensile capacity in the 1968 and 2008 NYCBC.

© 2016 Deep Foundations Institute

However, when we look at the 16" mini-caisson under the 2014 Code, its allowable tensile capacity is nearly half of its smaller diameter counterpart.

Unfortunately, the reasons for changes in the NYCBC are not always made clear to the local design community.

GEOTECHNICAL DESIGN: LOAD TRANSFER MECHANISM

The source of geotechnical capacity for any type of deep foundation element is derived from either side friction resistance, end bearing resistance, or some combination thereof. In the case of mini-caissons in NYC, the axial loads are mostly considered to be resisted by skin friction developed within the rock socket. Locally, the end bearing at the bottom of the rock socket is routinely ignored as it typically does not provide much capacity for smaller diameter casings and the area is often difficult to sufficiently clean and inspect (Tamaro et. al. 2000; Johnsen et. al. 2007). Although numerous methods exist to estimate the side shear resistance of mini-caissons socketed into rock (Rhyner et. al. 2010), the NYC building code has traditionally provided a single value of 200-psi[6] for the surface area of the grout-rock interface.

In terms of compressive geotechnical capacity, some local engineers also claim that the permanent steel casing terminating at the top of the socket sheds load directly to the rock. One school of thought argues that the entire allowable load carried by the steel casing transfers directly to bedrock, effectively reducing the required load for the rock socket (Johnsen et. al. 2007). Refer to Figure 5 for an illustration of this concept. In this case, very high compressive loads can easily be generated by mini-caissons. The length of the rock socket is then mostly a function of minimum code requirements or for uplift resistance.

Other engineers in our area take more of a measured approach to this notion and argue that only some percentage of the load in the casing can be transferred to the bedrock. For instance, Oweis and Hwang (2010) conducted a series of finite element analyses to create a "load dissipation or shedding parameter". They concluded that this parameter is directly related to rock quality and could be as high as 20% of the load in the casing. Still others have attempted to apply simplified bearing capacity equations by multiplying the casing area by the Code specified allowable bearing capacity of rock.

A third group of designers and professionals in NYC assert that none of the casing load should be considered transferring directly to the bedrock. Those objecting to this load transfer mechanism either reject the steel casing as a structural element altogether or claim there is insufficient knowledge or quality control regarding the casing-rock interface.

As those in the third group point out, there is very little published data for this issue. Even those who rely on all of the allowable load in the casing to shed into rock concede that they do not have the backing of published data or research.

[6] Source: 2014 New York City Building Code Section 1810.7.3, 1968 New York City Building Code Section 27-71(c)

© 2016 Deep Foundations Institute

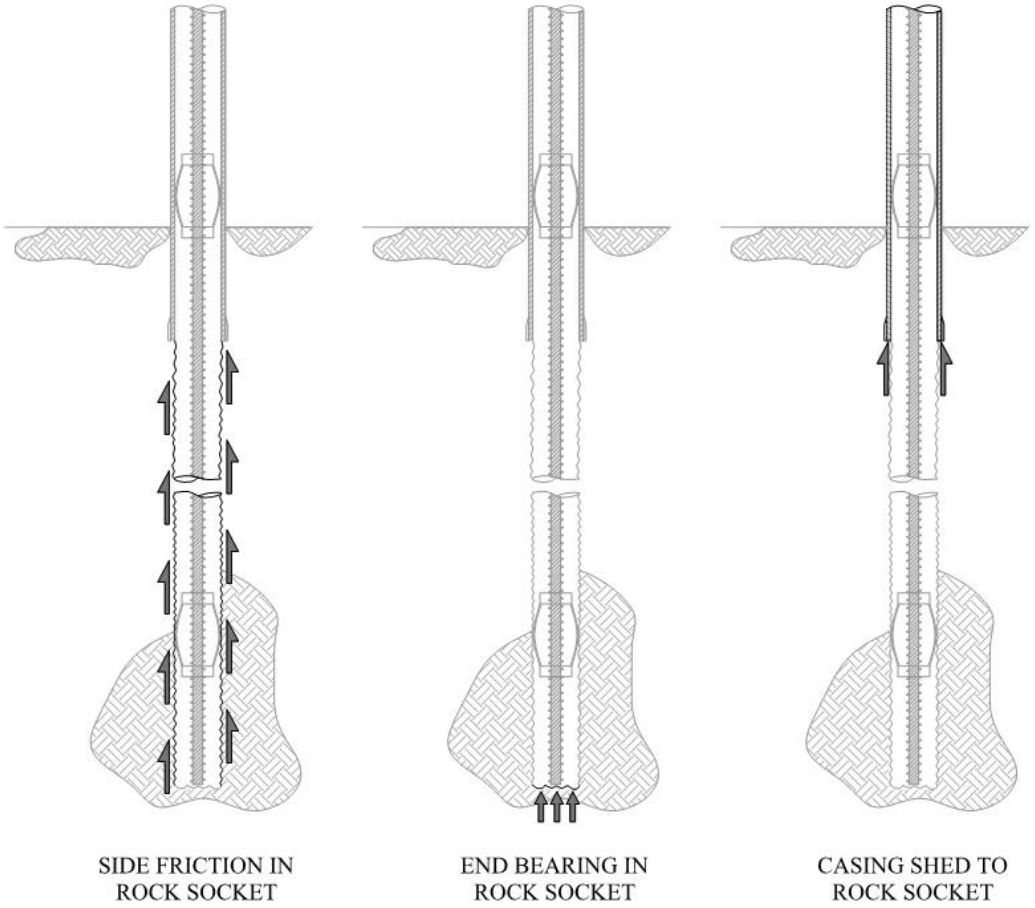


Figure 5: Typical Mini-Caisson Load Transfer Mechanisms

STRUCTURAL DESIGN: RELIABILITY OF STEEL CASING

As mentioned in the preceding section (and specifically noted by NCHRP 2006), the structural role of the steel casing in a mini-caisson is another issue not fully understood by the community. Traditionally in local practice, the steel casing has been permitted to take at least some portion of the compressive load as demonstrated by the various allowable stresses provided by the NYCBC over its iterations. Judging strictly by the changes in these values over time, there appears to be a trend in favor of limiting the amount of load carried by the casing.

The reasons for this apparent trend could be tied to constructability and installation concerns surrounding the casings themselves. Typically, casings are delivered to sites in machine threaded, 5- or 10-ft lengths. As the mini-caisson is being drilled through overburden soils and into rock, additional lengths of casing are tightened onto preceding sections by the drill rig. Although the interior of each mini-caisson is eventually inspected by video camera, it is unknown if the tightness of these threaded joints is sufficient to develop the required axial capacity. Some designers overcome this limitation by only considering the

© 2016 Deep Foundations Institute

reduced steel area at the threads for capacity calculations, as low as 25% of the full casing cross section. Another method is to fully weld the outside face of every seam between pieces of casing as the mini-caisson is being installed. This approach, however, often results in a drastically slower production rate for construction.

CONCLUSION

It is the authors' hope to generate discussion within the community which results in further research into these areas. Our conclusions and recommendations are as follows:

- The design parameters for mini-caissons in the 2014 building code requires clarification.
- Research is lacking in the area of load transfer between the mini-caisson and rock and casing and rock.
- Instrumented and load tests rock socketed mini-caissons may help shed light on proper design parameters in the NY area.

REFERENCES

JOHNSEN, L., J. Pastore, F. Ferrer, 2007. High Capacity Minicaissons in NYC. Structure Magazine, December 2007, pp. 9-12.

NCHRP, 2006. NCHRP Synthesis 360: Rock-Socketed Shafts for Highway Structures Foundations.

OWEIS, I., J. Hwang, 2010. Load Transfer to Micro Pile Rock Socket. Proceedings, American Society of Civil Engineers, GeoFlorida 2010: Advances in Analysis, Modeling, & Design.

RHYNER, F., J. Cahill, C. Huynh, A. Tognon, J. Moskowitz, 2010. Rock-Socketed Caissons in Yonkers Gneiss. Proceedings, American Society of Civil Engineers, The Art of Foundation Engineering Practice Congress 2010.

TAMARO, G., J. Kaufman, A. Azmi, 2000. Design and Construction Constraints Imposed by Unique Geologic Conditions in New York City. Proceedings, Deep Foundations Institute, DFI 2000 Conference.

© 2016 Deep Foundations Institute

DRILLED DISPLACEMENT PILES IN THE NORTHEASTERN UNITED STATES

W. Morgan NeSmith, Jr, PE Berkel & Company Contractors, Inc. Austell GA. USA, 770.941.5100, mnesmith@berkelapg.com

ABSTRACT

Drilled Displacement piles are a product of screw pile technology originally developed in Europe. The process involves rotating tool into the ground that displaces the soil laterally as it advances, then grouting or concreting through the hollow stem of the tool as it is withdrawn. They were first introduced in the United States in the 1990's and have become a mature and accepted technology since that time. They are now used to support a variety of heavily loaded structures including electric power and LNG facilities, stadiums and arenas, airports and mid- to high-rise commercial and residential facilities. In urban environments, the technique has a number of advantages including, low noise and vibrations, no removal of the existing soil, and reduced pile material cost due to the improved stress state of granular soils after installation (smaller or shorter piles can be used). For these reasons, displacement piles have been used to support various facilities in Northeastern United States (US). The paper presents case histories of the performance of displacement piles in the Northeastern US including the use of full displacement elements as a settlement limiting ground improvement system.

Keywords: Deep Foundations, Piles. Drilled Displacement, Auger Pressure Grouted Displacement, APGD

INTRODUCTION

"Drilled Displacement" (DD) is an industry umbrella term for a number of proprietary or commercially available cast-in-place pile installation systems which involve a hollow-stem tool that laterally displaces soil as it advances and the placement of grout or concrete through the hollow-stem tool as it is withdrawn. The systems include grout/concrete placement methods by both sand-cement grout pumped under pressure and tremie grout/concrete placement through bottom-hole discharge. The system discussed in this paper includes grout pumped under pressure, also referred to as Auger Pressure Grouted Displacement (APGD). A schematic of the APGD tool is shown in Figure 1. The tools require significant torque and downward force to advance; a typical installation platform is shown in Figure 2.

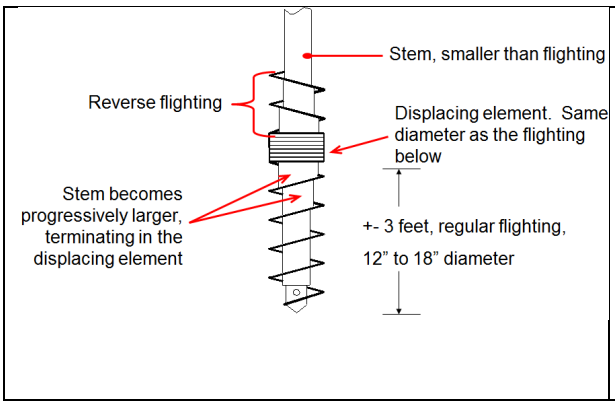


FIGURE 1 – APGD Displacement Tool

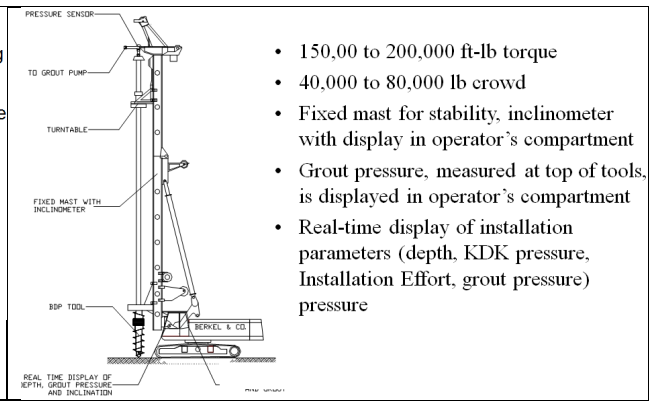


FIGURE 2 – APGD Installation Platform

Similar to Augered Cast in Place (ACIP) piles, DD piles are a single-pass process. The piles are drilled with one tool penetration and cast during the subsequent withdrawal. This can be more efficient when compared to other bored and cast-in-place piles (drilled shafts, micropiles) which are typically installed segmentally and require casing. Also, ACIP and DD piles are installed with low noise and vibrations when compared to driven piles and the price of grout/concrete compares favorably with driven steel piles on a per foot basis.

© 2016 Deep Foundations Institute

The general principal separating DD pile systems from ACIP pile systems is the soil improvement aspect of the installation of DD piles (densification of granular soil, low plasticity fine-grained soil or man-made rubble fill) that allows for increased shaft and toe resistances compared to ACIP piles. In improved soils, they can then support higher loads than ACIP piles, allowing for fewer piles; or they can support similar loads with smaller or significantly shorter piles. Additionally, since no soil is excavated during the process, DD piles can offer savings in some heavily contaminated soils, particularly in urban areas where soil removal from a site may be expensive, time-consuming and generally unwieldy.

Most DD pile installation platforms include standard Automated Monitoring Equipment (AME) that allows for the measurement and real-time display of drilling and grouting parameters as the piles are constructed. These parameters can include time, tool depth, calculated penetration and withdrawal rate, tool-rotation rate, the hydraulic pressure applied to rotate and apply downward force to the tools and grout pressure (grout flowcan be measured but is not considerd standard). Examples of the display of these parameters for an APGD system are presented in the case histories.

ENERGY FACILITY – DAGSBORO DE

The first project presented was an expansion to an energy facility in Dagsboro DE, near Indian River Bay on the Atlantic Coast. The site sits firmly in the Coastal Plain geologic region of the east coast of the US. An example Seismic Cone Penetration Test (SCPT) result from the site is presented in Figure 3 and shows soft upper sandy silt sediments underlain by loose sand and silt mixtures, transitioning to medium dense, relatively clean sands with depth. As loose to medium dense sands are most affected by the displacement process, this is an ideal setting for maximizing the load placed on a DD pile.

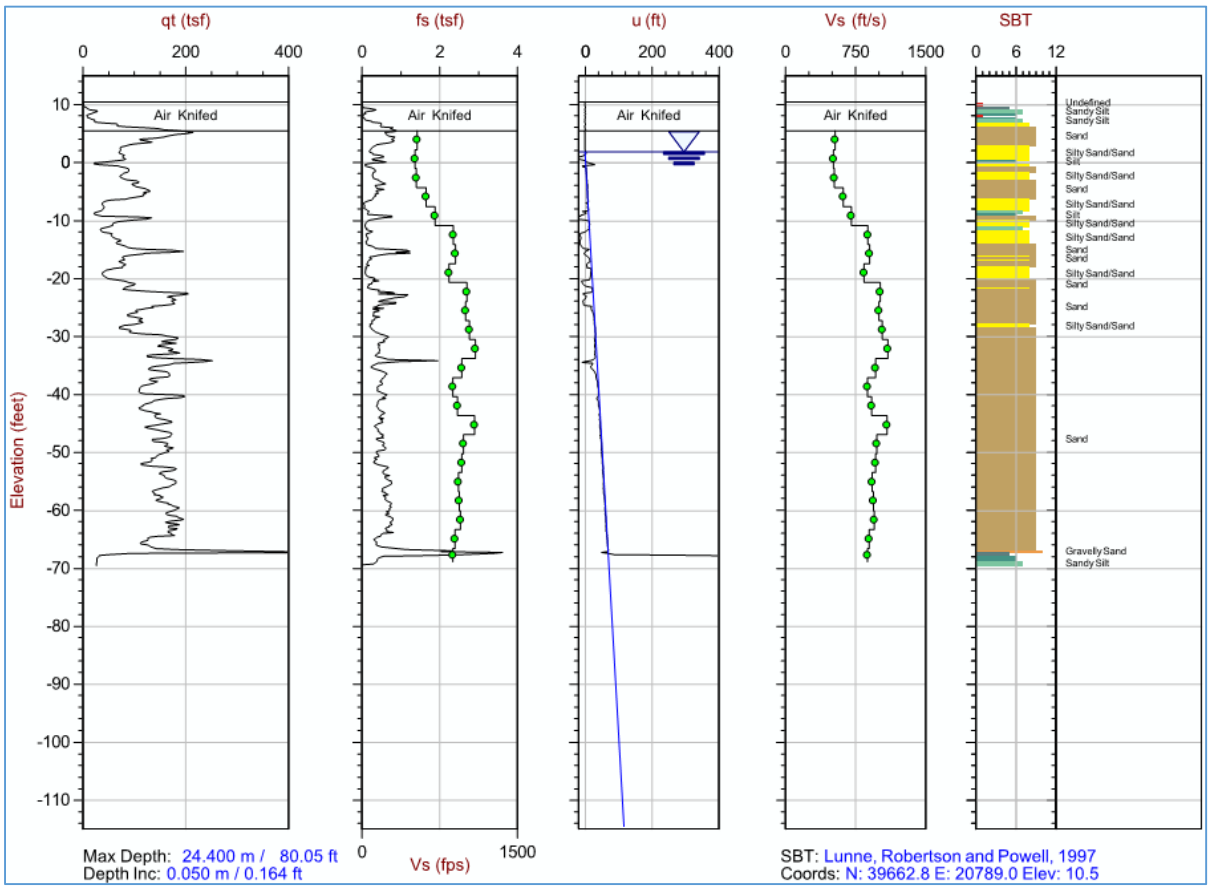


FIGURE 3 – Example Stratigraphy at Dagsboro DE

© 2016 Deep Foundations Institute

APGD piles were proposed to support compression loads of up to 150 tons. Preliminary analysis according to NeSmith (2002) indicated that 16-in piles installed 50-ft below the SCPT elevation could support these loads. A portion of the test pile installation record is shown in Figure 4. This information was available to the inspector and drilling contractor in real-time during the pile installation and, in general, shows a decrease in penetration rate and increase in hydraulic fluid pressure applied to the tooling (shown as KDK pressure in this example) with depth, as would be expected with the transition from loose to medium dense sand.

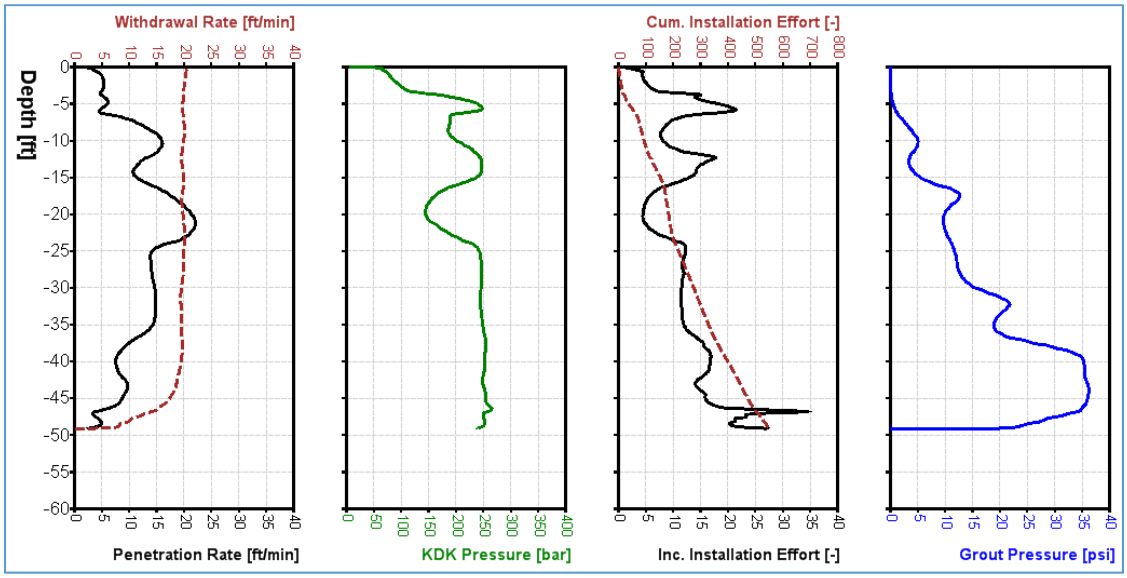


FIGURE 4 – APGD Pile Installation Record – Dagsboro DE

Also shown is an estimate of the energy expended by the installation platform to advance the tooling, both at 1-second intervals (Incremental Installation Effort, IE) as well as the total effort expended with depth (Cumulative IE, NeSmith and NeSmith, 2008). Figure 5 shows the compression load test results to the maximum applied load of 350 tons (at which load the pile broke) along with the estimated ultimate loads from the current International Building Code. A database of APGD pile capacities along with measured Cumulative IE is shown in Figure 6. Such a database can be used to establish a typically hyperbolic relationship between Cumulative IE and pile capacity for a given site. Production piles can then be installed to a specific stratum, using Incremental IE as an indicator (the higher the IE, the denser and more granular the soil) as well as to a specific energy level expended by the rig (similar to using hammer energy to establish driven pile toe levels) to take advantage of variations in density and stratigraphy across a given site, to maximize the efficiency of the system.

Also shown in Figure 6 are two examples of multiple test piles installed to different Cumulative IE values. One is from an alluvial flood plain and glacial outwash in ND and the other is from the Coastal Plain in central FL. They are examples of how a site specific IE value can be determined to provide a specific pile capacity and also an example of how geologic setting should be considered by an experienced design professional who is familiar with the performance of different types of DD piles.

At the subject site, final production pile lengths ranged between 45-ft and 55-ft depending on the density of the sand encountered at each facility. By comparison, 16-in diameter ACIP piles were to be about 70-ft in length across the site to support the same 150-ton design load. In this case, there was an average 20-ft reduction in pile length with a corresponding estimated 1.5 yd^3 less grout, along with a 25-ft shorter center-bar (#11, 75 ksi steel) per pile (about 1300 yd^3 of total grout and 18,000 l.f. of center bar). Additionally, no spoils were removed during DD pile installation eliminating the disposal of 4,500 yd3 of soil. The final foundation cost was 10% to 20% less expensive than a corresponding ACIP pile foundation.

© 2016 Deep Foundations Institute

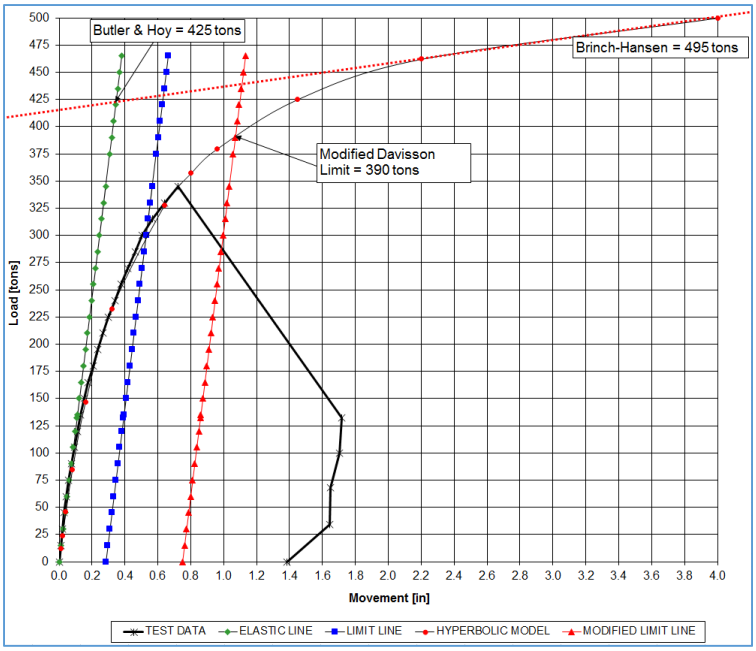


FIGURE 5 – Compression Load Test Results and IBC Ultimate Load Estimates – Dagsboro DE

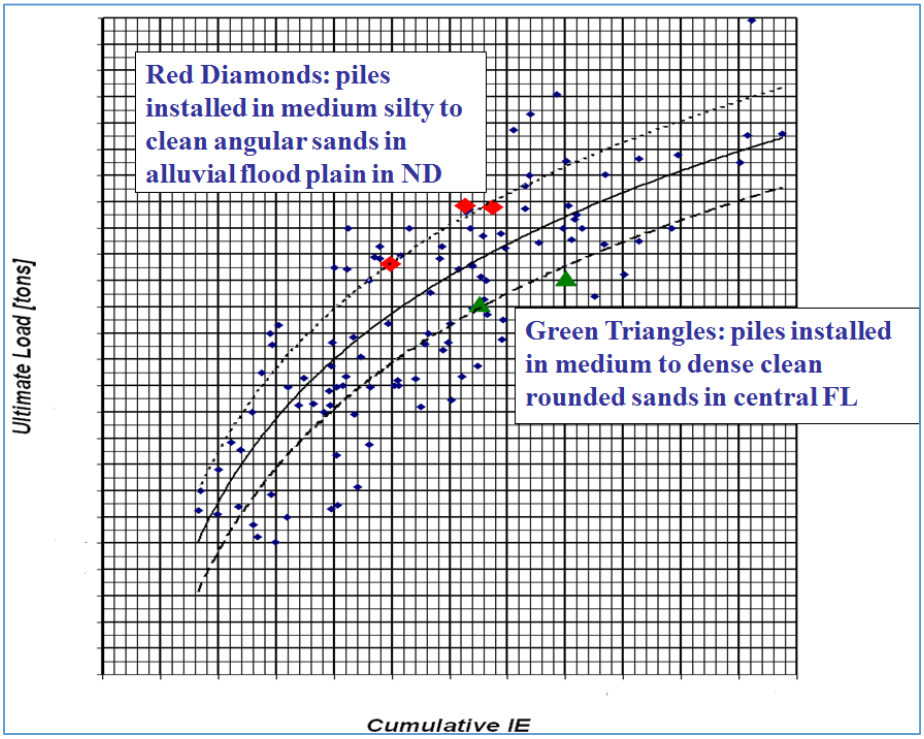


FIGURE 6 – Example Collection of Drilling Platform Installation Effort and APGD Pile Ultimate Load

MEDICAL FACILITY – CAMDEN NJ

The second example project was a large new medical facility in Camden NJ, relatively close to the Delaware River, just east of Philadelphia. The subsurface profile consisted of urban rubble fill over upper alluvial clay and sand deposits of variable density and stiffness.

© 2016 Deep Foundations Institute

Coastal plain sands underlay the alluvial soils. A table of N-Values from Standard Penetration Tests (SPT) as well as the generalized soil profile is shown in Figure 7.

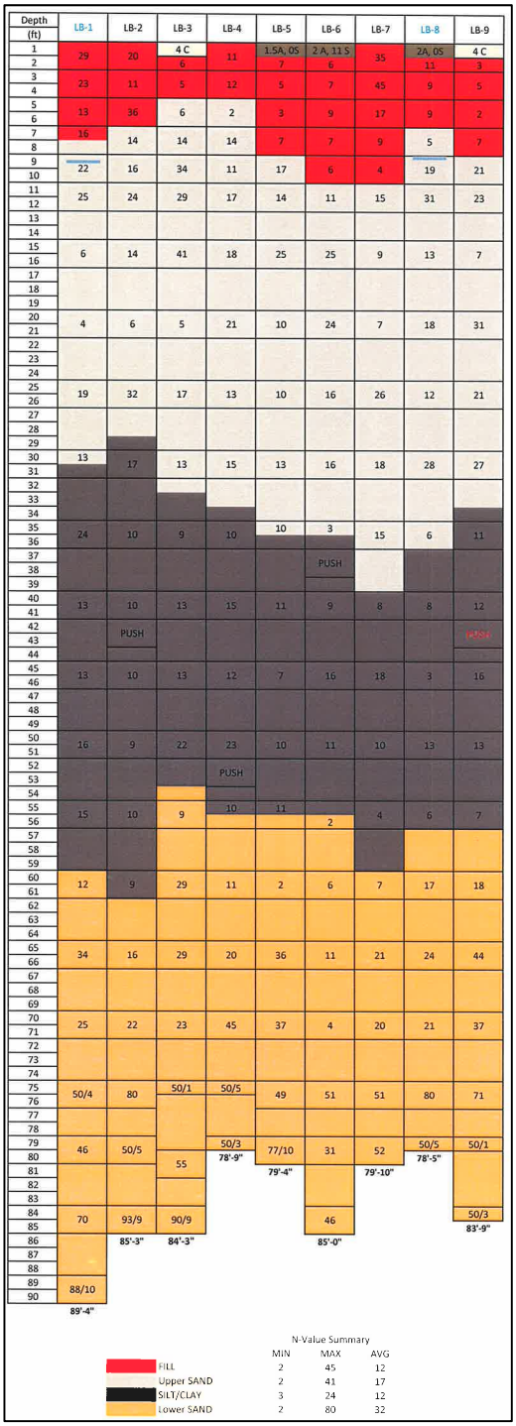


FIGURE 7 – Generalized Stratigraphy at Camden NJ Site

APGD piles were proposed to replace 90-ft long, concrete-filled, driven, closed-end steel pipe piles to support compression loads of 110 tons per pile. Preliminary analysis indicated that 14-in APGD piles could be used. A series of APGD probes were installed to collect drilling and grouting parameters prior to test pile installation. Based on the relatively similar IE values observed and the preliminary capacity analysis, the compression test pile was installed to 70-ft to exceed the required capacity of 220 tons, with the possibility of reducing production pile lengths based on the test pile results. Recorded installation parameters from the compression test pile installation are shown in Figure 8. Of note are the recorded grout pressures and volumes, the latter of which are significantly lower than might be expected for other grouted, cast-in-place pile systems. DD tools typically establish a pile diameter very close to plan in granular and firm to stiff fine-grained soils. Minimum incremental grout volumes for DD piles range from just greater than 100% of theoretical to a minimum of 105% of theoretical volume.

Load test results to the maximum applied load of 280 tons are shown in Figure 9 and evaluations of ultimate load are presented in Figure 10. The estimated ultimate loads are well in excess of the single pile requirements. For production, minimum Incremental and Cumulative IE values were employed to establish pile toes in the lower dense sands indicated on Figure 7 and by the Incremental IE towards the bottom of the compression test pile.

The efficiencies in this case were the elimination of the closed-end pipes and using slightly more grout vs. concrete per pile (90-ft x 12.75-in diameter pipe piles replaced with 70-ft x 14-in diameter DD piles). Elimination of the lead time for pile fabrication and delivery also advanced the construction schedule. Equivalent 14-in diameter APG piles were estimated to be about 85-ft in length.

© 2016 Deep Foundations Institute

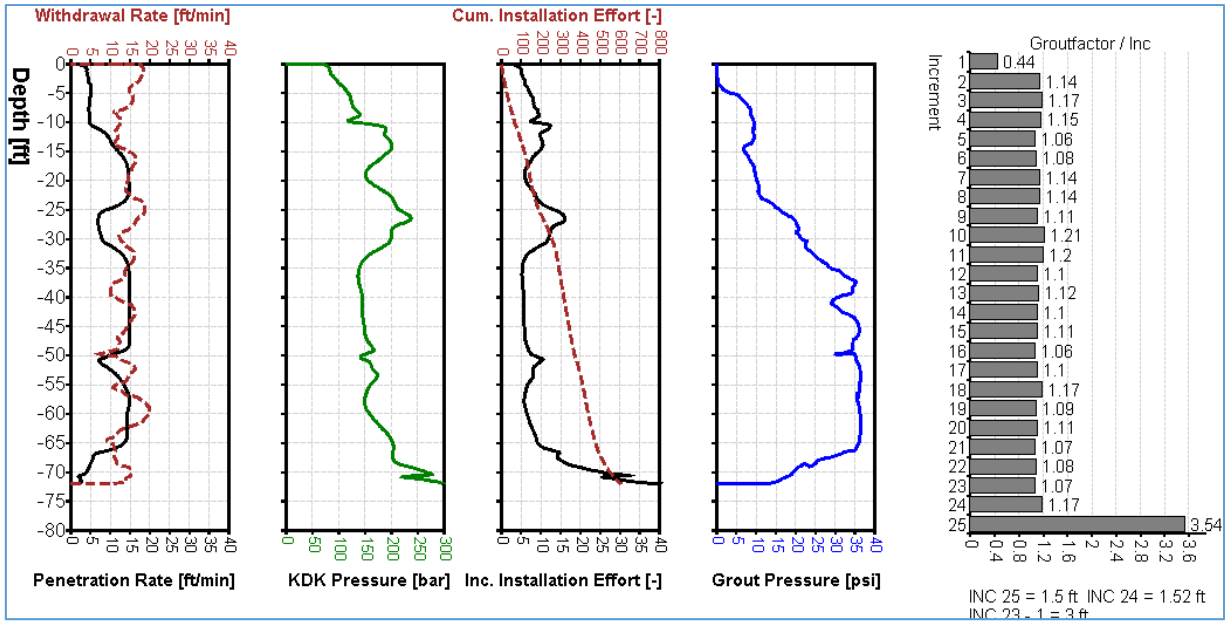


FIGURE 8 – Installation Parameters for Compression Test Pile – Camden NJ

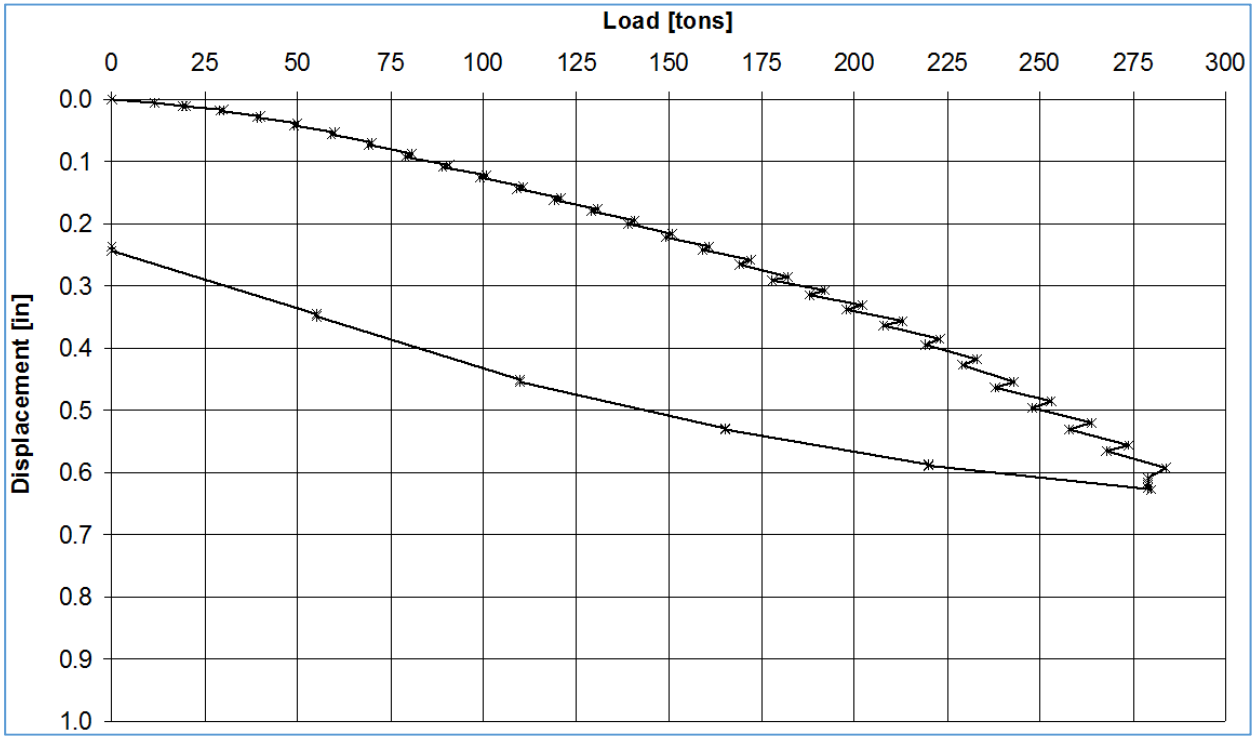


FIGURE 9 - Compression Load Test Results – Camden NJ

© 2016 Deep Foundations Institute

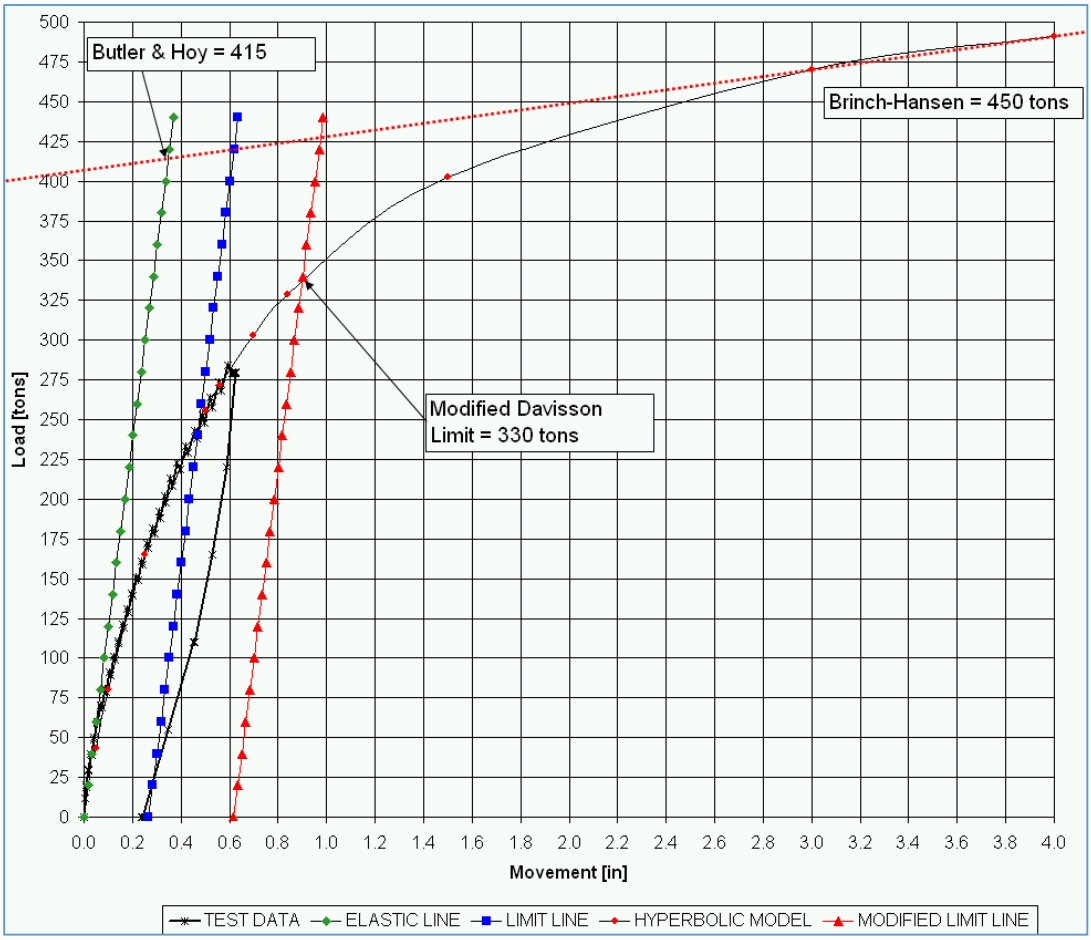


FIGURE 10 – Ultimate Load Estimates – Camden NJ

SETTLEMENT LIMITING ELEMENTS – WOODBRIDGE NJ

The final example project involved the use of APGD elements installed to limit settlement below a new energy facility in Woodbridge NJ, just west of the Raritan River and Sandy Hook Bay, as well as being west of the southern tip of Staten Island.

A generalized subsurface profile is shown in Figure 11 and consisted of urban rubble fill from the demolition of the previous structures at the site, loose to medium alluvial sands underlain by denser coastal plain sands and saprolite, weathered in place from the underling parent rock. The groundwater at the site was highly contaminated and a slurry wall had been previously installed around the site to contain the groundwater in the alluvial and coastal plain sands.

Any foundation system considered was to remove no soil or groundwater during installation. The system was also not to penetrate the saprolite, which was considered to be a natural lower barrier for the contaminated groundwater.

A review of the proposed structures indicated that due to their size and weight, they would predominantly be supported by large, significantly reinforced, concrete mats (Figure 12). APGD elements (commercially referred to as Cast-in-place Ground Improvement Elements or CGEs) were proposed to increase and standardize the density of the fill and loose sand to both increase the bearing capacity of the underlying materials and limit settlements to within tolerable project levels for a range of bearing pressures between about 3000 and 4200 psf.

© 2016 Deep Foundations Institute

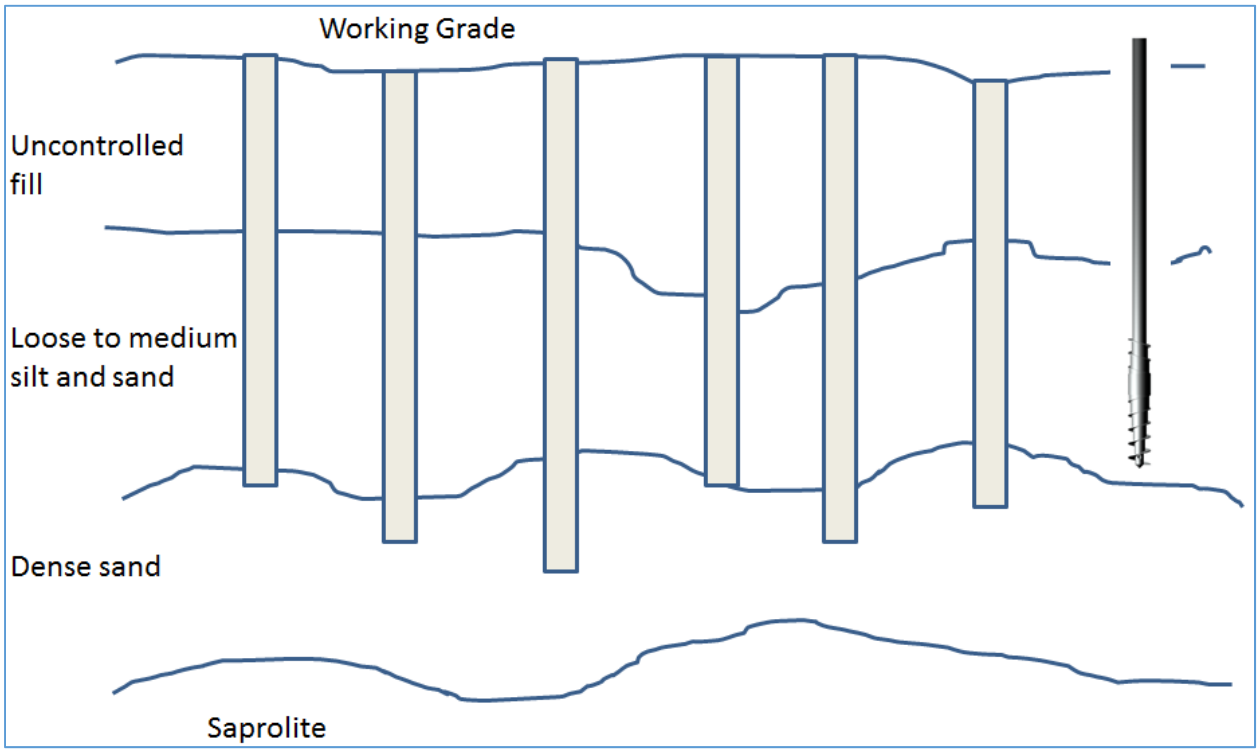
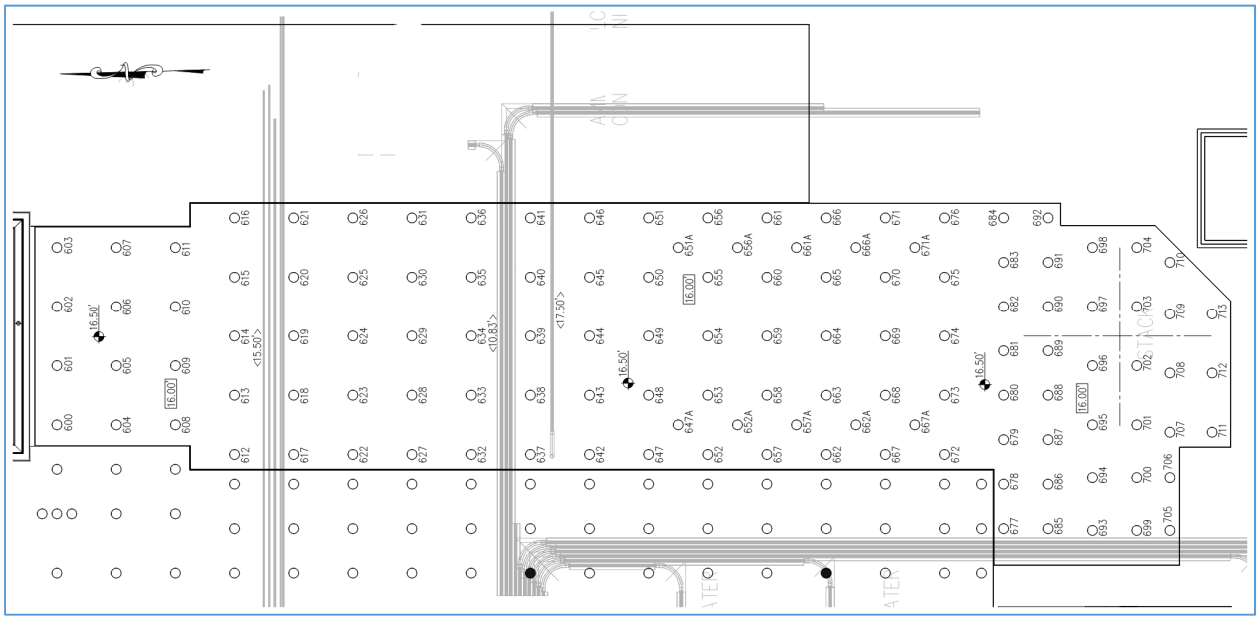


FIGURE 11 – Generalized Subsurface Profile – Woodbridge NJ

An example of the densification effect of a group of CGEs is shown in Figures 13 and 14. Two additional displacement elements were installed outside of an APGD compression test set-up to form a 6-ft square group (Figure 13). CPTs were performed at small distances from a single element as well as in the middle of the 6-ft square group. The increase in tip resistance from 3-diameters outside a single element (considered to be the pre-installation condition) and in the middle of the group is shown on Figure 14.


FIGURE 12 – Example Mat for One Structure for New Energy Facility – Woodbridge NJ

© 2016 Deep Foundations Institute

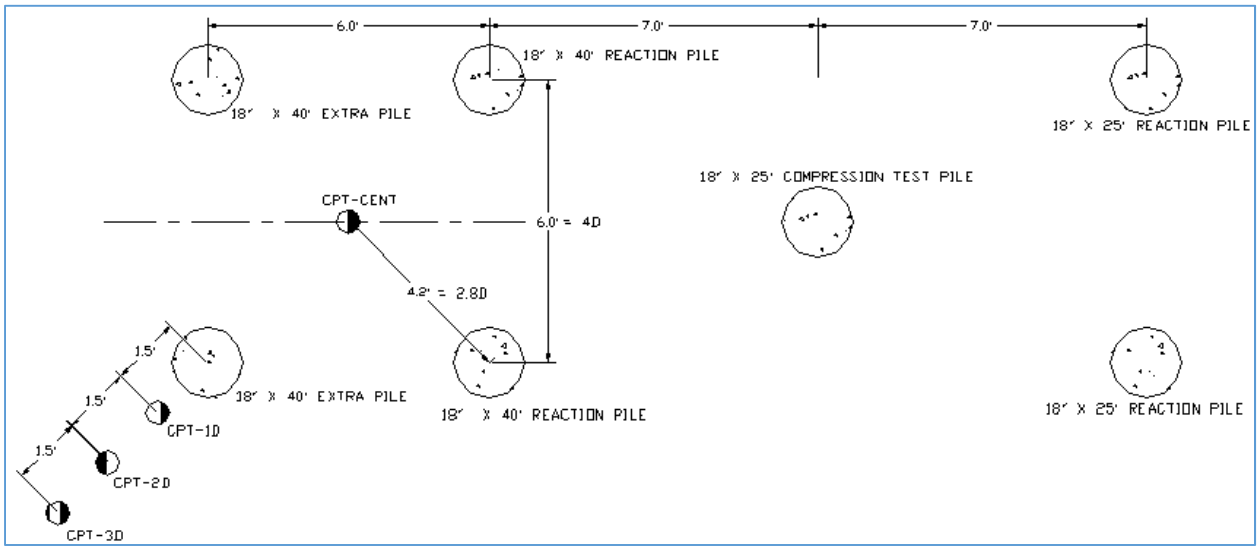


FIGURE 13 – APGD Test Pile Layout with Additional CGEs installed for Densification Testing

By using a database established from a number of these pre- and post-installation SPTs and CPTs, it is possible to predict the increased density of soils improved by CGE installation (Siegel et al, 2007a and 2007b). Considering CGE installation into the dense coastal plain sands above the saprolite, this database was employed at the subject site to establish appropriate CGE sizes and layouts under the various structures to provide the required allowable bearing pressures across the site. IE obtained from the AME system described previously was used to establish CGE toe levels in the dense sand above the saprolite. It is noted that a similar analysis can be employed for liquefaction mitigation in seismically affected regions.

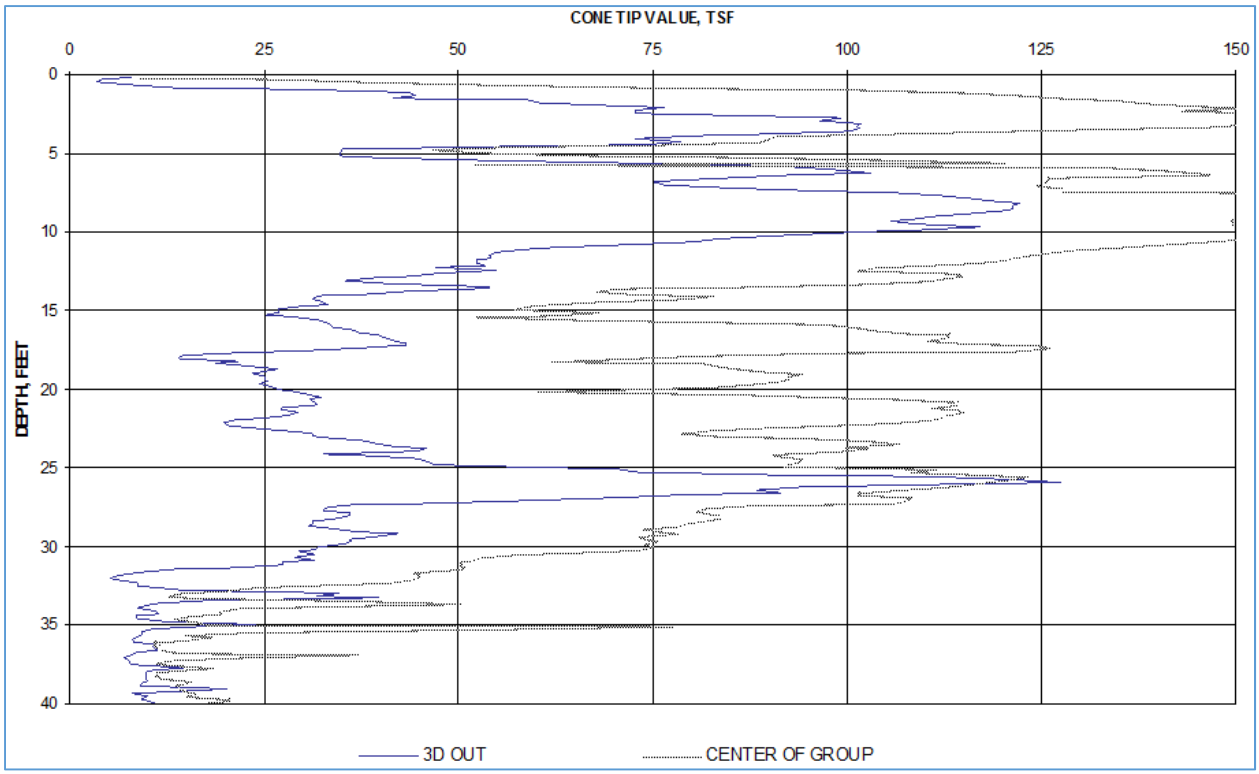


FIGURE 14 – CPT Tip Resistance Results in "Ambient" Condition and at Center of Pile/CGE Group

© 2016 Deep Foundations Institute

More recently, the ambient and increased shear wave velocity, Vs, have been obtained from both Seismic CPTs and refraction microtremor (ReMi) tests and used in a similar manner to establish increased resistance to liquefaction as well as increased allowable bearing pressure due to CGE installation. Measurement of Vs is considered to capture some of the effects of increased horizontal stress in addition to increased density that may not be captured by the tip resistance values from CPT tests alone.

CONCLUSIONS

Where they can be successfully installed, the single-pass nature of DD piles can reduce pile installation times when compared to segmentally installed, bored and cast-in-place piles. The densification and increase in horizontal stress that occurs upon installation in some alluvial and coastal plain sands and low-plasticity fine-grained soils can increase the load per foot that can be resisted by the piles, allowing for smaller diameter and shorter piles for equivalent ACIP piles, or fewer piles with larger loads.

The standard AME on board the installation platforms employed for DD pile installation can help maximize this efficiency by producing indications of stratigraphy and pile capacity in real-time to allow for variable toe levels to be set on a pile-by-pile basis taking advantage of the variation in stratigraphy across a given site. DD elements can also be effectively employed as a ground improvement system, either by bracing fine-grained soils or increasing the density and horizontal stress in urban fill and predominantly granular soils. The piles and elements can be particularly beneficial in heavily contaminated sites where spoil removal may be costly and time-consuming.

REFERENCES

Nesmith, W.M. (2002). “Static Capacity Analysis of Augered, Pressure-Injected Displacement Piles”. Geotechnical Special Publication No. 116. M.W. O’Neill and F. C. Townsend (Eds.). ASCE. February. Volume 1. pp. 1088 – 1097.

NeSmith, W.M. and NeSmith, W.M. (2008). Installation Effort: Current Calculation Methods and Uses in Design and Construction in the U.S. 5th International Geotechnical Seminar on Deep Foundations on Bored and Augered Piles. Ghent, Belgium. September 2008.

Siegel, T.C., Cargill, P.E., and NeSmith, W.N. (2007). “CPT Measurements Near Drilled Displacement Piles”, Proceedings, FMGM, Boston, MA.

Siegel, T.C., NeSmith, W.M., NeSmith, W.M., and Cargill, P.E. (2007), “Ground Improvement Resulting From Installation of Drilled Displacement Piles”, 32nd DFI Annual Conference, Colorado Springs, CO.

© 2016 Deep Foundations Institute

DRIVEN PILE FOUNDATION DESIGN AND CONSTRUCTION ISSUES FOR A HIGH-RISE BUILDING IN MANHATTAN

Sandy Larimer, P.E., Langan Engineering, Parsippany, New Jersey, USA, 973-560-4900, slarimer@langan.com
Satyajit Vaidya, P.E., Langan Engineering, Parsippany, New Jersey, USA, 973-560-4573, svaidya@langan.com
Rudolph Frizzi, P.E., G.E., D.GE., Langan Engineering, Parsippany, New Jersey, USA, 973-560-4703, rfrizzi@langan.com

ABSTRACT

This paper presents a case history in design and construction of a deep foundation system that included high-capacity open-ended driven piles constructed to support a high-rise building in Manhattan, New York. The project site is bordered by existing buildings, active streets, and critical public transportation infrastructure, which were considered in the new building's deep foundation and seismic design. This paper focuses on driven pile foundation design and installation through relatively loose soil deposits. Unique design aspects included seismic design considerations, and pile splice design for open-ended steel pipe piles subject to significant uplift and lateral loading. Unique construction aspects included quality assurance of open-ended steel pipe pile splices, and uplift and lateral load testing of driven piles installed in close proximity to other foundation elements installed for the project.

Keywords: driven pile, high-strength material, weld, weldability, carbon equivalency, seismic design, uplift, lateral, capacity

SITE CONDITIONS AND SUBSURFACE CONDITIONS

The project site is located in Manhattan, New York, and is bordered by existing buildings, active streets, and critical public transportation infrastructure that is located about 60 feet from the site. The existing sidewalk grades around the site are between about el 4 and about el 13; elevations are referenced to the North American Vertical Datum 1988 (NAVD88).

Subsurface conditions at the site generally consist of successive strata of historic fill, former river bottom deposits consisting of compressible clayey soils, and medium dense to dense sand, overlying mica schist bedrock. A generalized subsurface profile is shown in Fig. 1. The historic fill stratum is about 10 to 45 feet thick, and generally consists of loose to medium dense sandy soils with varying proportions of silt, gravel, and miscellaneous debris such as brick, concrete, and glass fragments. The underlying former river bottom deposit stratum is up to about 15 to 20 feet thick, and generally consists of very soft to very stiff clay and lenses of very loose to loose sand. Medium dense to dense sand was generally observed below the historic fill and former river bottom deposit strata and overlying bedrock. Top of bedrock was generally observed at about 80 to 105 feet (i.e. at about el -75 to el -100), except in the southeastern portion of the site where the top of rock was observed as deep as about 140 feet (i.e., at about el -135). Groundwater levels typically ranged between about el 1.5 and el -0.5.

Review of historic maps for the site area from 1842 indicate wharfs and piers associated with Manhattan's historic shoreline were once located across a portion of the site, and the site area was subsequently filled-in and several low-rise buildings were constructed on the made land. The foundations for these wharfs, piers, and buildings consisted of timber piles and timber cribbing filled with gravel. Isolated layers of dense gravel and wood obstructions were encountered in few of the borings scattered throughout the site and are believed to be the remnants of these old wharfs, piers, and building foundations.

© 2016 Deep Foundations Institute

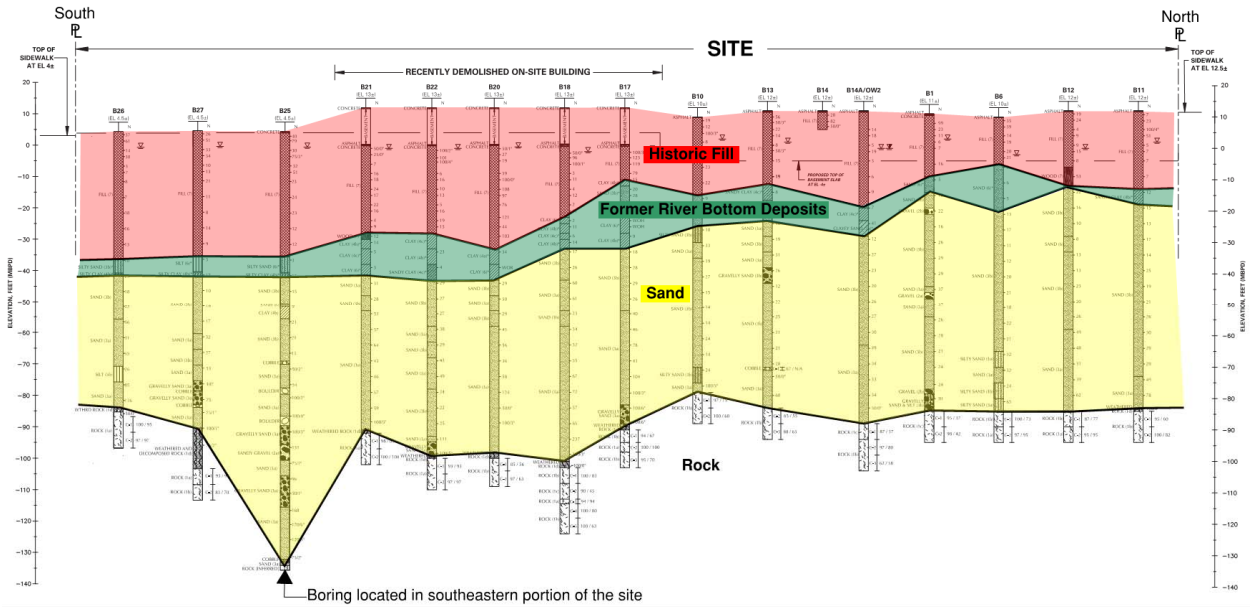


Fig. 1: Generalized subsurface profile.

DRIVEN PILE DESIGN CONSIDERATIONS

Considering the significant depth of the variable surficial fill and compressible former river bottom deposit materials considered nominally unsuitable for shallow foundation support, a deep foundation system was designed. The foundation system included driven end-bearing steel pipe piles.

The high-rise building superstructure and foundation design were initially performed per the requirements of the 2008 New York City Building Code (NYCBC) and its seismic design requirements. Since the site is located within 100 feet of critical public transportation infrastructure, the project was also checked considering a design earthquake event consisting of a 2,500-year (2% probability of exceedance in 50 years) Maximum Credible Earthquake (MCE) event with a magnitude of 6.25 (measured on the Richter scale) with a resulting Peak Ground Acceleration (PGA) of 0.36g. This level of ground shaking is significantly greater in magnitude as compared to that from a 2008-NYCBC-specified event, which is a magnitude 5.75 earthquake with a PGA of 0.147g.

A liquefaction assessment for the on-site soils was initially performed per the 2008 NYCBC requirements, and based on this criteria it was determined that liquefaction of the on-site soils under a 2008-NYCBC-specified earthquake was unlikely. Liquefaction assessment analysis indicated that under the MCE level of ground shaking, on-site soils in the upper 50 feet would potentially generate excess pore water pressures and undergo strength loss. Lateral spreading of the on-site soils was also considered under free field conditions (i.e., without considering the reinforcing effects of the proposed piles and surrounding infrastructure) in the foundation design analysis. As a consequence, 1.5 inches of theoretically calculated lateral spread movement was considered in the pile lateral analysis. When considering the applied lateral structural loads, the lateral analysis indicated that under liquefied soil and associated lateral spread conditions, the piles would laterally deflect up to 3 inches at the pile head. The project Structural Engineer confirmed the structure could tolerate the calculated lateral deflections at the foundation level. However, significant fixed head bending moments would need to be integrated into the design to account for the lateral pile-top deflections, with the pile-to-cap connections strengthened accordingly.

© 2016 Deep Foundations Institute

The driven piles were initially designed for a 200-ton compression capacity and a 45-ton uplift capacity, and consisted of a 12-inch-OD X 0.375-inch-thick, minimum 36 ksi steel, closed-ended pipe driven to bear on NYCBC Class 1c or better rock and completely filled with minimum 2,500 psi concrete. Lateral capacity analysis of the piles, considering group effects, indicated the piles could provide a lateral capacity of about 6.5 tons in the leading row and 4 tons in the trailing row under a fixed head condition; the structural design required a minimum capacity of 3 tons per pile. The initial design contemplated the piles to have no more than one shop or field splice, and the pile splices to be designed to provide the structural capacity of the pipe section.

Secondary oil casing pipe installed as an end-bearing open-ended pile was explored as a potential cost savings alternative. A Wave Equation Analysis was developed that identified open-ended pipes with outer diameters ranging between 13.75 and 14 inches with wall thicknesses ranging between 0.707 and 0.82 inch, when driven using a Junttan HHK-5S hammer (rated energy of 54.4 kips-feet) to an end-of-driving resistance of two consecutive 11 blows/inch could provide the required pile compression and uplift capacities. The open-ended secondary oil casing piles were to have minimum yield strength in excess of 50 ksi. The actual pipe material test data submitted by the supplier indicated the pipes typically had yield strengths in the range of about 130 to 140 ksi. Even when considering the allowable stress limitations in the 2008 NYCBC, the pile alternate section was considered to have higher structural capacity as compared to the initially designed pile section. The supplier however indicated that the piles would need to have up to 2 to 3 shop and field splices. Considering the potential economic benefit of the pile alternate, the pile alternate was considered favorably, provided the pile splices met or exceeded the 2008 NYCBC pile splice design requirements.

DRIVEN PILE DESIGN AND CONSTRUCTION

Pile Splice Design

To meet the project schedule, it was decided that the driven piles would be installed after excavating the site grade to about el 1 to 3 (i.e., a few feet above groundwater level). The available secondary oil casing pipe sections varied in lengths up to about 60 feet per section. The maximum pile lengths that could be transported to the site were limited to about 80 feet due to physical transportation constraints in Manhattan. Since the top of rock was typically about 75 to 100 feet below working grade level, multiple shop splices were necessary per pile and most of the piles also required at least one field splice.

The pile splices were designed and constructed to meet the splice design requirements in the 2008 NYCBC which required that pile splices meet the following two design requirements:

1. The splice shall be of adequate strength to transmit the vertical and lateral loads (including tension) and the moments occurring in the pile section at the location of the splice without exceeding the allowable stresses for such materials as established in NYCBC Section 1809.
2. In all cases, splices shall develop at least 50% of the capacity of pile in bending.

The following three types of pile splices were considered: (1) drive-fit sleeves welded at the top and bottom, (2) partial joint penetration (PJP) weld splice, and (3) complete joint penetration (CJP) weld splice. CJP welds have the same section modulus as the pipe pile section. Therefore, as long as a weld of sufficient strength is used, a CJP weld splice typically meets the above Code requirements. But, the section moduli and hence the bending moment capacities of the drive-fit and welded sleeve splices and PJP weld splices are less than the section modulus and bending moment capacity of the pipe pile section. Therefore, the sleeve and PJP splice designs had to be checked and modified where necessary to meet the NYCBC splice design requirements. As previously discussed, the piles were designed considering they could be simultaneously subject to axial compression and uplift loads, and bending moments, during an

© 2016 Deep Foundations Institute

MCE event. Therefore, the weld designs were checked to confirm that under the different combinations of pile axial loading and bending moments, the compression, tension, and shear stresses in the splices did not exceed the allowable stress requirements established in the 2008 NYCBC and American Welding Society (AWS) Design Manual D1.1.

Splice Weldability for High-strength Steel

Chemical analysis data for the high-strength secondary oil casing pipe material indicated the material had a relatively high carbon equivalency between about 0.58 and 0.73. These carbon-equivalency values indicated that the weldability of the material required special procedures (such as pre-heating) in order to accomplish a satisfactory weld. Test programs were developed for each proposed splice type.

The AWS D1.1 has a list of prequalified welds for specific base and weld materials and for various weld geometries. AWS D1.1 requires welds for materials comprising the secondary oil casing pipes to be designed, with test specimens fabricated and tested, to create a Procedure Qualification Record (PQR) to confirm the proposed weld can be performed on a production basis and can achieve the desired design capacity. A weld procedure specification (WPS) is then required to be developed based on the successful PQR. All welding is required to be performed by certified welders.

As part of the PQR process, two weld specimens were constructed for each type of splice and then two samples from these weld specimens were tested in a specialty material testing laboratory. Each weld was subject to nondestructive and destructive testing to correlate the nondestructive test results to those from the destructive test results, and to confirm the weld capacity. The weld specimens were prepared in accordance with the requirements of AWS D1.1. Each weld sample was first subject to nondestructive testing, which consisted of visual inspection (VI) during the welding process, ultrasonic testing (UT) in case of CJP welds, and magnetic particle testing (MPT) in case of a sleeve fillet welds or PJP welds. The weld specimens were then subjected to tensile and bending tests in accordance with the requirements of AWS D1.1. Based on the results of the PQR testing process and initial experience during pile installation, some of the weld design parameters were revised and PQRs repeated. The PQR process confirmed the parent pipe material required pre-heating to about 360^{o} F before performing welding. The test results generally indicated the high-strength steel pile material could be successfully welded to itself or to a lower strength steel section, and the weld could achieve the minimum required design capacities. Specific weld details for each type of splice are discussed in the paragraphs below.

The effect of quenching (i.e., rapid cooling) was also considered for the field-welded splices. Groundwater was present about 2 feet below the working site grade from where piles were driven. As previously discussed, pre-heating was necessary for satisfactory welding, and it was not practical to wait for a substantial time after welding a field splice to conventionally cool it before resuming pile driving, since this would delay pile installation. To study the effect of piles being driven right after the field splice was completed and inspected then becoming submerged while the pile section and weld were still at a high temperature (i.e. quenching), test specimens were prepared in the field using the different welded splice types, and select specimens were quenched with water immediately after welding was completed, while the rest were naturally cooled by air. Coupon samples were taken from the quenched and air-cooled weld specimens and microscopic observations and tension tests were performed on these samples to study the effect of quenching. The tests were conducted on the same day of welding and about 48 hours after quenching. Practically no differences were observed in the different test samples during microscopic observations and no loss of tensile strength was detected during tension testing. Therefore, it was concluded that quenching would have no significant effect on weld strength.

© 2016 Deep Foundations Institute

Splice-type Observations

Observations associated with the three splice types considered are discussed below:

1. Drive-fit sleeve welded at the top and bottom:

   Drive-fit sleeves of two different sizes were proposed. Steel for both types of sleeves had minimum yield strength of 60 ksi and an ultimate tensile strength of 90 ksi. Fillet welds of 0.3125-inch and 0.5-inch were proposed for the two sleeve sizes; details are schematically shown in Fig. 2 below. The proposed splices were designed based on a weld-electrode strength of 70 ksi and allowable stress factors provided in AWS D1.1 for welds subject to tension and shear. The calculations also considered a $^{1}/_{16}$-inch corrosion loss around the outside of the pipe, weld, and sleeve. The drive-fit sleeves were capable of providing the minimum required design tension capacity from the weld. Compression load on the pile was presumed to be transferred across the splice through end-bearing between the pile sections. The calculations also showed that the splices had a bending moment capacity that was adequate per the minimum requirements in the 2008 NYCBC for bending moments calculated under non-liquefied conditions. However, the splice capacity was not adequate for the calculated bending moments induced in the pile during the MCE seismic event and associated potential soil liquefaction. Therefore, the use of the drive-fit sleeve was permitted below el -60, because in this section of the pile, the calculated bending moment in the pile would be negligible.

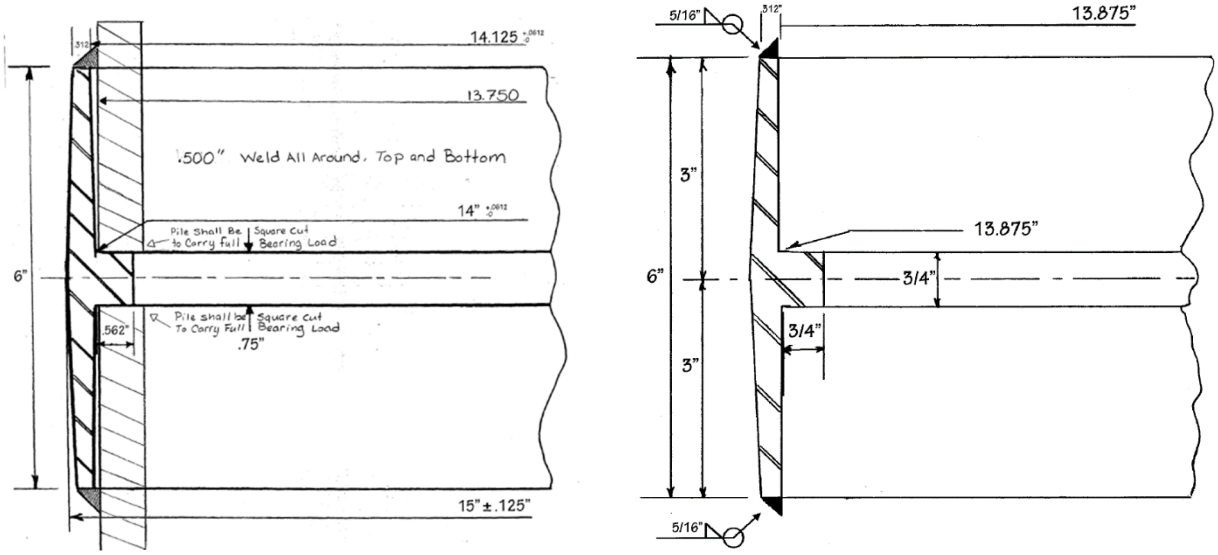


Fig. 2: Details for two sizes of welded drive-fit sleeves.

The drive-fit sleeves were installed on 18 index piles and each index pile was driven to the intended final driving resistance with pile dynamic analyzer (PDA) testing measurements. The welds were subject to VI and MPT. The welds on the piles were observed to be quenching as the welds were advanced a foot or two below ground surface and submerged below groundwater level. During the index pile driving process, PDA data showed anomalies during driving of three (3) of the 18 index piles. The anomaly locations generally coincided with the locations of the drive-fit sleeves.

To ascertain whether the observed anomalies in the PDA data were due to the quenching process, unidentified deficiencies in the welding process, or other factors, an investigation was conducted. One of the splices in question was located above pile cut-off elevation and was relatively shallow.

© 2016 Deep Foundations Institute

An excavation was performed around this pile to observe the condition of the welded splice. The splice in the second pile appeared to break during an uplift load test; the upper portion of the pile and splice was extracted from the ground using an excavator. The splice on the third pile was too deep to expose and observe. The accessible broken splice sections were visually observed and samples were collected from these sections for forensic testing. Photographs taken during forensic evaluation are presented in Figs. 3(a)-3(b). Forensic tests indicated that the damaged welds were caused by insufficient fusion between the weld material and the drive-fit sleeve. The lack of fusion was determined to be a result of inconsistencies in the sleeve material and foreign material, such as soil and debris, which were found between the weld and sleeve. Sufficient information could not be obtained from manufacturer's strength test results to confirm if variations in actual drive-fit sleeve materials existed. The drive-fit sleeve option was not used during production pile driving because the quality of the sleeve material could not be consistently verified, and the potential for field contamination during field welding existed. Select index piles spliced with the welded drive-fit sleeves were compression, uplift, and lateral load tested to confirm geotechnical capacity of the few piles used that were installed with drive-fit field splices.

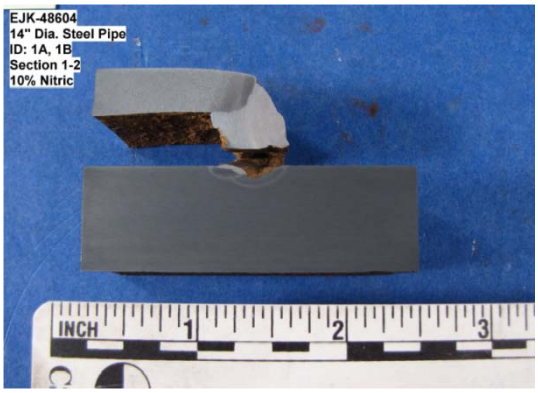


Fig. 3(a): Failed welded drive-fit sleeve splice.

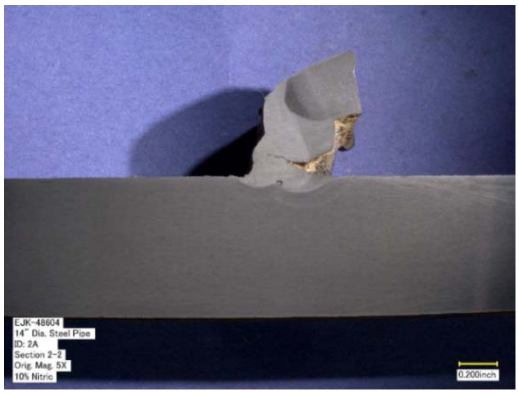


Fig. 3(b): Failed welded drive-fit sleeve splice.

2. PJP weld splice:

The PJP weld design alternate (in lieu of the drive-fit splice) consisted of 0.625-inch-thick welds performed using minimum 70 ksi electrodes. The design calculations considered $^{1}/_{16}$-inch of corrosion loss on the inside and outside of the pipe pile and weld. The calculations showed that the splice bending capacities were adequate per the minimum requirements in the 2008 NYCBC. However, the splice capacity was not adequate for the calculated bending moments induced in the pile considering the MCE seismic event and potential soil liquefaction. Therefore, the use of the PJP splice was permitted below el -60 because in this section of the pile, the calculated bending moment in the pile would be negligible. Plots showing calculated bending moment variation along pile length for the MCE soil model and seismic design parameters are presented in Figs. 4(a)-4(b) for shallow and relatively deeper pile cut-off elevations, respectively.

© 2016 Deep Foundations Institute

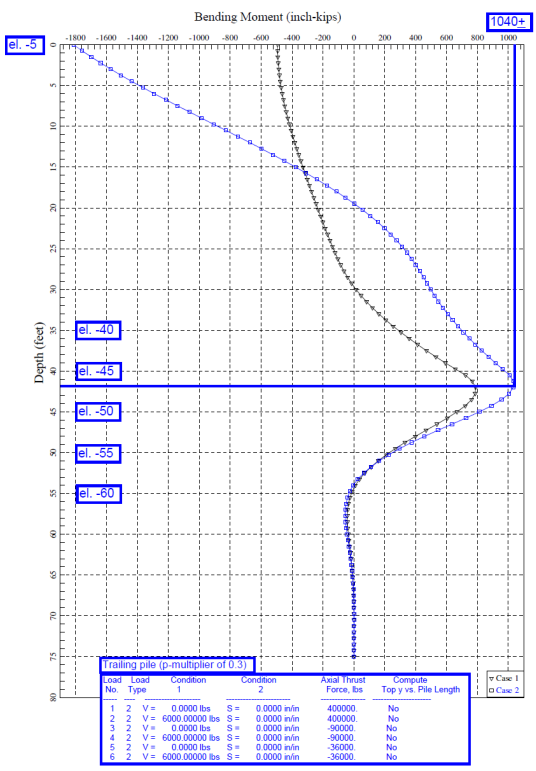


Fig. 4(a): Shallow pile cut-off.

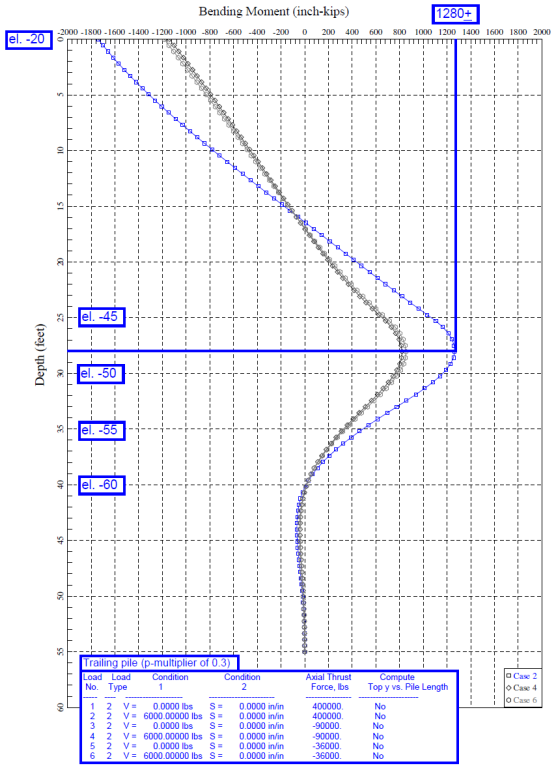


Fig. 4(b): Deeper pile cut-off.

The welding specialist for the project determined that the PJP welds were more practical to construct than the CJP welds. Per the project welding specialist, the PQR for the CJP weld could be used for the PJP welds, because PJP and CJP weld construction is generally similar and it is relatively easier to perform a PJP weld because of its relatively smaller thickness. No anomalies were observed during PDA testing performed during pile driving on piles with a PJP weld splice. All PJP splices were subject to VI and MPT.

3. CJP weld splice:

CJP weld splices were required for splices along the length of the pile above el -60. All the shop splices were also performed using CJP welds. The CJP weld splice design was based on a minimum 70 ksi weld strength; 110 ksi electrodes were used for field splicing. The CJP pile splice design accounted for $^{1}/_{16}$-inch corrosion loss on the inside and outside surface of the pile and weld. The design was reviewed for compliance with the 2008 NYCBC requirements for splices subject to design moments calculated for the MCE seismic event and resulting soil liquefaction. The PQR procedures, WPS, and design details and calculations for the CJP welds were submitted, reviewed, and approved during early stages of the submittal review process. All PDA-tested index piles had at least 1 or 2 CJP shop splices and eleven (11) PDA-tested piles also contained CJP field splices. The PDA test results did not show any anomalies at the shop or field CJP splice locations. All CJP welds were subject to VI and UT.

In general, field CJP weld splicing time in the field averaged at about 60 to 120 minutes per splice. Although it was demonstrated that quenching did not practically impact the weld, it was necessary to allow the weld to air-cool for up to about 40 minutes to allow the welds to be tested using the UT equipment; UT testing took about 10 minutes per splice.

© 2016 Deep Foundations Institute

Quality Assurance of Splice Welds

Shop CJP splices were performed in the supplier's yard prior to transporting to the project site. Field PJP and CJP splicing was performed at the site during production pile driving. Pile driving was performed using multiple pile rigs, and a total of about 105,000 linear feet of driven piles were installed. Pile sections were fabricated in the supplier's yard on a daily basis and shipped to the site. The welds were inspected and tested by the special inspection agency with test results provided to the special inspectors on a regular basis. Approved pile sections were marked at the yard prior to shipping so the Contractor and the on-site special inspectors could confirm pile sections picked for driving consisted of tested and approved spliced sections. In addition, inspection and testing of field splices was also performed on a daily basis. Results of the field testing were marked on the pile, and the on-site special inspectors were verbally informed of the results by the material testing agency on the same day. Any sections containing detected weld defects were removed and repaired in the supplier's yard or at the site, and then re-inspected.

Each weld was assigned a unique identification (ID) number after testing. These weld ID numbers, also referred to as piece marks (PM), were written on each pipe section directly adjacent to the weld and at the ends of the pipe section, and documented by the special inspection agency. Selected construction photographs from the weld observation, testing, and documentation process are shown in Figs. 5(a) and 5(b). Weld identification numbers were tabulated and provided to the project team on a periodic basis with language confirming if the weld was approved or if it needed to be repaired. Weld repairs typically consisted of removing the affected weld areas, re-grinding the two surfaces, pre-heating, and re-welding.



Fig. 5(a): Ultrasonic testing on a CJP weld.

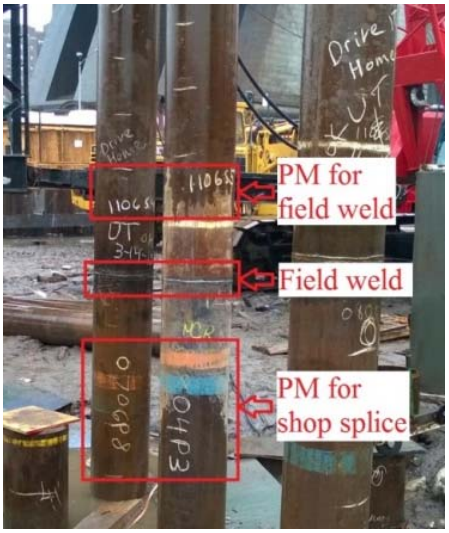


Fig. 5(b): PMs written on side of the pipe pile.

© 2016 Deep Foundations Institute

A schematic flowchart showing the weld quality assurance process is presented in Fig. 6.

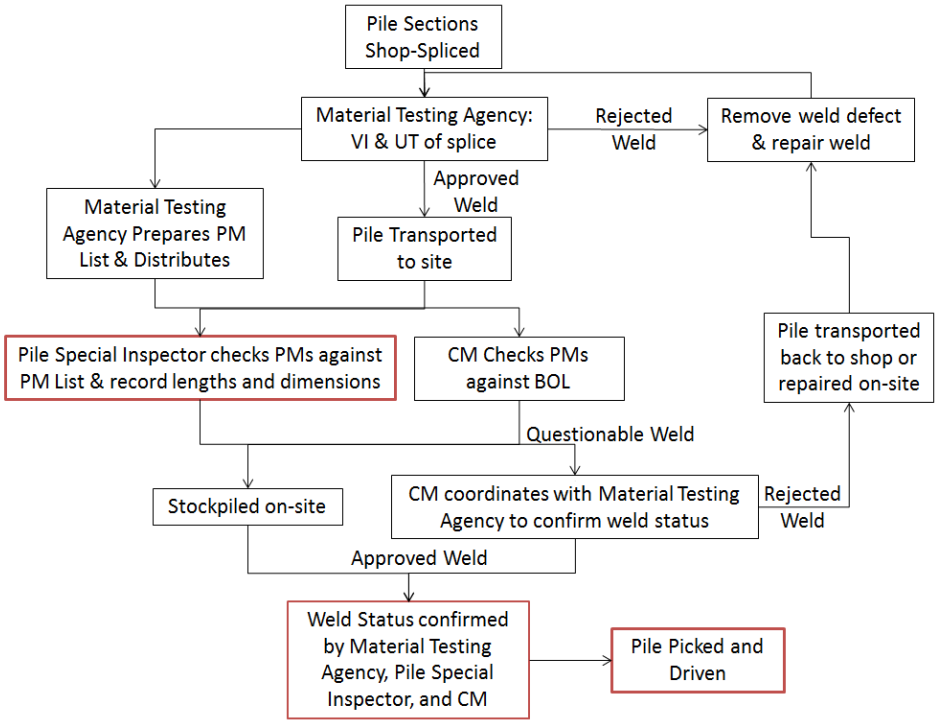


Fig. 6: Workflow for weld quality assurance process.

Pile Lateral and Uplift Capacity Verification

The new building foundations also included rock-socketed drilled piles, which due to project schedule constraints, needed to be installed concurrently with the driven piles. The drilled pile casings were installed using compressed air; during installation, external air flush was observed at the ground surface while drilling generally in the upper 50 feet of the soil stratum. Some driven piles were installed in close proximity to these drilled piles after they exhibited external air flush, and noticeable reduction in pile driving resistance was observed during the initial about 50 feet of pile driving. The driven piles resist compression loads through end-bearing on rock and therefore it was concluded that external air flush in soil would not have a significant impact on the pile compression capacity. However, since the piles relied on the surrounding soil for uplift and lateral capacities, it was necessary to explore how the uplift and lateral capacities of the driven piles could potentially be impacted by external air flush operation. Lateral and uplift load tests were performed on select driven piles around which external air flush was observed during adjacent drilled pile installation. No measurable reduction in the lateral pile capacity of the driven piles was observed during these load tests. The uplift and lateral pile capacities measured during these load tests were generally consistent with those measured during load tests in the other portions of the site. It was concluded that although external air flush may have resulted in some soil disturbance in the top about 50 feet, the lateral and uplift pile capacities were not significantly impacted.

© 2016 Deep Foundations Institute

CONCLUSIONS

The following conclusions are drawn from experience on this project:

1. The level of ground shaking resulting from a 2,500-year (2% probability of exceedance in 50 years) Maximum Credible Earthquake (MCE) event with a magnitude of 6.25 (measured on the Richter scale) with a resulting Peak Ground Acceleration (PGA) of 0.36g is significantly greater in magnitude as compared to that from a 2008-NYCBC-specified event.

2. The AWS D1.1 has a list of prequalified welds for specific base and weld materials and for various weld geometries. AWS D1.1 requires welds for materials comprising secondary oil casing pipes to be designed, with test specimens fabricated and tested, to create a Procedure Qualification Record (PQR) to confirm the proposed weld can be performed on a production basis and can achieve the desired design capacity. A weld procedure specification (WPS) is then required to be developed based on the successful PQR.

3. For materials that have high carbon equivalency, special welding procedures, such as preheating, are required. If a pre-heated weld is to be rapidly cooled during the construction process, the effect of such rapid cooling (i.e., quenching) on weld performance should be investigated and accounted for during the weld design process.

4. CJP welds have the same section modulus as the pile section and therefore can be used anywhere along the pile section when properly designed. However, CJP welds are more time consuming to construct and test when compared to typical PJP or fillet welds. The use of PJP or fillet welds is typically restricted to portions of the pile subject to relatively lower bending moments.

5. The PQR for a CJP weld can be used for a PJP weld of similar construction, because the PJP weld is performed using the same procedure and is relatively easier to construct because of the weld's smaller thickness.

6. Soil disturbance caused by adjacent construction, such as external air flush during drilled pile installation, can result in reduction in pile capacity when the piles rely on the disturbed soil zone for support. When signs of such potential impacts are observed, the pile capacities should be verified.

REFERENCES

American Welding Society, 2000. 17th Edition, AWS D1.1: Structural Welding Code – Steel, pp. 20-102, 265-268, and 341-342.

New York City Building Code, 2008. Chapter 16: Structural Design; Chapter 18: Soils and Foundations, pp. 328-326, 383-396, and 400-402.

© 2016 Deep Foundations Institute

FULL SCALE UPLIFT LOAD TESTING OF MICROPILES IN COHESSIONLESS SOIL

Maged A. Abdlrahem, Western University, London, Ontario, Canada, 226-224-4466, mabdlrah@uwo.ca
M. Hesham El Naggar, Western University, London, Ontario, Canada, 519-661-4219, melnagga@uwo.ca

ABSTRACT

Hollow bar micropiles have constructional advantages such as: fast and low-noise and low vibration installation process and small installation equipment, which allow access to tight places. In addition, they have efficient load transfer mechanism, which facilitates carrying considerable load in compression and tension. The common practice is to use diameter ratio of drill bit/ hollow bar (D_b/D_h) around 2 in their construction, and they are typically designed assuming type B as classified by the Federal Highway Administration (FHWA). In this paper, the performance and capacity of Hollow bar micropile with different (D_b/D_h) ratios are investigated. Full-scale micropiles were installed at a site in Ontario, Canada, and were tested in order to evaluate the uplift performance of Hollow bar micropile with different(D_b/D_h) ratios. Two micropiles with two different ratios 2.25 and 3 were constructed and tested. The total length of the micropiles was 6m with embedded length of 5.75m. The soil at the site was primarily medium dense to dense sand. The results of the load tests are presented and discussed. It was found that the uplift capacity of the micropile increased by about 19.5% as D_b/D_h increased from 2.25 to 3.

Keywords: hollow bar micropile, tension test, cohessionless soil.

INTRODUCTION

Micropile is a small diameter, less than 300 mm, drilled and grouted pile and is typically reinforced according to Federal Highway Administration (FHWA, 2005). The technology of micropile was introduced in North America in 1970's, but the growth in the east coast of United State was intense compared to all other cities around the globe (Bruce and Nicholson, 1989). Nowadays, micropile construction is used extensively worldwide as a viable solution that offers several advantages such as fast installation in low headroom, minimal disturbance to the adjacent structure efficient load transfer due to high grout to ground bond strength. As the method of grouting has major influence on the grout – ground bond strength, FHWA has classified the micropiles into four categories. Type A: the grout is placed under gravity and no pressure is required. Type B: The grout is typically pressurized under a pressure range from 0.5 to 1 MPa as the temporary casing is withdrawn. Type C: the grout is placed in two-step process. First, the grout is poured under gravity only as in Type A. Before the hardening of the grout, similar grout is pressured of at least 1MPa without the use of packer. Type D: Like Type C, it is a two – step process, the grout is placed under gravity as in Type A and sometimes pressurized as in Type B. After hardening of the initial grout, additional grout is pressurized between 2 to 9 MPa through sleeved pipe by using packers, as many times as needed. According to this classification, hollow bar micropile is usually designated as Type B. However, the construction technique is completely different from Type B. Recently; there is a trend to supplement the four types of micropiles by Type E as represent to hollow bar micropile (Timothy et al, 2012). The construction method of hollow bar micropile involves two main stages which can be performed in one–step process: advancing the drilling bit attached to a threaded hollow bar to the required depth; and pressurizing the grout through nozzles of the drill bit.

Han and Ye (2006) performed full-scale load tests on four micropiles; two were subjected to compression and two were subjected to tension loading. The nominal diameter and length were 150 mm and 8.0 m, respectively. According to the grouting method, micropiles in this study were considered as Type B as recommended by FHWA. The excavated hole was filled with aggregate finer than 25 mm and grout, utilizing a pressure up to 0.5 MPa. It was concluded that the ultimate load capacity of micropile subjected

© 2016 Deep Foundations Institute

to compression loading is higher than the ultimate capacity of micropile under tension loading conditions. Thompson et al. (2007) presented results of axial compression, uplift and lateral load tests on micropiles that were used to upgrade pier foundations. Based on the load test results, they concluded that the ultimate bond resistances of grouted micropiles provided by FHWA (2000) seem to be reasonable. Stuedlein et al. (2008) reported on compression and tension tests of micropiles installed in medium dense to dense, gravelly sand. The micropiles had a cased length of 3.05 m and 5.20 m bond zone length. The casing diameter was 140 mm with 13 mm wall thickness. The load–displacement curves indicated a stiffer response of micropiles subjected to compression loading than uplift. They noted that ignoring the contribution of end bearing resistance seems to be conservative. Abd Elaziz and El Naggar (2012) conducted a field study on four hollow bar micropiles installed in stiff silty clay deposit. The embedded length was 5.75 m while the OD and ID of the hollow bars were 76 mm and 48 mm, respectively. The load- displacement curves showed similar responses for both compression and tension loading conditions. The results demonstrated that the bond strength values suggested by FHWA considering hollow bar micropile as Type B underestimate the micropile capacity.

Despite it has been introduced in practice for more than 20 years, there has not been much information in the literature on the performance of hollow bar micropile with different diameter ratio of drill bit/ hollow bar (D_b/D_h) and the effect of grouting pressure. The work undertaken is a part of our research group to fill the gap in the literature on the behaviour of hollow bar micropile and the effect of several factors on its performance. One of the factors that can impact the performance of hollow bar micropile subjected to tension loads is the diameter ratio of drill bit/ hollow bar (D_b/D_h). This study focuses on evaluating the performance of hollow bar micropile with two different diameter ratios subjected to tension loads.

SITE INVESTIGATION

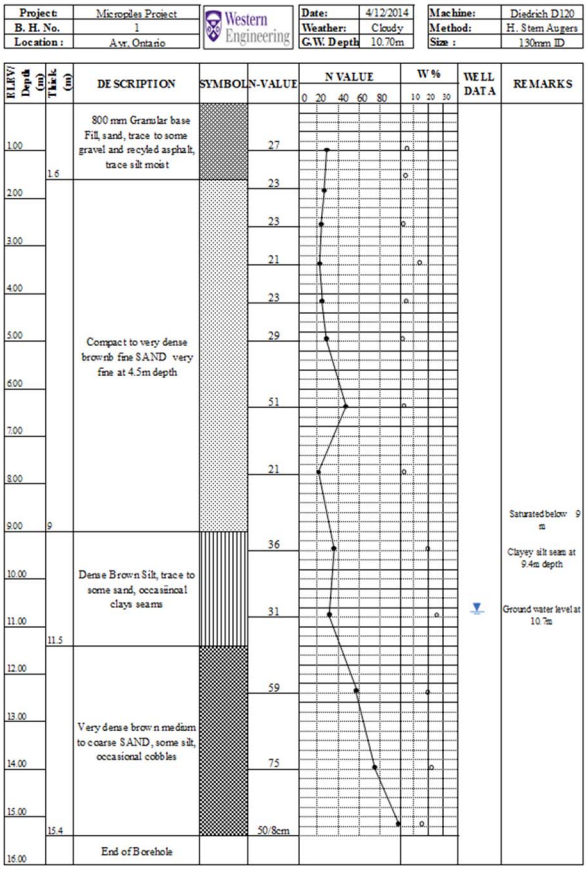
The site is located in Ayr, Ontario. An extensive site investigation was performed that included both in-situ and laboratory testing. Three mechanical boreholes were drilled to various depths using hollow stem auger of 130mm, followed by standard penetration test (SPT). Samples were extracted using split spoon sampling method and transported to the laboratory for further testing. Four CPT soundings were performed across the site. Figure 1 shows the SPT results for BH1 and BH2, including N values and water content for different soil layers. The first 400 mm consists of granular base fill with some gravel and recycled asphalt overlaying a layer of brown very dense sand up to 11m below ground surface. Seams of silt and silty clay were observed at different levels. The ground water table was observed between at 9.5 to 10.5m below ground surface. The results of CPT1 and CPT2 soundings are shown in Fig. 2. The average cone resistance corrected for pore water pressure (q_t) ranged from 10 to 30 MPa in the upper 6.5m and 30 to 45 MPa from 6.5m to 8m followed by a decrease in (q_t) with an average of 20 MPa. The soil behaviour type (SBT) as suggested by Robertson (1990) indicated that the soil is mainly sand with some seams of silty and sandy silt, that conforms with visual observations. Using the correlation proposed by Kulhawy and Mayne (1990), for the sand relative density can be established based on SPT and CPT data, i.e.

$$D_r = \left[\frac{(N_1)_{60}}{40}\right]^{0.5} \quad [1]$$

$$D_r = \left[\frac{(\frac{q_{c1}}{p_a})}{305}\right]^{0.5} \quad [2]$$

The computed relative density versus depth is plotted in Fig.3. There is a good agreement between the two test results, which indicated that the soil is mainly dense sand.

© 2016 Deep Foundations Institute



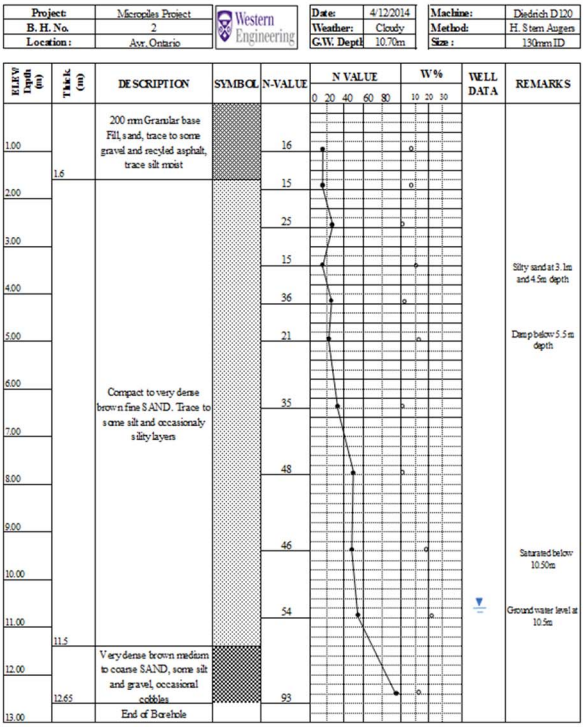


Fig 1. Boreholes 1 & 2, SPT N Value and water content.

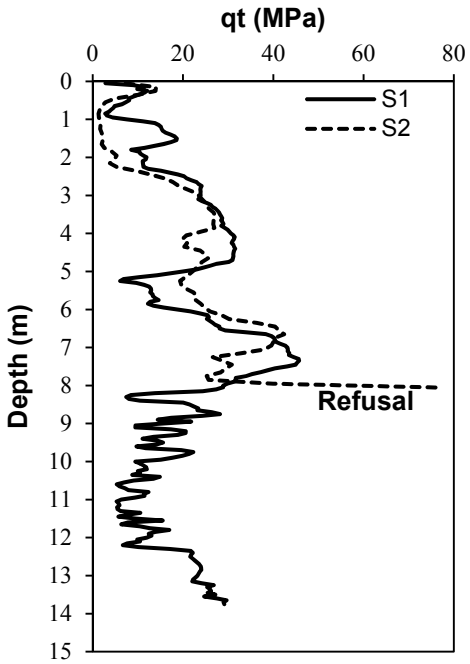


Fig 2. CPT test results for S1 and S2.

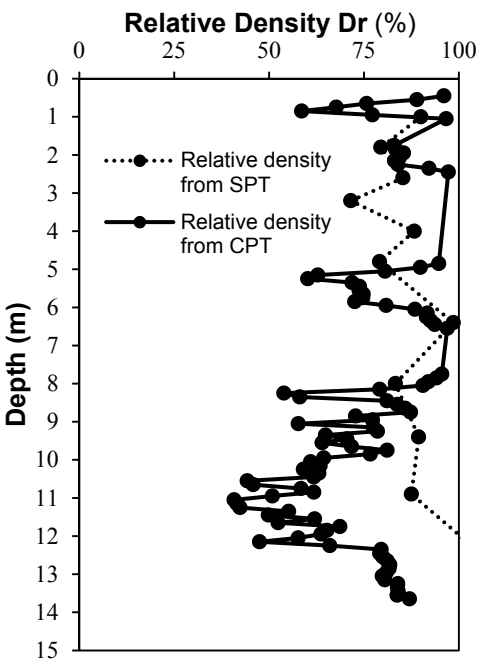


Fig 3. Relative density with depth.

© 2016 Deep Foundations Institute

MICROPILE MATERIALS AND INSTALLATION.

Six self-drilling hollow bar micropiles R51N were installed using an Ingersoll Rand ECM-350 drill rig. The outer diameter of the hollow bar is 51 mm and the inner diameter is 33 mm. Tungsten carbide cross cut drill bit was used as an excellent choice for granular soils. Figure 4 presents a plan view of the micropiles locations in the test site. Six micropiles were constructed and tested. In this paper, the test results of only two micropiles, denoted MP4 and MP5, are presented. MP4 was installed using drill bit with 115 mm diameter while MP5 was installed using 152 mm-diameter drill bit. The diameter ratio of drill bit/ hollow bar (D_b/D_h) is 2.25 and 3 for MP4 and MP5, respectively. The total length of the micropiles is 6m with 5.75m embedded length.

The drill bit attached to the hollow bar was positioned in the predetermined location. The verticality of hollow bar was ensured by attaching a 1m-long magnetic water level to the hollow bar. A rotary percussive drilling was employed simultaneously with grout flushing technique. A Nonstructural grout with specific gravity between 1.4 and 1.5 was employed as drilling fluid to drill the hollow bar to the required depth. Once the first segment of the hollow bar was installed, coupler was attached to allow the second segment to be installed. Upon completion the drilling, structural grout with specific gravity between 1.80 and 1.95 was injected employing pressure of 0.8 to 1 MPa. Grout cylinders were collected during the installation and were transported to a control room with a relative humidity of 100% and constant temperature of 23ºC. The average compressive strength after 28 days of the grout cylinders was 40 MPa and the average spilt tensile strength was 3.97 MPa. The compressive strength was determined according to ASTM C39 and the tensile strength was obtained in according to ASTM C496. The compressive strength meets the minimum requirement (28 MPa) set by FHWA (2005).

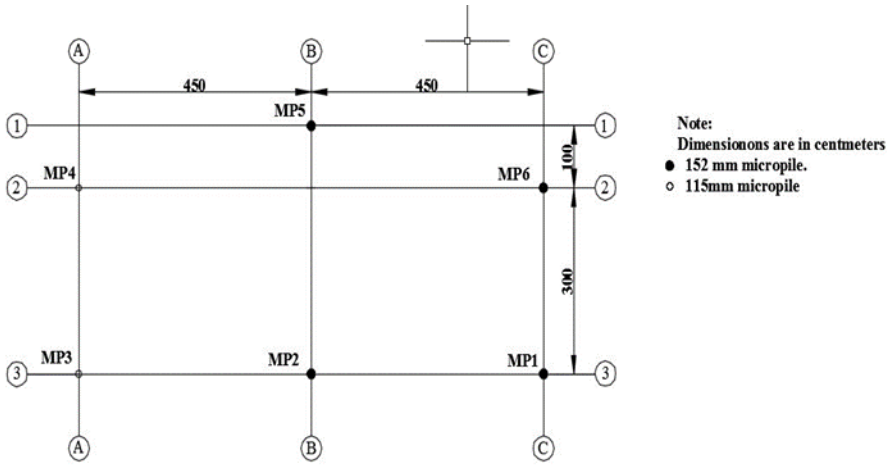


Fig 4. Plan view of micropiles locations.

TEST SETUP AND PROCEDURES.

A reaction frame system was employed for tension tests. It comprised a main steel reaction beam supported by cribbing. Shims were used to level and centralize the reaction frame. The reaction frame for tension tests is shown in Fig. 5. A hydraulic jack of 1100 kN advance capacity and maximum stoke capacity of 150 mm powered by a hydraulic pump was used. Four HLP 190 linear potentiometers were employed to record the vertical pile head movement and average value was taken. The HLP 190 has 100 mm stroke and an accuracy

© 2016 Deep Foundations Institute

of 0.01 mm. The potentiometers were attached to the loading steel plate in a square arrangement and clamped to two independent reference steel beams.

A quick load test method was employed in accordance with ASTM D3689/D3689M - 07 (Reapproved 2013) standard for tension tests. The load was applied in increments of 5 % of the anticipated failure load and maintained for 4-5 minutes before applying the next increment. The load was applied until the pre-specified load or failure is reached, once the failure is reached, unloading process took place in five approximately equal intervals.

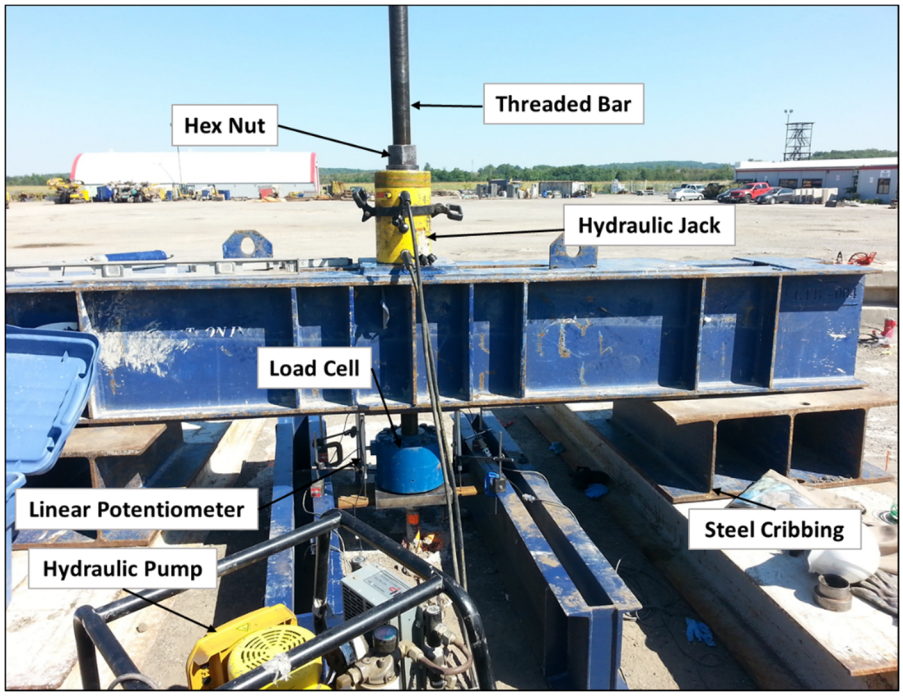


Fig. 5. Tension test setup

TEST RESULTS AND ANALYSIS.

Figures 6 and 7 present the load–displacement curves for MP4 with a diameter ratio (D_b/D_h) of 2.25 and MP5 with a ratio equal to 3. The two micropiles were loaded to the point where a small increase in the applied load resulted in continues increase in the vertical displacement. The observed MP5 response was stiffer that of MP4. Furthermore, MP5 showed higher ultimate capacity compared to MP4. The load displacement curve for MP4 shows a plunging failure at about 510 kN, while MP5 failed at 635 KN. Increasing the drill bit diameter from 115 mm to 152 mm resulted in an increase in the ultimate tension capacity of the micropile by about 19.5%. In addition to the observed plunging failure, three different Interpreted failure criteria were used to determine the ultimate capacity of the two micropiles.

Davisson (1972) proposed interpretation method for a driven pile that has three main components: elastic pile compression, intercept equal to 3.8 mm and tip resistance B/120 mm (For SI units) as in equation No 01. This method gained its popularity

© 2016 Deep Foundations Institute

$$\Delta = \frac{QL}{A_p E_p} + 3.8 + \frac{D}{120} \quad [1]$$

Where Δ = Displacement, Q = Applied load, L and D are the Pile length and diameter, respectively, A_p= cross-sectional area of pile and E_p = elastic modulus of pile.

Fuller and Hoy (1970) defined the interpreted failure load as the minimum load at which a rate of total settlement of 0.14 mm/kN occurs. This method is recommended by FHWA (2005).

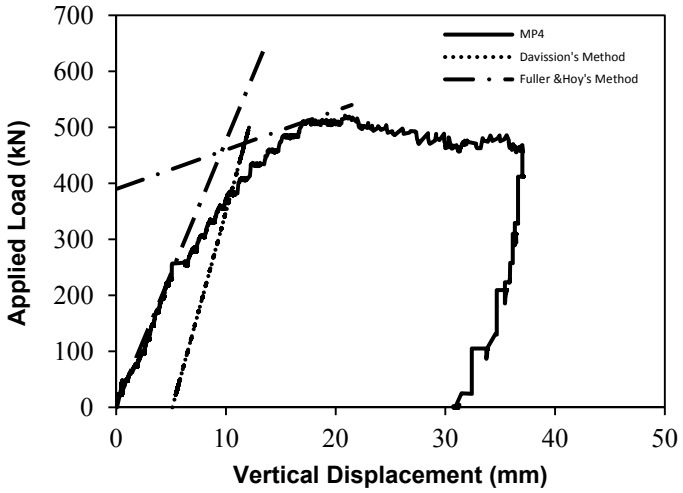


Fig 6. Load – displacement curve for MP4 with failure criteria.

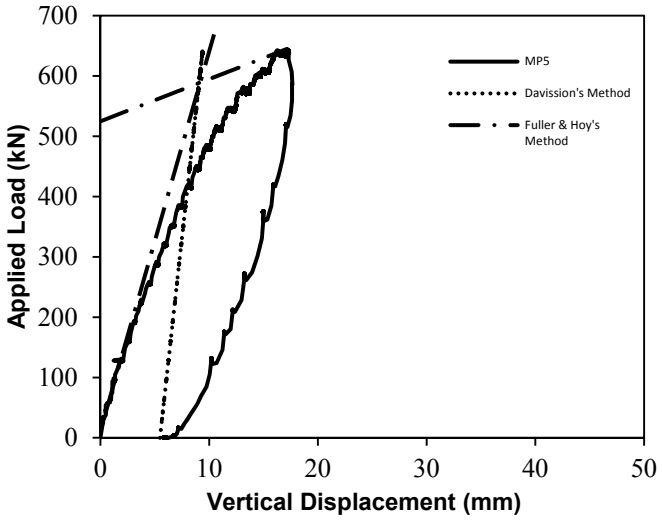


Fig 7. Load – displacement curve for MP5 with failure criteria.

The third interpreted failure criterion was proposed by Butler and Hoy (1977) in which interpreted the failure load as the intersection of 0.14 mm/kN slope with the line tangent to the initial straight line portion

© 2016 Deep Foundations Institute

of the load displacement curve. There interpreted failure load methods are presented in Table 1 and illustrated in Fig 6 and Fig 7.

Table 1. Comparison between Interpreted failure load methods.

Method	Interpreted Failure Load (kN)	
	MP4	MP5
Plunging	510	638
Davisson method	380	420
Fuller and Hoy's	512	635
Butler and Hoy's method	470	600

As it can be noticed from Table 1, Fuller and Hoy's method gives an interpreted failure load that is close to the observed plunging failure load, while Davisson's method seems to be overly conservative to interpret the failure load. Kulhway and Hirany (2009) noted that the Davisson method gives a conservative interpreted failure load compared to other interpreted failure criteria. It provides the lowest estimation of tension capacity of aforementioned methods.

Micropiles were exhumed and the actual diameters were measured. It was found that the average diameter of micropiles with drill bit 115 and 152 mm was 132 and 171 mm, respectively, i.e. the diameter increased by 12.8 % and 11.1 % over the diameter of the drill bit.

SUMMARY AND CONCLUSIONS

In this study, full-scale tests were conducted on two micropiles with two different D_b/D_h ratios, 2.25 and 3 to study the beneficial effect of increasing the ratio from 2.25 (the current practice) to 3. MP5 displayed a stiffer load–displacement response compared to MP4. The results indicated that the tension capacity of micropile increased by about 19.5% as the ratio of D_b/D_h increased from 2.25 to 3. The estimated ultimate bond strengths were back calculated and found to be 208 and 214 kPa for micropiles with drill bits of 152 and 115 mm, respectively, based on the actual effective diameter of exhumed micropiles. Comparing the three different interpreted failure criteria, it was found that Fuller and Hoy's method provides a better estimate of the failure load for micropile subjected to tension load. FWHA (2005) gives a wide range for grout–to–ground bond strength values for Type B micropile installed in medium to very dense sand between 120-360 kPa. The ultimate bond resistances of grouted micropiles obtained from this study lies within the wide range values provided by FHWA (2005). This study examined the behaviour of micropiles in medium dense sand. Similar study should be conducted in other type soil types to evaluate the effect of D_b/D_h on other soil profiles.

ACKNOWLEDGMENTS

The authors would like to acknowledge the support provided by HC MATCON for providing the materials, installing the micropiles and setting the reaction frames and NCERC for partially funding the project. Finally, the authors would like to thank the Libyan Ministry of Education for providing a scholarship to the first author.

© 2016 Deep Foundations Institute

REFERENCES

Abd Elaziz, A.Y., and El Naggar, M.H. 2012. Axial behaviour of hollow bar micropiles under monotonic and cyclic loading. Geotech. Test. J., 35(2), pp. 249–260.

ASTM International. (2013). ASTM D3689/D3689M – 07 (Reapproved 2013): Standard Test Methods for Deep Foundations under Static Axial Tensile Load. 13 p.

Bruce, D.A., and Nicholson, P.J. 1989. The practice and application of pin piling. ASCE Foundation Engineering Conference, Evanston, IL, 19pp.

Butler, H.D., and Hoy, H.E. 1977. User manual for the Texas quick-load method for foundation load testing. Federal Highway Administration, Office of Development, Washington, DC.

Davisson, M.T. 1972. High capacity piles. Proceedings, Soil Mechanics Lecture Series on Innovations in Foundation Construction, American Society of Civil Engineers, Illinois Section, Chicago, pp. 81–112.

FHWA. 2000. Micropiles design and construction guidelines- implementation manual. Federal Highway Administration (FHWA), U.S. Department of Transportation, Washington, D.C. Publication No. FHWA-SA-97-070.

FHWA. 2005. Micropiles design and construction. Federal Highway Administration (FHWA), U.S. Department of Transportation, Washington, D.C. Publication No. FHWA-NHI-05-039.

Fuller, F.M., and Hoy, H.E. 1970. Pile load tests including quick-load test method conventional methods and interpretations. Highway Research Board (HRB), Issue 333, pp. 78‑86.

Han, J., and Ye, S.L. 2006. A field study on the behavior of micropiles in clay under compression or tension. Canadian Geotechnical Journal, Vol. 43(1), pp 19‑29.

Kulhawy, F.H., and Mayne, P.W. 1990. Manual on estimating soil properties for foundation design. Research project No. 1493-6, EL-6800, Electric Power Research Institute. Palo Alto, Calif.

Kulhawy, F.H., and Hirany.A. 2009. Interpreted failure load for drilled shafts via Davisson and L_1-L_2. Internatioanl Foundation Congress and Equipment Expo. Deep Foundations. Pp. 127- 134.

Robertson. P.K. 1990. Soil classification using cone penetration test. Canadian Geotechnical Journal. 27(1), 151-158.

Stuedlein, A.W., Gibson, M.D., and Horvits, G.E. 2008. Tension and compression micropile load test in gravelly sand. Sixth International conference on case histories in geotechnical engineering, Arlington, VA.

Thomson, P., Leew, B., Zakeri, A., Becker, D., Bunce, C., and Dittrich, P. 2007.Axial compression, axial tension and lateral load response of pre-production micropiles for the CPR Mile 62.4 Nipigon subdivision bridge. Proc., 8th Int. Workshop on Micropile, Toronto.

Timothy, M. J., Bean, J. J. and Bolton, M. K. 2012. miniJET: A New Type of Micropile. Grouting and Deep Mixing, New Orleans, Louisiana: American Society of Civil Engineers (ASCE), pp. 1095-1104.

© 2016 Deep Foundations Institute

GROUND IMPROVEMENT BY DRY CONCRETE COLUMNS

Tatiana Tronda, Belarusian National Technical University, Minsk, Belarus, +375 29 2853422, t.v.tronda@gmail.com

ABSTRACT

The territory of Belarus is characterized by nonhomogeneous ground conditions. In some cases soft ground layers can reach tens of meters in depth. Application of piles and other conventional foundations is rather difficult and expensive in such complicated conditions. Alternatively for the first time dry concrete columns were applied to improve the saturated soft soils at two sites. As there is no design methods for calculation of bases improved by dry concrete columns static penetration and static load tests were carried out to check the bases on availability. Considerable increase of toe resistance and Young modulus was achieved for all types of soil. Practical application, technology and test results are described in the paper. According to comparative calculations the cost of foundations on the base improved by dry concrete columns can be 32-75% lower than the cost of conventional pile foundations depending on ground conditions.

Keywords: dry concrete column, ground improvement, characteristics, efficiency

INTRODUCTION

Pile foundations, sand cushions or dewatering are usually applied in complicated ground conditions which are caused by presence of saturated soft soils. If the depth of soft soils reaches 20 m or more, conventional foundations have limited application, high labor and construction cost. A rational solution in such conditions is a ground improvement of upper soft soils. It allows the loads to be transferred on upper ground layers and the stresses to be dissipated considerably before reaching underlying soft ground layers.

One of the effective ground improvement methods for saturated soft soils is the reinforcing by dry concrete columns (Fig. 1). The method allows saturated soft soils to be compacted and be drained at the same time. As a result strength and deformation characteristics of natural soils improve (Tronda 2013, Тронда 2014).

Unfortunately, there is no design and computing methods for the ground improvement by means of dry concrete columns. However, at present the methods are under development on the basis of theoretical and experimental researches.

TECHNOLOGY

The dry concrete columns are fulfilled in pressed wells according to technology of vibrostamped piles. Wells are pressed by vibratory hammer with the closed ended casing (Fig. 2) that provides compaction of surrounding soft soils. Then the casing is filled with dry concrete mix (Fig. 3). The casing end remains on the design depth and the casing is removed by vibratory hammer. The removing of the casing with vibration enables compaction of dry concrete mix inside the well. Dry concrete mix drains surrounding saturated soft soils improving its properties and the compaction speeds up the consolidation process. Over time the dry concrete columns fasten absorbing water from surrounding saturated soft soils that is need for hydration of cement (Fig. 4, 5).

© 2016 Deep Foundations Institute

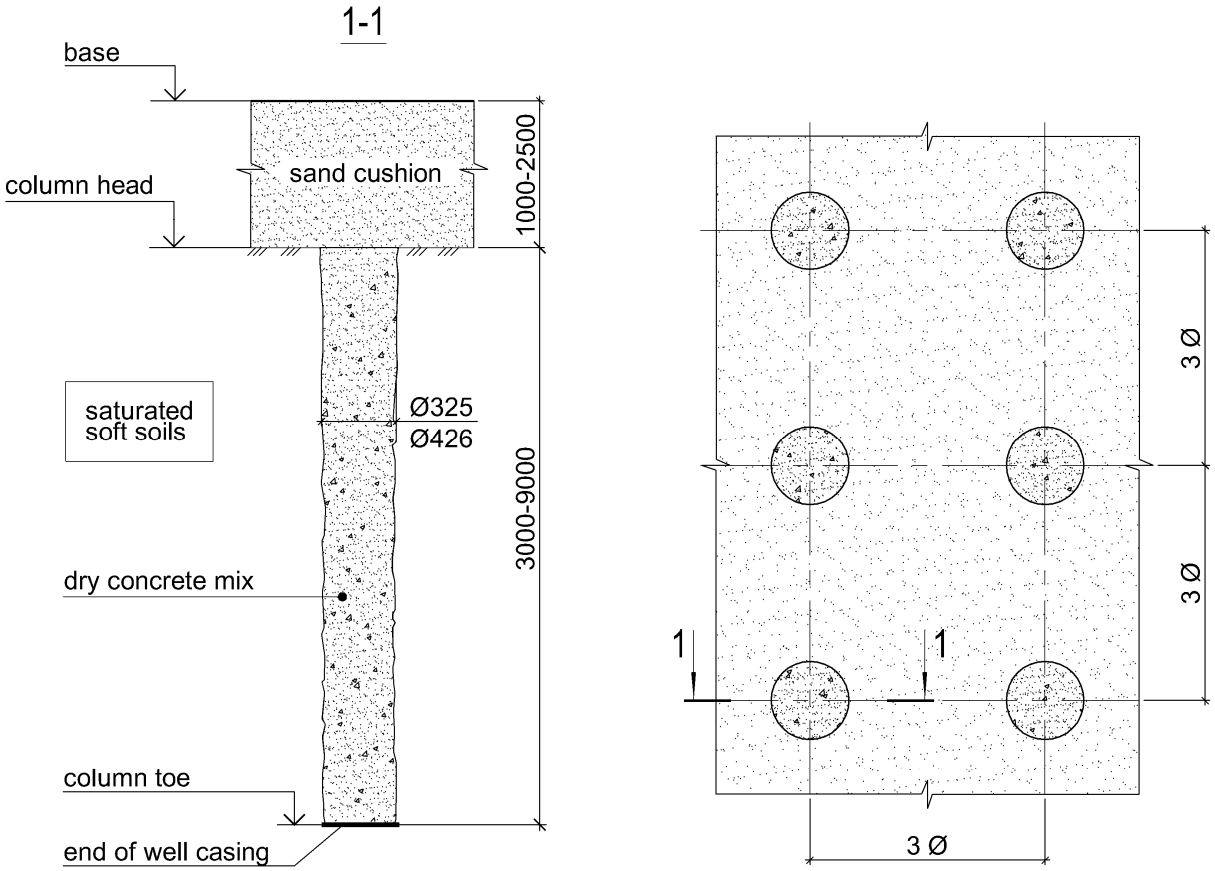


Fig. 1. Dry concrete columns

The arrangement of dry concrete columns is produced in two steps. In the first step each second column is produced in staggered-order. Second step columns are produced in three days after the first step. Over reinforcing columns the sand cushion is applied to distribute loads from upper structures or building. It creates an additional pressure that prevents the decompaction of soft soils and absorption of water.

There are no yet design methods for selection of suitable concrete mix for the ground conditions. But it is recommended to use the sulfate resistant cement or Portland slag cement for aggressive soils.

Dry concrete columns were applied at two sites with complicated ground conditions: in Kolodischi (Site A) and in Minsk (Site B). Since this type of ground improvement has never been used in Belarusian practice and no regulatory documents have any reference of them, its availability was checked by series of experiments such as static penetration and static load tests.

© 2016 Deep Foundations Institute



Fig. 2. Pressing the casing by vibratory hammer



Fig. 3. Filling of the casing with dry concrete mix



Fig. 4. The base reinforced by dry concrete columns



Fig. 5. Excavated dry concrete columns

© 2016 Deep Foundations Institute

SITE A

Ground conditions at the site are complicated (Fig. 6). There is a layer of soft loess sandy clay under the base of designed foundations. The layer reaches the depth of 3.0…8.5 m. A layer of medium- strength sand, clay soils with organic inclusions and peat lie below. Then medium-strength sand is located at the depth of 12.5…16.7 m.

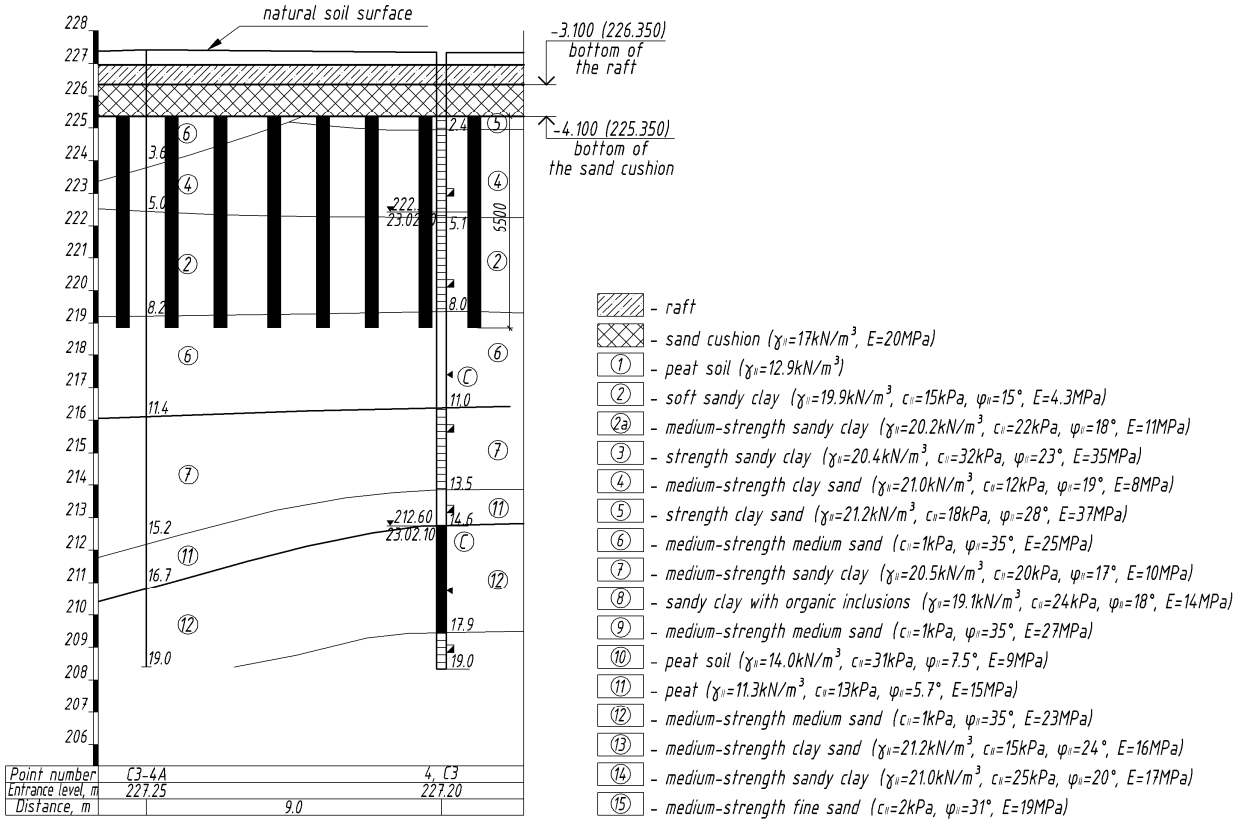


Fig. 6. Fragment of geological cross section. Site A

The application of sectional driven pile foundation was proposed by designers as the first variant due to the big thickness of soft soils. Piles were united by a raft under this project. The length of piles were from 25 to 33 m. As an alternate the cast-in-place reinforced raft over the sand cushion and dry concrete columns were proposed. Cost-performance comparison of variants showed that the cost of the raft on improved base is 32% lower than the cost of sectional driven pile foundation.

The dry concrete columns were made with diameter of 426 mm, step of 1.5 m and length of 4…7 m according to the technology described above. The dry concrete mix with the concrete class of C8/10 was used for the columns. Then the sand cushion with thick of 1.0 m was fulfilled layer by layer by shaking dynamic method.

For the control of soil compaction between columns the static penetration was carried out. Toe resistance q_s, MPa increased in 3.5 times for soils within the length of columns, from 1.7 to 6.1 times depending on type of soil. For soils within the length of wells toe resistance q_s, MPa increased in 1.7 times, from 1.1 to 2.2 times depending on type of soil and its location. One of the static penetration

© 2016 Deep Foundations Institute

points is shown at Fig. 7. Zones of influence under columns noticed on the graphs come to 3…7 diameters of the column. Changes of toe resistance and Young modulus for each layer on the Site A are shown at Table 1.

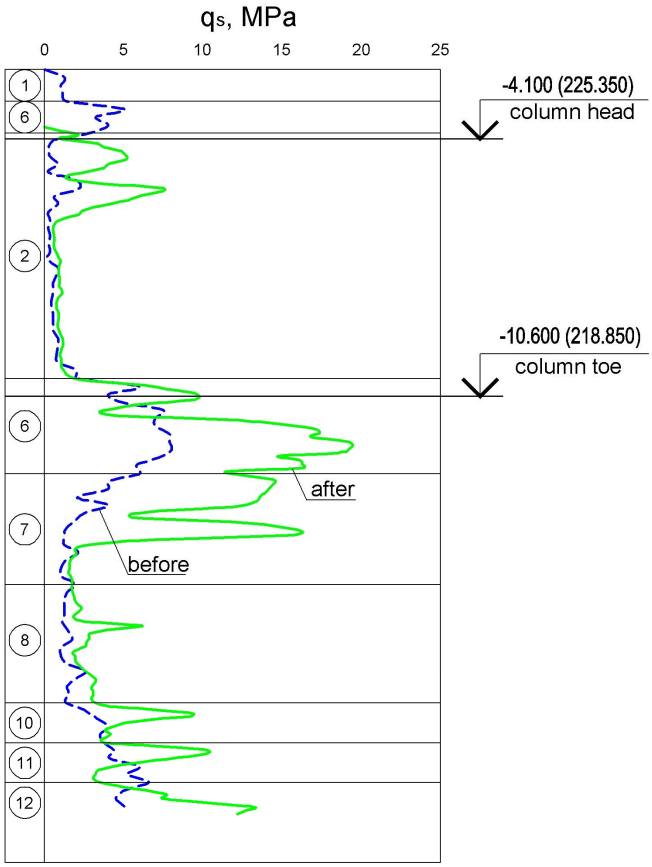


Fig. 7. Toe resistance q_s, MPa

Table 1. Changes of toe resistance and Young modulus for each layer on the Site A

Soil	Toe resistance q_s, MPa		Young modulus E, MPa	
	before	after	before	after
within the length of columns				
2	0.8	4.9	4.9	29.6
2a	3.3	5.5	20.2	33.5
4	1.5	6.5	8.6	37.3
6	4.3	7.4	19.7	33.8
within the length of wells				
6	6.1	12	28.1	55.1
7	2.0	4.3	12.4	26.0
8	1.9	3.4	10.9	19.2
10	3.6	4.8	9.3	12.2
11	4.6	4.9	14.4	15.5
12	4.6	7.0	21.0	32.3

© 2016 Deep Foundations Institute

Young modulus calculated according to the regulatory documents and results of static penetration averaged 36.1 MPa. Young modulus amounted to 10.3 MPa at these points before arrangement of dry concrete columns.

Static load tests were carried out after arrangement of the columns and compaction of sand cushion in order to determine Young modulus. The results showed increase of Young modulus on average up to 40 MPa that is equal to the results of calculation.

SITE B

Ground conditions at the site are complicated (Fig. 8). There is a layer of soft clay and filled-up soils at the surface. Then the soft clay layer with organic inclusions, marl, chalk and peat is located at the depth of 3.0...20.9 m from the base of foundation. Its total thickness reaches 26.8 m.

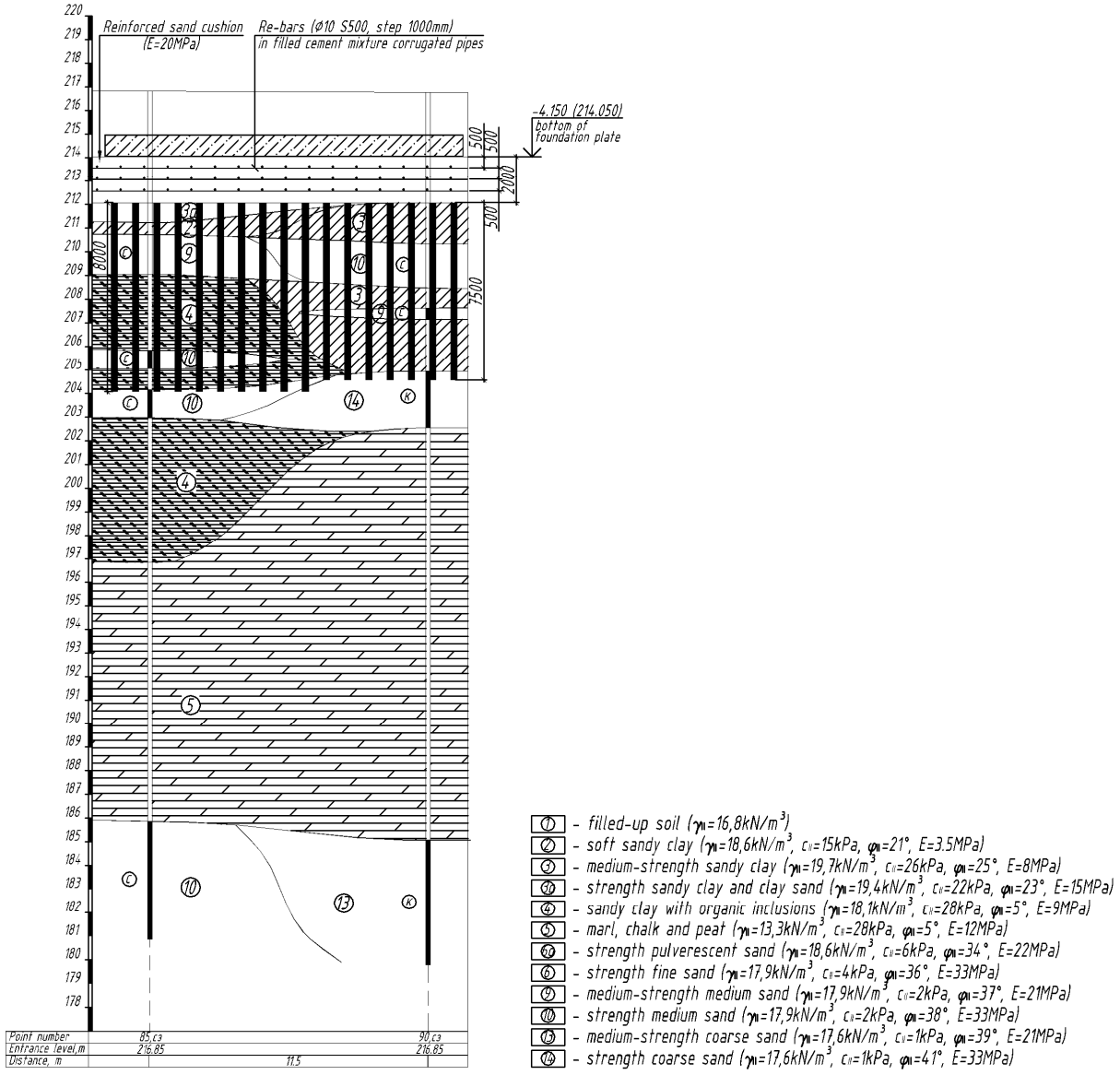


Fig. 8. Fragment of geological cross section. Site B

© 2016 Deep Foundations Institute

The first variant was a bored pile foundation. The application of long bored piles was unsuitable in this case due to the risk of high negative shaft resistance. The length of piles was from 25 to 33 m. The alternate such as a sand cushion is also unsuitable because its thickness was 12 m. The most reasonable decision in such ground conditions was to improve upper layers by dry concrete columns. Cost-performance comparison of variants showed that the cost of foundation slab with improved base is 75% lower than the cost of bored pile foundation.

The dry concrete columns were made with diameter of 325 mm, step of 1.0 m and length of 3…9 m according to the technology described above. The dry concrete mix with the concrete class of C12/15 was used for the columns. The load on the vertical reinforced base was transmitted through sand cushion with thick of 2.5 m reinforced horizontally in three levels.

The results of static penetration between the dry concrete columns showed that toe resistance q_s, MPa and Young modulus E, MPa increased in 2.5 times. Young modulus reached an average 20 MPa.

After the arrangement and compaction of the sand cushion second static penetration could not be carried out and move deeper than 2 m from the column heads. It indicates the strong compaction of surrounding soils.

The reinforced-concrete slabs were made after arrangement of the dry concrete columns and compaction of the sand cushion in order to determine Young modulus. According to the test results Young modulus averaged 55.8 MPa.

SUMMARY

Application of dry concrete columns is an effective ground improvement method that allows compacting and draining saturated soft soils at the same time.

The dry concrete columns affect not only surrounding but underlying soils at 3…7 diameters of the column from its toes.

Toe resistance and Young modulus of soft soils increase according to the results of static penetration and static load tests carried out at two sites.
Site A. Toe resistance increased on average in 3.5 times for soils between columns and in 1.7 times for underlying soils. Young modulus increased in 3.8 times from 10.3 MPa to 40 MPa.
Site B. Toe resistance increased on average in 2.5 times for soils between columns and Young modulus increased in 7 times from 8 MPa to 55.8 MPa.

The cost of the foundation on the base improved by dry concrete columns can be 32…75% lower than the cost of conventional pile foundations.

REFERENCES

Tronda, T., 2013. Actual experience with the geomassif in complicated soil conditions. Proceedings, 5th iYGEC, Paris, August 31-September 1, Vol. 2, pp. 151-154.

Тронда, Т.В., 2014. Натурные исследования упрочнения грунтов армирующими элементами из сухой бетонной смеси. Ресурсоекономні матеріали, конструкції, будівлі та споруди, збірник наукових праць, Rivne, Vol. 29, pp. 561-566.

© 2016 Deep Foundations Institute

This page left intentionally blank

© 2016 Deep Foundations Institute

HIGH CAPACITY DRILLED PILES IN BROOKLYN

Frederick C. Rhyner, P.E., Mueser Rutledge Consulting Engineers, New York, NY
Steven R. Lowe, P.E., Mueser Rutledge Consulting Engineers, New York, NY
Ahmed Elmekati, Ph.D., P.E., Mueser Rutledge Consulting Engineers, New York, NY

Abstract: The current phase of the Pacific Park development (formerly, Atlantic Yards) in Brooklyn involves constructing buildings on a platform over an existing LIRR rail yard. To preserve the maximum amount of space in the already congested yard and protect the yard which remains in service during construction, high capacity foundations are being designed well above previous capacities in the area. In addition to spread footings and small mats, various diameters of drilled piles are being used at design capacities ranging up to 600 tons. The piles are generally grouted at low pressure, up to about 50 psi. Load tests for various drilled elements, including piles, tiedowns and soil anchors, have confirmed allowable side resistance (bond) stresses in dense sand ranging from 20 to 30 psi. Testing with different rigs and operators has shown that down-the-hole hammers are feasible, but the installation techniques, types of equipment and size of the pile make a significant difference. The results show that more cost-effective foundations are possible when ample testing confirms expectations.

I INTRODUCTION

The Long Island Rail Road has operated a mainline on Atlantic Avenue since the 1800s, with a terminal at the intersection of Atlantic and Flatbush Avenues. In the early 1900s, the mainline was reconstructed in a cut and cover tunnel section. The LIRR's Atlantic Yard was constructed circa 1908 to service the terminal. It was depressed about 25 feet below street grade to coincide with the LIRR's mainline tunnel under Atlantic Avenue. Record drawings indicate that the gravity retaining walls lining the perimeter of the yard and other ancillary structures had been designed for an allowable bearing pressure of five tons per square foot (tsf). Perhaps by coincidence, the mat foundation for the tower of the Williamsburg Savings Bank was also designed for five tsf in 1929.

Figure 1 shows a typical geologic section through the site. The geology and subsurface conditions in this part of Brooklyn consist of fill generally five to 20 feet deep underlain by dense to very dense sand and gravel; in places, with numerous cobbles and boulders which make pile installation challenging. The sand strata that are on the order of 150 to 200 feet thick were laid down by glaciers during the last ice age and have been heavily precompressed. The sand strata are underlain in places by remnants of the Cretaceous-era Raritan Clay formation and Fordham Gneiss bedrock. Because of this, the sand strata generally provide excellent support for shallow foundations and the allowable bearing of five tons per square foot is usually easily justified.

The first portion of the Atlantic Yards project included the Barclays Arena, two adjoining residential towers, and improvements to the subway station all to the west of the present construction. The foundations of these structures were designed as spread footings and small mats using the historic allowable-bearing pressure of five tsf and conformed to the 1968 edition of the New York City Building Code. The current phase of the project includes constructing six buildings on a platform over the depressed LIRR Atlantic Yards and another six buildings at locations adjacent to the yard. The yard remains operational for the railroad service during construction. The yard itself is enormous, spanning two blocks for an overall size of approximately 200 feet wide by 1,700 feet long. The proposed buildings will be in the range of 20 to 40 stories tall, so the foundation loads are large. Moreover, the foundation loads are concentrated because deep girders spanning the platform transfer the loads to the limited space between the tracks in which to construct foundations.

© 2016 Deep Foundations Institute

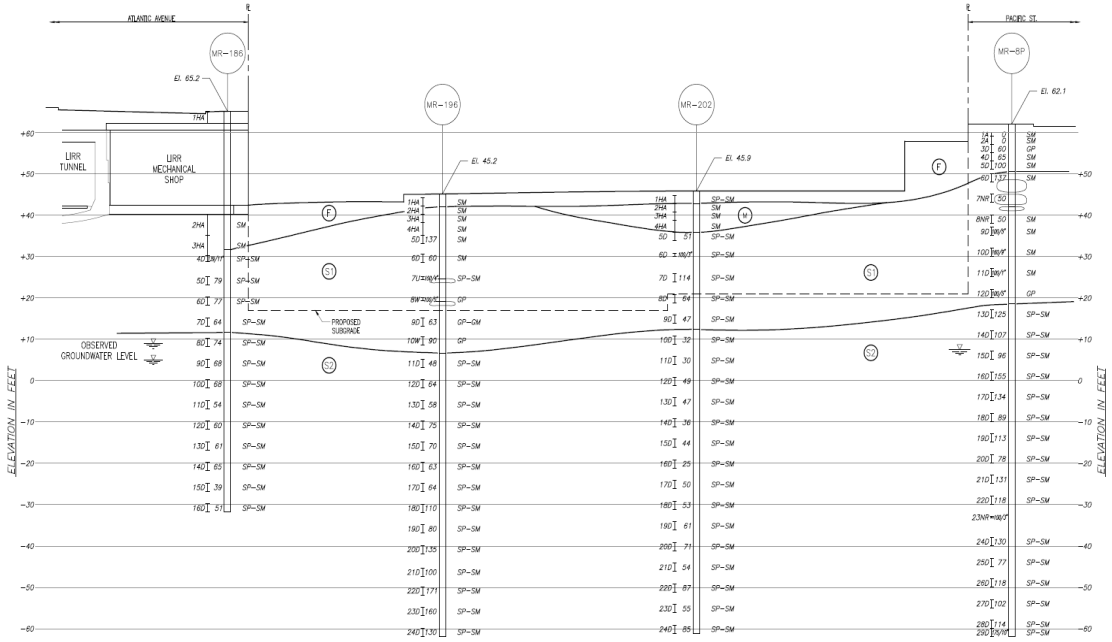


Figure 1: Typical Geologic Section for East Block of Site. For each boring, the section indicates the sample number, SPT N-value and Unified Soil Classification symbol.

© 2016 Deep Foundations Institute

Figures 2a and 2b show the west and east blocks of the Yard, respectively, and locations of pile foundations, isolated spread footings and small mats. The design team considered a large mat foundation early in the design phase, but a mat foundation needed to span the entire rail yard, about 200 feet wide by 825 feet long in each of the two blocks. The design team decided that high capacity drilled piles in combination with isolated spread footings and small mats were a more cost effective solution.

This paper describes the field testing programs and interpretation of results that enabled the use of high capacity drilled-in piles.

II HIGH CAPACITY DRILLED-IN PILES AND OTHER DRILLED-IN ELEMENTS

Two sizes of high capacity drilled-in piles were used for the project, a 13-3/8 inch diameter with an allowable capacity up to 295 tons and a 24 inch diameter with an allowable capacity of 600 tons. The bond zones for these piles ranged from 50 to 65 feet long. Given the site conditions both types of piles were installed with tips about 5 to 10 feet above the water table in the glacial sands. The piles were spaced at a minimum of 2.5 diameters center to center to minimize the footprint in the congested rail yard the pile cap capacity.

The 13-3/8 inch diameter piles were installed with a combination of a tri-cone roller bit and a down-the-hole-hammer (DTH). The roller bit was used to advance the pile until obstructions, or cobbles and boulders were encountered. A DTH hammer was then used to clear the obstruction(s) and the drilling then resumed with the roller bit. A plug was not maintained although the roller bit and hammer were kept within 3 to 6 inches of the bottom of casing. This technique was used because initial installation and test results using a DTH hammer alone indicated relatively low bond values. Piles were installed with polymer drilling fluid to facilitate removal of the casing. Once the piles were advanced to the final tip elevation, 65 to 75 feet below bottom of cap, they were tremie grouted with 8,000 psi grout, reinforced with two #24 thread bars and then pressure grouted to 50 psi in 10 foot increments as the casing was removed. Fifteen feet of casing was left in place to facilitate pressure grouting and to provide lateral capacity.

The 24 inch piles were installed using a starter casing of 28 inch diameter and 15 foot long, spun into the ground and cleaned with an auger. This casing provided the lateral capacity for the pile and to facilitate the grouting operation. The 24 inch diameter casing was telescoped inside the starter casing. A DTH hammer with a 24” diameter shroud around the drill string was advanced full length, 65 feet below bottom of cap. Once at the tip elevation, the pile was tremie grouted with 8,000 psi grout through the hammer, pressure grouted through the hammer using from 20 to 80 psi of pressure at five foot increments and then a cage of four #18 bars was installed. Original plans for secondary pressure grouting were abandoned due to difficulties with the system.

© 2016 Deep Foundations Institute

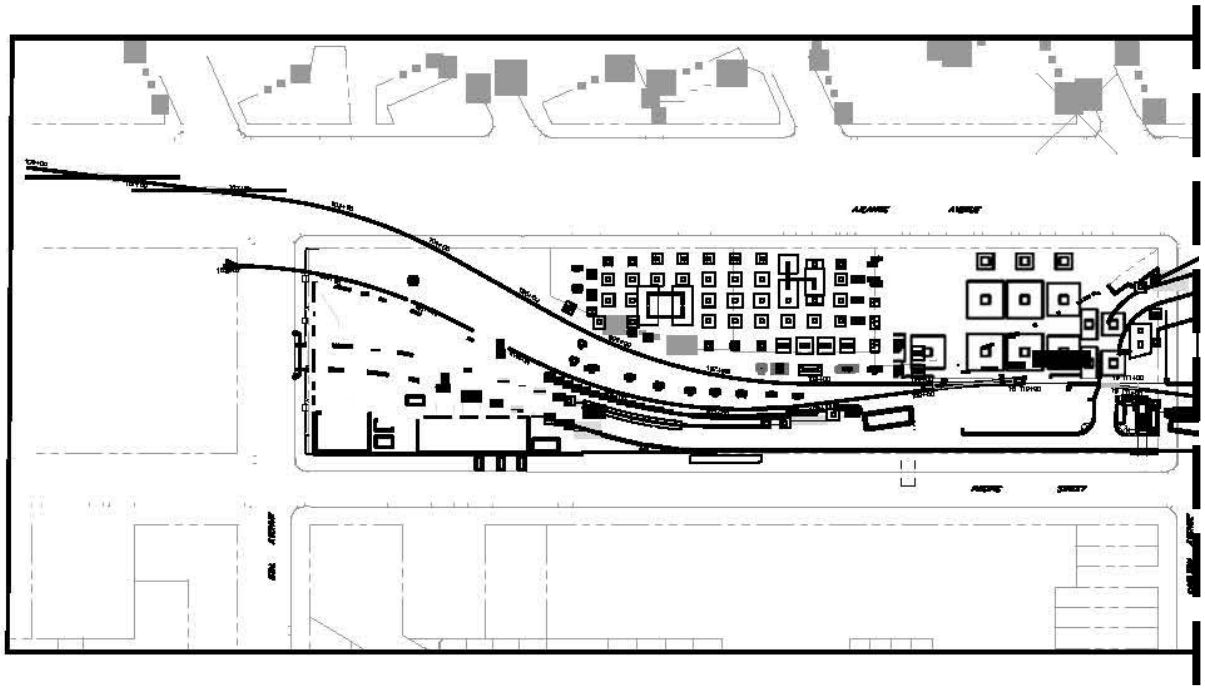


Figure 2 – a) West Block of the Yard



Figure 2 – b) East Block of the Yard

© 2016 Deep Foundations Institute

A. Drilled-in Pile Load Tests

A total of six successful static compression load tests were performed within the Yard footprint and another two piles in an adjacent site for one of the adjoining buildings. The load tests were performed according to ASTM D1143 and the New York City Building Code. Two load tests were performed on the 24" diameter piles. The piles were tested to 1200 tons. Figure 3 shows load versus settlement plot of the test results for the 24 inch diameter piles. Six load tests were performed on the 13-3/8 inch diameter piles (4 in the Yard, two each for two separate buildings, and two in an adjacent site). The piles were tested to 520 to 560 tons. Figure 4 presents the results for two of the 13-3/8 inch diameter piles.

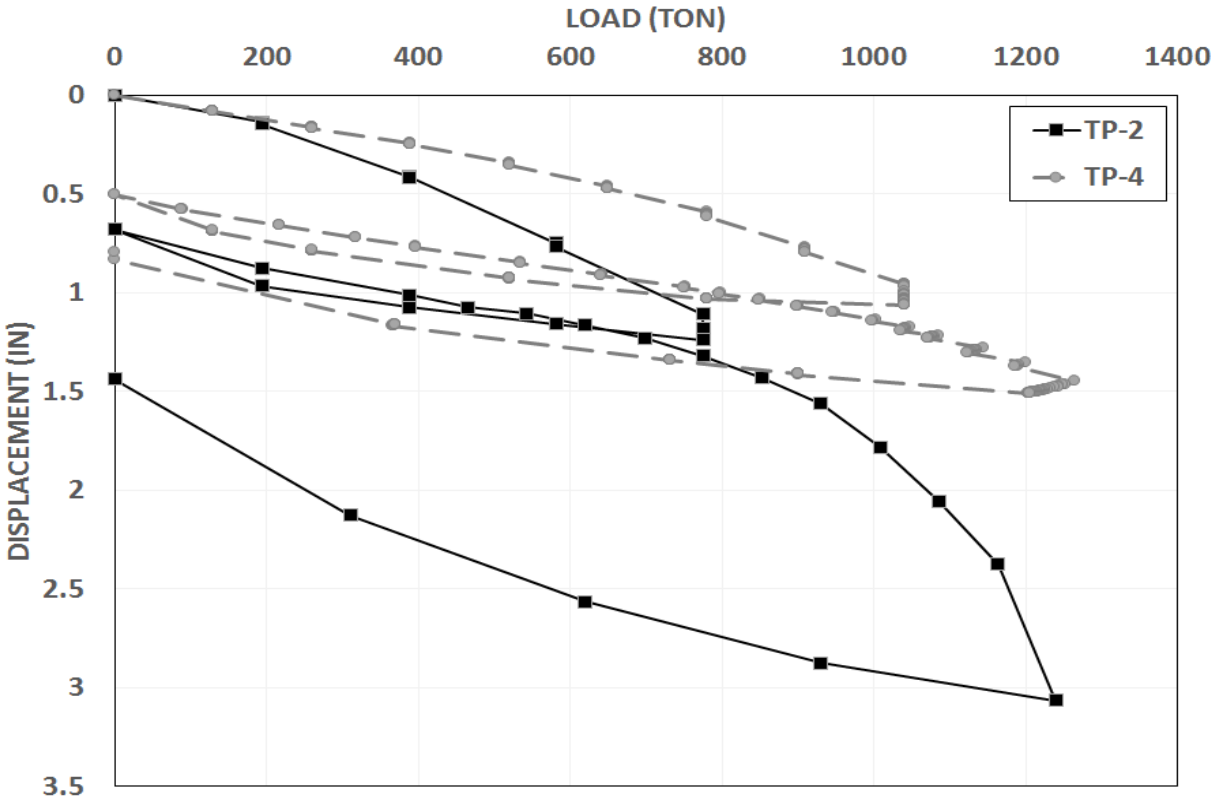


Figure 3 – Load vs. Settlement Plots for 24" Diameter Test Piles based on Axial Compression Test Results.

© 2016 Deep Foundations Institute

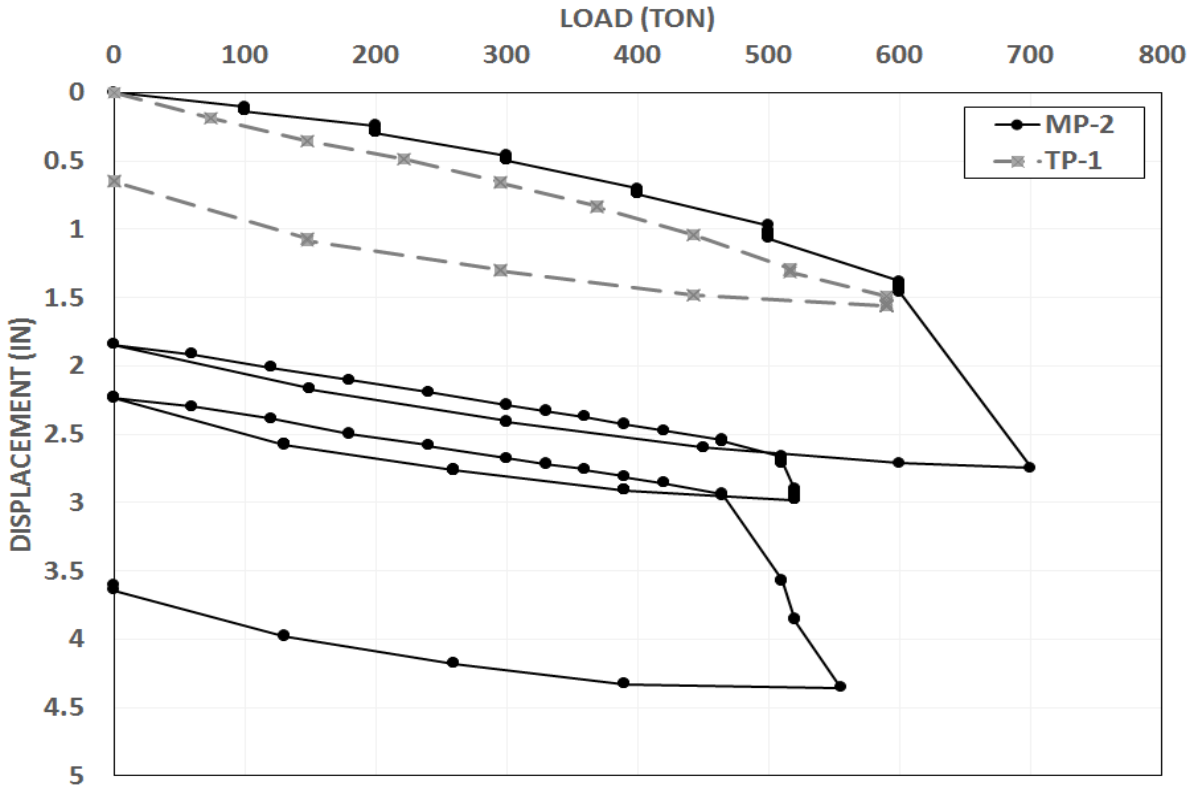


Figure 4 – Load vs. Settlement Plots for 13-3/8" Diameter Test Piles based on Axial Compression Tests Results.

B. Tie-Down Load Tests

Twenty-one permanent tiedowns were installed and tested in the Yard. The tiedowns were installed using a tricone roller bit to advance a 9-5/8 inch diameter casing and were pressure grouted in 10 foot increments at 50 psi. Tests were performed according to PTI recommendations and results indicated a minimum allowable 20 psi bond was achieved.

C. Soil Anchor Load Tests

Approximately 600 temporary soil anchors have been installed for support of excavation systems around and inside the Yard. All the anchors were installed using a lean grout drilling fluid to advance a hollow core bar with a sacrificial bit. The average hole size was about 6 inches in diameter and the bond zones ranged from 15 to 40 feet. The anchors were proof, performance and extended creep tested according to PTI recommendations and routinely indicated an allowable bond of 30 psi.

© 2016 Deep Foundations Institute

D. Summary of Load Test Results

Based on the results of the load tests, Table 1 shows the ranges of allowable bond stresses which were generally achievable. The load tests were not instrumented with strain gauges or telltales, thus end bearing could not be accurately determined. Nevertheless, the end bearing component was not anticipated to be a significant portion of the overall pile capacity. The allowable bond stresses incorporate a factor of safety (FS) of 2.0, based on the maximum test loads.

Table 1: Allowable Bond Stress using FS=2

Element	Allowable Load (tons)	Bond length (feet)	Allowable bond stress (psi)
13- 3/8 inch diameter drilled-in piles	260-280	50	20
24 inch diameter drilled-in piles	600	50	25
10-3/4 inch diameter tiedowns	70-85	25	15*
6 inch diameter soil anchors	70-115	15-35	30

* The conservatively-designed bond length resulted in the lower actual bond value for these elements.

E. Conclusions

Based on the load test results it appears:

- The practical limit for allowable bond for piles installed using a DTH hammer and roller bit in the glacial sands at the west end of the site are in the range of 20 to 25 psi.
- Drilled piles installed in prior phases of construction at the east end of the site, where significantly more cobbles and boulders were encountered, indicated allowable bond values exceeding 30 psi.
- When used as tiebacks, hollow core bars with sacrificial bits consistently provided bond values of 30 psi within the site. Based on test values and creep limits it appears that 30 psi is generally the upper limit of anticipated allowable bond strength for drilled-in elements.
- Installation techniques using a DTH hammer were feasible, but difficulties were encountered. The DTH hammer for the 24 inch diameter piles appeared to cause more ground disturbance than for the 13-3/8 inch diameter size. With either size, caving and poor capacities were occasionally encountered as well. Nevertheless, attempts at installing piles using different techniques and equipment, such as roller-bit drilling techniques, were generally unsuccessful because of the preponderance of cobbles and boulders.

© 2016 Deep Foundations Institute

This page left intentionally blank

© 2016 Deep Foundations Institute

HIGH CAPACITY GROUTED HELICAL PILES

Mohamed A. Mansour, Western University, London, ON, Canada; mmanso8@uwo.ca
Ahmed M. Soliman, Concordia University, Montreal, QC, Canada
M. H. El-Naggar, Western University, London, ON, Canada

ABSTRACT

Grouted helical piles allow significant increase in pile capacity with low additional cost over that of conventional helical piles. They can be particularly advantageous in sites where installation disturbance can reduce or even eliminate the pile shaft resistance. For helical piles with slender shafts, a grout column offers increased buckling resistance under compression loading, and may reduce the potential settlement required to mobilize the bearing component of their plates. This paper investigates the performance of grouted helical piles installed in loose sand. Grouted helical piles were constructed and tested in a controlled laboratory environment. Helical piles with hollow pipe shaft and single helix were grouted during installation. The grout was injected into the soil under high pressure through two nozzles placed above the piles helices. The load test results showed significant improvement in the performance and load carrying capacity of the helical pile due to the formation of a cylindrical grout column along the entire shaft leading to a higher shaft resistance contribution to the total pile capacity. The results suggest that grouted helical piles with slender hollow shaft could be used to support large structural loads.

Keywords: Helical piles, installation disturbance, grout injection, grouted helical piles

INTRODUCTION

Helical piles are widely used as a deep foundation system for different engineering applications. They represent an attractive foundation option because of their cost effectiveness, ease of installation even in limited access areas, low levels of noise and vibrations, and their ability to be installed through ground water without casing. In addition, they allow immediate loading upon installation. Helical piles are installed into the ground by applying a mechanical torque to the pile head. The installation torque monitoring provides a kind of quality control during the construction of helical piles. It could be used in predicting the ultimate pile capacity using several capacity-torque correlations (Livneh and Elnaggar 2008; and Hoyt and Clemence 1989).

However, helical piles installation can cause soil disturbance within the annular zone affected by the pile helices. This disturbance can introduce fissures within the pile cylindrical failure surface (Vesic 1971; Mooney el al. 1985; and Zhang 1999). Thus, the shear strength of the soil decreases along the affected zone. Bagheri and El Naggar (2013) evaluated the installation effects of helical piles in sand. They reported that as the helical blade proceeds into the ground, sand within the cylindrical path circumscribed by the helices experiences torsional and vertical shearing accompanied by sand displacement and stress changes. This process is more pronounced in the case of multi-helices and large diameter anchors. Bagheri and El Naggar (2016) evaluated the installation effects of helical piles in structured clay. They indicated that the behavior of the helical pile and its capacity are significantly affected by the degree of soil de-structuring induced by the penetration of the pile shaft and helices. In addition to the installation disturbance, helical piles have other drawbacks including; high potential settlement required to fully mobilize the bearing component of their plates, low buckling resistance of their slender shafts, and the incomplete rigidity of the coupling joints along the pile shaft that allow some lateral movement under compression loading (Vickars and Clemence 2000).

Pile grouting technology is advancing rapidly due to the continuous development of micropiles industry. The main advantage of pressurized grouting used in micropiles is that it serves as a ground improvement

© 2016 Deep Foundations Institute

technique which improves the grout-ground strength. Employing pressurized grouting to helical piles during their installation can mitigate their installation effects, and improve the contribution of the shaft resistance to the ultimate pile capacity.

Several grouting techniques were developed to inject grout into the surrounding soil through the helical pile hollow shaft after installation (Ratliff 1966; and Perko 2000). Vickars and Clemence (2000) introduced what is called the PULL-DOWN technique for grouted helical piles installation. In this technique soil displacement plates fixed at each coupling joint along the entire shaft, and a PVC or steel pipe sleeves were used to provide a cylindrical grout column around the pile shaft as the pile proceeds into the ground. Nasr (2008) patented a new grouting method that allows grout injection into the surrounding soil during helical piles installation using grout conduits extended through the helical pile hollow shaft.

Although grouted helical piles have been successfully used in many engineering applications with different soil conditions, the literature survey indicated that very little research effort has been focused on investigating the pile performance. In this study, a new grouting technique is proposed for grouted helical piles installation to overcome the drawbacks of conventional (un-grouted) helical piles. The improvement in the pile performance was evaluated by comparing the results of two helical piles constructed and tested in a controlled laboratory environment. One of these piles was installed without grouting, while the other was installed using the new grouting technique.

EXPERIMENTAL PROGRAM

Material properties

Ordinary Portland cement Type 10 (OPC 10) was used as a binder material for the grout mixture. The cement was mixed with water at a water/cement ratio of 0.45 according to ASTM C305. The flowability of the obtained neat cement grout was determined using the flow cone test (ASTM C939) and was found to be 17 seconds.

Geotechnical condition

The Piles investigated in this study were installed in a cylindrical steel tank with diameter 1.35 m, and depth 1.55 m. The steel tank was filled with sand in six layers each had a thickness of 25 cm. Each layer was compacted to maintain a consistent relative density of 28% in both tests. The Geotechnical properties of the used sand including; natural water content (ASTM D2216), specific gravity of soil solids (ASTM D854), maximum voids ratio (ASTM D4254), minimum voids ratio (ASTM D4253), and the angle of internal friction using direct shear test (ASTM D3080) were evaluated and are summarized in Table 1.

Table 1: Test sand properties

w_c %	γ_{bulk} (kN/m^3)	G_s	e_{max}	e_{min}	ϕ°
5.4	16.8	2.69	0.78	0.35	38

Piles installation

Two helical piles with hollow shaft were installed in loose sand to a depth of 80 cm. The piles had an outer shaft diameter 3.3 cm, an inner shaft diameter 2.8 cm, and a single helix with diameter 15 cm and pitch 3.5 cm. One of the tested piles was a conventional helical pile, while the other had two nozzles above the pile helix for grout injection as shown in Fig. 1. The grout nozzles had an inner diameter of 0.9 cm, wall thickness of 0.3 cm, length of 4.5 cm, and inclined with an angle of 45^o. The difference in elevation between the two nozzles was half the helix pitch to insure that every location in the soil will be injected twice.

© 2016 Deep Foundations Institute



a- Conventional helical pile



b- Helical pile with nozzles

Fig. 1: Tested helical piles a) conventional helical pile, and b) helical pile with nozzles

A guiding system was constructed as illustrated in Fig. 2, and a torpedo level was frequently used to insure the vertical alignment of the two piles during installation. For the grouted helical pile, 15 litres of neat cement grout was injected into the surrounding soil through the nozzles during installation under an average pressure of 60 psi (0.41 MPa). For full scale field applications, neat cement grout could be replaced with ready mix grout (containing some sand); however, the particles size of the used sand must be within the acceptable range in order not to plug the grout nozzles, and to allow the permeation of the injected grout into the surrounding soil (Warner 2004).

Test setup

To evaluate the load transfer mechanism, each pile was instrumented with six electrical resistance strain gauges (Vishay CEA-06-250UW-120) bonded to the pile shaft at three different levels. The pile head displacement was monitored by four independently supported linear variable displacement transducers (LVDT), with 0.1 mm accuracy and 100 mm stroke, placed at the corners of the loading plate. The applied load was measured using a calibrated load cell. The strain gauges, the LVDTs, and the load cell were connected to a data acquisition system to record the readings every 1 second.



Fig. 2: Guiding system for vertical alignment during piles installation

© 2016 Deep Foundations Institute

After installation, the grout was left to cure for one week, then the two piles were tested under static axial compression loading according to the quick maintained test procedure (ASTM D1143). The compression loads were applied to the tested piles through a hydraulic jack fixed to the pile head and acted against the cross beam of a steel frame. The piles were loaded in increments of 5% of their anticipated ultimate capacity. Each load increment was maintained for 5 minutes. Load increments were added until failure was reached without exceeding the safe structure capacity of the piles and the loading system. The final load was maintained for 15 minutes to monitor the creep behavior. The piles were then unloaded in 5 equal decrements. Each load decrement was maintained for 5 minutes. After applying the last decrement, the pile was left for 15 minutes to fully capture the rebound response. Figure 3 shows the compression test setup.



Fig. 3: Compression test setup

Results and discussion

The proposed technique for grouted helical pile installation is very similar to that used in the installation of micropiles. The two nozzles mounted to the pile shaft play the role of the drilling bit that creates a gab around the pile shaft with diameter 9.7 cm. This gab is filled with pressurized grout during installation. Therefore, an enlargement factor should be applied to the pile shaft to account for the increase in the grouted shaft diameter. Maclean (2010) recommended an enlargement factor of 1.3 for micropiles installed in sand, which is in a good agreement with the amount of grout used during installation. The resulting grouted shaft had an average diameter of 13 cm, and a length of 75 cm.

The applied load at the pile head and the corresponding average displacement obtained from the 4 LVDTs mounted to the loading plate were recorded for each load increment. Figure 4 presents the load-displacement curves for the grouted and un-grouted helical piles. As shown in Fig. 4, the grouted helical pile has a much better geotechnical performance, and a much higher load carrying capacity compared to the un-grouted one. Several criteria were used to calculate the ultimate capacity of the two piles using their load-displacement curves.

© 2016 Deep Foundations Institute

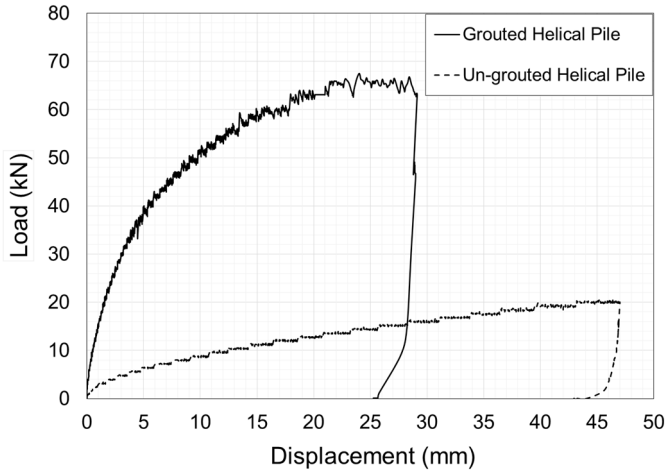


Fig. 4: Load-displacement curves for the grouted and un-grouted helical piles

One of the most widely used criteria to determine the pile capacity is the offset criterion (Davisson, 1972). According to Davisson's criterion, the ultimate pile capacity corresponds to a pile head displacement equal to the elastic deformation of the pile shaft (PL/EA) plus an offset as shown in Equation [1].

$$S = \frac{PL}{EA} + \frac{D}{120} + 4 \text{ (mm)} \quad [1]$$

Where S = pile head displacement, P = applied load at pile head, E = modulus of elasticity for the pile shaft, A = cross-section area of the pile shaft, and D = diameter of pile toe (D_{helix} in case of helical piles).

Butler and Hoy (1977) suggested another failure criterion which divided the load-displacement curve into three components. A linear segment followed by a non-linear segment, then a secondary linear segment with lower slope. Based on this criterion, the ultimate pile capacity is the intersection between the tangents to the first and secondary linear segments. Livenih and El-Naggar (2008) developed a failure criterion suitable for helical piles, where the pile ultimate capacity corresponds to a displacement equal to 8% of the helix diameter plus the elastic deformation of the pile shaft (PL/EA). Sakr (2009) introduced a failure criterion, where the ultimate pile capacity is defined as the load that causes a displacement equal to 10% of the helix diameter, which is in a good agreement with the findings of Terzaghi (1942). The ultimate capacities of the two piles determined using these interpreted failure criteria are summarized in Table 2.

Table 2: Ultimate capacities of the tested piles

Failure Criteria	grouted helical pile	Un-grouted helical pile
Davisson, 1972	40.0 kN	6.0 kN
Butler and Hoy, 1977	55.0 kN	7.5 kN
Livenih and El-Naggar, 2008	55.0 kN	10.0 kN
Sakr, 2009	58.0 kN	11.0 kN

Based on the results shown in Table 2, Davisson criterion was found to underestimate the pile capacity. Butler and Hoy (1977) was not accurate in estimating the capacity of the un-grouted pile due to the difficulty of drawing a tangent to its small initial linear segment. Livneh and El-Naggar (2008), and Sakr (2009) were found to be the most suitable criteria to determine the ultimate capacity for the tested piles. The ultimate capacity of the grouted helical pile was 55 kN, compared to 10 kN for the un-grouted one, with an increase of 550% in the total pile capacity.

© 2016 Deep Foundations Institute

The load transfer mechanism for the two piles was indicated using the electrical resistance strain gauges fixed to their shafts. For the un-grouted pile, the entire load was carried through its bearing plate, and its shaft resistance contribution was negligible (less than 2.5% of the total load). While for the grouted one, a shaft resistance of 42 kN and a bearing resistance of 13 kN were observed at failure as shown in Fig. 5. This jump in the pile shaft resistance could be attributed to the soil improvement due to grout injection, and the formation of a cylindrical grout column along the entire shaft, resulting in increasing the pile shaft diameter, and the angle of friction between the pile shaft material and the surrounding soil. On the other hand, the rise in the plate bearing component is due to the increase in the plate stiffness, and the enhancement in the mechanical properties of the soil below it under the effect of grouting.

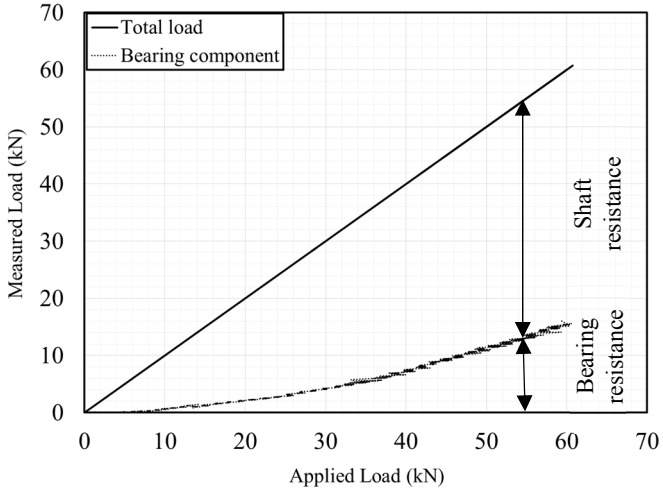


Fig. 5: Load transfer mechanism for the grouted helical pile

According to Vickars and Clemence (2000), the grouted column could be treated as a friction pile and its capacity could be calculated based on Equation [2].

$$P_{shaft} = \sum Fs*(\pi*D*L) \quad [2]$$

Where P_{shaft} = ultimate shaft resistance, F_s = is the unit skin friction along pile shaft, D = diameter of the grout shaft, and L = length of the grout shaft.

By substituting in Equation [2], the unit skin friction along the grouted shaft (F_s) was found to be 137 kPa. This value lies within the range of the grout-ground bond (α bond) for micropiles type B installed in loose sand according to the FHWA (2005). Thus, the resulting grouted helical pile using the proposed grouting technique will have a much better performance compared to the un-grouted one, as it depends mainly on its shaft component to resist the applied loads. It should be mentioned that the same grouting technique could be applied during the installation of helical pile with multi-helices. Consequently, the resulting grouted helical pile will be characterized by its high bearing and high shaft resistances. And hence, it will have the privilege over the existing deep foundation systems (micropiles, Augered cast in place piles, bored piles, conventional helical piles, and …., etc.) to support heavy structures.

CONCLUSIONS

A new grouting technique is proposed for grouted helical piles installation. The proposed technique is similar to what is used in the construction of micropiles. It includes grout injection into the surrounding soil under high pressure during helical piles installation. The pressurized grout is injected into the soil through

© 2016 Deep Foundations Institute

two nozzles located on the piles shafts above their helices. The new grouting technique produced a grouted helical pile having the same advantages of the conventional helical pile, plus a 550% increase in the total pile capacity with low additional cost. This jump in the pile capacity is attributed to the significant increase in the pile shaft resistance contribution to the total pile capacity, due to the formation of a cylindrical grout column around the pile shaft, which has a larger diameter, and a higher grout-ground bond. The results suggest that grouted helical piles with slender hollow shaft could be viable deep foundation option for high capacity applications.

REFERENCES

ASTM C305-14, 2014. Standard Practice for Mechanical Mixing of Hydraulic Cement Pastes and Mortars of Plastic Consistency. American Society for Testing and Materials, 3 p.

ASTM C939-10, 2010. Standard Test Method for Flow of Grout for Preplaced-Aggregate Concrete (Flow Cone Method). American Society for Testing and Materials, 3 p.

ASTM D1143-07, 2013. Standard Test Method for Deep Foundations under Static Axial Compressive Load. American Society for Testing and Materials, 15 p.

ASTM D2487-11, 2011. Standard Practice for Classification of Soils for Engineering Purposes (Unified Soil Classification System). American Society for Testing and Materials, 12 p.

ASTM D3080/D3080M-11, 2011. Direct Shear Test of Soils under Consolidated Drained Conditions. American Society for Testing and Materials, 9 p.

ASTM D4253-16, 2016. Standard test methods for maximum index density and unit weight of soils using a vibratory table. American society for testing and materials, 14 p

ASTM D4254-16, 2016. Standard test methods for minimum index density and unit weight of soils and calculations of relative density. American society for testing and materials, 9 p.

ASTM D7263-09, 2009. Standard Test Methods for Laboratory Determination of Density (Unit Weight) of Soil Specimens. American Society for Testing and Materials, 7 p.

ASTM D854-14, 2014. Standard Test Methods for Specific Gravity of Soil Solids by Water Pycnometer. American Society for Testing and Materials, 8 p.

Bagheri, F. and El Naggar, M. H., 2013. Effects of the Installation Disturbance on the Behavior of the Multi-Helix Anchors in Sands. 66th Canadian Geotechnical Conference, Montreal City, Quebec, Canada, 13 p.

Bagheri, F. and El Naggar, M. H., 2016. Effects of installation disturbance on behavior of multi-helix piles in structured clays, Journal of the Deep Foundations, 9(2), pp. 80-91

Butler, H.D. and Hoy, H.E., 1977. User's manual for the Texas quick load method for foundation load testing. FHWA-IP-77-8, Federal Highway Administration, Office of Development, Washington, 59 p.

Davisson, M. T., 1972. High capacity piles. Proceedings lecture series on innovations in foundation construction, Soil mechanics division Illinois section, ASCE, Chicago, pp. 81-112.

© 2016 Deep Foundations Institute

Elkasabgy, M. and El Naggar, M.H. 2015. Axial compressive response of large-capacity helical and driven steel piles in cohesive soil. *Canadian Geotechnical Journal*, 52(2), pp. 224-243.

Hoyt, R. and Clemence, S., 1989. Uplift capacity of helical anchors in soil, 12th International Conference on Soil Mechanics and Foundation Engineering, Rio de Janeiro. pp. 1019-1022.

Livneh, B. and El Naggar, M.H., 2008. Axial Testing and Numerical Modeling of Square Shaft Helical Piles under Compressive and Tensile Loading. Canadian Geotechnical Journal, 45, pp. 1142-1155.

MacLean, D. 2010. Typical case history of a Titan micropile. In Micropiles Seminar, Industry Trends and Developments DFI/ADSC, Mississauga, Ont., Canada, April 2010

Mooney, J. M., Adamczak, S. J., and Clemence, S. P., 1985. Uplift capacity of helical anchors in clay and silt. Uplift Behavior of Anchor Foundations in Soil, ASCE Convention Conference Proceedings, New York, USA, pp. 48-72.

Nasr, M.H., 2008. Method for Installing a Screw Pile, Application Publication, USA, Pub. No. US20080031695 A1.

Perko, H.A., 2000. Earth Anchors and Methods for their Use, Grant, USA, Pub. No. US6058662 A.

Ratliff, G.R., 1966. Method and Apparatus for Treating Soil, Grant, USA, Pub. No. US3243962 A.

Sakr, M., 2009. Performance of Helical Piles in Oil Sand. Canadian Geotechnical Journal, 46, pp. 1046-1061.

Terzaghi, K., 1942. Discussion on Progress Report of the Committee on Bearing Values of Pile Foundations, Pile Driving Formulas. In Proceedings of ASCE, Harvard Soil Mechanics Series 17, 68, pp. 311–323.

Vickars, R.A. and Clemence S.P. 2000. Performance of Helical Piles with Grouted Shafts. In New Technological and Design Developments in Deep Foundations, Proceedings of Sessions of GeoDenver 2000. GSP 100. American Society of Civil Engineers, Reston, Virginia, USA, 15 p.

Vesic, A.S., 1971. Breakout resistance for objects embedded in ocean bottom. Journal of Soil Mechanics and Foundation Division, ASCE, 97(SM9), 1183-1205

Warner, J. 2004. Practical Handbook of Grouting Soil, Rock and Structures, 1st ed., John Wiley & Sons, New Jersey, USA.

Zhang, D.J.Y., 1999. Predicting capacity of helical screw piles in Alberta soils. M.E.Sc. thesis, University of Alberta, Edmonton, Alberta, Canada. 334 p.

© 2016 Deep Foundations Institute

INNOVATIVE DEEP FOUNDATION SUPPORT USING DUCTILE IRON PILES

Doug LeDo, PE, GZA GeoEnvironmental, Inc. Providence, RI, USA doug.ledo@gza.com
Thomas Billups, PE, GZA GeoEnvironmental, Inc. Providence, RI, USA thomas.billups@gza.com
David Carchedi, PhD, PE, GZA GeoEnvironmental, Inc. Providence, RI, USA david.carchedi@gza.com
Brendan FitzPatrick, PE, DuroTerra, LLC, Braintree, MA, USA bfitzpatrick@duroterra.com

ABSTRACT

Working in urban environments presents unique logistical challenges beyond those typically associated with traditional geotechnical analysis and design. These challenges often include working on sites with limited access and laydown area, vibration concerns for adjacent structures and the need to work from variable elevations or within excavations. This paper describes the use of the modular Ductile Iron Pile system, a low-vibration driven micropile, on two urban projects on the Johnson & Wales University campus in Providence, Rhode Island. The paper describes the successful implementation of Ductile Iron Piles installed to develop capacity in end-bearing on one site and friction on the second site. Design, installation and quality control operations are all presented as well as the results of full-scale load testing performed on non-production test piles. This paper is of importance to the industry because it describes a versatile option for project teams as an alternative to traditional micropiles, helical piles or other deep foundation systems for urban sites.

INTRODUCTION

Working in urban environments presents unique logistical challenges beyond those typically associated with traditional geotechnical analysis and design. These challenges often include working on sites with limited access and laydown area, vibration concerns for adjacent structures and the need to work from variable elevations or within excavations. Two recent projects in downtown Providence, Rhode Island faced a combination of problematic soil conditions and urban construction challenges including vibration concerns. Both projects were a part of the Johnson and Wales University campus development. Figure 1 illustrates the urban locations of the sites.



Fig. 1. Project Site Locations

© 2016 Deep Foundations Institute

DUCTILE IRON PILE SYSTEM

For over three decades, European engineers and contractors have used specially-manufactured Ductile Iron Piles (DIPs) to provide a reliable and cost-effective alternative to more traditional deep foundation systems that address urban challenges. Ductile Iron Piles are a low vibration, driven pile system. The modular, small-diameter piles are manufactured in standard 5 m (16.4 ft) lengths to allow ease of installation on constrained sites (Fig. 2). A centrifugal-casting process is used to transform the lamellar graphite cast iron into spheroidal graphite or ductile cast iron to improve the strength and produce superior impact resistance for durability during driving. The DIP material exhibits a design yield stress of 46 ksi and modulus of elasticity of 24,600 ksi (TRM 2015). Each pile is cast with a bell and spigot to form a Plug-and-Drive connection mechanism. The connection develops strength through a combination of the tapered compression fit as well as a friction (cold) weld that occurs during the high-frequency driving process, thereby eliminating the need for field splicing. The piling material is delivered in compact bundles containing between 8 and 15 pile sections depending on pile diameters. The bundles can be easily transported to congested urban sites and offloaded into limited laydown areas as shown in Figure 3.



Fig. 2. Ductile Iron Pile Installation



Fig. 3. Ductile Iron Pile Material Stacked On-site

Installation

The system is installed using a medium-sized excavator and a hydraulic breaker hammer. The breaker hammer uses a modified shank that seats into the pile bell for driving, using the hammer's percussive energy. The hammer size (energy) is matched with the size of the Ductile Iron Pile and the driving conditions to develop the most efficient installation while not overstressing the pile material. Hammer sizes typically range from 3,000 ft-lb to 8,000 ft-lb class hammers for the range of pile sizes. The hydraulic hammers operate

© 2016 Deep Foundations Institute

at frequencies ranging from 250 to 500 cycles per minute, thereby delivering a much higher frequency content than traditional high-impact, low frequency driven piling systems. Vibration measurements recorded on various project sites with different pile diameters, all at distances of less than 1.5 meters (4.9 feet) from installation, are shown in Figure 4. The data has been plotted along with commonly used US Bureau of Mines criteria for limiting vibration levels to avoid damage to residential structures (Siskind et al. 1980). Results of the monitoring in close proximity to the pile installation illustrate that the majority of vibrations are less than 25 mm/second (1 in/s) and nearly all of the readings are below US Bureau of Mines criteria. Vibration levels rapidly decrease with distance from the pile location.

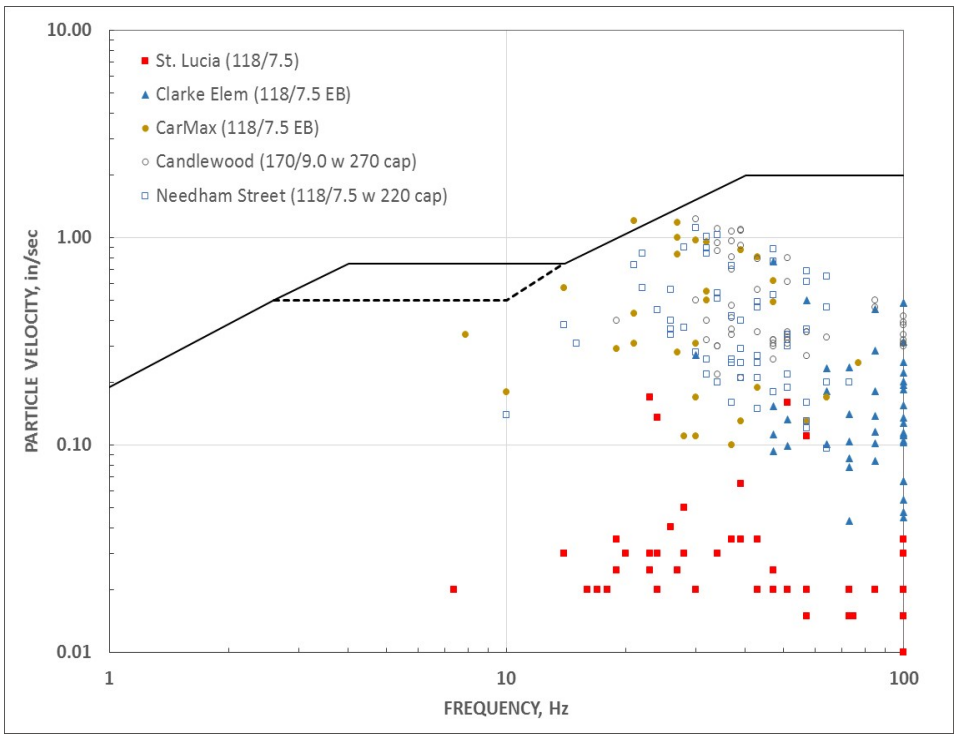


Fig. 4. Measured Vibrations in Close Proximity to Pile Installation

Ductile Iron Piles have the flexibility to be installed to develop capacity in either end bearing or in friction. End-bearing DIPs generate the load-carrying capacity through bearing on very dense soil or rock after reaching the project "set" termination criteria. Installation begins with the placement of a flat driving shoe or rock point on the ground at the pile locations. A 5-m long pile section is then positioned onto the shoe and driven into the ground using the vertical percussion energy. Using the same excavator, a second 5-m long pile section is swung into place to make the Plug and Drive (bell and spigot) connection and then driven. This process is repeated until the design length or pile termination criteria is reached. After driving, the pile is cut to elevation and filled with neat cement grout. A center reinforcing bar can be placed into the wet grout, if required by the design.

Alternatively, similar to a micropile, friction DIPs generate compression or tension capacity by creating a grouted bond zone within a competent soil layer. Piles designed for frictional resistance are installed by first installing an oversized conical grout cap over the end of the hollow pile. Conical grout caps range in diameter from 150 mm (5.9 in) up to 370 mm (14.6 in) depending on pile size and design requirements. The pile is then driven into the ground using high-frequency energy while continuously pumping sand cement grout through the interior of the pile. The grout exits through the grout ports in the conical cap, filling the annular space on the pile exterior during driving. The pile shaft becomes encapsulated in grout,

© 2016 Deep Foundations Institute

developing a bond zone. Additional pile sections are driven until the pile extends to the design length within the bond zone. A center reinforcing bar is then inserted if required for compression or tension capacity.

Quality Control

Field monitoring plays an important role during the installation process. Quality control/quality assurance monitoring is largely focused on pile alignment/verticality and recording penetration rates (length of time to drive 1 meter increments as marked on the pile section) during driving. The rates of penetration can be used as indicators of geotechnical resistance and pile capacity. For end-bearing piles, the pile is advanced until a particular rate of advancement or "set" is achieved. For example, a "set" criteria of less than 1 inch of movement in more than 50 seconds is a commonly used criterion that is confirmed by full-scale load tests. This criterion has developed through decades of experience and testing of the system in Europe and requires compatibility between hammer size (energy) and pile/cap dimensions for driving. For friction piles, the penetration rates are used to determine the depth which corresponds to the start of the bond length. The pile is then advanced a particular distance into the competent layer based on the penetration rates. In the event of very dense driving conditions that preclude the installation of the full bond length, the penetration rates can be used to verify the achievement of the set criteria for compression applications. The compression pile is deemed acceptable by meeting either 1) the required bond length or 2) achieving the set criteria.

Another important part of the quality control process is the performance of a full-scale pile load test on a non-production test pile. Load tests are often performed in compression (ASTM D-1143) or tension (ASTM D-3689) depending on the project requirements. Load testing is typically performed to 200 percent of the design load. Since friction piles rely on a bond zone of grout to soil for resistance to either tension or compression loads, it is typically more economical to test all piles in tension to confirm the grout to soil bond strength. A center bar would then need to be installed in the test pile(s).

Design - Overview

Both the composite strength of materials (structural capacity) and the geotechnical capacity are considered in the design of Ductile Iron Pile design. . With pile diameters ranging from 98 mm (3.85 in) to 170 mm (6.69 in) and wall thicknesses ranging from 6 mm (0.24 in) to 13 mm (0.51 in), designs can be tailored to achieve maximum efficiency for soil conditions and project loads. The system can also be designed to resist tension loads by inserting a high-strength center bar into grouted piles. Working capacities typically range from 25 tons to greater than 100 tons per pile in compression and 10 to 60 tons per pile in tension.

Design - Structural Compression Capacity

Ductile Iron Piles derive their structural capacity through contributions of the ductile iron strength, interior grout strength and the addition of a center reinforcing bar (if used). The allowable pile capacity (P_{dip}) is calculated as shown in Equation 1 for the separate contributions of strength:

$$P_{dip} = P_{ironpipe} + P_{grout} + P_{bar} \quad [1]$$

where $P_{ironpipe,}$ P_{grout} and P_{bar} are the allowable load resisted by the ductile iron pipe, the interior grout and the center reinforcing bar (if used), respectively. When grout and another material are to be used simultaneously to support a load in compression, the maximum strain is limited by the grout. In accordance with ACI guidelines, the maximum usable strain at the extreme concrete compression fiber is equal to 0.3 percent (2008). This is the maximum strain that the grout can experience before failure. However, the 46 ksi yield stress of the ductile iron pile is less than the typical values corresponding to the concrete stress

© 2016 Deep Foundations Institute

levels at 0.3 percent strain. As a result, the yield stress of the ductile iron is the controlling stress level in the composite capacity calculations.

The allowable load for the ductile iron material is equal to the final pile cross-sectional area ($A_{dip\text{-}final}$) multiplied by the yield stress ($F_{y\text{-}di}$) as shown in Equation 2.

$$P_{ironpipe} = uF_{y-di}A_{dip-final} \quad [2]$$

The final cross-sectional area of the DIP material may be reduced due to corrosion if applicable. The cross-sectional area for friction piles is equal to the manufactured area with no loss for corrosion since the interior and exterior of the pile is fully grouted. The yield stress reduction factor (u) is based on codified values for deep foundations (IBC 2009). Typical factors used for DIP design range from 0.4 to 0.5.

The contribution of the interior grout to the load carrying capacity is calculated as the allowable concrete compressive strength ($f'_{c\text{-}all}$) multiplied by the grout area (interior area within the pile) (A_{grout}) as shown in Equation 3 where the allowable compressive strength is limited to 0.33 of the ultimate compressive strength. Further limitations of the allowable compressive strength may be appropriate based on local building codes.

$$P_{grout} = f'_{c-all}A_{grout} \quad [3]$$

The allowable load for a center reinforcing bar (if used) is equal to the bar cross-sectional area (A_{bar}) multiplied by the yield stress as shown in Equation 4 where a yield stress reduction factor (u) of 0.4 is often used. The yield stress selected for design is often the lower of the center reinforcing bar or the ductile iron pile, based on similar design approaches for cased micropiles (FHWA 2005).

$$P_{bar} = uF_{y-bar}A_{bar} \quad [4]$$

The sum of the individual strength components are combined to develop the total allowable load resistance of the ductile iron pile from a structural perspective. The total allowable load resistance must be greater than the applied loading demand. Structural capacity calculations including buckling checks are also used in soft soil conditions to limit design capacities (FHWA 2005).

Design - Structural Tension Capacity

The allowable structural tension capacity of the Ductile Iron Pile is specifically related to the design of the high-strength center bar installed into the grouted pile. The tensile capacity is estimated as the product of the yield stress of the reinforcing bar ($F_{y\text{-}bar}$), a stress reduction multiplier (u) of 0.60 (IBC 2009) and the cross-sectional area of the center bar (A_{bar}) as shown in Equation 5.

$$P_{all-tension} = uF_{y-all}A_{bar} \quad [5]$$

Design - Geotechnical Capacity

The geotechnical capacity for Ductile Iron Piles is generated through either end-bearing on competent materials or friction along a grouted bond zone. For end-bearing piles, consideration of the type of bearing material and specific "set" criteria will influence the geotechnical capacity for design. Design approaches are empirical and based on significant load test experience. Results have shown DIPs driven with a hammer of suitable energy for the specific pile size and bearing on very dense soils (i.e. glacial till) or competent rock will typically achieve the required geotechnical capacity to match the allowable structural capacity with a set criteria of less than 25 mm (1 in) of movement in 50 seconds.

© 2016 Deep Foundations Institute

The geotechnical capacity for friction piles is a function of the grouted DIP diameter (related to the selected grout end cap used during installation), the estimated bond length (L_b) and the allowable soil skin friction along the DIP (α_{bond}) as shown in Equation 6. The bond length is estimated based on the anticipated penetration of the DIP into a layer capable of providing side resistance. The allowable skin friction values for design are determined based on the bond zone soil conditions. These bond zone friction values are consistent with accepted industry standards used for Micropiles – Type B (pressure grouted) as a result of the displacement installation and pressurized grouting operation (FHWA 2005). A check of the bond between the Ductile Iron Pile and the grout may also be performed, but is not typically a controlling factor.

$$P_{friction} = \pi d_{endcap} L_b \alpha_{bond} \quad [6]$$

GEOLOGY AND SUBSURFACE CONDITIONS

According to the 1956 Surficial Geology Map of the Providence Quadrangle, Rhode Island, the surficial soils in the vicinity of the site are comprised of artificial fill underlain by glacial outwash plains consisting of sorted sand, stratified silts and local deposits of gravel. The underlying bedrock is the Rhode Island Formation and is described as greywacke, conglomerate, sandstone, shale and meta-anthracite based on the 1959 Bedrock Geology Map of the Providence Quadrangle, Rhode Island. (GZA 2014)

The results of explorations performed at the actual project sites indicated the subsurface conditions were relatively similar at both sites. A layer of loose sand and silt "urban" fill containing construction debris (brick, concrete, asphalt, wood) was encountered up to 3.4 m (11 ft). The fill was underlain by up to 1.8 m (6 ft) of soft peat at some locations. More competent soils including medium dense to dense outwash sand and silt were then encountered and extended to 17.7 m (58 ft) followed by glacial till. Groundwater generally ranged between 4.6 m and 7 m (15 and 23 ft) below grade.

PROJECT 1 - JOHNSON & WALES UNIVERSITY - PHYSICIAN ASSISTANT STUDIES

Johnson & Wales University's new Center for Physician Assistant Health Sciences School (Fig. 5) was the first-of-its-kind facility in Rhode Island. The 1,672 m^2 (18,000 ft^2) facility houses lecture halls, active learning classrooms, labs and study spaces. The structure was constructed through renovations, modernization and addition to an existing 2-story building. Design loads were up to 150 kips for columns and 35 kips/foot on exterior walls.



Fig. 5. Photo of Center for Physician Assistant Studies

Geotechnical Design Approach

Geotechnical challenges for the project included the problematic urban fill and organic soil, but also included the practicality of construction of the new building addition while tying into the existing structure supported on shallow spread footings. Initial foundation support options under consideration were ground improvement, micropiles, compaction grout columns and helical piles which were also required for

© 2016 Deep Foundations Institute

underpinning of the existing building. Concerns with access limitations and vibrations generated from ground improvement and cost and speed of micropiles steered the project team towards a combination of compaction grouting for new construction and helical piles for underpinning of the existing building walls. The design team also considered and ultimately selected a Ductile Iron Pile solution to provide support for the new building foundations in concert with the planned helical anchors for existing building support where limited head-room restricted access with the on-site DIP installation equipment.

Installation and Testing

Ductile Iron Piles were designed for an allowable capacity of 70 kips using a 118/7.5 series pile (118 mm diameter with 7.5 mm wall thickness). The ductile iron piles were designed to develop capacity in end-bearing. The low-vibration piles were driven through the fill, peat and outwash sand/silt to terminate in the competent glacial till. Piles lengths ranged from about 20 to 27 meters (65 to 90 ft) to terminate in the sloping glacial till, a feature attributed to the nearby Providence River. The range of pile lengths was adjusted by simply adding additional pile sections. The piles were seated into the till or bedrock using a driving set criteria of less than 25 mm (1 in) of penetration per minute of driving. Prior to completion, the DIPs were then filled with grout during installation to further enhance the structural capacity and reduce the potential for corrosion on the pile interior.

Prior to installation of the production piles, a full-scale load test was performed to confirm the design capacity and performance. Results of the load test are shown in Figure 6. At the design load of 70 kips, deformation of the end-bearing DIP was limited to 12 mm (0.5 in). The deflection increased to 35 mm (1.38 in) at the 200% design load of 140 kips. A net deflection of 11.4 mm (0.45 in) was recorded upon rebound. The test results confirmed the performance of the system on the site.

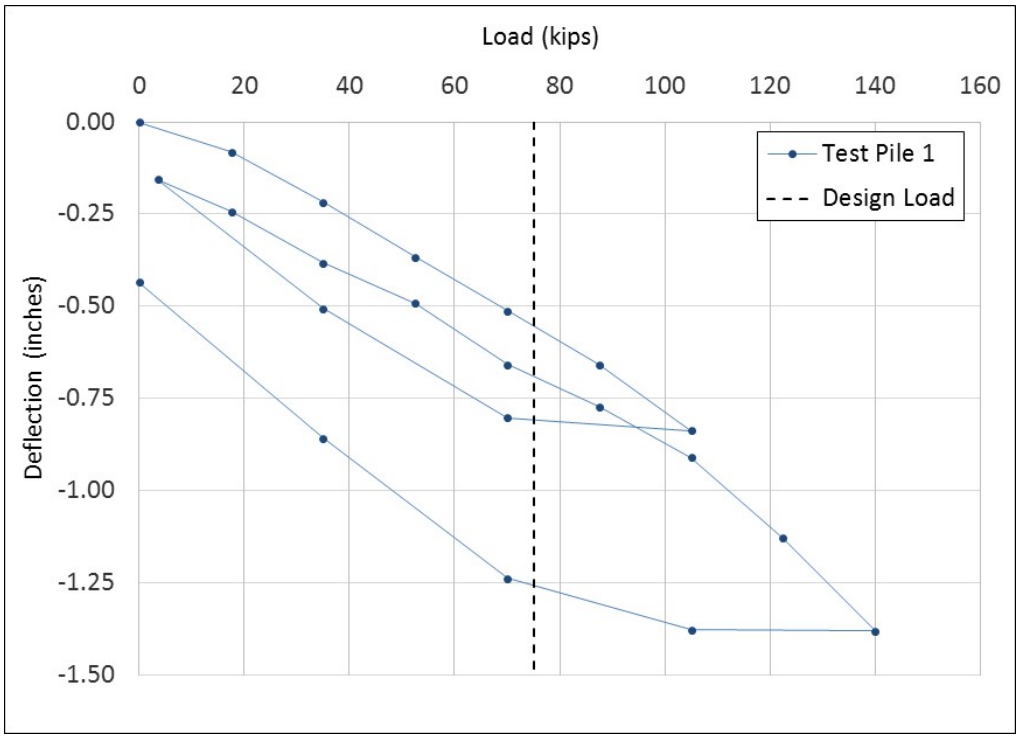


Fig. 6. End-Bearing Ductile Iron Pile Load Test Results

© 2016 Deep Foundations Institute

PROJECT 2 – JOHNSON & WALES UNIVERSITY – SCHOOL OF ENGINEERING & DESIGN

Johnson & Wales University's construction of a new $40M, 3-story School of Engineering & Design building (Fig. 7.) consisted of a 6,596 m^2 (71,000 ft^2) academic facility including classrooms, offices and labs. The project footprint was bordered on two sides by immediately adjacent Johnson & Wales buildings, requiring a solution to support foundations without adverse impacts to the existing buildings. Column loads in these locations of the building ranged from 150 to 600 kips with up to 45 kips of uplift (tension) at select locations.

Geotechnical Design Approach



Fig. 7. Photo of School of Engineering and Design

While the urban fill was present at the site, the organic deposit found at the previous project was not encountered. A cost-effective solution was developed to found the majority of the structure on improved ground with a design bearing pressures of 4,000 psf following Rapid Impact Compaction, a form of dynamic densification. However, vibrations generated during densification were expected (and confirmed) to be far too great to support building foundations immediately adjacent to the existing structures. With successful implementation of the Ductile Iron Pile system on the nearby Physician Assistant Studies building, the design team specified the system for the heavily-loaded, vibration-sensitive areas of the project to provide a cost-effective alternate to traditional solutions like drilled micropiles.

Installation and Testing

The use of 37.5 ton Ductile Iron Piles consisting of a Series 118/7.5 pile (118 mm diameter pile with a 7.5 mm wall thickness) was specified as part of the design. Although the design approach on the Physician Assistant Studies building required piles be installed through the fill and sands to terminate in end-bearing on dense glacial till or rock, a more cost-effective solution was designed using a friction DIP to develop both compression and tension resistance. Piles were designed with an oversized 220 mm (8.7 in) diameter conical grout cap to develop capacity with a friction bond zone in the sand underlying the fill. Pile lengths of 7.6 m (25 ft) were designed to resist the applied working loads of 75 kips. A #9 threaded, center reinforcing bar with a yield strength of 75 ksi was installed in certain piles to provide resistance to the tension loads.

A full-scale tension load test (ASTM D3689) was performed to confirm the design capacity and performance with the 4.9 m (16 ft) bond length. Results of the test are provided in Figure 8. At the design load of 75 kips (Cycle 2), upward deflection of the friction DIP was limited to 9.7 mm (0.38 in). The test was performed up to 200% of the design load (150 kips) where the total deflection was 19.3 mm (0.76 in) (Cycle 4). Following the final unloading, the test was reloaded to evaluate performance up to 225% (Cycle 5) where movement was still limited to only 22.3 mm (0.88 in) and maintained load resistance. Net deflection after unloading the pile was limited to under 10 mm (0.4 in).

© 2016 Deep Foundations Institute

The ductile iron piles were rapidly installed to extend through the fill and terminate in the sand. A minimum pile bond length of 4.9 m (16 ft) was maintained in the sand. A total of 66 piles were installed in 3 working days. Vibration levels were observed to be so minimal during installation that monitoring was discontinued.

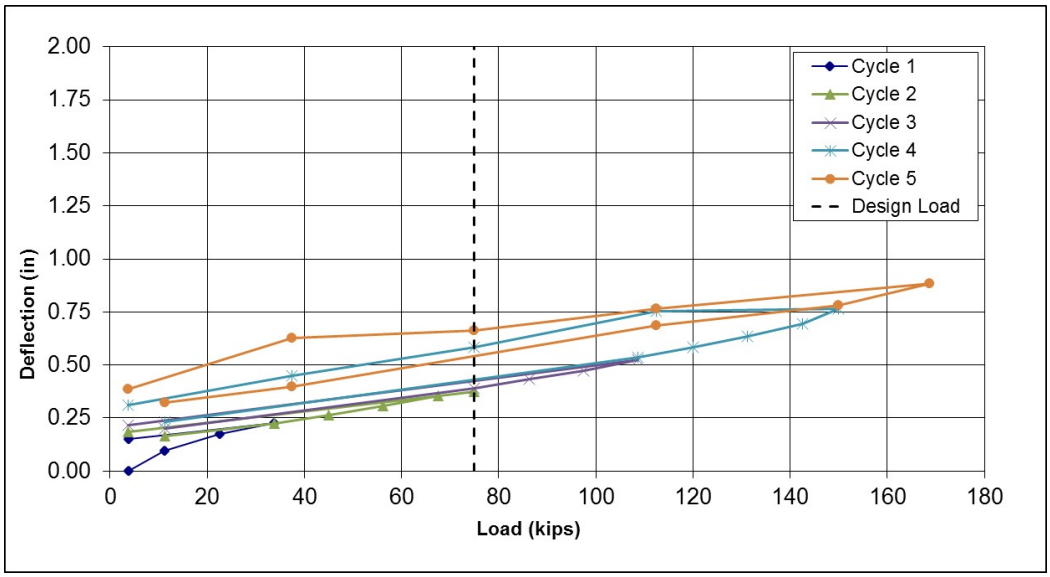


Fig. 8. Friction Ductile Iron Pile Tension Load Test Results

CONCLUSIONS

Ductile Iron Piles were successfully installed at two urban project locations in the Northeast United States where the benefits of the low-vibration, modular driven micropile system were realized. Selection of the system was made based on cost-effectiveness, low vibrations, rapid installation rate and the ability to work at constrained sites. The versatile pile system was designed to develop capacity in end-bearing on one site and through friction resistance for both compression and tension loads on the other site. Design approaches described herein and modeled after other traditional piles (driven piles, micropiles) provided an acceptable method for predicting capacity and performance. Load testing performed at both sites confirmed the design approach and anticipated capacities.

REFERENCES

American Concrete Institute (ACI) (2008). "Building Code Requirements for Structural Concrete (ACI 318-08) and Commentary. ACI. Farmington Hills, MI. p. 129.

Federal Highway Administration (FHWA) (2005). "NHI Course No. 132078: Micropile Design and Construction - Reference Manual. Publication No. FHWA-NHI-05-039. FHWA. Washington, D.C. p. 5-68, 5-69.

GZA GeoEnvironmental, Inc. (2013). "Geotechnical Report, Proposed PA Health Sciences School, 35 Claverick Street, Providence, Rhode Island." February 2013.

GZA GeoEnvironmental, Inc. (2014). "Geotechnical Report, Proposed Academic Building – Johnson & Wales University, Providence, Rhode Island." April 2014.

© 2016 Deep Foundations Institute

International Code Council, Inc. (ICC). (2009). International Building Code 2009. Country Club Hills, IL.

Siskind, D.E., Stagg, M.S., Kopp, J.W. and Dowding, C.H. (1980). "Report of Investigators 8507: Structural response and damage produced by ground vibration from surface mine blasting." United States Department of Interior - Bureau of Mines. P.73. 1980.

Tiroler Rohre Gmbh (TRM). (2015). "Piling Systems for Deep Foundations." October, 2014.

© 2016 Deep Foundations Institute

INNOVATIVE SSP DESIGN AND CONSTRUCTION FOR A COMPLEX SOIL REMEDIATION PROJECT

Mark C. Spence, P. Eng., Isherwood Geostructural Engineers, Burnaby, British Columbia, Canada, 604-428-7080, mark@isherwood.to
Matthew C. Janes, M. E. Sc., P. Eng., Isherwood Geostructural Engineers, Burnaby, British Columbia, Canada, 604-428-7080, matthew@isherwood.to

ABSTRACT

A former coal gasification site next to Rock Bay in Victoria, BC, Canada required a barrier to permit dewatering and excavation of the bay and surrounding property. The adjacent property owners had stringent requirements at the boundaries of their properties. Isherwood Geostructural Engineers designed a temporary steel sheet pile (SSP) water retention structure and excavation shoring system along the perimeter of the site. The project involved challenging geotechnical conditions in soft clay soils and a multi-faceted construction staging plan involving the diversion of two large storm water outfalls that drained into the bay. Despite a well-conceived design and construction plan, unexpected site conditions and delays led to significant changes in design and construction approach. Employment of the Observational Method and on-the-fly geotechnical investigation were instrumental in maintaining project momentum and schedule. The paper presents the geotechnical and geostructural design details and construction events as they transpired, highlighting the key issues, discussions and lessons learned.

INTRODUCTION

For over 100 years, the Rock Bay Site, in Victoria, British Columbia, Canada, had a legacy of contamination left behind from previous industrial activities. The site was the former location of a coal gasification plant that was in operation from 1862 to 1952. The site was also an infilling location for a nearby tannery and sawmill. The remediation of the Rock Bay Site involved the excavation and replacement of approximately 300,000 tonnes of contaminated soils on Transport Canada's property. The project commenced in 2004 and has occurred over several phases on multiple properties. In the third and final phase of the project, a temporary steel sheet pile (SSP) excavation shoring system and ocean barrier wall – required to seal off the bay – was employed to enable disposal and replacement of approximately 90,000 tonnes of contaminated soils from the shoreline and base of the bay.

PROJECT BACKGROUND

The Rock Bay site is located approximately 1.5 km north of the downtown core of Victoria, British Columbia Canada and is shown in Figure 1 below.

© 2016 Deep Foundations Institute

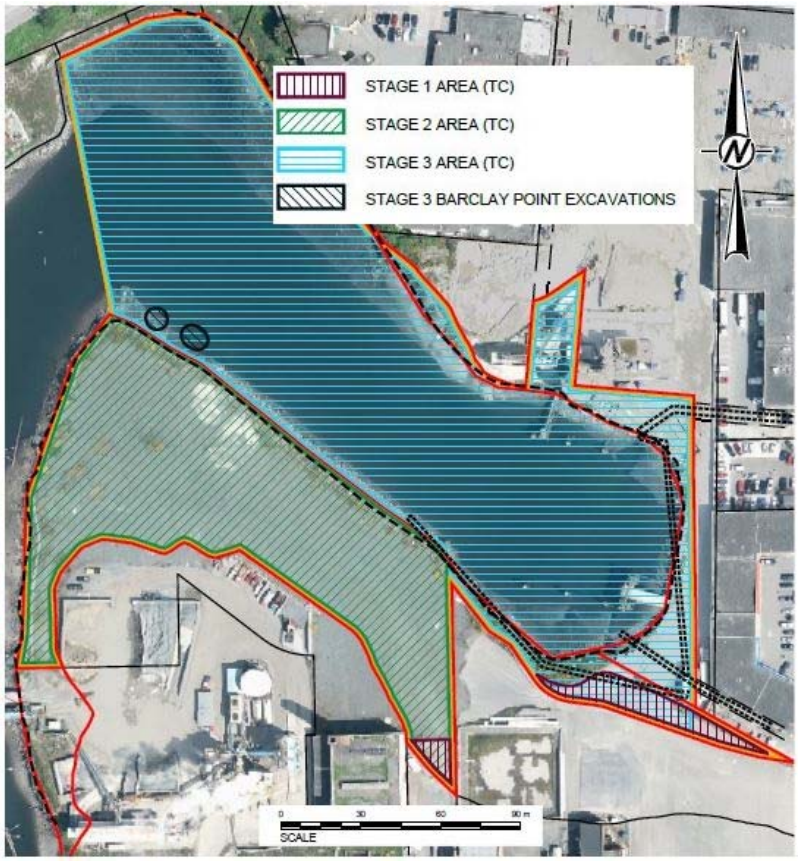


Fig. 1. Site Plan

The Stage 3 site covers a total area of approximately 4200 m^2 (45,000 $ft.^2$). The bottom of the bay varies from approximately -4.5 to -6 m geodetic, and the upland elevations vary from approximately 2 to 3 m geodetic. Generally, the contaminated soils extended to between -4 to -8 m geodetic along the perimeter of the site, requiring excavation shoring up to 11 m (36 ft.) in height. Much of the contaminated soils were submerged within the harbour floor, thus, the bay had to be sealed and drained to allow excavation and removal of impacted materials in dry conditions. The project requirements also mandated that the contaminated soils be removed to the full extent of the site boundaries, leaving zero percent residual contamination along the property line.

The site contains two major stormwater outfalls that drain into Rock Bay, located at the northeast and southeast corners of the site measuring 1800 mm and 900 mm in diameter, respectively. These two outfalls are designed to discharge up to 16,720 L/s (4,417 gal/s) of storm water into the bay and were to remain operational throughout the excavation and remediation works. The outfalls were temporarily diverted and would be re-installed following completion of the remediation works.

GEOTECHNICAL CONDITIONS

Results of the project geotechnical investigation confirmed that there are four distinct sediment layers overlying bedrock within the basin at the head of Rock Bay. The first sediment layer consisted of marine sediments which comprised soft to very soft organics, silts and clays deposited in recent time as a result of alluvial action and detritus from the stormwater outfalls entering the site from the east. Underlying the marine sediments was a layer of stiffer clay referred to as weathered Victoria Clay. The weathered

© 2016 Deep Foundations Institute

Victoria Clay is much weaker than the underlying Grey Victoria Clay. Below the Grey Victoria Clay lay a very dense sandy till material underlain by hard, undulating bedrock typical of the Victoria area.

INITIAL GEOSTRUCTURAL DESIGN

Excavation Shoring

The material of choice for both the excavation shoring and the temporary dam was steel sheet piling. In addition to supporting lateral earth loads, design of the shoring was to accommodate excavation to the edges of an irregular-shaped property line. This proved problematic for the corrugated profile of sheet piles since the contractor was not permitted to excavate outside of the site property. The sheet piles were fitted with backing plates, creating a "bin" to allow excavation to the property line by hydro-vacuum to the required depths as shown in Figure 2.

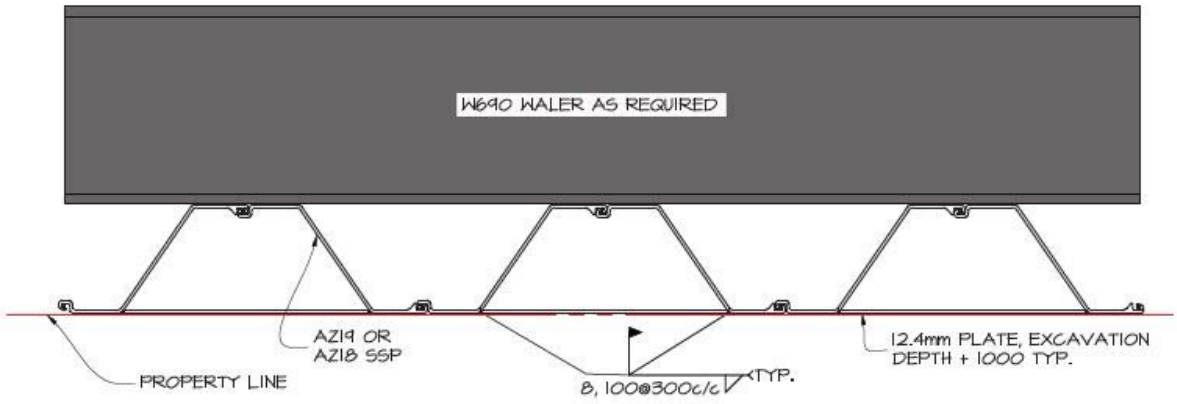


Fig. 2. Binned Sheet Pile Detail

The excavation contractor planned to excavate and backfill along the site perimeter via slot-cuts once the bay was sealed off and drained. The constrained project schedule, however, called for an innovative solution to the problem of delaying significant excavation until completion of the dam and dewatering of the bay. The design-build team conceived a shoring scheme that would allow for advance excavation and diversion of the stormwater outfalls with a significant schedule savings. Refer to Figure 3 below.

© 2016 Deep Foundations Institute

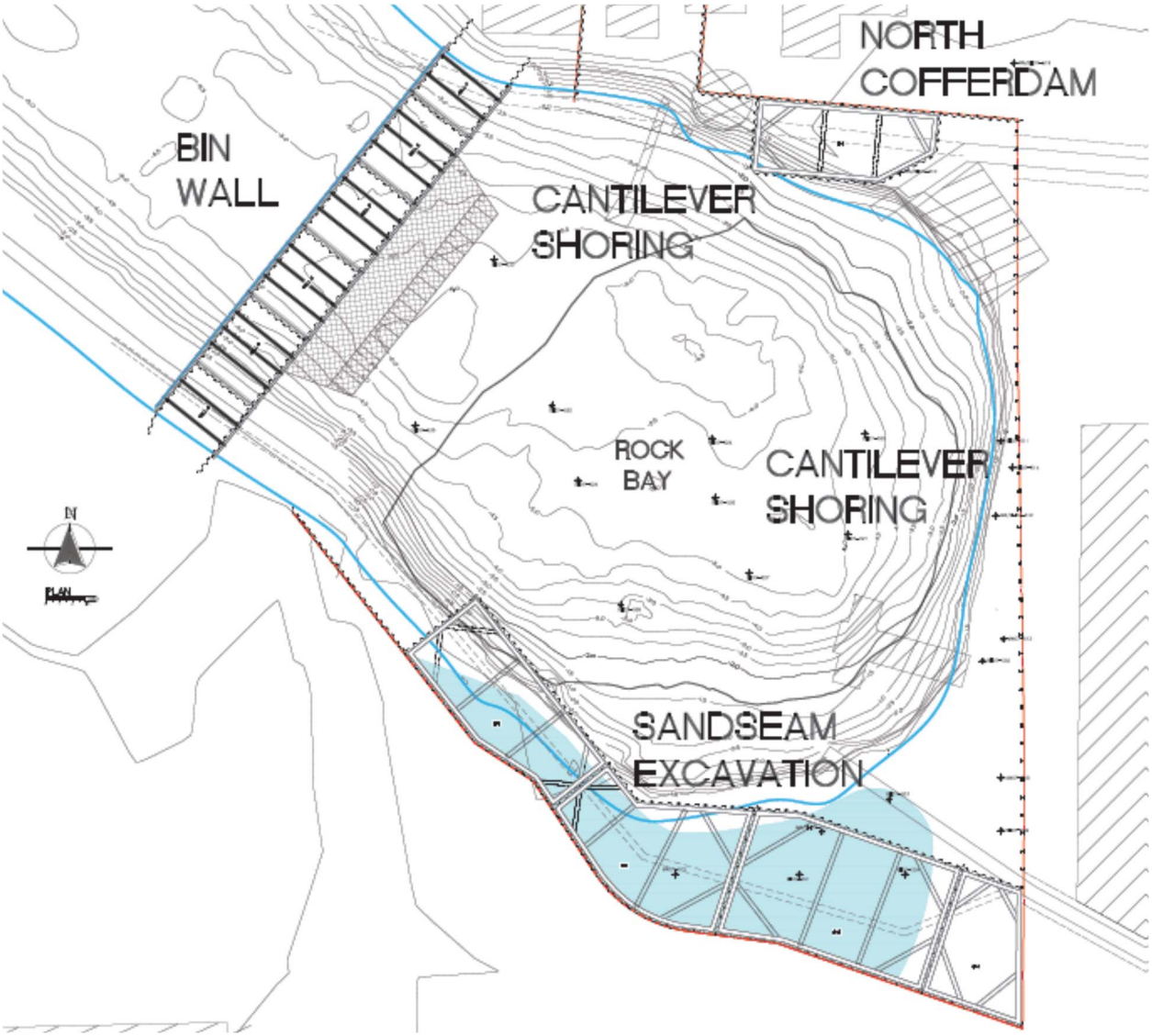


Fig. 3. Shoring and Bin Wall Plan

Per the initial design concept, which was subsequently modified, the series of internally-braced cofferdams along the south property line were to be installed, excavated and backfilled concurrently with the installation of the bin wall. The 11 m (36 ft.) deep cofferdams were generally designed with two levels of W610 (W24) walers braced by pipe struts between 610 and 915 mm (24 to 36 in.) in diameter. To minimize the amount of sheet piling required, the boxes were to be installed in a leap-frog fashion from west to east.

Bin wall

The bin wall was designed to seal the bay during dewatering and subsequent remediation works. The design was based on the US Army Corps of Engineers Manual on Design of Sheet Pile Cellular Structures. High tide elevation was predicted by the Canadian Hydrographic Service to be 1.02 m geodetic, resulting in a static water head of 6.02 m (19.75 ft.) as the primary externally applied force on

© 2016 Deep Foundations Institute

the bin wall. No wave action was anticipated, though tidal fluctuations were expected to range up to 2.45 m (8.04 ft.) during the service life of the dam.

The cell fill was selected as 75 mm (3 in.) crushed rock with zero percent silt to prevent siltation of the remediation area. This free-draining material would allow for a low seepage line that provided several structural benefits to the bin wall including reduction of the sheet pile interlock forces, increased effective stress at the base of the cells thereby augmenting sliding resistance, and increased internal shear resistance. The same material was selected to comprise a rock berm on the drained side of the bin wall to provide additional sliding and overturning resistance. Refer to Figure 4 below.

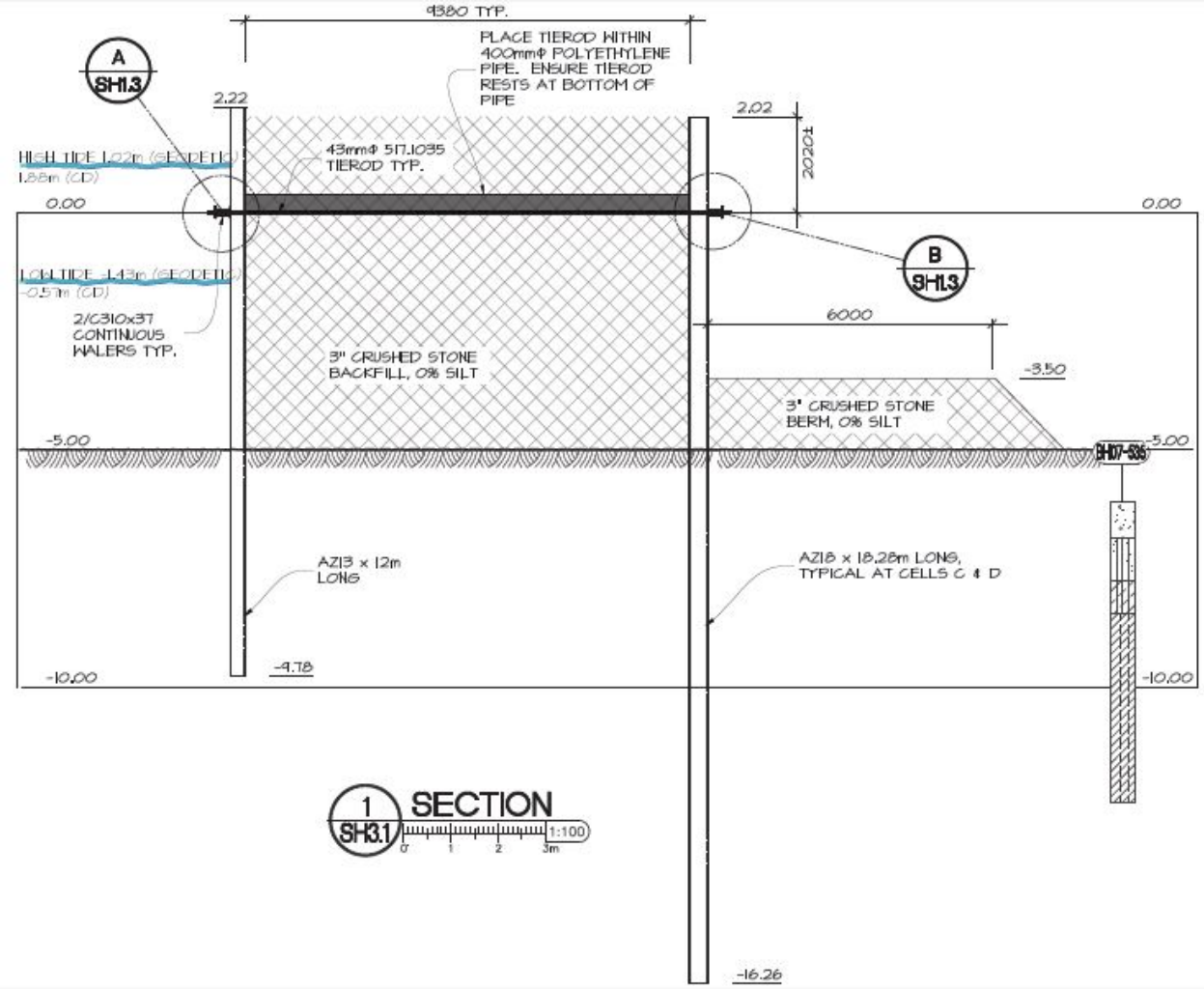


Fig. 4. Bin Wall Section

Monitoring Programme

In order to verify shoring performance during construction, the design was predicated on a monitoring programme including inclinometers and visual survey. The plan included four inclinometers; two located within the bin wall and two along the south property line where excavation was planned to the deepest elevation of -8 m. The inclinometer casings were strapped directly to the sheet piles and protected by a steel angle enclosure. Following driving of the sheet piles, the casings were grouted in place. Survey

© 2016 Deep Foundations Institute

targets were established at the top of shoring along the shoring perimeter and along the east face of the bin wall.

INSTALLATION OF EXCAVATION SHORING AND BIN WALL

The piling contractor commenced sheet pile installation of the bin wall and south cofferdams in August 2014. The AZ13 and AZ18 sheet piles were driven with an APE 200 vibro hammer. The bin wall cells were sectioned off with bulkhead walls, a 0.6 m (2 ft.) layer of sand placed and backfilled with 75 mm (3 in.) minus crushed stone. The two walls of the bin structure were connected via 43 mm (1¾ in.) diameter tie-rods and continuous double channel walers. Due to concerns of consolidation of the marine sediment layer under the weight of the backfill material, which could cause bending of the embedded tie-rods, the bars were placed in 400 mm (16 in.) hollow pipes.

Installation of the perimeter sheet piles along the south property experienced immediate delays. The contractor encountered controlled density fill (CDF) that was placed during previously completed remediation works on the neighbouring property to the south. Furthermore, once the sheet piles were driven through or past the CDF, driving rates seemed to indicate stronger clays than were anticipated based on the findings of the geotechnical investigation. The delays resulted in the first half of the bin wall being installed in the time required to complete the sheet piling of only the first of four south cofferdams. The delays foretold completion of the bin wall well before the south cofferdams could be backfilled and form the bedding for the outfall bypass pipe. The design-build team reacted quickly, re-envisioning the design to suit the changing construction timing. The three remaining south cofferdams were eliminated from the design, leaving only the sheet piles along the south property line as shown in Figure 5. The deepest contaminants lay along the south edge of the property, thus, lateral bracing was required to provide adequate working room for excavation equipment as shown in Figure 6. As encroachment into the neighbouring lands was prohibited, raked struts bearing on sheet pile footings were the preferred solution designed by Isherwood.

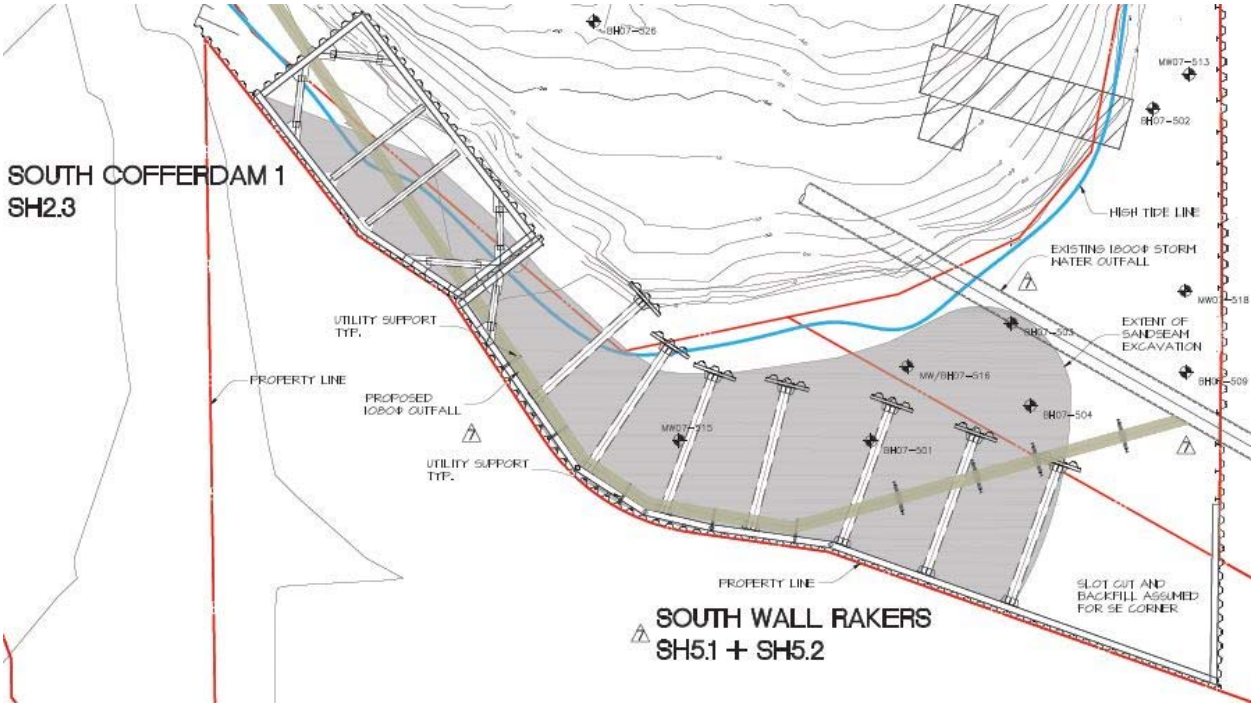


Fig. 5. Revised South Wall Shoring Plan

© 2016 Deep Foundations Institute

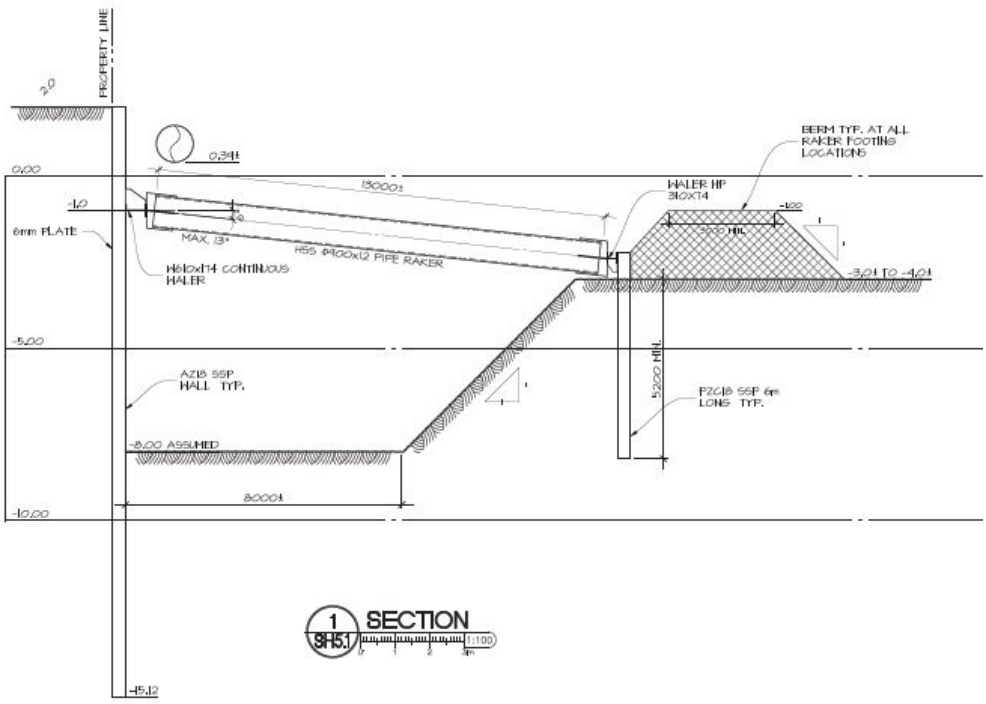


Fig. 6. Revised South Wall Section

As redesign of the south wall shoring was taking place, installation of the bin wall and western south cofferdam were ongoing. During installation of the second cell of the bin wall, bedrock was encountered at an unexpectedly high elevation. The surface of the bedrock appeared to slope upwards toward the north. The contractor performed a probing program to ascertain the profile of the undulating rock surface in advance of installation of the next cell. It was confirmed that the rock surface was sufficiently high that passive resistance of the pile toe was deemed to be insufficient. Isherwood designed a toe-pin detail that would provide a shear connection between the sheet pile tip and underlying bedrock. Each pair of sheet piles was outfitted with a 114 mm (4½ in.) diameter pipe prior to driving. The toe pins were installed through the pipes, 1 m (3 ft.) into the bedrock and grouted in place as shown in Figure 7 below.

© 2016 Deep Foundations Institute

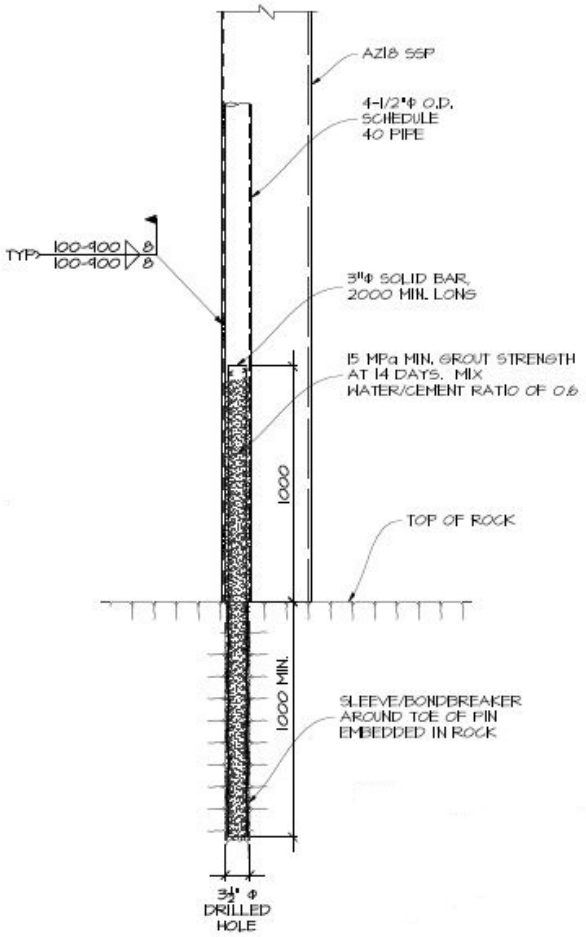


Fig. 7. Toe Pin Detail

Based on driving conditions encountered by the piling contractor, the design-build team performed supplementary geotechnical investigation consisting of in-situ hand vane shear tests within the first southern cofferdam. The vane tests indicated clay soils with shear strength between 30 and 200+ kPa, at approximately -2 m geodetic. These strengths proved to be significantly greater than indicated in the initial geotechnical data.

Inclinometer data was collected at the south cofferdam twice per week during excavation below the top level of bracing as shown in Figure 8.

© 2016 Deep Foundations Institute

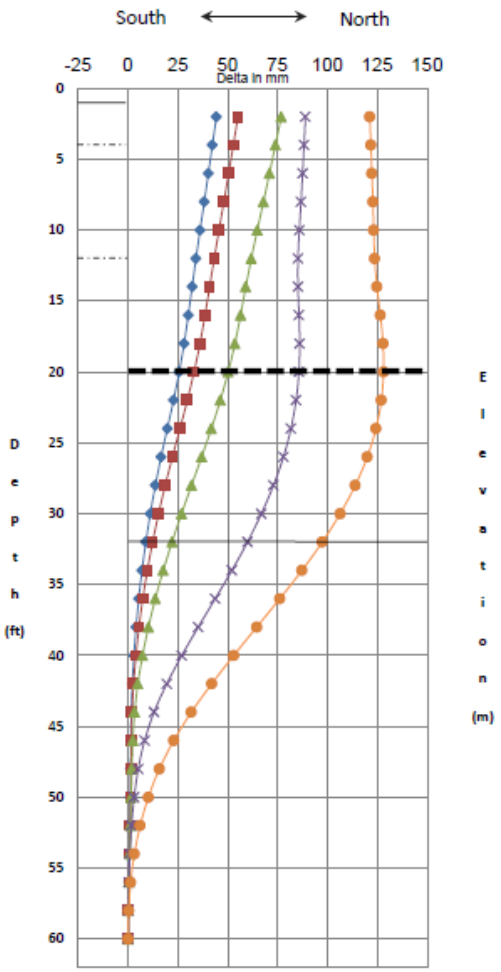


Fig. 8. South Cofferdam Inclinometer Plot

The gradual progression of lateral movements, correlated to excavation progress, indicated better than expected performance of the cofferdam walls. Based on the evidence of stronger clay soils and verification of cofferdam performance, and by carefully planning the slot-cutting and backfilling within the cofferdam, the design-build team was able to eliminate the lower level of bracing, saving significant constructions costs and schedule.

One of the challenges of the south wall redesign involved the need to temporarily reroute the two storm water outfalls to discharge on the ocean side of the bin wall. The storm water outfall was rerouted into a steel welded pipe designed to traverse the soon to be excavated region. The pipe was supported on piles and eventually by brackets hung from the south sheet pile wall. Excavation of the south wall proceeded using the raked struts supported by sheet pile buttresses. The timing and placement of the sheet pile buttresses was complicated by the schedule for the excavation of the material around the struts and buttresses. The buttress area was pre-excavated of contaminated soils and backfilled using 75 mm (3") minus fills. The fills required compaction in order to adequately support the sheet pile buttresses. The buttress supported struts were preloaded and provided support to the south sheet pile wall via a continuous waler. This provided for the deep excavation required to remove the contaminated sands 11-12 m below grade. Figure 9 shows the south shoring wall prepared for excavation.

© 2016 Deep Foundations Institute



Fig. 9. South Wall Bracing Installation and South Outfall Bypass Supported

On the north perimeter of the site the storm water outfall was also re-routed into a large diameter steel welded pipe. As a cost saving the steel pipe diversion was shortened and a sheet pile wall was driven perpendicular to the bin wall, parallel to the outfall, as a south training wall. Flows in both outfalls raised and dropped rapidly due to fast run off and collection of urban storm water.

DEWATERING AND EXCAVATION

Following completion of the bin wall and diversion of the two outfalls, dewatering of the bay commenced on March 3, 2015. Dewatering of the bay proved to be straightforward. The clay soils surrounding the bay ensured low groundwater recharge. As the water was lowered within the bay, the sheets of the bin walls and the northern training wall became stressed and the joints tightened and closed.

Two slope inclinometers were installed on the east (dry) side of the bin wall. Lateral movement of the bin wall was closely monitored in keeping with the Observational Method. This enabled the design-build team to proactively augment the granular berm in support of the bin wall as the full hydrostatic load was gradually added to the system. Figure 10 shows the progressive lateral deflected shape of the bin wall as the site was dewatered.

© 2016 Deep Foundations Institute

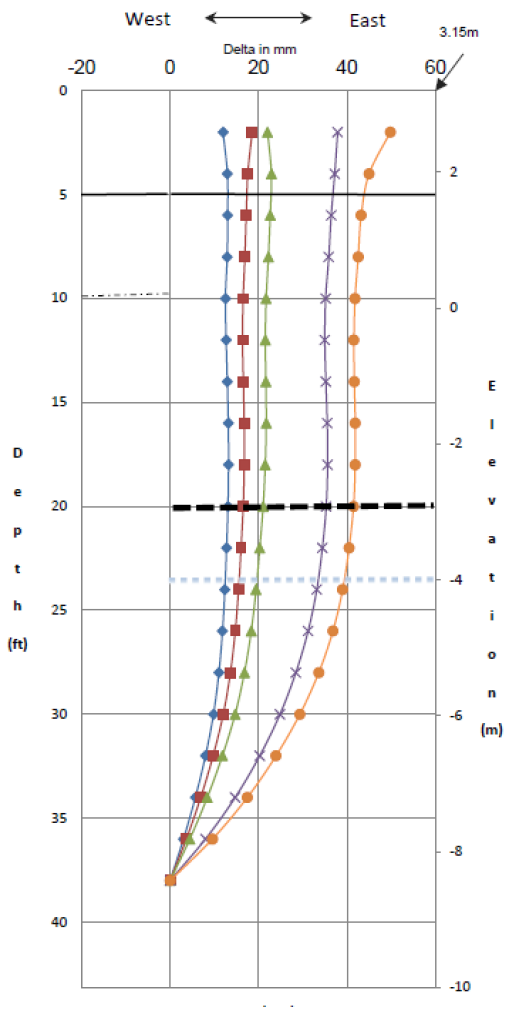


Fig. 10. Bin Wall Deflection during Bay Dewatering

SUMMARY

Remediation of the Rock Bay site was challenged with complicated geotechnical conditions, encroachment restrictions and an aggressive project schedule. A temporary sheet pile bin wall water retention structure permitted dewatering of the bay, and a sheet pile excavation shoring system along the perimeter of the site enabled excavation up to 12 m (40 ft.) to remove contaminated soils and replace with clean fill. Two major storm water outfalls were rerouted into steel pipes supported along the north and south perimeters and discharged on the ocean side of the bin wall structure. The design-build team overcame unexpected site conditions and delays with adaptations in design and construction approach. Employment of the Observational Method and on-the-fly geotechnical investigation were instrumental in maintaining project momentum and schedule.

© 2016 Deep Foundations Institute

This page left intentionally blank

© 2016 Deep Foundations Institute

INSTALLATION OF SECANT PILE WALL IN ROCK ADJACENT TO FRAGILE BUILDING

Chu E. Ho, Arup, New York, New York, USA, chu.ho@arup.com
Alfredas Daugiala, Underpinning and Foundation Skanska, Maspeth, New York, USA, alfredas.daugiala@skanska.com
Nicola Ebanks, Underpinning and Foundation Skanska, Maspeth, New York, USA, nicola.ebanks@skanska.com

ABSTRACT

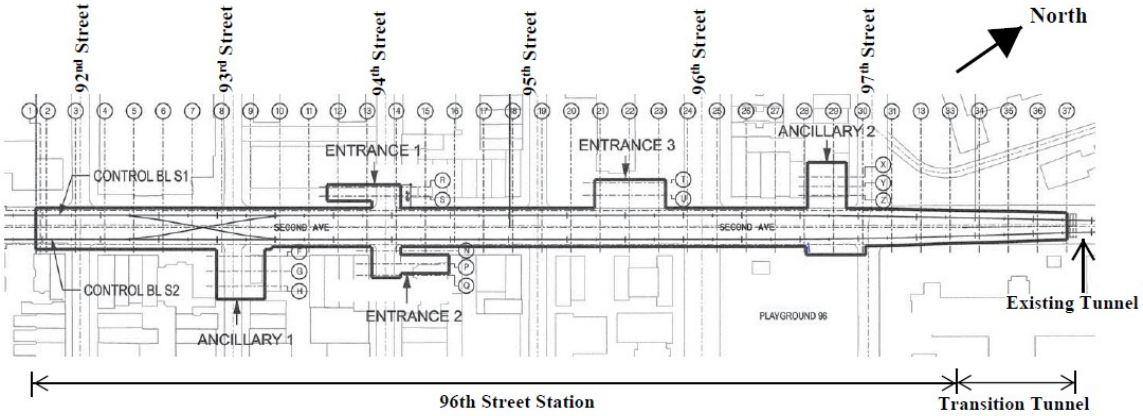
The construction of an ancillary structure for the new Second Avenue Subway Line in Manhattan, New York City involved a deep excavation in highly variable rock conditions adjacent to a fragile masonry building. The maximum difference between the lowest and highest rock elevations was about 30 feet, which posed a problem for the installation of secant piles that formed the supporting retaining wall for the excavation. At certain areas, the rock levels were higher than the top of the invert slab of the ancillary structure. To avoid disturbance to the adjacent fragile building, the secant piles were fully cased for drilling through the overburden soils and the rock sockets were formed using non-vibratory technique. This paper discusses the design and installation details of the secant pile wall and the contingency measures that were considered to mitigate the highly variable rock conditions. Monitoring of the adjacent fragile building showed that impact of pile installation were controlled within tolerable limits and safety of the building was not compromised.

Keywords: deep excavation, secant pile wall, rock socket, rock drilling, fragile building

INTRODUCTION

The 96th Street Station forms part of the newly constructed Second Avenue Subway Line on the East side of Manhattan Island, New York City (Figure 1). During construction of this station, several deep excavations were carried out adjacent to existing fragile buildings (Arksman et al. 2012, Grigson et al. 2016). These fragile buildings were typically four to five stories high, with a single rubble wall basement supported on timber piles or seated directly on the fill. The timber piles were often found to be in a poor condition and connections to the footings were compromised due to rotting of the timber within the zone of water table fluctuation. Several of these fragile buildings had to be strengthened and underpinned to improve the stability of the structures prior to commencement of excavation for the new subway station box (Trabold et al. 2012, Ho and Pena-Iguaran, 2013). The situation was most challenging at Ancillary Buildings 1 and 2 located at 93rd and 97th Street respectively, where secant pile walls were located merely 2 feet away from the adjacent property line, due to architectural space constraints. While mitigation of excavation induced ground movements can be controlled by the adoption of a stiff excavation support system, a more concerning factor was the uncertainty associated with the impact of the secant pile wall installation on the stability of the existing fragile buildings. This was particularly difficult at Ancillary 1 where the secant piles encountered highly variable rock levels that intruded into the excavation space. The following sections discuss the design and installation of the secant pile wall and contingency measures that were considered at Ancillary 1.

© 2016 Deep Foundations Institute



.

Fig. 1. Plan of 96th Street Station

GROUND CONDITIONS

The subsurface profile at Ancillary 1 consisted of fill overlying organics, silty sand, varved silts, glacial till, decomposed rock and the Manhattan Schist bedrock (Figure 2). Water table was located approximately 10 feet below ground. Figure 3 shows the Standard Penetration Test (SPT) blow counts, N_{60} obtained for the overburden soils based on borings within and around the site. The fill was up to 20 feet thick and generally consisted of backfilled sandy soils from prior construction. The fill was loose to medium dense with N_{60} ranging from 10 to 40 blows/foot. The organics layer was 15 to 25 feet thick with overconsolidation ratios ranging from 1.0 to 6.4 and N_{60} between 3 and 9 blows/foot.

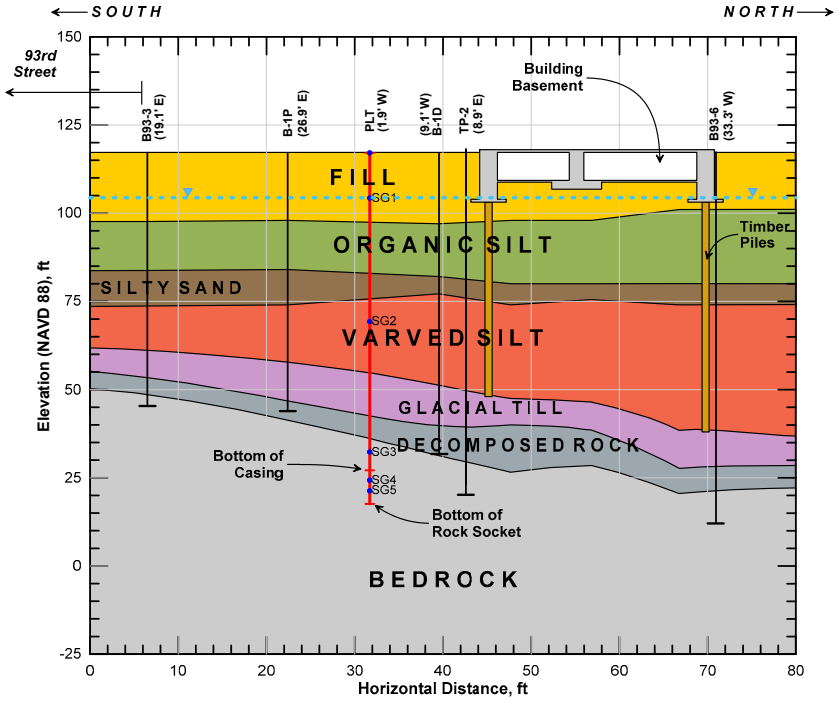


Fig. 2. Subsoil profile across the site at Ancillary 1

© 2016 Deep Foundations Institute

There was a layer of medium dense to dense silty sand (N_{60} = 20 to 50 blows/foot) about 15 to 25 feet thick below the organics layer. The thickness of varved silts ranged from 15 feet to as large as 35 feet in the vicinity of the site. The N_{60} values appeared to decrease with depth within the varved silts from about 20 to 40 blows/foot to slightly less than 10 blows/foot at depth of 60 feet. The glacial till was 7 to 10 feet thick, comprising mainly medium dense to dense fine to coarse gravel and sand, with some silt and trace of mica. The decomposed rock was a very dense micaceous fine to medium sand, with some silt and rock fragments. The bedrock was moderately hard to hard, fresh to slightly weathered, medium to coarse grained, quartz-mica-garnet schist, with thin horizontal to vertical foliations and rough very closely to closely spaced joints and fractures. The rock quality was highly variable and generally decreased with depth (Figure 3). The limited information provided by a small number of deep boreholes around the perimeter of the site prior to construction indicated that the top of rock elevations may vary significantly within the site.

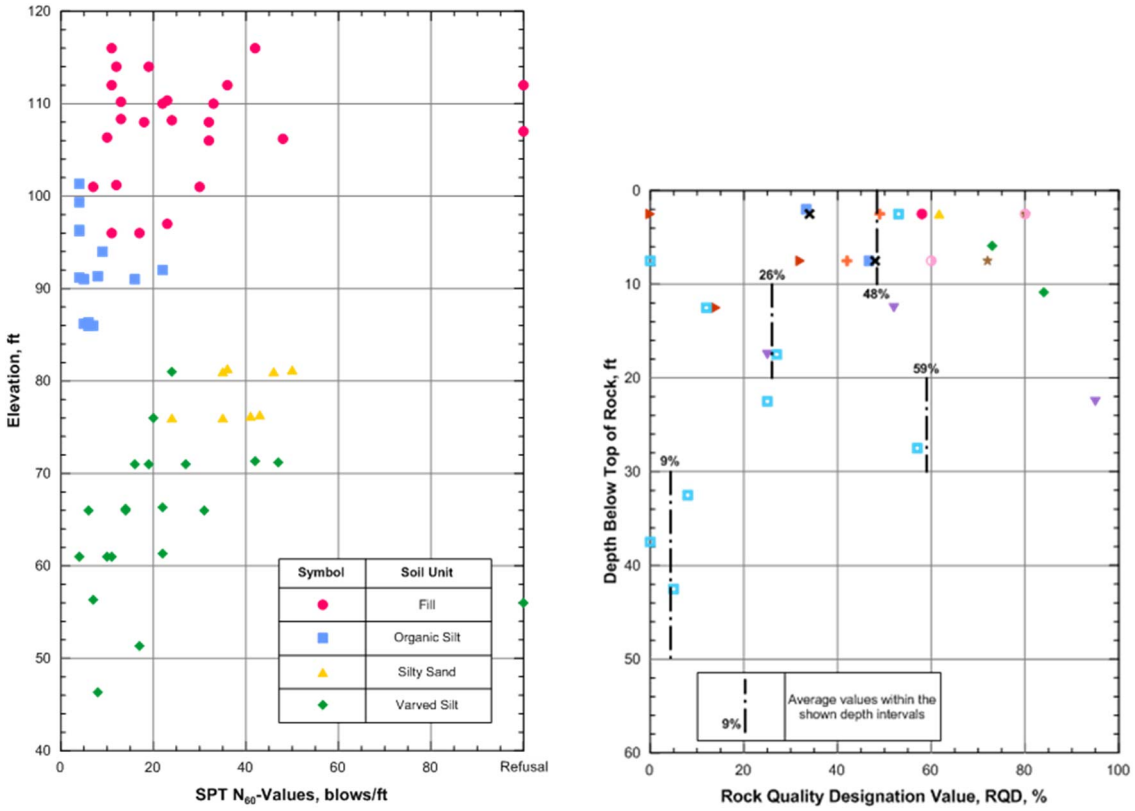


Fig. 3. Standard penetration test in overburden soils (left); rock quality (right)

EXCAVATION SUPPORT SCHEME

Ancillary 1 was located at the junction of Second Avenue and 93rd Street. The ancillary structure was located mostly underground and occupied the space beneath 93rd Street and the existing sidewalks on each side, including the empty lot of land immediately north of 93rd street. The existing ground surface elevation was approximately at EL+118ft. An above-ground structure for the ancillary building rises from the underground space on this lot to about 4 stories high next to an existing four story building. The invert slab was 6 feet thick, and underlain by a waterproofing membrane and drainage layer. The top of the

© 2016 Deep Foundations Institute

invert slab was located at elevation EL+60.29ft. The average final excavation level was approximately at EL+52.62ft and was located mostly within the competent glacial till or decomposed rock, except at the southeastern corner of the site where shallow bedrock was encountered.

Initially, a slurry wall scheme was envisaged to provide a rigid support wall system for controlling excavation induced ground movements. However, a significant portion of the slurry wall would have to be excavated well below the top of the shallow rock area, requiring heavy chiseling to penetrate the rock or the use of a hydraulic milling machine. Due to concerns about installation disturbances that may damage the adjacent fragile building, the slurry wall scheme was subsequently replaced by a permanent secant pile wall scheme with an internal cast-in-place wall (Figure 4). The secant piles were designed to resist all temporary earth and water loads during excavation, including surcharge from the adjacent building. In the permanent condition, it was assumed that the secant pile wall may leak through the joints, and hence the internal CIP wall was required to resist the full hydrostatic water pressure. The walls were connected together via a capping beam at ground level. Both walls were also designed to carry permanent vertical loads.

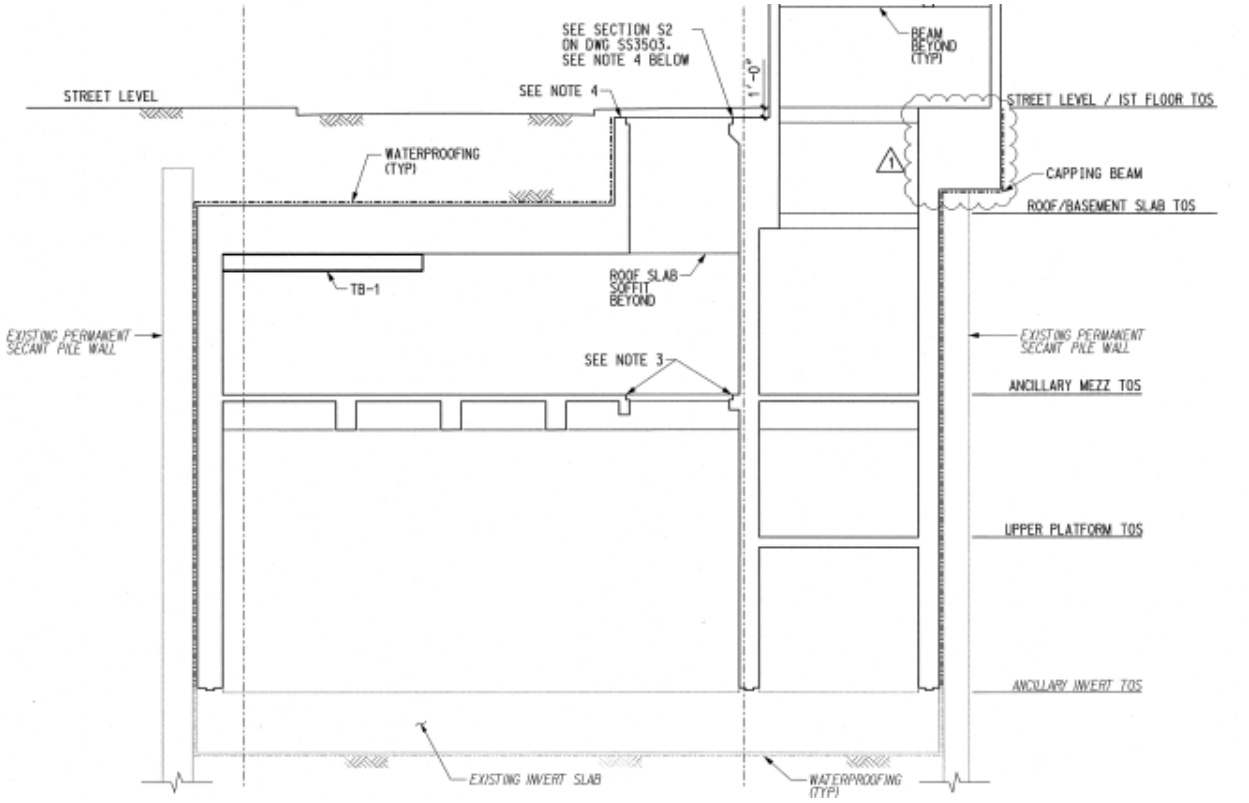


Fig. 4. Permanent secant pile wall scheme with internal cast-in-place wall

Figure 5 shows the plan layout of the permanent secant pile wall at Ancillary 1. The primary (P) and secondary (Type A and B) piles were designed for a nominal diameter of 34.5 inches. Two types of core beam sections were adopted for the secondary piles. Type A secondary piles, located along the southern site boundary and up to about the middle of the eastern site boundary, consisted of a standard W18 x 258 lb/ft steel core beam spaced 49 inches center-to center. Type B secondary piles consisted of a W18

© 2016 Deep Foundations Institute

x 258 lb/ft core beam with an additional 10 inches x 0.5 inches thick steel plate welded to both external faces of the flanges to increase the bending capacity of the steel section. Type B piles were spaced at 47 inches and ran along the northern site boundary (adjacent to the fragile building approximately between gridlines F to H) and the eastern site boundary to link up with the Type A piles. The transition between Type A and B piles was located at primary pile P32. Yield strength for the steel sections and plates was f_y = 50ksi. The total length of wall comprised of 31 Type A and 29 Type B secant piles and 60 primary piles. The design concrete strength for primary piles was 1000psi, while that for secondary piles was 4000psi. The toe of each pile was required to be installed at least 2 feet below the final excavation level with at least 2 feet embedment into sound rock. Sound rock was defined as rock with rock quality designation (RQD) greater than 50%. The excavation was supported by five tiers of temporary bracing, including the traffic deck (Figure 6).

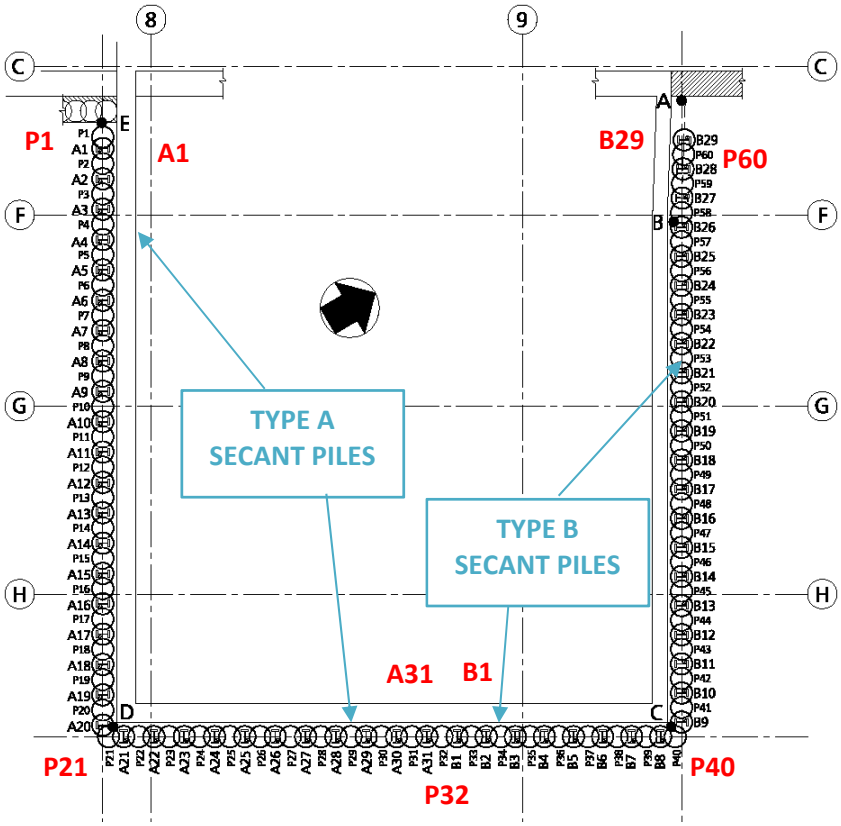


Fig. 5. Layout plan of Type A and Type B secondary piles and primary (P) piles

VARIABILITY OF ROCK LEVELS AND CONTINGENCY MEASURES

Prior to the start of construction, the adjacent fragile building was underpinned using micropiles for protection against potential ground movements arising from the excavation for the ancillary structure (Ho and Pena-Iguaran, 2013). As the secant pile wall was located only 2 feet away from the adjacent building, the method of installation was restricted to cased drilling to the top of rock, with the socket in the rock achieved using a rock drill. Down-the-hole hammering for penetrating the rock was not permitted to avoid loosening the foundation soils immediately below the basement and around the micropiles.

© 2016 Deep Foundations Institute

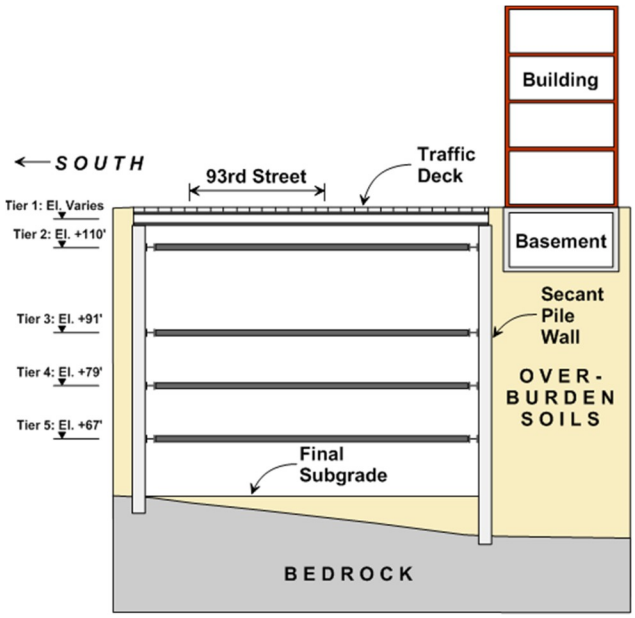


Fig. 6. Braced secant pile wall for temporary excavation support

To minimize uncertainty in the top of rock elevations, twelve supplementary probe holes were cored along the line of secant pile walls on the northern, eastern and southern boundaries of the site to establish the anticipated rock levels. Using the existing boring data, the results of these probes, together with the top of rock levels encountered during the micropile installation, a contour of the top of rock elevation was obtained to guide the secant pile wall construction, particularly those adjacent to the fragile building (Figure 7).

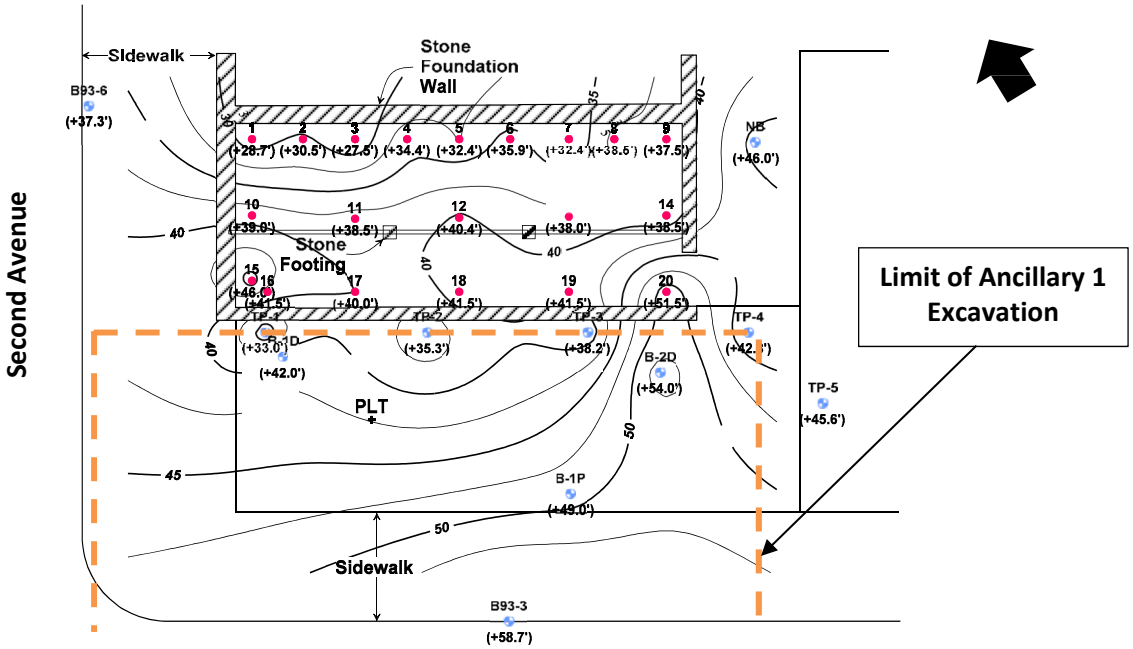


Fig. 7. Inferred top of rock contours adjacent to fragile building

© 2016 Deep Foundations Institute

Figure 8 shows the developed section along the secant pile wall. As can be seen, the probe results indicated that there was a zone where the rock rose as much as 9 feet above the bottom of the excavation. It was determined that the length of rock drilling may be up to 16 feet for the highest elevations of rock on the southeastern corner of the site. This situation may prove problematic for the drilling operations and may cause potential delay to the secant pile installation program.

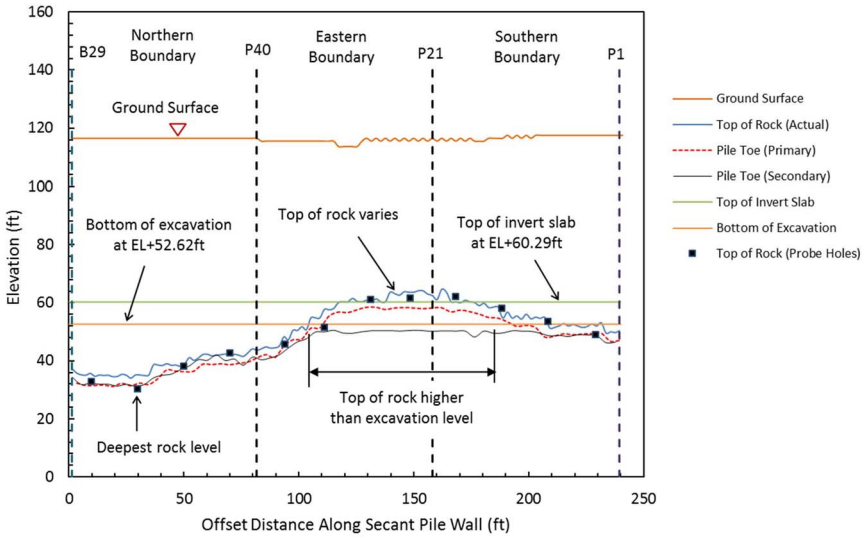


Fig. 8. Top of rock elevations obtained from probes and observed during pile installation

Alternate solutions to the excavation support design were therefore explored as a contingency in case the rock drilling operations proved to be too difficult during pile installation. This included the introduction of a pair of toe anchors drilled into the rock at locations where the secondary pile toe levels could not be completed to the original design elevations and terminated above the invert slab level, even if the nominal rock socket length of 2 feet had been achieved (Figure 9). The rock anchors were required to prevent a toe kick out situation during excavation below the pile toe level.

Another consideration was the potential lack of interlock between the piles where the rock was deep. For a drilling tolerance of 1:200, the anticipated deviation at the deepest rock level at EL+30ft was 5.28 inches (Figure 10). The overlap between the cased portions of adjacent piles could reduce from 11.5 inches (with no deviation) to just 1 inch. For the rock socket, the overlap could similarly reduce from 7.625 inches (with no deviation) to a clear gap of 3 inches between the rock sockets. However since the rock was generally of good quality and relatively impermeable, the small gap between the rock sockets would have no significant impact on excavation stability, hence no mitigating measure was required.

PRODUCTION PILING

Production pile installation was carried out over a seven month period, commencing from the southern site boundary away from the fragile building as a safeguard against any unexpected problems during rock drilling. The row of secant piles along the northern boundary in front of the fragile building was installed towards the end of the piling period. The secant piles were constructed using a Bauer BG40 drill rig

© 2016 Deep Foundations Institute

(Figure 11). A temporary double-walled heavy duty steel casing was used for drilling through the overburden soils. The casing outer diameter was 34.625 inches (880 mm) and the wall thickness was 1.575 inches (40mm). The casing was outfitted with a starter shoe with replaceable bi-directional tungsten carbide teeth for embedment into the rock (0.5 feet minimum). The diameter of the rock core barrel was 30.75 inches (780 mm).

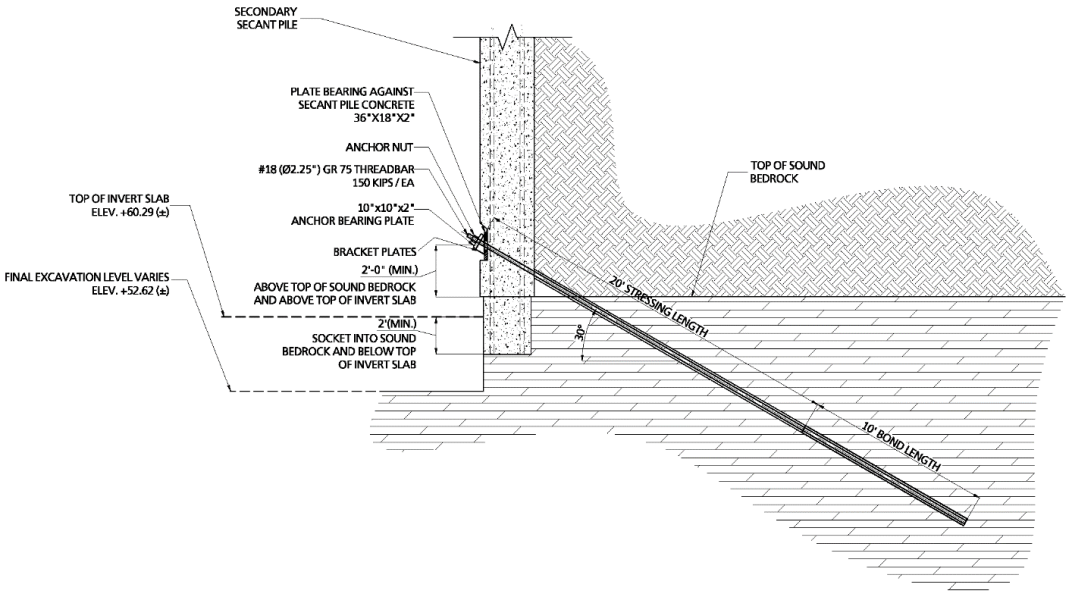
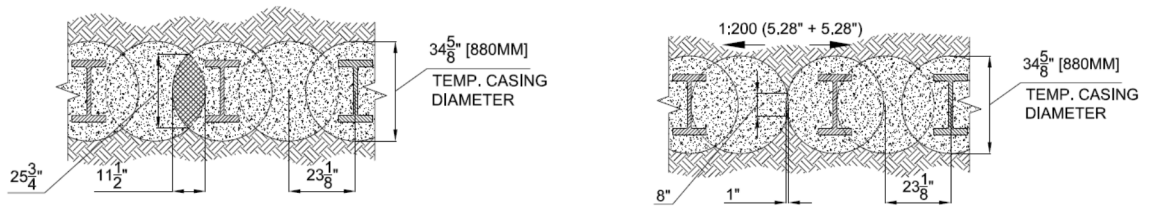
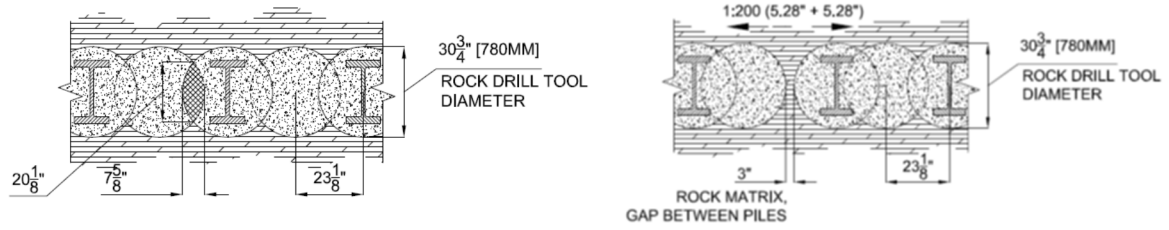


Fig. 9. Contingency rock anchors for stabilizing short secant piles at high rock areas



(a) At bottom of temporary casing



(b) At rock socket

Fig. 10. Interlock condition between piles at deep rock areas (EL+30ft)

Eventually, rock drilling was successfully completed without needing to activate the contingency plan to introduce toe anchors at areas of high rock. However, an adjustment to the toe embedment criteria was

© 2016 Deep Foundations Institute

made. At areas where rock levels rose above the bottom of excavation, the primary pile toe was allowed to be terminated just 1 foot below the top of the invert slab level provided the minimum 2 feet embedment in the rock had been achieved. However, the secondary piles (with the steel core beam) were still required to be installed to 2 feet below the bottom of excavation and embedded at least 2 feet into rock.



Fig. 11. Secant pile installation adjacent to fragile building (left); rock core barrel (right)

Figure 12 compares the actual top of rock elevations encountered in the primary and secondary piles, and the rock elevations extrapolated from the probe data shown in Figure 8. As can be seen, the probe data gave a reasonable indication of the actual rock levels encountered. The actual overburden drilling length for both primary and secondary piles varied between 51.4 and 82.5 feet, with a mean value of 66.4 feet. The length of rock drilling ranged from 2.1 to 6.7 feet for primary piles and 1.6 to 13.6 feet for secondary piles. The mean drilled length in rock of 3.4 feet for primary piles was larger than the nominal 2 feet rock socket that was specified.

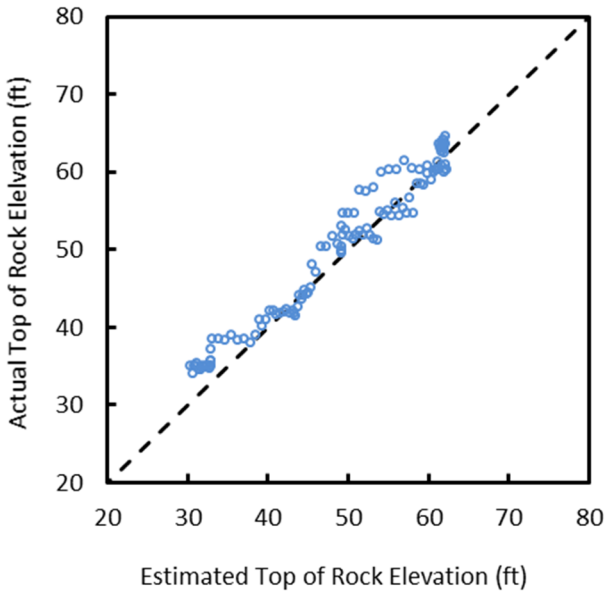


Fig. 12. Predicted rock levels based on probes and actual top of rock levels encountered in piles

The overall production rate varied between 1 and 2 days per pile, including drilling to the pile toe, placing

© 2016 Deep Foundations Institute

the core beam and filling with concrete. Typical production rate for drilling through the overburden soil varied between 10 to 15 feet per hour and penetration through the rock ranged from 3 to 5 feet per hour. Primary pile installation was generally faster due to relatively easy drilling in soil matrix and a shorter rock socket length. Secondary piles took longer as they were advanced through a stiffer matrix consisting of primary pile concrete and soil, as well as a longer rock socket.

The adjacent fragile building was monitored during production pile installation. Registered vibration levels were well within the specified limit of 0.5mm/s for a fragile building. Displacements read by automated motorized total stations for optical prisms mounted on the building indicated settlements ranging from 0.1 to 0.175 inches during the period of pile installation, with no significant horizontal displacements. The largest settlements were observed during installation of piles along the northern site boundary near the south-west corner of the fragile building (at gridline F). The most significant settlement at this corner was 0.05 inches observed during drilling of primary pile P59. Tilt of the building was generally small. Tilt sensors installed on the west basement wall indicated in-plane tilt of 1:1122 to 1:885 (0.892 to 1.13mm/m) toward the secant pile wall, while that installed on the east basement wall indicated in-plane tilt of 1:481 (2.08mm/m) away from the secant pile wall. The small observed displacements indicated that the adjacent fragile building was not adversely impacted by the secant pile wall construction and the mitigating measures implemented were successful.

CONCLUSIONS

This paper discusses the installation of secant pile walls for a 65 feet deep excavation in highly variable rock conditions adjacent to a fragile masonry building. The original design criteria required both the primary and secondary secant piles to be installed 2 feet below the bottom of excavation and embedded at least 2 feet into sound rock. Alternate schemes incorporating additional toe anchors to secure the secondary piles were considered in case the terminal depths of the piles could not be achieved. Supplementary probe holes cored along the length of the secant pile wall were helpful in providing guidance during pile drilling. To avoid unnecessary rock drilling, the primary piles were allowed to be terminated just 1 foot below the top of the invert slab level provided the minimum 2 feet embedment in the rock has been achieved. All piles were fully cased in the overburden soils and rock sockets were formed using a core barrel. Monitoring of vibrations and displacements indicated that pile installation was controlled to within tolerable limits and resulted in no adverse impact on the safety of the fragile building.

REFERENCES

Aksman, B., Grigson, R., and Giffen, R., 2012. Second Avenue Subway Project, New York: design of new underground stations. Proceedings of the Structures Congress 2012, Chicago, ASCE.

Grigson, R., Ho, C., and Lemus, P., 2016. Second Avenue Subway Project: deep excavation support of a cut-and-cover station. Proceedings of the Geotechnical and Structural Congress 2016, ASCE, 402-415.

Ho, C. E., and Pena-Iguaran A., 2013. Underpinning using micropiles for fragile building adjacent to deep excavation in Manhattan, New York. Proceedings of the 7th International Conference on Case Histories in Geotechnical Engineering, Wheeling, IL, Paper No.2.47.

Trabold, M., Aksman, B., and Giffen, R., 2012. Second Avenue Subway Project, New York: repair and refurbishment of existing structures adjacent to deep excavations. Proceedings of the Structures Congress 2012, Chicago, ASCE.

© 2016 Deep Foundations Institute

MICROPILES IN AN URBAN SETTING – TBTA VERRAZANO NARROWS BRIDGE HOV/BUS RAMPS, BROOKLYN, NY AND NYSDOT KOSCIUSZKO BRIDGE REPLACEMENT, BROOKLYN, NY

Brian T. Felber, HNTB Corporation, Parsippany NJ, USA, 973-434-3100, bfelber@hntb.com
M.D. Riegel, HNTB Corporation, Parsippany NJ, USA, 973-434-3100, mdriegel@hntb.com

ABSTRACT

Construction of foundation elements in an urban environment is often complicated by multiple constraints such as existing foundations, utility conflicts, maintenance and protection of traffic on high volume roadways, low overhead clearances, and vibration and displacement monitoring to reduce risks of impact to existing facilities. Micropiles are commonly a preferred foundation alternative in an urban setting to mitigate some of these risks. This paper presents examples in which micropiles helped reduce risk in an urban setting on the two subject infrastructure improvement projects. The case studies presented include the Verrazano Narrows Bridge HOV and Bus Ramp Improvements in Brooklyn, NY and the Kosciuszko Bridge Replacement in Queens and Brooklyn, NY. The paper details the micropile design, how risks were mitigated, and the complications to each of these projects associated with the urban setting.

Keywords: micropile, urban construction

INTRODUCTION

The paper begins with background information about the Verrazano Narrows Bridge HOV and Bus Ramp Improvements Project, followed by background information for the Kosciuszko Bridge Replacement Project. This introductory background information is followed by discussion of the urban site constraints, which controlled the foundation type selection for both projects. In closing, the paper discusses the micropile design process, load testing, and construction.

VERRAZANO NARROWS BRIDGE HOV & BUS RAMP IMPROVEMENTS BACKGROUND

Project Scope

The project consists of two new ramps; one designated for HOV / Bus traffic between Staten Island and the Gowanus Expressway, and one to be utilized for storing the barrier transfer vehicle. Also included is the complete reconstruction of Ramps B and F to accommodate horizontal and vertical alignment clearances from the new ramps, removal of the median of the upper level to add one lane, utilities improvements, stormwater improvements, and miscellaneous structural repairs. The new HOV / Bus Ramp was designed for reversible traffic flow to accommodate the demand of the peak traffic direction by movable barrier.

Geotechnical / Foundation Engineering Scope

The geotechnical work included a desk study review of existing plans, geotechnical reports, and geologic maps. This data was subsequently supplemented with a subsurface exploration program. Once completed, foundation design was performed for 25 proposed bridge substructures. Four existing battered pile-supported foundations and two shallow foundations were evaluated for increased loading. Upon completion of the foundation design, foundation plans, specifications, and an engineer's estimate were prepared. Foundation installation was observed on a part-time as needed basis.

Geologic Setting

The Verrazano Narrows Bridge site is located in the Atlantic Costal Plains Physiographic Province. Surficial soils include Artificial Fill and Holocene Salt Marsh Deposits. 150 to 180 feet of Terminal Moraine till deposits (Upper Pleistocene Deposits) placed by the Harbor Hill ice front during the Wisconsinin glaciation underlie the fill or Salt Marsh Deposits (Buxton 1999; Weidlinger 2007). The till

© 2016 Deep Foundations Institute

is underlain by 60 to 90 feet of Gardner Clay of the Pleistocene Epoch (Buxton 1999), which is highly plastic with SPT-N values ranging between 5 and 23 (Weidlinger 2007). Jameco Gravel deposits of the Pleistocene Epoch underlie the Gardner Clay (Buxton 1999), which is supported by Weidlinger (2007), where 25 to 80 feet of sand, gravel, cobbles, and bounders were encountered underlying the Gardner Clay. Precambrian gneiss bedrock underlies the site at a depth of roughly 350 or more feet (Buxton 1999; Weidlinger 2007).

Subsurface Conditions

Given the considerable thickness of the till deposits, which extend more than 160 feet below the ground surface, underlying soils are beyond the zone of interest for the foundation evaluation and design. Design stratification included 6 to 44 feet of fill at the surface, generally consisting of brown coarse to fine sand with varying amounts of gravel and silt with an average SPT N_{60} value of 29 blows per foot (bpf). The fill was underlain by a discontinuous stratum of black peat or fine grained organic soils generally between 0 and 8 feet thick, with an average SPT N_{60} value of 6 bpf. A discontinuous layer of low plasticity clay was encountered below the fill or peat, generally between 0 and 24 feet thick with an average SPT N_{60} value of 11 bpf. A discontinuous stratum of silty sand varying between 0 and 18 feet thick was encountered below the fill, peat, or low plasticity clay with an average SPT N_{60} value of 22 bpf. The underling till, which the micropiles were bonded in, was encountered at a depth between 8 and 45 feet below grade, on average 24 feet. The till was primarily brown well sorted mixture of coarse to fine sand, gravel, and fines, with an average SPT N_{60} value of 80 bpf. Groundwater was generally observed between 5 and 20 feet below the ground surface.

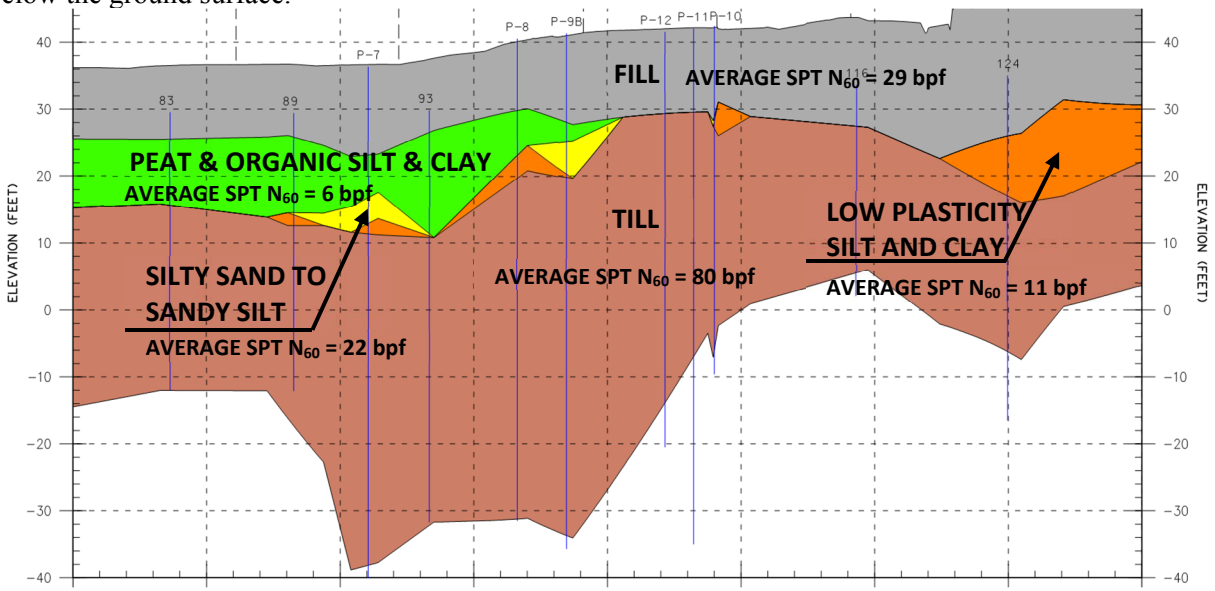


Fig. 1. Subsurface Profile Excerpt from Verrazano Narrows Bridge Project

KOSCIUSZKO BRIDGE REPLACEMENT BACKGROUND

Project Scope

HNTB served as the lead designer for the Skanska/Kiewit/ECCO III (SKE) team on the Kosciuszko Bridge Replacement Project Phase I design-build contract for the New York State Department of Transportation (NYSDOT). Phase I of the project involves the design and construction of the new eastbound structures of Interstate 278 over Newtown Creek from Brooklyn to Queens. The project runs between Morgan Avenue in Brooklyn and the Long Island Expressway Interchange in Queens (approx. 1.1 miles) and includes the staged demolition of the existing structures. This paper focuses on three micropile-supported abutments located at the Brooklyn Connector, identified as the Station 10+93 Abutment, the Morgan Avenue Begin Abutment, and the Morgan Avenue End Abutment.

© 2016 Deep Foundations Institute

Geotechnical / Foundation Engineering Scope
The geotechnical scope performed relevant to this paper included; review of soil borings, subsurface profile, soil properties, and settlement vs. depth plot prepared by the geotechnical design team. Axial and lateral analysis of the micropile group which included a deadman system to resist lateral loads, were performed to allow SKE to select the preferred foundation alternative based on cost, constructability, schedule, and risk reduction. Contract drawings, specifications, and an engineer's estimate were prepared. Proof and verification load tests were observed by the consultant.

Geologic Setting
The project site is situated in the Atlantic Coastal Plains Lowlands physiographic province, immediately east of the Manhattan Prong of the New England Upland province. The site is underlain by Cambrian-Ordovician Age metamorphic bedrock of the Hartland Formation, primarily gneiss of varying quality with a zone of highly weathered and decomposed rock of varying thickness overlying the competent rock. Intermittent, schist and marble bedrock have been reported to be present on site.

Overlying the bedrock is Cretaceous Raritan Formation soils, which exist as a confining layer, and are generally described as a light to dark gray, brown-red, pink red and gray white clay, silty clay and clayey to silty fine sand. The advance of the Wisconsinin glaciation roughly 15,000 years ago deposited Harbor Hill moraine across the site, overlying the Raritan Formation. The till of this moraine is comprised of an unsorted mixture of clay, silt, sand, gravel, cobbles and boulders. Surficial soils are variable in the upper 10 to 30 feet of the profile due to miscellaneous urban fill material that is comprised of a mixture of silt, sand, gravel and construction debris (e.g. brick, wood, trash, concrete and other materials). Groundwater levels at the three abutments were observed approximately 0 to 5 feet below the bottom of fill.

Subsurface Conditions
The surficial existing urban fill material is a highly variable mixture comprised of silt, sand, gravel, cobbles, brick fragments and wood. The average SPT N_{60} value is 17 bpf, which corresponds to a relative density of medium-dense. At the Station 10+93 Abutment, the Morgan Avenue Begin Abutment, and the Morgan Avenue End Abutment, the thickness of the fill was approximately 20 feet.

The fill is underlain by glacial till, predominantly silty sand with gravel, cobbles, and boulders (Cadwell 1989). The average SPT N_{60} value is 40 bpf, which corresponds to a relative density of dense. The thickness of the till was approximately 45 feet thick at the three abutments.

The contract required that foundations be limited in depth to remain a minimum of ten feet above the top of the underlying Raritan clay, for environmental reasons.

URBAN SITE CONSTRAINTS CONTROLLING FOUNDATION TYPE
Verrazano Narrows Bridge HOV / Bus Ramp Improvements
The Verrazano Narrows Bridge HOV / Bus Ramp Improvements project foundation design was in part controlled by the urban setting, which resulted in the following constraints:

- Limited options available for horizontal and vertical alignment of proposed HOV/Bus Ramp within TBTA Right-of-Way (ROW) due to limited clearances between numerous existing ramps
- Numerous existing foundations and utilities are present, limiting the footprint available for proposed foundations
- Existing battered pile supported foundations and battered pile supported retaining walls reduce available footprint further
- Existing shallow foundations in close proximity increase the risk of construction impact to existing foundations while in service

© 2016 Deep Foundations Institute

- Fort Hamilton Military Base access had to be maintained further limiting the potential foundation locations
- Existing ramps provided limited overhead clearance in some locations
- The need to maintain existing lanes in operation during construction
- Ability to erect structural steel given the congestion of the site and ramps in service

Accordingly, shallow foundations were considered but deemed inappropriate for a number of reasons. A spread footing solution would require excavation to a depth below the soft compressible soils to provide tolerable settlements, which would also require dewatering. Given the limited footprint between the existing and proposed foundations, sloped excavations were generally not feasible and temporary excavation support would be required. Clear distance from the existing battered piles or shallow foundations to the proposed foundations was limited proving problematic for temporary excavation support thereby increasing the risk of construction impact to the existing foundations. In addition, the lateral demands from braking, wind, and seismic loads were considerable given the pier heights in excess of 80 feet, resulting in considerable eccentricity and large footing sizes required to maintain stability. The additional excavation associated with shallow foundations was also a risk from a material disposal and archeological impact perspective due to the proximity of Fort Hamilton and the historic fills throughout the project site.

Driven piles were considered but deemed not the preferred alternative primarily because of drivability concerns given the presence of cobbles and boulders, and the potential for vibrations to affect existing foundations. Driven piles were also not preferred because of limited overhead clearance at some locations.

Drilled shafts were the second most viable foundation type considered, but were ultimately not selected due to overhead clearance, vibration, and limited working space for drilling equipment.

Reuse or retrofit of the existing battered concrete filled pipe piles, which were located in close proximity to the proposed Ramp B alignment was considered, but not advanced given the uncertain nature of the as-built foundations (multiple pile sections shown on record plans rendering it unclear which section was installed at a given location). Additionally challenges in establishing corrosion loss of existing piles to determine remaining service life provided another element of uncertainty and risk into the reuse approach.

Based on these constraints, micropiles were deemed the preferred foundation type given their ability to be installed in low overhead clearance, their small footprint, their ability to be advanced through cobbles and boulders, minimal installation vibration, large nominal unit side shear resistance, minimal excavation required for a shallow cap, and efficient ability to resist tensile loads. Micropiles were also advantageous because conflicts with existing footings required deep foundation elements be installed through existing pile caps and shallow foundations, through oversized core holes.

During the construction phase, two modifications to the proposed foundation layout were prepared to help accelerate the contractor's schedule. Proposed foundation J7 was originally designed such that several micropiles would be installed through the existing shallow foundation SPW-1 upon demolition of Pier SPW-1. The redesign of Pier J7 included two foundations and two piers constructed outside of the existing pier footprint, allowing construction to begin prior to demolition to accelerate the schedule.

Foundations J5/RB-1, J6/RB-2, and RB-3 originally required existing vertical and battered piles which were in conflict with the proposed micropiles, be removed after demolition of existing Piers SPWL-1, SPWL-2, and SPWL-3. The contract documents also included a performance-based requirement for the contractor to restore and verify the soil surrounding the piles, which were removed, was as dense as or

© 2016 Deep Foundations Institute

denser than shown by the pre-construction phase soil borings. However, to help accelerate schedule, the contractor demolished the existing piers and footings, exposing and surveying the pile heads. With this additional information, the design team was able to modify the proposed micropile array to avoid the existing battered and vertical piles and satisfy the axial, lateral, and structural demand.

Kosciuszko Bridge Replacement

The Kosciuszko Bridge Replacement project foundation design at the Station 10+93 Abutment, the Morgan Avenue Begin Abutment, and the Morgan Avenue End Abutment was controlled by the urban setting, which resulted in the following constraints:

- Low overhead clearance beneath the in service I-278 Brooklyn Queens Expressway (BQE)
- Proposed foundation elements need to be spaced to avoid proposed staged earth-filled embankments utilizing prefabricated modular retaining wall (T-Wall®) stems
- Proposed foundation elements need to be spaced to avoid or penetrate through existing shallow foundations without affecting these existing facilities, which remained in service during construction.
- Site specific rate of corrosion to steel elements was high, resulting in substantially reduced resistance to axial and lateral loads
- Contract requirements limited maximum depth of foundation elements, to remain a minimum of 10 feet above the top of Raritan Clay due to environmental constraints
- Proposed fill results in downdrag in existing and proposed fill from elastic settlement
- Preference to minimize excavation due to environmentally sensitive nature of the site

Shallow foundations were not viable due to the footprint of the existing shallow foundation, temporary excavation support, potential dewatering, and excavated material disposal reasons.

Driven piles were not preferred due to drivability concerns from cobbles and boulders, potential to impact existing shallow foundations from vibration, inefficiency associated with sacrificial steel rate, need to core through existing shallow foundation to accommodate pile driving at some locations, and most critically low overhead clearances.

Drilled shafts were not preferred due to the low overhead clearance, limited footprint available between existing shallow foundations and T-Wall® stems, and potential to impact existing shallow foundations from vibration.

Based on these constraints micropiles were deemed the preferred alternative, and the following micropile design alterations were compared:

- Downdrag in proposed fill might be reduced or eliminated by installing isolation casing, coating, or wrap.
- Downdrag in the existing fill was included in the micropiles axial demand, with the following alternatives considered to minimize its effects:
    - Pre-augering and installing a non-structural isolation casing through the existing fill, this was ultimately not selected due to cost and schedule impacts.
    - Coating the piles was ultimately not preferred due to survivability concerns and potential impacts to the grout-to-ground bond resistance. Bitumen and Slickcoat™ were considered as coating materials.
- Lateral resistance was ultimately resisted by a deadman system, but the following alternatives were also considered
    - Use of metallic MSE-type straps connected to the backwall to resist lateral load.
    - Battered micropiles which were ultimately not viable due to footprint and overhead space constraints, and p-delta effects exacerbated by downdrag. Therefore, the consultant

© 2016 Deep Foundations Institute

considered using vertical micropiles to resist the lateral demand, but due to the project's corrosion constraints, this alternative required an oversized casing be installed with the annular space filled with grout so that the inner casing could be relied upon. The micropile casing section properties would need to be reduced for thread reduction because the overhead clearance prohibited a continuous section of casing. The additional micropiles required to satisfy the lateral demand were not favorable from a cost and schedule perspective. The use of an inner casing to resist bending was not investigated for this project.

Based on these constraints, micropiles were proposed to resist axial demand only at the Station 10+93 Abutment, Morgan Avenue Begin Abutment, and the Morgan Avenue End Abutment. Axial demand from downdrag was included from the existing fill stratum, but not from the proposed fill stratum because the micropiles were isolated with sheets of polyethylene wrap in this zone prior to placing the proposed fill. The lateral resistance was provided by a reinforced concrete deadman tied to the abutment stem with steel tie rods. Figure 2 below shows the sequence of how the micropiles were installed and the deadman configuration utilized.

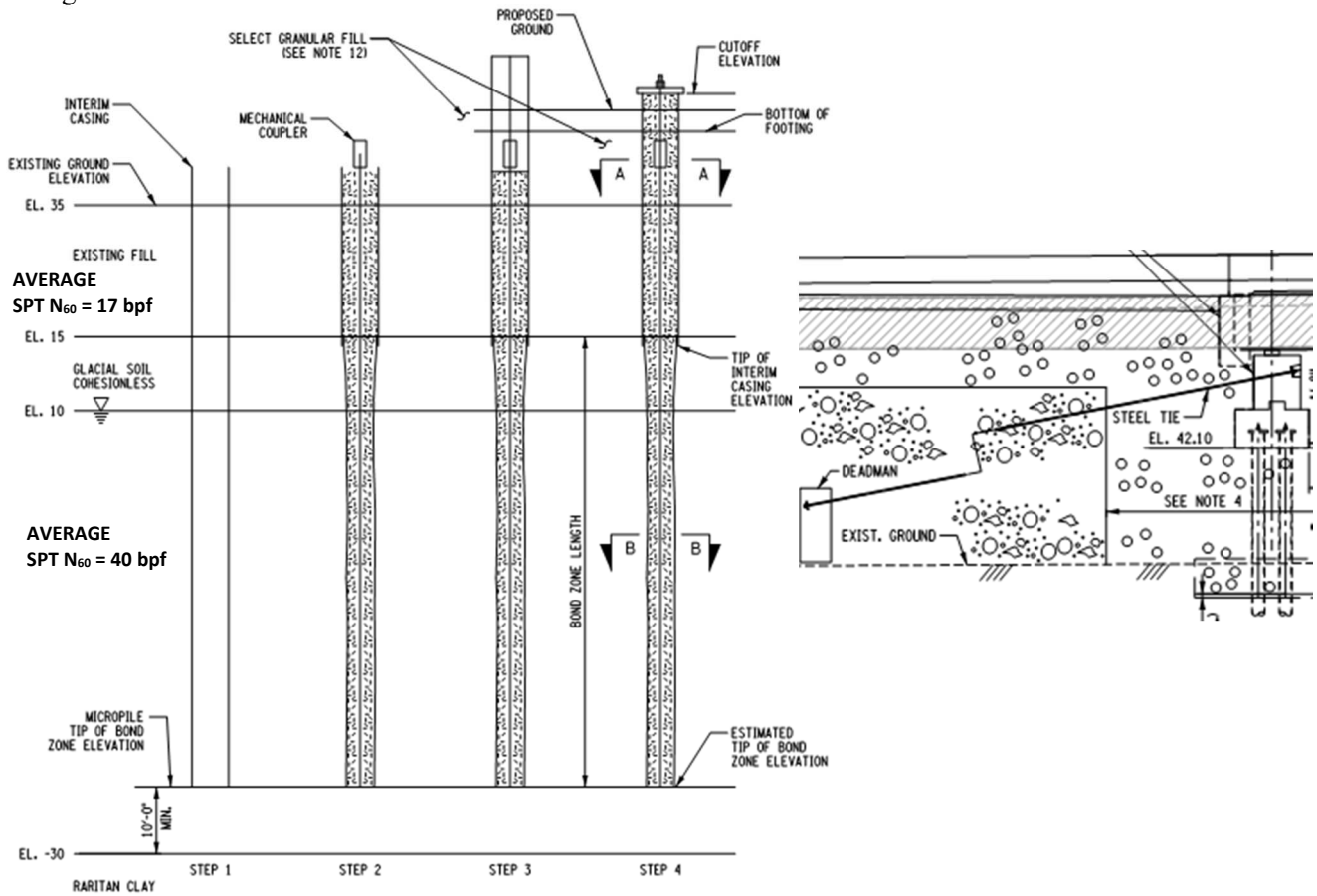


Fig. 2. Micropile Sequential Elevations and Reinforced Concrete Deadman Elevation

The micropile installation began by spinning casing from the existing ground surface to the bottom of bond zone elevation and cleaning out the casing (Step 1). Then the bar was placed in the hole and the micropile was tremie grouted up to roughly the existing ground elevation (Step 2). Subsequently, additional bar was coupled on and additional casing was spun on, to reach the micropile cutoff elevation (Step 3). The exposed portion of casing was double wrapped in sheets of polyethylene wrap to minimize the downdrag (Step 3). Upon completion of construction of the micropile cap and abutment stem,

© 2016 Deep Foundations Institute

MICROPILE DESIGN METHOD

Geotechnical Axial Resistance

Both projects were designed in accordance with AASHTO LRFD Bridge Design Specifications and used Type B, pressure grouted, micropiles bonded in dense to very dense glacial till, primarily sands with varying amounts of gravel and silt. Presumptive nominal unit grout-to-ground bond resistance values provided in AASHTO LRFD Bridge Design Specifications Table C10.9.3.5.2-1for this material and grouting method vary from 2 to 7.5 ksf. Presumptive nominal unit grout-to-ground bond resistances of 4 and 5 ksf was used for the estimated bond lengths shown on the Verrazano Narrows Bridge HOV/Bus Ramp and Kosciuszko Bridge Replace Contract Drawings, respectively.

The nominal grout-to-ground bond resistance (R_S) was calculated using equation 1 below.

$$R_S = \pi d_b \alpha_b L_b \quad [1]$$

Where, d_b = diameter of micropile drill hole through bonded length (ft)
A_b = nominal micropile grout-to-ground bond resistance (ksf)
L_b = micropile bonded length (ft)

A resistance factor (φ_{stat}) of 0.7 for the grout-to-ground bond resistance was used because verification load testing was proposed, in accordance with AASHTO LRFD Bridge Design Specification Table 10.5.5.2.5-1. Tip resistance was neglected. Therefore, the factored grout-to-ground bond resistance in compression and tension was calculated using equation 2 below.

$$R_R = \varphi_{stat} R_S \quad [2]$$

Structural Resistance

Plunge length was not relied upon to reduce the demand at the top of the bond length, therefore, the structural axial compressive resistance and axial tensile resistances were controlled by the bond length.

The nominal axial compressive structural resistance was calculated using Equations 3, and the factored axial compressive structural resistance was calculated using Equation 4.

$$R_{n\,CU} = 0.85\,[0.85\,f'_c A_g + f_y\,A_b] \quad [3]$$

Where, f'_c = specified compressive strength of micropile grout at 28 days (ksi)
f_y = specified minimum yield strength of reinforcement bar or stress in steel reinforcement bar at a strain of 0.003, whichever is less (ksi)
A_g = cross-sectional area of grout within micropile (in^2)
A_b = cross-sectional area of steel reinforcing bar (in^2)

$$R_{CU} = \varphi_{CU}\,R_{n\,CU} \quad [4]$$

Where, φ_{CU} = resistance factor for the uncased section in compression = 0.75

The nominal axial tension structural resistance was calculated using equation 5, and the factored axial tension structural resistance was calculated using equation 6.

$$R_{n\,TU} = f_y\,A_b \quad [5]$$

Where, f_y = specified minimum yield strength of reinforcement bar or stress in steel reinforcement bar at a strain of 0.003, whichever is less (ksi)
A_b = cross-sectional area of steel reinforcing bar (in^2)

$$R_{TU} = \varphi_{TU}\,R_{n\,TU} \quad [6]$$

Where, φ_{TU} = resistance factor for the uncased section in compression = 0.80

© 2016 Deep Foundations Institute

In addition, the combined axial and flexure resistance was checked, where applicable, in accordance with AASHTO LRFD Bridge Design Specifications:

$OD_i = Casing\ Outside\ Diameter\ (not\ considering\ corrosion\ and\ thread\ reduction)(in)$ [7]

$t_i = Casing\ Wall\ Thickness\ (not\ considering\ corrosion\ and\ thread\ reduction)$ (in) [8]

$t = \frac{ti}{2} =$

$Casing\ Wall\ Thickness\ Accounting\ for\ Thread\ Reduction\ if\ Corrosion\ not\ Controlling\ (in)$ [9]

$OD = \frac{OD_i}{2} = Casing\ Outside\ Diameter\ Accounting\ for\ Thread\ Reduction\ (in)$ [10]

$d_{bar} = Diameter\ of\ Reinforcing\ Bar\ (in)$ [11]

$n = \frac{Elastic\ Modulus\ of\ Steel}{Elastic\ Modulus\ of\ Grout} = Modular\ Number\ (dim.)$ [12]

$S_{casing} = \frac{\pi(OD^4-(OD-2t)^4)}{32\ OD} = Elastic\ Section\ Modulus\ of\ Casing\ (in^3)$ [13]

$S_{bar} = \frac{\pi(d_{bar}{}^3)}{32} = Elastic\ Section\ Modulus\ of\ Reinforcing\ Bar\ (in^3)$ [14]

$S_{concrete} = \frac{\pi(((OD-2t)^4)-(d_{bar}{}^4))}{32\ (OD-2t)} = Elastic\ Section\ Modulus\ of\ Concrete\ (in^3)$ [15]

$S_{ccomposite} = S_{casing} + S_{bar} + \frac{S_{concrete}}{n} Elastic\ Section\ Modulus\ of\ Casing\ (in^3)$ [16]

$Z_{casing} = \frac{(OD^3-(OD-2t)^3)}{6} = Plastic\ Section\ Modulus\ of\ Casing\ (in^3)$ [17]

$Z_{bar} = \frac{d_{bar}{}^3}{6} = Elastic\ Section\ Modulus\ of\ Casing\ (in^3)$ [18]

$P_u = Axial\ Compressive\ Load\ per\ Micropile\ (kips)$ [19]

$A_c = \pi[(\frac{OD}{2})^2 - [(\frac{(OD-2t)}{2})^2] = Cross\ Sectional\ Area\ of\ Casing\ (in^2)$ [20]

$R_{ncc} = 0.85\ f'c\ A_g + f_y(A_c + A_b) =$

$Nominal\ Structural\ Resistance\ of\ Cased\ Section\ in\ Compression\ (kips)$ [21]

$\phi_c = 0.8 = Resistance\ Factor\ for\ Axial\ Compression\ (dim.)$ [22]

$P_r = R_{ncc}\ \phi_c = Factored\ Structural\ Resistance\ of\ Cased\ Section\ in\ Compression\ (kips)$ [23]

$M_{ux} = Factored\ Moment\ per\ Micropile\ about\ X\ Axis\ (kip-in)$ [24]

$M_{uy} = Factored\ Moment\ per\ Micropile\ about\ Y\ Axis\ (kip-in)$ [25]

$M_{ps} = f_{y\ casing}\ Z_{casing} + f_{y\ bar}\ Z_{bar} = Nominal\ Plastic\ Moment\ Resistance\ (kip-in)$ [26]

$M_{yc} = f_y\ S_{composite} = Nominal\ Yield\ Moment\ Resistance\ (kip-in)$ [27]

$M_n = M_{ps}\ if\ \frac{OD}{t} < 2\sqrt{\frac{E}{f_y}} = Nominal\ Moment\ Resistance\ (kip-in)$ [28]

$M_n = M_{yc}\ if\ 2\sqrt{\frac{E}{f_y}} < \frac{OD}{t} \leq 8.8\sqrt{\frac{E}{f_y}} = Nominal\ Moment\ Resistance\ (kip-in)$ [29]

$\phi_c = 1.0 = Resistance\ Factor\ for\ Flexure\ (dim.)$ [30]

$M_r = \phi_f\ M_n = Factored\ Flexural\ Resistance\ (kip-in)$ [31]

$if\ \frac{P_u}{P_r} < 0.2\ then\ \frac{D}{C} = \frac{P_u}{2P_r} + (\frac{M_{ux}}{M_r} + \frac{M_{uy}}{M_r}) = Demand\ to\ Capacity\ Ratio\ (dim.)$ [32]

$if\ \frac{P_u}{P_r} \geq 0.2\ then\ \frac{D}{C} = \frac{P_u}{P_r} + \frac{8}{9}(\frac{M_{ux}}{M_r} + \frac{M_{uy}}{M_r}) = Demand\ to\ Capacity\ Ratio\ (dim.)$ [33]

Geotechnical Lateral Resistance

For the Verrazano Narrows Bridge project, the micropile groups were modeled using Bridge Software Institute's FB MultiPier Software, which uses p-y, t-z, Q-z curves to model the micropile group's response to lateral and axial loading. Deflections and rotations at the center of cap elevation were transposed up to the bearing elevation assuming the piers were rigid. The FB Pier lateral analysis provided factored axial compressive load and factored axial uplift load per micropile, and factored

© 2016 Deep Foundations Institute

moments about the x and y axis per pile which were used to evaluate the geotechnical and structural resistance of the micropiles and micropile cap.

For the Kosciuszko Bridge project, longitudinal lateral loads in the direction towards the span were resisted with a reinforced concrete deadman system connected to the abutment stem with steel tie rods. Longitudinal lateral loads in the direction away from the span were resisted by the passive earth pressure acting against the backwall. An intermediate value of passive earth pressure between the at rest earth pressure and the full passive earth pressure was determined to satisfy force and moment equilibrium, and used to estimate the displacement required to mobilize the resistance required. The steel tie rods were tensioned to the service loads to minimize deflections.

LOAD TESTING

Verrazano Narrows Bridge HOV & Bus Ramp Improvements Load Testing Program

The Verrazano Narrows Bridge HOV & Bus Ramp Improvements load testing program included sacrificial micropiles for verification load testing. Two verification load tests were performed in axial compression in accordance with ASTM D1143, and one verification load test was performed in axial tension in accordance with ASTM D3689, to the nominal resistance. In addition, 32 proof load tests were performed to 0.7 times the nominal resistance in axial tension in accordance with ASTM D1143. The micropiles were constructed with 10.75" OD x 0.5" Wall API N80 Casing and a single 75 ksi no. 18 bar.

Kosciuszko Bridge Replacement Load Testing Program

The Kosciuszko Bridge Replacement Project included one sacrificial micropile of the same diameter and bond length as the production micropiles, installed immediately up station of Morgan Avenue End Abutment, and was considered representative of the Station 10+93 Abutment, Morgan Avenue Begin Abutment, and Morgan Avenue End Abutment subsurface conditions. The sacrificial micropile, referred to herein as Test Micropile 1, was tested statically in tension to verify the proposed nominal unit grout-to-ground bond resistance. This verification load test was conducted to 753 kips, 1.4 times the maximum nominal resistance required for the three abutments (536 kips at the Station 10+93 Abutment). In addition, three static axial tension proof load tests were performed; one on a micropile from each of the three abutments. These tests were conducted to 0.7 times the nominal resistance (Factored Resistance) to prove the grout-to-ground bond resistance is adequate.

Test Micropile 1 was installed with an as-built bond length and cased length are 35.7 feet and 21.5 feet, respectively. A bond zone diameter of 11.75 inches was achieved using the Type B Pressure Grouting methods. 11.75" OD x 0.534" wall API N80 casing was used. The verification load test was installed with a single uncoated 3" diameter grade 150 threaded bar.

Loads were applied in increments using a calibrated hydraulic test jack and pressure gauge, and the vertical movements of the test pile thread bar were measured. As a secondary monitoring system, a vibrating-wire load cell was used to measure the applied load at the top of the pile. Three dial gauges were used to measure the vertical movement of the bar under the load increments. The dial gauges were mounted to an independent reference frame system. A piano wire and machine scales were also used as backup optical monitoring methods for the test. The dial gauges were graduated in increments of 0.001 in. Test Micropile 1 was loaded in accordance with ASTM D3689, Procedure A.

Load Testing Results

Table 1 below summarizes the four verification load test results from both projects. None of the four tests was conducted to failure, so the values reported are the maximum load verified. These four verification load tests in conjunction with the 35 proof load tests in glacial till in Brooklyn suggest the nominal unit grout-to-ground bond resistance in this material for Type B, pressure grouted, is generally closer to the

© 2016 Deep Foundations Institute

upper bound or in excess of the presumptive estimates provided in AASHTO. However, the variable nature of till and the variation in installation methods could result in significant variation.

Table 1: Micropile Verification Load Test Summary

Project	Load Test Number	Nominal Unit Grout-to-Ground Bond Resistance Verified (ksf)
Verrazano Narrow Bridge HOV/Bus Ramps	TP-1	4.2
Verrazano Narrow Bridge HOV/Bus Ramps	TP-2	7.0
Verrazano Narrow Bridge HOV/Bus Ramps	TP-3	7.0
Kosciuszko Bridge Replacement Phase I	Test Micropile 1	6.9

Note: None of the above tests was conducted to failure; therefore, nominal unit grout-to-ground bond resistance may be in excess of the values reported.

CONCLUSION

The Verrazano Narrows Bridge HOV & Bus Ramps Improvements and Kosciuszko Bridge Replacement Projects are examples of why micropiles are well suited for sites with urban constraints, which include low overhead clearances, congestion of existing utilities, close proximity to existing foundation, ability to be installed through existing foundations, and ability to be installed below or offline to aid in maintenance and protection of traffic on high volume roadways. Although not discussed in this paper, a robust monitoring program (biaxial tiltmeters, automatic total station (AMTS) monitoring of optical survey prisms, settlement platforms, inclinometers, crack gauges, pre and post construction surveys, etc. as required) should be included during urban construction to reduce the risk of construction impacts to existing structures and utilities.

In addition, the load testing programs for Type B, pressure-grouted micropiles in glacial till from two sites in Brooklyn, NY suggests that the nominal unit grout-to-ground bond resistance is likely in excess of 7 ksf, but due to the variable nature of till and micropile installation methods should be verified on a project specific basis.

REFERENCES

AASHTO. “AASHTO LRFD Bridge Design Specifications”. 6th Ed. 2012.

Ammann & Whitney Consulting Engineers. “Triborough Bridge and Tunnel Authority Narrows Bridge Contract NB-12 Brooklyn Approach”. November 15, 1961.

ASTM. Designation D3689/D3689M – 07 (Reapproved 2013). “Standard Test Methods for Deep Foundations under Static Axial Tensile Load”. July 2013.

Baskerville, C.A. “Bedrock and Engineering Geology Maps of New York County and Parts of Kings County and Queens Counties, New York and Parts of Bergen and Hudson Counties, New Jersey: U.S. Geological Survey Miscellaneous Investigation Series Map I-2306 . 1994.

Buxton, H.T., Shernoff, K. “Ground-Water Resources of Kings and Queens Counties, Long Island, New York”. U.S. Geological Survey Water Supply Paper 2498. 1999.

Cadwell, D.H. “Surifical Geologic Map of New York - Lower Hudson Sheet”. 1989

FHWA. “Publications FHWA-NHI-05-039, Micropile Design and Construction”. December 2005.

NYSDOT. “Static Pile Load Test Manual”. GCP-18, Revision #3, April 2007.

Weidlinger Associates Inc. “Seismic Assessment of the Approaches and the Lilly Pond Ave. Bridge Report”. Triborough Bridge and Tunnel Authority Verrazano Narrows Bridge Project VN-17. May 30, 2007.

© 2016 Deep Foundations Institute

PILED-RAFT FOUNDATIONS IN BELARUS

Sernov V. A., Belorussian National Technical University, Minsk, Belarus, +375297693703, sernoff2@yandex.ru

Abstract. One of the ways to increase the bearing capacity of a piled foundation is to take into account soil resistance in the base of the raft. Piled raft is similar to shallow foundation and can transfer significant part of the load into the base. It allows reducing number of piles in the foundation or shortening their length. As a result building terms and foundation costs reduce considerably. However, nowadays in Belarus there is no reliable and suitable in design practice methods of calculation of piled-raft foundations. In order to devise such methods we have analyzed the results of piled foundation tests fulfilled by various authors up to date and have carried out series of field and laboratory investigations in Minsk. The most important results of the investigations are provided in the article. Methods of analysis of piled-raft foundations are described.

Keywords: pile, raft, foundation, settlement, efficiency.

INTRODUCTION

Pile foundations of late years are used extensively in connection with the increased number of storeys and load increment on the soil. Often pile foundations are applied in comparative favorable ground conditions at the surface of the base. In such cases the increase of the bearing capacity of foundations and the reduction of construction cost are questions of primary importance for designers. One of the ways to increase the bearing capacity of a piled foundation is to take into account soil resistance in the base of the raft. Piled raft is similar to shallow foundation and can transfer significant part of the load into the base. It allows reducing number of piles in the foundation or shortening their length. As a result, building terms and foundation costs are reduced considerably. However, nowadays there is no reliable and suitable in design practice methods of calculation pile foundations with bearing rafts. In order to devise such methods we have analyzed the results of piled foundation tests fulfilled by various authors up to date and have carried out series of laboratory and field investigations.

Long before the constitution of the first piled-raft foundations in the Soviet Union there were attempts to consider soil resistance in the basis of isolated and strip grillages. Such bases can be considered as separate fragments of the piled-raft foundation. Prof. A. A. Bartolomey had tested more than 70 pile foundations of natural size in different ground conditions. The length of piles was 3 … 12 m (Бартоломей 1995). The observed results show that the raft carries about 10 … 12% of the total load applied when length of piles is over 9 m and space between piles is a=3d. Bearing capacity of the raft is about 35 … 40% when the length of piles is 5 … 8 m and a=6d. Prof. Golubkov has tested 2 prismatic piles (cross section: 350x350 mm, L=3800 m) and 2 pyramidal piles (cross section: head - 600x600 mm, foot – 100x100 mm, L=3000 m). One of the piles was tested with a raft and the other one without a raft. Significant influence of the raft on total bearing capacity was determined, the more the settlement was the more it influenced on the raft. Bearing capacity of the raft was 27,5% in foundation with prismatic pile and 42% with pyramidal pile (Голубков et al. 1971).

Laboratory researches of soil stress conditions in the base of piled-raft foundations were executed by Kozachok (Козачок 1979). The researches show that distribution of vertical stress in the base of a raft is similar to a foundation plate on the natural basis. Stress diagram of different groups of piles with high and low rafts are given in fig. 1.

© 2016 Deep Foundations Institute

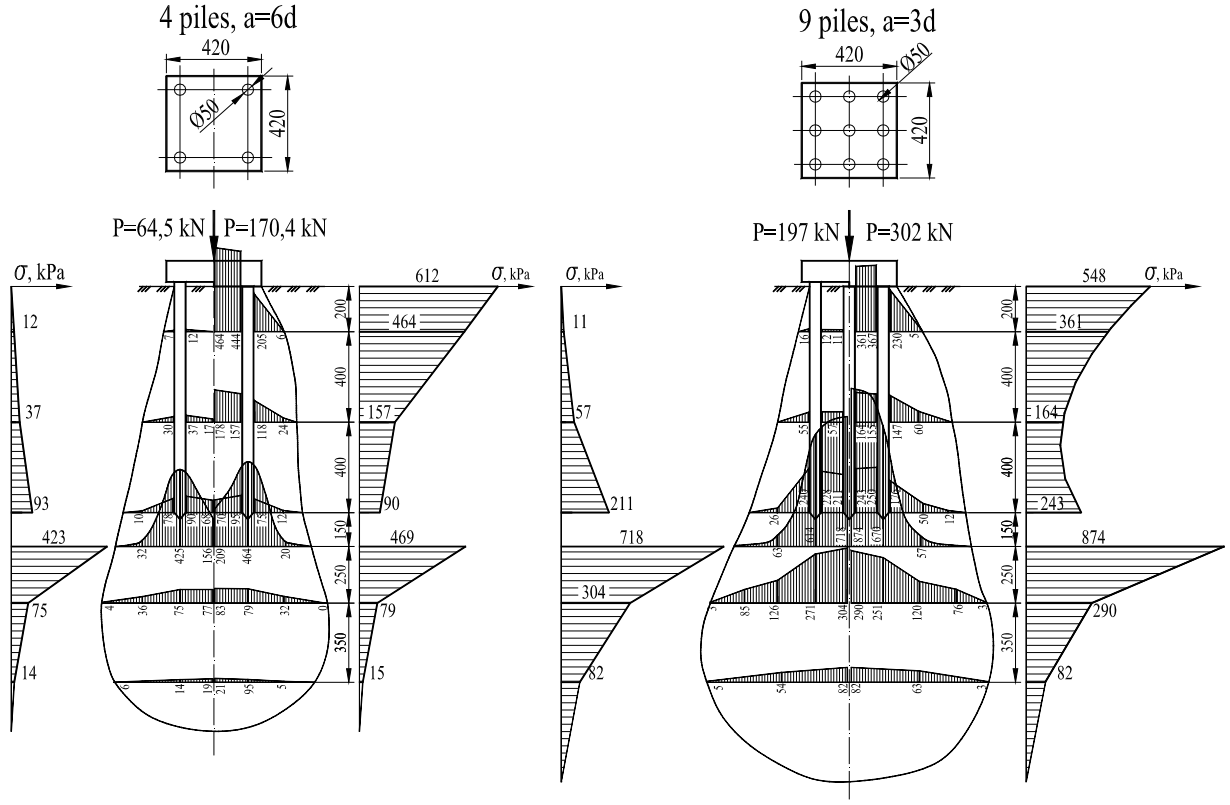


Fig. 1. Soil stress conditions in the base of piled and piled-raft foundations

The quantity of piles in group varied. At interaction of a raft with the base the part of loading is transferred to the top layers of the soil and the bearing capacity of the base is used more fully. Stress of the soil between piles is determined by friction forces along their side surfaces and the raft pressure upon soil. Friction forces increase with depth, stress from a raft, on the contrary, dissipates. As a result the saddle diagram with the minimum value in a point of equal tension from friction forces alongside surfaces of piles and resistance of a raft was generated.

MODEL TESTS

The part of the load that the raft carries increases when the pile length is reduced and the space between piles is increased. Some test results carried out by different authors confirm that their aim of the model tests was to determine the main factors of pile-raft-soil interaction. Model investigations were divided into small-scale and large-scale tests.

The object of the small-scale tests is to research the soil deformations under the raft in pile space. Models of driving piles (cross section 20x20 mm and length 150 and 300 mm) were tested in the sand-filled test rig with transparent front wall (Fig. 2). The soil was laid in the tray with layerwise compaction. Indicative strips were made of chalk through 50 mm. The load was applied with leverage and weights.

Deformations of the soil in the base were fixed persistent by means of photofixation in the time of pile driving and loading of the groups. Significant surface warp of indicative strips was detected during the process of pile driving.

After driving the pile tops were combined with the raft. Pile groups were subjected to static load. In the first place the high-raft pile foundations (without contact between the raft bed and the soil) were tested. Observational results show the slipping of the lateral surface of the piles relative to surrounding ground.

© 2016 Deep Foundations Institute

Additional minor displacements of the soil were found out only in the immediate vicinity of piles and they did not occur away from lateral surfaces (Сернов 2008).



Fig. 2. Test rig (on the left) and indicative strips warp in process of pile driving (on the right)

In the case of testing of the pile foundations with load-bearing raft the significant additional displacements of the soil in the pile space were observed. The settlement of the ground layers are diminished with depth similarly to shallow foundation (Fig. 3).

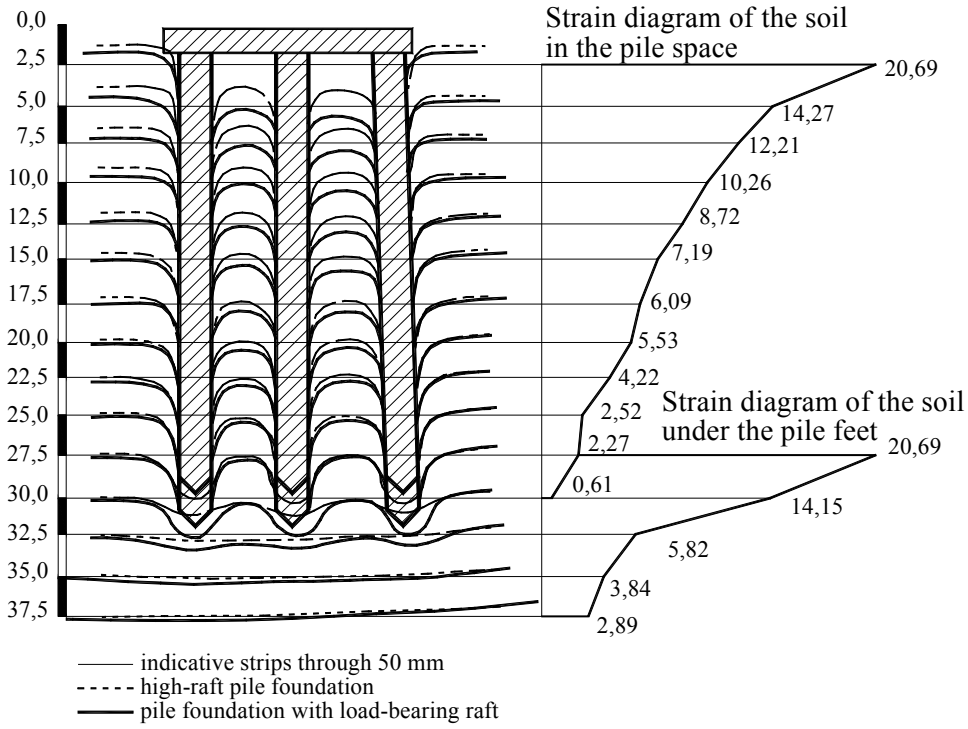


Fig. 3. Ground deformation in the base of pile foundation

The results of research show that the soil under the raft in the pile space does not settle side by side with a high-raft pile group and can resist a considerable part of the external load.

© 2016 Deep Foundations Institute

The aim of the large-scale tests is to estimate efficiency of the raft consist of bored piles in sandy soil. Investigations have been performed on the Test Site of Geotechnics of Belorussian National Technical University. Large-scale model tests of deep-raft and high-raft pile foundations are shown in fig. 4. The single piles, raft, groups of piles and piled-raft foundations were tested with static load.

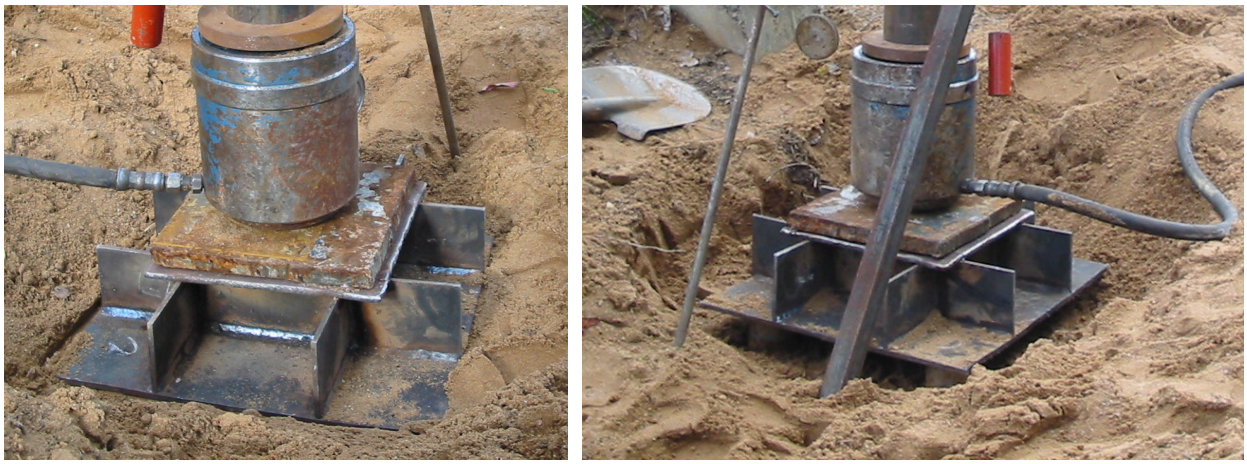


Fig. 4. Large-scale model test of the deep-raft (on the left) and the high-raft piled foundations (on the right)

The raft was made as rigid square metal stamp (b=500 mm). Pile foundations consisting of 1, 4, 6 and 9 bored piles with length of 1000mm and 2000mm and diameter of 60mm were tested both with deep and high rafts. The layout of piles in the groups is shown in fig.5. The results of pile foundation tests are represented in figures 6 and 7.

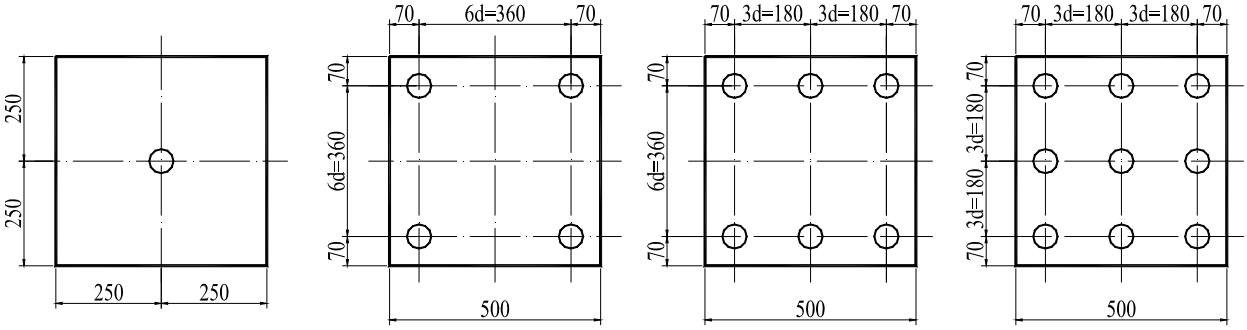


Fig. 5. The layout of piles in the groups of large-scale models of pile foundations

The large-scale model test results confirm high efficiency of raft-soil interaction in full band of size-shape factors of pile foundation. In case of deep-raft pile foundation (or piled raft foundation) bearing capacity is significantly increased. The major bearing factors influencing the raft interaction are pile length, pile space and settlement on the foundation.

The load-settlement diagrams presented in fig. 6 and 7 show that minimal increment of bearing capacity of the foundation occurs in case of 9 piles with length of 2000mm (by 18%). In other cases bearing capacity increases with pile length shortening, pile space extension and settlement rising.

© 2016 Deep Foundations Institute

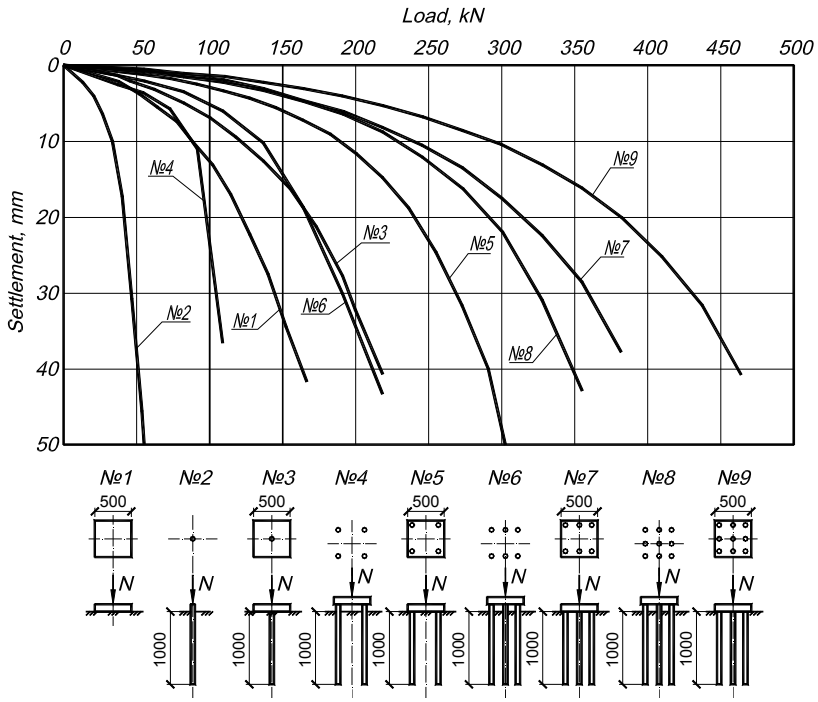


Fig. 6. The results of large-scale model tests of high-raft and deep-raft piled foundations consisting of bored piles with length of 1000mm

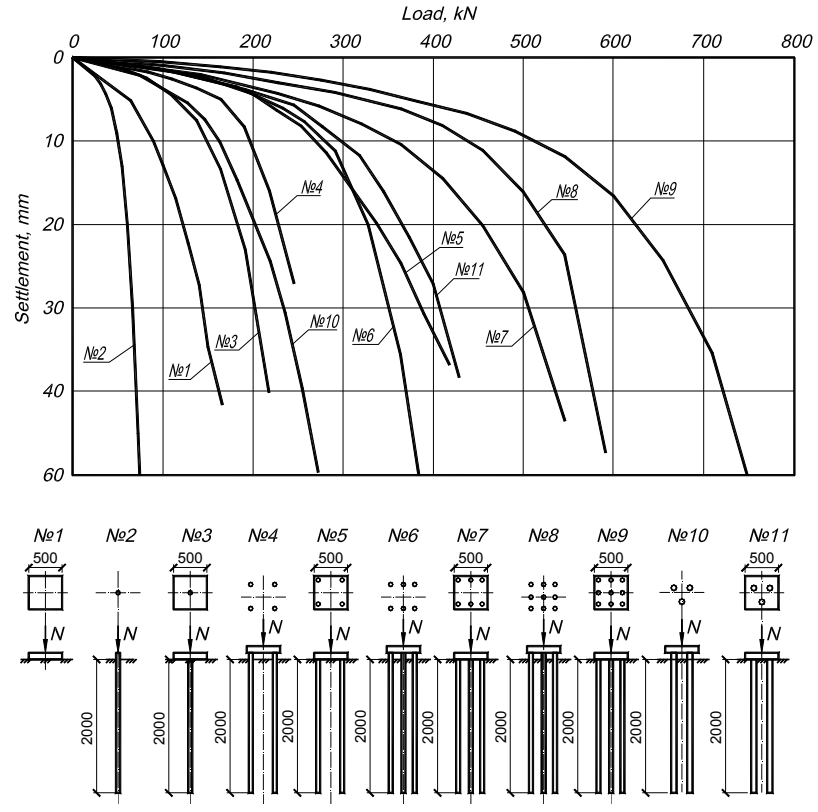


Fig. 7. The results of large-scale model tests of high-raft and deep-raft piled foundations consisting of bored piles with length of 2000mm

© 2016 Deep Foundations Institute

FIELD TESTS

Building sites of Minsk are characterized by complicated geological conditions. Quite often the firm soils are located at the surface but at a depth of 5-10m soft ground layers occur. Frequently filled-up ground is located at the surface. In these cases conventional long driven piles are used to transmit the load at deep-laid firm soil. The length of such piles could be 20m and more. The alternative foundation in such ground conditions consists of tapered piles with bearing raft. The sloping surfaces of tapered piles compact ground between piles and around the foundation. Bearing capacity of raft and lateral surface of piles considerably increases. Bearing capacity of the raft with tapered piles is much more than the bearing capacity of the raft with uniform cross-section piles. Stresses in the base of the foundation with tapered piles are dissipated in the top slices and do not reach soft ground layer at depth.

The results of tests prove efficiency of vibrostamped cast-in-situ tapered piles with bearing rafts when thick layer of filled-up ground is located at the surface. Strength characteristics of filled-up ground considerably improved due to consolidation. Sloping lateral pile faces eliminate negative friction. Compacted filled-up soil becomes the bearing layer both for piles and for rafts.
To estimate efficiency of piled foundations with bearing rafts static tests of single piles and couples of pile with the raft were carried out at different sites of Minsk in various ground conditions (Сернов 2009).

At the site in Belsky street 148 in Minsk firm loam soils were located at the surface but at a depth of 10m and more a soft loam soils with peat layers were found. There were two alternate versions of foundations. The first one was long driven prismatic piles with the length of more than 12m to transmit the load at deep-laid firm soil. The second alternate was short vibrostamped cast-in-situ tapered piles (L=3-4m) with rammed dry concrete mix at the pile foot and bearing rafts to transmit the load at the surface layer of firm soil. Technical and economic assessment shows that the cost of the second alternate is far less. Bearing capacity of vibrostamped tapered piles was increased by 80% by means of ramming dry concrete mix at the pile foots and then by 30% by means of bearing raft (fig. 8). Raft ratio (Kr=Fpr/Fp= bearing capacity of piled-raft foundation/ bearing capacity of piled foundation) in such case Kr=1.30.
The subsoil in the site in Prityzky Street consists of loessial loam, fine sand and peat layers. The first alternate versions of foundation was driven prismatic piles with length up to 20m. The second alternate was vibrostamped cast-in-place tapered piles with widening at the pile feet (the length of the piles is 3 and 4 m, diameter at the pile top is 0.5m, diameter at the pile foot is 0.3m).

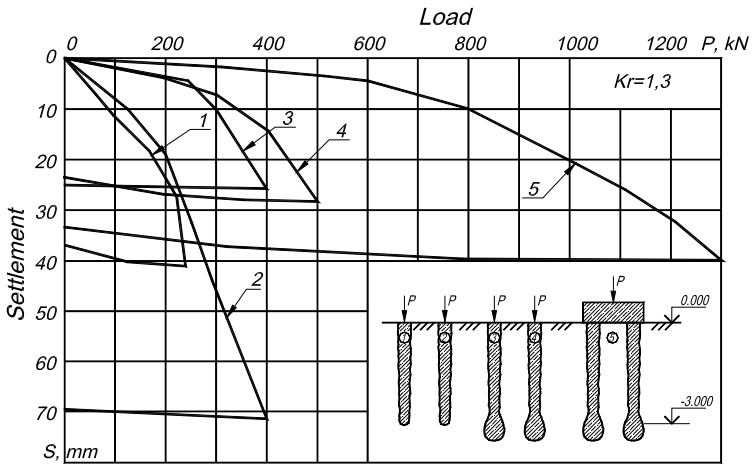


Fig. 8. The results of tests of single piles and 2 piles with raft in Belsky Street 148: 1, 2 — single piles; 3, 4 — single piles with widening at the pile foot; 5 — 2 piles with a raft (1.8x0.9 m)

© 2016 Deep Foundations Institute

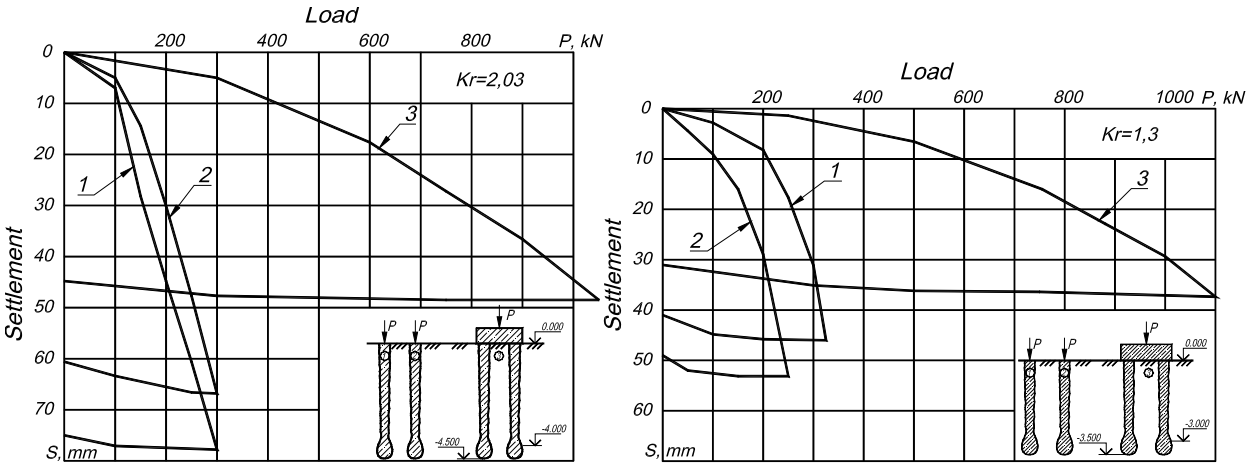


Fig. 9. The results of tests of single piles and 2 piles with raft in Prityzky Street: 1,2 — single piles; 3 — 2 piles with a raft 1.8m x1.2m (on the left) and 1.9mx0.4m (on the right)

Single tapered piles and two fragments of foundation were tested with static load. (fig. 9). Load-settlement diagram S = f(N) shows that the raft interacting with subsoil increases bearing capacity of the foundation by 30-103% (Kr=1.30÷2.03). The magnitude of raft ratio Kr depends on raft area and ground conditions in the base of the piles and the raft (Сернов 2009).

The similar results were obtained at the site in residential quarter of Burdeinogo Street and Jakubovskogo Street. two single bored piles and the same piles with a raft fragment were tested with static load (fig. 10).

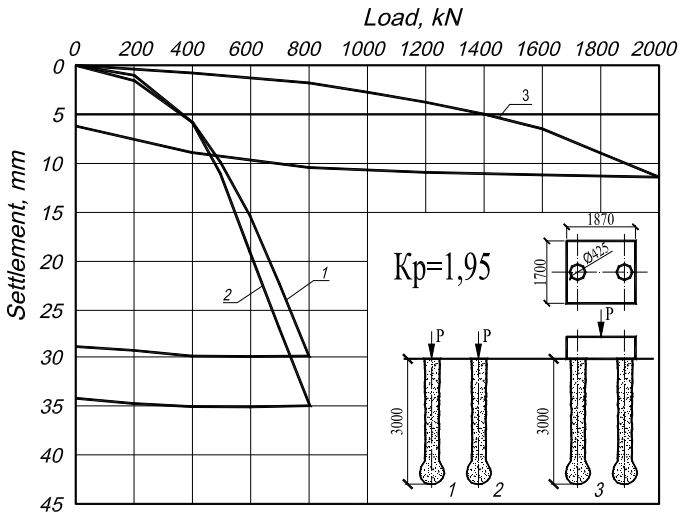


Fig. 10. The results of tests of single piles and 2 piles with raft in residential quarter of Burdeinogo Street and Jakubovskogo Street: 1,2 — single piles; 3 — 2 piles with a raft (1.7x1.87 m)

Load-settlement diagram S = f(N) shows that the bearing capacity of the foundation was increased by 95% (Kr=1.95).

METHODS OF ANALYSIS OF PILED-RAFT FOUNDATIONS

Analysis of model and field tests carried out in the Laboratory and Test Site of Geotechnics of Belorussian National Technical University as well as on various building areas in Minsk and other cities allows detecting the basic factors which affect the raft-soil interaction and determining range of applications of pile

© 2016 Deep Foundations Institute

foundations with load-bearing rafts. Design methods of ultimate vertical load and settlement of piled-raft foundations were developed (Сернов 2011). The results of theoretical and experimental researches performed by various authors were taken into consideration in development of the methods.

It has been found experimentally that the soil under the raft in the pile space does not settle with a pile group and in spite of traditional design approaches can resist a considerable part of the external load. Experimental total vertical stress diagrams in the base of various deep-raft pile foundations were carried out by Kazachok in the 1970s (Казачок 1979). Contrastive analysis of experimental data and estimated stress diagrams received with linearly elastic semispace theory show that the experimental curves are similar to theoretical diagrams. Calculating error is not more than 5%. Based on the results of our investigations we can draw a conclusion that stress and depth of compressed layer of the soil in the base of a raft and shallow foundation are similar and can be described with similar methods.

The ultimate vertical load carried by pile foundations with bearing raft is calculated:

$$N = N_r + N_{pf}\,, \qquad [1]$$

$$N_r = \gamma_{cr} p_r A_r\,, \qquad [2]$$

Were N_r = ultimate vertical load carried by pile group, N_{pf} = ultimate vertical load carried by the raft, p_r = average contact pressure under the raft bed depends on ground conditions and the assumed settlement of pile group, A_r = raft area without total cross-sectional area of the underlying piles, γ_{cr} = factor depends on ground surface preparation under the raft bed:

γ_{cr} =1.0 for compacted stone bed,
γ_{cr} =0.9 for compacted sandy soil,
γ_{cr} =0.8 for compacted clay soil,

The settlement of pile foundations with bearing raft is calculated:

$$S_{pf} = S_p + S_{add} \qquad [3]$$

S_p = settlement of pile group under the load N_r, S_{add} = additional settlement of pile group arising from additional vertical stress under the pile feet in case of $H_c > L$ (H_c = compressed layer of the soil, L – pile length).
Detailed description of computing methods of pile foundations with bearing rafts, range of applications, test and control methods are given in the article (Сернов 2011).

IMPLEMENTATION OF THE INVESTIGATION RESULTS

The experience of useing vibrostamped tapered piles was adopted at the site of Orthodox Church in Sukharevo district in Minsk (fig. 11).
Ground conditions under the raft:
1) - dust clay sand (E=18MPa, h=4m);
2) - soft sandy clay (E=6MPa, h=2m);
3) - sandy clay with organic residues (E=10MPa, h=1,5m);
4) - peat (E=3MPa, h=2,5m);
5) - firm sand (E=25MPa).
The first alternate was a foundation consisting of 480 driven prismatic piles with length of 14m and cross sections 0.3x0.3 and 0.35x0.35m.

© 2016 Deep Foundations Institute

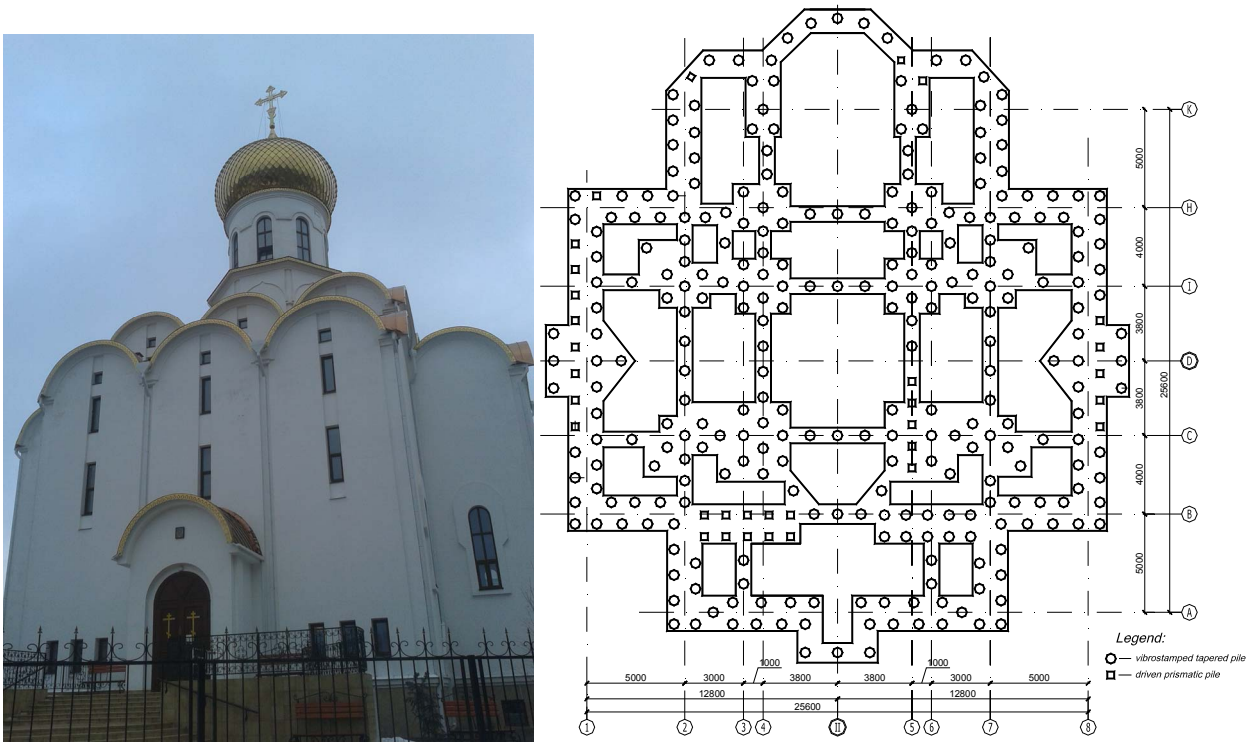


Figure 11. Orthodox Church: piled-raft foundation

The most reasonable decision in such ground conditions is to transfer load onto relatively firm upper layers of base. Calculation of the foundation according to [3] has shown that the raft transmits 40% of the load onto the base and the rest part of the load is transmitted by vibrostamped tapered piles with the length of 3m, top diameter of 0.5m and foot diameter of 0.3m. The layout of the piles is shown on fig. 11. The foundation consists of 285 tapered piles and 32 driven prismatic piles made before.
The cost of the foundation was reduced almost by two times by means of useing short vibrostamped tapered piles with bearing raft.

CONCLUSIONS

1. The raft has significant influence on the mode of deformation of the base. The large volume of the soil takes part in the work and increases bearing capacity of the base about 10 – 100% depending on size and shape of foundation and ground conditions of the site. The large reserve of bearing capacity of the base has not been sufficiently investigated.
2. When load is increased the settlement of piled-raft foundation occurs more uniformly than in piled foundation. There is no pronounced critical point and sudden loss of bearing capacity on the graphical char $K_p=f(N)$.
3. The basic factors which affect the work of the raft in foundation are ground conditions, quality and consolidation of soil under the raft, size and shape of the foundation (type of piles, pile length and space, width of the raft); load on the foundation.
4. Application of short vibrostamped tapered piles with widening at the pile foot and bearing rafts is more effective than conventional foundations consisting of driven prismatic piles. Compressing stress transmits into ground along the whole length of lateral pile faces without negative friction and by the raft. Upper layers of filled-up soil are compacted by means of sloping lateral pile faces and bearing capacity of this soil increases considerably.

© 2016 Deep Foundations Institute

5. Application of our investigation results in construction practice shows that taking into account soil-raft interaction can reduce the cost of pile foundation in certain cases by 30-50%.

REFERENCES

Бартоломей, А.А., 1995. Основы прогноза осадок свайных фундаментов. Основания, фундаменты и механика грунтов, Moscow, 3, pp 8-10.

Голубков, В.Н., Тугаенко, Ю.Ф., Хуторянский, Б.О., 1971. Исследование процесса формирования зоны деформации в основаниях одиночных. Основания и фундаменты, Kiev, 4: pp 9-13.

Козачок, Л.Д. 1979., Исследование распределения вертикальных напряжений в основании кустов висячих свай с низким ростверком. Диссертация на соискание ученой степени кандидата технических наук, Leningrad, 174 p.

Сернов, В.А., 2008. Исследование напряженно-деформированного состояния грунта в межсвайном пространстве. Сборник статей международной научно-технической конференции «Геотехника Беларуси: наука и практика». Minsk, October 20-22, pp 239 - 246.

Сернов, В.А., 2009. Эффективные конструкции свайных фундаментов с несущими ростверками. Сборник научных трудов XVI Международного научно-методического семинара, Brest, May 28-30, Vol. 2, pp. 174 - 178с.

Сернов, В.А., 2011. Расчет осадки свайного фундамента с учетом сопротивления грунта в основании ростверка. Строительная наука и техника. Minsk, 2. pp. 27-33.

© 2016 Deep Foundations Institute

PREDICTION OF AXIAL GEOTECHNICAL RESISTANCE OF BASE GROUTED DRILLED SHAFTS

Ehab S. Shatnawi, Ph.D., P.E, CH2M, Herndon, Virginia, 703-376-5062, ehab.shatnawi@ch2m.com
Emad Farouz, P.E, CH2M, Herndon, Virginia, 703-376-500, emad.farouz@ch2m.com

ABSTRACT

The increasing demand for small deformations and high-capacity drilled shafts without enlarging drilled-shaft diameters has motivated the development and increasing use of a base grouting (BG) technique. This technique has been demonstrated to improve drilled-shaft capacity, especially for shafts tipped into loose cohesionless soils. Nevertheless, there remains considerable uncertainty in predicting the performance of base-grouted shafts, particularly for shafts tipped into cohesive soils. To date, there are only two documented design methods for estimating the axial geotechnical resistance of base-grouted shafts: Tip Capacity Multiplier (TCM) and Axial Capacity Multiplier (ACM) methods. A comprehensive test program was carried out during the design phase of the Wisconsin Zoo Interchange project to help optimize the flyover ramp's foundation design. The test program included installing and testing one base grouted shaft and one ungrouted shaft at two sites with different ground conditions. Based on test results, it was concluded that prediction of the TCM method is well correlated with the measured values for both cohesive and granular soils; however, both methods tend to underestimate the axial resistance. Results also highlighted the importance of the base-grouting criteria in taking full advantage of the base grouting.

Keywords: base grouting, base resistance, grout pressure, drilled shafts, side resistance, Tip Capacity Multiplier, Axial Capacity Multiplier

INTRODUCTION

Base-grouted drilled shafts (BGDS), also known as post-grouted drilled shafts, consist of conventionally installed drilled shafts that contain access grout tubes placed within the shaft during construction. After installing the drilled shaft and achieving the pre-established concrete strength, grout is injected at the shaft tip through the access grout tubes to improve soil behavior around the drilled-shaft base. The tip grout injection improves the overall shaft capacity and reduces settlement through Densifying the in situ soils, compressing any debris left by the drilling process, preloading the soil beneath the tip to mobilize the shaft base resistance within service limits, increasing the tip area, and increasing the side resistance in the lower portion of the shaft.

© 2016 Deep Foundations Institute

Grouting injection techniques vary by the grouting method used to inject grout below the shaft base. There are two basic grouting injection distribution systems (Mullins and Winters, 2004): (1) simple compaction grouting, in which a sleeve-port system employs a network of exposed grout tips, and (2) mechanical grouting, in which one or two steel plates and an impermeable membrane are used, called the Flat-Jack.

There is no design method for BGDS included in AASHTO Bridge Design Specifications (henceforth the AASHTO method). There are two design methods widely used; one developed by Mullins et al. (2006) for cohesionless soils, called the Tip Capacity Multiplier (TCM) method, adopted by the Federal Highway Administration (FHWA) in their latest geotechnical engineering circular number 10 (Brown et al. 2010) (henceforth the GEC 10 method). The other method, developed by Ruiz et al. (2005), is called the Axial Capacity Multiplier (ACM) method, adopted by Synchro Pile, Inc.

In the TCM method, the shaft's overall grouted-shaft performance improved due to an increase in the base resistance. The TCM factor estimates the improved base resistance due to grouting. This factor is a function of the anticipated maximum grout pressure (GP_{max}), which is calculated as the ratio of the nominal-side resistance to the cross-sectional area of the drilled shaft and the nominal base unit resistance ($q_{BN,5\%}$) of the ungrouted drilled shaft corresponding to a displacement of 5% of base diameter and the permissible settlement (δt). The BGDS nominal unit base resistance ($q_{BN,\ grouted}$) is calculated as TCM × $q_{BN,\ 5\%}$. GEC 10 indicated that values of the TCM measured in field tests by Mullins et al. (2006) ranged from 3 to greater than 9, depending on grout pressure, quality of the equipment, and techniques used.

Mullins and Winters (2004) reported that shear stress reversal occurs along the shaft of a pile during grouting. They concluded that this effect also may contribute to the improved performance observed in BGDS. However, their research did not quantify the aforementioned stress reversal. This motivated Ruiz and his co-authors to develop the ACM method. ACM is a theoretical method in which three major factors are assumed to control the improvement in drilled-shaft capacity: (1) soil compression under the shaft tip, (2) shear stress reversal along the shaft due to grouting, and (3) and enlargement of the base area due to formation of a grout bulb. In this method the nominal axial resistance of the BGDS is estimated as the nominal resistance of the ungrouted shaft multiplied by ACM, where ACM is obtained from a design chart as a function of the nominal side resistance for the total length of embedded shaft and the anticipated maximum grout pressure. Synchro Pile, Inc. indicates that values of the ACM measured in the field range from 1.4 to 1.8 for dense sand, 1.7 for clay, and up to 2.6 for loose to medium sand.

DRILLED SHAFT LOAD TEST PROGRAM

The Drilled Shaft Test program consisted of installing and testing three pairs of drilled shafts at two sites, with diameters of 3.9, 6.5, or 8.2 feet. The range of diameters was selected using anticipated foundation loading requirements for the proposed bridges throughout the core and west leg of the Zoo Interchange. The shafts were extended to depths between 52.5 and 70.8 feet below ground surface. Depths were based

© 2016 Deep Foundations Institute

on the subsurface conditions at each shaft location, the shaft diameter, and the desired target geotechnical resistance. Table 1 lists the test shaft's diameters and depths. All six test shafts were equipped with an Osterberg Load Cell (henceforth referred to as "O-Cell") installed near the base of the shaft. In addition to the useful information regarding the drilled shaft side and base load transfers, the Drilled Shaft Test program provided very valuable information to quantify the advantages of BGDS. This was crucial because there is little field information available regarding BGDS extending into and bearing on the types of ground present in the Zoo Interchange area.

Table 1. Summary of Drilled Test Shafts

Shaft ID	Shaft Diameter (feet)	Shaft Length (feet)	Base Grout
CTS-1	8.2	69.5	No
CTS-2	8.2	69.5	Yes
CTS-3	3.9	53.3	No
CTS-4	3.9	52.5	Yes
WTS-1	6.5	70.8	No
WTS-2	6.5	70.2	Yes

Base grouting was performed on three shafts CTS-2, CTS-4, and WTS-2. Grout was injected throughout Crosshole sonic logging tubes as volume and pressure were recorded. Grouting was performed using a sleeve port, tube-a-manchette with top plate (Fig. 1). Vertical shaft movement at the top of the shaft was measured using an optical survey instrument. The grouting process was terminated after achieving the maximum allowed grout pressure, ranging from 550 to 850 pounds per square inch (shaft-specific), observing a vertical shaft movement of 0.75 inches, or by reaching a shaft specific target injected grout volume grout take, ranging between 12.6 and 52.8 cubic feet.



Fig. 1. Photographs for Base Grout Plate and Tube-A-Manchette Used for Test Shafts

Six soil borings, CTS-1, CTS-2, CTS-3, CTS-4, WTS-1, and WTS-2, were drilled for the six load tests. One pressuremeter test was performed at each site. Soils encountered at test shafts CTS-1, CTS-2, and CTS-3 consisted predominantly of stiff to very stiff lean clay with trace sand and gravel overlying medium dense

© 2016 Deep Foundations Institute

to very dense silty sand near the shaft bottom. Similar conditions exist at the CTS-4 location, although a thick layer of loose to medium dense silty sand was encountered at the ground surface. Soils encountered at test shafts WTS-1 and WTS-2 consisted predominantly of loose silt and soft clay, underlain by medium stiff to very stiff clay, which was underlain by medium dense silty sand and hard clay.

RESULTS OF THE AXIAL LOAD TEST

Results of the test program are summarized in Table 2 and presented graphically in Fig. 2 and Fig. 3. The base unit resistance corresponding to a 1-inch vertical shaft deflection was determined as the sustained O-Cell load, corresponding to the O-Cell base downward movement of 1 inch, subtracting the load taken in shear by the shaft section below the O-Cell, and divided by the cross sectional area of the shaft. For comparison to published guidance, the maximum base resistance was assumed to equal the base resistance (extrapolated) corresponding to a vertical shaft base displacement equal to 5% of the shaft diameter (i.e., an extrapolation was made on the mobilized end bearing graphs). The unit side resistances of the test shafts were estimated based on the strain gauge data and the computed shaft stiffness.

Table 2. Summary of Axial Loading Test Results

Shaft No.	Predominant Soil Below Tip	Average N60 or Su below Drill Shaft Base	Predominant Soil Above O-Cell	Applied/ Estimated Maximum Grout Pressure, psi	Base Unit Resistance @ 1″ and 5% D Base Deflection, ksf	Average Unit Side Resistance Above O-Cell, ksf
CTS-1	Medium dense to very dense silty sand	43 bpf 95 bpf	Very stiff clay	Not Grouted	32/55	1.7
CTS-2				160[a]/530	45/70	2.5
CTS-3	Medium dense to very dense silty sand	2.5 ksf 43 bpf	Silt and very stiff to hard clay	Not Grouted	98/155	2.4
CTS-4				300/880	135/190	3.3
WTS-1	Very stiff to hard clay w/gravel	95 bpf	Sand and very stiff to hard clay	Not Grouted	45/65	1.4
WTS-2				600/450	90/130	2.2

[a:] The reported applied grout pressure of 750 psi was due to equipment malfunction and does not agree with the base movement of less than 0.05'. The 160 psi was back calculated as the pressure required to move the drilled shaft 0.05-inch.
bpf = blow per foot. ksf = kips (thousands of pounds) per square foot, psi = pound(s) per square feet,
Su = undrained shear strength

© 2016 Deep Foundations Institute

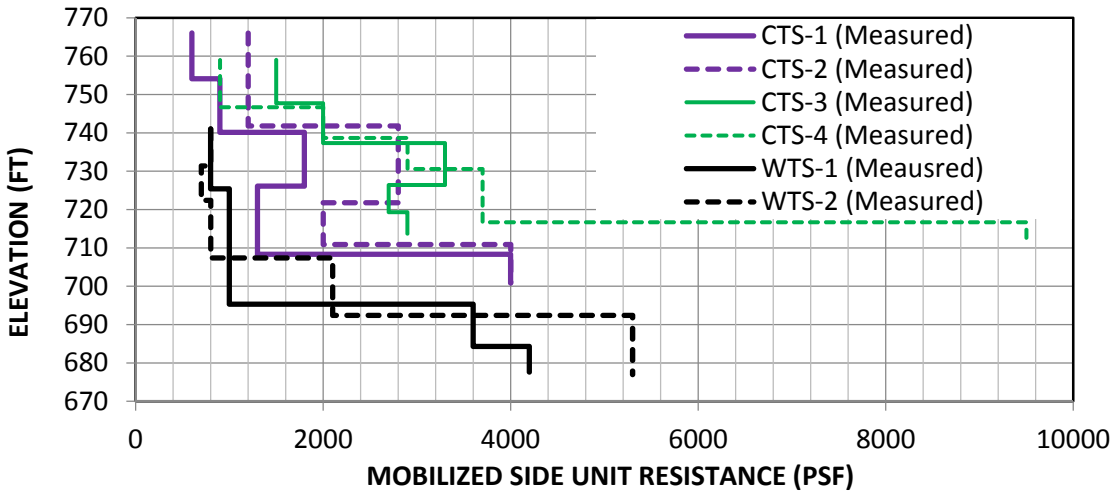
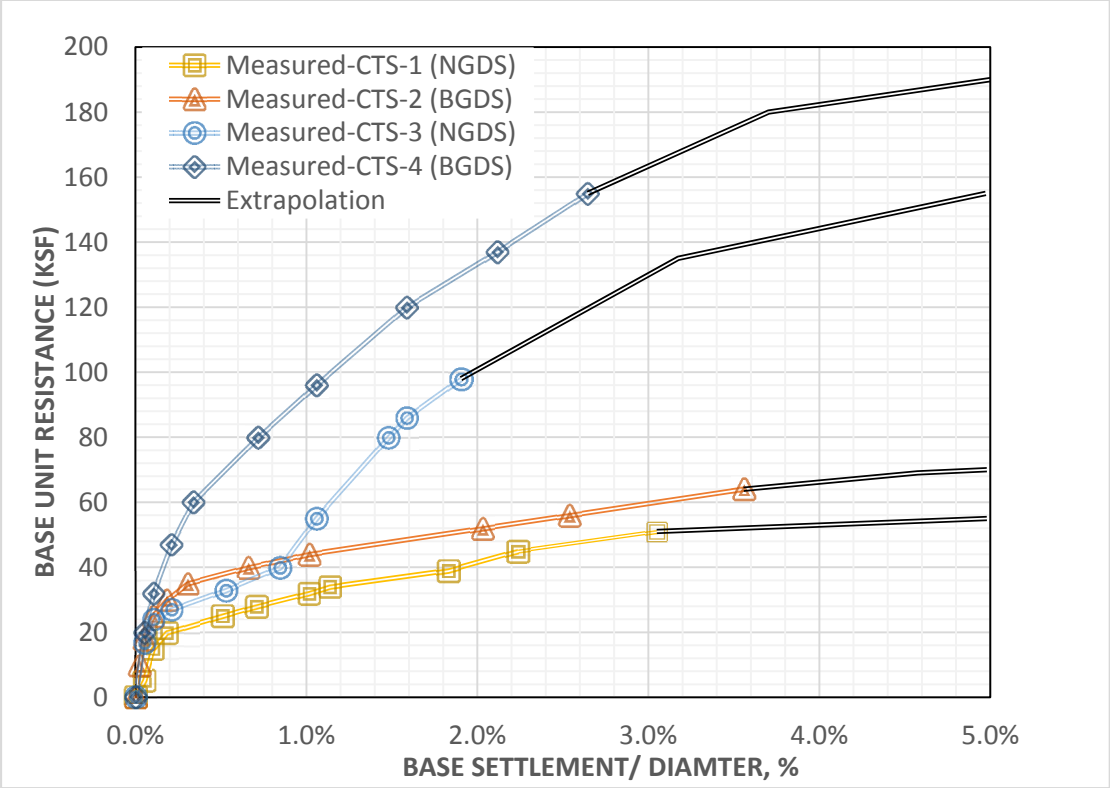


Fig 2. Measured Unit Side Resistance versus Eelvation

© 2016 Deep Foundations Institute



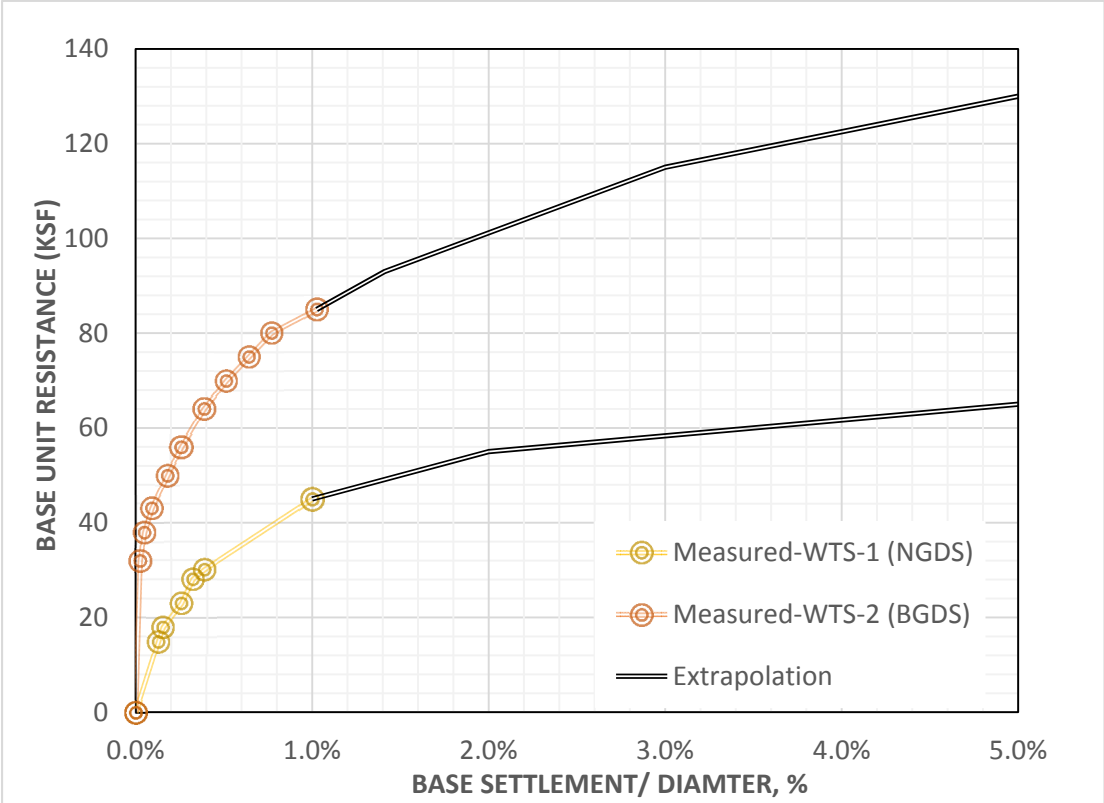


Fig 3. Measured Unit Base Resistance versus Base Settlement

© 2016 Deep Foundations Institute

INTERPRETATION OF THE AXIAL LOAD TEST RESULTS

Side Resistance for Ungrouted Shafts in Cohesive and Cohesionless Soils

Fig. 4 compares predicted unit side resistances of shaft intervals extending through cohesive soils or granular soils. For cohesive soils, the predicted unit side resistance, using the alpha method, correlate well with the measured values. As such, the alpha method of static analysis was recommended to estimate side resistance. For granular soils, Fig. 4 also shows that the GEC 10 beta method provides a prediction that generally agrees well with measured values. The GEC 10 method, however, overpredicts the side resistance for sands with high-blow count (N-value), since the effective friction angle correlation within GEC 10 is relatively high compared with other published relationships. The GEC 10 method was recommended for estimating the unit side resistance of cohesionless soils, but the internal friction angle was limited to 40 degrees.

Scattering in the measured versus predicted curves is still considered high. To investigate further, predicted profiles were plotted against measured profiles, which showed that the side resistance at shallow depths (above the top strain gauges) for all the test shafts was overpredicted. This occurs because soils at shallow depths are subjected to more disturbance during construction than deeper depths due to drilling, casing installation, and casing removal. Both AASHTO and GEC 10 guidance suggest ignoring the side resistance of the upper 5 feet of the drilled shaft to account for disturbance during construction, scour, moisture changes, and more. In doing so, the predicted side resistance for the three-test shaft agrees now with the measured resistance, but the side resistance for three shafts is still overpredicted within the top 10 feet. Consequently, limiting the unit side resistance to 1000 pounds per square foot in the top 10 feet was recommended.

Base Resistance for Ungrouted Shafts Bearing on Cohesive and Cohesionless Soils

Shaft CTS-1 had a maximum unit base resistance of 55 ksf. This value is approximately $1.2 \times N_{60avg}$, where N_{60avg} is the average standard penetration test corrected N-value within the zone of influence; this coincides with both AASHTO and FHWA methodologies. Shaft CTS-3 had a maximum base resistance of 156 ksf. This value is approximately $1.7 \times N_{60avg}$, which is greater than the $1.2\ N_{60avg}$ and the upper limit of 90 ksf prescribed by GEC 10.

The maximum unit base resistance for test shaft WTS-1, which was tipped in cohesive soils, is approximately 14.5 times the Su (i.e., measured bearing capacity factor [Nc] = 14.5). The calculated Nc factor using the FHWA and AASHTO methods is 14.5 (based on a Su of 4.5 ksf); however both manuals limit this factor to 9.0. Accordingly, it was recommended that the limiting bearing capacity factor, Nc, be increased from 9.0 to 12.0.

© 2016 Deep Foundations Institute

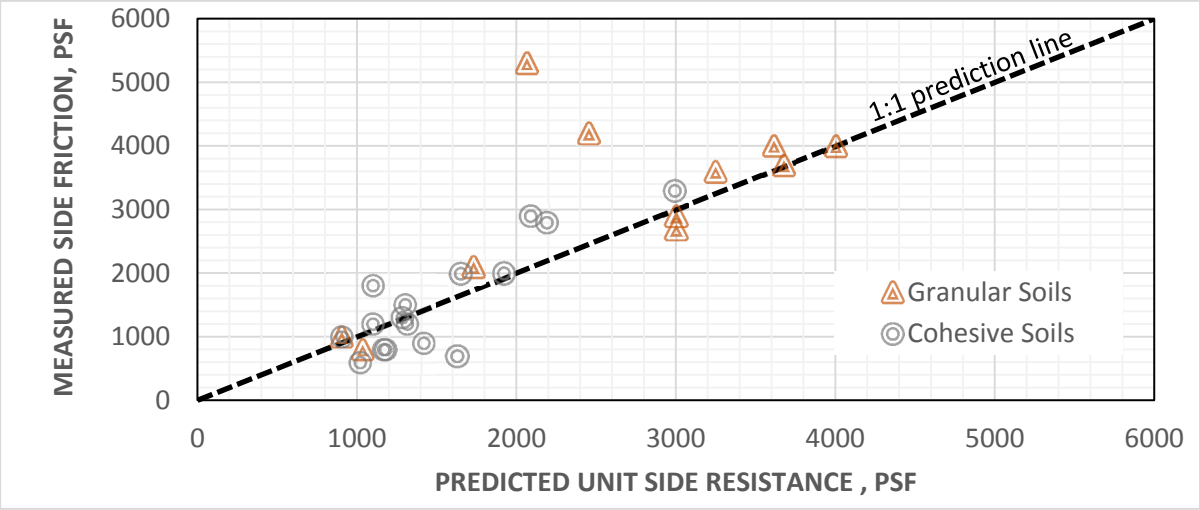


Fig. 4: Predicted versus Measured Unit Side Resistance

Axial Resistance for Base Grouted Shafts

Both the ACM and TCM methods were used to evaluate the axial resistance of the BGDS as compared with measured resistances. The TCM and ACM for three BGDS tests were back-calculated from the measured unit base resistance corresponding to a displacement of 5% of the shaft diameter, as well as displacement of 1 inch. The recommended methods for unit side and base resistances were used to estimate the maximum permissible grout pressure that can be applied at the base of the shaft. The estimated grout pressure values were compared to the applied pressure values in Table 1. Although the applied grout pressure for CTS-2 is more than the estimated value, the drilled shaft moved upward because BG was less than 0.05% diameter (D), at which roughly 20% of the side resistance would be typically mobilized. This indicates that the reported grout pressure of 750 psi may not accurately reflect what was applied on the shaft base. The grout pressure to mobilize 20% of the side resistance was back-calculated as 160 psi for CTS-2. The applied maximum grout pressure for CTS-4 is about one-third of the estimated grout pressure, and the drilled shaft movement due to BG is only 0.1% D, at which roughly 30% of the side resistance will be mobilized. WTS-2 was the only test shaft at which the BG was applied correctly to mobilize the nominal side resistance. The drilled shaft moved 0.4% D upward, and a significant portion of side resistance was mobilized.

Table 3 compares measured TCM values, predicted values based on applied grout pressure and maximum available grout pressure. It also presents the unit base resistances calculated from the axial compressive loading tests of the three BGDS (CTS-2, CTS-4, and WTS-2). Table 3 also shows the back-calculated ACM for the three BGDS, together with a comparison between the measured and predicted total axial resistances. Fig. 5 compares the ACM and TCM methods in predicting the total axial resistance. As shown, both methods underpredict the resistances mobilized at 1 inch of axial displacement and both methods generally overpredict nominal resistances. However, the relative differences in the TCM method are less than the

© 2016 Deep Foundations Institute

ACM method differences. Accordingly, the TCM method was recommended for estimating the BG contribution to the axial resistance.

Table 3. Back-Calculated TCM and ACM for BGDS

Shaft No.	Case	Base Unit Resistance, ksf		Total Axial Resistance, kips		ACM		TCM	
		@ 1"	@ 5% D	@ 1"	@ 5% D	@ 1"	@ 5% D	@ 1"	@ 5% D
CTS-2	Measured	45	70	5850	7170	0.8	1.0	0.8	1.3
	Predicted[a]	31	82	4854	9015	0.7	1.3	0.6	1.5
	Predicted[b]	71	152	11789	18724	1.7	2.7	1.3	2.8
CTS-4	Measured	135	193	3500	4206	1.2	1.5	1.3	1.8
	Predicted	100	160	2552	3969	0.9	1.4	1.0	1.5
	Predicted	170	270	7939	10774	2.8	3.8	1.6	2.6
WTS-2	Measured	90	131	6000	7361	2.0	2.5	3.8	5.5
	Predicted	75	134	4471	6260	1.5	2.1	3.1	5.6
	Predicted	60	106	5962	8943	2.0	3.0	2.5	4.4

[a] Based on the applied grout pressure.

[b] Based on the maximum computed grout pressure. The TCM method was used for the Base Unit Resistance prediction and the ACM method was used for the Axial Resistance.

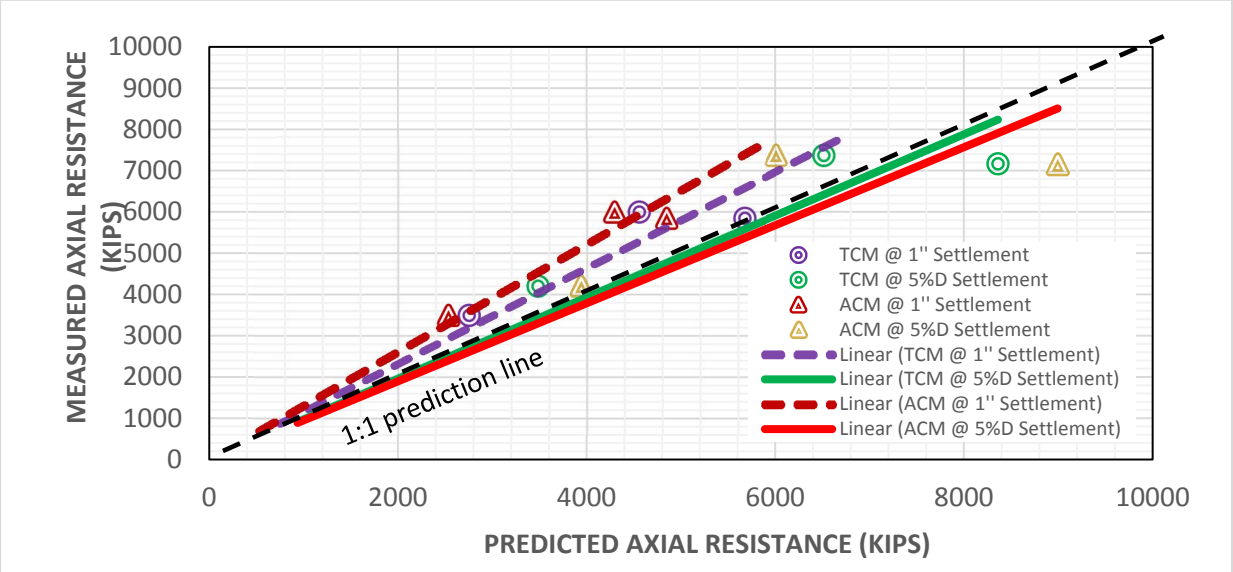


Fig. 5. Predicted versus Measured Axial Resistance for BGDS

Many researchers have indicated that BG may increase the side resistance near the shaft base due to transmission of grout externally above the shaft base. However, to date, no method is available to quantify this contribution. Results of the load test program indicate that in general BG improves the side resistance within a distance of one and one half shaft diameters above the shaft base. This distance approximately coincides with the lowest interval of strain gauges within each of the BGDS. Table 3-8 lists the improved

© 2016 Deep Foundations Institute

resistance at the bottom of each of the three BGDS. As shown, the unit side resistances within a distance of one and one half shaft diameters above the base were approximately 1 to 3.3 times the estimated resistance and, in the case of CTS-4, greater than the upper limit of 4 ksf specified in the AASHTO and GEC 10 guidance. Note that procedural irregularities encountered in BG CTS-2 and CTS-4 resulted in failure to achieve the grouting criteria. Such irregularities can be attributed to the lower performance of the two shaft pairs compared to the measured improvement of WTS-2 versus WTS-1. Consequently, and due an absence of other publications supporting this, it will be difficult to ensure that the BG bulb will extend above the shaft base. Therefore, considering BG contribution in side resistance is not recommended.

Table 5. Unit Side Resistance within 1.5 Diameters of the Base of BGDS

Shaft No.	Soil within bottom 1.5 D	Case	Average Unit Side Resistance within 1.5 × Shaft Diameter above the base, ksf
CTS-2	Medium dense to very dense silty sand	Measured	4.0
		Estimated	3.9
		Measured/Estimated, %	102
CTS-4	Medium dense to very dense silty sand	Measured	9.1
		Estimated	3.7
		Measured/Estimated, %	245
WTS-2	Very stiff to hard clay With gravel	Measured	5.3
		Estimated	1.6
		Measured/Estimated, %	331

Grouted versus Ungrouted Drilled Shaft

The Load Drilled Shaft Test program included installation of three pairs of shafts with the same diameter and extending to similar depths for the primary purpose of assessing the impact BG would have on base and total resistance. Table 6 compares the unit base resistance and the equivalent total resistance at a shaft top deflection of 1 inch. As can be seen, even with the procedural irregularities encountered in BG CTS-2 and CTS-4, the BG has been shown to provide a 25% to 100% increase in the base resistance and 27% to 43% increase in the total resistance.

Table 6. Base and Total Resistance Comparison—Grouted versus Ungrouted Shafts

Shaft Pair	Shaft Diameter, feet	Base Resistance @ 5% Base Deflection, kips	Increase with Base-Grout	Total Resistance @ 1″ Top Deflection, kips	% Increase with Base-Grout
CTS-1	8.2	56	25%	4400	33
CTS-2		70		5850	
CTS-3	3.9	156	24%	2760	27
CTS-4		193		3500	
WTS-1	6.5	65	100%	4200	43
WTS-2		131		6000	

© 2016 Deep Foundations Institute

SUMMARY AND CONCLUSIONS

Based on results of the Comprehensive Load Test program, base grouting has proven to improve the geotechnical axial resistance of drilled shafts effectively in both cohesive and cohesionless soils with a 25% to 100% increase over an ungrouted shaft; the lower end of this range is likely artificially low due to base grouting procedure irregularities. The following are major conclusions from this load testing program:

1. For ungrouted drilled shafts in cohesive soils, the predicted unit side resistances using the GEC 10 alpha method correlate well with measured values. For granular soils, the GEC 10 beta method generally agrees well with the measured values if the friction angle is limited to 40 degrees.
2. Redundant measurements of shaft upward movement during base grouting is of paramount importance.
3. The load test program shows that actual performance is highly dependent on shaft design requirements, such as shaft diameter, length, and serviceability criteria.
4. Base-grouting improves side resistance within one and a half diameters above the base of the shaft and possibly above that. Additional testing is needed to confirm this conclusion.
5. The TCM method was found to better predict the increase in the base resistance compared to the ACM method for both cohesive and cohesionless soils.

REFERENCES

American Association of State Highway and Transportation Officials. 2012. Sixth Edition, AASHTO LRFD Bridge Design Specifications.

Brown, D.A., Turner, J. P., and Castelli, R. J. 2010. Drilled Shafts: Construction Procedures and LRFD Design Methods. (GEC10), FHWA-NHI-10-016, NHI Course No. 132014,

Ruiz, M.E., Fernandez, A.L., and Pando, M.A. 2005. Bearing Capacity of Post Grouted Drilled Shafts Using a Load Transfer Approach. Proceedings of the 30th Annual Conference on Deep Foundations, DFI, Chicago, October 2005, pp. 139–49.

Mullins, G. and Winters, D. 2004. Post grouting Drilled Shafts Tips – Phase II. Final Report to the Florida Department of Transportation.

Mullins, G. Winters, D. and Dapps, S. . 2006. Predicting End Bearing Capacity of Post-Grouted Drilled Shaft in Cohesionless Soils. J. Geotechnical and Geoenvir. Engrg., 132(4): 478–87.

© 2016 Deep Foundations Institute

This page left intentionally blank

© 2016 Deep Foundations Institute

REMOVAL OF THE FORMER SAN FRANCISCO-OAKLAND BAY BRIDGE FOUNDATION CAISSON E3 BY MECHANICAL MEANS AND EXPLOSIVES

Michael Gebman, PhD, PE, COWI, Oakland, CA, USA, 510-267-7145, mclg@cowi.com
Jack Gerwick, PE, COWI, Oakland, CA, USA, 510-267-7172, jckg@cowi.com

ABSTRACT
With the opening of the new San Francisco-Oakland Bay Bridge East Span, the former bridge and its caisson foundations are being demolished. Caisson foundations are in the path of a future shipping channel and therefore need removal down to the mudline 50 ft below water (MLLW). For the first caisson to be removed (E3) a mechanical demolition was performed above the waterline and an implosion was done for the remaining caisson down to mudline. Mechanical demolition consisted of excavators operating from either on top of the caisson, from work platforms or from barges. The demolition was implemented on a trial basis with a successful implosion on November 14, 2015. The work was conducted in an environmentally sensitive area, with measures taken to protect fish, marine mammals and birds. This demolition technique was cost effective, faster to execute, and had a better environmental impact then an alternative option. The demolition, measures implemented to protect the environment, outcome, and lessons learned are presented.
Keywords: caisson, foundation, marine environment, demolition, implosion

INTRODUCTION
The California Department of Transportation needed a cost effective and environmentally friendly solution for removal of the remaining San Francisco-Oakland Bay Bridge (former East Span) caisson foundations, starting with caisson E3. This was necessary to clear a future shipping channel. One option was to construct a steel cofferdam around the caisson to allow demolition in the dry down to the mudline. This option would take years to complete, be cost prohibitive, and its noise would disrupt aquatic life and birds throughout the cofferdam construction and demolition. An alternative option was implemented on a trial basis to conduct a mechanical demolition of the caisson above waterline along with an implosion of the remaining caisson down to mudline. This had the clear advantage as a cofferdam was not needed, and the demolition project duration would be approximately 6 months, instead of several years for the cofferdam option. The potential impact on aquatic life and birds from the implosion was a concern, as the location is environmentally sensitive; however, measures were implemented to minimize these impacts. As presented in this paper, this demolition option was implemented on a trial basis for Caisson E3. The technique succeeded and will now be used on the remaining caissons.

BACKGROUND INFO ON CAISSON E3
The reinforced concrete Caisson E3 is the largest caisson which supported the former East Span of the Bay Bridge. It was constructed in 1934, with the Bay Bridge opening in 1936. Figure 1 shows the project location. The caisson had a cell arrangement of 7 x 2 above the mudline. Below mudline, the caisson had a cell arrangement of 9 x 4. A structural transition was made between the 7 x 2 and 9 x 4 cell arrangements with buttress walls. All cells were flooded, as underwater openings were included in the original caisson walls to equalize the hydrostatic pressure. Figure 2 shows the caisson layout with limits for mechanical demolition and for the implosion.

Overall caisson dimensions were 134 ft x 40 ft for the upper 7 x 2 cell group, and 167 ft x 80 ft for the overall 9 x 4 cell group. Wall thickness was 3 ft. On the top deck two 6 ft tall pedestals supported the former steel bridge towers. Each pedestal was centered over four caisson cells with a top slab thickness of 16.75 ft. Top slab thickness for the center six cells was 3.25 ft. The caisson top was surrounded by an apron slab with wing walls and a perimeter wall which supported fenders. The apron typically cantilevered 19.5 ft from caisson. Apron slab thickness was 18 inch, and had a slope of 1:4 (V:H). Caisson reinforcement consisted of square reinforcing bars, typically ¾ inch or 1 inch.

© 2016 Deep Foundations Institute

MECHANICAL DEMOLITION

All debris was required to be deposited within the caisson cells, which extend 164 ft below mudline providing sufficient capacity to contain all debris. Debris could not fall into the open bay, as this could disrupt local aquatic life and effect sea water chemistry. The caisson above water from EL +9 ft to its top at EL +37 ft was removed using three hydraulic excavators equipped with either:

- breaker units (for chipping through thick slabs or walls)
- concrete cutting jaws (for cutting through thin slabs or walls)
- catcher basket (a bin for debris containment)

These excavators were supported by the marine equipment shown in Fig. 3.

Pedestal Demolition

Demolition began with two excavators operating on the caisson top deck to chip openings into the caisson cells for debris placement into the cells. With the debris openings created the concrete pedestal supports at each end were removed down to the top deck surface. Figure 4 shows pedestal demolition underway.

Work Platform Fabrication

While pedestal demolition was underway, two steel fabricated work platforms were fabricated. Each platform, 20 ft x 40 ft, was designed to support two 50 ton excavators. Platforms were designed to be supported by three parallel caisson walls, as shown in Fig. 5. Platforms consisted of W18x97 beams at 20 inch spacing with gusset plates at the ends, and at midspan. Timber mats (12" x 12") were secured to the top flanges. Four pad eyes were welded to the beam flanges to allow lifting the platform. A safety railing was placed along the perimeter.

Work platforms were used to support excavators while the walls and top slab above the apron slab was removed as shown in Figures 5 and 6. After demolishing the caisson down to the apron (top) level, a thickened slab, approximately 8 ft deep, remained within the four caisson cells underneath each former pedestal. This thickened end slab along with the work platforms allowed the excavators to operate at this level for apron slab demolition.

Apron Demolition

Demolition of the cantilevered apron slab surrounding the caisson and its associated support walls could not be done with equipment on the apron slab because it was lightly reinforced and had a 1:4 (V: H) slope. Therefore one excavator equipped with a breaker unit operated at the caisson top level. Two excavators operated side by side from a barge (one with a catcher basket and the other with cutting jaws), as shown in Fig. 7. The barge was positioned so that debris landed on the barge deck. Debris material was placed into a large steel bin which was lifted by the crane to the caisson top and emptied into the caisson cells. The sloped apron slab was demolished by chipping with the excavator at the caisson top and by cutting using the excavator with a jaw unit.

The excavators made strategic cuts, which allowed an efficient removal of the apron wing walls and perimeter walls in large wall sections. Wall sections removed typically required using a torch to cut through bottom reinforcing bars before the section was completely free. When free, wall sections were lifted by the crane up to the caisson top level, broken into smaller pieces by the excavator (at the top level) and deposited into the caisson cells.

Pedestal Slab and Walls Demolition

Next, demolition of the remaining 8 ft thick slab in the four cells at each end (below former pedestals) was done by the excavators equipped with breaker units operating from work platforms. Demolition of the remaining caisson walls was done with excavators located on a barge and on the work platforms, as shown in Figures 8 and 9. Excavators operating from a barge required the use of a flexifloat barge between the

© 2016 Deep Foundations Institute

caisson and the excavator demolition barge to provide sufficient standoff distance for the excavators, and to catch any debris. The excavators were once again used to make strategic cuts to remove external walls in large sections. With the wall cuts in place, excavators on the barge were used to repeatedly hit the top of the wall until it toppled over and fell into the caisson cell. Wall demolition to EL +9 ft is shown in Figure 8 and 9. The completed mechanical demolition is shown in Fig 10.

PREPARATION FOR IMPLOSION

After all of the caisson walls were demolished to EL +9 ft, the remaining wall top surface was prepared for installation of a drill rig work platform to cover the entire caisson top. The remaining wall top surface was chipped to remove large surface irregularities. Reinforcing bars protruding from the remaining walls were removed with torch. The water surface in the caisson cells was cleared of floating formwork debris (from the original construction).

Steel beams from the two original work platforms were used with timber mats to cover the top surface of the remaining caisson cells. Grout pads were used to provide firm support points for the beams. This deck supported a 20 ton drill rig and personnel for explosives installation. The completed drill deck is shown in Fig. 11. The deck was kept in place for the implosion to serve as a blast containment mat. Further debris containment was provided by steel cable mats, which covered the perimeter walls to 1 ft below the waterline

The contractor's blast specialist designed the implosion. Explosive charges were installed into holes drilled 80 ft into the caisson walls at a 3 ft typical spacing. Twenty-two thousand pounds of explosive charges were installed in the holes. All of the holes drilled in the buttress walls (2 per wall) were wet. Buttress walls cracked over their lifetime providing a path for water to penetrate into the drilled holes. Twenty-six of the 135 holes drilled in the caisson walls were wet. The wrapping for the explosive charges was found to be potentially inadequate, and was changed and strengthened to ensure proper installation.

ENVIRONMENTAL MITIGATION

Prior to mechanical demolition, the caisson weep holes (open to the bay) were covered with steel plates and sealed with an aqua plug to contain cell water compromised by debris. As the water level within the caisson cells increased due to placement of debris inside the cells, the water was periodically pumped into Baker tanks for treatment off site. The impact on fish, marine mammals and birds had to be mitigated. Observers for marine mammals and birds were onsite during mechanical demolition.

The presence of a fish population in the site vicinity is difficult to quantify, therefore it was judged infeasible to quantify the impact on any given species from the implosion. The temporary impact of the implosion on the fish habitat was regulated with criteria. A dual criteria was established for potential take on fish from in water noise based on peak pressure and cumulative noise impacts. An impact threshold for injury to fish was set at 206 dB for peak pressure. The best measure to reduce and avoid impacts on the fish was determined to be seasonal avoidance. Fish species of concern are either not present, or present in their lowest numbers in early November. Early November was set for the implosion.

Marine mammals in the project vicinity could not be harmed or wounded. The presence of any marine mammal within the project vicinity was monitored during mechanical demolition, and prior to implosion. If any marine mammals were within the project vicinity immediately prior to the implosion, the implosion would have been delayed until the mammals were clear of the area.

Any birds that were potentially nesting in the project vicinity were allowed to be hazed by the contractor's biologist. Prior to the implosion, birds were hazed using hand held lasers pointed near the birds and with an acoustic deterrent device 1 minute prior to the blast.

© 2016 Deep Foundations Institute

The contractor installed a bubble curtain to attenuate the implosion pressure spike; manifolded compressed air nozzles on the seabed created a curtain of low-density water 50 feet from the caisson. Air compressors for the bubble curtain were located on two barges. The air compressors pushed 9,000 cubic ft of air per minute into the water, which can be seen by the white water in Fig. 12.

IMPLOSION DAY

Bridge traffic was stopped 20 minutes prior to the implosion to prevent any drivers from being startled by the implosion sound. Boaters were restricted to a distance of 1,500 ft from the caisson. Enforcement of these restrictions was performed by US Coast Guard, Highway Patrol, and San Francisco Police Department. The nearby BART commuter train tube was closed for the implosion. News media helicopters televised the event live. Ten aquatic life and bird observers were present for the implosion. These observers ensured no major aquatic life such as seals were in the area at time of blast, and studied the blast environmental impact.

IMPLOSION OUTCOME

At 7:17 am on Saturday, November 14, 2015, the blasting subcontractor detonated charges embedded in the caisson (Fig. 12). The implosion sent approximately 20,000,000 lb of debris into the bottoms of caisson cells below the mudline. A sonar image of the caisson before and after the implosion is shown in Fig. 13. Portions of the bubble curtains can be seen in the sonar image of Fig. 13, one of which (on the right side of the graphic) flipped over due to the blast. After the blast, some minor sections of the former caisson buttress walls remained slightly above the desired removal elevation. This debris was removed and deposited into the caisson cells with the aid of the floating crane and a cutting jaws attached to a pipe pile.

In a worst-case scenario, scientists predicted 1,500 fish could die because of the blast. The implosion impact on fish was studied with fish cages placed near the caisson. No impact was observed on the single test species; however, these results do not provide conclusive data that in-water implosions have no impact on nearby fish. Bird deterrence measures were successful as no take of birds was observed after the implosion. Experts concluded the implosion had a lower impact on fish and birds than originally predicted.

For the implosion, water quality measurements, hydro acoustic monitoring, and noise measurements were implemented.

COST

Caltrans performed extensive analysis of the demolition options for cost and environmental impact. The cost of the caisson mechanical demolition and implosion was $20 million. This was half of the estimated cost of the alternative using a cofferdam with mechanical demolition in the dry down to mudline. In addition, the demolition technique implemented lacked the significant additional risk due to water depths for the cofferdam alternative.

LESSONS LEARNED

Lessons learned and observations include:

1. The demolition technique implemented proved to be on time, and cost effective at half of the estimated cost of the alternative technique (cofferdam with mechanical demolition in the dry).
2. The demolition technique resulted in a limited and acceptable environmental impact. Regulations were satisfied for fish, marine mammals and birds. Carbon monoxide emissions from the demolition were a small fraction of the emissions that would have been generated from the alternative technique.
3. The implosion was highly effective at removing the caisson and sending debris into the cells as planned. Only a few small sections of the caisson buttress walls remained above mudline, which were later removed.

© 2016 Deep Foundations Institute

4. Supporting the work platforms on three walls was difficult due to the rough and undulating nature of the remaining walls top surface. Care had to be taken to ensure adequate bearing.
5. Work platforms originally included braced legs, which reacted on the caisson walls. This was intended to prevent the platform from lateral movement due to excavator demolition operations. This restraint was found to be unnecessary as the surface friction between the platform and wall tops was sufficient to prevent movement.
6. Operating equipment caused damage to the work platform edge beam flanges. This damage was not detrimental to the platform safety.
7. Demolition in a marine environment is a challenging task, requiring numerous coordinated moves of: barges, work platforms, excavators, fuel tanks, and access gangways.
8. Demolition work is tough on the equipment, especially on excavators equipped with breaker units. Numerous repairs to the breaker units was needed, and was performed by the skilled operators with spare parts readily available.
9. Prevailing wind direction should be taken into account when planning marine demolition to mitigate debris dust. The site was subject to a prevailing wind to the East, which was not desirable when the barges and crew needed to be located on the East side of the caisson to support demolition.

SUMMARY

The California Department of Transportation had two options for removal of Caisson E3 from the path of a future shipping channel. The first option, to construct a cofferdam for demolition in the dry would have been cost prohibitive, produced greater carbon monoxide emissions, and have an environmental impact on fish, marine mammals and birds over the several year project duration. The option selected, was mechanical demolition of the caisson above water and an implosion for the remaining caisson down to mudline. Using this option, excavators performed demolition from on top of the caisson, from work platforms, and from barges. Debris was deposited into the caisson cells, and in many areas strategic cuts were used to remove large wall sections. Environmental mitigation consisted of full time observers to monitor marine mammals and birds, treatment of caisson cell water displaced by debris, and a bubble curtain for the implosion. The remaining caisson, above mud line, imploded into itself on November 14, 2015, sending debris into the caisson cells below mud line. Environmental studies concluded the implosion had an acceptable environmental impact. This demolition solution, conducted on a trial basis, was declared a success and is being used on the remaining caisson foundations. This will provide the owner a solution that is cost effective, environmentally acceptable, safe, low risk, and schedule efficient.

ACKNOWLEDGMENTS

The authors would like to acknowledge the general contractor Kiewit/Manson (Joint Venture) and the owner: California Department of Transportation. Silverado conducted the mechanical demolition. Contract Drill & Blasting performed the implosion. Fredric Lausier of Kiewit, and David Nielsen of Manson are hereby acknowledged for their efforts leading the demolition construction team.

© 2016 Deep Foundations Institute

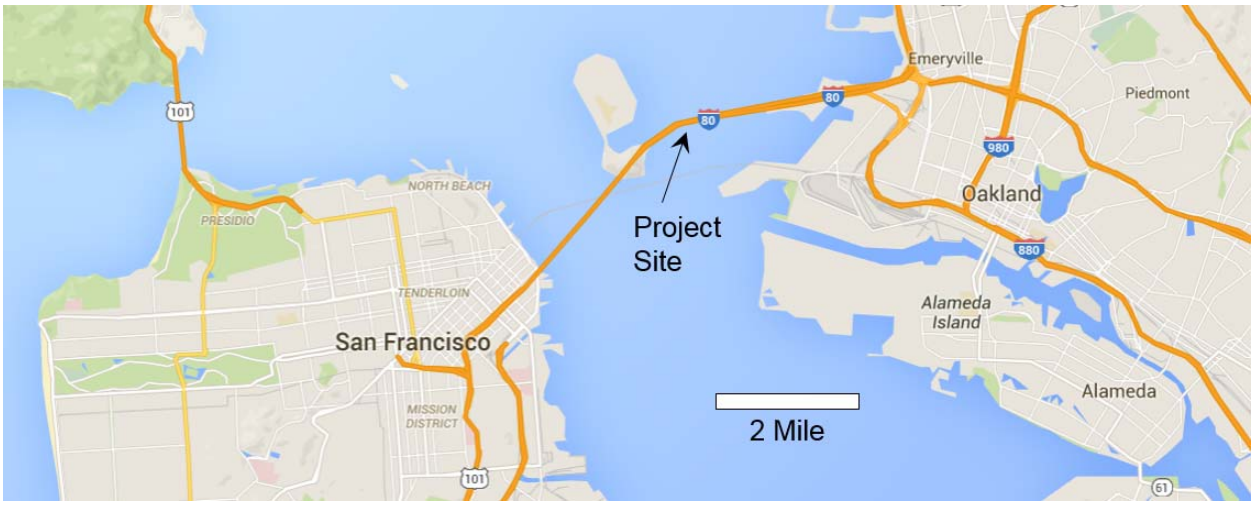


Fig. 1 Site Location

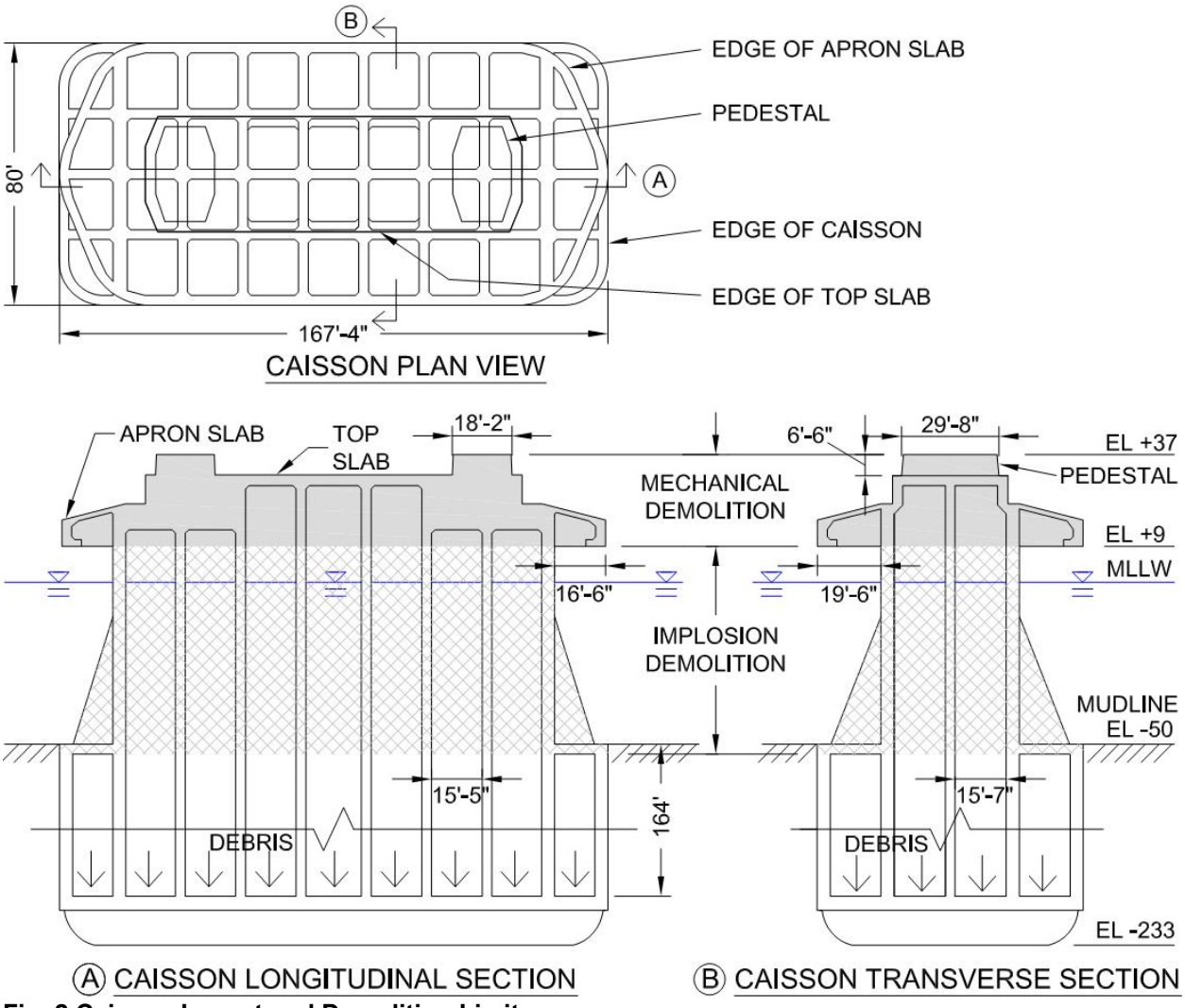


Fig. 2 Caisson Layout and Demolition Limits

© 2016 Deep Foundations Institute

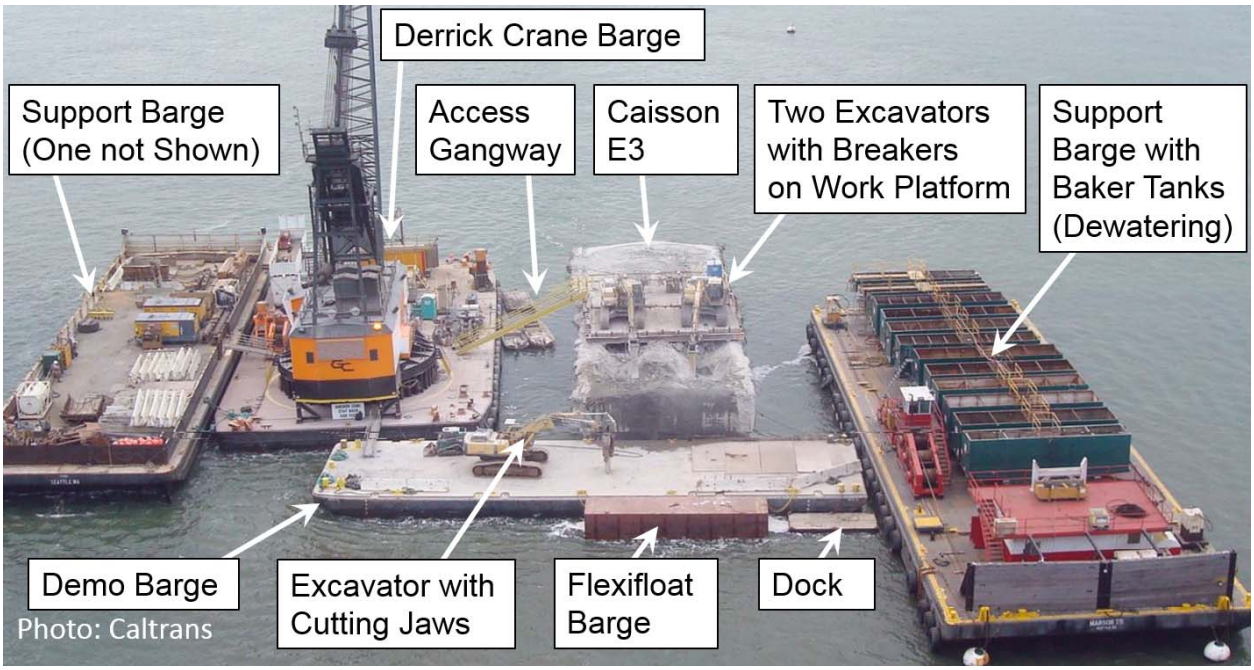


Fig. 3 Site Overview with Marine Equipment and Caisson E3 Apron Slab Removed



Fig. 4 Pedestal Demolition Well Underway

© 2016 Deep Foundations Institute



Fig. 5 Work Platform Spanning Two Caisson Cells

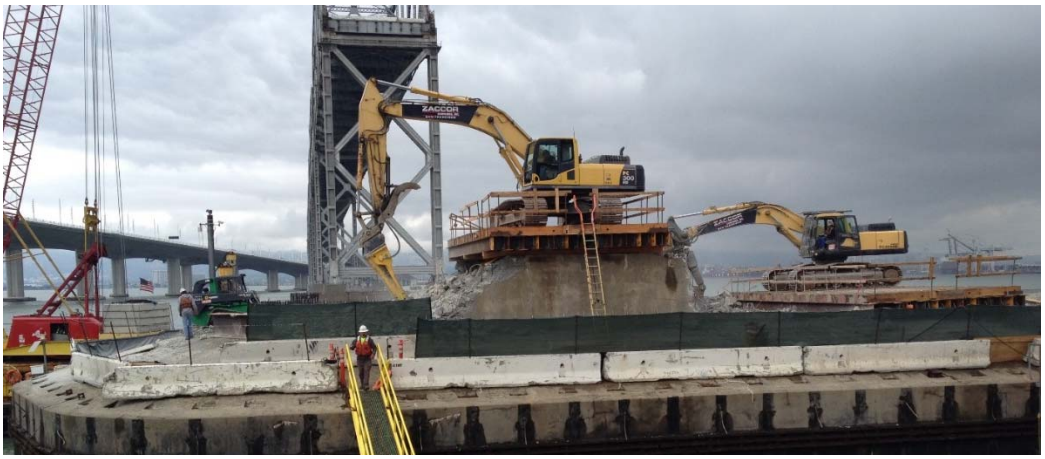


Fig. 6 Work Platforms in Use to Remove Caisson Walls above Apron Slab

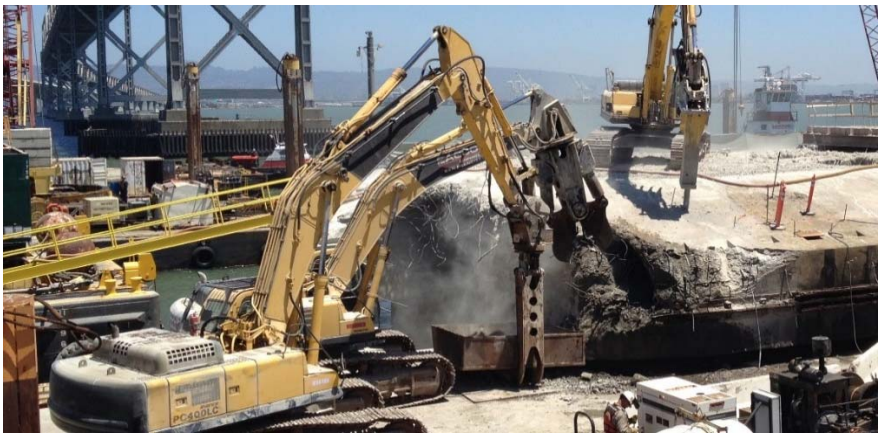


Fig. 7 Apron Slab Demolition Underway with Barge underneath Apron for Debris Containment

© 2016 Deep Foundations Institute



Fig. 8 Typical Removal of a Large Wall Section, Horizontal Cut almost completed

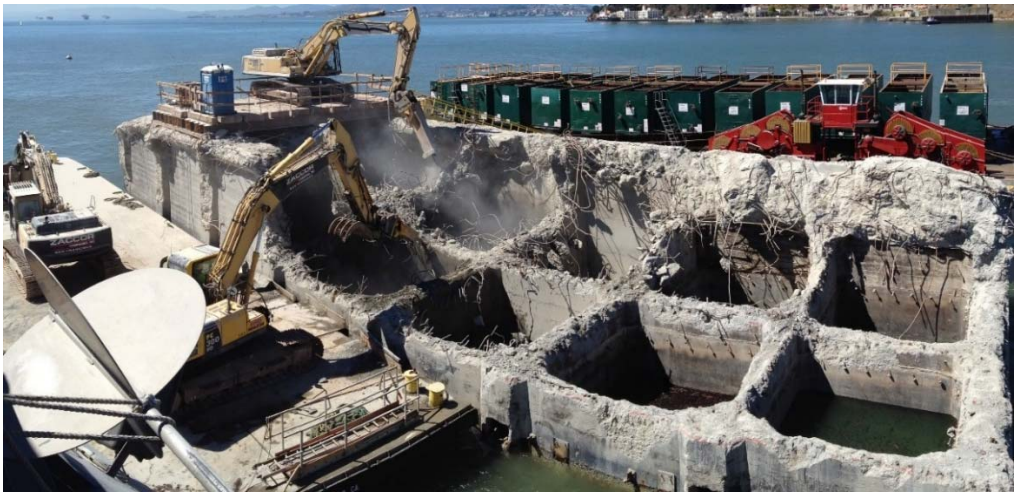


Fig. 9 Demolition Completed to EL +9 for Several Cells



Fig. 10 Caisson Mechanical Demolition Completed

© 2016 Deep Foundations Institute

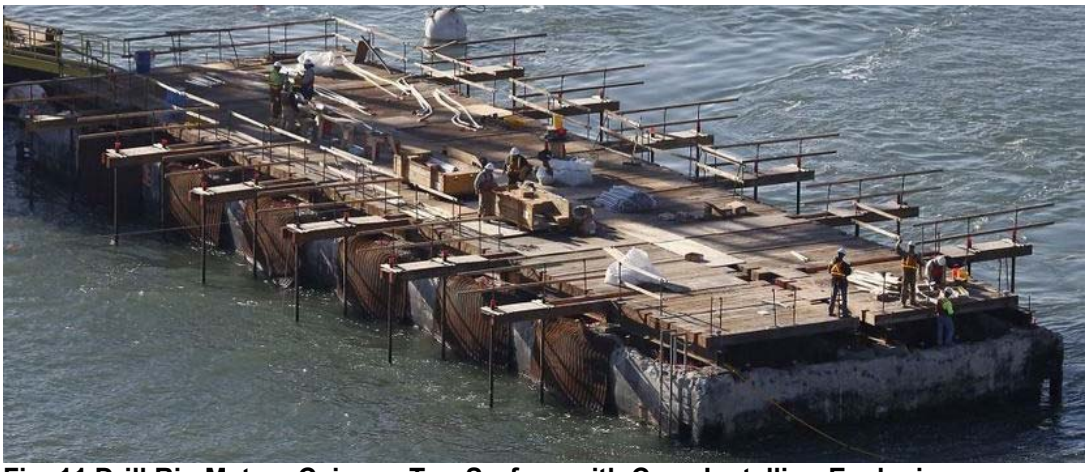


Fig. 11 Drill Rig Mat on Caisson Top Surface with Crew Installing Explosives



Fig. 12 Implosion Underway on 11/14/15 (Photo: Caltrans), Barge in background supports the Air Compressors for the Bubble Curtain System

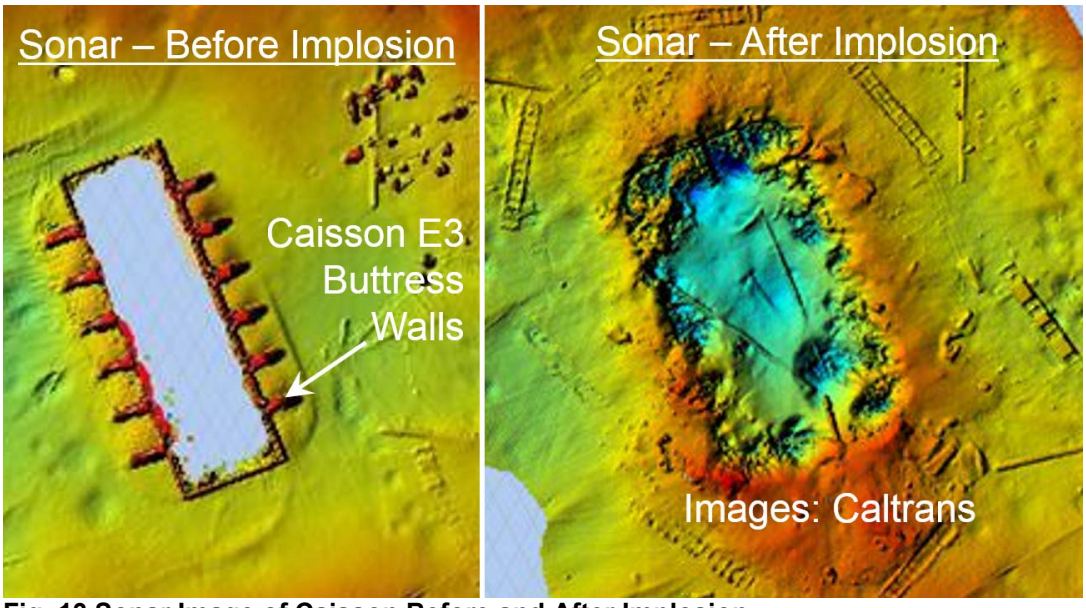


Fig. 13 Sonar Image of Caisson Before and After Implosion

© 2016 Deep Foundations Institute

REPLACEMENT OF THE KOSCIUSZKO BRIDGE BROOKLYN CONNECTOR: AN INTEGRATED DESIGN AND CONSTRUCTION APPROACH

Britain A. Materek, HNTB Corporation, Parsippany NJ, USA, 973-434-3128, bmaterek@hntb.com
M. D. Riegel, HNTB Corporation, Parsippany NJ, USA, mdriegel@hntb.com
P. B. Pizzimenti, Haley and Aldrich, Parsippany NJ, USA, ppizzimenti@haleyaldrich.com
E. M. Zamiskie, Haley and Aldrich, Parsippany NJ, USA, ezamiske@haleyaldrich.com

ABSTRACT

The Skanska/Kiewit/ECCO III team (SKE) in association with HNTB was awarded the design-build contract for Phase I of the Kosciuszko Bridge Replacement Project. As lead designer for the SKE team, HNTB was responsible for the design of the Brooklyn Connector which includes construction of approximately 2000 feet of new staged earth-filled embankments utilizing prefabricated modular retaining walls (T-Walls®). The proposed embankments will be constructed adjacent to and beneath the existing Brooklyn Queens Expressway (BQE) viaduct while the existing viaduct remains in service. Critical aspects of the settlement assessment relating to the soils supporting the existing BQE will be addressed, as their behavior drives the deformation of the viaduct. Furthermore, a construction monitoring program was used to enable the designer to assess settlement predictions and allow SKE to mitigate potential impacts to the existing BQE during construction. Additionally, the methodology for installation of the embankments in a limited access area underneath an active viaduct supported on settlement sensitive shallow foundations will be presented.

Keywords: Kosciuszko Bridge, T-Wall®, CPT, settlement, elastic modulus, shear modulus, construction monitoring, automated total stations

INTRODUCTION

Skanska-Kiewit-ECCO III Joint Venture, in association with HNTB was contracted by the New York State Department of Transportation (NYSDOT) to design and construct the Phase 1 replacement of the Kosciuszko Bridge Design-Build Project. Phase 1 of the project involves the design and construction of the new eastbound structures of Interstate 278 over Newtown Creek from Brooklyn to Queens. The project runs between Morgan Avenue in Brooklyn and the Long Island Expressway Interchange in Queens (approx. 1.1 miles) and includes the staged demolition of the existing structures.

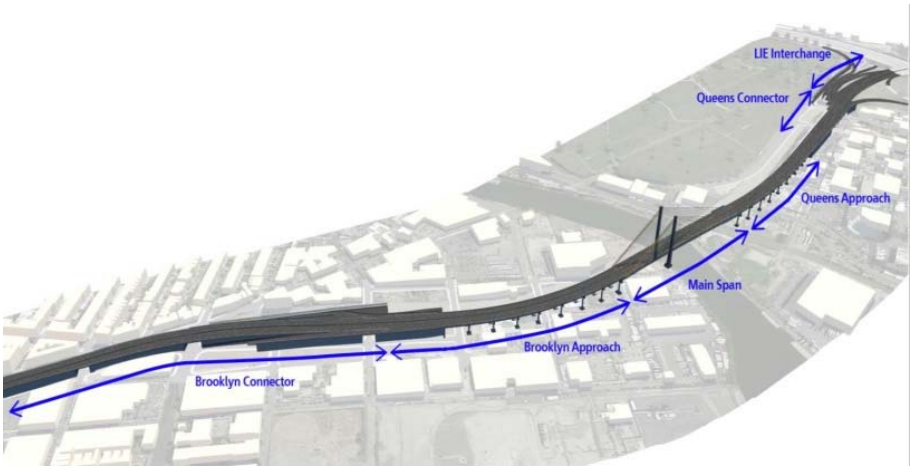


Fig. 1. Site Layout

© 2016 Deep Foundations Institute

This paper presents the challenges associated with the design of the Brooklyn Connector and details the design teams approach to managing the risks associated with the placement of up to 45 feet of fill adjacent to and below the existing Brooklyn Queens Expressway (BQE).

STRUCTURAL SETTING

The existing Brooklyn Connector extends from the Meeker Viaduct to the Brooklyn Approach and was originally constructed in1939 with modifications performed in 1971. The Brooklyn Connector consists of 78 rigid concrete spans supported by concrete piers on spread footings that are founded approximately 10 to 15 feet below the existing grade on the natural silty sand deposits. Portions of the original connector contain concrete closure walls with a brick veneer.

The connector structures are typically composed of a series of 3-span continuous rigid concrete frames in the longitudinal direction and two 2-span bents in the transverse direction. There is a longitudinal expansion joint between the eastbound and westbound halves, with the center pair of columns beneath the joint supported on a common footing. The transverse interior bents consist of a single row of columns and cap beams for the interior bents and double columns and cap beams at the expansion (end) bents. The pairs of columns at the transverse expansion bents are supported on common footings. Existing column heights through this section, with the exception of the columns supporting portions of the ramps, vary from approximately 11-feet to 39-feet.

GEOTECHNICAL SETTING

The project site is situated in the Atlantic Coastal Plains Lowlands physiographic province, immediately east of the Manhattan Prong of the New England Upland province. The site is underlain by Cambrian-Ordovician Age metamorphic bedrock of the Hartland Formation, primarily gneiss of varying quality with a zone of highly weathered and decomposed rock of varying thickness overlying the competent rock. Intermittent, schist and marble bedrock have been reported to be present on site.

Overlying the bedrock is Cretaceous Raritan Formation soils, which exist as a confining layer, and are generally described as a light to dark gray, brown-red, pink red and gray white clay, silty clay and clayey to silty fine sand.

The advance of the Wisconsin glaciation roughly 15,000 years ago deposited Harbor Hill moraine across the site. The till of this moraine is comprised of an unsorted mixture of clay, silt, sand, gravel, cobbles and boulders. The till is overlain by organic soils surrounding the Newtown Creek which extend both eastward and westward along the Brooklyn and Queens Approaches. Surficial soils are variable in the upper 10 to 30 feet of the profile due to miscellaneous urban fill material that is comprised of a mixture of silt, sand, gravel and construction debris (e.g. brick, wood, trash, concrete and other materials).

Groundwater levels were measured at monitoring wells where the groundwater table was found within the upper glacial deposits upland and just below the fill as it approaches the creek. The groundwater ranges in depth from approximately 10 feet below the existing ground surface near Newtown Creek, to 20 to 40 feet below the existing ground surface as the existing grade rises to the east and west of the creek.

Subsurface conditions generally consist of the following materials listed in descending order: Fill, Glacial Sand, Glacial Silt & Clay, Raritan Clay, Decomposed Rock and Bedrock as illustrated in **Fig. 2**. Based on the stresses induced from the proposed wall and embankment loads, settlements below approximately 70

© 2016 Deep Foundations Institute

feet are insignificant. Therefore, strata below the Glacial Sand were not impacted by the proposed wall and embankment construction and have not been addressed in this paper.

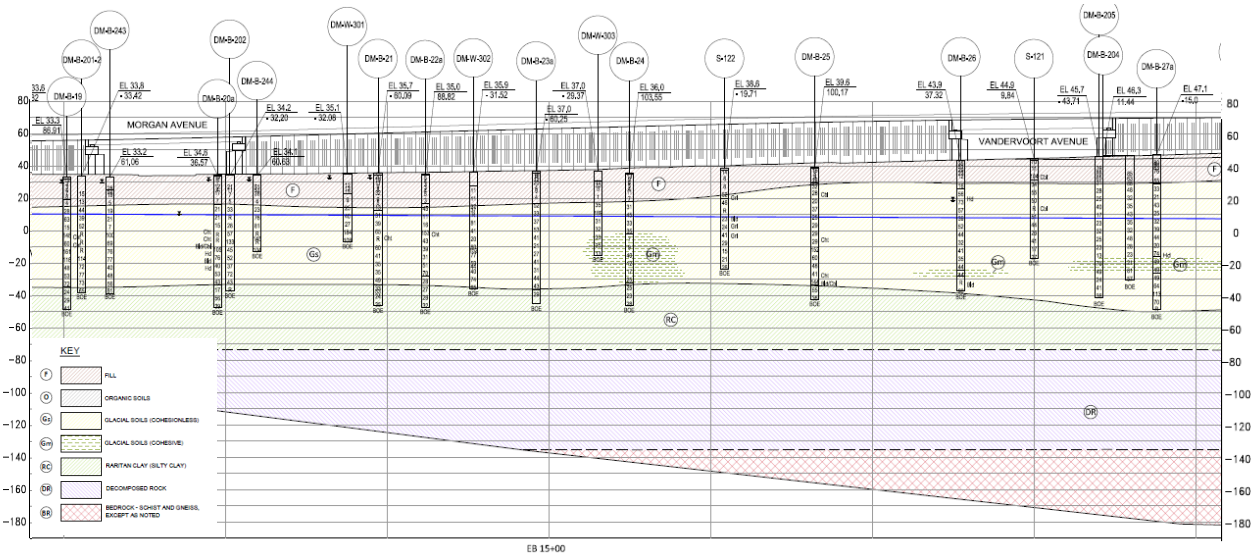


Fig. 2. Generalized Subsurface Profile

Stratum 1 - Fill

The surficial soils under the BQE and immediately adjacent are a variable mixture of urban fill comprised of silt, sand, gravel, cobbles, brick fragments and wood. The average standard penetration test (SPT) N60 value is 17 bpf, which corresponds to a relative density of medium-dense. This fill stratum occurs continuously along the alignment, but its thickness along the Brooklyn Connector alignment ranges between approximately 10 feet to 17 feet thick.

Stratum 2 – Glacial Soils (Silty Sand)

Silty sand glacial deposits generally underlie the fill throughout the Brooklyn Connector. Gravel, cobbles and boulders were encountered in this stratum. The average SPT N60 value is 40 bpf which corresponds to a relative density of dense. This Glacial Silty Sand stratum occurs continuously along the alignment. Where fully penetrated, the thickness varies from approximately 45 feet to 120 feet thick.

GEOTECHNICAL EVALUATION OF PROPOSED DESIGN

Overview

The critical component and the primary focus of this paper is associated with the settlement analysis performed for T-Wall® supported embankments where fill heights vary from approximately 13 feet to 45 feet. Constructing beneath and directly adjacent to the existing BQE presents some unique design challenges associated with construction in low overhead conditions and potential impacts to existing facilities which are supported on shallow foundations and will remain in service as embankment fills and T-Walls® are constructed. Geotechnical assessment of the soils supporting the existing BQE were a critical aspect of this design, as their behavior when subjected to additional stress beyond their current state drives the deformation of the viaduct.

Since the predominant strata being stressed by the construction of the T-Walls® is granular in nature, settlement was anticipated to be elastic and governed primarily by the elastic modulus of the soil. Several

© 2016 Deep Foundations Institute

methods to estimate the soil modulus from SPT and CPT tests were employed. Ultimately the design relied upon methods of correlating elastic modulus (E_s) values from CPT soundings.

Given the sensitivity of the existing structure to differential settlement, a detailed and thorough assessment was made of potential global variation as well as local variation of soil moduli. The E_s value was the single most important geotechnical engineering parameter in this assessment given the consequences associated with exceeding tolerable differential movements between adjacent columns of the existing BQE viaduct.

The geotechnical engineer approached this design initially through computations based on elastic settlements with soil parameters derived from SPT investigations. This approach was deemed inadequate to define and mitigate the obvious risks due to the high amount of gravel encountered and inaccuracy of SPT correlations to elastic soil parameters. These challenges led to the subsequent advance of a CPT/sCPT sounding program to better define the elastic parameters of the overlying urban fill and the glacial deposits below which encompass the zone of interest. To further validate and calibrate design methodologies the Designer also completed a static settlement load test. This in-situ load test and the adjacent sCPT soundings provided an opportunity for the design team to calibrate estimated elastic parameters.

Methodology

Cone Penetration Testing (CPT) and related correlations where used to refine the development of elastic modulus values for cohesionless soils subject to elastic settlement beneath the proposed Brooklyn Connector Embankments. Several published studies which contained relationships between elastic modulus and a range of assumptions and conditions were reviewed and assessed. Baldi et al., (1989) correlates secant elastic modulus for an average axial strain of 0.1% for a range of stress histories and aging based on the normalized cone resistance. Additionally, Robertson (1991) established methods to estimate the equivalent elastic modulus based on CPT results in sands based on the degree of loading and cone resistance, with corrections for aging. Although both these methods are valid, they have been dismissed in favor of more recent methods proposed by Robertson (2009), in which estimates of elastic modulus are based on correlations to shear wave velocity and the subsequent relationships between shear wave velocity, shear modulus and elastic modulus.

In order to assess the proposed methods of correlating CPT data and elastic modulus the following relationships between shear wave velocity, shear modulus and elastic modulus have been utilized:

$$V_s = \sqrt{G_o/\rho} \qquad [1]$$

where V_s is the shear wave velocity, G_o is the maximum shear modulus and ρ is the mass density (the total unit weight divided by the acceleration of gravity) of the soil.

$$E = 2\,(1+\nu)\,G \qquad [2]$$

where E is the elastic modulus, G is the shear modulus, and ν is the Poisson's ratio of the soil.

The accumulated experience over the last 25 years with sCPT results has led to the establishment of relationships between cone resistance and shear wave velocity, Vs, for a wide range of soils using the CPT SBTn chart as a basis. Robertson et al. (1992) developed a set of contours on the normalized SBTn Qtn-Fr chart of normalized shear wave velocity based on over 100 SCPT profiles combined with available published data. The contours originally developed in 1992 have been further evaluated and

© 2016 Deep Foundations Institute

verified using additional published data from other regions of the world (e.g. Schnaid 2005; Andrus et al. 2007) and can be approximated using the following equation (in m/s) from Robertson 2009:

$$V_s = [\alpha_{vs}(q_t - \sigma_v)/p_a]^{0.5} \quad [3]$$

where V_s is the shear wave velocity, α_{vs} is the shear wave velocity cone factor, q_t is the cone resistance, σ_v is the in-situ vertical stress, and p_a is the atmospheric pressure.

As the contour shapes for α_{vs} are similar to those for the soil behavior type index, I_c, (Robertson 2009) α_{vs} can be estimated using the following equation in $(m/s)^2$:

$$\alpha_{vs} = 10^{(0.55I_c+1.68)} \quad [4]$$

In order to verify the use of Robertson's method, results from six CPT soundings were correlated to shear wave velocity using Equations [3] and [4] using the software program CPeT-IT Version 1.7.6.19 from GeoLogismiki.

The results of the CPT correlated shear wave velocities were averaged and compared to measured average values of shear wave velocity determined from PS logging and sCPT results. The shear wave velocity values developed from CPT correlations were in general agreement with measured shear wave velocity values in both the fill and cohesionless glacial sands.

An additional assessment of measured shear wave velocity relative to correlated shear wave velocity was performed near Varick Avenue where a field load settlement test was performed. A seismic cone was used at multiple locations to obtain measurement of shear wave velocity at 5 foot intervals. The correlated values for shear wave velocity were compared to the measured values from the seismic cone tests, an example of which is included in **Fig. 3**. Overall, using the shear wave velocity correlations specified above appear to be somewhat conservative in relation to estimating elastic modulus for settlement analysis.

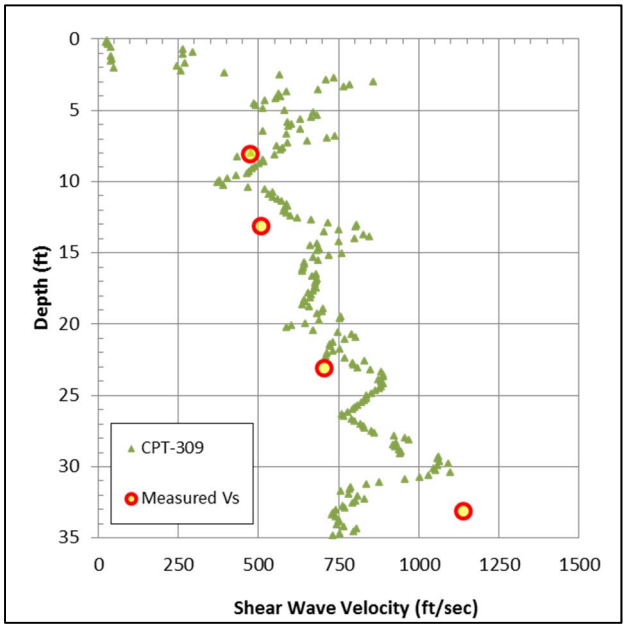


Fig. 3. sCPT Measured Shear Wave Velocity verses Correlated Shear Wave Velocity

© 2016 Deep Foundations Institute

In order to estimate the elastic modulus a relationship between the shear modulus and maximum shear modulus must be defined and Equation [2] is utilized. Assuming an average Poisson's ratio, ν, of 0.25 which is applicable to most course grained soils under drained conditions the following relationship can be developed between elastic modulus and shear modulus:

$$E = 2.5G \quad [5]$$

Thus far a methodology has been presented to estimate the maximum shear modulus, G_o, from Equation [1] which is related to the shear wave velocity and only applicable at very small strains. However, using the small strain modulus would not be appropriate for developing an estimate for an elastic modulus to assess embankment settlement, which is associated with much larger shearing strains. Therefore, there is a need to soften the initial shear modulus, G_o, associated with the shear wave velocity to a shear modulus, G, that corresponds to a strain level appropriate for design purposes to assess embankment settlement. In order to soften G_o and to relate Equations [1] and [2], a relationship between G/G_o is defined by assessing the generalized variation in shear modulus with shearing strain based on the work of Seed and Idriss (1970) and Winterkorn and Fang (1975).

An average axial strain of approximately 0.1% is reasonably representative for many well designed foundations (Lunne et al., 2001) corresponding to a G/G_o of approximately 0.3. This in in fact the assumption used in Roberston's method to correlate CPT results directly to elastic modulus. This correlation also assumes typical values for Poisson's ratio and unit weight in addition to G/G_o, which limits the ability of the correlation to account for alternate values.

Given the variability in the relationship between shear modules and shear strain illustrated by Winterkorn and Fang (1975), and given the need to estimate settlement caused by the proposed embankment construction which typically have larger shearing stresses associated with larger loading areas, deeper zones of influence, and larger relative deflections relative to a shallow foundation, a more flexible correlation is required to address these nuances. Therefore, an alternate method is recommended in Equation [6] which uses either the measured or correlated values of shear wave velocity to estimate the elastic modulus where unit weight, Poissons ratio, and G/Go are all assessed independently:

$$E = 2\,V_s^2\,(1+\nu)\,[\gamma/32.2]\,(G/G_o) \quad [6]$$

where Vs is in (ft/sec), γ is in (pcf) and ν, and G/Go are dimensionless.

Verification of Methodology

A settlement load test was performed using concrete blocks stacked approximately 15 feet high and loaded in stages. The plan dimensions of the loaded area is approximately 15 ft x 15 ft. Loading of the soil occurred in three stages consisting of a 450 psf load, a 1350 psf load and finally a 2250 psf load. Settlement was measured over time as the load was increased. In order to verify the recommended correlation methods, settlement was monitored using three survey points mounted to settlement plates bearing on the existing ground surface under the load.

To verify the correlation methods and calibrate the appropriate G/G_o ratio, settlement was estimated using the program Settle 3D by RocScience using elastic modulus values calculated using Equation [6] and using G/G_o ratios of 0.2, 0.25 and 0.3. Given that the purpose of the exercise was to attempt to match the results of the filed settlement load test using correlated data from CPT soundings at the location of the test, average values of shear wave velocity were used in the assessment.

Settlement was assessed at the center of the loaded area in Settle 3D and compared to the measured field results. Results of the analysis indicate that parameters developed using a G/G_o of 0.2 (summarized in

© 2016 Deep Foundations Institute

Table 1) are in good agreement with the results of the load test as illustrates in **Fig. 4**. Revisiting the work of Seed and Idriss (1970), a G/G_o or 0.2 corresponds to shearing strain levels that range from approximately 0.12 to 0.3 percent. This value also falls within the bounds of appropriate shear strain levels as illustrated by the work of Winterkorn and Fang (1975).

Table 1. Settlement load test soil parameters corresponding to G/Go of 0.20

Depth		Unit Weight (γ)	Poisson's Ratio (υ)	Shear Modulus Ratio (G/Go)	Shear Wave Velocity (Vs)	Elastic Modulus (E)
(ft)		(pcf)	(dim)	(dim)	(ft/sec)	(ksf)
0	10	109	0.34	0.2	523	496
10	20	109	0.34	0.2	698	884
20	30	122	0.27	0.2	819	1291
30	40	122	0.27	0.2	999	1921

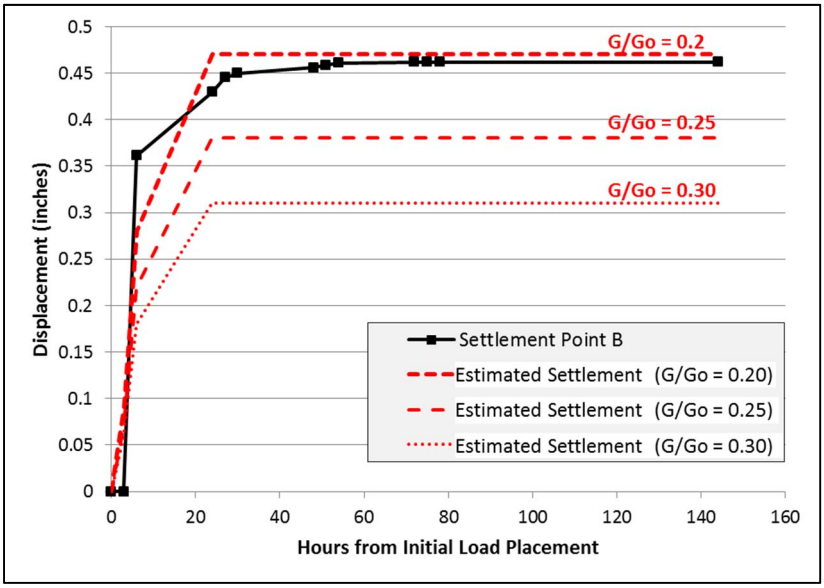


Fig 4. Settlement Load Test Results verses Settlement Estimates

Settlement Analysis

In assessing impacts to the existing viaduct as well as the proposed T-Walls, lower bound (LB), average and upper bound (UB) soil parameters were used to determine the anticipated total settlement and differential settlement (at grade for T-Wall assessment and at depth for existing foundation assessment). To capture the condition where soil parameters vary underneath adjacent existing columns, differential settlements were assessed using the unlikely scenario where LB parameters were present at one column and UB values were present at all adjacent columns. Upper bound and LB settlement estimates were conducted at each discrete existing column location to facilitate this assessment.

Although assessments were made comparing UB conditions directly adjacent to LB conditions, it should be noted that the variability observed during the investigation did not indicate this to be a likely condition. Therefore, additional assessment was also performed to assess potential differential settlement the UB to UB assessment of soil parameters and LB to LB for design purposes.

© 2016 Deep Foundations Institute

The software program Settle 3D version 2.011 was used to evaluate the settlement of the T-Walls and embankments. A staged analysis was performed to model the fill placement. A benefit of performing the staged settlement analysis is that it facilitates the evaluation of the cumulative total and differential settlement at any particular step as well as the incremental settlement between steps. **Table 2** presents the results of the settlement analyses for a portion of the embankment at the bearing level of the existing spread footings (approximately 12 feet below existing ground surface). This analysis corresponds to the anticipated vertical displacement that will be observed at the top of the existing pier columns.

Table 2. Maximum differential settlements between any two columns and total settlement

Stage	Maximum Differential Settlement Between Columns (in)				Max. Total Settlement (in)	
	LB vs. LB	LB vs. UB	UB vs. UB	ALL CASES	UB	LB
1D	0.46	0.79	0.12	0.8	0.88	0.21
2A	0.46	0.62	0.3	0.6	0.9	0.65
2D	0.7	0.76	0.51	0.8	1.23	0.9
3A	0.89	0.89	0.56	0.9	1.38	0.9

The results of the analysis performed suggests that the estimated maximum differential settlement for the existing footings, assuming lower bound and upper bound soil parameters are present at adjacent existing columns, is 0.9 inches. Maximum total settlement of the existing bridge footings was expected to be approximately 1.38 inches when LB elastic modulus values are used in the assessment.

STRUCTURAL IMPACTS

The existing structure was analyzed to evaluate its capacity to tolerate differential settlements during staged construction of the new retained fill structures. This analysis was performed for typical intermediate and expansion bents which are typical for the existing structure at the Brooklyn Connector in terms of structural configuration. The existing bent heights vary throughout the region and the bent heights analyzed are the shortest intermediate and expansion bents in this region. This is generally conservative for most of the bents in this region because shorter bents are inherently stiffer than taller bents. Hence, shorter bents develop higher shear forces and moments when subjected to relative displacements than taller bents.

The existing structures from Vandervoort Avenue to the West Approach Abutment are rigid frame cast-in-place concrete structures as previously detailed in the Structure Setting section of this paper and as illustrated in **Fig. 5**. Structural analysis was performed to determine the capacity of the existing Brooklyn Connectors to accommodate relative foundation displacements that may be expected during the staged construction of the new retained fill structures.

The nonlinear static analyses determined that the existing structure has sufficient displacement capacity to accommodate relative foundation settlements in excess of the anticipated geotechnical settlements without structural modifications. However, the existing bent cap beams were determined to have inadequate shear capacity for the combination of settlement with dead and live loads. Therefore, a retrofit scheme was designed and detailed to provide additional shear capacity for the existing bent cap beams. The retrofit consists of Fiber-Reinforced Polymer (FRP) wrapping which will be installed prior to the start of fill placement.

© 2016 Deep Foundations Institute

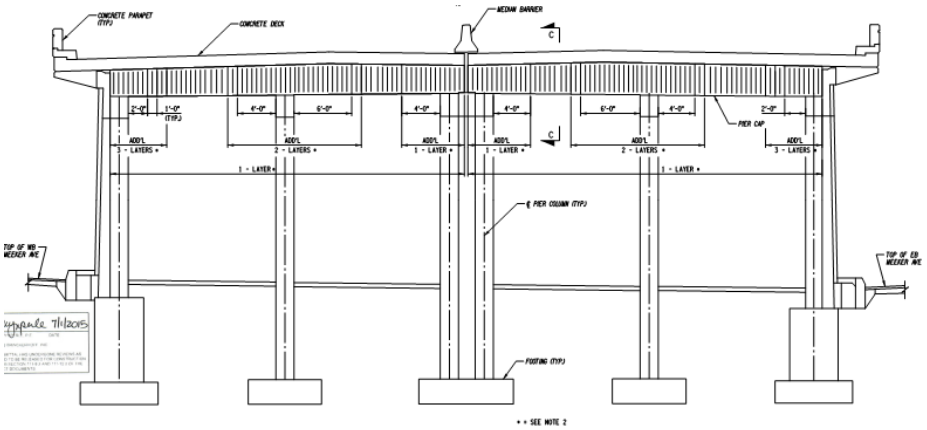


Fig. 5: **Typical Structural Cross Section**

MONITORING

Instrumentation and Monitoring Plan

Recognizing the importance to life-safety and essential service the BQE provides to daily New York City traffic patterns, the risk tolerance for a potential shut-down of the corridor was low. All parties involved recognized that a monitoring program that relies solely on the exceedance of an absolute value would not be satisfactory. Rather, an observational approach that considers both monitoring thresholds and an assessment of the potential for future deformation trends was used to assess the response of the existing structure to surcharge loads. The approach presented herein was designed to keep the Designer and builder informed as to the results of future actions and allows for adjustments to the program on a pro-active, rather than re-active basis.

Redundant optical monitoring systems were used as the primary instrument to measure absolute and relative positions of various fixed targets installed on structural elements and in the surrounding ground. The primary optical monitoring systems consisted of a series of automated total stations (AMTS) monitoring reflective mini-prisms installed at the top of each existing support pier column location where feasible. The monitoring program included automated reporting such that absolute and differential positions of each column supporting the BQE viaduct were uploaded to a controlled server that was available for NYSDOT, SKE, and Designer access in real time.

Observational approach methods were employed as the construction proceeded and monitoring data was observed, such that frequency of measurements and types and numbers of instruments were adjusted, either up or down as appropriate, to meet the needs of the activities being performed. The observational approach also allowed for adjustments to the construction operations in isolated areas where warranted.

The Designer assessed the observed settlement of the existing viaduct support piers and the movement of the ground surface on a regular basis through the progress of the build. Fill was cautiously placed by requiring a specific "Construction Hold Point" at each incremental 5–foot fill height level. The Hold Points allowed the Designer an opportunity to review the data collected and assess the predicted versus actual deformation and, if required, recommend adjustments to the build approach to maintain settlements within specified tolerances.

Monitoring thresholds were established based on the factored structural limits determined from the assessment of the existing viaduct support structure and are illustrated in **Table 3**. Data was reviewed, analyzed, and interpreted on an on-going basis with a focus on defining characteristic trending of

© 2016 Deep Foundations Institute

structural response to filling surcharge loads. Trend lines were used to predict the effect of additional fill placement and to prevent placing fills in excess of that which would exceed thresholds. The purpose of tracking the trends was to predict and inform the Designer and the builder of possible threshold exceedance levels before they actually occur.

Table 3. Monitoring Thresholds

Threshold Limit	Determination of Threshold Value	Threshold Value (in.)	Actions	
			Designer	Contractor
Alert	50% of factored structural limit	0.25 to 0.5	Process data. Predicts data trends.	Proceeds with caution. Prepares for remedial action.
Action	75% of factored structural limit	0.5 to 0.75	Assess structure. Determines courses of action and recommends repairs, if needed.	Stops work. Implements remedial actions if directed.

Figure 6 illustrates, in concept, the relationships between the threshold limits and theoretical deformation trends, against which actual observed data would be compared. The DB team utilized this approach to assess the monitoring results to proactively implement mitigation measures prior to achieving threshold limits. Based on the theoretical graph, the observed response at monitoring point "A" would indicate that filling is resulting in deformations that do not exceed predicted responses nor will approach thresholds. In contrast, the response at point "B" would support that if additional surcharge were to be placed, thresholds would be exceeded. In this case, actions can be taken before even the lowest threshold level is exceeded, or work may proceed with the knowledge that this area will require future modification to the work flow.

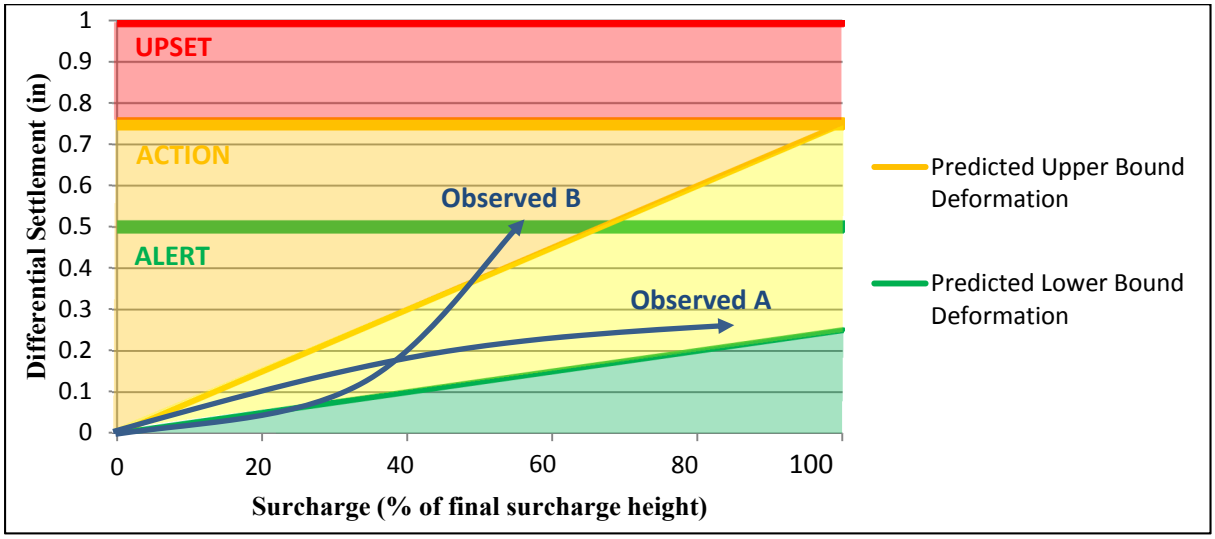


Fig. 6: Example Relationship between Threshold Limits and Theoretical Deformation Trends

Monitoring Approach and Analysis Results

Due the geometric arrangement of the existing viaduct which included 78 bents consisting of 6 to 8 columns each, there were approximately 500 mini-prisms being measured consistently. Differential measurements were automatically computed from ATMS data for both the transverse and longitudinal column pairs. Given the large number of measurements, it was necessary to develop a practical approach to assessing the data. The approach taken was a collaborative effort developed between the Designer,

© 2016 Deep Foundations Institute

SKE, and SKE's instrumentation subcontractor. The process used is is described herein with an example of data obtained for the portion of the Brooklyn Connector.

At all stages of filling, the Designer reviewed data to establish settlement trends in relation to geotechnical upper and lower bound predicted settlements for a given load stage. As previously discussed, theoretical estimates of differential settlement were assessed assuming lower bound modulus parameters existed adjacent to upper bound modulus parameters. Therefore, as long as the total settlement measured at any two adjacent columns trended in between the upper bound and lower bound estimates for total settlement, tolerance levels for differential settlement were not anticipated to be exceeded. Additionally, differential settlements were assessed directly relative to the percentage of fill height that had been placed.

The first challenge was maintaining accurate records of surcharge fill heights. Since it was not possible to automate measurements of fill height relative to time, these measurements required daily survey and reporting by SKE to the Designer. Fill heights were reported schematically on a daily basis during construction by general areas that were defined at the onset of earthworks. This allowed the designer to track the percentage of total fill placed relative to time and correlate these measurements to the design predictions.

Additionally, a daily snapshot report of the ATMS absolute measurements and averaged differential values between columns was provided in tabular form. The tabulation was hot-color coded as values approached threshold levels. These tabulations allowed the Designer to have an overview of areas where differential movements were relatively greater than other areas, and allowed the Designer to focus review efforts into areas with greater potential concern.

Based on the daily report and tabulated surcharge data, the Designer was able to generate specific trend plots, as originally proposed in the monitoring plan, to determine the relative performance of a given column pair and compare measured and predicted displacements. **Figure 7** shows a typical plot for a column pair in the Connector between Varick to Stewart Avenues. This observed trend line is a typical example of a pair that initially began to settle more than predicted, but as greater loads were placed, the settlement trend began to run under the predicted level. Although this column pair eventually exceeded the Alert threshold level, it was apparent by trend analysis that it would not reach the Action threshold. By this method, the Designer was able to agree to allow filling to continue without the need for SKE to begin preparations to implement remedial actions.

CONCLUSION

A CPT investigation was used to refine the development of elastic modulus values for the cohesionless soils present beneath the existing Brooklyn Connector viaduct in order to estimate values of total and differential settlement. The refined settlement analyses, in conjunction with the structural assessment allowed the design team to propose a structural retrofit on the existing bent cap beams that could withstand the anticipated forces generated by these anticipated differential settlements. Overall, the adopted design approach allowed SKE to move forward with the construction of the Brooklyn Connector embankment directly adjacent or underneath the existing viaduct while still in service.

The monitoring program was used to validate the predictive models, identify areas of concern, provide a rational means for decisions on construction process, maintain contractor's construction schedule and, most importantly, protect the public and health of the city's regional traffic flow. The monitoring program was developed with comprehensive and redundant measurement systems driven by the structural characteristics and importance of the Connector. In order to keep the construction operations moving

© 2016 Deep Foundations Institute

fluidly and reduce the "surprise" element of reaching critical thresholds requiring unexpected work stoppages, an observational approach including trend analyses was adopted. The trend analyses were used to determine if the settlements compared to the relative surcharge were below, as-expect, or above predicted levels. More importantly, the trend analysis was used to determine if the rate of settlements were accelerating or decelerating giving the Designer the ability to predict if critical thresholds would ever be reached.

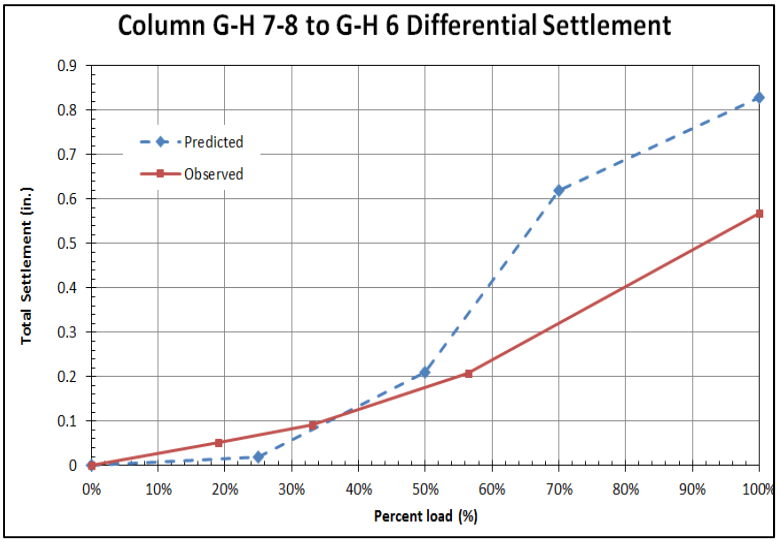


Figure 7. Typical Observational Trend Analysis of Differential Settlements at a Select Column of Brooklyn Connector between Varick and Stewart Avenues

Overall, the monitoring program in conjunction with the predictive analyses, gave confidence to the Designer that the filling operations could be controlled to maintain the structural integrity of the Approach, gave the SKE advance notice of where work could proceed and where remedial actions might be needed so that changes to the schedule did not come as a surprise, and gave NYSDOT the assurance that traffic patterns and life safety could be maintained on the existing bridge.

REFERENCES

Andrus, R.D., Mohanon, N.P., Piratheepan, P., Ellis, B.S., and Holzer, T.L. (2007) "Predicting shear wave velocity from cone penetration resistance". In Proceedings of 4th International Conference on Earthquake Geotechnical Engineering, Thessaloniki, Greece, 25-28 June 2007. Springer, New York. Paper No. 1454.

Baldi, G., Belloti, R., Ghionna, V.N., Jamiolkowski, M. and Lo Presti, D.F.C. (1989) "Modulus of sands from CPT's and DMTs". Proceedings of the 12th International Conference on Soil Mechanics and Foundaiton Engineering, Rio de Janerio, 1, 165-70, Balkema Pub., Rotterdam.
Baskerville, C.A, Earth Science in the City – Chapter 3 Engineering Geology of New York City. 2003.

Eslaamizaad, S., and Robertson, P.K. (1997) "Evaluation of settlement of footings on sand from seismic in-situ tests". In Proceedings of the 50th Canadian Geotechnical Conference, Ottawa, Ont., 20-22 October 1997. BiTech Publishers, Richmond, B.C. Vol. 2, pp. 754-764.

© 2016 Deep Foundations Institute

Lunne, T., Robertson, P.K., and Powell, J.J.M., (1997) “Cone Penetrometer Testing in Geotechnical Practice”. Spon Press, pp 93.

Robertson, P.K. (2001) “Estimation of Foundation Settlements in Sand from CPT”. ASCE Geotechnical Engineering Congress, Boulder.

Robertson, P.K., Woeller, D.J., and Finn, W.D.L. (1992) “Seismic cone penetration test for evaluating liquefaction potential.” Canadian Geotechnical Journal, 29(4): 686-695. doi:10.1139/t92-075

Robertson, P.K. (2009) “Interpretation of Cone Penetration Tests – A Unified Approach”. Canadian Geotechnical Journal, 46: 1337-1355. doi: 10.1139/T09-065.

Schnaid, F. (2005) “Geocharacterization and Engineering Properties of Natural Soils by In-Situ Tests”. Proceedings of the 16th International Conference on Soil Mechanics and Geotechnical Engineering, Osaka, Japan, 12-16 September 2005. Millpress, Rotterdam, Netherlands. Vol. 1, pp. 3-45.

Seed, H. B., and Idriss, I. M. (1970). “Soil moduli and damping factors for dynamic response analysis.” Rep. No. EERC 70-10, Earthquake Engineering Research Center, Berkeley, Calif.

Winterkorn, H.F., and Fang, H. Y. (1975), “Foundation Engineering Handbook.” Van Nostrand Reinhold Company, New York.

© 2016 Deep Foundations Institute

This page left intentionally blank

© 2016 Deep Foundations Institute

ROCK SOCKETED DRILLED SHAFTS FOR THE GOETHALS BRIDGE REPLACEMENT

John P. Turner, Dan Brown and Associates, PC, Laramie, WY, USA jturner@dba.world
Steven S. Dapp, Dan Brown and Associates, PC, Sequatchie, TN, USA sdapp@dba.world
Dan A. Brown, Dan Brown and Associates, PC, Sequatchie, TN, USA dbrown@dba.world

ABSTRACT

The Goethals Bridge Replacement (GBR) spanning the Arthur Kill Waterway between Elizabeth, NJ and Staten Island, NY consists of a dual-span 1,982.5-ft long cable-stayed bridge with approach spans of 2,545 ft on the NJ side and 2,788 ft on the NY side. The bridge is supported on over 200 drilled shaft foundations ranging in diameter from 4.5 ft to 10 ft and socketed into Passaic Formation siltstone. Drilled shaft resistances for design were based on load tests as described in a companion paper (Dapp et al. 2016). This paper presents the main foundation design considerations and challenges. The approach to construction of the rock sockets, with a focus on quality in order to support the use of high nominal values of side and base resistance, is described. Lessons learned from this project and their application to future similar projects are presented.

Keywords: drilled shaft, bridge foundations, load test, axial, lateral, bi-directional, Statnamic, rock socket

INTRODUCTION AND BACKGROUND

The Goethals Bridge Replacement (GBR) project is a Public-Private Partnership (P3) that represents a major milestone for the Port Authority of New York and New Jersey (PANYNJ) in its distinguished history of bridge building in the greater New York City metropolitan area. The new bridge will replace the existing Goethals Bridge, named after Major General George W. Goethals, Chief Engineer of the Panama Canal and the first consulting engineer for the Port Authority. The existing Goethals Bridge along with the Outerbridge Crossing and the Bayonne Bridge comprise the three Port Authority bridges connecting Staten Island with New Jersey. The existing Goethals Bridge and the Outerbridge Crossing are cantilever truss structures and both opened on the same day in 1928. They were designed by J.A.L. Waddell under the supervision of the eminent engineer Othmar H. Ammann (1879-1965), who was the designer of many other iconic bridges in the NY City area including the Bayonne Bridge (1931), the George Washington Bridge (1931), and the Verrazano Narrows Bridge (1964). The designer of record for the replacement Goethals Bridge is Parsons Corporation, which is the successor firm of Robinson & Steinman, whose principal David B. Steinman was also a notable NY area bridge designer and a contemporary and rival of O.H. Ammann.

The replacement Goethals Bridge is supported on over 200 rock-socketed drilled shaft foundations. Each main pylon tower is supported on a group of six 9-ft diameter drilled shafts and each anchor pier is supported by two 10-ft diameter shafts. Each approach pier consists of a two-column bent with each column supported on a rock-socketed drilled shaft. A rendering of the Main Bridge crossing the Arthur Kill is shown in Fig. 1.

© 2016 Deep Foundations Institute



Fig. 1. Rendering of Main Bridge segment of GBR. View is to the north (Photo courtesy of PANYNJ).

GEOLOGIC SETTING AND SUBSURFACE CONDITIONS

The GBR site is located geologically at the east margin of the Newark Basin, one of the many rift basins that developed in response to breaking apart (rifting) of the supercontinent Pangaea that began during the late Triassic Period, approximately 220 million years ago, and coincided with the opening of the Atlantic Ocean. Crustal extension in response to rifting resulted in down-faulting of crustal blocks, or grabens, bounded by normal faults. The Newark basin is a half-graben bounded by the Ramapo fault on the west and subsequently filled with sediments eroded from the adjacent uplifted footwalls. One of the resulting sedimentary units comprising the Newark Supergroup is the Passaic Formation, Lower Jurassic to Upper Triassic 'red beds' consisting of argillaceous siltstone, silty mudstone, very fine grained sandstone, and shale. The reddish-brown color derives from an abundance of oxidized iron minerals. At the GBR site, the Passaic Formation is predominately siltstone with occasional interbedded shale layers. Bedding is near horizontal and is observed in many core samples to be wavy or undulating.

Engineering properties of the Passaic Formation siltstone required for design and construction of rock-socketed foundations were evaluated through a comprehensive program of rock core logging, sampling, and laboratory testing. A total of 77 borings with rock coring were completed over the replacement bridge alignment. Most were targeted to be within the footprint or as close as practical to one of the pier locations, although this was not always achievable. In addition 23 probe holes were installed to establish top-of-rock elevations. Previous borings by the PANYNJ at the GBR site included rock core logs that were also relied upon to establish engineering properties of the rock.

An important feature of the rock profile is the thickness of weathered or decomposed rock overlying intact, or relatively unweathered, rock. Nominal values of rock unit side resistance were different for weathered rock (WR) and intact rock (IR). Socket axial resistance was assumed to begin at the elevation corresponding

© 2016 Deep Foundations Institute

to the tip of permanent casing. Casing was installed by vibratory hammer to refusal in rock. The target tip elevation was 2 ft below top of WR or to IR, whichever was encountered first. Since the actual casing tip elevation was not known until it was field-installed, and the actual thickness of WR was also not known precisely in advance at most locations, this approach required some flexibility in both design and construction to account for variations in the actual thickness of WR and in casing tip elevation. Over the bridge alignment, thickness of weathered rock varied from zero to 16 ft, with one isolated location (at Pier 2NY Westbound) where WR was 23 ft thick.

Overburden soil and weathered rock were sampled using standard SPT split spoon samplers, with rock coring initiated upon encountering relatively intact rock. The typical texture of the WR is shown in Fig. 2. The WR was characteristically friable and would disaggregate when removed from the sampler. The boring log description of the WR shown in the photo is "dense, red-brown coarse to fine gravel and coarse to fine sand w/ some silty clay; gravel is angular to subangular siltstone particles; relict bedding planes present".



Fig. 2. Typical weathered rock sampled by split spoon.

Typical rock core classified as intact rock (IR) is shown in Fig. 3. The first two core runs (C1 and C2) show high recovery but relatively low RQD, 33 and 58 percent respectively. This can be misleading, because the discontinuities that result in individual pieces being less than 4 inches in length are primarily horizontal. It was found that rock sockets could be excavated in this type of rock mass without caving or need for artificial support, thus preserving excellent side resistance. In the bearing zone beneath the tip, the horizontal discontinuities are in compression which results in excellent base resistance as determined by load testing described subsequently.

Other features of Passaic Formation siltstone that can be observed in Fig. 3 include occasional high angle discontinuities, calcite-filled veins, and some highly fractured zones.

© 2016 Deep Foundations Institute

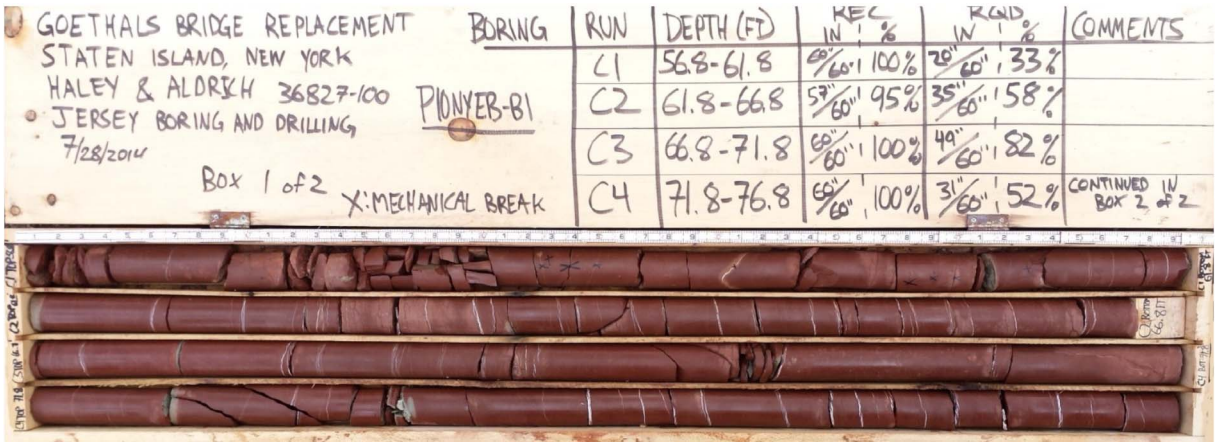


Fig. 3. Typical rock core showing variable RQD zones.

Laboratory strength testing of 87 intact rock core specimens, which included testing performed by the PANYNJ (52 tests) and NYNJ Link (35 tests) show the following parameters associated with rock uniaxial compressive strength (q_u):

Mean q_u:	8,230 psi	Standard deviation of q_u:	3,290 psi
Range:	2,170 to 18,060 psi	Coefficient of variation:	40%

Beginning at the ground surface, the overburden soil deposits include the following:

Fill: The fill varies in thickness from less than 1 ft to 18.5 ft and generally consists of very loose to very dense coarse to fine sand, coarse to fine gravel, and clayey silt with concrete, brick, and glass fragments.

Organic/Soft Soils: This layer is comprised of loose silts, soft peat, and fat clay with trace fine sand. These soils are highly organic, with water contents exceeding 100% and SPT-N values that are typically weight-of-rod (WOR) to 2 blows per ft. This layer is largely absent on the NJ Side with the exception of the NJ Inlet (Fig. 1) which at some time in the past was dredged down to rock, then subsequently filled in with soft organic soils to a thickness of approximately 15 ft. On the NY side, the organic/soft layer is as much as 28 ft thick near the Arthur Kill, but decreases in thickness toward the east until pinching out near the NY Abutment. For seismic conditions resulting in liquefaction of underlying loose sands this layer was assumed to undergo lateral spreading, imposing additional demand on the foundations. Owner-specified requirements state that lateral spreading forces be included for a distance of at least 700 ft from the Arthur Kill, which extends approximately to Pier 4 NY.

Marine Sand: This layer underlies the organic soils over the NY Approach between Piers 3 and Piers 11 and varies in thickness from 3 to 49 ft. This stratum typically consists of very loose to dense medium fine sand with silt and trace medium to fine gravel. This stratum is expected to be liquefiable under the design seismic loading. Effects on the foundations will include loss of lateral support in liquefied zones and liquefaction-induced lateral spreading of overlying layers. The marine sand was not encountered in borings on the NJ side or on the NY side from Piers 12 eastward to the NY Abutments.

Glacial Deposits: This stratum, believed to include both glacial till and glacial lake deposits, consists of loose to very loose coarse to fine sands with fine rounded to sub-angular gravel, or medium stiff to very stiff clayey silts to silty clays with fine gravel. These glacial soils are generally stronger and stiffer than the overlying deposits and provide significant lateral support to the drilled shafts. Over the NY Approach, between the Arthur Kill and Pier 9NY the glacial stratum ranges from zero to 15 ft thick. Between Pier 10NY and the NY Abutments the thickness ranges from 17 ft (at P11NY) to as high as 49 ft (at P14 NY). On the NJ Approach, the glacial stratum lies directly beneath the fill and ranges from 11 to 45 ft thick.

© 2016 Deep Foundations Institute

Figure 4 is a generalized subsurface profile over the alignment of the bridge. The main bridge tower structures in New York and New Jersey are identified as P1NY and P1NJ with the anchor piers designated as P2NY and P2NJ. The approach span piers are then numbered in an ascending order to the abutments on both sides of the anchor piers in NY (P3NY to P19NY) and NJ (P3NJ to P18NJ).

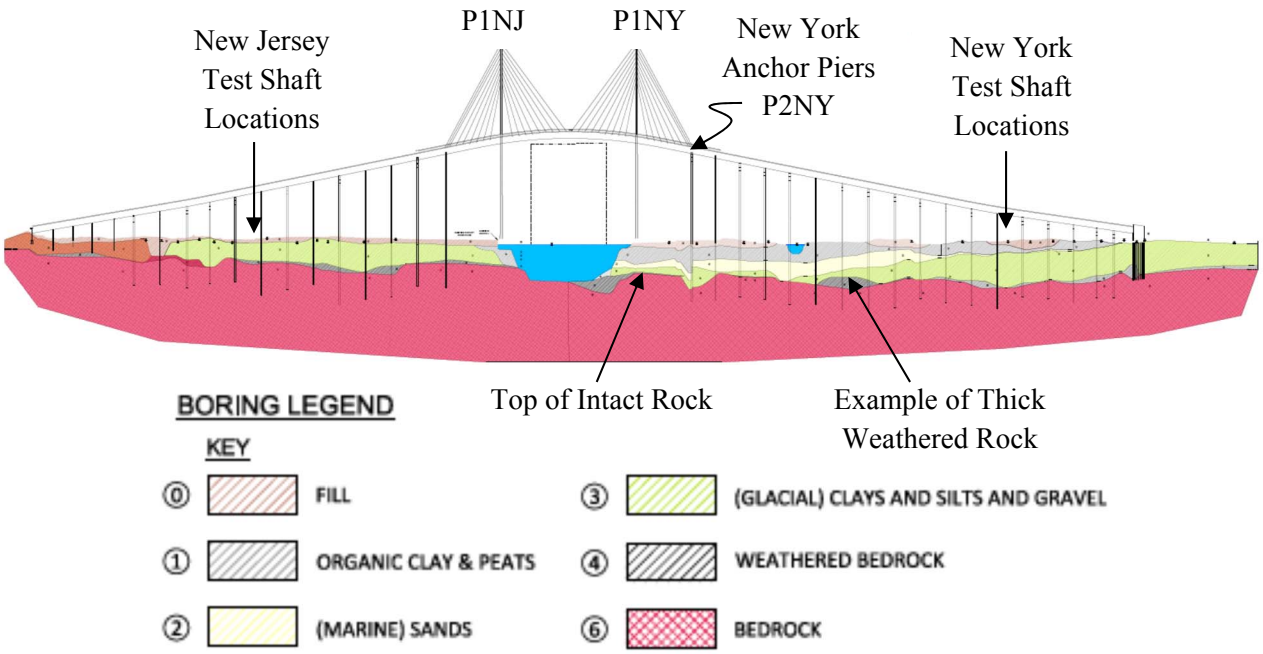


Fig. 4. Generalized subsurface profile, Goethals Replacement Bridge.

DRILLED SHAFT DESIGN

Rock-socketed drilled shafts provide a practical and cost-effective foundation type for the replacement bridge in comparison with other possible foundation types such as spread footings or driven piles. The relatively shallow depth to rock in combination with the magnitude of loads, especially where liquefaction and lateral spread potential exists (NY side), allows drilled shafts to take advantage of the ground conditions by transferring structural loads into the portion of the ground where geotechnical resistances are the highest (rock). From a constructability perspective, the rock was easily drilled with conventional rotary tooling. Drilled shaft design was based on the following criteria:

- Soil and rock layers over the full embedment length of the drilled shaft provide lateral geotechnical resistance, except in cases of scour and liquefaction.
- Axial geotechnical resistance is provided exclusively by foundation embedment in rock below the tip of permanent casing; axial resistance provided by overburden soils is neglected.
- Axial geotechnical resistance of rock sockets is based on the combined side and base resistances
- Pier scour elevations correspond to 100-yr scour and extreme event scour (500-yr)
- The contribution of permanent casing to the structural resistance of drilled shafts is: (a) neglected for axial and flexural strength; (b) considered for shear resistance; (c) considered for its confinement of the concrete; and (d) considered for its contribution to flexural stiffness.

© 2016 Deep Foundations Institute

Foundation design was carried out in accordance with the AASHTO LRFD Bridge Design Specifications. At each pier location, an idealized subsurface profile was developed. Soil and rock properties and nominal geotechnical resistances based on the subsurface investigation and load testing were assigned. Loads and structural characteristics of each shaft were provided by the bridge structural engineers. Each shaft was analyzed and designed to satisfy all applicable strength, service, and extreme event limit states. The following resistance factors were used to compute the factored axial resistance, and are based on AASHTO specifications applicable to bridge foundations where site-specific load testing is conducted:

- Strength load cases: $\varphi = 0.7$ (compression), $\varphi = 0.6$ (tension)
- Extreme Event load cases: $\varphi = 1.0$ (compression), $\varphi = 0.8$ (tension)

Resistance factors were reduced by 20 percent for the two-column piers to account for support of a single column by a single foundation element.

For preliminary design, axial and lateral geotechnical resistances were estimated using methods outlined in the FHWA Drilled Shaft Manual (Brown et al., 2010). In accordance with PANYNJ requirements for the GBR, a load testing program was carried out to validate and revise the resistances used in the final design. The load testing program is described in greater detail in a companion paper included in this conference (Dapp et al. 2016). Table 1 summarizes the final design values of nominal axial unit resistances provided by the rock-socketed portions of the shafts. All four load tests demonstrated average unit side resistance values exceeding 30 ksf at displacements not exceeding ½ inch. However, for design, the nominal side resistance was limited to the value given by the design equation provided in the AASHTO LRFD Bridge Design Specifications at the time the design was completed. This empirical relationship between unit side resistance and compressive strength of the rock is given by:

$$f_{sn} = p_a \, 0.65 \sqrt{\frac{q_u}{p_a}} \tag{1}$$

where f_{sn} = nominal unit side resistance, q_u = rock uniaxial compressive strength (limited to a maximum value corresponding to the concrete compressive strength), and p_a = atmospheric pressure in the same units as f_{sn} and q_u. In this case the design concrete compressive strength of 5 ksi is less than the rock uniaxial compressive strength of 8 ksi. Substitution of the concrete strength into Eq. 1 yields a nominal unit side resistance of 25 ksf, which was used for design, noting that the load tests demonstrate higher values and the design is therefore conservative with respect to this parameter. All four axial load tests, performed using the bi-directional load method, clearly demonstrated that side and base resistances were mobilized at compatible displacements and could be combined for calculating total axial resistance.

Table 1. Nominal axial resistances used in rock socket design

	Nominal Unit Side Resistance (ksf)	Nominal Unit Base Resistance (ksf)
Weathered Rock (WR)	6.0	--
Intact Rock (IR)	25	300

Using the nominal resistances in Table 1 and resistance factors stated above, drilled shafts were analyzed for each set of governing axial loads provided by the structural designer to determine the required socket length. PANYNJ project requirements specified a minimum socket length of two socket diameters (2D). Where weathered rock was thicker or where axial load demand exceeded the resistance provided by a 2D socket length, socket lengths exceed 2D. Each of the four main pylon towers is founded on a footing

© 2016 Deep Foundations Institute

supported by six 9-ft diameter shafts with 8.5-ft diameter sockets. All of these shafts have a socket length of 2D, or 17 ft, and all are capable of meeting the governing factored axial demand of 14,700 kips compression and 2,000 kips uplift.

At the two-column piers, shaft diameter was controlled by the diameter of the column being supported, with the shaft diameter six inches greater than the column. In general, column (and shaft) diameters decrease going from the main bridge toward the abutments. This occurs as the column heights decrease toward the abutments, decreasing the moment arm and therefore moment demand in the column and foundations. However, axial loads do not decrease proportionally because span lengths are approximately uniform and axial loads are dominated by the permanent load. As a result, the larger diameter shafts closer to the main bridge provide axial resistances well in excess of the axial demands with a 2D socket length. For example, at Pier 3NJ the factored axial demand is 5,450 kips and axial resistance is 14,000 kips (Resistance/Demand = 2.57) while at Pier 18 NJ (last pier before the abutment) the factored axial demand is 4,300 kips and the resistance is 4,400 kips (Resistance/Demand = 1.02).

Illustrative Design Example

Each of the four anchor piers for the main bridge segment consists of a two-column bent, with each column supported on a single rock-socketed drilled shaft foundation. Shaft diameters (OD of casing) are 10 ft with permanent casing to rock and a 9.5-ft diameter rock socket. Socket lengths for the NJ anchor piers are twice the socket diameter, or 19 ft, while socket lengths at both NY anchor piers exceed two diameters in order to locate the tips in competent rock. Fig. 5 illustrates the conditions at the NY Westbound anchor pier (P2NYWB) that required design socket lengths exceeding the owner-specified minimum of two socket diameters. A boring log at the south foundation shows weathered rock beginning a EL -40.3 ft and extending to the top of Passaic Formation intact rock at EL -63.3 ft (thickness of WR = 23 ft). The first six core runs show recoveries ranging from 32 to 60 percent and RQD values ranging from zero to 27. It was therefore necessary to locate the shaft tip in rock exhibiting low RQD. Side and base resistances were reduced to account for the lower quality rock, resulting in rock socket lengths of 29 ft (around three socket diameters) to satisfy LRFD design requirements for axial geotechnical resistance.

Lateral geotechnical resistance at the NY anchor piers was evaluated using revised *p-y* curve parameters that also reflect the lower strength rock mass. Under the governing seismic load case, the shafts at this location are subject to lateral spread loads resulting from liquefaction of the marine sand layer with associated spreading of the overlying soft organic soils and fill. In accordance with Owner-specified requirements, the drag force in the fill increases linearly with depth, while the drag load is uniform in the soft clay at 1,750 lb/in and uniform in the liquefied sand at 1,000 lb/in. Below elevation -35.5 ft the shaft is embedded in weathered rock. Figure 6 shows the assumed forces acting on the shaft, which is treated essentially as a free-standing column embedded in the glacial soil layer and rock below the liquefied marine sand, and subjected to the combined effects of Extreme Event I top-of-shaft inertial loads plus liquefaction/lateral spread flow loads. The resulting moment and shear demand on these anchor pier shafts are some of the highest foundation loads on the project. The design, performed with close collaboration between the structural and geotechnical engineers, provides structural and geotechnical resistances capable of meeting these severe demands while satisfying all AASHTO LRFD and owner-specified requirements.

© 2016 Deep Foundations Institute

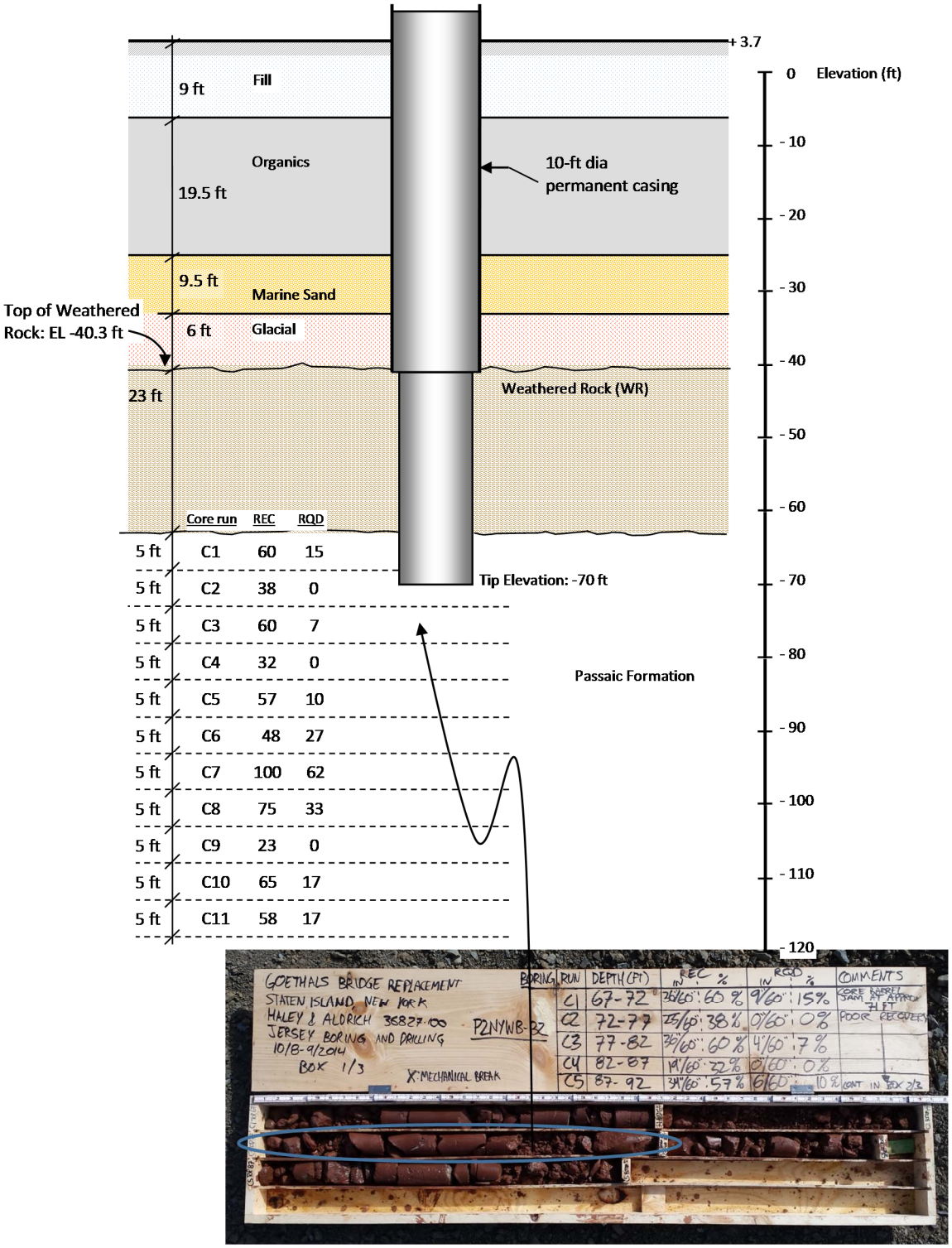


Fig. 5. Foundation and subsurface profile at NY westbound anchor pier.

© 2016 Deep Foundations Institute

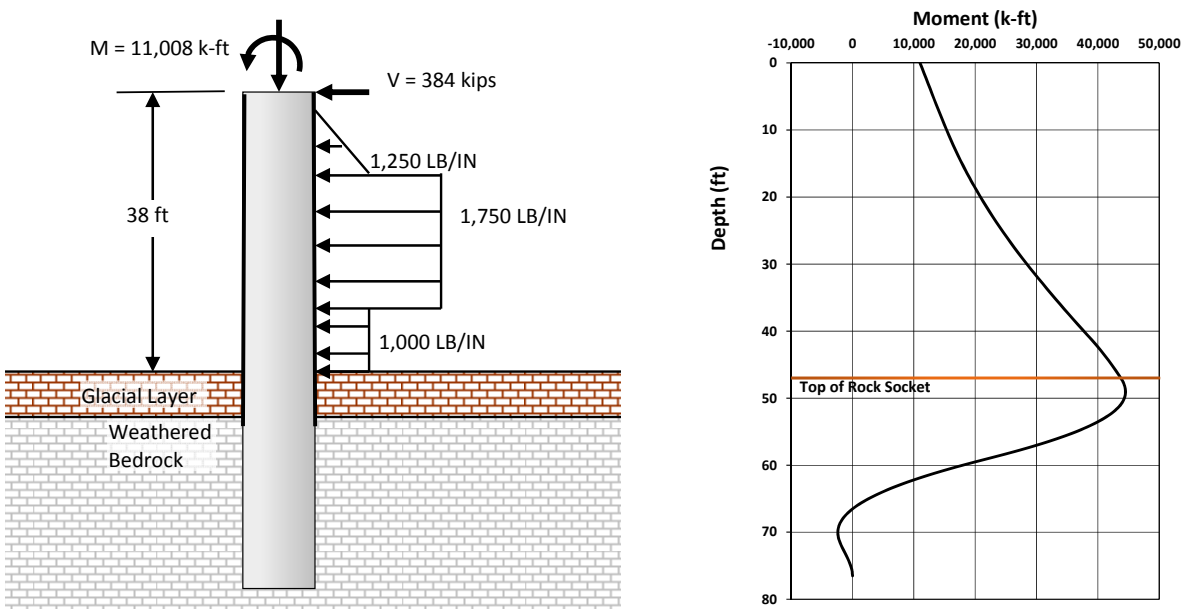


Fig. 6. Loading conditions and moment diagram considering seismic and lateral spread effects at P2NYWB.

CONSTRUCTION

Quality construction is a key factor when designing rock-socketed drilled shafts. In particular, when the design is based on the assumption that axial socket resistance is provided by combined side and base resistances, it is necessary to apply all applicable quality control and quality assurance tools to provide and verify a clean base prior to placement of concrete. Measures taken at the GBR project included:

- Development of Construction Specifications to provide minimum requirements for base cleanliness and inspection
- Submission and careful review (by the designer) of contractors' Drilled Shaft Installation Plan to ensure compliance with Construction Specifications
- Independent inspection by Construction Engineering Inspection (CEI) firm

Some of the specific requirements given in the Specifications aimed at assuring a clean base included a list of methods deemed acceptable for final base cleanout. For shafts constructed under wet conditions, which applied to most locations, use of cleanout buckets with a closing trap-door type bottom plate or airlifting was specified. Most production shafts utilized both of these methods. To verify bottom cleanliness prior to placement of the cage and concrete, inspection by mini-SID (Shaft Inspection Device) was required. This device provides a measurement of the sediment thickness at the base of the socket excavation. The requirement was for at least 12 of 15 measurements to be less than ½ inch of sediment and for zero measurements exceeding 1 ½ inches. All four of the load-tested shafts met this requirement and exhibited excellent mobilization of base resistance at small displacements, thus providing confidence that production shafts meeting the cleanliness requirements would also provide the base resistance mobilized in the load tests. Other quality control and assurance measures used on the GBR foundations included cross-hole sonic logging on every completed shaft, limits on the time between final mini-SID base inspection and concrete placement, and careful record-keeping by the contractor and the CEI firm.

© 2016 Deep Foundations Institute

One of the challenges on this project was associated with variations in the thickness of weathered rock. As noted above, the actual top of weathered rock elevation and the thickness of weathered rock was not known beforehand at every shaft location. The weathered rock thickness and variability in the how far the casing would penetrate into the WR meant that the casing tip elevation could not be known precisely until the casing was actually driven. The tip of casing defines the top of the rock socket. As a consequence, reinforcing cage lengths, and the elevations at which reinforcing changes occurred, had to be designed to accommodate a range of potential weathered rock conditions. These and other examples of design-construction challenges and measures taken to address them are described in greater detail in a companion paper by Daita et al. (2016).

SUMMARY

Foundations for the Goethals Bridge Replacement provide an example of how rock-socketed drilled shafts can provide a reliable and cost-effective means of supporting a major bridge by taking advantage of the high resistances that can be achieved. The key factors involved in taking advantage of rock sockets for this project were: (1) load testing to demonstrate high axial resistances (>30 ksf side resistance and >300 ksf base resistance), (2) utilization of all relevant construction QC/QA tools to ensure that rock sockets are constructed in a manner that is consistent with construction of the load-tested shafts that provide the basis of the design, (3) close collaboration between all members of the design-build team, and (4) adequate subsurface characterization, especially a thorough characterization of rock characteristics and their effect on socket resistances.

Load testing for this project demonstrates that side and base resistances can be used in combination to design rock socketed shafts for axial loading. This approach avoids the use of unnecessarily deep sockets, thereby minimizing the associated construction risks and costs.

ACKNOWLEDGMENTS

The GBR project developer is NYNJ Link Developer, LLC and construction is being performed by a joint venture of Kiewit-Weeks-Massman (KWM). Parsons is the bridge designer with Dan Brown and Associates as the foundation engineers. The authors would like to acknowledge and thank the many individuals in these firms who have made our participation possible. Special appreciation to Bobby Daita, Seth Condell, Jonathan Taylor, Serafim Arzoumanidis, Brad Pollock, Shawn Marlow, and Tom Spoth, all of Parsons Transportation Group. Haley & Aldrich, Parsippany, NJ performed the subsurface investigation under the able supervision Mr. Paul Pizzimenti.

REFERENCES

Brown, D.A., Turner, J.P., and Castelli. R.J., 2010. "Drilled Shafts: Construction Procedures and LRFD Design Methods," Geotechnical Engineering Circular No. 10 and FHWA/NHI Publication 10-016, 972 p.

Dapp, S.S., Turner, J.P., and Brown, D.A. (2016). Load Tests on Drilled Shafts at Goethals Bridge Replacement, *Proceedings*, International Conference on Deep Foundations, Seepage Control and Remediation, 41st Annual Conf. on Deep Foundations, DFI, NY.

Daita, B., Turner, J.P., and Jen, M. (2016). Goethals Bridge Replacement Foundation Design Modifications in Response to Field Conditions, *Proceedings*, International Conference on Deep Foundations, Seepage Control and Remediation, 41st Annual Conf. on Deep Foundations, DFI, NY.

© 2016 Deep Foundations Institute

SCREW AND STRAIGHT PILE BEHAVIOR UNDER CYCLIC COMPRESSIVE LOADING IN DENSE SAND

Adnan A. Malik, Ammico Contracting Co., Qatar, +97450789446, malikadnananwar@hotmail.com
Jiro Kuwano, Saitama University, Japan, jkuwano@mail.saitama-u.ac.jp
Shinya Tachibana, Saitama University, Japan, stachi@mail.saitama-u.ac.jp
Tadashi Maejima, Asahikasei Kenzai, Japan, maejima.tc@om.asahi-kasei.co.jp

ABSTRACT

The helical piling system provides solution to many geotechnical related problems due to its quick installation, higher compressive and pullout resistance, no wastage of material, workable in limited areas and reusability. However, its use as a foundation for bridges and high-rise buildings is still limited as compared to other piling methods. In the present study, the performance and load settlement behavior of screw and straight pile is investigated under cyclic compressive load in dense ground conditions. To achieve the set objectives, pile load tests were conducted in a cylindrical steel container. The model ground was compacted with dry sand at relative density of 80%. It is observed from the test results that screw and straight pile resistance reduced when the cyclic load is applied at allowable pile resistance state. The reduction in the ultimate pile capacity is more in straight pile than in screw pile. However, straight pile showed higher ultimate pile capacity than screw pile under similar pile tip diameter. The effect of helix bending deflection on load settlement behavior and ultimate pile capacity increases under cyclic loading.

Keywords: Model Pile Load Test, Screw Pile, Straight Pipe Pile, Cyclic Compressive Load

INTRODUCTION

Screw pile is one of the new developments in deep foundation, which is growing tremendously fast because of its quick installation technique, less noisy operation, no wastage of material and involvement of minimum manpower. Screw piles have an edge on straight pipe piles due to its high bearing capacity and uplift resistance. The installation mechanism of screw pile is different from straight pile. Torque and pressure is required to install the screw pile whereas hammering, pressure and vibration is required to install straight pile. As the installation mechanism is different between screw and straight pile, therefore, the ground disturbance that is produced during their installation is also different. The ground disturbance produced during the installation also depends upon the pile tip condition i.e. open or closed ended. Sakr, (2009) stated that the compressive capacity of screw pile in 3 to 5 times higher than driven piles having the same shaft diameter and length. The reason for this increase in pile capacity is due to helix, which is generally 2 to 2.5 times the pile shaft diameter. Larger helices can give higher end bearing capacity but it requires very powerful machinery to install in dense grounds. For instance, if large helix screw pile is installed in a dense ground then helix-bending deflection will start affecting the end bearing capacity (Yttrup and Abramsson, 2003; Malik et al. 2013 and 2015). According to Malik (2015), the equations of thin plate (Young and Budynas, 2002) with uniformly distributed load on the plate can give reasonable estimation of helix deflection due to dense ground conditions.

In the present study, the load settlement behavior of screw and straight pipe pile has been compared under cyclic compressive loading. The model ground conditions before the application of load is kept similar for both type of piles. The effect of helix bending deflection on the load settlement behavior and ultimate pile capacity under cyclic loading is also investigated. Fine-grained dense sand is used in this research.

© 2016 Deep Foundations Institute

RESEARCH METHODOLOGY

Model scale of pile load test is used to compare the performance of screw and straight piles under cyclic compressive loading. As the installation mechanism of both type of piles are different than each other and the ground disturbance associated with their installation is different too, therefore, to achieve the similar ground conditions for screw and straight piles both piles are placed, instead of their respective installation methods i.e. torque and pushing force for screw pile and vibration and hammering for straight pile. At first monotonic loading test is conducted on screw and straight piles to estimate the ultimate pile capacity. Then cyclic compressive loading tests are performed on both types of piles. The loading and unloading cycles are applied at allowable pile capacity i.e. 50% of ultimate pile capacity. After fifteen (15) cycles the loading is continued up to failure. Thin helical plates are also used to observe the helix bending deflection on the load settlement behavior under cyclic loading.

TESTING EQUIPMENT

Model Screw Piles

Model screw and straight piles having closed shaft tip was used in this study. The material of both type of piles were identical and is according to STK400 and SS400 steel standards. The tip diameter of screw and straight pile was also similar i.e. 60 mm (Fig. 1). However, the shaft diameter of straight pile was 2.8 times the shaft diameter of screw pile i.e. 60 mm > 21.7 mm. To achieve similar ground conditions for both types of piles, pile installation mechanism is not considered therefore, helix is modeled as a flat circular plate. The projected area of the helix will be similar whether it is flat or having a pitch and also end-bearing resistance has a direct relationship with the pile tip area. Therefore, helix with a pitch or without a pitch (flat) will not affect the end bearing resistance after pile installation during the loading stage. A slit of 5 mm is provided, which reflect the gap between the ends of the helix that generally exits in real piles, and also in the present study, it is used to insert different thicknesses of helices.



Fig. 1 Model screw and straight pipe pile with similar pile tip diameter (60 mm)

The length of screw and straight pipe pile is similar i.e. 500 mm. The dimensions of the helices that are used in this study are shown in Table 1.

Table 1 The dimensions of model helices for screw pile

Helix Diameter (D_h) (mm)	D_h/D_s	Helix Thickness (T_h) (mm)
60	2.8	1.0
60	2.8	2.0
60	2.8	6.0

© 2016 Deep Foundations Institute

Model Container

A cylindrical steel container having diameter of 592 mm and depth of 700 mm was used in this study (Malik et al. 2015) as shown in Fig. 2(a). The selected size of the container is according to the previous studies in which it is suggested that the zone in which soil affected by the loading is usually 3 to 8 times the pile tip diameter (Kishida, 1963; Robinsky and Morrison, 1964). Yang (2006) proposed that the influence zone in clean sand above the pile tip should be 1.5 to 2.5 times the pile diameter and influence zone below the pile tip should be 3.5 to 5.5 times the pile tip diameter (Yu and Yang, 2012). In the present study, the clearance around the pile was 13.7 times the pile tip diameter and the clearance below the pile tip was 400 mm (9.3 times pile tip diameter). The pressure on the wall and floor of the container was measured through pressure transducers. Toyoura sand was used to develop the model ground. The properties of Toyoura sand are as follow,

Condition	=	Dry, fine grain
Specific Gravity	=	2.645
D_{50}	=	0.20 mm
e_{min}	=	0.609
e_{max}	=	0.973

According to Garnier et al. (2007) and Rakotonindriana et al. (2010) if the ratio of pile tip diameter (D_h) to D_{50} is greater than 35 then there will be no scale effect for the tip resistance. In the present study, the D_h/D_{50} was 300.

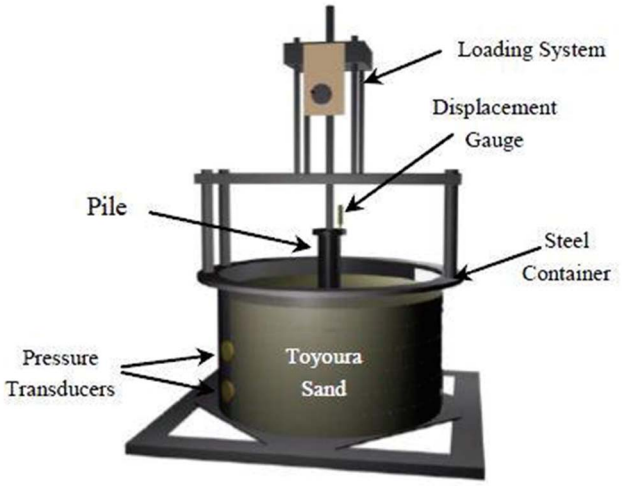


Fig. 2 Model cylindrical steel container

TESTING PROCEDURE

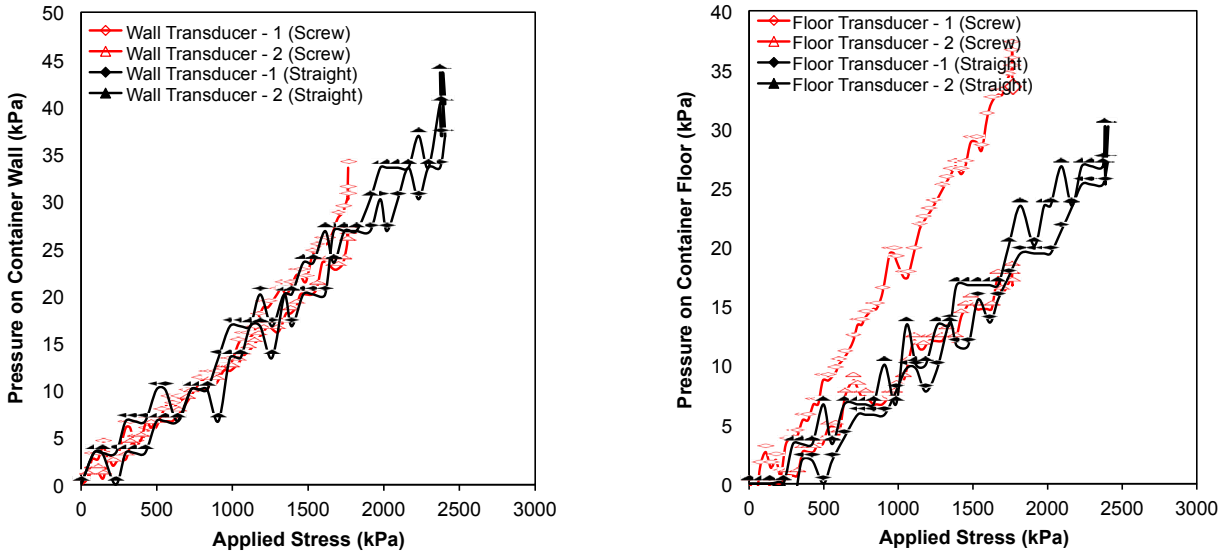
The Toyoura sand was compacted in six layers to develop the model ground. The relative density (D_r) after the compaction of each layer was approximately 80 %. The compacted thickness of each layer was 100 mm. The screw pile was placed after the compaction of the fourth layer i.e. 400 mm. The remaining two layers were compacted carefully around the screw pile. The settlement (S) of the screw pile was measured at the head through a displacement transducer. The applied compressive load (P) was measured with the help of load cell. The cyclic compressive load was applied in fifteen (15) rapid loading and unloading cycles. The time to complete one cycle was approximately 60 seconds.

© 2016 Deep Foundations Institute

RESULTS AND DISCUSSIONS

Pressure on Container Boundary during Pile Load Tests

The pressure on the wall and floor of the container was measured through pressure transducers, which was mounted on the container. It was observed that the pressure on the wall and floor of the container increased with the increase in applied stress as shown in Fig. 3. However, this increase in pressure on the wall and floor of the container was only 0.95 to 1.90 % of applied stress (at maximum applied pressure).



(a) (b)

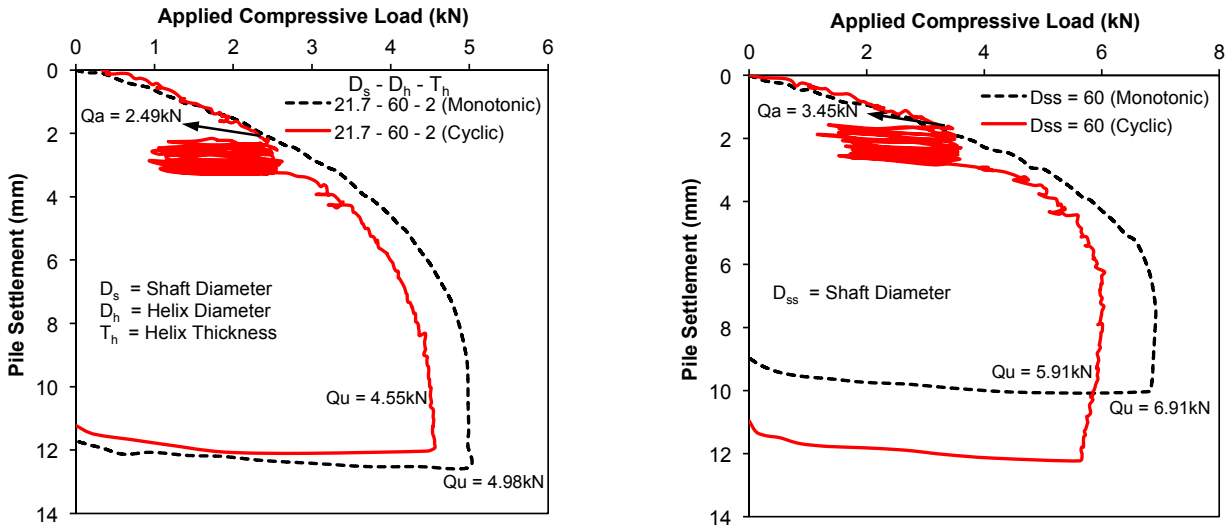
Fig. 3 Pressure developed on the container boundary (a) Wall (b) Floor

Performance of Screw and Straight Pile under Monotonic and Cyclic Loading

The pile load tests were conducted on screw and straight pipe piles with similar ground conditions (relative density 80 %) and pile tip diameter ($D_h = D_{ss} = 60$ mm) under monotonic and cyclic compressive loading. The cyclic load was applied as fifteen (15) loading/unloading cycles at allowable pile capacity (Q_a) i.e. 50 % of ultimate pile capacity (Q_u). At first, monotonic pile load tests were conducted on screw and straight piles and ultimate state was estimated. It was observed from the test results of screw and straight piles that load settlement curve changed after the application of cyclic loading, therefore, the ultimate pile capacity of both piles were reduced with respect to monotonic load tests as shown in Fig. 4. However, the reduction in ultimate pile capacity of screw pile was 8.6 %, which was lesser than straight pile whose reduction was 14.5%. The pile settlement during the loading/unloading cycles for both type of piles were similar i.e. approximately 1 mm. The reduction in the ultimate pile capacity might be due to the loosening of the dense sand around the pile tip area under repeated fast loading/unloading cycles. Which indicates that dense sand might becomes loose around the pile tip area if the loading conditions are cyclic with fast loading/unloading cycles. However, this need to be further explored in future research.

In only monotonic loading comparison, it was observed that straight pile ultimate capacity was 27.9 % higher than screw pile under similar pile tip diameter and ground conditions as shown in Fig. 4.

© 2016 Deep Foundations Institute



(a) (b)

Fig. 4 (a) Screw pile under monotonic and cyclic loading (b) Straight pile under monotonic and cyclic loading

Effect of Helix Deflection on Load Settlement Behavior under Monotonic and Cyclic Loading

The pile load tests were performed on screw piles with similar helix diameter (D_h = 60 mm) and ground conditions but different helix thicknesses (T_h) under monotonic and cyclic loading as shown Fig. 5. It was observed from the test results that cyclic loading altered the load settlement curve and reduced the ultimate pile capacity than the pile capacity under monotonic loading. In case of non-deformed piles (21.7-60-2, 21.7-60-6 and 21.7-60-2), this reduction in the ultimate screw pile capacity was about 17.3 %. Whereas, in case of deformed screw pile (21.7-60-1), this reduction was about 25.5 % as shown in Fig. 5.

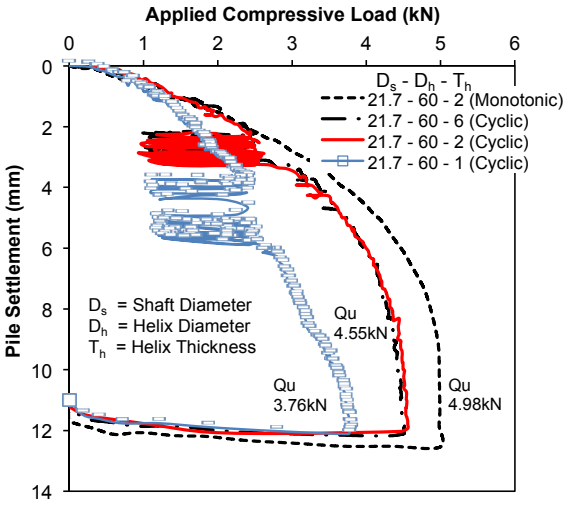


Fig. 5 Load settlement behavior of screw piles under monotonic and cyclic loading for deformed and non-deformed screw piles

© 2016 Deep Foundations Institute

In comparison of deformed screw piles under monotonic and cyclic loading, it was observed that the load settlement curve and ultimate pile capacity further decreased by 20.1 % as shown in Fig. 6. The pile settlement during the loading/unloading cycles for deformed screw pile was about 2mm as shown in Fig. 6. These results indicated that under cyclic loading the effect of helix bending deflection on the load settlement behavior further intensify, which further reduced the ultimate pile capacity of screw pile.

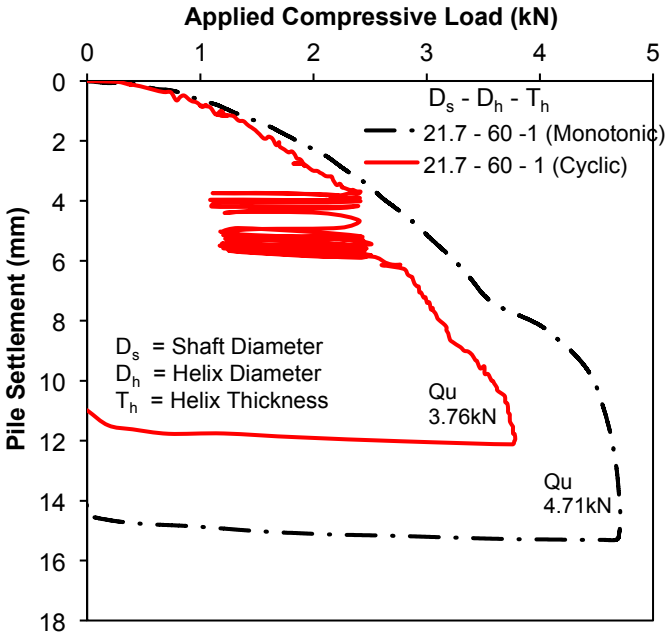


Fig. 6 Load settlement behavior of deformed screw piles under monotonic and cyclic loading

CONCLUSIONS

The model scale pile load tests were conducted on the single helix screw piles (close-ended) and straight pile (close-ended) under monotonic and cyclic loading with similar pile diameter and ground conditions. Following conclusions are drawn from the model experiments:

1) The load settlement behavior changes after the application of cyclic loading that reduces the ultimate pile capacity of screw and straight pipe piles under similar pile tip diameter and initial ground conditions.
2) The reduction in ultimate pile capacity of screw pile due to cyclic loading is lesser than straight pipe pile. However, the pile settlement during the loading/unloading cycles is almost similar.
3) It is believed that the reduction in the ultimate pile capacity is due to the loosening of dense sand around the pile tip area under rapid cyclic loading.
4) It is observed that the straight pipe pile has higher ultimate pile capacity than screw pile with similar pile tip diameter and ground conditions under monotonic loading.
5) It is also observed that the effect of helix bending deflection on the load settlement behavior and ultimate pile capacity is intensifying under rapid cyclic loading.

© 2016 Deep Foundations Institute

REFERENCES

Kishisa, H., 1963. Stress distribution of model piles in sand. Soils and Foundations 4(1): 1-23.

Malik, A.A., Kuwano, J., and Maejima, T., 2013. The effect of helix/wing plate deformation on end bearing resistance of screw piles. In Proceedings of 38th Annual Conference on Deep Foundations, Phoenix, USA, pp. 505-510.

Malik, A.A., Kuwano, J., and Maejima, T., 2015. Helix deflection effect on load settlement behavior of pile with increasing stress level. In Proceedings of 40th Annual Conference on Deep Foundations, Deep Foundation Institute, Oakland, USA.

Perko, H.A., 2009. Helical Piles: A practical guide to design and installation. John Wiley and Sons, New Jersey.

Robinsky, E.I., and Morrison C.F., 1964. Sand displacement and compaction around model friction piles. Canadian Geotechnical Journal 1(2) 81-93.

Rakotonindriana, M.H.J., Kouby, A.L., Buttigieg, S., Derkx, F., Thorel, L., and Garnier, J. 2010. Design of as instrumented model pile for axial cyclic loading. Physical Modeling in Geotechnics – Springman, Laue & Seward (eds), Taylor & Francis Group, London, pp. 991-996.

Sakr, M., 2009. Performance of helical piles in oil sand. Canadian Geotechnical Journal 46(9) 1046-1061.

Yttrup, P.J., and Abramsson, G., 2003. Ultimate strength of steel screw piles in sand. Australian Geomechanics 38(1): 17–27.

Yang, J., 2006. Influence zone of end bearing piles in sand. Journal of Geotechnical and Geoenvironmental Engineering 132(9) 1229-1237.

Young, W.C., and Budynas R.G., 2002. Roark's formulas for stress and strain. McGraw-Hill Companies, Inc., Two Penn Plaza, N.Y.

Yu, F., and Yang, J., 2012. Bearing capacity of open-ended steel pipe piles in sand. Journal of Geotechnical and Geoenvironmental Engineering 138(9) 1116-1128.

© 2016 Deep Foundations Institute

This page left intentionally blank

© 2016 Deep Foundations Institute

SILVER STAR MOTORS "TACKLES" BROWNFIELD SITE AND ADJACENT NYCT SUBWAY

Michael J. Chow, PE, Senior Consultant, GZA GeoEnvironmental of NY; 104 West 29th Street, 10th Floor, New York, NY; 212-594-8140
Dharmil Patel, EIT, Engineer I, GZA GeoEnvironmental of NY; 104 West 29th Street, 10th Floor, New York, NY; 212-594-8140

ABSTRACT

Construction progress is nearing completion at a Brownfield Site for a 100,000sf mixed-use 10 story building plus cellar for Silver Star Motors including a two-floor pre-owned Mercedes Benz showroom; high-end residential rental studios, 1, 2, and 3 bedroom apartments; and penthouses on the upper two floors. Excavation through impacted soil extended to 15ft depth. Project is approximately 7 ft north of a NYCT subway station, portions of the SOE are within inches of a 6ft diameter NYCDEP Sewer, and cellar extends below the depth of adjacent structures, requiring over 200 lf of underpinning.

A complex series of earth retention systems was utilized consisting of underpinning, drilled-in soldier piles (micro-piles), timber/concrete lagging, soil anchors and inclined rakers supported by a partially constructed foundation mat. Foundation mat subgrade was approximately 4 ft below the groundwater level creating more challenges during underpinning and achieving suitable foundation subgrades. All construction was undertaken on a non-union basis.

This paper describes the design, construction, and lessons learned for the multiple earth retention systems, Brownfield Remediation requirements, instrumentation, and monitoring used to manage complications of building adjacent to an active subway station, in close proximity to existing utilities, with underpinning and mat foundation installation below the water table.

Results of the instrumentation program are summarized which utilized an AMTS, monitoring prisms on adjacent structures, automated seismographs, and manual NYCT surveys.

Keywords: Earth Retention, Support of Excavation, Underpinning, Subway, Soil Anchors, Instrumentation, Monitoring, Automated Motorized Total Station (AMTS), Remediation, Brownfield, Environmental, New York City Transit, New York City Department of Environmental Protection.

© 2016 Deep Foundations Institute

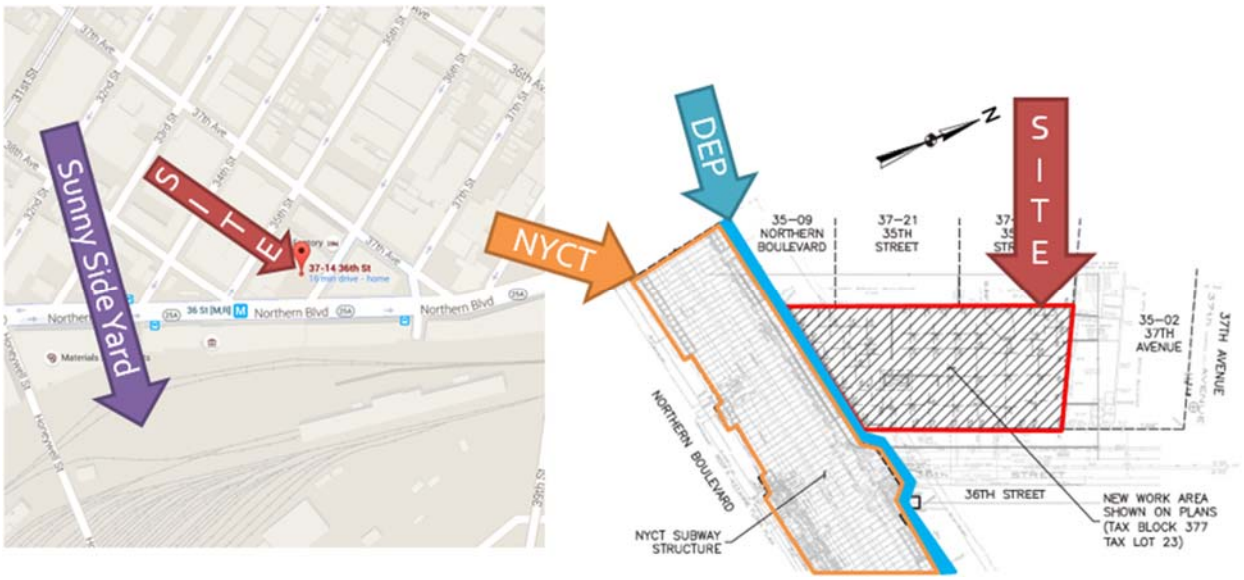


Fig. 1. Site location plan

BACKGROUND

Construction is nearing completion at a New York City Brownfield Site for a 100,000sf 10 story mixed-use building with a cellar, partially housing the new Silver Star Motors' Mercedes Benz dealership in Long Island City, Queens, NY. The structure will include a new two-floor Mercedes Benz showroom which not only incorporates Mercedes-Benz standards into the design, but also integrates with the industrial loft like facade above. The residential portion identifies itself with a prominent entrance on 36th Street and was developed as efficient but high-end studios, 1, 2 and 3 bedroom rental units. The top two floors are considered penthouses with 11 ft ceilings and terraces in four of the nine units. The amenity space includes a gym, outdoor recreation space and lounge. In addition, there is a recreational terrace space on the roof of the building (Figs. 1 and 2).



Fig.2. Architectural Rendering and June 2016 Progress photos

In February 2012 GZA participated in a construction networking organization, planned by a local attorney we have worked with in the past. At this event, we were approached by the initial Architect for the project with an opportunity to provide Geotechnical, Civil, and Environmental Services for the construction of a

© 2016 Deep Foundations Institute

mixed-use building that would house the Silver Star Mercedes car dealership and residential units. Through the initial Architect, we provided environmental due diligence services, negotiated the City of New York Office of Environmental Remediation (NYCOER) process and provided Preliminary Geotechnical Investigation Services. During this time, we established a very good relationship with the dealership owner.

Before the project could move into full scale design, the Owner brought on a Project Management & Equity firm and a new architect, MADGI. We were retained through the transition to continue to provide Geotechnical, Civil, and Environmental services. The new equity partner was receptive to entering the project into the NYSDEC Brownfield Cleanup Program (BCP) program to maximize tax credits resulting in additional investigation and remedial documentation requirements. The Owner then switched equity firms, construction management firms and general contractors several times. Through all this turmoil, our firm remained on the design team, and continued throughout the design and construction phase performing the scope of work as indicated herein. We were able to work with the General Contractor (GC) and the Owner through several design changes and our environmental work resulted in achieving the Certificate of Completion (COC) before January 1, 2016. The NYSDEC had expressed doubts on many occasions as to whether this was possible.

SCOPE OF WORK

GZA, the Geotechnical, Instrumentation, and Environmental Engineering Consultant for the Silver Star Motors team, conducted a phased subsurface investigation; provided recommendations and support for foundation design; designed the SOE systems including underpinning; performed preliminary dewatering analysis and design; acted as liaison with NYCT to obtain approval for the original 2014 and GC's 2015 Value Engineering revisions of proposed SOE and Underpinning schemes, performed NYCBC Special Inspections for Underpinning, SOE, and Subgrade inspections for Mat foundation/Underpinning; performed pre and post construction documentation and instrumentation installation; and developed and implemented the monitoring program to meet the project and NYCT requirements.

Geotechnical Investigation

GZA provided a preliminary subsurface exploration in April and May 2012 which consisted of 3 borings and 3 monitoring wells. Our final exploration program was performed in August and September 2013 which consisted of an additional 6 borings and 5 test pits, as shown in Fig. 3. Existing grade varied between El. 24 and El. 27 (NAVD88). At the west building a strip footing was found extending approximately between 8.5ft and 9.5ft below existing grade. The adjacent north foundation was not observed from the test pits but was observed to be at a similar level during construction.

© 2016 Deep Foundations Institute

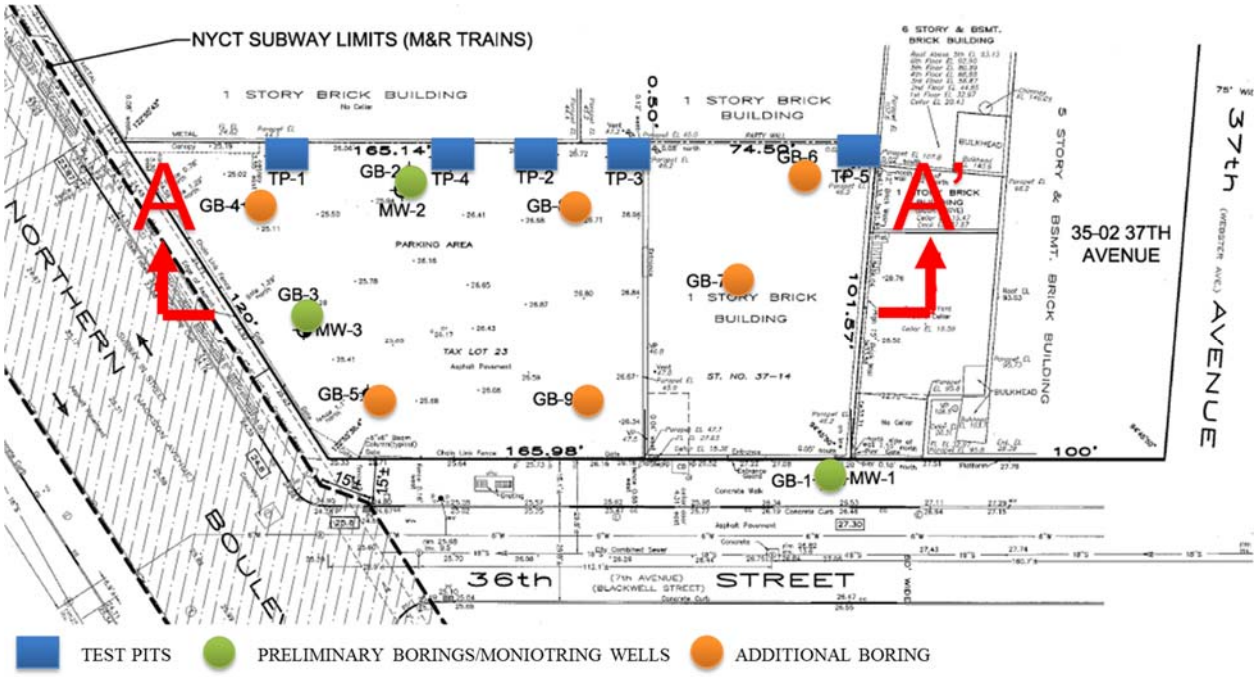


Fig. 3. Geotechnical Investigation

Our geotechnical report identified the soil stratification consisting of 9ft to 14ft of Fill, overlying very loose to very dense Sand (NYCBC Class 3a/3b/6) extending to 88ft. The Sand is underlain by a thin layer of very dense Silt (Class 5a) and hard Clay (Class 4a). The observed water level was between El. 14 and 15.4 (between 8.6ft and 13ft below grade). Based on these observations we recommended a design water level at El. 18, see Fig 4.

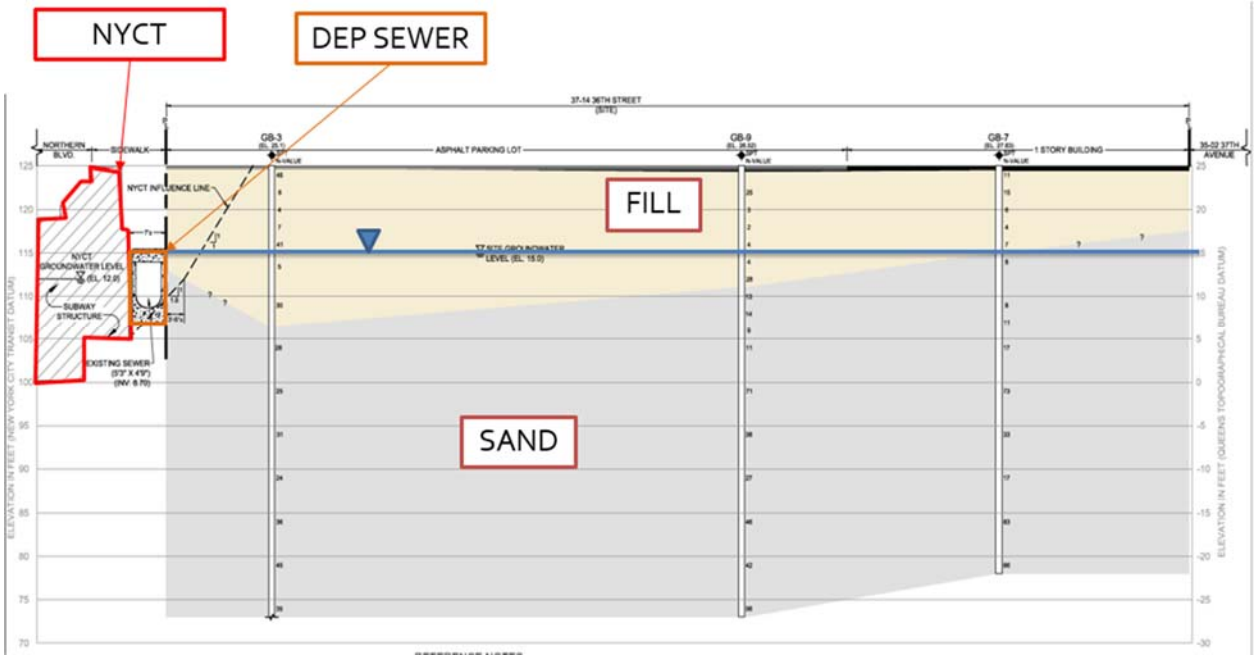


Fig. 4. Subsurface profile – Section A-A'

© 2016 Deep Foundations Institute

Support of Excavation and Underpinning

The foundation consists of a 3-foot-thick reinforced concrete mat slab throughout the entire footprint of the site requiring excavation to approximately 15ft depth in impacted soil up to 4 ft below the water table. The building is located approximately 7 ft north of a New York City Transit (NYCT) subway structure and the required Support of Excavation (SOE) is within inches of a large NYCDEP sewer which created challenging conditions for the design, and installation of the SOE system. The proposed cellar extends below the depth of adjacent neighboring structures requiring underpinning of over 200 linear ft of the adjacent structures. The mat level below the water table created more challenges in designing a suitable SOE system and achieving suitable subgrades for the foundation. The cellar required various temporary excavation support systems, dewatering, and a complex sequence of ground support installation:

The initial 2014 SOE/Underpinning approved by NYCT is shown in Fig. 5. The proposed 2014 excavation support scheme consisted of drilled-in HP14 soldier piles with 3-inch timber lagging plus 4-inch precast concrete lagging adjacent to the NYCDEP sewer structure. Lateral support adjacent to the NYCT Structure consisted of corner bracing supported by the ground level slab of the adjacent west building. Below the adjacent buildings up to 10 ft high, four ft. wide, underpinning piers were to be installed sequentially to not only re-support building walls below the zone of influence but also serve as SOE for foundation construction. Other SOE lateral support was to be provided by a combination of soil tiebacks and north-east corner bracing.

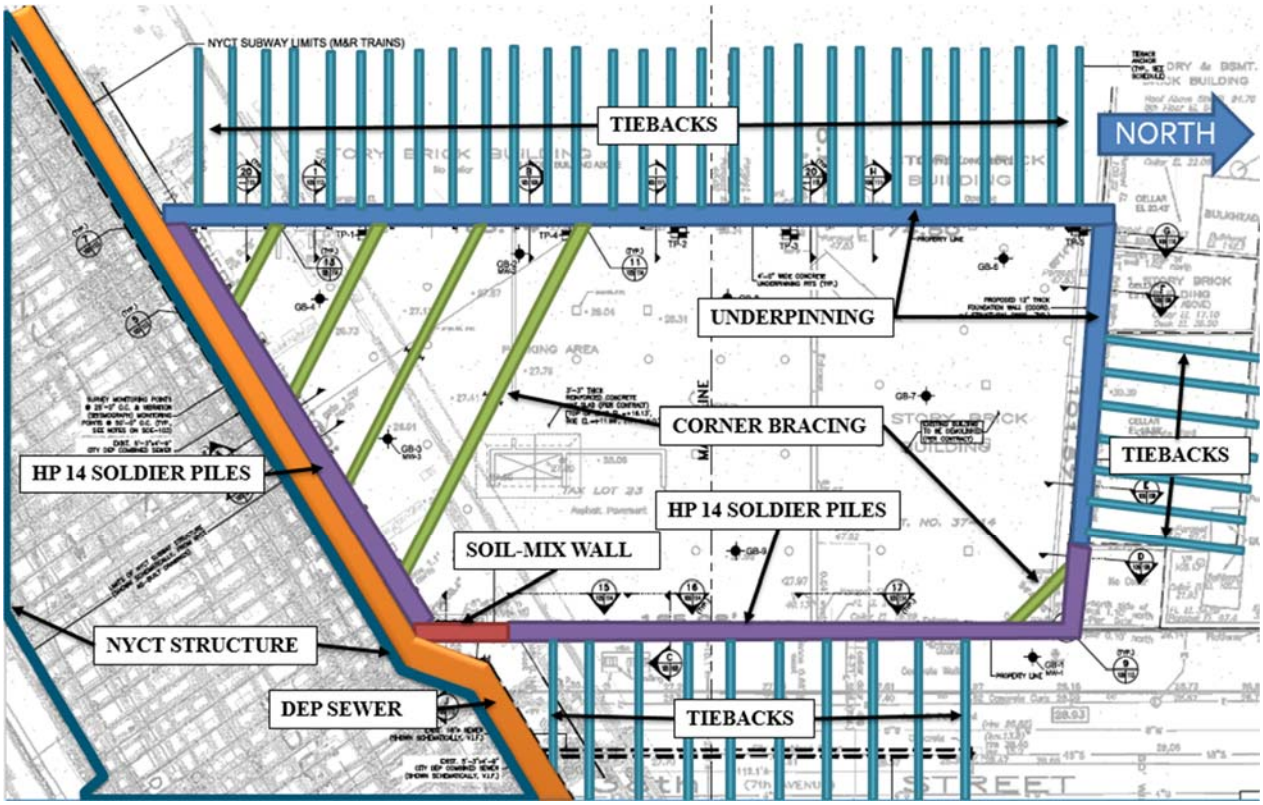


Fig. 5. Initial SOE/Underpinning plan view

© 2016 Deep Foundations Institute

The GC's 2015 Value Engineering Alternatives are as shown in Fig. 6. The GC proposed several Value Engineering (VE) Alternatives including substitution of 9-5/8 inch diameter micropiles in lieu of HP14 soldier piles placed within 24-inch diameter pre-drilled casing. Proposed lateral support adjacent to the NYCT Structure including using inclined HP12 steel rakers supported by the partially constructed mat foundation in lieu of corner bracing, as illustrated in Fig. 7. and shown in Fig. 8.

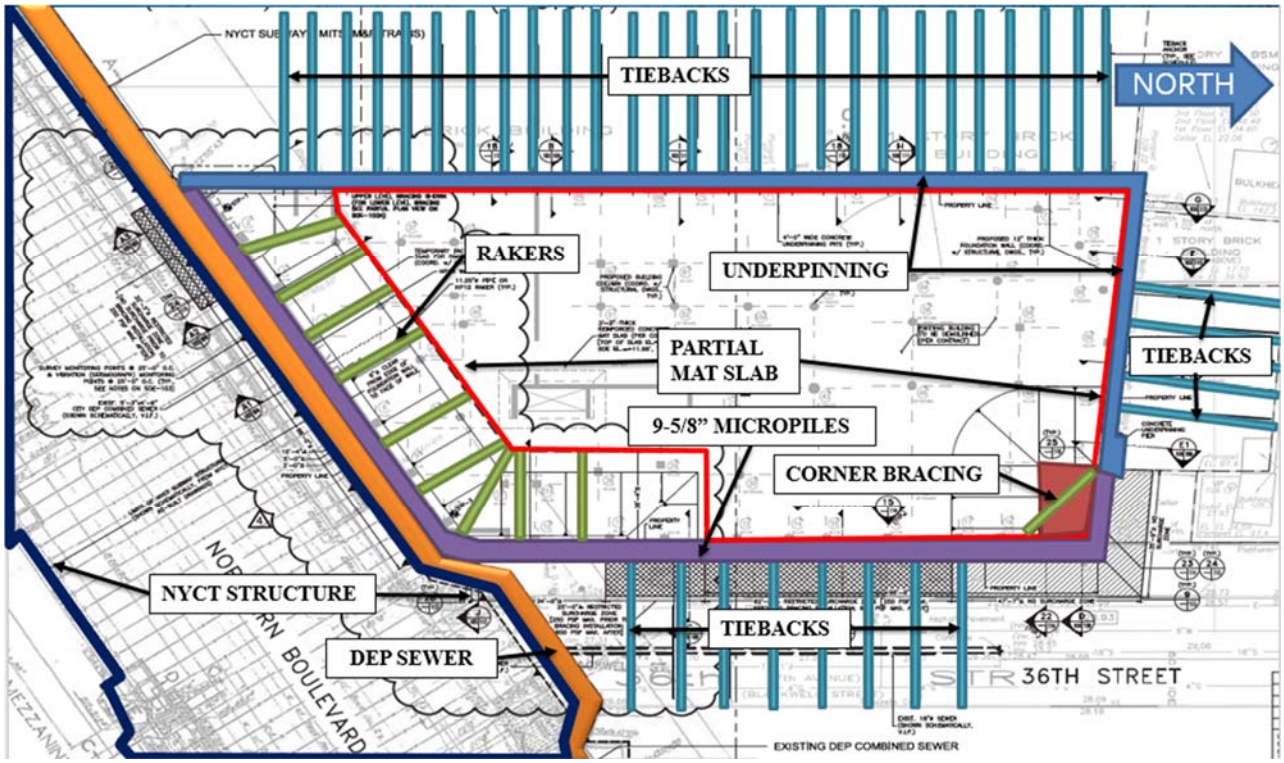


Fig. 6. Value engineering alternatives

To obtain timely NYCT approval(s), we acted as liaison with NYCT requiring frequent correspondence, negotiations, and preparation of multiple submittals and presenting not only the original 2014 SOE and Underpinning schemes but also the selected GC's proposed 2015 Value Engineering Alternatives which included presentation of NYCT Structure, Influence Lines, Dewatering Plans-Details-Requirements, Required Vibration and Optical Monitoring requirements.

Even though the GC proposed SOE changes in late 2nd Quarter, in order to obtain 2015 project eligibility for the NYC 421-a Tax Exemption, our firm expedited re-design and drawing preparation of signed and sealed drawings for the SOE System (micropile alternative, re-designing underpinning to eliminate tiebacks and bracing for a revised detention tank subgrade elevation) at the north-east corner in order to allow partial construction of the project to become eligible for the property tax credit, prior to proceeding with the remainder of the Value Engineering redesign.

© 2016 Deep Foundations Institute

Our proactive management of the design and drawing preparation assisted in maintaining the tight construction deadline proposed by the GC and saved the Owner on lost schedule and cost. This included incorporating multiple design changes made by the GC, providing phased design and sketches to allow GC to order material for long lead items, responding to inquiries from the GC and design team, expeditious review of submittals – sometimes on the same day.

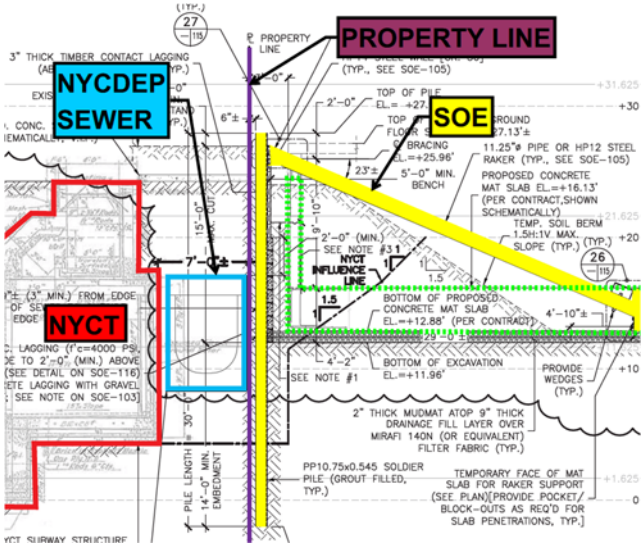


Fig.7. Section view adjacent to NYCT structure

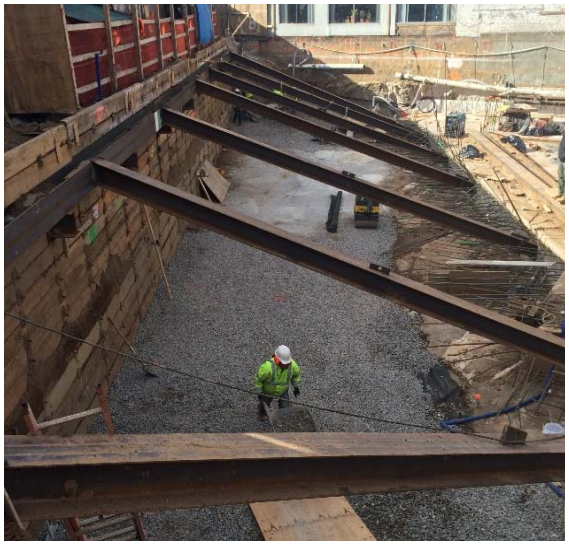


Fig.8. Photograph of raker installation adjacent to NYCT structure

Construction

Construction started in May of 2015 at the NE corner for detention tank for the project to qualify for the Phase 421a tax credit. The SOE for this partial foundation section consisted of three underpinning piers, micropile soldier piles, corner bracing system and contact timber lagging. Construction was delayed due to limitations in the dewatering system in place at that time.

Once NE corner construction was underway, the GC wanted to continue south along 36th Street outside of the NYCT Influence zone. After a quick turnaround of the re-design in this area, the GC could start soldier pile installation in early June, 2015.

Following installation of a sufficient dewatering system, the remaining underpinning piers and 50tn to 60tn tiebacks were installed between to accommodate for general site excavation.

The SOE system adjacent to the NYCT/DEP structures consisted of drilled in soldier piles with contact timber and pre-cast concrete lagging supported with inclined rakers bearing on a partial mat slab foundation. GC was not able to construct the partial mat foundation prior to November 2015, which was the deadline for the soil remediation. To meet the deadline, the GC performed marginal slot excavation adjacent to the soldier pile lagging supported by a temporary stabilizing berm prior to the installation of the rakers.

The dewatering system was incrementally removed as the foundation mat was poured. Once the portion of the mat supporting the rakers was poured, majority of the dewatering system had been removed. Subgrades adjacent to NYCT/DEP structure were initially disturbed due to the presence of groundwater. As we suggested the GC constructed a collection trench with a french drain to collect ground water and divert it away from foundation subgrades. The south portion of the mat was completed during early December, 2015.

© 2016 Deep Foundations Institute

Instrumentation

The instrumentation monitoring program designed and implemented by our firm consisted of, up to 11 automated seismographs and one Automated Motorized Total Station (AMTS) to monitor above the ground surface. The AMTS monitored a total of 16 prisms that were affixed to the adjacent structures which were underpinned or within the influence zone of the support of excavation system. Also 5 prisms were attached to the top of soldier piles adjacent to the NYCT/NYCDEP structures to monitor movement during berm excavation, partial mat construction, raker installation and foundation construction. We evaluated this data daily to evaluate the effects, of the SOE system, underpinning, dewatering, and foundation construction. As presented in Figure 9 settlement at underpinning piers was mostly negligible, with 0.35 inch maximum in an isolated area.

Nine of the seismographs were installed within the adjacent NYCT structure and automated so that alerts could be received at the construction site and our Manhattan office. A manual baseline optical survey and pre-construction condition survey was also performed at the NYCT Structure within the influence zone of the construction. The recorded vibrations were so low and NYCT was so satisfied with the construction that they did not require a post-construction condition survey.

The successful usage of this system was key during installation of underpinning and tiebacks in the adjacent properties, installation of drilled soldier piles adjacent to NYCT structures and during soil excavation to determine any possible damage to the adjacent structures. Because of the frequency of the data collection on site GZA personnel we were able to closely monitor settlement and determine the cause of the settlement and adjust the construction process to reduce overall settlement and lateral movement due to underpinning.

We developed and implemented a monitoring program to meet NYCT requirements; including pre-post optical surveys, automated vibration monitoring plans capable of providing real-time data and alerts to the project team. During the installation of the SOE system and construction of the Mat Foundation, vibrations recorded within the NYCT structure were below 0.2 inches per second (See Figure 10).

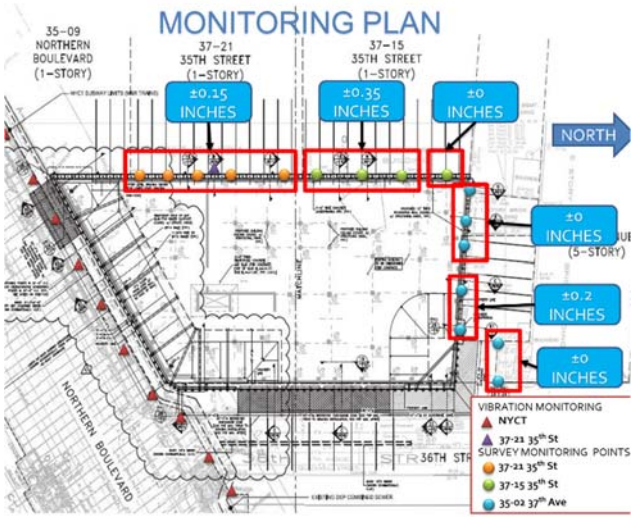


Fig. 9 – Settlement of adjacent structures due to underpinning and SOE construction.

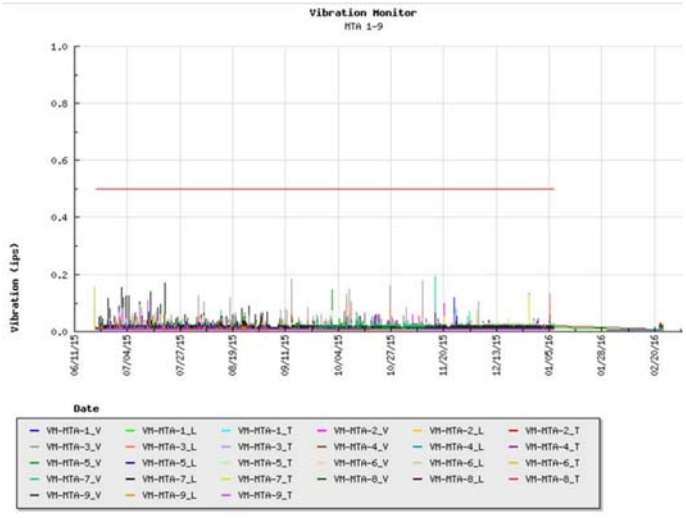


Fig. 10 – Vibration data collected from 9 seismographs in NYCT structure

© 2016 Deep Foundations Institute

Environmental

GZA also provided Environmental Consulting Services including: Assisting or Leading negotiations with NYSDEC, NYCOER, and NYSDEC; completing Phase I and Phase II ESAs; negotiating substantial redevelopment tax credits; preparing the RAWP; performing the CAMP; prepared a CHASP; Preparing Soil Waste Reports and Management Plans.

- Environmental Coordination with New York City Office of Remediation (NYCOER) Environmental (E) Designation, New York State Department of Environmental Conservation (NYSDEC) and New York City Department of Environmental Protection (NYCDEP)
- Performed Environmental Due Diligence under the NYCOER E-designation program
- Conducted Remedial Investigations to delineate on-site contamination and find the source of the off-site chlorinated solvent plume
- Prepared a RAWP, CAMP, SMP, FER
- Prepared applications for Long Island Well Permit and obtained Dewatering Permits from NYCDEP.
- Conducted full time remedial oversight and perimeter air monitoring services.

Lessons Learned

HP soldier piles installed within drilled-in temporary casing were originally specified. As previously discussed the GC proposed smaller diameter drilled-in micropile soldier piles in lieu of HP soldier piles. Installation of the casing and setting of the HP soldier piles would require larger equipment for drilling and placement than the implemented micropile alternative. Although tighter spacing is required, there appear to be more contractors, especially non-union firms, which have the ability to install micropile soldier piles rather than traditional drilled-in HP soldier piles. Drilled-in micropile soldier piles should also be considered in smaller projects in tight urban environments where driven soldier piles are not an option.

Corner bracing adjacent to the NYCT/NYCDEP structures was originally specified which we were more confident could be installed successfully than the proposed raker alternative implemented by the GC. Although successful for this project inclined rakers are reliant on a staged stabilizing soil berm adjacent to existing structures. During construction, contractors often do not or are unwilling to limit excavation operations to maintain the specified berms until the bracing is in place. With difficulty the stabilizing berms needed to be remediated for this project. Moreover, rakers rely on having part of the foundation mat or independent heel blocks be constructed and cured for base support which could delay bracing installation. Due to the reliance on foundation mat support for the rakers, to complete impacted soil excavation by the tax credit remediation deadline the GC implemented a riskier slot removal/replacement method for the impacted stabilizing berm. As was the case for this project, the presence of groundwater above final subgrade would have made installation of independent heel blocks below the foundation mat impractical.

Insufficient dewatering for the initial underpinning at the NE Phase 421a area created significant delays in the construction of those underpinning piers and generated concerns of loss of ground and associated settlement at the remainder of the underpinning and excavation below the water table. Prior to proceeding with the remaining underpinning the GC successfully focused their dewatering sub-contractor to provide sufficient dewatering expediting the remaining foundation work.

Provide frequent coordination, quick responses to inquiries, timely adjustments to design and drawing modifications to allow ordering of long lead items and maintaining tight construction schedule. In large part due to GZA's responsiveness the project was able to take advantage of not only 2015 421a Real Estate Tax Exemption credits but also soil abatement tax credits as described above.

© 2016 Deep Foundations Institute

The AMTS was located at the most suitable available location at this project. However, there were still line of sight limitations along the NYCT/DEP structures and 36th Street due to construction fencing and equipment. Attempts to monitor the micropile soldier piles adjacent to NYCT/DEP structures had limited success, due to on-going work and workers changing areas which disturbed prisms. Casing left extending above the ground surface or pipe embedded in the fresh micropile grout may have provided a more stable location for prisms. Also, intermittent manual survey monitoring can supplement the automated monitoring program.

Due to Owner delays caused by switching equity partners and general contractors, construction did not begin until the spring of 2015 with major earthwork not starting until the summer of 2015. In order to assure receipt of the Certificate of Completion (COC) and the substantial tax credits for 2015 all remediation activities were required to be completed by November 1, 2015 and the Final Engineering Report (FER) submitted on November 15th. Our firm provided full time remedial oversight during this period, obtained dewatering permits and prepared drafts of the NYSDEC required deliverables at the appropriate milestone deadlines well before remedial completion in order to assure the Case Manager had a quality document with minimal comments. Data was input into deliverable formats and evaluated as it was received and decisions regarding excavation limits were made in 24 hours from initial sampling. Soil manifests were tracked daily and entered into spreadsheets as they were received. Remedial construction was completed three days prior to the NYSDEC deadline and all reports were submitted in final format on November 15, 2015. The COC was received on December 22, 2015.

© 2016 Deep Foundations Institute

TBM RECOVERY SHAFT CONSTRUCTION - SR-99 TUNNEL

John Starcevich, PE, Malcolm Drilling Company Inc., Seattle, WA., USA
Lance Rasband, Malcolm Drilling Company Inc., Seattle, WA., USA
Richard Hanke, PEng, Malcolm Drilling Company Inc., Seattle, WA., USA

The 17.4 meter (57 ft) diameter tunnel boring machine (TBM), the world's largest at the time of her launch in 2012, locally referred to as "Bertha," is stuck. Incapacitated due to mechanical failure approximately 36 meters (120 ft) beneath downtown Seattle, situated precariously between the deteriorating Alaskan Way Viaduct and the failing Seattle Seawall. Accessing Bertha with a vertical shaft provides the best approach to address all facets needed for repairs and will allow the full removal of Bertha's cutter head and related inner workings. Limited area above the tunnel alignment and the physical restrictions of existing infrastructure, create significant challenges for the design of an otherwise symmetrical shaft, requiring special attention to design and layout. Consequently, the access/recovery shaft design required a combination of 3m, 2.5m, 2.2m, 1.5m and 1m diameter unreinforced drilled secant piles coupled with various ground improvement techniques and dewatering, to fully satisfy the shoring design requirements. This paper will describe the shaft installation procedures, equipment used and pitfalls encountered while undertaking access shaft construction of this magnitude.

INTRODUCTION

Tunneling on Seattle's SR99 tunnel project began in July of 2013. After slowly mining through a 4.5 m (14.76 ft) thick fiber-reinforced concrete headwall and the first of three stabilized "safe havens," Bertha would proceed along the proposed alignment through 122 meters (400 ft) of jet grout improved soil at a rate of slightly over 1.6 m (5.25 ft) per day. Once past the improved area, it was planned that "Bertha" – would be moving at a rate of about 11 m (36 ft) per day. By the end of October 2013, Bertha had mined roughly 131 m, (430 ft) averaging 1.4 m (4.6 ft) per day and had begun mining within native soils. By December 2013, tunneling had reached the 244 m mark and Bertha was averaging 3.6 m (11.8 ft) per day, achieving as much as 12.8 m (42 ft) of progress on given days. Unfortunately, on December 6th, 2013, Bertha began to stumble and all progress quickly came to a halt.

It was initially reported that an obstruction had stopped Bertha in her tracks. The preliminary investigation involved installation of 10 deep dewatering wells to reduce the hydrostatic pressure around the TBM, and allow visual inspection of the cutter head from within the TBM, and also to investigate for the presence of obstructions at the face of the cutter head. During this inspection, fragments of steel pipe were discovered entangled in the cutter head. The fragments were apparently from an abandoned 254 mm (10 in.) diameter monitoring well casing, previously installed by WSDOT to monitor ground water conditions for the design and planning of this tunnel project. After the steel was removed from the cutter head and cleared from Bertha's path, tunneling resumed. It was then discovered that Bertha was only able to generate a slow crawl.

The Contractor decided to more closely investigate the soil immediately in front of the TBM. At the Contractor's request, Malcolm Drilling, Inc. mobilized a Davey Drill 725 duplex rotary drill to install 18, 152 mm (6 in.) diameter probe holes on 1.5 m (5 ft) centers across the face of the cutter head. Of the 18 holes drilled, 6 obstructions were found at depths between 17 to 24 m (56 to 79 ft) (located between the top of the cutter head to near spring line). Small fragments of steel were found in several of the probe holes and the drill casing was not able to be advanced beyond the obstruction. Malcolm was then directed to drill 1.5 m diameter holes in 4 locations where the obstructions were encountered, to facilitate their removal. However, after these additional, larger exploratory holes were drilled, no additional steel fragments, nor obvious signs of obstructions were encountered. All additional exploratory work was completed by late February 2014, and the alignment was thought to be clear and ready for Bertha to continue moving forward.

© 2016 Deep Foundations Institute

However, once the TBM was cleared to resume mining, and the cutter head started turning again, a much larger issue was discovered. The machine's main bearing had been damaged so severely, it would need to be completely replaced, requiring removal of the TBM cutter head. This would require a monumental effort, with the fast-track design and construction of a structure over 36.6 m deep and more than 24 m in diameter; that would provide access to the TBM and allow the disassembly and removal of the entire cutter head.

SITE CONSTRAINTS

Malcolm was asked to assist with preliminary design and constructability of the access shaft required for the repair of the machine. Several challenges had to be overcome in designing an access shaft that would work for this project. Extremely limited access was the primary constraint (Figure 1). With the Puget Sound approximately 30.5 m (100 ft) to the west and the deteriorating Alaskan Way Viaduct (SR-99) immediately to the east, within feet of the proposed access shaft location, there were severe "at grade" access restrictions. Additionally, 1.5 m diameter tangent piles, spaced 0.46 m apart, (previously installed under the main tunneling contract) ran along the east and west edges of the tunnel alignment. These piles were required for settlement mitigation during tunneling and to protect the existing viaduct. A high groundwater table, only 2.4 m (~8 ft) below grade, also needed to be cut off. But probably most critical, was the schedule implications for building something effective and quickly enough to get this major project back on track.



Fig. 1: Site Layout/Access Constraints

© 2016 Deep Foundations Institute

RESCUE SHAFT DESIGN

Bertha's lack of progress has been the subject of much speculation, however one indisputable fact remained; the full cutter head and inner workings required removal to facilitate a complete repair of the TBM. A recovery shaft would need to be designed and installed immediately in front of the TBM to allow it to enter the shaft and provide access for repairs.

Malcolm Drilling, having extensive experience with secant pile compression rings, recommended a circular access shaft comprised of over-lapping secant piles that would provide excavation support, groundwater cut-off, and eliminate the need for horizontal anchors or braces maximizing space for removal of the cutter head. The original design included 2.13 m (7 ft.) diameter secant piles in a circular ring with jet grouting between the originally placed tangent piles. Moreover, jet grouting continued across the back of the machine to provide water cut-off for internal maintenance of the machine, as well as controlling water when the machine enters the access shaft.

Brierley and Associates designed the proposed access/recovery shaft and provided bid documents to select drilling contractors for bids. Upon review of the design, Malcolm suggested an alternate option; utilizing 3 m (9.84 ft) diameter drilled secant piles, requiring fewer secants and reducing the anticipated schedule. After a thorough review, Malcolm's proposed alternate was selected; and once awarded, Malcolm worked closely with Brierley in finalizing the design with the capabilities that could be brought to the project (Figure 2).

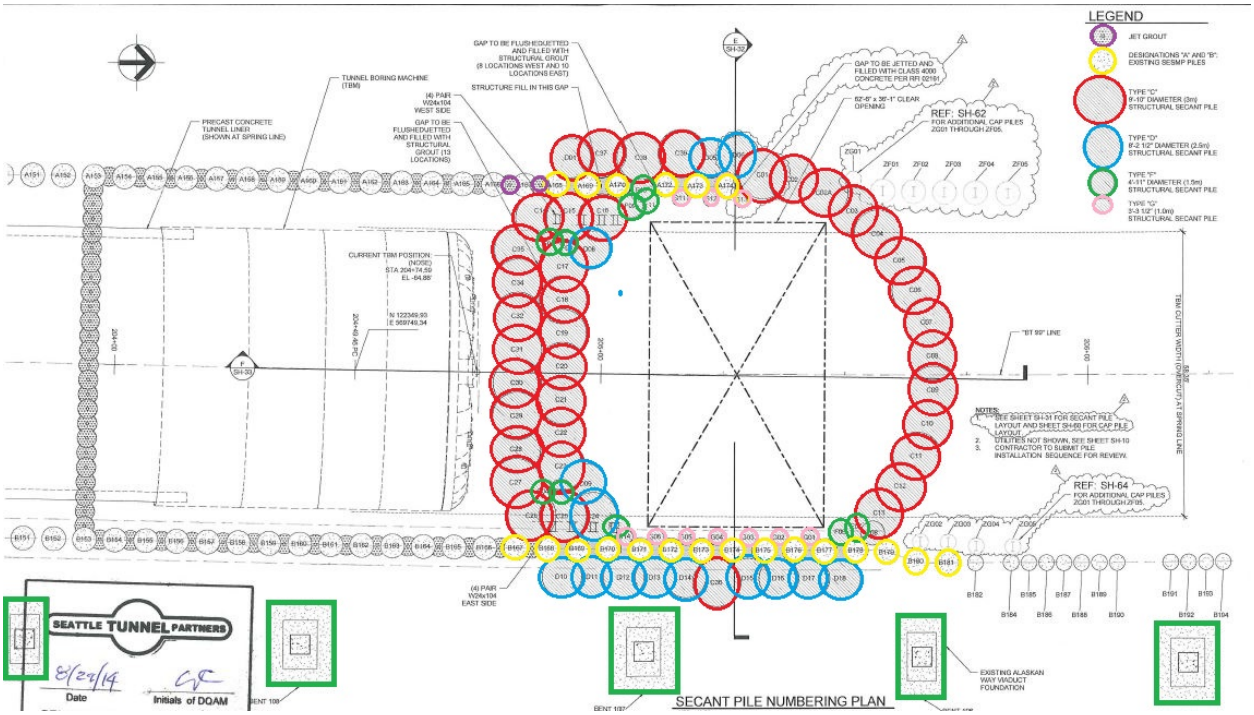


Fig. 2: Access/Recovery Shaft Layout - Note existing SR-99 footings, (green rectangles).

SUBSURFACE CONDITIONS

The south Seattle waterfront consists of reclaimed lands comprised of decades of undocumented fills, debris, and various organic deposits. The upper reaches of the soil profile contain numerous timber piles and railroad ties from buried trestles including sawdust and wood debris from previous milling operations. Various fill deposits overlie soft and loose marine sediments that lie on top of glacial till at depths of 12 to 27 m (39 to 89 ft).

© 2016 Deep Foundations Institute

The complex glacial stratigraphy controls the nature of the groundwater flow. The permeabilities vary by orders of magnitude in adjacent stratigraphic units. Consequently, there are multiple perched groundwater-bearing layers and multiple piezometric surfaces along the proposed tunnel alignment. Groundwater movement is governed by hydraulic gradients, which may increase, or decrease with depth; downward gradients typical of upland areas, and upward gradients often observed in water-bearing units close to discharge points. Soil borings near the south portal, with multiple piezometers installed, indicated multiple piezometric surfaces with variations in groundwater levels of up to 3 m (10 ft); some indicated artesian pressures of up to 1.5 m (5 ft) above the ground surface (Figure 3). Tidal influence was also observed to effect the groundwater level within the area of the recovery shaft, with groundwater levels observed as shallow as 1.5 m (5 ft) below grade.

Consistent with the known subsurface conditions at this reach of the tunnel alignment, there was an abundance of wood debris within the upper fill zone. Relic deposits of wood, pulp and decayed organic matter would be routinely encountered in vast areas where little to no natural granular soils were detected.

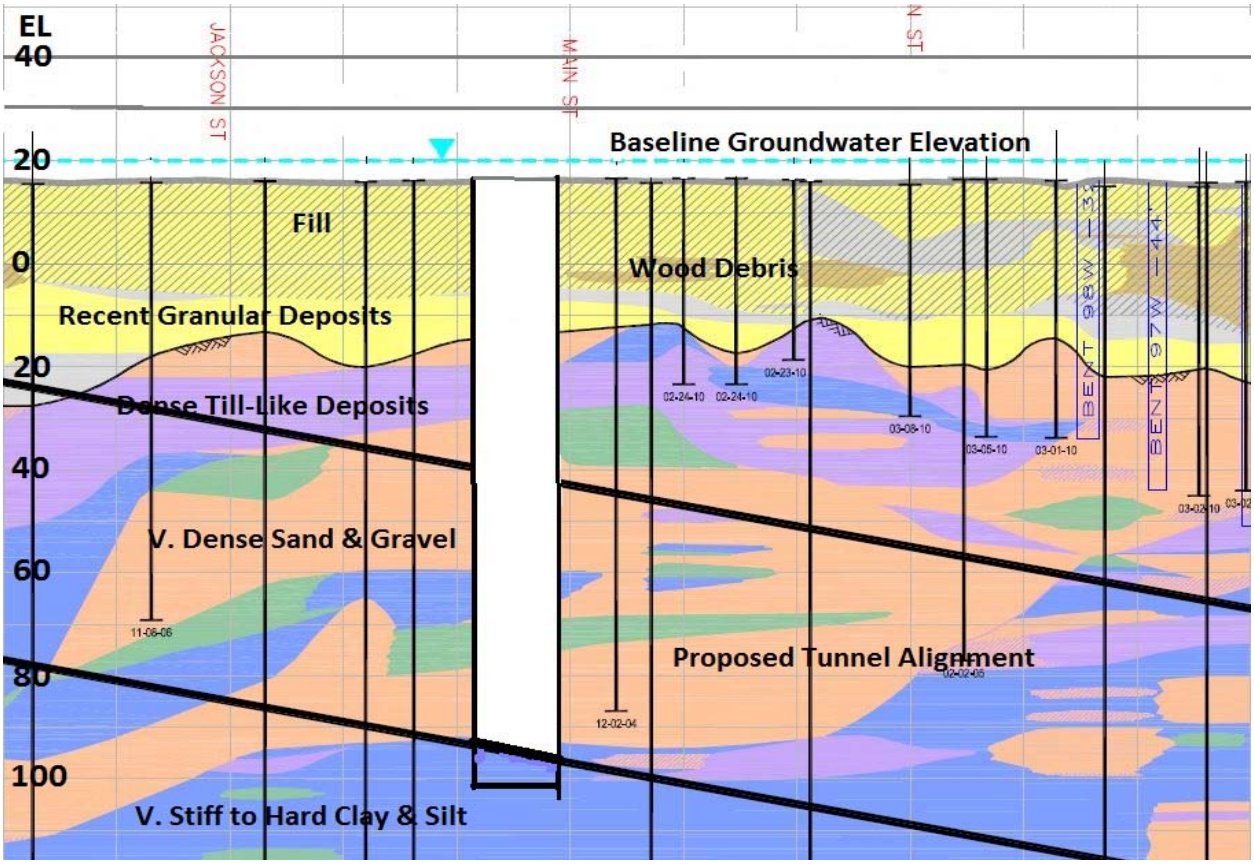


Fig. 3: Access/Recovery Shaft Subsurface Conditions

Additional geotechnical investigation within the vicinity of the recovery shaft revealed a deep aquifer with direct communication to, and encompassing, the silt deposit that constitutes a majority of the soil plug within and beneath the proposed access shaft. In addition, the presence of several large voids were confirmed, some that required more than 420 m^3 (550 CY) of controlled density fill (CDF) to fill, and some that had been previously filled with large crushed rock by the contractor.

© 2016 Deep Foundations Institute

DRILLED SECANT PILES

The original design for the TBM launch pit included two parallel rows of drilled shafts, one to the east, and one to the west, of the proposed tunnel alignment, and extend to the north, well beyond the tunnel headwall. They were designed to prevent lateral soil movement adjacent to the tunnel, and mitigate potential surface settlement; and were referred to as *South End Settlement Mitigation Plan (SESMP)* piles. Please note, for the purpose of our discussion, we will us the terms "drilled shaft" and "pile" interchangeably, to refer to the deep foundation and earth support elements used to construct both the recovery shaft and the original TBM launch pit. To incorporate the existing *SESMP* piles into the access shaft, smaller 1-meter diameter drilled shafts were constructed parallel to, and along the interior face of the existing SESMP piles. These drilled shafts help create a continuous outer wall along both the east and west sides of the access shaft, and to provide additional bearing capacity for the cap beams, required for support of the gantry crane. The work was completed with a Bauer BG-50 installing drilled shafts up to 40 m (131 ft) in depth. Once again there was difficulty with maintaining verticality that was specified to be within 152 mm (6 in.) at 40 m (131 ft), as checked with a SoniCaliper. The difficulty was a result of the concrete over-break of the existing SESMP piles (drilled shafts) and field adjustments had to be made to accommodate these issues. It was clear that the actual installation of the drilled shafts required to construct the access/recovery shaft was going to be significantly more challenging than designing it. Additionally, far more obstacles than anyone could have imagined during the planning and design phase were encountered. However, having the Designer's Field Representative on-site full-time provided the opportunity to quickly address challenges as they arose, allowing the project to move forward as quickly and efficiently as possible.

After the completion of the drilled shaft work, other equipment was mobilized to begin the large diameter work. Two spreads of equipment and crews began work in mid-June with Liebherr dig cranes and Leffer oscillators and rotators to start the 2.5 m (8.2 ft) and 3 m (~10 ft) diameter secant piles included in the final Brierley design (Figure 2). The work proved to be very difficult due to sequencing and the tight work areas on the job site (Figure 4). The greatest assets to the project were the two Leffer rotators. These machines proved to be the most efficient at installing the piles on location, maintaining verticality, and with the highest rate of advancement as opposed to just using casing oscillators for advancement. In the end, the shaft work was complete by the end of August 2014, leaving only the remaining grouting and dewatering work to be completed.

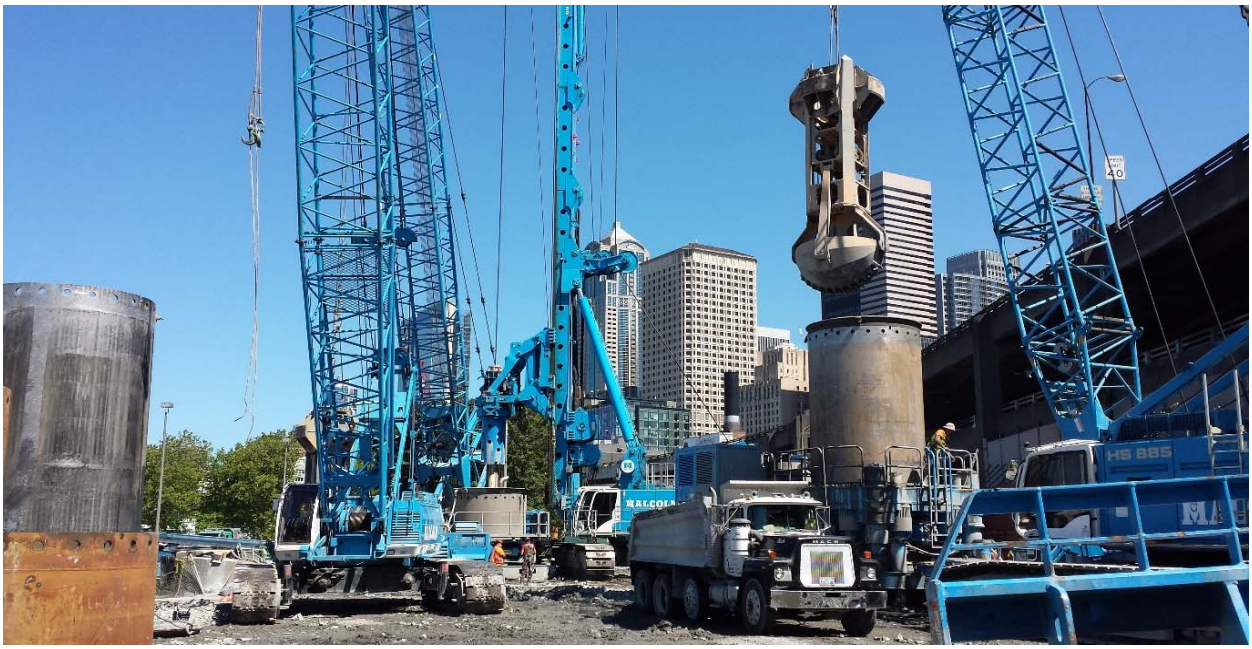


Fig. 4: Access/Recovery Shaft Construction– Confined work site.

© 2016 Deep Foundations Institute

JET GROUTING

Jet grouting was an integral part of the overall access/recovery shaft design. Jet grouting was required outside of the recovery shaft to provide a level of groundwater control at the machine "breakin," the location the TBM will bore into the recovery shaft. The SESMP piles, constructed previously, as part of the work for the original launch of the TBM, were located on both the east and west sides of the tunnel alignment, and were enhanced with jet grouting to act as cutoff walls, Figure 2. These SESMP piles consisted of 1.5 m (5 ft) OD drilled shafts, installed in two parallel lines, one to the east and one to the west of the proposed tunnel alignment. These drilled shafts were spaced approximately 1.9 m (6.23 ft) center to center, creating a gap of about 0.4 m (1.3 ft), requiring jet grouting to enclose the gap and provide groundwater cutoff. A transverse line of jet grout columns placed in secant fashion tied the two east/west cutoff walls together and encapsulated the TBM cutter head with the recovery shaft that was yet to be constructed. See Figure 5.

Jet grouting between the existing SESMP piles would have been extremely difficult, if not impossible, due to the large amount of concrete over-break resulting from the poor soil conditions. Accordingly, each proposed jet grout column was pre-drilled with 152 mm (6 in.) tooling, clearing a space for the jet grout monitor and casing to reach the designed depth. Upon completion of jet grouting along the SESMP pile lines, jet grouting efforts continued with construction of a transverse grout curtain, or cutoff wall, behind the TBM tail shield. The purpose of the cutoff wall was to control groundwater during the critical phase of shaft "breakin," as the TBM enters the access/recovery shaft.

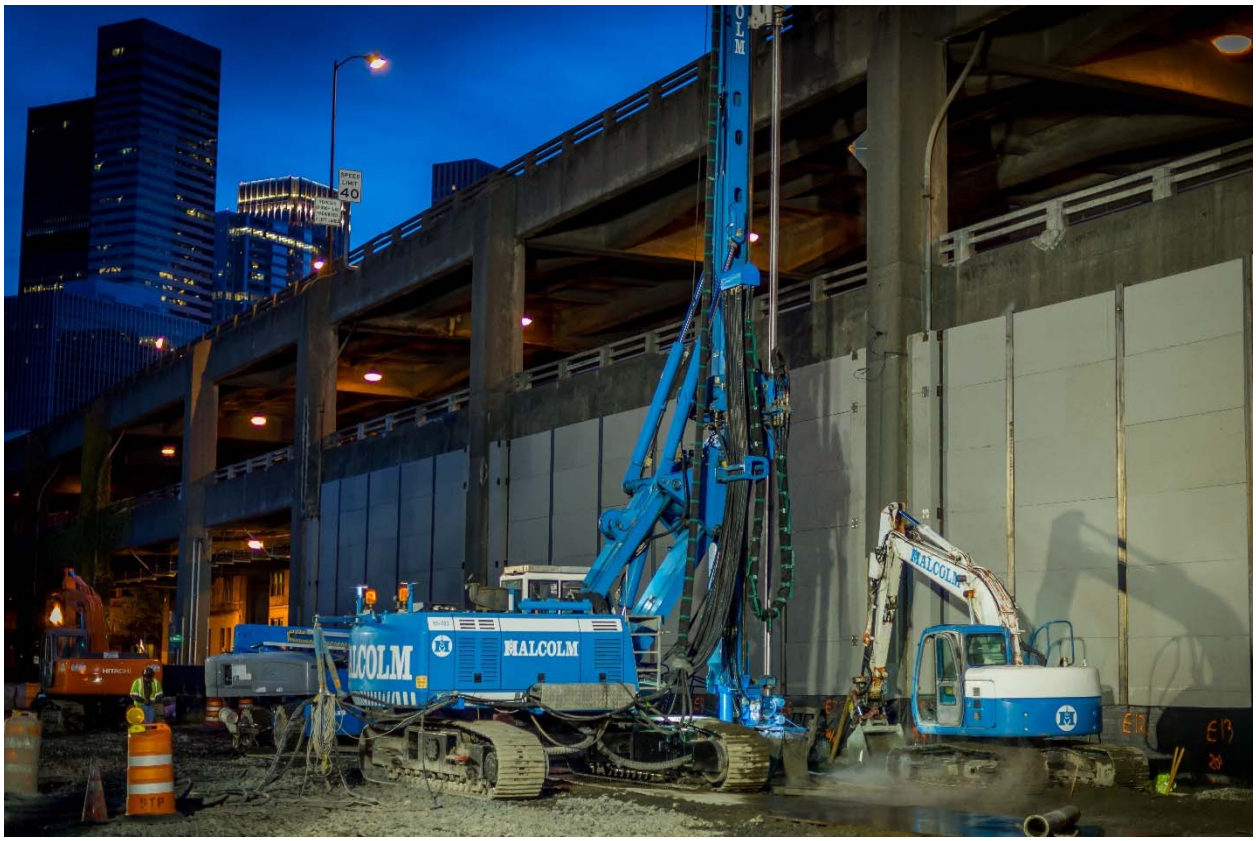


Fig. 5: Jet Grouting Operations adjacent to Alaskan Way (SR-99) Viaduct.

© 2016 Deep Foundations Institute

SESMP piles were located only on the east and west walls of the access shaft. The soil between them needed to be grouted in order to create a complete and continuous wall to withstand the extreme conditions anticipated throughout the various stages of the work. Continued dewatering, pressurizing of the TBM heading, and other work within the tunnel horizon caused soil loss and changes to the subsurface conditions. A sinkhole appeared in front of Bertha shortly after she first stopped that required backfilling, and required 420 m^3 (550 CY) of CDF. This was further evidenced by removal of vast quantities of TBM soil conditioner during drilled shaft excavation, at horizontal distances greater than 24 m (79 ft) to the NE of the TBM cutter face. A dynamic environment materially different than the rest of the project site had been created over a very short time. Consequently, during drilled shaft construction sink holes manifested to existing grade, requiring rapid evacuation of all heavy drilling equipment while the safety and stability of the working platform was assessed. After mass excavation and earthwork, a large volume of quarry spalls was imported to the site to create a safe and stable working platform, or mattress, for staging the drilling equipment. Subsequently, during the following drilled secant work, quarry spalls were carried deeper into the soil profile with each tooling penetration. As a result, the combined presence of a quarry spall mattress at grade along with quarry spalls throughout the vertical soil profile created an environment that was not conducive to jet grouting methods. As an alternative to jet grouting methods Malcolm mobilized two Foremost DR-24 vertical drill rigs to drill out and flush these confined spaces, between the SESMP piles and newly placed drilled secants, with high strength cement grout in hopes to treat the areas needed for the shoring design.

DEWATERING

Once the grouting work was completed the installation of the remaining dewatering wells commenced in addition to further geotechnical investigations and installation of instrumentation. The geotechnical investigation showed that the silt plug in the bottom of the excavation, previously assumed impermeable and to function as an aquiclude, actually had vertical silty sand seams thereby raising concern that the shaft bottom had potential to heave. This new obstacle was overcome by enhancing the current dewatering design. The current design was limited to 8 wells at 47 m (154 ft) in depth. To eliminate this potential bottom heave condition, 8 more wells, 4 at 47 m (154 ft) deep and 4 more at 62.5 m (205 ft) deep, were installed to depressurize the bottom plug for the final state of the excavation.

Prior to advancing the TBM into the access/recovery shaft, Malcolm was asked to install two horizontal drains, from within the access shaft, to relieve hydrostatic pressure behind the secant pile wall. The 15.25 m (50 ft) long drains were installed working from on top of the upper horizontal surface of the concrete cradle that was constructed in the bottom of the shaft to support Bertha upon entry, (Figures 6 and 7). The horizontal drains were comprised of 7.6 m (25 ft) of pre-pack PVC well screen, and 7.6 m (25 ft) of solid PVC pipe. The pre-pack well screen consists of a 152 mm (6 in.) diameter outer and 51 mm (2 in.) diameter inner slotted PVC well screen with filter sand in the annular space. One drain was located on each side of the TBM, at roughly the lower quarter-points of the tunnel, extending parallel with the alignment (Figure 6). An approximately 305 mm (12 in.) diameter hole was drilled through the secants and a 254 mm (10 in.) diameter pipe with a blow-out preventer (BOP) was installed at each location. The drains were installed within a 203 mm (8 in.) diameter borehole and equipped with a PVC ball valve to control flow.

Once the hydrostatic pressure surrounding the TBM was reduced to El. -85 (ft), essentially the elevation at which the horizontal drains were installed, the tunnel crew was given the approval to advance the damaged TBM forward, into the recovery shaft. However, prior to advancing into the recovery shaft, the perimeter of the anticipated penetration through the wall (of the recovery shaft) was pre-split with a long-reach, excavator-mounted hydraulic concrete breaker to both minimize the efforts of the TBM and to reduce the horizontal loading on the shaft headwall.

© 2016 Deep Foundations Institute

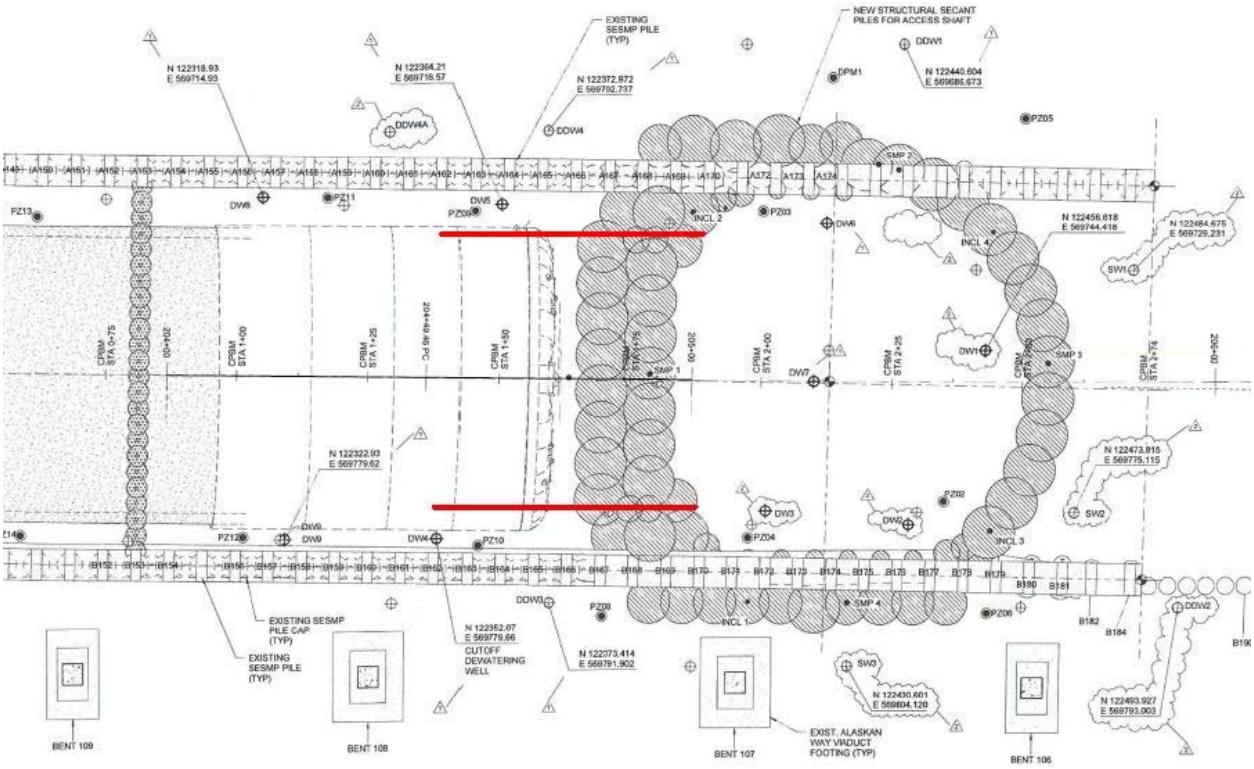


Fig. 6: Access/Recovery Shaft Dewatering – Horizontal drain layout.



Fig. 7: Access/Recovery Shaft Dewatering – Horizontal drain installation from within shaft.

CONSTRUCTION SUMMARY

Malcolm installed the following work to complete the access shaft:

17 - 1 meter (3.28 ft) diameter drilled shafts 40m deep
14 - 1.5 meter (4.92 ft) diameter drilled shafts 40m deep
16 - 2.5 meter (8.2 ft) diameter drilled shafts 40 m deep

© 2016 Deep Foundations Institute

25 - 3.0 meter (9.84 ft) diameter drilled shafts 40 m (131 ft) deep
1,951 m (6,400 ft) of jet grout column
16 - Dewatering wells up to 62.5 m (205 ft) deep
2 - Horizontal drains 152 mm (6 in.) diameter by 15.25 m (50 ft) long

SUMMARY

The work to create this access/recovery shaft was a monumental effort requiring precise coordination from the best in all disciplines and utilization of the most state-of-the-art foundation drilling equipment. There were many obstacles to overcome, as is the case in most emergency jobs, which required problem-solving "on the fly" to accomplish this monumental task within the extremely limited time available.

A broad range of geotechnical construction techniques were required for the construction of the TBM recovery shaft on the SR 99 tunnel. Difficult ground conditions along with a condensed work schedule contributed to the complexity of the work. Moreover, a highly "dynamic" underground environment created by TBM operation and maintenance, site preparation work and maintenance, and dewatering, added unforeseen challenges. State-of-the-art specialty foundation equipment was mobilized, which worked concurrently with Leffer casing rotators and oscillators, and Liebherr duty cycle dig cranes. Other applications included various jet grouting and dewatering scopes completed both at grade and from within the shaft excavation. This work tested the capabilities of existing equipment, pushing them to (and beyond) their previous benchmarks, and in doing so has defined new limits for secant shaft construction.



Fig. 8: Success – "Bertha" within the Access/Recovery shaft.

© 2016 Deep Foundations Institute

At the current time, “Bertha,” repaired and reassembled, has continued mining operations and is about midway along the proposed tunnel alignment, 4,135 ft of the 9,270 feet. Based on current production rates, tunneling operations should be completed by early to mid-2017. The current project schedule calls for the tunnel to be open to traffic in early 2019.

© 2016 Deep Foundations Institute

UB DIGS DEEP AND BUILDS OVER ADJACENT SUBWAY FOR NEW MEDICAL BUILDING HUB

Walter E. Kaeck, Mueser Rutledge Consulting Engineers, New York, NY, USA, wkaeck@mrce.com
Lisa R. Papandrea, P.E., Mueser Rutledge Consulting Engineers, New York, NY, USA, lpapandrea@mrce.com
David Chen, P.E., Mueser Rutledge Consulting Engineers, New York, New York, USA, dchen@mrce.com

ABSTRACT

Construction of the University at Buffalo's new School of Medicine and Biomedical Sciences (UB-SMBS) required excavation in variable ground to a depth of more than 40 ft adjacent to the NFTA Metro subway and Allen Street Station. Complicating the building design and construction, the new medical facility incorporates the at grade Station entrance building, requiring a combination of temporary and permanent excavation support structures, a complex sequence of ground support installation, and a mix of shallow and deep foundations to accommodate the large floor spans and concentrated column loads introduced by building over and adjacent to the Station entrance. Excavation and foundation construction was challenged by a stratified soil profile with interlayered and sensitive sands, silts and clays and complicated groundwater regime with perched and regional water tables. Efficient construction required ongoing coordination between the design team and contractor, careful field observation, and construction monitoring in several facets of below grade construction. This paper describes the design and construction of excavation support structures and foundations to manage the variable ground, congested site conditions, and complications of building adjacent and above an active subway station. Use of site instrumentation and monitoring data to provide guidance in construction when unanticipated field conditions arise is illustrated. Lessons learned in installation and sequencing of excavation support, groundwater control and foundation construction are also discussed.

Keywords: deep excavation, micropiles, groundwater control

INTRODUCTION

University at Buffalo President Satish K. Tripathi heralded the new School of Medicine and Biomedical Sciences (UB-SMBS) as a future linchpin of UB's downtown campus that will revitalize the area and enhance western New York's emerging bio-sciences corridor. The $375 Million, 628,000 square foot, eight story building with two basements is expected to house 2,000 faculty, student and staff allowing UB to increase class size from 140 to 180 students. It will be constructed above the Niagara Frontier Transportation Authority's (NFTA) Allen Street Station, creating a direct connection to Buffalo's light rail system. The 200 ft x 400 ft site is bounded by Main Street, High Street, Washington Street and the Roosevelt Apartments and adjoining parking lot at the west, north, east and south respectively, as shown in Figure 2. Groundbreaking for the new building was in October 2013 with the facility scheduled to open in early 2017.

UB-SMBS required excavation in variable ground to a depth of more than 40 ft adjacent to the NFTA light rail subway Station beneath Main Street and at grade Station entrance building occupying the southwest corner of the site. The subway proximity and integration of the Station entrance building into the new medical facility necessitated a combination of temporary and permanent support of excavation (SOE) structures, variable ground support and complex sequence of support installation, and a mix of shallow and deep foundations to accommodate the large floor spans and concentrated column loads introduced by building over and adjacent to the Station entrance. Excavation support system and foundation construction was completed in March 2015.

© 2016 Deep Foundations Institute

The UB-SMBS Master Planning Team is led by the New York State University Construction Fund (SUCF) with architect HOK and structural engineering consultant Ysrael A. Seinuk, P.C. (YAS). Mueser Rutledge Consulting Engineers (MRCE), the geotechnical engineering consultant for the team, conducted a subsurface investigation, provided foundation design assistance, designed the SOE systems, designed and implemented a monitoring program to evaluate construction effects, and performed controlled inspection of excavation support and foundation construction. The $52 Million contract for the first phase of construction, including excavation and shoring, foundations, and structural steel framing, was awarded to LP Ciminelli.

COMPLEX SUBSURFACE PROFILE

A geotechnical investigation was performed consisting of eighteen borings, six piezometers, and two observation wells to evaluate subsurface conditions for design and construction of foundations and temporary works. Four test pits were also made to determine the depth and condition of underground utilities, the footings supporting the Station entrance building, and the roof of the passageway connecting the entrance building with the underground Station. The test pits were also used to investigate the presence of remnant excavation shoring from the original subway construction.

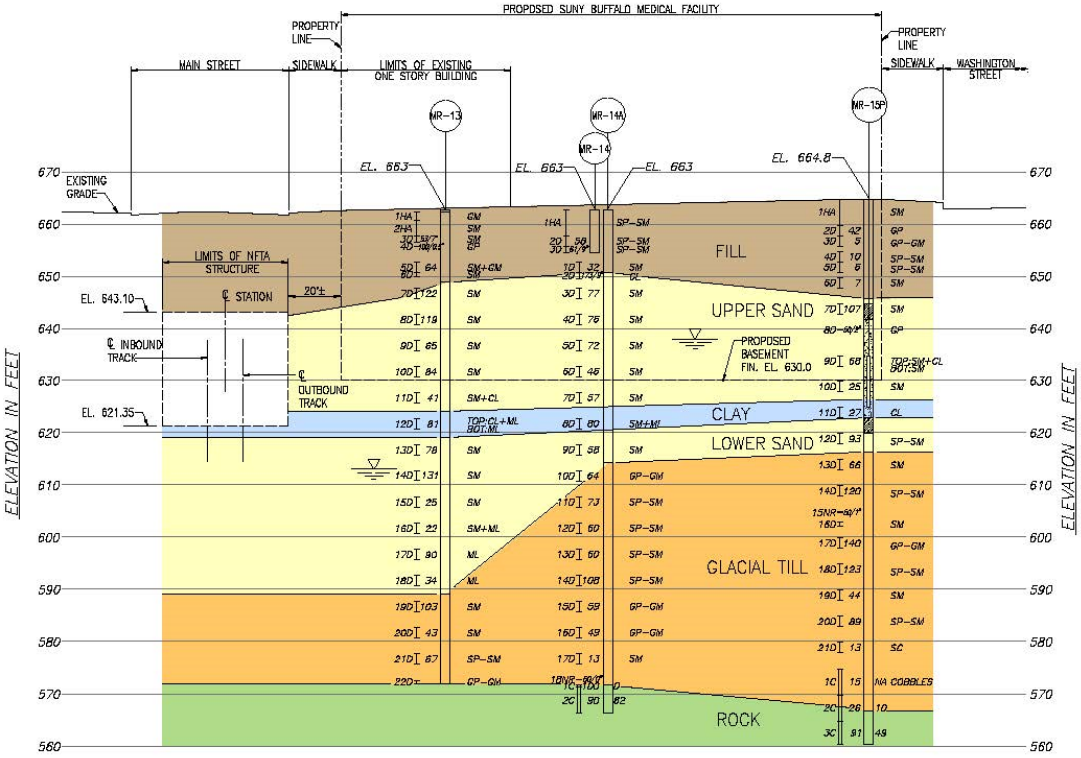


Figure 1: Geologic section looking north.

The borings reveal a complex subsurface profile consisting of 10 to 20 ft of predominantly loose granular fill (with deeper fill adjacent to the subway) overlying 30 to 50 ft of outwash deposits comprised of compact silty fine sands and silts interlayered with stiff to hard clays. The outwash is generalized into upper and lower sand layers with intervening clay as shown on Figure 1 based on predominant soil type and anticipated engineering behavior when excavating within each depth interval. However, the interlayering

© 2016 Deep Foundations Institute

of clays and silts within the sands is more complex with thinner and more frequent lenses and layers of clay and silt expected in excavations than indicated in the borings or portrayed on the geologic section of Figure 1. The clay is heavily over consolidated with an over consolidation ratio (OCR) greater than 4. The outwash deposits are underlain at a depth of about 50 to 70 ft by very compact glacial till consisting of sand, gravel, cobbles, boulders, and limestone rock fragments. A cherty limestone bedrock underlies the till deposits at a depth of 70 to 100 ft, or about Elev. 570. Elevations herein refer to the United States Coast and Geodetic Survey (U.S.C. & G.S.) Mean Sea Level Datum of 1988.

Because of the intervening low permeability clay between the sand layers, groundwater occurs at two distinct levels. A shallow perched water table exists above the clay within the upper sand at about 15 to 20 ft below ground surface, or about Elev. 640. The regional groundwater table is about 40 to 50 ft below ground surface, or about Elev. 610.

Basement construction required excavation to depths of 30 to 40 feet, or about Elev. 620, through primarily silty fine sands, sandy silts and stiff clays of the outwash deposits as shown on Figure 1. These sensitive fine grained soils in combination with the shallow perched water table were expected to pose significant challenges in foundation construction. Prior construction across High Street penetrating to just below the perched water table resulted in ground loss and softening of foundation subgrades when dewatering was attempted using sump pumping methods, indicating that the perched water table was laterally extensive and expected to produce sustained groundwater flow to excavations.

SITE CONSTRAINTS AND FOUNDATION DESIGN

The UB-SMBS facility encompasses the entire site footprint and includes a two level basement in areas outside of the existing NFTA Station entrance building as shown on Figure 2. The building superstructure spans over the entrance building and the station entrance is integrated into the new building. The lower basement has a finished floor at Elev. 630. Basement floor construction consists of a six inch topping slab, 18 inch thick sand layer for vibration isolation from the adjacent NFTA subway, and a 24 inch thick structural slab. The bottom of the basement slab is therefore at about Elev. 626, or about 25 to 40 feet below existing surface grades. Soils at this depth consist of either compact silty sands or stiff to hard clays. Spread footings therefore support the majority of the building except where concentrated loads exist along the northern and western perimeter of the building.

Construction of the UB-SMBS building superstructure above the NFTA Station entrance building required widely spaced, heavily loaded columns to span over and avoid interference with the existing structure. The concentrated loads, presence of relatively deep fill particularly where the site was disturbed by prior subway construction, and limited access for foundation construction within and adjacent to the Station entrance building required the use of micropiles for foundation support of this portion of the building. For similar reasons, micropiles were also required to support the at-grade portions of the SMBS building on the south side of the entrance building and adjacent to the Roosevelt Apartment Building.

VARIABLE GROUND SUPPORT

Surface grades at the site slope downward approximately 15 ft from Elev. 663 at High Street to Elev. 648 in the southeast corner of the site. Foundation excavation was needed to as low as Elev. 620, requiring perimeter excavation support retaining up to 43 feet of soil. In addition to the NFTA Station structures along Main Street, ground support selection and design would have to account for active sewer lines and water mains beneath the sidewalk and roadway of Washington and High Streets.

The initial building layout included foundation walls adjacent to both the east and north walls of the Station entrance building. For this configuration the basement excavation was within the influence zone of the

© 2016 Deep Foundations Institute

entrance building footings, which bear approximately 4ft below street grade. To protect the Station entrance and shallow footings, rigid secant pile walls laterally supported by external tiebacks or internal bracing were initially proposed to avoid Station underpinning. However, due to the high costs of the secant pile wall and increased risks of damage to NFTA structures, the Design Team opted to shift the basement walls along the entrance building 20 ft east, away from the influence zone of the existing footings as shown on Figure 2. This shift made soldier pile and timber lagging walls feasible for most of the site perimeter at a much lower cost.

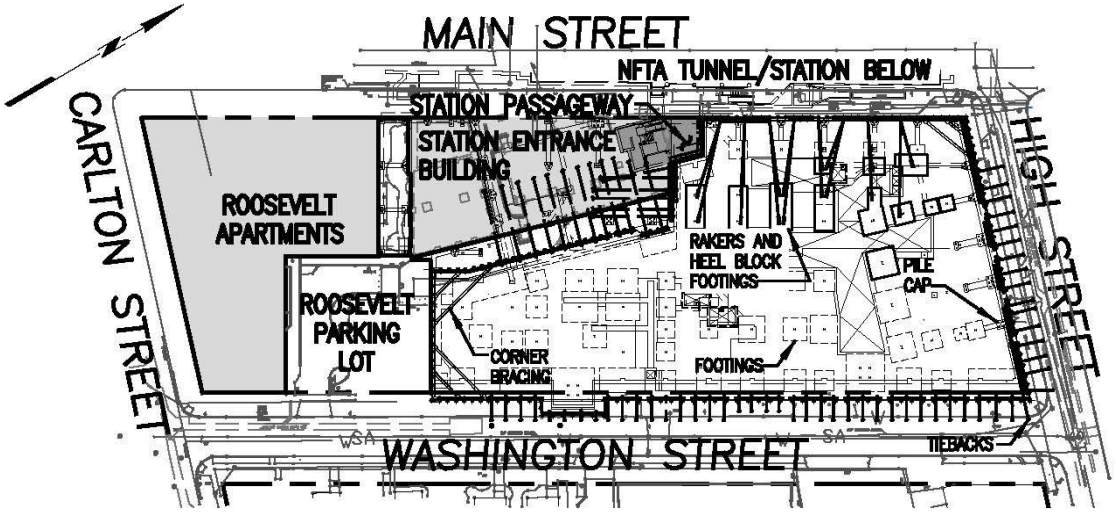


Figure 2: General site plan showing foundations and excavation support systems.

The final design of the excavation support system consisted primarily of drilled-in soldier piles and lagging. Drilled-in soldier piles were required within the influence (generally within 50 ft) of NFTA subway structures with driven soldier piles allowed elsewhere, however the Contractor elected to install drilled-in soldier piles at all locations. Where an approximately 40 ft length of the new structure remained adjacent to the NFTA Station entrance, a secant pile wall was designed to function as rigid SOE, avoid Station underpinning, and become part of the permanent structure's foundation wall.

The SOE walls were laterally supported by two to three levels of bracing with bracing types selected with consideration of site constraints, potential interferences to construction operations, and relative economy. Lateral support consisted of tiebacks along the majority of High and Washington Streets and where the west basement wall was shifted east adjacent to the NFTA entrance building to take advantage of the less restrictive work space provided by external tiebacks. The layout of tiebacks was carefully planned with tieback orientation varied to avoid existing sewers beneath both High and Washington Streets. Tiebacks were also desirable along the south side of the site but were not permitted by the adjacent property owner, so internal corner bracing was used. Along Main Street, where the subway box prevented the use of tiebacks, internal raker bracing laterally supported by permanent footings were employed as shown on Figure 3. These "heel block" footings were designed with shear keys to maximize the engagement of passive soil resistance behind the footings and increase the lateral resistance of the system. The varied SOE bracing systems are presented in Figure 2.

The secant pile wall was also supported by tiebacks, and due to the reentrant corner introduced by basement construction around the Station entrance building, these tiebacks crossed the paths of tiebacks supporting the soldier pile and lagging wall along the east side of the Station entrance building as shown in Figure 4.

© 2016 Deep Foundations Institute

This required careful layout of the tiebacks using a three dimensional Revit model. Vertical tieback angles and free lengths were adjusted to ensure tiebacks did not interfere with each other or share bond zones.

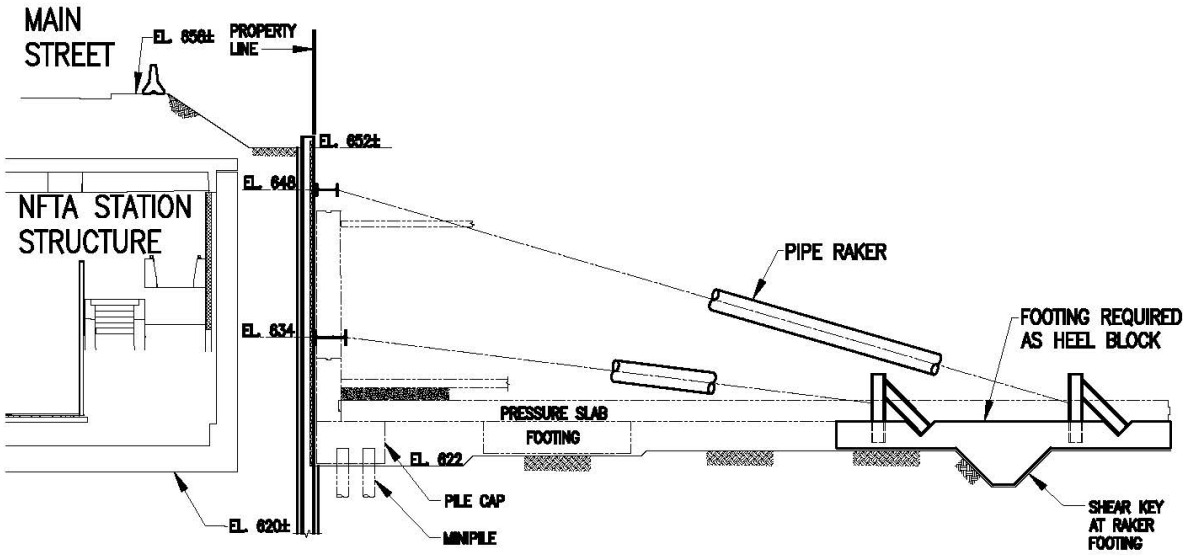


Figure 3: Soldier piles with raker bracing adjacent to NFTA station.

Where openings were present in the first level basement slab along the site perimeter, temporary bracing of the foundation walls was installed to provide the support of the missing floor slab. The temporary bracing allowed removal of the raker system along Main Street and corner bracing along the south end of the site and thereby avoid penetrations in the foundation wall and waterproofing by SOE bracing.

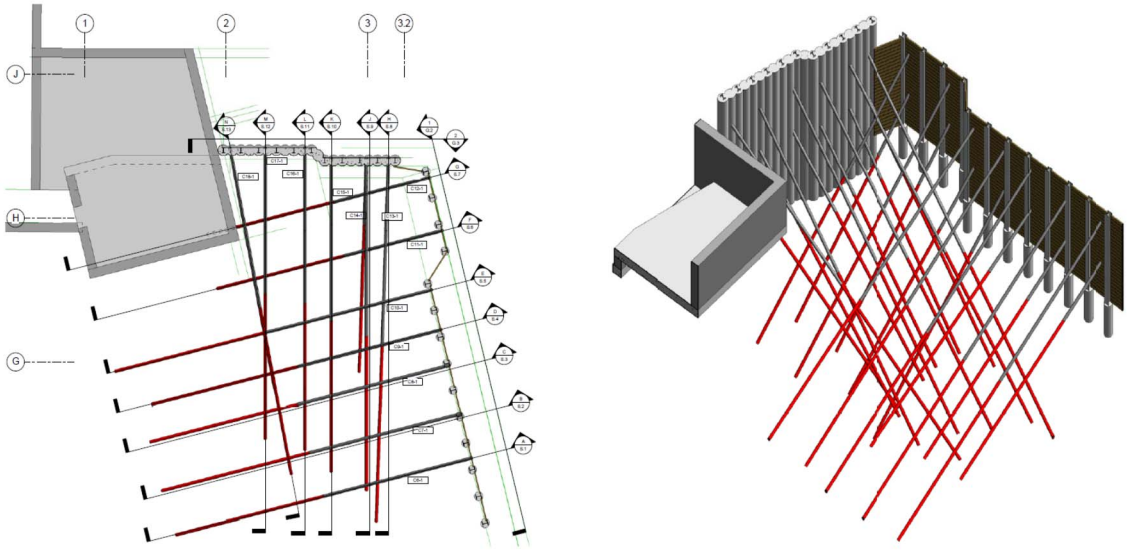


Figure 4: Three-dimensional model plan (left) and isometric (right) of overlapping tiebacks near the NFTA concourse.

© 2016 Deep Foundations Institute

FOUNDATIONS

The foundations consist of 107 rock-socketed micropiles, concrete footings of varying dimensions up to 26 ft x 26 ft x 4 ft, and a 2 ft thick structural slab designed to resist hydrostatic uplift. YAS prepared the contract documents for the foundations with geotechnical assistance from MRCE. Subgrade for footings and slabs were inspected and approved by an MRCE engineer and subsequently protected with a 4 inch mud mat prior to placing waterproofing and foundation reinforcement forms and concrete. Footings were designed for an allowable bearing pressure of 3 tsf.

The Contract documents specified micropiles with a 250 ton vertical capacity and 15 ton net lateral capacity for a fixed head condition after accounting for group effects. The micropile design required 13.375-inch diameter steel casing seated into rock and a 15 ft long rock socket with a full length core threadbar. Specifications required lateral and compression load testing to verify pile design loads.

The Contractor elected to redesign the micropiles using smaller 10.75-inch diameter casing with a 3-bar bundle "stub" core within the socket and extending 5 ft into the casing as shown on Figure 6. However, evaluation of lateral load testing data could only verify 8 tons fixed head lateral capacity for this smaller pile. To expedite the project, the design team re-evaluated lateral load demands at all columns and approved the use of the lower capacity piles at all locations with the exception of 16 piles supporting a shear wall within the Station entrance building. At these locations, 13.375-inch diameter micropiles were installed. A successful lateral load test was performed verifying the 15 ton lateral capacity of the larger diameter piles.

Micropiles were required within the Station entrance building and perimeter foundations along Main and High Streets. Micropiles were installed from street grade within and around the Station entrance building, and in some locations under low headroom conditions as depicted in Figure 5. Micropiles within the excavation were installed from just above the perched water table to allow drilling under a positive head and limit interference between micropile installation and raker bracing along Main Street.

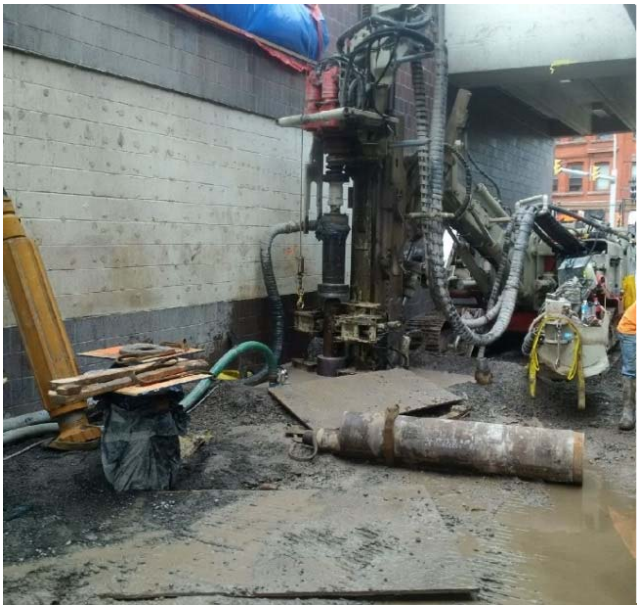


Figure 5: Low headroom micropile installation.

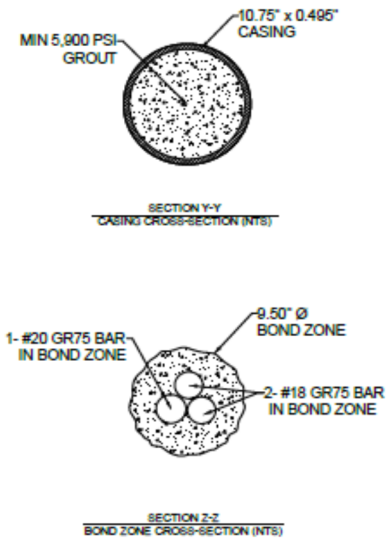


Figure 6: Typical micropile cross sections.

© 2016 Deep Foundations Institute

CHALLENGES DURING CONSTRUCTION

Placement of Micropile Core Steel

The method of placement of the 3-bar bundled "stub" core in the micropiles evolved with experience over the course of the work. The initial method of core steel placement proposed by the Contractor was to first tremie grout the full length of the micropile, then plunge (free-fall) the bundled bars unguided through the casing and into the socket. Following bar placement, a PVC probe pipe was inserted into the pile to locate the top of the bundle and confirm that the bars had reached design depth. MRCE expressed concern about the level of quality assurance of this method, and it was understood that piles with core steel not installed to the required depths must be replaced or repaired at no cost to SUCF.

After the first five micropiles were completed successfully by this method, the core bar bundle in the following three micropiles could not be verified to have reached the design depth. The "sounding" of the bundle with the PVC pipe indicated that the bundled bars were likely hung up on the rock ledge at the bottom of the casing and did not reach the socket. Although the Contractor quickly attempted to drill out the grout and re-set the bars, only the bundled bars within one of the three piles were able to be re-set to the tip of the socket. The other two piles were abandoned and replaced.

Because core steel placement and use of the PVC pipe to verify the top of the core steel proved difficult, primarily due to buoyancy in the grout and flexibility of the PVC pipe, the Contractor proposed to perform grouting of the micropiles in two "lifts," and plunging the bundled bars in between lifts to better facilitate bar placement to the tip of the socket. However, since the micropiles needed to be grouted by tremie method in order to displace the water in the hole, an interruption in tremie placement would risk creating a cold joint in the pile or could compromise grout quality by mixing with water during core steel placement.

Subsequently, the Contractor lowered the bundled bars prior to grouting using a winch line on the drill rig. The tremie pipe was taped to the bundle prior to lowering into the drilled hole, and the final top of bundle was verified with a weighted tape. This final method was implemented successfully for the majority of the remaining micropiles. Due to low headroom precluding use of the drill rig winch line within the NFTA Station entrance building, several of the larger diameter micropiles in this area were placed by the original "freefall" method with the understanding that a replacement pile would be required at the Contractor's expense if the bars did not reach the bottom of the socket. However, these bar bundles were installed successfully, most likely due to the larger diameter casing and socket.

Tieback Drilling Obstructions

As described previously, bracing of the excavation support walls at the reentrant corner around the NFTA Station entrance building required installation of two levels of overlapping tiebacks (see Figure 7 for a photo of this area). Secant pile tieback drilling encountered obstructions below the entrance building with steel fragments observed in the drill cuttings. The subway station and tunnel below Main Street were constructed in 1985 using cut and cover methods. Excavation support for subway construction consisted of a soldier pile and lagging wall with tiebacks, as confirmed during excavations at the site. It is possible that remnants of the abandoned soldier piles were encountered during tieback drilling. As a result, several of the overlapping tiebacks were offset in location or skewed horizontally to avoid these obstructions. Tieback offsets and skew angles were determined using the three-dimensional Revit model developed during the design phase of the project (see Figure 4). The Revit model was updated in real time to reflect

© 2016 Deep Foundations Institute

field conditions and provide assurance that adequate clearances between adjacent tiebacks and new micropiles were maintained.



Figure 7: View looking southwest at reentrant corner with soldier pile and lagging (left) and secant piles (right) and one level of tiebacks installed. NFTA Station entrance building is behind the SOE.

Sensitive Soils and Groundwater Control

Soils within the depth of excavation consisted of silty sands and sandy silts without cohesive binder and heavily over consolidated clays. Such fine grained soils are susceptible to softening and disturbance from construction operations particularly in the presence of water. Gravity drainage of these low permeability soils would be slow and application of vacuum to enhance gradients and accelerate drainage was expected to be beneficial. Perched groundwater was also expected at interfaces between the sands and clays that even with proper dewatering would require careful control to prevent ground loss during lagging installation. Records of prior construction indicated that the perched water table was laterally extensive and expected to produce sustained groundwater flow to excavations. Proper control of groundwater and surface water was therefore essential to safe and efficient excavation and foundation construction on undisturbed subgrade.

With groundwater perched on the clay and the regional water table below the excavation bottom providing no source of upward flow, groundwater inflow was expected to occur primarily at the excavation perimeter. The Contractor therefore elected to install vacuum wickpoints around the roughly 1200 ft site perimeter at average spacing of 9 ft. Wickpoints are a variation of conventional wellpoints with the solid PVC riser pipe and screen of a wellpoint replaced by flexible HDPE tubing and a dimpled plastic core inside a geotextile sleeve similar in construction to a wick drain used in ground improvement. The wick points were jetted through the clay layer to reach the lower regional water table. The annulus was then backfilled with filter sand to allow the perched water to drain vertically to the lower water table and the “wick” portion of the wickpoint. Unlike self-jetting wellpoints that allow for a continuous upward flow of water in the annulus to maintain hole stability during filter placement, filter placement in the wickpoint occurred through

© 2016 Deep Foundations Institute

a static water column with consequent potential for hole collapse or bridging of the filter sand and discontinuity in the filter column.

Installation of the wickpoint system began in August 2014, about three months after excavation had commenced. At this time, the site was excavated to the depth of approximately 10 feet below street grade. Wickpoints were installed in segments starting at the south end of the site, along Main Street, and at the northwest corner of the site, covering approximately 30% of the site perimeter. However, initial pumping showed that many of the wickpoints did not yield significant flows. The poor performance was attributed to the wickpoint design which required the wickpoints to penetrate through the clay layer with only a short (10 ft) length of screen at the bottom of the wickpoint. Under these conditions, the wickpoints simply functioned as widely spaced sand drains with maximum yield limited to the small annular flow through the filter column which was further reduced by the lack of a continuous sand column observed around many of the wickpoints during excavation.

Between the months of August and October 2014, piezometers along Main Street showed a drop in water level of only 6 feet. Another piezometer at the northwest corner of the site did not show any change. Fortunately, the relatively slow rate of excavation advance resulting from the large site and staged excavation and bracing installation provided the benefit of extended drainage time to deplete groundwater storage and control gradients at the site perimeter. This allowed water to gradually enter the excavation through the timber lagging where it was collected at the site perimeter using trenches and sumps and prevented from flowing across excavation subgrade. The vacuum dewatering system was never fully installed and the Contractor relied on local sumps for the remainder of the project. However, the presence and management of groundwater by sumping complicated construction. The lack of pre-drainage in advance of excavation required packing hay and filter fabric behind the lagging to prevent ground loss while allowing water entry below the perched water table. Several footings were over-excavated to remove sensitive site soils softened by groundwater infiltration. Along Washington Street, the rate of water entering the site was so great that the Contractor elected to install a row of sheet piling to cutoff water flow concentrated at the clay interface in order to complete the perimeter footings.

Brutal Winter Weather

Buffalo suffered a brutal winter in 2014-2015 with the coldest February (average temperature of only 10° F) ever on record and cumulative snowfall in excess of 110 inches. For perspective, it was twice as warm in Anchorage, Alaska in February 2015 (25 degrees on average) than Buffalo.

Protection of the sensitive soil subgrades from freezing and deterioration in this harsh weather environment proved quite a challenge. Subgrades were exposed for a minimum amount of time before sealing with a concrete mud mat and/or pouring concrete for foundations. Where subgrades were exposed overnight, frost blankets assisted by heating with glycol heat lines where necessary were placed to protect soils from freezing. All water was diverted away from and not allowed to collect in excavations. Backfill was placed around footings as soon as concrete had set.

INSTRUMENTATION AND MONITORING

An instrumentation and monitoring program was implemented to protect the Roosevelt Apartments, the NFTA entrance building and Allen Street Station and tunnel below Main Street, a water main running beneath the sidewalk along High Street, and the roadways around the site during installation of the excavation support system, site excavation and foundation construction. The program included

© 2016 Deep Foundations Institute

seismographs, tilt sensors and in-place inclinometers with automated data collection and remote monitoring, manually read crack gages, and manual optical surveys and laser scans by licensed surveyors.

Seismographs and tilt sensors were installed in both the Roosevelt Apartment building and NFTA entrance building and below grade Station to monitor vibrations and tilt, respectively. Deformation of adjacent structures and perimeter shoring was performed using laser scanning. Selected zones of structural relevance or possible deformations of the buildings were scanned using a laser scanner. Likewise, the exposed faces of the soldier piles were scanned as the excavation deepened. Each scan resulted in a point cloud which was then compared to the baseline readings and finally reduced to deformation values in the horizontal and vertical directions. Both the survey and scan data were provided to MRCE for evaluation.

A principal benefit of remote monitoring and automated data collection, made possible with wireless technology and the ever-expanding hard drive storage space, was that it enabled continuous monitoring of the instruments with minimal human interaction. All automatically collected data was uploaded to an off-site database and posted onto a centralized website to be viewed by the Contractor, Engineer and all other vested parties.

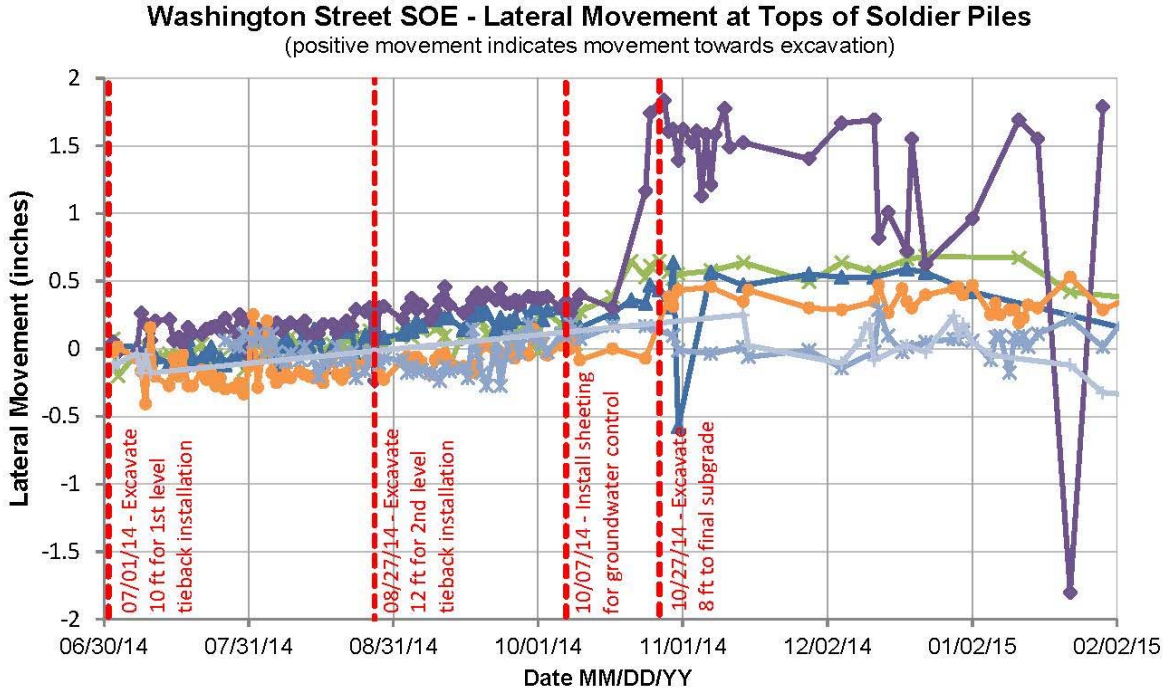


Figure 8: Plot of surveyed lateral movement with time for the tops of selected soldier piles along Washington Street, highlighting different stages during excavation.

Support of Excavation Performance

Prior to installation of the soldier and secant piles, three of the four in-place inclinometers were installed and actively monitored. The fourth inclinometer was installed next to a secant pile after the secant pile wall was installed. As excavation progressed deeper, laser scans of select soldier and secant piles were performed

© 2016 Deep Foundations Institute

on the exposed faces. Data was collected from these instruments and laser scans to continuously evaluate the performance of the excavation support system.

As the excavation progressed to the basement elevation, no significant movements were indicated by survey scans and inclinometers. However, sidewalk movement was seen on the Washington Street side of the site after the general excavation reached the final basement elevation. The laser scans of the soldier piles and surface settlement monitoring point surveys in the area also showed lateral movements of the soldier piles and settlement of the sidewalk. Upon further investigation, the movement was attributed to the installation of sheet piles near the bottom of the excavation for groundwater control. A plot of lateral soldier pile movement with time, with reference to different stages during excavation and sheeting installation is shown in Figure 8. After reviewing the data and with the concern of additional movement from removal of these sheet piles after the footing construction, the sheet piles were recommended to be left in place rather than extracted. Because the monitoring data was collected frequently, it provided significant value in determining the cause of movements and understanding movement trends such that timely modification in work plans were made to mitigate construction effects where necessary.

CONCLUSIONS

The most valuable lessons learned from excavation and foundation construction at UB-SMBS are those relating to quality assurance and the different ways a designer or inspecting engineer can be confident that quality has been maintained throughout all stages of a project. In the early design phases, a comprehensive subsurface investigation and geotechnical report provided an understanding of site conditions and directed foundation and excavation support design. Moreover, the geotechnical report was an important tool for quality assurance during construction, helping the Contractor and Design Team understand and predict groundwater issues and soil behavior. During construction, innovative ways of performing quality assurance were implemented, including three-dimensional modeling of tieback interferences and automated performance monitoring of SOE, to minimize the cost and time of performing remedial measures without compromising structural integrity. A thorough and continuously active monitoring program assured that potential movement trends of the excavation support would be identified, investigated, and remediated at their early stages. These different aspects of quality assurance were achieved with frequent and collaborative communication between the Design Team, Inspecting Engineers, and Contractors.

© 2016 Deep Foundations Institute

This page left intentionally blank

© 2016 Deep Foundations Institute

USE OF APG PILES FOR SUPPORT OF NEW HOSPITAL REPLACEMENT WING IN A SITE SUSCEPTIBLE TO EXCESSIVE GROUND SETTLEMENT VENTURA, CALIFORNIA

Justin Ray, PE; jray@langan.com; (510) 874-7058
Maria Flessas, PE, GE; mflessas@langan.com; (415) 955-5257
Langan Treadwell Rollo, San Francisco, California, USA

Danielle Steinmetz, PE; ds@berkelwc.com
Brian Zuckerman, PE; bz@berkelwc.com
Berkel & Company Contractors, Inc., San Francisco, California, USA

ABSTRACT

The Ventura County Medical Center Hospital Replacement Wing project consists of the construction of a 2- to 3-story building with a basement encompassing the entire footprint and two corridors connecting the new hospital wing to existing buildings. The site is located in the Ventura Basin where strong ground shaking has been observed during moderate to large earthquakes on nearby faults. The upper 90 feet of the soil consists of loose to medium dense fine-grained sands and low plasticity silts that are potentially susceptible to liquefaction, seismic densification, and hydroconsolidation. Ground settlement associated with a large seismic event on a nearby fault is estimated at 20 to 26 inches. To account for the anticipated ground settlement, auger pressure grouted (APG) piles gaining support below the potentially liquefiable soil were selected for the support of the proposed structure. Challenges for pile design included the anticipated earthquake-induced ground settlement, high downdrag loads, low soil lateral capacity during strong ground shaking, and the effect of pile installation on the performance of the existing adjacent buildings and the installed shoring system. The replacement hospital is supported on over 600 APG piles, with lengths varying between 120 and 140 feet. Axial pile capacities were verified with an extensive indicator pile installation program and dynamic pile load testing.

Keywords: liquefaction, augercast, APG, deep foundation

INTRODUCTION

The Hospital Replacement Wing (HRW) project is at the Ventura County Medical Center (VCMC) in Ventura County, Southern California (Figure 1). The VCMC consists of three interconnected hospital buildings (Buildings 303, 304, and Fainer Building), the Medical Laboratory/Cafeteria Building, two mental health buildings, a medical office building, an emergency generator building, and surface parking lots. The HRW is near the center of the campus, adjacent to several existing buildings.

The HRW is a 2- to 3-story structure, with a 15- to 20-foot-deep basement beneath the entire 95,000-square-foot building footprint. The HRW project includes a Loading Dock, a four-level corridor to the Fainer Building (Fainer connector), and a two-level corridor to the Medical Laboratory/Cafeteria Building (Café connector). The corridors are structurally separated from the existing buildings. Typical dead plus live load column loads for the HRW range from about 635 kips to 935 kips and total loads range from about 860 kips to 1,295 kips.

© 2016 Deep Foundations Institute

Excavation for the basement was performed prior to foundation installation. The excavation for the basement and adjacent improvements were retained using a soldier-pile-and-lagging system with tiebacks. The implemented survey monitoring system consisted of over 200 survey points on top of solider beams, on existing buildings, and on control points away from the excavation. Because of the proximity of the excavation to existing improvements and the depth of the excavation, weekly survey readings were performed as excavation began. Survey readings were processed and compared to the baseline readings taken prior to excavation.



Figure 1: Site Location Map

GEOLOGIC SETTING AND SUBSURFACE CONDITIONS

The VCMC is in the Ventura Basin, south of the southern flank of the Ventura Hills within the Transverse Range geomorphic province. The province is characterized by the east-west trending Transverse ranges that include mountain ranges extending from Point Conception at the western tip of Santa Barbara County to the east end of the San Jacinto Mountains in Western Riverside County.

The Ventura Basin is structurally controlled by reverse faults including the Red Mountain and San Cayetano faults to the north, and the Oak Ridge fault to the south. The Ventura fault zone transects the basin with an east-west trend, on the southern side of the Ventura Hills.

Subsurface conditions are generally uniform beneath the hospital site. The HRW building site is underlain by alluvial deposits consisting of interbedded layers of silty sand, sandy silt, and sandy clay, with lenses of gravel. The sand and clay in the upper 90 feet is generally loose to medium dense and soft to stiff, respectively. Below a depth of 90 feet (Elevation 69 feet, NGVD1929 datum), stiff to hard clay interbedded with lenses of medium dense to very dense sand is present. The high groundwater level at the project site is near a depth of about 35 feet below the existing ground surface (bgs), corresponding to Elevation 125 feet.

A summary of subsurface conditions (five alluvial units) beneath the HRW site is presented in Table 1 along with typical energy-corrected SPT blow counts (N_{60}).

© 2016 Deep Foundations Institute

Table 1: Summary of Subsurface Conditions beneath HRW

Unit Designation	Unit Classification	Typical N_{60} (blows/ft)	Approximate Elevation Range (feet)
Upper Coarse- Grained and Non- Plastic Fine-Grained Unit	SM to ML	4 to 15	Ground Surface to El. 127
Upper Low Plasticity Fine-Grained Unit	ML to CL	2 to 10	El. 127 to 110
Interbedded Coarse- Grained and Non-Plastic Fine-Grained Unit	SM to ML with thin interbedded layers of CL	5 to 30	El. 110 to 69
Lower Low Plasticity Fine-Grained Unit	CL to ML	20 to 50	El. 69 to 38
Interbedded Low Plasticity Fine-Grained and Coarse-Grained/Non-Plastic Fine-Grained Unit	CL with interbedded layers of SM and ML	35 to 100	Below El. 38

GEOLOGIC AND SEISMIC HAZARDS

During its history, the site has been subjected to strong to very strong ground shaking from moderate to large earthquakes on the Ventura-Pitas Point, Oak Ridge, Simi-Santa Rosa, and Red Mountain Faults, and future strong ground shaking should be expected. Strong shaking during an earthquake can result in ground failure such as that associated with soil liquefaction and seismic densification. In addition, hydroconsolidation has historically affected the project site.

Liquefaction

When a soil liquefies during an earthquake, it experiences a significant temporary loss of strength. Flow failure, lateral spreading, differential settlement, loss of bearing, ground fissures, and sand boils are evidence of excess pore pressure generation and liquefaction. The HRW project site is within a designated liquefaction hazard zone as indicated by the California Geological Survey (CGS) on the map titled *State of California Seismic Hazard Zones, Ventura and Saticoy Quadrangle, Official Map*, dated 14 February 2003.

The results of the available subsurface information were used to evaluate liquefaction potential at the project site. Empirical liquefaction analysis procedures described in Youd et al. (2001) were used in analysis. The evaluation was based on a Moment Magnitude, M_w=7.3 earthquake and a peak ground acceleration of 0.47g (corresponding to the Design Earthquake ground motion). The results of the analyses indicate the presence of potentially liquefiable soil layers within the saturated portion of the Upper Low-Plasticity Fine-Grained Unit (Elevation 110 to 125 feet) and within the Interbedded Coarse-Grained and Non-Plastic Fine-Grained Unit (Elevation 69 to 110 feet). The results of liquefaction analyses indicate up to 12 to 15 inches of total liquefaction settlement could occur during strong shaking on a nearby active fault.

Seismic Densification

Seismic densification (also referred to as cyclic densification and differential compaction) can occur during strong ground shaking in loose, granular deposits above the water table, resulting in ground surface settlement. Loose to medium dense silty sand above the design groundwater level was encountered in the exploration points performed at the site. Seismic settlement of unsaturated soil at the project site may be on the order of ½ to 5 inches during a major earthquake on a nearby active fault.

© 2016 Deep Foundations Institute

Collapsible Soil (Hydroconsolidation)

Soil collapse is the densification of sediments resulting from significant increases in their moisture content. This process typically results from moisture infiltration into the subsurface caused by poor surface drainage, irrigation water, or leaking pipes. This phenomenon is more prevalent in low-density, silty, sandy soil deposited in semi-arid and arid climates where the soil has not been subjected to saturation. Previous geotechnical studies for the VCMC campus and other sites in the Ventura area document hydroconsolidation potential for the primarily fine-grained silty soil on the order of six inches or more. Structural damage was observed east of the HRW site related to up to seven inches of hydroconsolidation of the near-surface soil (upper 35 feet of soil) above the groundwater level.

Summary of Potential Geohazard-related Settlements

If liquefaction, seismic deformation, and hydroconsolidation occur simultaneously due to strong ground shaking, the cumulative settlement may be on the order of 20 to 26 inches; however, the potential for settlements from seismic shaking (liquefaction and seismic densification) to occur in combination with hydroconsolidation settlement is unlikely to occur. For example, if one of the phenomena occurs, the volume change will make it less likely for the other phenomena to occur. A design earthquake-induced settlement of up to 20 inches was used for the design of the HRW project and its associated improvements.

FOUNDATION SYSTEM

Large-diameter drilled shafts gaining support below the liquefiable soil and a shallow foundation system with soil improvement consisting of cement deep soil mixing (CDSM) were evaluated in previous reports for the support of the new hospital. Large-diameter drilled shafts (6 to 8 feet in diameter) extending through the potentially liquefiable soil would require the use of drilling fluid (and likely casing) to stabilize the drilled shaft during the entire drilling operation. Large-diameter drilled shafts were not a viable economic solution because they would need to be 140 to 150 feet long in order to support the anticipated building loads and high downdrag loads. A shallow foundation system with CDSM extending through the potentially liquefiable soil was also evaluated. CDSM, defined as soil blended with cementitious materials injected through hollow, rotated mixing shafts with some type of cutting tool, creates vertical shafts of improved soil. For the support of the proposed hospital, 100 percent soil replacement was required. The CDSM would extend about 75 feet below the existing ground surface. Remaining liquefaction settlement of the soil below the improvement depth was estimated at 4 to 5 inches. In addition to having to account for the remaining settlement, this foundation system was also very costly.

To mitigate the anticipated ground settlement, it was recommended that the HRW structure, including the basement slabs, be supported on auger pressure grouted (APG) piles gaining support in the competent clay and sand below Elevation 69 feet. The APG pile foundation system was selected for the support of the hospital structure for its cost effectiveness, short installation schedule, and limited impact on site constraints.

APG piles are generally constructed following these four essential steps: 1) A hollow-stem auger with a diameter equivalent to that of the pile being constructed is advanced into the ground to the desired pile tip elevation; 2) once the desired pile tip elevation is reached, injection of fluid grout into the base of the pile is initiated by pumping of grout down the hollow stem of the auger and out through a grout port located near the tip of the auger; 3) following placement of an initial volume of grout at the base of the pile, or once a the target initial grouting pressure is reached, withdrawal of the auger is initiated, and the rate of auger withdrawal is coordinated with the rate of grout injection by means of automated installation monitoring equipment such that the volume of grout pumped in each successive increment of pile length meets or exceeds the target value throughout the pile grouting process; 4) once the grout column is fully formed and the auger removed, the grout level in the pile is raised or lowered relative to the working grade either by placing and filling a column former at the top of the pile or by removing fluid grout from the hole to reach the design pile cutoff elevation. Reinforcing steel is then placed within the fluid grout column utilizing special centralizers to maintain proper positioning and necessary clearance from the pile wall. A photo of the auger drill tip used for the project is shown on Figure 2.

© 2016 Deep Foundations Institute



Figure 2: Hollow stem auger drill tip with grout port

The design axial compressive capacities for 18-inch-diameter APG piles are presented in Table 3. The capacities were developed for a single pile, extending 60 feet below the bottom of the potentially liquefiable soil (below Elevation 69 feet), for a pile tip near Elevation 9 feet. The required pile capacity takes into account downdrag loads from the anticipated earthquake-induced ground settlement (up to 20 inches). Downdrag is the additional load transferred to the pile when the soil surrounding the pile settles and will impose negative (downward) frictional stresses on the pile. Downdrag loads were determined assuming a downdrag force equal to the frictional resistance resulting from downward soil movement relative to the pile above Elevation 69 feet.

Table 2: Axial Compressive Capacities: Single, 18-inch-Diameter, APG Pile

Building Area	Pile Cutoff Elevation (feet)	Maximum Design Building Load per Pile (DL+LL) (kips)	Downdrag Load (kips)	Required Pile Capacity (kips)
HRW	134.0	250	300	800
Loading Dock	142.0	150	410	710
Café Connector	151.5	100	550	750

Uplift resistance was calculated using an allowable frictional resistance of 500 pounds per square foot (psf). Per California Building Code 2010 (CBC) Section 1810A.3.3.1.4, if a maximum value of 500 psf is used to determine the uplift capacity of the piles, uplift load testing is not required. Because uplift would not control the design of the piles, the maximum code value of 500 psf was used for pile design, and uplift pile testing was not performed.

To design for lateral loading, lateral resistance from piles, pile caps, and grade beams was utilized. A series of lateral analyses for various axial loads on piles were performed. The stiffness for each pile reinforcing type was computed at various levels of axial loading and analyzed for various imposed deflections in the software program LPILE, considering fixed-head behavior and using soil parameters based on the geotechnical investigation. Rebar cages were required to

© 2016 Deep Foundations Institute

extend about 10 feet below the layer susceptible to liquefaction. The passive resistance on the vertical face of the pile caps and grade beams was computed in the direction of loading. The passive resistance of the perimeter grade beams was calculated using the length of each section of the perimeter wall and an average value for ground surface elevation along the applicable length. In the computation of passive pressure, it was assumed that no lateral resistance will be developed in the upper 20 inches of the pile cap due to the potential for seismic-induced settlement.

PILE LOAD TESTING PROGRAM

To confirm the values used in design, a load testing program was performed prior to beginning production. Test piles were installed with the same equipment and methodology used to install production piles. The load test program consisted of testing ten piles installed two weeks prior to testing. Test piles were tested in compression per ASTM D4945 Standard Test Method for High-Strain Dynamic Testing of Deep Foundations, which requires impacting the pile top with a substantial ram mass so that the pile undergoes a small permanent set. Dynamic load testing was selected to help provide a load distribution over the length of the pile as a way of differentiating the support above and below Elevation 69 feet. It was important to select a hammer large enough to induce settlement of the pile under the largest drops. The impact hammer selected for this project was a 16-ton, two-ram, drop-hammer. During the dynamic test, high strain dynamic pile measurements were collected and processed with a Pile Driving Analyzer (PDA) for ram drop heights ranging from 36 inches to 78 inches.

The results of the testing program included evaluation of the soil resistance along the pile activated at the time of testing. To evaluate bearing capacity and assess shaft resistance development, the Case Pile Wave Analysis Program (CAPWAP) method was used. CAPWAP analysis was performed for each test pile at a selected hammer blow (either 72-inch drop or 78-inch drop). The blows used in the analysis were selected based on data quality, pile integrity, and energy transfer. The results of the CAPWAP provided the skin friction distribution along the pile shaft and measured displacement under the transferred energy. The results of the CAPWAP are summarized in Figure 3 below. The measured permanent displacement under the transferred energy was between 0.25 and 0.35 inches.

© 2016 Deep Foundations Institute

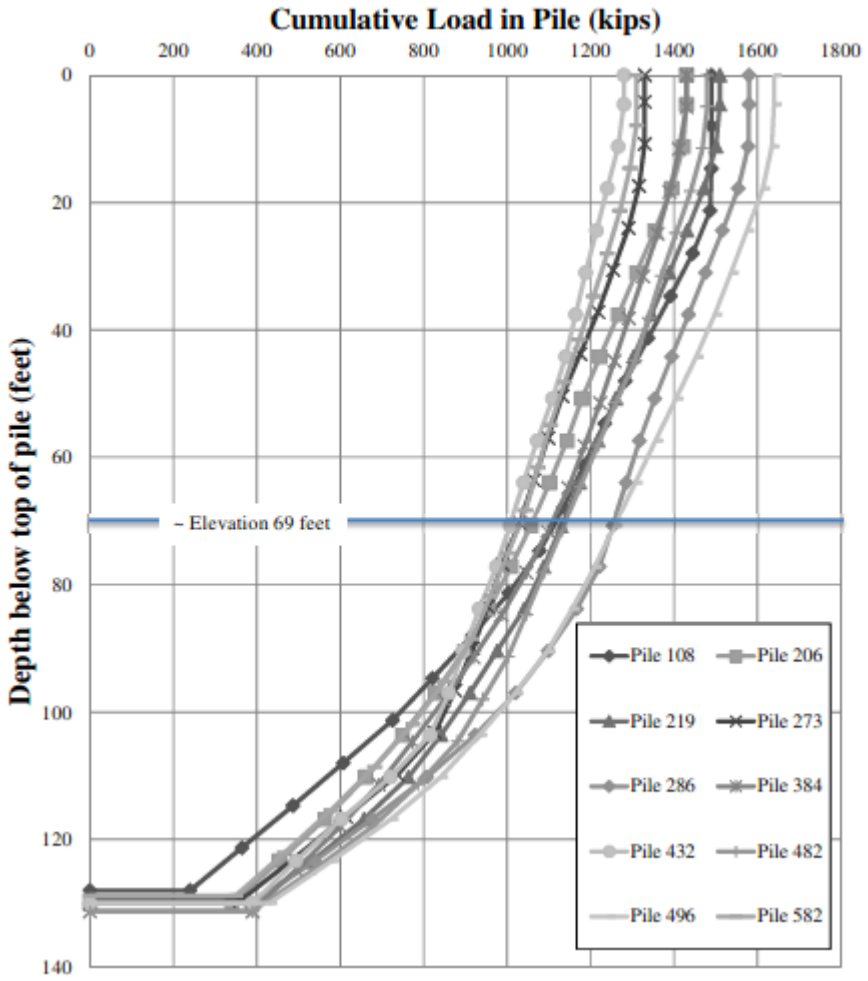


Figure 3: Results of CAPWAP on Test Piles

The average skin friction for the test piles above Elevation 69 feet was about 1,000 psf; the average skin friction below Elevation 69 feet was about 2,650 psf. End bearing in the test piles ranged from about 240 to 430 kips, with an average of about 350 kips. All tests were well above the design values presented in Table 2.

PRODUCTION PILE PROGRAM

Although the main requirement was to reach the design tip elevation, torque and rotation rates were recorded as the auger was advanced and grout flow, pressure, and field grout factor (actual grout pumped / theoretical grout required) were recorded as the auger was retracted and grout was pumped. The recorded parameters were used as a way of comparing the production pile soil conditions to those of the test piles. The foundation contractor created real-time quality control and quality assurance monitoring with their automated data acquisition system. This system allowed the drill rig operators and field engineers to observe the entire pile installation process and address any observable issues with installation. As expected from the subsurface investigation performed prior to construction, the observed subsurface conditions were relatively uniform across the site.

© 2016 Deep Foundations Institute

During production, one specific difference between the test piles and the production piles was observed. In about 10 percent of the production piles, appreciable grout settlement was observed (up to eight feet in some of the piles). Where grout settlement occurred, the pile was re-grouted to the cutoff elevation. The areas where grout settlement was observed were erratic and did not align with any of the recorded parameters. To confirm the capacity of the piles with significant grout settlement, the project team recommended three additional load tests be performed on piles with grout settlement. The additional dynamic tests were performed consistent with the methods in the previous section. The test results, shown in Figure 4, indicate the ultimate capacity of the tested piles is similar to the capacity of the other tested piles; in addition, all tests exceed the required pile capacity. Based on the load test results the project team did not recommend a reduction in axial capacity for the piles with grout settlement, provided they were re-grouted to the cutoff elevation. In total, 604 APG piles were installed for support of the HRW building and associated improvements.

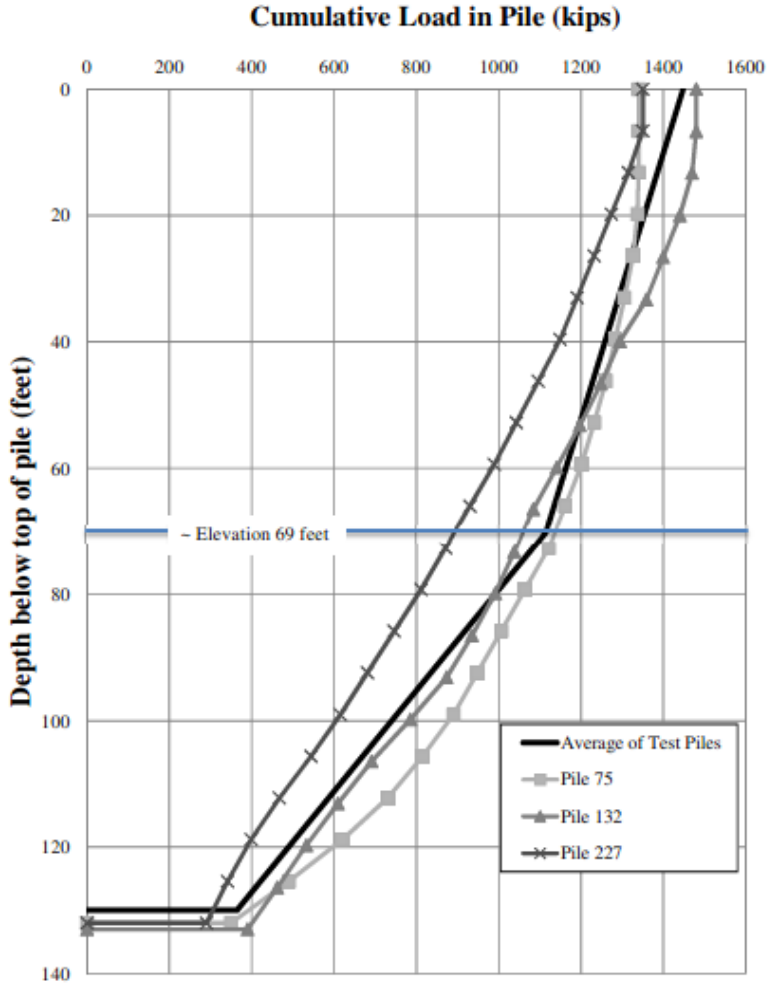


Figure 4: Results of CAPWAP on piles where grout settlement was observed

OBSERVATION AND MITIGATION OF MOVEMENT OF SHORING

The production pile program included installation of piles and pile caps adjacent to a shoring wall directly bordering an existing hospital building. The building directly south of the HRW excavation was supported on pre-cast 12-inch-sqaure concrete piles extending about 37 feet below the existing ground surface (about 5 feet below the bottom of the shoring piles and 108 feet above the bottom of the HRW piles). New APG piles were installed about 3 feet from the face of the shoring and 8 feet from the existing concrete piles.

© 2016 Deep Foundations Institute

During the installation of production piles, lateral and vertical movements of the shoring and existing building adjacent to APG piles were observed. The immediate action, as decided by the project team, was to cease pile installation operations adjacent to the wall and to increase survey monitoring to daily measurements. Additional survey monitoring points were also installed at the face of the building opposite the excavation and at the mid-point of the shoring wall where movement was observed. The structural engineer also conducted weekly site visits to observe the condition of the existing building. No significant damage of the adjacent building was observed.

The foundation contractor's original plan for pile installation adjacent to the shoring walls included installing one APG pile per pile cap per day. Over the course of a week, all the piles in adjacent 3-pile and 4-pile pile caps were installed. Survey readings were taken on Monday and Friday. Lateral movements of the shoring wall were on the order of ¼ to ½ inch during the period of installation. Vertical movements were on the order of ¾ inch during the period of installation. Lateral and vertical movements of the adjacent building were on the order of ¼ to ½ inch during the period of installation. Figure 5 shows an example of the recorded vertical movement of the shoring piles where APG pile installation occurred. The period of APG installation adjacent to the shoring piles occurred between the first two recorded points shown on the graph.

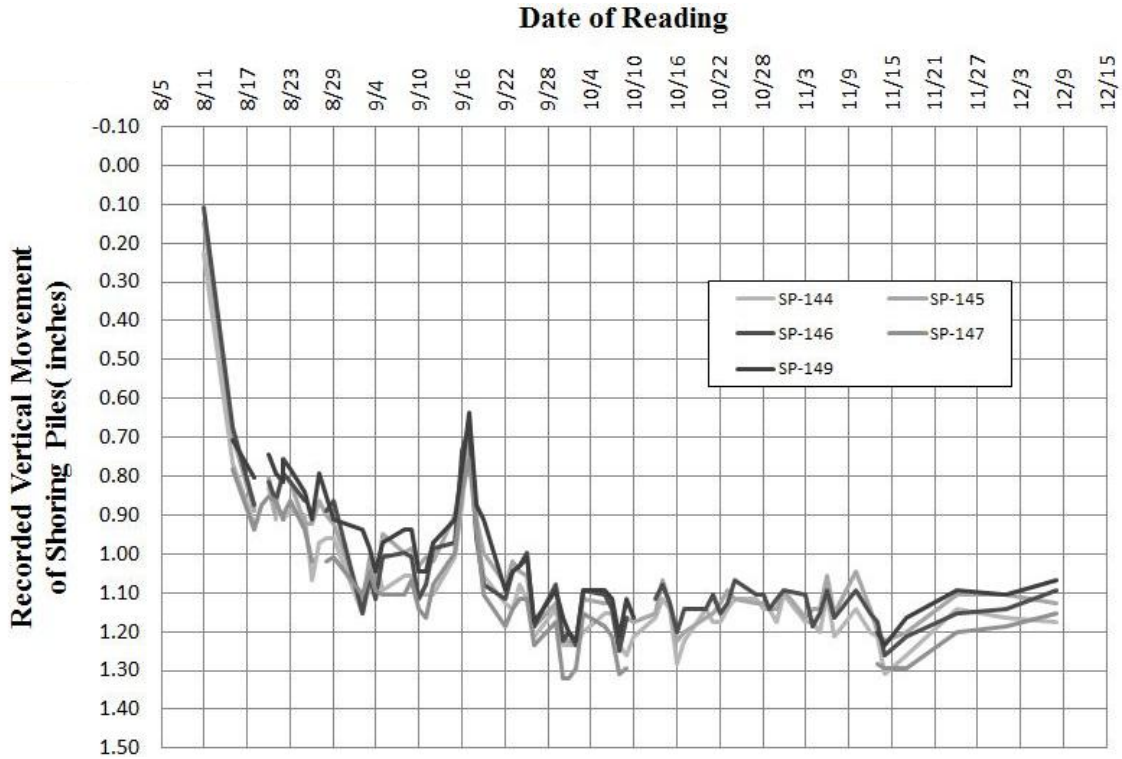


Figure 5: Recorded vertical movement of shoring piles during APG installation

After collecting and reviewing additional survey monitoring, the project team decided that it was acceptable to continue with installation. Survey readings indicated that although there was some additional creep of the shoring, movement had begun to stabilize from the movement that occurred during the initial pile installation.

The foundation contractor and the construction team proceeded with caution when pile installation continued adjacent to the shoring walls. As installation continued, the foundation contractor elected to install one APG pile per pile cap per day in alternating pile caps along the wall. Survey monitoring continued to be performed and reviewed daily. In addition, the project team set limits for lateral and vertical movement where additional actions would need to be performed. The structural engineer also continued weekly site visits to observe the condition of the existing building adjacent to the shoring.

© 2016 Deep Foundations Institute

Ultimately, the revised installation plan was successful. Daily survey monitoring continued in areas where APG piles were being installed. While some movement was still observed adjacent to where piles were being installed, the plan of staggering installation to every other pile cap kept movements within a more manageable range and damage was not observed in any of the adjacent buildings.

SUMMARY AND CONCLUSIONS

The development of a site susceptible to excessive ground settlement proved to be a unique challenge. The HRW site was especially unique because of the potential for both static settlements from hydroconsolidation and deep seismic-induced settlement. Ultimately, an earthquake-induced settlement of up to 20 inches was used for the design of the HRW project and its associated improvements

After the consideration of several deep foundation systems, APG piles provided an efficient and constructible solution for the difficult site. In addition, the use of dynamic pile load testing allowed the project team to develop skin friction profiles along the pile. Dynamic pile load testing was critical to determining the capacities above and below the bottom of the potentially liquefiable layer, allowing the team to differentiate load capacity from resistance that would contribute to downdrag (above Elevation 69 feet) and resistance that could be relied on (below Elevation 69 feet). An important aspect of the testing was making sure to conduct the test with a large enough hammer to induce settlement of the pile under the largest drops. On previous projects, the full capacity of piles during dynamic testing has not been achieved because the energy being transferred to the pile was not enough to utilize all of the potential resistance.

During construction, unexpected problems with horizontal and vertical movement of the shoring occurred as the result of APG pile installation. Because of the attentiveness of the project team, the issue was recognized quickly and dealt with before damage to adjacent improvements occurred. It is important to note that non-displacement pile installation adjacent to shoring and improvements can potentially induce settlement. With proper planning and monitoring, the issue was kept in a manageable range of movement and without damage. By staggering pile installation, the project team was able to keep movement within a tolerable range with minimal delay to the project.

Innovative design practices and attentive problem solving allowed the HRW project to be successful. During design and construction, constant communication was kept between the project team. This allowed for considerable attention to detail as issues arose and timely solutions.

ACKNOWLEDGMENTS

Ventura County Public Works Agency
Clark Construction Group
Langan Treadwell Rollo
Berkel & Company Contractors, Inc.
Simpson Gumpertz & Heger
GRL Engineers, Inc.

REFERENCES

California Geological Survey, 2003. State of California Seismic Hazard Zones, Ventura 7½-Minute Quadrangle, Official Map, 2 July 2003.

Fugro Consultants, Inc., 2011. “Geotechnical Site Characterization Study, Replacement Hospital Wing, Ventura County Medical Center, Ventura, California, Volume I”, 14 September 2011.

Fugro Consultants, Inc., 2011. “Foundation Evaluation, Shallow Foundations and Cement Deep Soil Mixing, Replacement Hospital Wing, Ventura County Medical Center, Ventura, California, Volume II”, 19 September 2011.

GRL Engineers, Inc., 2014. “Dynamic Pile Measurements, VCMC HRW, Ventura CA”, 5 August 2014.

Treadwell & Rollo, A Langan Company, 2013. “Geologic Hazard Evaluation and Geotechnical Investigation, Hospital Replacement Wing, Ventura County Medical Center, Ventura, California, 8 April 2013.

© 2016 Deep Foundations Institute

BORED PILE CONSTRUCTION CHALLENGES IN HIGHLY VARIABLE LIMESTONE FOR A SUPERTALL BUILDING

Seth K. Martin, Langan Engineering, Environmental, Survey and Landscape Architecture, D.P.C., New York, NY, USA, 212-479-5541, smartin@langan.com

Alan R. Poeppel, Langan Engineering, Environmental, Survey and Landscape Architecture, D.P.C., New York, NY, USA, 212-479-5405, apoeppel@langan.com

Konstantinos Syngros, Langan Engineering, Environmental, Survey and Landscape Architecture, D.P.C., New York, NY, USA, 212-479-5459, ksyngros@langan.com

Tony Nichlany, Langan Engineering, Environmental, Survey and Landscape Architecture, D.P.C., New York, NY, USA, 305-546-6605, tnichlany@langan.com

Keywords: bored pile, drilled shaft, Kenny Hill, karst, limestone, Osterberg cell

ABSTRACT

This paper presents a case study on bored pile construction in challenging karst conditions below a supertall building in Kuala Lumpur. Innovative design and construction techniques helped keep the project moving through very difficult and unpredictable geological and drilling conditions. The development encompasses about 12,400 square meters and includes a 77-story tower, a 59-story tower, a five-story podium, and four contiguous basement levels. The site is underlain by a residual soil derived from a siltstone/claystone (the Kenny Hill formation), then limestone bedrock. Subsurface conditions are relatively uniform within the Kenny Hill and highly variable at the limestone surface. Extreme cases included 40-meter-tall underground caverns, 40-meter-tall pinnacles, and a 50-meter-tall underground rock ledge. Local piling practice in Kuala Lumpur involves deriving pile capacity entirely in the Kenny Hill formation to avoid the unpredictable limestone surface. However, the massive tower foundation loads and relatively shallow bedrock required the piles to be socketed in the limestone. The 77-story tower will be supported by 2.0- and 2.2-meter-diameter bored piles 50 to 100+ meters long, socketed in limestone, with working loads between 40 and 70 Meganewtons. Two Osterberg-cell load tests were used to develop a site-specific rock socket skin friction correlation with RQD. Exploratory rock probes were drilled at each pile location to design the rock socket length based on the rock quality and sloping rock conditions. The rock mass was pressure-grouted during each rock probe to improve the rock quality and fill voids in the rock.

INTRODUCTION

The Kuala Lumpur City Centre, home of the Petronas Towers and the world's deepest foundations, will be the future home of a new supertall tower. The 77-story tower will be supported by a piled-raft foundation that relies on piles terminating in the highly erratic, karstic Kuala Lumpur limestone formation. The high building loads coupled with relatively shallow limestone across the majority of the tower footprint forced the piles to extend into the limestone.

The unpredictable and very hard Kuala Lumpur limestone caused significant project delays despite extensive design- and construction-phase subsurface investigations. Even greater delays were avoided by by implementing a pre-construction pressure-grouting program in the rock mass. Exploratory rock probes (i.e. proof-drilling) were drilled at each pile location to 25 meters into bedrock to assist the piling contractor and the design engineer in finalizing pile length requirements. The initial pile design was

© 2016 Deep Foundations Institute

adjusted using the proof-drilling results and then finalized during pile construction. The rock variability was such that the results of the proof-drilling were found to be unreliable in several cases.

This paper focuses on the project's success made possible by: the owner's willingness to perform extensive subsurface investigations during design and construction, finite element analysis of the variable conditions, thorough quality control and assurance measures, and most importantly communication between the designer and the contractor during construction.

PROJECT DESCRIPTION

The project site is comprised of two lots encompassing a total footprint of about 12,400 square meters. Two towers will be located within a seamless five-level podium and five below-grade levels. The subject 77-story tower weighs about 3,800 meganewtons (about 15 percent more than Manhattan's Empire State Building) and occupies a footprint of about 3,500 square meters.

The site is less than 500 meters from the Petronas Twin Towers, which are supported by a similar foundation system consisting of rectangular barrette piles extending down about 60 to 130 meters below grade and into the same limestone formation (Drumright et al., 1998). The site plan is presented as Fig. 1 below.

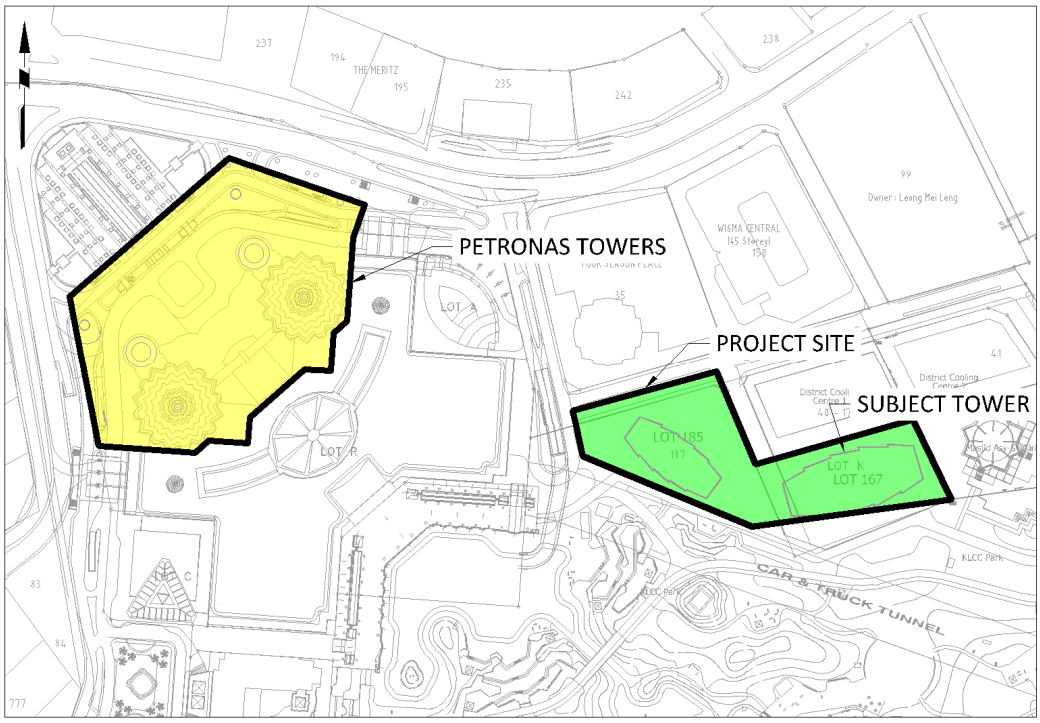


Fig. 1 – Site Plan

SUBSURFACE INVESTIGATION

The subsurface investigation for tall towers in this region requires multiple phases and extensive field and laboratory testing considering the variable conditions and the scope of the project.

The design-phase borings were performed in two phases, totaling 40 borings, drilled about 50 to 150 meters below grade, and 25 standpipe piezometers. The third phase of the subsurface investigation was

© 2016 Deep Foundations Institute

performed during construction and consisted of proof-drilling and pressure-grouting each of the 108 pile locations during construction alongside the piling activities. Details of the proof-drilling and grouting program are included in a subsequent section. Intact rock core samples were subject to unconfined compressive strength testing with Young's modulus measurements.

SUBSURFACE CONDITIONS

The Phase 1 borings indicated that the rock surface was relatively level at about 50 to 75 meters below grade within the tower footprint. One boring from the initial investigation suggested an area of shallow rock rising up to about 30 meters below grade. The Phase 2 borings were more focused to the limits of the tower and helped define the limits of the shallow rock as well as an area of deep rock 95 meters below grade. Rock quality was also highly variable with rock quality designations between 0 and 100 percent. Rock cavities, pinnacles and ledges were encountered in both phases of the investigation. Table 1 presents a summary of our representative soil and rock index parameters. A generalized subsurface profile based on the design-phase borings is presented as Fig. 2 below.

Table 1. Soil and Rock Engineering Design Parameters

Parameter	Surficial Soils	Kenny Hill	Limestone
Unit Weight (kN/m^3)	18.9	18.1	26.5
Drained Friction Angle (deg.)	29	31	n/a
Poisson's Ratio	0.17	0.17	0.16
Unconfined Compressive Strength (MPa)	n/a	n/a	90
Modulus of Deformation (MPa)	35	90	14,000

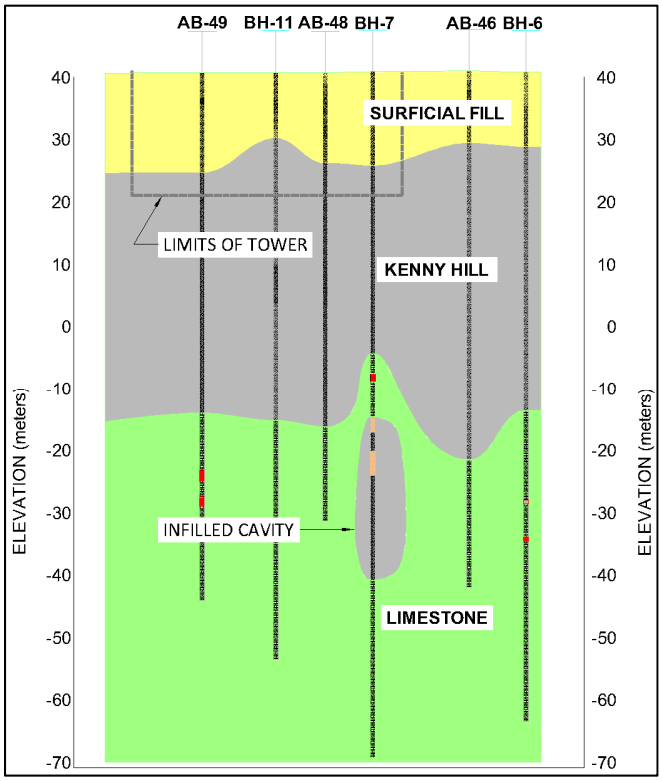


Fig. 2 – Subsurface Profile through Tower

© 2016 Deep Foundations Institute

Slump Zones and Cavities

Deep zones of loose/soft Kenny Hill residual soil, locally referred to as slump zones, were encountered in four borings near the limestone surface. Slump zones are defined as zones of soil with SPT N-values less than 10 blows per 30 centimeter (cm). Slump zones were encountered between about 50 and 80 meters below grade and ranged between about 2 and 10 meters thick.

Rock cavities 0.5 to 1.5 meters thick were encountered in four design-phase borings between about 50 and 100 meters below grade. Infilled cavities up to 40 meters thick were encountered at 35 proof-drilling locations. The average infilled cavity thickness encountered during proof-drilling was about 6 meters thick. About one-third of the design- and construction-phase borings encountered cavities in the limestone.

FOUNDATION DESIGN

The tower will be supported by a 4-meter-thick reinforced concrete mat over a field of 108 2.0- and 2.2-meter-diameter reinforced concrete bored piles. The bored piles supporting the 77-story tower are socketed into the limestone to satisfy both overall foundation capacity and limit tower settlement.

Geotechnical Pile Capacity

The pile socket lengths were proportioned assuming the load was transferred through skin friction in rock and bearing at the pile toe. The pile capacities were developed based on published correlations and empirical values used frequently in the region. The ultimate skin friction ($f_{s,ult}$) in the limestone was initially estimated based on the following empirical correlation developed by William and Pells (1981):

$$f_{s,ult} = \alpha \times \beta \times q_u \quad [1]$$

Where α = rock reduction factor (taken as 0.06), β = joint reduction factor (taken as 0.45), and q_u = uniaxial compressive strength (taken as 60 MPa).

The equation above yields an ultimate skin friction of about 1.6 MPa, or an allowable skin friction of about 640 kPa using a typical factor of safety of 2.5. This allowable skin friction is consistent with an empirical correlation by Neoh (1998), which recommends an allowable skin friction of 600 kPa for Malaysian limestone with a rock quality designation (RQD) between 25 and 70 percent.

The bearing capacity at the pile toe was calculated based on a unit base resistance of 1.5 MPa, about 1 to 4 percent of the unconfined compressive strength of intact rock. The end-bearing resistance of 1.5 MPa was adopted based on the load test results, which showed the mobilized end-bearing resistance was relatively low at the working skin friction loads.

Load Test Program

The rock socket friction and base resistance were verified through full-scale load tests on two production piles, CP2-1 and CP2-2 using Osterberg-cells (O-cells). Each test was performed using two levels of O-Cells within the rock socket. The O-Cells delivered a maximum load ranging between about 46 and 75 MN to the pile, mobilizing an average unit skin friction between 580 (CP2-2) and 1,560 kPa (CP2-1) and an end-bearing resistance of approximately 8 MPa in both load tests. The lower bound mobilized skin friction values were the result of poor construction practices as described below. Fig. 3 presents the mobilized unit skin friction versus deflection in the rock socket.

© 2016 Deep Foundations Institute

At test pile CP2-2, about 4 meters of the rock socket was backfilled with cohesive drill cuttings after loss of polymer slurry occurred during drilling within the rock mass. The cohesive drill cuttings appeared to reduce the skin friction in the rock socket. The average mobilized skin friction in this portion of the socket was about 450 kPa where the average RQD was about 54 percent.

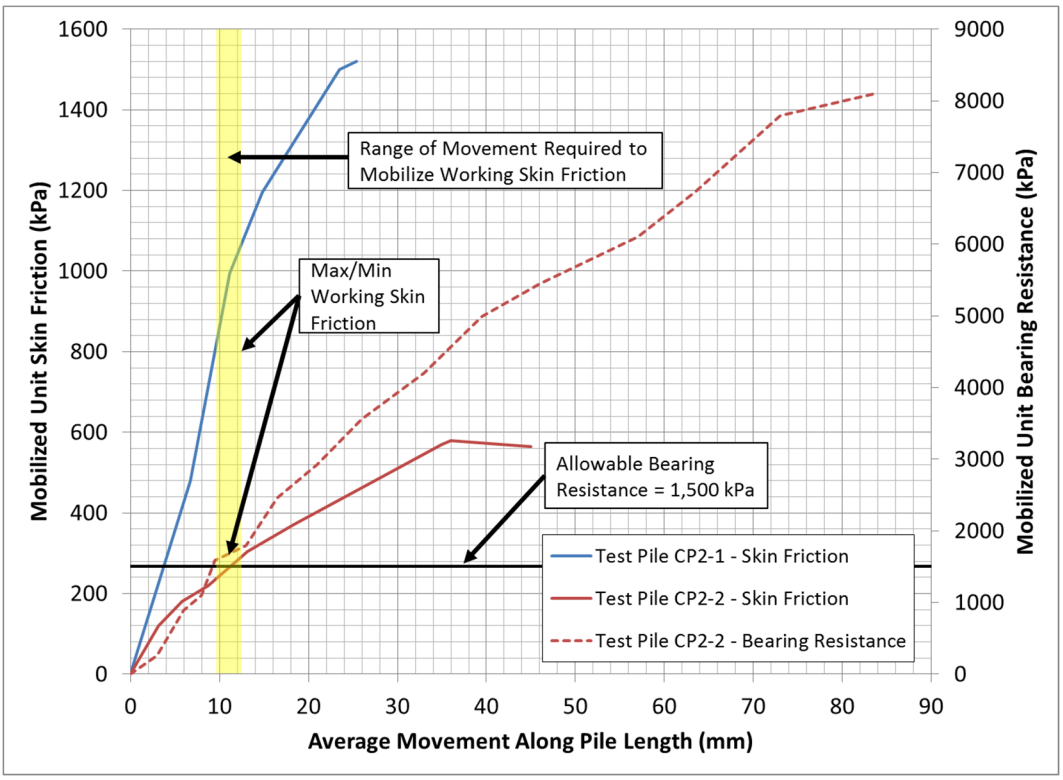


Fig. 3 – Unit Skin Friction in Rock vs. Pile Deflection

Unit Skin Friction vs. RQD

The results of the load tests and proof-drilling were used to confirm the use of published correlations between RQD and unit skin friction by Neoh (1998) and Tan (2009) and make site-specific adjustments to the relationships. Each test pile was proof-drilled providing a rock quality profile along the center of the pile's socket length, which was then correlated with the mobilized skin friction within the rock. The rock mass at both test piles was pressure-grouted in the same manner as the production piles. A comparison of the load test results, the site-specific correlation adopted for the pile design and published correlations is presented in Fig. 4 below.

© 2016 Deep Foundations Institute

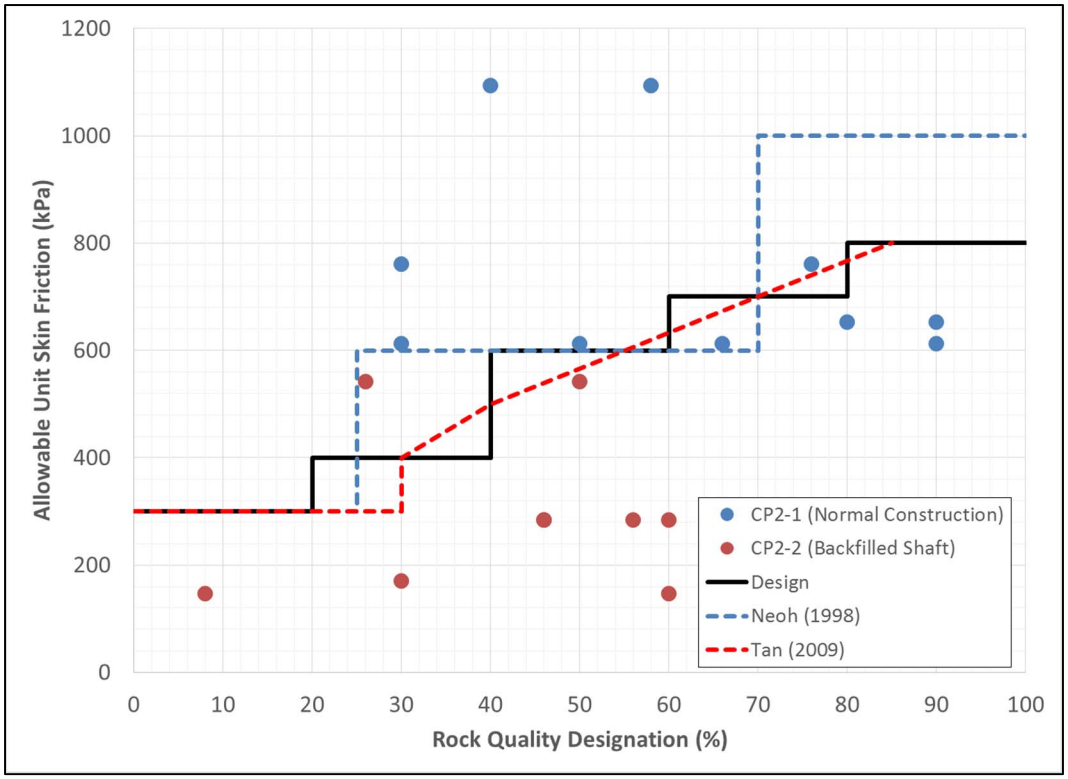


Fig. 4 – Allowable Unit Skin Friction vs. RQD

PILED-RAFT FOUNDATION FINITE ELEMENT ANALYSIS

We performed 3-D finite-element-method (FEM) analyses using the software package midasGTS to estimate the settlement response of the foundation raft and develop criteria for socketing piles into steeply-sloped rock.

The full piled-raft models incorporated the sloped stratification at the interface between the Kenny Hill and limestone layers. The piles were modeled using the "embedded pile" option, which employs beam elements to model the structural characteristics of the piles and interface elements to model the interaction between the pile and the surrounding soil/rock. Table 2 presents our best-estimate parameters for the soil and rock compressibility and the pile interface capacity. The piled-raft and limestone surface from our FEM model are presented in Fig. 5 below.

Table 2. FEM Modeling Parameters

Material	Modulus of Deformation, E_{def}	Ultimate Unit Skin Friction, f_s
Kenny Hill	90	100 kPa
Limestone	14,000	1,100 kPa

© 2016 Deep Foundations Institute

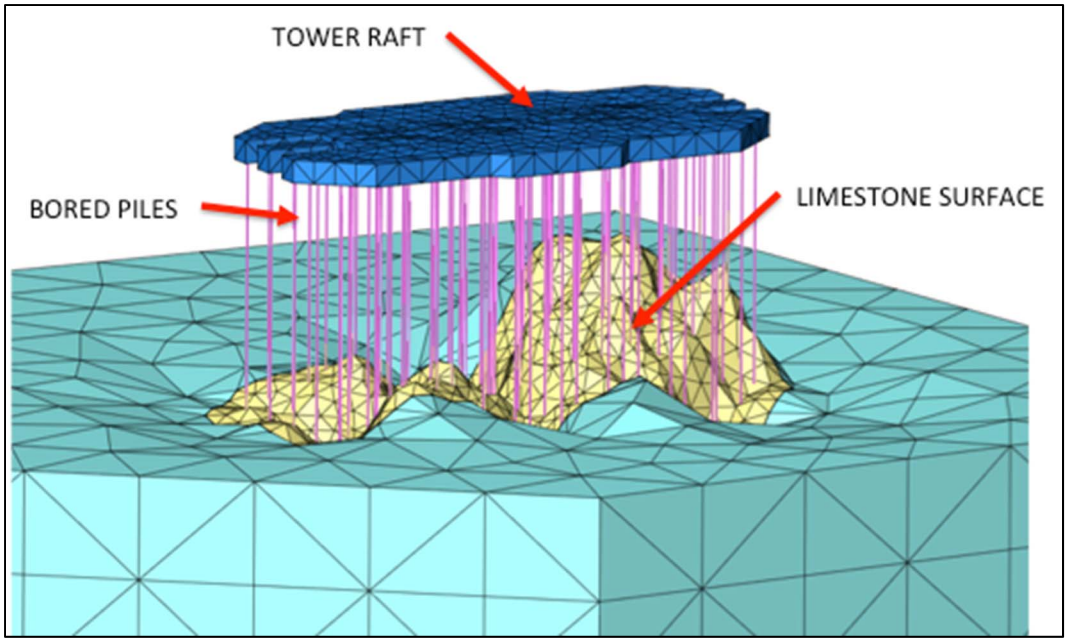


Fig. 5 – 3-D Finite Element Model

A simplified construction-stage process was modeled consisting of an initialization stage, an excavation stage, a piling stage, and finally a raft construction and tower loading stage. Soil settlement and heave was reset after the initialization and excavation stage, respectively. An iterative procedure was employed in coordination with the structural engineer to achieve convergence for the raft settlement magnitudes, the overall shape of the settlement contours, the pile loads, and the tower loads.

Rock Socket Length Criteria in Sloping Rock

Sloping rock was a constant issue across the tower footprint; the concern being that the rock socket length would include some length where rock was not present around the full pile circumference. We used a 3-D finite element model to analyze a single pile subjected to a 60 MN axial load and a rock surface dipping at 65 degrees from horizontal to help establish criteria for the rock socket length. The pile and soil layers were modeled with 3-D volume elements and 2-D plane interface elements between the pile and surrounding soil and rock. The results presented in Fig. 6 below indicate that the rock deformation occurs primarily within a distance of about one-half pile diameters from the top and within the top three pile diameters from the top of the rock socket. Accordingly, we specified that the rock socket length should start from the point where rock extends horizontally around the pile circumference out to at least one-half pile diameter from the pile edge. Fig. 7 presents a diagram of the rock socket length criteria adopted for the project.

© 2016 Deep Foundations Institute

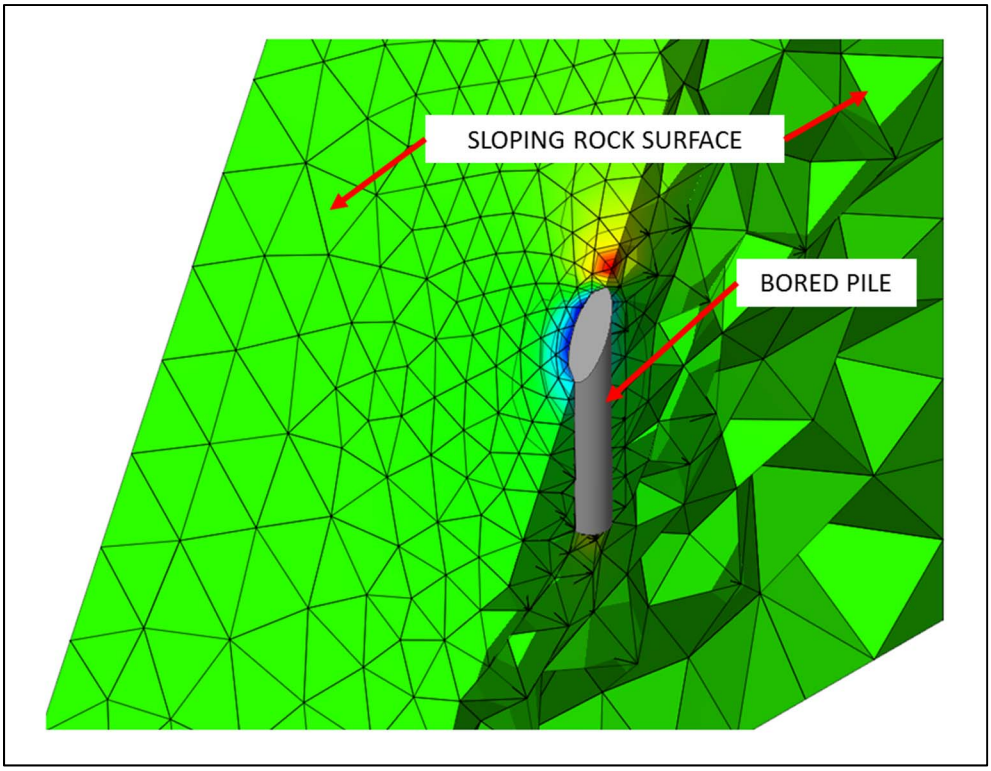


Fig. 6 – FEM Model of Single Pile in Sloping Rock

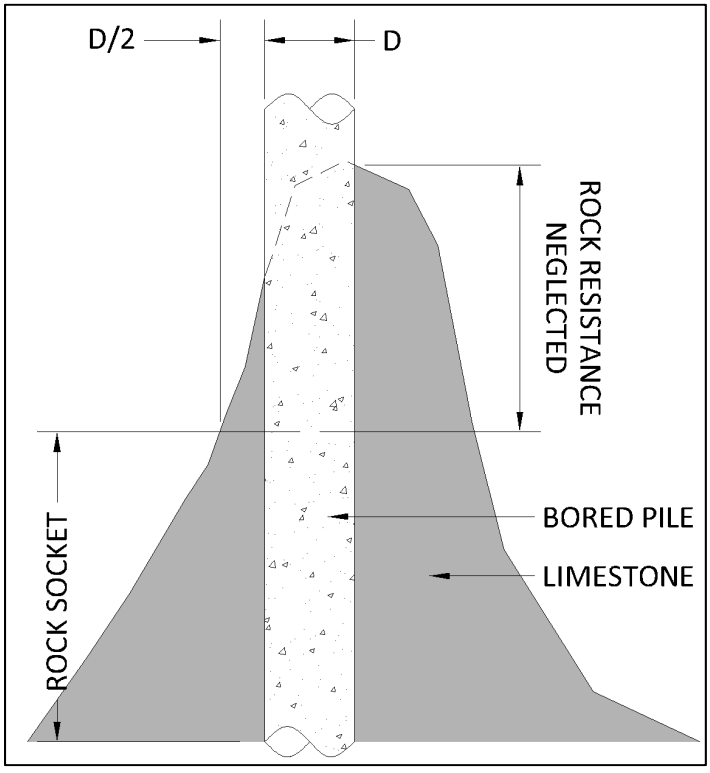


Fig. 7 – Socket Criteria in Sloping Rock

© 2016 Deep Foundations Institute

PRODUCTION PILE CONSTRUCTION

The pile construction phase required intensive oversight and communication between both the inspecting engineers, the designers and the contractor. The piles were drilled typically with a Bauer BG40 drill rig equipped with a telescoping Kelly bar and a variety of core barrels, cross-cutting bits, and digging/cleaning buckets. Bored piles were socketed between 6.5 and 24 meters (14 meters on average) into the hard limestone at depths up to 102 meters below grade.

The pile construction and field re-design process consisted of simultaneously proof-drilling and pressure-grouting at each pile location, evaluating the rock conditions to determine socket elevation and length, and final pile construction. Ultimately the owner's design team specified the rock socket lengths based on review by field inspectors, on-site designers and senior management both on and off site. The proof-drilling and piling operations were overseen and documented by a team of geologists and engineers employed by the piling contractor and the owner.

Pile socket lengths were estimated based on the site-specific correlation between rock capacity and RQD from the proof-drilling results then finalized during pile installation based on a combination of observed drilling rates, drill cuttings, and shaft inspections. The final rock socket was cleaned thoroughly using a tool with a flat plate and bucket to scrape off cuttings at the bottom of the socket. Immediately before placing concrete, the polymer slurry was air-lifted from the bottom of the borehole while new slurry was added from the top. The socket was inspected for depth and soundness by the field team. Shaft inspection devices (e.g. Sonicaliper®) were used as needed.

Proof-drilling and cavity treatment

Exploratory rock probes (i.e. proof-drilling) were performed at the center of each pile location and consisted of mud-rotary drilling to the top of rock then coring rock using an NX-sized core barrel to a minimum of 25 consecutive meters into competent rock, about 10 meters below the typical pile toe. Rock cores retrieved from the borehole were characterized by the contractor's field geologist and were subjected to point load tests. The RQD and point load index were used to determine the required socket length at each pile. The rock surface was mapped as proof-drilling progressed so that the top elevation of each rock socket would satisfy the sloping rock criteria.

Once the proof-drilling was complete, the borehole was grouted under pressure using a neat cement grout, with a compressive strength of 35 MPa and a water-cement ratio of 0.45. Each borehole was grouted until a backpressure of 10 bars was attained. In the most extreme case, over 1,800 bags of cement were used to grout a single borehole, equating to approximately 570 times the borehole volume. In total, more than 1,800 cubic meters of grout were pumped into the rock, which equates to about 0.5 meters of grout across the entire tower footprint.

The top elevation of each rock socket from the design-phase investigations was verified and revised as needed during construction. The top of rock socket was first estimated using interpolated rock slopes between adjacent proof-drilling points, and finalized during pile drilling by sounding the bottom of the borehole, observing the drilling cuttings and reviewing drilling rates. The sloping rock was so severe in some cases that the pile circumference would not be fully seated in rock for several meters below the rock level encountered during proof-drilling. The elevation of the rock socket top, as determined from proof-drilling, was lowered at nearly every pile based on the conditions encountered during pile construction.

The final pile lengths typically were about 5 to 10 percent longer than the lengths estimated based on proof-drilling. Only two piles exceeded the proof-drilling pile length estimate by more than 20 percent,

© 2016 Deep Foundations Institute

one of which required an 85 percent increase in pile length. This outlier was the result of an underground rock ledge falsely identified as the rock bearing level during proof-drilling. The rock ledge became apparent as proof-drilling nearby encountered rock significantly deeper and the field team noted faster piling rates not indicative of sound rock. The large-diameter pile appeared to be straddling the rock ledge requiring the socket to be relocated to the bottom of the ledge.

Deep Rock Levels

Several piles were required to bypass an upper thin rock layer and socket into a lower rock layer. In the most extreme case, the upper rock layer was encountered about 45 meters below grade and was 10 meters thick, followed by a 30-meter-thick infilled cavity extending to about 85 meters below grade where the lower rock layer was encountered. The upper rock level was generally not thick enough to support the pile's working load in friction and there were concerns of excessive settlement or geotechnical failure of the rock under the pile's working load. The lower rock layer extended so deep that the required pile toe elevation was below the maximum reach of the drill rig at 102 meters below grade, resulting in a reduced rock socket length. There were five piles where the reduced rock socket lengths of these five piles would be reduced such that the socket capacity was less than the required working load. The piled-raft performance was not significantly affected by terminating five of the 108 piles at 102 meters below grade, above the rock surface.

Polymer Slurry Issues

Polymer slurry was used to stabilize the borehole during drilling. Polymer slurry was specified instead of bentonite slurry to avoid issues with filter cakes forming on the sides of the rock socket. Because of high costs and limited supply, the piling contractor recycled the polymer slurry across multiple piles. The polymer slurry was typically refreshed several times during pile installation as most piles took nearly a month to construct. Refreshing the slurry involved vacuuming the old slurry out of the borehole as new slurry was pumped into the borehole. The slurry was pumped back into holding tanks to allow the sediment to settle out. The slurry was tested daily within the boreholes for sand content, Marsh Cone viscosity, pH, fluid loss, shear strength and specific gravity. As the piles were concreted, the slurry was pumped from the top of the pile and mixed with the rest of the batch. The quality of the slurry declined through recycling the slurry across multiple piles and from apparent contamination by fresh proof-drilling grout nearby.

The work area within the tower footprint became extremely congested with pile rigs and proof-drilling rigs working side-by-side. There were cases where proof-drilling and grouting was underway at a pile location adjacent to an open borehole. The pressurized grout traveled through the fractured rock and entered the adjacent pile borehole and was observed being excavated from the borehole. The polymer slurry density decreased significantly, which resulted in boreholes collapsing into the rock socket. Pile drilling was halted to allow the proof-drilling and pressure-grouting to be completed at this location.

The slurry issues were noted when several piles were found with 6 to 16 meters of sediment in the bottom of the borehole. In one case, the open borehole sat for three days without refreshing polymer slurry. The borehole partially collapsed into the socket, which required additional socket length because of concerns regarding reduced skin friction. In other cases, the material appeared to be caused by a combination of high sand content and soil sloughing off the sides of the boreholes. The piling contractor understood the risk of having multiple boreholes collapsing causing further delays and ultimately replaced all the polymer on site.

© 2016 Deep Foundations Institute

CONCLUSIONS

The quality of the constructed piles and overall foundation system was achieved through extensive design- and construction-phase investigation and testing, a full-scale load test program, pre-construction grout treatment of the limestone, pile installation oversight by the contractor's and the owner's engineers, post-installation integrity testing, and most importantly communication between the contractor and the designer. Open communication between the piling contractor, the field engineers and designers was critical in developing on-the-fly design and construction solutions to address variable field conditions and keep the project moving.

The extensive three-phase subsurface investigation helped develop geotechnical engineering parameters and refine the resolution of the variable rock profile. The investigation set the stage for a detailed foundation design and FEM analysis that included modeling the performance of the entire piled-raft, as well as developing criteria for socketing the piles in steeply-sloped rock. The construction-phase proof-drilling investigation allowed the designers to estimate pile lengths for the contractor that were typically within 5 to 10 percent of the as-built lengths. The proof-drilling also allowed for pressure-grouting the rock, which provided a more competent rock mass and minimized the potential for borehole instability in the rock and loss of costly polymer drilling slurry.

Two O-cell tests performed in variable rock quality profiles were used to develop a site-specific correlation between RQD and unit skin friction in rock.

Quality control and assurance were provided through extensive field oversight and testing by the contractor's engineers, the owner's local engineers, the owner's foreign designers. The comprehensive oversight effort allowed the team to stay ahead of construction issues, such as pile installation behavior contradicting the proof-drilling results, polymer slurry issues, boreholes collapsing, and extraordinarily deep rock levels.

This project exemplifies the importance of maintaining a design presence through construction challenges and how open communication between the contractor and the engineer results in more efficient construction and a better quality finished product.

REFERENCES:

1. Drumright, E.; Joseph, L.M.; Azam, I.T.; Baker Jr., C.N., 1998. Foundation Design and Performance of the World's Tallest Building – Petronas Towers. Fourth International Conference on Case Histories in Geotechnical Engineering.

2. Neoh, C.A.; Design & Construction of Pile Foundation in Limestone Formation, 1998. Journal of Institution of Engineers, Malaysia. Vol. 59(1), pp. 23-29.

3. Williams, A. F.; Pells, P. J. N., 1981. Side Resistance of Rock Sockets in Sandstone, Mudstone, and Shale. Canadian Geotechnical Journal, Canada. Vol. 18(4), pp. 502-513.

© 2016 Deep Foundations Institute

This page left intentionally blank

© 2016 Deep Foundations Institute

BUTTRESSING BERMS FOR STABILITY OF CANTILEVER SHEET PILES – LIMIT EQUILIBRIUM AND FINITE ELEMENT APPROACHES

Meena L. Viswanath, Geosyntec Consultants, 1255 Roberts Boulevard NW, Suite 200, Kennesaw, GA, 678-202-9593, mviswanath@geosyntec.com
Mustafa B. Erten, Ph.D., P.E., Geosyntec Consultants, 11490 Westheimer Rd, Suite 150, Houston, TX, 281-810-5071, mberten@geosyntec.com
Ali Ebrahimi, Ph.D., P.E., Geosyntec Consultants, 11490 Westheimer Rd, Suite 150, Houston, TX, 281-810-5025, aebrahimi@geosyntec.com
Ming Zhu, Ph.D., P.E., Geosyntec Consultants, 1255 Roberts Boulevard NW, Suite 200, Kennesaw, GA, 678-202-9538, mzhu@geosyntec.com
John F. Beech, Ph.D., P.E., Geosyntec Consultants, 1255 Roberts Boulevard NW, Suite 200, Kennesaw, GA, 678-202-9506, jbeech@geosyntec.com

ABSTRACT

Excessive deformation of a cantilever sheetpile wall can occur due to dredging, excavation, backfilling, or long-term creep behavior of soil. A buttressing berm constructed in front of the wall can be considered as a mitigation technique to prevent or decrease the deformation by increasing the passive earth pressure and thus improving the wall stability. The effect of the buttressing berm on the stability and deformation of a sheetpile depends on the berm geometry (i.e., the thickness/depth and the width) as well as the properties of the sheetpile and the adjacent soils. A parametric study was conducted using a conventional limit equilibrium method. Design charts were prepared to evaluate the effect of a buttressing berm and the soil friction angle on the wall stability and deformation. These charts can be used as a tool by geotechnical engineers to make a quick estimate of the required size of a buttressing berm in case of calculated or unexpected excessive deformation of a sheetpile. An analysis of the effect of a buttressing berm on the stresses and deformation of a sheetpile was also compared with the results from finite element analysis. The results of this comparison are discussed.

Keywords: cantilever sheetpile, deformation, buttress, limit equilibrium method, finite element analysis

INTRODUCTION

Cantilever sheetpile walls are commonly used to support excavations. Sheetpiles are hot rolled or cold formed sections of steel made to interlock with adjacent sections to form a continuous structure providing lateral support. Sheetpile walls can be cantilever walls or anchored with tiebacks. To construct a cantilever sheetpile wall, sheetpiles are driven by pile drivers or vibrated in to a design depth sufficiently below the depth of excavation. Excavation can then proceed in front of the sheetpile wall, which resists the earth pressure loading from behind the wall. The design depth and geometry of the sheetpile wall depend on the soil conditions, the depth of excavation, and the tolerable deformation. In certain cases, when a small buttress of soil can be left immediately adjacent to the sheetpile wall, the required depth or geometry of the sheetpile wall can be reduced or adjusted, which can significantly decrease the cost of procuring and installing the wall. Such a buttress can also serve as a short-term or long-term remedy in case of observed excessive deformation in a constructed wall. Traditional methods of analyzing the stability of a sheetpile wall do not account for the passive pressure effects of this small buttress. In this paper, a parametric study was performed for a variety of soil types and wall and buttress geometries by implementing traditional limit equilibrium methods in commercial software and design charts were created illustrating the effect of a buttressing berm on sheetpile deflection. Selected cases were then modeled in a finite element software to compare the results with the traditional limit equilibrium method. The resulting design charts can be used as a tool by geotechnical engineers looking to reduce the design geometry of a sheetpile wall or address observed excessive deformation in a constructed sheetpile wall.

© 2016 Deep Foundations Institute

METHODOLOGY

In the traditional limit equilibrium analysis method for sheetpile walls, cantilever walls can be modeled as flexible beams fixed at one end, subject to the loads generated from the surrounding earth pressures. Proper design of a cantilevered sheet pile wall must consider stability with respect to the forces and moments applied to the wall, moment capacity with respect to the applied moments, and any deflection criteria. Force and moment stability are attained by including sufficient embedment in the design of the cantilever, while moment and deflection are a function of the material and shape of the specified sheet pile as well as applied forces and moments. All three design criteria are dependent on correctly modeling the earth pressures surrounding the sheet pile wall. For a purely frictional material, with a geometry as shown in Fig. 1, the distribution of earth pressures at depth z would be as follows:

$$P(z) = \begin{cases} K_a \gamma z, \ active\ pressure\ for\ z \geq 0 \\ K_p \gamma (z - EH), \ passive\ pressure\ for\ z \geq EH \end{cases} \quad [1]$$

Where γ is the unit weight of the soil, EH is the depth of excavation, and K_a and K_p are earth pressure coefficients, defined using Rankine theory.

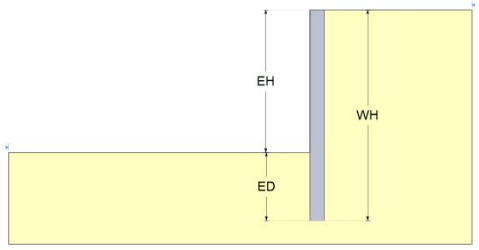


Fig. 1. Geometry of a cantilever sheetpile wall

The required depth of embedment is the depth at which both force and moment equilibrium are satisfied. Since moment equilibrium is usually more critical than force equilibrium, the calculation for moment equilibrium is performed first. The equation for moment equilibrium is as follows:

$$\frac{1}{2} K_a \gamma (ED + EH)^2 \cdot \bar{z}_{active} = \frac{1}{2} K_p \gamma (ED)^2 \cdot \bar{z}_{passive} \quad [2]$$

Where ED is the depth of embedment, $\bar{z}_{active}$ is the active moment arm, and $\bar{z}_{passive}$ is the passive moment arm. Once the equation is solved for ED, force equilibrium can be checked by comparing the active and passive pressures slightly below the required embedment depth, as follows:

$$K_p \gamma ((ED)) > K_a \gamma (ED + EH) \quad [3]$$

The recommendation of the USS Steel Sheet Piling Design Manual is to increase the depth of embedment by 20 to 40 percent (USS Steel Sheet Piling Design Manual, 1984). The AASHTO Standard Specifications recommend increasing the depth of embedment by 30 percent for temporary shoring and 50 percent for permanent shoring (AASHTO, 2002). The minimum depth of embedment is also recommended to be at least 1.5 m (5 ft) to 3.0 m (10.0 ft) regardless of the calculated minimum depth of embedment (CivilTech Software, 2014).

© 2016 Deep Foundations Institute

Once the required depth of the sheetpile is known, a section and material must be selected based on moment and deflection criteria. The maximum moment resulting from the earth pressures can be calculated from the earth pressure distribution behind the wall. The calculated maximum moment must be less than the allowable moment capacity of the selected sheet pile, which is calculated as follows:

$$M_C = \frac{M_y}{FS} = \frac{S \cdot \sigma_y}{FS} \quad [6]$$

Where M_c is the moment capacity of the section, M_y is the yield moment of the section, S is the section modulus, σ_y is the yield strength of the material, and FS is the factor of safety applied to the yield moment. Deflection criteria, which depend on the Young's modulus and the moment of inertia of the section, must also be checked.

LIMIT EQUILIBRIUM ANALYSIS

Geometry and Material Properties

Although the theoretical calculation given above is straightforward for simple geometries, it quickly becomes unwieldy when any additional factors, such as stabilizing berms, are considered. There are a number of software packages which implement the above equations numerically to calculate the required depths of embedment and maximum moment for a variety of geometries, including the one used for this study, Shoring Suite V8.15 (CivilTech Software, 2014). The geometry used to model a cantilever wall stabilized by a berm is shown in Fig. 2.

The berm was assumed to have a 2 horizontal to 1 vertical (2H:1V) slope as shown in Fig. 2. Both the berm height (BH) and the berm top width (BW) were varied in increments of 0.5 m (1.6 ft) or 1 m (3.3 ft). The excavation height (EH) was varied from 2 m (6.6 ft) to 5 m (16.4 ft).

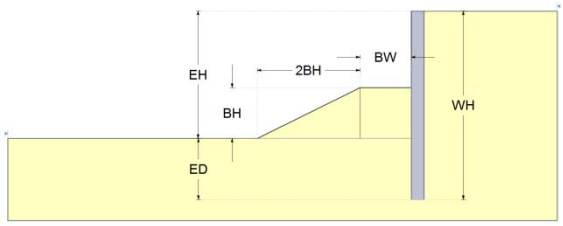


Fig. 2. Geometry of analyzed sheetpile wall with a berm

The earth pressure distribution was calculated by the EarthPres module in Shoring Suite, which modeled the distribution with a triangular apparent pressure envelope for unbraced walls. As is appropriate with a flexible wall, K_a was used for the soil pressure on the active side. The soil on both sides of the excavation was modeled as a sand with a unit weight of 20.8 kN/m^3 (131.7 pcf) and no cohesion. The friction angle of the soil was modeled as 25 and 30 degrees. For the purpose of this study, the soil was assumed to be dry on both sides of the wall, with no seepage or water table present. Consistent with the Rankine theory, no wall friction was assumed, and no multipliers were applied to the active or passive pressures. For simplicity, the same material properties were used for the foundation soil and the berm material. The program used a wedge analysis to determine the numerical solution, using the standard Terzaghi and Peck apparent envelope conversion method. The entire depth of the wall was considered for the purposes of passive pressure. No surcharges or earthquake pressures were considered.

The resulting earth pressure distribution was used in the Shoring module of Shoring Suite to calculate the required embedment depth (ED) and corresponding wall height (WH) and maximum moment. The wall

© 2016 Deep Foundations Institute

was modeled as a continuous span beam with a factor of safety of 1.0 without the stabilizing effect of the pile moment capacity. Deflections were calculated for a PZ-22 sheetpile section, which has a yield strength of 248 MPa (36 ksi), a moment capacity of 159 kN·m (117 lbf·ft), and a moment of inertia of 11,500 cm^4/m (84.4 in^4/ft). In cases where the PZ-22 sheetpile section did not have sufficient moment capacity for Shoring Suite to calculate a deflection, the wall was modeled using a PZ-27 or a PZ-40 sheetpile section, which have moments of inertia of 25,200 cm^4/m (184.2 in^4/ft) and 67,000 cm^4/m (490.9 in^4/ft). A normalized deflection was calculated by dividing the calculated deflection by the moment of inertia of the modeled sheetpile section. An equivalent deformation of a PZ-22 sheetpile section was then calculated by multiplying the normalized deflection by the moment of inertia of the PZ-22 section. The calculated wall heights include the recommended 20 percent increase in embedment, as mentioned above.

FINITE ELEMENT MODELING AND ANALYSES

Geometry and Material Properties

A similar group of cases were implemented in a finite element model for comparison. The 3-m, 4-m, and 5-m (9.8-ft, 13.1-ft, and 16.4-ft) excavation cases were analyzed for berm heights varying in increments of 0.5 m (1.6 ft) or 1 m (3.3 ft). The width of the berm in these cases was kept constant at 0 m. In addition, for the 5-m (16.4-ft) excavation case with 1 m (3.3 ft) of berm height, the width of the berm was varied between 1 m (3.3 ft) and 5 m (16.4 ft) to evaluate its effect on the wall behavior. The PZ-22 type of sheetpile was used in all cases. The soil and wall properties used in the finite element model are given in Table 1. Although the soil was assumed to be coarse grained, a small cohesion of 1 kN/m^2 was assigned to prevent any numerical complications in the finite element analysis.

Table 1. Soil and Wall Properties

Property	SI Units	Imperial Units
Foundation Soil and Berm Material:		
Unit Weight, γ	20.8 kN/m^3	131.7 pcf
Friction Angle, ϕ	30 degrees	
Dilatancy Angle, ψ	0 degrees	
Cohesion, c	1 kN/m^2	0.15 psi
Modulus of Elasticity, E_{50}	15,000 kPa	2176 psi
Poisson's Ratio, v	0.28	
Wall:		
Axial Stiffness, EA	2.74×10^6 kN/m	1.88×10^5 kip/ft
Bending Stiffness, EI	23,000 $kN \cdot m^2/m$	1,576 $kip \cdot ft^2/ft$
Soil/Wall Interface Strength, R_{int}	0.65	

Constitutive Model

The same geometry that was used in limit equilibrium analyses (i.e., from Fig. 2) was implemented in Plaxis (Plaxis, 2012), as a plane strain model using 15-node triangular soil elements and 5-node plate elements. The models consisted of approximately 600 soil and 10 plate elements. For more accurate calculations, a finer mesh was assigned around the sheet pile wall. The soil was modeled as a linearly elastic perfectly plastic material using the Mohr-Coulomb model, which is widely used for geotechnical modeling (Potts and Fourie, 1984 and 1985). The finite element model in this study represents the case where the berm was left in place during the excavation stage rather than placed after the excavation.

© 2016 Deep Foundations Institute

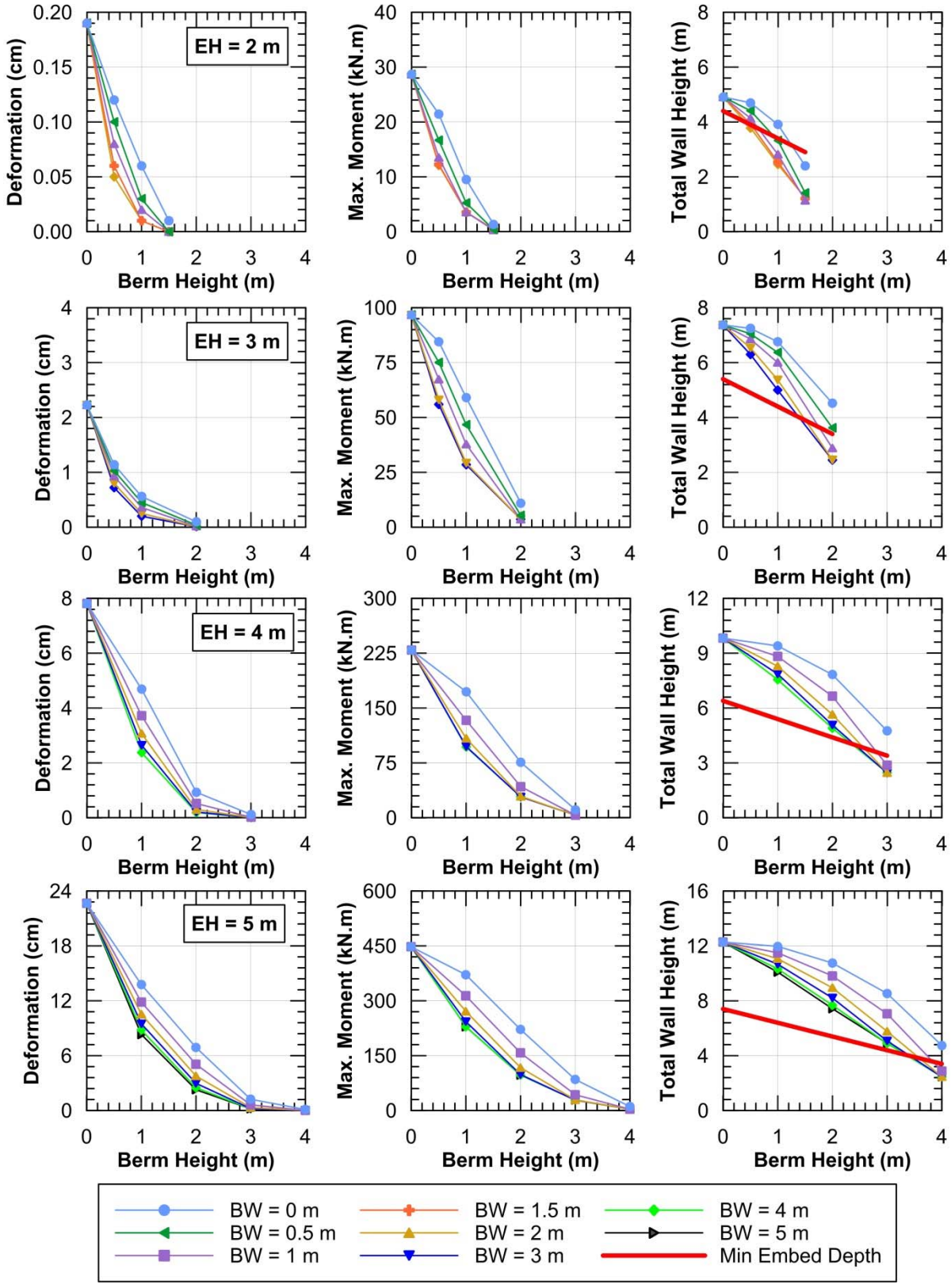


Fig. 3. Design charts for varying excavation depths and berm heights and widths for a soil with ϕ'=25 degrees (no water table)

© 2016 Deep Foundations Institute

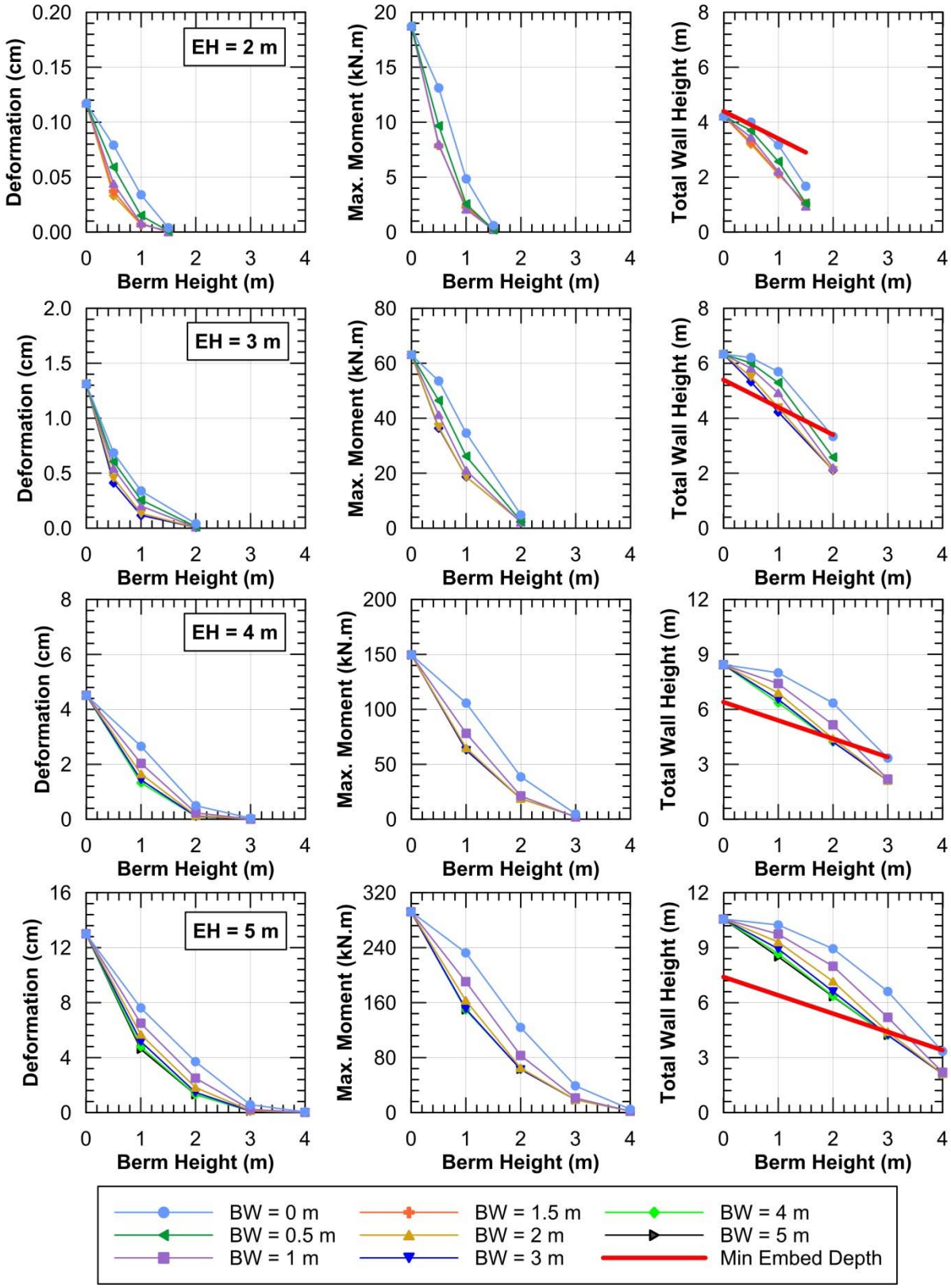


Fig. 4. Design charts for varying excavation depths and berm heights and widths for a soil with ϕ'=30 degrees (no water table)

© 2016 Deep Foundations Institute

RESULTS AND DISCUSSION

Limit Equilibrium Results

The design charts resulting from the limit equilibrium analysis are shown in Fig. 3 and 4. The design charts also show a line corresponding to a minimum recommended embedment depth of 2.4 m (7.9 ft). In both cases, whether the soil has a friction angle of 25 or 30 degrees, placing a berm adjacent to the sheetpile wall significantly decreases the maximum moment and top horizontal deflection of the wall. Increasing the height of the berm by a relatively small amount can reduce the required embedment depth, maximum moment, and top horizontal deflection by a relatively large amount. For example, in a 30-degree soil, a 4-m (13.1-ft) excavation, which would usually have a calculated deformation of 4.5 cm (1.8 in.) with a PZ-22 sheetpile, would have a deformation of 2.7 cm (1.1 in.) when a small berm 1 m (3.3 ft) high with zero top width were added, i.e., a decrease of 1.8 cm (0.7 in.) in wall deformation. However, each additional increment of buttressing berm height has a successively smaller impact on the maximum moment and top horizontal deflection; for example, while the same 4-m (13.1-ft) excavation with a 2-m (6.6-ft) high berm would have a deformation of 0.5 cm (0.2 in.), a 3-m (9.8-ft) high berm would result in a deformation of 0.04 cm (0.02 in.), i.e., a decrease of only 0.46 cm (0.18 in.). Increasing the width of the berm also reduces the required wall height, maximum moment, and top horizontal deflection; however, the effect is smaller than that of increasing the height of the berm. For example, the 4-m (13.1-ft) excavation showed a deformation of 2.7 cm (1.1 in.) with a small berm of 1-m (3.3-ft) height and zero top width; if the berm width is increased to 1 m (3.3 ft), the deformation would be reduced to 2.0 cm (0.8 in.), which is an additional reduction, but not as great a reduction as increasing the height by an additional 1 m (3.3 ft), which, as mentioned, would reduce the deformation to 0.5 cm (0.2 in.).

Comparison of Limit Equilibrium and Finite Element Results – Effect of Berm Height

Fig. 5 shows a comparison of the top of the wall deformations and maximum moments calculated using the limit equilibrium and the finite element analyses for the 3-m, 4-m, and 5-m (9.8-ft, 13.1-ft, and 16.4-ft) excavation cases in 30-degree soil with varying berm heights. For different excavation heights, the top of wall horizontal deflection varied between 0.04 cm (0.02 in.) and 13 cm (5.1 in.) in the limit equilibrium analyses and between -3.2 cm (-1.3 in.) and 18.7 cm (7.4 in.) in the finite element analyses. For taller berms,

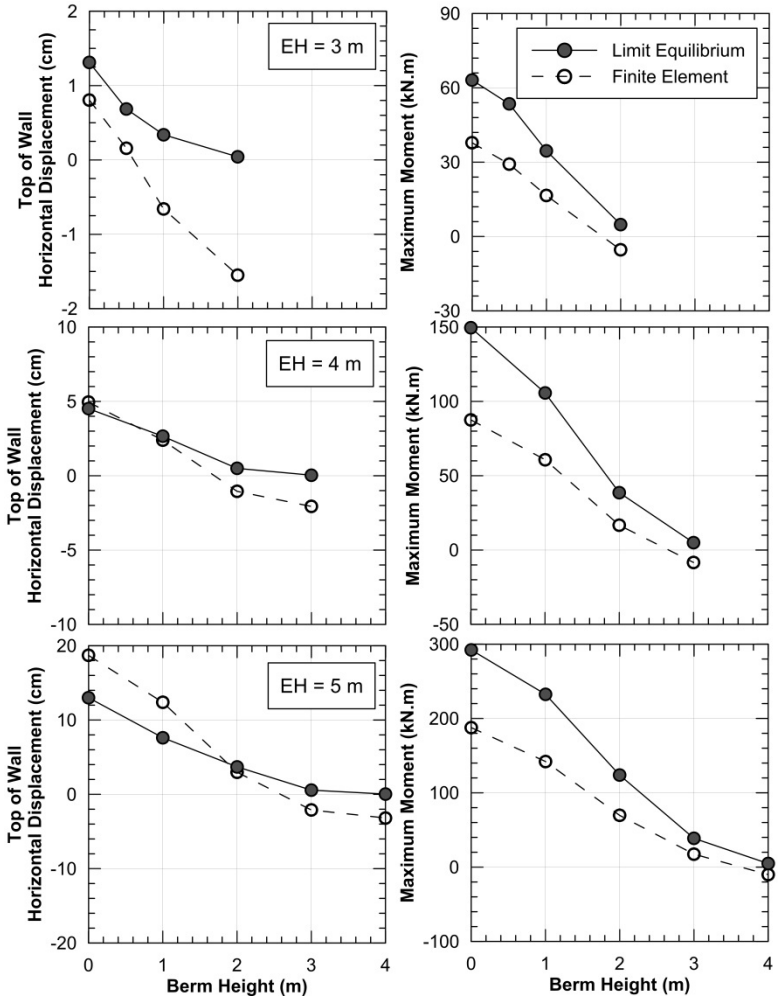


Fig. 5. Maximum top of wall deformation and maximum wall moments for EH=3 m, 4 m, and 5 m

© 2016 Deep Foundations Institute

the finite element analysis results show that the top of wall deflections are negative, which implies that the top of the wall moves away from the excavation. This phenomenon can be better examined in Fig. 6, which shows a comparison of the final deformed wall shapes for the 5-m (16.4-ft) excavation with various berm heights.

As seen in Fig. 6, for increasing berm heights, in the final condition, the top of the wall moves away from the excavation since it is restricted by the berm in front of the wall. The deformations in the embedded portions do not differ significantly for the various berm heights. Fig. 5 also shows that the maximum bending moments decreased with increasing berm heights in all cases. The maximum bending moments calculated by the finite element model were always smaller than the ones calculated with the limit equilibrium analyses. In addition, the maximum bending moments were negative for the tallest berm height. As shown in Fig. 6, with increasing berm height, the wall moves away from the excavation rather than towards the excavation. The change in the direction of the movement of the wall results in maximum bending moments occurring in the opposite direction.

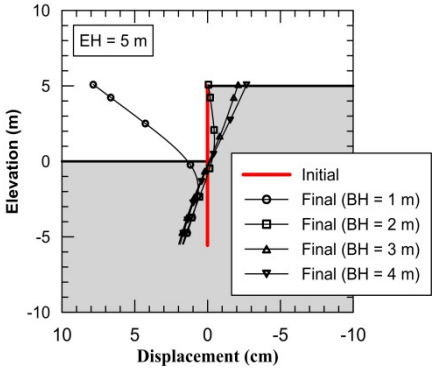


Fig. 6. Deformed wall shape for EH=5 m and BW=0 m with various berm heights

Comparison of Limit Equilibrium and Finite Element Results – Effect of Berm Width

In this analysis, the berm width was only increased until it equaled the excavation height. In looking at the design charts, it is clear that a berm width equivalent to the excavation height was sufficient to fully relieve the sheetpile wall from the active moment induced by that section of wall. For example, a sheetpile wall for a 4-m excavation in 30-degree soil with no berm experiences a maximum moment of 18.7 kN·m (13.8 kip·ft) and a deflection of 1.3 cm (0.5 in.) and requires a total wall height of 6.3 m (20.7 ft). A sheetpile wall for a 3-m excavation in 30-degree soil with a 1-m high and 3-m wide berm experiences the same maximum moment and deflection and requires the same embedment. However, this effect begins to become apparent in certain cases even before the berm width equals the excavation height. Since this effect is likely due to the effect of the passive wedge, the critical berm width at which additional berm width does not decrease the deflection or the moment would depend on the required embedment and the frictional strength of the material. However, based on the analyses presented here, a rule of thumb could be proposed for the modeled range of soils that a berm with a width corresponding to the total depth of the excavation will effectively reduce the height of the excavation by the height of the berm such that a traditional limit equilibrium analysis could be performed.

Additional finite element analyses were performed to investigate the influence of the varying berm width on the sheet pile wall behavior, as shown in Fig. 7. In all analyses, the excavation depth was 5 m and the height of the berm was 1 m. The berm width varied between 0 m and 5 m. The results show that the finite element model predicted more deformation when the berm width was less than 2 m and less deformation

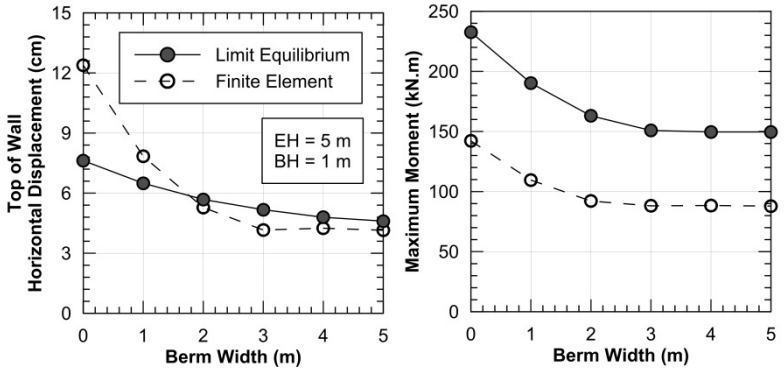


Fig. 7. Top of wall horizontal displacement and maximum moments for EH=5 m and BH=1 m

© 2016 Deep Foundations Institute

when the berm width was more than 2 m for the analyzed case. In general, the maximum moments calculated by the limit equilibrium analyses were larger than those calculated by the finite element analyses. However, the trend is the same as observed in the limit equilibrium analysis results, that after a certain critical width, the maximum moment does not decrease further.

Example Use of the Design Charts

The following is an example of how to use the design chart. A sheetpile wall designer is asked to design a sheetpile wall to support a 4-m (13.1-ft) excavation. The geotechnical investigation reveals that the site consists of sandy materials with a drained strength of approximately 25 degrees, while the water table is well below the excavation depth. All the other geotechnical parameters are similar to the ones modeled here. A traditional limit equilibrium analysis indicates that the wall will need to be 9.8 m (32.2 ft) tall and will have a maximum moment of 229 kN·m (169 lbf·ft). In order to select a sheetpile, the wall designer investigates the moment capacity of a PZ-22 pile and a PZ-27 pile. The yield strength for steel is assumed to be 248 MPa (36 ksi). The elastic section modulus of a PZ-22 pile is 973 cm^3/m (18.1 in^3/ft), while the section modulus of a PZ-27 modulus is 1,620 cm^3/m (30.2 in^3/ft). The moment capacity of each pile is the section modulus multiplied by the allowable bending stress, which is generally taken as 0.66 of the yield strength. The moment capacity of the PZ-22 pile is therefore calculated to be 159 kN·m (36 kip·ft), while the moment capacity of the PZ-27 pile is 266 kN·m (60 kip·ft). The designer therefore selects a PZ-27 pile for this project. The client then indicates that the cost of the proposed design is higher than the budgeted amount, and requests solutions for reducing the cost of the sheetpile wall. As a screening level tool, the designer looks at the design charts, as shown in Fig. 8, and identifies that a buttress with a 1-m (3.3-ft) width and a 1-m (3.3-ft) height may be effective in reducing the required height of the wall to 8.8 m (28.9 ft). The buttress might also allow the use of a PZ-22 pile, as the maximum moment may have been reduced to 133 kN·m (98 lbf·ft). This revised design would then fit into the client's budget. The designer then proceeds to undertake a detailed design for this case.

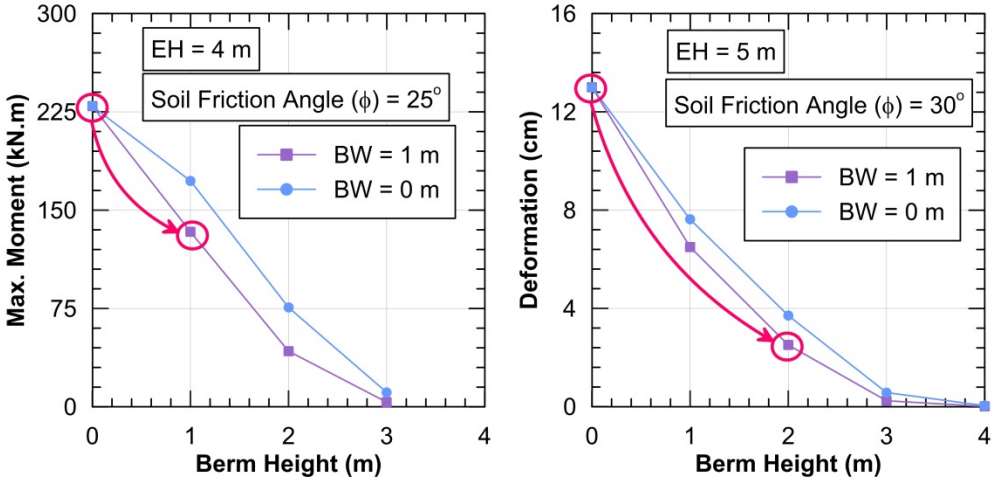


Fig. 8. Using the design charts to reduce the maximum moment (left) and excessive deformation (right)

A second example involves the case where a PZ-22 sheetpile wall is designed and installed at a 5-m (16.4-ft) deep excavation. Due to project constraints, the allowable deformation is approximately 2.5 cm (1 in.). During the course of the excavation, the sheetpile wall shows signs of excessive deformation. A geotechnical investigation reveals that the sandy soils have a strength of 30 degrees, and the water table is deep. Other geotechnical parameters are similar to the ones modeled in this paper. As a screening level tool to identify an emergency solution to the excessive deformation, the wall designer uses the design

© 2016 Deep Foundations Institute

charts as shown in Fig. 8 to identify that a 2-m (6.6-ft) high berm with a top width of 1 m (3.3 ft) may keep the deformation within approximately 2.5 cm (1 in.). The designer then proceeds to undertake a detailed design for this case.

CONCLUSIONS

The effects of placing a berm with a varying height and width on sheetpile wall behavior for a 2-m, 3-m, 4-m, and 5-m (6.6-ft, 9.8-ft, 13.1-ft, and 16.4-ft) deep excavation were evaluated in this study using limit equilibrium and finite element methods. Based on the geometry and the parameters used in this study, the main findings from this research are as follows:

- An increase in berm height results in a decrease in the required embedment depth, top of wall deflection, and the maximum bending moments;
- An increase in the berm width only reduces the top of wall deformations and the bending moments to a point. If the berm width is increased beyond this critical width, the reduction in top of wall deformation and bending moments do not continue to decrease; and
- The top of wall deflections and the maximum bending moments calculated by the finite element model are usually lower than the ones calculated by the limit equilibrium analyses.

The results presented in this study can be used as a preliminary screening tool for sheetpile wall and berm design or for emergency response under similar geometry and soil conditions.

REFERENCES

American Association of State Highway and Transportation Officials (AASHTO) (2002). Standard specifications for highway bridges, 17th edition. Code: HB-17. AASHTO, Washington, D.C.

CivilTech Software (2014). Shoring Suite Version 8.15. CivilTech Inc., Mountain View, CA.

Plaxis (2012), Two-Dimensional Finite Element model for Geotechnical Application Version 2012.01, Plaxis BV, Delft, The Netherlands.

Potts, D.M. and Fourie, A.B. (1984). The behavior of a propped retaining wall: results of a numerical experiment. Geotechnique, 34(3), 383-404.

Potts, D.M. and Fourie, A.B. (1985). The effect of wall stiffness on the behavior of a propped retaining wall. Geotechnique, 35(3), 347-352.

USS Steel Sheet Piling Design Manual, 1984. United States Department of Transportation/Federal Highways Administration, Washington, D.C.

© 2016 Deep Foundations Institute

DEEP FOUNDATION SUPPORT FOR THE ICONIC NEW YORK WHEEL

Quadri Owokoniran, Langan Engineering, Parsippany, NJ, USA, (973)560-4900, qowokoniran@langan.com
Satyajit Vaidya, P.E., Langan Engineering, Parsippany, NJ, USA, (973)560-4573, svaidya@langan.com
Rudolph Frizzi, P.E., G.E., D.GE., Langan Engineering, Parsippany, NJ, USA, (973)560-4703, rfrizzi@langan.com

ABSTRACT

This paper presents a case history in the design and construction of high-capacity drilled shafts for the iconic New York Wheel presently being constructed along the St. George area waterfront in northern Staten Island, New York. Although the site is located in an area that offers views of the Statue of Liberty, the Manhattan skyline, and New York Harbor, the variable and challenging subsurface conditions at the site and the structural loading requirements for Wheel erection and service conditions presented geotechnical design and construction challenges. The paper focuses on site and subsurface conditions, drilled shaft design and construction details, results of Osterberg-cell and lateral load testing, and load test data analysis and evaluation.

PROJECT DESCRIPTION

The proposed 630-foot (190 m) -tall New York Wheel (the Wheel) is projected to be one of the tallest observation wheels in the world. Upon completion, the Wheel will be capable of carrying over 1,400 passengers in its 36 capsules. The Wheel site is located along New York Harbor offering views of the Statue of Liberty, the Manhattan skyline, and the New York Harbor; see Fig. 1. The Wheel structure is sited along the waterfront, and served by a 3-story terminal located south of the Wheel in the eastern portion of the site and having a footprint area of about 34,250 sq-ft (3,180 sq-m). A 4-story parking Garage, with a footprint of about 112,840 sq-ft (10,480 sq-m), is to be constructed south of the Wheel in the central and western portions of the site.



Fig. 1. The New York Wheel

SITE AND SUBSURFACE CONDITIONS

The site's close proximity to the New York Harbor presented geotechnical challenges because the site is located in an area that was once beyond the historic shoreline of Staten Island. The site is an about 350,000-sq-ft (32,500-sq-m) parcel generally bounded by the Richmond County Bank Ballpark to the southeast, the 9-11 Memorial to the east, Bank Street to the north and northeast, and Richmond Terrace and an associated retaining wall to the southwest and south. A 50-ft (15-m) -wide New York City Transit Easement, with an active on-grade service area and tracks, is located in the southern portion of the site. See Fig. 2 for site location and approximate location of the Wheel foundation footprint.

Geotechnical subsurface investigations performed at the site consisted of drilled borings, seismic and piezometric cone penetrometer test (CPT) probes, and ReMi shear-wave-velocity measurements. The site subsurface conditions generally consist of successive strata of typically loose to medium dense surficial sandy fill with miscellaneous debris, a 5-to-50-ft (1.5-to-15-m) -thick soft to very soft clay and silt stratum (inferred former river bottom deposits) that increases in thickness towards the New York Harbor, natural dense to very dense sandy and gravelly soils with varying amounts of silt and clay, and weathered Serpentinite bedrock. The bedrock was encountered at depths ranging from about 10 ft (3 m) below existing grade in the southeastern portion of the site to about 80 ft (24 m) below existing grade in the northern portion of the site. Within the Wheel foundation footprint, depth to bedrock ranged from about

© 2016 Deep Foundations Institute

30 to 65 ft (9 to 20 m) below site grade. The top several feet of weathered bedrock was relatively soft, such that it was possible to advance the borings through it using conventional mud-rotary drilling techniques with SPT N-values obtained. Rock coring techniques were used to advance the borings through more competent bedrock. Groundwater was encountered between about el 0 to 2 (all elevations in this paper refer to the NAVD88 datum), which generally corresponds to the water level in the nearby New York Harbor. See Fig. 3 for a generalized site subsurface profile.

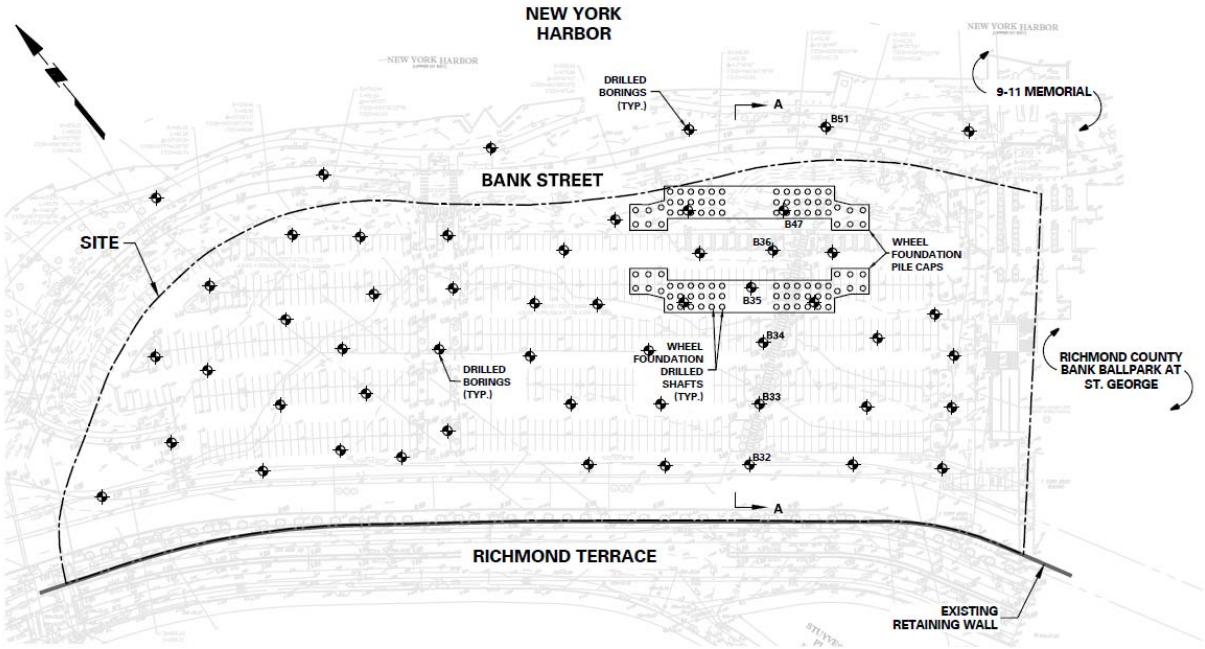


Fig. 2. Location plan

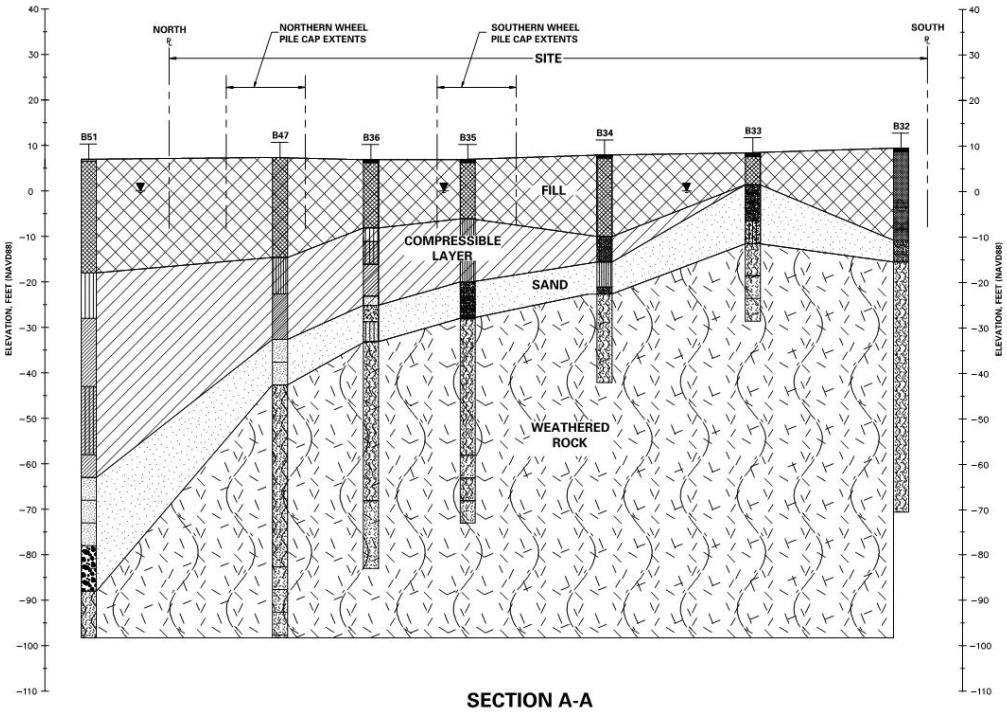


Fig. 3. Generalized site subsurface profile

© 2016 Deep Foundations Institute

Laboratory soil testing performed for the project consisted of soil grain size analysis, moisture content analysis, index property testing, and UU tri-axial testing. Laboratory testing of intact bedrock samples consisted of Brazilian Splitting Tensile Tests and Unconfined Compression Tests.

As part of the geotechnical investigation, liquefaction and lateral spreading potential was assessed. The liquefaction assessment followed 2014 New York City Building Code (NYCBC) seismic design requirements and consisted of a comparison of the Cyclic Stress Ratio to the Cyclic Resistance Ratio of the underlying soils within the top 50 ft (15 m) below ground surface. This assessment indicated probable liquefaction of loose sandy soils encountered in the borings performed in the northern portion of the site, including those within the Wheel footprint, under the NYCBC-defined seismic event. A site-specific seismic study was therefore performed in accordance with the NYCBC requirements and seismic design parameters were developed for use in the geotechnical and structural analysis. The site-specific study indicated that excess pore-water pressure ratios (r_u) of up to 0.8 could be generated in the liquefaction-susceptible soils during the NYCBC-defined seismic event.

An analysis was performed to evaluate the potential for liquefaction-induced soil lateral spread (Youd et al. 2002). Because of the relatively gently sloping waterfront and river bottom grades, the calculated lateral spread values were negligible in magnitude (less than 0.25 inch) for the NYCBC-defined seismic event. Therefore, considering the Wheel foundation was to be located at least 50 ft (15 m) away from the shoreline, lateral spreading was not considered during Wheel foundation design.

WHEEL FOUNDATION DESIGN

The Wheel structure is designed to be supported on four legs, with the associated drive units supported on four restraining towers. Due to the presence of potentially liquefiable soils and compressible former river bottom deposit soils beneath the Wheel footprint, and considering the significant Wheel erection and service loads, the Wheel structure was designed to be supported on four 11-ft (3.5-m)-thick reinforced concrete caps, each supported on 24 drilled shafts socketed into the Serpentinite bedrock. Each drilled shaft was designed to resist a maximum compression service load of 1,000 tons (9.8 MN), a maximum service uplift load of 540 tons (5.3 MN), and a maximum service lateral load of 155 tons (1.5 MN). Due to site constraints, the drilled shafts had to be spaced at a maximum center-to-center spacing of 11 ft (3.5 m). The Wheel design engineer specified a maximum lateral deflection tolerance of 1 inch (25 mm) under service loading conditions.

Drilled Shaft Structural Design

The drilled shaft casing and cased-zone reinforcement design were governed by lateral capacity and stiffness considerations. Lateral analysis considered the 20-to-50-ft (6-to-15 m)-thick strata of soft compressible soils, liquefaction-susceptible sandy soils, and cohesive soils susceptible to pore-pressure build-up and loss of shear strength. In addition, group effects were considered given the relatively close drilled shaft spacing. The lateral analysis was performed using commercially available L-PILE computer software program (Isenhower and Wang, 2015). The soil and bedrock properties used in the L-PILE model were estimated from on-site boring and laboratory test data and correlations published in the geotechnical literature (Kulhawy and Mayne, 1990).

When analyzing the lateral behavior of the drilled shafts under seismic loading, liquefaction and cyclic softening effects were considered. Loss of strength of the liquefaction-susceptible sandy soils was modeled using p-multipliers (Ashford et al. 2011) estimated using recommendations by the California Department of Transportation (Caltrans 2012) based on a range of back-calculated p-multipliers obtained from several load tests performed in liquefied soils. For soils undergoing partial liquefaction, the p-multipliers were scaled considering the site-specific seismic study results by dividing by 0.8. The strength loss in the soft compressible soils due to cyclic softening was determined by calculating the expected residual undrained shear strength of these soils during a NYCBC seismic event (Idriss and

© 2016 Deep Foundations Institute

Boulanger 2007 and 2008). The procedure (Idriss and Boulanger 2007) uses equivalent clean-sand-corrected SPT-N values to estimate residual strength; a residual shear strength value of 85 psf (4 kPa) was calculated and used in the analysis. Group effects were considered using p-multipliers recommended by AASHTO (AASHTO, 2008) for the lead, second, and trailing rows of shafts. When considering the combined effects of partial liquefaction and group conditions, effective p-multipliers for lateral analysis were obtained.

The drilled shaft reinforcement details in the cased and bedrock socket section were subsequently designed using the derived geotechnical loadings and to satisfy the allowable material structural stress requirements of the 2014 NYCBC.

Drilled Shaft Bedrock Socket Lengths

Given the bedrock variability, multiple approaches were used to develop preliminary ultimate side shear values for initial design. The methods utilized included: the Beta method (FHWA, 1999), the Modified Beta method (FHWA, 2010), and the Horvath and Kenny method considering weathered rock (FHWA, 2010). The initial ultimate side shear values ranged from 7.2 ksf (345 kPa) to 22.3 ksf (1,067 kPa), with the Beta method giving the lower value, and the Horvath and Kenny method giving the higher value. For initial sizing of the test drilled shafts, an ultimate unit side shear of 14.8 ksf (708 kPa) was used.

Drilled Shaft Design Summary

Based on above design considerations, the recommended drilled shaft design consisted of a 60-in (1.5-m) OD x 1-in (25.4-mm)-thick, minimum 36 ksi (248 MPa) steel casing extending a minimum of 5 ft (1.5 m) into NYCBC Class 1d or better rock; a 30-in (0.75 m)-diameter, minimum 35-ft (11-m)-long rock socket extending below the casing; and minimum 5,000 psi (34.5 MPa) concrete fill. The recommended drilled shaft reinforcement consisted of 24 full-length #18 Grade 75 bars, with nine additional #18 bars in the rock socket and extending at least 10 ft (3 m) above and below the casing tip.

A drilled shaft design alternate consisting of a 67-in (1.7-m)-OD x $^{15}/_{16}$-inch (24-mm)-thick, 42 ksi (290 kPa) steel casing, reinforcement consisting of a single full-length W18X158, 42 ksi (290 kPa) steel core beam, and a 35-inch (0.9-m)-diameter rock socket was considered during the Contactor submittal review process. The alternate drilled shaft design exceeded the structural axial and bending capacity of the originally specified section. The Contractor proposed a mechanical splice detail for the core beam to transfer the design compression, uplift, and lateral loads in the core beam across the splice. However, since the mechanical splice was not designed to provide substantial moment resistance, it was required to be placed at least 5 ft (1.5 m) below the casing bottom.

TEST SHAFT INSTALLATION

Four test drilled shafts were installed in two diagonally opposite pile caps. One of the test shafts, Shaft 37, was installed in the northeastern portion of the Wheel footprint, where the soft compressible soils were expected to be relatively thicker and top of rock was expected to be relatively deeper. A second test shaft, Shaft 81, was installed in the southwestern portion of the Wheel footprint, where top of rock was expected to be relatively shallower. These two test shafts were subject to Osterberg-cell (O-cell) load testing to simultaneously verify the test shafts' compression and uplift load-carrying capacities. The remaining two test shafts, Shafts 38 and 82, were installed immediately adjacent to the O-cell-tested shafts and subject to lateral load testing. The O-cell-tested shafts were used as reactions during the lateral load tests. The test shafts were installed using a Liebherr LB-44 drill rig. The test shaft construction sequence was as follows:

1. An 84-in (2.1-m)-OD temporary casing was spun to a depth of about 25 ft (7.6 m) below grade.
2. The casing was subsequently cleaned out using a 76-in (1.9 m)-diameter drilling bucket.

© 2016 Deep Foundations Institute

3. The casing was filled with polymer slurry.
4. The 67-in (1.7-m)-OD permanent steel casing was lowered and centralized inside the temporary casing, and advanced at least 5 ft (1.5 m) into NYCBC Class 1d or better rock.
5. The permanent casing was cleaned out using a 5-ft (1.5-m)-diameter auger and drilling bucket.
6. A 39-in (1-m)-OD temporary casing was lowered inside the 67-in (1.7-m) casing and advanced about 2 ft (0.6 m) below the bottom of the 67-in (1.7-m) casing. The 39-in (1-m) casing was centralized inside the 67-in (1.7-m) casing, so it could act as a verticality and alignment guide during rock socket drilling.
7. A 35.5-in (0.9-m)-diameter rock socket was drilled through the 39-in (1-m) casing to the specified tip elevation. Either an auger bucket or a rock auger was used to advance the socket.
8. The 39-in (1-m) casing was removed and any loose sediment at the bottom of the rock socket was removed using a 28-in (0.7-m)-diameter clean-out bucket.
9. After the rock socket was cleaned, a Sonicaliper™ (Loadtest, 2016) was used to obtain a cross sectional profile of the drilled shaft, and confirm that the shaft verticality was within the specified 0.5% of the shaft length and a minimum 35-in (0.9-m)-diameter shaft was constructed throughout.
10. The shaft bottom was observed using a mini-SID (AFT, 2016) to confirm that the amount of sediment present at the bottom of the drilled shaft was no more than 0.5 in (12.7 mm) over at least 50% of the shaft bottom and no more than 1.5 in (38 mm) at any location. If more sediment was observed, the shaft was cleaned again and the mini-SID observation repeated until satisfactory results were obtained. Soundings with a weighted tape measure were also made immediately after each mini-SID observation to calibrate the weighted tape soundings with the observed and measured sediment thickness.
11. After confirming the shaft bottom cleanliness, the W18X158 core beam reinforcement was lowered into the shaft and carefully centralized and oriented. The core beams for the O-cell shafts were instrumented with the O-cell assemblies and the specified number of strain gauges, tell tales, and extensometers. In the laterally load-tested shafts, a manual inclinometer casing and an automated shape array inclinometer casing were installed prior to concrete placement.
12. The test shaft was then tremie-concreted to about 4 ft (1.2 m) above the design cut off elevation.
13. Once the concrete achieved initial set, the annular space between the 67-in (1.7-m) and 84-in (2-m) casings was filled with tremie-placed cement grout, and the 84-in (2-m) casing was removed while the grout was fluid.

See Fig. 4 for photographs taken during drilled shaft installation. The polymer slurry consisted of four primary components identified as SlurryPro CDP, Enhanclt 100, Enhanclt 200 and SlurrpPro MPA. The slurry pH, specific gravity, and sand content were measured within the top, midpoint, and bottom of the drilled shaft at least twice each day during the drilling process and immediately prior to concrete placement to confirm the slurry properties met the minimum requirements established in FHWA GEC-10 (FHWA, 2010). It was noted that softer rock conditions were observed when drilling the rock socket for test Shaft 81 as compared to test Shaft 37. Concrete was placed in the test shafts within 54 hours of start of socket drilling and within 24 hours of socket drilling completion.

© 2016 Deep Foundations Institute

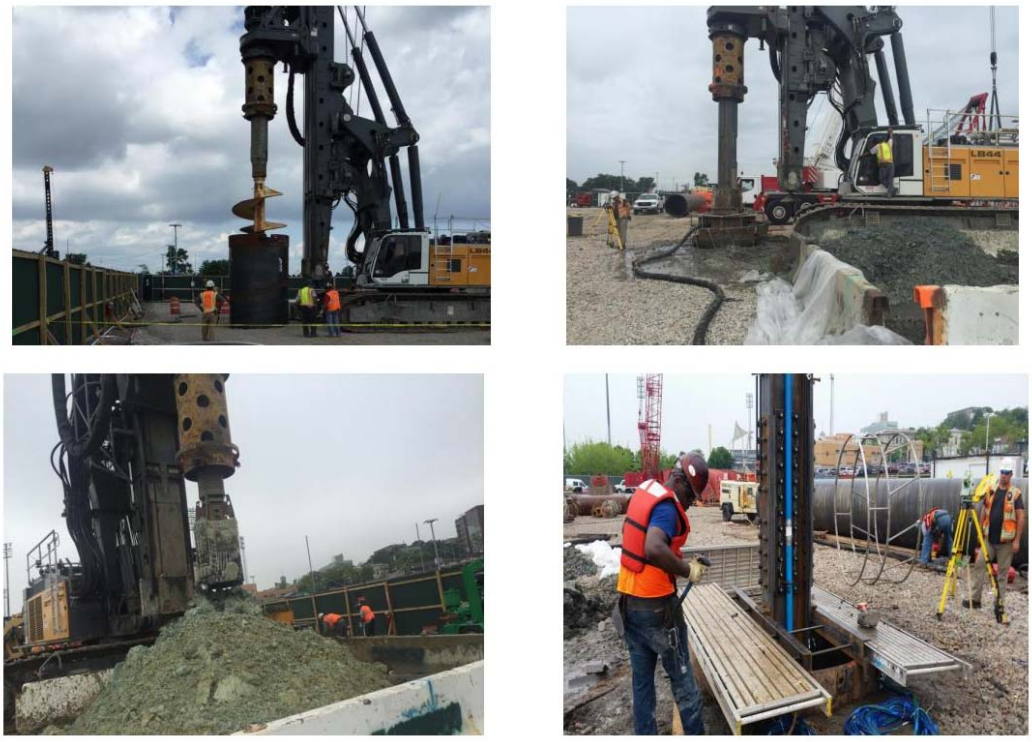


Fig. 4. Drilled shaft installation.

OSTERBERG CELL (O-CELL) LOAD TESTING AND DATA ANALYSIS

O-cell testing

After the compressive strength of concrete placed in the test shafts was confirmed to be greater than the design compressive strength, the O-cell load tests were performed. The O-cell test shafts were instrumented with pairs of sister -bar vibrating-wire strain gages attached to the core beam. In each test shaft, the strain gauges were installed in the rock socket at four specified levels below the O-cell and at six specified levels above the O-cell. In addition, four tell-tales were installed in two pairs in each test shaft to measure shaft deflection; two tell-tales were installed between the top of the test shaft and the top of the O-cell and the other two tell-tales were installed between the bottom of the O-cell and the tip of the test shaft. Refer to Fig. 5 for a schematic showing O-cell and instrumentation locations in test Shaft 37.

The O-cell load tests were performed following the Quick Load Test method specified in ASTM D1143. The O-cell was loaded in twenty equal increments up to a maximum load of 1,133 tons (11.3 MN) in each direction; each load increment was held for 15 minutes and the maximum test load was held for minimum 2 hours or until the rate of shaft deformation extrapolated over 12 hours was less than 0.012 in (0.3 mm). Each load test was unloaded in five equal decrements, with four minutes between each decrement. During each O-cell load test, real-time load, strain, and deformation data was acquired using an automated data-acquisition system and analyzed in real time. See Fig. 6 for the load distribution curves obtained for test Shaft 37.

© 2016 Deep Foundations Institute

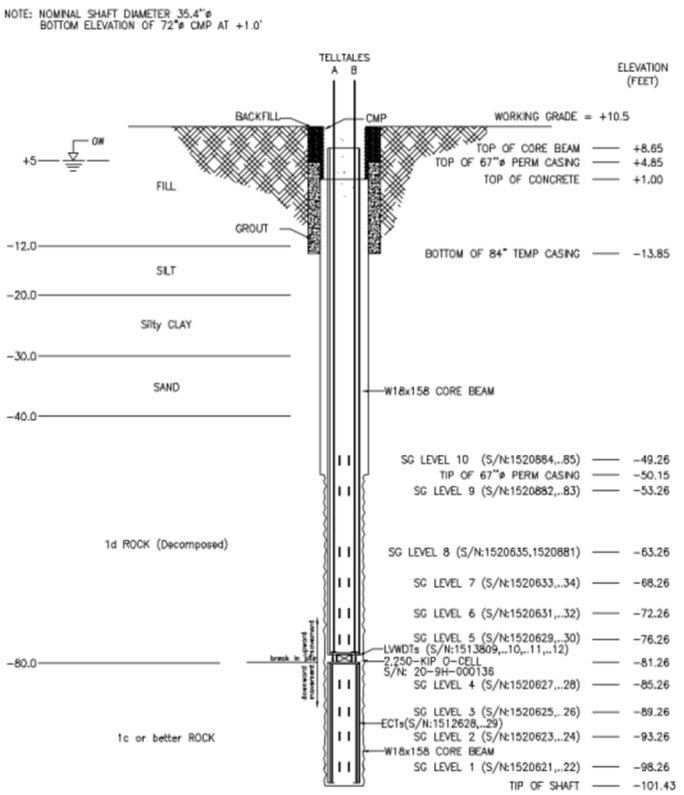


Fig. 5. O-cell and instrumentation locations for test Shaft 37

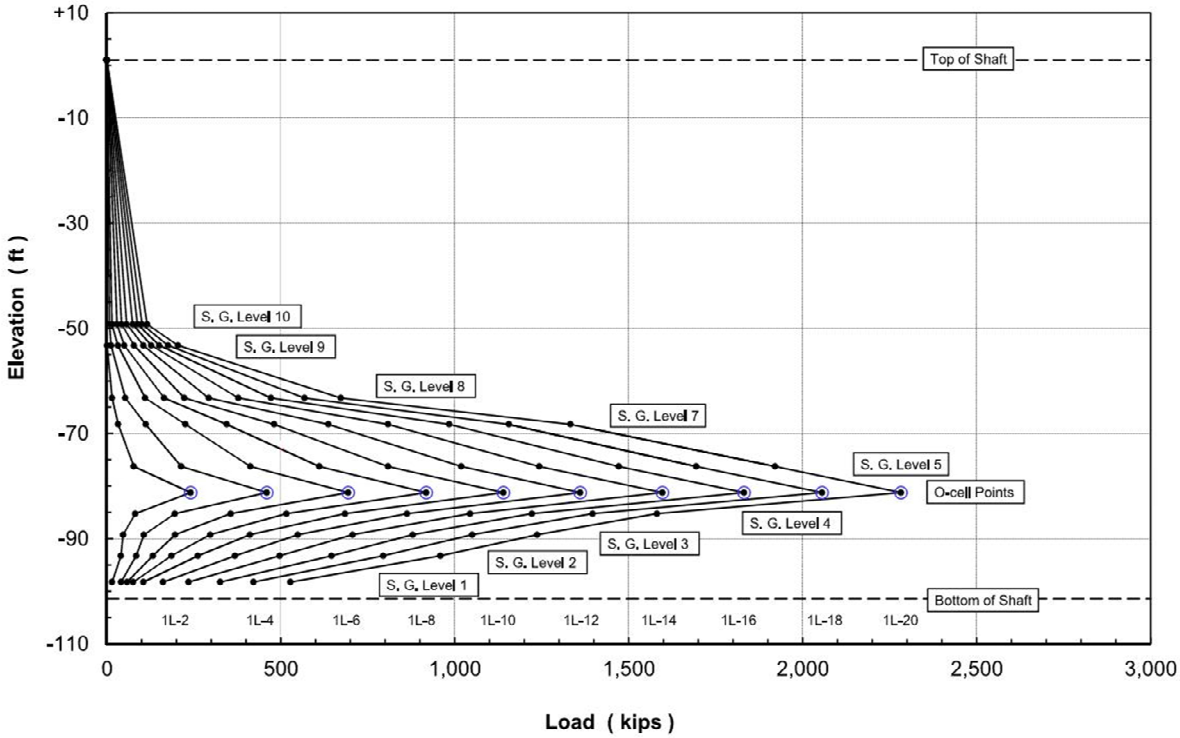


Fig. 6. Load distribution from O-cell load test performed on test Shaft 37

© 2016 Deep Foundations Institute

O-cell Test Data Evaluation

The strain gauge and tell-tale data from the O-cell tests was evaluated to determine the mobilized side shear values in compression and uplift, and to evaluate appropriate ultimate and allowable parameters for use in design.

The mobilized unit side shear resistance along the shaft socket zone between adjacent levels of strain gauges was calculated by dividing the difference in the transferred load at the two strain gauge levels by the socket circumferential area between the strain gauge levels. A unit side shear mobilization curve was determined for each socket zone by plotting the mobilized side shear values against the applied test load. From the shapes of the mobilized unit side shear plots for both test shafts, it was determined that the ultimate side shear was not mobilized during O-cell load testing. Considering the fractured and weathered nature of the Serpentinite rock, an analysis was therefore performed using normalized load transfer curves for deflection-softening behavior (FHWA, 1999) to extrapolate ultimate unit side shear in each rock socket zone in each test shaft.

Figure 7 presents calculated ultimate unit side shear resistance values from the O-cell testing for the different rock socket zones versus depth in the upper portions of the rock sockets where the rock was observed to be relatively more weathered. A range in the ultimate unit side shear values calculated based on the Beta procedure (FHWA, 1999) and the Modified Beta procedure (FHWA, 2010) are shown. For comparison, a criterion by Cole and Stroud (Cole and Stroud 1977) is also shown. SPT resistance values ranging between 60 blows/foot and 100 blow/foot were used in the Beta procedure calculation, and SPT resistance values ranging between 60 blows/foot and 300 blows/foot (equivalent extrapolated SPT N-value of 25 blows/inch) were used in the Modified Beta and Cole and Stroud procedure calculations. For the upper portion of the rock socket, the ultimate unit side shear values calculated based on O-cell data compare well with the range of values calculated using the Modified Beta procedure. There was considerable variability in the Cole and Stroud procedure results, and in most cases the procedure less conservatively predicted side shear.

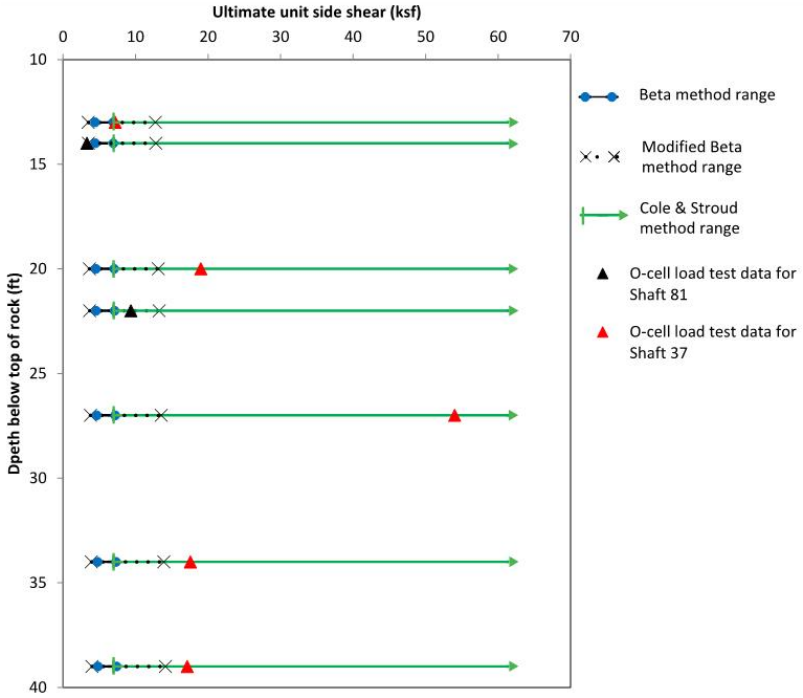


Fig. 7. Calculated Ultimate unit side shear vs. depth

© 2016 Deep Foundations Institute

Figure 8 presents calculated ultimate unit side shear resistance values for the different rock socket zones in relatively less weathered rock versus the RQD values measured at respective depths in the nearest on-site borings. This plot also shows the ultimate unit side shear values calculated using the Horvath and Kenny procedure (FHWA, 2010) and site-specific measured rock unconfined compressive strength. As expected, the load test data shows generally increasing ultimate unit side shear with increasing RQD. However, it appears for the materials encountered at this site, the Horvath and Kenny procedure (FHWA, 2010) tends to more conservatively predict side shear at higher RQD.

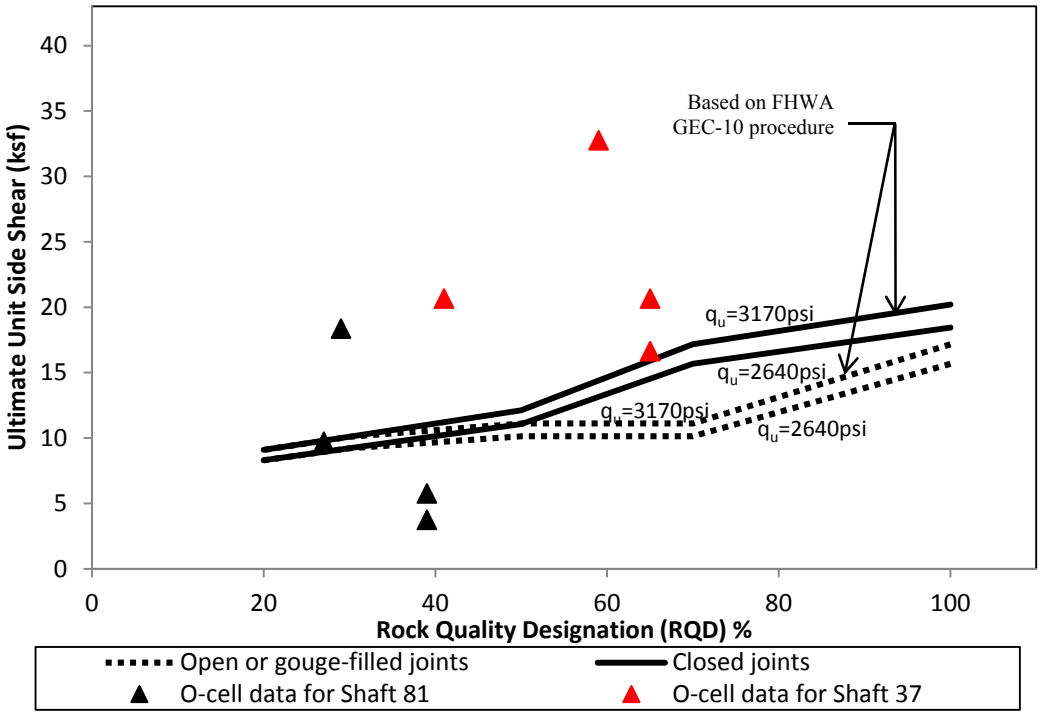


Fig. 8. Calculated ultimate unit side shear vs. RQD

Mobilized end bearing values of about 25 ksf (1,197 kPa) and 30 ksf (1,435 kPa) were measured in test Shafts 37 and 81, respectively, at about 0.05 in (1.3 mm) deflection. In test Shaft 81, a unit end bearing of 170 ksf (8140 kPa) was mobilized at a deflection of 0.15 inch (3.8 mm). A comparison of the load test data to the FHWA 2010 procedure for estimating end bearing in cohesionless soil indicates that the FHWA 2010 procedure conservatively estimates ultimate end bearing for the weathered rock encountered at this site.

The ultimate unit side shear values observed in the O-Cell tests capture the variability in the Serpentinite bedrock at this site, and are consistent with the observations during rock socket drilling for the test shafts. A comparison of the observed values to the range in theoretically calculated values presented in Figs. 7 and 8 indicates: (1) the bedrock in the upper portions of the rock sockets, in which relatively softer drilling conditions were observed, tended to behave more like a cohesionless intermediate geo-material, and (2) the bedrock in the lower portions of the rock sockets, in which relatively harder drilling conditions were observed, tended to behave more like rock material. Drilled shaft rock sockets were sized to address the specific bedrock depths, drilling conditions, individual design compression and uplift loading, and allowable side shear and end-bearing.

© 2016 Deep Foundations Institute

LATERAL LOAD TESTING AND DATA ANALYSIS

Lateral Load Testing

Lateral load tests were performed on test Shafts 38 and 82 installed adjacent to O-cell-instrumented test Shafts 37 and 81, respectively. The lateral load tests were performed following cyclic loading procedures outlined in ASTM D3966. The ground surface within 10 ft (3 m) of the test and reaction shafts was lowered to 1 ft (0.3 m) below the production shaft cut-off elevation, in order to closely simulate the service conditions. Each lateral-load-tested shaft was instrumented with an automated slope inclinometer array and a manual-read slope inclinometer to a depth of about 60 ft (18 m) below the top of the shaft, to facilitate shaft lateral deflection measurements with depth. The test shafts were laterally loaded until sufficient amount of shaft deflection was measured immediately below the bottom of the liquefaction-susceptible soil layer. The test Shafts 38 and 82 were loaded cyclically to maximum test loads of about 195 tons (1.9 MN) and 230 tons (2.3 MN), respectively. At test Shaft 38, a maximum lateral deflection of 2 in (51 mm) was measured near the ground surface, and a lateral deflection of about 0.5 in (12.7 mm) was measured at the bottom of the liquefaction-susceptible soil layer about 25 ft (7.6 m) below lateral load application level. At test Shaft 82, a maximum lateral deflection of 2.5 in (63.5 mm) was measured near the ground surface, and a lateral deflection of about 0.6 in (15.2 mm) was measured at the bottom of the liquefaction-susceptible soil layer about 14 ft (4.3 m) below lateral load application level. Negligible shaft deflections were measured for both test shafts about 10 ft (3 m) below top of rock.

Data Analysis and Evaluation

The lateral load test data for each test shaft was analyzed using the following procedure to study the expected production shaft behavior under service conditions:

Step 1: The initial LPILE analysis model for the drilled shafts was re-analyzed for a single drilled shaft under free head condition using soil and rock properties used in the initial lateral analysis; the modeled shaft was loaded to the actual maximum lateral test load. Soil and rock parameters in the initial LPILE model were refined and the analysis repeated until the lateral deflection vs. depth from the revised LPILE model matched the load test measurements.

Step 2: The LPILE model was further refined to account for service conditions by modeling head fixity, applying a $^{1}/_{16}$-in (1.6 mm) corrosion loss around the shaft's steel casing, including the previously discussed p-multipliers representing group effects and soil shear strength loss due to liquefaction and seismically-induced cyclic shear softening.

The results of the above analysis indicated the drilled shafts would be capable of resisting the anticipated individual lateral loads, while maintaining shaft head deflections under the maximum allowable deflection limit of 1 in provided by the Wheel design engineer.

PRODUCTION SHAFT INSTALLATION

All four test shafts were incorporated into the foundation as production shafts; the O-cells and all instrumentation tubing were grouted in place using minimum 5,000 psi (34.5 MPa) grout. Production shafts were installed using the same means and methods used for construction of the successfully-tested O-cell and lateral test shafts. The drilled shaft installation work was subject to quality assurance observation and verification. The following production shaft installation criteria were followed based on observations during test shaft installation and the results of the O-cell load tests:

- Rock socket drilling times were carefully observed to confirm they were in agreement with correlated specific rock socket material and design side shear.

© 2016 Deep Foundations Institute

- The drilled shafts were typically concreted within 54 hours of start of socket drilling work, and within 24 hours of rock socket drilling completion. In isolated cases when the Contractor was unable to meet the above rock socket exposure requirements, the subject shaft's rock socket was roughened using a slightly larger diameter drilling bucket.

- In order to utilize the end-bearing, cleanliness of the socket bottom was verified prior to concrete placement.

The installation rate for the production shafts was about one drilled shaft per rig per day.

CONCLUSIONS

The following conclusions were drawn from the drilled shaft design, load testing, and construction experience on this project.

- The bedrock in the upper portions of the rock sockets, in which relatively softer drilling conditions were observed, tended to behave more like a cohesionless intermediate geo-material. The bedrock in the lower portions of the rock sockets, in which relatively harder drilling conditions were observed, tended to exhibit behavior more comparable to rock-like material.

- For bedrock behaving like a cohesionless intermediate geo-material, the ultimate unit side shear values calculated based on O-cell data compare well with the range of values calculated using the Modified Beta procedure (FHWA, 2010). It however appears that for the materials encountered at this site, the Cole and Stroud procedure tends to more variably and less conservatively predict side shear.

- For relatively less weathered bedrock, the load test data shows generally increasing ultimate unit side shear with increasing RQD. However, it appears for the materials encountered at this site, the Horvath and Kenny method (FHWA, 2010) tends to more conservatively predict side shear at higher RQD.

- A comparison of the load test data to the FHWA 2010 procedure for estimating end bearing in cohesionless soil indicates that the FHWA 2010 procedure conservatively estimates ultimate end bearing for the weathered rock encountered at this site.

- Given the variable rock conditions at the site, careful measurement and recording of socket drilling resistance was emphasized as part of the production drilled shaft quality control and quality assurance program requirements.

REFERENCES

AFT, 2016. Miniature Shaft Inspection Device (mini-SID). http://www.testpile.com/#!services/aboutPage.

American Association of State Highway and Transportation Officials, 2008. AASHTO LRFD Bridge Design Specifications. Washington, D.C., 160 pp.

Ashford S.A., Boulanger R.W., Brandenberg S.J., 2011. Recommended Design Practice for Pile Foundations in Laterally Spreading Ground. Pacific Earthquake Engineering Research Center (PEER) 2011/04, 68 pp.

California Department of Transportation, 2012. Guidelines on Foundation Loading and Deformation Due to Liquefaction Induced Lateral Spreading, 44 pp.

Cole K.W., Stroud M.A. (1977). Rock Socketed Piles at Coventry Point, Market Way, Coventry. Piles in Weak Rock, Institution of Civil Engineers, London, 47-62 pp.

© 2016 Deep Foundations Institute

FHWA, 1999. Drilled Shafts: Construction Procedures and Design Methods, FHWA Publication No. IF-99-025.

FHWA, 2010. Drilled Shafts: Construction Procedures and LRFD Design Methods, FHWA Publication No. NHI-10-016, FHWA GEC-10, 972 pp.

Idriss I.M., Boulanger R.W., 2008. Soil Liquefaction During Earthquake, Earthquake Engineering Research Institute (EERI), 243 pp.

Idriss I.M., Boulanger R.W., 2007. Residual Shear Strength of Liquefied Soils, Proceedings of the 27th USSD Annual Meeting and Conference, Modernization Optimization of Existing Dams and Reservoirs.

Isenhower W.M., Wang S.T., 2015. Technical Manual for LPILE 2015. Ensoft, Inc.

Kulhawy F.H., Mayne P.W., 1990. Manual on Estimating Soil Properties for Foundation Design. Electrical Power Research Instirute, EL-6800, Research Project 1493-6, 308 pp.

Loadtest, 2016. A calipering Device for Deep Foundation Excavations. http://www.sonicaliper.com/soni.

Youd T.L., Hansen C.M., Bartlett S.F, 2002. Revised MLR Equations for Predicting Lateral Spread Displacement, Proceedings of the 7th US-Japan Workshop on Earthquake Resistant Design of Lifefline Facilities and Countermeasures Against Soil Liquefaction, Washington, Seattle.

© 2016 Deep Foundations Institute

DESIGN, CONSTRUCTION CHALLENGES AND QUALITY CONTROL OF A DEEP SOIL MIXING SYSTEM FOR WATERFRONT SLOPE STABILIZATION

Yan Lap J. Kan, GE, CEG
ENGEO Incorporated, San Ramon, CA, USA (925) 866-9000, jkan@engeo.com

ABSTRACT

A waterfront stabilization system consisting of Deep Soil Mixing (DSM) columns, vinyl sheet pile fascia, and concrete flood walls supported on shallow footings was designed and constructed for a high-density waterfront development in Northern California. The project site is underlain by soft, compressible organic soil locally known as Bay Mud that has been capped with loose sand and imported fill. The waterfront stabilization system constructed at the site mitigates liquefaction, consolidation settlement and seismic potential slope deformation along the waterfront; the system was designed to reduce lateral displacements to tolerable amounts for the proposed structures. This paper presents the general design methodologies, construction challenges and quality control of this waterfront stabilization system.

Keywords: waterfront retaining structure, deep soil mixing, vinyl sheet pile, compressible soil, lateral spreading, liquefaction

INTRODUCTION

Urban development in Northern California is fueling innovations in geotechnical engineering as more complex sites are developed. ENGEO Incorporated introduced a deep soil mixing technology from Japan to the US and designed a waterfront stabilization system for a high density waterfront development project in Redwood City, California. The approximately 12½-acre project site, as shown on Fig. 1, is surrounded by water on three sides, with an inner marina at the center of the site.



Fig. 1. Aerial Photograph of the Project Site

The project site is located in the seismically active San Francisco Bay Area in California. The San Andreas Fault, the Monte Vista-Shannon Fault, the Hayward Fault and the San Gregorio Fault are major active faults located within 25 miles of the site. Once a former marshland with a major slough until the late 1950s, the site was reclaimed by placing imported fill over the native compressible clay deposits, locally known as Bay Mud.

© 2016 Deep Foundations Institute

SITE CONDITIONS

Two phases of geotechnical explorations were performed. The first phase of geotechnical exploration consisted of deep borings and Cone Penetration Tests (CPT) extending to a maximum depth of 120 feet (36.6 meters) below the ground surface (bgs). The explorations showed the project site was capped with 5 to 7 feet (1.5 to 2.1 meters) of fill over 13 to 20 feet (4 to 6 meters) of Bay Mud. Concrete and brick fragments were encountered within the surficial fill layer. Below the Bay Mud, potentially liquefiable medium dense sand deposits approximately 5 to 8 feet (1.5 to 2.4 meters) thick were encountered. Below the sand, we encountered stiff to very stiff alluvial deposits that extended to the terminal depths of the borings and CPTs.

The second phase of geotechnical exploration consisted of a geophyscial survey utilizing multi-channel analysis of surface waves (MASW) to estimate the limits and depth of the historic slough. Shallow test pits were also excavated to further characterize the surficial fill. Figure 2 shows the locations of the geotechnical explorations as well as cross-section locations used for waterfront slope stability analyses.

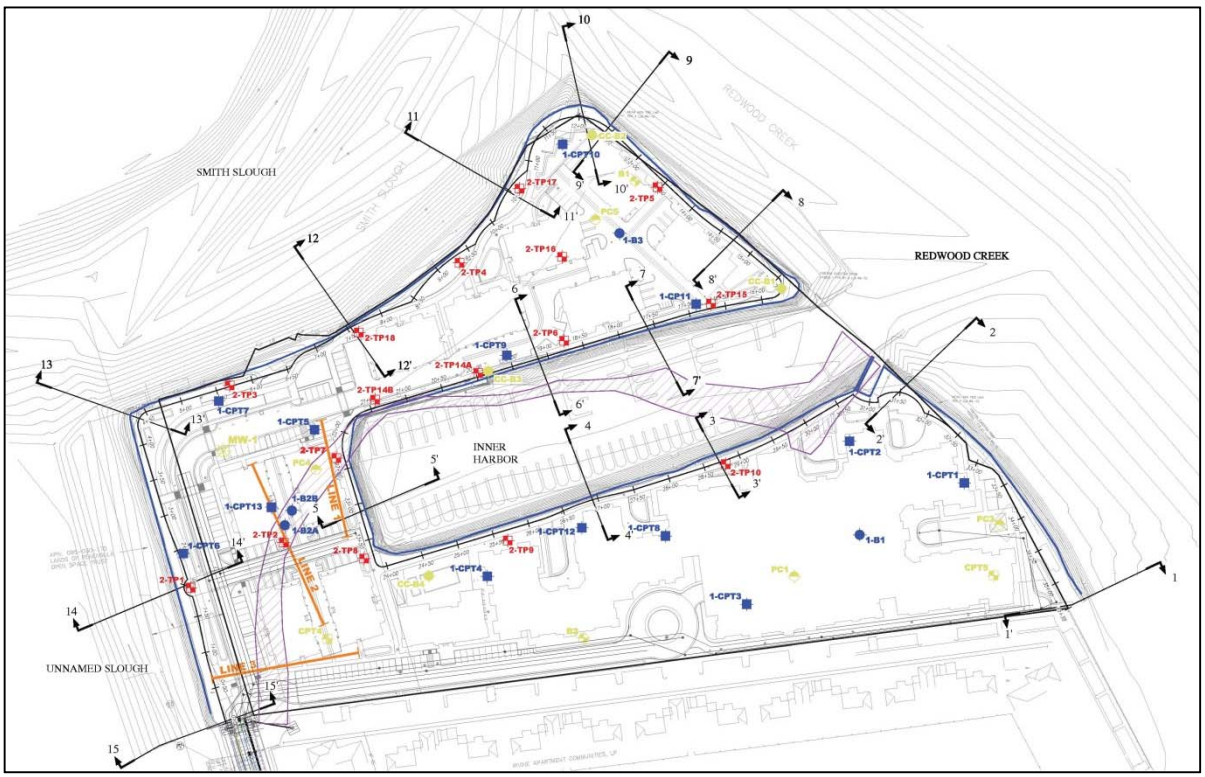


Fig. 2. Geotechnical exploration plan showing locations of 15 cross sections used for waterfront slope stability analyses

WATERFRONT SLOPE STABILITY ANALYSIS

Slope stability analysis on 15 cross-sections along the project's waterfront were performed with consideration of the seismic design criteria and ground motions set forth in the 2013 California Building Code (CBC). Bathymetry data of the surrounding water channels and the proposed future filling of the area was used to develop the geometric cross-sections for limit-equilibrium stability analyses. Under static conditions, our preliminary stability analyses showed waterfront factors of safety (FS) greater than 2.

© 2016 Deep Foundations Institute

To model seismic conditions for the waterfront slopes, we performed pseudo-static and Newmark Displacement analyses in accordance with California Geologic Survey Special Publication 117A. The potentially liquefiable sands below the Bay Mud were modeled with liquefied residual undrained strength correlations presented by Olson and Stark (2002). The 2013 CBC mapped "Maximum Considered Earthquake" (MCE) Geometric Mean peak ground acceleration (PGA_M) for this site is 0.571g; this seismicity is predominantly governed by a magnitude 7.9 earthquake generated from the nearby San Andrea Fault. Our pseudo-static analyses indicated that under seismic loading, the waterfront slope FS falls below 1.0. Using the simplified methods outlined in Bray & Travasrou (2007), we calculated lateral seismic deformations under these conditions to be in the range of 10 to 30 inches. It is important to note that the Bray & Travasrou's simplified methods are only indices of expected seismic performance and are not intended to predict the actual slope displacement amount or the location of displacement. Supplemental pseudo-static analysis indicated that when the unimproved waterfront slope was flattened to a 6:1 gradient, the FS increased to above 1.0.

EVALUATION OF WATERFRONT EDGE CONTAINMENT SYSTEMS

To mitigate seismic shoreline deformation, waterfront edge containment systems such as installation of steel sheet pile bulkheads, installation of closely spaced auger-cast pin piles, as well as interlocking deep soil mixing (DSM) were considered. With 3,500 linear feet (1.1 kilometers) of waterfront shoreline that had to be mitigated and the high steel price at the time of project design, steel sheet piles were considered less economical than auger-cast pin piles and DSM. An construction of auger-cast pin pile system was considered too long for the project schedule, especially considering downtime due to hole caving and casing installation. As a result, an interlocking DSM approach was selected as the preferred alternative.

A waterfront edge containment system of DSM columns provided the following benefits to this project:

- The project site was planned to be raised by 5 feet (1.5 meters) to maintain the site above future sea-level rise. DSM spoils generated were used as engineered fill to raise site grades, which lowered total construction costs by reducing the amount of expensive import soil.

- The DSM edge containment system consisted of interlocking DSM columns and panels that acted as a below-grade gravity wall to resist potential seismic lateral forces. This allowed shallow foundations with higher bearing capacity to be used near the waterfront, reducing foundation construction costs.

- The DSM edge containment system reduced the potential lateral deformations to tolerable amounts for the structures and improvements planned within the project site.

DESIGN METHODOLOGY OF THE DSM SLOPE STABILIZATION SYSTEM

The waterfront slope stabilization system includes construction of a continuous DSM edge containment system along the 3,500-foot long waterfront shoreline. The DSM system acts as a below-grade gravity retaining structure resisting both static and seismic loads. A wet-mixing method was used to blend the soils with a slurry of cement and/or binder. This method increases the strength of the existing soft clay and liquefiable sands along the waterfront. In addition, the treated soil will not consolidate or compress under new loads imposed by new fills.

Undrained soil strengths based on in-situ tests, laboratory test results of soil samples, and loading history of the project site were used to design the DSM system. In addition, bench-scale laboratory tests on Bay Mud samples were performed by mixing target ratios of water and cement into the soil samples to achieve

© 2016 Deep Foundations Institute

a minimum 28-day compressive strength of 150 pounds per square inch, psi (1034 kilopascal, kPa). Since bench-scale laboratory testing was performed in a controlled environment by inserting higher mixing energy, a FS of 5 was applied to the laboratory test results when evaluating the appropriate mix design.

We performed internal and external stability analyses in accordance with design procedures provided in the Federal Highway Administration Design Manual for Deep Mixing for Embankment and Foundation Support (FHWA, 2013). We augmented the FHWA procedure by applying seismic soil and inertial loads to the slope stability analyses model. The seismic design methodology was conducted consistent with the National Cooperative Highway Research Program Report 611 (NCHRP_611) "Seismic Analysis and Design of Retaining Walls, Buried Structures, Slopes and Embankments" (2008). The design of the DSM buttress consisted of the following stability evaluations.

Slope stability

The critical failure surfaces and corresponding factor of safety of the DSM system, referred to as a DSM buttress herein, were evaluated. Three modes of failure were considered under seismic loading conditions, with potential sliding surfaces:

1) Passing beneath the DSM buttress
2) Passing through the DSM buttress
3) Passing partially through and partially below the DSM buttress

A limited equilibrium slope stability analysis using the analytical software (Slide) was performed to model potential failures under seismic conditions. A minimum FS of 1.1 was considered acceptable. Based on California Geologic Survey Special Publication 117A and the simplified method of Blake et. al, (2002), a factored peak horizontal ground acceleration of 0.24g was applied to pseudo-static models to simulate a deformation threshold of 2 inches (5 centimeters). Loading from proposed buildings was applied onto the top of the DSM buttress. The passive resistance loading on the outboard side of the DSM buttress was modeled as a seismically deformed 6H:1V slope. Figure 3 illustrates one of the pseudo-static slope stability analysis output of the DSM buttress model.

Combined overturning and bearing capacity

The overturning and bearing capacity of the DSM buttress was also evaluated in accordance with the FHWA guidelines. Furthermore, we applied an inertial loading on the DSM buttress that was a function of seismic ground motion and weight of the buttress. A FS of 1.1 was applied in the determination of the active loading forces. In addition, we also applied load combinations that were consistent with Section 1807.2.3 of the 2013 CBC.

Crushing of the deep mixed shear walls at the outside toe

FHWA guidelines recommend evaluating the risk of crushing at the outside toe of the DSM buttress where the deep mixed ground overlies a hard bearing stratum. This is because the lateral loads applied on the DSM buttress could produce toe pressures that exceed the capacity of the deep mixed ground. Since lateral seismic earth pressures and inertial force of the DSM buttress were applied to the DSM buttress, we evaluated the risk of crushing to achieving a minimum FS of 1.1.

© 2016 Deep Foundations Institute

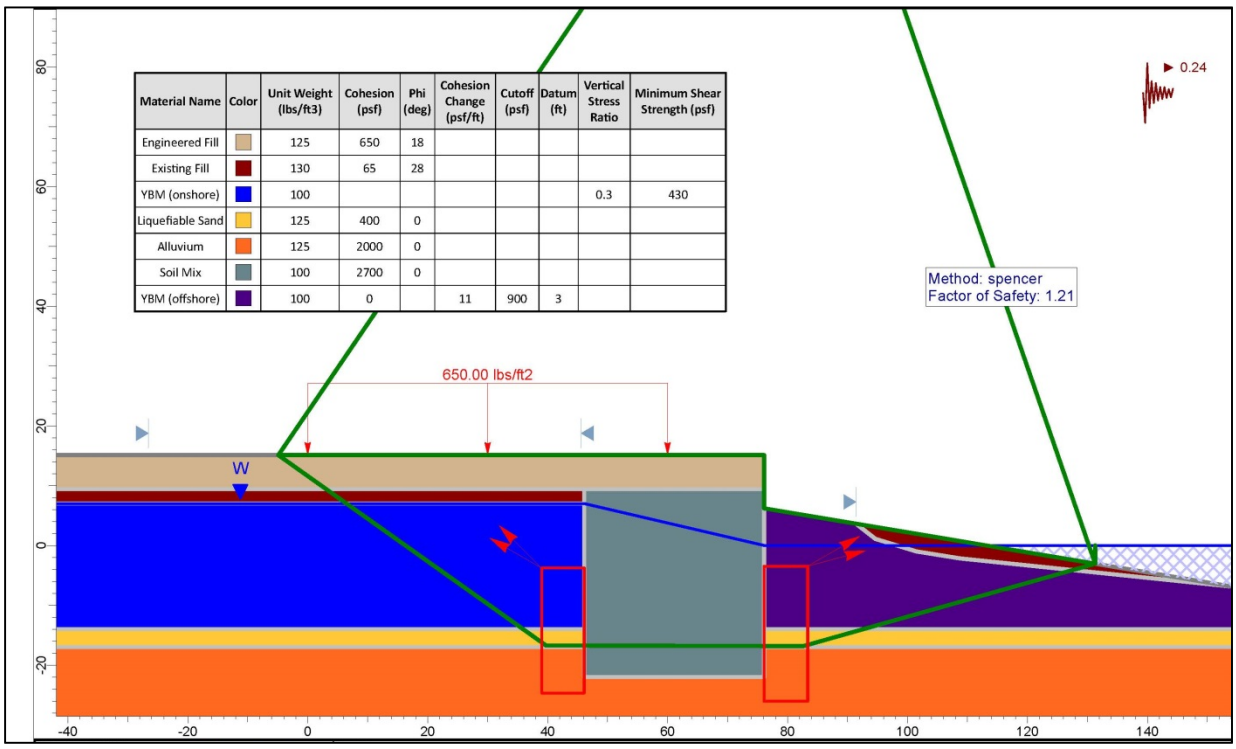


Fig. 3. Pseudo-static Slope Stability Analysis Output of the DSM Buttress Model

Shearing on vertical planes in the deep mixed shear walls

If the overlap between adjacent DSM columns is insufficient, the DSM panels and buttress wall may experience racking-like failure. For this evaluation, we utilized a minimum FS of 1.3 as recommended in the FHWA guidelines.

Exposure of DSM walls to scouring and or seismic regression of the waterfront

Under a major seismic event or due to long-term scour, the water channel slope may deform or degrade to a 6H:1V gradient and expose the upper 3 to 5 feet (1 to 1.5 meters) of the DSM buttress to the San Francisco Bay water. Our research and discussion with industry professionals concluded that it is not recommended for DSM treated soil to be in direct exposure to saltwater and wave scour action. Therefore, a protection system consisting of a vinyl sheet pile fascia was planned to be installed in front of the DSM wall. As shown on Fig. 4 and 5, the vinyl sheet piles were driven into the untreated soil in front of the DSM columns. Standard vinyl sheet piles of 15 and 25 feet long (4.5 and 7.6 meters) were driven into the untreated waterfront slope and embedded 5 to 15 feet (1.5 to 4.5 meters). A flood wall designed to retain 3 to 5 feet (1 to 1.5 meters) of engineered fill was constructed behind the vinyl sheet piles. Therefore, the vinyl sheet pile fascia was only subject to lateral earth pressures imposed by the DSM spoils placed between the top of the DSM buttress and the bottom of the floodwall footing. The vinyl sheet pile fascia also provided a more uniform and visually appealing waterfront edge to the project.



Fig. 4. Vinyl sheet pile with forms set up for shotcrete flood wall

© 2016 Deep Foundations Institute

FINAL DSM BUTTRESS DESIGN

For this project, the final DSM buttress design consisted of 5-foot (1.5-meter) diameter overlapping DSM columns with a center-to-center spacing of 3.5 feet (1.1 meters). The bottom of the DSM columns extended at least 1 foot into stiff alluvial deposits below the Bay Mud. The design considered full mobilization of the DSM to occur at 90 days after initial mixing. Continuous double-roll DSM panels were required to maintain stability against over-turning. Figure 5 illustrates two typical details of the project's waterfront stabilization system.

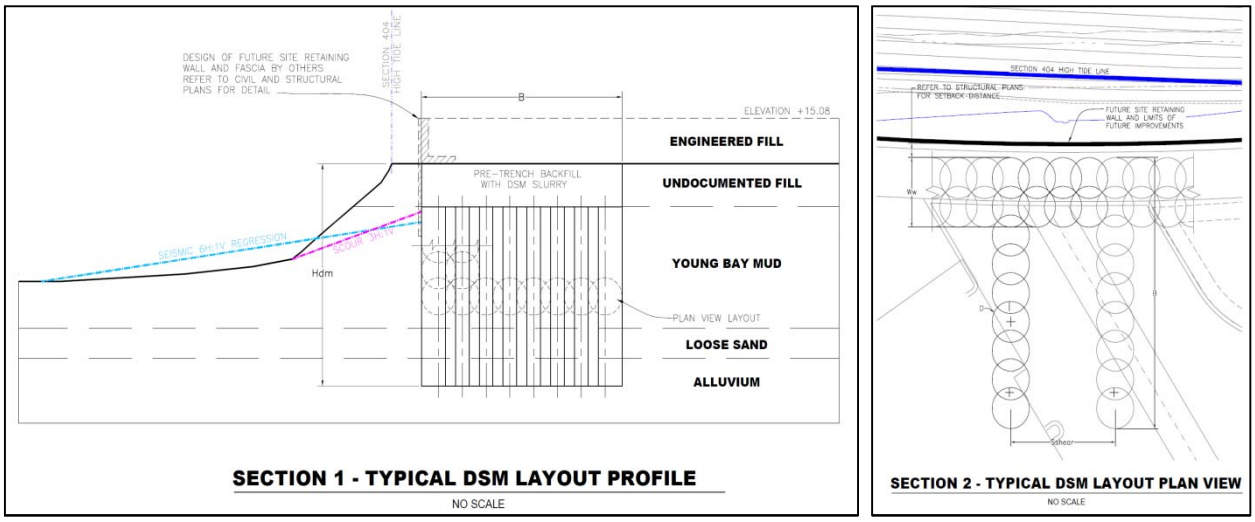


Fig. 5. Typical details of the DSM waterfront edge stabilization system

CONSTRUCTION CHALLENGES

Many technical and logistical challenges were faced and overcome during the installation of DSM walls along the project's shoreline. The site was narrow and confined by shorelines under tidal influence. This special site geometry posed challenges for siting of silos, staging of construction materials and sequencing of the DSM installation. In addition, other construction activities were also underway at the site. Utmost care and coordination was critical to keeping all the contractors working efficiently and on schedule.



Fig. 6. Crack Developed During Initial DSM Installation

The DSM installation was planned to be located approximately 5 feet (1.5 meters) from the waterside crest of slope. Due to the sensitivity of the underlying soft Bay Mud and the steep waterfront slope, shoreline deformation and instability under the heavy DSM equipment was high. Timber mats were used at all times to lower the equipment contact pressures and reduce stability issues.

During the initial DSM installation activities, tension cracks developed in the upper few feet of the shoreline (Fig. 6). This was apparently due to the lack of passive resistance against the lateral pressure exerted by the force of the soil-slurry and the fluidized ground. To reduce the lateral pressure and occurrence of tension cracks, pilot trenches were excavated ahead of the DSM installation. The pilot

© 2016 Deep Foundations Institute

trenches ranged from 4 to 6 feet deep (1.2 to 1.8 meters) and extended 7 to 10 feet (2.1 to 3 meters) ahead of the DSM equipment.

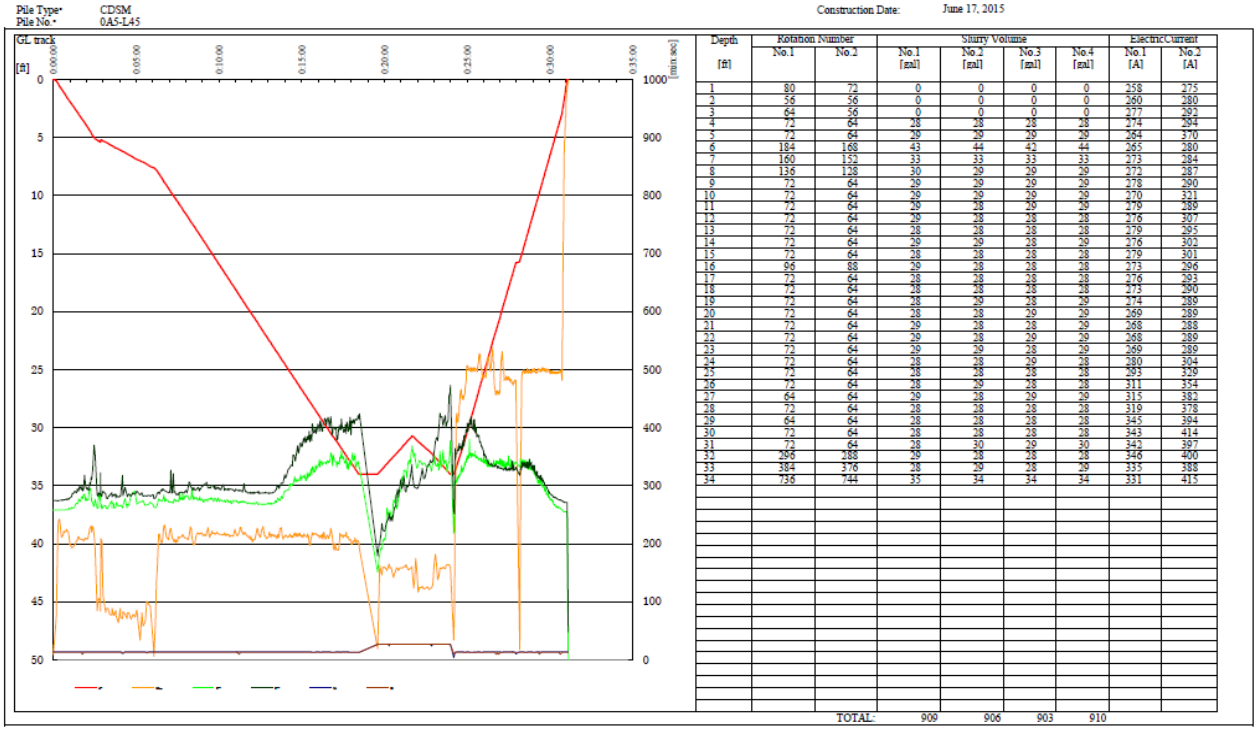
The pilot trenches occasionally encountered old wood pilings, concrete rubble, laced tires and gravel within the upper 5 to 10 feet. These were apparent remnants of the original site reclamation and filling performed in the late 1950s. Occasional obstructions were still encountered during the installation of DSM beneath the excavation depth of the pilot trench. Deeper obstructions were removed using an excavator and the DSM columns were redrilled to complete installation.

As the DSM installation proceeded toward the inner harbor, buried retaining structures within the former marina were encountered. These buried retaining structures shifted outwards towards the water as the DSM was installed so steel sheet piles were temporarily installed 25 to 40 feet deep (7.6 to 12.2 meters) to prevent further deformation of the buried retaining structure. This allowed the DSM to be successfully installed in where these buried structures were encountered.

QUALITY CONTROL

Real-time construction monitoring

Care was administered to assure that quality control was performed at every phase of the project from field validation tests and the final production phase. Real-time monitoring of the mixing parameters was performed for each element installed using a computer-operated quality control system. Daily quality control reports (Fig. 7) were prepared that documented the progress of construction, the installation time, element identification numbers, top and bottom elevation of the elements, type of mixing tool and specific gravity measurement records of the grout. In addition, these reports presented the real-time monitoring of



Depth [ft]	Rotation Number No.1	Rotation Number No.2	Slurry Volume No.1 [gal]	Slurry Volume No.2 [gal]	Slurry Volume No.3 [gal]	Slurry Volume No.4 [gal]	Electric Current No.1 [A]	Electric Current No.2 [A]
1	80	72	0	0	0	0	258	275
2	56	56	0	0	0	0	260	280
3	64	56	0	0	0	0	277	292
4	72	64	28	28	28	28	274	294
5	72	64	29	29	29	29	284	370
6	184	168	43	44	42	44	265	280
7	160	152	33	33	33	33	273	284
8	136	128	30	29	29	29	272	287
9	72	64	29	29	29	29	278	290
10	72	64	29	29	29	29	270	321
11	72	64	29	28	29	29	279	289
12	72	64	29	28	28	28	276	307
13	72	64	28	28	28	28	279	295
14	72	64	29	29	28	29	276	302
15	72	64	28	28	28	28	279	301
16	96	88	29	28	28	28	273	296
17	72	64	28	28	28	28	276	293
18	72	64	28	28	28	28	275	290
19	72	64	28	29	28	29	274	289
20	72	64	28	28	29	29	269	289
21	72	64	29	28	28	29	268	288
22	72	64	29	28	29	29	268	289
23	72	64	29	29	28	29	269	289
24	72	64	28	28	29	28	280	304
25	72	64	28	28	28	28	283	329
26	72	64	28	29	28	28	311	354
27	64	64	29	28	29	29	315	382
28	72	64	28	28	28	28	319	378
29	64	64	28	28	28	28	345	394
30	72	64	28	28	28	28	343	414
31	72	64	28	30	29	30	342	397
33	296	288	29	28	28	28	346	400
33	384	376	28	29	28	29	335	388
34	736	744	35	34	34	34	331	415
		TOTAL:	909	906	903	910		

Fig. 7. Typical daily quality control report

the parameters such as penetration and withdrawal speed of the mixing shaft, rotation speed of the mixing blades, grout injection volume and average amperage of the mixing motors recorded at every 1 foot interval along the depth of the column installed. The contractor was careful to monitor the average

© 2016 Deep Foundations Institute

amperage of the mixing motors during penetration to assure that the element reached the required depth of key-in into the competent stratum.

Core sampling and strength testing

The quality of the product was verified by coring and testing 3 percent of the total elements installed. Coring was performed after 21 to 28 days of installation. A total of 70 full depth continuous cores were obtained. Each full depth core consisted an average of six 5-foot (1.5-meter) long core runs. The core runs were retrieved, logged and photographed. Cylindrical core samples, each 2.5 by 5 inch (6.35cm by 12.7cm) were then cut from the full depth core runs, wrapped and protected with moist burlap paper, stored in 3 by 6 inch (7.6cm by 15.2cm) plastic cylinders with lid and transported to the laboratory for strength tests (Fig. 8).



Fig. 8. Cored DSM sample

Project specifications required the average 90-day unconfined compressive strength of the core samples as determined by ASTM D2166 to be 180 psi (1240 kPa) and no more than 10 percent of the samples tested with a 90-day UCS of less than 110 psi (758 kPa). All results were tracked and analyzed as a quality control measure to determine that every core met the specification requirements. Results from the 205 tested core samples showed an average strength between 199 psi to 738 psi (1372 to 5088 kPa) at 28 days; none of the samples fell below 110 psi (758 kPa) at 90 days.

PROPERTIES OF DSM SPOILS

On this project, the DSM installation generated approximately 35 percent spoils. The DSM spoils were used to raise the site grade by approximately 5 feet (1.5 meters) to achieve the desired design elevation. Laboratory tests were performed on the DSM spoils to evaluate the engineering properties. Table 1 provides a comparison between in-situ untreated Bay Mud deposits and DSM spoils generated predominately by mixing cement and/or binder to Bay Mud deposits.

Table 1. Comparison between Bay Mud deposits and DSM spoils

	Bay Mud Deposits	DSM Spoils
Dry Density (pcf)	50 to 60	50 to 60
Moisture Content (%)	75 to 85	65 to 75
Plasticity Index	70 to 75	27*
R-Value	<5	13*

*Only one test was performed

© 2016 Deep Foundations Institute

CONCLUSION

This paper is intended to present how earth mechanics principals can be applied to widely acceptable design guidelines published in SP117A, CBC and FHWA to properly design a deep soil mixing buttress system to reduce post-seismic lateral deformation along waterfront slopes. It also outlines construction challenges and associated mitigation measures, such as excavation of pilot trenches and installation of temporary sheet piles. Results from a robust quality control program are also presented, indicating that DSM installations result in uniform mixing and reliable strength results. Lastly, laboratory test results of the DSM spoils also indicated that engineering properties of the in-situ soils were enhanced and DSM spoils can be considered acceptable engineered fill materials.

ACKNOWLEDGEMENTS

The authors would like to thank Mr. Paul Powers and Mr. Joseph Wilson of The Pauls Corporation for their consideration and selection of this innovative engineering solution on this project. We are also grateful for Mr. Matt Salmon and Mr. Mike Lisle of the Pauls Corporation for their leadership on the numerous construction activities at the site.

The following project team members and reviewers all contributed to the success of designing and implementation of this DSM edge containment system:

Design Team
Mr. Leroy Chan of ENGEO for project management and geotechnical engineering designs; Mr. Bruce Chu and Mr. Justin Davison of Sandis for civil design; Mr. Matt Gruber of Callendar Associates for waterfront landscape architectural design and permitting efforts; and Mr. Jim Lentfer of Rinne & Peterson for structural design of the flood wall and fascia.

DSM Construction Team
Mr. David Yang, Mr. Sushil Kafle, Mr. Subash Shrestha and Mr. Ralph Griffin of JAFEC USA, Inc for their professionalism during DSM installation, detailed and punctual daily reports and coordinated coring and testing process.

Construction Monitoring Team
Mr. Tony Villalobos, Mr. Greg Hudson and Mr. James Yang of ENGEO for providing quality assurances services during construction of the DSM edge containment system.

Technical Review Team
Mr. Mark Gilbert of ENGEO for providing technical review on this paper. Mr. Logan Medeiros of Rockridge Geotechnical and Mr. Deron van Hoff of Geotechnical Consultants Incorporated for providing peer review on the geotechnical aspects of the DSM design.

REFERENCES

1. ASTM, 2011, American Society for Testing and Materials http://www.astm.org/

2. Blake, T. F., Hollingsworth R.A., and Stewartm J. P., 2002, Recommended Procedures for Implementation of DMG Special Publication 117-Guidelines for Analyzing and Mitigating Landslide Hazards in California: Committee organized through the ASCE, Los Angeles Section Geotechncial Group, Document published by the Southern California Earthquake center, 101p.

© 2016 Deep Foundations Institute

3. Bray, J. D. and Travasarou, T., 2007, Simplified Procedure for Estimating Earthquake Induced Deviatoric Slope Displacements, Journal of Geotechnical and Geoenvironmental Engineering, ASCE, V.133(4), pp. 381-392, April 2007.

4. California Building Code (CBC) 2013.

5. California Geologic Survey (formerly CDMG), 2008, Guidelines for Evaluating and mitigating seismic Hazards in California, Special Publication 117A.

6. FHWA; Federal Highway Administration Design Manual: Deep Mixing for Embankment and Foundation Support. Publication No. FHWA-HRT-13-046; October 2013

7. NCHRP; National Cooperative Highway Research Program, Report 611; Seismic Analysis and Design of Retaining Walls, Buried Structures, Slopes, and Embankments; 2008

8. Olson, S.M. and Stark, T.D., 2002, Liquefied strength ratio from liquefaction flow failure case histories, Canadian Geotechnical Journal, 39, 629-647

9. Rocscience, Slide 7.0 Software https://www.rocscience.com

10. Youd, T.L., C.M. Hansen, and S.F. Bartlett, 2002, Revised multi-linear regression equations for prediction of lateral spread displacement." Journal of Geotechnical and Geoenvironmental Engineering, 128 (12), 1007-1017.

© 2016 Deep Foundations Institute

SETTLEMENT EVALUATION OF LARGE WATER STORAGE TANKS UNDER CHALLENGING CONDITIONS

Yogesh Prashar, East Bay Municipal Utility District, Oakland, CA, USA (510) 287-0520
Ben M. Lewis, Kyoto University, Kyoto, Japan, bmlewis@ucdavis.edu

ABSTRACT

The East Bay Municipal Utility District (EBMUD) is a major water utility service providing water to over 1.3 million people in the eastern San Francisco Bay Area. EBMUD manages 28 dams at 5 terminal and 23 open-cut reservoirs within a 331-square-mile customer service area. As part of a 2012 update on EBMUD's Infrastructure Rehabilitation Plan for Distribution Reservoirs, EBMUD has decided to replace Central Reservoir, a 152.8 million-gallon open cut reservoir, with optimally sized tanks. This paper presents the results of an analytical comparison of various foundation reinforcement solutions for the proposed tanks including: Cement Deep Soil Mixed (CDSM) columns, vibro stone columns, rammed aggregate piers, and lightweight cellular concrete fill. The computational program GeoMat (www.ensoftinc.com) was used to perform simplified soil structure interaction analyses. Settlement estimates were developed for each alternative with the proposed loading and compared to an allowable differential settlement criterion established at 0.3-inches over a 50 foot length. The authors wish to present the importance of considering mat and soil interaction along with various settlement mitigation methods considered for this challenging project.

INTRODUCTION

Project Background

Central Reservoir is an operational open-cut reservoir located north of the intersection of 25th Avenue and East 29th Street in Oakland, California. The reservoir is bound by 23rd Avenue to the west, Sheffield Avenue to the east and Interstate Highway 580 to the north. Originally, the Central Reservoir site was a drainage swale incising into weathered bedrock formed from Pleistocene alluvial deposits. The reservoir was first constructed in 1910 by excavating a basin below grade and constructing an embankment dam on the south and cutting/filling the bedrock and alluvial deposits from the drainage swale. The main dam at the Central Reservoir site is also a DSOD (Department of Safety of Dams) jurisdictional dam and as such is regularly monitored by the EBMUD Materials Engineering Section and the California DSOD.

In a 2012 update to EBMUD's Infrastructure Rehabilitation Plan for Distribution Reservoirs, Central Reservoir was identified as a critical facility that has reached the end of its useful life and must be replaced due to: a failing panel craft lining which contains polychlorinated biphenyls in the interior coating, a roof that does not meet the current seismic code, and reduced operating levels due to potential leakage in the upper portions of the panel craft lining. Furthermore, Central Reservoir is about three times larger than required and is located at a lower elevation than other regional reservoirs in the pressure zone resulting in increased labor-intensive operational challenges and water quality operations.

This project presents some challenging geotechnical demands – the site is founded on weakly consolidated Holocene Alluvium overlying weathered bedrock, the proposed structural loads are large, and the new Central Reservoir is to be placed on a pad at an elevation of 182 feet, required placement of up to 30 feet of fill over the current basin. Additionally, the project aims for a long-term foundation solution that will outlive the new replacement tanks and accommodate future site upgrades. In order to meet this goal, the differential settlement criterion for the tanks was ¼ inch over 50 feet length. Lastly, the project also aims to address EBMUD's increasing trench spoil stockpiles by recycling discarded trench spoils as fill for the proposed tank pad.

There are five potential storage structure alternatives currently under consideration for the replacement of Central Reservoir, detailed in Table 1 and pictured in Figure 1. The District's Materials Engineering Section, to which the author belongs, was tasked with evaluating the five superstructure alternatives along with eight foundation alternatives from a geotechnical standpoint in order to assist with the selection of the preferred replacement alternative. This paper details the method and results of settlement analyses performed for the seven foundation

© 2016 Deep Foundations Institute

alternatives summarized in Table 2 as a part of the value engineering study for the selection of the preferred superstructure-foundation alternative combination.

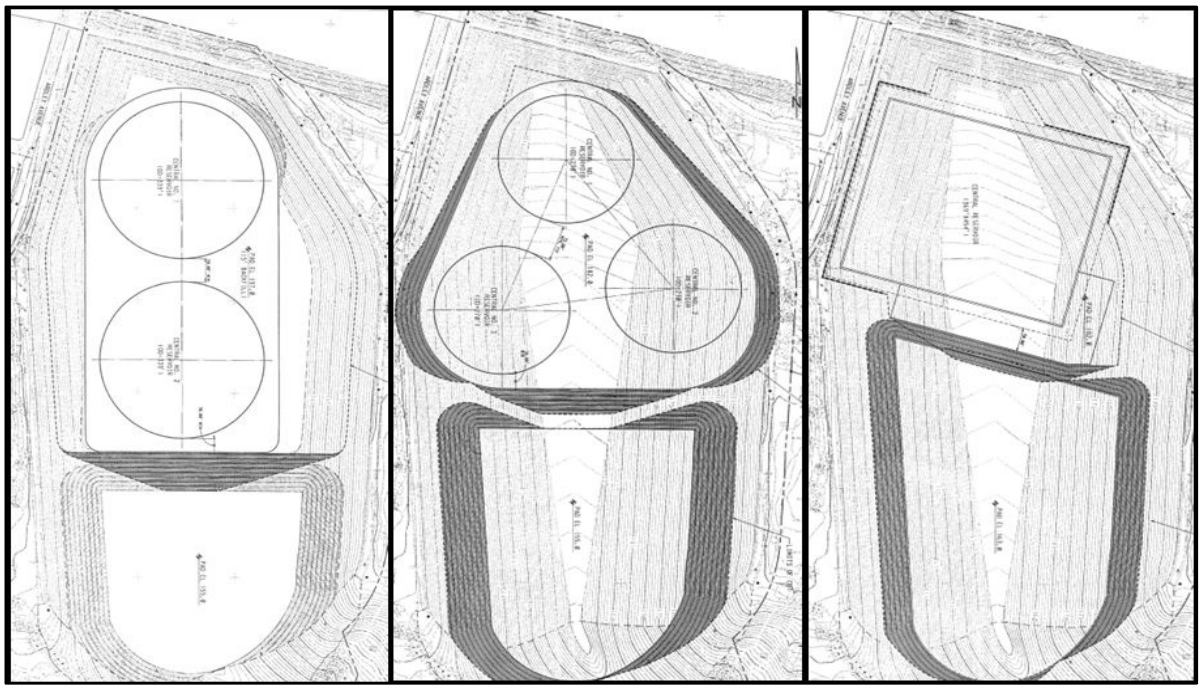


Figure 1 A: Two 25 MG Tanks **1 B: Three 17 MG Tanks** **1 C: One 50 MG Basin**

Table 1 – Superstructure Configurations and Alternatives			
Alternative	**Superstructure**	**Configuration**	**Reference Figure**
1	Steel DN Tanks	Two 25 MG Tanks	1A
2	Concrete DN Tanks		1A
3	Steel DN Tanks	Three 17 MG Tanks	1B
4	Concrete DN Tanks		1B
5	Concrete Basin	One 50 MG Basin	1C

© 2016 Deep Foundations Institute

Table 2 - Foundation Alternative Study Substructure Alternatives		
No.	**Alternative**	**Description**
1	Unreinforced Marginal Soils	Fill with trench spoils/site soils
2	LCC Fill	Leave underlying alluvium as is, place tanks on Lightweight Cellular Concrete (LCC) Fill.
3	RCC Fill	Leave underlying alluvium as is, place tanks on Roller Compacted Concrete (RCC) Fill.
4	Rammed Aggregate Piers (RAP)	Fill with trench spoils/site soils and reinforce fill and underlying alluvium with Geopier® rammed aggregate piers.
5	Cement Deep Soil Mixed Columns (CDSM)	Fill with trench spoils/site soils and reinforce fill and underlying alluvium with Cement Deep Soil Mixed Columns (CDSM).
6	Vibro Stone Columns	Fill with trench spoils/site soils and reinforce fill and underlying alluvium with Vibro Stone Columns.
7	LCC Fill over RAP Reinforced Subgrade	Reinforce underlying alluvium with RAP and fill to tank pad elevation with LCC Fill.

Subsurface Conditions

The anticipated subsurface conditions (See Figure 2) at the site consist of Holocene Alluvium, old fill placed during the original construction of the reservoir, and claystone/sandstone bedrock comprised of Pleistocene alluvial deposits (Upper San Antonio Formation). Embankment fill materials are generally comprised of excavated and compacted Alluvium. A portion of the proposed site is founded on old fill that was placed during the original construction of the reservoir. The material properties, based on a 2008 Seismic Stability Evaluation of Central Reservoir conducted by EBMUD, are summarized in Table 3 (Ref # 5). The subsurface stratigraphy is complex; it is anticipated that the original streambed was incised into Upper San Antonio Formation bedrock and that the distribution of Alluvium across the site is heavily dependent on the fluvial geomorphology of the original stream.

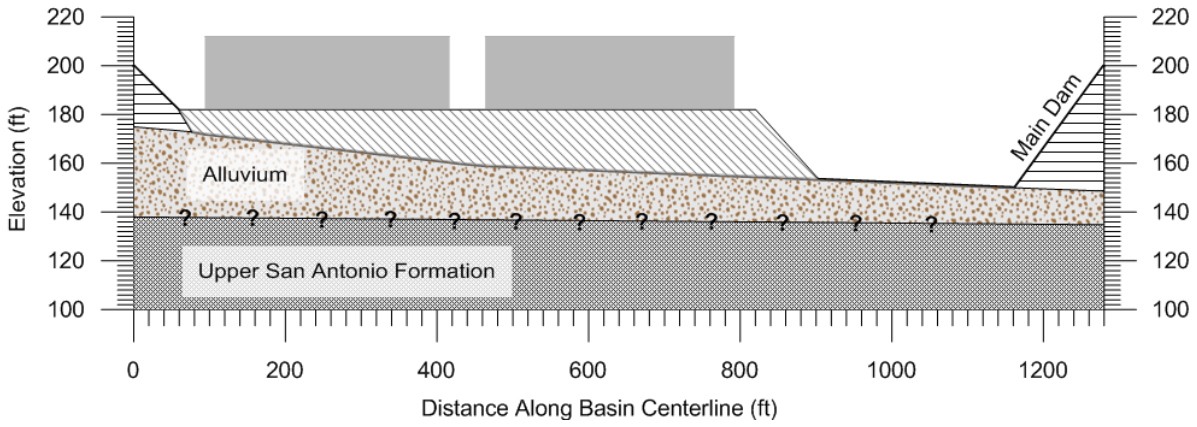


Figure 2: Site North South Profile

© 2016 Deep Foundations Institute

Table 3: Table of Material Properties (From 2008 EBMUD Report)							
	Friction Angle	**Cohesion**	**Unit Weight**	**Elastic Modulus**	**Poisson's Ratio**	**Shear Wave Velocity**	**Unconf. Compressive Strength**
	ϕ (deg)	**c (PSF)**	**γ (PCF)**	**E (PSF)**	**ν**	**Vs (Ft/sec)**	**s_u (PSF)**
New Fill (Assumed)	29.4	172	130	3.90E+05	0.35	875	500 - 2500
Alluvium	29.4	172	130	3.90E+05	0.35	1025	500 - 2500
Bedrock (Upper San Antonio)	38.7	0	130	7.50E+06	0.45	>1100	>3000

Fill: All fill materials at the site will likely be comprised of materials excavated from the main dam, over excavation of the surrounding slopes, and (if necessary) import materials from the District's stockpiled trench spoils site. For the purposes of this feasibility-level work, the proposed fill was assumed to have the same properties as the alluvium described below. Aggregate base was also identified as a potential fill material for the RAP and Geogrid alternatives, and while it was not considered in-depth at this stage, it is a viable alternative for reducing settlement.

Alluvium: The alluvium layer primarily consists of low to medium plasticity, weakly consolidated stiff sandy clays and clayey sands with silt, gravel, and occasional Franciscan pebbles. Due to great spatial variability in the subsurface profile, the alluvium-Upper San Antonio interface is complex and often difficult to identify, but is typically present at an elevation of around 135 to 150 feet. From a settlement standpoint, the alluvium layer is considered more sensitive due to its relatively higher compressibility. Reinforcement of alluvium will be an integral part of effective foundation solutions at the Central Reservoir site.

Upper San Antonio Formation: The Upper San Antonio Formation consists of completely weathered sandstone and claystone, in some borings overlain by stiff to very stiff medium plasticity silty clay. Due to the presence of heavily weathered sandstone and claystone, it is thought that an erosional unconformity lies at the boundary between the Upper San Antonio and the alluvium, suggesting that the Upper San Antonio is likely to be heavily consolidated. The Upper San Antonio can be further subdivided by shear wave velocity measurements into an upper member and a lower member characterized by markedly increased measured shear wave velocity.

Purpose

The purpose of this study was to evaluate the proposed superstructure and foundation alternatives from a geotechnical engineering standpoint, provide settlement estimates for all permutations of superstructure and foundation alternatives, and provide earthwork quantities to facilitate the selection of the preferred replacement alternative for Central Reservoir. Settlement estimates were to be compared to a differential settlement criterion of ¼ inch over 50 feet length in order to characterize the degree of earthwork required to achieve desirable settlement results.

SETTLEMENT ESTIMATION METHOD

For settlement estimation purposes, foundation reinforcement alternatives were broadly categorized into two categories based on settlement estimation method: 'Rigid Inclusion' alternatives, which involved insertion of stiff members into the foundation, and 'Engineered Fill' alternatives, which involved placement of a stiffer, non-consolidating fill on grade. Settlement estimates for the former were prepared using a rudimentary iterative decoupled soil-structure interaction analysis, while settlement calculations for the latter were prepared solely using 1-D spreadsheet calculations.

© 2016 Deep Foundations Institute

Calculation Methods

For all alternatives, initial settlement estimates were prepared using a spreadsheet based in *Theory of Elasticity* equations for estimating elastic settlement and the consolidation equation with Skempton's correction factor for 3-D effects for estimating consolidation settlement (Ref #1 & 4). Incremental changes in stress state after excavation, fill, and tank construction were estimated assuming a Boussinesq stress distribution. In the case of rigid inclusions, initial estimates were prepared for three cases:

1. 0% Replacement Ratio - Tank on unreinforced fill. (Fill assumed to have same properties as Alluvium)
2. 100% Replacement Ratio - Tank on completely reinforced fill (Fill and Alluvium assumed to have same stiffness as rigid inclusion)
3. Tank on partially reinforced fill (Fill and Alluvium assumed to have stiffness equivalent to plan-view area weighted average of alluvium and rigid inclusion stiffness)

Using the results from the (hypothetical) cases 1 and 2, values of the subgrade modulus for an Alluvium subsurface and a rigid inclusion subsurface were obtained. These values were then applied to a finite element model of a two-way slab supported by linear elastic soil springs, with the subgrade modulus from case 2 used for elements supported by rigid inclusions and the subgrade modulus from case 1 used for elements supported by the soil matrix. The computer program GeoMat (Ref #3) was used to perform all computations. The results of the finite element analysis were then used to estimate the bearing pressure on the soil matrix. Using this bearing pressure, the subgrade modulus for the soil matrix (case 1) was re-calculated and the process was repeated until convergence.

A simplified overview on the decoupled soil-structure settlement estimation methodology is outlined below.

The total settlement of the superstructure has two components:

1. Immediate (elastic) settlement; and
2. Consolidation (long-term) settlement.

In the case of soil reinforced by 'rigid inclusions' (Geopiers, CDSM columns, stone columns), elastic settlement was estimated by treating the reinforced layer as a uniform layer with a stiffness equal to the area-weighted average of the soil and reinforcement stiffnesses. However, in the case of consolidation settlement, no significant consolidation occurs within the rigid inclusions, which carry a greater load than the soil matrix. As such, to accurately estimate the consolidation settlement of the soil matrix the load carried by the soil matrix must be estimated. In order to address this issue, a procedure was developed to estimate the load carried by the soil matrix for rigid inclusion alternatives. For initial settlement calculations, immediate settlement was estimated using equations from Timoshenko and Goodier's Theory of Elasticity for settlement of a uniformly loaded elastic half-space, and consolidation settlement was estimated using conventional methods founded in Terzaghi's consolidation equation and Skempton and Bjerrum's 3-D consolidation correction factor. Settlement estimates for Geopier, stone column and CDSM column alternatives were then calibrated in three steps listed and depicted in the figure 3 below.

1. Spreadsheet estimation of immediate and consolidation settlement
2. 2-D finite element analysis of concrete slab on soil springs using subgrade moduli calculated from spreadsheet estimates (Using GeoMat™ software by Ensoft, Inc.)
3. Iteration of resulting soil matrix loading into spreadsheet to recalculate consolidation settlement

© 2016 Deep Foundations Institute

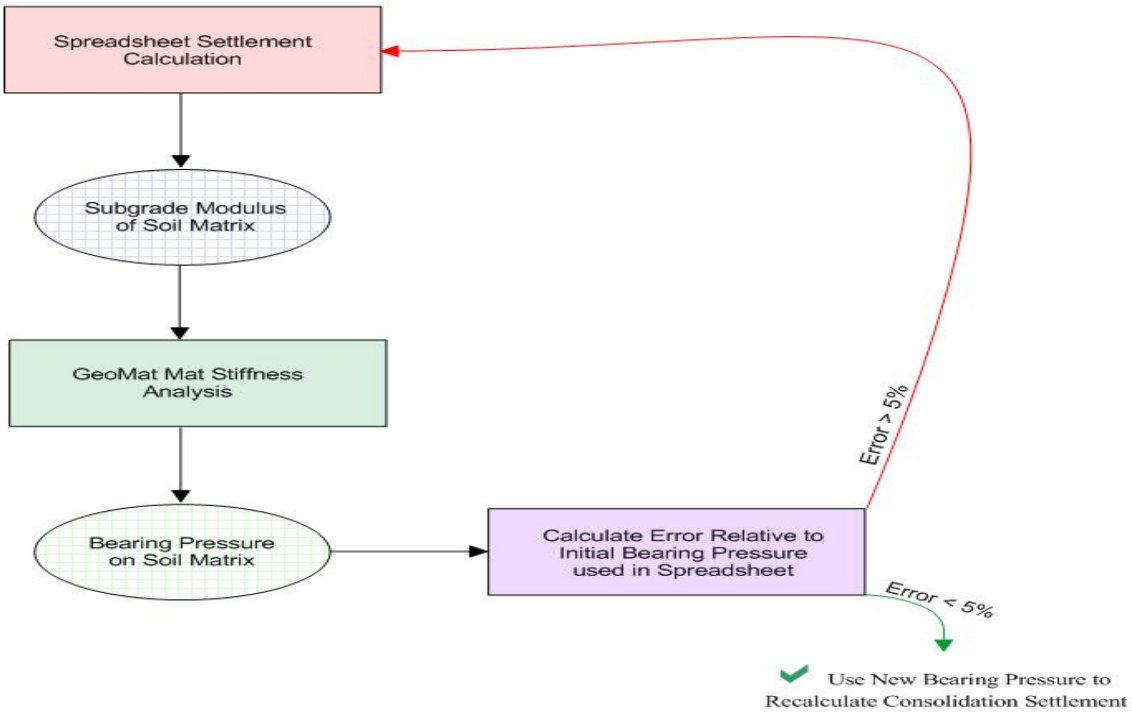


Figure 3: Decoupled Soil Structure Settlement Calculation Illustration

Accuracy of Method and Applicability to Problem

The settlement estimation method outlined in this paper has significant deviations from the physics of the problem – soil settlement is modeled as summation of a linear elastic component and a 1-D consolidation component with a simple correction for 3-D effects. Consequently, the settlement estimates outlined herein are not design-level estimates. Rather, they are intended for rapid evaluation of a large set of foundation alternatives, many of which are relatively new and do not have simple unified methods of evaluation of appreciable accuracy. Hence, evaluating all alternatives by a consistent calculation method allows for a more equitable comparison. Additionally, the method applied herein offers a simplified consideration of soil-structure interaction between the soil, rigid inclusions, and mat foundation.

Material Properties

The material properties used in the settlement analyses are summarized in Table 4 below. Properties for RAP and LCC fill were estimated using information provided by the manufacturers, while properties for CDSM columns were estimated using stiffness values from previous work performed for EBMUD using CDSM columns in clayey soils. Elastic properties for stone columns were estimated using an assumed stiffness equivalent to CDSM columns, along with a 50% increase in stiffness of the soil matrix due to installation, which was recommended by the RAP manufacturer (Tensar Corp.) for modeling settlement on RAP-reinforced soils with reinforcement spacing of 6 feet or less.

© 2016 Deep Foundations Institute

Table 4 – Material Properties Used for Settlement Estimation						
	Elastic Modulus	Poisson's Ratio	Moist Unit Weight	Void Ratio	Virgin Compression Index	Recompression Index
	E (psf)	ν	γ_m (pcf)	e	C_c	C_s
Alluvium	3.90E+05	0.35	130	0.65	0.15	0.04
Upper San Antonio	7.50E+06	0.45	130	0.78	X	0.022
Repurposed Fill	3.90E+05	0.35	130	0.65	0.15	0.04
LCC (31pcf)	7.40E+06	0.2	31	X	X	X
LCC (41pcf)	1.50E+07	0.2	41	X	X	X
RAP (Geopier)	4.00E+06	0.35	X	X	X	X
CDSM Column	1.00E+07	0.2	X	X	X	X
Stone Column	1.00E+07	0.35	X	X	X	X

Elastic parameters for the site soils (Alluvium and Upper San Antonio Formation) were estimated using historical data collected at the site. The value for the Upper San Antonio Formation elastic modulus was initially estimated using results of pocket penetrometer tests from historical borings, but was later increased to ~50% of the dynamic modulus in keeping with field observations that the Upper San Antonio was weathered bedrock. Because the stiffness of the Upper San Antonio rapidly increases with depth, settlement was only considered within the upper 26 feet of the layer. Elastic properties for the Alluvium were estimated using results of 33 CU triaxial compression tests performed during the 2008 seismic stability study of the main embankment. The test results were recompiled and reorganized for this project into Elastic Modulus vs. Vertical Strain scatter plots and contour plots for the Alluvium and embankment fill. While these plots provide more information than necessary for the rudimentary methods employed to date, as the project proceeds to the design phase they will provide valuable information for the more rigorous analysis methods employed at that point.

Settlement Assumptions

Due to the large degree of uncertainty regarding the deformability of the subsurface strata, settlement estimates were prepared for four possible cases of subsurface deformability conditions outlined in Table 5. These assumption cases also served a dual purpose of covering foundation solutions not directly considered – for example, treating the alluvium with cement would create conditions similar to case 4 by removing the alluvium's potential for consolidation settlement. Additionally, four cases of settlement assumptions allows for selection of an appropriate settlement estimation as the project evolves and more information is acquired on the subsurface conditions through borings or geophysical surveys.

Table 5 - Cases of Settlement Assumptions		
Case	**Alluvium Settlement**	**Upper San Antonio Settlement**
1	Elastic and Consolidation	Elastic and Consolidation
2	Elastic and Consolidation	Elastic
3	Elastic and Consolidation	None
4	Elastic	None

© 2016 Deep Foundations Institute

RESULTS

Elastic Modulus of Alluvium

Using recompiled CU triaxial compression tests (See Figure 4) from the 2008 seismic stability evaluation of Central Reservoir, (Ref #5) a scatter plot and contour plot were synthesized to evaluate the effects of confining pressure and vertical strain on the stiffness of the alluvium, pictured in Figure 3. Using Figure 3, the Alluvium Elastic Modulus was estimated to be 3.9E05 psf for an assumed vertical strain of 1% and a confining pressure of approximately 6 ksf.

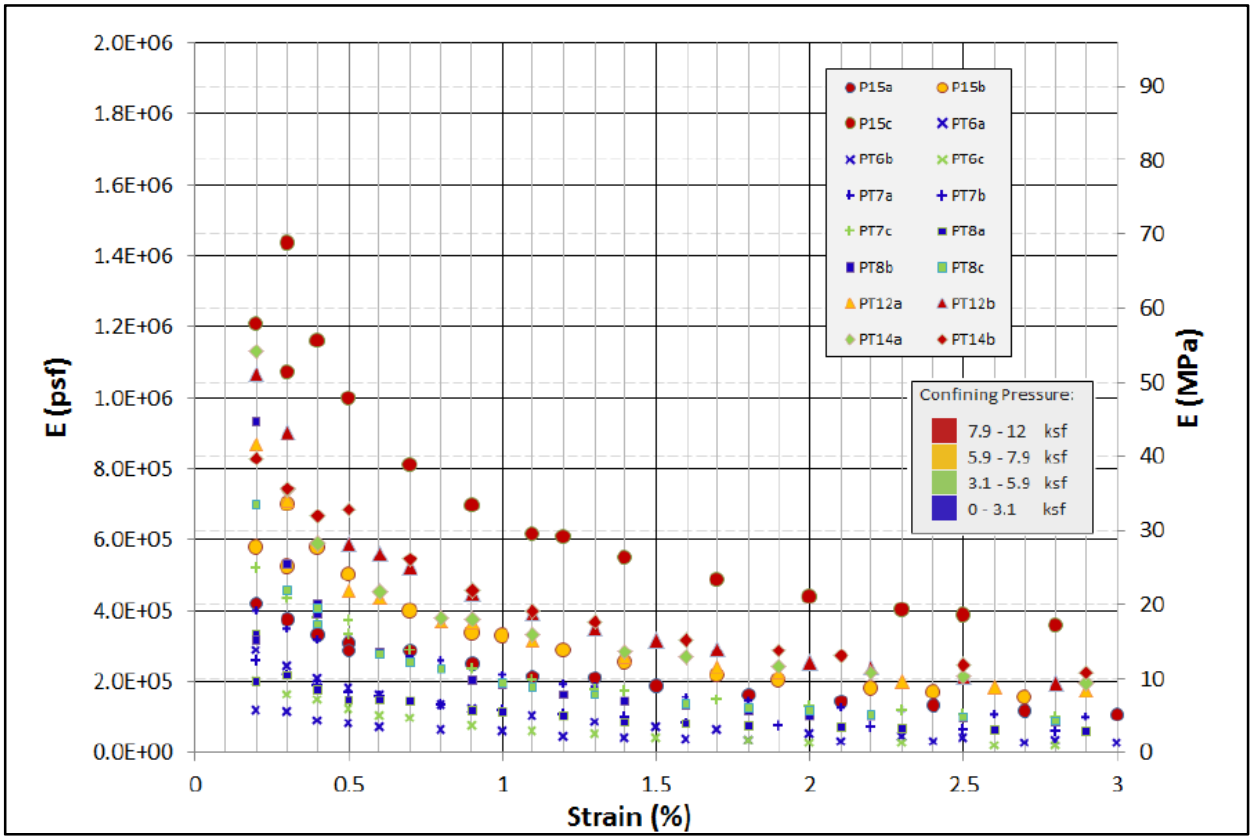


Figure 4: CUTriaxial Extracted Young's Modulus Versus Axial Strain Sensitivity

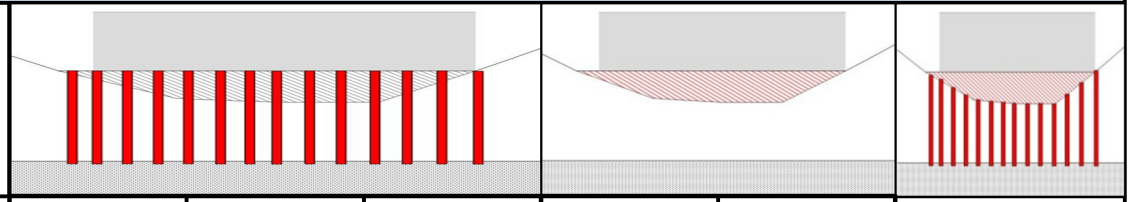
Settlement of Proposed Tanks

The results of settlement analysis, presented in Table 6, demonstrate the relative effect of different sources of settlement on the total and differential settlement of each alternative. The LCC fill over RAP-Reinforced Alluvium alternative was the only alternative to yield acceptable settlement for all settlement assumption cases, with 0.53 to 0.81 inches of maximum total settlement and 0.14 to 0.31 inches of maximum differential settlement. CDSM and stone columns were also effective over a wide range of settlement assumptions, yielding 0.31 to 2.12 inches of total settlement and 0.1 to 0.98 inches of differential settlement.

© 2016 Deep Foundations Institute

© 2016 Deep Foundations Institute

Table 6 - Breakdown of Settlement Estimates for Each Case (in inches)



Case		Settlement Type	Marginal Fill (Do Nothing)		Geopier 4' Spacing		CDSM 4' Spacing		Stone Col. 4' Spacing		RCC Fill		LCC Fill		LCC + Geopier in Alluvium	
Case 1	Total	Fill Elastic	8.69	1.13	2.63	0.27	2.08	0.16	2.12	0.15	4.12	0.00	3.43	0.01	1.18	0.01
		Alluv. Elastic		1.18		0.29		0.17		0.16		2.18		2.18		0.52
		Alluv. Consol		5.41		1.78		1.49		1.54		1.67		0.90		0.45
		USAF Elastic		0.07		0.07		0.07		0.07		0.06		0.06		0.06
		USAF Consol		0.91		0.22		0.20		0.20		0.21		0.28		0.14
Case 2	Total	Fill Elastic	7.78	1.13	1.46	0.27	0.85	0.16	0.85	0.15	3.91	0.00	3.23	0.01	0.80	0.01
		Alluv. Elastic		1.18		0.29		0.17		0.16		2.18		2.18		0.52
		Alluv. Consol		5.41		0.84		0.46		0.47		1.67		0.98		0.21
		USAF Elastic		0.07		0.07		0.07		0.07		0.06		0.06		0.06
		USAF Consol		-		-		-		-		-		-		-
Case 3	Total	Fill Elastic	7.72	1.13	1.24	0.28	0.60	0.16	0.60	0.15	3.84	0.00	3.16	0.00	0.70	0.01
		Alluv. Elastic		1.18		0.29		0.17		0.16		2.18		2.18		0.52
		Alluv. Consol		5.41		0.67		0.28		0.29		1.67		0.98		0.17
		USAF Elastic		-		-		-		-		-		-		-
		USAF Consol		-		-		-		-		-		-		-
Case 4	Total	Fill Elastic	2.24	1.12	0.57	0.28	0.33	0.16	0.31	0.16	2.18	0.00	2.19	0.01	0.53	0.01
		Alluv. Elastic		1.12		0.29		0.17		0.16		2.18		2.18		0.52
		Alluv. Consol		-		-		-		-		-		-		-
		USAF Elastic		-		-		-		-		-		-		-
		USAF Consol		-		-		-		-		-		-		-

* NOTE: Settlement breakdowns are at the location of MAXIMUM settlement for each case-foundation permutation.

DISCUSSION

The settlement breakdowns in Table 6 indicate that at the Central Reservoir site, some degree of reinforcement or improvement of the existing site soils is necessary to achieve the desired settlement. RCC and LCC fill, while stiffer than all rigid inclusion alternatives, are not sufficient to mitigate settlement due to the degree of elastic settlement estimated in the alluvium. It is also worth noting that there is a large spread of settlement across deformation assumptions, indicating the importance of further site investigation and laboratory testing to refine the deformability of subsurface strata.

By comparing the settlement estimations with computed soil matrix pressures in Table 7, the correlation between the soil matrix pressure on the alluvium and the total settlement of the superstructure is apparent. Cases 1 and 2 show the greatest difference in soil matrix pressures and also the greatest difference in total estimated settlement. Comparison of the settlement breakdown of the two cases also shows that consolidation of the Upper San Antonio greatly increases settlement in the alluvium – this is due to an increased alluvium soil matrix load allowed by settlement of the supporting base for the rigid inclusions. Hence, while the only difference between case 1 and 2 is consolidation of the Upper San Antonio layer, the difference in settlement between the two cases is not explicitly Upper San Antonio consolidation settlement, it is settlement of the Alluvium caused by Upper San Antonio consolidation settlement. These results indicate that accurate estimation of the rigid inclusion tip settlement will be a critical factor in selecting an acceptable foundation solution for central reservoir.

Table 7 - Computed Soil Matrix Pressures

Case	Settlement Considered		Geopier @ 4' Spacing	CDSM @ 4' Spacing	Stone Col. @ 4' Spacing
Case 1	Alluvium Elastic Settlement: Alluvium Consolidation Settlement: Upper San Antonio Elastic Settlement: Upper San Antonio Consolidation:	✓ ✓ ✓ ✓	**884.00**	**726.00**	**753.00**
Case 2	Alluvium Elastic Settlement: Alluvium Consolidation Settlement: Upper San Antonio Elastic Settlement: Upper San Antonio Consolidation:	✓ ✓ ✓	**390.00**	**206.00**	**214.00**
Case 3	Alluvium Elastic Settlement: Alluvium Consolidation Settlement: Upper San Antonio Elastic Settlement: Upper San Antonio Consolidation:	✓ ✓	**313.00**	**123.00**	**127.00**

© 2016 Deep Foundations Institute

CONCLUSIONS

Preliminary settlement estimates were developed for six proposed foundation solutions for the planned replacement of Central Reservoir. Using finite-element analysis of a two-way slab and conventional spreadsheet methods, settlement estimates were compared to total and differential settlement criteria and the results were interpreted to identify primary drivers for settlement at the site. The results of this preliminary analysis have identified three crucial aspects to consider for this project as it moves into the design stage:

- **Site Investigation and Testing:** Quantification of consolidation potential of the Upper San Antonio will serve to clarify the degree of potential tip settlement for rigid inclusion, which this paper has suggested to be a critical factor in estimating settlement. Ideally, clarification of consolidation potential variability with depth would provide valuable information for planning depths of rigid inclusions.
- **Reinforcement of Fill and Alluvium:** Settlement results presented in this paper have demonstrated that elastic settlement of Alluvium is expected to exceed total settlement criteria unless some degree of reinforcement is performed. In particular, rigid inclusions are a promising solution for reducing both elastic and consolidation settlement of the Alluvium.
- **Settlement at Tip of Rigid Inclusions:** This study has identified a potential for settlement at the tip of the rigid inclusions to transfer structural loads into the Alluvium layer, causing large increases in settlement. Accurate estimation of rigid inclusion tip settlement will be a crucial component of estimation of the settlement of the proposed tanks.

REFERENCES

1. Bowles, Joseph E. (1996). *Foundation Analysis and Design, 5th edition,* McGraw-Hill, New York, New York

2. Central Reservoir – A Report of the Conditions In and Immediately Adjacent to the Reservoir, East Bay Municipal Utility District Internal Report Dated April 1955, Oakland, California

3. Ensoft Incorporated (2014). User's Guide – *GeoMat v2014 – Analysis of a Soil-Supported Mat or a Structural Slab*, Austin, Texas.

4. Salgado, R. (2008). *The Engineering of Foundations*, McGraw-Hill, New York, New York.

5. Seismic Stability Evaluation Report Central Reservoir Main Dam, East Bay Municipal Utility District Internal Report Dated July 2008, Oakland, California

© 2016 Deep Foundations Institute

This page left intentionally blank

© 2016 Deep Foundations Institute

FRASER HEIGHTS BRIDGE – COMPARISON BETWEEN PDA TESTS AND PILE CAPACITY ESTIMATION METHODS

Ali Azizian, Tetra Tech EBA, Vancouver, BC, Canada, (604) 685-0275, ali.azizian@tetratech.com

Brian Hall, Tetra Tech EBA, Vancouver, BC, Canada, brian.hall@tetratech.com

ABSTRACT

Driven piles were selected to support the Fraser Heights Bridge bents. Piles were a key component of the top-down construction approach, which was adopted for minimizing potential impacts on an environmentally sensitive wetland. Project requirements mandated verification of pile capacities using dynamic methods. More than 40 Pile Driving Analyzer (PDA) tests were performed. The subsurface conditions were highly variable. On the east side, piles extended through loose sands, soft silts/clays, and two peat layers and were founded in glacial till-like soils at about 45 m depth. However, on the west side, till-like materials were so shallow that it was difficult to drive the piles sufficiently deep to obtain the necessary lateral support. This paper provides an overview of the geotechnical considerations of the bridge design and top-down construction approach, and expands on the presentation of PDA results and how they compared to pile capacity estimation methods and parameters recommended in the applicable design codes.

Keywords: Driven Piles, PDA Testing, Top-Down Construction, Difficult Soils, Till-like Materials

INTRODUCTION

The Fraser Heights Bridge (FHB) was a component of the Fraser Heights Connector (FHC), a 2 km section of the South Fraser Perimeter Road (SFPR), constructed as part of the Port Mann/Highway 1 (PMH1) Improvement Project. The FHC is located in northeast Surrey BC (Fig. 1).

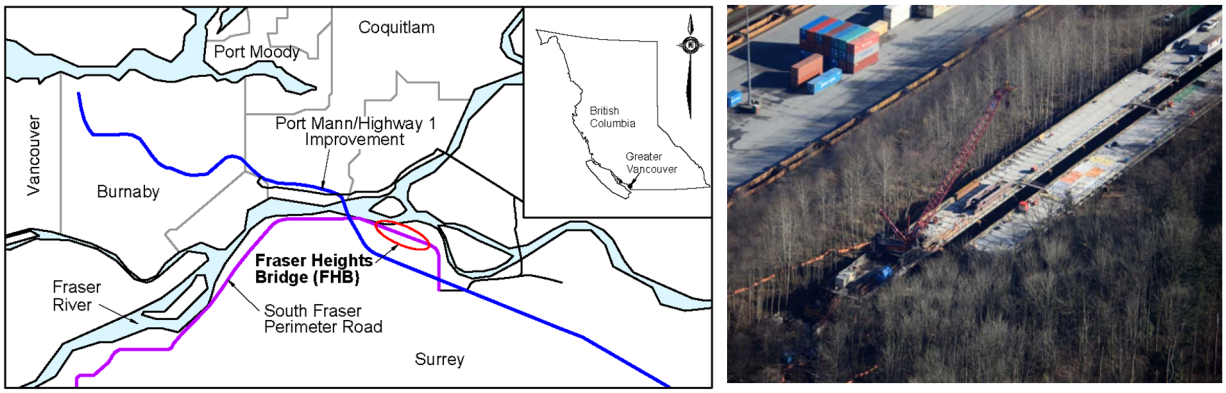


Fig. 1. Site location and aerial view of the bridge under construction.

Two major design and construction determinants were: 1) a mandated tight schedule to provide a non-tolled alternative to a new toll bridge; and, 2) an obligation that construction had to occur with minimal impact on the environmentally sensitive wetland the FHB crossed, including limiting the footprint of the permanent and temporary works to less than 45 m^2, and prohibiting construction access onto the wetland. Construction equipment was only allowed on the wetland on temporary trestles or on the finished structure. This latter requirement resulted in the bridge being constructed span by span, using a top-down approach.

© 2016 Deep Foundations Institute

Hall et al. (2015) presented the geotechnical considerations of the top-down construction approach and the performance-based design approach used for seismic design of the bridge. This paper will expand on the presentation of PDA test results and how the results compared to pile capacity estimation methods and parameters recommended in the applicable design codes.

Construction commenced in April 2011 and the bridge opened to traffic in December 2012. The estimated construction value of the bridge was $25 Million.

SITE CONDITIONS

Description

The site extended from the Fraser Heights glacial uplands in North Surrey out over a peat wetland in the floodplain of the Fraser River. A Canadian National (CN) Railway Intermodal yard bounded the north side of the site, which had been built about 20 years before by pumping dredged river sand onto the peatlands. This hydraulic fill extended partly onto the footprint of the east approach fill and intermittently along the bridge alignment.

Subsurface Soils

The soil profile varied significantly along the bridge as shown in Fig. 2.

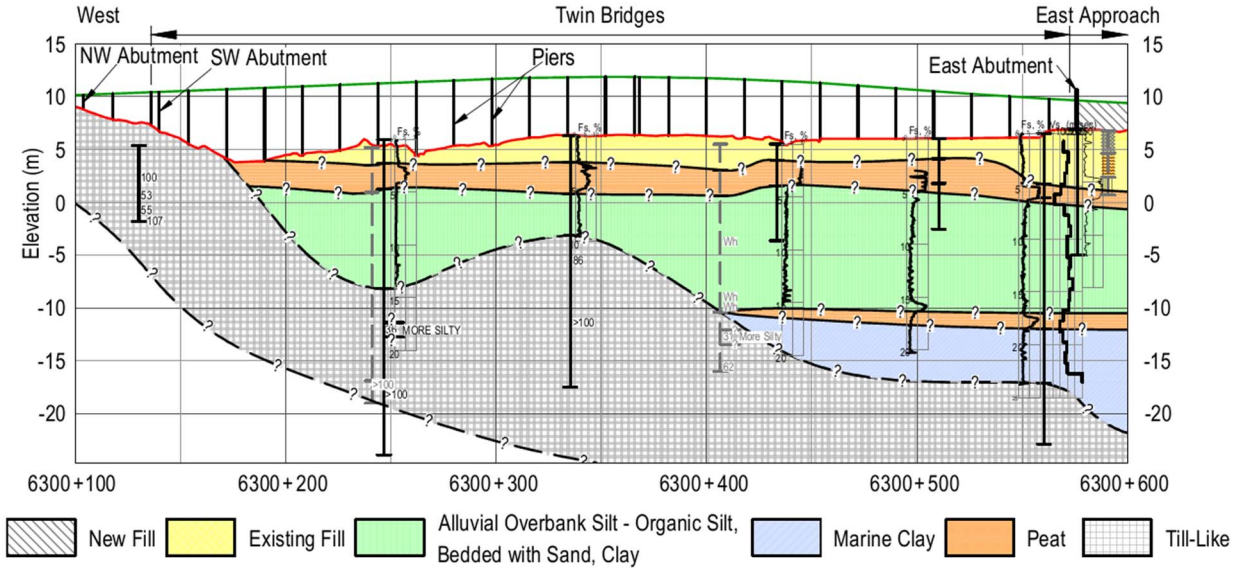


Fig. 2. Soil profile.

As a result of the environmental access restrictions onto the wetlands, 6 boreholes spaced at about 80 m intervals were available along the alignment. Particulars of the subsurface profile (Fig. 2) were:

- West: Dense glacial materials at shallow depth.
- Central: Variable thin fill over up to 4 m of peat, over 3 m to 10 m of soft overbank silt, over dense glacial material.
- East: Between 1 m to 5 m of loose hydraulically placed sand fill, over about 3 m of peat, over about 13 m of soft overbank silt, over a thin buried amorphous peat, over up to 5 m of soft sensitive marine clay, over dense glacial material.
- The glacial materials were described as till-like as they tended to be more silty and in places had lower and more variable Standard Penetration Test (SPT) N-values than was normally associated with local glacial till.

© 2016 Deep Foundations Institute

Groundwater

Standing water and flowing watercourses were present, and in addition to seasonal fluctuations related to flood stages in the Fraser River, beaver activity resulted in unexpectedly sudden changes in surface water levels. Excess piezometric heads of up to 12 m above ground surface were measured near the contact between dense glacial material and the overlying clay deposits.

BRIDGE STRUCTURE

The FHB consists of two parallel, 472 m and 436 m long, low-height, pile-supported trestles with steel girders and 250 mm full-depth precast concrete panelized decks (Fig 1.). Each trestle is 11 m wide and carries two travel lanes plus shoulders. The trestles are separated by a gap of approximately 4 m to allow sunlight through to the wetland habitat below.

The bridge has relatively short 18 m spans which were selected to avoid excessive reach demands on the construction crane. The west end spans were reduced to approximately 14 m length, and the east end span is a special 18 m long simple span which incorporates jacking provisions to compensate for possible long-term settlement of the 4 m high east approach fill.

As shown in Fig. 3, the intermediate support bents consisted of two (per trestle), 762 mm diameter by 19 mm wall thickness, driven, steel pipe piles, with specified yield strength of 310 MPa. The piles were extended above ground and connected to steel box-section cap beams. The piles and their connections were reinforced and filled with concrete. There were a total of 112 piles.

To obtain continuous, joint-free superstructure lengths of up to 250 m between the single, mid-bridge expansion joint and abutments, without applying excessive displacements to the supporting piles under thermal straining, laminated elastomeric bearings were placed beneath the girders. The bearings absorb much of the thermal strains via shear deformation, with the remainder of the strain being accommodated by flexure of the steel pipe piles. The relative distribution of these strains between bearings and piles varies significantly with the extended pile lengths and the variation in soft soil depth above the dense till-like material.

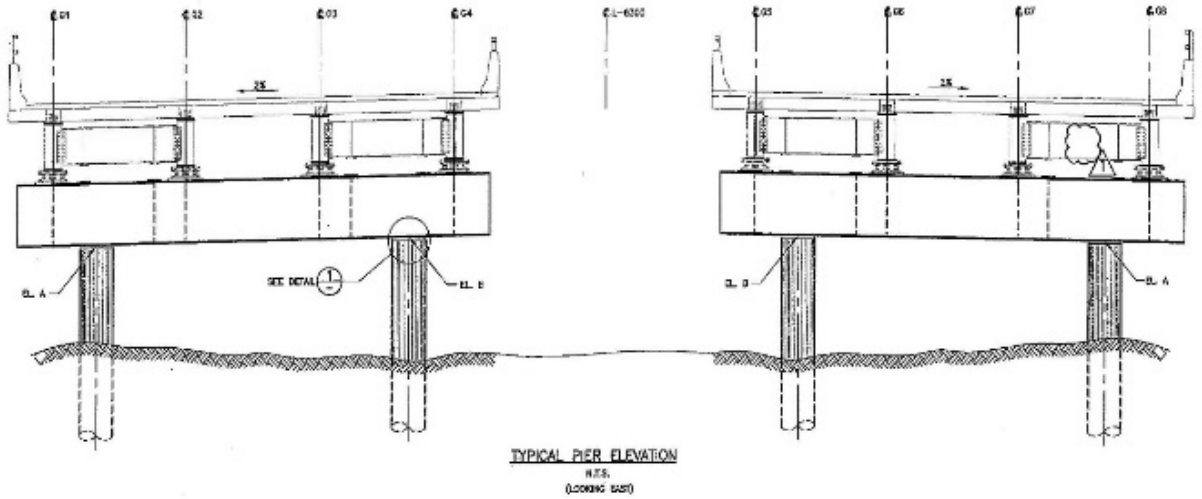


Fig. 3. Typical bridge elements

© 2016 Deep Foundations Institute

GEOTECHNICAL DESIGN

East Approach

The east approach required particular considerations because improvement of the soft compressible soils was necessary to avoid static/seismic embankment instability and to mitigate long-term settlement; but, at the same time, provide access for top-down bridge construction. A further consideration was that the anticipated settlement and lateral soil displacements during surcharging would impose large and unacceptable lateral loads on the abutment piles. The east span was constructed as a rotating span to allow adjustments by jacking in the event of long-term settlement. See Hall et al. (2015) for additional discussion.

Geotechnical Resistance Factors

A resistance factor of 0.5 was used for static loading based on PDA capacities and the 475-year seismic event (BC MoT Supplement, 2007). In addition, based on AASHTO (2007) and MCEER/ATC-49 (2003), a resistance factor of 1.0 was recommended for the 975- and 2475-year as well as the Subduction events.

Pile Details

The calculated maximum service load was 2,100 kN. The maximum factored load was 2,700 kN, which corresponded to the static load case (i.e. design was governed by service conditions). This resulted in a required unfactored ultimate geotechnical capacity of 5,400 kN for each pile.

The upper 11.5 m of each pile was concrete-filled, except that for shorter piles, the concrete fill was placed to within 1.5 m of the pile tip. A rebar cage with 2.6% longitudinal reinforcing steel was placed inside the pile to form the cap connection, as the steel pipe was curtailed 50 mm below the soffit of the pile cap. This connection was intended to form a plastic hinge if sufficient seismic displacement occurred in order to capacity-protect the pile cap.

The nominal spacing of each pair of trestle piles was 7 m; the cut-out was extended 300 mm transversely to accommodate the pile tolerance of 150 mm. This tolerance was found to be reasonable during installation and the maximum deviation was 100 mm. Kennedy et al. (2013) present further details of the capacity-protected pile-to-cap connection.

Pile Axial Capacity

Open-ended pipe piles were selected in order to facilitate penetration into the dense glacial till-like material and to make it easier to maintain tolerances. The Meyerhof (1976) and effective stress (Beta) methods as outlined in CFEM (2006), CHBDC (2006), and AASHTO (2007) were used to estimate unfactored Ultimate Limit State (ULS) capacities.

Pile penetration into dense glacial till-like material in the order of 3 m to 6 m were anticipated for plugged piles. For unplugged or partially plugged conditions (e.g. Randolph et al., 1991), the required penetration was anticipated to be about 6 m to 8 m. In addition, a minimum embedment depth of 4 m in till-like material was required for the piles near the west end to develop the required fixity to resist lateral loading.

CONSTRUCTION

General Sequence of Top-Down Construction

The construction was arranged so that the 250 tonne erection crane was supported by a work platform resting on the permanent trestles. The crane travelled along the westbound (northern) trestle which allowed the parallel eastbound trestle to be utilized for access and delivery of construction materials. At each location the crane installed the four piles beneath the next trestle. Figure 4 presents the top-down construction schematic and the arrangement of the two bridges with the erection and pile driving crane working from the construction platform.

There was minimal time available to address construction issues as delivery was required one year after start of construction to provide the non-tolled alternative. Two parallel spans had to be complete and operational every 10 days. Every construction component was on critical path.

© 2016 Deep Foundations Institute

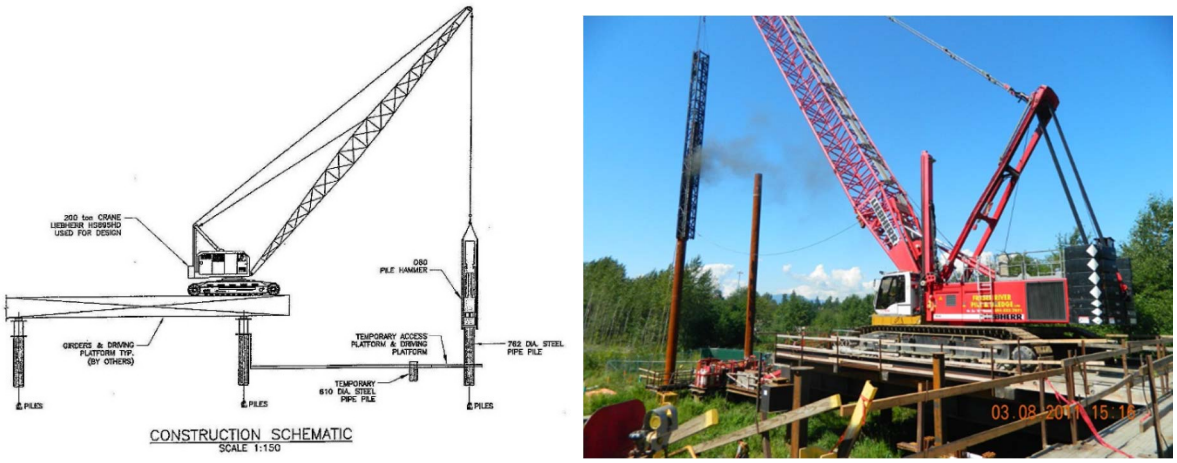


Fig. 4. Top-Down construction schematic, pile driving crane and hammer

Pile Drivability and Installation Methodology

From the outset, it was recognized that pile installation would be difficult and that there was significant risk of piles encountering obstructions and/or not obtaining sufficient penetration into till-like materials to satisfy lateral loading demands.

In top-down construction, the appropriate selection of the pile installation equipment is crucial because the hammer size and weight determine the crane capacity, which can affect the design of the bridge. Furthermore, if a pile is obstructed or damaged, performing remedial work is difficult and expensive because access onto the wetland requires special environmental permissions and has major schedule impacts.

The following installation risks were identified:

- Variable depth to dense glacial material: Because of the limited number of boreholes along the alignment, this was a risk with no simple mitigation.
- Obstructions: These included both boulders in the glacial soils and large tree trunks or root balls in the peat and overbank silt deposits.
- Pile layout: The pile layout was such that additional piles could not be installed without affecting seismic performance of the bridge.
- Artesian pressures: Open-ended pipe piles driven into artesian layers would be difficult to clean out if the artesian layers were not sealed off and/or the piles do not plug.
- Dynamic pile testing: The hammer must be sufficient to mobilize the piles during dynamic testing otherwise the results may not demonstrate that adequate axial capacity has been achieved

Ultimately, based on drivability studies and contractor input it was decided that the pile installation should consist of open-ended piles vibrated to dense material, followed by impact-driving to set using a D80 diesel hammer. The hammer was specifically oversized to handle obstructions and mobilize piles sufficiently during dynamic testing. The crane was operated on a temporary work platform which was supported by the permanent substructure. Providing a work platform was more cost-effective than strengthening the complete westbound superstructure to carry the heavy loads imposed by the construction crane.

Pile cleanout proved very time-consuming, and was undertaken using a clamshell bucket as the originally intended method of using vacuum excavation proved ineffective because of the fibrous nature of the peat. Concerns of encountering artesian conditions during pile cleanout did not materialize, likely because the piles penetrated and sealed potential artesian layers.

© 2016 Deep Foundations Institute

Obstructed and Damaged Piles

Variations in driven pile lengths are shown on Fig. 5. A total of 16 piles (about 14%) stopped on obstructions or were damaged and had to be drilled out, replaced or remediated. The obstructions consisted primarily of large boulders in the till-like deposits but on two occasions shallow refusal occurred on buried logs in the peat and overbank silt deposits.

Shallow boulders near the west abutment outside of the wetland area were removed relatively easily using an excavator. Where deeply buried boulders obstructed pile driving, prevented achieving sufficient pile capacity , or damaged the piles, an HP 360x174 pile (referred to as a stinger pile) was driven down the inside of the pipe piles to supplement the bearing capacity. Stinger piles were successfully installed at two locations (Piers 7 and 25) to remedy obstructed piles. In a third case (Pier 19), a stinger could not be installed inside the pipe (due to damage); therefore, two outside HP piles were installed. Stinger piles extended about 1 m, 9 m and 16 m below the bottom of the pipe piles at Piers 7, 19, and 25, respectively.

Five obstructed piles were extracted and after cutting off the damaged ends, were re-driven in conjunction with drilling out. Inspection of the extracted piles indicated that in most cases, the damage took the form of the piles folding in on themselves. This had the effect of making it necessary to extract a pile and cut off the damaged end before undertaking remedial work such as drilling-out or driving stinger piles.

In many cases plugging did not occur and this was considered to result from "fluffing" up of the soils within the pile during driving, possibly because of the effects of artesian pressures.

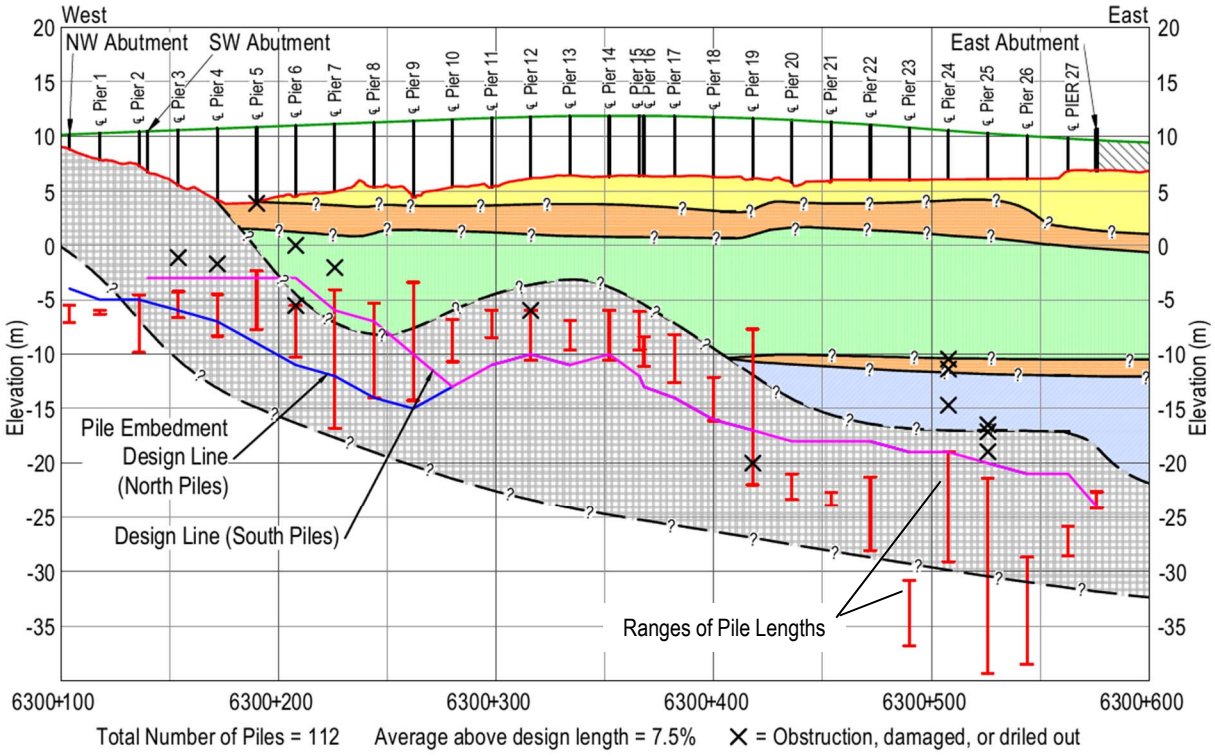


Fig. 5. Variations in installed pile lengths.

© 2016 Deep Foundations Institute

PDA Results vs. Design Codes

Fig. 6 summarizes the Pile Driving Analyzer (PDA) test results along the alignment. More than 40 PDA tests were performed on 12% of the piles to satisfy the design requirements as per AASHTO (2007). The PDA capacities were estimated using the Case Pile Wave Analysis Program (CAPWAP). The data are presented for End of Initial Drive (EOID) and Beginning of Re-drive (BOR).

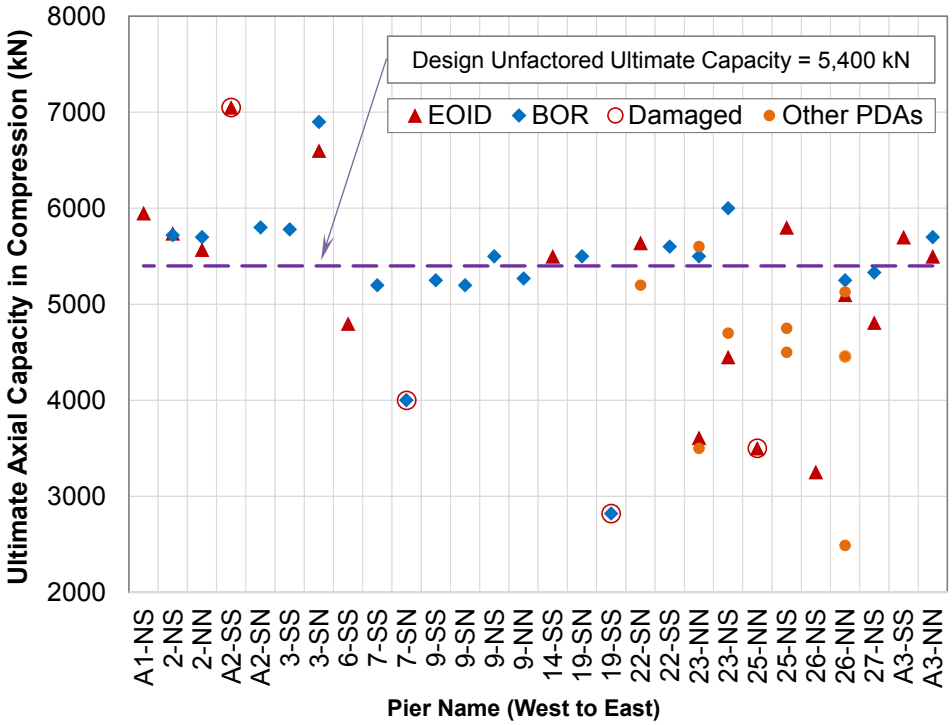


Fig. 6. Summary of PDA test results.

Figure 7 shows the variations in the unit shaft and toe resistance obtained from the CAPWAP signal matching process. Figure 8 shows the back-calculated Beta and N_t coefficients. Data are shown for three groups of piles (where PDA was available): 1) Abutment 1 to Pier 7 (western section), 2) Piers 9 to 14 (central section), and 3) Pier 19 to Abutment 3 (eastern section). Figure 8 also shows the ranges of Beta and N_t coefficients recommended in CFEM (2006) and CHBDC (2006) design codes for comparison with the back-calculated values.

Figure 9 shows the ranges of back-calculated Beta values for each pile but only within the till-like material for comparison with the code values. Because the depth to till-like soils varied across the site (longitudinal and transverse to the bridge) and the extracted ranges for Beta within till-like layer were based on the depth range indicated in the nearest testhole, the lower end of the Beta ranges may not necessarily reflect the actual Beta values in the till-like soils. Figure 10 shows the back-calculated N_t coefficients for each pile along the bridge (where PDA was available) for comparison with the code values. Figure 11 shows the statistical distribution of these coefficients in till-like soils for selection of representative values (e.g. 50th percentile).

© 2016 Deep Foundations Institute

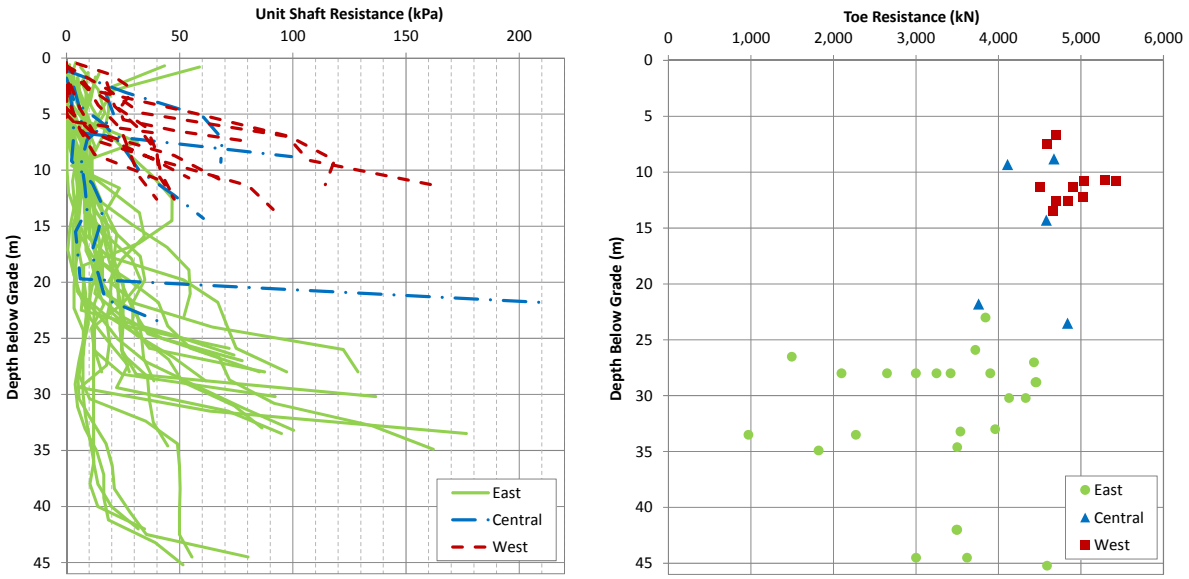


Fig. 7. Unit shaft and toe resistance (kPa) from CAPWAP.

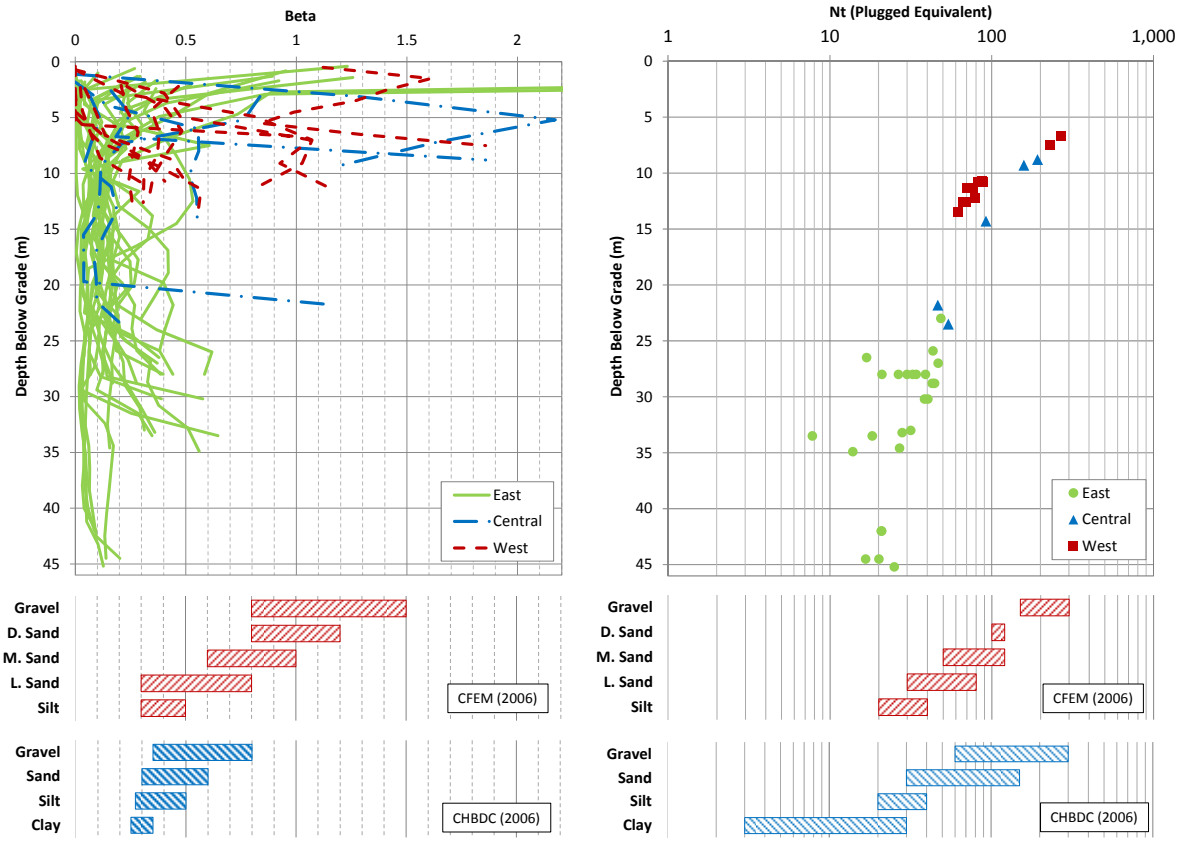


Fig. 8. Back-calculated Beta and N_t coefficients for three sections along the bridge.

© 2016 Deep Foundations Institute

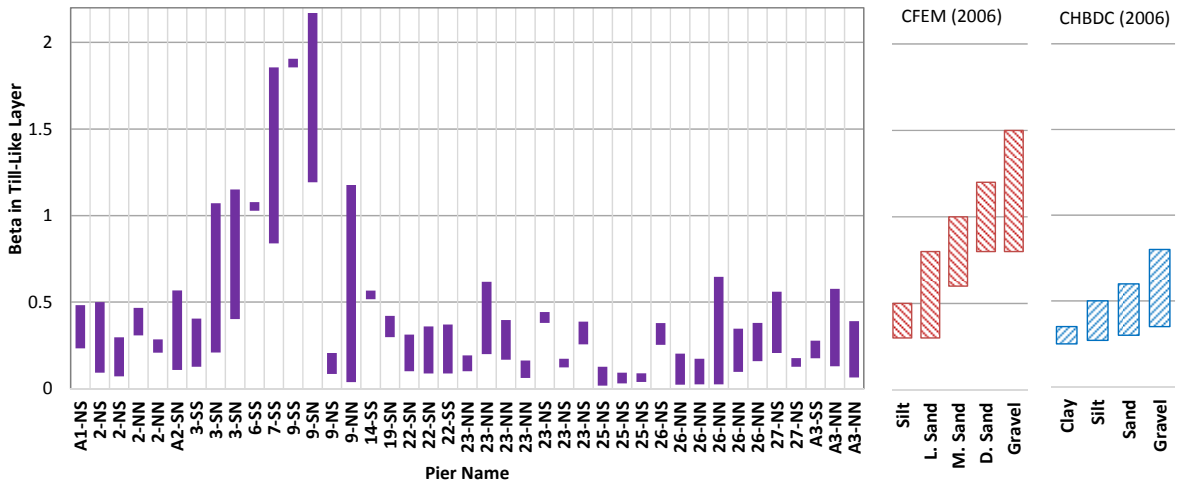


Fig. 9. Back-calculated Beta coefficients in till-like layer for each pile along the bridge.

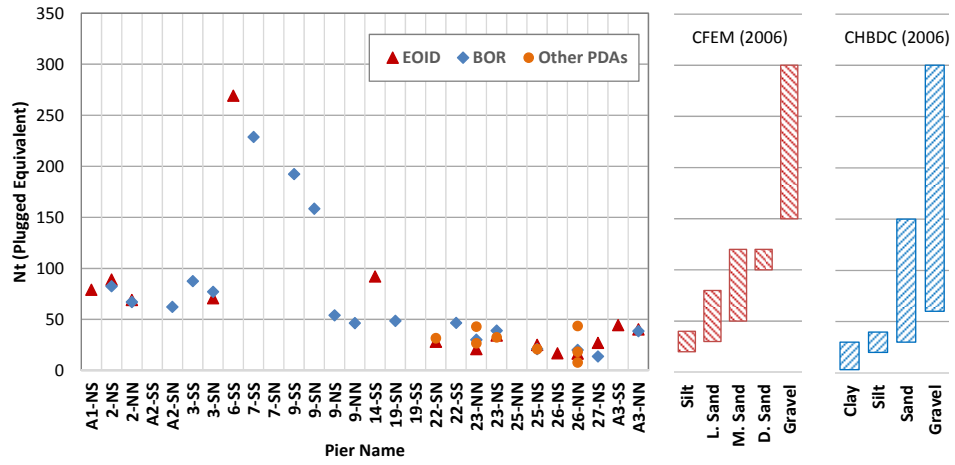


Fig. 10. Back-calculated N_t coefficients for each pile along the bridge.

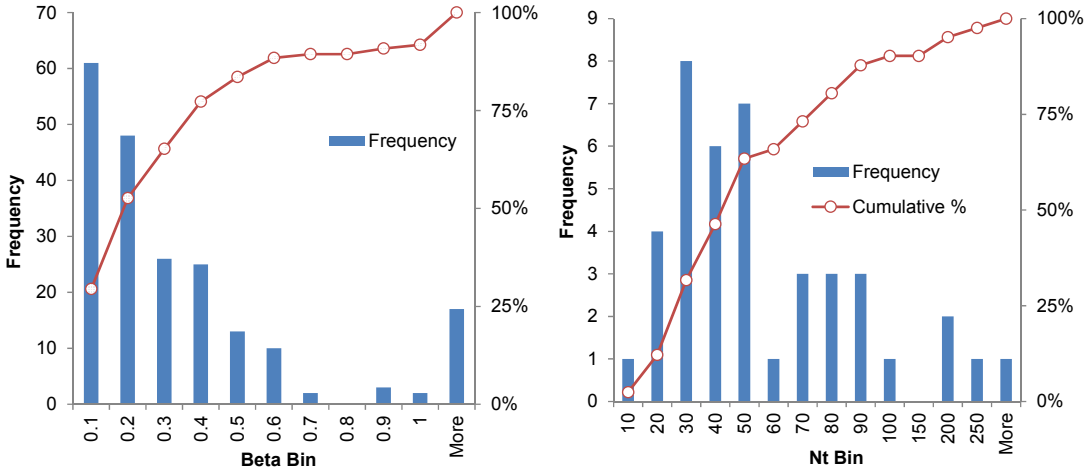


Fig. 11. Statistical distribution of back-calculated Beta and N_t coefficients.

© 2016 Deep Foundations Institute

These results indicate the following:

- Unit shaft resistance in till-like soils rarely exceeded 100 kPa; typically ranged from 25 kPa to 75 kPa; but, could be as low as 15 kPa over a significant length of pile embedment.
- Unit toe resistance in till-like soils calculated for an equivalent plugged condition (closed-ended pipe area of 0.45 m^2) typically ranged from 10,000 kPa to 12,000 kPa in the western section; and, from 6,000 kPa to 10,000 kPa in the eastern section, but with values as low as 2,000 kPa.
- Unit shaft and toe resistance did not have a direct correlation with increasing depth (or vertical effective stress). However, for a given pile, the unit shaft resistance generally increased with depth.
- Back-calculated Beta values for till-like soils typically ranged from 0.3 to 1 in the western section (where till-like soils are at shallow depths); and, from 0.05 to 0.3 in the eastern section (where these soils are at great depths). For comparison, the recommended range in CFEM (2006) for driven piles in "Dense sand" is 0.8-1.2.
- Back-calculated N_t values for till-like soils typically ranged from 60 to 200 in the western section (where these soils are at shallow depths); and, from 20 to 50 in the eastern section (where these soils are at great depths). The recommended range in CFEM (2006) for driven piles in "Dense sand" is 100-120.

SPT-Based Toe Resistance

CFEM (2006) presents two equations for pile capacity estimation based on Standard Penetration Test (SPT). The first equation (Meyerhof, 1976) equates the toe resistance (in kN) to 400 times the SPT index at the pile toe. The second equation (Decourt, 1995) is similar to the first but is based on 4 factors of 100, 165, 205, and 325 for clay, clayey silt, sandy silt, and sand, respectively. These factors apply to driven/displacement piles. Figure 12 presents the variability of the SPT blow counts in the till-like layer and the corresponding toe resistance using Meyerhof (1976) method. Comparing Figs. 7 and 12 indicates that the SPT-based resistance is significantly higher than the tip resistance back-calculated from PDA data.

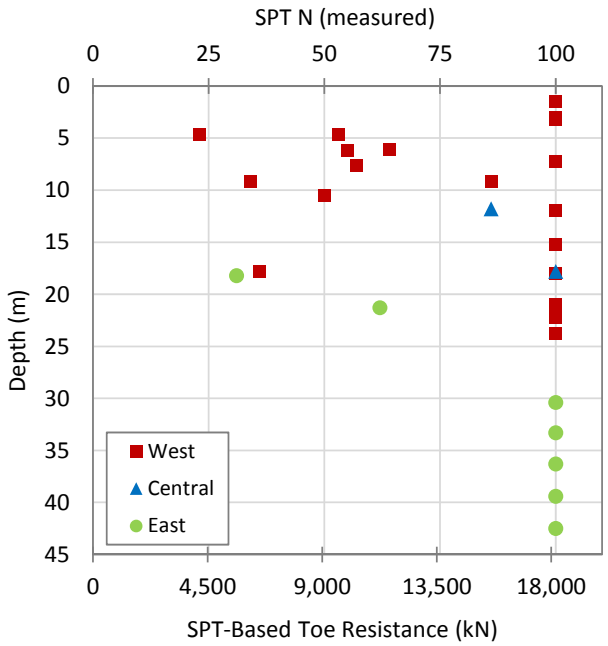


Fig. 12. Variation of SPT N-values and toe resistance using Meyerhof (1976) method.

© 2016 Deep Foundations Institute

Pile Setup vs. Time

Figure 13 presents the percent increase in pile resistance with time. As shown, in 5 cases, there was only a small increase after 3-4 days. However, in one of these 5 cases, the PDA capacity further increased by 80% after 4 additional days. In 3 other cases, up to 50% increase was noted in less than 2 days.

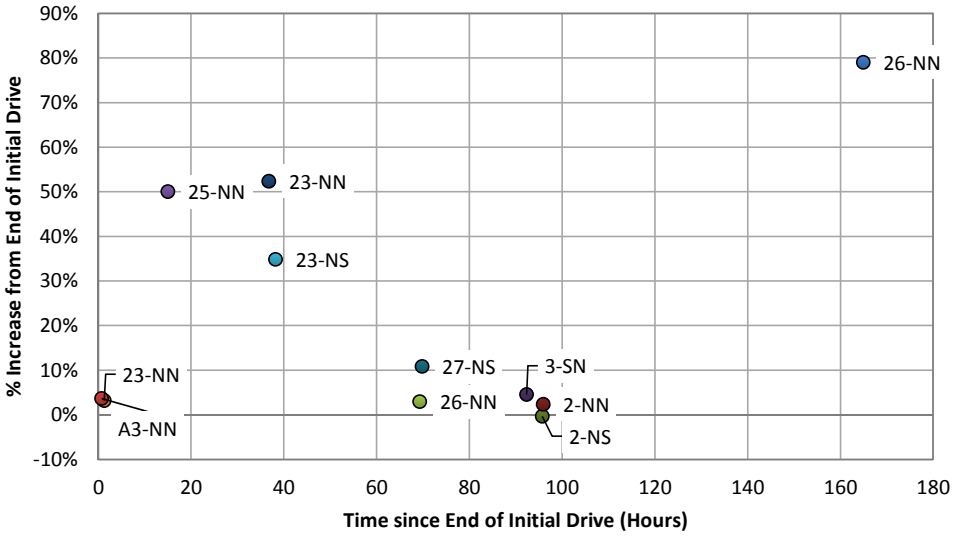


Fig. 13. Variation of PDA resistance with time (setup).

CONCLUSIONS

Difficult soil conditions, environmental restrictions prohibiting access onto the wetland, stringent seismic performance criteria, and mandated tight schedule were the main competing requirements for design and construction of the FHB. These requirements were addressed by adopting a top-down construction approach and extensive interaction between the designers and bridge constructors to integrate structural and geotechnical engineering with construction methodology.

Trestle-type piers, consisting of driven pipe piles (two piles per trestle), were a key component of the design. Insufficient geotechnical borings (due to access restrictions) and highly variable soil conditions resulted in significant variability in the estimated pile capacities during the design phase. In addition, demonstrating that the target capacities had been achieved proved to be challenging. This was further complicated by the fact that the recommended parameters for pile capacity estimation in the applicable design codes over-estimated the capacity when compared to the PDA results. Construction was not altered because of the PDA findings; however, actual pile lengths varied from the design (predicted) lengths. In an extreme case, the actual pile length was about 18 m longer than the design length of 27 m (i.e. 67% longer). On average, actual pile lengths were 7.5% above the design length.

Glacial till-like soils were relied upon as the major contributor to pile resistance. Code parameters for shaft and tip resistance (Beta and N_t coefficients, respectively) in dense sand or gravel are typically selected for till-like soils. However, back-calculated Beta and N_t coefficients from PDA results were found to be significantly lower than the code values. Ranges provided in the codes for silt and loose to medium dense sand were found to provide a better match with the PDA data for till-like soils at this site. Tip resistances estimated based on SPT data were also found to be significantly higher than those indicated by PDA.

Undertaking a detailed preconstruction pile test program to assess pile installation methodology and drivability, to verify applicability of pile capacity estimation methods to the soils present at the site, and to develop pile setup versus time relationships, could alleviate some of the difficulties of facing unexpected conditions during construction.

© 2016 Deep Foundations Institute

ACKNOWLEDGMENTS

The contributions of the following and permission to publish this paper are gratefully acknowledged: The BC Ministry of Transportation and Infrastructure (through Transportation Investment Corp.); Kiewit/Flatiron General Partnership, and Gateway Infrastructure Group as the bridge sub-contractor; H5M – a joint venture of Hatch Mott MacDonald and MMM Group Limited as prime consultant and Brybil Projects, a subsidiary of Associated Engineering (AE) Group Ltd., as bridge designers; and, Tetra Tech EBA as the geotechnical engineers. In particular, the contributions of the following individuals are appreciated: D. Harvey (structural design lead at AE), B. Miner (RMDT PDA testing), S. Northcutt (formerly of Tetra Tech EBA), A. Fell (Tetra Tech EBA), R. Osmus (Kiewit), K. Seabloom and J. Steele (Fraser River Pile & Dredge), and U. Wexler (formerly of AE).

REFERENCES

AASHTO. 2007. LRFD Bridge Design Specifications, 4th edition, *American Association of State Highway and Transportation Officials*.

BC Ministry of Transportation (MoT) Supplement to CHBDC (Canadian Highway Bridge Design Code) S6-06. 2007. Bridge Standards and Procedures Manual.

CFEM. 2006. Canadian Foundation Engineering Manual, 4th edition, *Canadian Geotechnical Society*.

CHBDC CAN/CSA-S6-06. 2006. Canadian Highway Bridge Design Code (CHBDC), *Canadian Standards Association*, ON.

Decourt, L. 1995. Prediction of load-settlement relationships for foundations on the basis of the SPT-T. Ciclo de Conferencias Internationale. Leonardo Zeevaert, UNAM, Mexico, 85-104

Hall, B., Azizian, A., Harvey, D. 2015. Fraser Heights Bridge – Geotechnical Considerations for Top-Down Construction on Difficult Soils. Canadian Geotechnical Conference, Quebec City.

Kennedy, D., Cook C., and Wexler, U., 2013. Seismic Design Using Isolation Bearings for Rapid Construction of the Fraser Heights Bridge, *7th National Seismic Conference on Bridges and Highways*, Oakland CA.

MCEER/ATC-49. 2003. Recommended LRFD Guidelines for the Seismic Design of Highway Bridges.

Meyerhof, G.G. 1976. Bearing Capacity and Settlement of Pile Foundations. *Journal of Geotechnical Engineering*, ASCE, Vol. 2, 195-228.

Randolph, M.F., Leong E.C. and Houlsby, G.T. 1991. One-dimensional Analysis of Soil Plugs in Pipe Piles, *Geotechnique*, 41(4): 587-598.

© 2016 Deep Foundations Institute

GOETHALS BRIDGE REPLACEMENT FOUNDATION DESIGN MODIFICATIONS DUE TO FIELD CONDITIONS

Bobby Daita, P.E., Parsons Corporation, New York, USA, bobby.daita@parsons.com
John P. Turner, Dan Brown and Associates, PC, Laramie, WY, USA, jturner@dbaworld.com
Mark Jen Ph.D., P.E., Parsons Corporation, New York, USA, mark.jen@parsons.com

ABSTRACT

The Port Authority of New York and New Jersey is replacing the existing Goethals Bridge built in 1928 which is deemed to be functionally obsolete. The replacement bridge will consist of a dual cable-stayed Main Bridge crossing the Arthur Kill with elevated approach spans connecting Elizabeth, New Jersey and Staten Island, New York. The main bridge towers are supported on a group of six nine-foot diameter drilled shafts that transition into a pier cap. The anchor and approach piers are supported on two column bents with each column supported on a single drilled shaft. The 4.5 to 10 feet diameter drilled shaft foundations have permanent steel casing to rock and socketed into bedrock. Subsurface conditions consist of Passaic Formation bedrock overlain by varying thicknesses of overburden soils. The foundation design assumes permanent casing extending a minimum 2 feet into the weathered bedrock. Rock socket lengths below the permanent casing vary between one to two shaft diameters based on the quality of the bedrock. The reinforcing design was based on AASHTO LRFD minimum requirements, force demands, seismic detailing requirements and also considering the continuity between the shaft and socket.

The bridge is currently under construction with approximately 70 percent of the foundations installed. Several field conditions encountered at various stages of shaft construction between casing advancement and concreting required design and construction modifications. Based on the driving method and the quality of the bedrock, the tip of the permanent casing hit refusal either above or below the design elevation, requiring modifications to the drilled shaft design and its reinforcement. This paper provides an overview of the general subsurface conditions at the site and its impact on foundation design and discusses the detailing worked into the design to accommodate tip elevation variations, as well as various foundation design modifications in response to actual conditions encountered during construction.

INTRODUCTION

The existing Goethals Bridge was constructed by the Port Authority of New York and New Jersey (PANYNJ) in 1928. The existing bridge is a steel truss cantilever with a 672 feet long central span over the Arthur Kill. Including the approaches, the bridge is 7,109 feet with a width of 62 feet and has four lanes for traffic. The 10-foot wide lanes in each direction do not meet the 12-foot requirement of modern highway design standards. Additionally the bridge has no shoulders for emergency access, or pedestrian walkways or bike paths. Considering these factors and given present-day traffic volume and commercial growth, the existing bridge is functionally obsolete. PANYNJ is therefore replacing the Goethals Bridge with a new bridge that will consist of more and wider lanes and will include shoulders, sidewalk/bikeway, provide improved safety conditions, and utilize state-of-the-art smart bridge technology. In addition, the new bridge will include a central corridor to accommodate future transit service. The new bridge will be located just south of the existing bridge which will be demolished upon completion of the replacement bridge.

A total of 19 elevated dual approach spans in New York (NY) and 18 elevated dual approach spans in New Jersey (NJ) along with the 3 dual spans of the Main Bridge over the Arthur Kill form the replacement bridge that connects Staten Island, NY and Elizabeth, NJ. The Main Bridge is a dual cable-stayed bridge providing a 138-ft clearance permitting passage of deep-sea vessels through the Arthur Kill.

© 2016 Deep Foundations Institute

The main bridge consists of a primary span between the eastbound and westbound tower structures in New York and New Jersey (identified as P1NY and P1NJ) and a secondary span between the towers and anchor piers (identified as P2NY and P2NJ). The approach span piers are numbered in an ascending order to the abutment on both sides of the anchor piers in NY (P3NY to P19NY) and NJ (P3NJ to P18NJ). The anchor and approach piers consist of two column bents while the abutments are under a pier cap footing. The eastbound and westbound bridges have separate abutments in both NY and NJ. Figure 1 shows the existing bridge with several of two-column bents under construction.



Fig. 1. Existing Goethals Bridge (right) and Replacement Bridge under construction. View is from NY side looking east.

GEOTECHNICAL CONDITIONS

The subsurface conditions are fairly consistent along the bridge and consist of overburden soils and varying thickness of weathered rock overlying competent bedrock. Overburden soils on the NJ side consist of man-made fill and glacial deposits and on the NY side consist of man-made fill, glacial deposits, marine sands, and tidal marsh deposits. The man-made fill thickness varies from about 2 feet to up to about 25 feet. The Wisconsin age glacial till deposits consist of un-stratified clay, silt, sand, and gravel and the outwash deposits consist chiefly of stratified fine to coarse sand and gravel. The Holocene tidal marsh deposits consisting of organic peat, silt, and clay that have accumulated in low lying areas created after the retreat of the glaciers are largely absent on the NJ side of the bridge. The thickness of this stratum generally decreases from west to east with thicknesses varying between 5 feet and 35 feet. Areas where the organic deposit is thinnest generally correspond with areas of thicker fill, indicating that the organic soil has likely been compressed by the overlying fill. The marine sand deposits were formed when the sea breached the terminal moraine left by the glacier and consist of loose to medium dense sands. This stratum extends eastward from Arthur Kill for a distance of about 3,200 feet. Some of the marine sands encountered in NY are susceptible to liquefaction under the design seismic ground motions.

© 2016 Deep Foundations Institute

The sedimentary bedrock which underlies the bridge site is part of the Passaic Formation in the Newark Supergroup, consisting of red and reddish brown shale, siltstone, and sandstone. These thin-bedded sedimentary rocks have ripple marks and mud cracks indicating a shallow-water depositional environment. The thickness of decomposed or weathered rock overlying competent rock varies between less than 1 foot to up to 10 feet in NY and up to 21 feet in NJ. The top of competent bedrock varies between El. -17 and El. -45 feet in NJ and between El. -38 and El. -61 feet in NY. Depth to bedrock is generally greater in NY than NJ. A companion paper (Turner et al., 2016) provides additional information on characteristics of the weathered and intact rock and a generalized subsurface profile.

The groundwater table was encountered at shallow depths due to the low lying topography along the bridge alignment. The groundwater table ranges from about El. 0 to El. 6 feet. The groundwater table in the vicinity of Arthur Kill is tidally influenced.

FOUNDATION DESIGN

Per Requirements for Provision of Work (RPW) document provided by PANYNJ, the replacement bridge foundations shall be founded in rock. Based on the relatively shallow depth of competent bedrock and the anticipated structural loading, drilled shafts socketed into competent bedrock were identified as the most suitable foundation type for supporting the replacement bridge. The main bridge towers are supported on a group of six (6) 9-foot diameter drilled shafts that transition into a pier cap. The two-column bents of anchor and approach piers are each supported on a single drilled shaft with diameters varying between 4.5 and 10 feet. Each abutment is supported on a group of three shafts with a diameter of 4.5 feet in NJ and 5 feet in NY. All the drilled shafts have permanent steel casing to rock with a nominal rock socket diameter 6 inches less than the permanent casing diameter. Permanent steel casings are assumed to extend a maximum of 2 feet into weathered bedrock prior to encountering refusal. In locations where the thickness of weathered rock is less than 2 feet, permanent steel casing was assumed to encounter refusal on top of intact rock. Design of the rock-socketed drilled shafts was based on the following considerations:

- Socket lengths shall be at least twice the rock socket diameter (2D) in areas where average Rock Quality Designation (RQD) within the rock socket zone is less than 75% and shall be at least equal to the socket diameter where average RQD within the rock socket zone is greater than 75%.
- Rock socket begins at the tip of the permanent casing and extends into both weathered and intact bedrock. At least 4 feet of rock socket length shall be within the intact rock. Socket lengths exceeded twice the rock socket diameter at some locations in both NY and NJ in order to completely penetrate the weathered rock and to meet the 4 feet into intact rock criterion.
- Soil and rock layers over the full length of the drilled shaft provide lateral geotechnical resistance; except in locations subjected to scour, liquefaction, and lateral spread flow loads.
- Axial geotechnical resistance provided by overburden soils is neglected and is exclusively provided by foundation embedment in rock below the tip of the permanent casing.
- Axial resistance of rock sockets is based on the combined side and base resistances.
- The contribution of permanent casing to the structural strength of drilled shafts is conservatively neglected; however, the increased strength of the concrete due to confinement provided by the casing is taken into account for lateral analyses.
- The contribution of permanent casing to increased flexural stiffness of drilled shafts is taken into account.
- In order to account for corrosion, the casing wall thickness in NY was decreased from 0.75 inches to 0.58 inches above El. -7 feet and to 0.23 inches below El. -7 feet for strength and service limit state load combinations. Under earthquake loading, the steel casing corrosion loss values are reduced to one-half of these values, *i.e.* 0.29 inches above El. -7 and 0.12 inches below El. -7 feet.

© 2016 Deep Foundations Institute

Nominal values of unit side and base resistances are based on AASHTO specifications, recommendations in the FHWA Drilled Shaft Manual (Brown et al., 2010), and axial load tests performed at the GBR Project site. Four axial load tests provided the basis for establishing the following nominal resistances used in final design: 25 ksf for unit side resistance in intact rock and 6 ksf in weathered rock, and 300 ksf for unit base resistance. The load test results demonstrated the validity of these design values even in locations at which the shaft base was bearing on rock with relatively low Rock Quality Designation (RQD) values. Resistance factors for strength and extreme event load cases were based on AASHTO specifications and were further reduced by 20% for the two-column piers to account for support of a single column by a single foundation element. The factored axial resistances calculated using these nominal side and base resistances at each shaft supporting the bridge exceeded the factored axial demand calculated using the governing strength limit state loads. The load testing program and its application to design are discussed in detail in a companion paper (Dapp et al., 2016).

Foundation reinforcing design was based on AASHTO LRFD Bridge Design Specifications, force demands, seismic detailing requirements, and considering the continuity between the shaft and socket. Reinforcing cages consist of two sections – a lower drilled shaft section with non-epoxy bars and an upper column transition section with epoxy bars. Permanent casing is assumed to protect the shaft reinforcement from corrosion, but the uncased column reinforcing steel is epoxy coated in order to meet design life requirements. The upper transition section consisting of epoxy coated Grade 60 longitudinal and transverse hoop bars is referred to as the "jumper cage". The upper and lower sections are connected using Type 1 mechanical couplers at staggered locations approximately 2 to 5 feet below top of permanent casing. The lower section consisted of non-epoxy coated Grade 80 longitudinal reinforcement with Grade 60 transverse spiral reinforcement and access tubes for cross-hole sonic logging (CSL) held together with a bracing system. Transverse reinforcement consists of spiral with pitch varying between 5 and 12 inches. Locations with a change in cross-section such as the column/shaft connection and top of rock socket have high stress concentration and potential for plastic hinge development. The spiral reinforcement with tighter pitch was at these potential plastic hinge locations or where maximum bending moment is anticipated within the shaft. The zones with tighter pitch occur near the top of the shaft and several feet above and below the top of rock socket (near the bottom of the casing). Figure 2 shows a drilled shaft reinforcing cage with the various features described above.

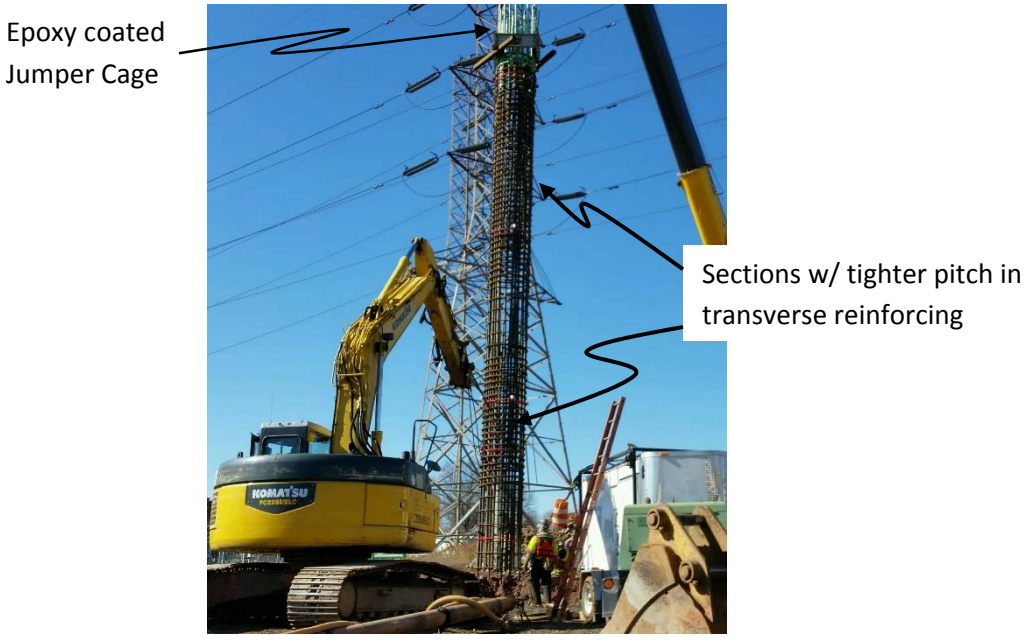


Fig. 2. Typical reinforcing cage.

© 2016 Deep Foundations Institute

FOUNDATION CONSTRUCTION

Construction of drilled shafts began with advancing the permanent steel casing to top of rock by vibratory hammer driving. Use of a rotator and/or oscillator for twisting the casing into the ground or telescoping drill techniques were initially identified as means of advancing the casing in the event of obstructions or the inability of the vibratory hammer to advance the casing. Overburden materials within the casing were then drilled using conventional augers and digging buckets. Upon reaching top of bedrock at the tip of casing, the rock socket excavation was advanced using a combination of rock core barrels, rock augers, and rock digging buckets. Considering the shallow groundwater table, water was added when the excavation extended reached 10 feet above the bottom of casing and maintained at a level above the groundwater table. While it may have been possible to construct some shafts "in the dry", flooding the casing was adopted as a means to reduce the risk of caving and provide positive seepage pressures against the walls and base of the excavated borehole. Once an excavation reaches the target socket tip elevation, mechanical clean out buckets are used initially to remove solids from the shaft excavation. An air lift consisting of a 6-inch diameter steel pipe with a 1-inch air supply line attached to the inlet of the pipe is lowered to the shaft bottom and used to remove solids from the bottom of the shaft (Figure 3). The air supply at the bottom of the shaft creates a substantial flow of solids and water rising inside the airlift and a constant water supply is added at the top of the shaft to maintain equalized pressure inside and outside shaft during airlift operation. The shafts are considered to be built in "wet condition" considering the presence of a column of water inside the shaft until concreting operation. The cleanliness of the shaft bottom is verified using a Mini Shaft Inspection Device (MiniSID) camera. Upon passing the MiniSID verification, the reinforcing cage is lowered into the shaft and held in place with a picking frame. Concrete is introduced into the shaft using a tremie pipe lowered to the bottom of the shaft. CSL tests are performed on all shafts at least 96 hours after placement of concrete.



Figure 3. Airlifting drilled shaft excavation at Pier 1 NY.

© 2016 Deep Foundations Institute

DESIGN AND CONSTRUCTION METHOD MODIFICATIONS

Field conditions encountered at various stages of shaft construction between casing advancement and concreting required design and construction modifications. These field conditions can be anticipated at other project sites and therefore the design and construction method modifications made at GBR project can serve as guidelines for other projects. The following paragraphs provide examples of conditions that have required modifications to both design and construction methods of the foundations. Specific examples for the GBR project are summarized in a tabular format later in the paper.

Alternate Method for Casing Advancement

The permanent casing is advanced using vibratory hammer initially for some of the approach piers in NJ. However, the existing fill soils with occasional cobbles and boulders and the very stiff/dense glacial overburden soils require tremendous effort during casing advancement using vibratory hammer. A revised casing advancement procedure consisting of using a rotator and/or oscillator was approved. As part of this revised casing advancement procedure the following guidelines were developed

- The shaft can be drilled unsupported up to a maximum depth of 10 feet to clear shallow obstructions and stand the casing upright.
- After this initial predrilling, the permanent steel casing with welded teeth to assist advancement of casing is placed in the excavation.
- The drill rig then simultaneously rotates and uses downward force to advance the casing into the overburden.
- If the casing encounters resistance or refusal, relief drilling is allowed to excavate soil from inside the casing. During relief drilling a 10-ft plug of soil must be maintained within the casing if water is not introduced.
- In order to advance the casing, drilling within the 10-ft soil plug above the casing tip is allowed only if the casing is flooded with water to at least 5 feet above the groundwater table.
- Drilling is allowed beyond the tip of the casing for up to 1 shaft diameter. However, the material drilled beyond the casing tip will be mudded (*i.e*. mixed with water and softened to allow advancement of casing) but left in place to prevent caving below the casing.
- If casing retraction is needed during installation (for example to ensure the casing is plumb and is within tolerance for its location), the casing will be backfilled first with soil cuttings and water to at least 5 feet above the target retract elevation prior to casing retraction.

This alternate casing advancement procedure was used at several shaft locations in NJ. A template was used to ensure the shaft was within location tolerance limits.

Casing Out of Location

Project specifications require the axis of the shaft measured at the top of the shaft to be within 3 inches of the plan location and for shafts to be plumb to within 1.5 percent of the length based on total shaft length. Some of the casings advanced with vibratory hammer or by twisting resulted in locations exceeding the 3-inch tolerance. However, all shafts were within the verticality tolerance. If the out-of-tolerance shaft was located in an area with a relatively tall column, the cage was offset 3 inches, which is the maximum possible in order to stay within the minimum concrete cover for the cage. The remainder of the out-of-tolerance width was compensated at the column/beam junction. At short column locations the casing was re-seated by pulling it up and re-advancing to meet the tolerance limits. In order to retrieve an already advanced casing, it was required for the casing to be flooded and to maintain a minimum 5-ft soil plug inside the casing above the casing tip in its retrieved condition.

© 2016 Deep Foundations Institute

Variations in Casing Tip Elevation

The top of weathered bedrock along the bridge varies in both NJ and NY. Thickness of the weathered rock zone and its competency are also quite variable along the bridge. It was not deemed feasible to perform a test boring or sounding at each shaft location, thus creating some uncertainty regarding top of weathered rock and intact rock elevations. The casing tip refusal elevation was found to depend on the competency of weathered rock and the method of casing advancement. For design, based on observations during installation of the test shafts, the casing was assumed to penetrate 2 ft into weathered rock. During construction, casings encountered refusal both above and below the estimated design tip elevations. Like most projects, reinforcing cages were pre-fabricated prior to drilling operations. The fabrication initially provided an allowance of an additional 3 ft of tight-pitch spiral reinforcing zone above the design top of socket elevation. This allowance was modified later to provide additional tight-pitch spiral both above and below the design top of socket elevation. The following design modifications were made for variations in casing tip elevation.

Case 1) Casing refuses above the design estimated tip elevation within overburden soils: Upon drilling inside the casing if it was determined that the casing refused within the overburden soils then the casing could be driven further to refuse within weathered bedrock in order to avoid caving-in of the soils between the tip of casing and bedrock. Relief drilling of soils within and below the casing assists in re-driving the casing into weathered rock. Rock socket length is then calculated beginning from the new casing tip elevation and the socket tip elevation is lowered to meet the design criteria (2D length and 4 feet in intact rock), if necessary. The need for reinforcing cage modifications can then be evaluated based on the field-modified casing tip elevation and socket length.

If the casing is left at the original refused location within the overburden soils, the reinforcing cage may need to be lowered if the top of weathered rock is below the design casing tip elevation. Modifications to the spiral reinforcement may be required if the elevation difference between the casing bottom and top of weathered rock exceeds the tight pitch spiral allowance provided in cage fabrication. This condition was encountered at several shafts in both NY and NJ. However, in most locations the casing refused in cohesive glacial soils within 2 feet of weathered rock. At two locations, casing encountered refusal within soils that have potential to cave-in. Additional details of these locations are provided in Table 1.

Case 2) Casing refuses above the design estimated tip elevation within weathered bedrock: Considering variations in the top of weathered bedrock, some casing encounters refusal above the estimated design tip elevation. Although it may result in longer than required socket length, the bottom of rock socket was unchanged to match the original design elevation so that the full length pre-fabricated reinforcing cage was useful. Also, a minimum 4 feet of rock socket within intact rock was confirmed. The additional tight pitch spiral reinforcement provided above the design casing tip elevation was sufficient to meet the design requirements in most locations considering the allowances provided in spiral reinforcement. However, at locations where the spiral reinforcement did not meet design requirements despite the allowance, modifications were made to the reinforcing cage. The modifications consisted of readjusting the pitch of spiral reinforcement such that the tight pitch spiral reinforcement meets the design requirement above and below the top of rock socket.

Although this condition was encountered at several shaft locations in NY and NJ, significant design changes were not required as the socket length is more than adequate and the additional spiral reinforcement allowance near design casing tip has allowed the shaft to meet design requirements. Design changes were required at two locations as described in Table 1.

Case 3) Casing overdrives and refuses below estimated tip elevation within weathered bedrock: Based on the competency of weathered bedrock, casing may sometimes advance below the estimated tip elevation.

© 2016 Deep Foundations Institute

In such a case the top of rock socket begins at the new bottom of casing elevation. The bottom of rock socket should be lowered to meet the design criteria (2D length and 4 feet in intact rock). If the reinforcing cage with spiral reinforcement allowances meets the design requirements, no changes are required. If the overdriving results in lowering bottom of rock socket by greater than 3 feet, the reinforcing cage was extended at the bottom with the use of Type 2 mechanical couplers. For cases where the overdriving resulted in lowering the bottom of rock socket by less than 3 feet, the reinforcing cage was lowered by extending the column reinforcing into the shaft and the spiral reinforcement readjusted to meet the design requirements.

This condition was encountered at several shafts in both NY and NJ and at almost all locations the overdriven casing refused within weathered bedrock. However, at P5NJEB South shaft weathered bedrock was encountered approximately 2.5 feet below the bottom of casing. Additional details of this case are provided in Table 1.

Based on the above modifications made for the initial shafts, cage fabrication for the remainder of the project shafts allowed for greater allowances in tight pitch spiral reinforcement to make the cage suitable for field conditions involving casing encountering refusal both above and below the design tip elevation.

Drilling in Dry Condition

Piers 16 and 17 of the bridge in NJ are located in the median of Interstate 95 and its ramp and provided the challenge of limited work space and difficult access to water. Addition of water into the shaft during drilling and airlifting operations would require a portable source of water and additional work space including lane closures. Therefore, the possibility of drilling the overburden soils and rock sockets in the "dry" *i.e*. without adding water or other drilling fluids was explored. Considering the shallow groundwater table at the site, drilling in the dry would only be feasible if the permanent casing provides a water tight seal and the bedrock is relatively impermeable during rock socket drilling. The following guidelines were developed for drilling in the dry:

- The casing will be either impact driven or twisted into bedrock to achieve a water tight seal. If casing is advanced by twisting method, the guidelines previously provided in this paper for this method should be followed. A heavy influx of water into the shaft excavation during drilling operations may potentially indicate a poor seal at the bottom of the casing, requiring additional measures to provide an adequate seal.
- The operation of drilling the rock socket and concreting the shaft should be completed within a 48 hour period. Additionally, upon completion of rock socket drilling, concreting of the shaft should take place within 24 hours. Therefore during casing advancement and drilling, a minimum 5 feet of soil plug should be left undrilled inside the casing unless preparations are made to drill the rock socket and place concrete within 48 hours. If concreting does not take place within the prescribed time limits, the shaft should be flooded and constructed using the "wet" method.
- Upon completion of rock socket drilling, the shaft will be subjected to an acceptance testing to qualify as "dry" despite minor water infiltration or use of mudding during casing installation. The acceptance test is performed over a 2-hour window by first de-watering the shaft excavation to within 3 inches of tip elevation and then obtaining depth to top of water inside the shaft at both the beginning and end of both hours. The shaft is accepted as dry if the water infiltration rate is less than 12 inches per hour. However, if the water infiltration rate exceeds 12 inches per hour then the shaft should be flooded immediately and constructed in the wet. Base inspection of a shaft accepted as dry shaft can be performed using a mini-SID device.

Shafts supporting the NJ Abutment were attempted in the dry. However, a water tight casing seal could not be achieved and all shafts were installed following the wet method of shaft construction.

© 2016 Deep Foundations Institute

Overdrilling of Rock Socket

Overdrilling below the design bottom of rock socket elevation was necessary at some locations in order to meet the design criteria of having at least 4 feet of socket within intact rock. Bottom of rock socket elevations were also deeper at some locations considering the size of the tools used during drilling operations. Also, base cleanout by airlifting tends to increase the socket lengths slightly. At some locations, the bottom of rock sockets was up to 4 feet below design elevations. The project specifications require terminating the reinforcing cage 6 inches above the bottom of the rock socket. The pre-fabricated reinforcing cages were not made to accommodate these overdrilled rock sockets. A design modification was made to allow leaving a portion of the rock socket at the bottom of the shaft unreinforced. Based on a review of the lateral shaft analysis, the shafts are subjected to negligible shear and bending moment within the bottom 3 feet of the rock socket. Therefore, a maximum 3 feet was allowed to be left unreinforced for shafts greater than 5 feet in diameter and a maximum 2 feet was allowed to be left unreinforced for shafts less than 5 feet in diameter.

Modifications to Reinforcing Cages

During shaft construction, a transition zone of epoxy coated column reinforcement identified as "jumper cage" was installed along with shaft reinforcing steel for facilitating future column construction. The jumper cage extends to within the upper 2 to 5 feet of the permanent casing. However, variations in casing tip elevation required lowering the column reinforcement more than design depths into the drilled shaft. This resulted in use of Gr. 60 epoxy coated steel to greater depths inside the shaft instead of Gr. 80 steel as designed. This design modification was possible as the maximum bending moment within the shaft occurs deeper and away from the interface with the column. Additionally, standard cross-sectional structural analysis was performed to evaluate the strength of the shaft with the modified reinforcing design.

Shaft locations where casing overdriving resulted in lowering the bottom of socket by greater than 3 feet required extending the shaft reinforcing cage at the bottom. A Type 2 mechanical coupler was used for connecting the Gr. 80 steel reinforcing cage and extension bars. A Type 2 coupler was preferred to Type 1 coupler in order to meet AASHTO requirements of having a yield strength that is 125% of the yield capacity of a Grade 80 bar.

Select Examples of GBR Design Modifications

Table 1 provides specific examples of locations where the above described field conditions were encountered and required design modifications. The foundations for the project are currently under construction and these examples will be updated at the end of foundation construction.

SUMMARY AND CONCLUSIONS

Construction of drilled shafts socketed in bedrock with a permanent casing in overburden soils presents challenges in the field that may require design modifications. Conditions encountered in the field during shaft construction from casing advancement to concreting that required design and construction method modifications at GBR project are summarized. Guidelines developed for construction modifications during casing advancement to rock and drilling are applicable to other projects with similar subsurface conditions. As reinforcement cages for shafts are fabricated prior to drilling at most projects, the design modifications made to the reinforcing cages at GBR due to field conditions can be used to make allowances in cage fabrication on future projects. As a minimum, the tight pitch spiral reinforcement required at the top of rock socket should be fabricated with sufficient allowances to account for variations in casing tip refusal elevations and variations in rock elevations anticipated in the field.

© 2016 Deep Foundations Institute

Table 1. Summary of Design and Construction Modifications due to Field Conditions at GBR Project

Field Condition	Locations	Design/Construction Modification
Casing out of location	P13NYEB S P7NJWB N	Top of casings exceeding location tolerance by 0.6 to 2 in. Cage was offset 3 in. to west to meet minimum concrete cover; remainder of tolerance width compensated at column/beam junction.
	P18NJEB 3	Top of casing out of location by 4 in. Casing was pulled up approximately 2 ft and re-twisted into location tolerance; 18 ft of soil plug maintained while position was corrected.
Case 1 : casing tip within overburden soils and above the design tip elevation	P3NYWB S	Casing initially refused in marine sands 7 ft above top of weathered rock. Contractor planned to proceed without further driving. During base cleanout, soils within the 7-ft zone caved. Casing was eventually advanced to refuse on weathered rock. Socket length was calculated based on the casing tip elevation upon re-driving.
	P2NJWB S	Casing initially refused 0.8 ft above rock due to irregular surface and lack of weathered rock. Shaft is located within water of NJ inlet. During airlifting water level could not be maintained inside the casing due to lack of seal. As the permanent casing was already cut to design shaft top elevation, the socket was grouted and re-drilled to achieve a water tight seal.
Case 2: casing tip within weathered bedrock but above design tip elevation	P10NYEB N & S P14NJEB N & S	Modified the spiral reinforcement to have adequate tight pitch spiral reinforcement near soil bedrock interface.
Case 3: casing tips in weathered bedrock below the design tip elevation	P2NYEB N & S P7NYWB N & S P9NJWB S	The reinforcing cage was extended at the bottom with use of Type 2 mechanical couplers.
	P4NJEB N & S	The reinforcement cage was lowered into the shaft so that the Gr.60 column bars extend deeper into shaft and the spiral reinforcement requirements are met at the top of rock socket.
	P6NJEB N &S P6NJWB N & S P11NJWB N & S P10NJWB N & S	Due to high RQD of the bedrock below the casing tip, rock socket was allowed to terminate at/near the design bottom of socket elevation.
Case 3: casing tips in weathered bedrock below the design tip elevation	P4NYWB N & S P5NYWB N & S P9NYWB N P12NYWB S P3NJWB S P13NJWB S	The overdriven length was 1 ft or less. The bottom of rock socket was lowered but no changes were made to the reinforcing cage. Any overdrill at the bottom of shaft to meet 2D length requirement was left unreinforced.
	P3NYEB N & S P4NYEB S P5NYEB N & S P8NYEB N & S P10NYEB N & S P11NYEB S NYEB Abutment P9NJWB S	The reinforcing cage was fabricated after drilling operations. The cage was made longer to meet the design requirements considering the field conditions without the use of any couplers.

© 2016 Deep Foundations Institute

Field Condition	Locations	Design/Construction Modification
Allowing Unreinforced Tip	P11NJEB S	Casing refused within overburden soils above design elevation and weathered rock was 7 ft below casing tip. The final bottom of rock socket was 2.5 ft deeper than design elevation. Reinforcing cage was terminated at original design elevation resulting in 2.8 ft of unreinforced socket.
	P5NJEB S P3NJEB N	The overdriven casing refused in glacial till with weathered rock below casing tip (1.1 to 2.5 ft). Also bottom of socket was over 4 ft below the design elevation. Based on engineering analysis, no changes were made to the reinforcing cage and some portion of the rock socket was allowed to be left unreinforced. At P3NJEB N the CSL tubes were required to be extended in the unreinforced section.

REFERENCES

Brown, D.A., Turner, J.P., and Castelli. R.J., (2010). "Drilled Shafts: Construction Procedures and LRFD Design Methods," Geotechnical Engineering Circular No. 10 and FHWA/NHI Publication 10-016, 972 p.

Dapp, S.S., Turner, J.P., and Brown, D.A. (2016). Load Tests on Drilled Shafts at Goethals Bridge Replacement, *Proceedings*, International Conference on Deep Foundations, Seepage Control and Remediation, 41st Annual Conf. on Deep Foundations, DFI, NY.

Kiewit-Weeks-Massman (KWM JV), (2016). Field Design Change (FDC) Library, Goethals Bridge Replacement Project.

NYNJLink, (2014). "Drilled Shaft Installation Plan Rev 4", Goethals Bridge Replacement Project.

Turner, J.P., Dapp, S.S., and Brown, D.A. (2016). Rock Socketed Drilled Shafts for the Goethals Bridge Replacement, *Proceedings*, International Conference on Deep Foundations, Seepage Control and Remediation, 41st Annual Conf. on Deep Foundations, DFI, NY.

`

© 2016 Deep Foundations Institute

This page left intentionally blank

© 2016 Deep Foundations Institute

GOETHALS BRIDGE REPLACEMENT PROJECT - PERFORMANCE-BASED DESIGN OF THE DRILLED SHAFT FOUNDATIONS

Chunli Wei, Parsons Corporation, New York, NY, 212-266-8562, Chunli.Wei@parsons.com

Mark Jen, Parsons Corporation, New York, NY, 212-266-8387, Mark.Jen@parsons.com

Xiaojun Wang, Parsons Corporation, New York, NY, 212-266-8557, Xiaojun.Wang@parsons.com

ABSTRACT

After more than 85 years of service, a critical link between New York and New Jersey, the Goethals Bridge over the Arthur Kill waterway, is being replaced with two new parallel bridges. Each bridge includes 1,650 feet long signature steel composite cable-stayed bridge, a 2,789 feet long New York approach and a 1,889 feet long New Jersey approach. The superstructure of each approach is supported on a series of two-column concrete piers and each column is supported on a single large diameter drilled shaft varying from 4.5 to 9 feet in diameter and anchored 45 feet below ground into the underlying rock.

A performance-based methodology was followed for the strength and extreme event limit states design of the drilled shaft foundations. The design for seismic loads has been performed using the AASHTO Guide Specifications for LRFD Seismic Bridge Design. For all strength and service loads, the AASHTO LRFD Bridge Design Specifications were used. Since the longitudinal and confinement requirements in the two specifications vary, the minimum longitudinal reinforcement was based on the more stringent requirements of the two codes. A design example is presented to illustrate the methodology in bridge deep foundation design using nonlinear time-history global analysis results with soil-pile interaction represented by sets of horizontal and vertical nonlinear soil springs along the drilled shaft, based on the soil and rock properties from the boreholes test results. In this paper the design methodology implements strain limits related to earthquake intensities and damage levels to calculate the capacity using XTRACT analysis, which aids designers to adopt applicable provisions that meet specific design requirements.

Keywords: performance-based design, drilled shaft foundation, finite element analysis, soil-pile interaction

INTRODUCTION

After more than 85 years of service, a critical link between New York and New Jersey, the Goethals Bridge over the Arthur Kill waterway, is being replaced with two new parallel bridges designed to carry vehicular traffic and a future mass transit corridor. They include two 1,650 feet long signature steel composite cable-stayed bridges with 260 feet tall V-shaped concrete gateway towers (Figure 1). The approaches consist of continuous pre-stressed concrete girders. The New York approach is a single structure consisting of 18 continuous spans, sloping at 4% for a total length of 2,789 feet without expansion joints. Similarly, the longest continuous portion on the New Jersey approach, with a similar slope, consists of 11 spans for a total length of 1,889 feet without expansion joints. The superstructure of each approach is supported on a series of two-column concrete piers that vary in height from 121.3 feet near the cable-stayed bridges to 11.8 feet near the abutments. Each column is supported on a single large diameter drilled shaft varying from 4.5 to 9 feet in diameter and anchored 45 feet below ground into the underlying rock.

© 2016 Deep Foundations Institute



Figure 1. Skyview of the New Goethals Bridge

As shown in Figure 2, Approach pier columns are founded on single, large diameter drilled shafts filled with reinforced concrete and socketed into the underlying bedrock. Permanent steel casing is used as armor for corrosion protection and excellent durability. The casing increases the predictability of the construction process, further assuring that the foundations will provide the required quality and strength. By eliminating pile caps on all the approaches, we gained significant project advantages and reduced the environmental impacts due to using fewer materials, limiting excavation, and reducing exposure to potentially hazardous materials.

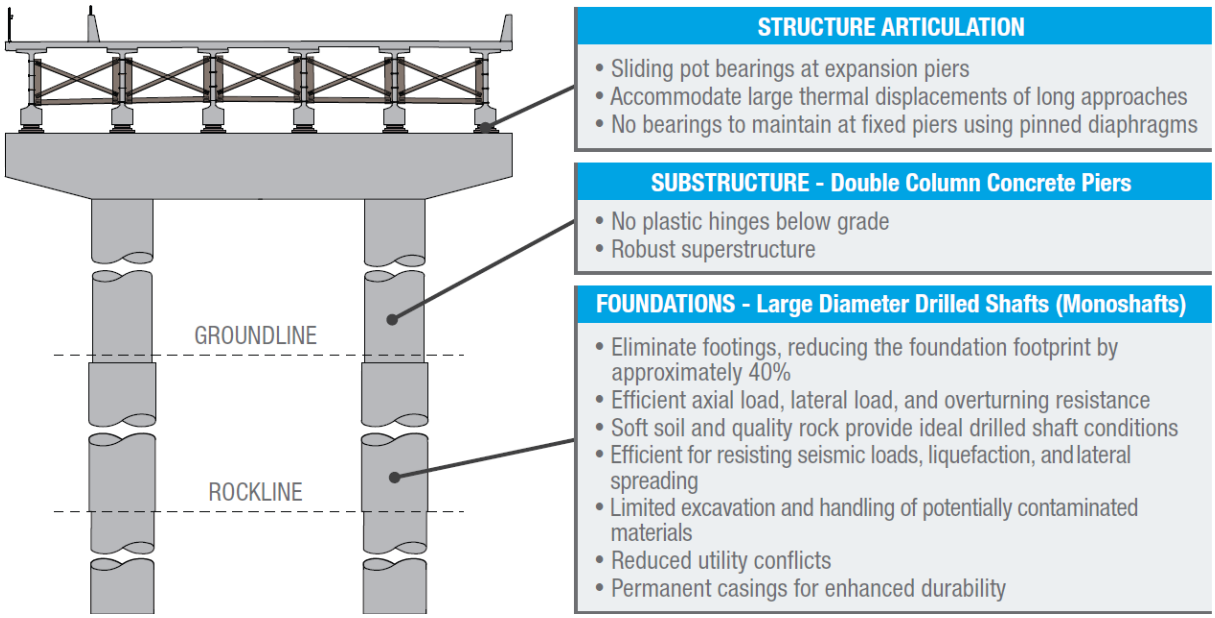


Figure 2. Sketch of Substructures of the Approach

The design of the drilled shaft follows the provisions of the AASHTO Guide Specifications for LRFD Seismic Bridge Design that includes the displacement-based design philosophy and performance-based seismic design criteria. The seismic analysis of the new bridge, a designated seismically critical structure in Seismic Design Category B, followed a sophisticated time history approach incorporating non-linear concrete properties, large displacements and advanced soil-structure interaction by applying sets of two

© 2016 Deep Foundations Institute

horizontal and one vertical nonlinear soil springs along the drilled shaft. The strain limits of the reinforced concrete corresponding to the damage level of a structural component are incorporated to aid designers adopt applicable provisions that meet specific design requirements.

GEOTECHNICAL CONDITIONS

Geotechnical conditions and design parameters are interpreted from logs of borings completed by NYNJ Link in 2014 and boring logs and reports contained in Exhibit 13 of the Project Agreement.

The New York Approach bridges extend from the eastern shore of the Arthur Kill to the NY Abutment on Staten Island. The NJ Approach bridges extend from the west end of the New Jersey Inlet (boat slip) westward over the NJ Turnpike, terminating at the NJ Abutments.

The subsurface consists of bedrock of the Passaic Formation (stratum 6) and several feet of decomposed rock (stratum 5) overlain by varying thicknesses of overburden soils. As shown in Figure 3, the overburden soils include Pleistocene glacial deposits (stratum 4) overlain by marine sands (stratum 3) and Holocene tidal marsh deposits (stratum 2). Several feet of man-made fill (stratum 1) is present at the existing ground surface. The existing ground surface ranges from approximately 2 to 9 feet above sea level.

Stratum 3, marine sand, is only encountered in the NY side. The loose sands are expected to be liquefiable under the design seismic loading. Liquefaction effects on the approach foundations will include loss of lateral support in liquefied zones and liquefaction induced lateral spreading of overlying layers. Passaic Formation rock (stratum 6) is the founding stratum for the drilled shaft rock sockets that will support all of the piers of the Goethals Replacement Bridge. This rock is described as red and reddish brown shale, siltstone, and sandstone.

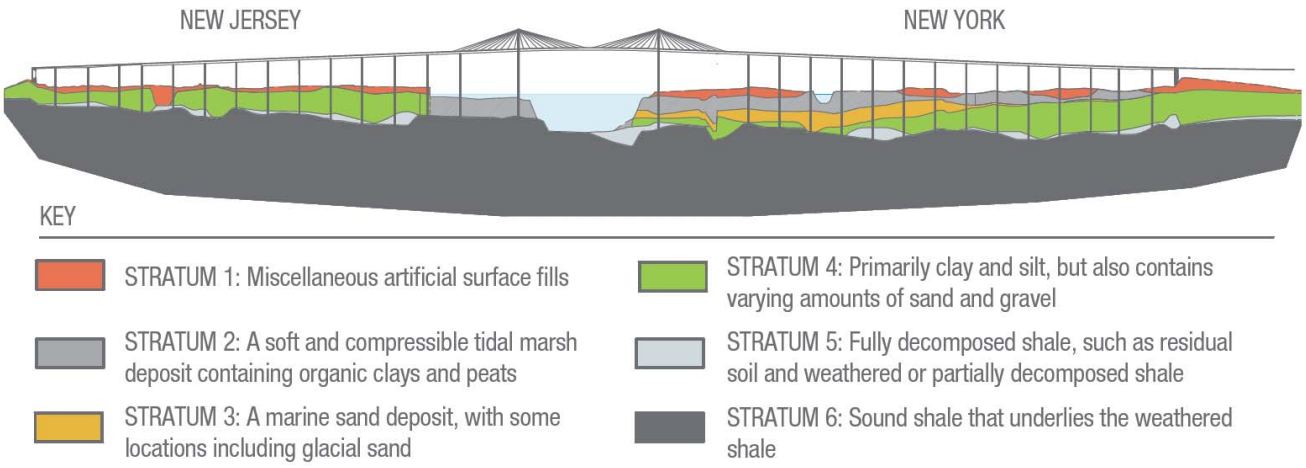


Figure 3. Subsurface Exploration and Borings

FOUNDATION DESIGN

The approach piers of the bridge are founded on large diameter drilled shafts which penetrate the soil layers and are anchored in the rock. The drilled shafts vary in diameter from 9.0 feet corresponding to the tallest piers to 5.0 feet for the shorter piers. Each shaft is encased in a steel casing extending along the entire length of the shaft and varying in thickness from 0.75 inches for the larger diameter shafts to 0.71 inches for the rest. The casing is used as formwork during construction of the shaft and afterwards as a means of providing

© 2016 Deep Foundations Institute

extra concrete confinement to the shaft (after allowing for corrosion loss). The portion of the shaft anchored in the rock provides axial resistance and, in some cases, also bending resistance.

Performance-based Design Criteria

The intent of the performance-based design concept is to achieve the expected performance (damage) levels which are expected to be achieved, or at least not exceeded, when the structure is subjected to earthquake ground motion of specified intensity.

Two-level-performance-based design approach was adopted in the project, which included both the lower-level functional evaluation earthquake (FEE) and the upper-level safety evaluation earthquake (SEE). The FEE is defined as the seismic event having a 10-percent probability of exceedance in 100 years, or a mean return period of 1,000 years. The SEE is defined as the seismic event having a 4-percent probability of exceedance in 100 years, or a mean return period of 2,500 years.

The Replacement Bridge has a critical importance classification and must provide immediate access to all vehicles following the FEE. After the SEE, immediate access shall be available to emergency vehicles with full access restored within a few months. Seismic performance levels, expressed in terms of damage levels, are defined in Table 1.

Table 1. Structural Damage Levels

Component	FEE	SEE
Piles/Drilled Shafts	No Damage	Minimum Damage
Pile Caps	No Damage	No Damage

"No Damage" is defined for structural members as the nominal capacity as described in AASHTO LRFD Bridge Design Specification. Nominal, not expected, material properties shall be used, and increased member strength due to the effects of confinement steel shall be ignored. "No Damage" is defined as full serviceability without repair or replacement.

"Minimal Damage" allows minor inelastic response, post-earthquake damage is limited to narrow cracking in concrete and inconsequential yielding of secondary steel members. Damage to nonstructural components of the cable system would be allowed.

Codes and Specifications

All concrete components were designed and the reinforcement was detailed following the requirements of two primary codes, the AASHTO Guide Specifications for LRFD Seismic Bridge Design (AASGTO Seismic Guide) and the AASHTO LRFD Bridge Design Specifications (AASHTO LRFD BDS). Seismic detailing requirements are also considering the continuity between the shaft and socket, and continuous reinforcement cage from the column to rock socket was adopted, as shown in Figure 4. Where deemed necessary, design directives where issued to clarify the requirements and procedures of the codes and those to be followed. The design directives address the following issues.

© 2016 Deep Foundations Institute

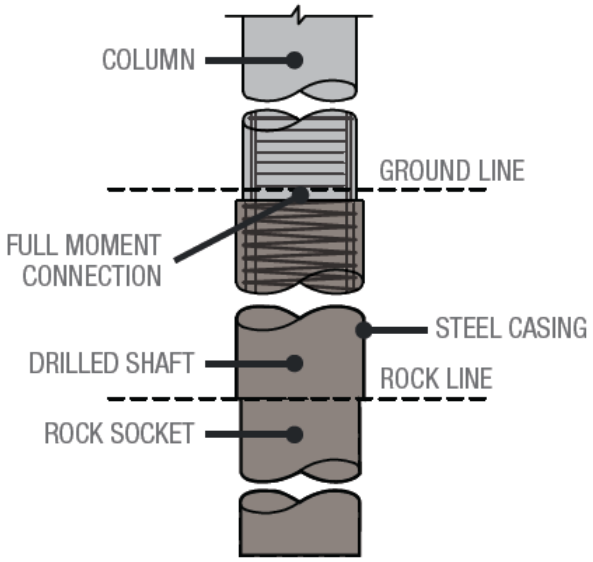


Figure 4. Sketch of Reinforcement in Column, Drilled Shaft and Rock Socket

Longitudinal and Confinement Reinforcement Requirements for Drilled Shafts

The longitudinal reinforcing design had the minimum steel constraint from AASHTO LRFED Bridge Design Specifications, and the transverse reinforcing design was followed the AASHTO Guide Specifications for LRFD Seismic Bridge Design. The longitudinal and transverse reinforcement requirements based on the AASHTO LRFD Bridge Design Specifications are shown in Table 2, and those requirements based on the SSHTO Guide Specifications for LRFD Seismic Bridge Design are shown in Table 3.

Table 2. Longitudinal and Transverse Reinforcement Requirements from the AASHTO LRFD Bridge Design Specifications

	LONGITUDINAL REINFORCEMENT		TRANSVERSE REINFORCEMENT	
Strength Requirement	$\frac{A_s}{A_g} \geq 0.135 \frac{f_c'}{f_y}$	5.7.4.2-3	$\rho_s \geq 0.45\left(\frac{A_g}{A_c} - 1\right)\frac{f_c'}{f_{yh}}$	5.7.4.6-1
Seismic Zone 1	No additional requirement	5.10.11.2	the transverse reinforcement requirements at the top and bottom of a column shall be as specified in Articles 5.10.11.4.1d and 5.10.11.4.1e	5.10.11.2
Seismic Zone 2	$0.06 \geq \frac{A_s}{A_g} \geq 0.01$	5.10.11.3	$\rho_s \geq 0.12 \frac{f_c'}{f_{yh}}$	5.10.11.4.1d-1
Seismic Zone 3, 4	$0.04 \geq \frac{A_s}{A_g} \geq 0.01$	5.10.11.4.1a	$\rho_s \geq 0.12 \frac{f_c'}{f_{yh}}$	5.10.11.4.1d-1

© 2016 Deep Foundations Institute

Table 3. Longitudinal and Transverse Reinforcement Requirements from the AASHTO Guide Specifications for LRFD Seismic Bridge Design

	LONGITUDINAL REINFORCEMENT		TRANSVERSE REINFORCEMENT	
SDC A	No additional requirement	8.2	the transverse reinforcement requirements shall be as specified in Articles 8.6.5 for SDC B	8.2
SDC B	$0.04 \geq \frac{A_s}{A_g} \geq 0.007$	8.8.1-1&8.8.2-1	$\rho_s \geq 0.003$	8.6.5-1
SDC C	$0.04 \geq \frac{A_s}{A_g} \geq 0.007$	8.8.1-1&8.8.2-1	$\rho_s \geq 0.005$	8.6.5-3
SDC D	$0.04 \geq \frac{A_s}{A_g} \geq 0.01$	8.8.1-1&8.8.2-2	$\rho_s \geq 0.005$	8.6.5-3

Based on the site-specific hazard analysis, the Goethals Replacement Bridge shall be assigned to Seismic Design Category (SDC) B as defined in the AASHTO Guide Specifications for LRFD Seismic Bridge Design. Herein the minimum ratio of longitudinal reinforcement shall not be less than 0.7% based on requirement in Section 8.8.2. However, the minimum ratio of longitudinal reinforcement is 0.84% based on Section 5.7.4.2 of AASHTO LRFD Bridge design Specifications shown as following:

$$\frac{A_s}{A_g} \geq 0.135 \frac{f_c'}{f_y} \quad [1]$$

Where f_c' = 5 ksi of concrete compressive strength and f_y = 80 ksi of longitudinal reinforcement yielding strength. So 0.84%, the minimum ratio of the longitudinal reinforcement per AASHTO LRFD Bridge Design Specification, was determined in this project.

Based on the AASHTO Guide Specifications for LRFD Seismic Bridge Design, the minimum ratio of transverse reinforcement is 0.003 in the Section 8.6.5, while it is 0.01 based on the equation in Section 5.10.11.4.1d-1 of AASHTO LRFD Bridge design Specifications as following. The requirement is too stringent for column design, hence the AASHTO Guide Specifications for LRFD Seismic Bridge Design was used for transverse reinforcement design. To be consistent, it is also used for drilled shaft transverse reinforcement design.

$$\rho_s \geq 0.12 \frac{f_c'}{f_{yh}} \quad [2]$$

Where f_c' = 5 ksi of concrete compressive strength and f_{yh} = 60 ksi of transverse reinforcement yielding strength.

Casing

The steel casings are not counted for the strength during the shaft design, but counted for the confinement of concrete requested by the design codes.

© 2016 Deep Foundations Institute

Rock socket design

Considering the continuity between shaft and rock socket, the continuous reinforcement was designed with satisfactory of the minimum requirement from the AASHTO LRFD Bridge Design Specification.

FINITE ELEMENT ANALYSIS

Global Modeling

In order to obtain the seismic response of drilled shafts foundations of the bridge, the global finite element model of the bridge was developed using ADINA program. This non-linear behavior of drilled shafts was modeled with bending moment-curvature (M-C) relationships that vary with the level of applied axial forces. The M-C relationships were calculated with XTRACT by TRC Solutions Inc., using Mander's stress-strain relationship for confined concrete. These frame elements with M-C stiffness relationships allow the calculation of the varying stiffness of these shafts and approach pier columns due to concrete cracking and potential formation of plastic zones. Numerous short frame elements are modeled at the potential plastic hinge zones to capture the plastic zone length. In addition to material non-linear response (shafts, approach pier columns and soils), the analysis captures the effects of non-linear large deflections of the bridge.

Soil-Structure Interaction

Approach Pier Foundations: For the approach pier foundations consisting of single drilled shafts, three springs (two horizontal and one vertical) are located at the center of each soil layer stratum to represent the interaction between the shaft and the respective soil layers. Non-linear hysteretic horizontal force-displacement relations with gap properties are computed from the PY curves, see Figure 5, generated by the program LPILE, version 7.02 by Ensoft Inc. The nonlinear vertical force-displacement relationships are computed from T-Z curves generated by the program APILE, version 5.024 by Ensoft Inc. The P-Y curves have hysteretic properties to provide damping from the surrounding soils and also gap properties to account for the effect of soil gap formation as the drilled shafts repeatedly push against the soils.

Tower Foundations: The underlying soils consist of tidal marsh deposits and loose sands and a thin stratum of glacial till overlying the rock. Therefore, the loose soils are ignored as inconsequential and the drilled shafts are modeled as columns fixed at the top of the rock.

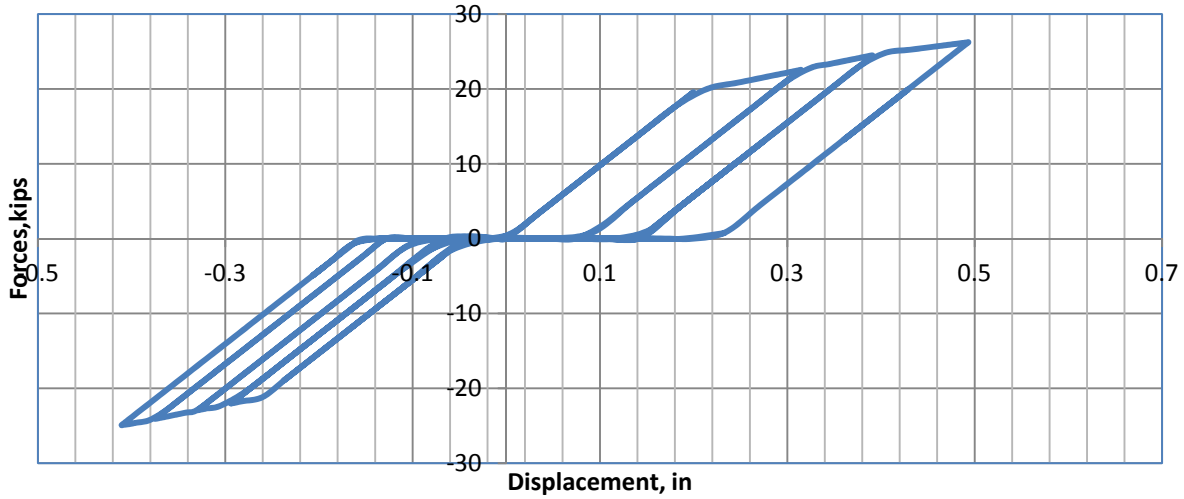


Figure 5. Typical Force-Displacement Relationship for Soil-Structure Interaction Foundation Spring

© 2016 Deep Foundations Institute

Pushover Analysis

A pier-by-pier pushover analysis was conducted through ADINA program to demonstrate that the piers have sufficient displacement capacity and also that plastic hinges do not develop in the shafts. To determine the ultimate capacity and hinge formations, the ultimate limit values (strains) of materials were used. The moment - curvature relationship was used to represent the nonlinear behaviors of the columns, shafts and cap beams. The joints between column and capbeam were assumed rigid. Moment - axial force interaction was considered in all reinforced concrete members.

The pushover analysis results show that the development of plastic hinges that occurs at a level of forces much higher than the actual seismic forces on the approach piers, and the displacement capacity of the piers in the transverse and longitudinal directions of the piers is significantly higher than the seismic displacement demand.

SUMMARY AND CONCLUSION

The overall scope of the bridge foundation design has been described in this paper, and the design directives per performance-based design criteria were presented to develop LRFD resistance for bridge pile foundations and reinforcement detail requirements with the consideration to reliability theory, focusing on the strength limit state and extreme limit state.

Here we may draw the following conclusions.

1. The design of a bridge or any other structure with more than one code gives a difference in the design due to the nature of using this code. In this paper, it can be seen that there are more reinforcement area with design in the AASHTO LRFD BDS compared with the AASHTO Seismic Guide.
2. The AASHTO could address the design of structures with such issue in a better way to aid designers adopt applicable provisions that meet specific design requirements
3. The transverse reinforcement as confinement component with the consideration of the casing participation is practical. But the casing participation is not considered for strength design, which may not be the most economical.
4. The analysis of the long sloping continuous spans can be best achieved by using advanced non-linear procedures and that the standard code analysis with equivalent cracking properties for the concrete columns is not sufficiently accurate to produce a refined component design when considering the above described configuration.
5. The analysis with 3D finite element program gives accepted results compared with that calculated by using the LPILE analysis. This provides more check for the design of the bridge and gives more agreement and suitability for the design.

ACKNOWLEDGE

The authors acknowledge the Port authority of New York and New Jersey (PANYNJ), Kiewit-Weeks-Massman, AJV (KWM) as well as the contributions of Parsons Project Manager Seth Condell and Engineer of Record Tom Spoth.

REFERENCES

AASHTO LRFD Bridge Design Specifications, 6th Edition, 2012.

© 2016 Deep Foundations Institute

AASHTO Guide Specifications for LRFD Seismic Bridge Design, 2nd Edition, 2011.

Goethals Bridge Replacement Project, Design Criteria.

Geotechnical Engineering and Structure Foundation Report, New Jersey Approach Foundations, Rev. 1, Dan Brown Associates, PC, June 7, 2014.

Geotechnical Engineering and Structure Foundation Report, Eastbound New York Approach Foundations, Final Design, Rev 1, Dan Brown Associates, PC, April 30, 2014.

LRFD Bridge Design Specifications, EI 11-021, NYSDOT.

PANY&NJ Goethals Bridge Replacement Project Requirements and Provisions for Work.

© 2016 Deep Foundations Institute

This page left intentionally blank

© 2016 Deep Foundations Institute

INCLUSION OF OVERBURDEN SOILS RESISTANCE INTO SHAFT NOMINAL CAPACITY FOR SIGNIFICANT ECONOMIC SAVINGS – AN OSTERBERG CELL LOAD TEST CASE STUDY

Aditya Ayithi, Ph.D., P.E., Loadtest USA, Gainesville, FL, USA, (352) 327-3698, Aditya@loadtest.com
Dean Herbst, P.E., Iowa DOT, Sioux City, IA, USA, (712) 239-1367, dean.herbst@dot.iowa.gov
William G. Ryan, Loadtest USA, Gainesville, FL, USA, (352) 327-3698, bill@loadtest.com

ABSTRACT

For rock socketed drilled shafts, it is a common practice not to include the frictional resistance of overburden soils into the nominal capacity estimation. The primary reason often being cited is "overburden soils resistance is negligible compared to that of rock socket resistance." However, in certain geological conditions, where the rock layer is located at greater depths, friction resistance from overburden layers can be significant. In addition, at such great depths, shaft drilling becomes very complicated and expensive. In these situations, considering the resistance of the overburden layers can be an economic alternative.

This paper presents a case study of an Osterberg cell (O-cell) load test conducted on a 161.8 feet long and 78-inch diameter instrumented test shaft. Based on initial designs, a 72-inch diameter rock socket of lengths 23 and 26 feet was required to provide a LRFD factored friction resistance of 3,200 kips. The load test results revealed that the material in the 72-inch diameter socket does not represent a true rock. However, the test results also proved that the factored friction resistance of overburden layers is greater than the required design resistance. Based on the load test results, it was decided to allow the overburden soils frictional resistance to be considered in the shaft design, resulting in significant economic savings.

Keywords: overburden soils, friction resistance, O-cell test, test shaft, load test program, economic savings

INTRODUCTION

Rock socketed drill shaft design guidelines of various State Department of Transportation (DOTs) agencies allow friction and/or end bearing resistance of only the rock socket portion into the design capacity estimation. It is typical to neglect the frictional resistance of overburden soils. However, in certain geological conditions where the rock layer is at greater depths, friction resistance of the overburden soils can be significant. In this case the friction resistance of overburden soils was verified via the specified instrumented O-cell test program and then used as part of the design capacity.

PROJECT DESCRIPTION

As part of I-29 improvement project, Iowa Department of Transportation (Iowa DOT) planned to replace the dual four lane bridges that cross the Floyd River in Sioux City, Iowa with dual six lane bridges (Fig. 1). Expected benefits from this improvement include improved safety, traffic operations and roadway infrastructure conditions.

BRIDGE SUBSTRUCTURE

The project consists of two individual bridges; a new south bound bridge and a new north bound bridge. The south bound bridge is 646-ft long and the north bound bridge is 644-ft long. Both are six-span, pre-tensioned and pre-stressed concrete beam bridges of varying width. Bridge foundations were designed such that the abutments of both bridges will be supported on driven steel piles and the bridge piers will be on drilled shaft foundations.

© 2016 Deep Foundations Institute

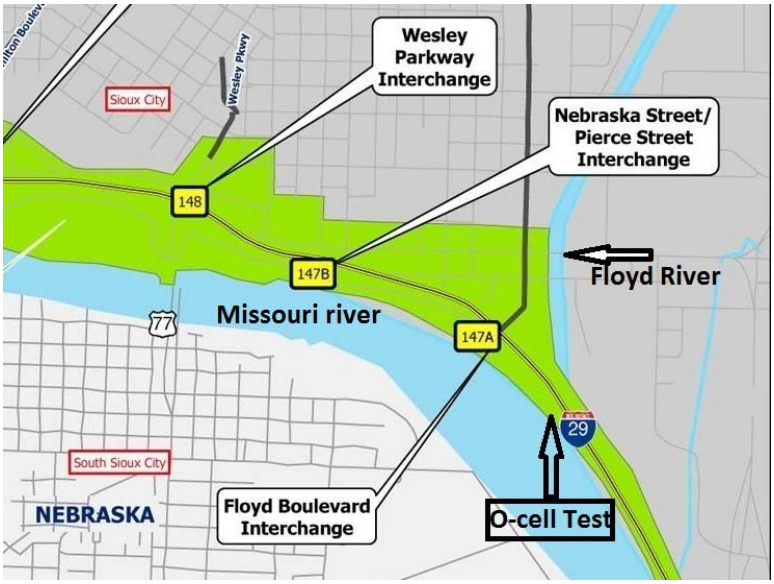


Fig. 1 Project site location map

GEOTECHNICAL EXPLORATION

A geotechnical exploration program was conducted to characterize the corridor soil properties and the data was to be used for the design and analysis of various geotechnical structures such as retaining walls, embankments, deep foundations etc. Based on the initial site exploration, visual classification and lab testing the general soil stratigraphy at the project site was characterized as having an upper sand layer with some silt and gravel, underlain by shale and sand stone (Figs. 2 and 3). Limestone was also encountered in a few locations. For sand layers, the SPT 'N' value varied from N=2 near the ground surface to N=40 at bottom of the layer. Once the N value reached refusal (i.e. N>50), based on visual observation and past experience at a nearby bridge site, it was classified as rock and rock core samples were collected (Fig. 3). For the rock core samples, the Recovery ratio (REC) varied from 0 to 100% and the Rock Quality Designation (RQD) varied from 0 to 90%. The unconfined compressive strength of selected rock core samples varied from 90 psi to 880 psi in shale, and320 psi to 760 psi in sandstone. The average Rock Mass Rating (RMR) was about 42.

BRIDGE PIERS PRELIMINARY DESIGN

The Iowa DOT LRFD Bridge Design Manual allows bridge piers to be supported on drilled shafts, where drilled shafts are economical and advantageous. Typically drilled shafts for bridge piers are required to be socketed into rock and are designed so that only the skin friction of the rock socket is considered. To minimize the effects of construction issues, drilled shafts are to extend an additional 12" into the rock beyond what is required for geotechnical capacity. Skin friction of the overburden soils is not allowed to be used in shaft capacity calculations.

Based on structural design estimations, the maximum allowable LRFD strength design axial load will be 3,200 kips for the interior bridge foundations and 2,200 kips for the exterior bridge foundations. For the anticipated design loads of a 78- inch diameter drilled shaft extending through the overburden to the top of bedrock with a72-inch diameter rock socket extending into the bedrock, the required rock socket lengths for both bridge piers would vary between be 23 feet and 31 feet. With these rock socket lengths, the total depth of the shafts ranges from 152 feet to 164 feet, depending on depth of rock layer from ground surface. It is worth noting here that it requires special tooling, methods and experience for a drilled shaft contractor to successfully construct such deep shafts.

© 2016 Deep Foundations Institute

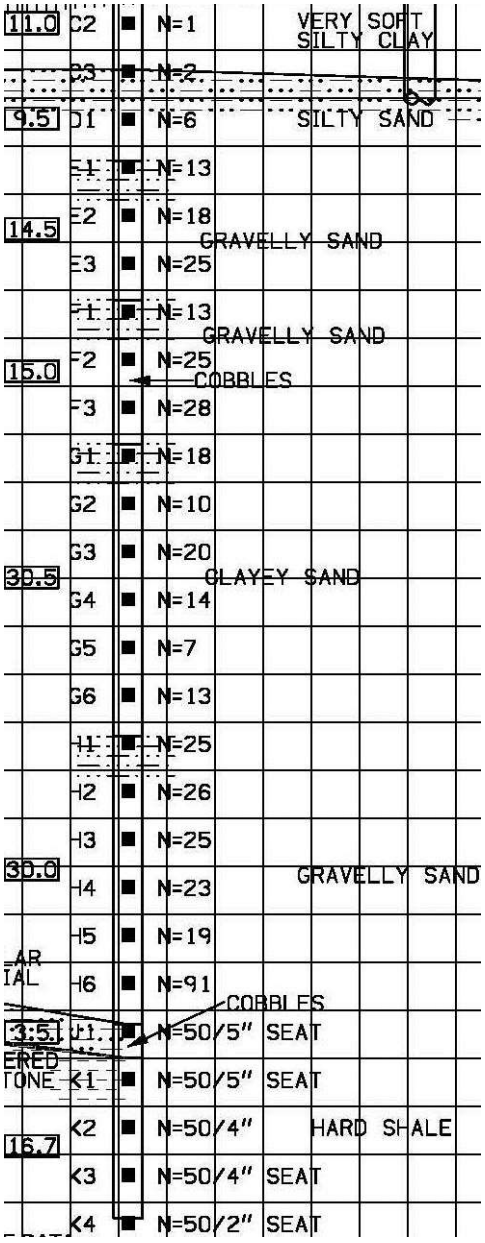


Fig. 2 Representative borehole log



Fig. 3 Rock core samples

DRILLED SHAFT LOAD TEST PROGRAM

The IOWA DOT Bridge Design Manual requires a static load test be conducted on a test shaft via O-cell test method in order to use LRFD methods. This test program was to serve two purposes: first to demonstrate the drilled shaft contractor's construction capabilities and second to confirm the soil design parameters. The test shaft was specified to be constructed in the vicinity of the north abutment of the proposed southbound bridge. Based on the initial geotechnical report, the test shaft depth was estimated to be around 174 feet from ground surface extending into rock socket.

© 2016 Deep Foundations Institute

Bi-directional O-cell Load Test

The O-cell is a highly specialized, sacrificial bi-directional loading device that the Engineer can have installed anywhere within the length of the reinforcement cage of a drilled shaft, auger cast pile (Fig. 4) or driven pile. It applies all of the axial compressive static loading within the shaft and requires no external reaction system or dead load at the top of the shaft. As the O-cell expansion occurs, the end bearing and side shear below the O-cell provides reaction for the side shear above it, and vice versa, until reaching the ultimate capacity of one of the components or until the O-cell reaches its rated capacity. Fig. 4 also shows the instrumentation of a typical O-cell test shaft. Vibrating wire strain gages are installed,

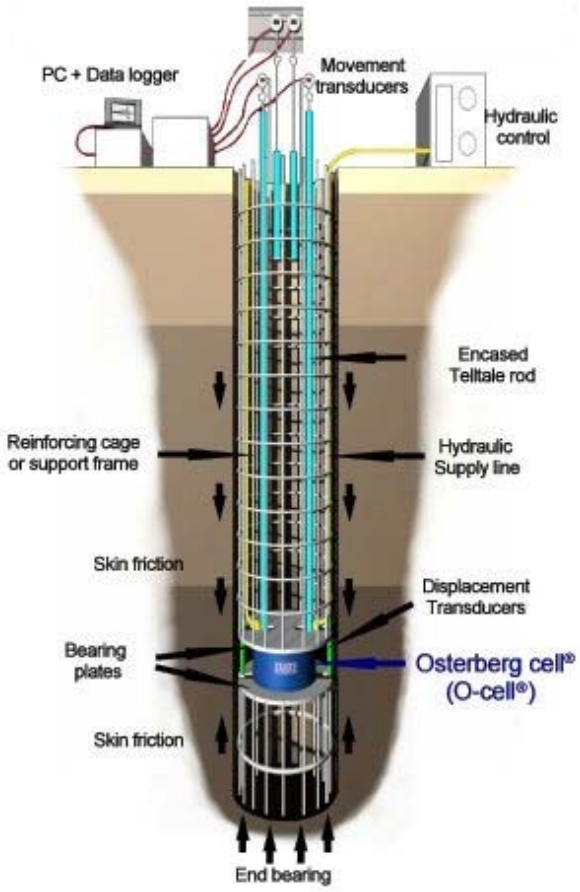


Fig. 4 General schematic representation of an O-cell test shaft (courtesy www.loadtest.com)

typically, at the top of each layer, to measure the strain (ε) and from which the load distribution (a.k.a. load shedding) for each layer can be calculated. O-cell expansion, shaft compression and top of shaft movements that occur during the load test are measured from the installed electronic expansion gages, which are connected to a computerized data acquisition system. A detailed description of O-cell testing and its advantages can be found at Osterberg (1998) and Ayithi et al. (2013). Because of its capabilities to apply extremely high loads, full scale load test on high capacity drilled shafts can be performed successfully, possibly to ultimate in side shear or end bearing.

Test Shaft Confirmation Boring

Iowa DOT requires confirmation soil borings to be taken at test shaft locations to verify soil stratigraphy and geotechnical parameters to finalize the test shaft plans and to optimize design calibration with the test results. The initial confirmation soil boring for the plan test location indicated the rock stratum to be deeper than anticipated. This deeper rock required a test shaft length of 200 feet deep to obtain the designed rock socket of 31 feet. The contractor indicated that this would require larger, not readily available, equipment

© 2016 Deep Foundations Institute

to construct a test shaft to that depth. Because of this complication, Iowa DOT moved the test shaft closer to and in alignment with Pier 5. This allowed for construction of the test shaft with the same equipment planned for use to construct the production shafts.

The second confirmation soil boring, performed at the Pier 5 location, identified a bearing layer, refusal 'N' values, that did not represent the rock material identified in the design geotechnical report. While this layer was encountered beneath the sand layer, as was the rock, it was identified as "residuum" and classified as very dense sand with clay and silt. The rock, as discussed earlier, identified in the initial geotechnical exploration and at a nearby bridge site generally indicate the same N values (e.g. 50/1", 50/3") as the "residuum". Considering a socket of 31 feet in the refusal blow count residuum materials allowed the test shaft to be constructed at a reduced length of 161.8 feet.

However, following commonly accepted drilled shaft design & construction theory, a change of material classification from rock to residuum significantly influences shaft design capacity. With the initial drilled shaft design based primarily on rock socket frictional resistance, use of the normally considered residuum lower friction values as compared to rock friction values the design would require deeper drilled shafts to achieve the same capacity. This would again push drilled shaft depths past 170 feet toward 200 feet or greater significantly increasing construction difficulty and construction costs.

This points to the importance of the load test and how critical its planning and results were for calibration of the site material geotechnical parameters and shaft capacity designs.

Test Shaft Instrumentation and Construction

A schematic section of the instrumented test shaft is shown in Fig. 5. The test shaft was equipped with a loading assembly consisting of three (3) 3,000 kip O-cells (i.e. 12,000 kips total in upward and downward directions) placed 21 feet above the shaft base (Fig. 6). Six (6) expansion transducers were attached to the loading assembly to measure the assembly's expansion. Eight (8) levels of strain gages with four (4) gages per level were attached to rebar cage. Strain gage data collected during shaft loading is used to estimate the load distribution in shaft. Four telltale casings were installed to measure concrete compression in the shaft above the loading assembly.

Case Foundation Company and Cramer & Associates jointly constructed the test shaft. 78- inch tooling was utilized down to the bottom of sand layer. Then 72- inch tooling was used to create the socket of the 183- foot deep shaft. An auger and digging bucket were used for drilling, and a cleaning-bucket for cleaning the base. A 102-inch O.D. temporary outer casing and 90-inch O.D. temporary inner casing were inserted as the drilling progressed. After cleaning the shaft base, a SONICALIPER was used to profile the shaft. At the end of concrete pour, the temporary casing was replaced with a corrugated metal casing with its tip below the design scour elevation of +1057 ft.

TEST RESULTS & ANALYSES

A maximum sustained load of 6,649 kips in both upward and downward directions combined, was applied in 12 increments. At this maximum load, the top and bottom of the loading assembly moved 1.030 inches and 4.106 inches, respectively. Also, the top of shaft movement was 0.834 inches. Subtracting a buoyant weight of 587 kips for the shaft above the loading point, a total shaft resistance of 12,711 kips was mobilized during the test. Fig.7 shows the upward and downward movement curves at each load increment. An equivalent top load (ETL) curve developed based on Fig. 7 is shown Fig. 8. Strain gage data was used to estimate the load shed in side shear between each strain gage level (Fig. 9) and corresponding unit side shear curves (a.k.a. t-z curves) are shown in Fig. 10. The maximum unit side shear mobilized for a zone average displacement of ½ - inches was 8.4 ksf and has occurred between strain gage level 2 and the loading assembly.

© 2016 Deep Foundations Institute

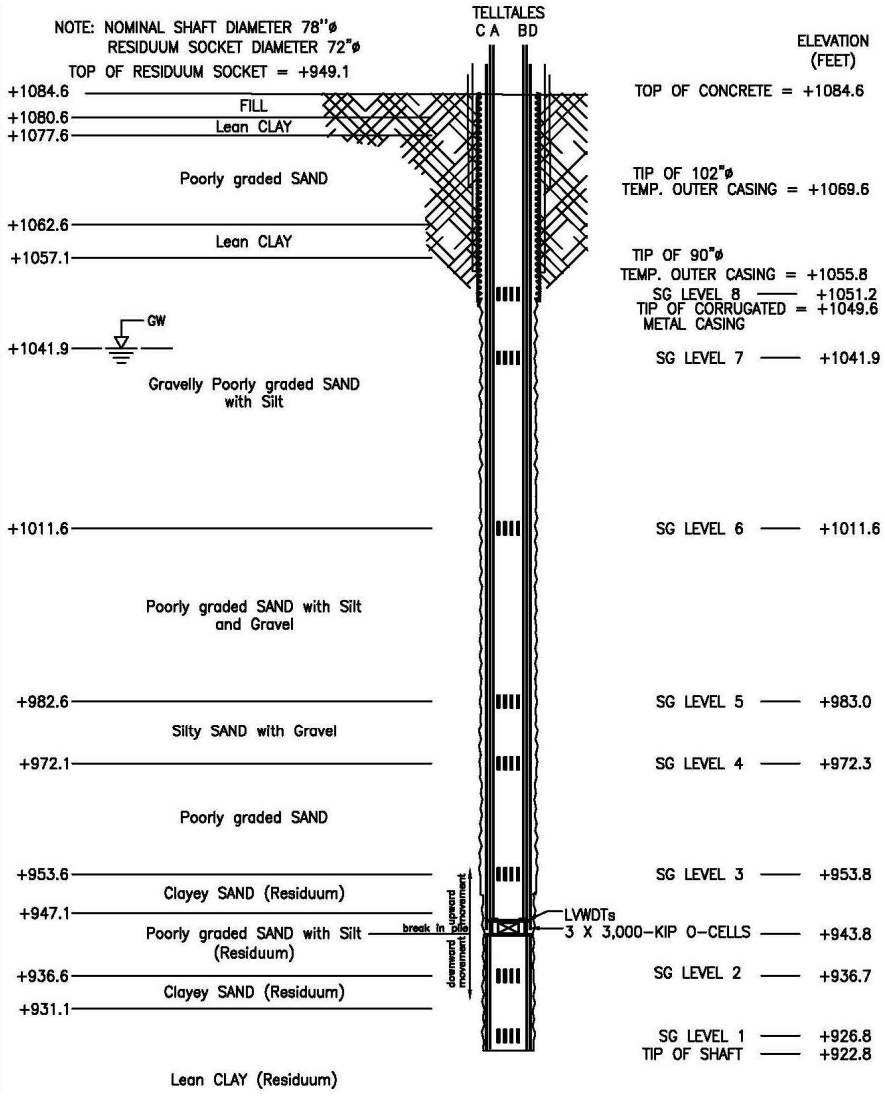


Fig. 5 Schematic section of O-cell test shaft.



Fig. 6 O-cell assembly inside the rebar cage

© 2016 Deep Foundations Institute

The maximum downward displacement of about 4.4 inches for the lower portion of the shaft below the O-cell assembly (Fig. 7) clearly indicates that the material in the 72-inch socket does not represent a true rock material. Therefore, since there is no rock layer, the drilled shaft designs based on rock socket friction cannot be applicable. However, the major positive finding from the test is that the shaft has a resistance of 7,500 kips at 1.0-inch downward displacement (Fig. 8). It is worth to note here that all the resistance is mobilized from the soils only, which would be considered as overburden soils for a rock socketed drilled shaft and is not allowed to be considered as part of design capacity, per Iowa DOT LRFD design specifications.

Based on load distribution from Fig. 9, the mobilized resistance of the shaft above scour design elevation +1057.0 ft. is estimated to be about 497 kips. After subtracting 497 kips from the total net mobilized resistance of 6,064 kips for the shaft above the loading level, the final mobilized resistance of the upper shaft comes out to be 5,565 kips at about 1-inch displacement. After applying a LRFD resistance factor of φ=0.7, the factored allowable capacity of upper shaft is 3,895 kips. This capacity is 695 kips more than specified LRFD maximum design load of 3,200 kips. In addition, resistance of lower shaft below the O-cell assembly would result in a much higher available shaft resistance than required and the back calculated resistance factor φ would be less than 0.5.

For this specific project the testing results helped in concluding two points. First, the test shaft confirmation boring findings were correct in that the materiel in the socket does not represent a true rock type material. Secondly, although there was no rock layer, the drilled shaft, as currently designed, will have much more resistance than the structural design requires.

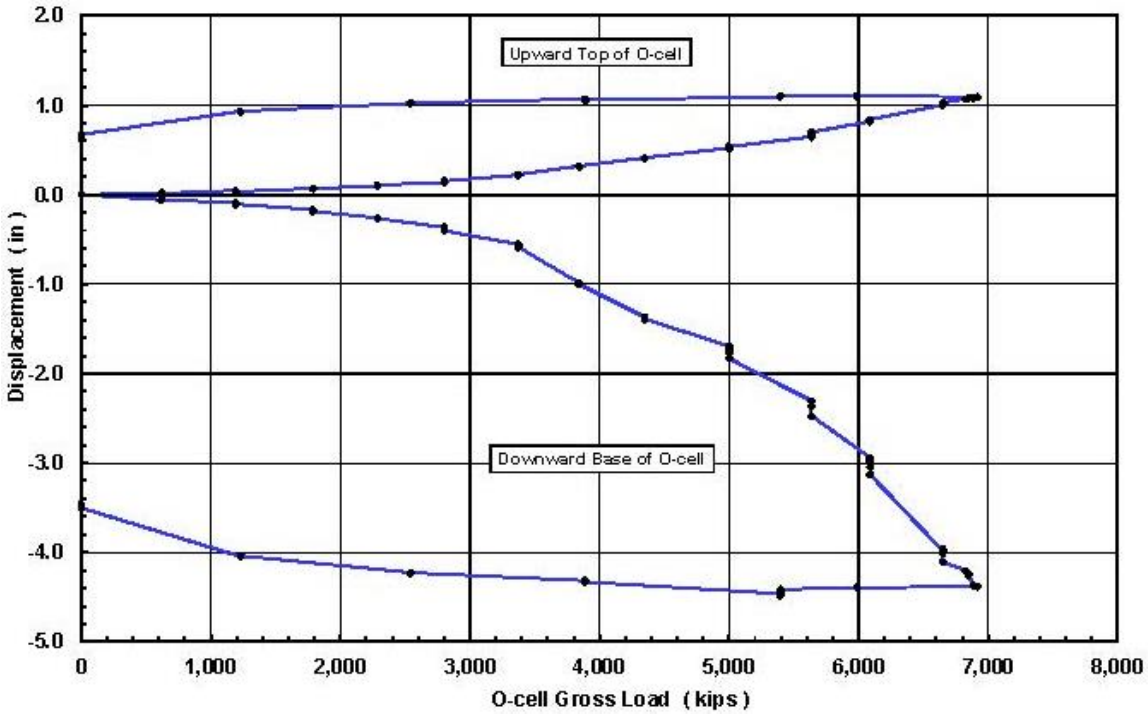


Fig. 7 O-cell load vs displacement curves

© 2016 Deep Foundations Institute

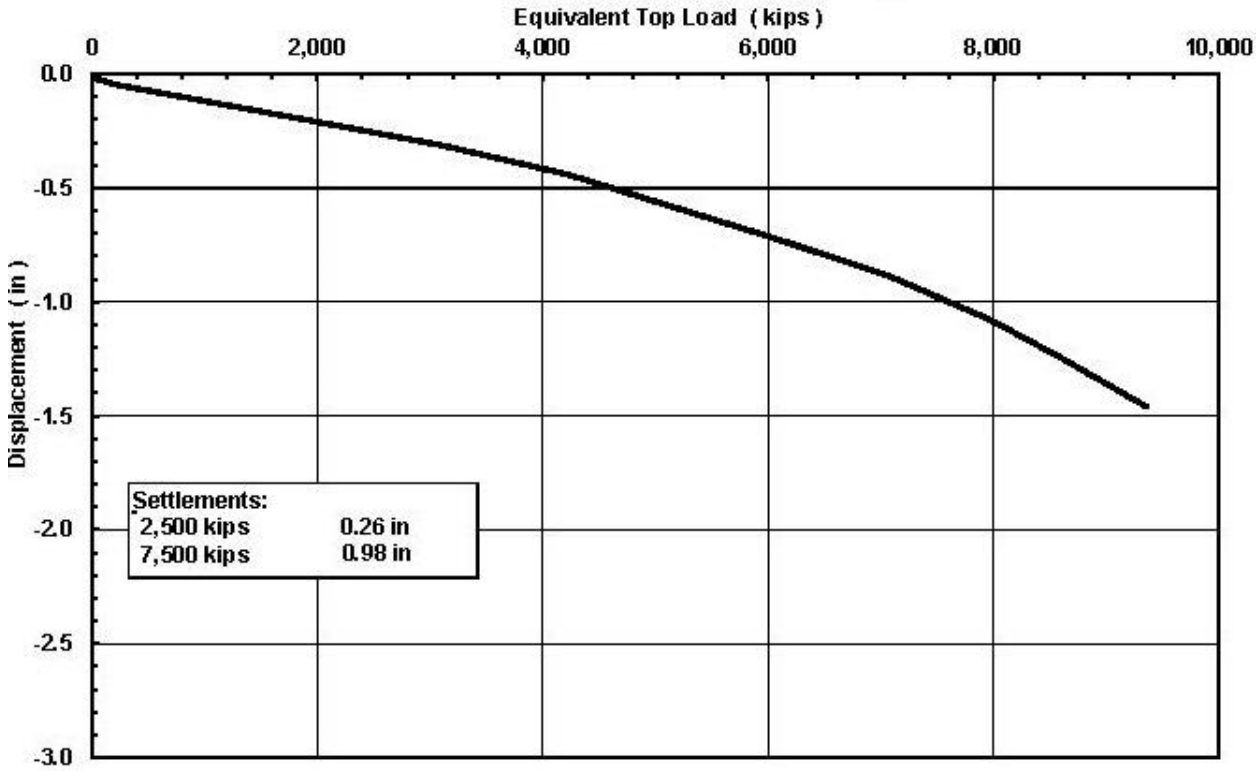


Fig. 8 Equivalent top load curve

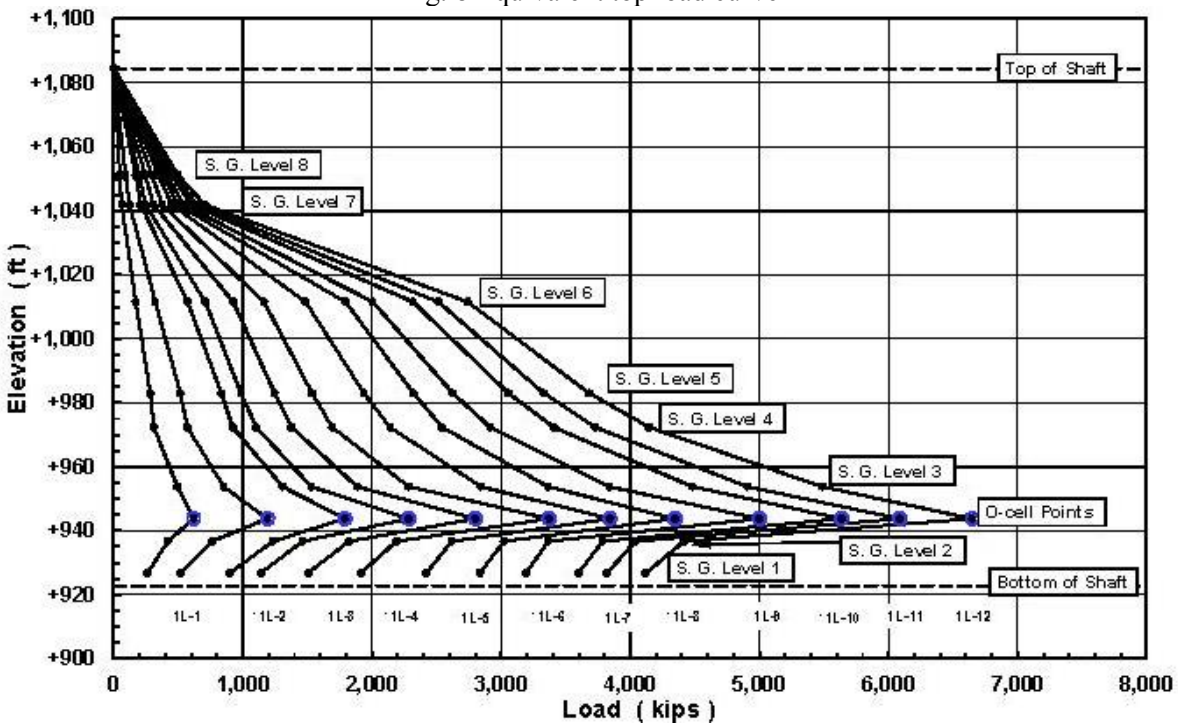


Fig. 9 Strain gage load distribution

© 2016 Deep Foundations Institute

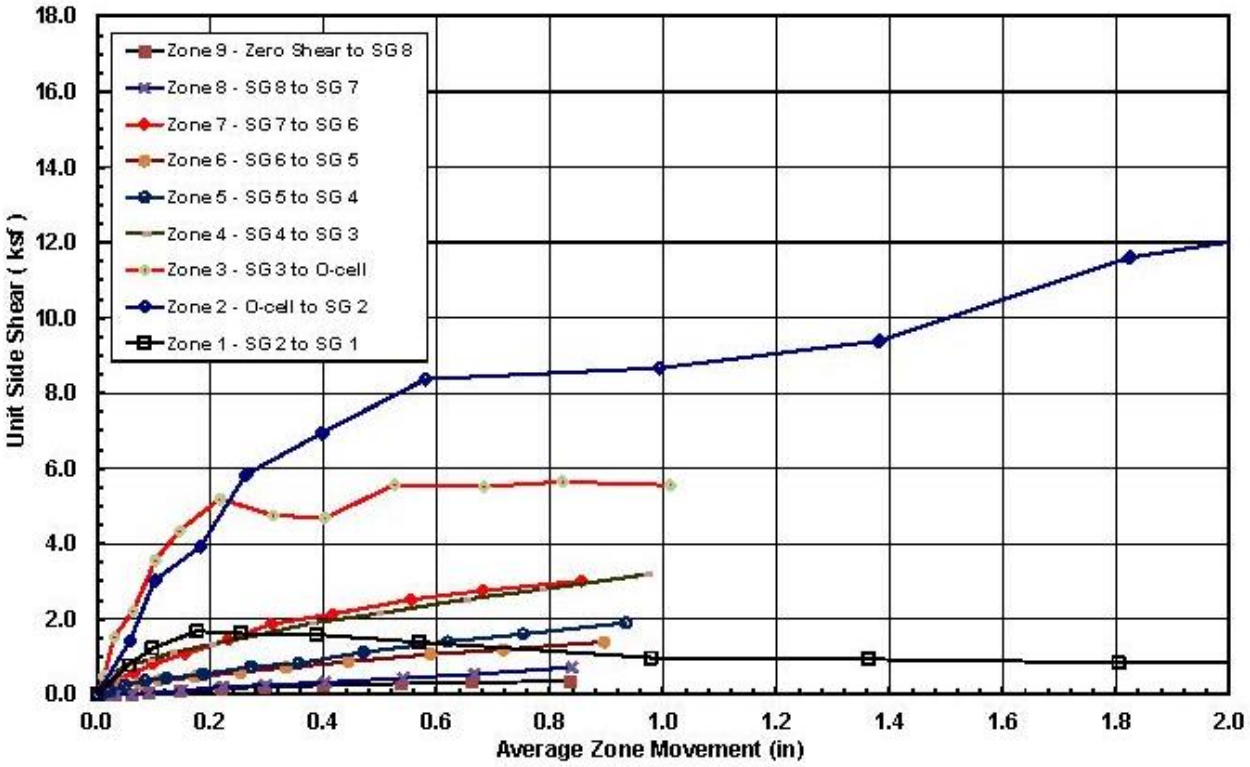


Fig. 10 Unit side shear curves

PROJECT SPECIFIC ECONOMIC BENEFITS FROM O-CELL TEST

Per the geotechnical exploration report, considering only rock socket friction, initial LRFD based shaft design lengths were in the range of 180 feet below ground surface. Development of contractual documents and final contract award for drilled shaft construction were completed based on these design lengths.

However, during preparation for the test program, it was found out that no rock layer exists at this design depth. Building of rock socketed drilled shafts, per the design guidelines, with a rock socket of 31 feet, would require drilled shafts deeper than 200 feet, minimum. For drilled shafts deeper than 200 feet, construction costs grow exponentially as depth increases. They would also require special construction equipment and methods. Based on the drilling contractor's approximate estimation for this project, adding additional shaft drilling depth to 200 feet would be approximately $500,000. Additional materials quantities such as rebar, concrete, plus larger capacity cranes etc. were broadly estimated, to add a minimum of another million dollars to construction costs.

FHWA design guidelines allows the design of drilled shafts in soils with no rock sockets. Applying value engineering principles, the O-cell test results proved that the drilled shaft constructed in overburden soils, at the current design lengths, provide more frictional resistance than the structure design requirements. Additionally, the load test results provided design and soils parameter calibration, allowing application of a higher resistance factor. This higher resistance factor reflects an increase in design reliability confidence and knowledge of construction procedure influences for establishing production shaft dimensions. Considering the above, the friction resistance of overburden soils was applied to the production drilled shaft resistance designs. This allowed production shaft construction to proceed at plans dimensions with no design modifications, preventing significant project cost overruns.

© 2016 Deep Foundations Institute

SUMMARY AND CONCLUSIONS

For rock socketed drilled shafts, design guidelines of the various agencies do not consider the frictional resistance of overburden soils as part of the design resistance. Iowa DOT geotechnical design guidelines require that drilled shafts be advanced into rock sockets, with the resistance estimated from rock socket friction only. Resistance from over burden soils is not allowed to be considered as part of design capacity.

In this paper, results of a load test conducted on a drilled shaft, as part of a I-29 replacement bridge over Floyd River are presented. Based on the initial geotechnical exploration, the material at about 140 feet below the ground surface were classified as rock and the drilled shaft initial designs were initially developed considering rock socket frictional resistance only. Development of contractual documents and final contract award for drilled shafts construction were done based on these designs.

However, during the load test program, it was realized that the material classified as rock does not represent a true rock material. The load test results confirmed that the factored frictional resistance of the overburden soils were much more than the required design capacity. Based on the results, it was decided to consider the frictional resistance of overburden soils into the design, resulting in significant cost savings. The O-cell test program conducted for this project not only fulfilled the requirement of a full-scale load test, but also served as value added engineering tool.

At times, the frictional resistance of the overburden soils is significant and can be verified by instrumented O-cell load test. When appropriate, considering the overburden soils friction resistance as part of design resistance can result in a significant cost savings. Application of overburden soils resistance can also justify shaft dimension reductions providing additional economic value.

REFERENCES

Osterberg, J.O., 1998. The Osterberg load test method for bored and driven piles: The first ten years. Deep Foundations Institute, Proceedings of Seventh International Conference on Deep Foundations, Vienna, Austria.

Ayithi, A., Bullock, P.J., Khoo, H.S. and Ramana, G.V., 2013. Technical and economic benefits of O-cell load testing for deep foundation in India. Proceedings of Indian Geotechnical Conference, December 22-24, 2013, Roorkee, India.

LOADTEST USA, 2015. Report on drilled shaft load testing (Osterberg method): Test shaft-1 - I-29 over Floyd River, Sioux City, IA (LT-1289). LOADTEST USA, Gainesville, FL.

LRFD Bridge Design Manual, 2016. Iowa Department of Transportation, Des Moines, IA, 1006 p.

© 2016 Deep Foundations Institute

INFLUENCE OF SURFACE REPLACEMENT LAYER ON BEHAVIOR OF LATERALLY LOADED LARGE BORED PILES IN SOFT CLAY: PILE LOAD TESTS AND NUMERICAL INVESTIGATION

Mamdouh M. Hamza, Suez Canal University & Hamza Associates, Egypt, hamza@hamza.org
Marawan M. Shahien, Tanta University & Hamza Associates, Egypt mshahien@hamza.org
Hayel M. El-Naggar, Housing and Building National Research Centre, Egypt, hayelelnaggar@gmail.com
Mohamed Sobhi, Tanta University, Egypt, masli2010@yahoo.com

ABSTRACT

This paper presents the results of two lateral load tests on large bored piles in soft clay deposit for a major site in northern Egypt. The tests are carried out on 0.8 m diameter piles. One of the tests is carried out on the pile where the clay starts from the ground surface. The other test is carried out on a pile after surface improvement by replacing the top 1.50 m of the clay deposit by compacted granular soil. The results of the tests show the influence of the surface replacement layer on the lateral load versus lateral displacement relationships of the loaded pile. The results of the two tests are used to calibrate a 3D Finite Element Analysis model for the pile. The model is used to investigate the influence of the thickness and lateral extent of the surface replacement layer on the behavior of laterally loaded large bored piles.

KEYWORDS: Large bored piles, lateral pile load test, surface replacement layer, and Finite element analysis.

INTRODUCTION

Lateral loads for piles are produced by seismic events, wind, wave action, ship impact, traffic, and land slide forces. The lateral resistance of a pile is controlled by the stiffness and the strength of the material of the pile and the soil surrounding the upper portion of the pile. In most situations, the soil surrounding the upper portion of the pile is too weak to sustain the design lateral loads. Thus there is a need to increase the lateral resistance of the pile or groups of piles. Such an increase may be achieved by either increase number of piles or increase pile diameter. Alternatively, an economic way to increase the lateral resistance is to improve the soil surrounding the upper portion of the pile (Rollins and Brown, 2011; Faro et al., 2015).

Ground improvement has the ability to increase the lateral resistance of the pile by increasing the passive resistance of the soil surrounding the upper portion of the pile. The ground improvement techniques have the potential for being more cost-effective and reducing construction time. In spite of this fact, such techniques are rarely implemented in practice. Further, there are relatively few tests or records available in the literature to guide engineers in evaluating the actual effectiveness of this approach. In addition, there is no standard or methodology to aid engineers in designing increase of lateral resistance with surface ground improvement. There are specific improvement methods for each soil type, whether it is loose cohesionless soil or soft cohesive soil and these methods are provided by Michell (1981), Tershai and Juran (2000), ASCE (1997), and Rollins and Brown (2011). Furthermore, there are number of case histories that add a new hole in the sight, such as the cases provided by Brown et al. (1987, 1988), Mokwa and Duncan (2001), Rollins et al. (2005), Rollins and Cole (2006), Cole and Rollins (2006), Rollins, Snyder et al. (2010) , Rollins, Gerber, and Kwon (2010), Rollins and Nasr (2010), and Gerber et al. (2010).

© 2016 Deep Foundations Institute

This paper describes two tests on trial piles with the same dimension (diameter and length). The first test (case 1) is carried out on a pile that is surrounded by natural ground of soft to firm clay, whereas the second test (case 2) is conducted on a pile that is surrounded with the same soil except for 1.5 m thick replacement layer. The results of the two pile load tests are used to calibrate a 3 D finite element model. The calibrated model is then used to carry out parametric analysis studying two major variables; thickness of surface replacement layer and the lateral extent of the replaced layer.

SOIL CONDITIONS AT TEST SITE

A comprehensive site investigation program was conducted in the site. The program included drilling boreholes down to depths of about 60m below ground surface, piezocone penetration test, and field vane tests. Laboratory testing are carried out on Shelby tube "undisturbed" samples including unconsolidated undrained and consolidated undrained triaxial tests. Fig. (1) shows the geotechnical profile encountered at the site. It consists of a fill layer that is 0.5 m in thickness. The fill is underlain by 24.0 m of soft to firm clay (upper clay). Poorly graded sand layer with silt (upper sand) underlies the upper clay. The upper sand layer is 1.5 m in thickness. The upper sand layer is followed by 11.50 m of very stiff clay (middle clay). The middle clay is underlain by 5.50 m of very dense silty clayey sand (lower sand). A stiff to very stiff clay layer underlies the lower sand and continued to end of boring. The ground water table is encountered at about 1.0 m below ground surface. Geotechnical parameters of soil formations are shown in Fig. (1).

TESTED PILES PROPERTIES

Two lateral load tests are carried out on two trial piles. The two piles are reinforced concrete bored piles. The two piles are identical in both diameter and length. The embedded length of the piles is 38m. Both piles are embedded in the natural soil profile described above and shown in Fig. (1). The top 1.5 m of the soil profile is improved by replacement with compacted sand layer around the second pile as shown in Fig. (1). Table (1) presents the geometrical and design information of the two piles.

Table 1. Geometric and design information of the tested piles (Lateral Loads)

Test No.	Shape	Diameter (mm)	Length (m)	Design Load (kN)	Test Load (kN)	% (T.L / D.L)
Pile 1	○	800 mm	40.0 m	85	170	200
Pile 2		800 mm	40.0 m	150	225	150

LATERAL LOAD TESTS

The loading jack obtains reaction from a stiff steel girder that is 10 m in length. The girder distributes the jack reaction load on 9 concrete blocks. The blocks are resting on the natural soil. The blocks are constrained by a vertical cut of natural soil with height equal to block size of 1.0m. The blocks gain additional weight by 8 blocks bearing on top of the lower blocks.

One dial gauge is used for measuring the lateral displacement of the pile. The dial gauge is mounted on the pile on the axe of the hydraulic jack. The dial gauge is supported on a reference beam. The dial gauge used to measure lateral displacement is located at 150 mm above the ground surface. The load cell is used for load measurement. The pressure in the hydraulic jack is increased when drop in pressure occurs. The load is kept constant during the time of loading within accuracy +/- 2 %. The testing procedure, load and unload sequence and duration of readings are in accordance with ASTM D 3966.

© 2016 Deep Foundations Institute

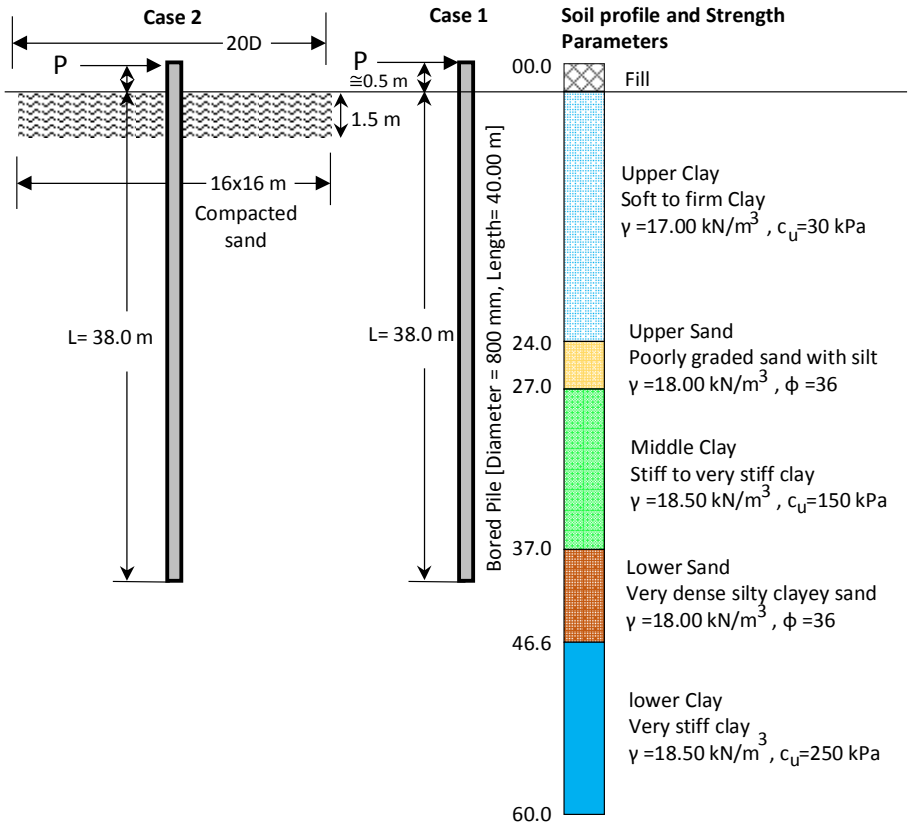


Fig. 1. Geometrical profile and properties of the site and information on the tested piles

FIELD TEST RESULTS

The relationship between lateral load and lateral displacement during loading and unloading of the two tests (test 1 referred to as case 1 and test 2 referred to as case 2) are shown in Fig. (2). For test 1, the maximum horizontal displacement at maximum lateral load (170 kN) is 21.55 mm. Upon unloading, the horizontal displacement reduced to 6.72 mm, i.e the pile recovered horizontal displacement of 14.83 mm. During loading of test 2, the lateral displacement at maximum lateral load (225 kN) is 8.46 mm. The recovered displacement during unloading is 6.48 mm reducing the lateral displacement to 1.98 mm. The observed performance during testing indicates no concrete failure occurred in the pile with considered elastic response under the range of loads in the tests.

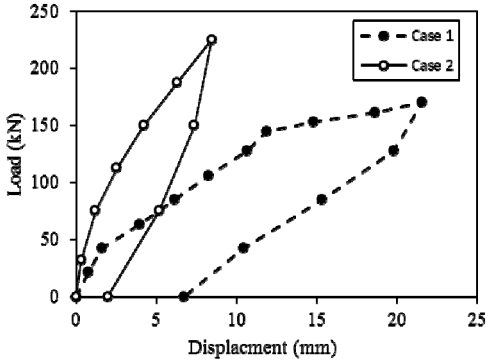


Fig. 2. Load versus horizontal displacement for the two tested piles

© 2016 Deep Foundations Institute

NUMERICAL ANALYSIS VERIFICATION

Three dimensional Finite Element Models are built for the two tests. The 3 D meshes of the two models are shown in Fig. (3). Table (2) shows summary of geotechnical parameters used in the analysis presented in this paper.

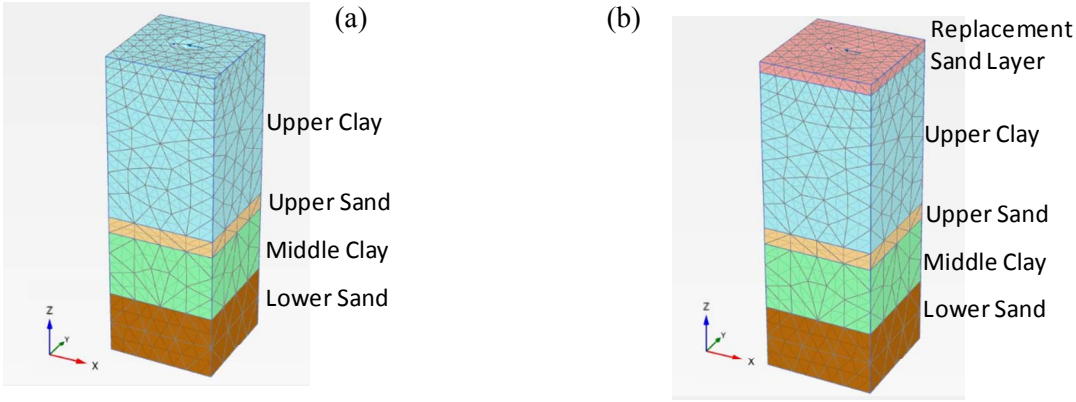


Fig. 3. Three dimensional mesh for pile in (a) natural soil profile and (b) the same soil profile with surface replacement of 1.5 m thick sand layer

Table 2. Geometrical parameters used in the analysis.

Layer	Depth Below Ground Surface m	Unit Weight kN/m^3	Effective Stress Shear Strength c'=0, ϕ' Degree	Drained Deformation Modulus kPa	Undrained Shear Strength, c_u kPa	Undrained Deformation Modulus kPa
Upper Clay	24.5	17.0	-	-	30	9000
Upper Sand	27.0	18.0	36	30000	-	-
Middle Clay	37.0	18.5	-	-	150	45000
Lower Sand	46.6	18.0	36	40000	-	-
Lower Clay	60.0 (EOB)	18.5	-	-	250	60000
Replacement Sand Layer	Top layer	19.0	38	50000	-	-

The observed load versus displacement relationship in each case (test) is compared to results of the finite element analyses. The main objective of the comparisons is to calibrate the built numerical model with the parameters in Table (2). Such calibration would allow for further use of the model for carrying out parametric analysis as shown in the following sections. The comparisons of results or calibration are shown in Fig. (4). The comparisons in Fig. (4) show excellent agreement between the results of analysis and the observed behavior.

© 2016 Deep Foundations Institute

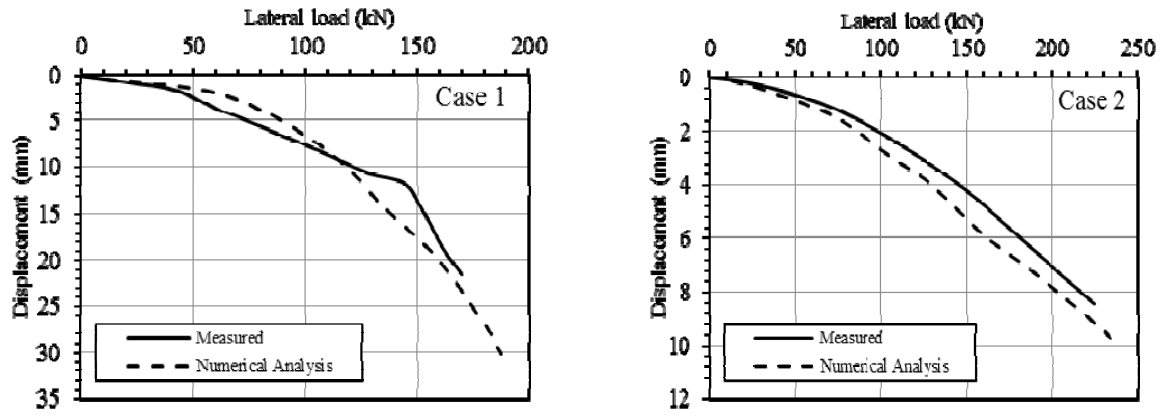


Fig.4: Comparison between the field data and 3D Finite Element Analysis results for the load versus displacement curves for case (test) 1 (without surface replacement) and case (test) 2 (with 1.5 m surface replacement)

PARAMETRIC ANALYSIS

The 3D finite element model of case (test) 2 with soil replacement is utilized to carry out parametric analysis. Table (3) shows the variables and range of values considered for each variable of the parametric analysis.

Table 3. Variables Considered in Parametric Study.

Variable	Symbol	Units	Range of Values	Normalized Symbol	Range of Values
Thickness of surface replacement layer	Z	m	0.0, 0.5, 1.0, 1.5 & 2.5	Z/D	0.0, 0.625, 1.25, 1.875 & 3.125
Horizontal extent of replacement layer around the pile	X	m	0.0, 4.0, 8.0 & 16.0	X/D	0.0, 5.0, 10.0 & 20.0

Two series of computer runs are carried out. In the first series, the value of X is varied in the range shown in Table (3) while keeping the value of Z constant at 1.5 m corresponding to Z/D of 1.875. During the second series, the value of Z is varied in the range shown in Table (3) while keeping the value of X constant at 16.0 m corresponding to X/D of 20.0.

RESULTS AND INTERPRETATIONS

The results in terms of horizontal load versus lateral displacement relationships for the first and second series are shown in Figs. (5) and (6), respectively. The results in Figs. (5) and (6) are presented in terms of relationships between secant stiffness K versus normalized displacement in Figs (7) and (8) for the first and second series, respectively. The secant stiffness K is defined as horizontal load divided by lateral displacement. The normalized displacement (δ/D) is defined as the lateral displacement divided by pile diameter. Shown also on Fig. (8) are the results of the measured data during the pile load tests.

© 2016 Deep Foundations Institute

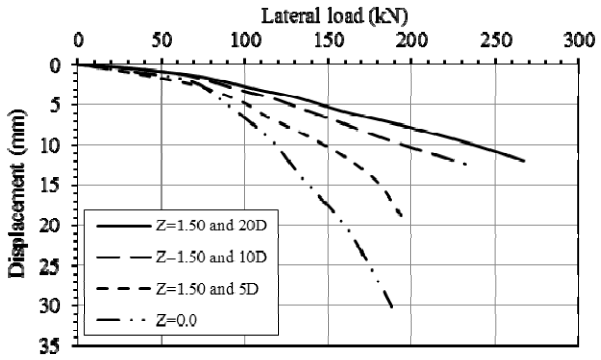


Fig. 5: Load versus Displacement curves for 1.5 m thick surface replacement with different values of horizontal extents around the pile (First Series).

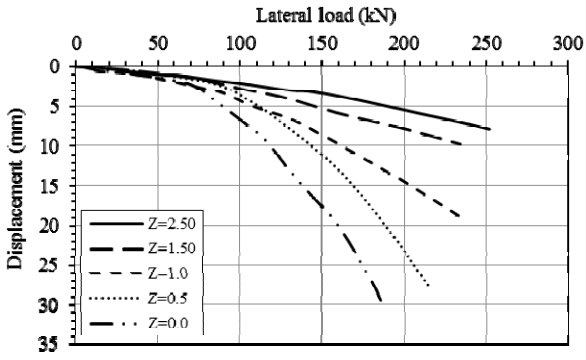


Fig. 6: Load versus Displacement curves for different thicknesses of surface replacement (Z/D) with horizontal extents X/D of 20 around the pile (Second Series).

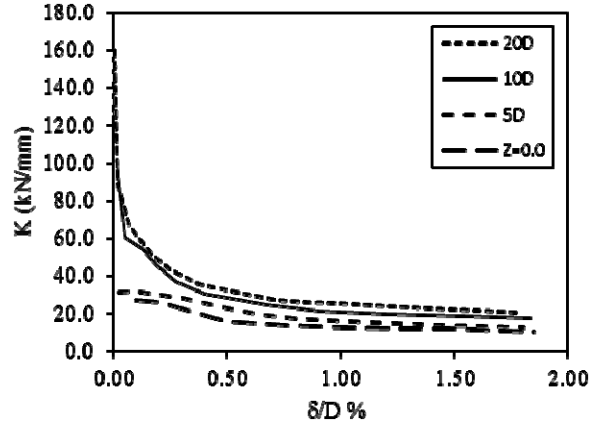


Fig. 7: Secant stiffness versus normalized displacement curves for 1.5 m thick surface replacement with different values of horizontal extents around the pile (First Series).

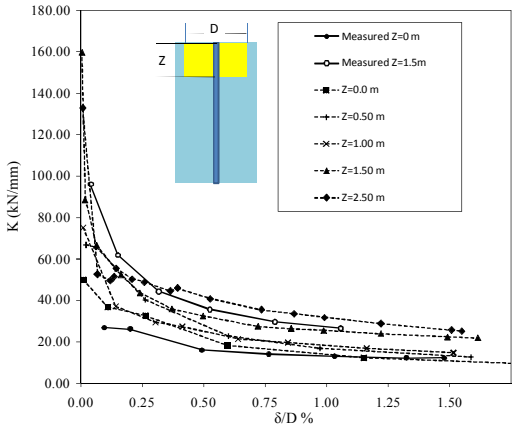


Fig. 8: Secant stiffness versus normalized displacement curves for different thicknesses of surface replacement (Z/D) with horizontal extents X/D of 20 around the pile (Second Series).

Furthermore, the results in terms of deflection, shear force, moment and soil reaction along the shaft depth for the second series only are shown in Figs. (9) due to the limited spacing. The results in Figs (9) correspond to horizontal load of 170 kN.

The following four parameters are introduced for sake of comparisons:
K is stiffness that is defined as H/δ, where H is the horizontal load and δ is the horizontal displacement.
Vmax/H is the ratio of maximum shear force along the pile length to horizontal load H.
Mmax/HD is the ratio of maximum bending moment along the pile shaft to HD, where D is pile diameter.
Rmax/H is the ratio of maximum reaction along the pile shaft to horizontal load H.

The four parameters are plotted versus X/D for the first series in Fig. (10) while the same four parameters are plotted versus Z/D for the second series in Fig. 11.

© 2016 Deep Foundations Institute

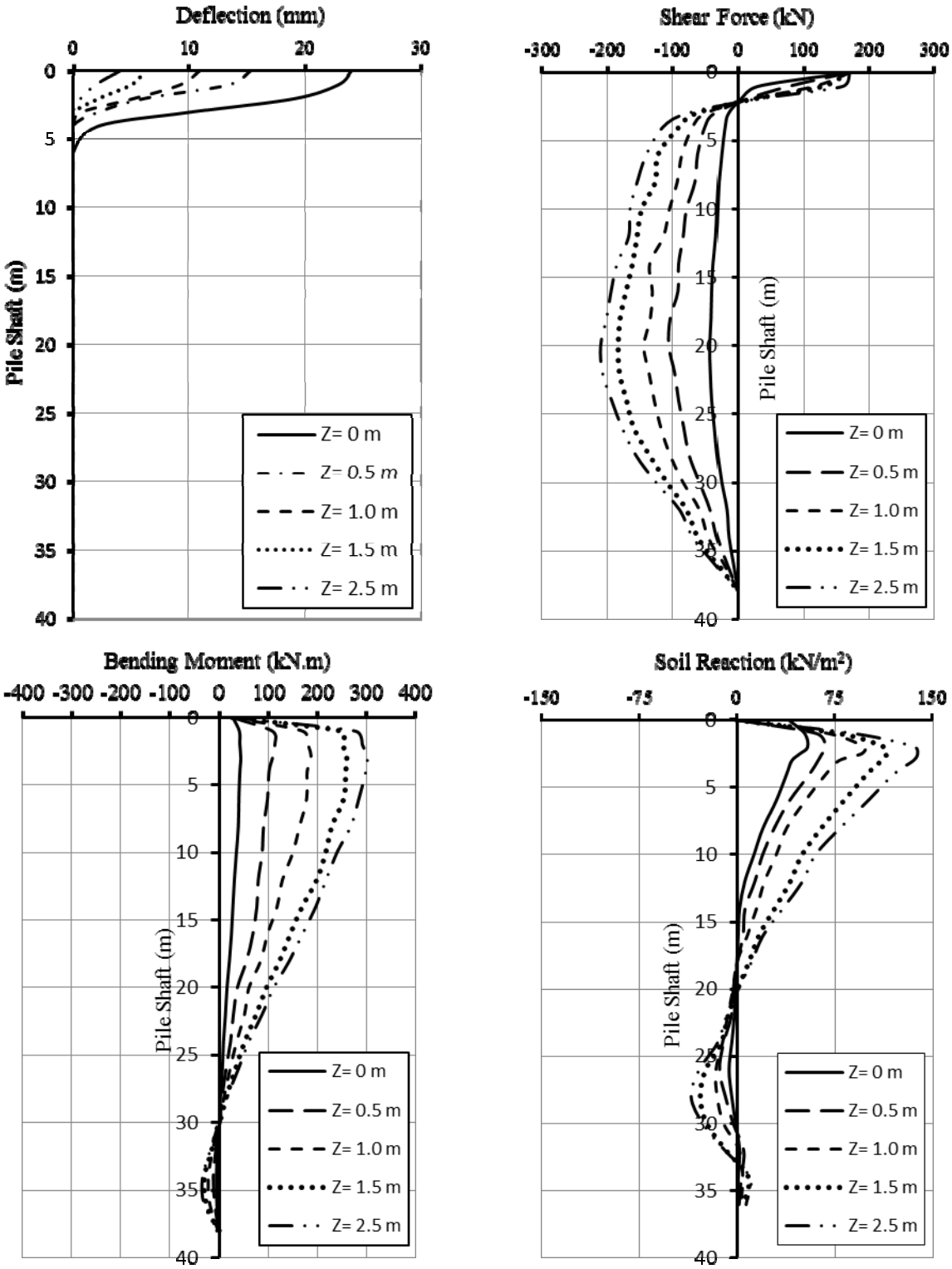


Fig. 9: Deflection, shear force, moment and soil reaction along pile depth for different thicknesses of surface replacement (Z/D) with horizontal extents X/D of 20 around the pile (Second Series). The data correspond to horizontal load of 170 kN.

© 2016 Deep Foundations Institute

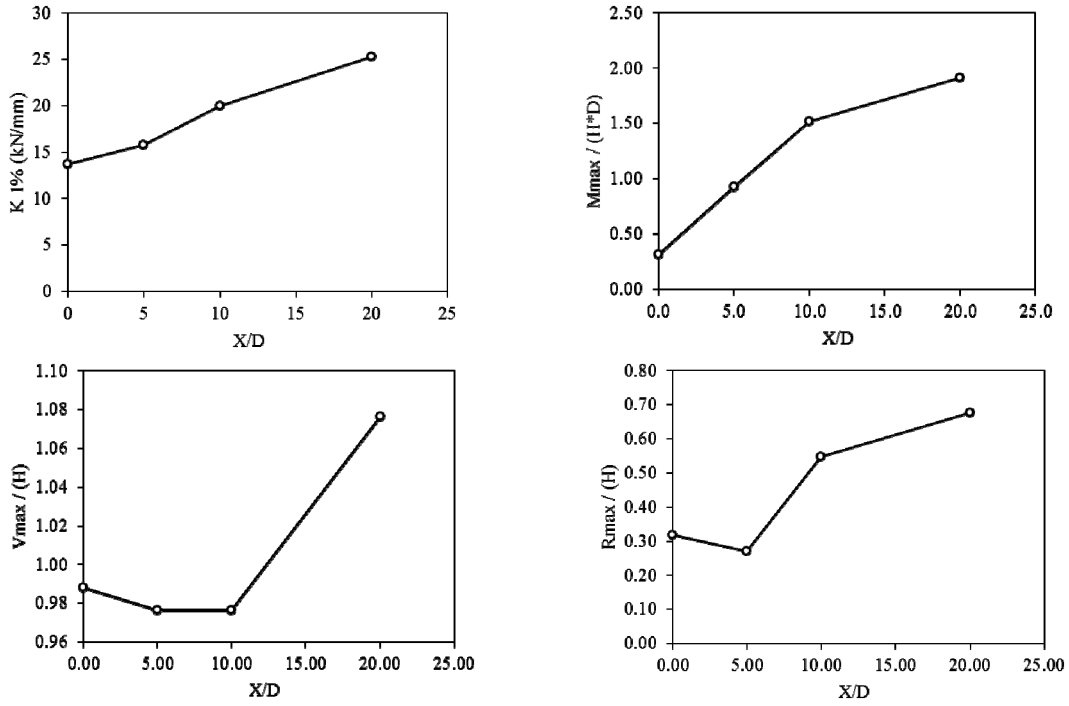


Fig. 10: Parameters K, Mmax/HD, Vmax/H and Rmax/H versus various values of X/D for First Series – Horizontal Load H =170 kN.

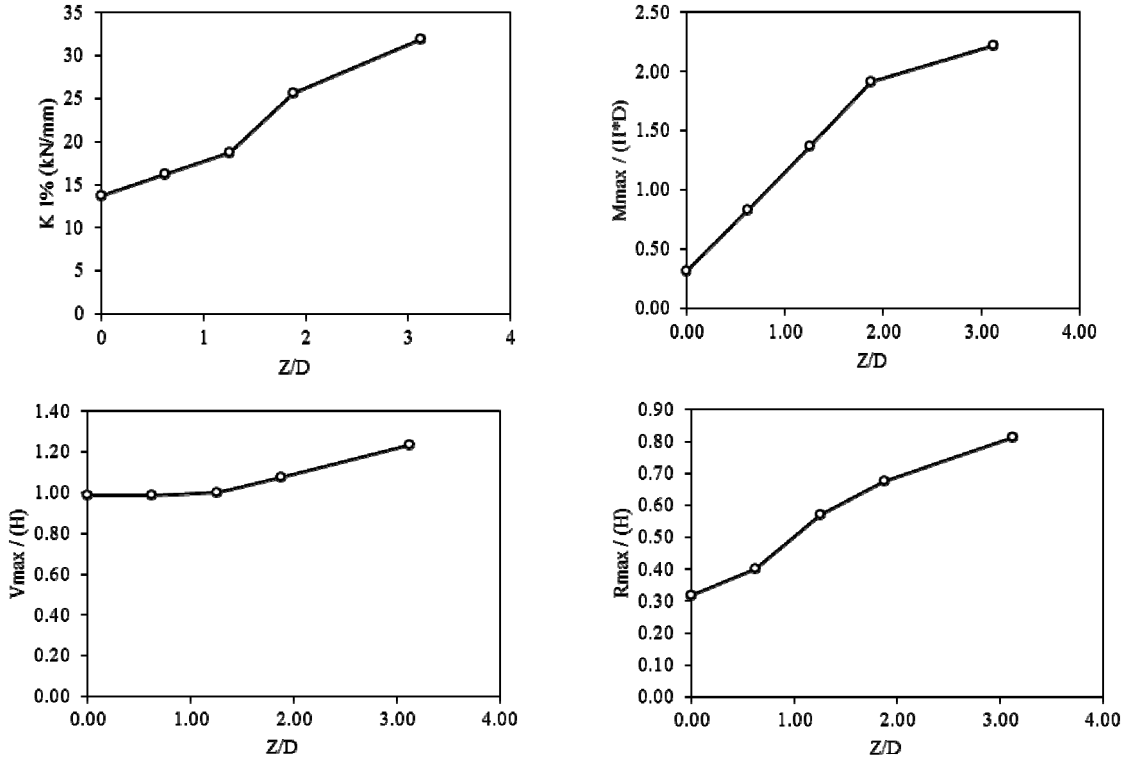


Fig. 11: Parameters K, Mmax/HD, Vmax/H and Rmax/H versus various values of Z/D for Second Series – Horizontal Load H =170 kN.

© 2016 Deep Foundations Institute

DISCUSSIONS AND CONCLUSIONS

Considering the results in Figs (2) and (4), it is clear that the overall behavior of the pile is improved by the presence of the sand replacement layer of 1.5 m in thickness. For instance, at certain displacement equal to 1% of the pile diameter (8mm), the corresponding load in the case of natural soil (case 1) is 106 kN while the load in the case of surface improvement (case 2) is 225 kN. The load increased about 112%.

Considering the results in Figs. (5) and (7), in general the lateral behavior of pile improves with the increase in the lateral extent of surface replacement. This can be explained by the fact as the lateral extent of surface replacement increases, there is enough space behind the pile that allows for better development of passive resistance in the surface layer. It should be noted that the improvement in the lateral behavior of the pile within lateral extent in the range of 10D to 20D is not as significant as within the range of 5D to 10D. This is due to the fact that for depth of improvement of about 2D (Z=1.5 m), only distance of 10D is required to fully develop the passive resistance in the soil surrounding the pile. Any further increase in lateral extents in the surface replacement layer does not significantly contribute to any additional passive resistance. It is consistent with the observation made by Rollins and Brown (2011).

Considering the results in Figs. (6) and (8), in general the lateral behavior of pile improves with the increase in thickness of surface replacement. This is due to the increase in passive resistance with the increase in thickness of surface replacement layer. It should be noted that the improvement in lateral behavior of the pile increases with the increase in thickness of surface replacement layer until it reaches certain thickness (in this case 1.50m) and the increase in the behavior decreases with the increase in thickness of surface replacement layer.

Considering the different parameters along the shaft of the piles in Figs (10) and (11), in general, the presence of surface replacement layer acts as surface constrains to the head of the pile limiting the surface displacement, increasing the maximum bending moment.

As passive resistance (soil reaction) increases at or near the top of the pile either due to increase in lateral extent or thickness of surface layer, the location of the maximum shear moves from the pile head to mid depth of the pile.

For the data and analysis presented in this paper, the following conclusions can be drawn.

- The use of surface replacement compacted sand can significantly improve the performance of laterally loaded piles.
- The increase in lateral behavior of pile is a function of the combined effects of the lateral extent of surface replacement and depth of the thickness of surface replacement layer, as well as the ratio between the shear strength of the surface layer and that of natural soils.

REFERENCES

ASCE (1997), “Ground Improvement, Reinforcement and Treatment: A Twenty Year Update and Vision for the 21st Century,” ASCE Geo-Institute Conference, July 1997 (Geotechnical Special Publication No. 69).

Brown, D. A., Reese, L. C., and O’Neill, M. W. (1987), “Behavior of a Large Scale Pile Group Subjected to Cyclic Lateral Loading,” Journal of Geotechnical Engineering, ASCE, 113(11): 1326–1343.

Brown, D. A., Morrison, C., and Reese, L. C. (1988), “Lateral Load Behavior of a Pile Group in Sand,” Journal of Geotechnical Engineering, ASCE, 114(11): 1261–1276.

© 2016 Deep Foundations Institute

Cole, R.T and Rollins, K.M. (2006), “Passive Earth Pressure Mobilization During Cyclic Loading,” Journal of Geotechnical and Geoenvironmental Engineering, 132(9): 1154–1164.

Duncan, J. M. and Mokwa, R. L. (2001), “Passive Earth Pressures: Theories and Tests,” Journal of Geotechnical and Geoenvironmental Engineering, ASCE 127(3): 248–257.

Faro, V., Consoli, N., Schnaid, F., Thomé, A., and da Silva Lopes, L. (2015). "Field Tests on Laterally Loaded Rigid Piles in Cement Treated Soils." J. Geotech. Geoenviron. Eng., 10.1061/(ASCE)GT.1943-5606.0001296, 06015003.

Gerber, T. M., Rollins, K. M., Cummins, C. R., and Pruett, J. M. (2010), Dynamic Passive Earth Pressure on Abutments and Pile Caps. Final report prepared for Utah Department of Transportation Research Division Lead Agency for Pooled-Fund Study. Unpublished raw data.

Mokwa, R. L. and Duncan J. M. (2001). “Experimental Evaluation of Lateral-Load Resistance of Pile Caps,” Journal of Geotechnical and Geoenvironmental Engineering, ASCE 127(2): 185–192.

Rollins, K. M., Snyder, J. L., and Broderick, R. D. (2005), “Static and Dynamic Lateral Response of a 15 Pile Group,” Proceedings, 16th Intl. Conf. on Soil Mechanics and Geotech. Engineering, Millpress, Rotterdam, The Netherlands, Vol. 4: 2035–2040.

Rollins, K. M. and Cole, R. T. (2006), “Cyclic Lateral Load Behavior of a Pile Cap and Backfill,” Journal of Geotechnical and Geoenvironmental Engineering, ASCE 132(9): 1143–1153.

Rollins, K. M., Olsen, R. J., Egbert, J. J., Jensen, D. H., Olsen, K. G., and Garrett, B. H. (2006), “Pile Spacing Effects on Lateral Pile Group Behavior: Load Tests,” Journal of Geotechnical and Geoenvironmental Engineering,ASCE 132(10): 1262–1271

Rollins, K. M., Gerber, T. M., and Ku Hyun Kwon (2010), “Increased Lateral Abutment Resistance from Gravel Backfills of Limited Width,” Journal of Geotechnical and Geoenvironmental Engineering, ASCE 136(1): 230–238.

Rollins, K. M., Snyder, J. L., and Walsh, J. M. (2010), “Increased Lateral Resistance of Pile Group in Clay Using Compacted Fill,” Proceedings, GeoFlorida 2010: Advances in Analysis, Modeling and Design, (Geotechnical Special Publication No. 199) ASCE 1602–1611.

Rollins, K. M. and Nasr, M. (2010), “Numerical Analysis of the Effectiveness of Limited Width Gravel Backfills in Increasing Lateral Passive Resistance.” Dynamic Passive Earth Pressure on Abutments and Pile Caps. Final report prepared for Utah Department of Transportation Research Division Lead Agency for Pooled-Fund Study.

© 2016 Deep Foundations Institute

INNOVATIVE EARTH RETENTION PROJECT FOR A PARKING GARAGE

Dipl.-Ing, Andreas Brandner, IB-Brandner, Karl-Schoenherr-Strasse 8, A-6020 Innsbruck – Austria, Phone +43 512 563 3320, Fax +43 512 563 3324, Email office@ib-brandner.com

ABSTRACT

A world famous Wintersport resort in the Alpine planned to build a parking garage for more than 600 cars and busses situated between a torrent, a district road and the village.

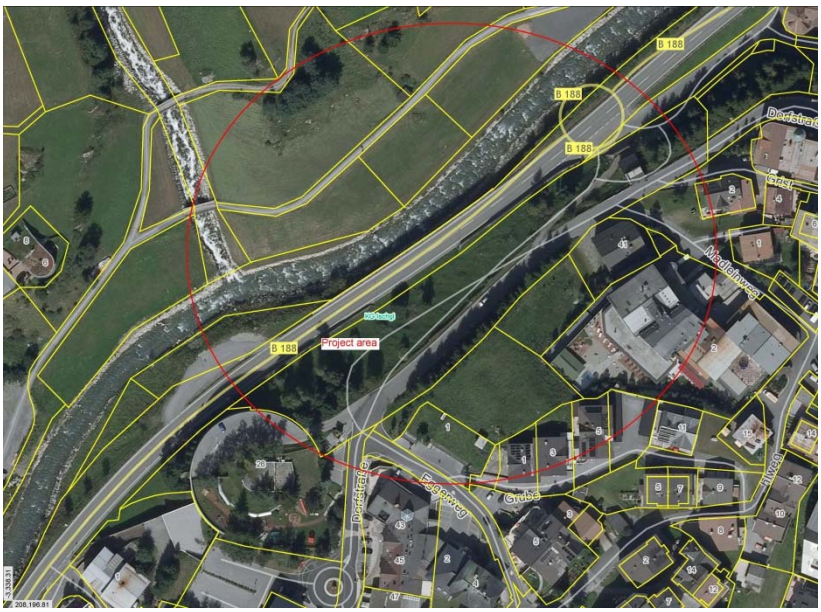


Figure 1 – project area

A nearly 200 m long building giving place for 6 parking levels and a maintenance level for busses and trucks is situated alongside a hill causing excavation height between 20 and 25 meters, which had to be secured. Due to restrictions – neighbours did not allow the client to drill anchors for retention – we designed a solution combining micropiles, strand anchors, shotcrete and nails as permanent earth retention not exceeding the space of 7 meters provided by the local street. Soil conditions were as challenging - reaching from backfill to moraine with boulders of more than 20 m³ volume – as the construction period of total 12 months for the whole project, which was opened mid of November 2015.

The innovative solution outperformed the client´s project from the technical and commercial aspect and helped the contractor to save time and money.

The design process with its difficulties as well as erection process is described in the following paper.

© 2016 Deep Foundations Institute

1. GENERAL PROJECT DESCRIPTION

The village of Ischgl in Tyrol published tender documents for the erection of a big garage. A General Contractor together with the geotechnical and structural designer worked on an alternative solution for the support of excavation and structural design as well. Based on a site investigation consisting of 11 test boreholes and geotechnical tests – shear test, triaxial compression test, seepage test – the geotechnical and structural design was part of the tender documents for the garage worked out by AST general contractor.

The planned garage was situated in public property. The adjacent owners demanded their property free of obstacles down to a depth of 12 m leaving a strip of only 7 meters as anchorage zone. The challenge was the excavation height of nearly 25 meters close to buildings along the village road allowing max deformations of 50 mm horizontally.

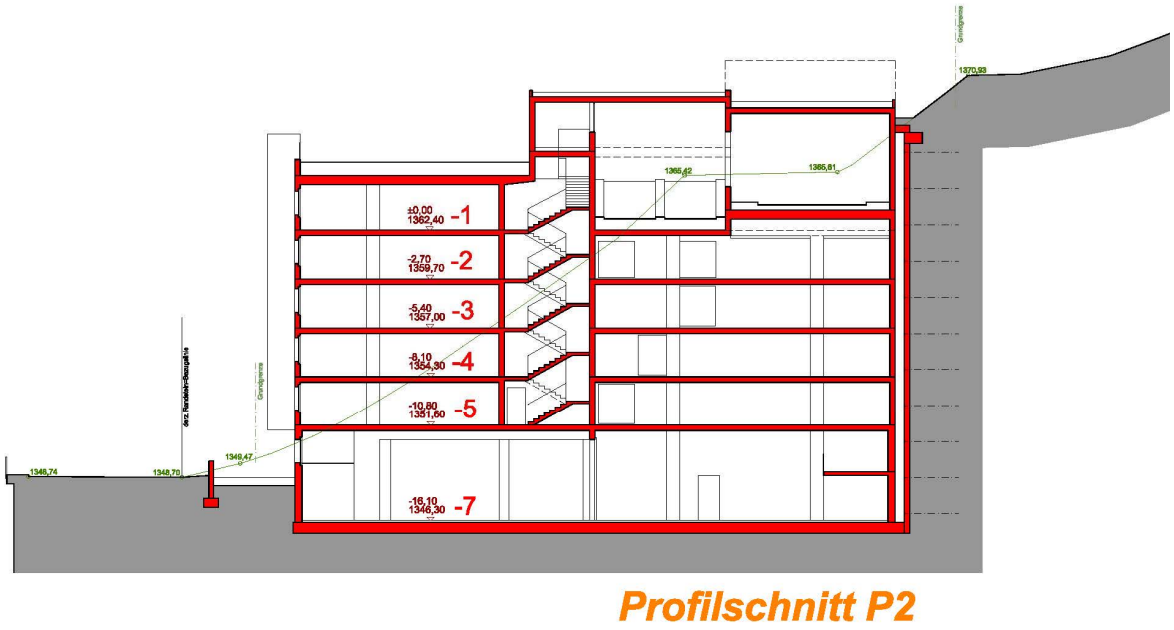


Figure 2 – section 2 of the garage showing excavation height

To gather some more soil data for the design and execution additional test drillings down to a depth of 35 meters were executed in early spring 2013 and led to the final geotechnical design.

After long discussions with several geotechnical contractors borepiles of diameters 60-120 cm were not chosen due to soil conditions –huge boulders bedded in very inhomogeneous matrix of clay, silt, sand, gravel – in fear of severe difficulties while drilling. Another problem was the lack of space for the necessary anchors. These conditions lead to a solution for the support of excavation consisting of micropiles, tieback piles – prestressed - and soil nailing within the 7 meter strip.

© 2016 Deep Foundations Institute

The choice to execute a permanent support of excavation saved a lot of money for the garage building as well and led to the award of the tender to AST General Contractor in spring 2013.

2. GEOLOGY

The site is situated in a narrow valley in Tyrol in the central part of the Eastern Alps.

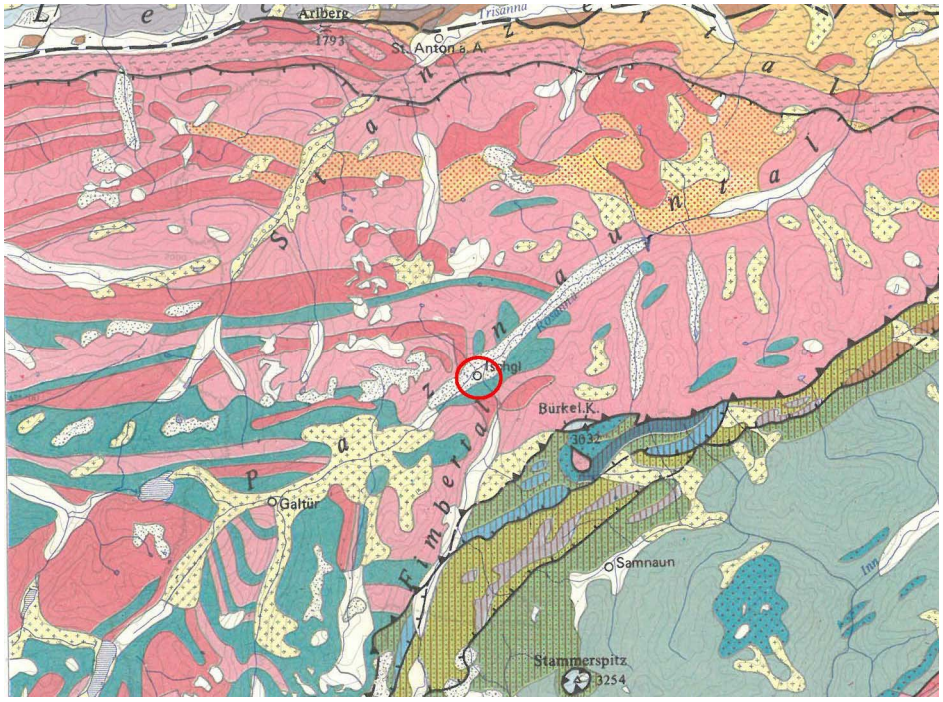


Figure 3 – geological overview 1:50000

The valley of the Trisanna creek leads in northeast direction from the Silvretta massif to the valley of the Inn River. The southern slopes are belonging to the Penninikum – Amphibolite whereas the northern slopes are Granite and Gneiss. The valley bottom shows several layers of sediments – silt, sand, gravel and boulders. These strata were medium dense to loose and showed a strong inhomogeneity across the building site as shown in figures 7 and 8. The site is situated at the exit of the Fimber valley where the Fimber creek deposited huge boulders and sediments – medium dense to very dense mixture of sandy-silty gravel.

As the new garage was jointed to the old existing garage backfill of sandy-silty gravel had to be secured.

Ground water level was about 3,40 meter below foundation but there was expected some seepage from the southern slope.

As soil parameters following data were provided by the client´s geotechnical consultant:

Friction angle	$\varphi' = 35°\text{-}37°$
Cohesion	$c' = 0$ kN/m²
Weight density	$\gamma = 21\text{-}22$ kN/m³
	$\gamma' = 11\text{-}12$ kN/m³
Stiffness modulus	$E_s = 80\text{-}150$ kN/m² increasing with depth
Modulus of subgrade reaction	$k_s = 30.000$ kN/m³
Permeability	$k_{f,u} = 1{,}0 * 10^{-4}$ m/s

© 2016 Deep Foundations Institute

The site check during excavation work showed that these values were only partly correct as in the eastern part of the building site the density was deteriorating to medium dens to loose and the backfill showed to be not compacted as it should have been.
STP tests across the site showed an inhomogeneous compactness in the river sediments, which did not correspond to the date given by the client. The variation of the subgrade modulus reached from 10.000 to 40.000 kN/m³.

3. GEOTECHNICAL AND STRUCTURAL DESIGN

Based on the soil parameters given and corrected the whole project was designed according to Eurocodes – EN 1990, EN 1991-2, EN 1992-2, EN 1993-2, EN 1997-1, EN 1537, EN 14199 and additional national regulations and approvals. These codes allow the design following the semi probabilistic safety concept using partial safety coefficients. For a major part of the garage avalanche impact had to be taken into account as additional horizontal pressure.
During the whole design process we followed the 4-eye principle – design was independently checked and released by a technical supervisor. Permanent site supervision by designing engineer provided maximum safety of this spectacular support of excavation and building.

3.1 Support of excavation

To stabilize the 25 meters of excavation a combination of vertical micropiles – GEWI 63,5 – inclined tieback micropiles GEWI 63,5 with a post grouted bonding length of min. 6 m and soil nails hollow bar type R32-250 and R38-500 with a reinforced shotcrete cover was used. With this combined system a mass bloc was created, which was anchored into subsoil. Nails were used to improve soil and form the theoretic soil block. The nails did not have an influence on the bending moment of the “cantilever beam” formed by the A-frame pile raft. The top of the vertical pile and the battered tieback pile was fixed in a pile grille of reinforced concrete and the battered pile was prestressed to reduce deformation at the top of the support of excavation due to skin friction of tieback pile.
Analysis was carried out in several steps:

- Stability analysis – overturning, sliding of the reinforced soil system
- Stress analysis for the tieback piles
- Stress analysis for the nails and shotcrete cover
- Global stability analysis for the whole system, which was carried out according to JANBU with curved slip lines and JANBU with polygonal slip lines.

All steps were carried out using geotechnical software tools by CUBUS AG.

© 2016 Deep Foundations Institute

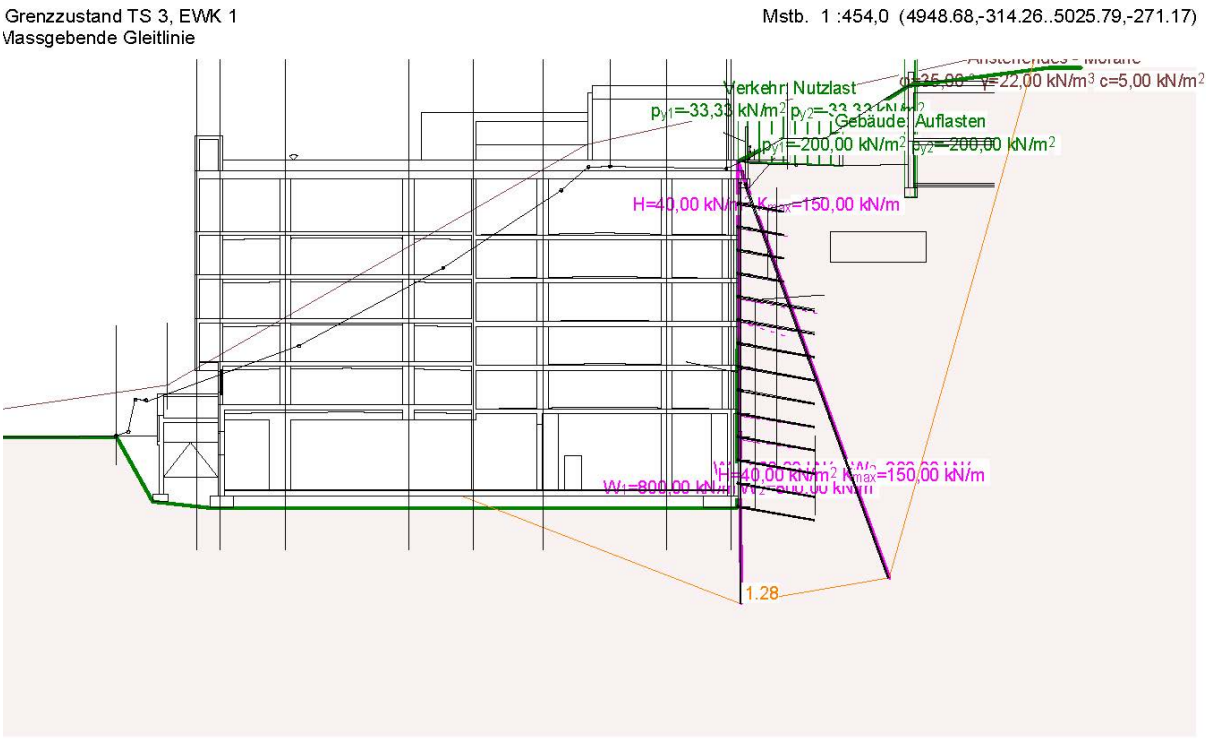


Figure 4 – global stability of 1.28 > 1.00 – JANBU

3.2 Foundation

As compactness was very inhomogeneous across the site a pile foundation – ductile driven iron piles diameter 170 mm, wall thickness of 9 mm including injection were proposed to bring down the high loads – up to 4000 kN beneath the columns without any settlement issues. A shallow foundation would have led to foundation dimensions of approximately 4 by 4 meter and a thickness of 1,20 m without having solved settlement differences due to inhomogeneous compactness.

To use the maximum utilisation factor of the piles a permanent measurement of driving progress during battering brought the necessary information. With these data the length of the piles was determined and fixed on site. The single pile load was fixed to 1200 kN

According to the data gathered on site during battering the length of the piles varied between 6 and 12 m.

The decision for this flexible system helped to increase the working progress by minimizing the excavation amount and also concrete works including reinforcement.

Therefore a close cooperation of our structural design department with the geotechnical department was necessary to obtain an optimized foundation solution.

© 2016 Deep Foundations Institute

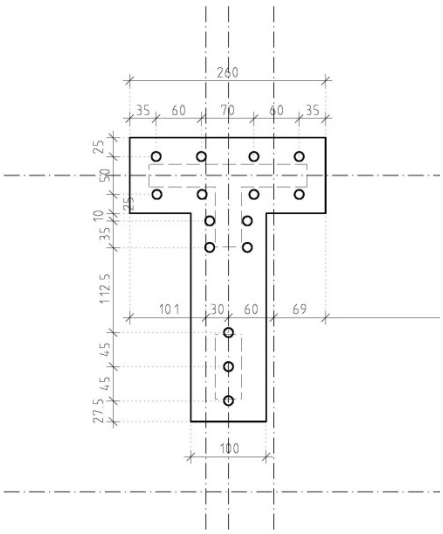


Figure 5 – sample of pile foundation

4. ERECTION PROCESS

A challenge for the contractor was the time schedule which allowed works between begin of May to middle of November each year. A total erection time of 20 months starting in late spring 2013 was planned.

Before starting excavation and support of excavation the village road had to be shifted from the site to provide traffic without disturbance during erection period.

Drilling works for the micropiles and inclined tieback piles started in summer 2013 after site cleaning including relining of waste water line, electricity lines and gas pipeline was finished. The first part of support of excavation area of more than 1600 m² including 2550 m of micropiles and more than 4000 m of soil nails R32-250 was finished by middle of November 2013. After the winter break till May works started again in May 2014 and were continued till late autumn 2014. Meanwhile the client decided to build a new municipality building adjacent to the garage, which increased the length another 40 meters. Support of excavation works for the increased project could be finished by end of July 2015 leaving a total area of more than 4500 m² of support of excavation.

A major problem and challenge were the big bloc which were embedded in the soil matrix not only for the drilling team but also during excavation as they reached into the pit and had to be removed with caution – hydraulic splitting was the best thing we could do, without harming the shot concrete cover.

A tight geodetic survey program – survey points on top and across the wall were checked twice a week – was carried out during excavation works and showed maximum deformations of 45 mm on top close to the old garage building due to bad backfill works – Figure 6 right edge. Deformations of survey point across the wall decreased from top to bottom.

© 2016 Deep Foundations Institute

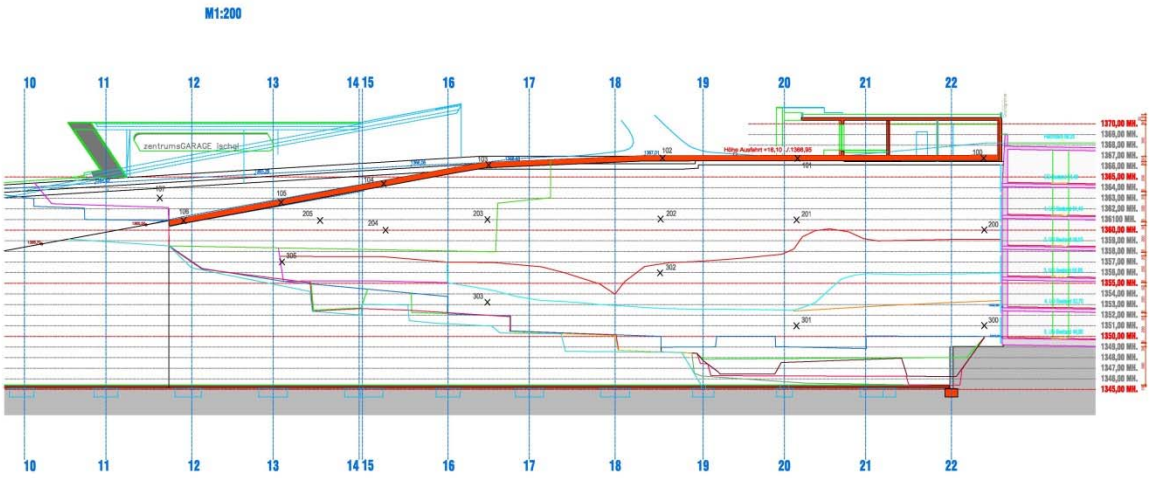


Figure 6 – excavation plan 1 part – survey points

Due to continuous geodetic survey, soil conditions and the local access street just at the edge of the excavation we decided not to use inclinometers.



Figure 7 – site view – drilling of hollow bar through boulders in the wall with air instead of injection

Part of the project was the relining of the district road near the river Trisanna and a roundabout as entrance to the garage and access street to the village.

© 2016 Deep Foundations Institute



Figure 8 – site view in July 2014 – half of support of excavation finished, relining of district road in progress

Support of excavation works in the first section could be finished in June 2014 and pile driving for the foundation started.

© 2016 Deep Foundations Institute



Figure 9 – pile driving works

Concrete works started immediately after pile driving and lying of drainage pipes and waste water lines beneath the floor slab had been finished by mid of July 2014.



Figure 10 – concrete works in July 2014

© 2016 Deep Foundations Institute

In winter 2015 the client decided to build a tunnel as direct entrance to the new built ropeway 10 m south of the garage. Support of excavation had to be adapted and the reinforcement for the tunnel provided.



Figure 11 – tunnel entrance

The support of excavation for the widened project could be finished in July 2015 and concrete works for the garage and the new municipality building were finalized in September 2015.
The garage was opened as planned mid November 2015.

5. SUMMARY

We learned several lessons in that project:

- Total view and integrated design of geotechnics and structural work brings high benefit and cost reduction.
- Sophisticated support of excavation systems combining different methods can be adapted to differing needs of client
- Design has to be adapted flexible to site conditions such as underground conditions, surface, etc. – often very short term work
- Design has to follow the needs of the site – possibilities of transport, drilling, concreting
- Tight survey program accompanying geotechnical work is essential for secure working and success of chosen solution
- Thorough site supervision and close cooperation with assessor discussing the problems in advance reduce design process time

© 2016 Deep Foundations Institute

Two interesting and challenging years for all, who were involved – client, structural and geotechnical designer, contractor – ended under blue sky without any accidents or major problems.

References:

Deutsche Gesellschaft für Geotechnik e.V. 2012 *EA-Pfähle*

Empfehlungen des Arbeitskreises "Pfähle"; Recommendations on Piling, Ernst & Sohn

EN 1990 *Basis of structural design*

EN 1991-*2 Actions on structures – Part 2: Traffic loads on bridges*

EN 1992-2 *Design of concrete structures — Part 2: Concrete bridges — Design And detailing rules (consolidated version)*

EN 1997-1 *Geotechnical design — Part 1: General rules (consolidated version)*

EN 1537 *Execution of special geotechnical work – Ground anchors*

EN 14199 *Execution of special geotechnical works — Micropiles*

FSV – *Austrian Association for Research on Road - Rail - Transport*

© 2016 Deep Foundations Institute

This page left intentionally blank

© 2016 Deep Foundations Institute

JET GROUTED FOUNDATION FOR 57-STORY TOWER

Robert Alperstein, P.E., D.GE, L.M.ASCE, Consultant, RA Consultants LLC, New York, NY, USA 609-918-9614, bob@raccllc.com
Nidal AbiSaab, P.E., M.ASCE, Partner, RA Consultants LLC, New York, NY, USA 646-484-3253, nidal@racllc.com
Joe Pastore, Vice President, Hayward Baker Inc., West Caldwell, NJ, USA, 201-489-1700, JAPastore@haywardbaker.com

ABSTRACT

This paper describes the design and construction aspects of the foundation support for a 57-story building currently under construction in lower Manhattan. The site is located near the East River with subsurface conditions consisting of about 40-ft [12.2-m] of unsuitable historic fill and soft plastic clay underlain by about 130-ft [39.6-m] of dense sand resting on bedrock. A mat foundation supported on unsuitable soils improved by jet grouting was selected for the project. Design concepts and selection of the engineering properties of the improved and natural foundation soils are discussed. The results of quality control testing and methods to verify design parameters during construction are presented.

Keywords: jet grouting, soil improvement, foundations

INTRODUCTION

New York City (especially Manhattan) is known for its skyline of high rise structures. The geologic conditions in the New York Metropolitan Area influence the selection of foundations and feasibility of high rise construction as noted by Horvath (2013). These conditions include varying depth and quality of bedrock, multiple glacial events during the Pleistocene Epoch, and the effects of human modifications to the subsurface environment. Clusters of relatively taller buildings are generally located in Lower and Midtown Manhattan where sound crystalline bedrock is at relatively shallow depth beneath the ground surface and shallow foundations rest on the bedrock surface. In recent years the use of more costly high capacity driven piles or drilled caissons and deep basements has enabled the high skyline to spread to other areas.

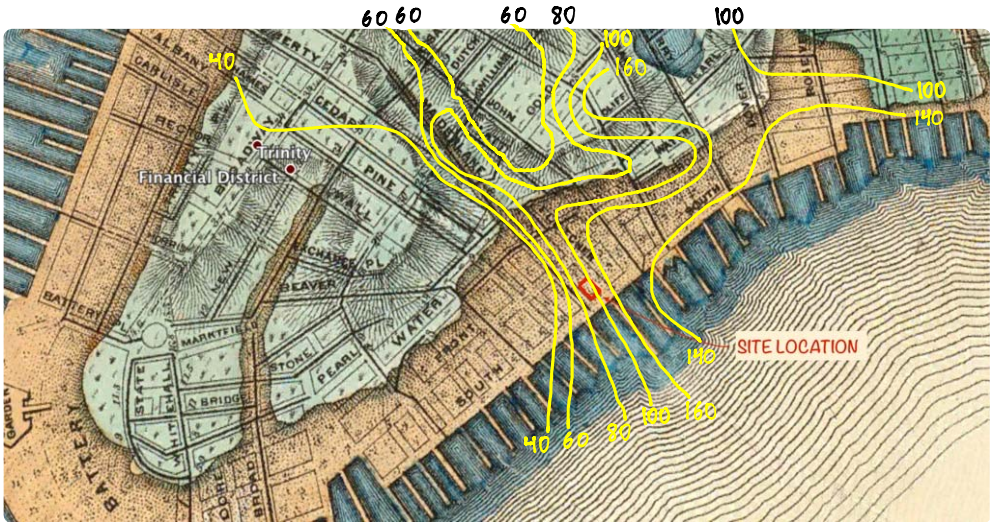


Figure 1

Site Location superimposed on Viele Map (1867) with depth of rock contours in ft based on Baskerville (1994)

The location of the project that is described in this paper is shown in Figure 1. It is on the lower East side of Manhattan near the South Street Seaport in an area of deep rock. Here Pleistocene events caused the

© 2016 Deep Foundations Institute

development of variable and soft natural subsoils, thick deposits of uncontrolled man made fill exist (East of the original Manhattan shore line), and the groundwater is relatively shallow because of the site's proximity to the East River. It might be considered ill-suited to high-rise construction. Nevertheless, a 57- story tower without basement and occupying a relatively small footprint of about 4,835-ft^2 [380-m^2]. was designed and currently is under construction.

SUBSURFACE CONDITIONS

Subsurface Conditions were described in an earlier paper (Alperstein et al, 2013) and are repeated as follows. Figure 2 shows the site location and surrounding properties. The surrounding properties (except for the immediately adjacent vacant property on the western site boundary) are located at least 25-ft [7.6-m] from the site because of streets between the properties, and the structures existing on the properties are known or believed to be pile supported. A lower hi-rise structure (about 30-stories) will be designed by others for construction on the adjacent vacant property shortly after the construction of foundations for the 57-story tower. At this writing we understand that deep drilled piles will be used for the adjacent structure.

Several borings were made or were available on the site and adjacent site. Just before construction began several cone penetration test soundings (CPT) were advanced. Subsurface conditions as interpreted from the boring and CPT logs are illustrated in Figure 3. They generally consist of as much as 28-ft [8.5-m] of uncontrolled Fill. The Fill was comprised of gravel, sand, silt, pieces of concrete, asphalt, steel, bricks, and wood. The fill is largely the result of demolition of previous structures that once occupied the site. Typical N-values were around 20-blows/ft, but much higher values were recorded while penetrating the construction debris. About 10-ft of wood was encountered below the uncontrolled fill in two borings. The wood may have been part of old ship wreckages or buried bulkhead cribbing dating to the 18th Century when this part of Maiden Lane was a dock or ship slip.

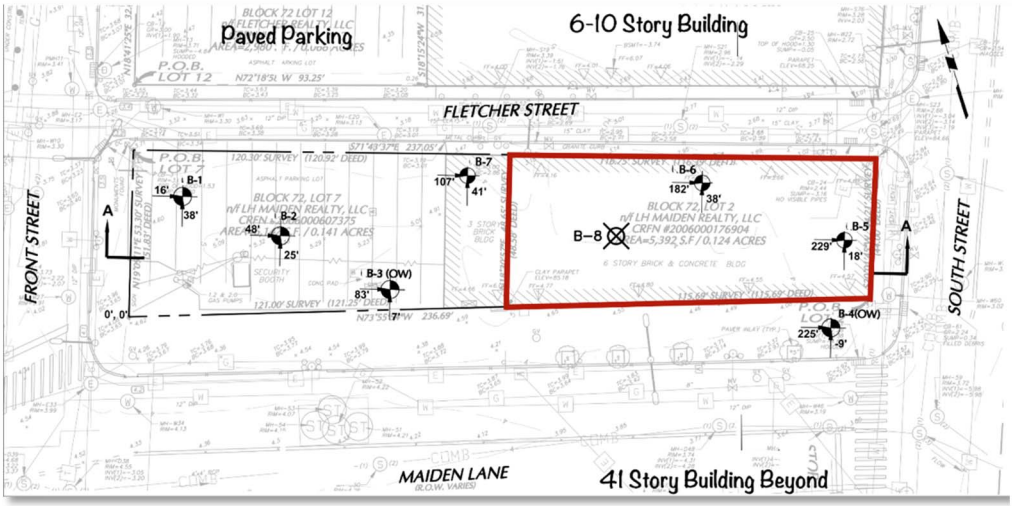


Figure 2

Site Location and Surrounding Properties

Underlying the Fill to a depth of about 35-ft [10.7-m] below grade were about 5- to 14-ft [1.5- to 4.3-m] of compressible deposits of peat, organic silt and organic clay and generally characterized as Organic Clay (OH, per Unified Soil Classification System). N-values varied from Weight of Hammer to about 5-blows/ft indicating a very soft to medium consistency. The Organic Clay most likely was deposited in an estuarine or tidal marsh environment during lower stages of the East River.

The OH deposit was followed by up to 130-ft [39.6-m] of sand deposits (Sand). The sands, generally poorly graded (SP and SP-SM) are believed to be glacial outwash as they sometimes contain thin silt or

© 2016 Deep Foundations Institute

clay lenses. Typically, the Sand is dense to very dense with N-values usually exceeding 30-blows/ft. However, occasionally lower N-values were encountered near the upper Sand surface. About 55-ft [16.8-m] below ground surface the Sand becomes more silty (typically SP-SM or SM) and denser with N-values mostly above 50-blows/ft. We believe that at the lower depths the Sand stratum probably is a till deposited by advancing and retreating glaciers some 12,000-14,000 years ago. The bottom of the till varied from about 129- to 162-ft [39.3- to 49.4-m] below ground surface.

Sporadically, up to about 25-ft [7.6-m] of Decomposed Rock was encountered below the Sand. N-values in the Decomposed Rock were very high (exceeding 100-blows/ft) and when the stratum was cored with an NX core barrel very little recovery and zero RQD was obtained. Bedrock consisting of hard mica schist with quartz was encountered at depths varying from about 132-to 166-ft [40.2- to 50.6-m] below ground surface. Core recovery and RQD were 100 percent or slightly lower.

Groundwater was encountered about 5- to 8-ft [1.5- to 2.4-m] below ground surface and appeared to be tidally influenced.

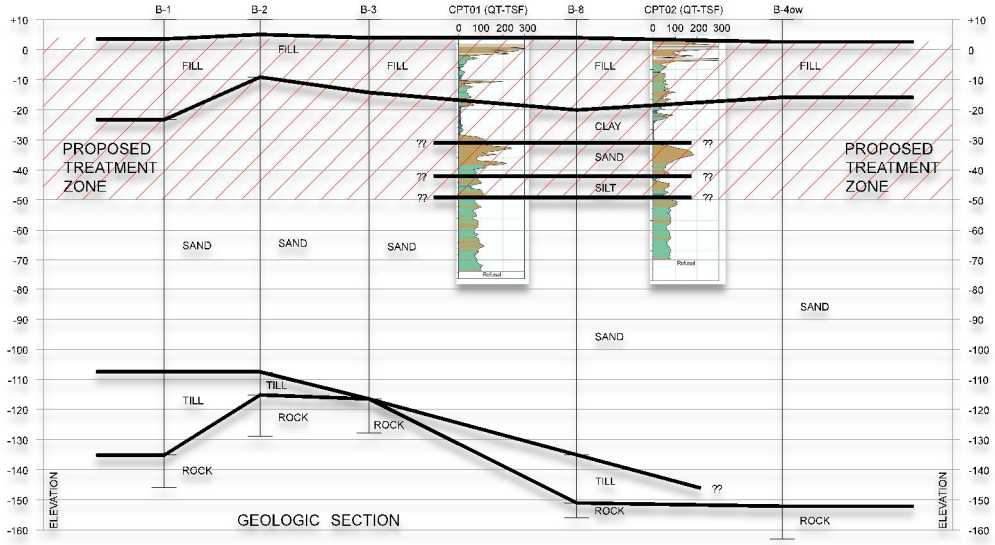


Figure 3

Geologic Section

FOUNDATION SELECTION AND DESIGN

The proposed 57-story structure would have an average footprint area load greater than 5-tons/ft^2 [0.48-MPa]. We judged the highly variable uncontrolled Fill and the variable and highly compressible Organic Clay strata as incapable of supporting the proposed structure without excessive settlements or bearing capacity failure. The Owner had no need for a deep basement bypassing the unsuitable strata and wanted to avoid dewatering. Therefore deep foundations consisting of either caissons drilled into the bedrock, drilled piles into the dense Sand, or high capacity piles driven into the dense Sand seemed appropriate.

Preliminary designs were developed for the three options. These included various diameter caissons with design capacities in the order of 4,000-kips [17,793-KN], drilled piles with design capacities of about 200-kips, and driven Taper Tube piles with capacities around 500-kips [2,224-KN]. These designs were discussed with several local contractors. Because of the caisson depths and possibly other risk factors the contractors were reluctant to bid on the drilled caissons design. The result was extremely high price quotes that were substantially above the Owner's budget.

© 2016 Deep Foundations Institute

The lower capacity deep foundation options (drilled or driven piles) also were expensive, but more importantly would occupy so much footprint area as to be impractical. Therefore, the foundation selection was re-evaluated.

During the re-evaluation we re-visited the deep basement option. The Owner reiterated its lack of interest in a basement and concerns about dewatering. Further, the cost and difficulty of transferring the structural loads to the basement mat was a negative factor. However, the concept developed of transferring the foundation loads to the competent sand strata by substantially improving the Fill and Organic Clay strata. Considering the height of the proposed structure, the nature and thickness of the Fill this was an innovative approach to a difficult foundation situation. Because of the high foundation loads, especially constant gravity and transient wind, the need for a relatively incompressible and well controlled improved soil became apparent.

Potential settlements/uplift due to wind loads are addressed through installation of pre-stressed rock anchors. They consist of steel casing with internal reinforcing threadbars socketed into rock. The rock anchors were divided into two groups. One group was locked against the steel casing under the mat foundation. The other group will be locked on top of the mat foundation (within pockets) and re-locked once the building reaches 75% height.

Preliminary discussions with the specialty foundation contractor (Hayward Baker Inc. (HBI)) suggested that a cost savings (compared to deep foundation elements) of several million dollars could be realized by utilizing jet grouting for ground improvement with a 10-ft [3-m] thick structural mat foundation supported on the improved soil. Jet grouting improves the existing soils by mixing them in place with cement grout. The grout is pumped under high pressure through a pipe with nozzles that is inserted into the soil to the desired depth of improvement. The pipe is rotated as it is removed from the ground and the grout flows under pressure through the nozzles forming high velocity jet streams that erode the soils and mix them with the grout. The resulting cured improved ground is a "soilcrete™" having unconfined compressive strengths in the range of 350- to 1,000-lbs/in^2 [2.4- to 6.9-MPa]. The range in unconfined strength was estimated by HBI based on their experience and the geotechnical characterization of the Fill and Organic Clay strata.

We established the acceptability of the proposed design by estimating the potential settlements of the proposed structure and foundation system using finite element method (FEM) of analysis (Alperstein, et al, 2013). We assumed that the site would be contained by tangent or secant piles also constructed by the jet grouting method. Generally, the estimated potential settlements ranged from about 2- to 3-inches [5.1- to 7.6-cm] due to dead and live loads. Since the dead loads comprised about 88 per cent of the service loads and the subsoils are mostly granular most of the potential settlements are expected during construction. Consequently, these settlements can be accommodated during the construction process.

Uncertainties always exist when evaluating the probable performance of foundations. For this project the major uncertainties were in the estimated engineering properties of the foundation materials that were input to the FEM analyses and the effects of obstructions on construction (discussed later). Probable engineering properties of the soilcrete™ were estimated based on HBI's several decades of experience with jet grouting. That experience includes properties as determined on samples collected from production work and from lab prepared samples. The lab prepared samples were composed of site soils mixed with grout in proportions to those expected to be achieved when jet grouting.

Typically, jet grouting has been used for structural support and reduction of water flow. Therefore, unconfined compressive strength (UCS) and permeability are most often tracked. The properties of

© 2016 Deep Foundations Institute

soilcrete™ created with soil mixing techniques also have been collected. This project is unique in that the modulus of elasticity of the soilcrete™ is a critical parameter in the design.

HBI's experience regarding modulus generally indicated that it could be estimated as about 200 to 400 times UCS (both in same units). The estimated values of Young's modulus for design purposes are shown in Table 1.

We estimated the engineering properties of the natural subsoils based on our experience and evaluation of N-values shown on the boring logs. The estimated properties are summarized below. At inception of construction several cone penetration soundings were conducted, with results shown in Figure 3.

Table 1 Design Values of Young's Modulus

Material	**Young's Modulus lbs/in^2 [MPa]**	**UCS lbs/in^2 [MPa]**
soilcrete™ (Fill)	69,444 – 152,780 [479] – [1,053]	300 – 600 [2.1] – [4.1]
soilcrete™ (Clay)	40,250 – 100,700 [278] – [694]	200– 500 [1.4] – [3.4]
soilcrete™ (Sand)	118,055 – 298,600 [814] – [2,059]	400 – 1,000 [2.8] – [6.9]
Natural Sand	6,950 – 13,890 [48] – [96]	N/A

Assuming that Young's modulus can be represented as 2 times the cone penetration resistance (Schmertmann 1970) generally confirmed the design properties as reasonable based on N-values for the natural Sand below the proposed improvement (treatment) zone.

SOIL IMPROVEMENT DURING CONSTRUCTION

The grouting operations were conducted in three phases:

- First Phase: Field Testing
- Second Phase: Production Grouting of all planned improvement columns
- Third Phase: Verification of grouting sufficiency and additional improvement

HBI mobilized a grout batching plant consisting of one silo, augers, calibrated load cells, agitator tank, jet valve mixer and a high pressure pump capable of generating pressures up to 5,000-lbs/in^2 [34.5-MPa]. The thoroughly mixed grout was pumped under pressures of up to 4,500-lbs/in^2 [31.0-MPa] to the grouting drill rig. Grout flow rates and pressures, rotation rates, and withdrawal rates were recorded and displayed by a Data Acquisition System at the rig providing the rig operator with real-time information to control and modify grouting operations. During grouting the specific gravity of the grout was tested approximately every 20 minutes.

A second drilling rig was available for pre-drilling through anticipated obstructions in the fill layer.

First Phase: Field Testing

A field testing program was initiated to establish the appropriate drilling parameters to achieve the required design conditions. Proposed production grouting locations were planned as shown in Figure 5. Three column sets (two columns each) were evaluated in the perimeter and three column sets (three

© 2016 Deep Foundations Institute

columns each) were evaluated in the intended mat foundation area. Specific gravity, jet grouting rotation rate (RPM), Jet grouting head withdrawal speed (cm/min) were varied in the six sets, but were maintained constant for the full depth of the profile. Typically, the specific gravity ranged from about 1.45 to 1.6; the withdrawal speed ranged from 10- to 40-cm/min; and the rotation rate ranged from 3- to 15- RPM.

Two grout sample types were collected from the various grout columns:

1. Samples from the spoils pile generated during grouting.
2. Samples from a drill hole using a custom sampler (Figure 4) attached to the grouting rods on the drilling rig.

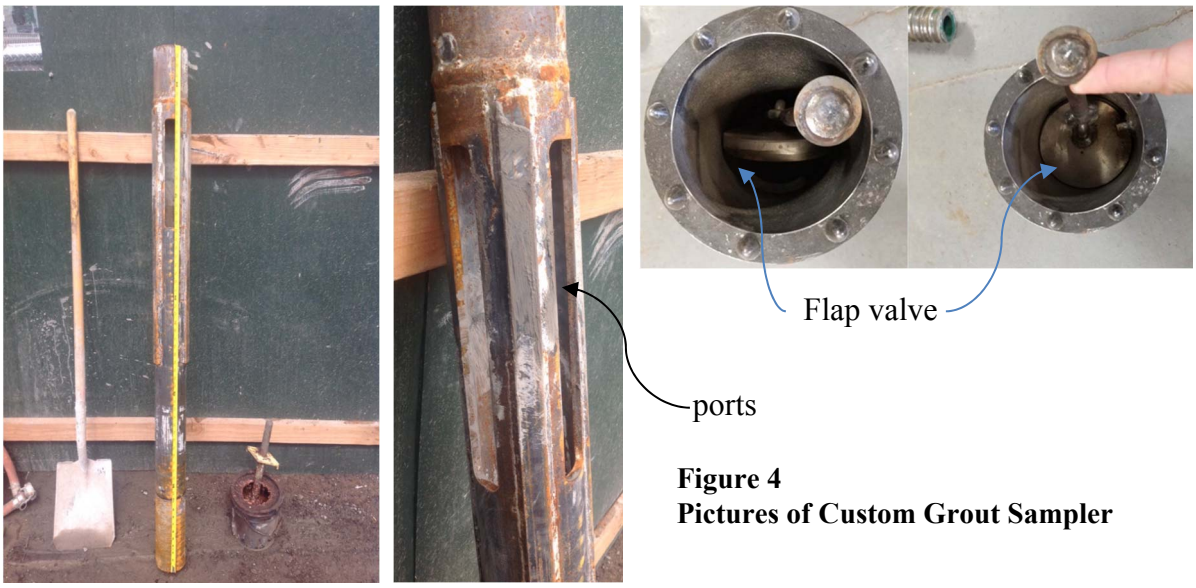


Figure 4
Pictures of Custom Grout Sampler

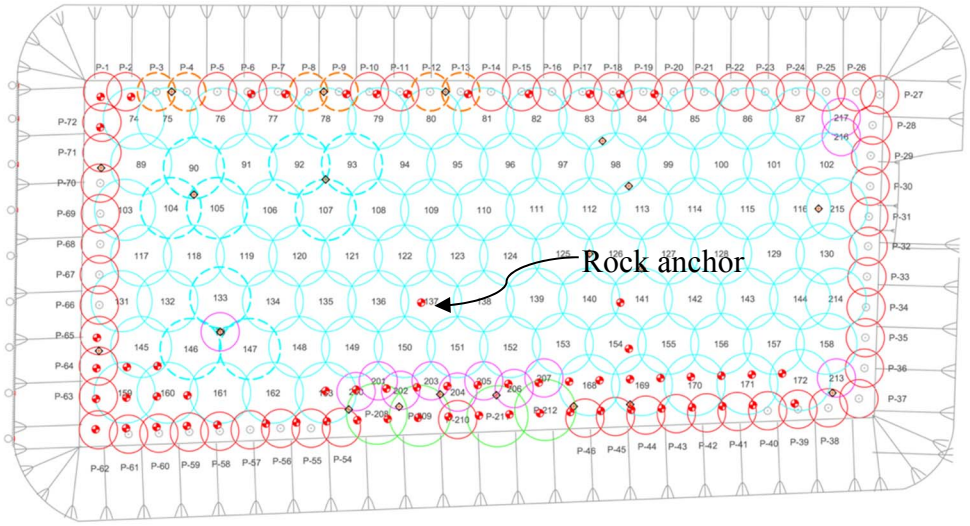


Figure 5
Grouting Plan Showing grout columns

Legend
5-ft diam.
8-ft diam.
5-ft diam.
8-ft diam.

Samples were obtained at approximate depths of 5, 9 and 15 meters below ground surface (bgs) covering the three generalized strata in the grouting treatment zones (Fill, Clay and Sand). The samples were tested in the laboratory for UCS. The sampler has a flap valve or gate at the bottom allowing grout to enter it

© 2016 Deep Foundations Institute

and flow out the side ports as the sampler is pushed to the desired level. When the sampler is pulled up for removal the gate closes trapping the grout in the sampler below the ports and above the gate.

Core drilling was used to evaluate the general extent and distribution of the jetted grout in the ground. Coring was done with a wireline double tube core barrel at 10 locations. The ten core borings were completed to a depth of approximately one foot above the bottom of the grouted region. Several core samples were tested for UCS.

The need for pre-drilling became apparent as obstructions (mainly wood, concrete, steel, bricks, shells and other debris) in the fill layer hindered the drilling and grouting operations.

The field test data were evaluated with respect to desired compressive strength and Young's modulus as determined in the design phase, ability to obtain the desired column diameter with distribution of the grout and possible influence of obstructions. Young's modulus was calculated from the laboratory UCS results. The calculations indicated that modulus is related to the UCS as follows:

Table 2 Lab Results (First Phase, Field Testing): Young's Modulus / UCS

Material	Average Young's Modulus E at 28-days lbs/in^2 [MPa]	Average UCS at 28-days lbs/in^2 [MPa]	Ratio E/UCS
soilcrete™ (Fill)	290,000 [2,000]	675 [4.6]	429
soilcrete™ (Clay)	191,000 [1,300]	470 [3.2]	407
soilcrete™ (Sand)	365,000 [2,500]	620 [4.3]	588

Comparing the Young's modulus shown in Table 2 to those in Table 1 indicates that the design conditions were achieved. However, except for the Sand stratum the *insitu* ratio of E/UCS was lower than those used for obtaining design values of E, mainly because the achieved values of UCS were higher than expected. The test results (Figure 6) at varying curing times suggest that although UCS increases with time the modulus is essentially unchanged but has large variations.

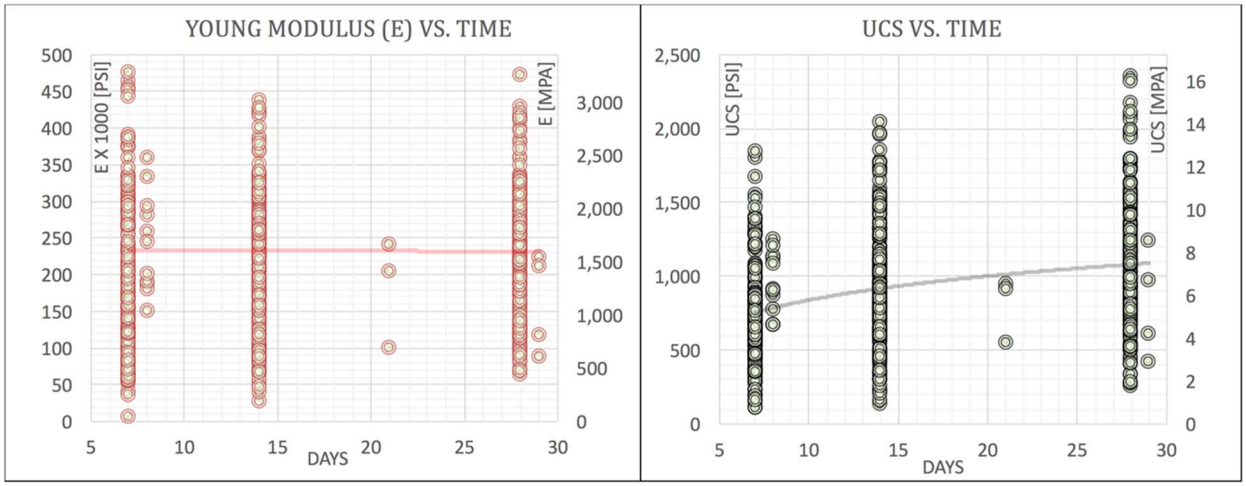


Figure 6: Laboratory Test Results (Test Program and Production Piles)

Evaluation of the field testing indicated that during production grouting:

- Grout should have a specific gravity of 1.56 to maintain desired grout strength.

© 2016 Deep Foundations Institute

- Perimeter columns could be installed with withdrawal and rotation speeds such that 4-ft [1.22-m] center to center grout column spacing would result in 5-ft [1.52-m] influence diameters.
- Mat columns could be installed with withdrawal and rotation speeds such that 7-ft [2.13-m] center to center grout column spacing would result in in 8-ft [2.44-m] influence diameters.
- Drill hole samples would be used for UCS quality control testing purposes since test results on spoil samples were unrepresentative and could not be relied upon. All presented samples in this paper are from the in-situ sampler. The spoil samples were unrepresentative likely due to the sampling technique and the mixing of soilcrete with water and other impurities at the ground surface.
- Further verification coring should be conducted after grouting operations are completed.

Second Phase: Production Grouting

Production grouting was accomplished in two stages with two rigs, as necessary:

1. Predrilling through the fill layer with the first rig at grout column locations with an 8-in [20.3-cm] diameter bit down-the-hole pneumatic hammer. Air was the primary flush with water added to the line to suppress dust.

2. Continuing drilling through the clay and sand layers to the specified elevation with the grouting rig (second rig) using a nominal 6-in diameter tricone roller bit with water flush and jet grouting proceeding from the bottom up. Occasionally grout was used as the drill fluid. The grout flush was used only if wet-to-wet columns were installed on the same day or if difficulty was being encountered lifting drill spoils from the bottom of the hole with water flush. One hundred seventy eight (178) columns were jet grouted.

Quality Control

Laboratory UCS tests were conducted on samples collected from at least one of two columns grouted per day, or as deemed necessary.

The grout quality was monitored by collecting samples from holes drilled in the fresh grout with the drilling rig. Samples were obtained with the custom built sampler at approximately 5, 9, and 15 meters bgs. Also, the specific gravity of the grout was tested approximately every 20 minutes. Necessary adjustments were made to the water-cement mix to maintain a specific gravity of 1.56.

Laboratory UCS results and Young's Modulus during production grouting are summarized in Table 3.

Table 3 - Laboratory 28-Day Test Results (Second Phase, Production Grouting)

Stratum	Design Compressive Strength lbs/in^2 [MPa]	Minimum Compressive Strength lbs/in^2 [MPa]	Average - 1 Std. Deviation lbs/in^2 [MPa]	Average Compressive Strength lbs/in^2 [MPa]	Average Young's Modulus E at 28-days lbs/in^2 [MPa]	Ratio of E/UCS
Fill	300 – 600 [2.1] – [4.1]	273 [1.9]	586 [4.0]	1,002 [6.9]	212,000 [1,500]	211
Clay	200 – 500 [1.4] – [3.4]	286 [2.0]	699 [4.8]	1,121 [7.7]	234,000 [1,600]	209
Sand	400 – 1,000 [2.8] – [6.9]	494 [3.4]	755 [5.2]	1,183 [8.1]	252,000 [1,750]	213

© 2016 Deep Foundations Institute

At several locations the hole collapsed during the sampling process limiting the number of collected samples. Corrective actions consisting of additional grout columns and/or testing were developed when insufficient samples were obtained.

The laboratory test results indicate that the jet grouted strata achieved the compressive strengths generally higher than design values. Further, the laboratory values of Young's modulus were somewhat higher than the design values. The modulus to strength ratio (E/UCS) was closer to the lower design ratio, whereas in Phase 1 it was closer to the higher design ratio. We suspect that the significantly larger number of test samples in Phase 2 than in Phase 1 contribute to these variations. Our design estimates were prudently based mainly on the lower design ratio range.

Third Phase: Verification of grouting sufficiency and additional Improvement

A second coring round (9 additional locations) was implemented at the end of the second phase to verify the grout efficiency and distribution.

After evaluating the results of the 9 cores, 5 cores were added to verify the grout in two identified critical areas.

Evaluation of the results of the verification coring indicated that additional grouting and other remedial actions should be undertaken in two identified potential weak zones. In our judgment the "potential weak zones" were caused by interference effects of obstructions in the Fill. This had been our concern from the start of the project and a remedial action program was available for implementation. The program consisted of additional grouting to strengthen the soilcrete in the mat areas to a depth of 70 ft (21.3-m) below ground surface (grouting from -70 to -48 feet (21.3- to 14.6-m)) and locally structurally bypassing the Fill layer.

Twelve locations were identified requiring grout strengthening below the original design bottom of grout (53-ft. bgs, 16.2-m bgs) and installation of a bypass device. The bypass device consisted of a 9 5/8 –in outside diameter steel pipe (filled with concrete having a strength of 5,000-lbs/in^2, 34.5-MPa from ground surface to a depth of 30-ft (9.1-m) bgs (bypassing the Fill) and with #8 reinforcing bar extending to 50-ft. (15.2-m) depth bgs. Two locations were identified requiring the bypass device without additional grouting.

Grouting is completed and the structure is under construction. Settlements at the top and bottom of the jet grout layer are being monitored allowing an evaluation of performance of the jet grouted foundation and the underlying natural Sand. If necessary, structural adjustments will be made to accommodate settlements.

CONCLUSIONS

We conclude that:

1. High rise structures can be founded on deep dense soil deposits with due consideration of potential settlements.
2. Poor near surface foundation soil conditions can be improved with jet grouting. The properties of the improved soils must be considered in the foundation design and consideration of potential settlements.

© 2016 Deep Foundations Institute

3. The elastic modulus of the soilcrete™ is related to the UCS. The relationship should be determined for the site specific soil conditions.
4. Field testing is required to establish production grouting parameters that will result in the desired ground improvement.
5. Quality control procedures are necessary to assure that design conditions have been achieved. For the subject project UCS testing of drill samples, specific gravity testing of grout, and core drilling after grouting were effective quality control procedures.
6. Corrective actions may be required after reviewing quality control test results.

ACKNOWLEDGEMENTS

The authors thank the Fortis Property Group, especially Mr. Akiva Kobre, Senior Vice President, Development, for permission to present this paper. We also thank and acknowledge the project's structural engineer, WSP Cantor Seinuk; Messrs. Jeffrey Smilow, P.E. and Patrick Chan, P.E. in particular.

REFERENCES

ALPERSTEIN, R, N. AbiSaab, J. Pastore, and R. Guo 2013 "52-Story Tower with Jet Grouted Foundation Bearing on Sand" American Society of Civil Engineers, ASCE, Metropolitan Section, Annual Seminar.

BASKERVILLE, C.A. 1994 Bedrock and engineering geologic maps of New York County and parts of Kings and Queens Counties, New York, and parts of Bergen and Hudson Counties, New Jersey. U.S. Geological Survey, U.SD. Department of the Interior.

HORVATH, J. S. 2013 "Foundation challenges in the New York City metropolitan area caused by nature, humans, and their interaction**"** American Society of Civil Engineers, ASCE, Metropolitan Section, Annual Seminar.

SCHMERTMANN, J. H. 1970 Static cone to compute static settlements over sand. American Society of Civil Engineers, ASCE Journal of the Soil Mechanics and Foundations Division, Vol. 96, No. SM3, pp 711-731

VIELE, E.I. 1867. Sanitary topographic map of the City and Island of New York

© 2016 Deep Foundations Institute

KOSCIUSZKO BRIDGE MAIN PYLON DEEP FOUNDATION SOLUTION

Coleman, D, Underpinning and Foundation Skanska, Maspeth, New York, USA,
david.coleman@skanska.com
Daugiala, A, Underpinning and Foundation Skanska, Maspeth, New York, USA,
alfredas.daugiala@skanska.com

ABSTRACT

In 2014 the New York State Department of Transportation (NYSDOT) awarded a Design-Build contract to the joint venture team consisting of Skanska which is the managing partner; Kiewit Corporation and Ecco III (SKE) and HNTB as the lead design firm. The design build team employed methods to provide schedule savings and commercial benefits to the owner NYSDOT. This paper presents the design approach and construction methods used to accelerate drilled shaft installation supporting the main span foundation for the cable stayed bridge. The drilled foundation contractor Underpinning and Foundation Skanska, a division of Skanska was responsible for assisting with design, budgeting and construction of the drilled shaft foundation construction. As part of the Request for Proposal (RFP) bid process, Alternate Technical Concepts (ATC) was encouraged by the NYSDOT. The JV team proposed an ATC which involved a scaled production shaft testing method to simulate the ultimate load level, commonly referred to as the "Chicago Method" was used in the rock socket employing the Osterberg Cell (O-Cell) testing procedures. To the authors knowledge this was the first NYSDOT project where this approach was utilized on a Demonstration/Production installation to validate construction procedures and load bearing capacities. Construction procedures, challenges and solutions are discussed in detail. Upon completion of successful drilled shaft construction, concrete integrity is verified using two methods – Cross Hole Sonic Logging (CSL) and Thermal Integrity Profiling (TIP). A comparison from the contractor's perspective is provided. Finally the drilled shaft rock socket is tested to ultimate end bearing values while rock socket side shear stresses are not exceeding the service level loading. Lateral load test was also a RFP requirement; the test arrangement and performance are discussed in detail as well. The Kosciuszko Bridge location poised unique geotechnical challenges on many levels shifting towards an extreme boundary of parameters encountered in New York City Area for drilled shaft construction. The JV team and specialty drilled shaft contractor actively participating in the shaft design and construction practice coordination and working with NYSDOT yielded a successful foundation solution which provided cost and schedule savings to the project.

Keywords: deep foundation, drilled shafts, rock socket, rock drilling, O-Cell test

INTRODUCTION

The Kosciuszko Bridge Replacement involves a cable-stayed structure that will span the Newtown Creek replacing the existing Kosciuszko Bridge on Interstate I -278 which is locally known as the Brooklyn-Queens Expressway or BQE. A site location map is provided in Figure 1. The bridge connects the boroughs of Brooklyn and Queens, New York. The new bridge is being constructed in two phases. Phase 1 construction (Design/Build) involves construction of Queens/Brooklyn or eastbound bridge constructed adjacent to the existing bridge. The existing eastbound structure will then be demolished and all traffic will be shifted to the new bridge. The new bridge is expected to open sometime in 2017. Then in Phase 2 construction (Design/Bid/Build) for the westbound bridge will be bid and constructed in a future contract. An illustration, Figure 2 provides a depiction of the new bridge constructed in Phase 1. This paper provides a summary of the design and construction of the drilled shaft foundations to support the main pylon towers.

© 2016 Deep Foundations Institute

The new bridge will have a total span length of approximately 1.1 miles. The bridge deck rises to a height of 90 feet (27.4 meters) above the navigational channel of Newtown Creek. The main span pylon for Phase 1 construction is located on the Brooklyn side near the Newtown Creek. The pylon towers supporting the bridge deck will rise to a height of 289 feet (88.1 meters).

The main pylon for the bridge is supported on large diameter drilled shaft foundations drilled through approximately 160 feet (49 meters) of overburden with rock sockets embedded into Gneiss/Schist bedrock.

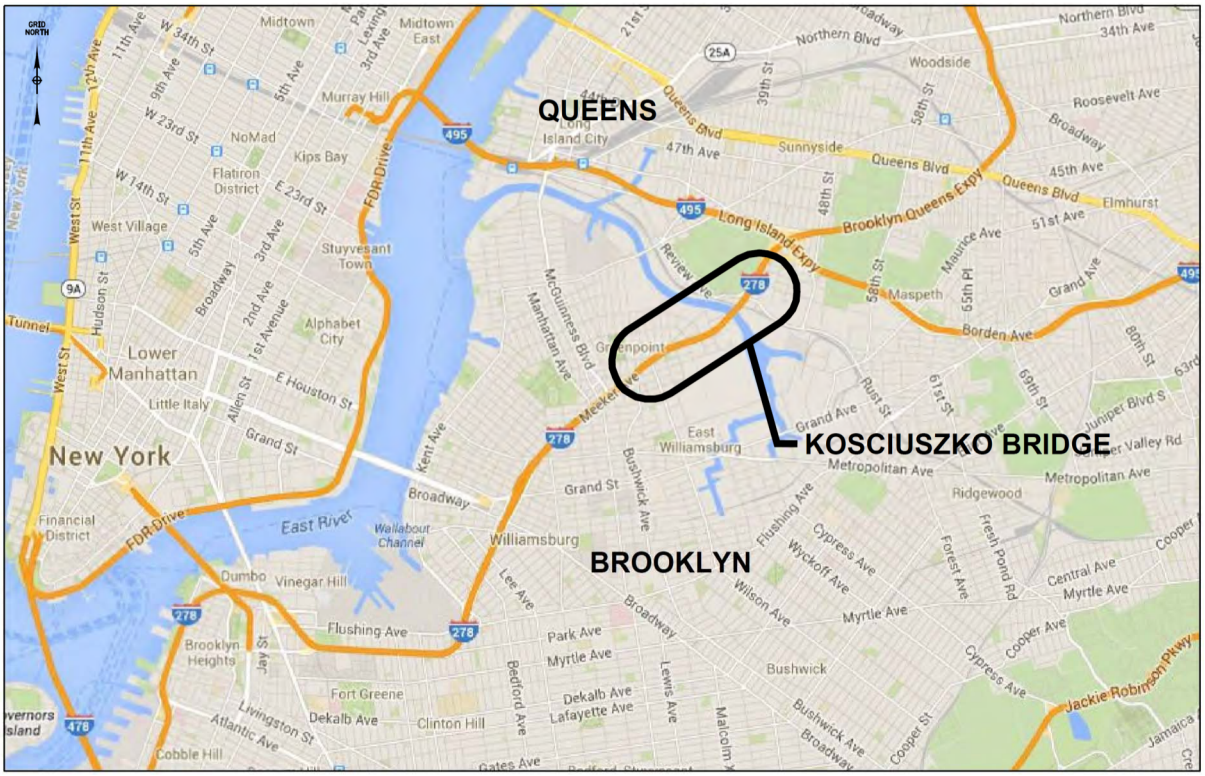


Fig 1. Site Location Map (Reference: Google Maps)

SUBSURFACE PROFILE

The subsurface conditions at Kosciusko Bridge main span pylon location consists of six major strata as identified and profiled by Haley and Aldrich:

- Stratum 1 – Fill (mixture of silt, sand, gravel and cobbles, brick fragments and wood)
- Stratum 2 – Organic Deposits (organic silt and clay localized within the Newtown Creek floodplain)
- Stratum 3 – Silty Sand (silty sand glacial deposits with layers of silty clay and clayey silt)
- Stratum 4 – Silty Clay (Raritan formation consisting of clay and silt mixtures with occasional silt and fine sand lenses and/ or gravel)
- Stratum 5 – Decomposed Rock (fine sandy and/ or gravelly silts and clays)
- Stratum 6 – Bedrock (Primarily Gneiss along with Schist and Marble generally Class II Good Rock)

© 2016 Deep Foundations Institute

The noted strata were developed based on three borings provided for the North and South pylon foundations by NYSDOT. The site geology profile was augmented by an additional five borings installed post-award by SKE. This strata profile with plan location for pre-award and post-award bores is detailed in Figure 3 and 4. SKE installed additional soil/rock borings to provide supplemental information for the Demonstration/Load Test shaft location and to verify top of rock due to concerns of a sloping rock condition. The profile consists of overburden soils to a depth of 160 feet (48.8 meters) below ground surface (BGS), where a layer of decomposed rock is encountered above the Gneiss/Schist bedrock. The water table is approximately 15 feet (4.6 meters) BGS. The rock dips in a northerly direction at 5 - 9 %. The rock is characterized as follows:

- Gneiss / Schist
- Brownish black & Very light gray to very dusky red
- Fine grained to coarse grained
- Moderately fractured to slightly fractured
- Very hard to Extremely hard
- Unconfined compressive rock strengths as high as 23,560 psi (162 MPa) , or an average compressive strength of 16,500 psi (114 MPa).
- Rock Quality Designation (RQD) averaged 82% and Rock Recovery Designation averaged 95%

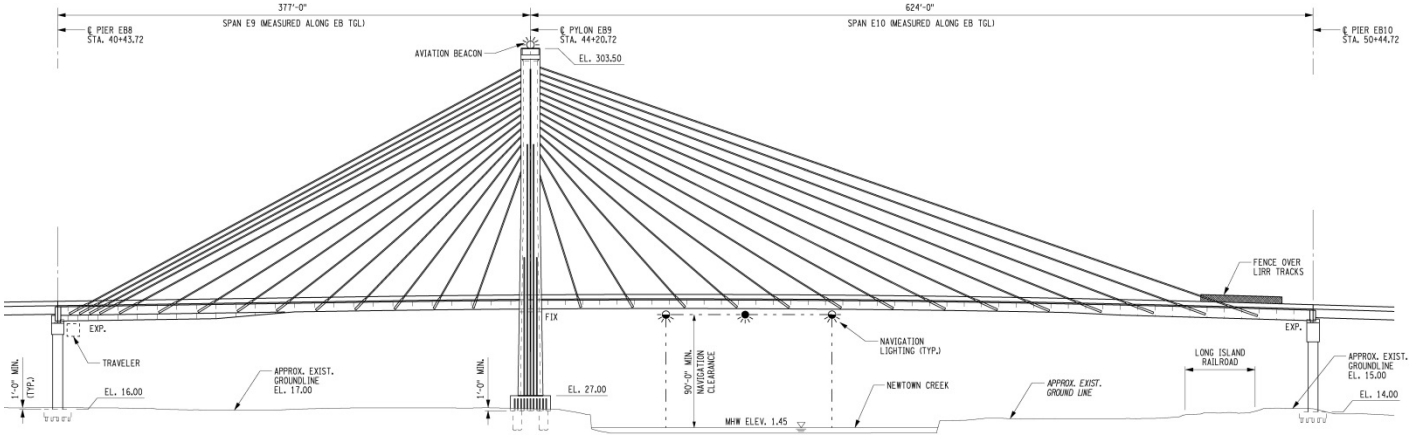


Fig 2. New Bridge Phase 1 – Elevation view

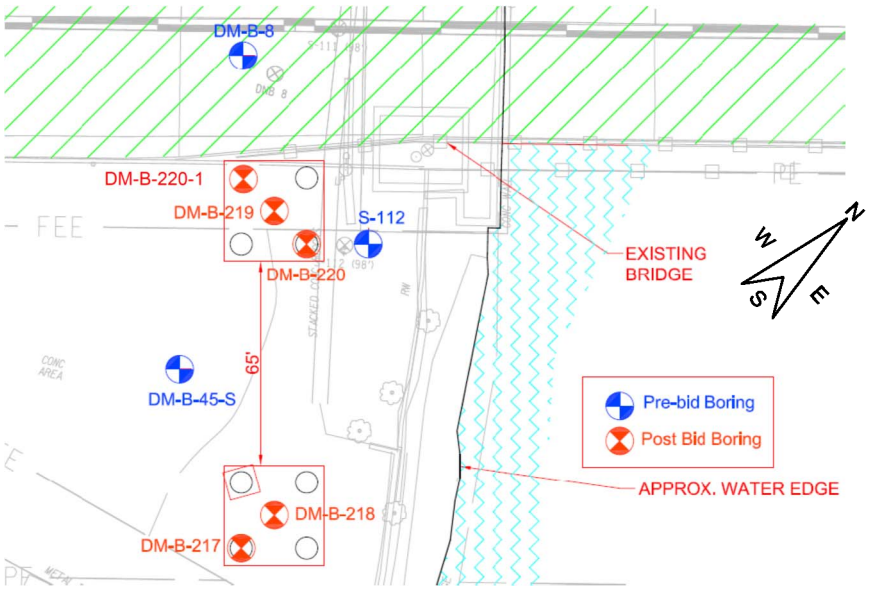


Fig 3. Phase I Bridge Pylon Shafts and Borings – Plan View

© 2016 Deep Foundations Institute

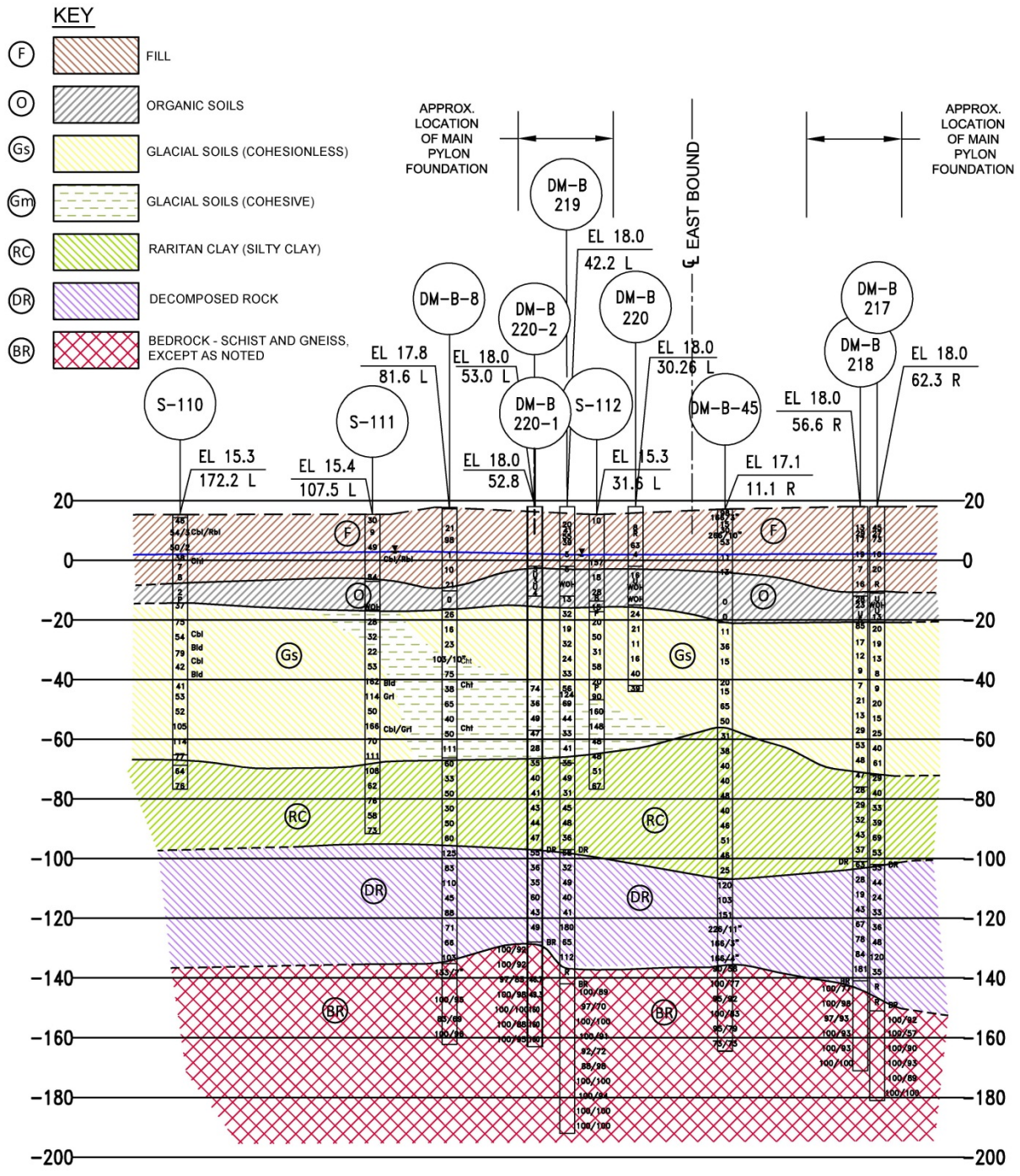


Fig 4. Soil Profile at Main Pylon Foundation (Vertical datum NAVD 88. Ref: Haley & Aldrich, Geotech. Design Memorandum[8])

DRILLED SHAFT CONSTRUCTION

The main span pylon foundation consisted of two heavily reinforced footings that measured 32 by 32 feet (9.8 by 9.8 meters) and 12 feet (3.7 meters) thick, supported by two groups of four each drilled shafts for each leg of the pylon. Refer to Figure 3 for foundation layout schematics. Drilled shafts were constructed

© 2016 Deep Foundations Institute

with a temporary oversized top casing which was required by the RFP. This oversized top casing requirement was necessary to isolate contaminated soil and groundwater consisting of Tetrachloroethylene and Trichloroethene contaminates located in the upper overburden Fills above the organic silty/clay strata. A Temporary top casing was installed at 9 feet (2.7 meters) diameter and a secondary casing at 8.5 feet (2.6 meters) diameter into the silty clay to obtain a casing seal. Temporary casings were installed with a vibratory hammer or by twisting into place with the drill Kelly bar and a casing twister tool to depths of 10 and up to 43 feet (3 up to 13 meters) BGS. Environmental concerns required the isolation and removal of the contaminated soil and water to avoid any contamination leakage migration outside the identified hot zones. The soils from the contaminated zone was removed from the site and disposed of at an off-site disposal facility. Water was treated on site in a SKE provided treatment facility and disposed of on site. Drilled shaft excavation continued at 8 feet (2.4 meters) diameter open shaft to a depth ranging from 160 to 170 feet (49 to 52 meters) BGS utilizing polymer drill slurry to maintain borehole stability to top of bedrock. The sloping rock was leveled prior to setting the permanent casings. The shaft was excavated with a combination of tools involving earth/rock augers and digging buckets. Permanent casings at 84 inches diameter by 5/8 inches wall thickness (2133.6 mm x 15.9 mm) was installed in two or three piece lengths varying from 45 to 80 feet (14 to 24 meters) in length and were spliced together using a complete joint penetration weld (CJP) on location at the shaft and lowered to top of rock. The casing was then screwed and advanced into the Gneiss/Schist bedrock to obtain a seal. Due to rock hardness, having an average compressive strength of 16,500 psi (114 MPa) and a severe sloping condition of 40% to 50% across the shaft area a grout plug was placed in the rock socket and several feet into the casing to facilitate a casing seal.

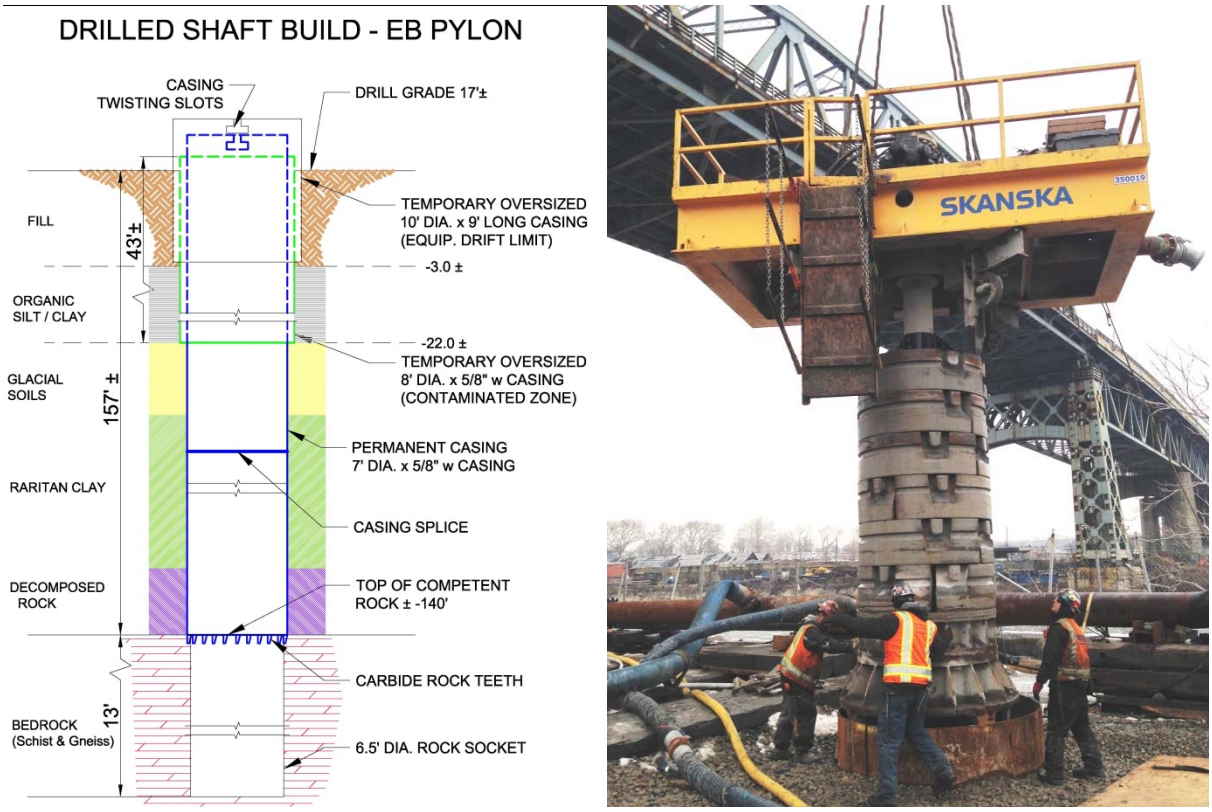


Fig 5. Shaft Built Schematics and Reverse Circulation Drill (for rock socket drilling) - RCD

© 2016 Deep Foundations Institute

The severe sloping rock condition was not a known condition at time of bid, as SKE was anticipating a 5% to 9% condition. This situation was of grave concern to the SKE team as this condition may prevent the advancement of the casing, seating and ultimately a seal to allow the successful operation of the Reverse Circulation Drill (RCD) excavation method selected for rock socket excavation. This will be discussed in more detail in the Construction Challenges and Solutions section of this paper. During shaft excavation and upon completion of overburden drilling, shaft verticality was monitored with the Sonicaliper device to determine how much the shaft was deviating out of the plumb position and to determine if corrective action would be required prior to permanent casing placement. This was important as there was concern if the shaft was drilled out of plumb it may not be possible to set casings on location and in compliance with the verticality requirements of 2% of shaft length. If the shaft was on location, plumb and the permanent casing sealed into bedrock the 6 inch (152 mm) casing annulus was grouted to grade with a 200 psi (1.4 MPa) grout in two stages. A two stage grout placement was required due to concern of casing collapse due to outside and inside pressure differential[1].

The temporary top casings were then extracted and re-used. The polymer slurry was then removed, stored in tanks on-site for re-use and then replaced by potable water. The grout plug and rock socket was then drilled at 6.5 feet (1.98 meters) diameter extending into the Gneiss/Schist bedrock at 13 feet (3.96 meters) using a SM Hain-120K pile top RCD. The drill cuttings were flushed up the drill string into a discharge pit and then the water was returned to the shaft. The decision to use a RCD drill platform was based on the depth of the shaft, shaft diameter and the compressive strength of the bedrock. The rock socket was then inspected using Mini-Sid inspection device to verify bottom cleanness to the required specification requirement of no more than 1.5 inches (38 mm) of loose soil at any location across the bottom of the shaft and no more than 0.5 inch (13 mm) of soil in 50% of the area of the shaft. The noted requirement was achieved by using a bottom clean out bucket (muck bucket) and by airlifting the rock socket bottom. Once shaft bottom was approved a full length reinforcing cage weighing as much as 35 tons (311 kN) was placed in sections. Cages were placed in three sections and spliced together on location with barlock couplers. The two splice requirement was necessary to accommodate site constraints and shaft lengths up to 180 plus feet (55 + meters). Concrete placement followed using a 6,000 psi (41.4 MPa) tremie mix, using a 10” gravity tremie pipe. A total of 255 cubic yards (195 cubic meters) were typically placed in each drilled shaft.

QUALITY ASSURANCE / QUALITY CONTROL

Drilled shafts were subjected to multiple levels of quality control measures. Open shaft verticality through overburden soils was measured by the drilling rig alignment control and dedicated Sonicaliper profiling for each shaft, this confirmed shaft verticality of the order of 0.5 -1% was achievable in the given geological setting and build method used. Sonicaliper verified shaft volumes for the theoretical annulus grout volume evaluation. The casing annular space grouting had to be carried out in two stages to prevent the 5/8 inch (15.9 mm) thick casing buckling due to pressure differential[1,5,6]. Once the casing and rock socket drilling is completed a mini shaft inspection device (mini – SID) was used to confirm the rock socket base cleanliness using a five spot sediment checking criteria (50 % less than 0.5”, no location exceeding 1.5” (13mm, 38 mm)). Next, construction quality control involved concrete integrity testing using Ultrasonic Crosshole Testing (CSL)[2] and thermal integrity profiling (TIP) using embedded thermal couple wire sensors. Both CSL and TIP validated concrete mix design and placement practices to produce quality drilled shaft foundation.

© 2016 Deep Foundations Institute

ALTERNATE TECHNICAL CONCEPTS - ATC

The design build team proposed the following drilled shaft foundation alternate technical concepts to the NYSDOT during the RFP response period for the purpose of saving schedule and construction costs. ATC covered following items:

- Elimination of the demonstration shaft
- Using a production shaft as a test shaft to obtain the design parameters of rock socket
- Utilizing the modified O-Cell test to obtain high end bearing stress (ultimate level) while the rock socket friction is kept to service level stresses; i.e. “Chicago Method”.

ATC was accepted and brought mutual benefits to the owner and Design Build team.

CONSTRUCTION CHALLENGES & SOLUTIONS

Surface Obstructions: Prior to the start of dilled shaft construction for main span pylons, pre-excavation were performed at each drilled shaft location to remove surface obstructions to -10 feet (3 meters) BGS. This was done to facilitate temporary casing placement as required to isolate contaminated soils and water. During foundation installation man made obstructions consisting of large pieces of concrete debris was encountered below the 10 feet (3 meters) of pre-excavation, which prohibited the installation of temporary casing installation with the vibratory hammer. A photograph of the obstruction removal operation is provided in Figure 6. The casing procedure was modified using a two staged approach with a top casing and a secondary casing that could then be installed with the drill rig, this allowed obstructions to be removed during excavation and the advancement of the casings. Temporary casings were advanced by twisting and crowding into place thus maintaining intimate contact with the soil and isolation of soil and water contaminates.



Fig 6. Surficial Obstruction Removal

© 2016 Deep Foundations Institute

Sloping Bedrock: the pre-bid bore information represented a moderate bedrock sloping condition of 5% to 9 % or approximately 8 inches (203 mm) across the area of the shaft. This was not considered a serious matter with the tooling and equipment that was planned for the project. When the results of post-award bores were analyzed and confirmed that a much more serious problem existed as the rock appeared to be sloping severely at approximately 55% or an estimated 47 inches (1194 mm) across the area of the shaft. The problem simply stated was how to advance the 7 feet (2.13 meters) diameter casing 4 feet (1.2 meters) into very hard rock and achieve a casing seal. Once this casing was spliced together it was in some cases 180 feet (55 meters) long and weighed in excess of 50 tons (445 kN) and was not going to be easily moved if at all if any contact with the bore hole sidewall or if collapse occurred. A remedial plan was developed revising the proposed bid-build method. This required additional tooling to be mobilized to the site to remove and level the sloping rock in advance of setting permanent casings. The following problems were identified and remediation plans developed to address each prior to mobilization to the project site.

- Inability to advance permanent casing to rock: The open hole shaft design diameter was increased from 7 feet (2.13 meters) diameter through the overburden soils to 8 feet (2.44 meters) diameter. This was done to reduce the risk of side shear friction build up which would prohibit the advancement of the steel casing to rock. Specifically, we were concerned that the casing could not be placed plumb and on location, as the casing would have tendency to walk off in the direction of the rock slope. By increasing the shaft diameter this provided better opportunity to level the rock, cut a casing kerf and set/seal casing on location to allow the RCD to excavate the rock socket with minimal risk of blow in or ground collapse at the soil/rock interface.

- Inability to seat or seal casing to rock: A pre-cored relief kerf was drilled into rock at 72/78 inch (1829/1981 mm) diameter to relieve rock for removal with rock augers using conventional rotary drill methods. This procedure was required to level the rock to maintain casing plan location. Additionally this rock leveling was required to avoid burning out carbide rock cutters on permanent casing and to minimize the risk of casing freeze before obtaining a full circumferential seal into the rock strata.

- Casing buy lengths are too short: Additional casing was ordered to avoid additional splicing on location and delay. Based on pre-bid bore information casing lengths were estimated at 1,296 linear feet (395 meters) with waste for embedment and working conditions. At the completion of post-bore logs, rock was encountered at elevation -152.3 feet which is 14 feet (4.3 meters) deeper than what was the estimated (elevation -138 feet). The casing buy length was increased to 1,368 linear feet (417 meters).

- Safety / logistic concerns for placing casing in lengths in excess of 170 feet (52 meters) utilizing one splice: Due to casing lengths in excess of 170 feet (52 meters), additional casing splices were added to the bid-build method. Specifically 6 of the 8 locations were spliced with two splices instead of the bid plan of one each.

- Inappropriate tooling to remove and level sloping rock: The original build scheme was to provide conventional tooling that would fit inside the 7 feet (2.13 meter) diameter casing to level or address any rock concerns associated with the 9% slope as required to prepare the rock for seating and sealing of the permanent casing. SKE procured and mobilized additional tooling consisting of 6.5 and 8.0 feet (2.0 and 2.4 meters) tooling sets to drill rock kerf and remove rock at the larger diameter of 8.0 feet (2.4 meters).

© 2016 Deep Foundations Institute

- Casing not sealed, reverse circulation drill (RCD) cannot operate, blow in occurs: At completion of rock leveling a concrete plug of approximately 8 feet (2.4 meters) or 10 cubic yards (7.65 cubic meters) was placed in all shafts; concrete was placed on leveled rock surface and up into the casing. The concrete plug was installed to secure casing on location, in contact with rock and to provide a seal for the RCD equipment. This bulb plug outside of the casing at rock /soil interface would help hold the RCD in place until seated full face across the rock profile. Failure of the concrete seal to hold could lead to collapse of the rock/soil interface into the shaft, not allowing the RCD to advance the rock socket.

Proposed bid method does not work: Due to severe sloping rock (40% to 55%) and hardness of the rock strata (Gneiss/Schist with unconfined compressive strengths exceeding 23,000 psi (159 MPa)) SKE was very concerned that the casing could not be advanced to required depth; installed on location; installed to specified vertical tolerances and seated into the rock to allow rock excavation using RCD methods.

Verticality: the contract specifications allowed the drilled shafts a 2% verticality tolerance which was not a major concern of SKE. Of concern was that if the shaft was drilled within the 2% tolerance the casing may hit the borehole side wall during installation and not advance to rock. This concern was eliminated with the use of the Sonicaliper to profile the shaft during excavation and at completion of the overburden excavation. If the shaft was deviating out of tolerance the drill operator would know and correction would be made to re-plumb the shaft.

LOAD TEST RESULTS

Osterberg Load Test[6,7] was conducted on a demonstration/production shaft utilizing the concept of "Chicago Method" using a Loading Procedure A – Quick Test of ASTM D1143[3]. The Chicago load test method uses the test configuration where the rock socket test is conducted by loading the end bearing unit area to the ultimate stress levels while engaging a rock socket peripheral side shear reaction at the levels not exceeding the service load magnitudes since this test shaft is also a production shaft. The O-Cell test using a reduced end bearing plate of diameter of 38 inches to load the rock socket prescribed bearing contact area to the level of 681 ksf (32.6 MPa) while the mobilized side shear resistance of value of 27.4 ksf - 190 psi (1.31 MPa) utilizing a single 6000 kip (27000 kN) hydraulic jack O-Cell assembly. It has been demonstrated the construction methods employed enable the design team to utilize high end bearing resistance design and prescribed side shear resistance values. Based on the O-Cell test performance the rock socket length could have been reduced accordingly, however, such effort has not been exploited given the quantities involved did not warrant revisiting the drilled shaft design methodology. Additionally the RFP required rock socket length to extend two diameters. Figure 7 & 8 depicts the load displacement curves and Chicago method schematics and actual jack configuration used.

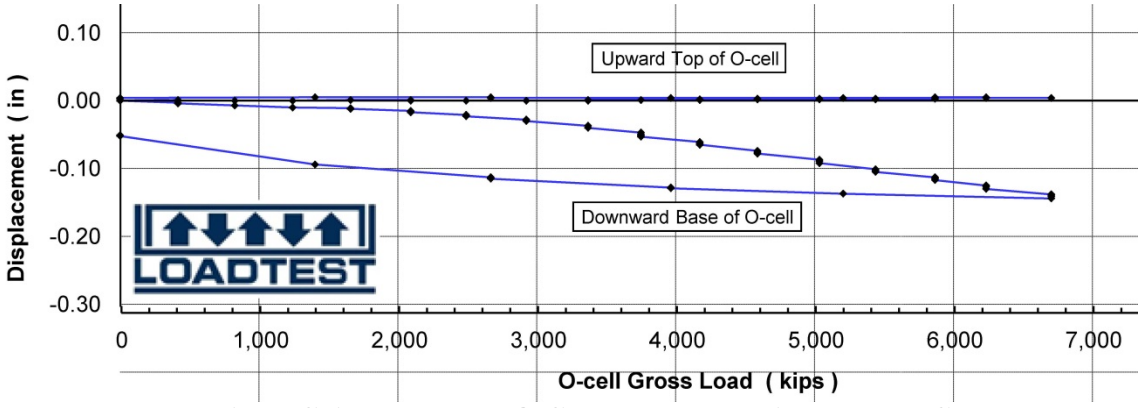


Fig 7. Chicago Method O-Cell Test - Load Displacement Curves

© 2016 Deep Foundations Institute

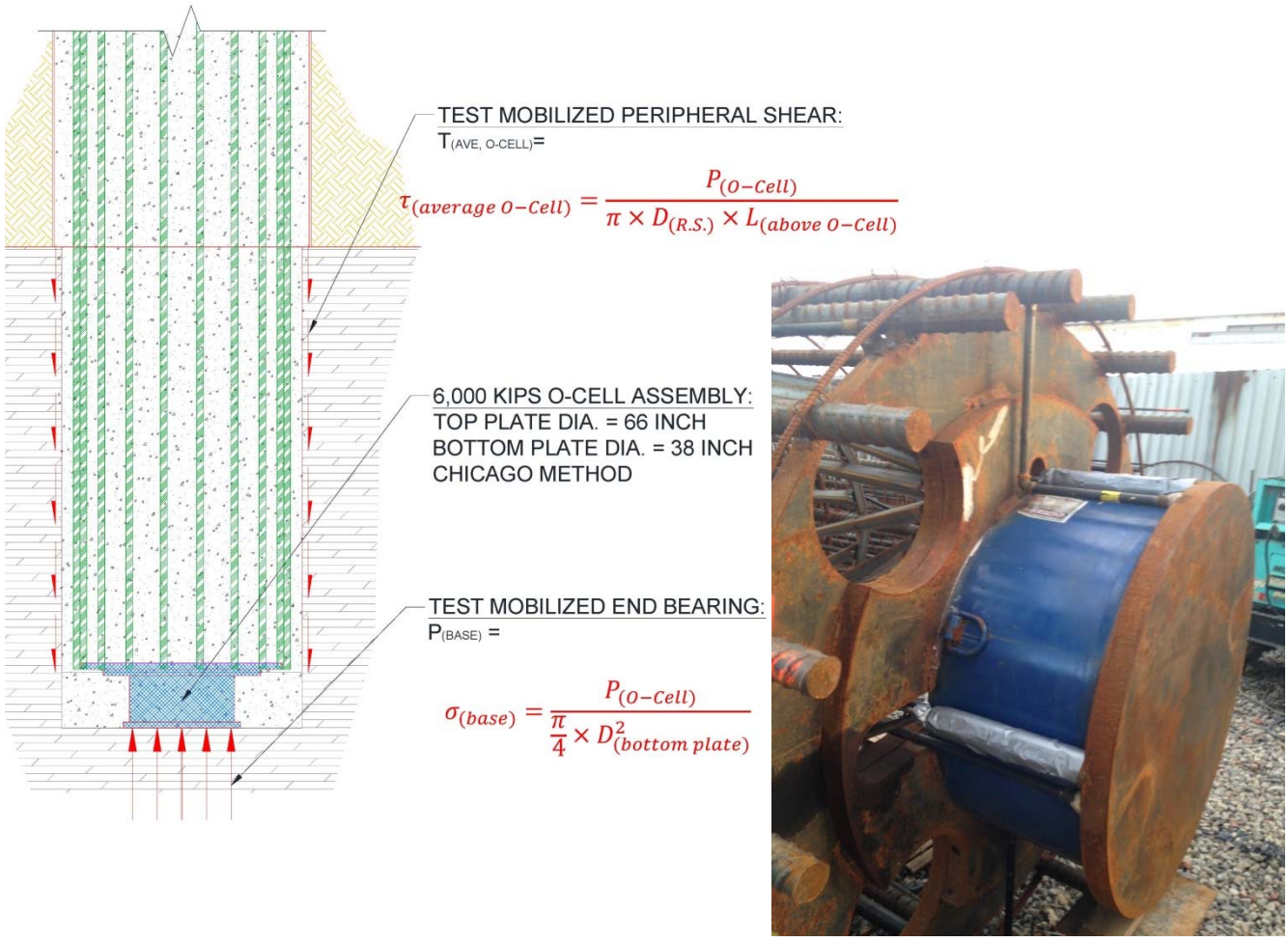


Fig 8. Chicago Method Rock Socket Testing Configuration

Lateral Load Test[4] was conducted at completion of all eight drilled shafts, integrity testing and accepted by NYS DOT. Since this is a design built project the drilled shaft lateral load demand evolved with the design development progress. During the initial design iteration, lateral load demand was considered to be in the order of 500 tons (4448 kN) and in the final stage the free head configuration test load was established at 350 tons (3114 kN). The lateral loading response was monitored by the direct head movement measurement and the use of shape accel array inclinometer (shape tape) for deformation with depth and lateral load influence / soil engagement depth determination. Lateral load test has proven the annular space grouting successfully reinstates the drilled shaft – soil interface contact, lateral load depth of influence is in the order of 60 feet (18.3 meters) below the grade surface, load deformation response uniformity between two shafts tested and head deformation magnitudes of the order of 0.5 inch (13 mm). Since the tested shafts were production shafts, care of load transfer had to be exercised to distribute the lateral load of 350 tons (3114 kN) without causing a localized plastic zones at the bearing / contact points. Frame with designated stiffness path element utilization was used to distribute the applied load adequately. Figure 9 depicts the lateral load test configuration and the head deflection plots.

© 2016 Deep Foundations Institute

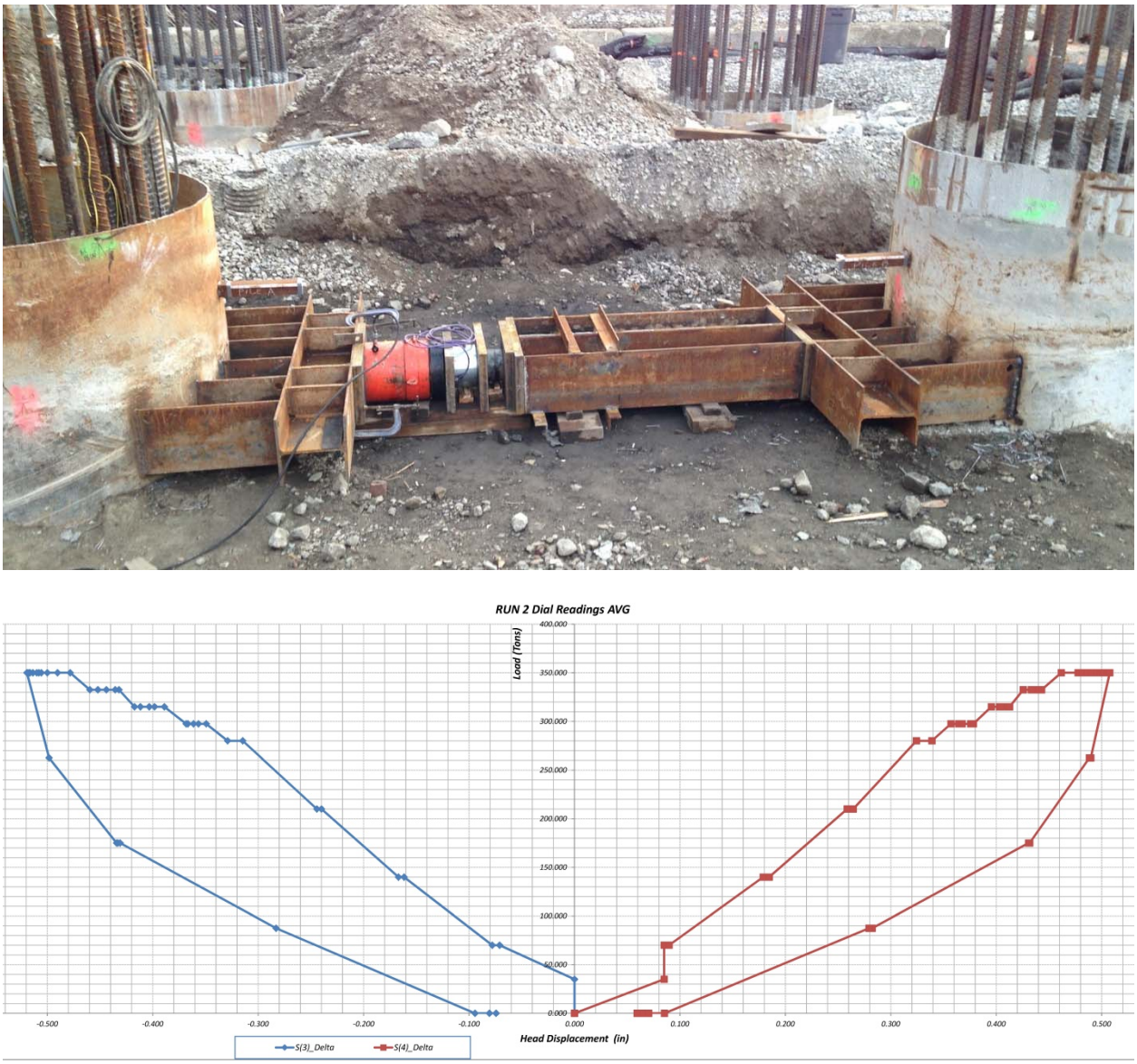


Fig 9. Lateral Load Testing Configuration and Head Deflection Plots

CONCLUSIONS

The contract design-build delivery approach for the installation of a difficult and challenging drilled shaft foundation installation as required by JV design appears to have been the right choice. This can be concluded as constructability issues, concerns and risks were addressed in preparation of design drawings and specifications. This paid dividends during shaft construction by the elimination of potential problems, providing specifications that were project specific and development of a collaborative spirit between contractor, designer and the owner. The ATC provision was utilized successfully and to everyone's benefit, by eliminating the Demonstration/Loadtest shaft from a sacrificial shaft to a production foundation element and the acceptance by NYSDOT of a unique Osterberg load testing method which

© 2016 Deep Foundations Institute

went against local practice and custom. In regards to Design-Build vs. Design-Bid-Build contracts specific to the foundation construction there are always surprises as design plans are generally not at the 100% completion stage and therefore there are unanticipated costs. Lastly and probably most importantly the preemptive actions taken by SKE to address the unanticipated severe sloping rock condition prior to site mobilization worked. All drilled shafts were constructed within prescribed tolerances, no shaft blow-ins or loss of ground occurred. This aside it is the authors' opinion for the Kosciuszko Bridge project the benefits of Design-Build far outweighed the post-award surprises.

ACKNOWLEDGEMENTS

The authors would like to thank the New York State Department of Transportation for providing the Alternate Technical Concept (ATC) provision in the Kosciuszko Bridge RFP and accepting our proposed ATC for the Osterberg Load test approach. Further thanks goes out to The Underpinning and Foundation Skanska operations team consisting of Nolan Kealy P.E.: Project Manager, Superintendent: Mario Francese, Project Engineer: George Rittman, Estimators: Jinseop Kim P.E., Engineering: Alfranio Prado P.E., Scheedie Russell. The authors also wish to thank Shing Pang P.E. of Loadtest, Matthew Riegel P.E. of HNTB for their advice and support in preparation of the Osterberg Load test method ATC. Others: KB Technologies, SM Hain Company, Berkel & Co. Contractors, Inc. and the "Windy City"

REFERENCES

1. American Petroleum Institute, 2010. Recommended practice for planning, designing and constructing fixed offshore platforms-working stress design.21st Edition.

2. American Society of Testing and Materials (ASTM), 2008. Standard Test Method for Integrity Testing of Concrete Deep Foundations by Ultrasonic Crosshole Testing, ASTM D6760-08.

3. American Society of Testing and Materials (ASTM), 2007. Standard Test Methods for Deep Foundations Under Static Axial Compressive Load, ASTM D1143-07.

4. American Society of Testing and Materials (ASTM), 2007. Standard Test Methods for Deep Foundations Under Lateral Load, ASTM D3966-07.

5. American Concrete Institute (ACI), 2014. Report on Design and Construction of Drilled Piers. ACI 336.3R-14 American Concrete Institute, Farmington Hills, MI.

6. FHWA, 2010. Drilled Shafts: Construction Procedures and LRFD Design Methods, Publication No. FHWA-NHI- 10-016, NHI Course No. 132014.

7. Duncan C. Wyllie, 1999. Foundations on rock. 2nd Edition. E & FN SPON London and New York.

8. Matthew Riegel P.E. (2013), Kosciuszko Bridge Replacement, Geotechnical Foundation Design Memorandum.

© 2016 Deep Foundations Institute

LATERAL PRESSURE RELIEF BY GEOTEXTILE ENCASED COLUMNS (GECs) AT PILED BRIDGE ABUTMENTS: TWO CASE STUDIES

Dimiter Alexiew, HUESKER Synthetic GmbH, Gescher, Germany, +4925427010, dalexiew@huesker.de
Lilma Schimmel, HUESKER Inc., Charlotte, USA, +1704588 5500, lschimmel@hueskerinc.com
Sven Schröer, HUESKER Inc., Charlotte, USA, +1704588 5500, sschroer@hueskerinc.com

ABSTRACT

The Geotextile Encased Columns (GEC) deep foundation system for embankments on soft soils was introduced some 20 years ago and is now considered State-of-the-art worldwide.
The GECs consist of compacted granular fill, similar to common gravel columns, with one decisive difference: they are confined in a high-strength low-strain flexible geotextile "cylinder" (encasement). This engineered element provides a very efficient tool to control and optimize the behavior of the system. GECs perform very well even in extremely soft soils ensuring bearing capacity (stability) and reducing settlements. Due to the encasement, they also provide high lateral ductility. A wide range of fills including sands can be used.
The remarkable reduction of vertical stresses in the soft soil surrounding the GECs results in a decrease of lateral pressure as well. Such reduction combined with the lateral ductility allow GECs to be also used for lateral pressure-relief adjacent to sensitive foundations, e.g. rigid piles. The application of GECs as lateral pressure relief was recently used in Brazil and Germany where bridge abutments were built on concrete reinforced-piles. The GECs below the bridge approaches and adjacent to the piles decreased the lateral pressure to acceptable values.
This paper presents two case studies for which the most relevant parameters, the geotechnical conditions, specific problems, engineering philosophy, final solution and lessons learned are discussed.
Furthermore, instrumentation programs were applied in both projects. The most important results in terms of displacements and stresses are shown, evaluated, summarized and commented upon, focusing on the lateral stress-relief, followed by conclusions and recommendations.

Keywords: stress relief, soft soils, bridge approaches, geotextile encased columns, measurements

INTRODUCTION

Bridge abutments on soft soils can be founded on piles of different types. Being generally rigid non-ductile elements, the piles are quite sensitive to high asymmetric lateral pressure from the surrounding soil, for example as pressure generated by adjacent bridge approaches (embankments). For taller approaches and/or very soft soils, the lateral pressure is significant (also classically known as Tschebotarioff-effect, Tschebotarioff 1973). The problem can be avoided by building the embankment first and installing the abutment piles after sufficient soft soil consolidation under the embankment load has occurred. However, due to different reasons, such as construction logistics, this is not always possible. Another alternative is to provide support (e.g. by piles) adjacent to the embankment to equalize settlements in the contact embankment/abutment (Fig. 1, left and Alexiew 2005). Additionally, geotextile encased columns (GECs) can be applied as supporting elements (Fig. 1, right) (Details regarding principles, design, execution and experience with GECs are not herein presented but can be found in Alexiew et al. 2005, 2014, 2015). The main function of the system, to control the stability (Ultimate Limit State - ULS) and deformation behavior (Serviceability Limit State - SLS) of the embankment is similar to piles, however the elements are softer and more ductile. A verified codified design has been developed (EBGEO 2011).

© 2016 Deep Foundations Institute

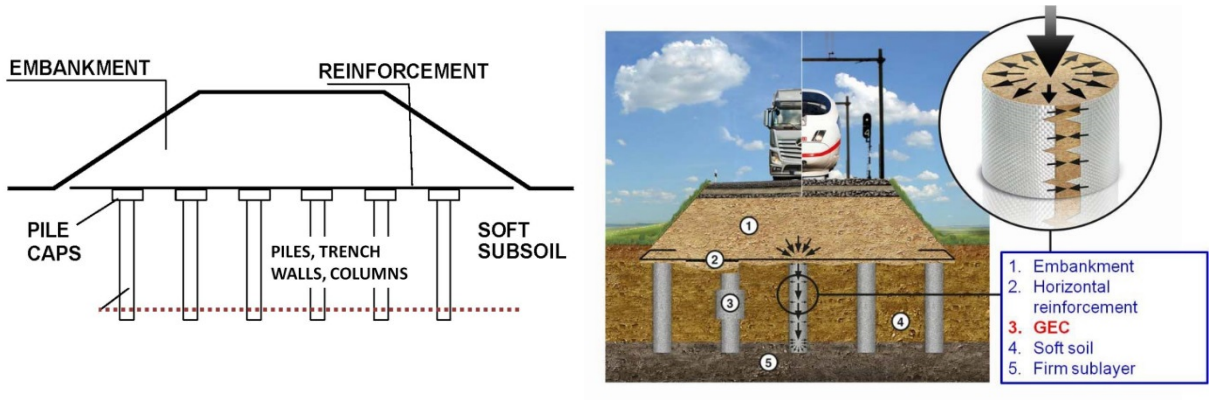


Fig. 1. Embankment on piles (left) and on Geotextile Encased Columns (GEC) (right).

The GECs attract typically 75 to 85 % of the vertical load correspondingly reducing the stresses in the soft soil around them and the horizontal normal (lateral) stress. The latter effect can be used for lateral stress relief on adjacent buried structures in the soft soil. The possible application for the relief of lateral stress was realized long ago, but was only adopted in real projects quite recently in Brazil and in Germany. Note, that although the GEC technique is now well established, no research has yet been undertaken on its use for reduction of the induced horizontal earth pressure acting on pile foundations embedded in soft soils. This aspect is neither directly handled in EBGEO (2011).

PROJECT IN BRAZIL 2013 - 2014

Overview

Bridge abutments for a new high traffic road project in the Brazilian State of Rio Grande do Sul, near Porto Alegre, had to be founded on reinforced concrete piles in very soft soil. The pile foundations and the abutments were constructed prior to the addition of the 8 m high embankment approaches. Thus, a solution was conceived to protect the existing pile foundations from the lateral soft soil pressure under the embankments.

The geotechnical investigation revealed a sedimentary deposit of 5 to 8 m soft clay layer overlaying dense sand. Near the surface, there was an over consolidated crust approximately 1 m thick and within the depth affected by seasonal variations of the water table. The hydrostatic pore-pressure corresponds to the regional water level (Schnaid et al. 2014). The groundwater level is close to the surface, after heavy rainfall the terrain becomes flooded.

The final optimized foundation solution for the embankments comprised the installation of four rows of GECs next to the bridge, a geogrid horizontal reinforcement on the top of the columns and two rows of GECs beyond the bridge edge. The design was performed according to EBGEO (2011). Some engineering judgement and modified methods had to be applied to calculate the lateral pressure variation along the length of the foundation.

GECs 0.8 m in diameter with a 2.4 m spacing in a triangular pattern were placed in the clay underneath the embankment through the clay layer. Such layout corresponds to an area replacement ratio of 0.1. The displacement method of installation was used (Alexiew et al. 2015) and poorly graded sand sourced from the Guaíba River was used as fill. A seamless high-modulus geotextile encasement, Ringtrac 100/200, with a tensile modulus in the "ring" direction of about 2000 kN/m was used (Fig. 1, right). The geosynthetic encasement not only provides the radial confinement required, but it also allows a quite fast drainage of pore water into the column during loading by embankment construction.

Figure 2 shows an overview, stages and aspects of the execution. (Note, that due to the high-strength encasement the compacted sand columns can stand alone "in air" without surrounding soil).

© 2016 Deep Foundations Institute



Fig. 2. Execution: installation behind the bridge abutment and top of installed GECs (right).

Instrumentation program

Due to the lack of research and experience regarding the lateral pressure variation with depth and also due to the importance of validation of assumptions and design calculations, a monitoring program was planned and implemented at one of the abutments. Instrumentation, comprising total pressure cells, electrical piezometers, inclinometers and settlement plates was installed. Pressure cells and piezometers were placed between the first GEC row and the piles, 0.5 m from the edge of the first row of bridge piles, vertically, in three different depths. The pressure cells were fixed on structural steel H beams. Two inclinometers were installed between the columns to monitor horizontal displacement fields within the soft soil layer. The monitoring program was maintained until the excess pore pressure was dissipated, a period of about 154 days (from 08 Aug 2013 to 09 Jan 2014). The embankment was built from day 27 to day 91 (final height of 8 m).

Measurement results and comments

For brevity, only some results and graphs are herein provided.
The horizontal displacements perpendicular to the embankment axis reached a maximum value of 65 mm at a depth of 3 to 4 m (approximately at the middle of the clay layer). Rates of displacements have decreased substantially at final construction stages and were close to stabilization at final readings.
In Figure 3, the height of embankment versus time is depicted; the increase in height and therefore incremental loading is relevant for all figures. The development of total horizontal (lateral) normal stress (pressure) $\sigma_{h\ tot}$ is displayed over the depth and for different stages from the beginning of construction (day 27) until day 110, i.e. twenty days after end of construction (day 91). This is the total lateral pressure at the first row of abutment concrete reinforced piles.
For comparison, the graph corresponding to the theoretical initial K_0 value of the clay is shown as well. The first curve for day 27 (beginning of construction) is very similar to the K_0-graph; it seems to be an indication of the proper functioning of pressure cells. The maximum pressures occur at about 4 m of depth; this corresponds approximately to the max lateral displacement, see above, and seems plausible. Bulging at a significant part of the curves occurs in the later stages of construction. That increase in the ratio of pore water pressure to total pressure is due to the contribution of the pore water pressure u (Fig. 4, left). For brevity, no u-graph is shown. Instead, Figure 4 left shows the ratio of increase of water pressure Δu to the increase of total horizontal stress $\Delta\sigma_{h\ tot}$ allowing a better understanding of the behavior of the GEC system.
The max value of $\Delta u/\Delta\sigma_{h\ tot}$ is about 0.3, indicating proper functioning of the GECs as "megadrains" quickly dissipating excess pore water pressure (Alexiew et al. 2014, 2015). Note that for non-supported embankments on saturated soft soils, this value can be as high as 0.8 (Blume et al.2006).
At day 130 (40 days after end of construction) the pore water pressure is almost completely dissipated i.e. the primary consolidation of embankment is completed.

© 2016 Deep Foundations Institute

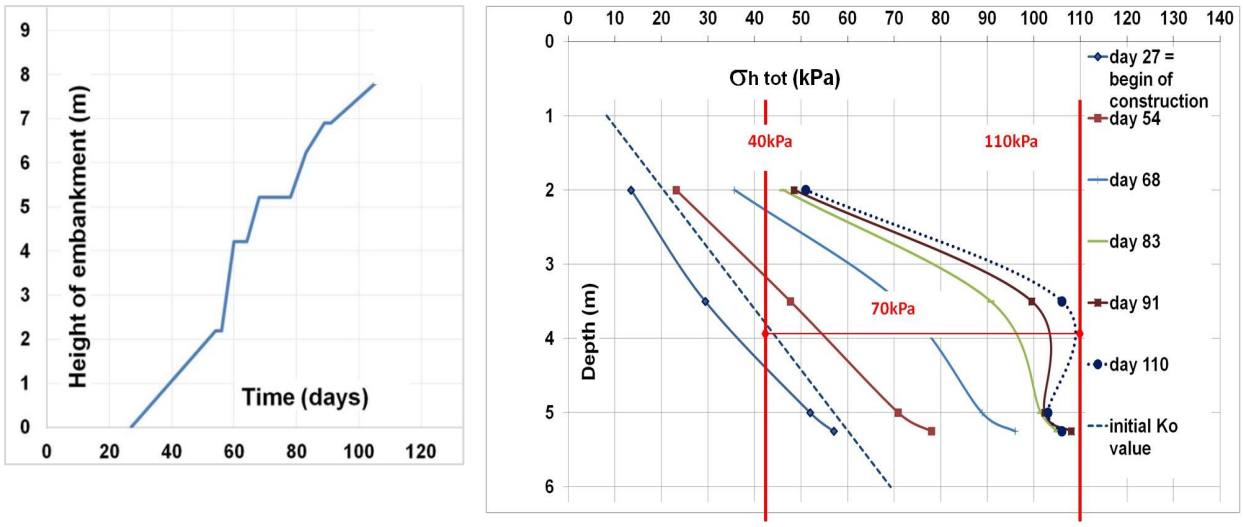


Fig. 3. Embankment height over time (left) and development of total horizontal stress (lateral pressure) on the piles of bridge abutment (right).

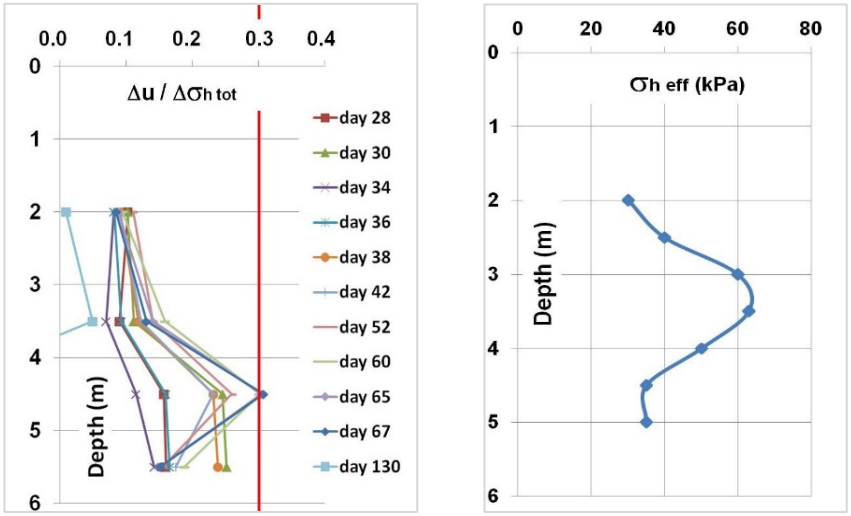


Fig. 4. Ratio of pore water pressure to total horizontal stress (left) and effective horizontal stress (lateral pressure) on the piles of bridge abutment (right).

Considering the asymmetric lateral pressure on the reinforced concrete-piles, which is the focal point herein, the excess pore water pressure u is not really critical, because it generates an almost axial-symmetric "circular" hydrostatic load on the (impermeable) pile. More critical and thus from real interest is the effective horizontal stress $\sigma_{h\ eff}$ which is much more asymmetric and thus creating bending and shearing of the piles. The average value of this stress based on approximate evaluation of all data is depicted in Figure 4, right. They are in the range of 30 to 60 kPa and were found to be non-critical for the reinforced concrete piles. This is less than 50% of the values to be expected according to the empirical earth pressure proposed by Tschebotarioff (1973) for asymmetric loading conditions under an embankment without GECs.

The concept and solution proved to be successful. After this conclusion was achieved and to save costs, the monitoring program was ceased after five months, although further monitoring would have been enriching from the scientific point of view.

© 2016 Deep Foundations Institute

PROJECT IN GERMANY 2013 - 2015

Overview

The new German Federal Road (Bundesstrasse) B212n in the northwest of Germany was conceived as a bypass of the City of Berne. Note that the allowed driving velocity on a Federal Road is 100 km/h, thus the requirements in terms of serviceability are quite stringent. The route of B212n comprises nine bridges and viaducts with high embankment bridge approaches. Construction started in 2009 and the entire road has to be put into operation in 2017. Soils in the Northwest region of Germany are typically soft saturated soils (clay and peat) with thickness ranging from 10 to 15 m, underlain by sandy layers; the ground water level (GWL) is almost at the surface. A common solution in such cases is to build the road embankments with high-strength basal geosynthetic reinforcement in combination with strip drains and temporary surcharging (Alexiew & Blume 2010). However, at Berne this scenario could not be applied especially for the higher embankments (typically the bridge approaches). The tight schedule of the project did not allow sufficient time for consolidation under preloading. Furthermore, there would be the risk of non-acceptable post construction creep settlements.
Finally, foundation on GECs for the approaches was found to be the optimal solution due to technical, technological, financial, scheduling and ecological arguments.
For the northern approach embankment at river Hunte, two problems had to be solved: the crossing of an old landfill and the reduction of the lateral pressure with depth on the piles of the bridge abutment (similar to the project in Brazil described above). The latter challenge is the focal point herein. For more on the "crossing the landfill issue" see Alexiew et al. (2016) which includes also detailed geotechnical information.
Figure 5, left shows a plan view, and Figure 5, right a longitudinal cross section of bridge approach and abutment. Typical values of the undrained unconsolidated shear resistance s_u of peat and clay are in the range of 10 to 15 kPa, the drained internal friction angles ϕ' are in the range of 20° to 25°. The old landfill was extremely heterogeneous (Alexiew et al. 2016).

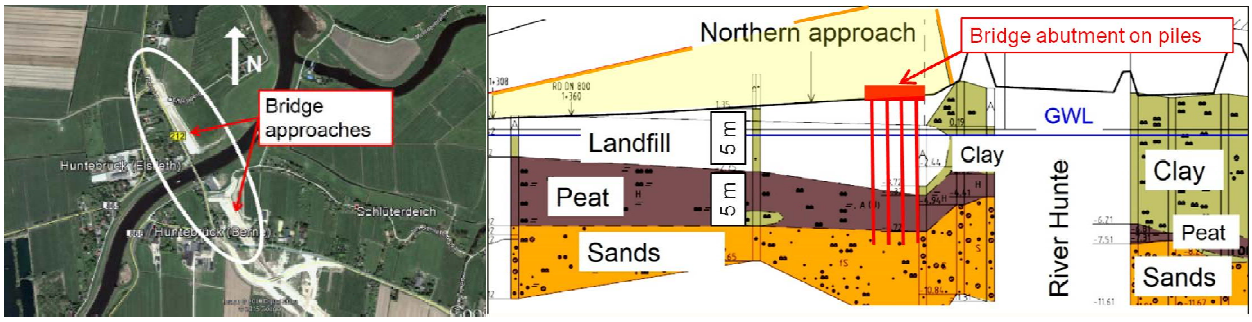


Fig. 5. Plan view of the river Hunte crossing (left) and simplified longitudinal cross section (right); GWL (average ground water level)

The height of the embankment at the abutment is about 7 m.
Design for the GEC foundation system was performed according to EBGEO (2011) which is until now the only code worldwide that addresses the system. GECs with a diameter of 0.6 m were installed in a triangular pattern with an area (replacement) ratio of 12.4%, resp. 17.5% (Fig. 6). Generally, the area ratio for GECs ranges from 10 to 20% (Alexiew et al. 2014, 2015).

© 2016 Deep Foundations Institute

Very high-strength high-modulus geotextile encasements, Ringtrac 100/500 PM, made from PVA (Polyvinylalcohol) yarns were adopted with a tensile modulus in the "ring" direction (Fig. 1) of more than 7000 kN/m (more than three times stronger than the material for the project in Brazil described above). This resulted from the very stringent deformation limitations for German Federal Highways.
Due to the intended additional function as lateral pressure relief system for the abutment concrete reinforced piles, a group of six rows of GECs with the higher area ratio of 17.5% mentioned above was installed adjacent to the abutment. The layout is marked in grey in Figure 6.
The German pile design recommendations EA Pfähle (2007) comprise a simplified procedure to assess a pile group safety regarding lateral pressure from an adjacent embankment. The requirement is that the factor of safety (FOS) for the global (external) stability of the embankment in direction to the piles is at least 1.4. A global stability analyses according to EBGEO (2011) was performed resulting in the GEC group shown. The same type of columns and geotextile encasement were kept as in the "standard" case below the rest of approach embankment, only the number of GEC rows and the area ratio were increased to achieve a FOS > 1.4. Additionally, based on regional experience, it was decided that the $\sigma_{h\ tot}$ had to be limited to max 50 kN/m². A simplified FEM analyses was performed as well. The goal was to reduce the lateral pressure to less than 50% in comparison to a non-supported solution. The final area ratio amounts to 17.5% instead of 12.4% for the remainder of the embankment.

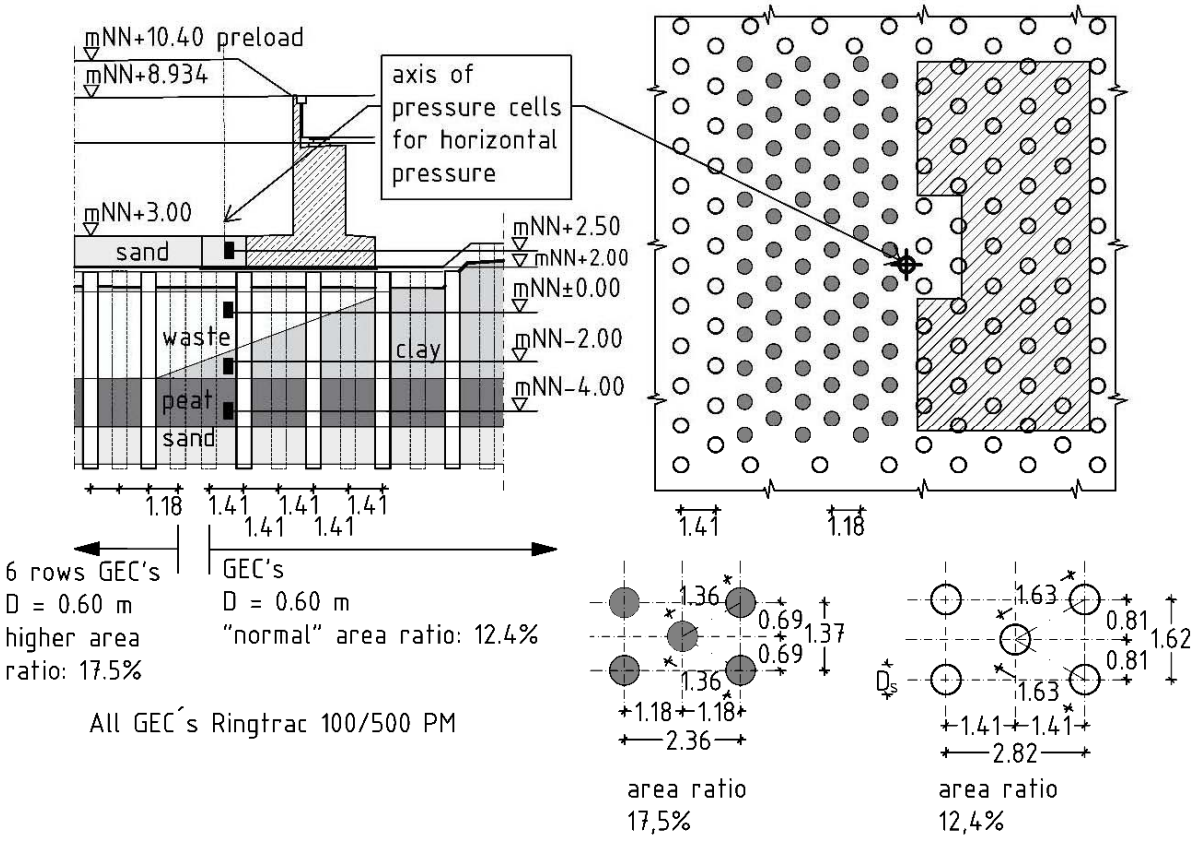


Fig. 6. GEC foundation near the abutment: longitudinal cross-section (left) and plan view (right).

© 2016 Deep Foundations Institute

Instrumentation program

A monitoring program was implemented due to similar reasons as in Brazil: lack of research and experience regarding the lateral pressure variation with depth and also due to the importance of validation of assumptions and design calculations. The instrumentation was more extensive than in Brazil because of the sensitive "old landfill crossing issue" (beyond the scope of this paper; for details see Alexiew et al. (2016)) and because of the very strict requirements of the bridge designers in terms of acceptable lateral pressure on piles. The program generally included the same types of gauges, but in greater quantities and in additional positions.
For brevity, we will focus only on the earth total pressure cells installed between the GEC stress-relief group and the abutment piles. They were installed in a vertical axis at the centerline of embankment - the zone of highest loads - at four levels in the four soil materials represented: the sand fill of the working platform, the waste, the clay and the peat. Details are depicted in Figure 6 ("mNN" means average sea level, the values are in meters).

Measurement results and comments

For brevity, only simplified graphs of $\sigma_{h\ tot}$ development are shown in Figure 7. The main stages/periods of embankment construction and the corresponding heights are shown as well.

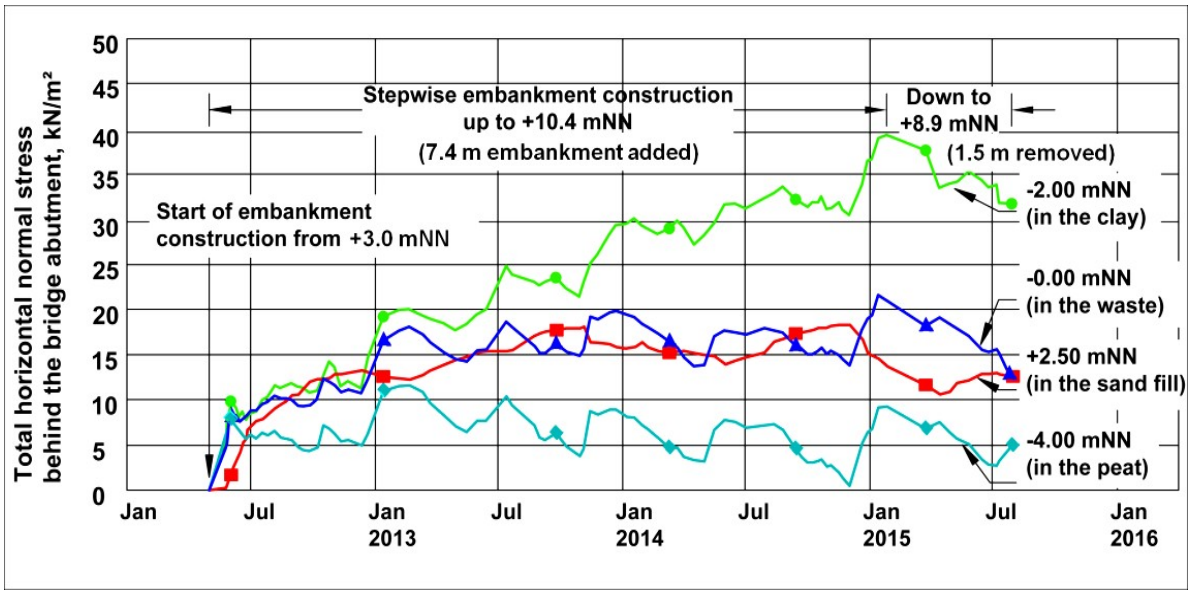


Fig. 7. Total horizontal stresses $\sigma_{h\ tot}$ at four levels in four different layers behind the bridge abutment over time (see also Figure 6).

The local deviations of the graphs reflect seasonal deviations of ground water level (GWL); they change the pore water pressure u as a part of $\sigma_{h\ tot}$. Note that since the sand fill at mNN+2.50 is quite above the average GWL at mNN±0.00 (varying by about ±0.5 m) the total $\sigma_{h\ tot}$ is not influenced by GWL changes. Instead it undergoes less deviations and the σ_h graph is smoother when compared to the other lower levels/layers. This is an indication of the proper installation and functioning of the earth pressure cells. It can be assumed that in this sand fill layer the registered σ_h is not the total but rather the effective σ_h.

© 2016 Deep Foundations Institute

From the practical point of view, the most important fact is that the highest total σ_h of 40 kN/m² (as it has to be expected in the clay) is less than the half of total σ_h to be expected without the stress relief offered by the GEC group (predicted by EBGEO 2011 and the simplified FEM analyses) demonstrating the correctness of design approach and the suitability of GECs as a lateral pressure relief measure. This was the case also in the Brazilian project. The stress is also quite below the max allowed value of 50 kN/m².
It seems that the GEC system has proved to be an efficient solution also as a stress relief system.
Generally the "total σ_h behavior" of the clay and of the peat meets the expectations taking into account their position and permeability. The monitoring program for this instance is still ongoing. Of special interest are the measurement results for the old waste being something of a rarity and its behavior between the behavior of the clay and of the peat. More detailed evaluations, analyses, comparisons and hypotheses will be presented elsewhere.

FINAL REMARKS

For two projects in typical soft soil areas in Brazil and Germany with bridge abutments supported on piles the approaching embankments were founded on Geotextile Encased Columns (GEC). Beside their common functions of ensuring embankments' global stability and controlling settlements in these projects, the GECs also had to perform as lateral stress relief systems protecting the piles of the abutments from excessive lateral asymmetric pressure along their lengths. These are the first instances on which GECs were applied with such a function worldwide and no prior experience was available.
Both projects were designed and executed approximately at the same period 2013-2015. Geotechnical circumstances, philosophy and design approaches were similar.
In both cases, monitoring programs were applied with the additional specific focal point of registration and evaluation of total and effective horizontal (lateral) stresses adjacent to the piled abutments.
Useful information was collected in terms of validation of engineering philosophy and design approaches.
In both cases the solutions proved to be successful and efficiently met the requirements and expectations.
Concisely, GECs' additional function as a lateral stress relief system for adjacent buried structures in soft soils is efficient and can be used as a standard solution.

ACKNOWLEDGEMENTS

Many parties participated in these innovative GEC "stress-relief" projects: consultants, researchers, investors, officials and supervisors. The authors, being only a part of this engineering constellation, would like to express their appreciation to all participants for their activities and efforts.

REFERENCES

Alexiew, D. 2005. Piled Embankments: Overview of methods and significant case studies. *Proc. 16 ICSMGE,* Osaka, pp. 1819-1822.
Alexiew, D., Brokemper, D., Lothspeich, S. 2005. Geotextile encased columns (GEC): Load capacity, geotextile selection and pre-design graphs, *Proc. Geofrontiers 2005*, Austin. CD GSP-131, pp. 1-12.
Alexiew, D. and Blume, K.-H. 2010. Two reinforced embankments on soft soils: Experience after more than twenty years, *9th International Conference on Geosynthetics ´10,* Guaruja, Brasil, pp. 1851 - 1854.
Alexiew, D., Thomson, G. 2014. Geotextile encased columns (GEC): why, where, when, what, how? *Proc. International Symposium on Advances in Foundation Engineering (GEOMATE 2014),* Brisbane. pp. 484-489.
Alexiew, D., Raithel, M., Schimmel, L., Schröer, S. 2015. Geotextile encased columns (GEC) as pile-similar foundation elements: basics, specifics, case studies. *Proc. DFI Annual Conference 2015*, Oakland, October 2015, no pages.

© 2016 Deep Foundations Institute

Alexiew, D., Blume, K.-H., Raithel, M. 2016. Bridge approach on GEC in Northern Germany: measurement program and experience. *Proc. GeoAmerica 2016 3rd Panamerican Conference on Geosynthetics*, Miami Beach (to be published).
Blume, K.-H., Alexiew, D. and Glötzl, F. 2006. The new federal highway (Autobahn) A 26 in Germany with high geosynthetic reinforced embankments on soft soils. *Proc. 8th International Conference on Geosynthetics´06,* Yokohama, Japan, pp. 912-916.
EA-Pfähle. 2007. Empfehlungen des Arbeitskreises "Pfähle", *German Geotechnical Society (DGGT)*, Ernst & Sohn, Essen-Berlin.
EBGEO 2011. Recommendations for design and analysis of earth structures using geosynthetic reinforcements - EBGEO (English version). *German Geotechnical Society (DGGT)*, Ernst & Sohn, Essen-Berlin. 313 p.
Raithel, M. 1999. Zum Trag- und Verformungsverhalten von geokunststoffummantelten Sandsäulen. *Schriftenreihe Geotechnik*, Heft 6, Universität Gesamthochschule Kassel, Kassel, Germany.
Raithel, M., Kempfert, H.-G. 2000. Calculation models for dam foundations with geotextile coated sand columns. *Proc. International Conference on Geotechnical & Geological Engineering GeoEng 2000*, Melbourne, p. 347.
Schnaid, F., Winter, D., Silva, A.E.F., Alexiew, D., Küster, V., Hebmüller, A. 2014. Geotextile encased columns (GEC) under bridge approaches as a pressure-relief system. *Proc. 10th International Conference on Geosynthetics*, Berlin. CD, no pages.
Tschebotarioff, G.P. 1973. Foundations, Retaining Walls and Earth Structures, 2nd ed. McGraw-Hill, New York, 642 p.

© 2016 Deep Foundations Institute

This page left intentionally blank

© 2016 Deep Foundations Institute

LOAD TESTS ON DRILLED SHAFTS AT GOETHALS BRIDGE REPLACEMENT

Steven S. Dapp, Dan Brown and Associates, PC, Sequatchie, TN, USA sdapp@dba.world
John P. Turner, Dan Brown and Associates, PC, Laramie, WY, USA jturner@dba.world
Dan A. Brown, Dan Brown and Associates, PC, Sequatchie, TN, USA dbrown@dba.world

ABSTRACT

The Goethals Bridge Replacement (GBR) spanning the Arthur Kill Waterway between Elizabeth, NJ and Staten Island, NY is supported on over 200 drilled shaft foundations ranging in diameter from 4.5 ft to 10 ft and socketed into Passaic Formation siltstone. Four drilled shafts, two on each side of the bridge (NJ and NY), were load tested using the bi-directional axial load method. Axial test results demonstrate that RQD, taken by itself, is not necessarily a reliable indicator of side or base resistance. High recovery with low RQD can be a function of horizontally bedded siltstone and shale where the individual pieces of core do not exceed four inches, but may still provide very high side and base resistance. Axial testing was followed by a lateral rapid-load test (Statnamic) on each of the same four shafts. In addition, one of the shafts was subjected to a static lateral load test to validate the rapid-load method as being representative of static loading conditions. Results of the axial load tests provide the basis of unit side and unit base resistances used in the LRFD design of the rock sockets for axial loading, while results of the static and Statnamic lateral load tests were used to calibrate *p-y* curve parameters used for design under lateral and moment loading. This paper describes implementation of the load testing program and its role in the design process.

Keywords: drilled shaft, bridge foundations, load test, axial, lateral, bi-directional, Statnamic, rock socket highest

INTRODUCTION

Design of drilled shaft foundations for the Goethals Bridge Replacement (GBR) required load testing in order to validate the parameters used for calculating geotechnical axial and lateral resistances. The bridge, including foundations, was designed in accordance with the AASHTO LRFD design specifications, 6th Edition (2012). The bridge owner is the Port Authority of New York and New Jersey (PANYNJ). One of the PANYNJ project requirements was stated as follows:

> "Perform a minimum of two (2) separate axial compression load tests (one [1] in New York and one [1] in New Jersey) for each demonstration shaft of different size and construction methodology to verify the design assumptions and construction procedures. At a minimum, one (1) demonstration shaft is required to be representative of production shafts with a diameter within one (1) foot above or below the demonstration shaft diameter.
>
> Conduct a minimum of two (2) lateral load tests (one [1] in New York and one [1] in New Jersey) for each demonstration shaft of different size and construction methodology. At a minimum, one (1) demonstration shaft is required to be representative of production shafts with a diameter within one (1) foot above or below the demonstration shaft diameter."

Based on preliminary design, diameters of the production shafts ranged (initially) from 5 ft to 10 ft. The above requirement for demonstration/test shafts to represent production shafts of diameters within $\pm$ 1 ft results in a minimum requirement of two test shafts on each side (NJ and NY): a 6-ft diameter shaft to represent production shafts with diameters from 5 to 7 ft, and a 9-ft diameter test shaft to represent production shafts with diameters from 8 to 10 ft.

© 2016 Deep Foundations Institute

Load testing provides benefits beyond simply meeting the project requirement stated above. Load testing of rock sockets provides the opportunity to demonstrate very high axial resistances. Lateral load testing of four drilled shafts on a single project allows calibration of soil and rock *p-y* curve parameters while accounting for as-built structural characteristics of the test shafts, thereby increasing the reliability of lateral load analyses used for design. Use of the Statnamic test method for lateral loading provided insight into foundation lateral response to rapid loading, an important consideration in the design for extreme event seismic loading. Finally, within the AASHTO LRFD design specifications, a higher resistance factor is allowed for design based on load testing, which provides more cost-effective designs, especially on a project such as the GBR with over 200 drilled shafts.

LOAD TEST PROGRAM

Two test shafts were installed and tested within the alignment of the NY Approach, and two within the alignment of the NJ Approach. One test shaft on each side is a 9-ft diameter shaft, designated as TS1-NY and TS3-NJ, with permanent casing seated into rock and a 8.5-ft diameter rock socket. The second test shaft on each side is a 6-ft diameter shaft with permanent casing to rock and a 5.5-ft diameter rock socket. The 6-ft diameter shafts are designated as TS2-NY and TS4-NJ. Test shaft designations, dimensions, and locations are summarized in Table 1. Note that the socket lengths of the test shafts exceed the design lengths of production shafts of the same diameters. The increased socket lengths were needed for bi-directional load testing which relies upon side resistance of the shaft above the O-cell to provide the reaction necessary to develop base resistance. The socket lengths in Table 1 were selected to mobilize the anticipated base resistance of the Passaic Formation rock, estimated to be at least equal to 300 ksf.

Table 1. Summary of Load-Tested Drilled Shafts, Goethals Bridge Replacement

Test Shaft	Diameter		Lengths		Location
	Shaft (in)	Socket (in)	Total[(1)] (ft)	Socket (ft)	
TS1-NY	108	102	96.7	33.4	NY Approach, South of N. Washington Ave., between Piers NYWB 14 and 15
TS2-NY	72	66	86.1	25.8	NY Approach, South of N. Washington Ave., between Piers NYWB 14 and 15
TS3-NJ	108	102	63.6	28.9	NJ Approach, Krakow St., north and west of Pier 9NJWB
TS4-NJ	72	66	52.8	20.8	NJ Approach, Krakow St., north of Pier 9NJWB

(1) Total length is from grade elevation to tip of socket

SUBSURFACE CONDITIONS AND TEST SHAFT INSTALLATION

An overview of the geologic and geotechnical conditions for GBR Project is presented in a companion paper (Turner et al., 2016) included in this proceedings. Borings with rock coring were performed at the location of each test shaft. Beginning at the ground surface, conditions at the 9-ft diameter TS1-NY show 8 ft of fill overlying 5 ft of organic clay exhibiting WOH resistance, underlain by 48.5 ft of medium stiff to very stiff glacial clay and medium dense clayey sand. Weathered rock at a depth of 61.5 ft is approximately 4.5 ft thick and is underlain by Passaic Formation siltstone. All seven core runs showed recoveries of 100% and RQD varies from 45% to 100%. Conditions at the 6-ft diameter TS2-NY show 8 ft of fill overlying 3 ft of organic clay, underlain by 45 ft of medium stiff to stiff glacial clay and loose to medium dense clayey sand. Weathered rock at a depth of 56 ft is approximately 7 ft thick and is underlain by Passaic Formation siltstone. Rock core recovery ranged from 78 to 100%, with RQD ranging from 7 to 52%. The lower RQD

© 2016 Deep Foundations Institute

values at TS2-NY (relative to RQD at the other test shaft sites) provided an opportunity to assess the influence of low RQD on side and base resistances.

On the NJ side, the boring at the location of the 9-ft diameter TS3-NJ, shows 5 ft of fill underlain by 26.5 ft of glacial clay and sand, underlain by 4.5 ft of weathered rock, then siltstone bedrock. The rock core exhibits high recovery (98 to 100%) with RQD ranging from 62 to 100%. Core photographs at this shaft provide strong visual evidence of excellent rock mass characteristics for foundation support. The boring for the 6-ft diameter test shaft (TS4-NJ) showed 4 ft of fill overlying 24 ft of glacial clay and sand with fine gravel, underlain by 2.5 ft of weathered rock, and then intact Passaic Formation siltstone. Rock core exhibited relatively high RQD (63 to 92%) over the depth of coring. In general this boring also showed excellent rock mass for foundation support, an observation consistent with the RQD values cited above.

The load test sites were selected to represent a range of conditions expected over the project with respect to: (1) depth to rock, (2) thickness of weathered rock, and (3) the presence of soft overburden soils, which are largely absent on the NJ side but are present on the NY side. By encompassing this range of ground conditions, the load test locations were optimized to provide results applicable to the design of production shafts over the range of conditions expected over the bridge alignment.

Test shaft installation can be summarized as follows. Permanent casing was driven to refusal at the top of rock using the APE Model 400 Vibratory Driver/Extractor, as is shown in Figure 1. The casing penetrated into weathered rock in order to achieve a hydraulic seal. Overburden soil was then excavated by an auger from inside the casing using a rotary drill rig. During excavation the casing was flooded so that the water level inside the casing was sufficient to offset the groundwater pressure.

When a hydraulic seal could be verified, the rock socket was excavated to tip elevation, while maintaining the water level inside the casing above the groundwater elevation. Rock augers were primarily used and the spoils appeared as ground up bits of rock and rock fragments, as is shown in Figure 2 (typical). Occasionally core barrels were used through the more massive layers of the intact rock socket material; a retrieved core piece is shown in Figure 3, and the circular grooves left by the preceding rock auger pass are seen on top of the core.

Following base cleanout, the bottom was sounded with a weighted tape and inspected using the mini-SID (Shaft Inspection Device). Prior to concreting, a shaft profiling device (SONICALIPER) was used to determine the shape and extent of the shaft excavation. Concrete was placed in the wet, using a tremie embedded into the freshly placed concrete at all times. Cross-Hole Sonic Logging (CSL) was conducted after concrete curing to assess the quality of the as-placed concrete inside the reinforcing cage. Figures 1-3 illustrate several of the test shaft installation procedures.

RESULTS

Axial Load Tests

The axial load tests were designed to measure the unit side and unit base resistances of sockets in Passaic Formation rock. These results are summarized in Table 2. Figure 4 shows the bi-directional load-displacement curves for TS1-NY, which is representative of all four tests where the shafts lower section resistance was well balanced against the upper. The following general aspects of socket response are noted:

- Base resistance in every case was mobilized at small displacement and achieved values exceeding 300 ksf at displacements ranging from 0.21 to 0.60 inches (less than 0.5 percent of diameter).
- Unit side resistances exceeded 30 ksf in all cases at displacements of less than ½ inch.

© 2016 Deep Foundations Institute

- Side and base resistances can be combined for LRFD limit state design; there is no issue associated with ‘strain compatibility’ for combining side and base resistances.
- The maximum loads in every case were governed by the O-cell capacity, not the geotechnical resistances; it is clear that all four shafts could provide higher values of resistance than those mobilized and reported in Table 2.



Fig. 1. Vibro-driving casing at TS3-NJ.



Fig. 2. Typical Intact Rock Cuttings.



Fig. 3. Cored Intact Rock.

© 2016 Deep Foundations Institute

Table 2. Summary of Resistances and Displacements Mobilized in Axial Load Tests.

Test Shaft	Mobilized Unit Side Resistance, (ksf)	O-cell Upward Displacement (in)	Mobilized Unit Base Resistance (ksf)	O-cell Downward Displacement (in)
TS1-NY	32.5	0.33	359	0.21
TS2-NY	30.6	0.11	319	0.21
TS3-NY	36.1	0.49	335	0.60
TS4-NY	34.2	0.16	340	0.32

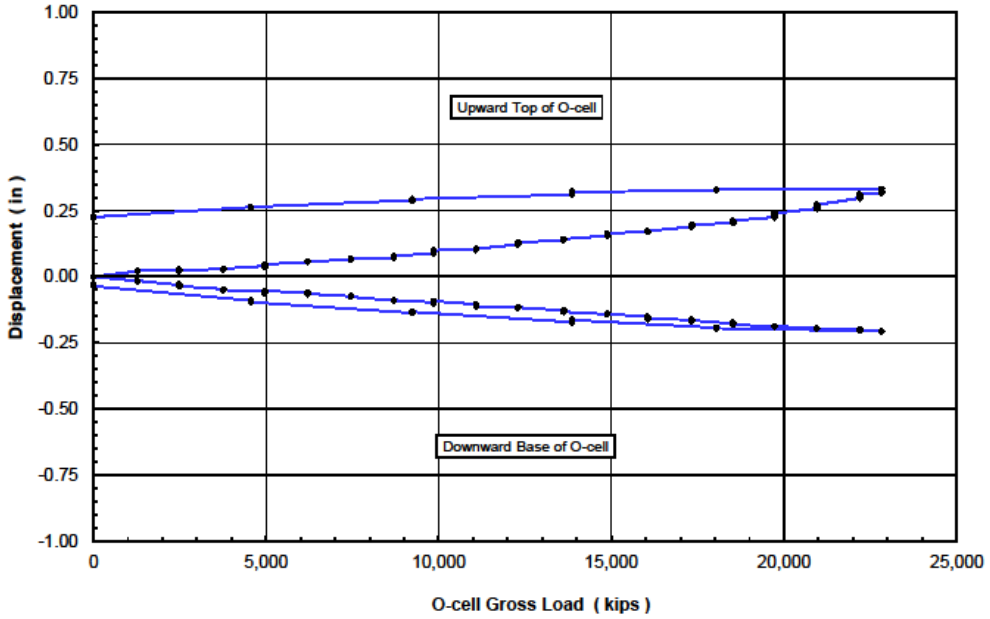


Fig. 4. Bi-directional load-displacement curves, TS1-NY (9-ft dia).

The measured axial resistances at TS2-NY (6-ft diameter) provide useful information regarding the influence of rock mass characteristics on socket resistances. Figure 5 shows the stratigraphy over the length of the socket at TS2-NY. The 6-ft diameter casing was driven to the top of weathered rock, which is 7-ft thick and is underlain by Passaic Formation siltstone and shale. The cored rock exhibits relatively high recovery (78 to 100 percent) but relatively low values of RQD. The entire socket is embedded in rock for which the RQD does not exceed 50 percent.

Over the depth of cored rock, from the O-cell to strain gage level 3 which is located at the interface between intact and weathered rock, the average unit side resistance was 30.6 ksf at an upward displacement of 0.11 inches. The weighted average RQD over this interval is 29. The maximum mobilized unit side resistance occurred between the O-cell and strain gage level 1, which lies predominately in the zone of core run C3 where RQD = 7. These test results demonstrate that RQD, taken by itself, is not necessarily an indicator of side resistance. The core photograph shows that the zones of high recovery but low RQD are a function of horizontally bedded siltstone and shale where the individual pieces of core do not exceed 4 inches in length, but side resistance of the socket was apparently not impacted adversely as long as the socket can be drilled without caving. The load test on TS2-NY clearly demonstrates this is the case.

© 2016 Deep Foundations Institute

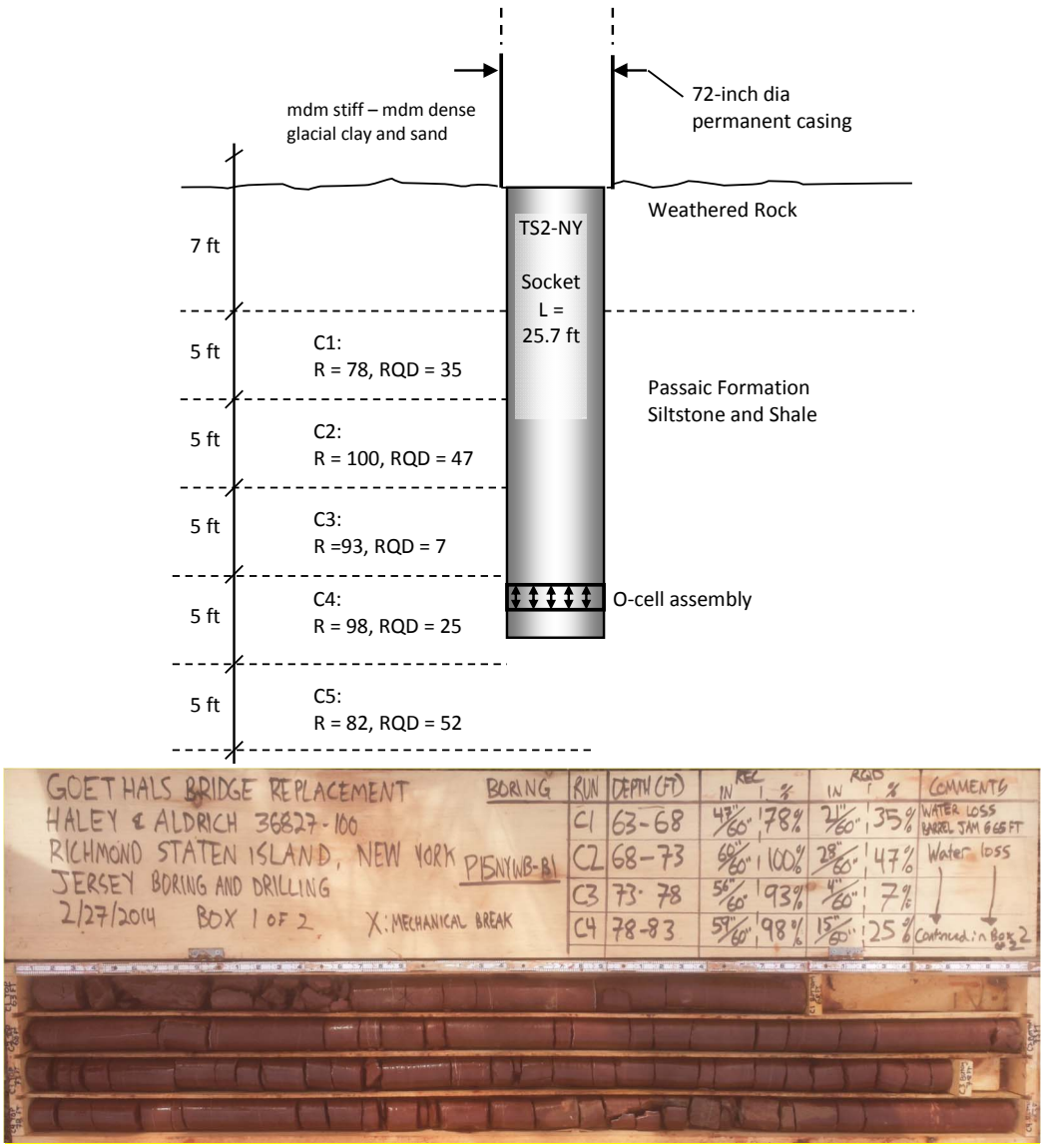


Fig. 5. Subsurface Profile and Rock Core at TS2-NY.

Similarly, the RQD of the rock immediately beneath the tip of the socket is relatively low. In core run C4, RQD is 25%, and the weighted average RQD over one socket diameter below the tip is 46%. Despite these low RQD values, the test results show a mobilized unit base resistance of 319 ksf at a downward displacement of 0.21 inch. The horizontal bedding planes in the rock are loaded in compression, which apparently does not adversely affect the bearing resistance. The lesson is that RQD alone may not be the best indicator of rock socket base or side resistance, but must be considered within the context of other rock mass characteristics, such as orientation of discontinuities relative to the direction of loading and the ability to excavate the rock socket without caving.

Lateral Load Tests

The static lateral load test was performed on TS4-NJ (6-ft diam.) utilizing TS3-NJ (9-ft diam.) for reaction prior to conducting any Statnamic lateral load testing. Figure 6 shows the overall arrangement, with the insert details the dynamometer load cell (pin connected at each end to a clevis) and the dial gages at the elevation of the applied load and attached to a stationary reference beam behind the shaft.

© 2016 Deep Foundations Institute

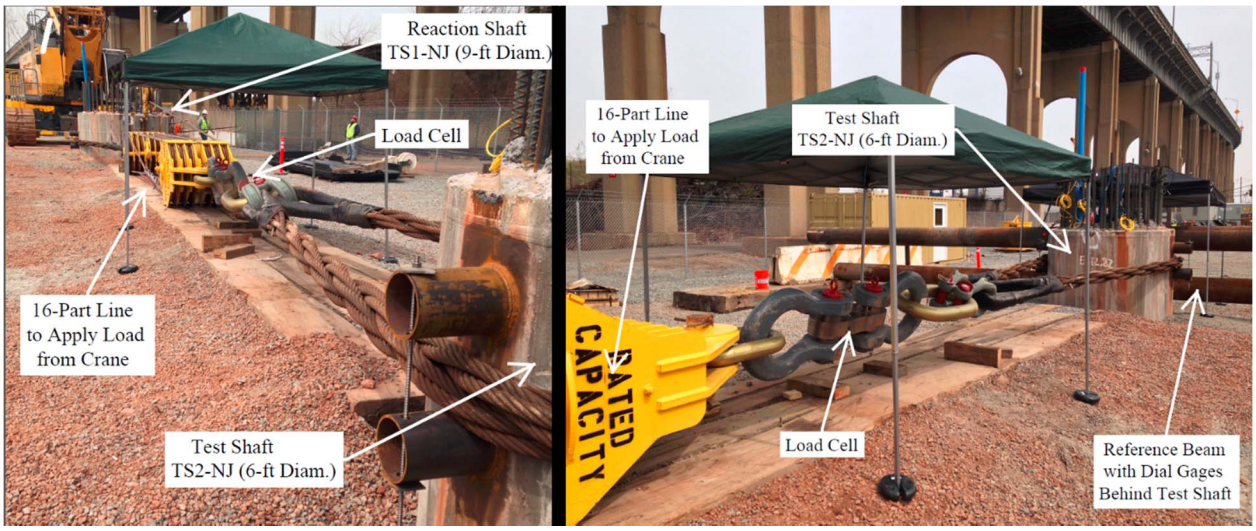


Fig. 6. Static Lateral Load Test Set-Up.

Each of the four test shafts was instrumented with strain gages and accelerometers along the length of the shaft to allow deflection and strain profiles to be established. Unlike the axial tests where the zone of interest is exclusively the rock socket, lateral response is affected significantly by the mobilized soil resistance provided by the overburden soils. Accelerometer readings were double integrated to yield the displacement profile of each shaft, while strain gages distributed over the shaft length provided the ability to establish where and when the shaft experiences the initiation and onset of cracking. The lateral load at the top of the shaft was measured directly by a calibrated load cell.

For the static test, the shaft was loaded in 10 increments up to the maximum of 425 kips and then unloaded in 4 decrements (ATSM D3966-07). Load increments were sustained for 10 minutes for the first two increments, 15 minutes for the third, and 20 minutes for all subsequent increments except that the maximum load of 425 kips was maintained for 60 minutes. Each load decrement was sustained for 10 minutes. At the maximum applied lateral load (425 kips) the measured lateral displacement was 1.26 inches and upon unloading the residual displacement (permanent set) was 0.33 inches.

The Statnamic lateral load tests were conducted with the device oriented laterally to produce the force against the top of the shaft, as is shown in Fig. 7. Load is generated by a combustion process in which the reaction mass (mounted on a sled) is pushed away from the shaft horizontally and thus delivers an equal but opposite force to the top of shaft. The load impulse lasts approximately 0.5 seconds.

Interpretation of lateral rapid-load test results requires the use of an analytical model that captures the soil structure interaction mechanisms of the test and incorporates those mechanisms into analyses used for design. The generated force has three components: (*i*) the static response (*ii*) soil damping, and (*iii*) an inertial force effect which can either reduce the load during acceleration or increase the load during deceleration.

Each test was modeled using commercially available software based on the *p-y* curve method of analysis. Input includes the stratigraphy at the test location, soil and rock *p-y* curve parameters for each soil or rock layer, and structural characteristics of the test shaft. The soil strength and stiffness characteristics (the *p-y* soil or rock model) were adjusted to provide agreement between the modeled responses and the actual measurements of load versus deflection at the top of shaft, as well as the deflection versus depth for each load. This back-fitting procedure provides site-specific calibration of *p-y* curve parameters used for design.

© 2016 Deep Foundations Institute

Table 3 summarizes the *p-y* curve parameters obtained through back-fitting of the four rapid-load and single static lateral load tests, and subsequently used for design of the shafts for the GBR.

Note that for *p-y* calibrations to be valid, it is important that the structural strength and stiffness properties of the shaft be representative of the actual *as-built* conditions (as opposed to the design values). For example, concrete strengths based on cylinder tests, which typically exceeded 6,000 psi, should be used in lieu of the concrete design strength of 5,000 psi. Underestimation of the structural stiffness of the shaft would lead to an overestimate (unconservative) of the strength and stiffness of the soil model in order to compensate.

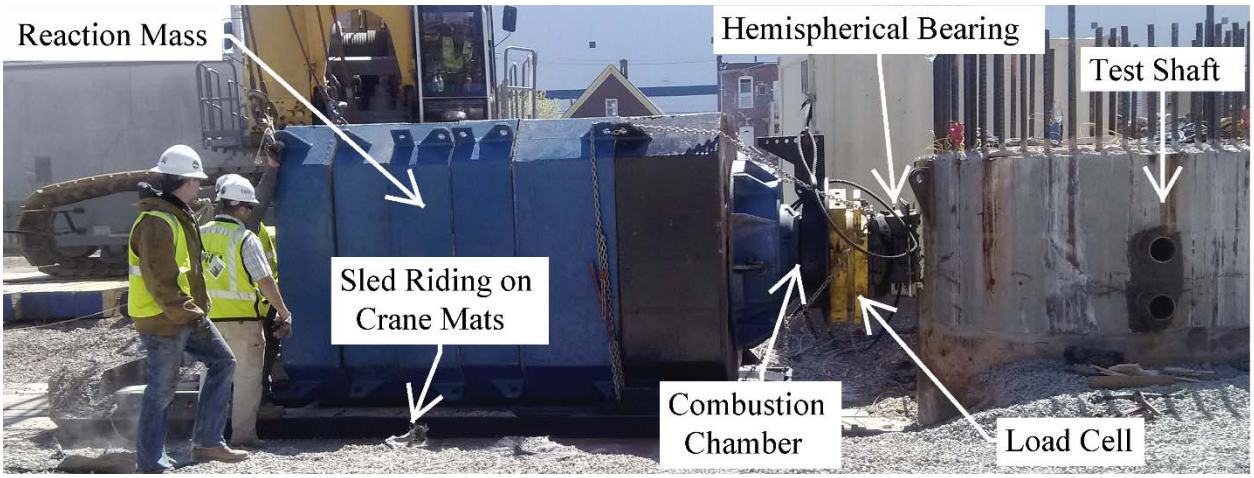


Fig. 7. Lateral Statnamic Load Test Setup.

Table 3. Soil and Rock Lateral Parameters.

Stratum		Model Parameters			
Organic Clays and Peat		Soft Clay (Matlock)	Effective Unit Weight =	50	pcf
			Undrained Cohesion "C" =	175	psf
			Strain Factor E_{50} =	0.015	
Marine Sands		Sand (Reese)	Eff. Friction Angle =	30 °	
			p-y Modulus "k" =	100	pci
Glacial Till	SPT N < 8 b/ft	Stiff Clay w/o Free Water(Reese)	Undrained Cohesion "C" =	600	psf
			Strain Factor E_{50} =	0.004	
	SPT 8 ≤ N ≤ 14 b/ft		Undrained Cohesion "C" =	2,500	psf
			Strain Factor E_{50} =	0.004	
	SPT N > 14 b/ft		Undrained Cohesion "C" =	4,000	pcf
			Strain Factor E_{50} =	0.004	
Weathered Rock		Weak Rock (Reese)	Youngs Mod., Er =	100,000	psi
			Comp. Strength =	500	psi
			RQD =	50%	
			k_rm =	0.0005	
Intact Rock		Weak Rock (Reese)	Youngs Mod., Er =	300,000	psi
			Comp. Strength =	2,000	psi
			RQD =	50%	
			k_rm =	0.00005	

© 2016 Deep Foundations Institute

Figure 8 illustrates a typical lateral load versus displacement curve from the rapid-load test, in this case for TS3-NJ (9-ft dia.). The measured response is compared to two models: (1) linear elastic shaft and (2) non-linear. The initial portion of the measured response curve is best captured by a linear elastic model until significant cracking develops. Beyond the onset of cracking, the measured response trends towards that predicted by a non-linear model at higher loads. Presumably the measured results would lie along the non-linear model predictions at loads higher than shown, or for longer load durations. Our recommendations for this project, as well as from numerous lateral Statnamic testing at other sites, were to bound the tested results by the linear elastic and non-linear models (both using the same soil and rock parameters), then utilize the non-linear model for design.

The lateral load testing at GBR afforded the unique opportunity to compare static and Statnamic lateral tests on a 6-ft diameter shaft at very high lateral loads. The static and equivalent static from Statnamic testing results for TS4-NJ are compared to the modeled behavior in Fig. 9. The Statnamic curve is offset by 0.33 inches to account for the permanent set at the end of the static test. At the maximum static test load of 425 kips, the deformation measured in the Statnamic test is reasonably close (within 7%) to that obtained from the static test, especially considering the 60 minute static hold time at this increment.

The nonlinear model, established by back-fitting of all four Statnamic tests, provides a good fit to the static load test results, and was used subsequently for design of the drilled shafts. The Statnamic results are initially stiffer along the re-load portion, but at greater loads the behavior is bound by the linear elastic and non-linear models. Comparison of the Statnamic results at the higher loads to the nonlinear model predictions (lying along then extending from the static curve) provides a means to account for time-dependent creep associated with the longer hold periods of the static test, ranging from 10 to 60 minutes.

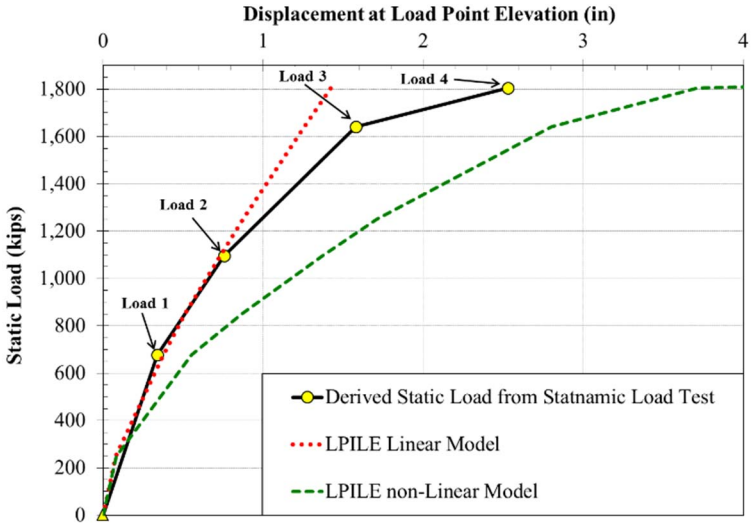


Fig. 8. Statnamic Lateral Test Results at TS3-NJ (9-ft diam.), Typical.

The Statnamic "equivalent static" behavior accounts for inertial and damping resistances; however, these results do not account for the time dependent soil displacement under constant load that occurs with hold periods as in the static load test. These creep effects are small at displacements of one inch or less but become more pronounced at larger displacements. However, creep adjustment is accounted for when the non-linear model of the reinforced concrete shaft is used, and therefore provides a means to account for time-dependent behavior that is not directly measured in a Statnamic test. The equivalent static response for Statnamic testing is representative of the shaft response to rapid loading that may occur Extreme Event load cases (*e.g.*, earthquake or vessel impact).

© 2016 Deep Foundations Institute

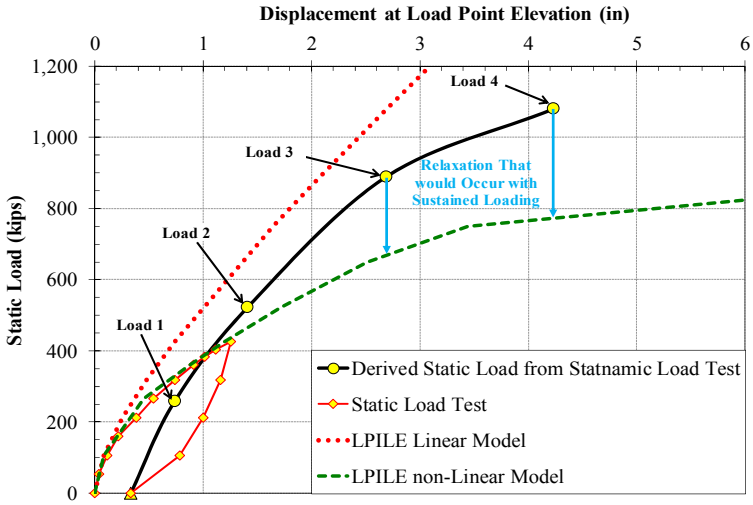


Fig. 9. Static and Statnamic Lateral Test Results at TS4-NJ (6-ft Diameter).

SUMMARY AND CONCLUSIONS

A program of axial and lateral load testing on drilled shafts for the Goethals Bridge Replacement Project is described. Axial load tests using the bi-directional load test method were aimed at establishing nominal values of unit side resistance and unit base resistance of sockets founded in Passaic Formation siltstone. Four load tests were performed and all of them yielded unit side resistance values exceeding 30 ksf and unit base resistance values exceeding 300 ksf. More importantly, the load tests demonstrated that side and base resistances are mobilized at compatible displacements and can be combined for LRFD design. Relatively high side and base resistances measured at a test location where rock RQD values were low (7 to 47 percent) illustrate that RQD, taken by itself, is not necessarily a relevant indicator of rock socket behavior. RQD is an index property, and must be considered within the context of other rock mass characteristics such as orientation of discontinuities, degree of weathering, direction of loading, stability of the excavated socket, and other relevant factors. Application of the test results design is described further in Turner et al. (2016).

Lateral load tests on the same four shafts by the lateral rapid-load method, or Statnamic test, were used to calibrate *p-y* curve parameters for each soil and rock layer encountered over the GBR alignment. A single static lateral test on the 6-ft diameter NJ test shaft was used to verify that the Statnamic test provides information sufficient to establish the equivalent static response of the shaft, in addition to simulating the shaft response to rapid loading that may result from seismic or impact loading.

ACKNOWLEDGMENTS

Bi-directional load testing was performed by Loadtest, Inc. of Gainesville, FL, under the supervision of Mr. Shing Pang. Lateral Statnamic testing was performed by Applied Foundation Testing, Inc., of Green Cove Springs, FL under the supervision of Mr. Don Robertson. The static load test was fabricated and performed under the supervision of Mr. Brannin Beeks of KWM. The authors wish to thank these individuals for their expertise and professional service in carrying out the GBR load testing program.

REFERENCES

Turner, J.P., Dapp, S.S., and Brown, D.A. (2016). Rock Socketed Drilled Shafts for the Goethals Bridge Replacement, *Proceedings*, International Conference on Deep Foundations, Seepage Control and Remediation, 41st Annual Conf. on Deep Foundations, DFI, NY.

© 2016 Deep Foundations Institute

PHYSICAL MODELING AND DEVELOPMENT OF DESIGN CRITERIA FOR MAINTAINABLE DRAINS FOR EARTH RETENTION SYSTEMS

Andrew Z. Boeckmann, University of Missouri, Columbia, MO, USA, 573-884-7613, boeckmanna@missouri.edu
J. Erik Loehr, University of Missouri, Columbia, MO, USA, eloehr@missouri.edu

ABSTRACT

Poor drainage is a common cause of poor performance of earth retention systems, resulting in burdensome serviceability problems that can progress to outright failure of the retention system if not addressed. A drainage system consisting of filtered conical drains that can be installed through the face of an existing retaining wall and readily maintained was evaluated through tests of physical and numerical models. The physical models were constructed with different backfill materials in a container measuring 8 ft wide by 4 ft tall by 15 ft long. Tests were conducted by saturating the backfill under a constant water elevation atop the model, and then maintaining the water elevation until seepage from the drains reached a steady state condition. Pore pressures within the backfill and outflow from the drains were measured to facilitate calibration of numerical models that accompany the physical models. Results from the calibrated finite element models were used to develop design criteria for the drains. The design criteria establish the required drain spacing as a function of the height of groundwater above the drains and the diameter of the drain.

Keywords: retaining wall, drainage, physical model, numerical model

INTRODUCTION

Many retaining wall performance problems are a result of poor drainage of the wall backfill. Consequences of poorly drained backfill include displacement and rotation of the wall face, including the extreme case of collapse, and seepage through the face of the wall, which is in turn associated with damage from corrosion, dry rot, and other forms of deterioration. A common approach to improve drainage of an existing wall is the installation of drainage features (e.g. "weep holes") in the face of the retaining wall. Weep holes facilitate controlled seepage through the face, which relieves water pressure within the backfill and directs seepage to known locations in the wall face. Although installation of weep holes is relatively common, engineering methodologies for selecting the size (diameter) and spacing (along the wall) of facial drainage features are uncommon if not altogether non-existent. This paper documents tests of physical and numerical models of retaining walls with facial drainage features, including conventional weep holes as well as maintainable drains installed through the face and extending into the wall backfill. Results of the testing were used to develop generic design criteria, which establish the required drain spacing as a function of the height of groundwater above the drains and the diameter of the drain.

PHYSICAL MODELING

Large-scale physical model retaining walls measuring 8 ft wide by 4 ft tall were constructed in the University of Missouri's large-scale geotechnical modeling laboratory. Silty sand was used as wall backfill for the first series of tests, and a clean sand was used as backfill for the second series of tests. Drainage features of varying size were installed at various spacing in the face of the retaining wall. To test the performance of the drains, a constant height of water was impounded behind the wall backfill while measuring outflow from the drains and pore pressures within the backfill. This section documents the various components of the testing before describing the stages of testing and presenting results.

Maintainable Drains

Drainage features for the physical models included conventional weep holes as well as conical drains that are installed through the wall face and extend into the backfill. The conical drains can be installed during

© 2016 Deep Foundations Institute

construction of a new wall, or through the face of an existing wall. As shown in Fig. 1, the conical drains consist of two pieces: an outer cone that is permanently affixed to the wall face, and an insert cone with geotextile filter that attaches to the outer cone. The insert piece can be removed to clean or replace the geotextile filter (hence "maintainable drain"). The geotextile used in the filters for testing is specified with an apparent opening size equivalent to the No. 30 sieve and a permittivity of 1.5 s^{-1}. Permittivity is defined by ASTM D 4491 (2016) as "the volumetric flow rate of water per unit cross sectional area per unit head…in the normal direction through a geotextile." Three size conical drains were tested, with nominal wall face openings of 2.5 in., 4 in., and 6 in. The conventional weep holes consisted of the same geotextile installed across wall face openings of the same nominal sizes as used for the conical drains.

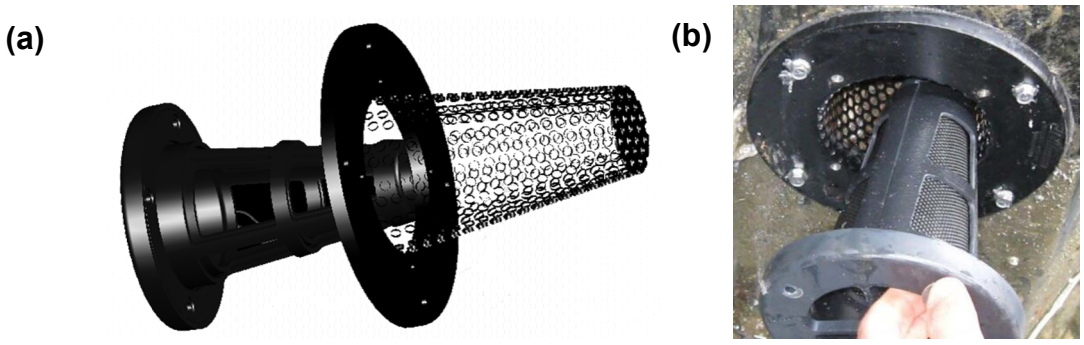


Fig. 1. Maintainable drains used in the physical and numerical models: (a) schematic representation, (b) photograph of drain installed through a concrete retaining wall.

Model Container and Water Control

The retaining wall was built inside the model container shown in Fig. 2. The container is 8 ft wide by 15 ft long with 4 ft sidewalls. A water control system consisting of 30 nozzles is fixed above the container. During testing, flow to the nozzles was controlled by a solenoid valve connected to a float switch inside the container to maintain a constant height of water. The data acquisition system records the time of operation during testing, so the total volume of water into the model container was approximately known.

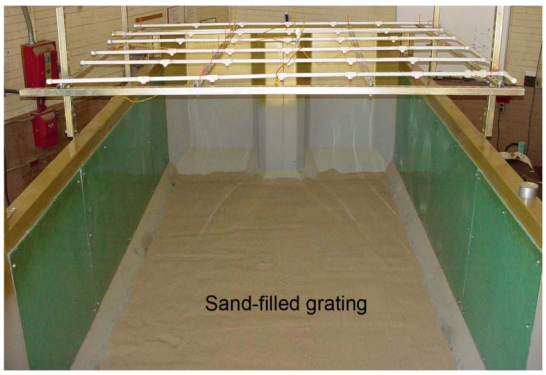


Fig. 2. Photograph of model container in which test retaining wall was built. Water control system shown above the container was used with a float switch to maintain a constant water level.

Test Soil Characteristics

Two test soils were used for the retaining wall backfill. The first series of tests was performed on a wall with silty sand backfill. The second series of tests was performed on a wall with fine sand backfill. Both test sands have the same source material, but the fine sand has been washed and screened to produce a more uniform gradation as shown in Fig. 3(a). Standard and reduced Proctor compaction curves for the silty sand

© 2016 Deep Foundations Institute

are shown in Fig 3(b). To account for the method of compaction used during construction (described below), a reduced Proctor test was performed to accompany the standard Proctor test. Both tests were performed according to ASTM D698 (2012), but the reduced Proctor test used 10 blows per lift instead of the specified 25. Additionally, the hydraulic conductivity of compacted specimens was measured according to ASTM D5856 (2015). For reduced Proctor compacted specimens with water contents from 5 to 9%, the hydraulic conductivity was approximately $3x10^{-6}$ ft/s ($1x10^{-4}$ cm/s). Hydraulic conductivity of the fine sand was measured with a constant head test (ASTM D2434, 2006) to be $2x10^{-3}$ ft/s ($6x10^{-2}$ cm/s).

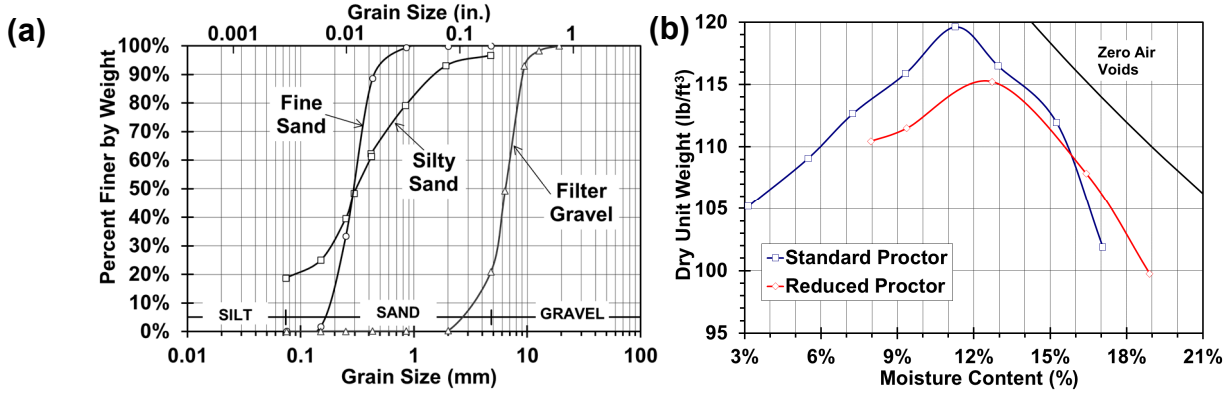


Fig. 3. (a) Grain size distributions for test soils and (b) Proctor compaction curves for the silty sand. Reduced Proctor specimens were compacted with 10 blows per lift.

Instrumentation

Testing of the model retaining wall included instrumentation to measure outflow from the drains and pore pressures within the wall backfill. Outflow was measured with tipping-bucket style gages. A magnetic counter records the number of times the bucket tips, which corresponds to a known volume of water. During testing, flow rates interpreted from the tipping-bucket gages were verified by weighing the volume of seepage from the model during 10-min. intervals.

Flexible tube tensiometers were used to measure pore pressures throughout the retaining wall backfill. The operating principle of the tensiometer is that unsaturated soil imposes a negative pressure (suction) on the saturated porous ceramic tip. The suction is transferred through the flexible line to a reservoir and pressure gage at the opposite end of the instrument. Tthe tensiometer gages were mounted atop the container to allow positive pore water pressures to be measured in addition to suction. The tensiometers were equipped with both electronic pressure transducers and Bourdon tube gages to allow for visual inspection of pore pressures and to verify output from the voltage transducers. Locations of the 14 tensiometers used during testing are shown in Fig. 4.

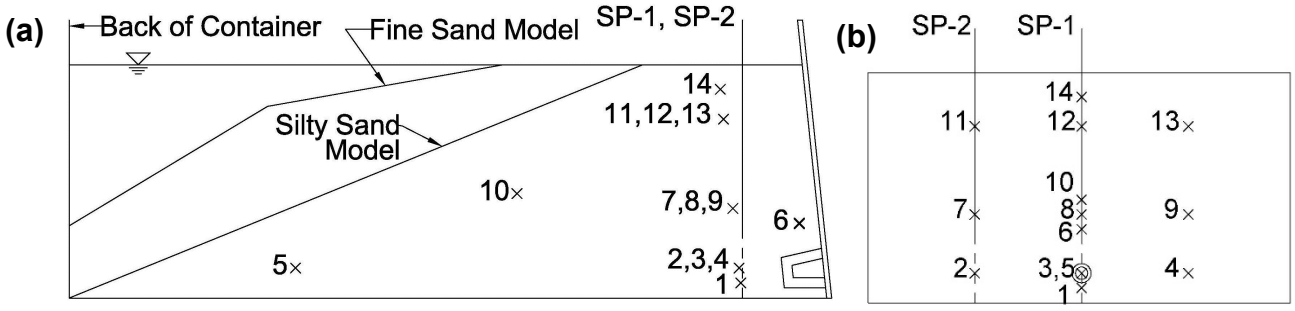


Fig. 4. Instrumentation locations: (a) cross section of retaining wall and (b) front view of retaining wall. "SP" designates standpipe piezometers and "x" designates a tensiometer location.

© 2016 Deep Foundations Institute

In addition, two standpipe piezometers were installed to measure the phreatic surface during testing. The PVC standpipes were installed full-depth and were located 2 ft behind the face of the retaining wall as shown in Fig. 4. The bottom 1-ft increment of each standpipe was slotted so that water levels in the standpipes correspond to pore pressures in the backfill approximately 1.5 ft behind the drain. A filter fabric covered the slots to prevent material from entering the pipes.

Construction of Model Retaining Wall

Photographs from construction of the physical model wall with silty sand backfill are shown in Fig. 5, and a photograph of the constructed wall with water impounded behind the backfill is shown in Fig. 6. For the first model wall, the silty sand backfill was placed in approximately 9-in. thick lifts. The backfill was dry of optimum during placement, and several samples were taken from each lift to measure water content. Lifts were compacted using a 400-lb smooth drum roller. For the second model wall, the fine sand backfill was placed without compaction using the bucket attachment of a small skid-steer loader. As shown in Fig. 4(a), the fine sand model was constructed with a greater total volume of backfill than for the silty sand model. The volume was increased for the second model to increase the seepage flow path distance and promote greater drawdown. The effect of backfill geometry is discussed in the results and numerical modeling sections.

The face of both model walls consisted of wood boards measuring 1.5-in. thick by 11.25-in. tall, with the boards placed in advance of the backfill lifts. Wood boards were selected for the wall face to facilitate simple laboratory construction. In reality, the maintainable drains generally can be installed in any type of wall face capable of supporting a hole extending to the backfill (e.g. steel sheet pile walls, concrete cantilever walls, etc.). Plastic sheeting was used to reduce the volume of water that would leak along the sides and bottom of the model container as well as the amount of seepage through the retaining wall face. Additionally, the inside of the bottom of the face was sealed with expansive polyurethane foam. During testing, some seepage was observed through the face of the model wall (e.g. Fig. 6), but the rate of seepage was too small to be measured. During construction of the model wall with silty sand backfill, one 4-in. diameter maintainable drain was installed in the center of the retaining wall face just above the bottom of the wall. The outer cone of the maintainable drain was surrounded with approximately 2-in. of gravel as shown in Fig. 5(b). During testing of the silty sand model wall, additional drains were installed closer to the sides of the model container, but these drains were inserted without gravel. For the fine sand model wall, both maintainable and conventional weep holes were tested, and all drains were installed without gravel. Additional details about drain spacing and diameters during testing are presented in the next section.

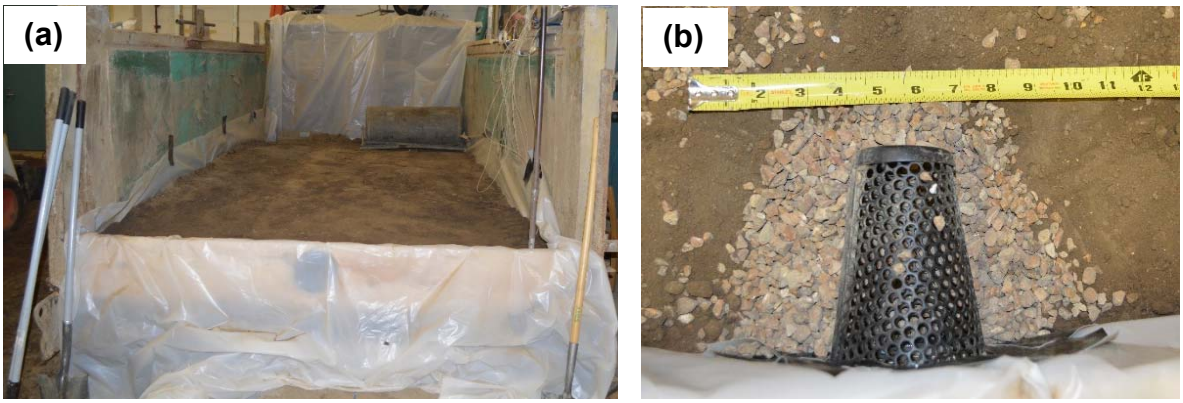


Fig. 5. (a) Inside of model container during construction, showing 400-lb smooth drum roller used for compaction and (b) maintainable drain installed through center of retaining wall face during construction. Gravel was placed around the outer cone of the drain during construction.

© 2016 Deep Foundations Institute

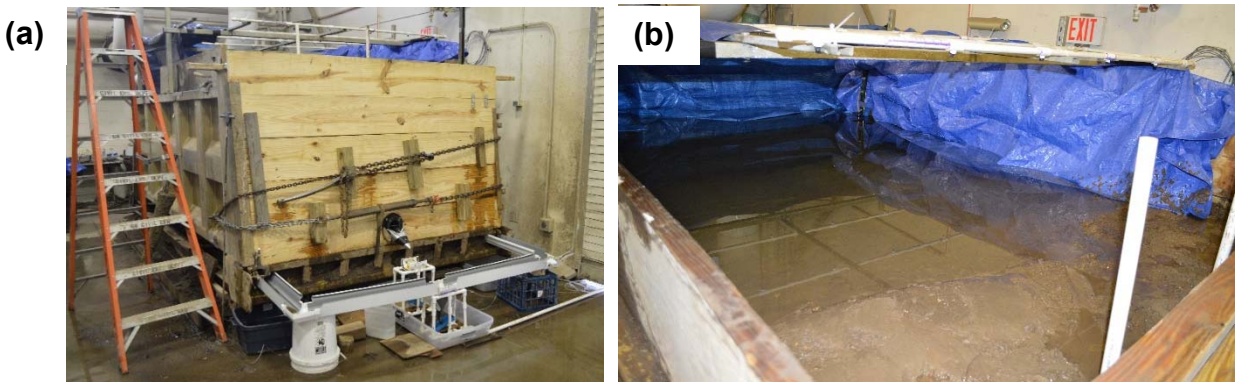


Fig. 6. Final constructed retaining wall: (a) front and (b) top with water impounded behind backfill.

Testing and Results

Testing of each model retaining wall consisted of several stages, which are described in Table 1. Drain type, diameter, and spacing were varied between stages. Steady state flows from the drains are also listed in Table 1, along with the corresponding drawdown values observed in the standpipe piezometers. The drawdown values are the vertical distance between the elevation of the water surface ponded behind the backfill and the elevation of the water in the standpipes located 2 ft behind the face of the model walls.

During the first stage for the silty sand model wall, a single 4-in. maintainable drain was installed in the center of the retaining wall face. As shown in Fig. 5(b), the outer cone of the 4-in. drain was surrounded by approximately 2-in. of gravel during construction. After testing the 4-in. center drain, a 2.5-in. maintainable drain was inserted inside the 4-in. drain outer cone. With this configuration, the center drain had the same size within the backfill as the 4-in. drain with gravel, but the face of the drain was equal to a 2.5-in drain. During Stage 3 of the silty sand model wall test, the center drain was sealed and two 2.5-in. maintainable drains were installed. The drains were located at outer quarter points along the wall face to test a spacing that is effectively half of that from Stages 1 and 2. Testing of the fine sand model wall consisted of seven stages, with three testing conventional weep holes and four testing maintainable drains. Between each test stage, a submersible pump was inserted in a well approximately 12 ft behind the wall face to dewater the backfill and facilitate swapping of the drains without significant loss of backfill through the wall face.

Table 1. Physical model test stages. For test stages with two drains, the outflow value listed is the sum of flows from both drains.

		Drain Information					Total Drain Outflow Rate, gpm	Drawdown, in.	
Model Wall	Test Stage	Type	Diameter, in.	Number	Effective Spacing, ft	Gravel around Drain?		Center	Quarter point
Silty Sand	1	Maintainable	4	1	8	Yes	0.035	6.6	3.3
	2	Maintainable	2.5	1	8	Yes	0.032	4.8	3.3
	3	Maintainable	2.5	2	4	No	0.010	3.3	3.7
Fine Sand	1	Weep	2.5	1	8	No	0.30	7.1	6.9
	2	Maintainable	2.5	1	8	No	0.32	7.9	7.8
	3	Maintainable	4	1	8	No	1.00	11.7	11.6
	4	Maintainable	6	1	8	No	1.47	16.0	15.8
	5	Weep	6	1	8	No	0.67	9.0	8.9
	6	Weep	2.5	2	4	No	0.78	12.3	12.8
	7	Maintainable	2.5	2	4	No	0.71	11.5	12.0

© 2016 Deep Foundations Institute

Several noteworthy observations arise from the results of Table 1:

- Drain outflows from the fine sand model were one to two orders of magnitude greater than drain outflows from the silty sand model. Drawdown in the fine sand backfill was also considerably greater than in the silty sand model. Backfill material was not the only difference between the models; the fine sand model wall had a greater volume of backfill material (Fig. 4(a)), which produces a longer flow path and therefore more head loss.
- For the silty sand model, the total drain outflow was nearly the same for Stages 1 and 2. This indicates the permittivity of the 2.5-in. drain was not controlling the second stage of the testing. If the permittivity were controlling, a more significant reduction in outflow between the first and second stages would be expected. Stage 3 resulted in notably less outflow than from the first two stages, which is likely a result of the smaller drain size into the backfill, especially with the absence of gravel around the 2-in. drains.
- Results of tests of the fine sand model indicate drain outflow and drawdown within the backfill both increase with drain size.
- Both weep and maintainable drains were tested for the fine sand model. The effect of drain type depended on drain size. For 2.5-in. diameter drains installed at the same effective spacing, the outflow and drawdown values were similar regardless of drain type. For 6-in. diameter drains, the outflow and drawdown were approximately twice as great for the maintainable drain as for the conventional weep hole. A likely explanation for the difference between drain types is that the conical maintainable drains have greater surface area than the planar weep holes, and the greater surface area promotes more drainage. The surface area effect is muted for smaller diameter drains, not only because the difference in surface area is less but also because most of the increased surface area is contained in the wall face opening as opposed to being in contact with the backfill soil.

NUMERICAL MODELING

Three-dimensional finite element models were created to evaluate the results of the physical models. Additional models were created to evaluate the effect of facial drainage features on a generic retaining wall. The numerical models were created with *RS*^{3} (Rocscience, Inc., 2014; Version 1.021). Results are presented in the sections below.

Numerical Model of Retaining Wall Test

The *RS*^{3} model of the test of the silty sand physical model is shown in Fig. 7. The model includes three materials: silty sand backfill, gravel, and a material used to represent the drain. Hydraulic conductivity of the backfill was adjusted to calibrate the model as discussed below. The gravel material was used to model the gravel behind the drain (Fig. 5(b)) as well as the empty space within the cone-shaped drain to avoid including a void in the numerical model. The value of hydraulic conductivity used for gravel in the model is 3×10^{-2} ft/s (1 cm/s). The thickness and hydraulic conductivity of the region used to represent the drain were selected to equal the permittivity of the geotextile inside the drain, 1.5 s^{-1}.

Boundary conditions are depicted in Fig. 7(a). A total head boundary corresponding to the water level in the model container was applied to the exposed face of the backfill. No-flow boundaries were applied along every other boundary except for the face of the drain, where a seepage face was modeled. Seepage through the face of the retaining wall was therefore not included in the model; this is a reasonable approximation considering the small rate of seepage that was observed through the model wall face. The three-dimensional mesh is shown in Fig. 7(b) and consisted of ten-noded tetrahedrons. The *RS*^{3} model of the fine sand physical model is similar to the numerical model of the silty sand wall, but with slightly different backfill geometry to match the final constructed surface of the fine sand model, a different hydraulic conductivity value for the backfill, and drain inputs adjusted to match the configurations described in Table 1.

© 2016 Deep Foundations Institute

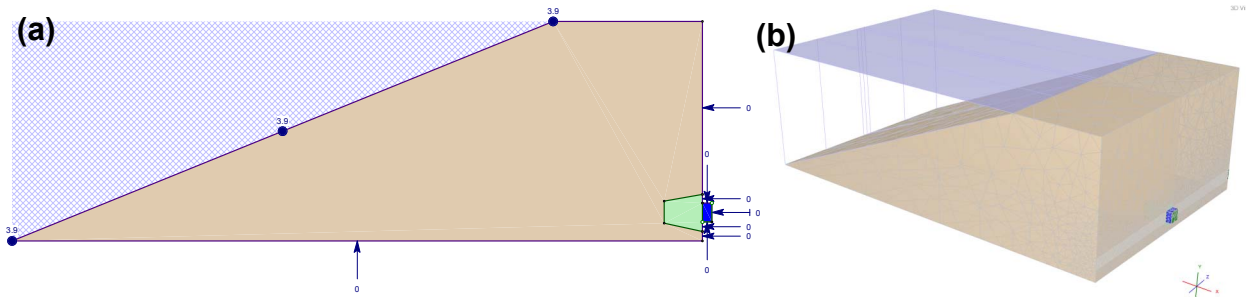


Fig. 7. Rocscience *RS*^{3} numerical model of silty sand retaining wall test: (a) in 2-D and (b) in 3-D.

Calibration of the *RS*^{3} models was achieved by adjusting the hydraulic conductivity of the backfill until the numerical model predicted values of drain outflow and drawdown that reasonably match those listed in Table 1. Drawdown was primarily evaluated based on standpipe piezometer data, but tensiometer results were also considered. Evaluation of various trial models during calibration confirmed that drain outflow is sensitive to changes in backfill hydraulic conductivity. The same evaluations also revealed that drawdown is less sensitive to changes in backfill hydraulic conductivity and is affected more by changes in model geometry, with longer flow paths resulting in greater drawdown. This observation was the basis for increasing the volume of backfill used to construct the fine sand physical model in order to promote greater drawdown. Because drain outflow is sensitive to backfill hydraulic conductivity but drawdown is not, outflow measurements were more critical to calibration of hydraulic conductivity values than piezometer or tensiometer measurements. For the silty sand model, the calibrated hydraulic conductivity of the backfill is $2x10^{-5}$ ft/s ($6x10^{-4}$ cm/s), which is approximately seven times greater than the value measured by ASTM D698. For the fine sand model, the calibrated hydraulic conductivity of the backfill is $8x10^{-4}$ ft/s ($2x10^{-2}$ cm/s), which is 2.5 times less than the value measured according to ASTM D2434. The differences between calibrated and laboratory hydraulic conductivity values are significant but not unreasonable considering the variability of hydraulic conductivity measurements for compacted soils.

Figure 8 shows interpreted values of the phreatic surface from tensiometers and piezometers as well as the phreatic surface predicted by the numerical model for Stage 1 of the silty sand model and Stage 3 of the fine sand model. Both stages included one 4-in. maintainable drain. The phreatic surfaces predicted by the numerical model are reasonably close to the locations observed in the physical model, especially the piezometer observations. Locations interpreted from tensiometer pressures are more variable, but generally consistent with results of the numerical model. As discussed above, the pore pressure regime predicted by the numerical model is strongly influenced by the geometry of the backfill and drain and influenced less by the backfill hydraulic conductivity.

Numerical Models for Full-scale Retaining Walls

A separate *RS*^{3} model was created to evaluate drainage feature design criteria for full-scale retaining walls. The numerical model is simple, including three components: the drain, backfill, and a groundwater source behind the wall. The drain was modeled with gravel, similar to the model described above. The backfill was modeled with hydraulic conductivity of $3x10^{-5}$ ft/s ($1x10^{-3}$ cm/s), which is similar to the fine sand used in the second physical model. Other values of hydraulic conductivity were evaluated but did not affect design criteria results significantly, as discussed below. The location of the groundwater source (essentially the length of the finite element model) is an important parameter. If the location is relatively close to the face of the retaining wall, it greatly influences the drawdown resulting from the drains. A series of models with varying source distances was evaluated to determine an entry distance that appropriately balanced the impact on model results with the computational demand of the model. An entry distance of 1000 ft was selected; the effect of this distance on model results is small, and greater entry distances have impractically high computational demand.

© 2016 Deep Foundations Institute

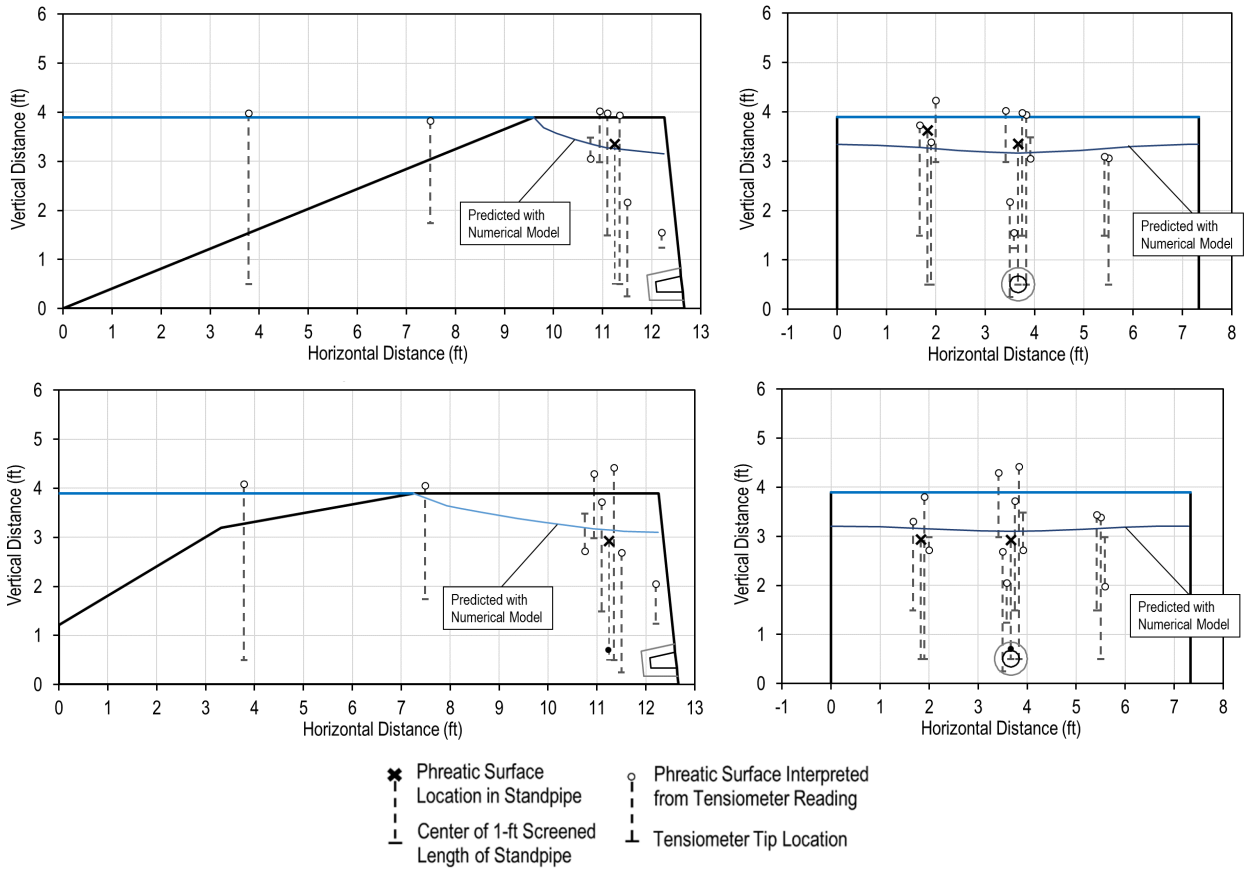


Fig. 8. Phreatic surface observations from physical models and phreatic surface locations predicted by calibrated *RS*^{3} models: (a) cross-section through center of silty sand model, Stage 1; (b) front view of wall for silty sand model, Stage 1; (c) cross-section through center of fine sand model, Stage 3, and (d) front view of wall for fine sand model, Stage 3.

DESIGN CRITERIA

To develop design criteria, several variations of the model described above were evaluated. Three drain sizes were considered: 2.5-in., 4-in., and 6-in. diameter. In addition, two drain types were considered: conical drains (such as the maintainable drains) that penetrate the backfill and conventional weep holes that do not penetrate the backfill. For each drain configuration, multiple heights of groundwater above the drain were considered. For each combination of drain configuration and groundwater height, the drain spacing was varied to determine the effect of spacing on the pressure head on the face of the retaining wall and on the flow from the drain. Example results are shown in Fig. 9. As shown in Fig. 9(a), the pressure head on the face of the retaining wall increases linearly as spacing increases, with greater pressure experienced between the drains compared to the cross-sectional plane of the drains. For closer spacing, no pressure develops in the plane of the drain (e.g. spacing of 10 ft and below in Fig. 9(a)). The results of Fig. 10(b) show drain outflow increasing linearly with spacing; that there is no reduction in flow indicates the permittivity of the drains does not control for any of the configurations considered. Fig. 9 includes results for sandy backfill with hydraulic conductivity of $3x10^{-5}$ ft/s ($1x10^{-3}$ cm/s) as well as clayey backfill with hydraulic conductivity of $3x10^{-8}$ ft/s ($1x10^{-6}$ cm/s). The effect of hydraulic conductivity on the pore pressures predicted by the model is negligible, as demonstrated in the results of Fig. 9(a). The drain outflow predicted by the model is directly proportional to backfill hydraulic conductivity: as shown in Fig. 9(b), the predicted drain outflow values from the model with sand backfill are 1,000 times greater than the corresponding values in the model with clay backfill. These observations regarding the effect of backfill material on pore pressures and flow are consistent with observations from the physical models.

© 2016 Deep Foundations Institute

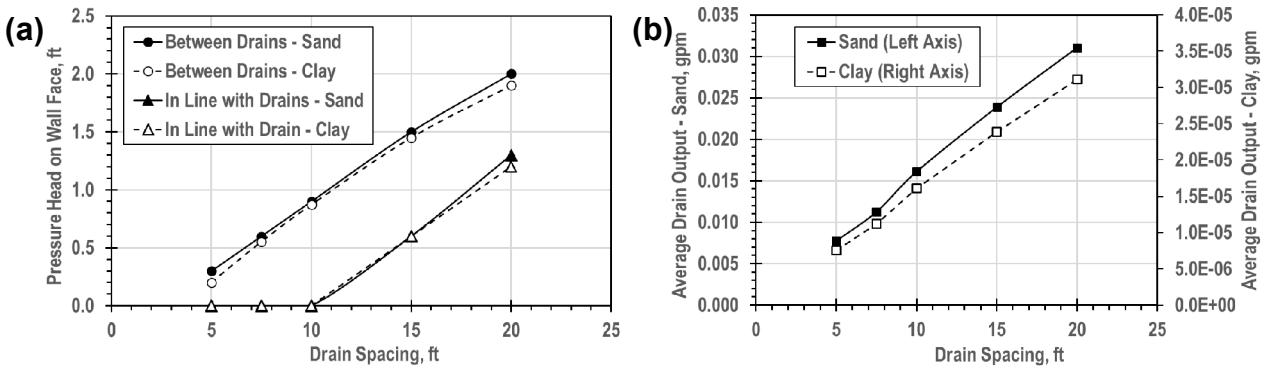


Fig. 9. Results of design evaluation analysis for 4-in. conical drains and groundwater 20 ft above drain: (a) pressure head on wall face versus spacing and (b) drain outflow versus spacing. Note drain output values are plotted on separate axes; drain outflow values from the clay model are 1,000 times less than values from the sand model.

Design criteria were developed by determining the spacing at which no pressure develops above the drain elevation on the face of the retaining wall (e.g. spacing of 10 ft and below in Fig. 9(a)). From a stability perspective, this is a relatively conservative criterion since it typically corresponded to less than 2 ft of pressure head on the face of the wall between the drains. However, the criterion is prudent for maintenance and general performance considerations. More aggressive criteria could be developed based on other considerations such as external and global stability for design of individual retaining walls. Other considerations that would require project-level analyses include walls with more than one row of drains (to determine the required vertical and horizontal spacing) and walls with drains consisting of geotextiles having permittivity not equal to 1.5 s^{-1}. Lastly, the design criteria do not consider filter compatibility with backfill material, which would more adversely affect the conventional (non-maintainable) weep holes.

The proposed general design criteria for each drain are shown in Fig. 10, with points showing values determined from the numerical model analyses and lines interpreted by the authors. Two sets of design criteria are presented, Fig. 10(a) for the conical drains penetrating the backfill and Fig 10(b) for drains that do not penetrate the backfill. The difference between the two sets of criteria is considerable, with backfill penetration corresponding to greater drawdown and therefore greater allowable spacing compared to drains that do not penetrate the wall backfill. The difference in the two criteria is consistent with observations from the physical model tests.

Several other comments regarding the design criteria are noteworthy:

- The allowable spacing was capped at 30 ft to include a practical limit that accounts for local variations in groundwater conditions and any other potential considerations that could impact wall performance for greater spacing.
- The maintainable drains modeled for this study (Fig. 1) should only be designed according to Fig. 10(a) if the wall face thickness is sufficiently thin to facilitate penetration of the backfill; otherwise (e.g. for thick concrete cantilever walls), the maintainable drains should be designed according to Fig. 10(b). All conventional weep holes should be designed according to Fig. 10(b).
- The horizontal axis of Fig. 10 was defined to allow designers some flexibility in vertical placement of the drains (rather than conservatively but impractically assuming the drain is at the base of the wall). As a result of this definition, the backfill material below the drain will be saturated and water pressure will be exerted on the wall face below the drain.
- For most values of groundwater height, there are several drain size-spacing combinations that satisfy the design criterion, leaving designers the option of specifying a greater number of small drains or a lesser number of large drains. Selecting the option of smaller drains at closer spacing is

© 2016 Deep Foundations Institute

perhaps associated with greater reliability compared to larger drains at greater spacing, but the smaller drain design option is also likely associated with greater installation and maintenance costs. Designers should consider these impacts when selecting their design configuration.

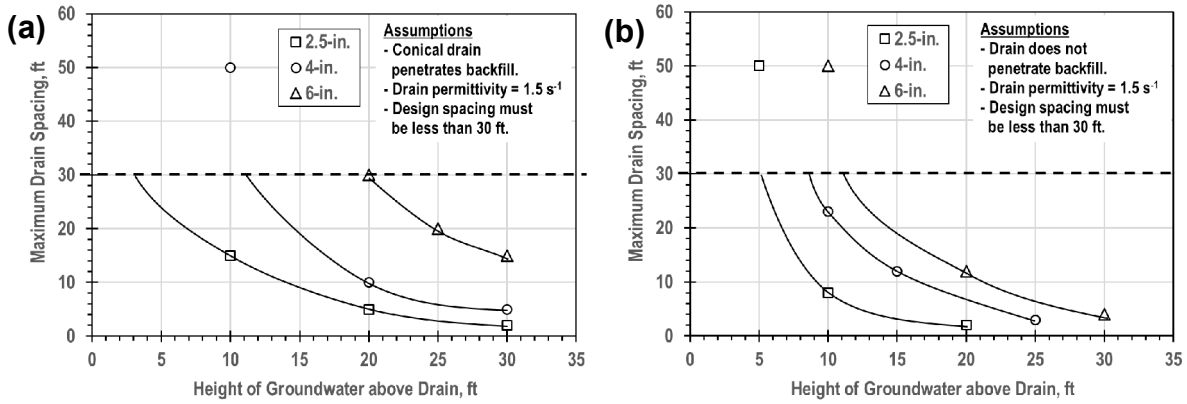


Fig. 10. Design criteria results for (a) conical drains which penetrate backfill and (b) drains that do not penetrate backfill. Results of design criteria analysis are shown with open symbols. Lines represent proposed design criteria.

SUMMARY AND CONCLUSIONS

Tests of physical models and numerical models of retaining walls with facial drainage features indicate such features effectively reduce water pressures that develop on the face of retaining walls. Results of both physical and numerical models indicate backfill hydraulic conductivity controls the volume of seepage through the drains but has less impact on the drawdown within the backfill. Drawdown within the backfill is controlled by geometric considerations, including the distance to the groundwater source, the size of the drain, and penetration of the drain through the wall face into the backfill. Each of these effects was observed in results of both the physical and numerical models. The effects are also reflected in the design criteria that were developed using the numerical models. Design criteria were developed for maintainable conical drains that penetrate the wall backfill as well as for drains that do not penetrate the wall backfill, including conventional weep holes. The latter set of criteria is associated with closer recommended drain spacing. The design criteria are general and do not address all situations, notably situations when permittivity controls, backfill is not compatible with the drain geotextile, or multiple rows of drains are included.

REFERENCES

ASTM Standard D698, 2012. Standard Test Method for Laboratory Compaction Characteristics of Soil Using Standard Effort, ASTM International, 13 p.

ASTM Standard D2434, 2006. Standard Test Method for Permeability of Granular Soils (Constant Head), ASTM International, 6 p.

ASTM Standard D4491, 2016. Standard Test Methods for Water Permeability of Geotextiles by Permittivity, ASTM International, 8 p.

ASTM Standard D5856, 2015. Standard Test Method for Measurement of Hydraulic Conductivity of Porous Material Using a Rigid-Wall, Compaction-Mold Permeameter, ASTM International, 9 p.

Rocscience, Inc., 2014. RS^3 1.0: 3D Finite Element Analysis for Rock and Soil, Version 1.021, August 10, 2016.

© 2016 Deep Foundations Institute

PRACTICAL CONSTRUCTION CONSIDERATIONS FOR RUNWAY EXTENSION AND TAXIWAY EXPANSION OVER SOFT/ORGANIC SOIL USING A COLUMN-SUPPORTED LOAD TRANSFER PLATFORM

Brian T. Nereson, P.E., GeoInsight, Inc., Manchester, New Hampshire, USA; Ph (603) 314-0820 and Michael C. Penney, P.E., GeoInsight, Inc., Manchester, New Hampshire, USA; Ph (603) 314-0820

ABSTRACT

This technical paper was prepared to describe the general process by which the authors designed a column-supported load transfer platform (LTP) for support of asphalt-paved runway and taxiway embankment areas over soft organic soils, the major tasks and observations made during construction of the system, and the outcome of the system design and construction. The LTP system was designed using the method described in the BSI Standards Publication Code of Practice for Strengthened/Reinforced Soils and Other Fills, BS 8006-1:2010 (BS8006), to achieve performance objectives for the project. The design also used other criteria based upon the authors' engineering experience and understanding of the expected interaction between soils, structures and geotextiles. The design and construction process described herein resulted in a successful project. The authors identified that full-time engineering oversight during construction was of high importance and provided a high degree of value to the project. The authors' intimate knowledge of the potentially adverse effects of variations in construction practices promoted timely identification of construction deficiencies that could have affected the reliability of the system. This resulted in corrections and modifications being made, while materials were still accessible, to protect the intended performance of the finished system.

INTRODUCTION

The site is located in Marshfield, Massachusetts. The surrounding area is flat and contains significant wetlands with a water table at or near the ground surface. Prior to the improvements described herein, the site was already developed as an existing municipal airport with an approximately 3,000 linear-feet asphalt-paved runway oriented in a northeast/southwest direction (northeast end referred to as Runway 24 and southwest end referred to as Runway 6; Fig. 1). The site is located approximately 0.5 to 1 mile (Runway 24 and Runway 6, respectively) from the Atlantic Ocean.

The improvement project included total extension of approximately 550 linear feet of asphalt-paved runways and taxiways over existing wetlands that consisted of soft, organic soils with varying but significant depths (Fig. 2). An initial geotechnical assessment performed for the project identified that the subsurface conditions were not suitable to support the proposed runways and taxiways in their existing state.

The project constraints included, but were not limited to, previously-prepared wetland environmental impact approvals that strictly limited the allowable project boundary to the edge of planned construction areas. Therefore, soil excavation and its associated extended soil sloping beyond the footprint of the runway limits was not feasible. Post-construction settlement was required to be negligible so that the transition between the old and new runways and taxiways would be imperceptible.

Runway 24 was at approximately elevation (El.) 0 feet and Runway 6 was at approximately El. 9 feet. The approximately 100 linear feet of Runway 24 extension and approximately 50 linear feet of Runway 6 extension were surrounded by wetlands on three sides at approximately El. -1 feet (Runway 24) and El. 5 feet (Runway 6). Additionally, approximately 400 linear feet of taxiway widening was bordered on one

© 2016 Deep Foundations Institute

side by wetlands. Groundwater was generally at or just below the ground surface, which significantly added to the sitework challenges.



Figure 1: Aerial Site Image Prior to the Project



Figure 2: Aerial Site Image After the Project

SUBSURFACE CONDITIONS

Subsurface conditions generally consisted of shallow surface fill underlain by an organic wetland deposit, a marine sand deposit, a marine fines deposit, a thin glacial till deposit and bedrock. The organic wetland deposit was observed to maximum depths of approximately 22 feet below ground surface (bgs), and was generally described as very soft to soft organic silt with varying amounts of organic root fibers and trace amounts of fine sand. The marine sand deposit was observed to depth ranging from approximately 20 to 37 feet bgs, and was generally described as very loose to loose, fine to medium sand with trace amounts of gravel and silt. The marine fines deposit was observed to range from approximately 3 to 7 feet in thickness and was generally described as very soft to medium stiff, elastic silt or clay with trace amounts of fine sand. The top of the glacial till deposit was observed at depths ranging from approximately 33 to 40 feet bgs, was approximately 6 to 12 feet thick, and was generally described as medium dense to very dense, heterogeneous mixture of fine to coarse sand and gravel with little to trace amounts of silt. Refusal surfaces indicative of bedrock were encountered at depths ranging from approximately 39 to 50 feet bgs.

EMBANKMENT SUPPORT ALTERNATIVES

The authors considered various economical geotechnical solutions as being feasible alternatives if some degree of risk (i.e., potential settlement) was acceptable to the client, including support of the embankments and pavements on soils improved with rammed aggregate piers or controlled-modulus columns, or partial excavation of unsuitable soils and replacement with light-weight structural geofoam blocks. The authors considered the use of structural sheeting, cantilevered soldier beams and lagging, or structural sheeting with tie-back anchors to allow for complete over-excavation of the unsuitable soil and replacement with compacted structural soil. However, subsurface conditions were such that over-excavation and replacement methods were uneconomical due to the cost of shoring, dewatering, and unsuitable material management. The client considered soil improvement methods or partial over-excavation and replacement alternatives to carry too much risk. Preloading of the expansion areas with a surcharge was also considered, but the client would not allow the runways to be out of use for the time period needed to cause significant compression of the organic deposits, and some additional long term settlement would still be possible with this approach, so it was eliminated from consideration. As such, the authors proposed supporting the new runway pavement systems and adjacent embankments on load transfer platforms (LTPs) supported by timber piles. It should be noted that rigid inclusions such as controlled modulus columns or stone columns are also technical feasible for supporting the LTP; however, timber piles were chosen based upon the client's familiarity with timber piles.

© 2016 Deep Foundations Institute

This alternative was highly beneficial with respect to eliminating the need for soil management, nearly eliminating dewatering, and mostly eliminating adverse impacts to the surrounding wetlands. Activities performed to improve the runway expansion areas were conducted entirely within the limits of allowed wetland disturbance boundaries. Greater than 2,000 timber piles were installed to support approximately 5,500 square yards of LTP. Embankment fill and pavement layers, as well as adjacent vegetated runway safety areas, were constructed above the LTPs. Measureable or observable settlement of the pavement and turf areas constructed above the extent of the LTPs was not identified after construction of the structures. Nearly two years after construction of the improvements, airport staff have not observed noticeable airport runway pavement deformation.

LOAD TRANSFER PLATFORM DESIGN

General

The LTP generally consists of a relatively stiff structural "mattress" layer that can be constructed using geogrid or geotextile confining reinforcement and select internal aggregate materials that are part of an overall system used to support and transfer loads past an unsuitable bearing zone to a suitable bearing layer. The LTP performs in a three-dimensional manner in which vertical loads applied to the surface of the mattress, which is the platform, are transferred on the horizontal plane by the tensile capacity of the geogrid/geotextile confining reinforcement layer(s). The mattress-supported loads are then transferred past the unsuitable bearing layer to a suitable bearing layer via closely-spaced vertical support columns (Fig. 3).

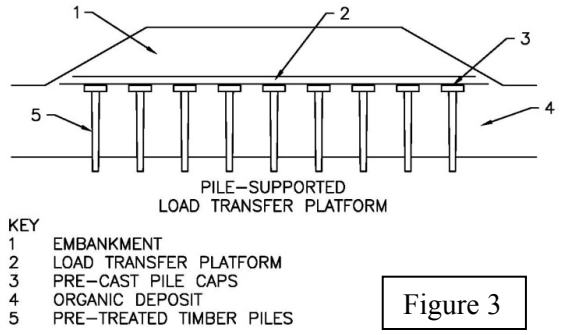


Figure 3

Design of the LTP was performed using the BSI Standards Publication Code of Practice for Strengthened/Reinforced Soils and Other Fills, BS 8006-1:2010 (BS8006). Other LTP design methods are known to exist that were considered as appropriate design methods (including the new German method, the Dutch method, catenary and beam methods, and others); however, other design methods are not discussed herein. In the U.S., LTP design methods commonly use catenary and beam methods.

For the purposes of this project, the mattress platform was constructed using an upper and lower very high-strength woven geotextile encapsulating a dense-graded structural fill. The mattress was constructed on top of pre-cast pile caps and the embankment fill materials were installed directly on top of the mattress. The vertical columns were designed and constructed as timber piles acting in end-bearing and side friction in the inorganic materials below the organic layer. Timber piles were designed and installed to achieve vertical download capacities ranging from 16 to 20 tons, as required to support up to approximately 5 feet of compacted select aggregates and the relatively low live loads associated with moderately-sized aircrafts. Geotechnical design of timber pile capacity is well documented in the field of geotechnical engineering, and further discussion of timber pile vertical and lateral capacity design is not included herein.

Primary considerations for the LTP design included:

- design vertical loads on the LTP resulting from embankment loads, applied dead loads and live loads;
- pattern and spacing of vertical support columns and width of pile caps, which controls the unsupported geotextile length between pile cap edges;

© 2016 Deep Foundations Institute

- sequencing of the work to properly prepare the subgrade for the LTP, including soil removal and placement, and dewatering;
- tensile loads in the geotextile developed due to vertical loads, and unsupported geotextile lengths and the geotextile strain from the resulting tensile loads;
- behavior of the LTP in a three-dimensional manner thus requiring tensile forces to be considered in biaxial directions along the plane of the geotextile layers;
- termination details for the LTP at the edges of the embankment/limits of work, which typically required design of anchors on top or adjacent to exterior vertical columns rather than extending the LTP over suitable soils to construct anchorage; and
- selection of appropriate factors of safety for various system components (i.e., applied loads, geotextile reinforcement, vertical support column capacity, etc.).

It should be noted that evaluations of the specific design parameters discussed in the following sections are a general summary of the primary design parameters and evaluations performed by the authors for this project. Additional evaluations and calculations were performed that are not discussed in whole or in part in this paper.

Pile Spacing, Orientation and Pile Cap Design

Pile spacing selection is a critical consideration for design of the LTP. In general, greater pile spacing results in lesser total piles to be installed (and thus lower vertical support columns costs). However, the spacing must be considered in conjunction with the tensile load that the reinforcement layer must carry. Greater spacing also increases the load at each pile location. Calculation of the reinforcement tensile load is discussed in the sections that follow. The ramifications of increasing the pile spacing include significant increases in tensile loads on the reinforcement layer and potentially unacceptable strains. In fact, the availability of high-strength geotextile reinforcement may be a limiting factor in pile spacing (i.e., at some given pile spacing, the tensile load in the reinforcement layer will be greater than available geotextiles can resist within tolerable strain limits).

For this project, the authors used an iterative approach whereby various pile spacing and pile cap widths were analyzed and the resulting tensile load in the reinforcement layer was determined until a given pile spacing and cap dimension resulted in a suitable maximum reinforcement tensile load at a pre-determined allowable strain limit. The resulting design consisted of piles oriented in a square grid with a center-to-center spacing of 5 feet in each direction, and pile cap dimensions of 2 feet by 2 feet square (Fig. 4).

The pile cap design was also given consideration. Larger pile caps favorably decrease the unsupported span of the geotextile, but then become subject to higher internal stresses, requiring more reinforcing steel and a thicker section. Larger caps were also considered to be more susceptible to accidental vertical displacement by equipment travelling over the caps.

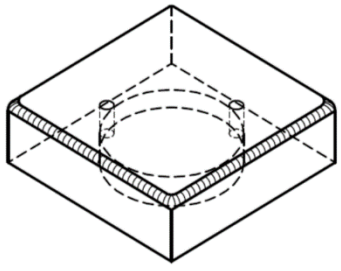


Figure 4: Typical Pre-Cast Pile Cap

Specific considerations included how the pile caps would be connected to the pile butts, and constructing the pile caps with rounded edges to reduce the potential for sharp pile cap edges to damage the overlying geotextile reinforcement layer. The pile caps were constructed with two ports through the cap and into the pile butt socket to allow for grout to be injected into the sockets to secure the pile caps to the pile butts.

© 2016 Deep Foundations Institute

Vertical Load Determination

Vertical loads on the vertical support columns and LTP were determined using Marston's formula as described in BS8006, where the vertical stress on the pile caps is equal to:

Equation 1: $$p'_c / \sigma'_v = [C_c a / H]^2$$

Where: p'_c = vertical stress on the pile caps
$\sigma'_v = (f_{fs}\gamma H + f_q w_s)$ and is the factored average vertical stress at the base of the embankment
f_{fs} = partial factor for soil unit weight
γ = unit weight of the embankment fill
H = height of the embankment
f_q = partial load factor for external applied loads
w_s = uniformly distributed surcharge load
a = width of the pile caps
C_c = arching coefficient

and the distributed load carried by the reinforcement between adjacent pile caps is equal to :

For $H > 1.4(s-a)$:

Equation 2: $$W_T = [1.4sf_{fs}\gamma(s-a) / (s^2-a^2)][s^2-a^2(p'_c/\sigma'_v)]$$

For $0.7(s-a) \leq H \leq 1.4(s-a)$:

Equation 3: $$W_T = [s(f_{fs}\gamma H+f_q w_s) / (s^2-a^2)][s^2-a^2(p'_c/\sigma'_v)]$$

Where: W_T = distributed load carried by the reinforcement between adjacent pile caps
s = pile spacing between adjacent piles

An important note in the resulting distributed load carried by the reinforcement between adjacent pile caps calculated by the above equations is that the load does not necessarily increase directly with an increase in embankment height. Due to the effect of soil arching, at some given embankment height (dependent on the span between edges of pile caps), additional loads applied by increased embankment height is transferred directly to the pile caps rather than being carried as a distributed load by the unsupported length of the geotextile layer(s). However, the effects of soil arching depend upon the pile cap spacing. The critical pile spacing (i.e., pile spacing to embankment height) is approximated as:

Equation 4: $$H \geq 0.7(s-a)$$

As such, for this design, the embankment is relatively thin which resulted in the need for relatively close pile spacing to maintain loads on the geotextile within reasonable magnitudes.

Tensile Load Determination and Strain Evaluation

The tensile load per unit length carried by the geotextile reinforcement, T_{rp}, was determined as discussed in BS8006:

Equation 5: $$T_{rp} = W_T(s-a) / 2a\sqrt{1 + 1/6\epsilon}$$

Where: T_{rp} = tensile load per unit length carried by reinforcement
ϵ = strain in the reinforcement

© 2016 Deep Foundations Institute

For the purposes of the LTP design for this project, minimizing the reinforcement strain was considered of high importance due to the relatively low height of the embankment overlying the LTP (and thus potential for settlement of the embankment surface to be realized at finished grades due to minimal potential for soil bridging effects) and the possibility that relatively small settlements could result in cracking of the surficial pavements. For this project, the authors selected a relatively conservative maximum allowable strain of two percent in calculating the resulting tensile loads. The authors expected that the geotextile reinforcement would achieve the design strain value during placement of embankment fill over the LTP and prior to construction of the asphalt-paved runways and taxiway. Figure 5 displays the characteristic relationship between the load and strain calculated by the T_{rp} equation (strain range between one and ten percent). The graph indicates that at low strain values (such as the two percent design value for this project), the resulting load is relatively high.

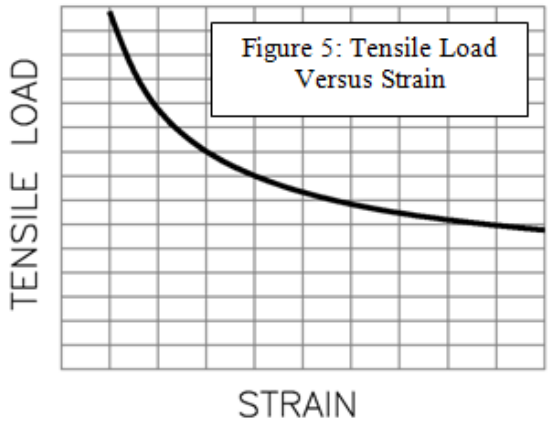


Figure 5: Tensile Load Versus Strain

In order to reduce the potential for damage to the geotextile layer directly overlying the pile caps, the caps were cast with rounded chamfers along their top outside edges (sharp pile cap edges could tear the geotextile). In addition, the authors designed the system to include a two-inch layer of sand to be placed over the top of the pile caps to create a cushion. The combination of the chamfer and the soil cushion layer slightly increased the unsupported length between the caps, but was important in providing a more predictable load condition. In determining the tensile load in the reinforcement layer, the authors considered the unsupported length of the geotextile factor (i.e., the [s-a] factor in the T_{rp} equation) to be:

Equation 6: $(s\text{-}a)_{corrected} = (s\text{-}a)+2t_{sand}$

Where: t_{sand} = thickness of sand cushion over the pile cap

The $2t_{sand}$ factor was added to account for the 1 horizontal to 1 vertical bearing lines from the geotextile layer to the top of the pile cap, which slightly increases the unsupported geotextile length. Other bearing line angles ranging to up to 75 degrees are documented in studies performed by others. The result of this additional unsupported geotextile length factor increased the tensile load on the geotextile layer. The design for this project resulted in a maximum tensile load on the geotextile reinforcement of approximately 10.5 kips per foot per foot width of geotextile at the selected 2 percent strain, which included factors of safety applied to dead and live loads on the LTP.

Geotextile Selection

The evaluation process for selecting an appropriate geotextile generally included reviewing manufacturer data and engaging in discussions with the suppliers' engineers on high-strength geotextiles for critical design parameters, which included: whether the material was biaxial or uniaxial (due to the system being required to carry loads in a three-dimensional manner as previously discussed); manufacturer's reported design strength at two percent strain; manufacture's actual test data collected during the material stress/strain testing; the potential long-term creep of the material; and other factors.

Based upon the evaluation of potential geotextiles and manufacturers, it was determined that the most economical approach for the project was to design the LTP as using two uniaxial geotextile layers (with strong-axes in perpendicular directions) rather than a single biaxial geotextile layer. In addition to the

© 2016 Deep Foundations Institute

economical benefits of using two uniaxial geotextile layers, the authors considered that using two geotextile layers would build some amount redundancy into the LTP design and, therefore, the realized strains in the geotextile layers would be likely be less than the selected maximum allowable strain value of two percent.

BS8006 discusses minimally the effects of using multiple geotextile layers in LTP design. In general BS8006 indicates that the tensile capacities of successive layers of geotextile beyond the first layer are not summed equally to determine their combined load-carrying capacity. BS8006 recommends that when multiple geotextile reinforcement layers are used in the LTP design, the layers be of equal strength and stiffness. BS8006 recommends that a factor of 1 be applied to the first geotextile layer tensile strength, a factor of ≤ 1 be applied to the second geotextile layer tensile strength, and a factor of ≤ 0.5 be applied to any subsequent geotextile layer to sum the system's total tensile load capacity.

For the purposes of the LTP design for the project, the authors selected a geotextile that was capable of carrying the design tensile load as a single layer. Due to the selected geotextile being a uniaxial material, the combination of the two perpendicular geotextile layers were considered to be capable of carrying the design tensile force in two horizontal-plane directions of the LTP.

Seaming/Overlapping

In designing a LTP using biaxial reinforcement, a major consideration is seaming of reinforcement layers along the sides of the reinforcement rolls or where a roll of reinforcement terminates. The tensile capacity of the system may be limited to the strength that can be developed at the seams. For this project, two layers of uniaxial reinforcement were used. As such, the most critical location of the reinforcement was located where a roll of reinforcement terminated (i.e., the strong-direction of the reinforcement was parallel to the roll length).

The authors considered whether the critical overlap locations should be field seamed to maximize the strength of the reinforcement overlaps, or whether overlapping the successive reinforcement rolls would be sufficient for the LTP design. Based upon our evaluation, we determined that overlapping the successive rolls would be sufficient, provided the overlap lengths were centered over a row of pile caps and extended to at least the centerline of the previous and subsequent pile caps. Overlap distance along the weak axis of the reinforcement was determined to be less critical (the perpendicular reinforcement layer would be capable of carrying the full design tensile load in that direction) and therefore were designed to be 18-inch overlaps.

Geotextile and Aggregate Layers

As discussed herein, the LTP design included utilizing two uniaxial geotextile reinforcement layers. In designing the LTP using two reinforcement layers, consideration had to be given to whether the geotextile layers should be laid directly on top of each other or separated with a layer of aggregate. Additionally, if the reinforcement layers were to be separated by a layer of aggregate, it would be necessary to consider the thickness of the aggregate layer (and resulting separation distance between the reinforcement layers) and how the separation may affect the load(s) that would be applied to the individual reinforcement layers.

The authors determined that laying the reinforcement layers directly on top of one another was not appropriate for the project. Major considerations that affected this decision included that the interaction between the two layers would result in a relatively very low sliding coefficient that could jeopardize the reinforcement pull-out capacity at overlaps, as well as the difficulties that would be realized during construction of the layers. Construction complications would have included possible difficulties in

© 2016 Deep Foundations Institute

maintaining the layers taut and free of wrinkles (discussed later in this paper) as workers walked across the lower layer while placing the upper layer.

As a result of the evaluations and considerations, the LTP was designed to include a 16-inch layer of select aggregate between the geotextile reinforcement layers. The selected layer thickness was considered to be an appropriate thickness for placement and compaction to create a relatively rigid LTP that would not result in a significant increase in the design tensile load in the reinforcement layers while allowing the two layers in combination to perform similar to a biaxial reinforcement material.

Anchorage

In general, LTPs can be designed with the reinforcement layers extending a design distance over suitable bearing subgrades that have sufficient vertical downloads (from overlying cover) to create a suitable anchorage condition and resist pull-out of the reinforcement layers. As discussed herein, the majority of the outer perimeter of the LTP was at the edge of the allowable construction area. The outer perimeter of the LTP was adjacent to existing wetlands that were not permitted to be disturbed. As such, the limits of the LTP where adjacent wetlands were present had to be terminated using an alternative anchor design.

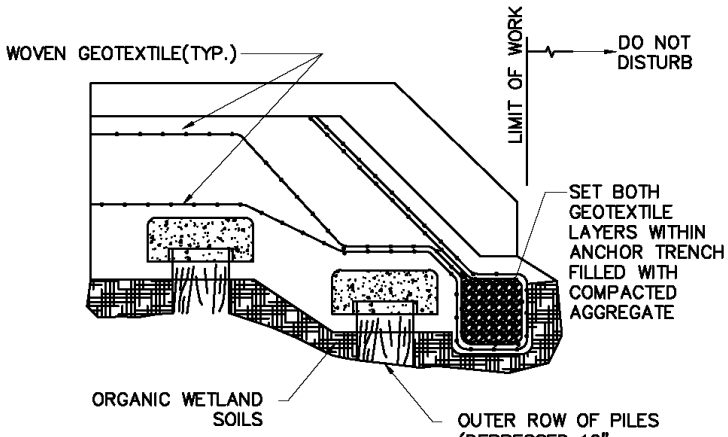


Figure 6: Reinforcement Anchor

For this project, anchorage at the termination limits of the reinforcement layers adjacent to the wetlands was designed and achieved by using a buried aggregate anchor bar wrapped in the geotextile reinforcement (Fig. 6). The wrapped-geotextile anchor was designed to rely on lateral capacity of the outer row of piles to resist the reinforcement pull-out force.

Where anchorage was required adjacent to suitable bearing soils (such as the junction of conventional soil-supported runway areas and the LTP), the reinforcement layers were extended a horizontal design distance of 10 or 14 feet over the suitable bearing soils to develop the design pull-out resistance.

INSTALLATION OF TIMBER PILES AND CONSTRUCTION OF THE LTP

Subgrade Preparation

Prior to installation of piles, the LTP footprints were cleared of existing pavements or vegetation, and excavation was performed to achieve an appropriate elevation below the design pile cut-off elevations. A layer of crushed stone was placed over the LTP footprint prior to pile driving activities in order to create a working platform for the construction crews, and dewatering activities were performed where necessary so that pile installation and other construction stages could be performed “in the dry.” After installation of the piles, a non-woven geotextile separation fabric was placed over the crushed stone in preparation of placement of the overlying sand “cushion” layer surrounding and over the pile caps.

© 2016 Deep Foundations Institute

Pile Installation

Strict locational tolerances were implemented regarding the installation of piles (Fig. 7), which required the piles being located not more than 3 inches off from the planned 5-feet center-to-center spacing after installation. The accuracy of the pile locations was considered of high importance due to the significant increase in tensile loads (and consequent increase in strain values) when the unsupported reinforcement span distance increased by even a matter of a few inches. Field inspection engineers monitored each pile during installation for location accuracy. Where piles were installed outside the specified tolerances, modified (larger) pile caps were installed (discussed in the following section). It is important to note that the authors believe that without direct oversight of the pile installation by the design engineers, the resulting level of attention paid to installing the piles within the specified tolerances may not have been achieved which could have been detrimental to the performance of the LTP.



Figure 7: Installation of Timber Piles

Pile Cap Construction

Upon completion of pile installation, field inspection engineers measured the center-to-center distance between each pile butt in order to determine whether the piles were installed within the specified tolerances. Where pile butts were located outside the specified tolerances, cast-in-place pile caps were constructed with greater widths so that the resulting edge-to-edge pile cap spacing was not greater than 3 feet (the design perpendicular unsupported reinforcement length between caps). Pile caps (Fig. 8) where piles were installed within the specified tolerances consisted of precast units. Each of the precast units was secured to the pile butt by pumping grout into two pre-formed ports in the top surface of the pile cap (Fig. 9). Field inspection engineers were particularly careful to identify any precast or cast-in-place pile caps that were cast with sharp edges (rather than suitable beveled edges) and to identify those conditions to the contractor so that those edges could be grinded to an appropriate bevel.



Figure 8: Pile Cap Placement

As described previously, a sand cushion was placed over and between pile caps to provide additional protection against damage to the geotextile layer. The sand layer also provided a more convenient working surface for the contractor and helped to stabilize the caps in place.

The entire layer was compacted in-place after achieving the final elevation above the pile caps. Field inspection engineers measured the thickness of the sand layer throughout the LTP areas to verify that the sand layer was not greater than 2 inches above the top of the caps. As discussed in the design portion of this paper, further increasing the thickness of the sand layer would have resulted in increasing the design unsupported reinforcement length, and thus an undesired increase in tensile loads (and consequently increased strain values). Benefits of full-time oversight of the pile cap construction by the engineer included the ability to identify: pile caps that were spaced outside of the design tolerance; pile caps that were not placed in a square alignment to adjacent caps; pile caps that were not set level on top of the piles; cast-in-place caps that were not constructed with appropriate bevels; and areas of the sand cushion where the thickness exceeded the design value. The



Figure 9: Pre-Cast Pile Cap Placement and Socket Grouting

© 2016 Deep Foundations Institute

authors believe that without direct full-time oversight by the engineer, these items may not have been paid their due attention, and excessive geotextile strain could have resulted.

Geotextile Reinforcement Construction

Field inspection engineers oversaw placement of all geotextile reinforcement for the project (Fig. 10 and Fig. 11). The authors considered the proper placement of the geotextile reinforcement of utmost importance to constructing a reliable LTP. Specific geotextile reinforcement placement requirements included verifying: each roll of geotextile was the approved material and in good condition (i.e., not damaged prior to placement); each layer and roll of geotextile was placed and pulled taut (free of wrinkles); proper overlaps were constructed and that critical strong-axis overlaps were located centered over pile caps; placement of aggregate layers over the geotextile did not create wrinkles in the geotextile; and anchor lengths and anchor trenches were properly constructed.

Engineering oversight of the geotextile reinforcement placement was vital to the LTP construction. While on-site, field inspection engineers identified on multiple occasions where construction practices could have negatively affected the reliability of the system if not recognized and corrected at the time of geotextile placement. These conditions were usually subtle and not something most earthwork contractors would otherwise have paid close attention to. For example, in some instances the engineer identified portions of the geotextile that, once laid out, included wrinkles that the engineer required the contractor to address prior to placement of fill. In other cases, placement of the fill on the geotextile resulted in the formation of wrinkles (sometimes simply due to the direction the fill was being placed and spread), which field inspection engineers identified and required correction of prior to proceeding with fill placement.



Figure 10: Geotextile Reinforcement Placement



Figure 11: Geotextile Reinforcement Pulled Taut

Placement and Compaction of Aggregates

Aggregate layers were placed and compacted between the two geotextile reinforcement layers (Fig. 12) and above the upper geotextile layer to support the overlying embankment materials and asphalt-paved runway. Aggregates were compacted using heavy vibratory rollers. Thorough compaction using a heavy vibratory roller was considered important in order to develop tensile resistance in the geotextile which would purposefully cause initial straining of the reinforcement layers at this stage of the LTP and embankment construction (rather than strains being developed at later stages, such as during or after asphalt pavement placement, which could result in settlement and cracking of the pavement).



Figure 12: Compacting Gravel over Lower Geotextile Layer

© 2016 Deep Foundations Institute

The mattress layer select fill was installed in two 8-inch thick layers. During the compaction activities, field inspections engineers observed the subgrades for evidence of yielding that could indicate excessive strain of the geotextile layers. The aggregate layers were also tested in the field for percent compaction. A compaction criterion of 100 percent of the maximum dry density was specified by the Federal Aviation Administration for the project. Based upon the testing, the aggregate layers achieved 100 percent compaction, which was an indicator that the reinforcement layers were providing adequate subgrade support. Additionally, the subgrades were observed to be unyielding and therefore the authors were satisfied that the geotextile reinforcement was of adequate strength and exhibited relatively low strains, which was expected based upon the relatively low allowable strain value in the LTP design.

Performance Monitoring

After placement of the upper geotextile reinforcement and compaction of the overlying aggregate layer, field inspection engineers excavated to the top of the upper geotextile layer and constructed several settlement monitoring platforms (Fig. 13). The purpose of the platforms was to allow assessment of the performance of the LTP over time. The platforms consisted of a 2-feet by 2-feet plywood base with a 3-inch diameter polyvinyl chloride (PVC) pipe extending to the final embankment elevation, and an outer 4-inch diameter PVC sleeve (to allow the platform to settle and not be influenced by friction of the riser against the surrounding soil). The platforms were constructed over the unsupported spans of the geotextiles (between pile caps).



Figure 13: Settlement Monitoring Platform Construction

Field inspection engineers surveyed monitoring points to assess the approximate top geotextile layer elevation after each lift of soil was placed over the LTP during construction of the embankment. Based upon the survey results, negligible movement of the upper geotextile layer was observed. The authors considered this finding to indicate that the LTP was designed and constructed in a manner that was capable of supporting the design loads, and that the BS8006 design method may have resulted in a conservative LTP design.

CONCLUSIONS

Design of the LTP system was performed using the methods described in BS8006. Based upon the successful completion of the project, the authors considered the BS8006 design method to result in a reliable LTP system design. The authors identified that providing full-time oversight throughout the pile installation and LTP construction process was of extreme importance and provided a high degree of value to the project. Having performed the design for the LTP system and having intimate knowledge of the influence of various alterations to the design allowed the engineers to identify potential construction practices that could have been detrimental to the performance of the system and correct those potential issues prior to them impacting the finished project. Among various conditions that were corrected by inspection engineers in the field during construction included: timber piles that were not driven to sufficient depth to achieve the vertical capacities or which were damaged during driving; timber piles that were installed outside locational tolerances, which resulted in pile caps being outside locational tolerances; pile caps that were installed out of alignment or constructed without proper beveled edges; insufficient geotextile reinforcement overlaps; and, geotextile reinforcement that was not placed and pulled taut sufficiently for to achieve the strict design requirements. Full time oversight by trained engineers allowed these (and other potential construction defects) to be addressed. Without full-time direct oversight, there are many intricacies of LTP construction that may not have been paid detailed attention to during construction that could have detrimentally affected the reliability of the system, which could have been very costly to repair if settlement occurred after pavement construction. In particular,

© 2016 Deep Foundations Institute

excavating and repairing portions of the LTP would have been extremely difficult and would likely compromise other portions of the LTP. The potential for post-construction failure of the system was greatly reduced by engineering oversight to correct the identified issues during construction, rather than post-construction.

REFERENCES

BS 8006-1:2010, 2010. Code of Practice for Strengthened/Reinforced Soils and Other Fills, British Standards Institution, London, England.

© 2016 Deep Foundations Institute

PRESSURE-GROUTING IMPROVES PERFORMANCE OF HELICAL PILES: A PRODUCTION CASE HISTORY, STATIC LOAD TEST RESULTS, AND COMPARISONS TO PREDICTED LATERAL DEFLECTION AND AXIAL RESISTANCE

Karen J. Dawson, P.E., CH2M, Bellevue, WA USA (425) 233-3340 Karen.Dawson@ch2m.com
Francisco Johnson, American Piledriving Equipment, Kent, WA USA (253) 872-0141
FranciscoJ@apevibro.com

ABSTRACT

Pressure-grouted high strength helical displacement piles are a recently developed pile type that can be useful in conditions where noise or vibrations must be low or where access or clearance is limited. However, there is no information in the literature that can be used to estimate the soil resistance of these piles or production rates. To fill this information need, this paper presents a New Jersey installation case history and the results of static axial and lateral load tests on both pressure-grouted and ungrouted high strength helical piles at the case history site and trial installation locations in New Jersey and Washington State. Piles between 25 and 50 feet long comprised of steel shaft diameters of 4.5, 5.5, and 7 inches with equivalent grout column diameters ranging from 12 to 22 inches were tested. Lateral loads of up to 100 kips and axial compression loads of up to 700 kips were applied. The results of the load tests are compared to predictions of lateral deformation and axial resistance.

Keywords: pressure-grouted, helical, displacement pile, load test

INTRODUCTION

Helical piles have long been recognized as a useful foundation type in situations where noise and vibrations must be limited, or where there are access or clearance restrictions. Relatively well-documented design methods and torque to capacity correlations have been developed for the most commonly used helical piles, which are relatively small (typically shafts of 6 inches or less) with corresponding low load carrying resistance.

With the increased need to construct in congested urban environments, there is incentive to develop helical piles with higher axial resistance. Seismic and other loading conditions also require lateral resistance, which is low for the typically small helical pile shafts. One method of increasing the soil resistance, both axially and laterally and at relatively low cost, is to place grout around the shaft. Injecting the grout under pressure through the hollow helical pipe section and out a grout port or ports located near the toe of the pile has the potential to increase the pile resistance significantly above that which can be achieve by gravity grouting. Not only does the pressurized grout push out against the surrounding soil, but the rotating helix helps to distribute the grout laterally. Unfortunately, little information is available in the literature to help designers estimate the resistance of grouted helical piles in general and none is available regarding pressure-grouted helical piles.

This paper provides information to begin to fill the grouted helical pile information gap, first by presenting a brief case history on the use of pressure-grouted helical piles and second by comparing the resistance measured by static load tests to resistance predicted by analytical methods used for helical piles, augercast piles, and micropiles. The comparisons are made for the case study and trial installations at test-only sites in Sayreville, New Jersey and Kent, Washington; all three of the sites involved testing of both pressure-grouted and ungrouted helical piles so that the relative increase in performance associated with grouting can be seen.

JERSEY CITY CASE HISTORY

Background

The project owner, Jersey Avenue MM LLC of Jersey City, NJ proposed to construct a multi-story mixed retail and residential structure covering an area of approximately 16,000 square feet. The building was originally designed with driven 9-5/8-inch x 0.352-inch wall pipe piles for foundation support. Service

© 2016 Deep Foundations Institute

loads were 160 kips per pile and ultimate loads were 320 kips per pile. Based on the advanced age of the existing buildings and their location within a few feet of the proposed new building, the construction contractor decided that driven piles were not a constructible foundation option.

Site Conditions

The site is located near the intersection of Jersey Avenue and Christopher Columbus Drive in Jersey City, NJ. This is a developed urban area with mixed residential and commercial buildings, many with brick cladding, as shown in Figure 1. The working elevation for pile installation was excavated 12 feet below the street level.

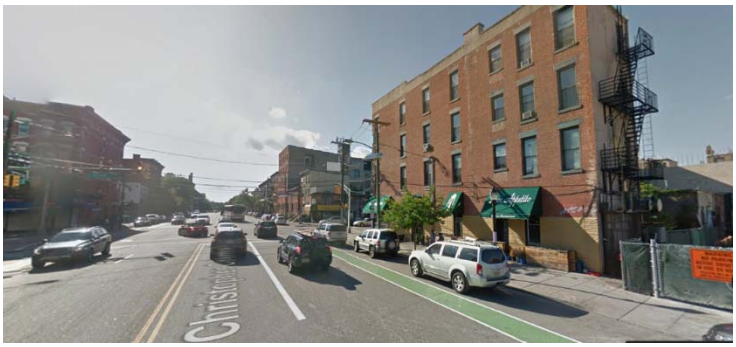


Fig. 1. Jersey City street view

Subsurface Conditions

The subsurface exploration was conducted by M&Z Engineering Associates of Monmouth Junction, New Jersey. The subsurface below the pile installation grade consisted of approximately 5 to 10 feet of soft silt underlain by a poorly graded sand with occasional interbeds of silty sand, sandy clay, and clayey gravel. The granular materials were typically medium dense, but randomly varied from loose to very dense. The borings were drilled with hollow stem auger, so there is a possibility that heave resulted in overstatement of some of the Standard Penetration Test (SPT) N-values. The apparently random low SPT values at depth suggest that the higher SPT values may be overstated due to the presence of gravel. Rock was encountered at depths ranging from about 63 to 72 feet below the pile installation grade. Groundwater was encountered about 2 feet below the pile installation grade. Estimated geotechnical design properties of the material penetrated by the piles are provided in the load testing portion of this paper.

Helical Pile System

FM Home Improvements (FM) of Orange, NJ, contracted with American Piledriving Equipment (APE) to supply installing equipment, piles, and technical assistance for high strength helical pile (HD^{TM}) support of the structure. FM subcontracted the pile installation to Caporaso Excavating Inc. of Union, NJ.

The APE HD^{TM} piles were made from re-certified secondary market oil field casing, with a tensile yield strength ranging from 80 to 100 ksi. The casing was provided in 20-foot starter section with 10- and 20-foot extension sections. Each section was fitted with threaded couplings, creating a constant interior diameter pile with no reduction in tensile, compression, or bending strength at the joint relative to the casing. A drawing of the starter pile section is shown in Figure 2. The extension sections utilized the same shaft and couplings as the starters but did not have helixes or grout ports. The ungrouted test piles were identical to the grouted piles but without the end closure plate or grout ports.

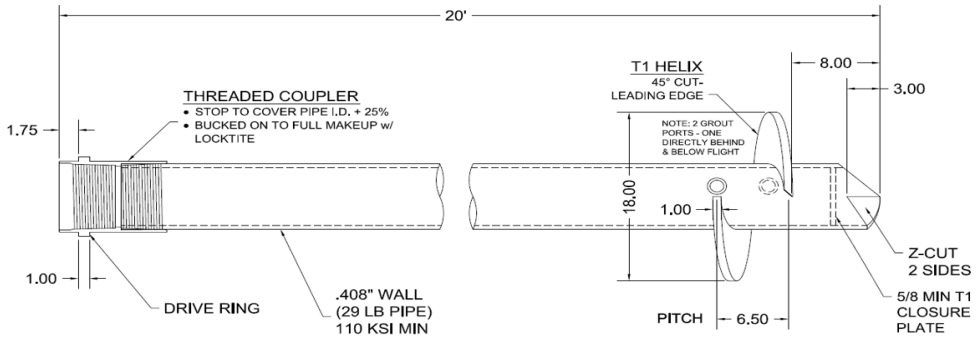


Fig. 2. Jersey City grouted pile starter section schematic

The installation equipment was plumbed to allow grout to be pumped through the hydraulically powered drive head and the interior of the helical pile as it was twisted into the ground. Grout exited the pile through grout ports at the leading and trailing edge of the bottom helix. Test cubes of the grout showed unconfined

© 2016 Deep Foundations Institute

compressive strengths of 9900 psi. Grouting pressures ranging from 500 to 3200 psi were measured at the grout pump during installation.

Pre-Production Static Load Testing

Pile installation began with a pre-production static load test program. The pre-production program was intended to verify the preliminary estimates for pile diameter, minimum depth, and installation criteria. The equipment supplier provided the load testing frame, jack, load cells, measuring equipment, and personnel to set up and conduct the static load tests. The tests were conducted in accordance with the ASTM D1143 Quick Test procedure except as noted below.

The compression load test frame consisted of three cross-beams anchored by eight 20-foot-long helical piles of the same dimensions as the test pile. Figure 3 shows a typical load frame set-up. Because the reference beam was supported at locations slightly less than 6 diameters from the grouted test pile, it was surveyed before, after, and at intervals throughout the test; the reference beam did not move.



Fig. 3. Typical load frame set-up

Initially, three ungrouted piles were installed to depths ranging from 28 to 38 feet below the excavated basement level. The ungrouted test piles were not filled with concrete for testing. The static load tests on these piles showed unfactored resistance (Davisson offset method) ranging from 105 to 290 kips; these resistances were below the target resistance of 320 kips.

Rather than extending the piles deeper or adding helixes, the design and construction team elected to grout the piles. A fourth pre-production test pile was installed 25 feet deep with a net grout volume equivalent to a 22-inch diameter composite grout/steel element. The termination depth was based on a marked increase in grouting pressure from 2500 psi to 3200 psi over the last 2 feet of penetration and torque approaching the 150,000 foot-pound nominal capacity of the drive head. Static load testing of this pile showed an unfactored resistance in excess of the 320 kip target.

Load versus deformation plots from the static load tests are shown in Figure 4**.** Although the grouted pile was not loaded to failure, the load versus deflection plots show that the deflection in the grouted pile at design load was only 10 to 50 percent of that exhibited in the ungrouted piles**.** If the resistance at a deflection of 0.35 inches, the deformation at the maximum tested load for the pressure-grouted pile (&G-4 in Figure 4) is compared for all four test piles, we see that the ungrouted piles had 95, 150, and 220 kips of resistance (in piles 7U-1, 7U-2, and 7U-3 respectively) - or 30, 47, and 69 percent of the resistance of the pressure-grouted pile, despite being 3 to 13 feet longer than the pressure-grouted pile.

Production Installation

Production pressure-grouted helical pile installation equipment included:

- APE HD^{TM} 150 drive head
- Caterpillar 349EL excavator for drive head mount
- Putzmeister BSA 14000 grout pump with rated pressure of 3,200 psi and 93 cubic yards per hour
- Two 1400 cubic feet per minute air compressors
- Skid steer for pile handling

© 2016 Deep Foundations Institute

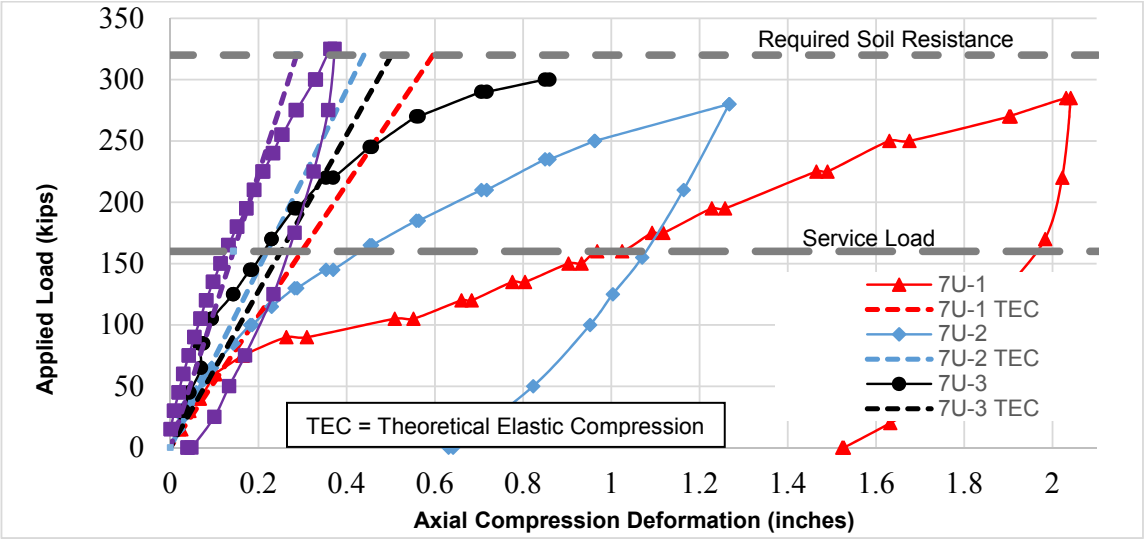


Fig. 4. Jersey City pre-production load vs. deformation curves

Production installation of the grouted piles involved a crew of four, including the excavator/drill operator and grout pump operator. Over 250 piles were installed between January and February. Typically, production ranged from 15 to 17 piles a day, working an 8 hour shift. Termination was based on an increase in grouting pressure and torque similar to the pre-production test, and commonly occurred at a depth of about 25 feet.

COMPARISON OF PILE RESISTANCE MEASURED IN LOAD TESTS TO PREDICTIVE METHODS

Different analytical methods were used to predict the axial compression and lateral resistance of the pressure-grouted piles at the two New Jersey sites and the Washington State site. These predicted capacities were compared to the capacities determined from static load test results. The predictive methods and comparison of results are described in the following subsections.

Axial Compression

Three methods were used to predict axial compressive resistance:

Hybrid Micropile Method

This method utilizes the bond resistance of a pressure-grouted micropile to estimate the shaft resistance, or skin friction, and predicts toe resistance using a common driven pile method (Fellenius, 1991).

$R = R_t + R_s$, [1]

Where R = Total Resistance, R_t = Toe Resistance, R_s = Side Resistance

$R_t = A_t * (N_c * c_u + \sigma'_v)$ for cohesive soils, [2]

$R_t = A_t * N_q * \sigma'_v$ for cohesionless soils [3]

A_t = area of toe = $\pi * D_{helix}^2/4$ [4]

Where N_c = deep foundation bearing capacity factor = 9, c_u = undrained cohesion, σ'_v = effective stress at pile toe, N_q = deep foundation bearing capacity factor for cohesionless soil (function of soil friction angle)

$R_s = A_s * \alpha_{bond}$ [5]

Where A_s = Side area = $\pi * D_{shaft} * L$, D_{shaft} = shaft diameter, L = shaft length, α_{bond} = bond strength for a Type B, pressure-grouted micropile (Sabatini, et al, 2005).

Two alternatives were examined for D_{shaft}; one with the diameter equal to the steel shaft diameter, and one with the diameter equal to the equivalent grout column diameter.

© 2016 Deep Foundations Institute

Steel Screwpile Method

The steel screwpile approach utilizes methods for calculating toe resistance and side resistance similar to those developed for driven piles, such that:

$R = R_t + R_s$, [1]

Where R, R_t, and R_s are as defined for the hybrid micropile approach above and R_t is calculated as described for the hybrid micropile approach. However, with the screwpile approach, side resistance is calculated as follows:

$R_s = A_s * \sigma'_{v_{ave}} * K_s * \tan\phi$ For cohesionless materials [6]

Where $K_s = \beta/\tan\delta$, $\delta = 0.6 * \phi$ for steel against sand, $\delta = 1.0 * \phi$ for pressure grout against soil, β = skin friction factor for displacement piles in sand, such as described by the Canadian Foundation Engineering Manual (CFEM) (2006).

$R_s = A_s * c_u * \alpha$ For cohesive materials [7]

Where α = adhesion factor, such as recommended by the CFEM or API.

Side resistance within 1 shaft diameter of the pile toe and ground surface is ignored. This method is also reported in Tappenden and Sego (2007). The shaft resistance was applied to the effective diameter of the grout for the cases examined.

Drilled Displacement Pile Method

The drilled displacement pile approach uses the method recommended by the FHWA (Brown et al, 2007), which is based on load test result correlations in conditions where the spoils were displaced into the borehole wall during construction. This method relies upon CPT or SPT correlations.

$R_t = A_t * q_t$ [8]

Where $q_t = 0.4*q_c + W_T < 200$ tsf, where qc is the uncorrected CPT tip resistance [9]

q_t (tsf) $= 0.19 * N_{60} + W_T$ for $N_{60} \leq 50$ [10]

W_T = constant =0 for $q_p \leq$ 75 tsf and uniform, rounded materials having up to 40% fines

W_T = 14 tsf for $q_t \leq$ 89 tsf and well-graded angular materials having up to 10% fines.

N_{60} = Standard Penetration Test blow count corrected for hammer efficiency but not depth

$R_s = A_s * f_s$ [11]

$f_s = 0.01q_c + W_s$ for $q_c < 200$ tsf [12]

f_s (tsf) $= 0.05 * N_{60} + W_s$ for $N_{60} < 50$ [13]

Where W_s = correlation constant = 0 and $f_s < 1.7$ tsf for uniform, rounded materials having up to 40% fines. This relationship was used for estimating the resistance in fine-grained soils at both test sites.

$W_s = 0.5$ tsf and $f_s \leq 2.2$ tsf for well-graded angular materials having up to 10% fines, and W_s for soils between these two ranges can be linearly interpolated.

Load Test Results

The two test sites with axial compression load test data presented in this paper are the Jersey City site described in the case history and the APE yard in Kent, Washington. The Kent site consists of over 150 feet of alluvial deposits. A summary of material descriptions and interpreted engineering properties for both the Kent and Jersey City sites are provided in Table 1.

© 2016 Deep Foundations Institute

Table 1.

Summary of Subsurface Conditions and Interpreted Engineering Properties

Description	Depth (feet)	N_{60} range	γ' (pcf)	ϕ' (deg)	c_u (psf)	N_q	α	β	α_{bond} (psi)
Kent, Washington									
Fill. Silty sand with gravel	0-7	5-29	130	37	0	100	0	0.7	20
Firm sandy silt with interbeds of loose to med. dense silty sand and poorly graded sand with silt	7-43	6-29	43	32	0	40	0	0.2	15
Medium dense to dense poorly graded sand with silt	43-55	55-60	62	37	0	100	0	0.7	35
Jersey City, New Jersey									
Stiff silty clay with gravel, moist	0-2	30-45	90	-	1000	9	0.9	-	10
Stiff silty clay with gravel, wet	2-9	2-6	28	-	1000	9	0.9	-	10
Loose to medium dense silty sand to poorly graded sand, occasionally with gravel	9-40	5-67[(1)]	58	30	-	40	-	0.15	15

[(1)] Highly variable, discounted highest values in analysis.

Figure 5 shows static test load versus deformation plots for the three sizes of grouted helical piles tested in Kent. The static test load versus deformation plots for the Jersey City piles are shown in Figure 2. Table 2 compares the resistance determined from interpretation of the static load tests with estimated resistance calculated by the three methods described above.

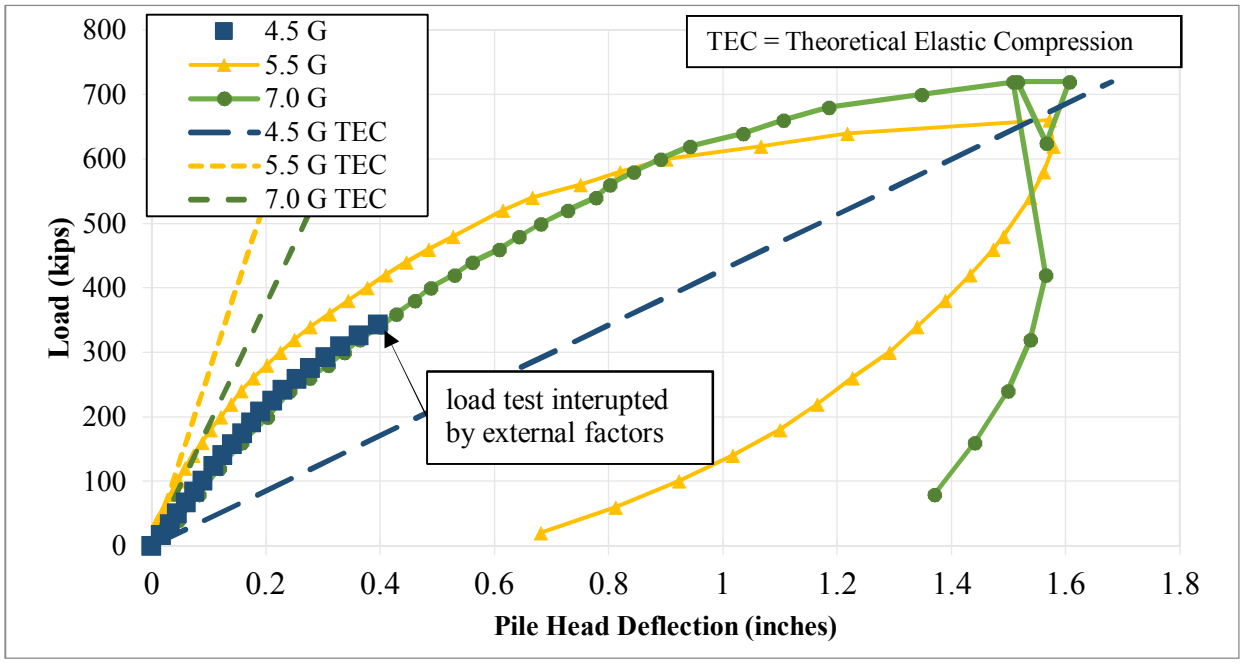


Fig. 5.Static compression load test results from Kent, Washington

© 2016 Deep Foundations Institute

Table 2.
Comparison of Predicted and Measured Pile Capacities in Axial Compression

Pile Name	Test Pile Geometry Summary					Ultimate Resistance				Back-calculated K_T[4] (ft^{-1})
						Inter-preted from Static Load Test (kips)	Calculated from Interpreted Subsurface Data as a Percentage of the Static Load Test Value			
	Pipe O.D (in)	Helix Diameter (in)	Effective Grout Diameter Based on Volume (in)	Pile Toe Depth (feet)	Install-ation Torque at End of Driving (ft-lb)		Hybrid Micropile Approach [1]	Steel Screw-pile Approach [2]	Drilled Displace-ment Approach [3]	
Kent, Washington										
4.5 G	4.5	14	18	49	32,000	>350 [4]	<125%	<125%	<165%	>10.9
5.5 G	5.5	16	18	49	44,000	600	95%	90%	105%	13.6
7.0 G	7	18	15	51	47,000	680	105%	95%	90%	14.5
Jersey City, New Jersey										
7U-1	7	18	NA	38	64,000	105	NA	180%	250%	1.6
7U-2	7	18	NA	28	NR	180	NA	70%	125%	NR
7U-3	7	18	NA	32	110,000	290	NA	50%	85%	2.6
7G-4	7	18	22	25	NR	>320 [5]	<135%	<50%	<105%	NR

[1] Type B micropile bond applied to steel diameter/equivalent grouted diameter, Nq mid-range for toe bearing
[2] mid-range for Nq values, skin friction as for driven steel piles. End bearing calculated from the larger of steel helix or effective grouted diameter at toe.
[3] Shaft diameter = steel shaft for piles 7U-1, 7U-2, & 7-U3. = effective grout diameter for all grouted piles.
(4) Backcalculated empirical correlation factor commonly used for ungrouted, small diameter helical piles such that $R=K_T * T$, where T is the final installation torque
[5] pile not loaded to failure
NR=not recorded
NA=not applicable (not grouted)

Lateral

Lateral resistance of the pressure-grouted piles was predicted with the P-y method, implemented by use of the finite difference program LPILE (Ensoft, 2015). Two methods were used to model the composite steel/grout section:

- Ignoring the strength of the exterior grout, but accounting for the equivalent diameter for soil resistance (labeled cracked section in load vs. deflection plots)
- Using the full strength of the grout over the full equivalent grouted diameter (labeled "uncracked" in load vs. deflection plots).

Lateral load tests were conducted at the Kent, Washington site, and at a Sayreville, New Jersey site. A grouted (pile 7.0G) and an ungrouted 7-inch steel pile were tested in Kent. Tests were in accordance with ASTM D3966 and the load was applied and deflections were measured at the ground surface. The 7-inch ungrouted pile in Kent is not listed in Table 1 because it was installed to a depth of 77 feet, so is not directly comparable with the grouted piles in axial compression. The ungrouted pile was not filled with concrete.

The lateral load versus deformation plots are shown for the Kent site in Figure 6. The Kent materials were modeled in LPILE as Reese Sand. Deformations measured during the load tests and predicted using LPILE are shown for the grouted and ungrouted 7-inch steel pile. As is evident from the data in Figure 5 the tested pile exhibited considerably stiffer response than LPILE calculated for an uncracked section.

© 2016 Deep Foundations Institute

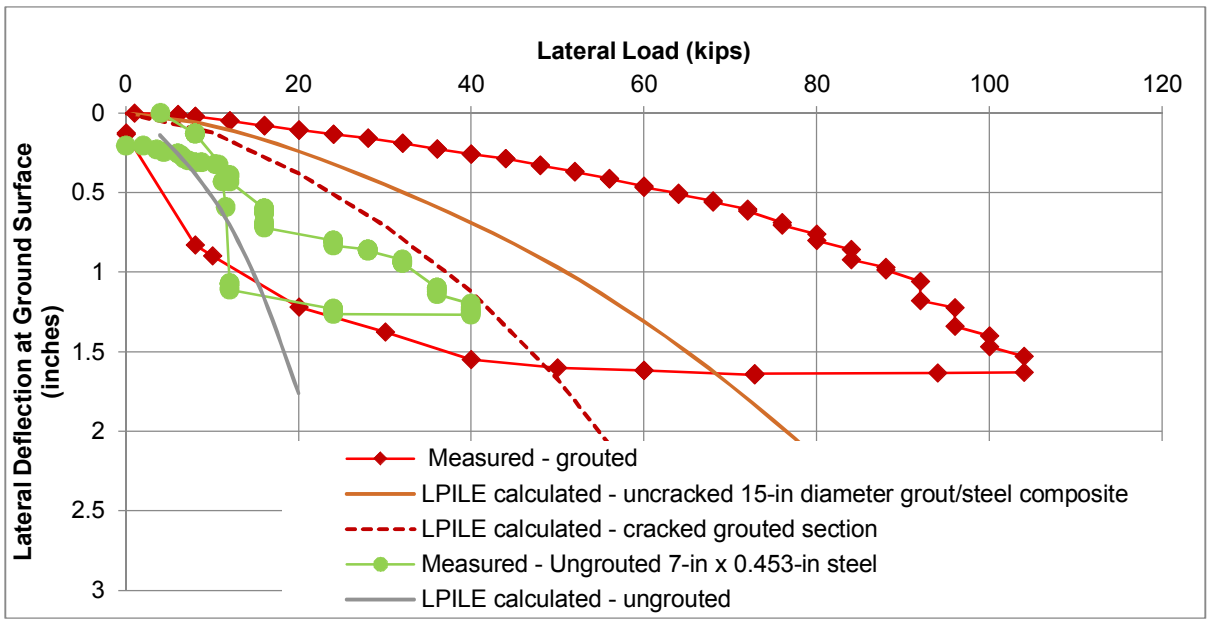


Fig. 6.Measured and Predicted Lateral Load vs. Deformation at Kent

The Sayreville site consisted of approximately 2 feet of dense sand with silt and gravel underlain by 8 feet of very stiff silt with a trace of fine sand, underlain by a stiff to very stiff silty clay with trace of file sand. The upper materials were modeled in LPILE as API sand, and the clay was modeled as a stiff clay with free water. Both 4.5- and 7.0-inch steel piles with equivalent grouted diameters of 12 and 16 inches, respectively, were tested laterally. The measured and predicted lateral load vs. deformation plots are shown in Figures 6 and 7.

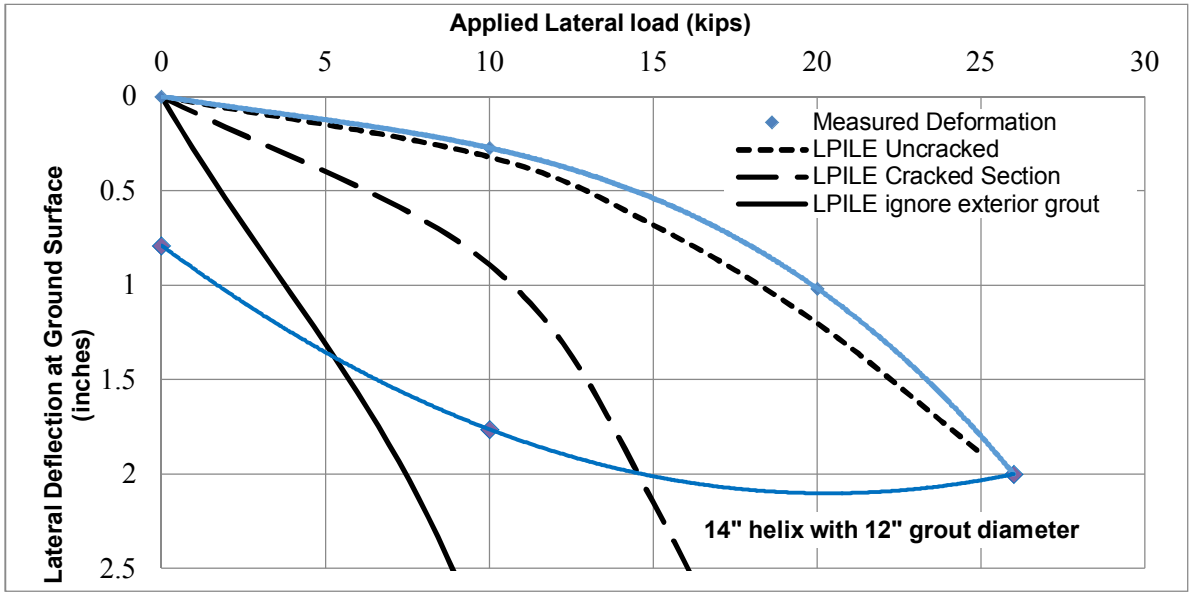


Fig. 7.Measured and Predicted Lateral Load vs. Deformation in 4.5-inch pile at Sayreville

© 2016 Deep Foundations Institute

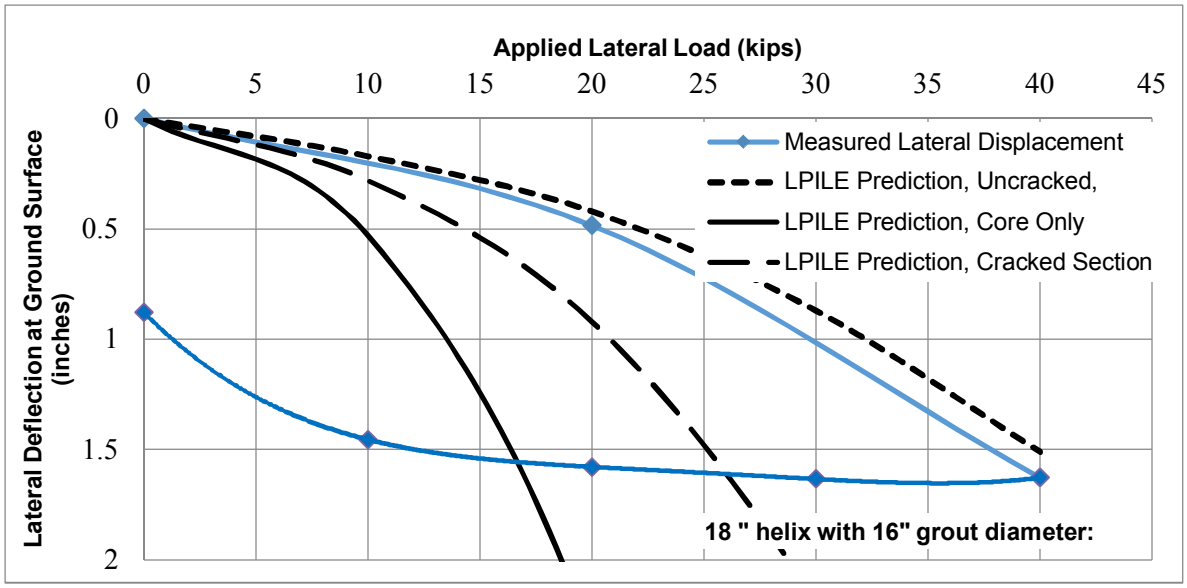


Fig. 8. Measured and Predicted Lateral Load vs. Deformation in 7.0-inch pile at Sayreville

SUMMARY

The following can be summarized from the Jersey City case history:

1. A pressure-grouting system was used to increase the axial compressive resistance of a 7- x 18-inch helical pile founded primarily in loose to medium dense silty sand to poorly graded sand to well above 320 kips
2. Grouting decreased the deflection under service loading by 50 to 90 percent relative to that of an ungrouted pile with the same steel section. Viewed another way, at a deflection of 0.35 inches, the pressure-grouted pile had a resistance that was 140 to 330 percent higher than the resistance of the ungrouted piles.
3. The pressure-grouted piles were installed with no damage to adjacent vibration-sensitive structures.

The Kent trial installations showed that pressure-grouting increased the lateral resistance by approximately 300 percent at a 1-inch allowable deflection.

The comparison of static load test with predicted pile resistance or deflections showed:

1. Predicted axial compressive resistance ranged from less than 50 percent to 250 percent of the measured value, with the Steel Screwpile method providing the most consistently conservative results
2. There was no clear best or worst method for predicting axial compression resistance.
3. The empirical relationship, $R=K_T * T$, between torque at the end of installation and resistance was not consistent among the piles tested.
4. Lateral behavior of the Sayreville "uncracked" section prediction nearly matched the measured deflection for the grouted 4.5- and 7.0-inch piles. A P-multiplier of almost 3 was needed for the Kent uncracked section prediction to match the measured deflection. Cracked section modeling significantly overpredicted measured deflections.
5. The best method for predicting deflections under lateral loading appears to be by using an uncracked composite grout/steel section to represent the pile in a P-y analysis.

© 2016 Deep Foundations Institute

CONCLUSIONS

Although pressure-grouting will increase the axial compressive resistance in all subsurface conditions, it will be most economical in conditions without a definitive bearing layer, in highly variable and layered stratigraphy, or where a stiffer lateral response is needed. Site specific load testing will be recommended until a large, well-documented database of test results for a variety of conditions is developed, but in the right soil conditions, pressure-grouting might be expected to result in significant increases in axial and lateral resistance compared to the ungrouted condition.

Many well-documented load tests are needed to determine the best analytical methods for predicting axial compression and lateral resistance of the pressure-grouted piles. Until a large data base is in place, any one or all of the three methods examined could be used for preliminary predictions of resistance, but a generous resistance factor or factor of safety factor should be applied. Preliminary predictions must be refined by pre-production load testing.

ACKNOWLEDGEMENTS

The authors would like to thank the Jersey City project team: the owner Jersey Avenue MM LLC, the geotechnical engineer MZ Engineering, the general contractor FM Home Improvements, and Thomas Campbell for their contributions to the case history.

REFERENCES

Brown, D.A., Dapp, S.D., Thompson, W.R., and Lazarte, C.A 2007. Geotechnical engineering circular No. 8, Design and Construction of Continuous Flight Auger (CFA) Piles. FHWA-HIF-07-03

Ensoft, 2015. LPILE A program for the analysis of deep foundations under lateral loading, Version 8.

Fellenius, 1991. Pile Foundations. In: Foundation engineering handbook, Second Edition. H. Fang Ed., pp. 511-536.

Sabatini, P.J., Tanyu, B., Armour, T., Groneck, P., and Keeley, J. 2005. Micropile design and construction. FHWA-NHI-05-039. National Highway Institute and Federal Highway Administration U.S., Department of Transportation, Washington, D.C.

Tappenden, K.M., and Sego, D.C. 2007. Predicting the axial capacity of screw piles installed in Canadian soils. Proceedings: OttawaGeo2007, pp. 1608-1615.

© 2016 Deep Foundations Institute

PROTECTION OF WATERFRONT PROPERTIES BY PRESSED-IN SHEET PILE SEAWALLS

Ian Vaz, Giken America Corp.; Orlando, Florida; (407) 380-3232 ivaz@gikenamerica.com
Rafael Holcombe, Tetra Tech; Long Beach, CA; (562) 257-1589 rafael.holcombe@tetratech.com
Takefumi Takuma, Giken America Corp.; Orlando, Florida; (407) 380-3232 ttakuma@gikenamerica.com
Chris DellAringa, Blue Iron, Inc.; West Sacramento, California; (949) 265-5991 chris@blueironinc.com

ABSTRACT

This paper will discuss the successful installation of seawalls for the first phase of a project in Long Beach in California known as the Naples Island Permanent Seawall Repair – Phase 1. How an unconventional method of pile driving resulted in the reduction of the duration of the project while using less space and maintaining minimal noise impacts to accommodate neighbors will also be discussed. Included in the paper will be how non-vibratory equipment used on this project also significantly minimized the risk of disturbances as well as settlement on residential properties; which in turn greatly reduced the risk of damage to existing structures. The first phase of a 6-phase project along a section of the canals with tight clearances and proximity to residents included the installation of a 1,912 linear-foot steel sheet pile wall system in front of the existing deteriorating walls from January until March 2015.

Keywords: press-in, sheet pile, seawall

INTRODUCTION

This project was located in the Naples Island neighborhood of Long Beach in southern Los Angeles County, California. After 80 years of the same seawall structures lining the canals of this beautiful neighborhood, the City of Long Beach Department of Public Works decided that it was time to better protect the area's multi-million dollar homes by repairing its crumbling seawalls. The City realized that the walls will only become worse due in part to several concerns, including bending failure for the already deflecting walls. According to the City, certain sections of the walls had a significant risk of global failure if the area experienced a "moderate" near-source earthquake (City of Long Beach, CA, 2014b). Although the seawalls were in need of major repair, this would not be simple. Due to the tight clearances of the seawalls between the homes and canals, installation would be difficult with heavy, conventional construction equipment.

Phase 1 of the project involved installing sheet piles on the water side in front of existing and aging vertical concrete seawalls between the Ravenna and Toledo Bridges along the Rivo Alto Canal. See Figure 1 for the General Plan for Phase 1. Financing for this project by the City's Tidelands Capital Improvement's Division allowed the construction to begin in a timely manner. However, the challenges for the City included regulatory restraints that further complicated the construction in terms of the duration of the project due in part to numerous regulations from several regulatory agencies.

The seawalls of Naples Island have been restored numerous times since the 1930's to address erosion caused by weeping of soils through the wall due to the repetition of tidal changes, subsidence on the land area inland of the seawalls, and structural issues also related to the tidal changes. Various construction techniques were used in an attempt to shore the ground behind the seawall including mud jacking and pressure grouting. Repairs to existing tie-backs and installation of new tie-back anchors were intended to shore the existing concrete and extend the life of the walls.

© 2016 Deep Foundations Institute

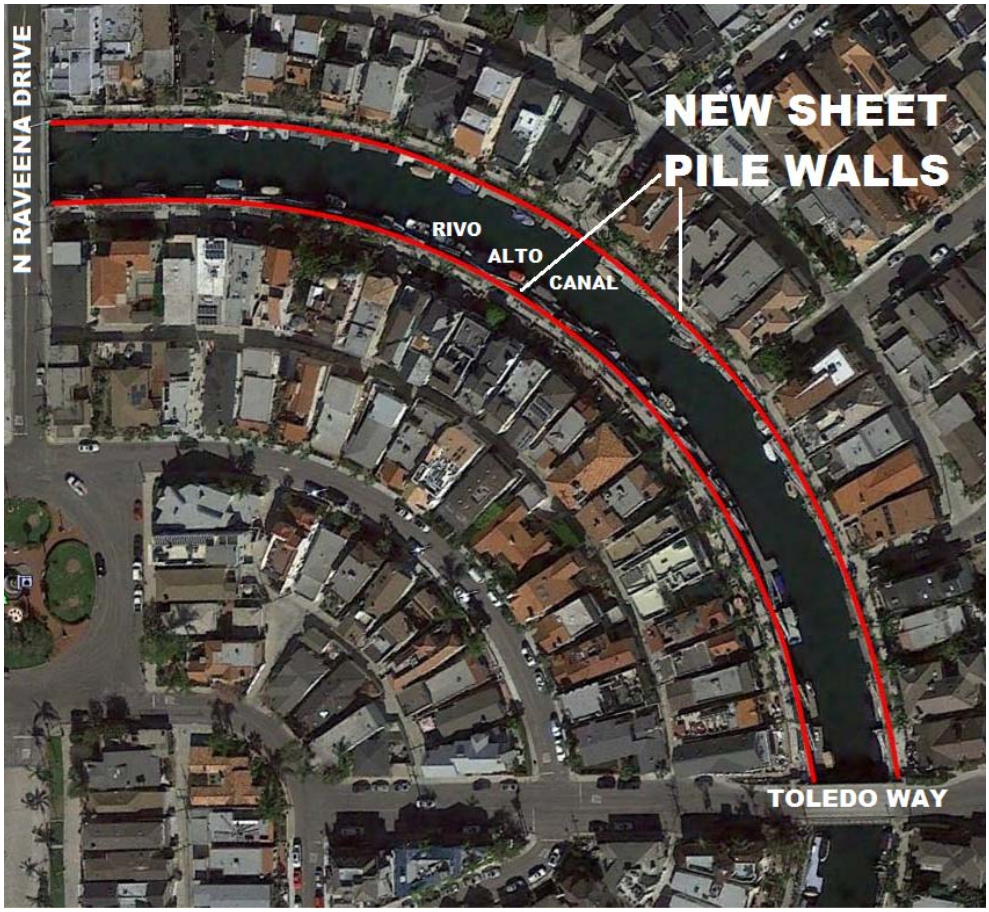


Fig. 1 General Plan Phase 1 Seawalls

DESIGN

During the permitting process, the City investigated the feasibility of many seawall upgrade or repair options with the focus on how to install a new wall on the landside of the existing wall to reduce impact to sensitive marine life habitat. The City successfully argued against the California Coastal Commission that a new wall on the landside of the existing wall was not feasible due to site constraints not limited to pre-existing buried structures, soil conditions, and accessibility to the site. Sheet piles installed with the Press-in Driving Method was the final design recommendation from the City's design consultant, Tetra Tech, Inc., who also designed the seawalls to accommodate the expected sea level rise for the 75-year life of the wall. This decision was predicated on horizontal clearance restrictions which were barely outside the backyards of residences. There was simply no room for any other types of operation and the low impact nature of the press-in pile driving procedures eliminated the issues with noise and vibration.

The 1,912 linear feet of sheet pile seawalls for this beginning phase at the time was considered as the phase that would set the standard for the remaining five phases of the project; signifying this phase's importance. The new seawalls on both sides of the Rivo Alto Canal were to extend 18 inches from the existing concrete seawalls into the channel which resulted in fill of approximately 1,727 square feet of submerged soft-bottom habitat. In order to mitigate this issue, the northern bank and north arm of a 17.7-acre tidal lagoon located approximately 1 mile northwest of Naples Island known as Colorado Lagoon was excavated to create approximately 20,908 square feet of submerged soft-bottom habitat to mitigate the loss for this phase and

© 2016 Deep Foundations Institute

the remaining 5 future phases of this project. The new seawalls also had to be designed in such a way to enhance the public's ability to access the waterway since they would narrow the canal by approximately 3 feet and fill public trust lands.

An epoxy coating was applied to approximately 25 feet of the exposed side of the 42-foot-long sheet piles for corrosion protection and aesthetic purposes. The City's pre-design survey of the surrounding neighborhood indicated the residents preferred a grey finish to an unfinished or rusted look. The design of the seawall relied on extra thickness of the steel sheet pile to provide enough cross sectional thickness to allow for sacrificial corrosion over the 75 year expected lifespan of the seawalls. The new seawalls were designed as shown on the section view in Figure 2 and the plan & elevations views in Figure 3 to repair the seawalls. The Press-in Pile Driving Method was used to press in the sheet piles (City of Long Beach, CA, 2014a). The Commission did stipulate Special Conditions that were designed to mitigate the effects that the seawall repair was expected to have on the surrounding environment and wildlife. In order for the City to complete Phase 1 of the project, it had to abide by certain plans imposed by the Commission. These plans or programs included the Colorado Lagoon Soft Bottom Mitigation Plan, the Eelgrass Mitigation Program, relocation of motile native marine invertebrates, silt curtains, floating booms, and best management practices.

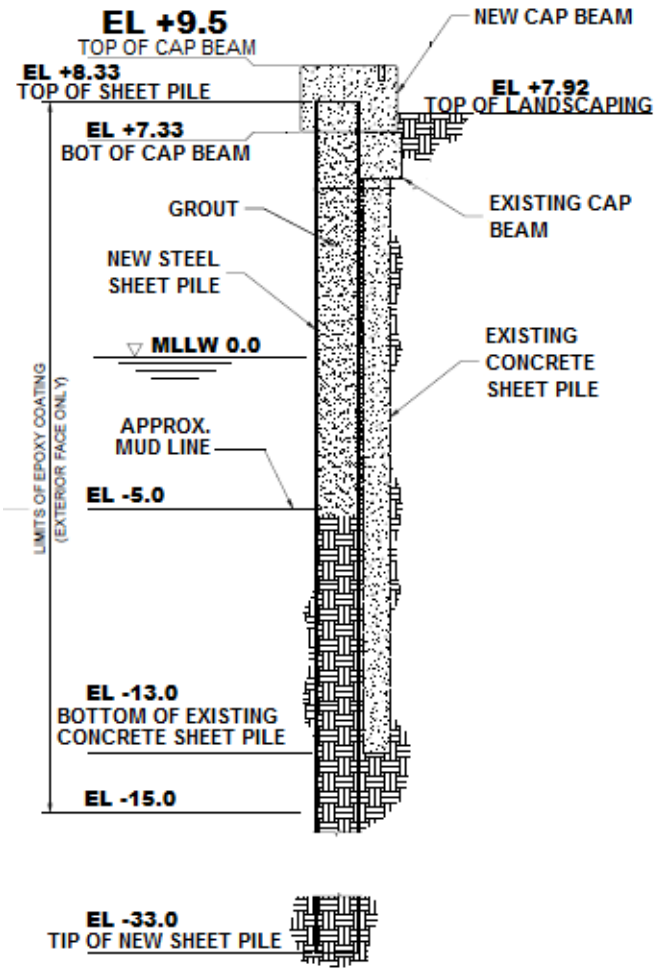


Fig. 2 Section View of Sheet Pile Walls

© 2016 Deep Foundations Institute

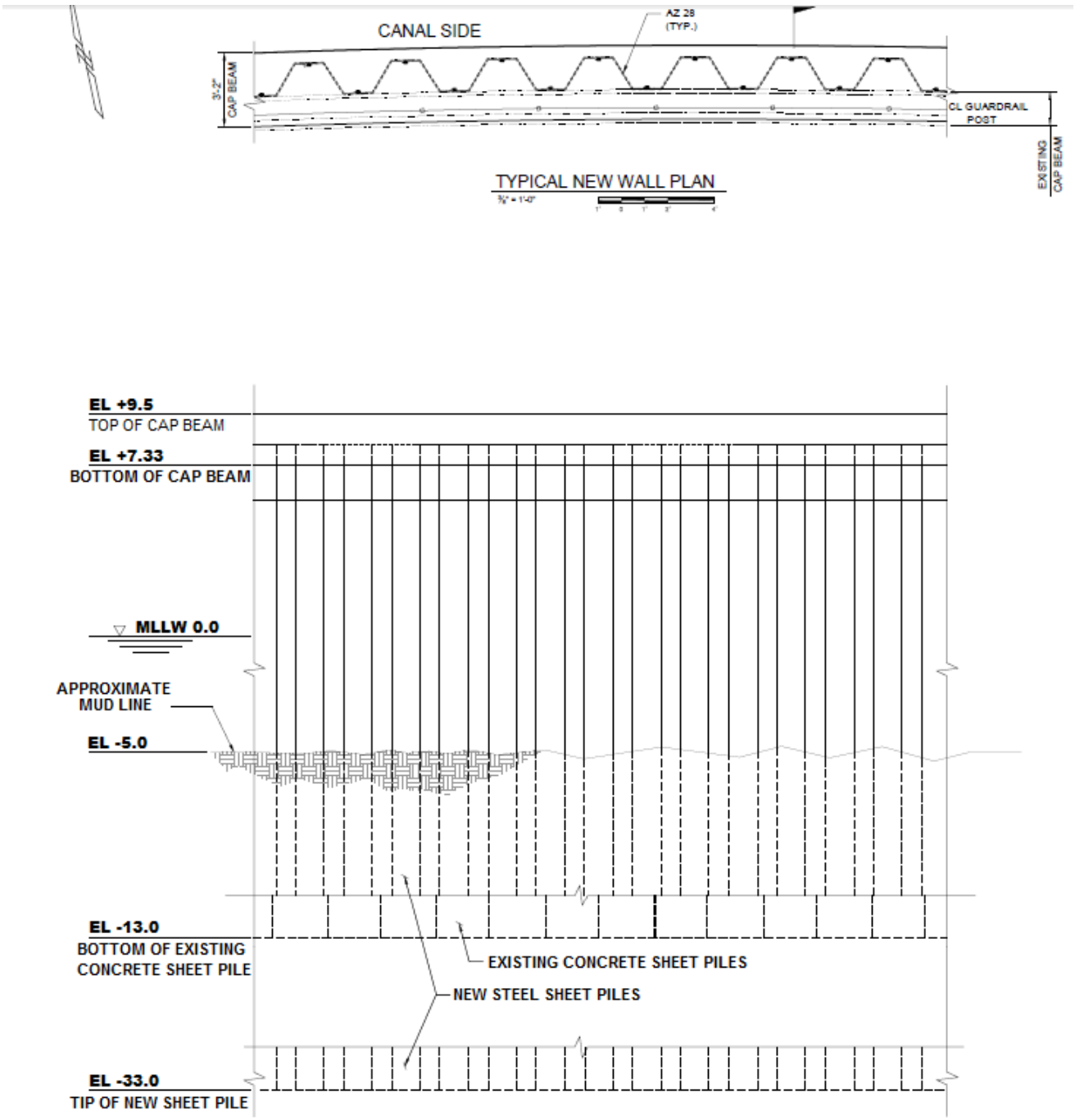


Fig. 3 Plan & Elevation Views of Sheet Pile Walls

© 2016 Deep Foundations Institute

THE PRESS-IN PILE DRIVING METHOD

The Press-in Pile Driving Method typically utilizes a reaction force derived from a few previously installed piles to hydraulically press in the next pile. The press-in pile driving equipment of this type works on top of already installed piles and moves forward on its own as shown in Figure 4. Due to the fact that this method does not use vibratory or percussive force to install the pile, it is regarded as an environmentally-friendly pile driving method. See Figure 5 for the sheet pile driving by the press-in equipment on the project. Its advantages are:

1. Low noise and practically vibration free. It enables pile driving projects close to houses, schools, hospitals, and other sensitive structures as well as in the areas where sensitive fish and/or animals are around. These features were the primary reason that the method was chosen for the project surrounded by houses and sensitive structures.
2. The equipment size is relatively small and its clamping point is much lower than those of other pile driving methods. This fact enables the equipment to work in physically tight working conditions, both horizontally and vertically. It worked out well for the construction of the seawalls consturced on this highly confined project. (Takuma, 2015)
3. It can achieve much more accurate and safer pile installation due to a combination of better control of the piles and lower clamping points compared with other pile driving methods. Driving the 42-foot-long sheets was successfully achieved on this project.

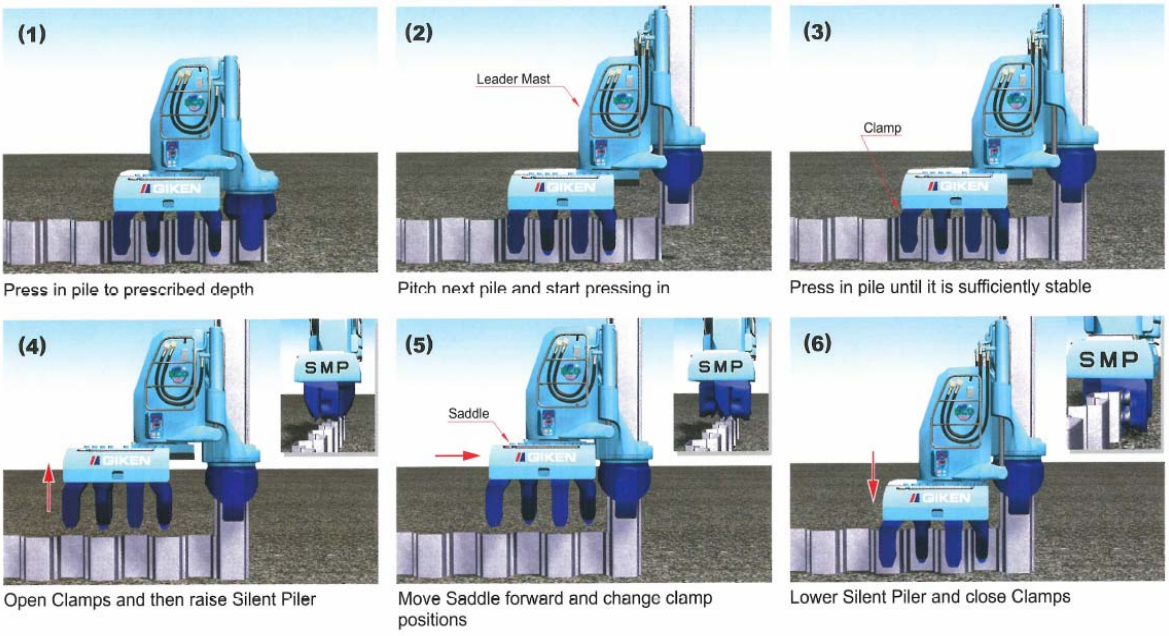


Fig. 4 "Self-walking" Sequence with the Press-in Pile Driver

© 2016 Deep Foundations Institute



Fig. 5 Sheet Piles Pressed in with the Press-in Pile Driver

The California Coastal Commission's stipulation within the specifications stated that "noise from pile driving and other activities shall not exceed 65 dB within 500 feet of any active nesting site for various types of birds and other sensitive species" and that "if constrcution noise exceeds 65dB, then alternative methods of pile driving or other sound mitigation measures shall be used as necessary to achieve the required dB threshold levels." Further on into the specifications stated that "the new sheet piles would be installed on the waterside of the existing vertical concrete seawalls using a hydraulic press (Giken Silent Piler)" (City of Long Beach, CA, 2014a). In comparison to press-in pile driving equipment, conventional pile driving equipment such as diesel & vibratory hammers would not have been as suitable for this project because they generate much higher level of noise and vibration (White, et al. 2002) than press-in pile drivers while taking into account the project location being in the middle of a residential nighborhood. There are other types of press-in pile driving equipment which consist of a heavy crawler rig and tall leads with a press-in attachment. This type of equipment is approximately 3 times as large in footprint, 5 times as tall, and twice to 4 times as heavy as the "larger" of the press-in machines that was utilized on this project. The use of pile driving equipment equipped with heavy crawler rigs and tall leads would not have been feasible because of the surcharge it would have imposed on the existing sheet pile wall during construction in addition to the tight jobsite conditions. At the start of the project, vibration and noise monitoring were conducted on the Press-in machine at the site from a distance of 20 feet. There was no noise recorded over 70 decibels. No vibration was recorded from that distance as well. Settlement monitoring of sturctures was also conducted, which resulted in no movement shown.

SEAWALL CONSTRUCTION

Seawall repair for the Rivo Alto Canal required a number of steps to be taken before actual sheet piling commenced. These steps included the disconnecting and removal of private dock floats, access platforms, and gangways. The faces of the existing seawalls were pressure washed to remove marine growth and to reveal cracks & holes so that no decomposition would occur after the grout would be poured. The top portion of the existing seawall caps were also demolished before the steel sheet piles were to be installed. After the upper portion of the cap was removed, the contractor was required to remove the front face of the remaining cap to be flush with the vertical concrete sheet piles in order to minimize the impact to soft

© 2016 Deep Foundations Institute

bottom habitat and narrowing of the canal. Once those caps were removed, a Giken Silent Piler ECO 1400S hydraulic press-in pile driving machine was used to install AZ 28-700 steel sheet piles in interlocked pairs. A typical Silent Piler is capable of installing a pair of hot-rolled sheet piles at up to 150 metric tons of press-in force. For the seawall repair, an average of 80 metric tons of force was used to install the sheet piles. Approximately 14 pairs of sheets were installed each 8-hour workday and were installed well within the required installation deviation tolerance which was a maximum of 1 inch. The sheet pile section was chosen by the contractor. See Figure 6 for the typical soil conditions and Figure 7 for the proximity of sheet piles to one of the existing concrete walls.

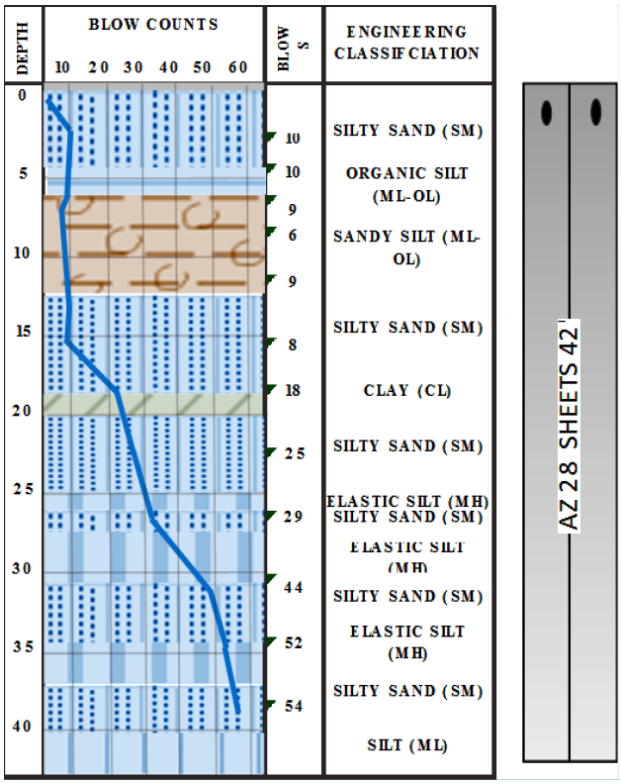


Fig. 6 Soil Conditions

The sheet piles were delivered by truck to the job site. They were then unloaded by crane onto the onsite barge. The barge used on site had to be a flexifloat barge since a conventional barge could not get under the 2 low bridges located at Ravenna Drive & Toledo East. The crane had to be walked on the barge from an alley. The press-in pile driver was also assembled from another alley. All concrete and grout was pumped from the 2 alleys to placement.

© 2016 Deep Foundations Institute



Fig. 7 Front View of Wall Installation

After sheet pile installation was completed, neat cement grout was pumped into the gap between the old, existing concrete walls and the newly installed sheet pile walls by using a low pressure ChemGrout pumping plant. New concrete seawall caps were created to encapsulate the top of the new walls together with the existing seawalls. Although the new seawalls were installed without tie-backs, they were linked to the existing seawalls by the new concrete caps. New guardrails, landscape beds, sidewalks, an improved drainage system, and relocated street lighting complemented the construction. Residents actually had the opportunity to take a survey to decide which type of seawall cap design would be placed on the walls after installation was complete. Construction work done after sheet pile installation was possible from the City's Tidelands Fund, which provided the money that was used for the public access improvements.

UNFORESEEN CHALLENGE

Along the North Wall of the Rivo Alto Canal was a weir structure that would present itself as the biggest challenge for Phase 1 of this project. The project's design called for the demolition (to the old cap elevation) and reconstruction of The Cordova Pump Station Weir Box (see Figure 8) before installing the new seawall. When the pile driver reached this point, the construction crew encountered a portion of the structure that would not allow them to install the sheet piles properly. The crew would eventually find out that a combination of concrete overspill from the original weir construction along with old timber from the original seawall dating back to before 1910 interfered with the sheet pile installation. Since there was difficulty installing the sheet piles at this point, the crew decided to demobilize the equipment and move to the other side of canal for efficiency. While sheet piling continued on the other side of the canal, contingency plans were being developed regarding how to handle pressing in the sheet piles around the weir structure. One idea was to bring in a 20-inch drill rig to break through the concrete and the wooden panel. However, a drill rig was not necessary since a simpler plan would prove sufficient. A breaker bar was used with a vibratory hammer to spud the wood panel. The panel was then jetted with high water pressure to locate the extents of the obstruction. With the concrete and wooden panel no longer being a disrupting factor, sheet piling was able to continue until completion of the project. Despite this obstacle, the project was completed 2 weeks ahead of schedule; thanks in part to the Press-in Method. Figure 9 illustrates an example of how the project turned out aesthetically.

© 2016 Deep Foundations Institute

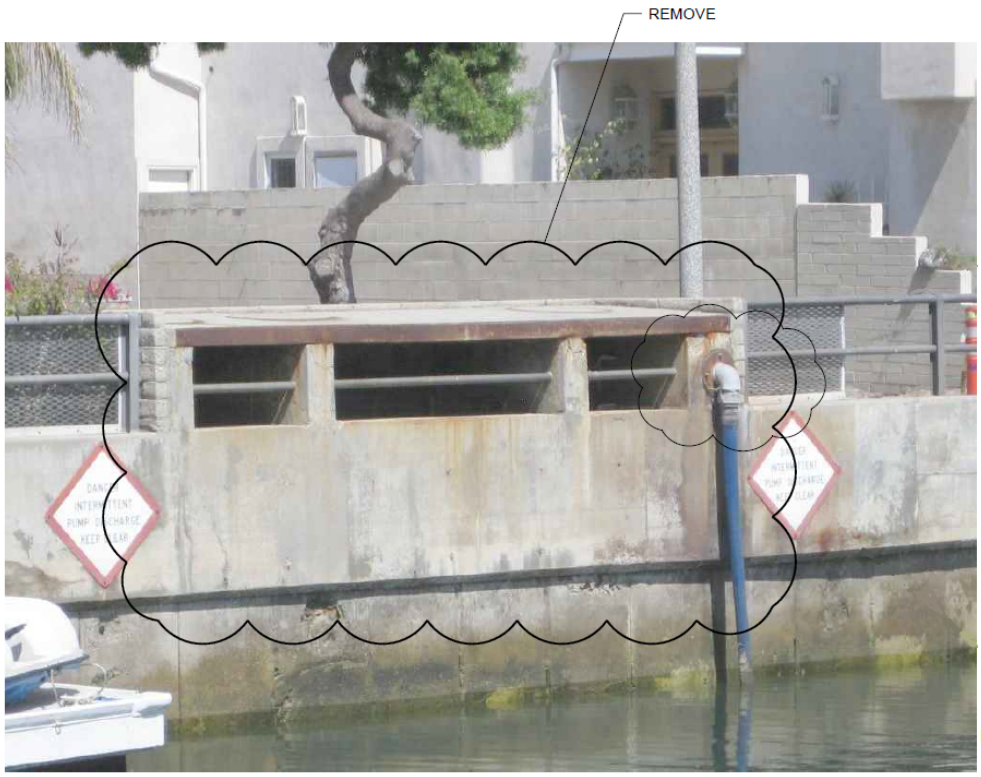


Fig. 8 Cordova Pump Station Weir Box at Rivo Alto Canal



Fig. 9 Completed Installation

© 2016 Deep Foundations Institute

CONCLUSION

The success of this project was entirely dependent on executing the construction within a tight footprint directly adjacent to homes without damage or unnecessary disruption to the residents living in these homes. The press-in pile driving system was the most feasible way this work could have been accomplished given the site constraints. The press-in system is non-vibratory yet very effective at driving long piles as was demonstrated in such difficult conditions. The system was able to work within very confined areas and required little in preparation work and disruption outside the footprint.

ACKNOWLEDGEMENTS

The authors acknowledge Shigeru Kambe of the Giken America Corporation for providing his insight as well as informative documents & images for this paper.

REFERENCES

City of Long Beach California Tidelands Capital Improvement Division and Department of Public Works, 2014a. Contract Document Plans and Specifications.

City of Long Beach California Tidelands Capital Improvement Project Office, 2014b. Naples Seawall Repairs Phase One. PowerPoint Presentation for a community meeting, October 16.

Takuma, Takefumi, 2015. Low Noise and Low Vibration Press-in Piling Method in Soft Soil in Congested Urban Areas. Proceedings of the 3rd International Symposium of Deep Foundations, Mexico City, November 11-12.

White, D., Finlay, T., Bolton, M., and Bearss, G. (2002), Press-in Piling: Ground Vibration and Noise During Piling Installation, ASCE Special Publication 116.

© 2016 Deep Foundations Institute

RISK ASSESSMENT AND QUALITY CONTROL ON GROUTED WATER-RETAINING LAYERS BY OBSERVATIONAL ENGINEERING

Bartho J. Admiraal, Volker Staal en Funderingen BV, Rotterdam, The Netherlands, +31102992288, b.admiraal@vsf.nl

Falco A. van Dijck, VolkerInfra Design BV, Woerden, The Netherlands, +31348435100, fvandijck@volkerinfradesign.nl

ABSTRACT

As part of the Schiphol-Amsterdam-Almere project, the largest aqueduct in Europe is being built in order for the A1 motorway to cross the Vecht river. The A1 consists of 12 lanes and the total width of the aqueduct will be 65 m (213 ft). The total length of the structure will be 620 m (2035 ft). Speed of construction is essential for the DBFM-contract, which forms the primary reason for choosing a building method with a horizontal water retaining barrier created by low pressure grouting. After final checks on the water tightness of the silica based layer (softgel), excavation to a depth of approximately 12 m (40 ft) below the water table could be started in order to build the aqueduct.
This paper presents a new approach for the calculation of the required grout volumes needed to ensure a "softgel" layer without gaps or holes. The approach applies measurement of deviations due to execution aspects in a probabilistic model. With this model, one is able to study the effects in a field application, i.e. multiple rows of grouted spheres. The results are visualized in order to analyze the risk of holes more easily. It is evident that the existence of a hole means a major leakage. By completing multiple runs, the strategy for grout volumes can be adjusted to minimize this risk.

Keywords: grouted layer, execution deviations, probabilistic model, seepage, visualizing multiple grouting

INTRODUCTION

The Dutch Department of Waterways and Public Works invests over € 4 billion between 2012-2020 to increase the capacity of 63 km (41 mi) motorways of one of Holland's major corridors. The A1/A6 will be transformed over a distance of 20 kilometers (13 mi). Near Muiden, the current drawbridge on the A1 for crossing the Vecht river will be replaced by a new aqueduct to be located slightly south of the existing bridge.



Fig 1. Artist Impression of the Aqueduct Vecht

© 2016 Deep Foundations Institute

The overall project includes the expansion of motorways between Schiphol (Amsterdam Airport), Amsterdam and Almere (SAA). This makes SAA the largest motorway project undertaken in the Netherlands in at least the last few decades. The length of the aqueduct itself will be nearly 200 m (655 ft) to support both the river as well as an eco-friendly zone at the western side of the Vecht. Future traffic will cross the Vecht river nearly 10 m (33 ft) below water level causing the total length of the structure to be 620 m (2035 ft). By accommodating 12 lanes a width of 65 m (213 ft) is needed making aqueduct Muiden the widest in Europe.
To build the aqueduct building pits with excavation levels of up to 12 m below surface level are needed. In general, the soil profile near Muiden consists of a Holocene (mainly peat and clay) top layer of around 8 m (27 ft) thickness with Pleistocene sand-layers below, see figure 2.

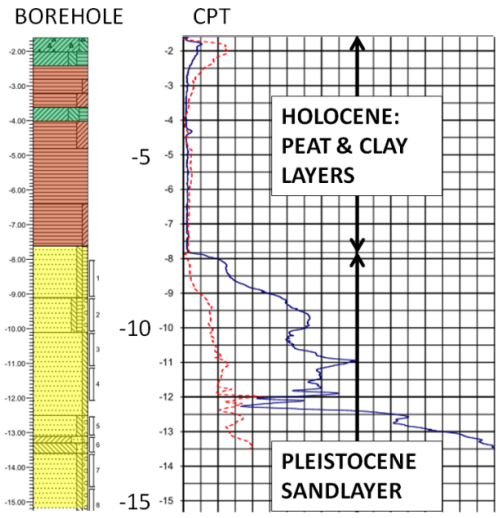


Fig. 2. Typical Borehole and CPT

(Ground)water levels are almost equal to the surface level. To create deep but dry building pits, the Pleistocene sand-layer (aquifer) needs either extensive dewatering or an anthropogenic sealing. Dewatering of the entire aqueduct is not an option since the amount of groundwater that has to be extracted during the building period exceeds the legal limit of 3 million m^3 (110,000,000 ft^3) in 3 years.

Since building speed is essential for the financial result of the DBFM-contract, a building method has been chosen in which a deep horizontally watertight barrier is created in the building pit using low pressure grouting. After this silica based layer (softgel) has been installed a total number of 5300 piles (vibro-combination and prefabricated concrete piles) have been driven through the “softgel” establishing the foundation for the actual concrete bridge structure. For retaining walls anchored sheet piles are used.
The use of low pressure grouting for this kind of structure is more or less standard practice in the Netherlands. However, the required depths of the water retaining barrier [19 to 24 m (62 to 78 ft)] minus working level) is not standard and needs extra care for design and execution. Deviations in the execution may lead to excessive differences compared with the design position of every grout injection element. For deep applications, these deviations will have a greater impact. As a result the risk regarding the permeability of the grouted layer enhances accordingly.
To control these specific risks, a new approach was developed. On previous projects a method for the grout volumes was used based on measurements on sites combined with semi-probabilistic equations. For this project a more sophisticated model is made, incorporating the interaction between grout spheres and completing multiple calculation runs based on measured deviations (= observational engineering).

© 2016 Deep Foundations Institute

GENERAL DESIGN OF A GROUTED LAYER

The principle for permeation grouting is a uniform, 3-dimensional flow of a grout from a single injection point. In a homogeneous porous soil, a near perfect sphere with a constant radius will be formed. Assuming that the soil complies with this condition, a horizontal grid for the injection points and the grout volumes will be chosen in order to achieve a minimum layer thickness and a minimum overlap of the spheres at the critical spots. See Figure 3.

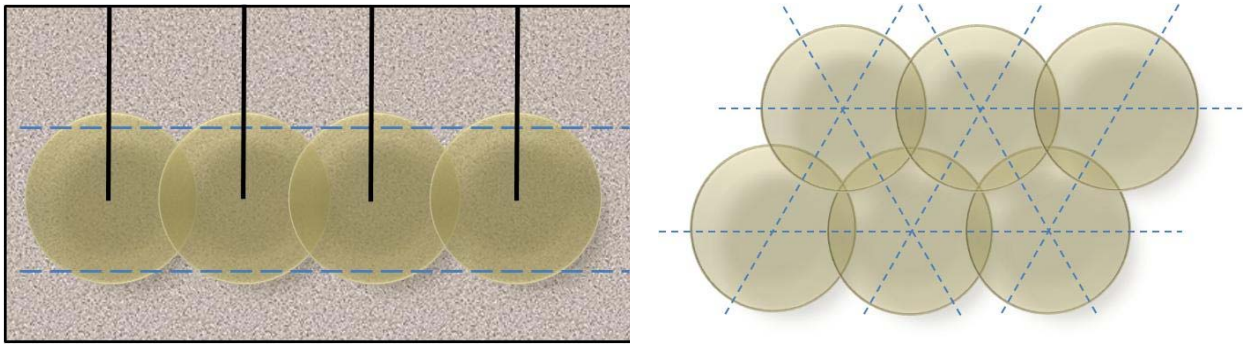


Figure 3: Basic design of a layer by permeation grouting. Cross-section and top view

For a regular triangular grid the required volume of grout can be calculated by the following equations:

$$Vgr \geq {}^{4}/_{3}\,\alpha n\pi r^{3}\,, \qquad [1]$$

$$r \geq Rtg/2cos({}^{\pi}/_{6}) \qquad [2]$$

and

$$Vgr \geq \alpha n h_{min} sin({}^{\pi}/_{3}) Rtg^{2} \qquad [3]$$

Where V_{gr} = grout volume, α = safety factor, n = porosity, r = radius of the grouted sphere, R_{tg} = rib length of the triangular grid and h_{min} = minimum required layer thickness.

The suitability of a soil layer for permeation grouting should be checked by a suitable and sufficient geotechnical soil investigation. This has to be done to analyze the homogeneity and continuity of a layer as well as to determine the grain size distribution. Thereby the presence of such suitable layer should be ensured and the choice for a certain type of grout is confirmed. Fortunately, like in most delta areas, the soil in the Netherlands generally consists of a top layer (0 - 20m) of Holocene cohesive materials like peat and clay above a massive layer of Pleistocene sands. So soil investigation can be done relatively easily with multiple CPT's and additional boring.
For the purpose this paper, as example the following parameters for one of the building pits are taken:
n=0.36, R_{tg}=1.2 m (4 ft), h_{min}=1.0 m (3.3 ft), depth D=22.5m (74 ft).

A safety margin of at least 10% extra grout volume is commonly added. So equations [1], [2] and [3] with a safety factor of 1.1 lead to
r=0.69m (2.26 ft), Vgr≥ max (0.552 ∨ 0.494) = 0.55m^3 (19.4 ft^3)

© 2016 Deep Foundations Institute

EXECUTION ASPECTS

In a proper design, deviations between theory and application also have to be considered. Especially for water retaining layer this is of great importance. The leakage through a hole or a number of holes in a "softgel" layer with a surface in total 1 m^2 (11 ft^2) equates easily to the seepage through 1000 m^2 (11000 ft^2) of well grouted sand. Consequently, potential deviations due to execution have to considered in the design-calculation of the grout volume.
The first potential deviation concerns the precision of the location of each grout position at working level. The method of survey at the working level of the chosen grid should be selected according to the type and risk sensitivity of a project. But even if this is done properly, the accuracy of placement has its limitations.
The second deviation to be considered is the inclination of the installation tool before placement of the elements. The elements for grouting – a simple small diameter hose connected to a "manchette-device"- are usually installed drilling a rod or vibrating a steel profile to the designed depth. Vertical positioning of the installation equipment before placement of the elements can be done quite precisely. Installation equipment with a guiding mast is preferred, but monitoring of verticality before placement of each element is mandatory.
The third deviation is aberration during driving or drilling. Even by minor changes of inclination during driving at depth, deviations in x-y directions will occur. At depths of more than 12m (40 ft), the influence of these deviations can be significant.
The fourth deviation is related to depth. Not only does the method of placement and the craftsmanship of the workers have its own limitations, but there is also a risk of rise of the elements during extraction of the profile. This latter item depends mainly on the shape of the manchette-element.

QUANTIFICATION OF DEVIATIONS AND EFFECTS DURING GROUTING

Measurements on site

Due to the depths of the retaining grouted layer in this project, it was decided to measure the above mentioned deviations. The found maximum x-y deviations at working level were up to 50 mm (2 in): mean value ~25 mm (1 in), standard deviation ~15 mm (0.6 in).
Each position was checked by a state-of-the-art survey (total station) and the vertical position of the installation profile was ensured by using an accurate carpenters level.
Deviations regarding the verticality during installation is dependent on the stiffness of the profile or rod, the rotation speed (drilling), soil conditions, presence of obstacles even small and, of course, the installation depth. Research with inclination measurements on this project, combined with results from prior projects, have shown the following values for the relative deviations at depth:

Table 1: x-y deviations due to profile inclination during installation in percent of depth

Installation method	mean value	standard. deviation	number of measurements
drilled	0.66	0.49	97
vibrated	1.02	0.62	44

It should be noted that the mean values and standard deviations presented above are calculated as a percentage of the depth. Any deviations in verticality of the installation tool prior to placement are combined in these values.
For the deviations in depth, the following values were found: mean value 50 mm (2 in) upwards, standard deviation 60 mm (2.36 in). Unnecessary to is that the works have been executed by the use of skilled professionals.

© 2016 Deep Foundations Institute

Overlap of spheres

The consideration for deviations in the design will undoubtedly lead to a larger required radius of the grouted spheres and accordingly to a larger volume of grout. However, there are also advantageous aspects for grouting effects like overlapping of spheres. Where a sphere has been formed by grouting, grouting from an adjacent element can't flow into the same pores. So grout from a neighboring element will be limited in certain directions and due to the additional flow resistance preferred currents in other directions will develop. The volume driven grouting process will therefore result in a bigger sphere than the start radius in Equation 1 . See Figure 4.
A second beneficial effect is the difference in permeability in distinguishing directions. Depending on the geological origin and history of the soil in a delta area, the permeability in horizontal directions is often larger than in vertical direction. Consequently the horizontal radius of a grouted sphere will be larger and therefore also the overlap of the spheres will be greater. One should be careful accounting for this in design because the presence of natural inclined soil layers might lead to a negative effect and thereby a smaller overlap.

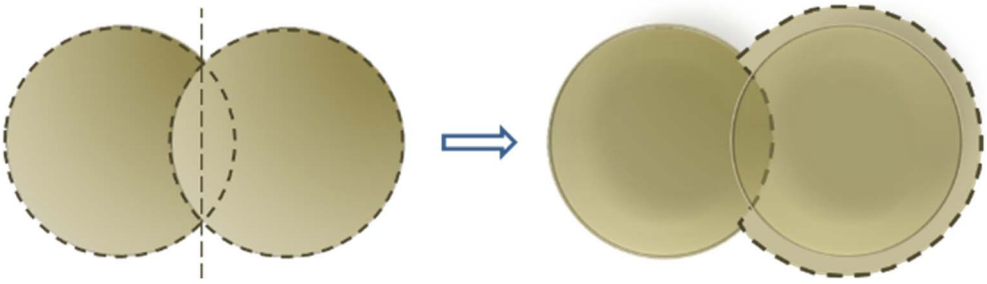


Fig. 4: Effect of overlapping spheres.

A third beneficial effect comes from blending with dissipated groundwater in the pores of the sand layer. Due to this effect the water content in the grout will increase, mainly in the outer zone of the forming sphere. This will lead to a larger volume, although with a minor adverse effect on the quality. Enlargement of the real grout volume by 10% or more is known for low viscous silica-gels.

DETERMINATION OF GROUT VOLUMES BY OBSERVATIONAL ENGINEERING

Design based probabilistic models

When statistical values of the deviation at depth of the grouting are known, the calculation of the grout volume per element can be modified. For this project, a standard distribution of the deviation in magnitude as well as in direction is chosen. However, in practice this depends to the method of installation of the elements and the measured values, so can be different for other projects. For a first conceptual model, the x-y deviations in the most negative direction from the center of the triangular grid were considered. However this results in a quite conservative model, since every element is surrounded by 6 neighboring elements. The situation that all 6 neighboring elements will have a major deviation in the most negative direction from the center element is not likely to happen. Although the direction of the deviations is random, here a simplified approach is considered. Instead of using upper limit values, a comparison is made by using modified probabilistic equations.
In delta areas composed of soft soils, Equations 1 to 3 are normally suited till depths of 12 m (40 ft). Well documented measurements should be used to determine the upper limit value or modified equations for deeper grouting applications, e.g.:

© 2016 Deep Foundations Institute

$$Vgr \geq {}^{4}/_{3}\, n\pi r^{3} \quad [1] \quad ,$$

with

$$r \geq {}^{R_{tg}}\Big/_{2\,cos\left({}^{\pi}/_{6}\right)} + {}^{1}/_{2}\left(\delta_{max.surf} + \mu_{incl,depth} + T_{inv}(2 \times 5\%; n-1)\sigma_{incl,depth}\right) \quad [4]$$

and/or

$$r \geq {}^{R_{tg}}\Big/_{2\,cos\left({}^{\pi}/_{6}\right)} + {}^{1}/_{2}\left(\delta_{mean.surf} + \mu_{incl,depth}\right) \quad [5]$$

and still applies:

$$Vgr \geq nDsin({}^{\pi}/_{3})Rtg^{2} \quad [3]$$

Where $\delta_{max,surf}$ = maximum or 95% value of the deviation in placement on working level,
$\mu_{incl,\ depth}$ = mean value deviation at defined depth due to inclinations,
$\sigma_{incl,\ depth}$ = standard deviation at defined depth due to inclinations and
T_{inv} = distribution factor Student-T method

This approach is based on expert judgement and therefore subjective to a certain degree. However, this has proven to be reliable on previous projects.
In Table 2 the required volumes of grout have been calculated using Equations 1 to 5 and the parameters included in this paper.

Table 2: Minimum grout volumes according equation 1, 3, 4 and 5 in m^3

$V_{gr\ -22.5m}$	[1]	[3]	[4; 1]	[5; 1]
drilled	0.552	0.494	0.830	0.707
vibrated	0.552	0.494	0.973	0.824

But an even more accurate determination of the grout volume per element can be calculated when the beneficial effects are also incorporated. So a more sophisticated model was the subject for a new research.

Influence of overlapping on the size of spheres

As mentioned in this paper, overlapping of grout will lead to the formation of larger spheres. Increase of grout volumes in order to compensate for deviations in the exact position of the injection elements will enhance this effect. This effect is often noticed in the field where pump pressures will increase during the progress of the project, resulting in the so called formation of a grout front. This side effect is often used to ensure full contact between the retaining wall and the grout layer. In the case of extreme formation of a grout front, fracturing or "fracking" can be a negative consequence. Fracturing will lead to leakage of grout and weakens the soil locally, which will have a negative effect on the development of a number of grout spheres. So, the use of an extra volume of grout may not lead to extra safety, but instead to extra risks due to locally far less effective grout layers.
Therefore a design model has been developed to incorporate the beneficial effects mentioned earlier in this paper.
The equation calculating the volume of grout in the overlap of two spheres can be written as:

© 2016 Deep Foundations Institute

$$V_{overl} = \frac{n\pi}{12d}\left(r_1 + r_{2,0} - d\right)^2\left(d^2 + 2d\left(r_1 + r_{2,0}\right) - 3\left(r_1 - r_{2,0}\right)^2\right) \quad [6]$$

Where r_1 = radius sphere 1, $r_{2,0}$ = radius sphere 2 (starting value), d = center to center distance with $d < r_1 + r_2$ and V_{overl} = volume of the 2 sphere caps = overlap.

Under the assumption that the volume in the overlap will lead to an enlarged diameter of the sphere being grouted, a model can be formed determining the amount of grout needed to avoid a gap in the grout layer. The new radius $r_{2,1}$ can be calculated by:

$$r_{2,1} = \sqrt[3]{\frac{3}{4n\pi}\left(V_{gr} + V_{overl}\right)} \quad [7]$$

The enlarged radius of the developing new sphere will lead to an increase of the calculated volume of the overlap. So iterations are needed, converging to an acceptable limit value of $r_{2,x}$.
A remark has to be made for the effect of three overlapping spheres. Where the overlap of three spheres interfere, the volume of the mutual overlap will be calculated twice. This effect has to be discounted on the development of the radius and overlap.
In Equation 6 and 7, the enlarged size of a sphere due to differences in permeability between horizontal and vertical direction and dilution of the grout in the outer zone are still not incorporated. Since there is not much known about the differences in permeability this effect is yet not used. For this project, this effect is used as compensation for the double calculated volumes where three spheres overlap. Also the calculation of overlap volumes of ellipsoidal spheres is a quite complex exercise. So we need a model in which -except for a single point of injection- each neighboring grouting is influenced by overlapping and will influence the size of a new adjacent grouted sphere. Putting these effects in a mathematical model like Equations 4 and 5 forms a major challenge, so another method is considered.

Visualizing results in a field

Referring to the deviations, the main influence in the development of overlapping spheres probably comes from the unknown distance between the centers of two neighboring spheres. However, the probabilistic characteristics of the deviations are known by measurements. Therefore, the potential variation in distances between injection elements can be used to set up a probabilistic analysis. For every injection point, the deviations are chosen independently and randomly according to a standard distribution. By multiple calculations, the risk of holes in a layer can be calculated as well as the number and sizes of possible gaps. Deviations in accuracies of the depth of the injection elements can also be incorporated in Equation 6. Every grouting point will be given coordinates according to the position in the grid adjusted by combined deviations. These new x-y-z coordinates are used in multiple iterations on Equation 6 and 7.
In the developed field model it is even possible to choose a specific sequence of grouting in order to study the effects on front formation and the influence on the scale of risks for leakages. For the building pits in the aqueduct project Muiden, analyses have been performed based on these principles. The results have been visualized in order to have a better overview. An example is given in Figure 5.

The model was set up for a field of 31 x 22 elements, ~34 x 22m^2 (366 x 237 ft^2). For this project, installation of the manchette-elements by vibration of a sheet-pile profile is chosen and according to the distribution of the several measured values the parameters in deviation have been calculated.
Grouting row by row was modelled in order to analyze the effects in case of formation of a grout front. This strategy creates more certainty on forming intimate contact between the grouted “softgel” layer and the sheet-pile retaining wall.
In this respect, the influence of variations in grout volume was investigated, especially the effect of using larger grout volumes in the first few rows.

© 2016 Deep Foundations Institute

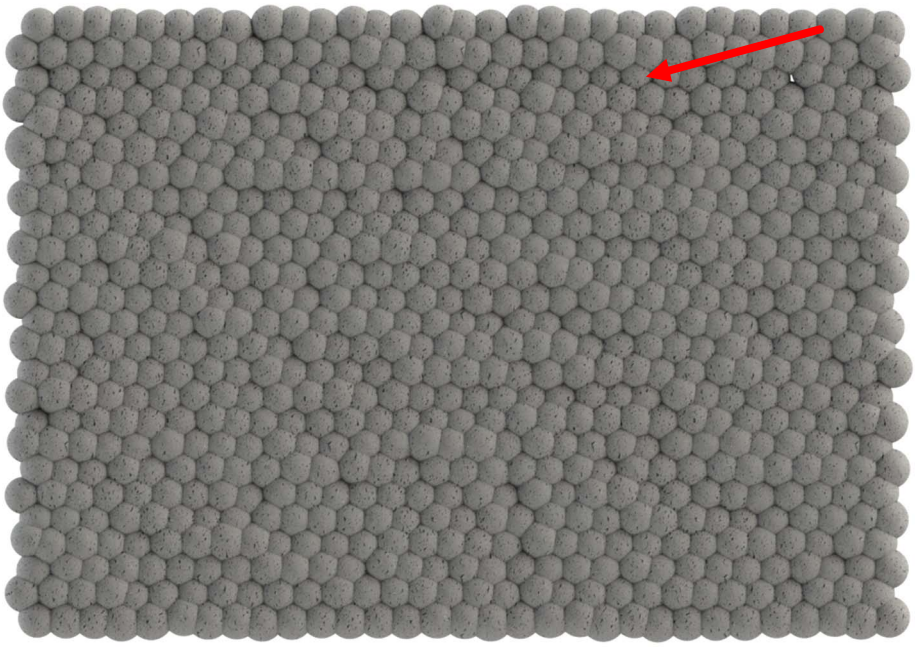


Figure 5: Visualization of a run. Grouted layer, volume 0.875m^3 first 2 rows, 0.675 m^3 following rows

After a number of runs the following grout volume per element was chosen: first two rows 0.900 m^3 (31.8 ft^3),
third and fourth row 0.800 m^3 (28.3 ft^3), rest of the field 0.675m^3 (23.8 ft^3).
For a total field area of more than 20,000 m^2 (215000 ft^2) this new way of modelling is not only meant for savings on execution time and costs, but most importantly results in an improved understanding of the risks and influences of applied grout volumes and sequence of grouting.
This model is considered as a first step in a new approach. Therefore improvements will certainly be made in the future. In addition, more measurements of the deviations during installation of the elements and better understanding of the effects of permeability differences in horizontal and vertical directions would be most valuable. Developments in inclination measurement for all installed elements might even result in a fitted strategy and grout volume per element, still using the calculation of overlap volumes.

THE PROOF OF THE PUDDING

For the dewatering permit, predictions of the flow rates through the horizontal and vertical barriers, the total dewatering quantities and the environmental impacts of the dewatering had to be determined. To estimate these as accurately as possible, conservative values for the permeability from laboratory tests results were used as input to the hydrological model.
Construction activities at site started with installation of sheet piles directly followed by injection of the soft-gel. Within the deepest pit driving of the piles started in February 2014 and lasted until July 2014.
While monitoring the variations in water levels inside and outside of the pit and the inclination of the sheet pile walls, dewatering and excavation started in July 2014 and was completed in August 2014.

Excavation of the first compartment started in July 2014 while the variations in water levels in and outside the building pit, inclination of the sheet pile walls and dewatering quantities were monitored. The aqueduct was opened in 2016. In general, with the exception of local leakage, the soft-gel layer has proven to be sufficiently watertight for dewatering the pit. Although the gel layer has been penetrated by more than 4000

© 2016 Deep Foundations Institute

piles, the actual quantities from the dewatering were well within the permitted limits. The result is shown in Figure 6.



Figure 6. Building pit September 2015

SUMMARY AND CONCLUSIONS

For the construction of Europe's largest aqueduct multiple deep building pits were needed with excavations up to 10 m (33 ft) below the water table. In order to keep the dewatering within the legal limits, low pressure grouting –soft gel- was chosen as a water retaining barrier between sheet-pile walls. These barriers had to be installed to depths of 24m (78 ft). For a well performing sealing, accurate placement of the grouting elements at the designed depths is needed. But even then, deviations will have a major impact on the minimum required volumes of grout. The size of adjacent grouted spheres will determine whether there will be "holes" in the grouted barrier or not. But on the other hand, too much grout will lead to a fast growing front of grout with potential fracturing and leakages as a result. In addition over-grouting will result in extra time for the execution and waste of materials. So, the selection of the volumes of grout should be made with great care.

The scale of the project urged, but also gave possibilities, for measuring the deviations, mainly focused on the precision of placement of the elements. While it is not feasible to do this for each individual element, a probabilistic analysis can be implemented. To determine the required size of the grouted spheres, mathematical calculations were made to find the influence of overlapping spheres. Since the volume of overlap results in an increase of the radius, multiple interpolating calculations have to be performed. For other types of deviations or side effects assumptions are being made. Different types of deviations are identified in this study.

In order to create a better insight in effects and risks of leakages, a model for a (part of the) field has been built. The biggest advantage of this model is the possibility for visualizing the results of choices in grouting (sequence and volumes). This can be an important tool for analyzing grouting strategies and for explaining to other participants the potential risks and reason regarding certain choices.

© 2016 Deep Foundations Institute

As indicated, assumptions regarding potential deviations in the size or shape of the spheres need improvement. For the deviations in the installation of grouting elements, it would be a large improvement if measurements could be made for each element.

ACKNOWLEDGEMENTS

The authors would like to express their gratitude to the Delft University of Technology as well as the laboratory of Volker Staal en Funderingen for their research by experiments on the influence of pile driving through grouted layers. We would also like to thank the participating companies within the project for making it possible to conduct these studies and presenting the results in this paper.

© 2016 Deep Foundations Institute

ROCK EXCAVATION AND UNDERPINNING BELOW A 19-STORY BUILDING

Steven C. Highfill, PE, Thornton Tomasetti, Inc., New York, NY, USA, 212-367-3072, shighfill@thorntontomasetti.com
Kevin P. Gleckler, Judlau Contracting, Inc., New York, NY, USA, 347-386-2458, kgleckler@judlau.com

ABSTRACT

Escalators to access platforms for the Second Avenue Subway Station at 72nd Street in Manhattan are to be installed in the basement of an existing 19-Story residential building. The escalators, which extend below the existing building foundations, require excavation of an inclined rock cavern up to 80-feet deep. Underpinning of columns within the 19-story building as well as a stone masonry party wall and columns for an adjacent 5-story building was completed prior to excavation of the rock cavern to ensure structural stability.

This paper will discuss the analysis and design of the underpinning system, the installation and load transfer procedures and the cavern excavation immediately below. The underpinning system was subject to very strict deformation limits and to electronic monitoring prior to and throughout the load transfer and construction process. Key details such as the load transfer mechanism between the reinforced concrete column and the temporary structural steel underpinning frame will be discussed. The challenging rock excavation process will be described which utilized conventional equipment and pattern drilling with Da-mite rock splitting mortar.

Keywords: underpinning, transfer, monitoring, jacking, subway, rock, excavation

INTRODUCTION

Phase 1 of the Second Avenue Subway is being built by MTA Capital Construction (MTACC) to improve subway service on the east side of Manhattan. Entrance 1 for the 72nd Street Station of the Second Avenue Subway is located on the east side of 2nd Avenue at the corner of E 69th Street in New York City. Access to the station mezzanine, approximately 80-feet below grade, is designed to be routed through the basement of an existing 19-story residential building. From the sidewalk, stairs and escalators within the width of sidewalk connect the riding public to a basement level mezzanine, which turns into the building at roughly 16 feet below grade (Fig. 1). Riders then connect to three long escalators to arrive at the station mezzanine. The escalators are to be installed within an inclined and arched cast-in-place (CIP) concrete lined rock cavern (Fig. 2). Construction of both the entrance into the basement and the escalator cavern require the transfer of columns within the 19-story building. Excavation of the escalator cavern also impacts the foundation support for columns and a load bearing party wall for the 5-story residential building immediately to the north. Two stages of

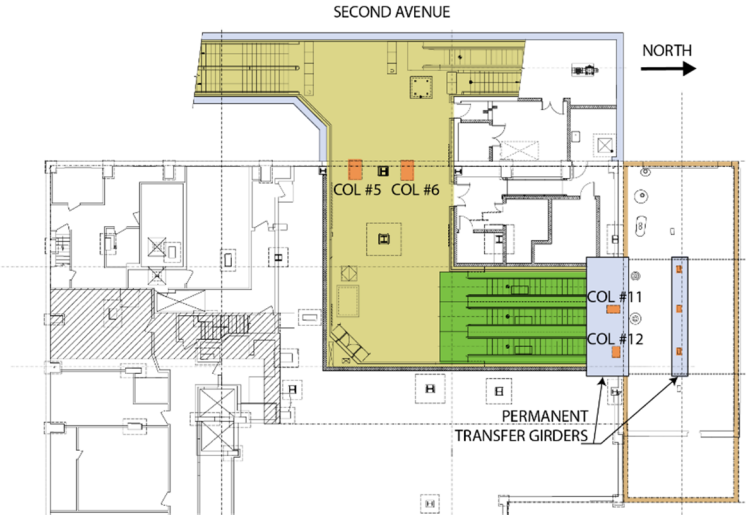


Fig. 1. Plan- Entrance Mezzanine

© 2016 Deep Foundations Institute

load transfer were used at each location. The Stage 1 transfer used a temporary underpinning system to unload the current structure which allowed for construction of the permanent transfer girders. Stage 2 transferred the load from the temporary system to the permanent transfer girders.

The process of transferring the location of large building loads has the potential to induce movement related stress in the structure and building finishes for which they were not designed or cannot tolerate. Stringent movement criteria were established by the project and subject to continuous monitoring throughout the load transfer sequence. Likewise, rock excavation adjacent to and below building foundations could cause unacceptable movement, noise, or vibration in the buildings.

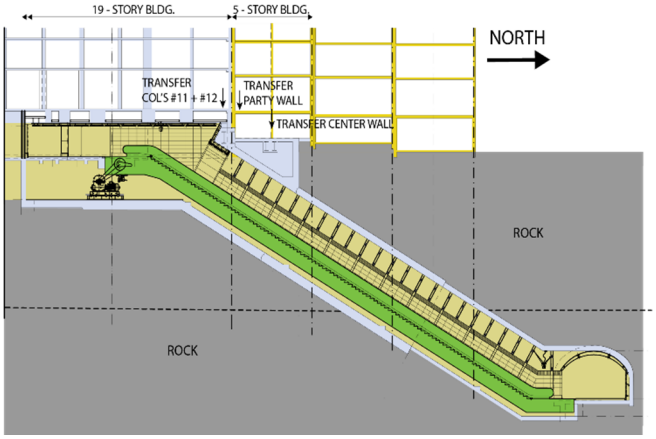


Fig. 2. Section- Entrance 1 Escalator Cavern

The design of the underpinning systems, the use of controlled load transfer procedures, and the use of controlled rock excavation methods are the subject of this paper.

Roles

The General Contractor for the construction of Entrance 1 was Judlau Contracting, with Kevin Gleckler served as Project Superintendent and jacking engineer. Steven Highfill of Weidlinger Associates, who recently merged with Thornton Tomasetti, was responsible for the design of the underpinning.

EXISTING BUILDINGS

Entrance 1 to the subway from the sidewalk was designed to be through the basement of a 19-Story building at the corner of 2nd Avenue and E 69th Street. The building, which was built in the early 1960's, was constructed of reinforced concrete flat slabs supported by reinforced concrete columns. Foundations below the basement level are spread footing supported on rock. Record drawings show that the flat slabs were designed using a lightweight aggregate concrete while other concrete in the building was normal weight. The building façade consisted of brick masonry backed up by terra cotta. The column schedule in the record drawings summarized the gravity loads for each column. Columns #11 and #12 on the north wall and #5 and #6 on the west wall were to be transferred. An independent column load takedown provided confirmation of the gravity loads in the four columns.

The age of the 5-story building immediately to the north is unknown but pre-dates the 19-story building. Field investigation found the structure to consist of wood framing spanning between a center wood bearing wall and masonry party walls on the north and south building limits. The party walls are constructed of brick masonry above ground but the basement walls are of rubble stone masonry. A wood girder at the ground floor supports the load bearing center wall, which transfers the wall load to brick masonry columns in the basement. The party walls and masonry columns are supported on rock. Foundations for the south party wall, adjacent to the 19-story building, and the center masonry columns require underpinning in order to safely excavate the escalator's rock cavern and construct the permanent concrete structure. The north party wall and foundations for additional low-rise buildings to the north, which are also above the escalator cavern, were found by the project to be outside of the zone of influence of the rock excavation and, therefore, did not require underpinning.

© 2016 Deep Foundations Institute

MOVEMENT LIMITATIONS

In order to limit stresses in the existing building frames and to reduce the possibility of impacts to building finishes, a controlled load transfer procedure is required. A detailed sequence of construction is necessary and pre-loading the temporary and permanent supports is a requirement of the project. The presence of brittle finishes such as brick, terra cotta, and plaster makes the limitation of movement particularly important and strict limitations are specified. Vertical movement of the existing buildings is limited to +/- 0.07 inches and rotation of existing building columns cannot exceed 0.003 inches per foot during the load transfer process.

DESIGN

The project required the use of four temporary underpinning frames, which are used to unload the existing structure and to allow construction of the permanent support. Underpinning Frame 1 is at the north side of the 19-story building and is designed to support Columns #11 and #12 and the adjacent party wall. Frame 2 supports the center wall within the 5-story building. Frames 1 and 2 are used to transfer building loads over the rock cavern and will be the primary focus of this paper (Figs. 3-4). The third and fourth frames supporting Columns #5 and #6 along the west wall of the 19-story building are outside of this paper's scope.

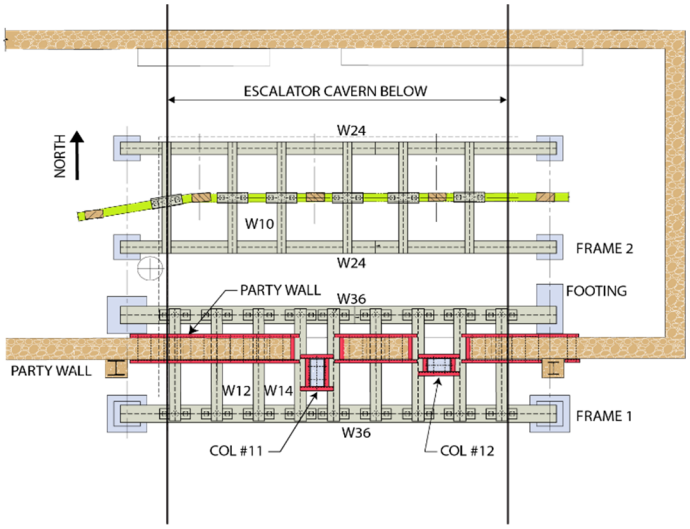


Fig. 3. Plan- Underpinning Frames

Underpinning Frames 1 and 2 are required to span the rock cavern, which has a maximum clear width of roughly 27'-2". The overall span for each frame was established as 32 feet which, based on footing sizes, provided approximately 1-foot clear between the face of rock and the closest face of a footing. Each frame utilized a pair of girders spanning the cavern, which were supported on footings bearing on rock. The existing structure was directly supported by needle beams, which spanned to the girders.

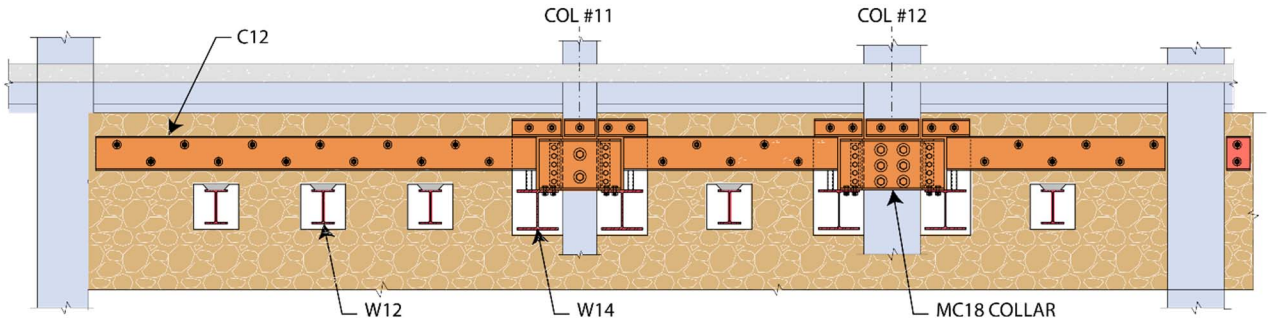


Fig. 4. Elevation- Party Wall and Underpinning Frame 1

© 2016 Deep Foundations Institute

Frame 1

The total loads at Frame 1 for Columns #11 and #12 were independently computed and determined to be 383 Kips and 234 Kips respectively. The design load for the party wall was determined to be 13 KLF. Frame 1 was designed to consist of a pair of W36 girders spaced 8-feet apart, a pair of W14 needle beams each at Columns #11 and #12, and W12 needle beams at roughly 3-feet on center to provide intermediate support to the party wall. The rubble party wall was sandwiched between C12's to provide stability to the wall and designed to span between needle beams. The C12's were interconnected using grouted through bolts providing essentially continuous support to the rubble wall.

The critical connection of the concrete columns to the W14 needle beams was resolved using a steel collar made of MC18's on the four sides of the columns (Fig. 5). The collars were grouted to the face of the columns using non-shrink grout and through bolted to the columns using high strength threaded rod equivalent to ASTM A490 bolts. A pattern of 6 bolts in the long face of the columns and 2 bolts in short face was used to transfer the column load to the channels. In order to avoid slippage between the channels and the column face, the threaded rods were to be pre-tensioned to create a friction connection similar to a slip-critical type connection in structural steel. The coefficient of friction was enhanced by roughening the surface of the columns and by blast cleaning the bearing surface of the channel. As redundant measures to prevent slippage, the annular space around the threaded rods was grouted after application of the pre-tensioning force and the washer\bearing plates welded to the MC18's.

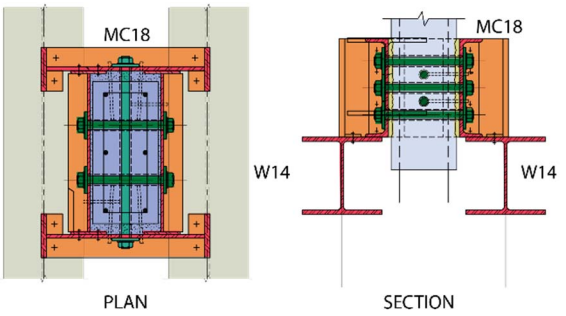


Fig. 5. MC18 Collar to Support Columns # 11 and #12

The Stage 1 sequence of construction for the frames was established to maintain the stability of the existing structure while constructing the temporary supports and implementing the load transfer as follows (Fig. 6);

1. Install C12's at the party wall; pre-grout the party wall to fill voids, core drill and grout anchors, erect C12's and grout to face of wall, and tighten anchors to a snug tight condition.
2. Cut openings in party wall for needle beams.
3. Prepare rock surface and install foundations.
4. Erect Frame 1 girders and needle beams.
5. Dry pack grout between needle beams and party wall.
6. Erect MC18 collars; roughen face of existing columns, core drill for anchors, erect MC18 collar and grout to column face, install anchors, and weld washer plates.
7. Pre-load frame using hydraulic jacks.
8. Install posts with tapered shims and remove jacks.
9. Remove the party wall and Columns #11 and #12 below the frame.
10. Install W8 infill beams and grout to party wall.

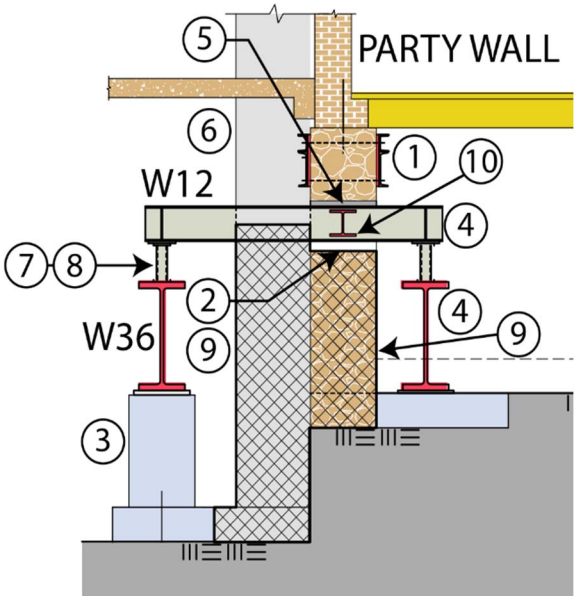


Fig. 6. Sequence of Construction- Frame 1

© 2016 Deep Foundations Institute

As noted above, the anchors at the MC18 collars are required to be pre-tensioned to develop a friction force and, to eliminate the possibility of slippage, the annular space between the anchors and drilled holes was to be grouted. In order to ensure that the friction force was fully developed and would not be reduced over time through creep, the grouting was to be completed after the pre-tensioning. Various options were considered to achieve this condition including the use of grout injection ports. However, the geometry of the collar and limited access points made this very difficult. The solution was to first install a slow setting epoxy grout in the holes, to spin the anchors into the grouted hole, and to pre-tension the anchors prior to grout set. This time sensitive process was completed one anchor at a time.

Frame 2

The three columns supporting the center wood girder which, in turn, supports the load bearing wall in the 5-story building, were estimated to support a total load of 58 kips each. Frame 2 was designed to consist of a pair of W24 girders spaced 8-feet apart and a pair of W10 needle beams was used to support the wood girder on each side of a column. The sequence of construction was similar to that of Frame 1.

Permanent Supports

The permanent support for the rock cavern was designed to be an inclined cast-in-place concrete cavern with an arch roof. The base design for the permanent supports of Columns #11 and #12, the party wall, and the center wall for the 5-story building was to be structural steel transfer girders. An alternative design was proposed to integrate permanent CIP concrete transfer girders with the arch roof, which was accepted (Fig. 7). Given the loads and depth available, the strength of the concrete transfer girders was not a major challenge but the strict performance requirements were more so. Initial deflection of the girders would be compensated for in the jacking process but live load and, more importantly, long term creep effects, needed to be considered. Detailed calculations were performed that took into consideration the varying depth of the girders from the shape of the arch and the use of compression reinforcing steel to limit creep which showed that the post-jacking deflections would be less than the project limit of 0.07 inches.

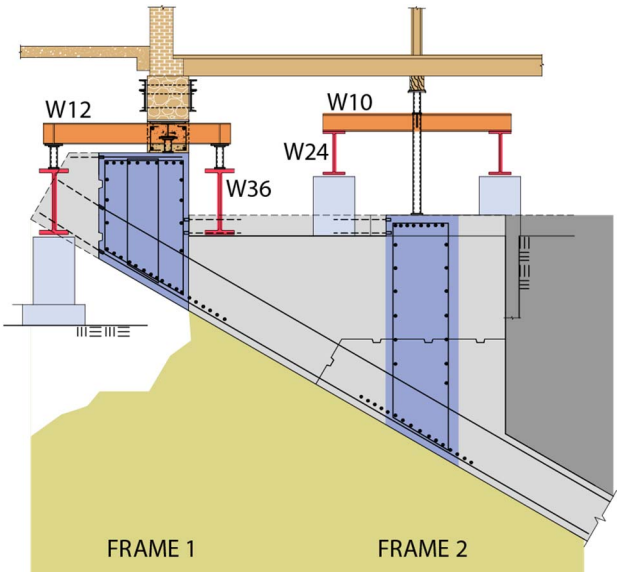


Fig. 7. Section- Permanent Supports

The transfer of load from the temporary frames to the permanent girders as achieved in the Stage 2 load transfer. Following the Stage 1 sequence of construction, these additional steps were required to complete the project at Frame 1 (Frame 2 similar);

11. Excavate the rock cavern and install the CIP liner and permanent girders.
12. Pre-load the permanent girders and unload Frame 1 using hydraulic jacks.
13. Install posts with tapered shims and remove jacks.
14. Remove temporary steel and foundations.
15. Splice reinforcing steel and infill concrete for Columns #11 and #12.
16. Infill concrete to underside of party wall.
17. Complete the escalator structure.

© 2016 Deep Foundations Institute

Load Transfer and Monitoring

Stress conditions in the existing structures were required by the project to essentially remain unchanged and strict limits on movement and rotation were established. In order to ensure this, a controlled load transfer process and continuous monitoring were required. The monitoring system consisted of the following;

- Liquid Level Sensors (LLS) utilize water and air in a system of hoses and pumps which are set under a constant pressure mounted on the existing structure and are used to observe vertical movements (Fig 8).
- Linear Variable Differential Transformers (LDTV), which read differential voltage, were connected between the existing structure above and below the Frames to directly observe 'liftoff'. These were removed after Stage 1.
- Tiltmeters were installed to observe rotation of the existing structure. Other Tiltmeters were installed on the temporary girders to monitor response.
- Accelerometers were installed on the building roofs to monitor the overall structural response.



Fig. 8. Photo- Liquid Level Sensor and Tiltmeters

The monitoring system was in place and baseline readings were established prior to the start of the Stage 1 load transfer. The monitoring was continuous and available through the web to MTACC, project engineers, the underpinning engineer, and contractor.

Prior to beginning a stage of load transfer, the underpinning engineer prepared a pre-jacking report to confirm that the underpinning frames, monitoring, special inspection reports, and jacking system were complete. He also confirmed that the condition of the existing buildings appeared to be unchanged.

The design load for each jack had been estimated by the underpinning engineer based on evaluation of the building weights and response of the underpinning frames. However, the Stage 1 jacking loads were to be incrementally applied, which allowed for adjustment of the final loading based on the response of the buildings during the jacking process. Loading increments were as follows; 25%, 25%, 15%, 15%, 10%, and then 5% increments until the final jacking load was established in the field by the underpinning engineer. Monitoring data was reviewed by the underpinning engineer after each load increment and a decision was made to continue or to modify the process. When monitoring of vertical building movement using the LLS' and LDTV's indicated that 'liftoff' had been reached, the jacking process was stopped. This occurred at roughly 90% of the expected load. Once the jacking was complete, temporary steel posts were installed adjacent to the jacks and the jacks removed. Confirmation that this was the correct load was observed after removal of original support in the ongoing monitoring, which showed minimal additional building movement.

© 2016 Deep Foundations Institute

Stage 2 jacking included the use of hydraulic jacks in the original Stage 1 locations and a second set of jacks below the permanent columns, the party wall, and at the permanent columns in the 5-story building (Fig. 9). The Stage 1 jacks were preloaded in 25% increments to the final Stage 1 loading in order to unload the temporary steel posts and the previously installed tapered shims were removed. The Stage 2 jacks were then loaded in 25% increments, while the Stage 1 jacks were simultaneously unloaded. As with the Stage 1 jacking, monitoring of the structural response was available throughout the jacking process and the results were reviewed by the underpinning engineer at each load increment. When all of the load had been transferred, temporary steel posts adjacent to the Stage 2 jacks were installed and shimmed tight. With the load then transferred to the permanent structure, the jacks and temporary underpinning frames were removed. Concrete was used to infill the party wall and concrete columns.

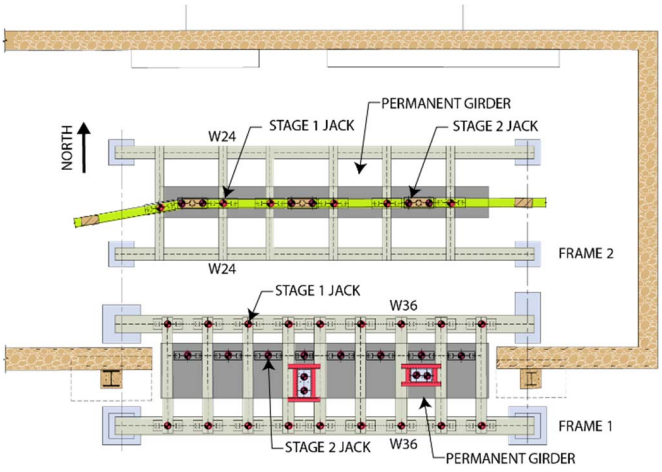


Fig. 9. Plan- Stage 2 Load Transfer

CONSTRUCTION

Construction of Entrance 1 required Judlau to excavate and remove bedrock and to selectively underpin and remove structural elements for the 19-story and 5-story buildings to house three 120-foot long escalators and to construct an Escalator Machine Room (EMR). The escalator cavern required a 30 degree inclined rock excavation, which would be lined with an arched roof CIP concrete structure. The escalator machine room itself required substantial additional rock excavation.

The project required excavation and removal of approximately 100 CY of existing concrete slab, 225 CY of soils, and 1,600 CY of rock beneath the residential structures. Construction of the concrete cavern and EMR required an estimated 225 Tons of reinforcing steel and 1,800 CY of concrete.

Underpinning

Before excavation could begin, underpinning the existing structures above was required. The new EMR and inclined arch would sit under the footprints of two residential structures, one of modern construction and one constructed of wood framing supported on rubble foundation walls. The design was developed that comprised of heavy steel girders, needle beams, and thru-bolted C-channels to support the structural columns and foundation walls. With the weight of the heaviest steel girder over 9,000 lbs. each, at lengths of up to

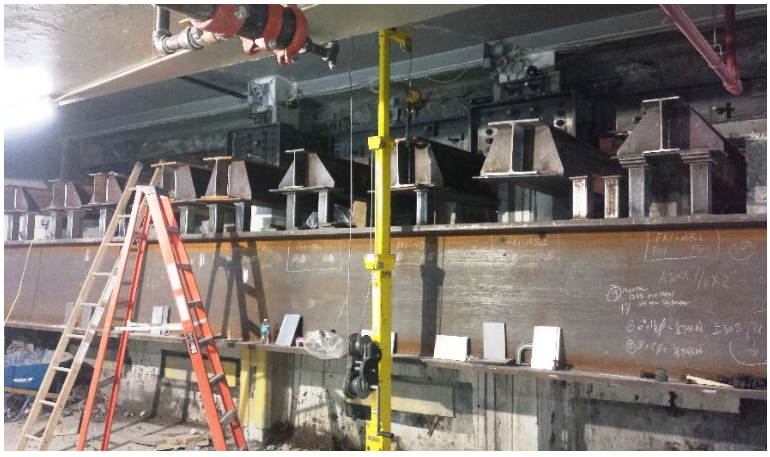


Fig. 10. Photo- Underpinning Frame 1 From Garage

© 2016 Deep Foundations Institute

32 FT, setting each piece carefully into position around the buildings foundations would prove a difficult task (Fig.10). Headroom into the existing structures garage was limited, creating another challenge getting the large pieces of steel into the area. The largest girder would sit along the south side of the north foundation wall of the garage of 301 East 69th Street. A special forklift, a JLG Lull TL 1255, was used for its low profile and max lifting capacity to drag the large girder in place and set atop the concrete footings, with the help of a mini-bobcat. The other three girders that made up the rest of Frame I & II needed to be dollied into the basement of 1322 2nd Avenue through the existing sidewalk hatches off 2nd Avenue. Each girder was spliced in two pieces, using chain falls and jacks to set each to its proper elevation.

Installing the needle beams was the next step in the sequence of the underpinning installation. This proved challenging because of the existing condition of the party wall that the beams needed to penetrate. The composite structure made points of entry through the wall critical in sizing, requiring additional engineering and temporary supports to enlarge the openings to allow installation of each beam through the party wall without compromising its integrity. Existing utilities under both structures (gas, electrical, sewer, steam, etc.) needed to be supported or rerouted to allow installation of the steel. When reroute was not a solution, the utilities were worked around or incorporated into the design of the frame.

Bolt-up of the underpinning frames were simplified using DTI washers and TC bolts, both direct tightening indicators that illustrate when structural bolts are properly tightened, eliminating the need for torque testing in tight locations. The ironworker crew needed to use extreme care when welding the beams to the girders, careful not to create any small fires or smoke-out that would affect the living areas directly above; the close proximity of the wooden substructure of 1322 2nd Avenue to the areas of welding made this a difficult task.

Upon completion of the two underpinning frames, Simplex jacks were brought in and set in place per the underpinning design. WB Equipment, the jack supplier, provided 3 full jack setups for the Stage 1 load transfer, when the temporary underpinning frames were activated, and 5 for the Stage 2 setup where the load was finally transferred to the permanent supports. 24 jacks were used for Stage 1 and an additional 18 used for Stage 2. Sequencing proved challenging and extreme care was taken when loading the jacks. This was especially the case during Stage 2 when the Stage 1 jacks were to be unloaded simultaneously with the loading of the Stage 2 jacks. Working in groups and under the direction of the jacking engineer, the jacks were activated in small increments to avoid unbalanced loading. Monitoring systems were checked prior to proceeding to the following load increment.

Excavation

Preparation of a Construction Work Plan (CWP) was necessary for such a delicate and extensive rock excavation. Planning would be crucial to complete the work under budget, while maintaining the aggressive schedule. The first step was choosing the right equipment for the excavation. The initial plan was to use a track drill (Fig. 11) with large button splitters (Fig. 12) to break the majority of the rock and to remove the broken pieces with a mini-excavator. 90-lb jackhammers and pneumatic rock drills/rock splitters would be used alongside the track drill to remove excess rock (tights) along the perimeter of the inclined shaft and escalator machine room pit. Creating an accurate staging and removals plan to ensure all overburden was removed without trapping the equipment was an important step in planning the excavation. The overburden needed to be removed in gradual lifts, careful not to



Fig. 11. Photo- Track Drill

© 2016 Deep Foundations Institute

create too deep of a pocket in one area of the limits that would trap the equipment, making it impossible to remove the spoils. Rock bolts and sand walls were installed after the completion of every 5 FT lift to stabilize the cut rock face.

The challenges faced were immediately realized prior to mobilizing and beginning the excavation. The garage entrance of the 19-story residential structure is down a steep driveway off 69th Street. Equipment size was limited by the 9-foot headroom at the existing roll down gate. Extensive research was conducted to find the biggest excavators and track drills in service, with the lowest headroom required.

Another challenge was the control of noise and dust expected with this type of excavation. As noted above, the excavation would take place beneath an active 19-Story residential building, with only a 6" thick concrete slab separating the construction from permanent residents above. A number of plans & procedures needed to be put into place prior to excavation and construction, including mitigation plans, installation of noise and monitoring equipment, and dust /noise suppression systems over/around the excavation site, as well as at the exit from the garage. Sound blankets covered all available ceiling and wall space around the construction limits and water mist systems were installed above the excavation and along the path out to the street to minimize dust. Working hours were limited to 8AM-7PM Monday thru Friday, with no work allowed on the weekends, leaving little room for error when planning and tackling the extensive removals.



Fig. 12. Photo- Button Splitter

Excavation and removal of the rock located beneath the residential structures, Class 1A Manhattan Schist, proved to be more difficult than originally anticipated (Fig. 13). Traditional means and methods of drilling & splitting in small areas and removing the rock with robotic demolition machines (Brokks) and mini-excavators were time-consuming and costly. Constant survey was critical during the excavation process; the crews needed to know the limits to which the rock needed to be cut back, but be careful not to over excavate, as every additional cubic yard removed was costly. When rock demo began, Judlau was removing an average of 25 CY of rock per week, at a cost of $2,000/CY.

Working with a large crew of drill runners and laborers who operated multiple pneumatic sinker drills (rock drills), the team worked in a tight pattern, drilling 1-3/4" dia holes into the rock at a depth of 3'-0" from the surface, careful to keep a maximum separation of 1'-0" between centers. This was focused around the perimeter of the excavation. A second crew operating pneumatic feather splitters (rock splitters), would follow closely behind, installing the feather splitter with grease to allow the splitter to expand, creating large cracks in the rock between the multiple holes. Additional equipment was used to drill and split the larger areas within the perimeter of the excavation. An Ingersoll Rand ECM 350 Track Drill was used to drill 3½"-diameter holes at a depth of 3'-0" at 18" centers in a staggered



Fig. 13. Photo- Excavation and Cavern Construction

© 2016 Deep Foundations Institute

pattern. Hydraulic button splitters were then inserted, splitting the rock between each hole.

Once drilling/splitting was completed, the Brokk 400 would be sent in, further loosening and breaking off the cracked rock in various sized pieces with its hoe-ram (hydraulic hammer). A CAT 304C mini track-excavator would then muck out the area with its bucket, stockpiling the rock in the back of the escalator pit. Often the rock would need to be double and triple handled to get all of the loose rock to the stockpile. At the end of each shift, the mini excavator would then muck out the stockpile to the top of the escalator pit, where a mini-bobcat CAT 232b would then scoop the rock in its bucket, stockpiling it in a loading bin in the back of the garage that would be cleaned out every 2-3 days into 20CY dumpsters in the street.

Although not much could be adjusted with the method of removal of overburden, the method of breaking rock used in the initial months of excavation proved to be costly and inefficient. To increase efficiency and production, a 2nd method was introduced, utilizing a special rock-splitting mortar, Da-Mite, to speed the breaking process. This mortar was used as an addition to the drilling and mechanical breaking; utilizing the same drilling pattern, but increasing the depth of the 3½"-diameter holes from 3'-0" to 5'-0", the crews would drill as many as holes as they could throughout the week, cleaning each with air and plugging as they moved. Each Friday afternoon, a mixing crew would mobilize, filling each hole, typically 150-200 of the 3½" dia. holes & 100-150 1¾" dia. holes, with this 2-part expansion mortar, and letting it set over the weekend. Come the following Monday, the rock would be split, ready for the Brokk 400 to loosen and the mini excavator to remove. After Da-mite was introduced, the volume of rock removed each week increased from 25 CY\week to roughly 60 CY\week while the cost per cubic yard for removal decreased form $2000/CY to around $800/CY.

The construction of the concrete cavern (Fig. 14) immediately followed the completion of excavation. A scaffold system was utilized to install the PVC membrane waterproofing system on the rock ceiling and walls. Rebar installation shadowed the installation of the waterproofing, using a specialized arch bender to bend the double-faced arched #9 bars and splicing them into place.

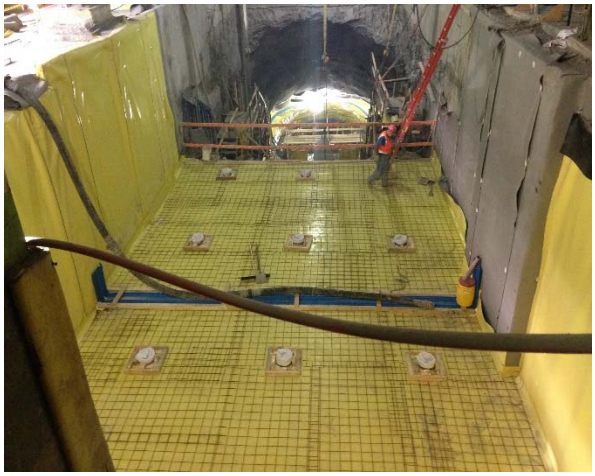


Fig. 14. Photo- Construction of Cavern and EMR

A consultant and fabricator were hired to develop and engineer a mechanical arch-formed system that would run on a set of rails on the 30 degree inclined slope. Fully collapsible by a system of large hydraulic pistons, raised and lowered down the incline by a hydraulic winch and cable, and set in place by a series of hydraulic brakes and jacks, the arch form allowed Judlau to accurately set and shape the arch in 20'-0" sections, working from the bottom, up. The finish was required to be an 'architectural finish'. To achieve this, the arched form was lined with a smooth liner of ½" thick sheet.

CONCLUSIONS

The success of a special project such as the construction of Entrance 1 is sometimes measured in what does not happen. In this case, the success is proven in the fact that the 19-story and 5- story buildings directly affected by the construction did not suffer any adverse impacts from the underpinning and re-support of major structural elements. Nor did the excavation of a major rock cavern negatively impact the building

© 2016 Deep Foundations Institute

structure or its residents. These outcomes can be attributed to careful engineering and construction planning as well as a commitment to meet or exceed strict project requirements.

ACKNOWLEDGEMENTS

Metropolitan Transit Authority Capital Construction (MTACC); responsible for building the project on behalf of New York City Transit.
Wang Technology and Straam; monitoring services
AECOM-Arup, A Joint Venture; prime design engineer
Parsons Brinkerhoff; construction quality management services

© 2016 Deep Foundations Institute

This page left intentionally blank

© 2016 Deep Foundations Institute

SLOPE REPAIRS IN A TIGHT FOOTPRINT: SLOPE STABILIZATION USING MULTIPLE TECHNOLOGIES

Dan Mahrt, PE

Abstract
In June of 2009, a slope failure occurred along River Road in Bismarck, North Dakota. The slope failure affected approximately 300 feet of River Road with vertical displacements up to 3 feet, resulting in closure of the road. River Road travels along the Missouri River in Bismarck in a geologic area riddled with historic slope failures of varying sizes. River Road is a city roadway which travels along the Missouri River. The toe of the failure extended into the Missouri River, therefore methods to repair the slope needed to be constructed within United States Army Corps of Engineers (USACE) requirements, and be acceptable to the City of Bismarck. As this is a scenic area along the river, the stakeholders desired to maintain the scenic landscape along the roadway as a part of the slope stabilization.

Due to the magnitude movement of the failure mass, the geometry of the failure was relatively easy to evaluate. In evaluating remediation options and collaborating with the USACE, the team determined that the scarp was situated primarily within the navigable portion of the Missouri River. This required USACE approval for any repair or remedial work downslope of the roadway. The City of Bismarck wished to reopen the roadway as soon as possible, therefore stabilization options were limited to working within the road right-of-way to avoid permitting for working within the navigable waterway.

The remediation solution for this project involved a combination of driven H-pile and placement of lightweight fill to re-construct the roadway at the original grades, and avoid impacting the navigable portions of the Missouri River. This paper discusses the unique project constraints and the innovative solution using multiple technologies to successfully stabilize the slope.

Background
In June 2009, Bismarck, North Dakota experienced two consecutive days of significant rain resulting in over 5 inches of precipitation in a 36-hour period. Shortly after these rain events, a slope failure was noted on River Road, a city street along the Missouri River in Bismarck. Initial findings noted the slope failure affected about a 300-foot long portion of the roadway, with vertical displacements of about 2 feet. The city of Bismarck closed the roadway and began evaluating repair solutions for the road.

Preliminary reconnaissance of the site that same week concluded that movement of the slope was still occurring. An engineering team from Braun Intertec Corporation formulated an exploration plan for the site, and worked with the city of Bismarck to initiate further studies of the area and of the affected portion of the roadway. The engineering team reviewed topography, the geologic setting, and available documentation of the area.

Figure 1 shows the general area of the project, and locations of other landmarks discussed herein.

© 2016 Deep Foundations Institute



Figure 1. Site Overview

Geology and Hydrology

The site lies on the east side of the Missouri River in Bismarck, North Dakota. In this vicinity of Bismarck, the geologic profile east of the Missouri River consists of loess-mantled decomposed bedrock; west of the river is a broad alluvial plain. The east bank of the Missouri River is characterized by steep cut-banks with localized colluvial deposits overlying decomposed bedrock.

The decomposed bedrock in this area of Bismarck consists of the Cannonball Formation. The Cannonball Formation is a tertiary deposit consisting of alternating beds of sandstone and mudstone. The sandstone is generally poorly cemented (Murphy, Surface Geology, Bismarck Quadrangle, North Dakota, 1997).

Based on gage measurements, depicted in Figure 2 (United States Geological Survey, 2016), south of the site on the Missouri River in the timeframe of the failure, riverine water levels did not appear to impact the slope failure.

© 2016 Deep Foundations Institute

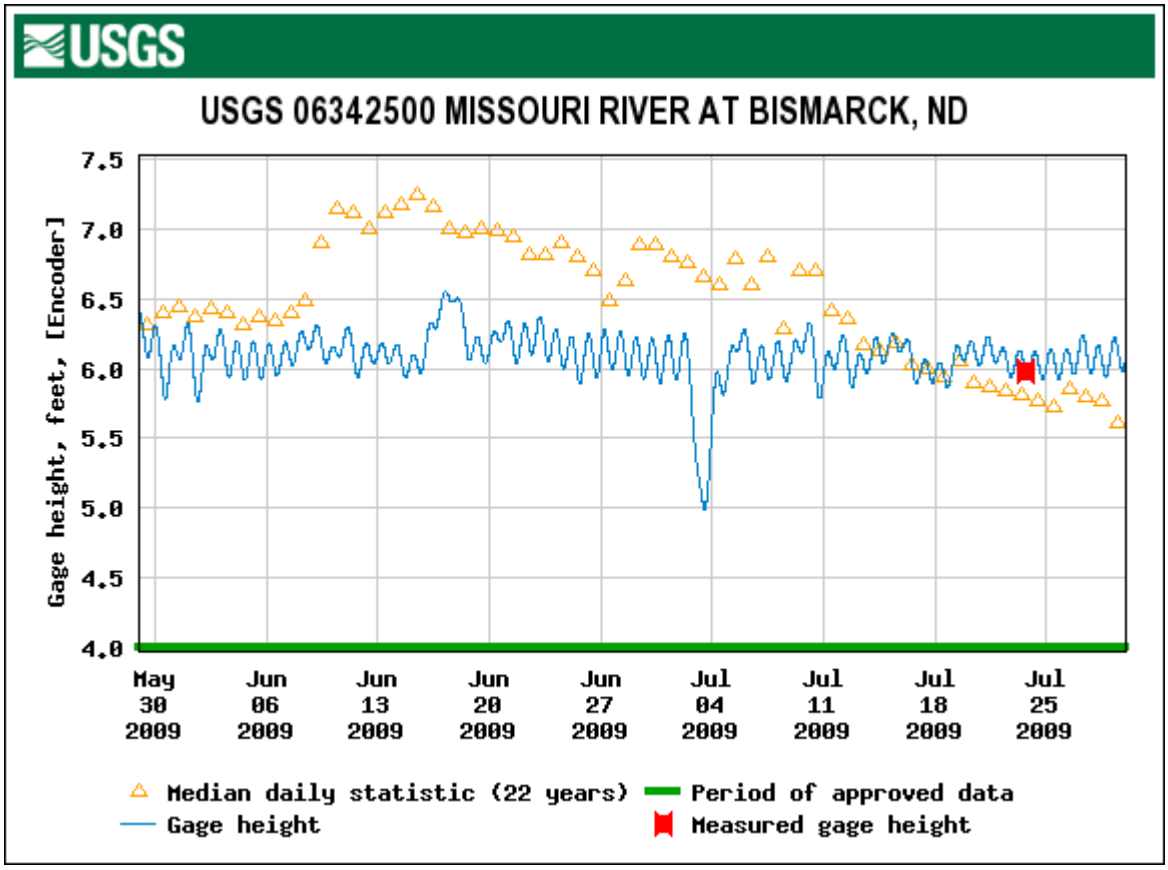


Figure 2. Stream Gage Measurements at Time of Slope Failure

History of Slope Failures

Numerous slope failures are present along the Missouri River and its tributaries in this area of North Dakota (Murphy, Areas of Landslides, Bismarck Quadrangle, North Dakota, 1997). One failure of particular interest impacted the Northern Pacific Railway Bridge over the Missouri River, which is located about 750 feet south of the failure along River Road and is depicted in Figure 1.

The Northern Pacific Railway bridge was constructed in the 1880s. George Shattuck Morrison, a prominent bridge engineer in that era, was the bridge engineer for the original construction of the bridge. In this area and at this period of time, the Missouri River had a rather wide alluvial plain, and Morrison noted that the river channel would likely meander through the plain over time. To reduce the required bridge length, Morrison decided to build a dike on the west side of the River, upstream from the bridge. The dike would serve to increase flow under the bridge, reducing sandbar deposition and reducing the likelihood of the channel meandering (Murphy, Ice Jams, Landslides and the Northen Pacific Railway Bridge at Bismarck, 2009).

Shortly after the bridge was constructed, the east bridge pier began moving. Railway engineers attempted numerous stabilization methods without success. In 1951, Dr. Ralph Peck was commissioned to evaluate the slope and devise appropriate stabilization. Dr. Peck hypothesized that the channelization of the river channel, in conjunction with trimming of the slope for the bridge, resulted in the slope failure. Dr. Peck's solution was to remove a significant portion of the hilltop above the bridge and recontour the base of the slope. This solution ultimately slowed the movement of the pier down to acceptable levels (Murphy,

© 2016 Deep Foundations Institute

Bismarck Landmark Railway Bridge, Volume 62, No. 2, Spring 1995). The bridge remains in use to this day, but has undergone several structural upgrades.

In reviewing the findings and geology of this famous failure and other failures in the area, many of the failures are associated with the Cannonball formation claystone/mudstone.

Initial Considerations and Goals

The city of Bismarck desired to repair the slope expediently to allow traffic back on the roadway. Entering the project, preliminary discussions of potential slope stabilization measures centered around expedient and "typical" repair methods consisting of sheet pile with tie-backs. As the team worked through details of the repair, the specific methods of repair and the constraints of the repair changed considerably.

Site Investigation

After reviewing geologic maps and literature regarding slope failures in the area, a team of Braun Intertec engineers visited the site. During the site visit, we selected strategic accessible locations to drill borings, measured characteristics of the scarp, and marked specific features to survey. Boring and inclinometer locations were selected during this site visit. The boring locations are indicated in Figure 3. Inclinometers were installed in Borings ST-1 through ST-4.

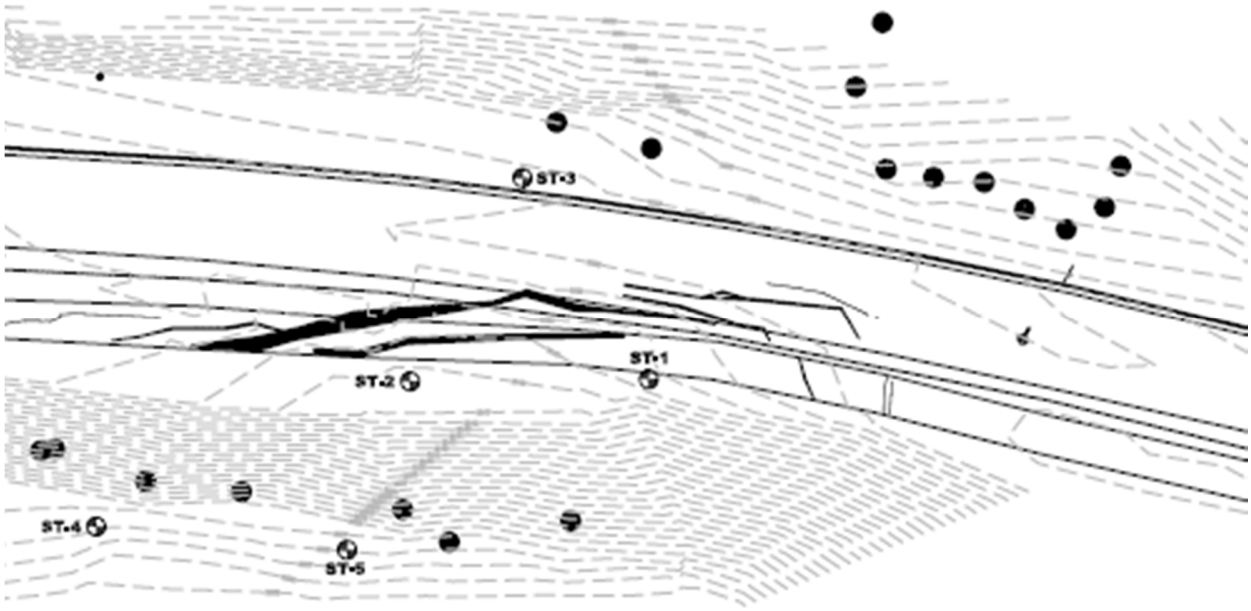


Figure 3. Boring Location Sketch

© 2016 Deep Foundations Institute

During site reconnaissance, the head scarp was evidenced by 2 to 3 feet of subsidence. The toe of the failure was not visible, but was believed to be within the Missouri River. The findings of the report and analyses were published in a Geotechnical Evaluation Report (Mahrt & Hubbard, 2009).

Subsurface Conditions

The borings encountered subsurface conditions generally similar to what was expected, however, the decomposed bedrock was encountered deeper than anticipated. The subsurface conditions are summarized in Table 1. In the roadway, 2 to 7 feet of variable fill was present, overlying mixed colluvium that extended to depths of 12 to 22 feet. Loess was encountered beneath the colluvium. Cannonball formation decomposed bedrock was present at the base of loess and extended to the boring termination depths.

At the toe of the slope, adjacent to the Missouri River, the borings encountered variable alluvium extending to about 12 feet underlain by Cannonball formation decomposed bedrock.

Thin-walled tubes were collected and Standard Penetration Tests (SPT) were conducted in the overburden. Standard penetration testing was conducted in the decomposed bedrock. The fill, colluvium, and alluvium typically consisted of interlayered fine and coarse-grained soils, making recovery of representative thin-walled tubes difficult.

Groundwater was observed at varying elevations in the borings, as much as 10 to 15 feet above river level, in the borings completed adjacent to the head scarp.

The interpreted subsurface profile through the west-to-east axis of the failure is shown in Figure 4. The colluvium, loess, and alluvium observed in the borings consist of mixed soils that, although variable on the whole, appear to have similar strength characteristics. These soils were therefore modeled as one unit of similar strength in the analyses. The piezometric surface was assumed to be 5 feet higher than levels observed in the borings. With the layered subsurface proflile, groundwater appeared to be collecting in discontinuous higher permeability layers. Using an elevated piezometric surface, the model accounted for water collecting at different elevations in the profile.

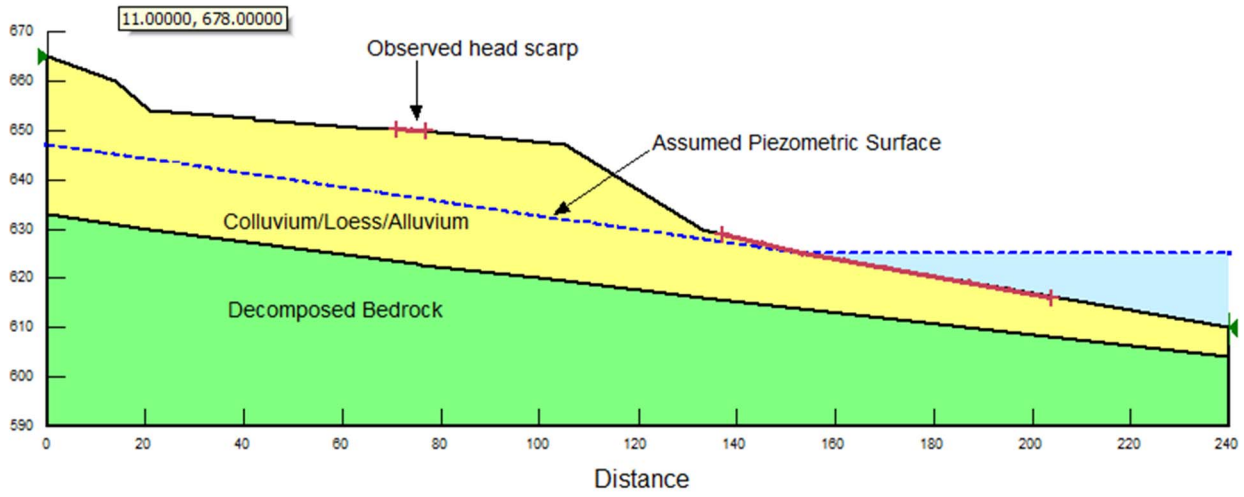


Figure 4. Simplified Cross-Section

© 2016 Deep Foundations Institute

Table 1. Summary of Subsurface Conditions

Location	Depth Zone	Material	$N_{(uncorrected)}$
Crown and Adjacent to Head Scarp	Extends 2 to 7 feet below ground surface	Fill (silty sand, lean clay, silty clay)	3 - 6
	Extends from fill to depths of 12 to 22 feet below ground surface	Colluvium (silty clay, fat clay, lean clay, clayey sand, silty sand)	WOH* - 7
	Extends from base of colluvium to depth of 23 to 32 feet below ground surface	Loess (lean clay, silt)	2 - 6
	Below Loess	Cannonball Formation decomposed bedrock (claystone/shale/sandstone)	15-52
Base of Slope	Extends 12 feet below ground surface	Alluvium (silty sand, clayey sand, sandy silt, lean clay)	2-5
	Below Colluvium	Cannonball Formation decomposed bedrock (claystone/shale/sandstone)	15-52

***Weight of Hammer

Laboratory Testing Program

The laboratory testing program selected for this project included comprehensive index and volumetric testing, as well as, two hydraulic conductivity tests, two consolidated isotropic undrained compression (CIUC) and one unconsolidated-undrained (UU) triaxial compression test. Summaries of the lab results are provided in Tables 2 and 3. The laboratory testing program was developed to characterize material index properties and the effective and total stress parameters. The final stabilization methods had not been determined when laboratory testing was selected, therefore a broad range of tests was selected.

Table 2. Laboratory Volumetric and Index Testing Result Summary

Material	Moisture Content (%)	Wet Unit Weight (pcf)	Dry Unit Weight (pcf)	Liquid Limit	Plasticity Index	P200 (%)
Fill	18	NA	NA	NA	NA	NA
Colluvium	23	103	84	62	40	92
Loess	29-37	121	93	34-47	12-32	80-96
Alluvium	22-26	NA	NA	NA	NA	NA
Decomposed Bedrock	25	124	99	NA	NA	NA

Table 3. Laboratory Strength and Hydraulic Conductivity Summary

Material	Hydraulic Conductivity (cm/s)	CIUC Triaxial		UU Triaxial	
		ϕ' (peak, deg)	c' (peak, psf)	ϕ_u (deg)	c_u (psf)
Colluvium	NA	NA	NA	23.5	1060
Loess	$1.4x10^{-6}$ to $4.8x10^{-8}$	28 to 32	20 to 280	NA	NA

© 2016 Deep Foundations Institute

Analyses

As data was collected in the field, subsurface models of the conditions were developed. Initial back-calculation was conducted based on the location of the observed scarp. As more data was collected and lab results were processed, the model was refined. Based on field observations of the failure surface and the subsurface profile developed from the drilling program, it appeared that the instability was occurring within the soil overburden, and not the decomposed bedrock, which was originally hypothesized as being the source of the issue, based on experience in the area. The borings indicated that the upper portion of the decomposed bedrock typically consisted of competent sandstone, with soft, saturated materials overlying the sandstone.

Due to the interlayering of the fine and coarse-grained soils in the soil overburden, it appeared that there were varying water levels and resulting seepage pressures generated by the rain events. However, as the interlayering was not continuous, modeling the seepage in the discontinuous layers was not practical.

In the months following the initial failure, rain events resulted in additional movement of the slope. The movement was observed in one of the inclinometers, within a month of installation and was observed in the remaining inclinometers, within 2 months of installation. We were therefore able to input the approximate failure surface into our models relatively quickly to verify our initial assumptions.

After establishing the cross-section from the borings, potential failure geometries were analyzed. During field reconnaissance, more than 2 feet of subsidence of River Road was observed at the head scarp. Constraints were established constraints in the analyses to force the failure plane through the observed head scarp, extending down towards the river. Stability of the cross section was analyzed by varying material properties until a factor of safety of about 1 was achieved; the resulting failure surface was similar to that noted in the inclinometers. The back-calculation resulted in a friction angle of 20 degrees for the colluvium/alluvium/loess unit. The friction angle of 20 degrees appears low based on the peak strength parameters from the triaxial tests conducted, but given the variability of the materials and piezometric conditions observed in the borings, the low value was justified. With the factor of safety near 1, additional forces acting on the slope such as seepage forces due to rain, would reduce the factor of safety and initiate slope failure. Multiple calculation methods were evaluated at this stage to evaluate differences in the analyses method or failure surface geometry impacted the back-calculation. However, these variations resulted in little difference in the back-calculated parameters. The performance of the stabilization design would ultimately depend on the shearing resistance along the failure surface, rather than the undisturbed soil strengths. Therefore, analyses proceeded using a friction angle of 20 degrees, and neglecting cohesion, to represent the post-failure conditions.

Constraints for Repair

Due to the urgency of the project, the team began discussing potential stabilization options and ideas even before the field exploration was complete. Initial ideas consisted of conventional methods of sheet pile with tiebacks or soil nails that local contractors could install relatively quickly.

As the site lies along the Missouri River, we began collaborating with the United States Army Corps of Engineers (USACE) prior to the field investigation. As we collected field data and discussed the project with USACE more, we learned that while the City of Bismarck owned the roadway (where the head scarp was present), the actual slope was governed by the USACE (where the majority of the failure mass was present). Because of this, any work done on the actual slope face would require USACE permitting and a public comment period which could take over a year. As the City of Bismarck intended to repair the slope and

© 2016 Deep Foundations Institute

open the road within a matter of months, the required comment period and permitting process would significantly delay re-opening the road. We therefore began evaluating alternative methods to stabilize the slope expediently that would not require the USACE permitting process.

While we had initially considered several potential stabilization options, the requirement of keeping the working platform and stabilization measures at the head of the scarp significantly reduced the alternatives. We considered additional drainage measures and lightweight fill solutions, however, adequate stabilization could not be proven without lowering the alignment of the roadway. The City of Bismarck determined that relocation of utilities, within the roadway (upslope of the head scarp) would not be practical or timely, so we evaluated other options.

Converging on a Solution

After preliminary evaluations of drilled shafts, micropiles, and driven piles, we elected to pursue a driven pile alternative to stabilize the slope. As we evaluated the alternatives, the City of Bismarck concurrently evaluated purchasing materials in advance of the stabilization contract to further reduce delays. The engineering and purchasing solutions converged on driven steel H-pile. The City was able to purchase the piles and take delivery almost immediately and multiple local driven pile contractors were available to bid the project and begin construction shortly thereafter.

After determining that driven steel pile would be a workable solution, we evaluated multiple configurations of driven pile. We ultimately chose a 50-foot long, HP14x73 pile section driven at a 7.5:12 (horizontal:vertical) batter, nearly parallel with the original slope. The piles were designed to be driven into the weathered bedrock, primarily sandstone. The design incorporated two rows of piles along the slope face. Piles were spaced at 5-feet, center-to-center in each row. The resulting layout is depicted in Figure 5

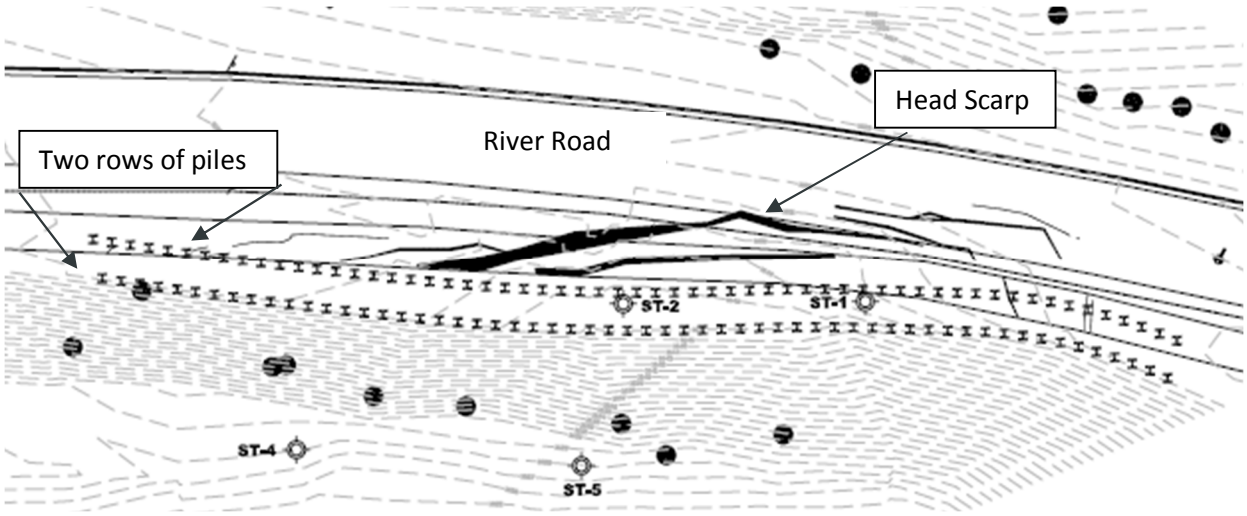


Figure 5. Pile Layout

The 7.5/12 batter was selected because it was achievable with local equipment and provided an efficient design with the slope geometry. The piles were modeled as a beam, providing shear resistance parallel to the failure plane. With this angle and the geometry of the failure mass, future movement of the slope would impart a significant axial compressive component to the piles, as well as, a smaller lateral component. As the piles were driven into the sandstone bedrock, they are able to resist the axial compressive component.

© 2016 Deep Foundations Institute

Evaluation of the lateral capacity of the piles was completed by first conducting lateral analyses of the piles at the failure surface. We first evaluated the lateral load imposed on the piles from additional movement of the failure mass. We then evaluated the pile response from these loads to develop estimated pile resistance.

While the analyses indicated that the piles would stabilize the failure mass, the roadway grade where the head scarp subsided needed to be raised up 3 to 4 feet. Stability and deformation analyses indicated that an acceptable factor of safety would not be achieved using conventional fill materials, and that the scarp would be subject to additional movement. We therefore incorporated a lightweight fill section to limit the net additional load on the head scarp. A subexcavation was completed in the head scarp area to allow placement of a 4-foot thick layer of lightweight fill. The combination of subexcavation of existing soils and placement of lightweight fill was balanced to result in a net loading increase of about 130 pounds per square foot in the head scarp area. Shredded tires were elected to be used as lightweight fill, as they were regionally available on short notice. The resulting cross-section is illustrated in Figure 6. For this geometry and repair condition, we calculated a factor of safety just less than 1.3.

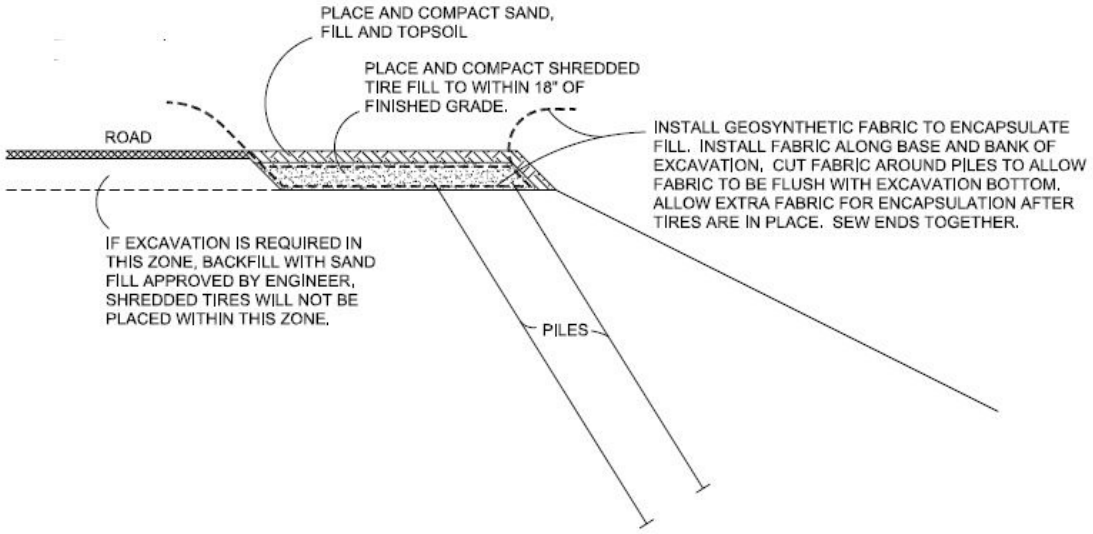


Figure 6. Cross-Section of Repair

The requirement to keep the repair solution outside of the slope face provided the added benefit of maintaining the natural setting of the slope face in the scenic Missouri River valley.

Implementation of the Design

Plans and special provisions were quickly developed so the bid for repairs could be let. The contractor was able to mobilize the week after being awarded the contract. The City of Bismarck had already taken delivery of the required H-piles on the site, so work could begin immediately.

© 2016 Deep Foundations Institute

After removing the pavement and subexcavating the roadway to 5 feet below the final pavement elevation, pile driving commenced. A Delmag D30-32 hammer was used to drive the piles. During pile driving, some additional subsidence of the head scarp occurred as the piles were driven through the failure mass. However, as the piles penetrated the weathered bedrock, the subsidence was noted to stop. This observation confirmed our evaluation of failure plane lying within the soil overburden.

Pile driving commenced near the end of October 2009 and was finished in about a week. The contractor subsequently placed the lightweight fill, subbase, and base and paved an initial lift of asphalt in November 2009. The surface course of asphalt was not placed, as we anticipated that some additional movement may occur as stresses from the failure mass and fill placement were transferred to the piles. The roadway was then reopened to traffic in November 2009, approximately 5 months after the initial failure of the slope.

We observed the repair area in the spring of 2009, prior to paving the surface course. Less than an inch of subsidence was noted in the area of the head scarp. Once the asphalt surface was placed, the road was reopened. Inclinometer readings taken in the Spring of 2009 indicated that the upper portion of the failure mass had moved less than an inch since the slope repairs were made. The inclinometers at the base of the slope indicated up to 2 inches of movement occurred between November 2009 and May 2010.

Subsequent Monitoring

We continued to monitor the inclinometers biannually through 2011 and observed performance of the repair during these trips. Only negligible movements were noted in the inclinometers after the May 2009 readings and no visible indications of additional slope movement were noted. Summer of 2011 brought significant precipitation and flooding to this area of Bismarck. River levels were over 12 feet higher than typical gage heights during the summer of 2011 (Figure 7). We took final readings on the inclinometers in November 2011 and again noted negligible movement in the inclinometers.

© 2016 Deep Foundations Institute

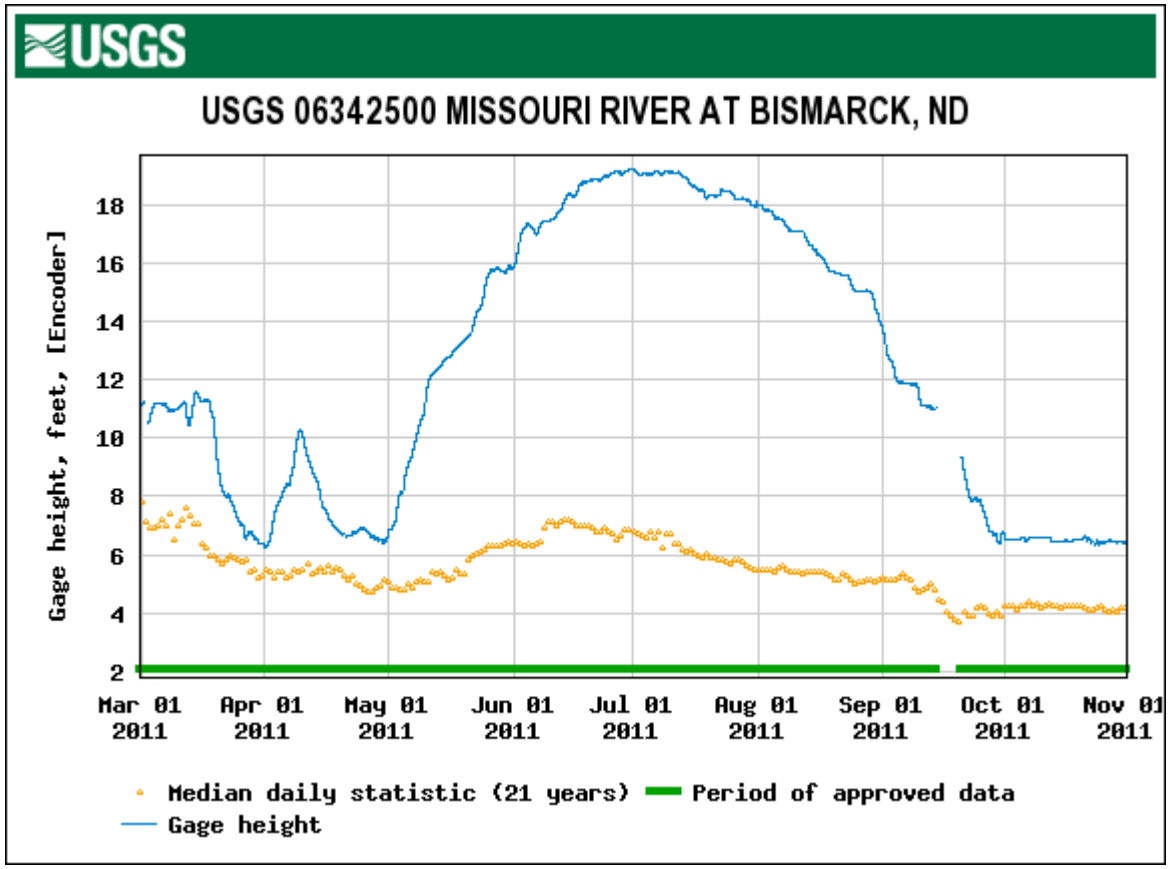


Figure 7. Stream Gage Measurements in 2011

The inclinometers were abandoned after the 2011 readings. In subsequent site visits, visible distress has not been observed.

Conclusions

This project presented unique constraints and challenges to stabilize a slope failure. The use of multiple stabilization technologies improved the resulting stability of the repaired section, and allowed the City of Bismarck to repair the slope and reopen the roadway without relatively quickly. The combined system proved resilient through significant flood events of 2011.

© 2016 Deep Foundations Institute

References

Murphy, E. C. (1997). *Areas of Landslides, Bismarck Quadrangle, North Dakota.* North Dakota Geological Survey.

Murphy, E. C. (1997). *Surface Geology, Bismarck Quadrangle, North Dakota.* North Dakota Geological Survey.

Murphy, E. C. (2009, July). Ice Jams, Landslides and the Northen Pacific Railway Bridge at Bismarck. *DMR Newsletter*, pp. 5-8.

Murphy, E. C. (Volume 62, No. 2, Spring 1995). Bismarck Landmark Railway Bridge. *North Dakota History Journal of the Northern Plains*, 2-19.

United States Geological Survey. (2016). Retrieved from National Water Information System: http://nwis.waterdata.usgs.gov/nd/nwis/uv/?referred_module=sw&search_station_nm=missouri&search_station_nm_match_type=beginning&county_cd=38015&site_tp_cd=ST&index_pmcode_00065=1&group_key=NONE&sitefile_output_format=html_table&column_name=agency_cd&colum

© 2016 Deep Foundations Institute

TURNING THE VALLEY OF ASHES INTO A TENNIS HAVEN: THE DEVELOPMENT HISTORY OF THE USTA SITE IN QUEENS, NY

Alfred H. Brand, Mueser Rutledge Consulting Engineers (MRCE), New York, NY, USA, 917-339-9300, abrand@mrce.com
Sissy Nikolaou, formerly MRCE, New York, NY, USA, s.nikolaou@outlook.com
Pablo V. Lopez, MRCE, New York, NY, USA, 917-339-9300, plopez@mrce.com
Athena C. Denivo, MRCE, NY, USA, 917-339-9300, adenivo@mrce.com
Michael McMaster, MRCE, New York, NY, USA, 917-339-9300, mmcmaster@mrce.com

ABSTRACT

The paper presents the history of development of the United States Tennis Association (USTA) site, focusing on geotechnical, geoseismic, and foundation engineering challenges associated with it. The site is located at the Flushing Meadows Corona Park area of Queens, New York. Now home to the Billie Jean King National Tennis Center (BJKNTC), the site used to be a biologically rich, tidal salt marsh that extended south from Flushing Bay and overlaid an ancient buried valley. In early 20th century, Brooklyn Ash Co. was contracted to fill the marshland with cinders and furnace ashes. F. Scott Fitzgerald describes the "Valley of Ashes" as *"a fantastic farm where ashes grow like wheat into ridges and hills and grotesque gardens; where ashes take the forms of houses and chimneys and rising smoke, and finally, with a transcendent effort, of ash-gray men who move dimly and already crumbling through the powdery air."* In 1939 the site was leveled and filled to host the World's Fair and refilled again for the 1964 World's Fair.

The USTA moved to the site in 1978 and in mid-1990's constructed the 23,000-seat Arthur Ashe Stadium (AAS). Currently, USTA has a Strategic Vision Plan venue with several interconnected construction projects including buildings, infrastructure upgrades and improvements to site circulation. In addition to a historical walkthrough, the authors will discuss technical challenges of supporting these developments through layers of fill, thick organic silty plastic clays and regional varved soils with bedrock found 300 to 400 feet deep. The subsurface is not only a weak foundation medium, but is susceptible to large amplification of seismic waves propagating from the bedrock during earthquakes. The developments are usually founded on project-specific pile foundations that carry static loads in deeper layers and accommodate lateral demands and performance objectives. Engineering innovations from the most recent development, the roof structure over AAS, will be discussed.

KEYWORDS: United States Tennis Association, Arthur Ashe Stadium, pile foundations, seismic design, Flushing Meadows, marshland, fill, organic clay, varved soils, geotechnical challenges

HISTORY

Long Island was formed during the last glaciation about 14,000 years ago. During that time the Laurentian ice sheet progressed southward covering all of today's Canada and New York State and terminating at the present position of Long Island. A terminal moraine formed at the leading edge of the glacier. That terminal moraine constitutes the high ground which makes up the central ridge of Long Island's topography. Prior to the last glaciation, an ancestral channel of the Hudson River is believed to have passed beneath what is now Flushing Meadow. As a result of a valley left by the river, glacial moraine deposits did not reach the same elevation within the Flushing

© 2016 Deep Foundations Institute

Meadow area as elsewhere. As the glaciers melted, large lakes were formed upland of the terminal moraine. The lake north of Flushing Meadow was known as Lake Flushing. Within that lake, deep deposits of varved silt, clay and fine sand were formed. The varves are the result of seasonal deposition related to the melting of the ice (Parsons, 1976). Warmer seasons produced more rapid flow and coarser deposits, while cooler seasons produced still water and finer deposits of silt and clay.

After the glacial lakes drained, a thick deposit of organic silt and clay formed (Moss, 2012). By the time Long Island was inhabited by man, the Flushing Meadow had filled with organic silt and clay and a stream known as the Flushing River meandered through the swamp deposits. A portion of an 1890 topographic map showing the Flushing Meadow swamp and the meandering Flushing River are reproduced as Figure 1. By the late 1800s the Flushing Meadow swamp had become an attractive area for the disposal of waste. Coal was being burned for heating of buildings in the NY metropolitan area. Coal burning produces a large amount of ash. Disposal of that ash was a major industry and the Flushing Meadow was an ideal disposal place. The Corona ash dump, west of Flushing Meadow, consisted of piles of ash which reached elevations in excess of 80 feet above sea level (Munshi-South, 2015). The Corona ash dump became famous in F. Scott Fitzgerald's book The Great Gatsby where the conditions through the Valley of Ashes are vividly described.



Figure 1. Flushing Meadow topography (1890).

By the 1930s New York City (NYC) planned to convert the Flushing Meadow and its Valley of Ashes to a public park. That coincided with the planning for the World's Fair to be held in 1939. Mueser Rutledge Consulting Engineers (MRCE), then known as Moran and Proctor, was engaged to explore subsurface conditions and develop site improvements and foundation criteria for World's Fair structures. Borings were made on the widely spaced grid throughout the Flushing Meadow area. Soil samples were obtained using the relatively new dry sample method by driving a split spoon sampler, now known as the standard penetration procedure. Larger diameter thin-walled tubes within a split spoon were used to obtain samples of cohesive soil for laboratory testing. Foundation criteria were developed for various buildings, highways and bridges. The early geotechnical work on site preparation for the park was described by George Freeman of Moran and Proctor in the proceedings of the 1937 International Conference of Soil Mechanics.

The meandering Flushing River needed to be straightened and controlled. A tide gate was designed and constructed near the north end of the proposed park development to control the level of water

© 2016 Deep Foundations Institute

in the Flushing River. That tide gate, built in 1936, which also functions as a roadway bridge, remains functional today.

Some of the structures for the World's Fair were intended to be temporary, serving only for the two-year life of the fair. Other structures were intended to have a longer life. As a result, different foundation solutions were employed. For temporary structures foundations were often placed on spread footings within the ash fill after it had been graded to the desired final configuration. For permanent structures, piles were driven to a bearing stratum below the organic soil. At that time, drilling technology was not capable of extending borings extremely deep. The borings typically ended in the first granular material encountered below the organic silt and clay (Brand, 1997).

The focal point and symbol of the 1939 World's Fair was the Trylon and Perisphere (USTA, 2015). That feature consisting of a sphere and a tall pylon were constructed on a foundation of driven timber piles. Another significant structure was the NYC Pavilion which was constructed on driven piles. The tide gate mentioned previously was founded on piles, as was a long boardwalk connecting the subway line north of the Long Island Railroad tracks to the entrance pavilion of the fair known as the Passarelle. A photograph of the 1939 World's Fair viewed from the north looking south, is included as Figure 2. At the conclusion of the 1939 world's fair most of the structures were dismantled. The Trylon and Perisphere was removed but the foundations were left in place. The Passarelle, boardwalk and tide gate remained, as did the NYC building.



New York World's Fair, 1939. FAIRCHILD AERIAL SURVEYS, INC.

Figure 2. View of 1939 World's Fair looking south.

By the 1960's a concept for another World's Fair evolved. The overall configuration of the 1964 World's Fair was not very different from that of 1939. Grand Central Parkway was widened, the Long Island Expressway was completed in an east-west direction bisecting the fairground and the Van Wyck Expressway was constructed as an elevated highway traversing along the eastern edge of the fairgrounds. The 1964 World's Fair again included both temporary and permanent structures, with focal point the Unisphere, a 140-foot diameter stainless steel globe which still remains as a focal point in Flushing Meadow Park. Following MRCE's design, the Unisphere was constructed on the pile foundations left in place from the original Trylon and Perisphere.

© 2016 Deep Foundations Institute

The NYC Pavilion was used again for the 1964 World's Fair. After the fair, that pavilion became a skating rink and continued to house a three-dimensional model of the entire five boroughs which was known as the diorama of New York. The NYC Pavilion has recently been renovated and now is the home of the Queens Museum.

One of the major structures of the 1964 World's Fair was the US Pavilion which was positioned towards the north end of the fairgrounds. The US Pavilion superstructure was founded on four large pile supported super columns. The structure was framed using giant trusses to cantilever from the four support points. Additional piles supported the entrance stairways and escalators beneath the center of the building. East of the US Pavilion, the open – air Singer Bowl was founded on spread footings bearing in the fill.

The 1964 World's Fair ran for two summer seasons, after which many of the structures were dismantled. Significant structures remaining today are the NYC Pavilion and the Unisphere, and site features including roadways, fountains and the iconic Art Deco style park benches. The fairgrounds are now a heavily used public park called the Flushing Meadows Corona Park.

The United States Tennis Association (USTA) had its home in Forest Hills at the West Side Tennis Club throughout much of the 20th century. By the early 1970's the US Open had outgrown the available space at the West Side Tennis Club and a larger venue was needed to accommodate the crowds and their transportation needs, as there was essentially no parking available within the Forest Hills community. The USTA accepted an opportunity to take over the existing Singer Bowl which remained from the 1964 World's Fair and reconfigured it as a two-court stadium, with Cantor Seinuk being the structural engineer for the renovations. Since the Singer Bowl was on spread footings the structure additions also had to be on spread footings and had to be designed to accommodate settlements. The thick organic silt and clay underlying the site continues to settle through a combination of primary and secondary consolidation mechanisms. Ground settlement within the park and for structures founded on fill is an ongoing problem. Special structural details needed to be developed to accommodate such settlements. The USTA Stadium opened in 1977 and has served its purpose well for many years. It was enhanced in 1997, and continues to function as the Louis Armstrong Stadium and Grandstand Stadium.

By 1995 the US Open event had grown and a new larger stadium was needed. The USTA engaged Mueser Rutledge for geotechnical studies and WSP Cantor Seinuk for structural design under the direction of architect Rossetti Associates to develop a new 23,000-seat stadium. For this new structure a very comprehensive boring program was undertaken to explore the character of the fill, organic soil and the glacial soils underlying the organics. The deepest boring extended approximately 225 feet and did not encounter a hard layer which would be characteristically considered a bearing stratum for end bearing piles. Below the 80 feet of fill and organic soil was a thin layer of glacial sand. That is underlain by a very thick layer of the glacial lake varved silt, clay and fine sand. Consolidation tests showed that the varved soil is pre-consolidated and thus could sustain the pile loads of a major stadium, albeit with some settlement (DeNivo et al., 2015).

One of the major difficulties in constructing the new stadium on piles and the surrounding courts and "outbuildings" on shallow foundations was that there were many instances where remnant foundations of previous 1939 and 1964 World's Fair structures interfered with future foundations.

© 2016 Deep Foundations Institute

Maps were developed using available information to document where prior structures existed and whether those prior structures were on spread footings or piles. Those maps have proven useful in understanding the issues during design and construction at the USTA campus.

The new stadium, which would later be named the Arthur Ashe Stadium, was constructed between 1995 and 1997. Construction was halted in the summer of 1996 to allow the US Open event to be played in the original stadium. By the summer of 1997 the stadium was complete for playing the US Open. By the mid 2000's the USTA was again in need of additional space so a new indoor facility was constructed on the east end of the campus. That facility was constructed on a combination of driven tapered piles and drilled- in- place friction piles. The drilled piles were used where driven piles posed a risk of damage to nearby structures which were on spread footings.

Over the recent several years, improvements were made to the USTA facilities by upgrading and replacing outdoor court facilities and concession buildings, but the major improvement is the construction of a movable roof over the Arthur Ashe Stadium to reduce the possibility of interruptions as a result of rain events. The roof structure construction has been done in conjunction with major reworking and rehabilitation and reconfiguration of the outdoor court facilities surrounding Arthur Ashe Stadium. Borings were made for the new roof in 2013. In addition to conventional split spoon sample and undisturbed sample borings, cone penetration with in-situ geophysical tests were performed to further characterize the soil conditions.

Piles for the roof were driven between the latter part of 2013 and early part of 2014. Construction was interrupted during the 2014 US Open and resumed after the open was completed. The major steel framework was installed between 2014 and 2015 and construction once again was halted for the 2015 US Open. The construction continues and it is anticipated that the 2016 US Open will be played under the new roof, which can be closed in the event of rain.

SUBSURFACE CONDITIONS

Many subsurface investigations have been made at the BJKNTC in Flushing Meadows dating back to its original use as the site of the 1939 World's Fair. More recently, MRCE has completed a series of subsurface investigations beginning with a site wide investigation for the construction of Arthur Ashe Stadium in the early 1990s and most recently an investigation in 2016 for the future reconstruction of Louis Armstrong Stadium. In total, the subsurface investigations include more than a hundred of borings completed across the entirety of the site.

The borings range in depth up to 200 feet below the ground surface and undisturbed samples have been obtained for laboratory testing. In addition to the borings, a series of Cone Penetrometer Tests (CPTs) ranging up to 200 feet in depth have been performed during several of the more recent investigations. CPTs include pore water dissipation tests and a series of in-situ downhole seismic shear wave velocity measurements at various locations throughout the site.

Starting in 2012, a series of 12 observation wells were installed throughout to monitor groundwater levels across the site. The groundwater levels are measured continuously through the use of data loggers in order to monitor seasonal variations and long term changes in the groundwater levels. Average groundwater levels at the site range from El. +0.0 in the northeast to El. +4.5 in the

© 2016 Deep Foundations Institute

southwest. Ground surface elevations across the site typically range between El. +6 and +16. Elevations are referenced to Local On Site Datum, where El. 0 is 2.36 feet above USGS Mean Sea Level Datum at Sandy Hook, NJ (1929, NGVD).

The general stratigraphy throughout the site consists of a layer of manmade fill called Stratum F overlying a series of four organic soil strata: O1, O2, O3 and O4. Stratum O1, consisting of brown peat, was encountered below the fill sporadically across the site and is typically less than 5 feet thick. The predominant layer underlying the Fill and Stratum O1, is Stratum O2 which consists of soft gray organic silty clay. This stratum typically ranges in thickness across the site from 40 to 60 feet, with the thickest layer of Stratum O2 existing in the southeast region of the site. Stratum O3, consisting of stiff brown and gray peat with traces of silty clay, underlies Stratum O2 and is present sporadically throughout the site. Stratum O4, which consists of organic clayey sand, underlies Stratum O3 and is not consistently present throughout the site. Underlying the organic soils are the Pleistocene era deposits grouped as Strata P-1A and P-1B strata. Stratum P-1A is a layer of outwash sands that varies in thickness across the site. This stratum consists of medium compact gray fine to coarse sand and ranges in thickness from less than 5 feet to up to 85 feet. Stratum P-1B consists of varved silts and clays and is present throughout the site typically at about El. -90. Figure 3 presents a generalized soil profile. Laboratory testing was performed on undisturbed samples to provide geotechnical design parameters. Table No. 1 includes ranges of unit weights and friction angles or undrained shear strengths for each layer.

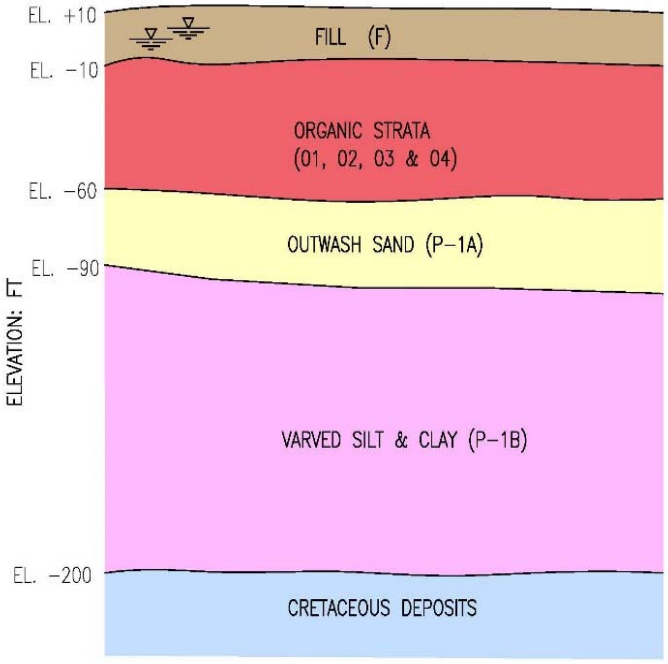


Figure 3. Generalized geologic section.

Table 1. Soil design parameters.

Soil Stratum	Unit Weight γ (psf)	Friction Angle ϕ (deg)	Undrained Shear Strength (psf)
Fill (F)	100-110	30 - 32	NA
Meadow Mat (O-1)	70 - 90	--	500 - 900
Organic Silty Clay (O-2)	85 - 100	--	300 - 1000
Peat (O-3)	70 - 95	--	700 - 2500
Organic Clayey Sand (O-4)	110 -120	29 - 31	--
Sand (P-1A)	120 - 125	32 - 36	--
Varved Silt & Clay (P-1B)	110 - 120	0	1500-3500

© 2016 Deep Foundations Institute

SEISMIC EFFECTS

Geo-seismic practice in Eastern US and NYC in particular has a relatively short history (Nikolaou et al., 2012) with the first seismic building code in effect in 1995 and updates in 2008 and 2014. The USTA site has unique geologic and tectonic characteristics that can create significant site amplification effects due to the high impedance contrast between the relatively soft overburden soils and stiff bedrock, the low strength and shear wave velocity and high plasticity index of thick clay layers (Strata O1, O2, O3, O4 and P-1B), and the vibrational differences between the predicted high-frequency bedrock motions and low-frequency vibration of the overburden soils.

The subsurface conditions at the site as presented in Figure 3, are typically characterized seismically as Class "F" sites due to the presence of thick and plastic clays. In this case the NYC Building Code requires a site-specific study is performed to derive seismic design parameters based on geologic, seismologic, and soil characteristics.

Site-specific seismic studies have been performed for the various structures on the USTA campus using the applicable NYC seismic code. The site-specific analyses were performed using the one-dimensional ground response analysis program (Schnabel, 1972). The program analyzes horizontally layered soil columns excited by vertically propagating shear waves originating from the bedrock (see Fig. 4; Nikolaou & Go, 2009). Input for the analysis includes the shear wave velocity (V_s) of the soil layers and rock, geotechnical properties for each soil stratum, and acceleration time histories at the bedrock level. Results from the Seismic Cone Penetration Test (sCPT) were used to derive a V_s profile with depth, and compared to correlations of V_s to the Standard Penetration Test (SPT) results for the granular soils and undrained shear strengths (S_u) for the cohesive layers. The V_s profiles were supplemented with Crosshole Seismic Test data MRCE performed at neighboring sites with similar subsurface conditions. The site-specific analysis is equivalent-linear, which uses appropriate strain-dependent shear modulus reduction curves (G/G_{max}) and damping (ξ) curves compatible with the overburden deposits to produce strain-compatible stiffness and damping (Nikolaou, 2008).

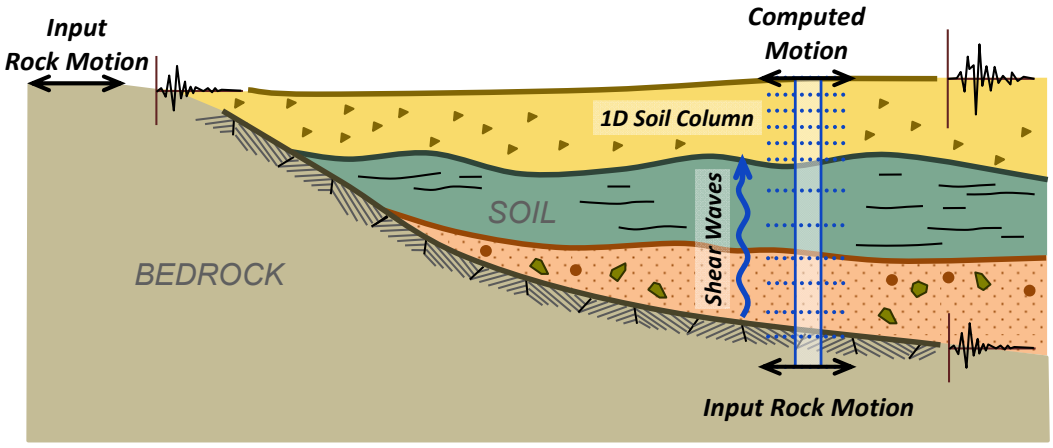


Figure 4. Simplified soil amplification modeling (after Nikolaou & Go, 2009).

A generalized profile studied is shown on Figure 5. For the ground motion input at the bedrock level, we used acceleration time histories compatible with the seismic hazard at the site for the Maximum Considered Earthquake (MCE) that has an approximate return period of 2500 years.

© 2016 Deep Foundations Institute

Several sets of acceleration time histories were developed to evaluate the variability in the site response. Each set has two orthogonal components of the ground motions. Parametric studies were also performed for the depth to bedrock that was varied between 250 to 400 feet below grade and for the V_s values of the soil layers that were varied within ±20% of the best estimate. For seismic design, the site-specific results were multiplied by two-thirds as required by the seismic code.

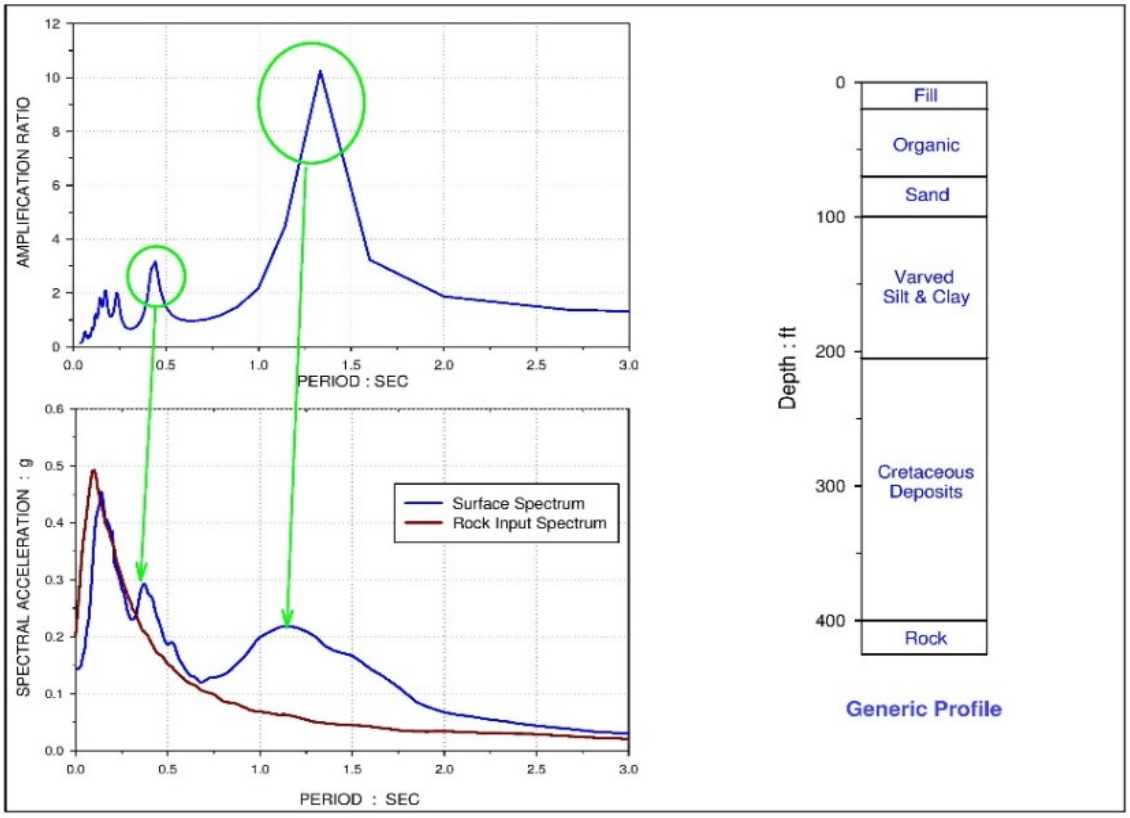


Figure 5. Seismic response of a typical soil column: Amplification ratio (top) and spectral acceleration (bottom) as function of the structural period.

The seismic response of a generic soil profile is shown in Figure 5. The bottom plot presents average results of Spectral Acceleration (SA) as function of structural period (T) of numerous individual analyses. The top plot is an example of the soil amplification ratio determined from a single representative analysis by dividing the calculated acceleration at the ground surface by the acceleration at the bedrock as function of structural period (T). The maximum soil amplification ratio takes place at the primary frequency of vibration of the soil column, approximately at T of 1.3 seconds (s). However, in absolute SA terms, the peak spectral value at the ground surface appears at the third and second modes of the soil column, at approximately T of 0.2 and 0.4 s, followed by a lower peak at the first mode at T of 1.3 s. This result is attributed to the larger acceleration values in the short periods; a characteristic of site response in Eastern US due to the high-frequency content of the bedrock input (Nikolaou et al., 2012).

As per code requirements, the liquefaction potential was also examined. The screening of overburden soils below the ground water showed a potential for the saturated fill layer to liquefy during the design earthquake at portions of the site. The effects of this potential were accounted

© 2016 Deep Foundations Institute

for by developing a reduction in strength and stiffness of this layer and calculating post-liquefaction dynamic settlements that were incorporated in the pile design. In areas with a potential for liquefaction effects, pertinent soil parameters in the foundation modeling were applied and structural solutions were developed to achieve the desired structural performance objectives.

PILE FOUNDATIONS

Since the start of redevelopment of the site in the 1990's with the Arthur Ashe Stadium and the practice and tournament tennis courts, major structures have been supported on piles driven into the P-1A/1B strata, while smaller structures are supported on spread footings bearing in the fill at 1 tsf. The piles in Arthur Ashe Stadium are Monotube™ and pipe composites as described in Table 2. The bottom 65 feet is comprised of 25-foot J taper Monotube™ section with an 8-in tip shop welded to a 40-foot long 14-in diameter Monotube™ extension. The remainder of the piles are 12 ¾ -in steel pipes. Piles have an allowable bearing capacity of 90 tons with tip elevations varied from El. -78.2 to -178.5. In addition, 40 tons of downdrag was included in the design.

In the early 2000's when USTA looked at replacing their indoor facility, a study was done to see if the new facility could be supported on spread footings. The footprint of the new structure was larger than the existing one. MRCE performed a settlement analysis which estimated large differential settlements between portions of the building over the existing footprint and the portions extending passed it. The decision was made to support the structure on piles with the interior tennis courts bearing on the fill. Concession stands which exist adjacent to the indoor facility are supported on spread footings. New columns adjacent to those stands were supported on drilled mini-piles while the remainder of the structure was supported on Monotube™ piles. Piles drilled near the existing concession stands had allowable axial capacities of 32.5 tons for 25-foot bond zone and 75-tons for 40-foot bond zones in the Stratum P-1A. Tip elevations for drilled piles varied from El. -87 to -100. The driven piles were 16-in in diameter Monotube™ piles having an 8-in tip and 33-foot long taper with 16-in diameter Monotube™ straight section extensions and 14-in diameter Monotube™ piles having an 8-in tip and 25-foot long taper with 14-in diameter Monotube™ straight section extensions. Monotube™ piles have an allowable structural design capacity of 60 tons and tip elevations varied from El. -83.3 to -130.6. Downdrag allowances of 40 tons for the 14-in piles and 50 tons for the 16-in piles are in addition to the structural design load.

The 2012 USTA Strategic Vision Plan aims at enhancing the current conditions at the site and preserving its stature as a world-class venue. This includes a roof over Arthur Ashe Stadium; reconstruction of practice and tournament courts and the Con Edison electrical substation; and a new transportation building, Chiller plant and Grandstand stadium; and a replacement of Armstrong Stadium. Some of the new structures will be supported on spread footings in the fill and others on piles like the Arthur Ashe Stadium Roof, Chiller Plant, and Substation.

The Arthur Ashe Roof is supported on composite Tapertube™ piles with the tapered pile section having a wall thickness of 0.25 inches (in) and measuring 8-in O.D. at the tip and tapering to 18-in O.D. over its 25-foot length. The tapered section is factory spliced to a 30-foot long straight pipe section with 18-in O.D. with a wall thickness of 0.25 inches. Pile lengths were extended as needed by fitting and splicing 0.375-in thick walled 18-in O.D. straight pipe sections using either a mechanical splicer or a full penetration weld. Pile have a 95-ton allowable structural design

© 2016 Deep Foundations Institute

capacity with tip elevations varying from El. -90 to -169. An additional downdrag capacity for 60 tons was included in the pile design. Figure 6 shows typical composite Tapertube™ piles.



Figure 6. Composite Tapertube™ piles.

The Substation and Chiller Plant which are at the north edge pf the facility are supported on composite Tapertube™ piles with tapered pile section with wall thickness of 0.25 in and measuring 8 in O.D. at the tip and tapering to 18 in O.D. over its 25-foot length. The tapered section is factory spliced to a 30-foot long straight pipe section with 18 in O.D. with a wall thickness of 0.25 in. Pile lengths were extended as needed by fitting and splicing 0.375 in thick walled 18 in O.D. straight pipe sections using either a mechanical splicer or a full penetration weld. Piles have allowable bearing capacity of 90 tons with tip elevations varying from El. -90 to -140.

Table 2. Summary of pile types and capacities.

Structure (Year)	Pile Type	Allowable Axial Bearing Capacity	Lateral Capacity	No. of Load Tests
Arthur Ashe Stadium (1996)	***Composite Pipe-Monotube Piles*** 14-in dia 3 gauge Monotube & 12¾ -in dia, 0.312-in wall steel pipe	90 tons	1 ton (as per code)	25 (compression)
Indoor Tennis Center (2006)	***Monotube Piles*** 8-in tip & 33-foot long taper wt 16-in dia Monotube™ straight section extensions 8-in tip and 25-foot long taper with 14-in dia Monotube™ straight section	60 tons	1 ton (as per code)	25 (compression)
	10-3/4" Drilled Minipile Steel pipe casing, 10-3/4" O.D. 1/2" wall	32.5 tons, 25-foot bond zone 75 tons, 40-foot bond zone	1.5 tons	6 (compression)
Arthur Ashe Stadium Roof (2014)	***Composite Tapertube™ Piles*** Tapered section 0.25 in wall & 8 in O.D. at tip; tapers to 18 in O.D. over 25 feet. Tapered section is factory spliced to 30-foot straight pipe with 18 in O.D. & 0.25 in wall. Pile extensions are 0.375 in walled 18 in O.D. straight sections.	95 tons	14 tons (non seismic)	5 (compression)
			25 tons (seismic)	2 (lateral)
			Fixed-head	
Con Edison Substation & Chiller Plant (2015-2016)	***Composite Tapertube™ Piles*** Tapered section has 0.25 in wall & 8 in O.D. at tip; tapers to 18 in O.D. over 25-foot length. Straight section with 18 in O.D. with wall thickness of 0.25 in.	90 tons	6 tons	2 (compression)
			Free-head	2 (lateral)

© 2016 Deep Foundations Institute

In addition to designing the piles for vertical capacities, lateral capacities of the piles also had to be analyzed for the newer structures. The pile response to lateral load was modeled for seismic and non-seismic loads with the software package LPILE by Ensoft, Inc. that models a single pile. An average p-y modification factor was used to account for the shadowing effect of the closely spaced piles. In areas where liquefaction of the fill below the water table was a concern, the fill was modeled as cohesive soil with low shear strength between 50 and 150 psf for seismic cases. Table 2 summarizes the pile types and capacities used throughout the site.

ACKNOWLEDGEMENTS

The authors gratefully acknowledge the United States Tennis Association (USTA) for entrusting us with the design responsibility of their structures. The collaborative spirit of the parties involved (ROSSETTI, WSP Group, Faithful+Gould, Hunt, Underpinning & Foundations Skanska (UFS) and MRCE) was essential in solving the design and construction challenges for the recent USTA projects. MRCE graciously allowed us time to prepare this paper and several of our colleagues assisted in its preparation; to all of which we are thankful.

REFERENCES

Brand, A.H. (1997). "Game, Set, and Match," ASCE Magazine, ASCE, May, 67(5):2A-8A

Canale, T., Nikolaou, S., Riemer, M. (2015). "Evaluating Liquefaction Risk for Varved Soils in Northeastern US," *6th Int. Conf. on Earthquake Geotechnical Engng*, Christchurch, NZ, Nov. 1-4

DeNivo, A.C., Lopez, P.V., Nikolaou, S., Brand, A.H.., Josef, R.G., Rahimian, A. (2015). "Rising to the Challenge: A Roof for Arthur Ashe Stadium," *Deep Foundations Institute (DFI) Magazine* Cover Story, Sept-Oct, 13-18

Fitzgerald, S. (1925). The Great Gatsby. New York: Charles Scribner's Sons

Moss, C.J. (2012). "Aspects of deglaciation in Flushing Meadows, Queens, NYC," Hanson, G.N., Chm., *21th Conf. on Geology of Long Island and Metropolitan NY*, SUNY at Stony Brook, 13 p.

Munshi-South (2015). "Early History: Swamp & Ash Dump," *Baruch College Seminar No. 3*, macaulay.cuny.edu/eportfolios/munshisouth10/group-projects/flushing-meadows-past/, 11/30/15

Nikolaou et al. (2012). "Geo-Seismic Design in the Eastern United States: State of Practice," *ASCE GeoCongress*, Geotechnical Engineering State of the Art and Practice, Oakland, pp. 828-854, 2012

Nikolaou, S. & Go, J. (2009). "Site-Specific Seismic Studies for Optimal Structural Design: Part II – Applications," *Structure Magazine*, December:12-16

Nikolaou, S. (2008). "Site-Specific Seismic Studies for Optimal Structural Design: Part I – General," *Structure Magazine*, February:15-19

Parsons, J.D. (1976). "NY Glacial Lake Formation of Varved Silt and Clay," *Journal ASCE Geotechnical*, 102(GT6): 605-638

Schnabel, P. et al. (1972). "SHAKE: Computer Program for Conducting Equivalent Linear Seismic Response Analyses of Horizontally Soil Deposits," Report EERC 72-12, UC Berkeley

Tamaro, G.J., Kaufman, J.L., & Azmi, A.A. (2000). "Design and Construction Constraints Imposed by Unique Geologic Conditions in NY," *DFI 8th Int. Conference*, NYC, October

United States Tennis Association, USTA (2015). "The History of the National Tennis Center," www.usta.com/About-USTA/National-Tennis-Center/Information/history_of_ntc/, 11/30/15

© 2016 Deep Foundations Institute

This page left intentionally blank

© 2016 Deep Foundations Institute

WASHINGTON AVENUE TUNNEL PROJECT: FORTIFYING AGING UNDERGROUND INFRASTRUCTURE

Andrew R. Klaetsch, Mueser Rutledge Consulting Engineers, New York, NY, USA, 917 339-9300
aklaetsch@mrce.com
Peter W. Deming, Mueser Rutledge Consulting Engineers, New York, NY, USA, 917 339-9300
pdeming@mrce.com

ABSTRACT

The Washington Avenue tunnel in Kingston, NY was completed in 1912 to convey combined storm water and sanitary sewage. Over a mile in length, the tunnel was driven almost entirely in bedrock, with the exception of an approximately 170 foot long brick arch segment constructed in soil. About 90 years after the tunnel was put into service, persistent subsidence problems and sinkholes were observed in Washington Avenue above the shield-driven soil tunnel segment, eventually causing the important traffic thoroughfare to be closed. Subsequent tunnel inspections revealed a breach in the brick arch and a significant volume of fine soil within the tunnel. A two-phase remediation program was implemented to control seepage, reduce soil migration, and remedy sinkhole problems. The first phase included in-situ soil densification by vibratory pile probe driving to improve density in shallow sandy soil loosened by ground loss. The second phase included installation of a continuous soilcrete arch structure over and alongside the tunnel, extending to rock or compact glacial till and spanning the length of the soil tunnel segment. Overlapping vertical soilcrete columns were installed through interlayered sandy and clayey silt by jet grouting to form a continuous arch structure, using grout parameters verified by full scale field testing.

KEYWORDS: seepage, tunnel, jet grouting, soil improvement, soil migration, sinkhole

PROJECT BACKGROUND

The Washington Avenue tunnel in Kingston, NY (Figure 1) was completed in 1912 to convey combined storm water and sanitary sewage to Rondout Creek by the Board of Water Supply of the City of New York. The tunnel is over a mile in length and constructed primarily in rock. Contract documents indicate the tunnel was designed with a horseshoe shape at least 3 ft wide and 5.5 ft high.

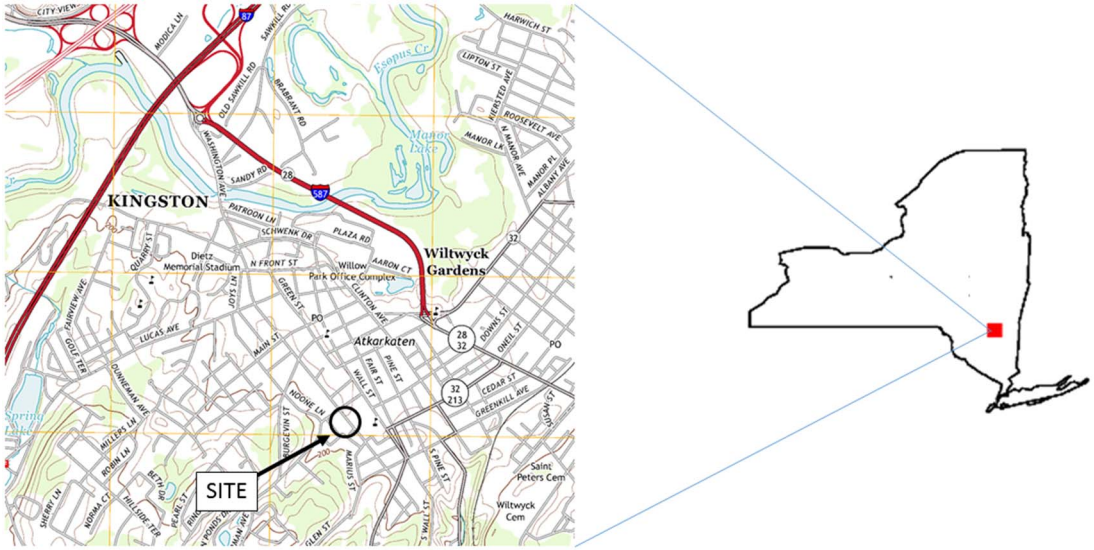


Fig. 1. Excerpt from 2013 USGS Kingston West Quadrangle.

© 2016 Deep Foundations Institute

In the vicinity of the project site, a cave-in occurred during tunneling as the heading advanced through a transition between rock and soil. After the cave-in, the tunnel was advanced in a shield under pressure for a distance of roughly 200 ft, where the heading again penetrated into rock (Hallinan, 1948). Through the shield driven section, the tunnel was lined with a concrete invert and walls with a brick arch crown. Construction drawings indicate the timber shield was left in place, and dry pack was placed to fill the space between the brick arch and timber.

The City of Kingston modified the Washington Avenue Tunnel in 1993. In order to separate storm water flow from sanitary sewer flow, a 24 inch diameter sanitary sewer pipe was embedded in concrete in the tunnel invert. The City also installed a vertical 30 inch diameter storm water shaft at the location of Tannery Brook (Figure 2) to divert surface flow from the brook into the tunnel. The new shaft penetrated the existing brick arch roughly 30 feet upstream of the segment of tunnel driven through soil.

PERFORMANCE PROBLEMS

Five years after the Tannery Brook storm water shaft was completed, ground settlement was observed south and west of the shaft. Between 1998 and 2010, the City of Kingston backfilled areas of subsidence near the Tannery Brook shaft and repaired pavement in Washington Avenue as new areas of subsidence appeared. Injection grouting was performed in 2011 to improve soil supporting a box culvert structure in the vicinity of observed subsidence, and later that year the street was closed due to the repeated appearance of sinkholes.

Remote camera inspections of the tunnel and manned entry were performed to assess the condition of the tunnel. Inspections revealed a breach in the tunnel crown a short distance downstream from the Tannery Brook shaft, and significant accumulation of fine soil within the tunnel. It was determined that the tunnel invert had settled about 16 inches in the vicinity of the crown breach. In addition, seepage was observed emanating from around the Tannery Brook shaft penetration at the tunnel crown.

INVESTIGATIONS AND REPAIRS

The City undertook an investigation program to determine the cause and extent of subsidence below Washington Avenue. The program included geotechnical borings, CPTs, groundwater observation wells, and robotic camera inspection of the tunnel.

Subsurface Conditions

Soil stratigraphy consists of less than 10 feet of fill underlain by a natural layer of fine to medium sand and silty sand up to 40 feet thick. Below the sand is an interlayered sequence of fine sandy silt and clayey silt up to 70 feet thick. A thin layer of glacial till was encountered over rock in some borings. Shale bedrock varied in depth from about 20 feet below grade upstream of the site to over 120 feet below grade at the deepest point. Generalized subsurface stratigraphy in relation to Tannery Brook Shaft and Washington Avenue Tunnel is shown in Fig. 2.

The 2012 and 2013 geotechnical boring and CPT data indicated a significant decrease in soil density above the tunnel beneath Washington Avenue when compared with data from exploratory borings drilled prior to installation of the Tanner Brook shaft. The zones of decreased density coincided with areas most affected by subsidence and sinkhole formation.

© 2016 Deep Foundations Institute

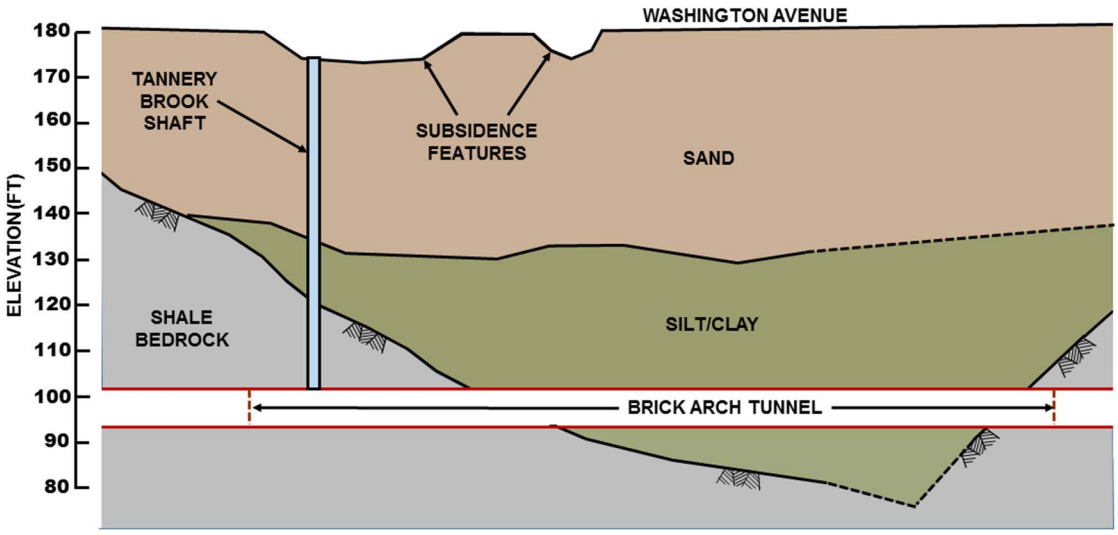


Fig. 2. General subsurface conditions and location of observed surface subsidence. Approximately 200 linear feet of tunnel shown.

Repairs

The City contracted to clean soil from the tunnel and install new liners. City engineers stated that up to 200 cubic yards of fine soil was removed from the tunnel with vacuum equipment. A 185 foot long segmented PVC liner was installed within the horseshoe shaped storm water tunnel, and a fiberglass slip liner was installed in the 24 inch diameter sanitary pipe embedded in the tunnel invert concrete. Each liner traversed the portion of tunnel constructed in soil.

Finally, chemical grout was injected around the 30 inch diameter steel shaft at Tannery Brook in an attempt to stop seepage into the tunnel. The grouting was conducted by drilling from the surface along the outside of the shaft to the top of bedrock, roughly 10 feet above the brick arch tunnel. Despite the repair work, sinkholes continued to appear and Washington Avenue remained closed to traffic.

SUBSIDENCE REMEDY SELECTION

The City of Kingston solicited proposals for remediation of subsidence-related performance problems in Washington Avenue. The work included three components: stabilization of the deep soil profile, installation of surface piping of Tannery Brook, and resurfacing Washington Avenue. This paper summarizes only the deep soil stabilization component of the project.

The City stipulated that the work area would be confined to a narrow zone within the street allowing residents access to homes fronting on Washington Avenue throughout the work. Where water, sewer, power, and gas service was to be removed in the work zone, temporary services were installed to prevent service interruptions to the homes. In addition, an overhead high voltage power transmission line crossing the work zone was to remain in place and temporarily de-energized only as needed during the work.

Given the generally sandy consistency of the uppermost 40 feet of the soil profile, vibrating pile densification was selected for ground improvement in the upper zone. Additional geotechnical borings were drilled and used in conjunction with available boring records and CPT data to delineate the zone of loosened soil requiring densification.

© 2016 Deep Foundations Institute

Installation of a soilcrete arch structure extending to bedrock by jet grouting was the selected method for stabilizing the lower zone, where the soil consists of interlayered sequences of sandy and clayey silt. The soilcrete arch would isolate the aging brick arch tunnel from soil overburden pressure and prevent migration of soils into the tunnel. The arch structure would span the length of the soil tunnel segment, and overlap the soil tunnel to rock tunnel transition zones at either end.

Meetings were held to inform residents of the nature of planned construction activities and discuss possible effects on the homes adjacent to the work site. The construction vibration threshold level was set at 0.5 in/s to reduce vibration damage to adjacent structures.

Alternative methods discussed during peer review of the initial design included installation of rammed aggregate piles in the upper zone. Due to depth limitations, rammed aggregate pile installation was not considered a viable alternative to densification. Contact grouting around the tunnel within the lower zone was discussed as an alternative to the soilcrete arch. Contact grouting was not selected due to risk associated with drilling and injecting grout under pressure in close proximity to the timber shield and brick tunnel arch, each of which were of unknown condition.

CONSTRUCTION

Vibrating pile probes were required to be conducted in a primary-secondary pattern covering the width of Washington Avenue and extending from the Tannery Brook shaft to about 80 feet downstream, where surface settlement and sinkhole formation were observed, and subsurface investigations indicated the upper zone was loosened. A series of settlement monitoring points were surveyed before and after densification to gage the amount of settlement induced. No soil was allowed to be brought into or removed from the work zone.

An initial test program included three primary and two secondary probes, driven as described above, located in the center of the probe pattern, most distant from any adjacent structures. The purpose of the test program was to ascertain if pattern spacing required adjustment based on the observed the size of settlement craters surrounding primary probes, and gage attenuation of construction vibrations with distance.

Geo Solutions, Inc. of New Kensington, PA performed production probes immediately after completing the test program, from which it was determined the probe spacing was adequate. The contractor used an ICE Model 22RF variable moment driver suspended from a telescopic boom crane to drive an H12x74 beam to a depth of about 40 feet, hold the beam at full depth with the hammer activated for 60 seconds, then retract the beam. A total of 114 probes were completed in six work days.

Upon completion of each probe, the diameter and depth of settlement craters forming around the probes were recorded. Settlement craters ranged from 2 ft to 7 ft deep and 1.5 ft to 4 ft in diameter. Other settlement features, such as tension cracks as shown in Fig. 3, were frequently observed forming radially around and up to 8 feet distant from groups of recently completed densification probes. The work area required frequent grading to provide level ground for placement of the crane.

Three portable seismograph units were placed in front of the homes nearest to the work each day, and operated continuously. The minimum distance between any densification probe and an adjacent building was about 35 feet. Recorded peak particle velocity remained below the 0.5 ips threshold throughout densification work.

After primary and secondary densification probes were completed, the work area was regraded and compacted with a vibratory drum roller. The final elevation survey of settlement monitoring locations indicated the overall settlement of the densification area was approximately 14 to 16 inches.

© 2016 Deep Foundations Institute



Fig. 3. Densification probe driving (left) showing high voltage power transmission line with orange shield installed. Tension cracks (right), indicated by arrows, frequently developed around groups of recently driven probes.

Soilcrete Arch

The soilcrete arch design consisted of a series of interlocking columns created by jet grouting to form a continuous arch over the existing tunnel extending alongside the tunnel to the top of rock. A minimum length of 180 feet was required to span the soil tunnel segment and overlap the soil tunnel to rock tunnel transition zones at either end.

Soilcrete geometry was constrained by the limits of the work zone described above and an estimated offset distance between grout columns and the existing timber support structure around the tunnel. Typical soilcrete arch geometry is shown in Fig. 4. Finite element modeling of the proposed arch determined a minimum jet grout compressive strength of 130 psi was required to support earth pressure.

The jet grouting design included a performance-based specification, leaving jet grouting parameters, equipment, and estimated column diameter to be determined and proven by the contractor. A jet grouting test program was developed to confirm the contractor's chosen grouting parameters and mix design. The program included installation of least three overlapping soilcrete columns within the work zone, compressive strength testing of cylinders molded from fresh soilcrete material, and confirmatory coring at the centroid of three overlapping columns after at 28 days. Geo Solutions, Inc. completed the test program by retrieving competent cores of the test columns 15 days after installation.

The contractor's jet grouting layout included 327 overlapping 5-foot diameter columns in eight rows. The contractor prosecuted much of the work using two drill rigs working simultaneously supplied by two jet grouting pumps. The rigs were equipped with Jean Lutz or Gamperl & Hatlapa data acquisition systems to monitor rotation and lift rates, grout and air pressure, and grout injection rate. Grout consisted of cement and water with specific gravity of 1.5, mixed in a batch plant erected on the site with a portable cement silo. Jet grouting operation in progress is shown in Fig. 5.

© 2016 Deep Foundations Institute

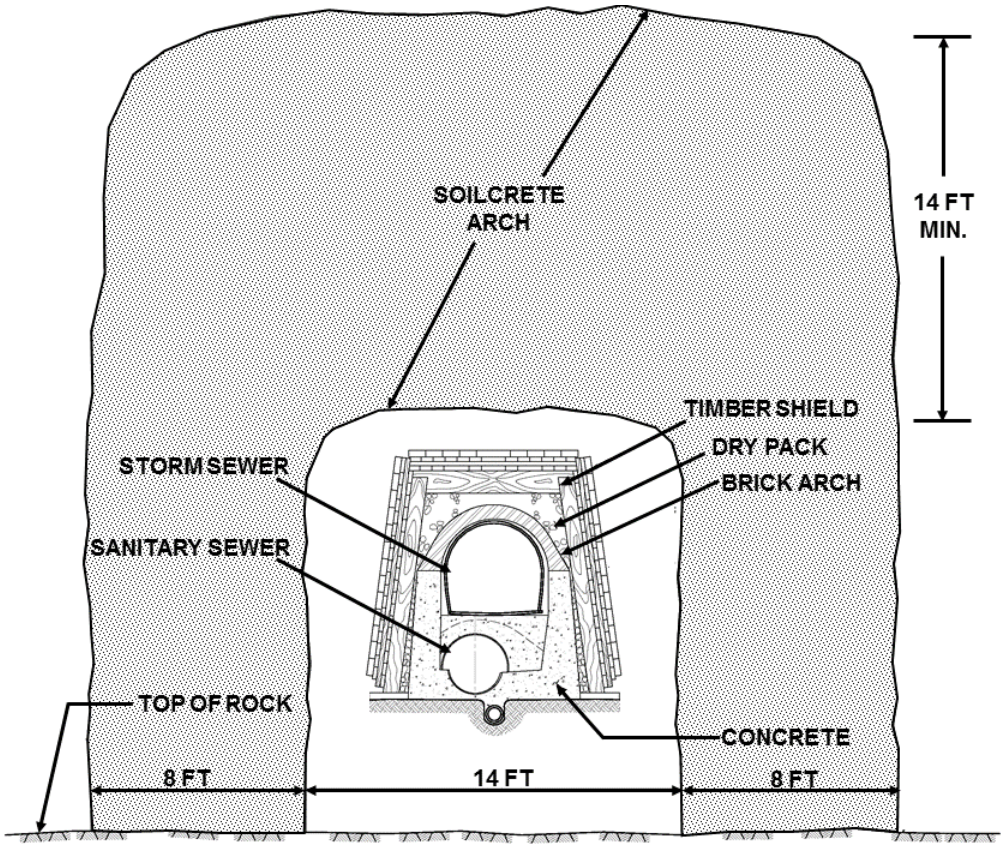


Fig. 4. Typical soilcrete arch geometry. 8 ft thick sidewalls extend to rock as deep as 40 feet below the tunnel invert.

Each planned soilcrete column location was surveyed at the start of the work day. Single-port, roller-bit jet grout monitors were advanced to the specified elevation above the tunnel or to refusal for columns extending to rock, at which point the jet pumps were activated. Jet grouting then proceeded continuously at a fixed rotation speed and lift rate until the specified top elevation was reached. The average grout injection rate was 68.5 gpm at an average pump pressure of 6,000 psi. Spoils were sampled at the ground surface for confirmatory strength testing. At its deepest point, the soilcrete arch supports extended to roughly 120 feet below grade.

Jet grouting was completed in 55 work days. The structure consisted of 326 overlapping soilcrete columns. An average core recovery of 83% was obtained with a triple tube HQ size core barrel from seven core locations. Unconfined compressive strength of molded soilcrete samples ranged from 175 psi to over 1,400 psi, with an average strength of over 700 psi. The minimum tested strength exceeded 130% of the design strength.

© 2016 Deep Foundations Institute



Fig. 5. Jet grouting in progress. One grouting rig and high pressure pump in foreground. Second grouting rig in left background. Photo captured from atop the grout batch plant cement silo.

SUMMARY AND CONCLUSIONS

A portion of Washington Avenue in Kingston, New York was repeatedly damaged by subsidence and sinkhole formation beginning in the 1990's. As subsidence continued, underground utilities and adjacent homes were damaged, and the city was forced to permanently close the street to traffic. It was determined that ground loss into an 80 foot deep, 100 year old brick arch sewer tunnel was the cause of the performance problems.

The City undertook a comprehensive remediation program intended to limit further subsidence and render Washington Avenue safe for public use. The remediation program included ground improvement by vibrating pile densification and construction of a soilcrete arch structure by jet grouting at depth to isolate the aging brick arch tunnel from soil overburden pressure and prevent migration of soils into the tunnel. The work was completed in the fall of 2015 and Washington Avenue was reopened to traffic after a 3 year closure.

REFERENCES

Hallinan, A.F., 1948. Location of Washington Avenue Tunnel, Kingston, New York. City memo. 3 p.

Kirby, P., 2016. After 5 years, road near Kingston sinkhole site reopens to traffic next Monday. Kingston Daily Freeman online article. May 19, 2016.

© 2016 Deep Foundations Institute

This page left intentionally blank

© 2016 Deep Foundations Institute

A RESILIENCE APPROACH FOR DESIGN OF EARTH RETAINING SYSTEMS WITH APPLICATION ON MSE WALLS

Rallis Kourkoulis, National Technical University of Athens, Greece, rallisko@yahoo.com
Fani Gelagoti, National Technical University of Athens, Greece, fanigelagoti@gmail.com
Irene Georgiou, National Technical University of Athens, Greece, irelimini@outlook.com
Sissy Nikolaou, WSP | Parsons Brinckerhoff, New York, USA, nikolaous@pbworld.com
George Gazetas, NTUA, Greece, gazetas@central.ntua.gr

ABSTRACT

The need to shift geotechnical design from a "factor of safety" to a "performance based" design (PBD) approach has increased rapidly in the past years following examples from structural engineering. PBD supports sustainable engineered systems that target project-specific geotechnical behavior objectives and results in more rational and, in most cases, less conservative solutions. Resiliency, efficiency, risk optimization, and cost-effectiveness are key components of this approach. For design of retaining walls, the concept of mechanically stabilized earth (MSE) systems combines these attributes, while being environmentally friendly and adaptive to variable construction conditions. Natural hazards, such as earthquakes, may drive the design of MSE systems whose reliability depends on their performance under extreme events. In this paper, the authors compare the seismic response of an MSE steel-reinforced vs. concrete-reinforced retaining wall. The MSE system is composed of a grid of longitudinal and transverse ribs which internally enhances the capacity of the soil backfill. Results of fully non-linear two-dimensional (2-D) numerical finite element analyses using two commercial programs with emphasis on the interface conditions are presented. The pull-out resistance of the grid used in the numerical simulation was evaluated from actual pull-out experiments. The results demonstrate a superior performance of the MSE system as compared to the concrete one, especially when subjected to strong seismic excitations.

Keywords: resilience, risk, mechanically stabilized earth, retaining wall, seismic, performance based design, sustainability

INTRODUCTION

The idea of performance-based geotechnical engineering is not new, and has been evolving as our perception for 'good' performance has also evolved (Kramer, 2008). In early practice, the only criterion for achieving good performance was to avoid failure; designers had only to ensure that the available capacity of the geotechnical system is sufficiently higher than the expected demand (i.e. Load and Resistance Factor Methodologies). Yet, even when the key design requirements against collapse are satisfied, the system may still be placed into a condition in which the deformation constraints are not met (Bolton, 2012). To address these issues, geotechnical design has been developing into a predominantly performance-based approach that correlates deformation considerations to the severity of the experienced loading. As such, in earthquake-related problems, the definition of good performance of a geotechnical system is no more unique; for a low intensity earthquake the system should remain serviceable (i.e., the developed deformations should remain low), whilst for the design earthquake the maintenance of life-safety is the single performance criterion.

Yet, this is still not enough as during the last 20 years, records of earthquakes that overly exceed the design standards keep increasing. A merely indicative list of recent events includes the earthquakes of Wenchuan (2008), the fatal M8.8 Chile (2010), and the sequence of seismic shocks in Christchurch, New Zealand with recorded accelerations on the order of 100% of gravity. Attempting to design for such extreme and unprecedented seismic actions would impose enormous demands to the structure and provoke a ludicrous squander of resources. Recognition of our inherent inability to control nature

© 2016 Deep Foundations Institute

(especially when resources are limited) has led the engineering community to pursue resilience as the most viable strategy to minimize the consequences of the inevitable disaster (Bruneau & Reinhorn, 2007). Resilience is often defined in terms of the ability of a system to absorb shocks, to avoid crossing a threshold into an alternate and possibly irreversible new state, and to regenerate after disturbance (Resilience Alliance, 2009). In the words of Holling (1996), a resilient system may be disturbed and still persist without changing function.

This paper aims to highlight the application of the very idea of resilience in the design of Earth Retaining Systems which is challenging as, by definition, our problem lacks measurable performance metrics. To overcome this obstacle, we have compared directly two conventionally equivalent retaining structures: a typical pile-wall system and a MSE wall.

Since the first Mechanically Stabilized Earth (MSE) wall construction in California in the early 70's, MSE systems have become increasingly popular due to their low cost and ease of construction especially when it comes to 'deep cuts.' Among their other important attributes, MSE systems have been found to perform equally or better than more rigid wall systems under seismic loading events. In strength-based terminology, both retaining systems are treated as totally equivalent; both are designed to attain identical Seismic Factors of Safety. These two 'equivalent' structures have been subjected to a variety of loading scenarios and the Resilience is quantified by their ability to:

(a) remain functional after medium-intensity earthquake events
(b) preserve their structural integrity under extremely strong earthquake events (far in excess of the design-earthquake)
(c) demonstrate redundancies
(d) recover from multiple earthquake incidents with minimum disturbance

PROBLEM DEFINITION – NUMERICAL MODELING

The problem investigates the behavior of a retaining wall supporting a 10m-tall backfill. Two alternatives were examined and compared: (i) a conventional bored pile retaining wall and (ii) a steel-reinforced MSE wall. The geometry and main characteristics of the two alternatives are shown on Fig. 1. Following the currently applicable codes, the two systems were designed to ensure the same static and seismic (pseudo-static) factors of safety (FS). An equivalency in static and seismic safety factors (FS_{static}= 1.8 and $FS_{seismic}$ =1.2 assuming a design ground acceleration of 0.16g) is achieved with the following alternatives:

(e) Tangent pile wall with pile diameter of 1.2 m (4 ft) and ultimate moment capacity M_{ult} = 1.7 MNm and height of 20 m (66 ft), with 10 m (33 ft) embedded and 10 m (33 ft) free wall.
(f) Rows of 7 m (23 ft) – long reinforcement grids at 0.6 m (2 ft) vertical spacing. The grid configuration consists of 10 mm (0.4 in) bars at 200 mm (8 in) spacing both in the longitudinal and transverse directions.

© 2016 Deep Foundations Institute

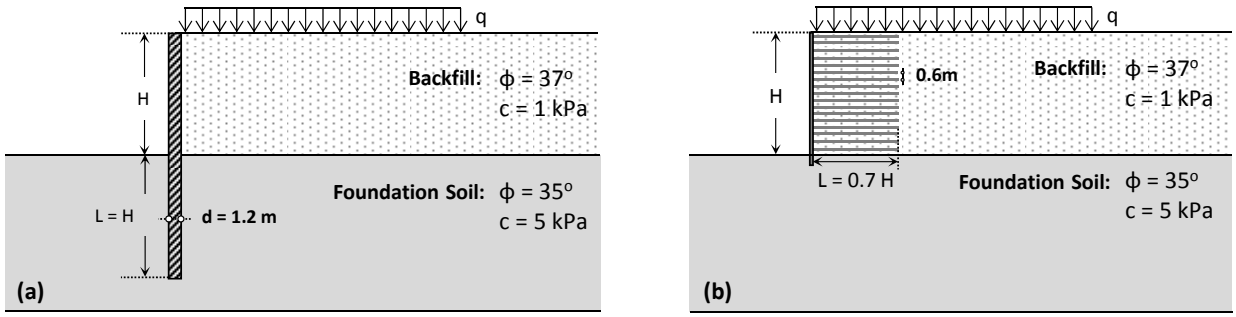


Fig. 1. Examined retaining systems: (a) conventional pile wall, (b) Mechanically Stabilized Earth.

Utilizing the finite element codes ABAQUS and PLAXIS, the analysis was performed assuming plane strain conditions and taking account material and geometric nonlinearities. As illustrated in Fig. 2a, the geometry is "mirrored" in order to ameliorate the lateral boundary effects and examine the effect of the inherent asymmetry of the accelerogram (the "polarity" effect) in a single dynamic analysis. The soil was modeled with nonlinear continuum elements, while the piles are modeled as 2D beam elements, circumscribed by plane-strain continuum elements of nearly zero stiffness. Thus, pile stiffness is introduced in the simulation through the central beam element, the nodes of which are rigidly connected to the circumferential solid element nodes at the same depth. Consequently, each pile section behaves as a rigid disc: rotation is allowed on the condition that the disc remains perpendicular to the beam axis, but stretching cannot occur. The moment-curvature relationship derived from section analysis is input for the simulation of the non-linear response of the concrete pile wall. Sliding and separation of the pile from the surrounding soil are captured through interface elements placed at the pile periphery.

In the MSE model, the concrete facing panels and the grid reinforcements are modeled through continuum and truss elements respectively. Each facing panel with thickness of 0.2 m (~ 8 in) and height of 0.6 m (~ 24 in) is pin-connected to its neighboring panels which allows relative rotation between panels, but restricts the horizontal and vertical degrees of freedom. Therefore, the actual connection between consecutive panels is simulated as realistically as possible. The truss elements simulating the steel reinforcement are in turn connected to individual facing panels.

As has been proven by means of several pull-out tests of grid steel reinforcements, the apparent friction coefficient f* at the sand/mesh interface decreases with the increase of embankment height. This behavior is characteristic of dilatant materials under low confining stresses and is attributed to the presence of the grid which restrains the tendency of the sane to dilate. According to Lajevardi et al. (2013), f* decreases from 1 at the surface to approximately 0.6 at the depth of 6 m (~20 ft) after which it remains constant. This is compatible with the french standard (NFP-96-270, 2009) recommendations of f* values of 0.9 and 0.4, respectively. Our study assumes the truss elements (representing the reinforcement grid) are in perfect contact with the surrounding soil elements. This means that the coefficient of friction at the soil-reinforcement interface is equal to $f^* = \tan\varphi = 0.75$, (where φ is the internal friction angle of the backfill) which, based on the aforementioned values, appears to be a conservative value for the upper rows of reinforcement. Lower f* values at the top layers of the MSE wall (where the length of the resisting anchoring zone is smaller) should be overpredicting seismic displacements. Yet, this low selection was deliberate in order to investigate the inherent resilience of MSE systems.

The soil behavior is modeled through a modified kinematic hardening constitutive model, encoded in the ABAQUS environment through a user subroutine. Developed by Anastasopoulos et al. (2011), it combines an extended pressure-dependent Von Mises failure criterion, with nonlinear kinematic hardening and associated plastic flow rule. The evolution law has two components: a nonlinear kinematic hardening component describing the translation of the yield stress in the stress space, and an isotropic

© 2016 Deep Foundations Institute

hardening component which defines the size of the yield surface σ_0 as function of plastic deformation. In this study, model parameters were systematically calibrated for various levels of overburden stress according to the experimental G-γ and ξ-γ curves of Ishibashi & Zhang (1993). Fig. 2b portrays typical comparisons between experimental and computed results for two levels of confining pressure.

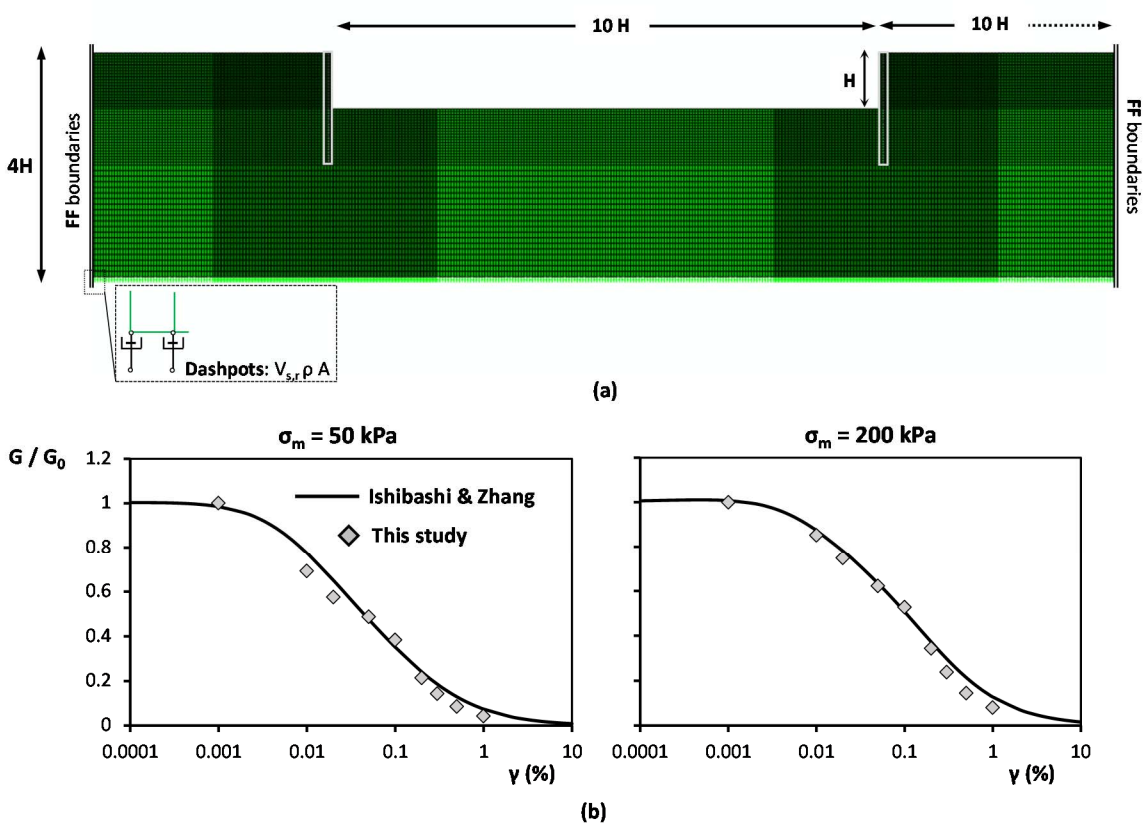


Fig. 2. (a) FEM of conventional pile-wall; (b) G-γ curves for two confining pressures (σ_m = 50 kPa – left, σ_m = 200 kPa – right): soil constitutive model calibration against Ishibashi & Zhang (1993).

A numerical simulation of the cyclic simple shear test was conducted with the low-strain shear modulus G_0 was estimated using Seed et al. (1986):

$$G_0 = 1600\ K_2\ (\sigma_m')^{0.5}$$

where σ_m is the confining pressure, K_2 is a characteristic soil parameter taken equal to 10 for the relatively dense sand adopted herein.

Interfaces between facing panels and soil, and between piles and soil were modeled with special contact elements that allow both separation and slippage, the latter controlled by coefficient of friction μ = 0.7. Kinematic constraints were assumed at the lateral boundaries of the FEM to simulate free-field response, while dashpot elements have been used at the base of the model to account for radiation damping.

PERFORMANCE UNDER STATIC LOADING

Before proceeding to the dynamic analyses, the retaining systems were examined under static loading. Note that installation effect on the soil was not taken into account and the models are assumed to be wished-in-place. This assumption, in accord with previous studies, has proven more conservative for the MSE system, since it overestimates both the plastic strains and the displacements at the facing.

© 2016 Deep Foundations Institute

Horizontal deformations under static loading, which consists of the application of gravity in conjunction with a uniformly distributed load of 10kN/m along a distance of 50m behind the wall, are represented in Fig 3. Although equivalent in terms of safety factors, the pile system flexibility is prominent, exhibiting an approximately 3-fold larger displacement (30 mm or 1.2 in) compared to the MSE alternative (10 mm or 0.4 in). Interestingly, more pronounced is the difference in the mode of deformation: deformations of the pile system decrease linearly with depth until the level of excavation and remain almost constant along the embedment part; on the contrary, the maximum MSE lateral deformation develops mid-height, resulting in a convex deformed shape of the facing. The observation agrees with previous experimental studies (Suberhamani et al., 2008), confirming the adopted numerical methodology.

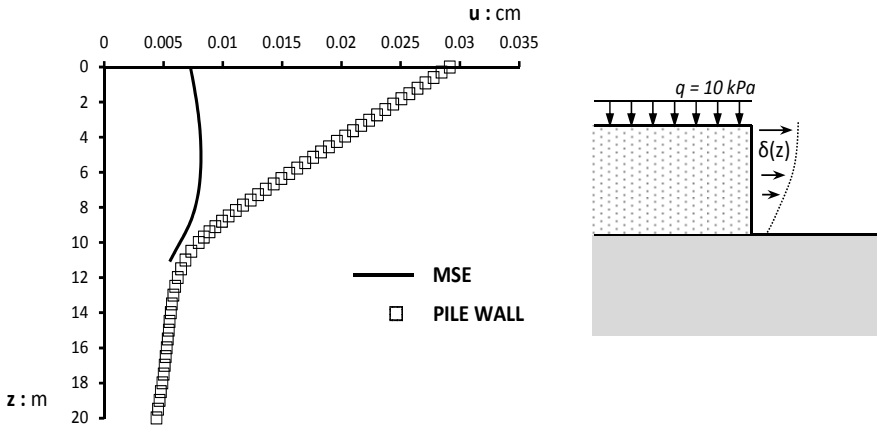


Fig. 3. Horizontal displacements under static loading on: (a) MSE and (b) concrete pile wall.

SEISMIC EXCITATION: RESPONSE UNDER EXTREME SHAKING

Resilience of retaining systems depends on their performance under extreme events, such as earthquakes exceeding the design levels. In this section we compare the response of the two systems presented previously under moderate and high-intensity earthquake scenarios.

To cover a range of realistic ground motion characteristics, the seismic performance was evaluated using four recorded accelerograms. The selected ground motions can be classified based on their frequency content into two categories: the high-frequency motions where a great portion of the earthquake energy corresponds to structural periods (T) lower than 0.3 s and the low-frequency motions, where spectral accelerations are maximized for T greater than 0.75 s. The acceleration time histories and their elastic response spectra are plotted on Fig. 4. The LPCC record of the 2011 M_s 6.3 Christchurch earthquake and the Gilroy record of the 1989 M_s 7.1 Loma Prieta earthquake belong to the first category, with peak ground accelerations (PGA) of 0.9 g and 0.4 g, respectively. The second one is the 2003 M_s6.4 Lefkada, Greece earthquake record, characterized by a sequence of roughly eight strong motion cycles with PGA = 0.4g, and the well-known Rinaldi (228) record of the 1994 M_s6.8 Northridge earthquake which is characterized by forward-rupture directivity effects with PGA = 0.8g.

Figure 5 summarizes the performance of the systems in terms of permanent outward horizontal displacements at the end of each earthquake excitation. Accounting for polarity effect the results are presented for the worst case (left or right wall). It is evident that both walls are less sensitive to the high-frequency excitations, while substantial deformations result from the low-frequency motions. Nonetheless, in all cases MSE exhibits remarkably lower lateral movements than the concrete pile wall. Considering the extreme case of the Rinaldi excitation, Fig. 6 compares the acceleration and displacement

© 2016 Deep Foundations Institute

time histories at the top of each system. It is shown that the MSE, due to its inertial characteristics, does not follow exactly the ground motion, thereby limiting the acceleration propagation towards the surface. On the contrary, the more flexible pile alternative follows the dynamic deformation of the backfill, allowing the propagation of even high-frequency acceleration pulses to the top. Note that at around time t = 4.9 s (i.e., the instant of the main pulse) the pile wall experiences significantly larger displacement than that of MSE; this displacement remains as irrecoverable residual deformation after the end of shaking, although the displacement attributable to the trailing pulses is practically same for the two systems.

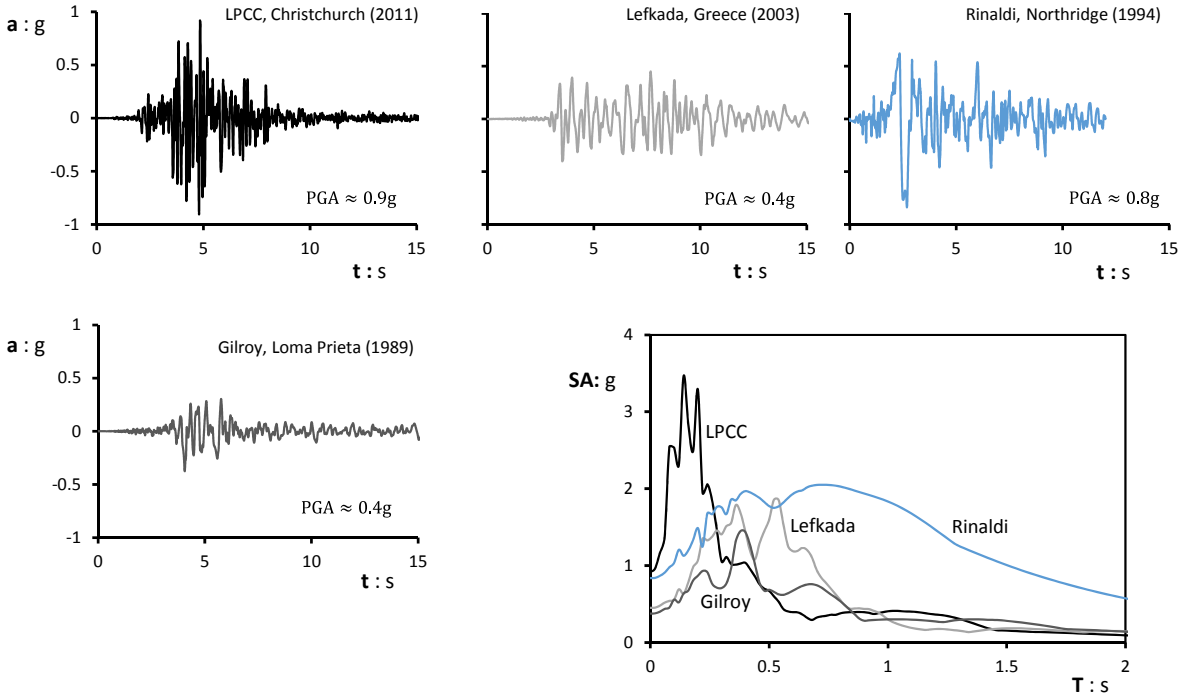


Fig. 4. Acceleration time histories used as seismic excitations for the dynamic analysis of the retaining systems and their elastic response spectra.

A typical result of the ABAQUS seismic analysis is portrayed in Fig. 7 in form of contours of plastic strains on the deformed shape of the system. The response of MSE under seismic excitation differs from the static one; the entire MSE wall responds as an almost rigid block governed by an overturning mode of deformation. As such, the maximum lateral movement occurs at the top of the wall, while the reinforced zone moves outwards and rotates imitating the pattern of a rigid block. In addition, the failure surface form behind the reinforced zone at the backfill and no internal plastic deformation may be observed. On the other hand, the pile deformations seem to follow their pattern under static loading conditions, caused by the formation of an active wedge behind the wall due to the lateral active earth pressures.

SEISMIC EXCITATION: WALL DEFORMATION AND DAMAGE

Fig. 8a presents horizontal displacements with depth following the Rinaldi excitation. Despite the severity of the event, the MSE wall was able to resist with relatively limited deformations of 270 mm (11 in), while the conventional pile wall top moved 500 mm (20 in). Although both systems seem to have avoided collapse, the behavior of the pile wall appears by performance standards. The superiority in behavior of the MSE system is also evident in terms of structural distress. Figure 8b presents the moment-curvature plot of the pile produced during shaking, superimposed with its monotonic M-k curve: the pile has developed large curvature values which have led it to expend its available strength, rendering it

© 2016 Deep Foundations Institute

threateningly vulnerable to a hypothetical aftershock. Unfortunately though, an aftershock of quite significant intensity would actually be a high probability scenario after such an extreme event as the Rinaldi shaking. On the other hand, the MSE wall displays a resilient performance: not only it sustained the shaking with about half the displacement of the pile wall, but it has done so while developing stresses well below the yield limit of 500 MPa (10,500 ksf) at all levels of reinforcement (Fig. 8c).

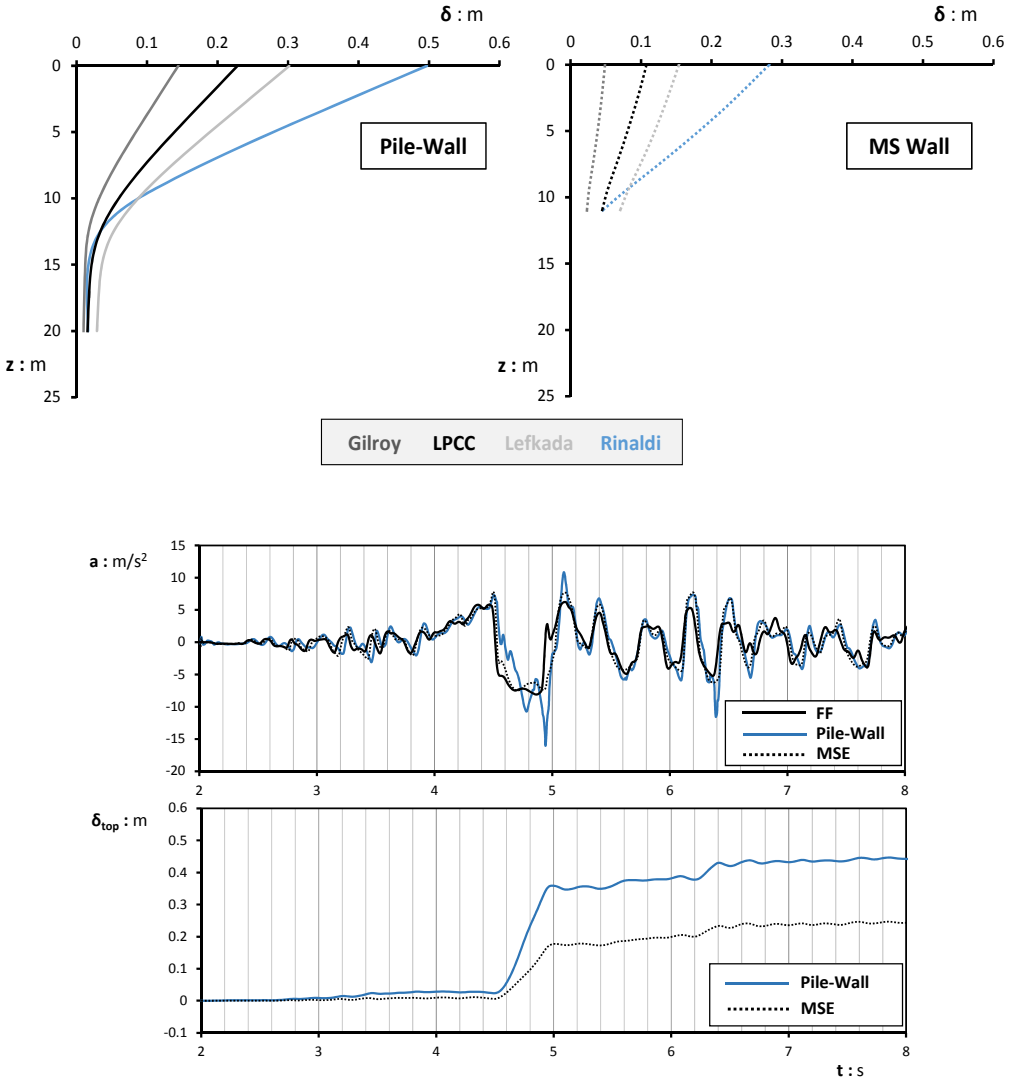


Fig. 6. Acceleration and displacement time-histories at the top of the retaining structures as a result of the Rinaldi excitation (Northridge, 1994).

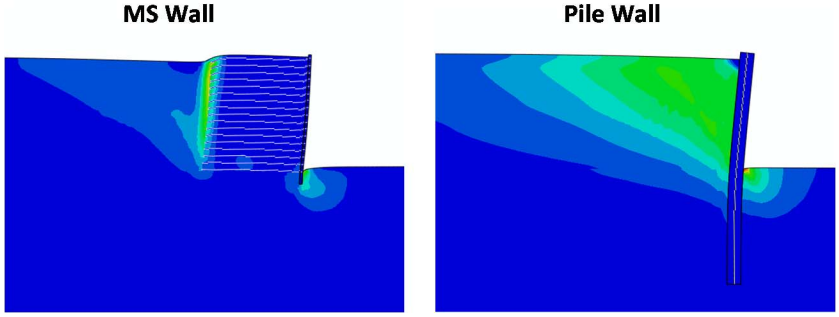


Fig. 7. Contours of plastic strains on the deformed mesh at the end of the seismic excitation.

© 2016 Deep Foundations Institute

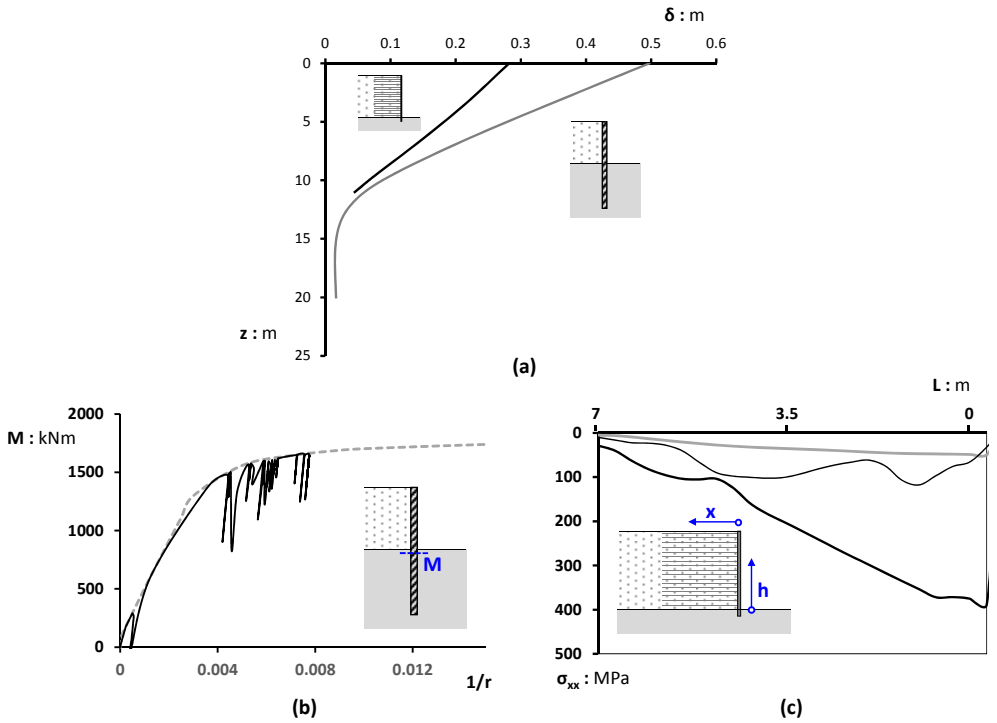


Fig. 8. Seismic Performance of the two systems subjected to the Rinaldi ground motion: (a) wall deformation, (b) Moment-curvature diagram at the point of fixity; (c) axial stresses along the rib length at three characteristic heights (h_1, h_2 and h_3).

MSE WALL REDUNDANCY

After highlighting the resilience of MSE retaining walls in terms of their ability to preserve their structural integrity under extremely strong earthquake events and remain functional afterwards, this section briefly addresses the redundancy accompanying this system. To this end, the MSE wall is again subjected to a mild (Gilroy record) and an extreme (Rinaldi record) earthquake shaking having preserved only half of the originally prescribed grids (i.e. grid reinforcements are now considered at vertical distances of 1.2m instead of 0.6m). This setup corresponds to a quite unrealistic scenario where half of the required reinforcements are unable to offer any resistance. Results are plotted in Figure 9 in terms of distribution of horizontal displacements along the wall, revealing a quite astonishing response. For both scenarios the increase in horizontal displacements is only marginal.

Although a surprise at first sight, this excellent response is the result of the transformation of the resisting mechanism: instead of the rigid block response observed in case of the properly designed MSE wall, the system now sustains severe plastic yielding in the "internal" soil (Fig. 9b) and obvious distress of the reinforcement bars. Indeed, when properly designed the bars are structurally "underexploited" (i.e. offer their resistance mainly via the friction mechanism) while the internal soil develops no serious strain. These are the two concealed safety fuses which are inherent in this system and provide it with redundancy. Of course, when considering the low intensity Gilroy record the tensile stresses developed are manageable, while in case of the Rinaldi scenario the bottom (more stressed) bar evidently reaches its capacity which is obviously a sign of imminent failure.

© 2016 Deep Foundations Institute

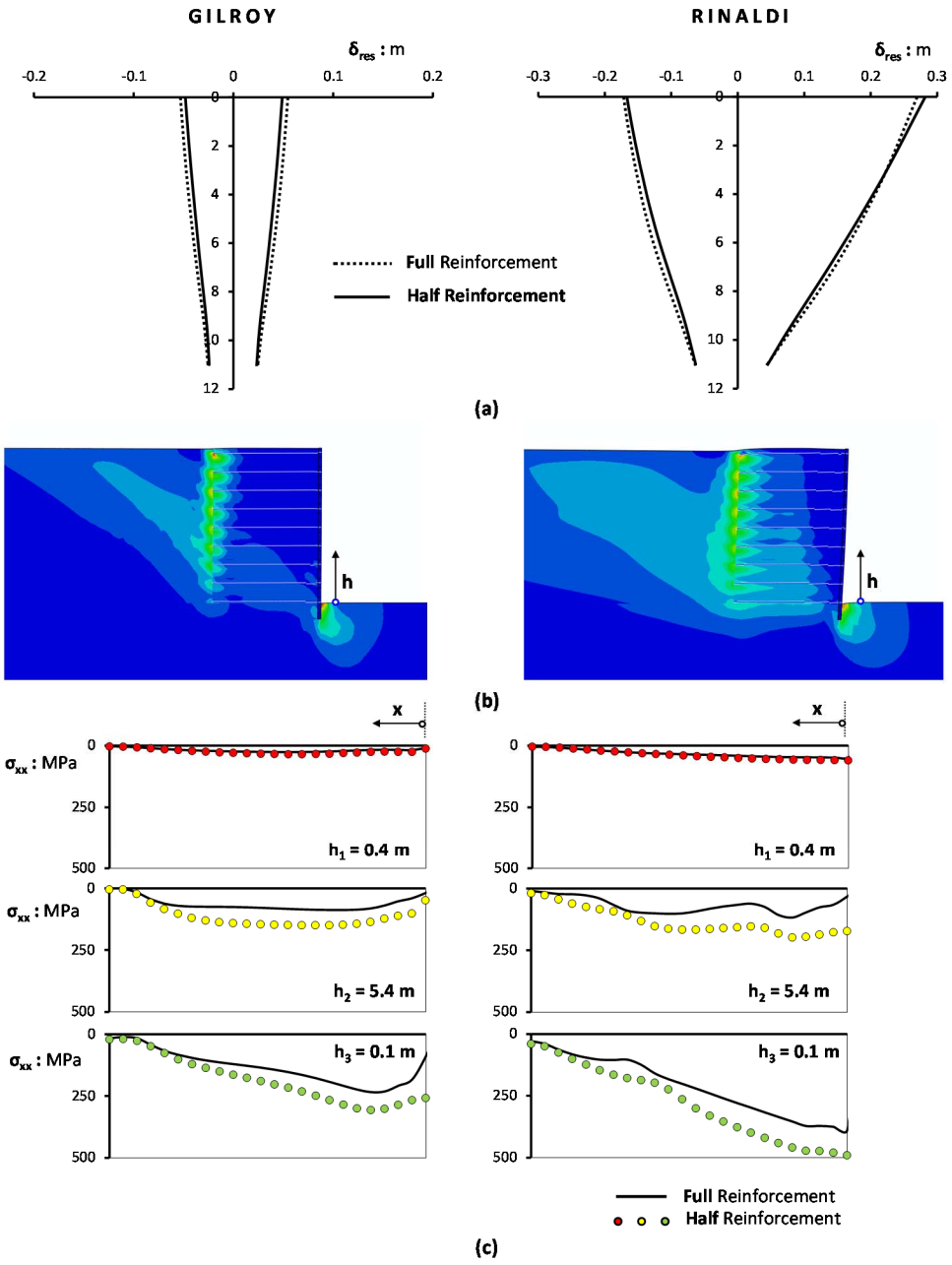


Fig. 9. MSE Wall redundancies when the cut is subjected to the Gilroy (left column) and the Rinaldi (right column) excitations: (a) residual displacements along the wall height; (b) plastic strain distribution at the end of the shaking (assuming that only half of the reinforcement is active); (c) axial stresses along the rib length at three characteristic heights (h_1, h_2 and h_3).

CONCLUSIONS

This paper has presented a comparison between a conventionally designed pile wall and a mechanically stabilized earth wall retainingn a vertical soil cut of height H=10m retaining system when subjected to several earthquake scenarios. It has been shown that despite the massive dimensions of the piles (diameter D=1.2m and depth L=20m), and despite the fact that both systems have been designed to meet the same state-of-the-art strength-based criteria, the lightweight MSE wall demonstrates a superior performance for all cases examined. The MSE system has been shown to experience apparently lower displacements while

© 2016 Deep Foundations Institute

maintaining the structural integrity of the reinforcement bars; on the contrary, the piled wall experiences almost double deformations –especially when subjected to extreme earthquake shaking, while its structural distress renders it extremely vulnerable to any potential aftershock.

Our analyses suggest that the MSE alternative constitutes a resilient retaining structure, owing not only to its superior performance in terms of performance-based indices such as deformation but also due to its ability to remain operable immediately after an earthquake and its inherent redundancies. The latter come in the form of additional robustness that may be offered by internal soil yielding and exploitation of the total available tensile strength of the reinforcement bars.

REFERENCES

Anastasopoulos, I., Gelagoti, F., Kourkoulis, R., & Gazetas, G., 2012. Simplified constitutive model for simulation of cyclic response of shallow foundations: Validation against laboratory tests. J. Geotech. & Geoenvironmental Engineering, ASCE, 137(12):1154-1168.

Bolton, 2012. Performance-based design in geotechnical engineering, 52nd Rankine Lecture, London, UK.

Bruneau M. and Reinhorn, A.M. (2007). Exploring the concept of seismic resilience for acute care facilities, *Earthquake Spectra*, 28(1):41-62

Holling, C. S. 1996. Engineering resilience versus ecological resilience. National Academic Press, Washigton DC, USA.

Ishibashi, I., and Zhang, X., 1993. Unified dynamic shear moduli and damping ratios of sand and clay, Soils and Foundations; 33(1):182-191.

Kramer, S., 2008. Performance-based earthquake engineering: Opportunities and implications for Geotechnical Engineering Practice, Geotechnical Earthquake Eng. & Soil Dynamics IV, Sacramento, CA

Lajevardi, S. H., Dias, D., and Racinais, J., 2013. Analysis of soil-welded steel mesh reinforcement interface interaction by pull-out tests, Journal of Geotextiles and Geomembranes, 40:48-57.

Seed, H.B., Wong, R.T., Idriss, I.M., and Tokimatsu, K., 1986. Moduli and damping factors for dynamic analyses of cohesionless soils, J. Geotechnical Engineering, ASCE, 112(11):1016-32.

© 2016 Deep Foundations Institute

CHALLENGING GROUND CONDITONS DURING FLOODING LEAD TO INNOVATIVE DEEP FOUNDATION DESIGN PROCESS AND LOAD TEST EVALUATION

James F. Mehnert, P.E., USACE, Kansas City, Missouri, USA, james.f.mehnert@usace.army.mil
Glen M. Bellew, P.E, USACE, Kansas City, Missouri, USA, glen.m.bellew@usace.army.mil

ABSTRACT:

The Kansas City District-United States Army Corps of Engineers has completed the design modification of a pile supported floodwall located along the Missouri River in Kansas City, Kansas. This deep foundation supported floodwall protects over 2 billion dollars in infrastructure, is approximately 17 ft (5.2 m) tall and is 1,446 ft (440.7 m) long. Design modifications included the addition of a row of drilled shafts and the addition of relief wells. Typically, deep foundation design is controlled by total stress analysis and undrained soil strength. Neither controlled design at this site, where effective stress and drained strength controlled. During high river stages, artesian pressures develop, leading to a reduction in both effective stress and pile capacity. Deep foundation analysis software available to the designer does not allow these effective stress conditions to be directly entered, so a unique way was developed to account for them. A load test was performed to verify the design. During load testing, the supporting ground was unsaturated and had effective stress conditions different from those that controlled the design. A load test evaluation process involving unsaturated soil mechanics was developed and performed. This paper will share both the effective stress design process used and the load test interpretation process performed.

Keywords: artesian, drilled shaft, effective stress, underseepage, unsaturated soil mechanics

INTRODUCTION

The Fairfax-BPU Floodwall is part of the Fairfax-Jersey Creek Flood Protection Unit in Kansas City, Kansas. The floodwall was built in the 1940s and currently provides Missouri River flood protection for over 2 billion dollars of infrastructure in the Fairfax Industrial Area. The floodwall averages 17 ft (5.2 m) in height, is 1,446 ft (440.7 m) in length and is divided into 35 separate monoliths. The originally constructed foundation support for each of these monoliths typically consisted of three rows of seven tapered steel monotube piles, each roughly 20 ft (6.1 m) in length. All monontube piles are tipped in sand, well above bedrock.

The highest flood to load the Fairfax-BPU floodwall occurred in 1993 when floodwaters rose to within 3 ft (0.9 m) of the top of the floodwall. In 2006, USACE performed a feasibility study that included the evaluation of the Fairfax-BPU floodwall. One conclusion of the study was that when floodwaters reached the top of the floodwall, foundation failure would occur. The factors driving this predicted failure included the increase in floodwall loading due to rising floodwater, and the loss of pile support. This loss of pile resistance is due to artesian pressures that are generated by floodwall underseepage.

The views expressed are those of the author and do not necessarily represent those of the US Army Corps of Engineers

© 2016 Deep Foundations Institute

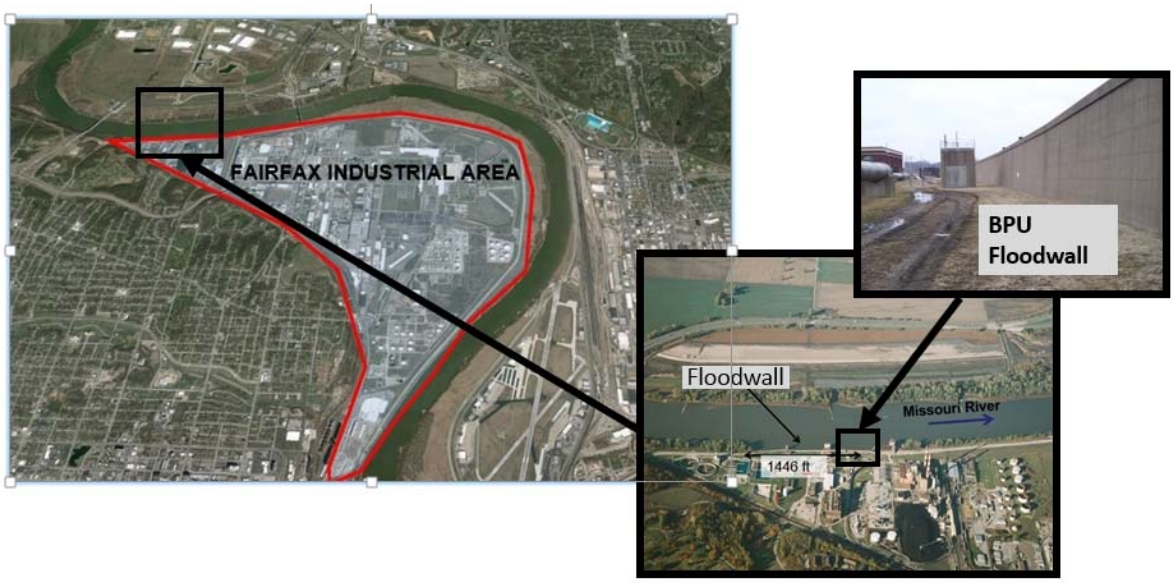


Figure 1. Fairfax-BPU Floodwall Location

THE IMPACT OF UNDERSEEPAGE ON FOUNDATION SUPPORT

Typical to the floodplain of the lower Missouri River, soil stratification at the Fairfax-BPU floodwall consists of lower permeability clays and silts overlying higher permeability sands that in turn extend to bedrock. The upper layer of less permeable soil is typically referred to as the blanket, and the more permeable sands below are typically referred to as foundation sands. By evaluation of historical pump tests and examination of boring logs, the ratio of foundation sand horizontal permeability to blanket soil vertical permeability at this site was determined to be approximately 1,000.

In the Missouri River channel, foundation sands are directly exposed to the river. Because of this direct exposure to the river, when floodwaters rise, the groundwater pressure in the foundation sand quickly reflects the river elevation. On the landside of the floodwall, where there is no flooded river, groundwater in the foundation sand becomes artesian and the effective stresses drop in both the foundation sand and the clay blanket. Drained soil strength controls this foundation design, so this loss of effective stress reduces both the axial and lateral soil resistance, at the time when pile loading is at its greatest.

DESIGN TO ELIMINATE FLOODWALL FOUNDATION DEFICIENCY

In 2013, the funding to eliminate the Fairfax-BPU foundation deficiency was obtained and the design phase was commenced. Two design approaches were used to increase floodwall foundation support, thereby eliminating the design deficiency. The first approach focused on reducing the underseepage generated artesian pressures. The second approach focused on the addition of deep foundation elements.

© 2016 Deep Foundations Institute

REDUCTION OF ARTESIAN PRESSURES IN FOUNDATION SAND

Two alternatives were considered to reduce underseepage pressures; a deep cut-off wall and relief wells. The construction of a cut-off wall was determined to be cost prohibitive for reasons that included the following: the existence of multiple utilities on the riverside of the floodwall, the limited construction access on the riverside of the floodwall, and a foundation sand thickness of over 100 ft (30.5 m). By elimination, relief wells became the selected alternative to reduce underseepage artesian pressures. Relief wells are commonly used to reduce artesian groundwater pressures in foundation sands behind flood protection (Fig. 2). A 14 well system was designed to reduce artesian pressure in foundation sand, increase effective stresses in the foundation sand and the upper blanket, and improve foundation support during flooding.

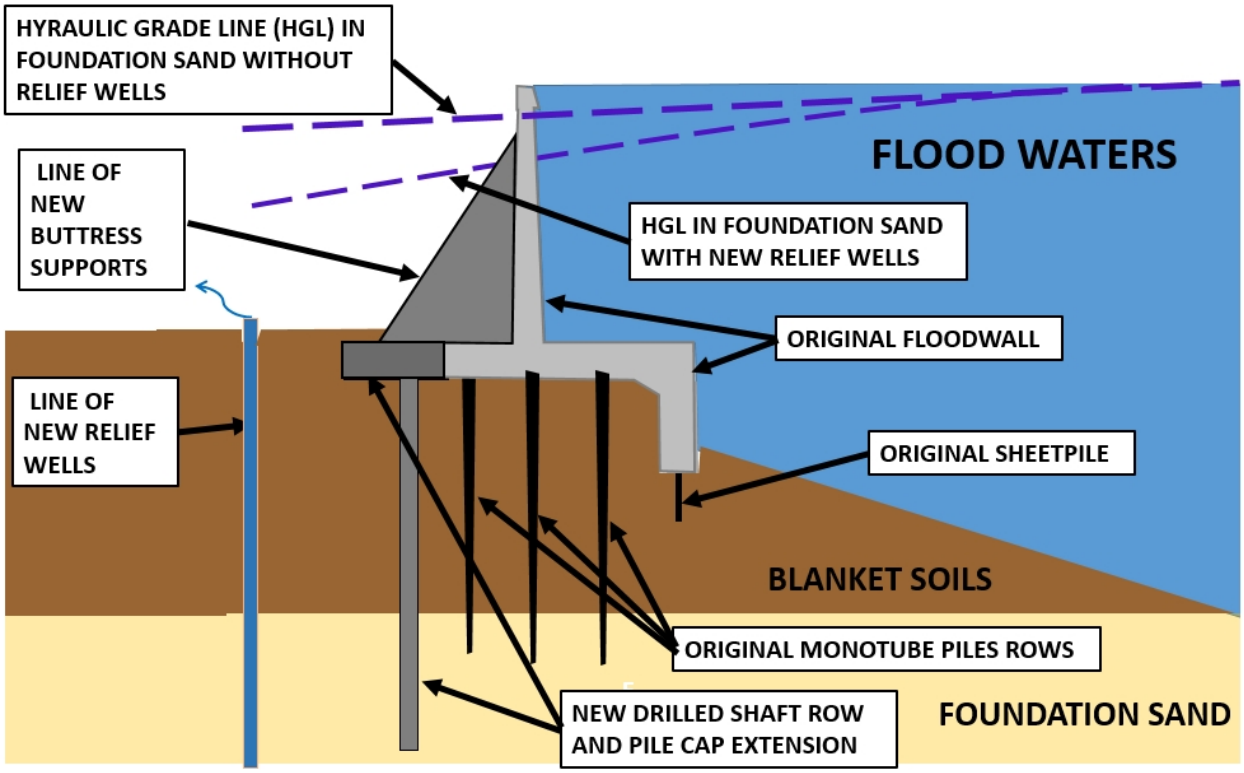


Figure 2. Cross-section of floodwall improvements

DEEP FOUNDATION SELECTION AND DESIGN PROCESS

As noted, the originally constructed floodwall monoliths were each supported by three rows of tapered steel monotube piles. Drilled shafts were selected to provide additional support because their installation would minimize disturbance to the ground and, they could be adequately reinforced to resist the large lateral loading that would occur when water reached the top of the floodwall.

The foundation analysis and design procedure required evaluation of both axial and lateral response of the existing monotube piles and the proposed drilled shafts. Axial analysis of the existing tapered monotobe piles was performed according to methods outlined in FHWA (1997), using the APILE software program. Axial analysis of the proposed drilled shafts was performed according to methods outlined by FHWA

© 2016 Deep Foundations Institute

(1999), using the SHAFT software program. Additionally, the axial capacity of drilled shafts was verified using methods described in FHWA (2010). Lateral analysis for all deep foundations was performed according to the p-y method, using the GROUP software application. Although short duration and undrained responses were evaluated, drained strengths and artesian effective stress conditions controlled the design. The analysis procedure followed is described in the following steps.

1. Determine underseepage conditions based on the previously designed relief well system.
2. Adjust the unit weight of the blanket soil to account for this underseepage, thus providing software with information necessary for it to correctly model the effective stress condition.
3. Perform axial analysis of monotube piles to determine both axial capacity and axial response.
4. Perform axial analysis on drilled shafts to determine both axial capacity and axial response.
5. Perform deep foundation group analysis using p-y methods.
    a. Verify that floodwall monolith group deflection does not exceed 1.5 inch (38 mm).
    b. Verify that deep foundation bending moments do not exceed allowable values.
    c. Verify that deep foundation shear values do not exceed allowable values.
    d. Verify that deep foundation axial loads are less than allowable capacities from step 4.

ADJUSTMENT BLANKET UNIT WEIGHT TO CAPTURE EFFECTIVE STRESS

Standard axial and lateral deep foundation analysis software packages do not allow the direct input of effective stress conditions or the input of the artesian groundwater pressures. The programs instead calculate effective stress conditions by applying user provided soil unit weight values, user provided groundwater elevations, and by assuming that groundwater is both static and unconfined. During flooding, the underseepage that flows landward beneath the floodwall is neither static nor unconfined. The unit weight of the fine grained blanket soil was reduced to account for the artesian conditions in the foundation sand (Eqn. 1). Entry of both the reduced blanket unit weight and the buoyant foundation sand unit weight into the aforementioned software packages, results in the correct modeling of the of effective stress conditions. Typical values calculated are shown in Table 1.

$$\gamma_{uplift} = [(\gamma_{bl} Z_{bl}) - (\gamma_w (h_p + Z_{bl}))] / Z_{bl} \quad [1]$$

Where γ_{uplift}= reduced unit weight of soil, γ_w= unit weight of water, γ_{bl} = total unit weight of blanket, Z_{bl}= blanket soil thickness, h_p= artesian head in sand measured from the ground surface.

Table 1. Typical Excess head and Modified Blanket Unit Weight

Total unit weight of blanket (pcf)	h_p in foundation sand (ft)	Z_{bl} (ft)	γ'_{uplift} (pcf)
119	13.1	22.5	20.3

RESULTING DRILLED SHAFTS DESIGNED TO ADDRESS THE DESIGN DEFICIENCY

To eliminate the floodwall foundation support deficiency required both the previously discussed relief well system and the addition of drilled shaft foundation support. This support consisted of a single row of 24 inch (610 mm) diameter steel cased drilled shafts, Fig. 3. The typical drilled shaft support added to each monolith consisted of a single row of seven drilled shafts reinforced with permanent steel casings and full length steel piles, typically HP 12 x 74 piles.

© 2016 Deep Foundations Institute

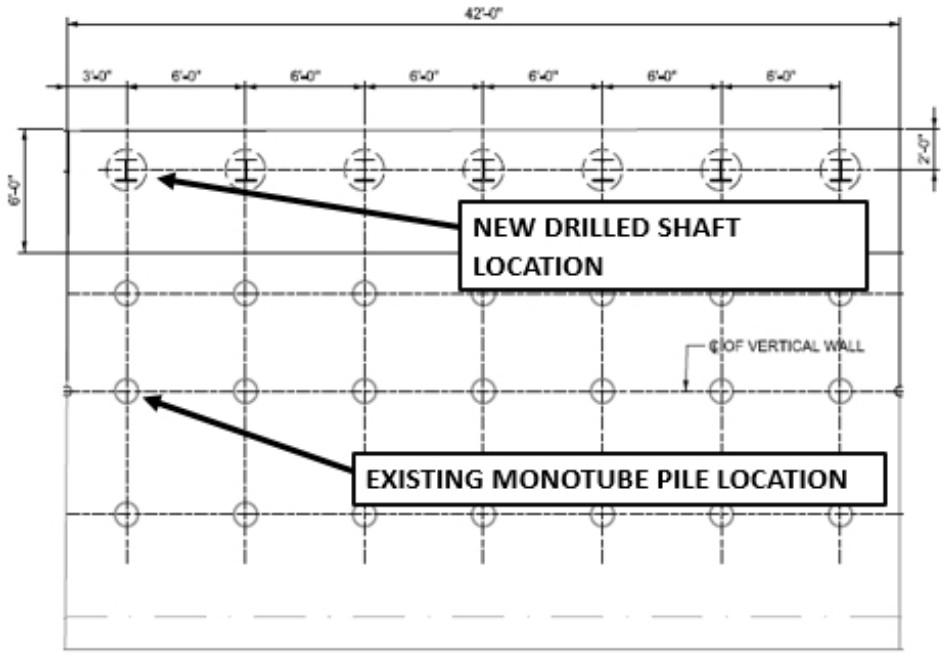


Figure 3. Plan View of Standard Pile Cap Layout Depicting Locations of Original Monotube Piles and the Proposed New Drilled Shafts

UNIQUE DRILLED SHAFT LOAD TEST DESIGN VERIFICATION PROCESS

Because of the unique analysis requirements, axial and lateral drilled shaft load tests were performed to verify the design results. Typically, drilled shaft design is controlled by undrained soil strength and total stress conditions, thus simplifying the interpretation of load test results. However, due to groundwater pressure from underseepage, the deep foundation design for this project was controlled by effective stress conditions and drained soil strengths. Adding to the complexity of using the load test results to verify the design, the effective stress conditions at the time of the load test were in a state of suction, a state much different from the controlling design case. As a result, the evaluation and application of load test data required a multi-step approach. The preliminary steps included the determination of unsaturated soil suction, determination of the effective friction angle at the load test site, the determination of the unsaturated blanket soil shear strength, the back calculation of soil/shaft friction angle, the determination of shaft axial capacities, the development of axial load response curves and the back calculation of the soil modulus. Finally, back calculated soil/shaft friction angles, axial response curves and soil modulus values were incorporated into the group foundation model to verify the design.

SOIL DATA COLLECTED TO INTERPRET LOAD TEST

A soil boring was completed within 15 ft (3.0 m) of the load test location one week prior to the performance of the load test. To allow the determination of matric suction at the load test site, laboratory testing of blanket soil samples included moisture content testing, density testing and testing to allow development of soil-water characteristic curves (SWCC). SWCC samples were collected from drying ground, and SWCC testing was performed according to ASTM D 6836. The SWCC plots and volumetric moisture content values were then used to estimate both the air-entry value (AEV) and matric suction of the cohesive blanket soil layer. The following figure is an example of the SWCC plots obtained.

© 2016 Deep Foundations Institute

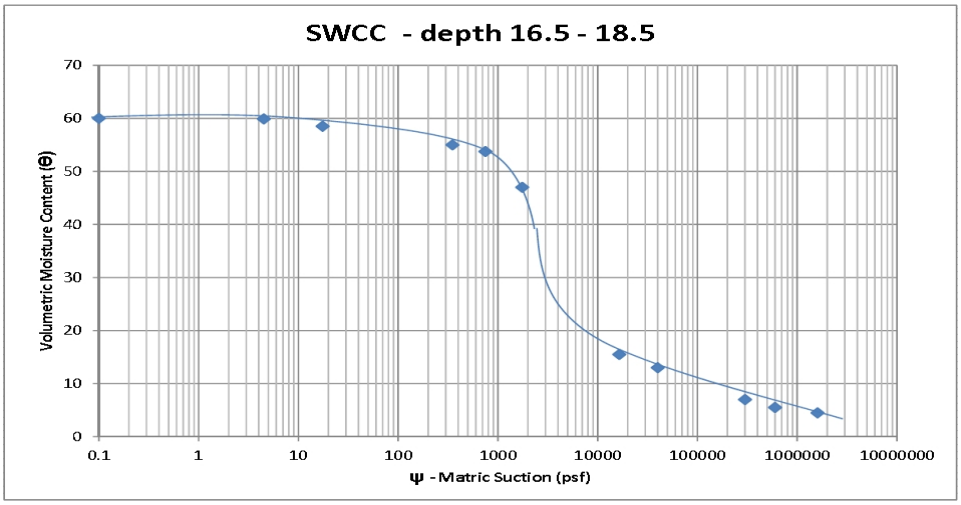


Figure 4. Example Soil Water Characteristic Curve (SWCC) determined for blanket soil

ESTIMATION OF UNSATURATED DRAINED SHEAR STRENGTH

At the time of the load test the blanket soil was unsaturated, a condition that increases the shear strength. The first step in calculating this increased shear strength was to calculate the effective stress. Equation 2 was used to calculate the effective stress at the time of the load test.

$$\sigma'_{vo} = \psi + \sigma_n \quad [2]$$

Where ψ = matric suction, and σ_n = net normal stress

Once the effective stress had been determined, the unsaturated shear strength of the blanket soil could be calculated. The unsaturated shear strength of the blanket soil was calculated using the Khalili and Khabazz (1998) method (Eqs. 3, 4 and 5).

$$\tau_s = c' + \sigma_n \tan\phi' + \chi\psi \tan\phi' \quad [3]$$

Where τ_s = unsaturated shear strength, c' = drained cohesion, ϕ' = drained friction angle, σ_n = net normal stress, ψ = matric suction , and χ = fitting parameter.

The fitting parameter for this method is written as follows:

$$\text{If } \psi > AEV, \text{ Then: } \chi = [(\psi)/AEV]^{-0.55} \quad [4]$$

$$\text{Otherwise: } \chi = 1 \quad [5]$$

The following table provides typical unsaturated blanket soil suction and shear strength results.

© 2016 Deep Foundations Institute

Table 2. Drained Shear Strength of Unsaturated Blanket Soil

Layer	$\emptyset'_{\text{triax.}}$	σ_n	ψ (psf)	*AEV* (psf)	χ	τ_s (psf)
Blanket	29	2079	2200	510	0.4475	1698

DETERMINATION OF SHAFT AXIAL CAPACITY AND AXIAL RESPONSE CURVES

Load test measurements of end bearing and side resistance were used to calculate axial capacity and, to generate axial response curves, assuming the design underseepage case. Ultimate drilled shaft capacity was calculated by adding ultimate side resistance and base resistance together. End bearing calculated using the Standard Penetration Test (SPT) method outlined in FHWA (2010) closely matched end bearing determined from the load test, making interpretation a simple mater. Interpretation of the axial load test to determine soil/shaft friction was a more complicated mater due to the presence of matric suction in the blanket soil. Drilled shaft load test side shear resistance values were used to back calculate the soil/shaft friction angles using the β-method (Eqs. 6-11). The β-method is described by O'Neill (2001).

$$R_{total} = R_{base} + R_{side} \quad [6]$$

$$R_{side} = f_s A_s \quad [7]$$

Where R_{total}, R_{base} and R_{side} = ultimate axial total, end bearing and side resistance, and A_s = Area of shaft perimeter.

$$f_s = \beta\,(\sigma'_{vo}) \quad [8]$$

Load Test Conditions: $\sigma'_{vo} = \psi + \sigma_n$ [9]

$$\beta = \left\{\left[(1 - sin\emptyset')OCR^{sin\emptyset'}_{as\ tested}\right]\ tan[\delta']\right\} \quad [10]$$

$$OCR = \text{overconsolidation ratio} = \sigma'_p/(\sigma'_{vo}) \quad [11]$$

Where σ'_p = past pressure, σ'_{vo} = effective stress, δ' = angle of friction between soil and drill shaft, and $\emptyset'$ = effective soil friction angle from testing.

Table 3. Comparison originally assumed δ' to value backcalculated using load test data

Soil Strata	Original Design Assumption δ'(deg)	Back calculated from load test δ'(deg)
Blanket Soil	33	33.6
Foundation Sand	36	34.6

© 2016 Deep Foundations Institute

With δ' known, flood state axial shaft capacities and axial response curves were generated (Fig. 5).

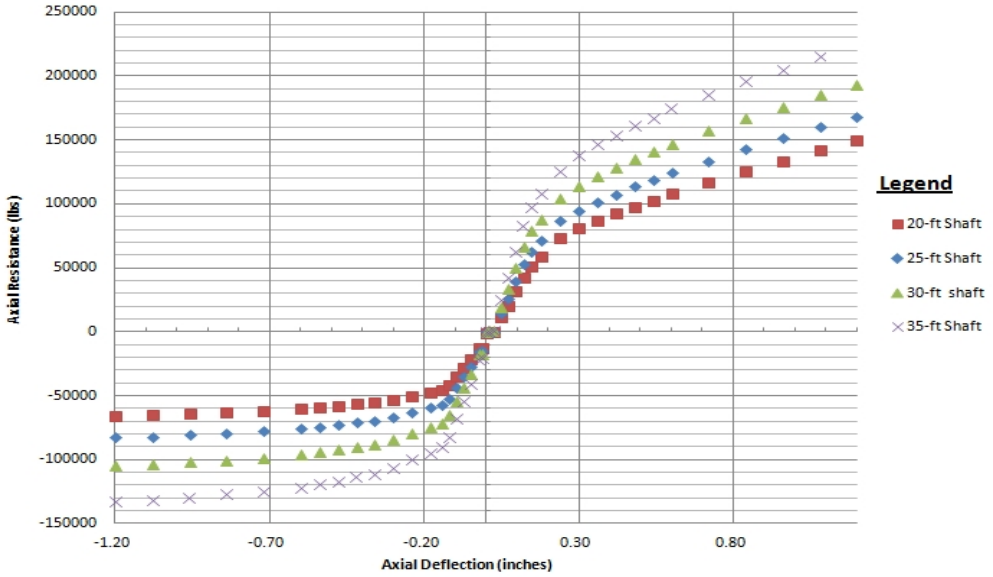


Fig. 5. Axial response curves developed using calibrated δ' values and groundwater pressures that reflect top of wall flooding after the construction of the designed relief well system

Both the load test back calculated soil/shaft friction angle and the shaft axial response curves were later incorporated into the original design group analysis model to verify the adequacy of the design.

CALIBRATION OF LATERAL SHAFT RESPONSE CURVES

Using the p-y method and varying the soil-modulus parameter (K) by trial and error, load test response curves were matched, and load test based K values determined (Fig. 6).

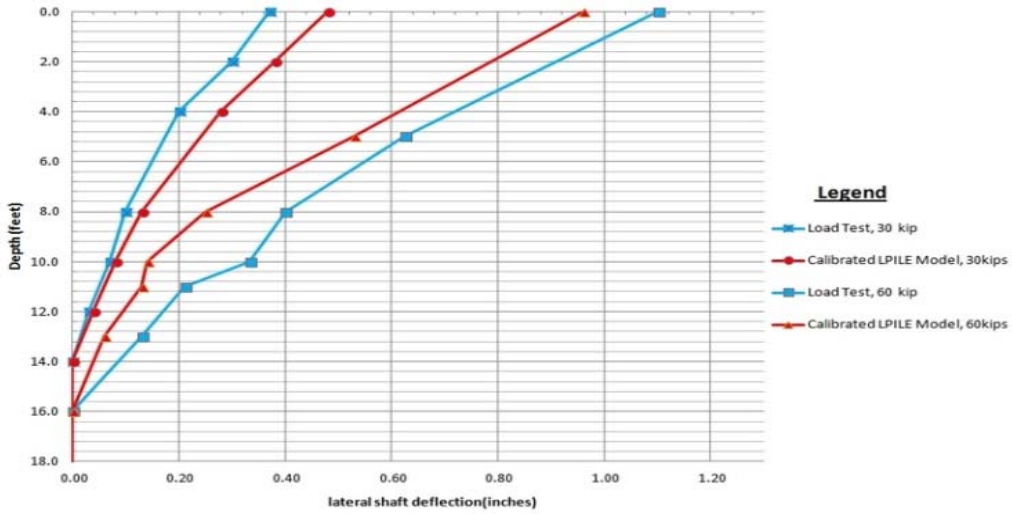


Fig. 6. Example shaft deflection versus shaft depth calibration curves

© 2016 Deep Foundations Institute

GROUP ANALYSIS DESIGN VERIFICATION

The last step in the load test design verification process was to incorporate the calibration results into the group analysis model of the original design, and then to run this model. Results from the model were then checked to determine if the design still met requirements. The incorporated calibration results included the axial load response curves, soil/shaft friction angles (δ') and the lateral soil-modulus values (K). Group analysis of monolith deep foundations allowed the determination of; the axial load carried by each deep foundation element, maximum internal moments of each deep foundation element, and maximum pile cap deflection of each floodwall monolith. All checks found that the original design was adequate (Table 5).

Table 4. Design Adequacy of Foundation Support Modification for Standard Monolith

CASE	Standard Floodwall Monolith Deflection	Axial Capacity FS For Standard Monolith		Structural Design Criteria Check	
		Tapered Monotube Piles	Drilled Shafts	Pile and Shaft Maximum Moments	Pile and Shaft Maximum Shear
Original Analysis of Modification	0.46	2.4	3.6	Yes	Yes
Analysis with Load Test Results	0.83	1.7	6.1	Yes	Yes

SUMMARY

In a previous 2006 study, the Fairfax-BPU floodwall was found to have inadequate foundation support to resist loading from floodwaters reaching the top of the wall. This deficiency was caused by increased loading and flood induced underseepage. A design to correct this deficiency included the addition of relief wells to reduce underseepage pressures, and the addition of deep foundations. The relief well system consisted of 14 wells. Deep foundations added consisted of a single row of 7 drilled shafts landward of the existing monotube pile support. These drilled shafts were 24 inch (610 mm) in diameter, permanently cased, typically 25 feet long and typically reinforced with HP 12 x 74 piles. Lateral and axial load tests were performed to verify the adequacy of the design modification. Analysis incorporating the load test results determined that the standard floodwall monoliths would deflect 0.83 in (21.1 mm) during flood loading, less than the 1.5 in (38.1 mm) allowed. The construction of additional deep foundation support was completed in 2014, as Phase I of the project (Fig. 7). Phase II of the design modification, consisting of the addition of 14 relief wells and a pumping plant modification, will conclude in the fall of 2016.

© 2016 Deep Foundations Institute



Fig. 7. Photo from 2015 of completed Fairfax-BPU floodwall modification

REFERENCES

Federal Highway Administration (FHWA), 1997. Design and Construction of Driven Pile Foundations, Report No. FHWA-HI-97-013, U.S. Department of Transportation, Washington, D.C. 453 p.

Federal Highway Administration (FHWA), 1999. Drilled Shafts: Construction Procedures and Design Methods, Report No. FHWA-IF-99-025, U.S. Department of Transportation, Washington, D.C., 790 p.

Federal Highway Administration (FHWA), 2010. Drilled Shafts: Construction Procedures and LRFD Design Methods, Report No. FHWA-NHI-10-016, U.S. Department of Transportation, Washington, D.C., 972 p.

Fredlund, D.G., Fredlund, R.D., and Rahardjo, H., 2012. Unsaturated Soil Mechanics in Engineering Practice. Wiley-Interscience, New York, 944p.

Khalili, N. and Khabbaz, M.H., 1998. A Unique Relationship for X for the Determination of Shear Strengths of Unsaturated Soils. Geotechnique, 48(5) 681-687.

O'Neill, M.W., 2001. The Thirty-Fourth Karl Terzaghi Lecture: Side Resistance in Piles and Drilled Shafts, Journal of Geotechnical and Environmental Engineering, 127(1) 1-2, pp 3-16.

U.S. Army Corps of Engineers (USACE), 2000. Design and Construction of Levees, Engineer Manual (EM) 1110-2-1913, Department of the Army, Washington, D.C., pp. B1-B18.

U.S. Army Corps of Engineers-Kansas City District, 2006. Review of Completed Project, Kansas City Levees, Kansas and Missouri, U.S. Department of the Army, Kansas City, Mo, pp. 45-46, pg. 57, pp. 7.1-7.64.

© 2016 Deep Foundations Institute

EXPERIMENTAL EVALUATION OF BUILDING SETTLEMENTS FOUNDED ON LIQUEFIABLE SOILS

Joseph A.W. Toth, University of Nevada, Reno, NV, USA, (775)-682-6450, josepht@nevada.unr.edu
Ramin Motamed, University of Nevada, Reno, NV, USA, motamed@unr.edu
Farshid Ghazavi, Arup, Los Angeles, CA, USA, farshid.ghazavi@arup.com

ABSTRACT

Post-disaster reconnaissance of areas affected by earthquakes has documented extensive damage to buildings with shallow foundations located in liquefaction-prone areas. Currently, estimation of liquefaction settlement is based on empirical correlations that evaluate settlement in the free-field environment and are based on one-dimensional consolidation. However, observations have shown that liquefaction settlement under buildings can be considerably greater. This research is based on a series of 1-g shake table experiments using a transparent soil box to reproduce liquefaction-induced building settlement. Building settlements were evaluated using a scaled model of a building foundation representing a 1-2 story building. Comprehensive parametric study was carried out to establish the effects of several parameters on free-field and building settlements such as building width and thickness of liquefiable soil layer. The experiments utilized accelerometers and pore-water pressure sensors to monitor ground accelerations and buildup of pore-water pressures in both the free-field and model building footprint. Results of these experiments are compared to available centrifuge tests and field observations and conclusions are drawn with respect to the potential scaling effects. Lastly, this paper discusses the feasibility of installing helical piles as a mitigation strategy to reduce the building settlements by presenting some of the exploratory experimental data obtained from this series of 1-g shake table tests.
Keywords: Liquefaction, building settlements, helical piles

INTRODUCTION

The 2010-2011 Canterbury earthquake sequence and the 2011 Great Tohoku earthquake are some of the most recent examples where large numbers of low-story structures sustained damage resulting from liquefaction-induced settlements. This damage has commonly been observed in residential and commercial areas developed over loose, unconsolidated and saturated coarse grained soils resulting from both natural and man-made deposits. Damages incurred from the 2010-2011 Canterbury earthquake sequence occurred in the largely unconsolidated fluvial environment bordering the Avon River in Christchurch (Henderson 2013). Similar damage was also incurred during the 2011 Great Tohoku earthquake where liquefaction of soils occurred in both young alluvial deposits and fill materials (Ashford et al. 2011). Figure 1 presents typical modes of failure to structures resulting from the effects of liquefaction. Current practices in evaluation of liquefaction settlement rely on empirical correlations (Tokimatsu et al. 1987; Ishihara et al. 1992) developed for liquefiable soils in the free-field environment (Dashti et al.

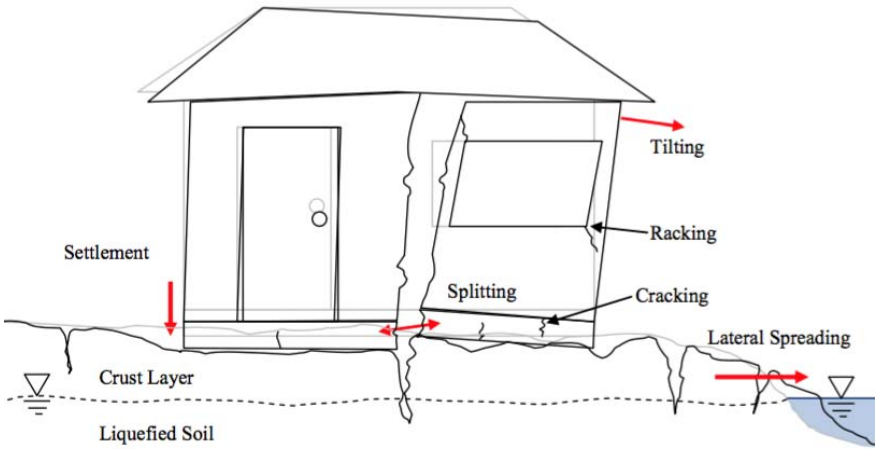


Figure 1. Modes of Failure Caused by Liquefaction (Henderson 2013)

© 2016 Deep Foundations Institute

2010a). However, recent observations of the performance of foundations suggest that settlement of rigid shallow foundations in liquefiable soils are commonly greater than those predicted in the free-field. Therefore, new correlations should be developed to better predict the degree of settlement of shallow foundations in liquefiable soils. Current research is beginning to focus on the mechanisms of settlement during liquefaction in regards to confining stress, pore-water pressure and shear stress induced from foundations (Dashti et al. 2010b).

This paper presents the results of a series of scaled 1-g shake table tests performed to evaluate the settlement of rigid shallow foundations over a uniform liquefiable sand. Each test evaluated the degree of settlement for both the free-field environment and building footprint. Results of the experiments are compared to available centrifuge tests and field observations drawing conclusions with respect to potential scaling effects. In addition, the feasibility of installing helical piles as a mitigation strategy to reduce building settlements is discussed and the results of one exploratory experiment that utilized a model footprint founded on a scaled helical pile foundation are presented.

1-G SHAKE TABLE EXPERIMENTS

A series of scaled shake table tests were performed to evaluate liquefaction induced settlement for rigid shallow foundations over a uniform deposit of liquefiable sand. Available scaling laws for 1-g testing were reviewed for our evaluation and are presented in Table 1. Similitude scales presented in Table 1 are derived from Iai (1989). Our evaluations used a scaled factor of 10 for all cases of unsupported shallow foundations and shallow foundations supported with helical piles. It should be noted that all results referenced henceforth in this paper are presented in model scale. The series were conducted on a liquefiable stratum that varied between 0.5 feet and 1.0 foot in thickness overlaying a non-liquefiable stratum of equal thickness. Each test evaluated degree of settlement for the model foundation and free-field environment. Circular concrete footprints were used in our testing and served as the model buildings. Each footprint assumed an equal contact pressure representative of a 1-2 story residential structure and varied in diameter (width). Testing included the use of a total of five accelerometers and one pore-water pressure sensor.

Table 1. Similitude Laws for 1-g Shake Tests

Variable	λ	For $\lambda = 10$
Length	λ	10
Density of Saturated Soil	1	1
Density of Water	1	1
Strain of Soil	$\lambda^{0.5}$	3.16
Time	$\lambda^{0.75}$	5.62
Frequency	$\lambda^{-0.75}$	0.18
Stress	λ	10
Effective Stress	λ	10
Pore-water Pressure	λ	10
Permeability	$\lambda^{0.75}$	5.62
Porosity	1	1
Displacement	$\lambda^{1.5}$	31.62
Acceleration	1	1

© 2016 Deep Foundations Institute

Soil Box

Our experiment utilized a transparent soil box fitting the model dimensions of 6.7 feet x 2.1 feet x 2.7 feet (*length* x *width* x *height*). The box was constructed of 1-inch thick clear acrylic and reinforced along the corners by a rigid steel frame. The inside base of the box was fashioned with additional 1-inch thick acrylic spacers and perforated 0.25-inch thick acrylic sheets that served as the base platform for the construction of the soil layers. The perforated acrylic had a veneer of woven geomembrane allowing the soil to drain freely while retaining the testing medium. Additionally, two valves were installed within the zone created by the acrylic spacers to assist in saturation and draining of the soil box.

Soil Properties

Shake table testing was performed using a fine to medium, poorly graded Sierra Silica #60 mesh sand (D_{50} ≈ 0.32 mm, C_u ≈ 1.75, C_c ≈ 1.04, e_{min} ≈ 0.73, e_{max} ≈ 1.01). Liquefiable and non-liquefiable layers were respectively prepared to approximate relative densities (D_r) of 30% and 60% as shown in Figure 2.

Model Configuration and Preparation

Configuration of our model was derived from a geotechnical project located in South Lake Tahoe, California that included retrofit of existing structures using helical piles over potentially liquefiable soils. Review of available boring logs and subsurface conditions concluded an approximate 10 foot thick layer of coarse saturated sands. The standard model configuration used in each test is presented in Figure 2 and includes the typical layout of instrumentation. In an effort to reduce boundary effects in the direction of simulated shaking, a 0.25-foot thick sheet of high density foam was placed at each end of the soil box. Each test was prepared by first constructing a moisture conditioned non-liquefiable layer. The non-liquefiable layer was conditioned to 5% moisture and then compacted in lifts within the base of the transparent soil box to a uniform thickness of 1.0 foot. Saturation of the non-liquefiable layer was then completed through use of a spigot located at the base of the soil box. Water was slowly introduced into the box, thus saturating the soil from the bottom up. Saturation continued until a sufficient height of standing water resided over the non-liquefiable layer, typically 0.5 feet or half the model liquefiable stratum thickness. The liquefiable layer was then constructed by means of pluviation through water. The sand was poured over a fine mesh screen situated over the transparent box assisting in uniform deposition and complete saturation of the liquefiable layer through the standing water. The phreatic surface was located at the surface of the liquefiable layer for all tests as shown in Figure 2.

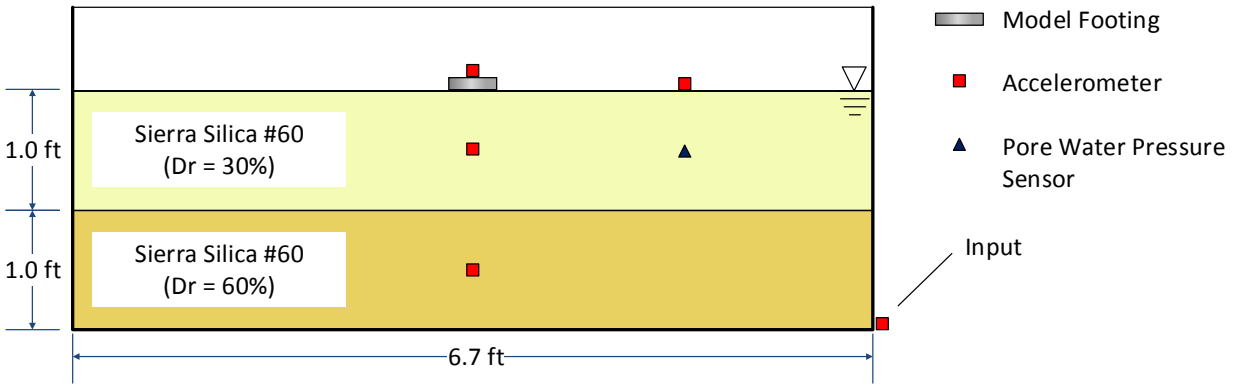


Figure 2. Scaled Model Configuration of 1-g Shake Table Tests

© 2016 Deep Foundations Institute

Accelerometers were placed throughout the soil stratum during preparation and their locations are shown in Figure 2. Each accelerometer was secured to a semi-rigid base and placed either within the soil stratum or on the ground surface to maintain proper orientation during model excitation. One pore-water pressure sensor was installed and secured at the center of the liquefiable layer beneath the free-field accelerometer as shown in Figure 2.

Ground Motions

Input motions were achieved using an eccentric-mass shaker that was centered on the top of the shake table. The eccentric mass shaker was configured to produce a 4Hz frequency oriented in a horizontal direction. Input motions were employed using the eccentric-mass shaker for a total of 20 seconds, at that point the input motion was ceased. Each test was recorded for a total of 40 seconds to ensure a complete record for both acceleration and pore pressure dissipation. An average peak ground acceleration (PGA) of 0.36g was achieved for the shake table tests presented in our experimental results.

To establish repeatability of the results in our evaluations, one shake table test was repeated three times. This test was re-evaluated using the same scaled configuration and model building thus ensuring similar results.

Rigid Mat Foundations

Circular concrete footings were employed in each test to serve as the model building foundation based on Table 1 Similitude laws. Each building, representing a typical 1-2 story structure, assumed an average contact pressure of approximately 125 psf (Perko 2009). A total of three different foundation widths were employed during testing and varied in prototype size from 2.5, 3.75 and 5 feet in diameter (model dimensions 0.25, 0.375 and 0.5 feet). It should be noted that based on the limited dimensions of the soil box, employing a realistic sized model foundation was not feasible. Although our model buildings induced an average contact pressure of 125 psf, the models themselves are more representative of an isolated concrete footing. Before commencement of each test, initial hand measurements of the ground elevation were recorded for the settlement evaluation. Measurements from the top of the soil box to the ground surface were recorded across the entire footprint of the soil box. A total of 34 initial measurements were recorded that included the model building footing, area within zone of influence from the model building footprint and free-field environment. Figure 3 presents a typical plan view of the shake table tests and the gridlines (oriented longitudinally) used to assess initial and final ground surface elevations for evaluation of settlement. Upon completion of each test, similar measurements were recorded at the same locations. Final settlements were determined and averaged using all 34 measurements comprising both the building footprint and free-field environment.

© 2016 Deep Foundations Institute

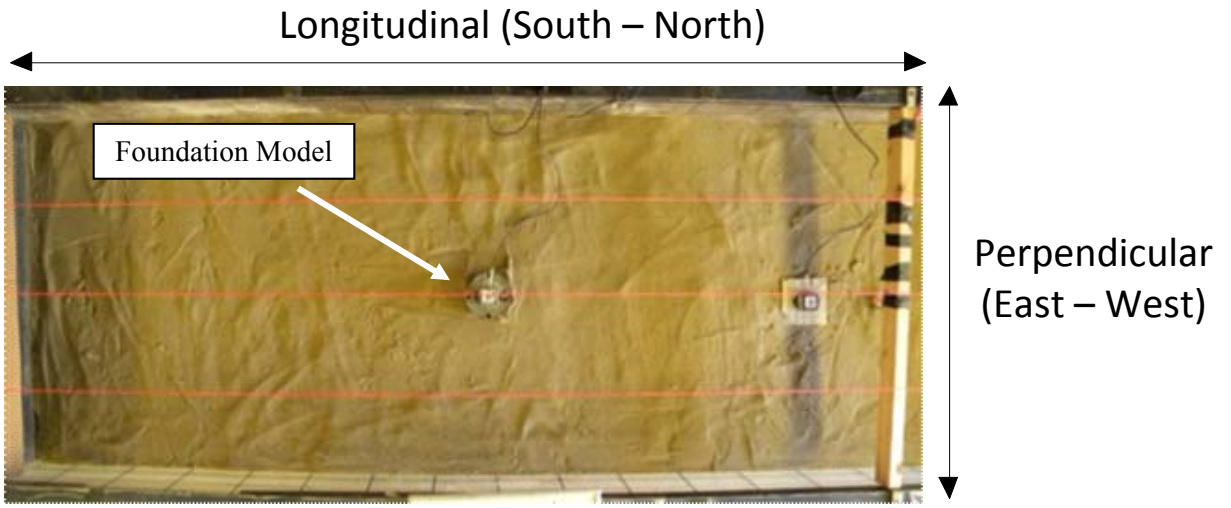


Figure 3. Plan View of 1-g Shake Table Test Showing Grid Pattern Used in Measuring Settlement

Helical Pile Supported Foundations

In regions where liquefaction susceptibility is high, there is a need for effective solutions in mitigating foundation settlement. For this study, helical piles were chosen as a mitigation strategy in reducing the excessive building settlements that occur in structures founded over liquefiable deposits. Compared to other conventional foundation and soil improvement methods (driven piles, deep soil mixing, etc.) helical piles are the most attractive from a constructability and economic standpoint. Installation of helical piles typically require less logistics during installation and can be employed in more spatially restrictive locations.

Using similarly constructed circular concrete footprints, helical piles were secured to the base and used to support the foundation. One preliminary test (Test #30) was performed using model helical piles to evaluate the reduction in liquefaction induced settlement. Design of the helical pile was completed in prototype dimension and scaled down to model size. The prototype dimension of the helical pile consisted of a 3-inch diameter circular shaft that included a single 12-inch diameter helix and 0.375-inches in thickness. The smaller shaft size was chosen for our design and was presumed to be typical for use in residential structures. Adhesion along the shaft was ignored in the design calculation. Four helical piles were secured to the footing; each being 1.6 feet in length with 0.3-inch circular shaft and one 1-inch diameter helix located at the pile tip. In order to secure each pile to the footing of our model, four plastic sleeves were embedded in the concrete footing and served as a crude pile bracket. Figure 4 presents photos of the design and configuration of the concrete footing and helical piles used in the evaluation. In addition, Figure 4 also shows the sleeves embedded in the footing and allowed the footing to rest directly on the ground surface. Each helical pile was embedded to a bearing depth of 1.5 feet or center of the non-liquefiable layer. Because of the crude design and construction of our helical piles, difficulties presented themselves during installation. Although each helix was of the approximate size and gauge thickness, the pitch of the helices could not be controlled. As a result reproducing installation of the piles as they would in common practice could not be achieved in the laboratory. Therefore, each pile was placed at the intended bearing depth during placement of the non-liquefiable layer rather than advanced into the bearing layer to target depth. Initial and final ground surface measurements, similar to the unsupported rigid mat foundations, were completed during the test. These measurements provided a good comparison of liquefaction-induced settlement between unsupported and supported shallow foundations.

© 2016 Deep Foundations Institute

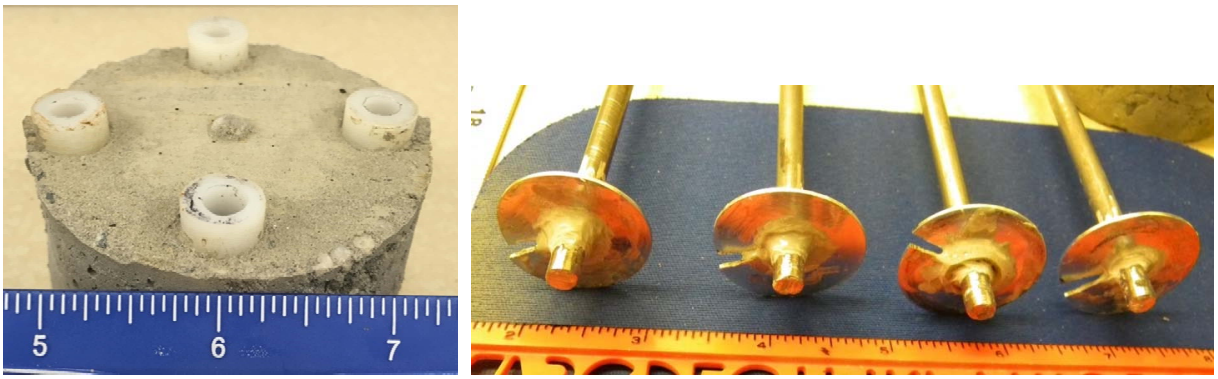


Figure 4. Model Concrete Footing and Helical Piles Used in 1-g Shake Table Tests

Figure 5 shows the helical piles embedded within the non-liquefiable layer and the concrete footing positioned on top of the pile shafts. In addition, Figure 5 also presents a basic configuration of the helical piles and instrumentation in profile. The area from the base of the concrete footing to the top of soil in the figure represents the thickness of the liquefiable layer just before saturation and pluviation. Future testing of helical pile foundations will include variation in depth of embedment of the pile as well as variation in diameter of helices.

EXPERIMENTAL RESULTS

Table 2 provides a summary of results based on the evaluations conducted for select tests #19 through 30. Each evaluation in the summary includes foundation diameter as well as average free-field and building settlements. These evaluations, with the exception of Test #30, were performed using an equal input frequency of 4 Hz and recorded similar peak ground accelerations. It should also be noted that Test #19 through 26 were evaluated as unsupported footings while Test #30 was supported using helical piles.

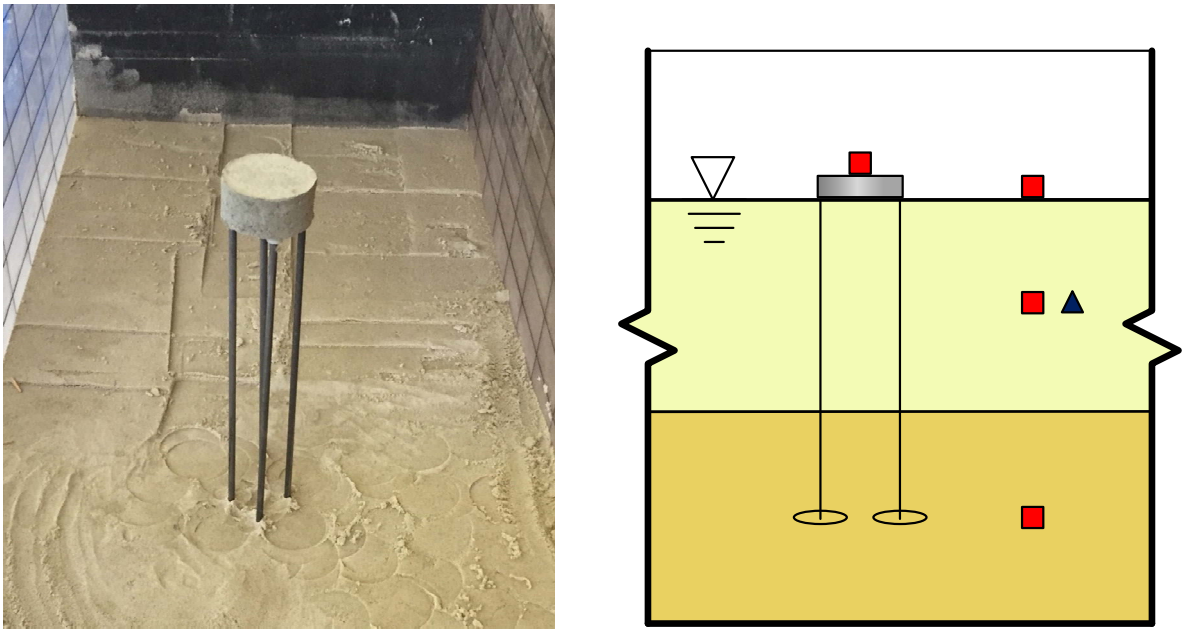


Figure 5. (Left) Photo of Scaled Helical Model Configuration in 1-g Shake Table Tests. (Right) Schematic Illustration of Helical Piles Installed.

© 2016 Deep Foundations Institute

Table 2. Summary of 1-g Shake Table Test Results

Test No.	Liquefiable Layer Thickness (ft)	Non-Liquefiable Layer Thickness (ft)	Foundation Diameter (ft)	Average Free-Field Settlement (ft)	Average Building Settlement (ft)
19	0.5	0.5	0.5	0.016	0.092
20	0.5	0.5	0.5	0.014	0.106
21	0.5	0.5	0.5	0.016	0.105
25	0.5	0.5	0.25	0.018	0.056
26	0.5	0.5	0.375	0.021	0.100
30	1.0	1.0	0.25	0.040	0.005

Time histories recorded for Test #19 and Test #30 are presented in Figure 6 and include all five accelerometers and one pore pressure sensor. Each accelerometer is labeled respectively to their depth or location within the soil box. It is evident in the recorded time histories that the ground accelerations within the non-liquefiable layer (D_r = 60%) closely parallel those of the input motion for each case of unsupported and supported shallow foundations. A steady increase in pore-water pressure develops in unison with each respective input motion for Test #19 and Test #30. Lastly, the sharp increase in pore-water pressure is indicative of the development of liquefaction phenomena. This phenomena is apparent in Test #19 for all recorded ground accelerations located within and on the surface of the liquefiable soil (D_r = 30%). However, in Test #30 the model footing is founded on helical piles secured in the non-liquefiable layer, translating to larger ground accelerations.

© 2016 Deep Foundations Institute

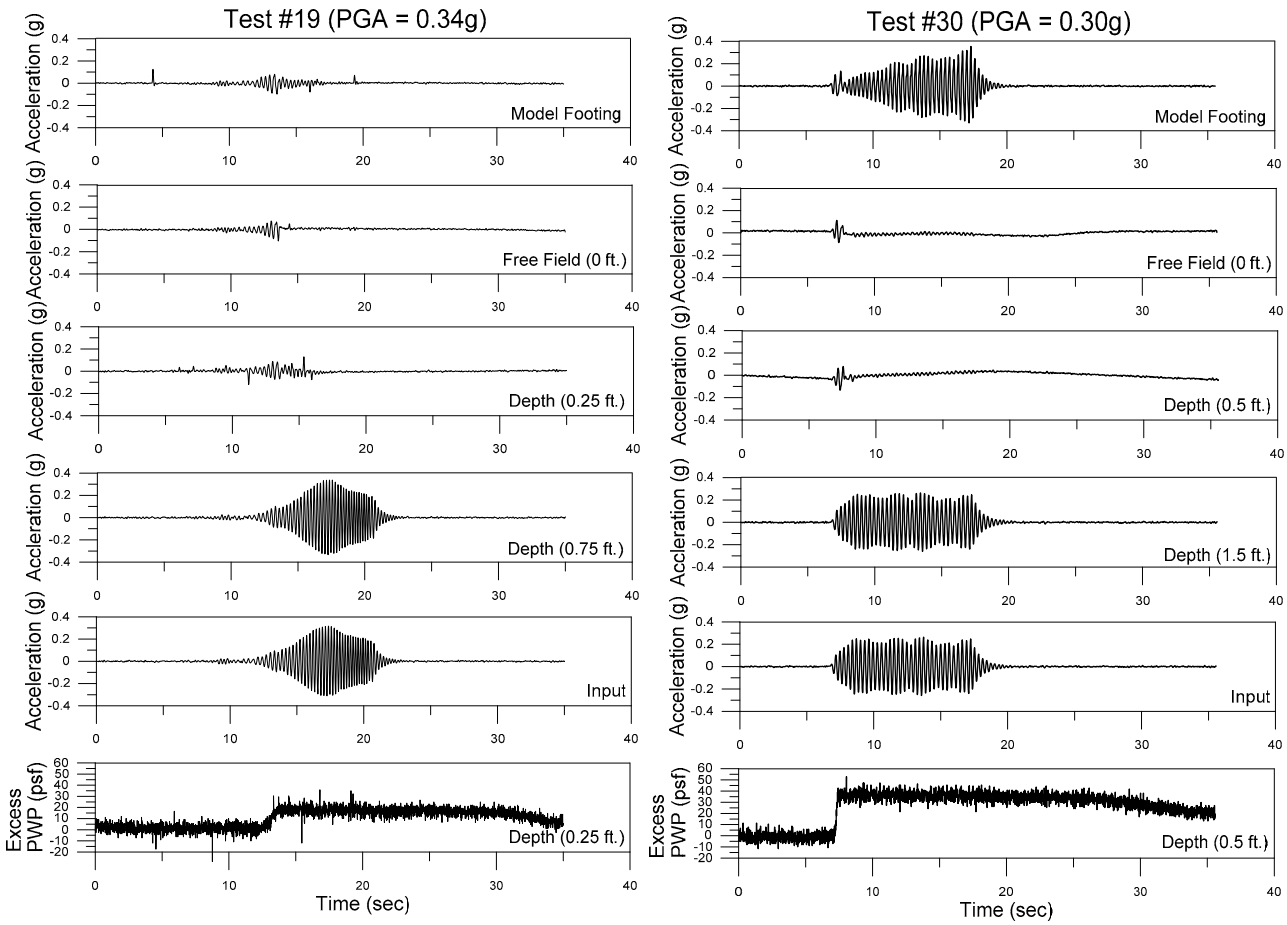


Figure 6. Typical Acceleration and Excess Pore-water Pressure Records for Cases of Unsupported Footing and Helical Piles during Experimental Testing Without and With Helical Piles as Mitigation Measure.

Settlements were measured and average values are presented for each test in Table 2. Measured settlements for Test #19 are presented in Figure 7 and show both areas within the free-field and model building environment. Measurements were recorded and plotted both longitudinally and perpendicularly to the long axis of the soil box. The longitudinal axis is plotted in three sections: centerline (which includes the model building), as well as the eastern and western sections off centerline. For further reference these lines are delineated in Figure 3. Perpendicular measurements were plotted in a similar fashion and include sections north and south of centerline. Figure 7 clearly shows an increase in measured settlement within the boundary and zone of influence of the model building for Test #19. Test #30 evaluated a model building supported on helical piles. Each helical pile was bearing at the same approximate tip elevation. Although Test #30 was performed at a larger scale under slightly different input motions, a considerable decrease in liquefaction-induced settlement was observed.

© 2016 Deep Foundations Institute

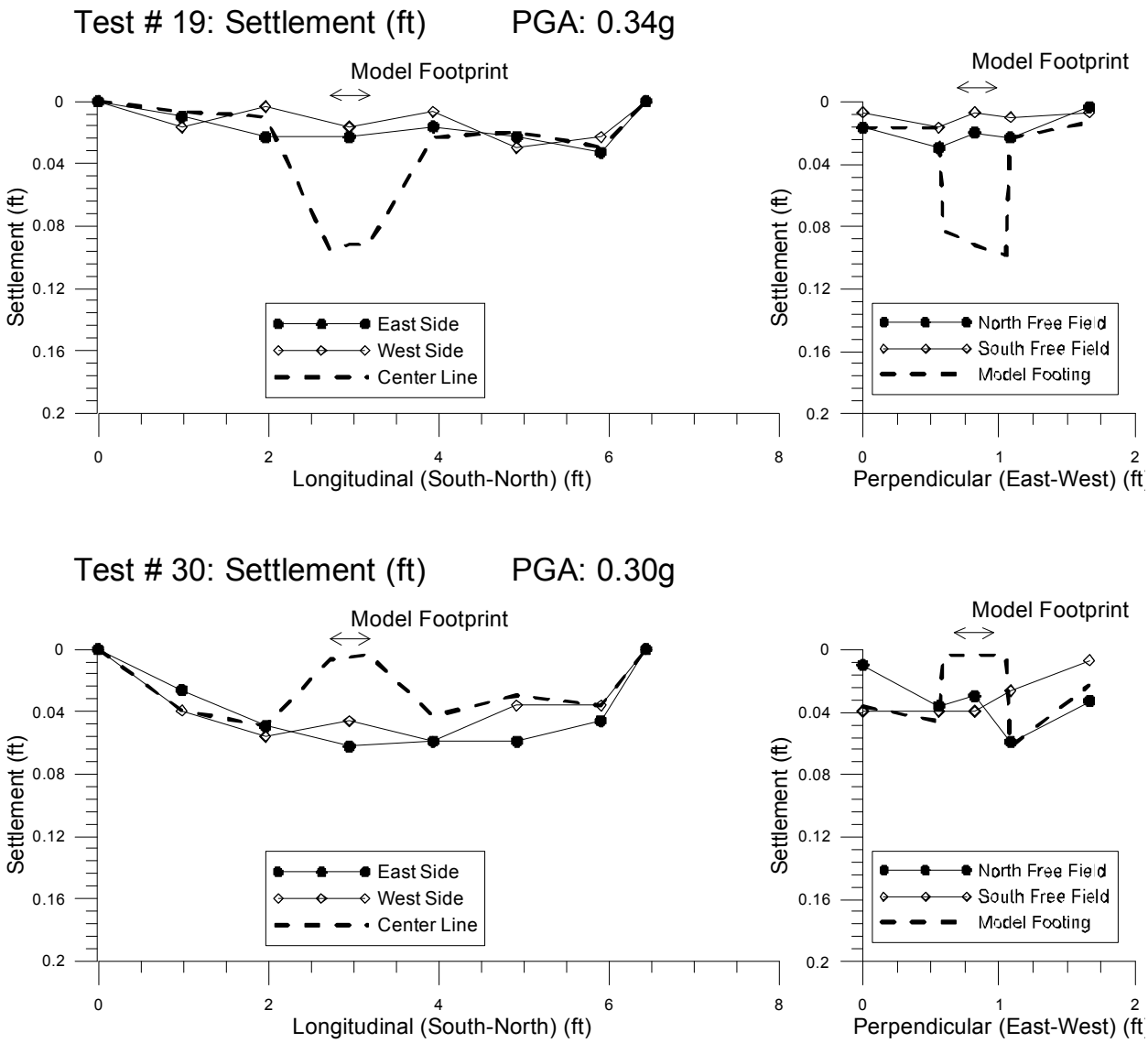


Figure 7. Typical Plots of Liquefaction Induced Settlement for Cases of Unsupported Footing and Helical Piles during Testing

Figure 8 presents our results in comparison to previous studies of liquefaction-induced settlement for shallow foundations. The plot provides a normalized comparison of foundation settlement in regards to building width. This plot was previously presented in Dashti et al. (2010b) and Bray and Dashti (2014) and has been updated to include the results of our experiments. The updated plot is comprised of a series of field observations, centrifuge and shake table test studies. The upper and lower bound plots are based on field observations. Liu/Dobry, Hausler, and Dashti plots are based on results from centrifuge testing. Yoshimi results are based on shake table testing. Results show a similar scatter of data for normalized foundation settlements based on the overall sources provided in the plot. However, our 1-g shake table tests resulted in a drastic reduction in building settlements with the use of helical piles (Test #30).

© 2016 Deep Foundations Institute

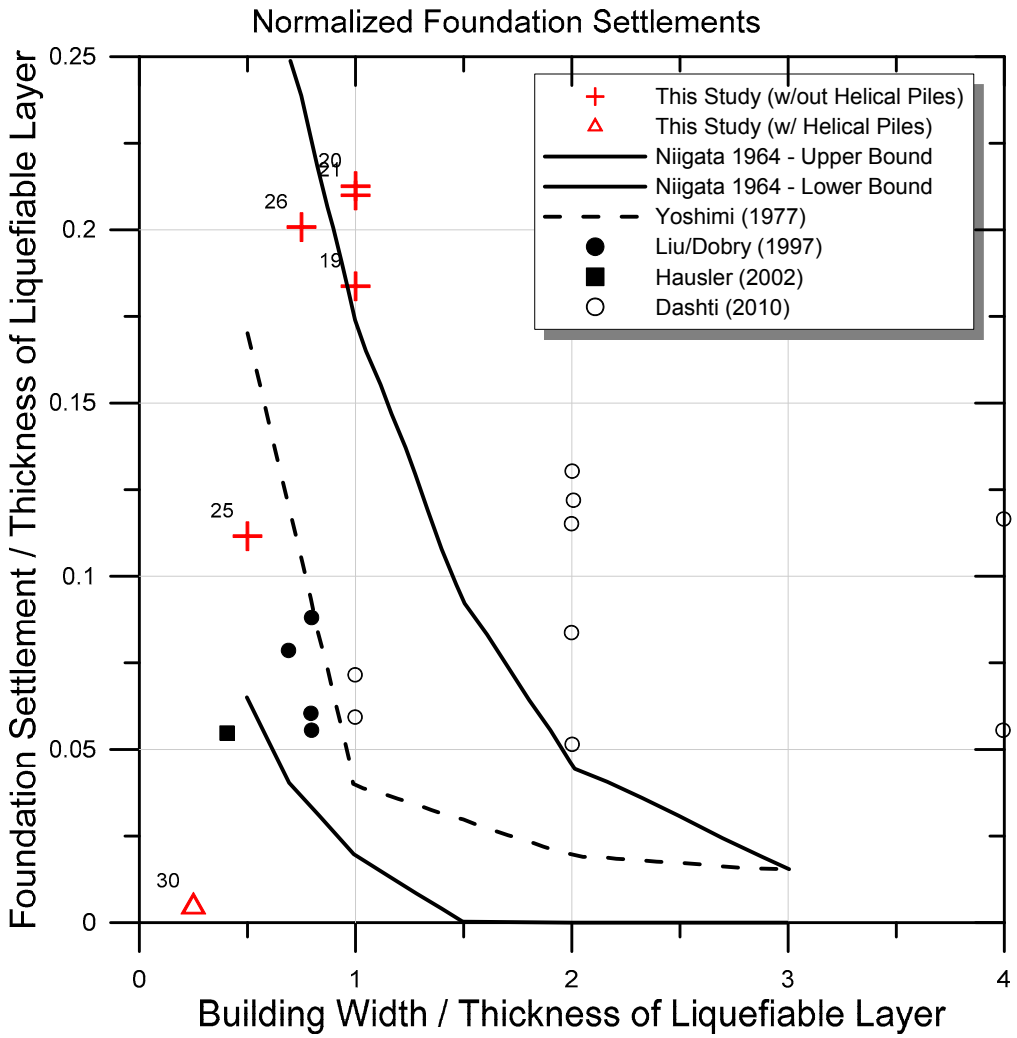


Figure 8. Comparison of 1-g Shake Table Results with Previous Research (Adapted from Dashti et al. 2010b)

SUMMARY AND CONCLUSIONS

In summary, these experimental evaluations have shown that liquefaction-induced settlement is considerably greater and far more complex than the conventional empirical approach based on one-dimensional consolidation settlement in the free-field. These results have been validated in comparison with available experimental centrifuge tests and field observations based on the 2010-2011 Canterbury Earthquake sequence and 2011 Great Tohoku Earthquake.

In this study helical piles were chosen as a solution in mitigating the settlements incurred by the effects of liquefaction. As our understanding of helical piles increases they are being implemented over a wider range applications in foundation design and repair. Research is currently underway to better understand their application in mitigating liquefaction induced settlement and response during seismic events.

The feasibility of helical piles was evaluated as a potential mitigation strategy in the reduction of liquefaction-induced settlement. Based on our evaluation, implementation of helical piles in supplementation with rigid shallow foundations showed a dramatic reduction in liquefaction-induced settlements.

© 2016 Deep Foundations Institute

ACKNOWLEDGEMENTS
The authors would like to thank Bob Fehling and RamJack for providing project geotechnical information used in developing the liquefaction model that served as the basis for this experimental evaluation.

REFERENCES

Ashford, S.A., Boulanger, R.W., Donahue, J.L., & Stewart, J.P. (2011). "Geotechnical Quick Report on the Kanto Plain during the March 11, 2011, Off Pacific Coast of Tohoku Earthquake, Japan. GEER Association Report No. GEER-025a, 1-20.

Bray, J., and Dashti, S. (2014). "Liqueaction-Induced Building Movements." Bulletin Earthquake Engineering., 12, 1129-1156.

Dashti, S., Bray, J.D., Pestana, J. M., Riemer, M.R., and Wilson, D. (2010b). "Centrifuge Testing to Evaluate and Mitigate Liquefaction-Induced Building Settlement Mechanisms." Journal of Geotechnical and Geoenvironmental Engineering, 136(1), 918-929.

Dashti, S., Bray, J.D., Pestana, J. M., Riemer, M.R., and Wilson, D. (2010a). "Mechanisms of Seismically-Induced Settlement of Buildings with Shallow Foundations on Liquefiable Soil." Journal of Geotechnical and Geoenvironmental Engineering, 136(1), 151-164.

Henderson, D. (2013). "The Performance of House Foundations in the Cantebury Earthquakes." (Master's thesis). University of Canterbury, August 2013, 1-448. HTTP://IR.CANTERBURY.AC.NZ/HANDLE/10092/8741

Iai, S. (1989). "Similitude for Shaking Table Tests on Soil-Structure-Fluid Model in 1-g Gravitational Field." Soils and Foundations, 29(1), 105-118.

Ishihara K, Yoshimine, M (1992). "Evaluation of Settlements in Deposits Following Liquefaction during Earthquakes." Soils and Foundations., 32(1), 173-188.

Perko, H.A. (2009). "Helical Piles: A Practical Guide to Design and Installation." Hoboken, New Jersey, Wiley.

Tokimatsu K, Seed HB (1987). "Evaluation of Settlements in Sands due to Earthquake Shaking." Journal of Geotechnical Engineering ASCE, 113(8), 861-878.

© 2016 Deep Foundations Institute

This page left intentionally blank

© 2016 Deep Foundations Institute

DESIGN BUILD OF THE NEW NY BRIDGE FOUNDATIONS

Chris J. Leykam P.E., Tappan Zee Constructors, LLC, Tarrytown, NY, USA, 914-606-3600 Chris.Leykam@gcinc.com
Scott. A. Jacobs P.E., Tappan Zee Constructors, LLC, Tarrytown, NY, USA, 704-526-3246, Scott.A.Jacobs@fluor.com

ABSTRACT

Construction of the New NY Bridge over the Hudson River 25 miles north of New York City is one of the largest civil infrastructure projects presently underway in the United States (formerly Tappan Zee Hudson River Crossing). The $3.14 billion Design-Build contract is also the largest ever awarded by the state of New York using an Alternative Project Delivery method, and the first major public project to use Design-Build. The new 3.1 mile long bridge will replace the existing Governor Malcolm Wilson Tappan Zee Bridge with a modern twin crossing featuring: Iconic side by side cable stay main spans; significant deck widths accommodating eight lanes of regular traffic, wide shoulders, and a shared use pedestrian and bike path; foundation with excess capacity to fully support a future rail bridge; more than 1,000 large diameter pipe piles driven in deep glacial deposits; drilled shafts installed through steep blast-rock slopes on the east shore landings. Geotechnical challenges included varied bedrock and glacial till surfaces with steep slopes and depths in excess of 750 ft.

The purpose of this paper is to highlight major features of the New NY Bridge project with specific focus on the design and construction of the foundations supporting the approach and main span structures from abutment to abutment, provide background on alternative project delivery in NY, as well as provide an overview of the design-build process as it was applied to foundation delivery.

Keywords: design-build, bridge, foundation, driven pile, drilled shaft, precast pile caps, sound attenuation.

The 3.1 mile Governor Malcolm Wilson Tappan Zee Bridge was constructed across the Hudson River connecting Nyack and Tarrytown (Rockland and Westchester Counties). Construction started in March 1952 and was completed in 1955 for a cost of $81 million. The seven lane crossing first opened to traffic on December 15, 1955 and coincided with the opening of a 28 mile segment of highway I-87 / I-287 between Suffern NY and Yonkers NY. The bridge is part of the extensive 574 mile New York State Thruway road system owned and operated by the New York State Thruway Authority (NYSTA).

Path to The New NY Bridge

The need to replace the aging and heavily used Tappan Zee Bridge became increasingly apparent to NYSTA by 1999, as costs to maintain and repair the structure and road decks multiplied while traffic demand remained high. The original design basis was for 100,000 vehicle trips per day, while current demand averages 140,000 vehicle trips per day with a peak of near 170,000. Costs for maintenance and repair were increasing substantially and forecast to be $750 million over next decade. Of additional concern the 3.1 mile bridge experiences approximately double the vehicle accident rate as the rest of the 574 mile Thruway system, and the bridge has no shoulder lanes available for disabled vehicles or emergency responders.

Plans for a replacement lagged due to many factors, chief among them were a difficult environmental review process and a desire by some constituencies to incorporate the bridge into a large new regional mass transportation system, light rail or bus rapid transit, all of which lead to uncertainties for scope and schedule. The New NY Bridge project was reinvigorated in late 2011 when NY Governor Cuomo made replacement of the bridge itself the principal priority, separating it from the need to concurrently build a mass transit system. Soon thereafter, the crossing was named to a White House short list of critical

© 2016 Deep Foundations Institute

national infrastructure mega-projects which qualified it for expedited permitting and environmental review as part of the "We Can't Wait Initiative", adding it to the newly created Federal Infrastructure Projects Dashboard (*www.permits.performance.gov*). Later that same year Governor Cuomo enacted the "Infrastructure Investment Act" which allowed a select group of state agencies, including NYSTA, to use Design-Build project delivery for contracts for a period of three years (*State Bills S50002-2011 and A40002-2011*). Historically the use of Design-Build or similar alternative project delivery in New York has not been an option on public projects as the prevailing law effectively required agencies to contract design services separate and apart from construction services (*N.Y. Educ. Law § 7200 et. seq. and § 6512-6516*).

Design-Build Process

Tappan Zee Constructors, LLC (TZC), a consortium of Fluor Enterprises, American Bridge Company, Granite Construction, Inc., and Traylor Brothers, Inc., was selected by NYSTA as the Design-Build contractor based on a proposal for $3.14 Billion to design and construct the new crossing and demolish the existing structures. The design team assembled by TZC is led by HDR Inc. and includes COWI/Buckland & Taylor, GZA GeoEnvironmental, and URS Corp., among many others. The contract was awarded with notice to proceed in January 2013.

The Design-Build process started for TZC from the very beginning of the pre-bid phase in early 2012. From the earliest stages during estimating a "Construction Driven" process was put in place to quickly converge on principal design elements and features (concrete vs. steel, segmental vs. full span, etc.) Key focus areas for achieving the pursuit goals included: developing early pricing on base work, overall constructability, quick turn-around of potential options, establishing low up-front costs, identifying technical solutions and innovations, consideration for maintainability of structures, mitigation of overall project risk, and keeping in touch with public opinion. The final design-build concept consisted of a lighter superstructure, fewer foundations spaced further apart, and less piles than those of the competitors. Major features included:

- Two independent 3.1 mile bridges, across 43 piers and 2 abutments.
- Eight 12 ft wide lanes for regular traffic, four shoulder/emergency lanes, space for dedicated bus lanes, and a shared use bike and pedestrian path with views to the North.
- Main spans of 0.4 mile long composite cable-stayed structure with 400 ft tall pylons (Fig. 1).
- Approaches of 2.7 mile in length comprised of 350 ft steel girder spans (Fig. 2), arranged in a Girder-Substringer system with thin precast deck for weight savings and polymer overlay for service life.
- Accommodation within the foundation elements and pylon structures for a future rail bridge.
- Erection by large pre-assembled units in full spans using the heavy lift marine shear leg crane *Left Coast Lifter* (*I Lift New York*) with below hook capacity up to 1900 Ton.
- Significant use of precast elements including pile cap foundations, pier caps, and bridge decks.
- A 100 year service life, before major maintenance is required, using probabilistic service life design approach methods with performance based durability modeling.
- Open end steel pipe piling both end-bearing on bedrock and friction in deep clays within the river.
- Foundations on the east land-side approach in steep blast-rock rubble slopes supported by drilled shafts end bearing on bedrock.

© 2016 Deep Foundations Institute

- Foundations on the west land-side approach supported by a combination of steel H-piles end bearing on bedrock and spread footings on improved ground.

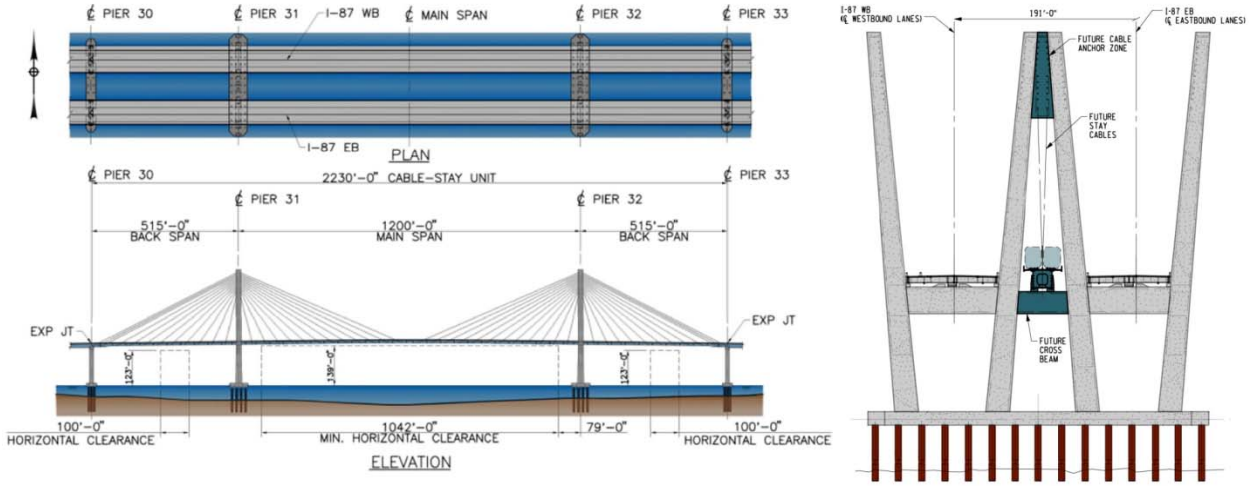


Figure 1: Plan, Elevation, and Section for New NY Bridge Main Span (NTS)

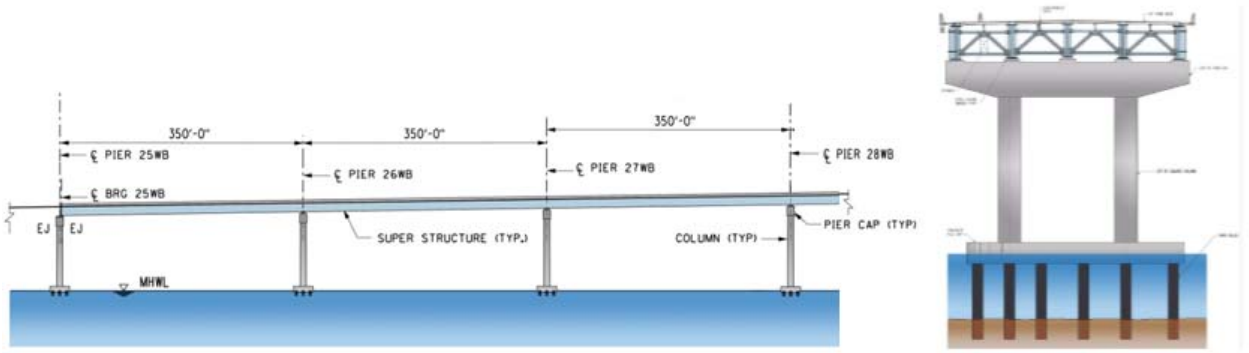


Figure 2: Elevation and Section for Typical Approach Piers (NTS)

After award of the project, TZC resumed the design-build process, with the design initiation phase starting in early January 2013. The design schedule set an aggressive 18 month goal for completion of "Released for Construction" (RFC) drawings and specifications, driven by the project construction dates for each work area. The schedule included an expediting process for "Early Construction Start" (ECS) packages for critical long-lead time materials and key activities, with bridge foundation construction and steel pile fabrication among the most important. The standard design sequence submitted design packages to TZC and NYSTA for review and formal comment resolution at four stages: Definitive (30%), Interim (60%), Final (100%), and RFC (100% signed and sealed). The ECS packages shortened the review process to three stages: Definitive (30%), ECS (100%), and RFC (100% signed and sealed). In between formal submissions, numerous informal reviews by TZC and NYSTA occurred during regular weekly technical meetings and special "over the shoulder" review sessions for complex components. At peak design there were 16,000 design hours per week produced by personnel from 35 firms in 5 countries. Using the expedited ECS review process, the first test piles driven in permanent production locations were installed in August 2013, and full production pile driving began in October 2013 at the large main span foundations, 8 to 10 months after NTP. Another four ECS packages covering half of all approach

© 2016 Deep Foundations Institute

piles and pile caps received RFC approval within the next two months, allowing production pile driving to proceed by December 2013. This demonstrates how effective use of alternative project delivery can advance a complex and large scale project from design to construction in relatively short time.

For design and construction planning purposes, the bridge was broken into eleven design units between the Rockland and Westchester Abutments, with ten units for Approach Structures, and the eleventh for Main Span (Fig. 3). Construction activities required multiple concurrent work fronts, or major equipment headings, through all phases of the project from foundation construction through superstructure erection.

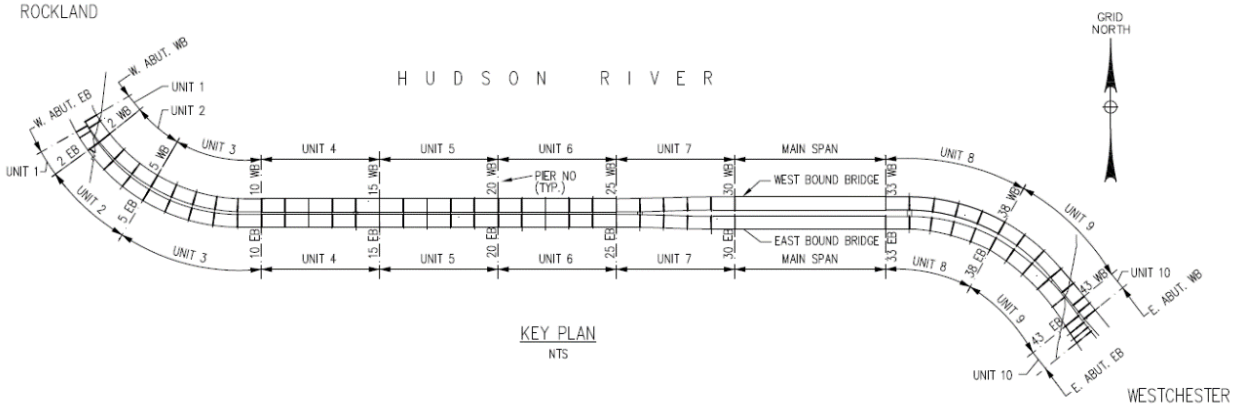


Figure 3: Project Design Unit Key Plan

Surface and Subsurface conditions

The Hudson River Estuary is the lower most section of the Hudson River and reaches from the mouth of the New York Upper Bay at the Verrazano Narrows in New York Harbor north approximately 180 mile through the Hudson Valley region to the dam at Troy, NY. The river experiences twice daily tide cycles along its length. It is characterized by brackish water, as sea water from the Atlantic Ocean migrates up river on high tides and mixes with fresh water flowing south. The area where the bridge crosses is the widest section of the river outside the harbor, a three mile wide by approximately nine mile long fetch called the Tappan Zee. It was so named a "Zee", or Sea, by early Dutch settlers as the expanse of water resembled a coastal sea rather than a river.

The estuary occupies deep valleys carved out of the bedrock over a series of glacial periods during the late Pleistocene. The Hudson River Valley experienced the last two advances of the Laurentide Glacier about 140,000-200,000 years ago and 22,000 years ago respectively. During the periods of glacial recession and re-advance that followed much of the Hudson River Valley including the Tappan Zee were submerged under glacial lakes (Lake Hudson then later Lake Albany), and steadily accumulated deep alluvial deposits of silts and varved clays interspersed with lenses of sands, overlying the glacial till deposits and bedrock below.

Subsurface explorations and laboratory data made available by NYSTA during the pre-proposal phase included soil boring records from the original 1950 – 1952 bridge design as well as contemporary investigations performed between 1992 and 2012 using Standard Penetration Test (SPT), Cone Penetrometer Test (CPT), Dilatometer, Pressuremeter, and Shear Vane test methods at more than 100 combined locations across the river and landings.

© 2016 Deep Foundations Institute

After project start, TZC's first priority for foundation design was mobilizing a supplemental subsurface exploration program focused in the footprint of the proposed new bridge foundations. The program consisted of 78 additional borings to depths of 440 ft, 9 Piezocone Penetration Test probes (CPTu), in-situ SPT testing and extensive laboratory testing of recovered samples. Results of the geotechnical data collected (Table 1) showed generally similar stratigraphy across the length of the proposed bridge, however with extremely variable bedrock surface elevations sloping in multiple directions and depths exceeding 750 ft within 1500 ft of the West shoreline. The typical profile in descending order was Organic Soils, Sand, Silt & Clay, Glacial Till, Decomposed Rock, Weathered Rock, and Bedrock (Fig. 4). Rock geology consisted of sandstone formations in areas west of the main span towards Rockland and gneiss formations east of the main span towards Westchester.

Table 1: Summary of Overburden and Rock Layers and Typical Properties

	USCS Class	Thickness (ft)	SPT-N / RQD	
Organic Soils	OH	18 to 169	WOR	Normal Consolidated
Sand	SP, SP-SM, and SM	2 to 82	WOR to 70	varied Very Loose to Very Dense
Varved Silt & Clay	CH and CL	35 to >300	WOR to 40	Over-Consolidated by 2500 psf at depths below 200 ft
Glacial Till	SM, SP, GP, SC, GM, and GC (varied)	3 to 45	40 to 100	varying density Sand, Gravel with 5 to 35 % mixed silts and clays
Decomposed Rock		3 to 16	100 / 6"	Penetrated by SPT spoon
Weathered Rock		2 to 9	RQD < 35 %	
Bedrock			RQD > 35 %	Sandstone (West) / Gneiss (East)

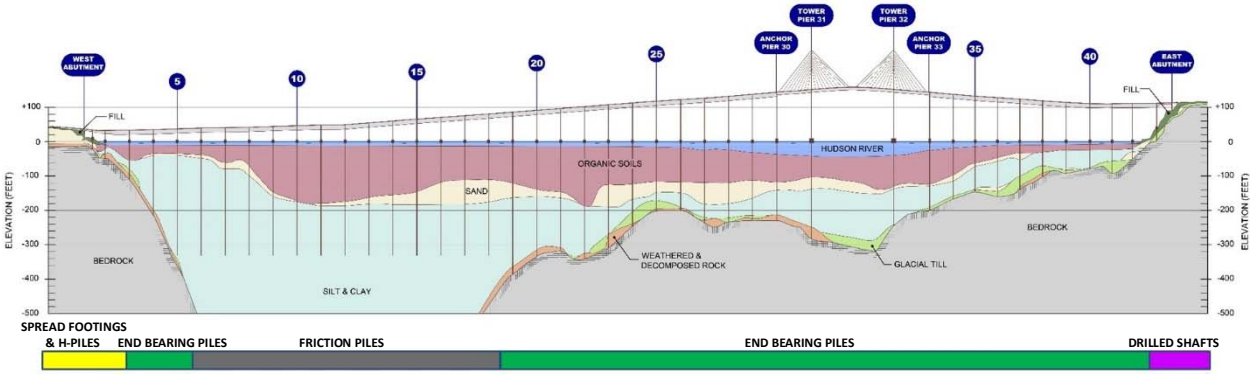


Figure 4: Project Longitudinal Subsurface Profile

Foundation Design

During design, capacity values for both piles and drilled shafts selected for the foundation were calculated using data obtained during a load test program performed by NYSTA (under separate contract in March 2012 as the "Pile Installation Demonstration Project" or PIDP) and traditional analytical calculation methods. The design capacities were confirmed through a series of pile load tests carried out by TZC in each bridge Design Unit between August 2013 and April 2014, prior to installing the associated production piles. In designing the foundation for the bridge, some of the major design challenges included the following:

1. Relatively deep rock over most of the alignment. Bedrock over the alignment was on the order of 200 to 300 ft with a large portion extending to beyond 750 ft below mudline.

© 2016 Deep Foundations Institute

2. In some areas, shallow hard rock made it difficult to obtain adequate lateral support and uplift capacity.
3. Glacial till layer overlying the bedrock introducing the potential for pile tip damage but also the potential to result in shallow refusal when near shore.
4. Steeply sloping bedrock in areas near the main span in addition to the abutments.
5. Extremely soft clay up to 200 ft or more in thickness. Most of the borings exhibited Standard Penetration Test (SPT) values of weight of hammer for most of the penetration with the exception of a somewhat thin sand layer and the glacial till layer.

The subsurface conditions required the use of both friction piles and end bearing piles. Friction piles relied purely on the varved clay present below the extremely soft organic clay. A fault line runs through the main span area of the bridge, thus end bearing piles to the east of the main span were terminated either in glacial till or on extremely hard gneiss bedrock while piles to the west were terminated in glacial till or in softer sandstone rock.

Methods used to estimate pile capacity include the Alpha, Beta, and Lambda methods as recommended by FHWA and AAHSTO. When comparing the analytical capacity estimates and the results of the PIDP load test program, the analytical methods appeared to over-predict the capacity. Therefore, the results of the PIDP were favored in estimating pile capacities and pile size/length selections. It was assumed that due to the PIDP dynamic tests having been performed on the same piles statically tested, pore water pressure played a part in the capacity reduction as compared to analytical capacity measurements. To account for this two piles were installed at each TZC test pile location, with dynamic testing performed on one pile and static testing on the other. Static piles were left undisturbed after installation until loaded during the test. However, the pore water effect did not appear to influence the static load test results as originally anticipated. The required nominal capacity values at preliminary design along with the static load test results are summarized in Table 2.

Table 2: Preliminary Required Nominal Capacity and Load Test Result Summary

Type	Size	Preliminary Required Nominal Axial Resistance, kips	Static Load Test Results, kips	
			End Bearing	Friction
H-Pile	HP14x117	1,100	-	-
Pipe Pile	36 inch Dia.	3,000 to 3,500	3,600 to 4,200	-
Pipe Pile	48 inch Dia.	3,800 to 5,400	4,700 to 6,300	3,900 to 4,400
Pipe Pile	72 inch Dia.	5,700 to 6,800	7,500	-
Drilled Shaft	48 inch Dia.	3,000	3,300	

In order to confirm the design, a total of 17 full scale static load tests were performed in addition to dynamically testing approximately 254 piles both during the test pile program and during production. In addition to the axial load tests, full scale lateral tests were performed as well. Load tests were performed anywhere from 3 weeks to several months following initial installation utilizing both reaction tension piles and static dead weight, with a maximum test load of 7500 kips. Each axial test pile was installed with several levels of vibrating wire strain gauges in addition to tell tales with protection angles. While the effort proved fruitful overall, a portion of the strain gauges were damaged during installation (mainly lower levels). Aside from the stressful environment of pile driving, the protection angles were only stitch-

© 2016 Deep Foundations Institute

welded and soil was able to penetrate the angles which may have contributed to the damage as well as lead to difficulty in the post-installation of the tell-tale rods.

Overall, the results of the pile load test program proved the nominal capacity of the pile within 5%. It should be noted that none of the end bearing test piles failed prior to reaching the capacity of the load frame. Therefore, values provided in Table 2 should not be considered ultimate for end bearing piles. For skin friction piles, the load test results matched the pile capacity estimates very well. Friction pile capacities experienced significant setup with values measured of eight to ten times the end of initial drive (EOID) values.

As noted, significant dynamic testing was performed on both test piles and production piles. A pile setup study was conducted to evaluate pile setup over time to identify the amount of time required to realize adequate pile capacity. After EOID, piles were re-struck at fifteen minutes, 1 hour, 24 hours, and then at 7 to 14 days. The data showed a very consistent capacity gain over time and permitted more informed decisions to be made during both the test pile program and during production. This was particularly useful in the few cases where piles may not have shown sufficient capacity at EIOD but later were shown to match the trend of pile setup established for the project (Fig. 5).

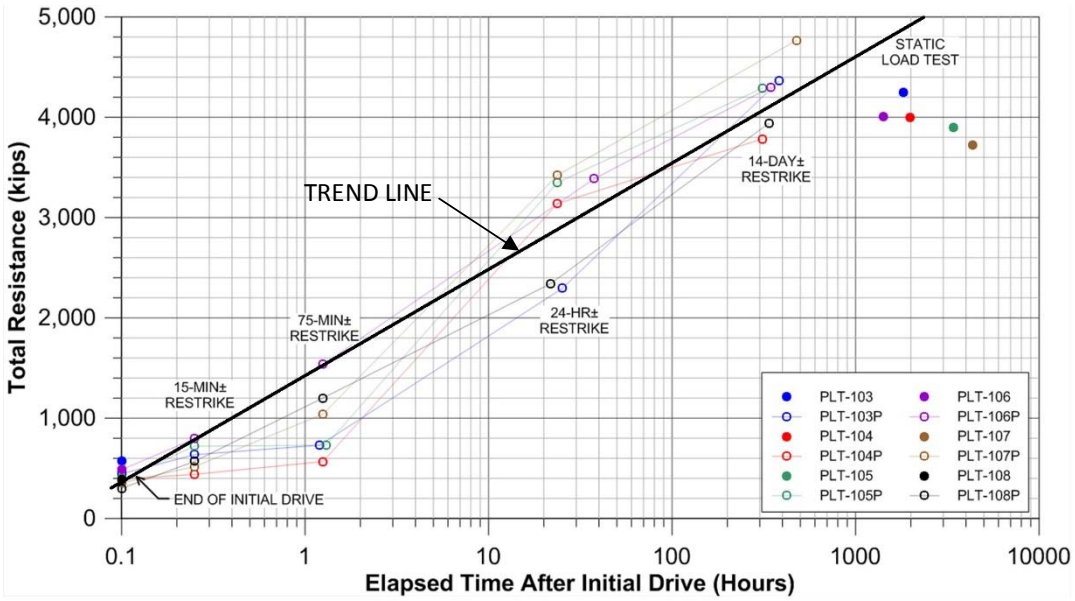


Figure 5: Friction Pile Setup Capacity (kip) vs. Log Time (hours)

Drilled shafts at the Westchester landing and abutments were designed utilizing both skin friction and end bearing, with a bi-directional load test performed on a production shaft to confirm the design parameters. In an effort to avoid failing the shaft, conservative values were selected and the shaft was loaded to a maximum load that confirmed the unit strength values used in the design. The PIDP program showed skin friction values as high as 50 ksf without failure, a unit value of approximately 18 ksf was required to meet the design loads. End bearing measured in the bi-directional load test was approximately 150 ksf.

© 2016 Deep Foundations Institute

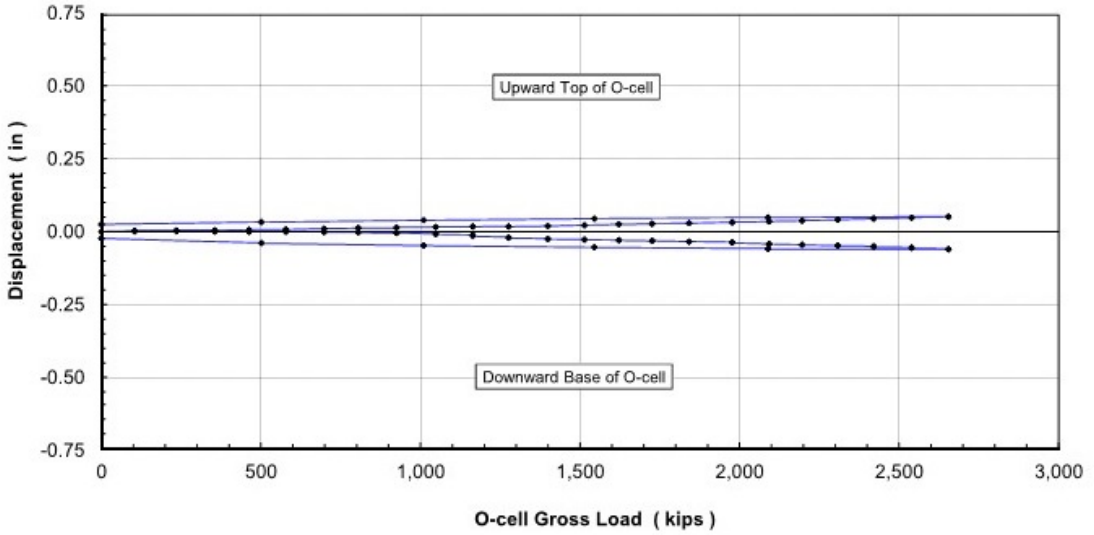


Figure 6: Drilled Shaft Displacement vs. O-Cell Load Capacity

Driven Pile Foundation Construction

Pile driving of the marine foundations was broken up into three areas: East/West near-shore approach foundations comprised of 36 inch OD x 1.25 inch wall pipe piles; approach foundations comprised of 48 inch OD x 1 inch wall and some 72 inch OD x 1 inch wall pipe piles, and main span foundations comprised of 72 inch OD x 1 inch wall pipe piles. Piles of all diameters designated for end bearing locations had an inside flange type cutting shoe welded to the tip. The bottom 10 ft of the 72 inch piles were increased to 2.5 inch wall pipe to maintain integrity during hard driving.

Construction of the near shore foundations was performed in two separate equipment headings using 300 Ton crawler cranes working from temporary steel trestles installed on the North side, which were necessary in the shallow water areas outside the limits of the project dredged access channel. At each west-bound foundation a temporary 45 ft x 100 ft cofferdam cell, comprised of 65 ft long AZ19-700 or AZ26-700 sheet pile pairs, was installed with 4,400 or 5,500 in-lb vibratory hammers to a depth +/- 50 ft below mudline. The 36 inch foundation piles were then installed either in one segment for lengths up to 170 ft, or two spliced segments for longer piles, inside the flooded cofferdam. For 2 segment piles, lower segments were driven with a 4,400 in-lb or 6,600 in-lb vibratory hammers to a maximum depth of 160 ft, and then stopped to allow splicing as necessary. Pile driving continued with IHC-S280 hydraulic impact hammers to final grade and achieving 10 bpi over 2 inch of driving or practical refusal at 10 bpi over 0.5 inch, with a 140-150 ft-k energy setting. After completion of driving, piles were cleaned to varying depths for later installation of pile reinforcing cages and concrete plugs. Pile cap construction proceeded with a temporary 2 ft tremie concrete mud-mat placed in the wet inside the cofferdam and cured. The cofferdam was then de-watered, piles cutoff, reinforced concrete pile cap was formed, and poured in the dry with conventional means.

At the Westchester approach the depth to bedrock was shallower in some locations allowing for single segment piles. However, due to a 20 to 30 ft thick till layer a modified driving protocol was necessary to prevent pile damage and avoid costly pilot drilling in the event a minimum tip elevation was not reached. A stepped procedure was used starting with pushing the pile to top of till using weight of the S280

© 2016 Deep Foundations Institute

hammer; initiating driving at 60-70 ft-k energy setting to 20 bpi; stepping up to 110-120 ft-k to 20 bpi; stepping up to 140-150 ft-k for completion to 7 bpi over 3 inch or practical refusal.
Construction of the main span and approach foundations began with two equipment headings driving 72 inch piles in October 2013, and gradually added three more headings driving 48 inch piles. A peak of five separate equipment headings between June and September 2014 completed an average 90 piles per month, using two 750 Ton and two 300 Ton barge mounted ringer cranes *Hank Hummel*, *Strong Island*, *Bob Hill*, and *Hoosier* as well as the 350 Ton derrick barge *Thomas W*. Pile driving at each location began with setting up a primary floating template with spud piles driven with a vibratory hammer, and locking off at a fixed elevation. Then a set of secondary grillage beams with tertiary pile template frames and guide rollers were installed and surveyed on location. A majority of the piles were installed in two spliced segments with total lengths up to 340 ft. The 48 inch piles at the deepest clay layers were installed in three segments up to 390 ft total length due to crane headroom limits. There were no issues observed for the impact hammers to break setup capacity gained over the pause for splicing, when driving resumed.

For typical 72 inch end bearing piles the driving criteria varied depending on the depth to top of rock and slope of rock between piles in order to prevent damage to pile tips. In areas were sloping rock was a concern driving began with a 17,200 in-lb vibratory hammer to a depth of 150 ft and stopped for splicing. Driving then resumed with an IHC-S800 hydraulic impact hammer at 140 ft-k energy and run up to 50 bpf. Driving continued at 275 ft-k energy up to 16 bpi, then stepped to 350 ft-k and up to 400 ft-k achieving 11 bpi or practical refusal at 10 bpi over 0.5 inch.

For the 48 inch friction piles in deep clay a modified driving procedure was used starting with a 6,600 to 17,200 in-lb vibratory hammer to a depth of between 160 to 180 ft and stopping for splicing. Driving then resumed with an IHC-S280 hydraulic impact hammer at 120 ft-k energy or greater and continued until minimum tip elevation was reached or exceeded. Four piles at each pair of bent caps were subsequently dynamic tested with restrikes occurring between 50 to 215 days later using the IHC-S800 hammer at 500 ft-k energy to validate pile setup. Using the Case Method the typical contribution of nominal pile resistance due to friction was determined between 80 to 98%, with remainder in end bearing. The maximum measured stresses at pile butt and tip were typically below 40 ksi.

Environmental Monitoring

Planning and executing the construction of the New NY Bridge required TZC to meet many project environmental permit conditions as well as Environmental Performance Commitments (EPCs) as part of the Final Environmental Impact Study (FEIS). Several of these applied specifically to airborne noise control during all pile driving operations, as well as underwater noise for marine pile driving in the river, including:

- Deployment of an underwater noise attenuation system (NAS) for all piles 48 inch diameter and larger, with underwater sound monitoring for 10% of the piles to verify attenuation levels were within the 206 dB peak SPL threshold for each pile diameter size.
- Deployment of an underwater array of up to 34 fish monitoring receivers for tracking movements of endangered Atlantic and Shortnose Sturgeon tagged with sonic transmitters in the project zone and an additional 6 monitors north and south outside the project area, as far as 8 to 16 miles.
- Maintenance of an underwater "acoustic corridor" for fish to travel through within which pile driving was limited to below 187 dB re 1 $\mu Pa^2 \cdot sec$ cSEL and 150 dB re 1 μPa rms SPL.

© 2016 Deep Foundations Institute

- Use of pile hammer sound mitigating shrouds to reduce airborne noise for all impact pile driving hammers, as well as use of movable noise barrier walls for land work.
- Impact pile driving limited to 20, 30 or 45 minutes per hour (pier dependent), and concurrent driving of piles was restricted for various zones in the river. Pile driving was limited to 7am - 7pm weekdays and 12 pm-6 pm Saturdays, with pile driving at the Rockland shore area further limited to 8am – 6pm weekdays.
- All construction activities including pile driving were limited to 70 dBA maximum at night (10pm to 6am), and until 12pm Saturdays, and all day Sundays.
- Vibratory pile hammers were required to be used "to the maximum extent practicable" as a means to reduce both airborne and underwater sound.

For underwater sound the EPC goals were to achieve at least 10 dB noise reductions below what was produced by pile driving without attenuation and to minimize the radius of the 206 dB re 1 μPa peak SPL isopleth. TZC elected to use an unconfined multi-tier air bubble ring system which met the goal based on field demonstrations performed by NYSTA during the 2012 PIDP, and validated by independent monitoring during impact driving of all project test piles and periodic monitoring on 10% of production piles. The unconfined system was comprised of a series of 2 to 5 inch rolled pipe rings which were lowered around each 48 inch or 72 inch pile exterior at maximum 10 ft vertical intervals, hung with wire rope rigging from below low water elevation to mudline. Each ring was ported with a series of 1/16 inch vent holes and supplied by an independent 1600 cfm oil-free air compressor / receiver at 40-80 psig pressure. The system was activated only during periods of impact pile driving and was typically installed on clusters of 6 to 10 piles at each pile template location after pile splicing.

Pile Cap Design and Construction

The pile cap substructures for the New NY Bridge made extensive use of precast elements on the approach foundations as well as the main span pile caps below the tower pylons and anchor piers. For the approach, monolithic precast tub elements were designed to form the permanent bottom and sides for the pile caps at 60 locations. Each precast cap tub ranged in weight from 340 to 507 Tons and in size up to 84 ft long, 36 ft wide, and 8 ft tall. The interior had ribs to support the thin floor and circular blockouts to allow the tub installation over top of the driven piles. Each tub was lifted and set on temporary steel hangers from four piles with the Hank Hummel or Left Coast Lifter marine cranes, with a maximum lifted load over 610 Tons below the hook. The pile blockouts were sealed with tremie concrete and tub was dewatered allowing pile cutoff and load transfer to continue in the dry. Finally each tub had hundreds of long vertical shear bars connected to anchors in the floor, top mat reinforcing bars installed, and was filled with up to 750 cy of cast in place concrete creating a final composite pile cap substructure.

The Design-Build process for the approach pile cap tubs in particular allowed the final design to be tailored closely to project equipment resources and fabricator capabilities in order to gain efficiencies during precasting and construction. By far the biggest advantage was implementing common dimensions for the precast tubs and standard details of individual embedded components and rebar. This not only maximized productivity inherent with repetition at all stages, but also allowed fairly rapid re-sequencing of tubs selected for delivery at the fabricator or which pier to install at the project site. The process was challenging with extremely close coordination necessary between multiple geotechnical and structural design teams to ensure common tub details satisfied the design criteria particular to each approach Design

© 2016 Deep Foundations Institute

Unit, and with the TZC construction team providing frequent constructability reviews of details and combined tolerances. Ultimately, the number of unique tub elements was reduced from eleven down to six types, with common pile spacing for friction pile units and common pile spacing for end bearing pile units. In addition, there was also the advantage of likewise reduction in number of pile driving template configurations required.

At larger than a football field each of the main span caps required more than 11,000 cy of concrete and 1,300 Tons of reinforcing. These caps were formed using a 21,000 sf concrete floor slab suspended from the piles and 14 ft tall steel side walls. The slab was designed for ease of erection using a series of 50 to 100 Ton precast floor panels and a composite cast in place concrete overlay. The precast floor panels were initially hung above high tide elevation with steel hanger beams over every 72 inch pile, and joined with concrete closure pour joints into a continuous slab. The steel side forms were installed and the complete tub form structure was lowered with 34 synchronized strand jacks to 7 ft below water. The pile blockouts were sealed with tremie concrete by divers, uplift bracing was installed, and the entire tub was dewatered. Next a secondary reinforced concrete slab was poured in composite with the precast to complete the foundation base support. The piles were cutoff, and construction continued with pile plug and foundation reinforcing placement comprised primarily of tightly spaced #18 bars in all directions. Each pile cap was then filled with concrete in four separate lifts in excess of 3,100 cy supplied by two floating batch plants operating nearly 24 hours per pour, and cured with thermal controls using internal water cooling pipes for a period of 5 to 7 days.

Summary

The 3.1 mile New NY Bridge crossing remains one of the largest infrastructure projects in the United States. It is notable both for being the first major project in the state of New York using Alternative Project Delivery methods and the single largest Design-Build contract awarded in the state by the New York State Thruway Authority. The foundation design required more than 1,000 large diameter pipe piles and drilled shafts installed in challenging subsurface conditions including steep varied bedrock surfaces with deep varved silts and clays with depths beyond 750 ft.

Pile capacities were estimated using methods recommended by FHWA and AASHTO in combination with data from a preliminary test pile program performed by NYSTA prior to project tender. Design for majority of bridge foundations was completed in less than a year after NTP and included an extensive pile load test program. TZC performed a series of seventeen full scale pile load tests, in addition to numerous dynamic testing, to confirm pile capacity within 5% of the required axial resistance.

Through the use of the Design-Build method aided by innovative design features, creative construction means and methods, and hard work by the Designer, Contractor and Owner's representatives, the first of the twin span is scheduled to be completed in 2017, and both spans will be fully operating by 2018.

References

Burdette, N., and Lamont, M., "Precast Substructure Elements for the New NY (Tappan Zee Hudson River Crossing) Bridge," International Bridge Conference Proceedings, June 2014 (IBC 14-54)

Permitting Dashboard Federal Infrastructure Projects "Tappan Zee Bridge Replacement" www.permits.performance.gov/projects/536302001 (Accessed April 2, 2016)

© 2016 Deep Foundations Institute

R. S. Markowitz and A. Winkler “New York Enacts Design Build Legislation” www.pecklaw.com/images/uploads/communications/Client_Alert-NYDesign-BuildLegislation.pdf (Accessed March 28, 2016)

R.T. Ward “Are Design Build Contracts Legal in New York?” February 2015 www.wbgllp.com/legal-alerts.php?id=97 (Accessed March 28, 2016)

Sirkin, L and Bokuniewicz, H., 2011 “The Hudson River Valley: Geological History, Landforms, and Resources,” *The Hudson River Estuary*, J.S. Levinton and J. Waldman eds. Cambridge University Press, New York, NY pp. 13-23

The New NY Bridge "About The Project The New NY Bridge to replace the Tappan Zee continues to make great progress on the Hudson River" www.newnybridge.com/about/ (Accessed April 2, 2016)

Westchester County Virtual Archives "Records of the Tappan Zee Bridge Construction, 1951 - 1955" www.westchesterarchives.com/ht/muni/tarrytn/tappanZee.htm (Accessed March 15, 2016)

© 2016 Deep Foundations Institute

SHEIKH JABER AL-AHMAD CAUSEWAY PROJECT IN KUWAIT - A CASE STUDY

Paolo Cavalcoli, Trevi SpA, Cesena, Italy, pcavalcoli@trevispa.com
Marco Chiarabelli, Soilmec North America, Fort Worth, TX, (401) 965-2575, m.chiarabelli@soilmec.it
Federico Pagliacci, Soilmec SpA, Cesena, Italy, f.pagliacci@soilmec.it

ABSTRACT

The Sheikh Jaber Al-Ahmad Causeway Project in Kuwait is estimated at approximately $US3.7 billion and consists of constructing a causeway across the Kuwait Bay, connecting the Shuwaikh Port with the northern Subiyah area, where the new "Silk City" will be established. The $US77 billion Silk City will revive the ancient "Silk Road" trade route and will become a major free trade zone linking central Asia with Europe. The new city will be completed in 2030, it will house about 700,000 people and, furthermore, it will include the tallest tower in the world. The Causeway will stretch approximately 23.3 miles and will be composed of a combination of low-level bridges, embankments and transition islands. A bridge of about 16.8 miles in length will span the navigation channel and a free flow interchange at the Shuwaikh Port will connect the causeway to the main road network in Kuwait City. The geo-construction portion of the project involves the execution of 1,200 drilled shafts with diameters of 98 inches and 118 inches embedded to a maximum depth of about 276 feet. Details are provided concerning the subsurface conditions, the geotechnical characteristics and the strength parameters, illustrating, as well, the installation technique implemented for the construction of the drilled shafts. In addition, particular attention is paid to the description of the challenges faced while constructing the drilled shafts at a distance of about 10 miles from the shore, such as the depth of the water above the midline (more than 160 feet), an underwater current and the tidal variation.

Keywords: bridge foundations, drilled shafts, polymer slurry.

INTRODUCTION

This paper presents an overview of the foundation works executed for a 37km causeway across the Bay of Kuwait, connecting Shuwaikh Port with Subiyah New Town Development. The project, in which Trevi is actively engaged, includes a 27 km low-level bridge across the bay, a main bridge with a span of 200 m, an overpass and a 5 km approach road onshore in Subiyah.

The main purpose of this report is to provide information about the nature and features of the applied technique of bored piles, including a description of each work phase and other related details, in order to aid in the design of the foundations for the proposed construction.

Works for the soil investigation were carried out in accordance with accepted geotechnical standards/guidelines. Brief descriptions of the methodology of the field are also provided in this report.

LOCAL CONDITION AND GENERAL GEOLOGY

Natural Setting and Climate

The State of Kuwait is situated at the north-eastern corner of the Arabian Peninsula. It comprises an area of approximately 17,800 km^2 extending between latitudes 28°30' and 30°05'N and longitudes 46°33' and 48°30'E (Fig. 1).

© 2016 Deep Foundations Institute

Kuwait is characterized by the predominance of a hot and dry climate. The temperature varies between 30°C and 54°C during the summer period (from June to September). Winter is rather cool, especially in January with a mean temperature of 12°C.



Fig. 1. General overview of the geography and location of the project.

Always from a climate point of view, Kuwait is characterized by scanty rainfall, totalling approximately 110 mm per year and frequent dust-storm events. The contribution of dust sedimentation in the north-western part of the Arabian Gulf amounts to 1 mm per year. The same thickness of deposition is assumed to be detected throughout the coastal areas of Kuwait.

Pronounced variations in humidity represent another common climate phenomenon in Kuwait with relative humidity ranging from 60.9% in January to 21.5% in June. Furthermore, evaporation is very high and varies according to locations and seasons. The mean amount of evaporation is 10.3 mm per day.

General Geology

Kuwait lies on the eastern edge of the deep sedimentary basin that forms the Arabian Peninsula and is underlain by a considerable thickness of sedimentary rocks. In the south of Kuwait, relatively young deposits of the Dibdibba formation (from Upper Miocene to Pleistocene, approximately from 2 to 10 million years old) outcrop at the surface. These deposits are underlain in depth by the Dammam formation (Upper Eocene Epoch, approximately from 38 to 42 million years old). The normally intervening deposits of the Fars formation are absent except in Northern Kuwait.

The Dibdibba formation typically consists of siliceous sands and gravels, with varying amounts of silt and some thin clay and gypsum bands. Cementation is only partial and relatively poor, consisting of calcium carbonate and gypsum.

In South Kuwait, the recent deposits overlying the Dibdibba formation mainly consist of windblown sand, forming sheets and low dune structures. Adjacent to the shoreline, calcareous deposits are locally present consisting of oolitic and bioclastic sands.

The low seasonal rainfall mostly evaporates or percolates into the ground. Therefore, little runoff ends up in the sea. The influence of evaporation predominates and the general movement of groundwater is upward. This leads to high concentrations of soluble material near the ground surface generally composed

© 2016 Deep Foundations Institute

of calcium carbonate, gypsum, etc. Gypsum predominates in North Kuwait, whereas in the South high concentrations of calcium carbonates are encountered near the ground surface.

SUBSURFACE INVESTIGATION AND GENERAL CONDITIONS

Overview of project phases

The project involved a soil investigation performed along the area between Shuwaichk port and Subiyah, as illustrated in Fig. 2.

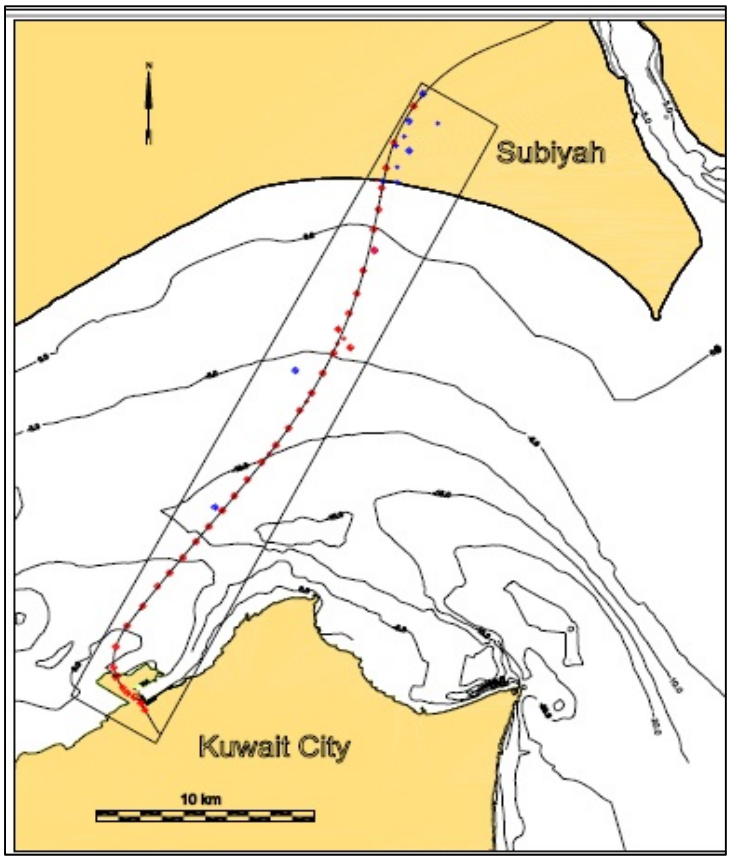


Fig. 2. A map showing where the soil investigation was carried out

For each investigation, a drill log was obtained providing the following information:

- Description of the soil
- Location
- Elevation
- Date of the investigation
- Coordination
- Depth

Starting from Shuwaikh port side, sand in very loose, medium dense and very dense condition was detected, while in the other side dense sand and very soft to medium clay were found.

Figure 3 shows some samples found during the onshore and offshore drilling.

© 2016 Deep Foundations Institute



Fig. 3. Samples found during the drilling phase: thickened gravel and sand; quartz gravel; cemented sand formation; cap rock with fossils; sand clay mixture with crystallization.

During the foundations works, rock layers, such as sandstone and flint, were also found.

PILE FOUNDATIONS

Trevi Foundations Kuwait is involved in the construction of offshore and onshore piles. The onshore piles have a diameter of 2,500 mm and 1,200 mm, while the offshore ones have a diameter of 3,000 mm, reaching a max depth of 84 m and 2,500 mm from the temporary bridge.

Onshore Piling

Trevi Foundations Kuwait is working as subcontractor for two different main contractors: Hyundai and Combined Group. A general overview of the onshore work is shown in Fig. 4.

Temporary bridge activity

For this area, activities have been carried out following two different approaches. With regard to the first area (finger area) the job was performed from fingers connected to the temporary bridge and about 50 piles of 2,500 mm were completed. As for the second area (Temporary Bridge), once the piles from the fingers were completed, the crew started to work on two small barges along the temporary bridge, where the execution of about 150 piles was foreseen. This part of the job is very difficult since it requires the driving of a double casing for each pile, one with 2,500 mm of diameter and an outer casing with 3,000 mm of diameter, employed as a guide for the inner case or as a dry tank when the head treatment of the pile is required. A general overview of the temporary bridge work is shown in Fig. 5.

© 2016 Deep Foundations Institute

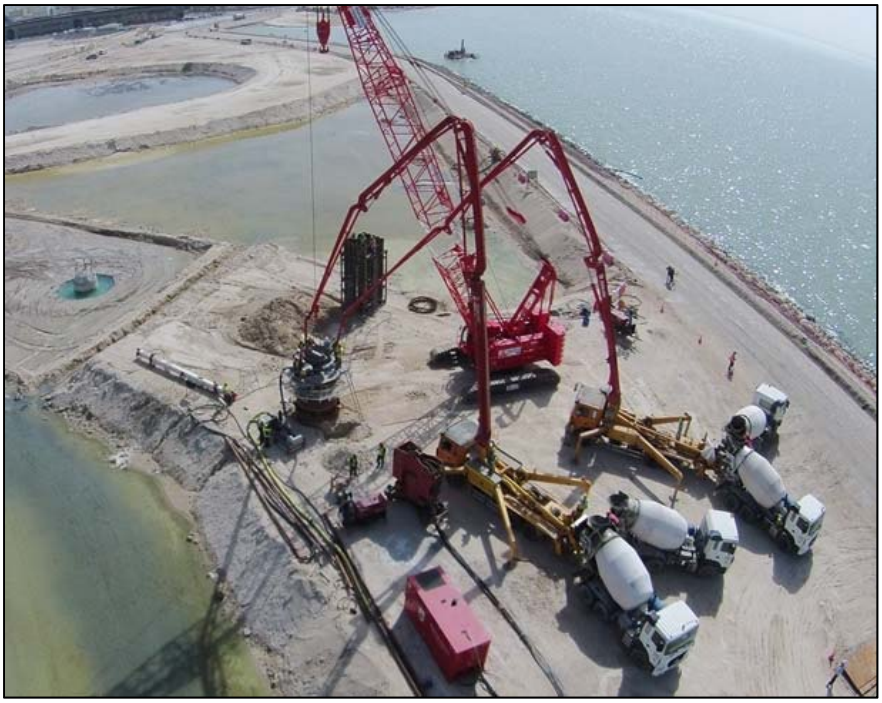


Fig. 4. General overview of the onshore work



Fig. 5. General overview of the temporary bridge work

Offshore Piling

Several difficulties have been faced and solved with regard to offshore activities. For this particular reason, this section of the paper focuses on the offshore production, which is quite different from onshore piling for many aspects, such as:

© 2016 Deep Foundations Institute

- Distance from land (the farthest pile is located 17 km from land)
- Depth of piles (between 50 and 84 m)
- Hydrostatic pressure and buoyancy
- Underwater currents
- Wave and swells
- Tidal variation (very strong in Kuwait) from 0 to 3.8 m
- Wind and sandstorm (very strong in Kuwait) up to 60 km/h
- Cyclone (rare in Kuwait)
- Existing navigation (limited in the area)

Piles with a diameter of 3,000 mm are requested with a maximum depth up to 84 m. The whole project includes 1,200 piles to be completed and Trevi Foundations Kuwait is in charge of about 230 piles offshore entrusted by the main contractor Hyundai Engineering and Construction Co. Ltd. Currently, more than 130 piles have been completed offshore. A general overview of the offshore work is shown in Fig. 6.



Fig. 6. General overview of the offshore work

Setting Barge

All the works are executed from a barge provided by Hyundai. The barge layout is shown in Fig. 7.

It is located at a distance of 1.60 m from the pile (casing) to drill. This distance is calculated from the drilling machine (Soilmec SC-120HD) and its boring kit Soilmec SA-40 which allows to operate at a certain distance.

The barge is fixed to the sea bed level thanks to 4 spud legs and 4 anchors, which ensure the stability during the work. It is not a self-elevated barge. Once the pile is completed, it is necessary to shift the barge to the following pile to be drilled. During this phase, anchor boat and tug boat are required in order to facilitate the shifting.

The technical specifications for the barge are shown in Fig. 8.

© 2016 Deep Foundations Institute

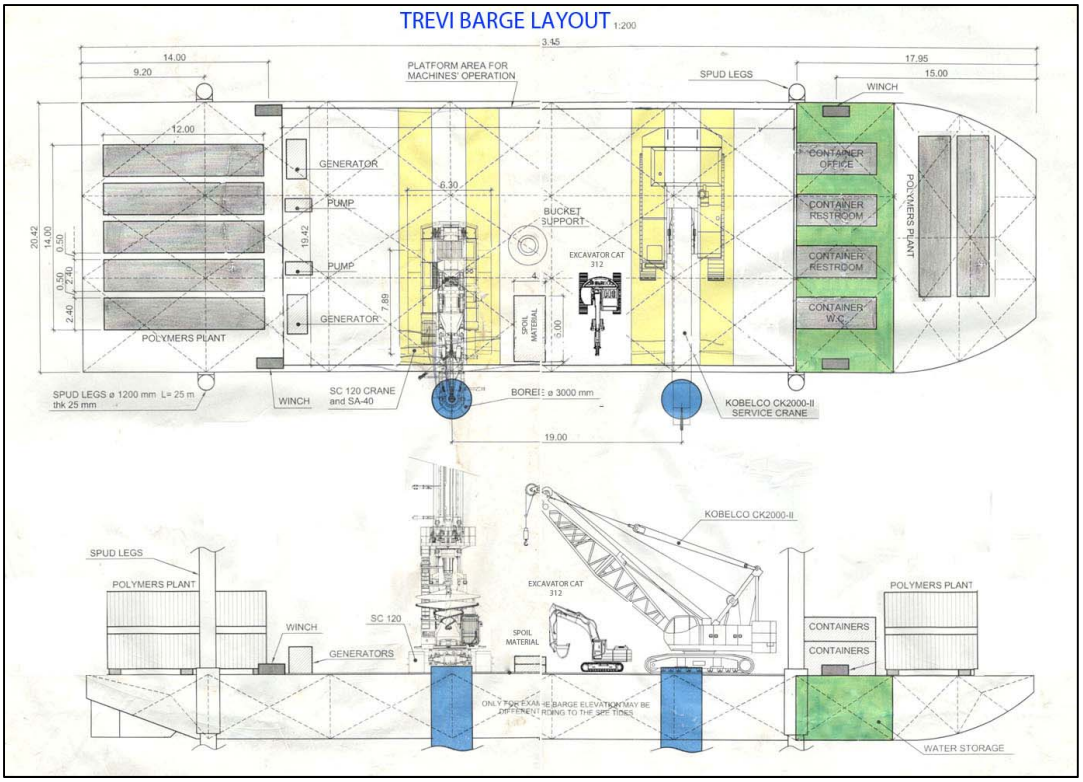


Fig. 7. Trevi barge layout

TYPE OF VESSEL	:	FLAT TOP DECK CARGO BARGE
FLAG	:	ST. VINCENT & GRENADINES
HOME PORT	:	KINGSTOWN
BUILT	:	2003 - MALAYSIA
REGISTERY NUMBER	:	10607
CLASS	:	B.V. 1 ✠ HULL
LAST SPECIAL SURVEY	:	MARCH, 2008
LENGTH	:	70.23 METERS
BREADTH	:	20.42 METERS
DEPTH	:	04.88 METERS
CLEAR DECK SPACE	:	64.50 X 18.50 METERS
DECK STRENGHT	:	10 TONS / M2 starboard
DWT	:	4500 TONS
GRT / NRT	:	1831 / 550 TONS
SIDEWALLS	:	3.00 MTRS SIDE WALLS (can be installed)
RAMP	:	9.10 MTRS LENGTH X 4.25 MTRS WIDE (can be installed)
DECK EQUIPMENT	:	- 16 STANCHIONS ON PORT AND STARBOARD SIDE EACH
		-11 X TWIN POST BOLLARDS OF 250 MM
		-2 X TOWING BRACKET AT FWD
		-1 X DIESEL ENGINE DRIVEN ANCHOR WINCH
		-1 X 780 KG STOCKLESS BOWER ANCHOR
		-1 X 165 MTR ANCHOR WIRE OF 32 MM DIA
		-1 X 12.5 MTR ANCHOR TAIL CHAIN OF 26 MM
		-3 X SOLAR NAVIGATION LIGHTS

Fig. 8. Technical specifications of the barge

© 2016 Deep Foundations Institute

The barge is composed by several and different water tanks under the deck, in order to ensure a better balance during the work time. As a matter of fact, the presence of the drilling machine, the crane, the backhoe, 13 polymer tanks with a capacity of 55 m^3 each and another tank used as office and store makes it necessary for the barge to maintain its horizontal position without leaning on one side, since this could compromise the verticality of the pile and give rise to several problems.

Further barges are used as support during the different activities, such as:

- Disposal barge
- Service barge
- Rebar cage barge

The disposal barge is used during the drilling phase and, in particular, is used for stocking all the materials took out during the excavation phase. The service barge, instead, is used as a support during all the activities since it provides an empty space where all the tools are disposed, such as second bucket, cleaning bucket, hanging bar etc., and it is always present during the activity. Furthermore, a rebar cage barge located near the barge is employed when rebar cage needs to be installed.

CONSTRUCTION PHASES

There are six main phases constituting the construction of bored piles:

- Driving casing (not in the offshore activity for Trevi, this operation is carried out by Sambo)
- Excavation
- Cleaning pile
- Placing of reinforcement
- Airlifting and flushing
- Casting concrete and pile head treatment

All these phases are characterized by different quality checks, such as the control of the pile verticality, polymer density, etc.

Polymer slurry

The construction phase was performed using polymer mud. Tools for mixing the polymer as shown in Fig. 9. This probably represents one of the most critical parts of the work and a special attention had to be dedicated to this aspect. The polymer mud was used to support the walls of the pile throughout the excavation phase and until the casting of the pile.

A good rule of thumb is to keep the level of polymer slurry at least 3 meters above the piezometric surface at all times. An equally good rule is to place the slurry in the borehole before the piezometric level is reached so that sloughing or raveling do not have a chance to start.

For the preparation of the polymer slurry some requirements need to be respected:

- Using clean water (not contaminated by organic material).
- Adjusting the initial water pH to 10 – 11.
- Avoiding to create agglomerates of polymer powders during mixing.
- Mixing the polymer powder to get an initial fresh slurry viscosity between 60 – 120 sec.
- Maintaining the re-circulation of the polymer with no centrifugal pumps.
- Correcting the re-used slurry adding new polymer and maintaining a viscosity between 50 and 100 sec.
- Recovering the slurry from the pile using progressive cavity pumps.

© 2016 Deep Foundations Institute

- Using a sedimentation tank to reduce the sand content into the recycled slurry.



Fig. 9. Tools for mixing the polymer

Nevertheless, there are also others guidelines to be followed: the handling and disposal of polymer slurries may also be subject to environmental regulations. Some jurisdictions require waste polymer slurry to be transported to a waste water treatment plant after obtaining the plant's approval. Concerns have also been raised over the potential effects of polymer-based slurries on drinking water aquifers.

Furthermore, during the excavation it is compulsory to check the polymer characteristics in presence of the inspector such as:

- Viscosity
- pH
- Density
- Sand content

Figure 10 shows photographs of polymer sampling techniques.

The sand content plays a very important role, especially before the casting of the pile. On the basis of the AASHTO 2009 which is present in the contract, after the air lifting process this value should be lower than 4%. Nevertheless, in this project the AASHTO 2010 is in use, reporting a value of the sand content lower than 1%.

© 2016 Deep Foundations Institute



Fig. 10. Collecting polymer samples

Driving off-shore casing

This procedure, as mentioned above, is carried out by Sambo. All the casings have already been installed deep into the ground (Fig. 11). Each casing is about 40 m long and the distance from pile to pile amounts to 60 m. On the other hand, Trevi is carrying out all the driving of the casings for the onshore work.



Fig. 11. Disposition of driven casing

Excavation

Once the casing is ready, an inspection is carried out by a surveyor to check the proper position in accordance with the latitude and longitudinal coordinates indicated by the project requirements. Only after the approval the excavation phase can start.

For the excavation offshore, a Soilmec SC-120HD with a SA-40 rotary kit and a Soilmec SC-100 are used and positioned on the temporary bridge. For the onshore work, the Company is employing the Soilmec SR-930. Different sizes of buckets are in use, according to the diameter of the piles. When all the

© 2016 Deep Foundations Institute

material is collected into the bucket, it is at first downloaded into an empty tank, then moved by a backhoe in a disposal area and finally collected by Hyundai.

The bucket represents a very important tool and, besides the features mentioned above, it is constituted by different lateral openings in order to allow the polymer to spurt out once full of material (Fig. 12).

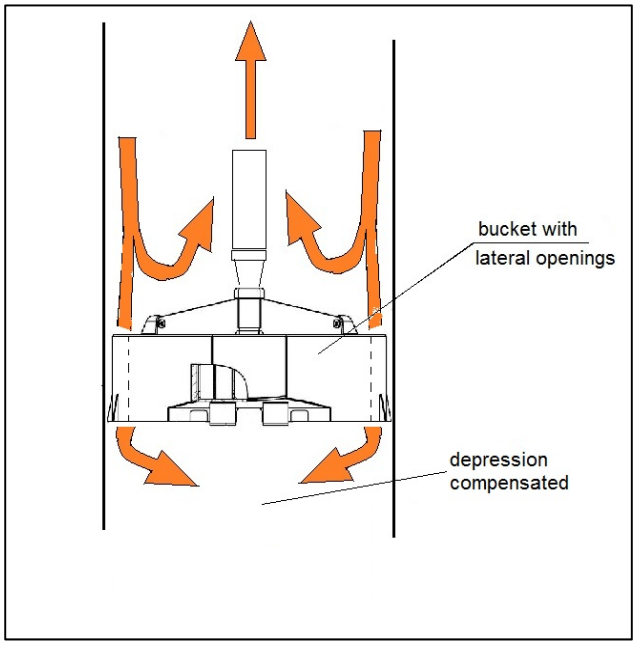


Fig. 12. Main futures of the bucket

Considering the offshore case, where about 130 piles have been completed, it is possible to define the cycle time related to the excavation. In particular, taking also into account the different layouts of soil which is possible to meet during this particular phase, 15 hours is needed to complete one pile at 65 m of depth. This is possible mainly thanks to different factors, such as:

- Dimension of the bucket in terms of H =0.4 m
- Diameter of 3,000 mm
- Very good quality and experience of the drilling operator

Photographs of different construction stages are shown in Fig. 13. The pictures illustrate that the polymer compensation represents another important tool introduced. It allows control of the polymer level into the casing, constantly ensuring an optimal condition in terms of pressure applied for the stability of the pile when it is open.

Rebar cage installation is shown in Fig. 14.

© 2016 Deep Foundations Institute

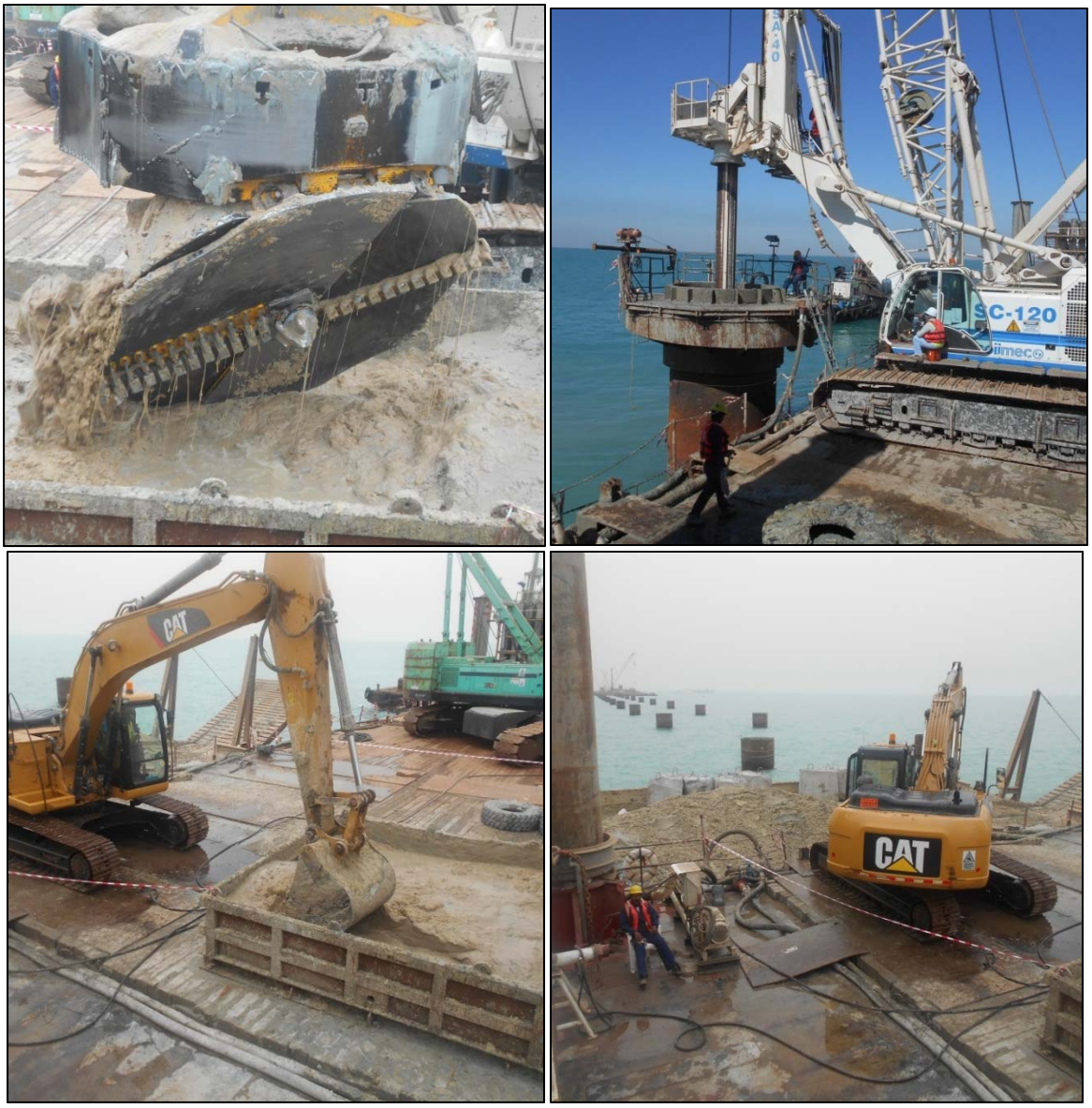


Fig. 13. Different phases during excavation

© 2016 Deep Foundations Institute



Fig. 14. People at work on the pile during the lowering of the rebar cage

Pile Stability Control

During the boring activity, it is mandatory (as required by the contract) to carry out different tests in order to certify a high-quality level and to constantly keep a very high standard of production. Several tests were implemented at the beginning of the project (preliminary test) while some of them are currently being carried out. All the tests gave and are giving excellent results. Sonic test, coring test, integrity test, camera test, O-Cell test for a pile test, and Koden test: these are some of the most important tests that this job includes.

The Koden test, for instance, is always carried out in both onshore and offshore activities (respectively 2500 and 3000 mm).

Once the excavation is completed, it is necessary to control the pile stability through a Koden test, which uses the principle of the ultrasonic wave travel from the sensor to the wall of the drilled hole and reflects to the sensor trough the polymer slurry. It is the most employed test for determining the verticality of the pile. Thanks to its examination, it is very easy to recognize the presence of collapse or cavity.

Another test included in the activity is the camera test (Fig. 15), which must be carried out after the air lifting process. It consists of a camera lowered at the bottom of the pile, with special tools which allow us to observe the bottom part of the pile and verify the presence of sedimentation. In this way it is possible to compare results within a certain range and if the result is under a fixed level it is possible to proceed with a casting phase.

© 2016 Deep Foundations Institute



Fig. 15. General overview of the camera test tools

Cleaning Pile

After the excavation phase, the surveyor's control and the Koden test, it is very important clean the pile with a cleaning bucket (bucket with no teeth) (Fig. 16) in order to clean the bottom of the pile from sedimentation matured during the first hours.



Fig. 16. Cleaning bucket used after the end of excavation

Rebar Cage Installation

When the previous phase has been completed, another important phase has to be carried out consisting of the installation of the rebar cage. On the basis of the depth of the pile, different segments are lowered in

© 2016 Deep Foundations Institute

the pile. Three main segments are installed and, due to a very limited space available (Fig. 17) and also to a non-perfect stability of the jobsite, this represents one of the most delicate phases throughout the work.

An important aspect is represented by the disposition of the three segments on the rebar cage barge, in consideration of the logistical problems mentioned above. The following disposition of the rebar cage on the rebar cage barge is always compulsory.

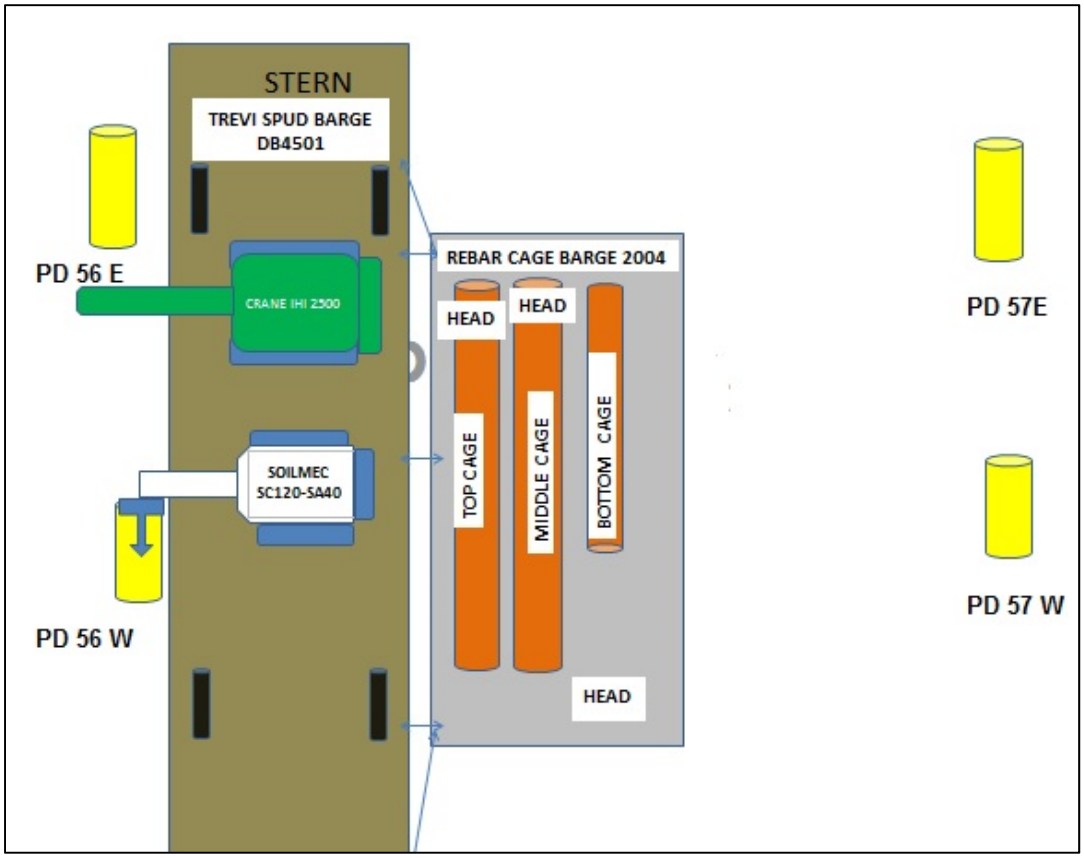


Fig. 17. Disposition of the 3 segments of cage on the rebar cage barge

The lightest segment must be positioned far from the crane, while the heaviest and the biggest ones must be situated very close to the barge, in order to be easily collected by the crane.

For instance, a segment of 24 m has to be lowered by two cranes, as shown in Fig. 18.

Due to its length, two cranes are necessary to move the rebar cage without any problem. Figure 19 shows a joint with a coupler which links two different steels. The maximum tolerance in terms of distance between each steel element is 5 mm.

© 2016 Deep Foundations Institute



Fig. 18. Lowering of a rebar cage with 24 m of length with two cranes



Fig. 19. Joint between two bars with coupler

Air Lifting Process

The air lifting process is a very important procedure for cleaning the bottom of a pile and it consists in 7 different steps, each one requiring about 20 minutes, that is why this procedure takes long time. It aims at removing debris and cleaning the base of pile bores acting, essentially, as an airlift pump by using compressed air. The setup of a typical airlifting operation (Fig. 20) is as follows: a hollow tube is placed in a certain position inside the pile bore and a side tube is connected to the end of the tube near the pile bottom for the passage of compressed air inside the tube. The upper end of the tube is linked to a

© 2016 Deep Foundations Institute

discharge tank for the circulation of pumped fluid from pile base. During airlifting, compressed air is piped down the tube and it returns up to the discharge tank carrying it with the fluid. It functions by imparting energy to the fluid and forces the fluid to move vertically upwards. The injected air mixes with the fluid, resulting in the formation of lower unit weight of the combined mixture when compared with surrounding fluid. This hydrostatic pressure forces the fluid/air mixture up to the discharge tanks.



Fig. 20. Air lifting tools

Casting concrete and pile head treatment

Once the airlifting process is carried out and following the control of the sand content by the inspector, the casting can start, employing the pump concrete method and with two marine batching plants parked near the barge. The pile is filled with concrete up to 3 m upper than the cut off level, which is why a pile head treatment is required to clean the overcast quantity of concrete casted. A special cleaning bucket (Fig. 21) with a diameter of 1,200 mm is used in order not to touch the rebar cage, which has a diameter of 2,800 mm. All the concrete taken out while lowering this cleaning bucket is at first collected in different steps and disposed in special container and finally sent to Hyundai.

© 2016 Deep Foundations Institute



Fig. 21. Cleaning bucket and details of surface cleaning

Once the cleaning is completed, a man basket with people is lowered inside the pile for cleaning and make the entire concrete surface uniform, especially the part between the casing and the steel, which is the most difficult to reach.

Construction photos are shown in Fig. 22.



Fig. 22. Actual bridge construction status

© 2016 Deep Foundations Institute

CONCLUSIONS

Since the beginning of the work, much progress has been achieved in terms of production, and it is currently possible to complete three piles per week. Trevi continues to seek possible solutions through research aiming at improving the current status and always maintaining a high quality standard. Even if the Company faced many challenges, due to the shortage of concrete and steel cages or adverse weather conditions, the production is quite good and may be increased in the close future, hoping in an optimal boundary condition.

© 2016 Deep Foundations Institute

This page left intentionally blank

© 2016 Deep Foundations Institute

VALUE-ENGINEERING OF H-PILE FOUNDATIONS IN KARSTIC GEOLOGY

Daniel J. Woeste, Geosyntec Consultants, Chicago, Illinois, DWoeste@Geosyntec.com
Rachael M. Fischer, Geosyntec Consultants, Chicago, Illinois, RFischer@Geosyntec.com
Terence P. Holman, Turner Construction Company, Chicago, Illinois, tholman@tcco.com

ABSTRACT

A new 50 MW biomass renewable energy power plant was planned for construction in southwestern Georgia. The original foundation design consisted of very conservatively designed H-pile groups with vertical and battered piles to carry the axial and lateral loads. The authors conducted a testing program to value-engineer the foundations with the goals of increasing the working axial pile resistance and reducing or eliminating battered piles. Seven test piles were installed and dynamically monitored with a Pile Driving Analyzer (PDA). Two lateral load tests and one tension load test were conducted. The results of our testing program allowed the project team to: (i) increase working pile resistances by factors of 1.5 to 2, reducing the total number of piles by more than 30%, (ii) eliminate the battered piles, and (iii) lessen overall project risk. Poor communication and documentation in a critical area of the site required some piles to be spliced and re-driven after additional PDA testing, establishment of new driving criteria, and consideration of long-term soil setup. This case study emphasizes the economic and risk reduction benefits of a design phase testing program, and the need for consistent communication between parties in the field.

Keywords: value engineering, risk mitigation, H-pile, karst, soil setup

INTRODUCTION

A new 50 MW biomass renewable energy power plant (Plant) was planned and constructed in southwestern Georgia. The Plant converts clean wood-based and paper-based waste from existing forestry and pulp operations, waste timber, and maintenance operations into steam that is used by an adjacent manufacturing facility. The Plant also generates electric power with limited greenhouse or particulate emissions for use by a local utility provider.

The project site (Site) is located in Dougherty County, in the Coastal Plain physiographic province of Georgia; an area of known karstic activity. Specifically, the Site is underlain at depths of 30 to 45 ft by the Ocala Formation, a light-colored fossiliferous limestone of the Eocene era. According to Watson (1981), the Ocala Formation is 125 to 200 ft thick in the vicinity of the Site and increases in thickness to the southeast. Due to differential weathering, this formation is characterized by an irregular upper surface that transitions from sandy clay/clayey sand into a dense to very dense silt and fine sand locally referred to as limestone. This subsurface stratum is most relevant to the foundation design of the Plant.

The Plant will be comprised of a number of major structures. The structures discussed herein include the following: Stacker/Reclaimer, Hog/Screen structure, Boiler structure, Turbine structure, Truck Tipper, and Water Treatment structure. Figure 1 shows the location of these structures. The owner's engineers designed a foundation system for the structures consisting of H-pile groups with vertical and battered piles to carry the axial and lateral loads. Vertical piles were designed to carry axial working loads of 110 to 140 kips. Battered piles were designed to carry all lateral loads; no lateral analysis was conducted. In total, approximately 700 piles were proposed in the original design.

Based on the large number of proposed piles and the potential impact of battered pile installation on project schedule, the EPC contractor retained Geosyntec Consultants, Inc. (Geosyntec) to evaluate the proposed foundation design and value-engineer the H-pile groups.

© 2016 Deep Foundations Institute

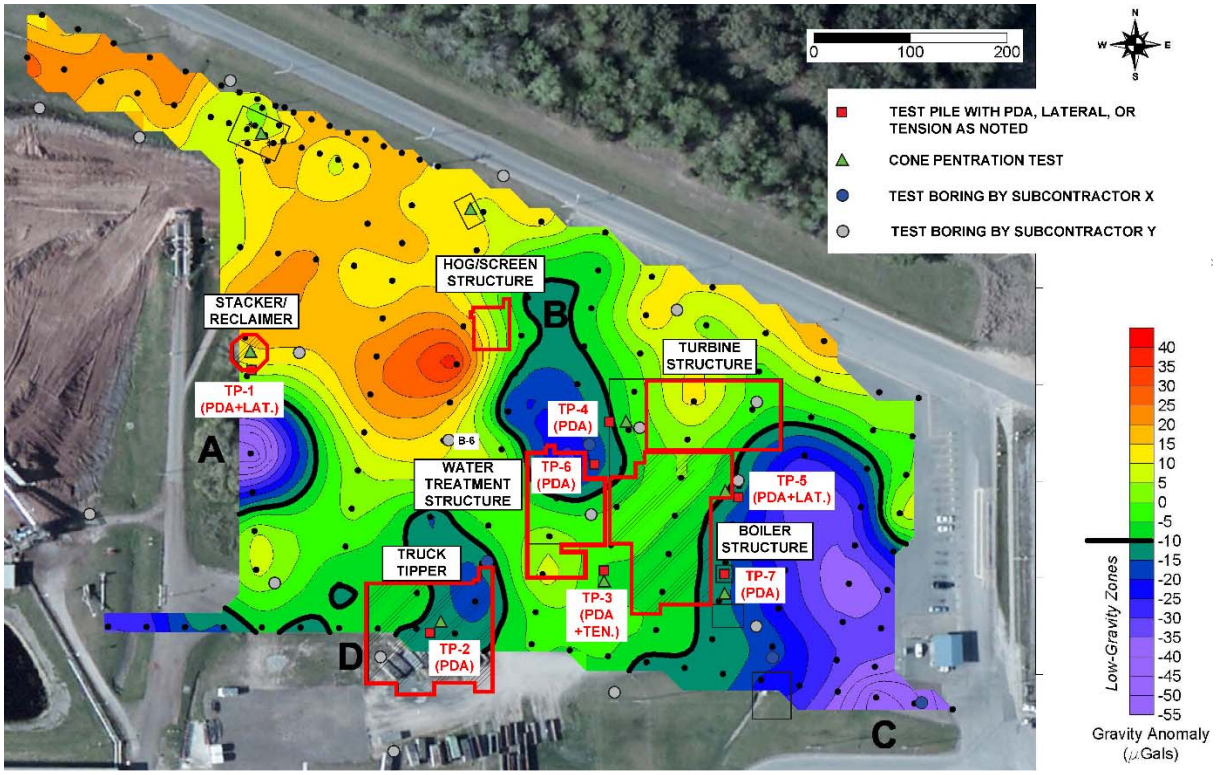


Fig. 1. Site layout showing Plant structures and testing locations

SUBSURFACE INVESTIGATION

The subsurface conditions for this project were initially assessed using site investigation data collected by others. Existing data included 17 Standard Penetration Test (SPT) borings drilled using mud rotary methods, 3 shallow hollow stem auger borings, and a shear wave velocity profile using the SeisOpt ReMi method. The SPT borings were advanced to depths ranging from 40 to 75 ft below ground surface (bgs) and typically terminated in the Ocala Formation; a layer with measurable and often erratic SPT values.

Geosyntec oversaw Cone Penetration Testing (CPT) at eight locations to further characterize the subsurface conditions and to accompany the subsequent deep foundation testing program discussed herein. The location of the CPTs are shown in Figure 1. During initial soundings in the northwest quadrant of the site, apparent voids near the point of cone refusal in the limestone were encountered; use of a weighted measuring tape indicated that an open karstic feature may exist to great depth. Geosyntec recommended the use of geophysics to evaluate the potential for karstic features following the information obtained during the CPT testing.

A site-wide microgravity survey was performed to map the lateral extent of potential karstic features by identifying variations in subsurface densities indicative of cavities, caves, or significantly looser zones. A contour map developed from the results of the microgravity survey is shown in Figure 1. Results of the survey indicate gravity anomalies in the eastern portion of the Boiler structure complex, the northeastern corner of the Truck Tipper and beneath the northern portion of the Water Treatment structure.

Four additional hollow stem auger test borings were conducted to a depth of 90 ft bgs to investigate the low-gravity zones. None of the four borings encountered variations indicative of the low-gravity findings in the microgravity survey. The authors attribute these findings to the difficulties with using a borehole to locate discrete spatial irregularities that may have contributed to the microgravity survey results.

© 2016 Deep Foundations Institute

Figure 2 shows the generalized subsurface profile established for the Site based on the site investigation data collected.

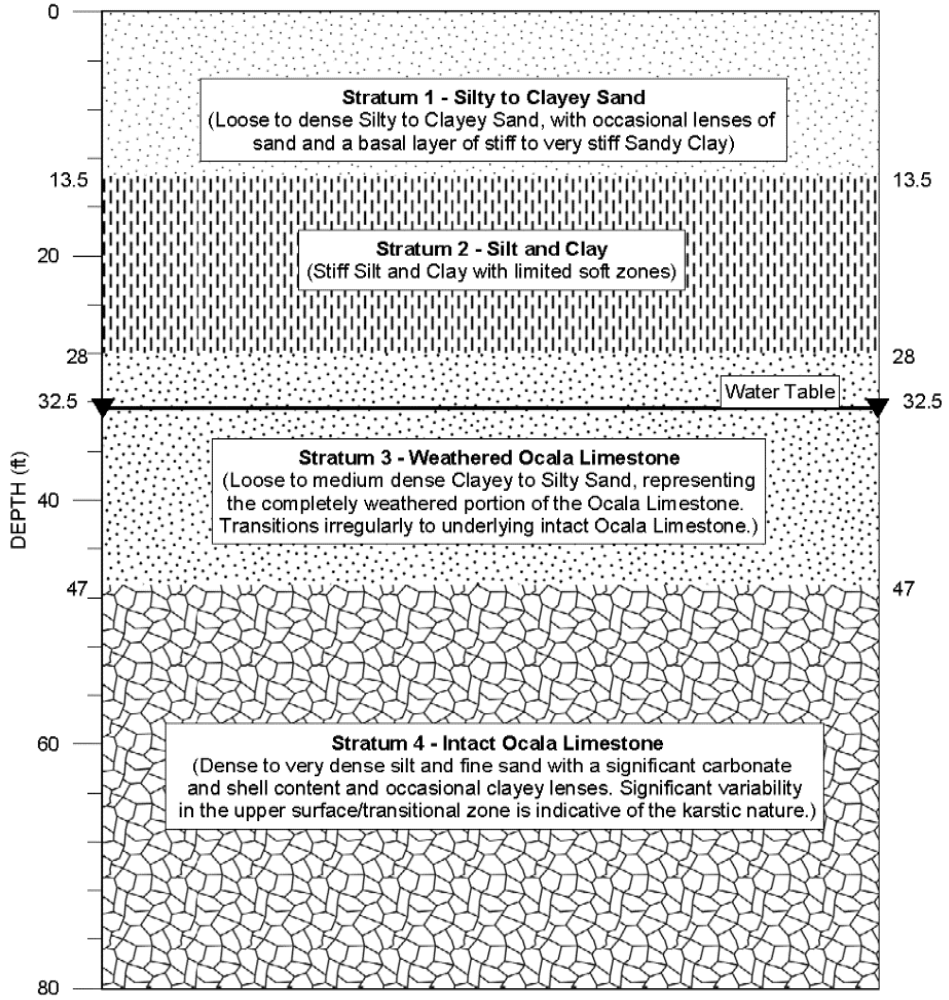


Fig. 2. Generalized subsurface profile

DEEP FOUNDATION TESTING PROGRAM

Geosyntec developed and conducted a pre-production deep foundation testing program to collect field data for use in value-engineering the H-pile groups. Design of the testing program was driven by the following goals: (i) increase the working axial pile resistance, (ii) reduce or eliminate the battered piles, (iii) confirm assumptions regarding pile tensile load capacity, and (iv) reduce overall project risk associated with a site located in an area of known karstic limestone. To accomplish these goals, the authors conduced dynamic pile monitoring, static lateral load testing, and static tension load testing. These tests are discussed in detail in the following subsections.

Dynamic pile monitoring

The initial dynamic pile monitoring program consisted of five HP14×73 test piles (designated as TP-1 through TP-5) driven to a depth of 70 ft bgs. This depth was selected based on achieving penetration into the dense to very dense, intact portion of the underlying Stratum 4. Test piles were installed using a Pileco D30-32 open-ended diesel hammer. Test pile locations are shown in Figure 1. Two additional test piles (designated as TP-6 and TP-7) were installed to a depth of 79 to 83 ft bgs to investigate areas in which the

© 2016 Deep Foundations Institute

microgravity survey had indicated potential deep anomalies, interpreted to be soft or loose, highly weathered zones above Stratum 4.

The dynamic testing subconsultant performed continuous dynamic monitoring using the Pile Driving Analyzer (PDA) from a depth of 30 ft to the approximate pile termination depth. They also performed Case Pile Wave Analysis Program (CAPWAP) analyses for representative hammer blows every 10 ft starting at approximately 40 ft bgs. The purpose of the CAPWAP analyses was to evaluate the specific dynamic ground model, refine the dynamic predictions of total ultimate compression resistance, and estimate the distribution of side and tip resistance. Restrikes were conducted 6 to 7 days after initial driving to evaluate soil setup, which is simply defined herein as the increase in ultimate resistance as a function of time after initial driving. Table 1 summarizes the ultimate geotechnical resistance and distribution of side and tip resistance at the end of initial driving and after restrikes. The apparent decrease in predicted tip resistance at the beginning of restrike (BOR) is due to the mathematical re-proportioning involved in the CAPWAP analysis. The increased side resistance after 6 to 7 days of soil setup resulted in lower interpreted mobilized tip resistance.

Table 1 - Summary of dynamic monitoring results

			End of Initial Drive (EOID)			**Beginning of Restrike (BOR)**			
Test Pile No.	Est. Tip Depth bgs (ft)	Approx. Tip Elev. (ft)	Shaft Resistance R_s (kips)	Tip Resistance R_t (kips)	Total Ult. Resistance R_u (kips)	Shaft Resistance R_s (kips)	Tip Resistance R_t (kips)	Total Ult. Resistance R_u (kips)	Final Set (in.)
TP-1	71	120.3	431	85	516	654	12	666	0.25
TP-2	70	116.8	281	75	356	427	21	448	0.25
TP-3	70	117.6	433	87	520	518	30	548	0.25
TP-4	70	120.0	280	69	349	494	5	499	0.50
TP-5	70	116.7	123	52	175	241	31	272	0.52
TP-6	78	107.0	299	35	334	-	-	441†	-
TP-7	81	104.3	351	31	382	-	-	504†	-

† Estimated BOR ultimate resistance based on measured average setup factor of 1.32

The dynamic testing data were used to develop a distribution of pile capacity with embedment depth for various areas of the site. Based on the data collected, the authors established that the overall pile setup factor, defined as the ratio between ultimate geotechnical resistance at BOR and ultimate geotechnical resistance at end of initial driving (EOID), was an average of 1.32 with a standard deviation of 0.17. Using this relationship, we estimated that the BOR ultimate resistance of test piles, TP-6 and TP-7, located within the low-gravity area would be about 441 kips and 504 kips, respectively. TP-6 and TP-7 were not restruck because the pile driving contractor had demobilized.

The CAPWAP analyses include an estimation of ultimate or mobilized side resistance along the embedded segment lengths of each pile. The estimated ultimate resistance in Stratum 3 and 4 is most pertinent to the final design of the HP14×73 piles for this project. The authors assumed that the BOR values were most representative of long-term conditions.

Static load testing

Two free-head lateral load tests and one axial tension test were conducted at the Site in general accordance with ASTM D3966 and ASTM D3689, respectively. For each load test, we used a combined loading sequence of Standard Loading and Excess Loading as defined in the two aforementioned ASTM standards.

© 2016 Deep Foundations Institute

Standard Loading typically refers to loading up to 2 times the anticipated working load and Excess Loading refers to loading to greater than 2 times the anticipated working load. Reaction frames, reference beams, hydraulic jacks, load cells, and instrumentation were provided and set up by the subcontractor. Geosyntec reviewed and approved the shop drawings for the load test assemblies.

We instrumented test piles with arc-weldable vibrating wire (VW) strain gauges on the tension side of each lateral test pile prior to driving. The strain gauges were situated at approximately 5 ft, 9 ft, 13 ft, 17 ft, and 21 ft bgs after completion of driving. A ShapeAccelArray (SAA) inclinometer was also used to measure lateral pile deflections during two free-head lateral load tests from the top of the test piles to approximately 20 ft bgs. For the tension test pile, we installed four pairs of VW strain gauges on the HP14×73 test pile; after installation, the gauges were situated at approximately 5.5 ft, 20.5 ft, 40.5 ft, and 60.5 ft bgs.

Lateral load tests

The authors performed lateral load tests on test piles TP-1, located in the footprint of the Stacker/Reclaimer, and TP-5, located adjacent to the Boiler Structure. The objective of the lateral load tests was to load the test piles in their strong axis to geotechnical failure, generally defined as lateral deflection at the pile head of about 3 inches. Test pile TP-1 was taken to the structural limit of the load cell, 50 kips, and test pile TP-5 was loaded to 80 kips after removing the load cell. Neither pile reached a point of apparent geotechnical failure. Load-deflection and SAA deflection plots for TP-1 are provided in Figure 3.

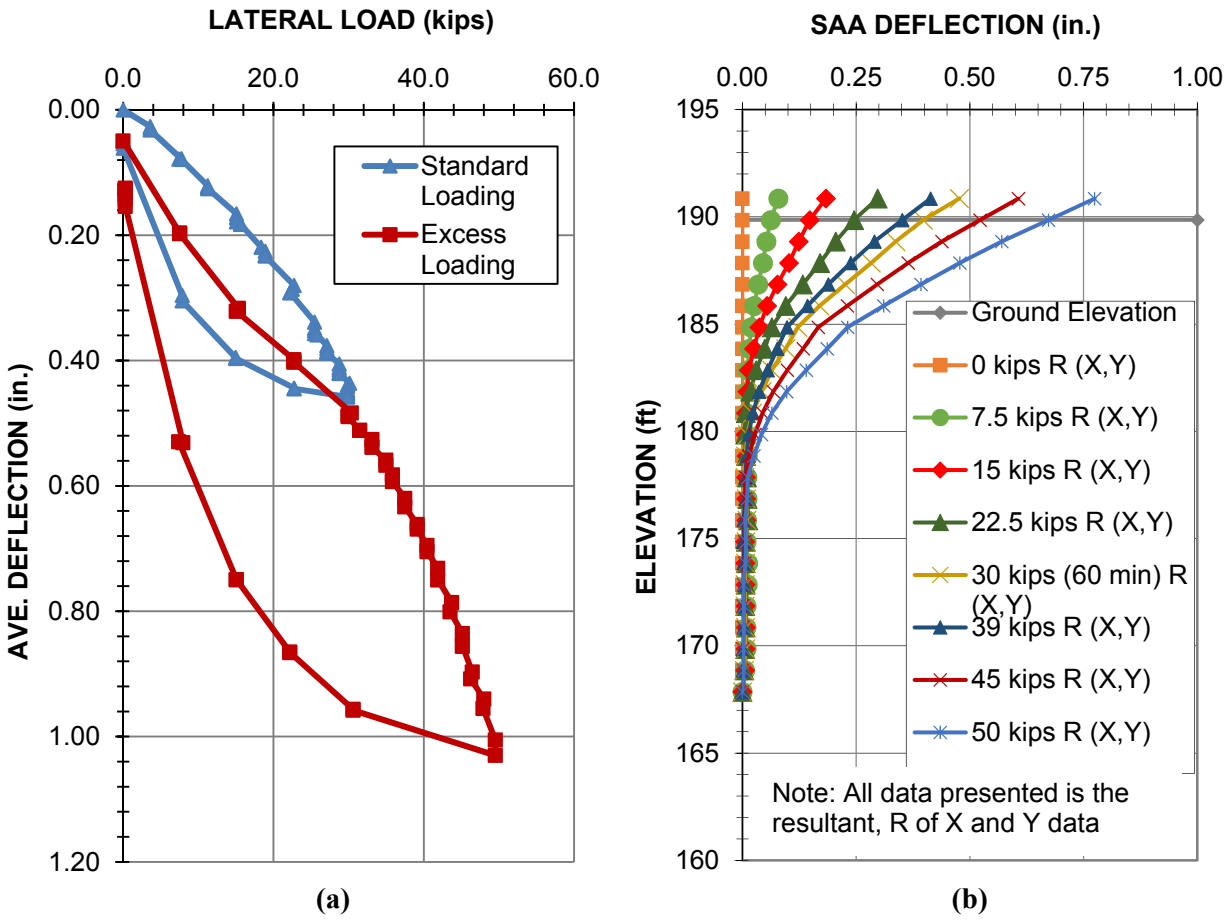


Fig. 3. (a) Load versus dial gauge measured deflection for the lateral load test on TP-1, (b) SAA measured deflection versus elevation for the lateral load test on TP-1

© 2016 Deep Foundations Institute

The results of the lateral load tests, interpreted using the methods contained in the International Building Code (IBC) (2012), indicate that single-pile service (working) lateral loads may range from 25 to 36 kips depending on location. This IBC criterion states that the single-pile service load is ½ of the load causing 1 in. of lateral deflection.

Tension load tests

We performed the axial tension load test on test pile TP-3, located adjacent to the Water Treatment Structure and Boiler Structure. The tension load test was requested by the owner's engineer with the objective of evaluating the ultimate geotechnical resistance in case it was needed for design. Test pile TP-3 was taken to the safe structural limit of the load frame, 270 kips, with a measured total upward deflection of 0.24 in. There were no indications of geotechnical failure in this load test.

The results of the tension load test, interpreted using the methods contained in IBC (2012), indicate that single-pile service (working) tension loads may range from 135 kips to 180 kips depending on whether the source of the tension loads is static or transient (wind, lateral, seismic, etc.), respectively. IBC (2012) does not address or provide an upward deflection value that corresponds to an ultimate condition similar to the code provisions for lateral loading.

DEEP FOUNDATION DESIGN RECOMMENDATIONS

Geosyntec developed the following recommendations for axial, lateral, and tension resistances based on our evaluation of the existing and new subsurface data, dynamic pile monitoring data, and static load testing results. A summary of the proposed production pile driving criteria based on our findings is also presented herein.

Axial compression resistance

Based on the dynamic monitoring data from EOID and BOR, the total ultimate resistance for the test piles ranged from 440 kips to greater than 500 kips for embedded pile lengths of 70 to 81 ft except at TP-5. In consideration of the quantity of pre-production testing and the recommended production pile testing program, we used a factor of safety ranging from 2.0 to 2.25 to develop the recommended working (service) axial compression resistances.

We recommended that for redesign of the pile groups, a working axial compression resistance of 220 kips for a single HP14×73 pile be used for all structures except the Truck Tipper; this represents an increase of approximately 60 to 100% over the original geotechnical engineering report recommendations. The tip to cutoff pile length necessary to develop the recommended working resistance ranged from 67 to 80 ft, and was dependent on the elevation and persistence of the dense to very dense, Intact Limestone. Variations in the cutoff elevations were expected, specifically in the areas of the Boiler/Turbine/Water Treatment Structures where the potential for irregular weathering patterns was established by the microgravity survey.

Lateral loading resistance

Based on the free-head lateral load test results, we concluded that a single-pile working lateral resistance of 25 kips be used for vertical piles also supporting axial compression loads in the foundation design. We conservatively estimated that lateral movements of the piles could range from 0.25 to 0.50 inches under the recommended working resistance.

© 2016 Deep Foundations Institute

Pile group efficiency values were estimated using the conservative recommendations presented in AASHTO (2012) and Hannigan et al (2006), as follows: (i) a value of 0.67 for small pile groups [4 to 9 piles (i.e. 2 to 3 rows)], and (ii) a value between 0.55 and 0.60 for larger groups with multiple rows of piles. Using these efficiency values, the revised recommended working resistance from each vertical pile is 17 kips for small groups and 14 kips for larger groups, assuming the average center to center pile spacing was maintained at 4 ft.

Axial tension resistance

Based on the results of the axial tension load testing (which did not reach a geotechnical failure condition), we recommended using a service (working) axial tension resistance of 135 to 180 kip for a single HP14×73 pile embedded a minimum of 70 ft bgs. The lower bound value (factor of safety equal to 2.0) would be used for static tension loading and the upper bound (factor of safety of 1.5) would be used for transient loading conditions.

Pile driving criteria

The authors assessed the driving records for the test piles along with the dynamic monitoring data to develop driving criteria based on the Pileco D30-32 open-ended diesel hammer used for the test pile program. Test piles were driven with this hammer, switching from Fuel Setting No. 1 (approximate energy of 35,000 ft-lbs) during initial drive and switching to Fuel Setting No. 2 (approximate energy of 51,000 ft-lbs) during penetration into the lower portions of Stratum 3 and continuing into Stratum 4. For the purpose of production driving, we proposed a single fuel setting, Setting No. 2, for consistent performance except at the Truck Tipper.

The primary driving criteria for all structures other than the Truck Tipper was established as follows: (i) install the pile to a minimum tip elevation using a Pileco D30-32 open-ended diesel hammer or similar, operating at Fuel Setting No. 2; and (ii) continue driving pile until resistance (blow counts) are a minimum of 30 blows per foot for the last 3 ft of driving.

For the 100-kip Truck Tipper piles, we proposed to, (i) install piles to a minimum tip elevation using a Pileco D30-32 open-ended diesel hammer, operating at Fuel Setting No. 1; and (ii) continue driving piles until the resistance (blow count) is a minimum of 20 blows per foot for the last 3 ft of driving.

CONSTRUCTION QUALITY ASSURANCE

The authors recommended dynamic monitoring of production piles, including initial driving and restriking, to verify that the proposed driving criteria or modifications would result in successful installation. We proposed that 3% of the production piles be dynamically monitored during initial installation and restriking, and that CAPWAP analyses be conducted for each. We also recommended that a Geosyntec field representative be on-site during production pile driving to perform construction quality assurance (CQA), however the foundation contractor hired an independent consultant for the CQA activities. Geosyntec was involved in the evaluation of driving records, construction progress, and modifications to installation procedures and criteria.

Problematic piles and corrective action

Production pile driving outpaced the delivery of field logs to Geosyntec. During our office review, it was discovered late that a number of piles in the area of the Hog/Screen and the critical Turbine structure displayed driving behavior different than that experienced during the test pile program from which the driving criteria were developed. These piles drove with very little resistance until the final 10 to 15 ft, at

© 2016 Deep Foundations Institute

which point blow counts increased to where they met the primary driving criteria. Further analysis using the CAPWAP-predicted side resistance distribution, confirmed the presence of soft, low side resistance zones along these piles. The dissimilar driving behavior went unnoticed by the CQA engineer and the piles were considered acceptable by field determination. This miscommunication led to these piles being prematurely trimmed to final cutoff elevations.

After discovering this issue, Geosyntec proposed additional dynamic monitoring and CAPWAP analyses to gather more data on these problematic piles. Unfortunately, due to piles having been accepted and cut off, splicing of production piles was required to facilitate further driving. Restrike PDA data for many of the suspect piles indicated that the ultimate geotechnical resistance was insufficient to provide the required factor of safety. Therefore, Geosyntec directed that a significant number of the production piles be driven to greater depths. New driving and restrike data were used to establish and refine soil setup values for the side resistance. With these new data, we assessed the ultimate geotechnical resistance using time-based soil setup theory.

The authors used the method proposed by Skov and Denver (1988), along with site-specific short term soil setup values calculated from the PDA and CAPWAP data, to estimate the ultimate geotechnical side resistance for the re-driven piles. The Skov and Denver method is believed to be conservative and uses the following predictive equation:

$$R_{s,ult(t)} = R_{s,EOID}\left[A \cdot log\left(\frac{t}{t_0}\right) + 1\right] \quad [1]$$

where $R_{s,ult(t)}$ is the predicted ultimate geotechnical resistance at time t after initial driving, $R_{s,EOID}$ is the short term side resistance at the end of initial driving, A is a constant, and t_0 is a constant typically taken as 1 day for piles in sand and 0.5 day for piles in clay.

We derived an average value of A equal to 0.2 for the Site from the CAPWAP analyses performed on initial driving and restrikes. This site-specific value is considered to be at the lower bound of the published range of values from A=0.2 for sands to A=0.6 for clays; however, a value closer to 0.4 would have been expected given that the weathered limestone soils at the Site are typically sandy clays and clayey sands.

Table 2 provides a summary of the calculated time-dependent values of $R_{s,ult(t)}$. We were able to demonstrate that all of the previously problematic piles were predicted to have a long-term axial capacity approximately equal to or greater than the target value of 440 kips.

Table 2. Time-dependent increase in R_{ult}

			$R_{ult,EOID}$ (kips)	**$R_{ult(t)}$ (kips), A=0.2**		**$R_{ult(t)}$ (kips), A=0.4**	
Structure	Pile No.	Final Pile Length (ft)	EOID†	90 days	365 days	90 days	365 days
Turbine Pedestal	1	139	267	509	541	560	625
	3	120	275	521	555	574	641
	11	122	178	367	388	401	444
	13	122	331	610	650	673	753
	14	121	190	386	409	423	469
	21	123	213	423	449	464	516
Hog/Screen	A3-2	90	363	589	633	731	819
	C3-2	103	358	582	625	722	809

†Ultimate resistance at the end of driving from CAPWAP analyses or estimated from driving resistance

© 2016 Deep Foundations Institute

SUMMARY AND CONCLUSIONS

A carefully designed and conducted pre-production testing program helped facilitate the value engineering of H-pile groups designed to provide foundation support for a new 50 MW biomass renewable energy power plant. The goals of our testing program were accomplished through dynamic pile monitoring, static lateral load testing, and static tension load testing. Analysis of the data collected allowed us to achieve the following:

- increase the working (service) axial compression resistances of individual piles to 220 kips; and increase from the originally proposed values of 110 to 140 kips by a factor of approximately 1.5 to 2.0;
- demonstrate the ability of vertical piles to carry a lateral load of 25 kips; thus eliminating the need for any of the originally proposed battered piles;
- reduce the total number of piles from approximately 700 to 484, a reduction of approximately 30%; and;
- reduce overall project risk; the scope and targeted nature of the pre-production pile testing program resulted in an increased level of confidence that the ground conditions were relatively well understood and that the recommended pile capacities could be achieved.

An oversight during production pile driving and miscommunication by parties in the field led to costly splicing of piles. However, critical examination and redesign of individual piles helped mitigate risk in the karstic geology. This project highlights the economic benefits of a design phase testing program and the significant increase in axial capacity that can be realized from time-based soil setup theory. This project also underscores the need for consistent communication between the field CQA engineer the design engineer.

ACKNOWLEDGMENTS

The authors would like to thank their client for the opportunity to be involved with this project.

REFERENCES

AASHTO 2012. LRFD Bridge Design Specifications, American Association of State Highway and Transportation Officials, Washington, D.C., 1661 p.

Hannigan, P.J., Goble, G.G., Likins, G.L., and Rausche, F.R., 2006. Design and Construction of Driven Pile Foundations – Volume 1, Federal Highway Administration Report No. FHWA-NHI-04-042, Washington, D.C., 968 pp.

International Building Code (IBC) 2012. IBC, International Code Council, Country Club Hills, 725 p.

Skov, R., and Denver, H. (1988). Time-dependence of bearing capacity of piles. Proc., 3rd Int. Conf. on the Application of Stress-WaveTheory to Piles, B. G. Fellenius, ed., BiTech Publishers, Vancouver, BC, 879–888

Watson, T.W. 1981. Geohydrogeology of the Dougherty Plain and adjacent area, Southwest Georgia. Georgia Department of Natural Resources, Hydrologic Atlas 5, 5 p.

© 2016 Deep Foundations Institute

This page left intentionally blank

© 2016 Deep Foundations Institute

A CASE STUDY OF MULTICHANNEL ANALYSIS OF SURFACE WAVES (MASW) AS A TOOL TO CHARACTERIZE UNKNOWN FOUNDATIONS

Siavash Mahvelati, Temple University, Philadelphia, Pennsylvania, United States of America, (215)204-7814, tuf60905@temple.edu
Joseph T. Coe, Temple University, Philadelphia, Pennsylvania, United States of America, (215)204-6100, joseph.coe@temple.edu
Philip Asabere, Temple University, Philadelphia, Pennsylvania, United States of America, (215)204-7814, tuf03655@temple.edu

ABSTRACT

Characterization of existing foundations remains an important issue as foundation reuse and rehabilitation continue to garner increased attention. In the case of unknown foundations, geophysical and nondestructive testing (NDT) methods have been utilized in the past to evaluate foundation geometry and could serve as useful tools in the case of foundation reuse. A comprehensive study was initiated in the late 1990's and early 2000's that evaluated the effectiveness of the available geophysical and NDT technologies to characterize unknown foundations for scour evaluation purposes. At the time of that study, the Multichannel Analysis of Surface Waves (MASW) geophysical method was in its infancy and not widely used. Since then, MASW has become increasingly prevalent in geotechnical applications as the method presents a number of potential advantages when characterizing the subsurface, including rapid testing, increased signal to noise ratio, and ability to resolve velocity inversions. This paper presents a case study that explores the abilities of MASW as an unknown foundation characterization tool. MASW was applied to determine subsurface stiffness at a bridge foundation site in the Philadelphia metropolitan area. One MASW survey line was performed immediately over the foundation of interest and another was performed over a control zone adjacent to the foundation to establish a baseline site profile. The purpose of this testing was to examine whether MASW could establish the geometry of the foundation at this site. This paper presents the site conditions and MASW testing procedures, followed by a discussion of data analysis and interpretation.

INTRODUCTION

Adequate knowledge regarding subsurface conditions is a difficult problem for transportation infrastructure, particularly for the more than 40,000 bridges across the United States with unknown foundations (Arneson et al., 2012; Collin and Jalinoos, 2014). An appropriate scour analysis cannot be performed for these unknown foundation bridges when they are located over waterways, which signifies that these bridges are classified as scour critical according to Federal Highway Administration (FHWA) guidelines. Moreover, it is extremely difficult to reuse the foundation for a bridge in the case of rehabilitation if its geometry and/or load carrying capabilities are unknown. In such cases, subsequent efforts to remove the existing foundation system from the subsurface can prove to be quite expensive and the inability to reuse the foundation represents a costly unnecessary expense. Since excavation efforts to expose a foundation and determine its properties are complex, costly, and potentially unsafe, evaluation of unknown foundations has traditionally been accomplished using geophysical and non-destructive testing (NDT) techniques. Olson et al. (1998) and Olson and Aouad (2001) summarize the results from one of the most comprehensive studies using geophysical and NDT methods to evaluate the geometry of unknown foundations. Wightman et al. (2003) also include an entire section devoted to unknown foundations in their seminal work regarding the use of geophysics for highway related issues. Olson et al. (1998), Olson and Aouad (2001), and Wightman et al. (2003) all acknowledge that subsurface borehole test methods (e.g., Parallel Seismic) are typically more accurate and versatile in estimating foundation geometry relative to surface methods (e.g., Sonic Echo/Impulse Response). However, surface methods are

© 2016 Deep Foundations Institute

less costly and more rapidly implementable. All current state-of-practice methods have limitations concerning the evaluation of unknown foundations, particularly for complex foundations (piles underlying a cap) (Olson and Aouad, 2001; Hertlein and Davis, 2006; McLemore et al., 2010). Thus there is still a need for the development and testing of new robust methods to estimate unknown foundation geometry and, ideally, load carrying capabilities and condition.

The multichannel analysis of surface waves (MASW) geophysical method presents an attractive alternative to evaluate unknown foundations due to its versatility, speed, and relationship to stiffness properties. MASW consists of analyzing the dispersive nature of surface waves generated from a seismic source on the ground surface (typically an impact from a sledgehammer) to develop an estimate of subsurface shear wave velocity (V_s) as a proxy for stiffness (Park et al., 1999). Dispersion refers to the fact that the different frequency components in the input surface wave sample different depths of the subsurface strata and will therefore travel at different velocities. Raw waveforms recorded from geophones placed on the surface can be post-processed to estimate a velocity-frequency relationship (i.e., dispersion curve) that summarizes the dispersion at the site. This curve can then be used in an inversion algorithm to estimate the most probable subsurface stiffness profile capable of generating the measured dispersion curve. The MASW method has become increasingly commonplace in the geophysical, NDT, and geotechnical community since its inception in the late 1990's (i.e. Park et al. 1999). MASW is utilized for several subsurface investigation applications including soil characterization (Park and Miller, 2005), anomaly detection (Xia et al., 2004; Miller et al., 2005), characterization of bedrock topography (Miller et al., 1999), and evaluation of seismic site amplification (Stephenson et al., 2005). However, MASW was in its infancy at the time of Olson et al. (1998), Olson and Aouad (2001), and Wightman et al. (2003) and has not been used to evaluate unknown foundations.

Given the strong signal-to-noise ratio of surface waves, fundamental underpinnings of the methodology, and field testing procedures, MASW presents a number of potential advantages when evaluating the subsurface for unknown foundations. For example, MASW is capable of resolving velocity reversals that can exist when the foundation is not located on a sufficiently stiff layer (e.g., frictional piles not driven to bedrock). This versatility may allow MASW to extend its applicability to sites not likely to be successful with other surface geophysical methods (e.g., seismic reflection, seismic refraction, etc.). Additionally, MASW field operations can proceed rapidly in cases where landstreamer systems are used. In this manner, multiple surveys can be performed to develop two-dimensional (2D) subsurface profiles within a day of testing at a site. The use of a 2D approach is very beneficial because it can provide information regarding the stiffness of the subsurface both in the immediate vicinity of the foundation elements and in the general area of the foundation. This ability to evaluate stiffness properties of the nearby soils can provide useful information about sites with limited results from previous subsurface exploration efforts (if indeed any were performed). When used in combination with estimates for the dimensions of the foundation (e.g., depth to foundation bottom), such subsurface stiffness information can help with estimating the load-carrying capabilities of the unknown foundation based on reverse engineering concepts (McLemore et al., 2010; Sayed et al., 2012). However, there are a number of questions that must be addressed regarding the applicability of MASW for the detection of subsurface anomalies such as foundations. One major concern is the resolution capabilities of MASW, both in the vertical direction and in the lateral direction. The velocity-based approach of MASW and dependence of depth resolution on wavelength means that estimates of layer thickness increases with depth. Therefore, the precision with which the depth to a foundation bottom could be identified would decrease the deeper the foundation is located. Additionally, data post-processing in MASW assumes a layered earth model with perfectly flat contacts between strata throughout the length of the receiver array. Any heterogeneity in the lateral direction (such as a long slender foundation element) can potentially undergo a smoothing effect that may mask their presence in the subsurface (Boiero and Socco, 2011). Thus it is uncertain whether MASW would be capable of adequate lateral resolution to detect foundation systems. Given these limitations, only a handful of studies have explored the use of MASW for anomaly detection (e.g., Miller et al. 2005;

© 2016 Deep Foundations Institute

Nasseri-Moghaddam et al. 2007; Lin et al. 2012; Parker and Hawman 2012), and none of them have addressed a bridge foundation as the target of interest. Therefore, the goal of this study was to establish a proof-of-concept case history where MASW was performed to evaluate an unknown bridge foundation so that the viability of this method could be tested.

FIELD TESTING

For this study, MASW was performed at a field site located at the interchange for the Betsy Ross Bridge to Interstate 95 (I-95) in northeast Philadelphia, Pennsylvania (Fig. 1). This site is part of ongoing multi-phase initiatives to rebuild and improve I-95 near Philadelphia and has been previously documented using various geophysical and NDT methods for unknown foundation evaluation (Coe and Kermani, 2016; Coe et al., 2014; Kermani et al., 2014). Soil conditions at the site are highly variable based on previous geotechnical borings. They primarily consist of silty sands near the surface, clayey soils at approximately 7 m – 12 m (23.0 ft – 39.4 ft), and gravelly, silty sands at depth. The bedrock at the site (primarily Pegmatite, Amphibolite, and Schist) is highly weathered and is typically located at approximately 15 m – 25 m (49.2 ft – 82.0 ft) below the surface. The ground water table is located approximately 3 m – 11 m (9.8 ft – 36.1 ft) below the surface with daily fluctuations due to tidal variations in the level of the nearby Delaware River. The foundation at the site supports pier 7 of ramp B (structure S-10295) at approximate station number 39. It consists of a reinforced concrete (RC) pile cap with dimensions of 7.3 m by 5.5 m (24.0 ft by 18.0 ft) supported on a group of 35 cast-in-place concrete piles with steel casings driven at approximately a 1:5 (H:V) batter angle (Fig. 2). Final as-built drawings and foundation construction records are unavailable for the site, which mimics a true unknown foundation case study. This implies an additional sense of uncertainty in the remaining discussion of the MASW results. However, based on the relatively shallow bedrock, method of construction, size and age of the structure, the foundation was confidently assumed to be founded on bedrock at the tested location. Borings performed when the original section of I-95 was constructed at the site contain subsurface information immediately adjacent to the foundation location. This boring was terminated at top of rock approximately 16.7 m (55 ft) below the ground surface, which provides an estimate for the foundation bottom.



Fig. 1: Betsy Ross field site and foundation location (courtesy of Google Maps) (adapted from Kermani et al. 2014).

MASW testing at the site was performed at two locations. The first location was centered directly over the foundation of interest and aligned with its largest lateral dimension (i.e., 7.3 m) (Fig. 1). A second survey

© 2016 Deep Foundations Institute

was performed at another location away from the foundation to serve as a baseline V_s profile. The results from this location allowed comparisons to be made regarding the effectiveness of MASW in identifying the foundation. Data was acquired at the site using a 24 channel Geometrics Geode seismograph connected to a field laptop running the Geometrics Seismodule Controller Software (SCS). GiscoGeo 4.5 Hz vertical geophones were planted into the ground and spaced at 1.0 m (3.3 ft) for a total spread length of 23.0 m (75.4 ft). The input surface wave was generated using impacts from a 20 lb sledgehammer source on a 25 mm (1.0 in) thick aluminum plate. A single hammer impact at one offset from the receiver array may not generate a sufficient range of frequencies to properly develop the dispersion curve for the site. Therefore, multiple source offsets were used on either side of the array to improve the resulting dispersion image. Triggering was performed with a Geometrics trigger switch to ensure accurate timing for each shot record. Stacking was also performed at each source offset, whereby multiple impacts were recorded and added together to improve signal to noise ratio. Each shot record typically consisted of 5 stacks that were recorded for a total of 2.048 s with a sampling interval of 0.125 ms.

Data analysis was performed with the Geometrics SeisImager/SW software package. The raw waveforms recorded at each source offset location were individually processed using the phase shift method (Park et al., 1998) to produce a dispersion image. Each dispersion image was then interpreted to select an appropriate fundamental mode dispersion curve. Each of the selected dispersion curves were then stacked and averaged to form a composite curve that best characterized the subsurface conditions beneath the receiver array. This composite dispersion curve was then inverted using the linearized inversion routine available in SeisImager/SW. This inversion algorithm uses forward modeling to develop a theoretical dispersion curve for a given trial subsurface stiffness profile. The misfit between the theoretical dispersion curve and the measured field dispersion curve is then computed in a least squares sense. The process then repeats in an attempt to match the most probably theoretical model of the subsurface based on misfit between the theoretical and measured dispersion curve. For both the control line and the line over the foundation, the inversion process converged to a solution within 5% root means square error (RMSE) after 7 iterations.

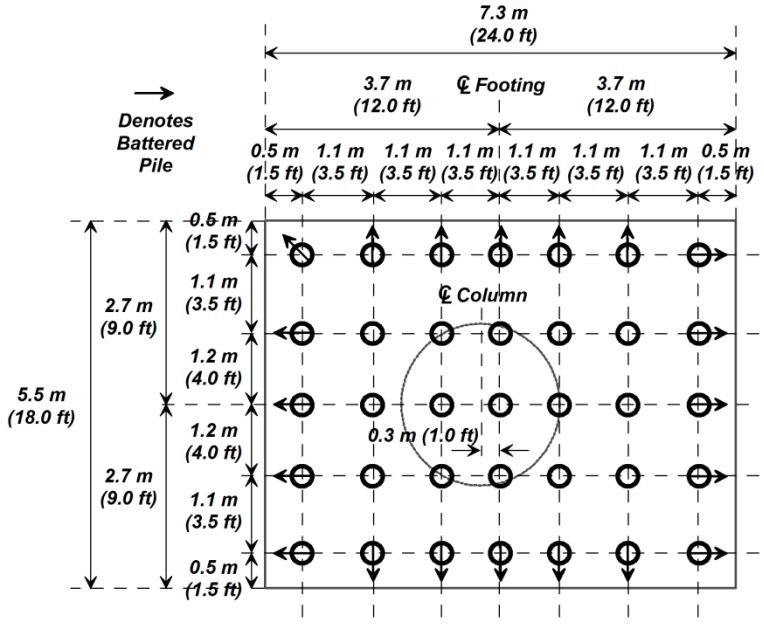


Fig. 2: Schematic of foundation system tested at Betsy Ross bridge site (adapted from Kermani et al., 2014).

© 2016 Deep Foundations Institute

RESULTS

Figure 3 presents the V_s profiles acquired using MASW at the test site. The results demonstrate an appreciable increase in stiffness for the array centered on the foundation. Therefore, MASW seems capable of detecting the presence of the underlying foundation. The initial increase in stiffness is approximately 15% in magnitude and is evident starting at 1.0 m (3.3 ft) below the ground surface, which roughly corresponds to the depth of the RC pile cap. The increase in stiffness is particularly notable below 5.2 m (17.1 ft) and the percentage with which the stiffness has increased compared to the baseline survey (about 35%) is relatively consistent throughout the remainder of the profile. A linear feature with consistent stiffness contrast relative to the soil (i.e., pile elements) may at least partially account for the observed stiffness increase. However, there are very few case histories where MASW has been used to estimate velocity over complex composite systems (e.g., long slender and stiff elements surrounded by variable soil conditions) that can provide definitive guidance about interpretation of the measured V_s profile. For example, the expected range of values for velocity of a composite soil-pile system is not entirely clear. Therefore, there is uncertainty as to whether the V_s increase evident in Fig. 3 is sufficiently large enough to indicate a foundation. However, given the relative proximity of the two MASW lines, little difference in the velocity structure is expected between the two sets of results. It is therefore very likely that the increase in velocity is at least partially attributable to the underlying foundation system since very little else can account for such a prevalent systematic feature in the measured profiles.

In addition to the preceding issues related to detectability of the foundation based on stiffness, the resolution of MASW was also explored in this study. The lowest frequency component of the dispersion curve is related to the deepest strata that can be sampled by the wavelengths present in the source surface wave. A typical approximation originating from the spectral analysis of surface waves (SASW) method is that the depth of investigation of surface wave testing is 1/3 to 1/2 the largest wavelength (Stokoe et al., 1994). Based on the baseline dispersion image generated at this site, the lowest measured frequency was approximately 9 Hz, which corresponds to a wavelength of approximately 36.1 m based on a V_s of 325 m/s. However, in the case of the array centered on the foundation, increased noise and incoherency in the dispersion images led to an increase in the lowest frequency recorded. For that survey, the lowest frequency recorded was approximately 17 Hz. Using the measured 440 m/s phase velocity at this frequency, the corresponding wavelength was 23.2 m. The depth of investigation at this site was therefore limited to approximately 12.0 m (39.4 ft) for the baseline and 7.7 m (25.3 ft) for the foundation. There is less confidence in the measured stiffness below these depths in the respective profiles. This unfortunately signifies that the actual depth to the foundation bottom cannot be distinguished, given the estimated depth of 16.7 m established from the existing boring logs. Another aspect to consider is that the depth resolution of MASW is directly related to the smallest wavelength measured by the equipment. This in turn is related to receiver spacing. As noted in Fig. 3, the smallest layer thickness is 1.0 m, which roughly corresponds to the smallest wavelength observed in the dispersion images at this site (i.e., approximately 0.9 m). However, the thickness of layers is typically increased for deeper strata to numerically stabilize the inversion algorithm in MASW. An examination of layer thickness in Fig. 3 shows that the deeper layers in the profile correspond to increased thicknesses of up to 1.3 m. Moreover, the final layer in the profile is modeled as a half-space with infinite thickness. Given the limitations in depth of investigation and in layer thickness resolution, a lower bound estimate of approximately 7.7 m can be made for the depth to the foundation bottom at this location. This, of course, assumes that the consistently larger V_s value in Fig. 3 very likely indicates the presence of a foundation. This estimate represents the top of the half-space layer and the maximum extent of sampling depth based on the wavelengths generated at this site. This depth to bottom information would prove highly beneficial to bridge owners were no information be readily available regarding this foundation.

© 2016 Deep Foundations Institute

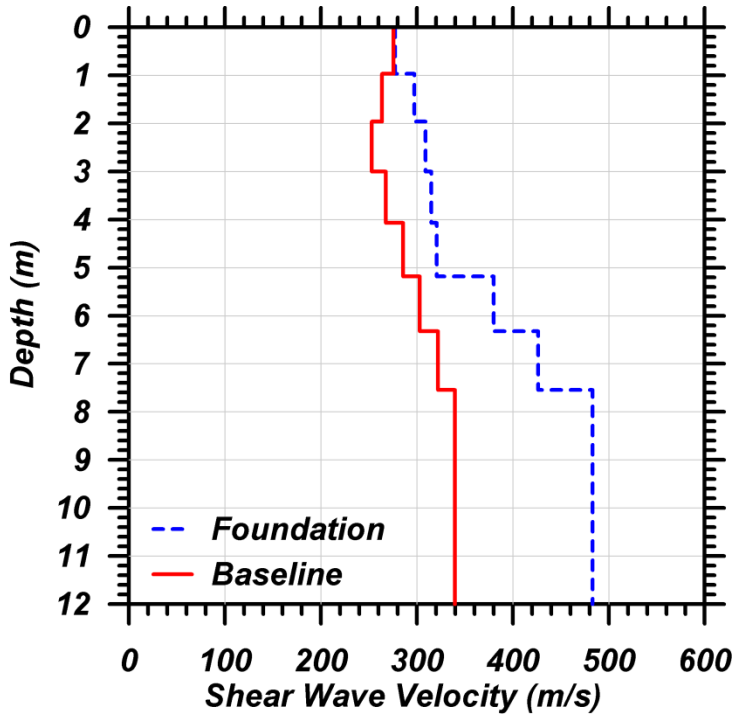


Fig. 3: V_s profiles for the MASW survey over the foundation and the baseline survey away from the foundation.

Finally, it should be noted that the results in Fig. 3 are dependent on the lateral resolution capabilities of MASW in relationship to the lateral extent of the foundation. The MASW survey centered on the foundation was aligned with the largest lateral dimension of the foundation (i.e., 7.3 m). This roughly represents a total length of 7dx, where dx is the spacing between adjacent geophones (1 m in this study). A foundation length of 7dx represents approximately 30% of the total array length. Fig. 4 shows the raw waveforms recorded from a single source offset shot record over the foundation. Apparent in Fig. 4 is the increase in signal noise for the waveforms recorded over the existing foundation, presumably as a result of increased reflected and refracted energy from the piles. This noise increase takes place between approximately 10.0 m – 15.0 m in lateral distance along the surface. The corresponding estimate of the foundation lateral dimension is therefore 5.0 m, which compares favorably with the known 7.3 m dimension from existing design plans. These results demonstrate the importance of lateral resolution as related to receiver spacing. The estimate of 5.0 m is only inaccurate by one receiver spacing on either side of the foundation and an estimate of 7.0 m would compare excellently with the 7.3 m known dimension. Had the MASW array used larger spacing between receivers, it is likely the case that lateral resolution would suffer and we would be unable to provide a reasonable estimate for lateral geometry. One final item of note is that the lateral extent of the foundation increased with depth due to the outer row of angled piles. By the anticipated bottom of the pile elements (i.e., 16.7 m below the surface), the pile group "footprint" may have increased to as much as roughly 12.6 m by 10.8 m (41.3 ft by 35.4 ft) assuming the bottom of the pile cap was located at approximately 2.0 m (6.6 ft) below the ground surface. Since the MASW array was aligned with the largest dimension of the pile cap, the lateral extent of the foundation bottom may have approached 12.6 m (i.e., at least half the total array length) towards the bottom of the soil profile. The fact that such a large lateral "heterogeneity" was located beneath the MASW array may have contributed to the success in measuring stiffness increases from the foundation in this study. The large dimensions of the foundation at deeper locations may have diminished the issues associated with the layered earth model assumed in the inversion algorithm.

© 2016 Deep Foundations Institute

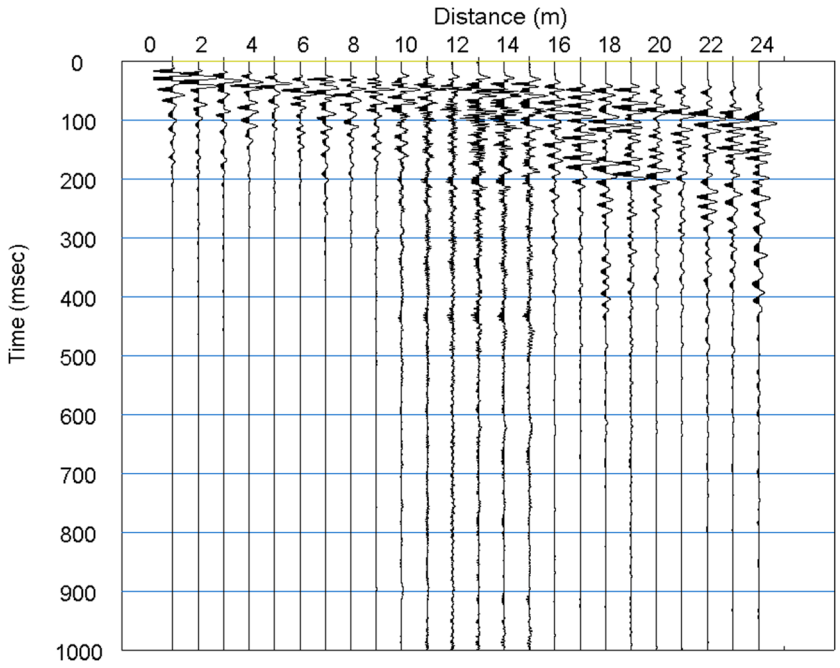


Fig. 4: Raw waveform record from the MASW array centered over the foundation at the Betsy Ross site.

CONCLUSIONS

The results in Fig. 3 and Fig. 4 are encouraging with regards to the use of MASW to detect and evaluate unknown foundations. We were clearly able to measure a systematic increase of approximately 15% – 35% in the stiffness/velocity structure for the MASW survey line performed directly over the foundation in relationship to the baseline profile. Based on this stiffness increase and the depth resolution capabilities discussed in this paper, the depth to foundation bottom could be estimated as 7.7 m. This did not compare favorably with the expected depth to foundation bottom of 16.7 m below the surface. However, such an estimate could still prove valuable in situations where no other information is available regarding foundation depth. It was shown that the depth resolution limitation of MASW clearly affected the capabilities of the method to accurately estimate foundation depth. Finally, a relatively accurate estimate of 5.0 m was obtained for the lateral extent of the foundation near the surface by examining the raw waveform records. These results indicate that the effects of a subsurface anomaly with lateral extent of approximately 30% - 50% of the total array length can be resolved using MASW. However, despite the promise demonstrated by MASW in this study, there are still numerous issues to explore regarding vertical resolution, lateral resolution, and guidance on appropriate soil-foundation composite velocities. Future testing should continue to evaluate the effectiveness and add to the existing case history database of MASW for unknown foundations. This is particularly relevant in the context of two-dimensional surveys and their abilities to resolve horizontal geometry (i.e., lateral extent) in addition to vertical geometry (i.e., depth to foundation bottom). As previously noted, such 2D surveys may provide a rapid and useful approach by which foundation geometry could be determined in addition to stiffness of the surrounding soils. Such an approach would allow an estimate of foundation load-carrying capabilities.

REFERENCES

Arneson, L.A., Zevenbergen, L.W., Lagasse, P.F., and Clopper, P.E. (2012). “Evaluating Scour at Bridges," HEC No. 18, 5th Edition, FHWA-HIF-12-003, Federal Highway Administration, Washington, D.C.

© 2016 Deep Foundations Institute

Boiero, D., and Socco, L.V. (2011). "The meaning of surface wave dispersion curves in weakly laterally varying structures." Near Surface Geophysics, 9, 561-570.
Coe, J. T. and Kermani, B. (2016). "Comparison of Borehole Ultrasound and Borehole Radar in Evaluating the Length of Two Unknown Bridge Foundations." DFI Journal: The Journal of the Deep Foundations Institute. doi: 10.1080/19375247.2016.1166313. (Article in Press).
Coe, J.T., Kermani, B., Nyquist, J.E., Berg, P.H., McInnes, S.E., and Sybrandy, L. (2014). "Use of P-wave Reflection Imaging and Other Nondestructive Testing Techniques to Evaluate Unknown Bridge Foundations." Proceedings ASCE Geo-Congress 2014, Atlanta, GA.
Collin, J.G., and Jalinoos, F. (2014). "Foundation Characterization Program (FCP): TechBrief #1 – Workshop Report on the Reuse of Bridge Foundations." FHWA-HRT-14-072, Federal Highway Administration, McLean, VA.
Hertlein, B.H., and Davis, A.G. (2006). Nondestructive Testing of Deep Foundations. John Wiley & Sons, West Sussex, England.
Kermani, B., Coe, J.T., Nyquist, J.E., Sybrandy, L., Berg, P.H., and McInnes, S.E., (2014). "Application of Electrical Resistivity Imaging to Evaluate the Geometry of Unknown Bridge Foundations." Proceedings Symposium on the Application of Geophysics to Environmental and Engineering Problems (SAGEEP) 2014, Boston, MA.
Lin, C., Lin, C., Dai, Y., and Chien, C. (2012). "Assessment of Ground Improvement with Improved Columns by Surface Wave Testing." Grouting and Deep Mixing 2012, 483-492.
McLemore, S., Zendegui, S., Whiteside, J., Sheppard, M., Gosselin, M., Demir, H., Passe, P., and Hayden, M. (2010). "Unknown Foundation Bridges Pilot Study." Federal Highway Administration & Florida Department of Transportation.
Miller, R.D., Xia, J., and Park, C.B. (2005). "Seismic techniques to detect dissolution features (karst) at a proposed power-plant site." in Near Surface Geophysics, Butler, D.K. (ed.), Society of Exploration Geophysicists, 663–679.
Miller, R.D., Xia, J., Park, C.B., and Ivanov, J.M. (1999). "Multichannel Analysis of Surface Waves to Map Bedrock, Kansas Geological Survey." The Leading Edge, 18(12), 1392-1396.
Nasseri-Moghaddam, A., Cascante, G., Phillips, C., and Hutchinson, D.J. (2007). "Effects of underground cavities on Rayleigh waves – Field and numerical experiments." Soil Dynamics and Earthquake Engineering, 27, 300–313.
Olson, L., Jalinoos, F., and Aouad, M.F. (1998). "Determination of Unknown Subsurface Bridge Foundations: A Summary of the NCHRP 21-5 Interim Report." Geotechnical Guideline No. 16, Federal Highway Administration, Washington, D.C.
Olson, L.D., and Aouad, M.F. (2001). "Unknown Subsurface Bridge Foundation Testing, NCHRP Project 21-05(2) Final Report." Transportation Research Board, Washington, D.C.
Park, C.B., and Miller, R.D. (2005). "Seismic Characterization of Wind Turbine Sites in Kansas by the MASW Method." Kansas Geological Survey, Open-File Report 2005-23, Lawrence, KS.
Park, C.B., Miller, R.D., and Xia, J. (1999). "Multichannel Analysis of Surface Waves." Geophysics, 64(3), 800-808.
Park, C.B., Miller, R.D., and Xia, J. (1998). "Imaging Dispersion Curves of Surface Waves on Multi-Channel Record." 68th Ann. Internat. Mtg. Soc. Expl. Geophys., Expanded Abstracts, 1377-1380.
Parker, E.H., and Hawman, R.B. (2012). "Multi-channel Analysis of Surface Waves (MASW) in Karst Terrain, Southwest Georgia: Implications for Detecting Anomalous Features and Fracture Zones." Journal of Environmental and Engineering Geophysics, 17(3), 129-150.
Sayed, S.M., Sunna, H.N., and Moore, P.R. (2012). "Rational Alternative to Positive Discovery of Pile-Supported Bridges with Unknown Foundation Depth." Journal of Bridge Engineering, 17(1), 173-181.
Stephenson, W. J., Louie, J. N., Pullammanappallil, S., Williams R. A., and Odum, J. K. (2005). "Blind Shear-Wave Velocity Comparison of ReMi and MASW Results with Boreholes to 200 m in Santa Clara Valley: Implications for Earthquake Ground-Motion Assessment." Bulletin of the Seismological Society of America, 95(6), 2506-2516.
Stokoe, II, KH, Wright, G.W., James, A.B., and Jose, M.R. (1994). "Characterization of geotechnical

© 2016 Deep Foundations Institute

sites by SASW method." In: Woods, R.D., Ed. Geophysical characterization of sites, A.A. Balkema/Rotterdam, 15-25.
Wightman, W.E., Jalinoos, F., Sirles, P., and Hanna, K. (2003) "Application of Geophysical Methods to Highway Related Problems." FHWA, Central Federal Lands Highway Division, Lakewood, CO.
Xia, J., Chen, C., Li, P.H., and Lewis, M.J. (2004). "Delineation of a Collapse Feature in a Noisy Environment Using a Multichannel Surface Wave Technique." Geotechnique, 54(1), 17-27.

© 2016 Deep Foundations Institute

This page left intentionally blank

© 2016 Deep Foundations Institute

COMPARISON OF NON-DESTRUCTIVE INTEGRITY TESTS ON EXPERIMENTAL DRILLED SHAFTS

Armin W. Stuedlein, School of Civil and Construction Engrg., Oregon State University, Corvallis, OR
Qiang Li, School of Civil and Construction Engrg., Oregon State University, Corvallis, OR
Jim Zammataro, Pile Dynamics, Inc., Cleveland, OH
Daniel Belardo, Pile Dynamics, Inc., Cleveland, OH
Bernie Hertlein, GEI Consultants, Inc., Vernon Hills, IL
Antonio Marinucci, Independent Consultant and Researcher, Brooklyn, NY

ABSTRACT

An experimental program focusing on four drilled shafts was conducted to determine the effect of high strength steel reinforcement bars on lateral resistance, steel casing on axial and lateral resistance, and steel casing without internal reinforcement on lateral resistance. Thermal Integrity Profiling (TIP) Thermal Wires and crosshole sonic logging (CSL) access tubes were installed in each shaft, and thereafter the corresponding non-destructive testing (NDT) was performed on each shaft to assess the integrity of the shafts and to compare the results from the different NDT methods. The results of the CSL tests using scored PVC tubes are compared against those conducted in 73/56 fully-threaded steel hollow bars, whereby the results indicated that the threaded bars served as a good host for performing the CSL tests. The data from the TIP Thermal Wires is compared against the results from the CSL tests for each of the four shafts, and the similarities and discrepancies between the two methods are discussed. This paper will serve as a reference to those interpreting the measurements and data obtained by performing non-destructive integrity tests on drilled foundations.

INTRODUCTION

Non-destructive tests (NDTs) embody a set of critical tools for the evaluation of the integrity of constructed deep foundations, particularly for cast-in-place foundation elements. Construction defects may require the rejection of the foundation element by the owner's representative, resulting in costly repairs or replacements and delays to the project schedule. The use and appropriate interpretation of the results from the NDTs provide the information required when evaluating the integrity of these constructed elements. A cooperative research program was conducted to assess the effects of various construction variables on the axial and lateral performance of drilled shaft foundations, which provided an opportunity to compare the established Crosshole Sonic Logging (CSL) test method to the newer Thermal Integrity Profiling (TIP) Thermal Wire method. This paper presents an overview of the experimental program performed at the geotechnical test site at Oregon State University (OSU), details of the CSL and TIP installation and testing methods, and the results of the NDTs on the constructed drilled shafts. Because one of the shafts was constructed with fully-threaded longitudinal steel hollow bars, this experimental program also allowed the assessment of the use of the hollow bars as access tubes for the CSL tests. Both the CSL and TIP test methods indicated that the shafts were of good quality and free from defects or anomalies; the data obtained using the TIP method also provided an estimate of the as-constructed shaft diameter and the reinforcement cage alignment, which will prove helpful when back-calculating axial and lateral load transfer during future loading tests.

SUBSURFACE CONDITIONS AT THE TEST SITE

The geotechnical test site at OSU has been used for over twenty years as the setting for full-scale geotechnical experimentation. The subsurface conditions have been the focus of numerous investigations, and are summarized by Dickenson and Haines (2006). The geotechnical engineering field research site is approximately 3.5 acres in extent and lies just west of the O.H. Hinsdale Wave Research Laboratory. The

© 2016 Deep Foundations Institute

native soil profile (Fig. 1) generally consists of stiff to very stiff, plastic Willamette Silt (ML/MH, and locally CL/CH) that was deposited in "upper" and "lower" units, separated by a thin seam of dense silty sand (SP/SM). A slightly thicker medium dense to dense sand layer separates the Willamette Silt deposits from a thick and deep deposit of stiff to very stiff, plastic silt and clay (MH/CH). The groundwater table varies from a depth of 0.9 m to 2.3 m (3 ft to 7.6 ft) below the ground surface throughout the year. In general, the plastic deposits communicate very little groundwater; water flows readily through the granular layers and has been observed to initiate caving due to water flow if the shaft cavities are constructed without the use of drilling slurry or temporary steel casing.

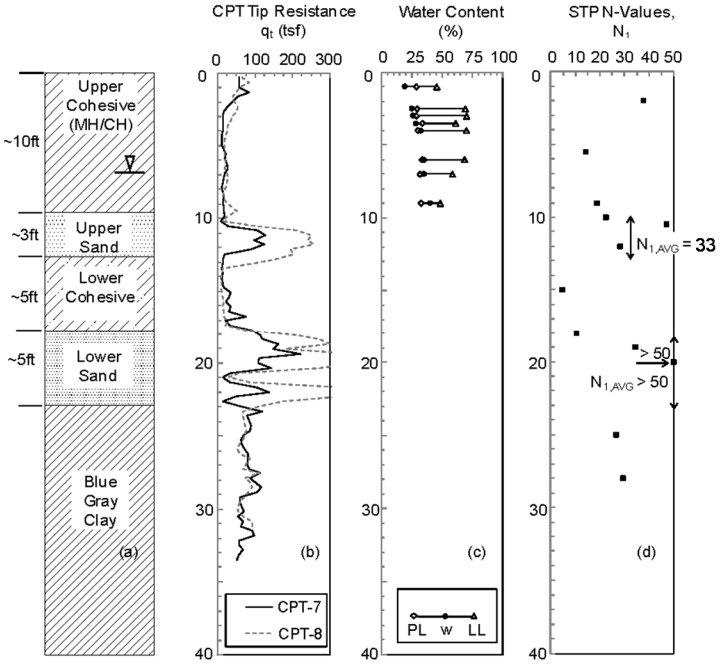


Fig. 1. General stratigraphy and subsurface conditions at the geotechnical test site at OSU (all depths in feet; after Nimityongskul 2011).

SUMMARY OF EXPERIMENTAL PROGRAM AND TEST SHAFTS

The global objectives of the cooperative research program are to study the impact of steel casing and high-strength steel reinforcement on the axial and lateral behavior of full-scale drilled shaft foundation elements and to evaluate the appropriateness of currently used design procedures. The axial and lateral capacity of the four instrumented drilled shafts will be evaluated, including axial load transfer (e.g., *t-z* and *q-z* behavior) and lateral load transfer (e.g., *p-y* behavior). This research aims to confirm the suitability of currently used design and analysis methods, or to suggest recommendations for changes to procedures to maximize the benefit of steel casing and high-strength steel reinforcement cages.

The test shafts were constructed with a nominal diameter of about 0.9 m (36 inches), lengths of about 19.8 m (65 ft), and an embedment of about 18.3 m (60 ft) below the ground surface. Owing to the planned lateral loading tests, the shafts were constructed to extend approximately 1.5 m (5 ft) above the ground surface. Based on discussions with ODOT Bridge Section engineers, one drilled shaft was selected to serve as a baseline shaft to represent the typical amount of internal steel used in drilled shaft foundations that support bridge superstructures. The longitudinal reinforcement for the "baseline" shaft consisted of nine No. 14, Grade 60 deformed steel bars resulting in a reinforcement ratio of about 2% for the longitudinal steel, and the shear reinforcement consisted of two No. 5 spirals at 150 mm (6 inch) spacing. Owing to the use of mild internal reinforcement for the reinforcement cage, this shaft was designated as MIR. The salient features of shaft MIR are summarized in Table 1, and its corresponding typical cross-section, indicating the location of the CSL access tubes and inclinometer casing, is shown in Fig. 2a.

The three remaining shafts were constructed using permanent steel casing and/or high-strength steel reinforcement, and were dedicated to investigating the axial and lateral responses compared to those of the MIR shaft. The shaft with the high-strength internal reinforcement (i.e., HSIR), was constructed with a nominal nine No. 11 Grade 80 (552 MPa or 80 ksi yield stress) longitudinal bars resulting in a reinforcement ratio of about 1.5% for the longitudinal steel, and with two No. 5 spirals of the same grade at 200 mm (8 inch) spacing for the shear reinforcement. The quantity of the longitudinal steel was selected to provide an equivalent magnitude of axial and flexural resisting force in the bars at yield so as

© 2016 Deep Foundations Institute

to make a direct comparison to MIR; thus, the product of yield strength and area of steel are equal for MIR and HSIR. For the HSIR shaft, three #11 bars were substituted with 73/56 (outside/inside diameter in mm) hollow fully-threaded Grade 80 (552 MPa or 80 ksi yield stress) bars that provided both the necessary structural requirements and the access for CSL testing. To prevent the intrusion into the hollow bar of drilling fluid and/or concrete during construction, the base of the hollow bar was capped with welded steel plate. The CSL testing was performed in general accordance with ASTM D6760 (ASTM 2014a)

Table 1. Summary of experimental characteristics of instrumented test shafts. The total and embedded length of each shaft is 19.8 m (65 ft) and 18.3 m (60 ft), respectively.

Test Shaft and Designation	Diameter m (in)	Casing Wall Thickness mm (in)	Internal and External Steel (%)	Actual Volume of Concrete m^3 (yd^3)
Mild Internal Steel Reinforcement (MIR)	0.9 (36)	0	2.00	16.1 (21.0)
High-strength Internal Reinforcement (HSIR)	0.9 (36)	0	1.50	15.3 (20.0)
Cased, Mild Internal Reinforcement (CIR)	0.9 (36)	12.5 (0.5)	7.20	13.3 (17.4)
Cased, No Internal Reinforcement (CNIR)	0.9 (36)	12.5 (0.5)	5.33	13.2 (17.3)

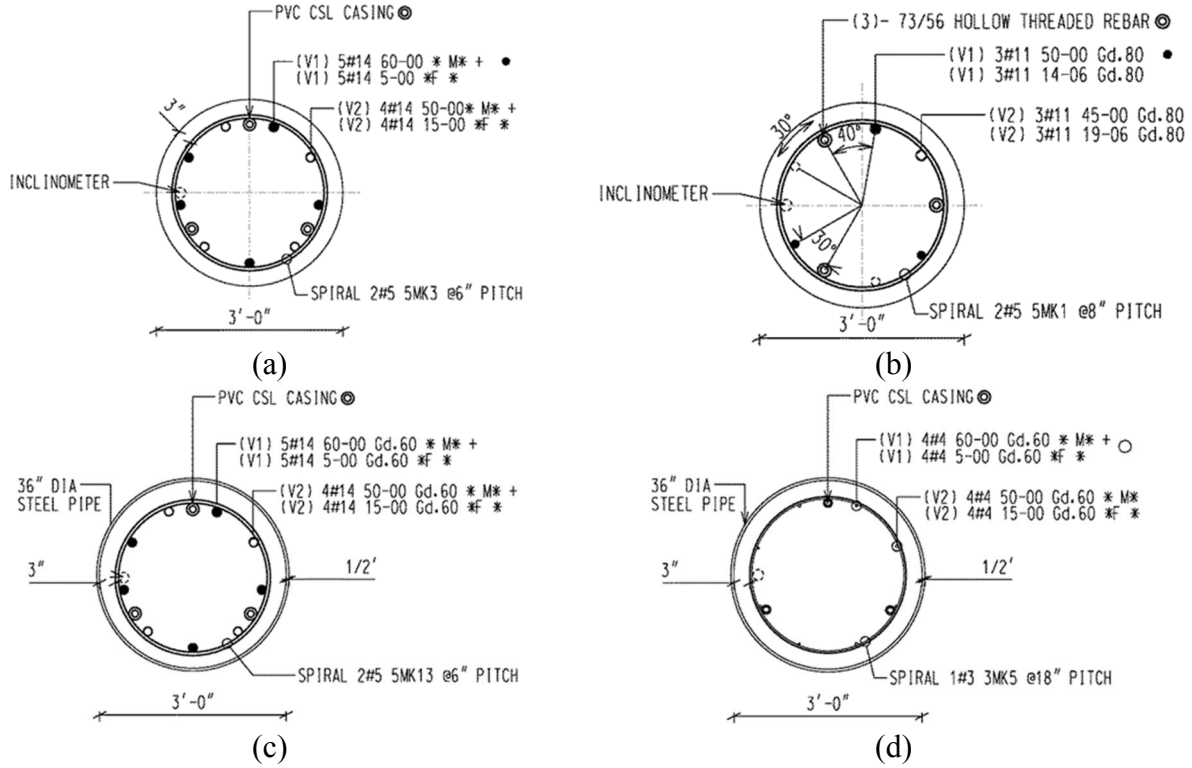


Fig. 2. Cross-section of proposed test drilled shafts: (a) MIR, (b) HSIR, (c) CIR, and (d) CNIR. Note: all units in imperial units; the outside diameter of steel casing was 37" (inside diameter shown in figure).

The main benefit expected from the use of Grade 80 longitudinal and spiral steel reinforcement in drilled shaft construction is to provide larger openings in the reinforcement cage compared to those realized with Grade 60 steel, allowing for enhanced flowability of the concrete and reduced frequency of shaft anomalies or defects. For the HSIR shaft, the hollow fully-threaded bars eliminated separate CSL access tubes, resulting in a significantly less congested reinforcement cage compared to the baseline shaft (Fig. 3a). A typical cross-section of the HSIR shaft indicating the locations of the hollow bars and inclinometer

© 2016 Deep Foundations Institute

casing and the experimental characteristics of the HSIR shaft are provided in Fig. 2b and Table 1, respectively. A photograph of the top of the as-constructed HSIR shaft is shown in Fig. 3b.

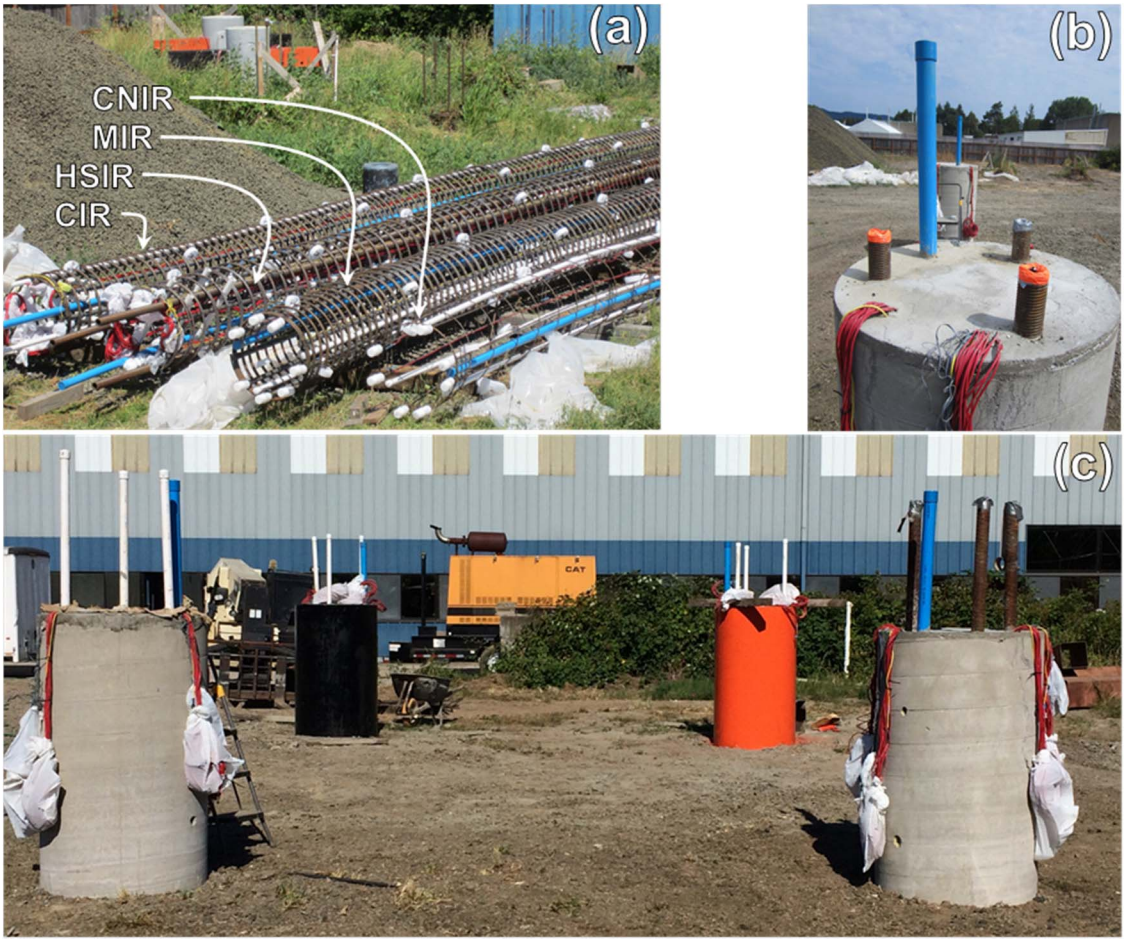


Fig. 3. Photographs indicating (a) the as-built, instrumented test shafts, (b) shaft HSIR with hollow threaded bar, and (c) shafts MIR, CNIR, CIR, and HSIR starting from the left proceeding right.

The two remaining shafts were constructed with permanent steel casing, which consisted of a 940 mm (37 inch) outside diameter with a wall thickness of 12.5 mm (1/2 inch). In addition to the permanent steel casing, one shaft was constructed using mild, Grade 60 reinforcing steel (yield strength of 414 MPa or 60 ksi) and a reinforcement ratio of 2% for the longitudinal bars, and is therefore similar to the MIR shaft except for the permanent casing. This shaft is designated CIR for "cased, internally-reinforced." The fourth shaft was constructed with permanent steel casing and an internal reinforcement cage (reinforcement ratio of 0.15%) consisting of just enough reinforcement bars (Grade 60) to deliver strain gages to the necessary elevations; the designation for this shaft is CNIR ("cased, no internal reinforcement"). Shaft CNIR was drilled using a 940 mm (37 inch) earth auger, whereas CIR was drilled using a 915 mm (36 inch) auger to evaluate the effect of subtle construction differences on axial resistance. For shafts CIR and CNIR, the main goal was compare directly the effect of internal and external steel reinforcement on the lateral response of drilled shafts. A typical cross-section for shafts CIR and CNIR is shown on Figs. 2c and 2d, respectively.

A photograph of the as-built and instrumented test shafts MIR, CNIR, CIR, and HSIR, respectively from left to right, is shown in Fig. 3c. Shafts MIR and HSIR were constructed with full-penetration access

© 2016 Deep Foundations Institute

tubes relatively parallel to the shaft's cross-section to facilitate connection of the hydraulic actuator that was used to perform the lateral loading test. Whether or not the voids from the access tubes could be detected by the various NDT methods described herein was of interest in this study, as was the suitability of the hollow fully threaded bars for CSL testing purposes.

NON-DESTRUCTIVE TESTING AND RESULTS

Description of Non-Destructive Test (NDT) Methods Evaluated

Crosshole Sonic Logging (CSL) - The test shafts were evaluated using two NDT methods: the Crosshole Sonic Logging method and the Thermal Integrity Profiling Thermal Wires method. The Crosshole Sonic Log (CSL) method is a downhole testing technique using ultrasonic pulse velocity (UPV), which is standardized in ASTM Standard D6760 (ASTM, 2014a). The UPV through concrete is a function of the density, age, and Young's modulus of the material, and can therefore be used to assess the as-constructed quality of the material. In this bottom-up method, a transmitter and receiver are simultaneously raised upward along the shaft within the access tubes, thereby allowing the measurement of the UPV along the ray path of the compressive *p*-wave signal. When a series of velocity measurements are made at uniform spacing (between transmitter and receiver) along a uniform path length, the measurements can be plotted graphically (e.g., in a "waterfall" plot) to permit a rapid visual assessment of material uniformity. It is critical that the access tubes be installed at uniform spacing along the entire length of the shaft. A rule of thumb for the minimum number of access tubes in a shaft is one tube per 0.3 m (1 ft) of shaft diameter but no less than 3 tubes (Brown et al., 2010), and this approach was followed for the test specimens evaluated herein.



Fig. 4. Instrumented reinforcement cage MIR showing scored PVC and Thermal Wires.

Access tubes are typically 51 mm (2 inch) in inside diameter, are either PVC or steel pipe, and are fixed to the reinforcement cage prior to placement in the excavated shaft cavity. Prior to concreting, the access tubes are filled with water to counter buoyancy, to facilitate maintaining uniform temperatures during the curing of the shaft concrete (which the potential of debonding of the pipe from the concrete), and to assist with the transmission and receiving of the UPV signal. *P*-wave velocities in good quality concrete will range from 3,600 to 4,400 m/s (11,800 to 14,400 ft/s) depending on the density, age, and Young's modulus of the concrete. One can identify anomalies by comparing the measured *p*-wave velocity to the expected velocity for the given concrete mix design and stiffness. Zones of concrete that have voids, contaminated concrete, segregation of aggregate from the paste, soil inclusions, or other possible anomalies will yield slower UPVs. The CSL method has been widely accepted as a NDT for integrity assessment and quality assurance of drilled shaft construction due to its relatively inexpensive cost and relatively rapid execution. Unfortunately, CSL testing can only measure the velocity of the material in a straight line between the transmitter and receiver, cannot test the material between the soil-shaft interface and the reinforcement cage, and cannot give, therefore, an indication of the thickness or quality of the concrete cover.

© 2016 Deep Foundations Institute

The CSL access tubes used in the test shafts were constructed using PVC pipes, which, as discussed above, are subject to debonding (Fig. 4). To mitigate the risk of debonding, the surface of each segment of PVC pipe was scored and roughened along its entire length by rotating and advancing the pipe through a scoring box. This approach produced a very rough surface intended to improve the bond strength of the pipe to the concrete. In general accordance with established best practices, each of the PVC pipes were filled with water soon after the installation of the reinforcement cages.

Thermal Integrity Profiling (TIP) Thermal Wires - Thermal integrity profiling uses the heat generated by the curing cement (i.e., hydration energy) to assess the quality of cast-in-place concrete foundations, such as drilled shafts, bored piles, augered cast-in-place piles, continuous flight auger piles, and drilled displacement piles. The expected temperature at any location depends on the shaft diameter, mix design, time of measurement, and distance from the center of the shaft. Anomalies such as soil inclusions, voids, segregated concrete, and alignment of the reinforcement cage can be determined by measuring the hydration temperatures during the curing phase. The relationship between the shaft diameter and hydration temperature tends to be linear in the region near the cage; therefore, the actual shape of the shaft can be estimated (Mullins, 2010). Because this method relies on the heat of hydration, TIP testing is performed near the time of peak temperature, generally taken between 12 and 48 hours after concrete placement, depending on the shaft diameter and mix design, and in accordance with ASTM D7949 (ASTM, 2014b).

For the test shafts, data was acquired using full length Thermal Wires® that were tied to the reinforcement cage (e.g., yellow wires in Fig. 4). Typical practice requires one wire for each foot of shaft diameter but with a minimum of four wires, which are installed prior to placement of the reinforcement cage and prior to concreting. Data loggers are attached to each wire at the top of the shaft and collect temperature measurements in 15 minute increments, typically until after the peak temperature has been reached and has begun to decay. TIP measurements that are cooler than the average indicate necking, inclusions, or poor quality concrete, whereas warmer than average measurements are indicative of bulges. In general, temperature variations of +/- 2 °C are within the normal range for TIP results due to variations in the cable location and unavoidable shifting or movement of the reinforcement cage during installation in the shaft excavation and during concreting. Anomalies are indicated by abrupt changes in temperature at a particular depth. Diametric variations of temperature across the shaft reveal misalignments of the cage. The recorded measurements can be imported into commercial software that graphs the temperature vs. depth data and that can generate a 3D model of the shaft geometry, which incorporates the actual volume of concrete poured.

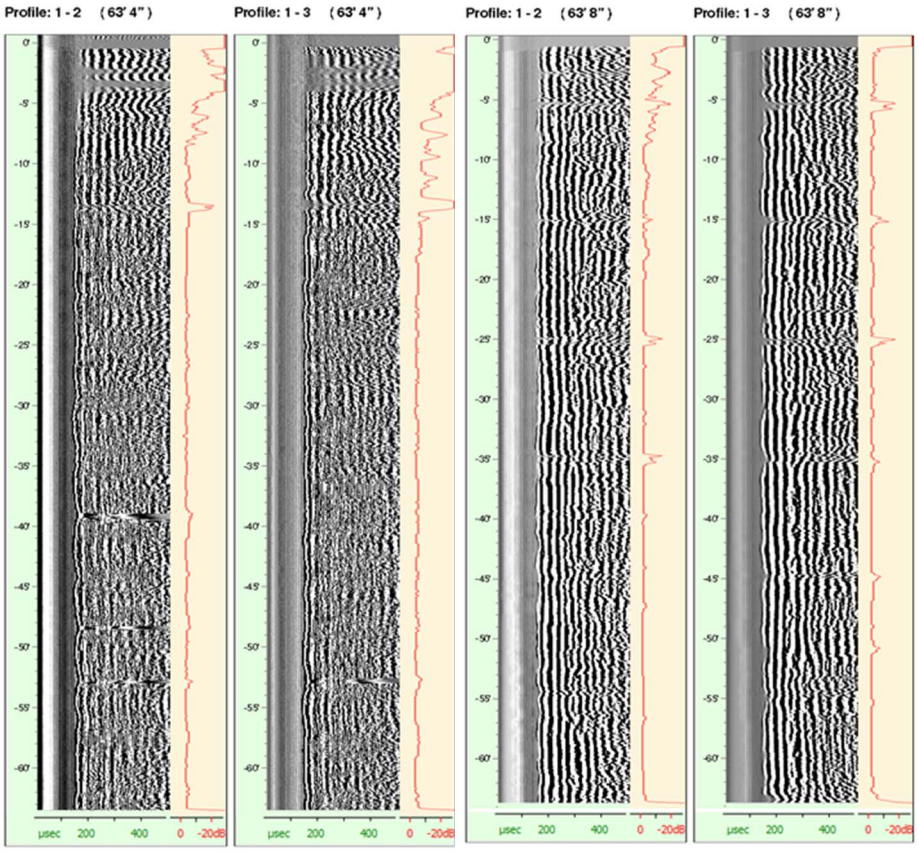
CSL Test Results

The drilled shafts were constructed on June 16 and 17, 2015, and the CSL tests were performed approximately 3 weeks later on July 6, 2015. The results from the CSL testing performed on shaft MIR indicated two thin zones of reduced pulse energy and velocity reductions on all three profiles at depths of about 1.2 m (4 ft) and 4.3 m (14 ft) below the top of the concrete. As shown on Fig. 5a, profiles 1-2 and 1-3 also revealed reduction in the velocity and energy at depths of about 0.6 m (2 ft) and 1.07 m (3.5 ft) below top of concrete. These velocity reductions were attributed to the horizontal, full penetration PVC pipes that were added to the shaft for connection of the hydraulic actuator for the lateral loading test. Some electrical interference was apparent as denoted by the horizontal streaks in the lower portions of profiles 1-2 and 1-3. The typical CSL pulse velocity was about 3,760 m/s (12,320 ft/s), and no significant anomalies were detected for the MIR shaft.

For shaft HSIR, the CSL test results indicated thin zones of reduced pulse amplitude and velocity reduction at multiple locations recurring at intervals of about 3 m (10 ft), starting at a depth of about 1.5

© 2016 Deep Foundations Institute

m (5 ft) below top of concrete, but there was no evidence of any significant anomalies (Fig. 5b). These regular indications of reduced UPV correlate to the location of couplers used to connect the segments of the 3 m (10 ft) long hollow fully threaded bars. Couplers have contributed to the partial segregation of the aggregate from the cement paste and/or to the partial consolidation of the concrete. The typical CSL pulse velocity for the HSIR shaft was about 3,770 m/s (12,360 ft/s).



(a) *(b)*

Fig. 5. Full depth sample CSL test results for (a) MIR, and (b) HSIR.

For the CIR shaft, the CSL profiles indicated minor variation in the first arrival time (FAT) of the pulse and in the pulse energy from a depth between about 0.6 m (2 ft) and 1.38 m (4.5 ft) below the top of concrete. Local, random electrical noise appeared to disturb the UPV signal in one of the profiles; however, no evidence of any significant anomalies was noted in the CIR shaft. The typical CSL pulse velocity for this shaft was approximately 3,910 m/s (12,830 ft/s).

Based on the CSL test results for the CNIR shaft, there was a thin zone located around a depth of about 1.07 m (3.5 ft) below the top of concrete where both the pulse energy and the velocity were diminished by as much as 50% of the pulse energy and velocity outside of this zone. Similar small zones were observed at multiple locations recurring at intervals of about 3 m (10 ft) along the length of the shaft, but these zones produced progressively less velocity reduction with increasing depth. These observations were attributed to localized zones of partial segregation or lack of consolidation associated with the PVC tube couplers. The typical CSL pulse velocity for the CNIR shaft was about 3,820 m/s (12,770 ft/s).

Of interest is the comparison of the signals from the CSL test results obtained using the PVC tubes and the hollow threaded bars. Representative wave forms obtained from within MIR and HSIR shafts are shown in Fig. 6. The signal generated within shaft MIR is erratic, complex, of higher frequency, and low amplitude; furthermore, such signals are more difficult to interpret. Conversely, the signal generated within shaft HSIR produced very clean, crisp, and well-defined waveforms that are clear and easy to interpret. The advantage of receiving clean signals may be observed in the comparison of waterfall plots, where the stacked signals are separated by thick, well-spaced parallel lines indicative of good signals for shaft HSIR (Fig. 5b) compared to muddled signals for shaft MIR (Fig 5a). Thus, the use of hollow threaded bars appears well suited as a quality control component, which could help alleviate congestion

© 2016 Deep Foundations Institute

within the reinforcement cage and could minimize the potential for anomalies or defects in a completed shaft.

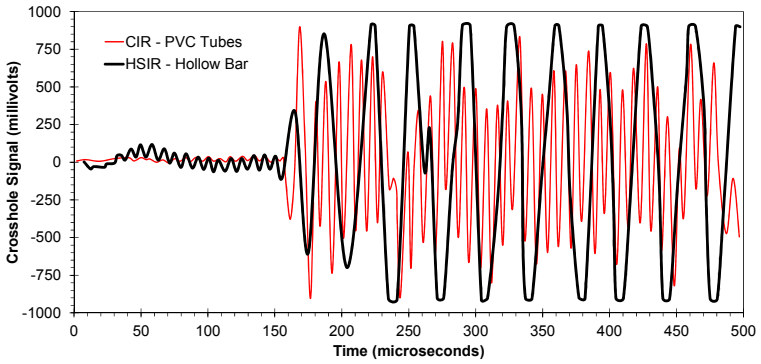


Fig. 6. Comparison of typical wave forms developed within PVC and hollow threaded bar.

TIP Test Results

The collection of thermal data using the TIP Thermal Wires® commenced several hours following the completion of construction on June 16 and 17, 2015, for shafts MIR and HSIR, and for shaft CIR, respectively. No TIP thermal data was collected for shaft CNIR. For each shaft instrumented with TIP Thermal Wires®, data was collected at 15 minute intervals for approximately five days. In general, the results from TIP included profiles of measured temperature and calculated shaft radius versus depth. The calculated shaft radius incorporates the measured thermal profile, the reported shaft length, and the actual volume of concrete used (Table 1). Given sufficient thermal measurement points, the calculated radius can be interpolated from the four Thermal Wires distributed around the perimeter of the reinforcement cage. Shafts MIR, HSIR, and CIR reached peak temperature approximately 46, 49, and 46 hours, respectively, after placement. The presence of the permanent casing in shaft CIR did not appear to affect the time required to obtain peak heat of hydration temperature.

Representative results from the TIP measurements obtained for shaft MIR are presented in Fig. 7. The reinforcement cage for shaft MIR was overlaid on a 2D color spectrum map to improve the visualization of the estimate radius profile (Fig. 7a). The average calculated radius is consistently larger than the design shaft radius of 0.45 m (18 inches), with a generally decreasing radius with depth. The shaft radius generally increases to a maximum of 0.58 m (23 inches) for depths between 6 to 7.5 m (20 to 25 ft), which is consistent with the location of the lower sand layer (Fig. 1). The thermal results also indicate that the reinforcement cage is slightly shifted along the instrumented length of the shaft; however, the concrete cover provided to the cage is never less than 75 mm (3 inches). The alignment of the reinforcement cage is shifted such that Wires 1 and 2 are closer to the center of the shaft (and therefore exhibit higher temperatures) and Wires 3 and 4 are closer to the shaft-soil interface (indicated by lower temperatures). Temperature reduction (termed "roll-off") was observed to begin at a depth of approximately 1.5 m (5 ft) below the top of the shaft, which is caused by heat loss due to the exposure of the concrete to ambient air temperatures. However, the high temperature above the ground surface was attributed to the insulating-effect of the cardboard sonotube form used to temporarily support the fresh concrete. Shaft

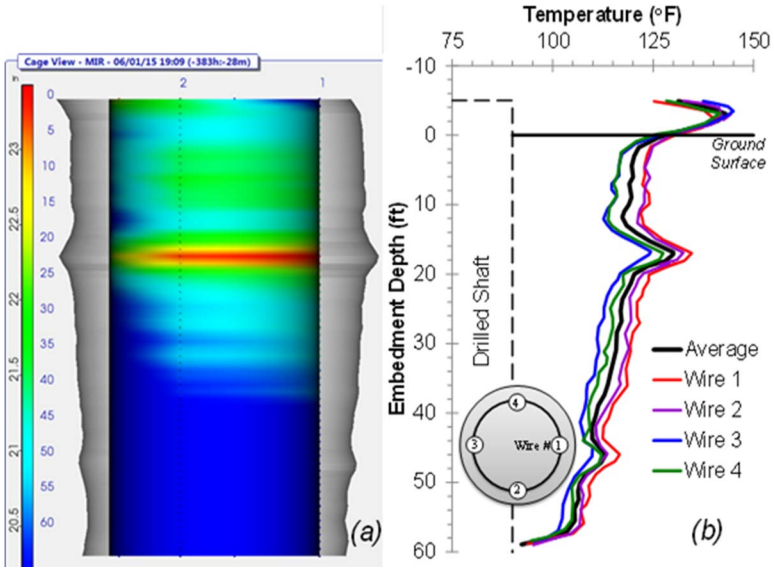


Fig. 7. TIP results for shaft MIR (a) variation of radius map with depth inferred from thermal measurements, and (b) actual depth profiles of temperature measured along four points on reinforcement cage. Note: figure (a) shows depth beginning at the top of shaft (1.5 m above ground surface).

© 2016 Deep Foundations Institute

HSIR also exhibited this temperature signature (Fig. 8), whereas shaft CIR did not, thereby indicating that the heat-conductive steel casing does not produce an insulating effect. Temperature roll-off also occurred at the bottom of shaft MIR, which was caused by heat loss at the shaft-soil interface at the base of the shaft. The shaft bottom temperature roll-off begins at a depth of approximately 1.5 m (5 ft) above the shaft base (Fig. 7b). No anomalies were identified around the base of the shaft.

The TIP results (i.e., average temperature- and radius-vs.-depth profiles) for the three TIP-instrumented shafts are compared in Fig. 8. Slight variations in temperature are noted between shafts MIR and HSIR, which can be due to slight differences in the concrete mix; however, the profiles are quite similar resulting in a similar estimate of radius with depth. Localized increases in radius in the sandy seams are consistent with caving susceptibility that was observed in other shaft construction at the OSU test site. The profile of the estimated radius provides excellent guidance for the back-calculation of unit side and lateral resistance derived from the planned axial and lateral loading test programs. The accuracy of the radius calculation can be observed in the computed radius for the cased shaft, as shown in Fig. 8b, which has a known, full-depth inner radius of 0.45 m (18 inches). Comparing the measurements of the individual thermal wires in shafts HSIR and CIR indicated that the cages were very well centralized within the casing. Shaft HSIR had, on average, more than 75 mm (3 inches) of cover along the entire depth, whereas shaft CIR yielded an even 75 mm of cover due to the permanent casing (Fig 8b). Interestingly, the average temperature profile produced by shaft CIR was smaller in magnitude along much of its depth than those of shafts MIR and HSIR, which may have resulted from the highly conductive steel casing forming the edge of the shaft. Compared to the rest of the temperature profile below ground surface, the temperature of shaft CIR between the ground surface and a depth of 1.5 m (5 ft) was slightly larger. An increase in temperature in uncased shafts typically indicates an increase in shaft radius; however, since shaft CIR was constructed with casing, this increase in temperature appears to be the result of an air gap located outside of the permanent casing, which acted as an insulator. The increase in temperature appears to terminate at a depth consistent with the ground water table. Based on the TIP results, it may be concluded that shafts MIR, HSIR, and CIR are of continuous construction and free from serious anomalies.

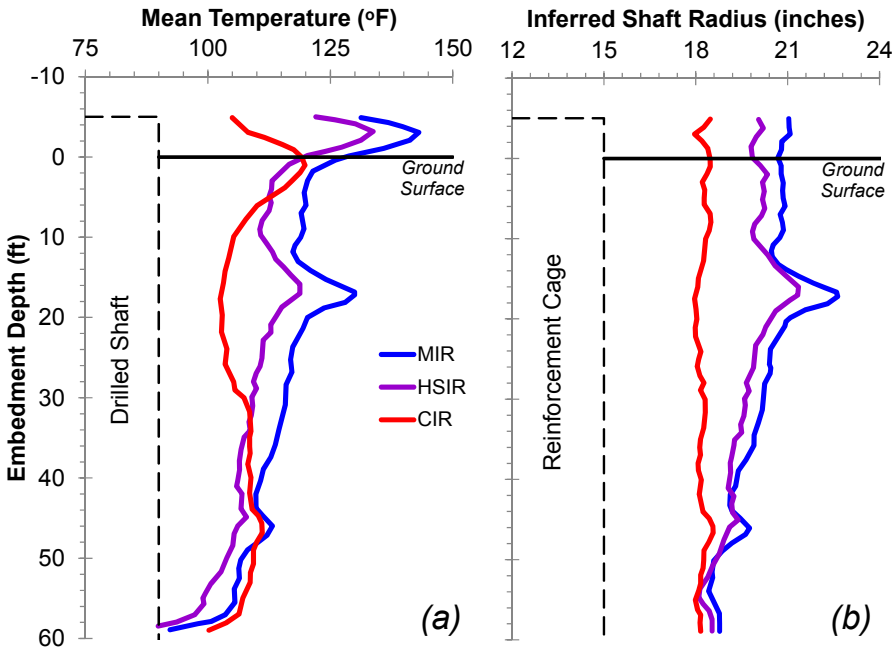


Fig. 8. Comparison of average (a) temperature-depth profiles, and (b) radius-depth profiles for shafts MIR, HSIR, and CIR.

CONCLUDING REMARKS

Four instrumented test shafts were constructed at the geotechnical engineering field research site at Oregon State University, and were evaluated for integrity using the well-established Crosshole Sonic Logging (CSL) and the new Thermal Integrity Profiling (TIP) Thermal Wires® non-destructive testing methods. The shafts were constructed with and without high strength steel reinforcement bars (shafts

© 2016 Deep Foundations Institute

HSIR and MIR, respectively), and with permanent steel casing with and without internal reinforcement steel (CIR and CNIR, respectively). Based on the results from the integrity tests, the four shafts were constructed without significant anomalies. Significantly cleaner *p*-wave velocity signals were produced for the CSL tests performed using hollow fully threaded steel access tubes compared to those tests using roughened PVC access tubes, thereby resulting in improved clarity in the waterfall plots. These results indicate that there are no barriers to the use of hollow threaded bars in both structural applications and quality control. In addition, the locations of pre-fabricated voids that were used for mounting the hydraulic actuator for the lateral loading tests were identified by the CSL measurements.

The TIP results indicated that the reinforcement cage of shaft MIR was slightly misaligned, but that the entire reinforcement cage had sufficient concrete cover along the length of the shaft. For shafts HSIR and CIR, the TIP results indicated that these shafts were well-centralized and had sufficient concrete cover. Using the TIP method, the thermal measurements will be exceptionally useful in determining the shaft radius with depth, which will facilitate accurate back-calculation of axial and lateral load transfer. Unfortunately, the TIP Thermal Wires® were not able to identify the small, pre-fabricated voids in shafts MIR and HSIR; however, these voids would not be likely to cause rejection of production shafts.

ACKNOWLEDGEMENTS

The authors wish to acknowledge the many agencies, firms, and individuals who have contributed to the ongoing research effort. The authors are grateful for support from the Oregon Department of Transportation through grant SPR 765 and from the Pacific Northwest Transportation Consortium (PacTrans) through grant DTRT12-UTC10. The West Coast Chapter (WCC) of the ADSC contributed funds to help offset material costs associated with the construction of the test shafts, with critical coordination efforts and guidance provided by John Starcevich (Malcolm Drilling, Inc.), Becky Patterson (WCC ADSC), and Rick Walsh (Hayward Baker, Inc.). Malcolm Drilling, Inc. constructed the test shafts; Pacific Foundation, Inc. installed the reaction piles; and Ralph's Concrete donated the concrete pumping services. The Grade 80 solid and hollow steel reinforcement bars were donated by ConTech Systems, whereas the Grade 60 steel reinforcement bars and all cage fabrication was donated by PJ's Rebar. The permanent steel casing was donated by Skyline Steel, and the Grade 150 steel reinforcement bars for the reaction anchors were contributed by Williams Form, Inc. Spacers and bar boots were provided by Foundation Technologies. Crosshole sonic logging services was donated by GEI Consultants; and Thermal Integrity Profiling Thermal Wires® and logging services were provided by Pile Dynamics, Inc.

REFERENCES

ASTM (2014a) "Standard Test Method for Integrity Testing of Concrete Deep Foundations by Ultrasonic Crosshole Testing," *ASTM D 6760*, ASTM International, West Conshohocken, PA, 7 pp.

ASTM (2014b) "Standard Test Methods for Thermal Integrity Profiling of Concrete Deep Foundations," ASTM D 7949, ASTM International, West Conshohocken, PA, 7 pp.

Brown, D.A., Turner, J.P., & Castelli, R.J. (2010) "Drilled shafts: Construction procedures and LRFD design methods," *Report No. FHWA-NHI-10-016*, US Department of Transportation, Federal Highway Administration, Washington, D.C.

Dickenson, S.E. and Haines, B.Z. (2006) "Characterization of the Geotechnical Engineering Field Research Site at Oregon State University," *3rd Edition*, Oregon State University, 231 pp.

Mullins, G. (2010) "Thermal Integrity Profiling of Drilled Shafts," *Journal of the Deep Foundations Institute*, 4(2), pp. 54 – 64.

Nimityongskul, N. (2011) "Effects of Soil Slope on Lateral Capacity of Piles in Cohesive Soils," *PhD Thesis*, School of Civil and Construction Engineering, Oregon State University.

© 2016 Deep Foundations Institute

ANALYSIS OF STRUCTURAL CAPACITY AND STIFFNESS OF DRILLED SHAFTS WITH CONSTRUCTION DEFECTS AND REPAIRS

Benjamin J. Turner, Dan Brown and Associates, Arroyo Grande, CA, bturner@dba.world
John P. Turner, Dan Brown and Associates, Laramie, WY, jturner@dba.world

ABSTRACT

Non-destructive testing and evaluation (NDT/NDE) methods have become standard tools as part of the post-construction quality assurance of drilled shaft foundations. In responding to anomalies, foundation designers, owners, and contractors face a number of choices, including: (i) acceptance of a shaft with known anomalies, (ii) further investigations of integrity (*e.g.*, concrete coring), (iii) repair schemes, and (iv) reject and replace. To assist in selecting the best option, analyses are often performed that involve assessing the structural performance of reinforced concrete shafts that may include defective concrete or voids. Currently, the analytical tools for predicting the flexural strength and stiffness of drilled shafts with defective concrete located in discrete regions of the cross section are limited. This paper presents a robust moment-curvature analysis tool for drilled shafts based on the fiber-element discretization method. The tool allows for consideration of anomalous or defective concrete regions in the shape and location that they are believed to exist in the shaft while considering explicitly the nonlinear material behavior of the intact regions based on expected material properties. A case study is used to illustrate the practical application of the analysis to drilled shaft projects.

Keywords: drilled shafts, anomalies, construction defects, defective concrete, structural design of foundations

INTRODUCTION

Imperfections such as defective concrete or accidental eccentricity of reinforcing cages are an inherent part of the drilled shaft construction process that will occur occasionally even when construction best-practices are followed. Petek et al. (2002), O'Neill and Sarhan (2004), Poulos (2005), and others have described the effects that construction defects can have on the axial and lateral performance of drilled shafts. Our industry has seen rapid progress in recent years in the development and improvement of tools for detecting drilled shaft anomalies, such as gamma-gamma and crosshole-sonic logging, sonic-echo testing, thermal integrity profiling, and even visual inspection with invasive video cameras. Nonetheless, in most cases the wealth of data from these tests is used by foundation engineers to make a fairly "black or white" decision—should the defects be repaired, or should the shaft be rejected? A third option that is not typically considered is to directly analyze the section, including anomalies, and compare the reduced strength and/or ductility to the actual project demands. This option takes full advantage of the data collected during integrity testing, and may provide a justifiable means for avoiding further construction costs and delays, whether for repair or replacement.

One of the reasons this alternative is not commonplace is that conventional analysis tools do not provide a means for analyzing the structural resistance (*i.e.*, strength), and load-versus-displacement (*i.e.*, stiffness and ductility) characteristics of reinforced concrete sections that include defects. This paper presents a method for quantifying the lateral-load response of drilled shafts through finite-element analysis of a fiber model, sometimes referred to as "fiber-element" or "fiber-section" analysis. Following an explanation and

© 2016 Deep Foundations Institute

verification of the method, a case study is presented in which the tool was used to develop a realistic alternative to a costly repair scheme.

FIBER-ELEMENT ANALYSIS METHOD

The authors developed a finite-element program to analyze a circular drilled shaft section including zones of defective concrete. The program is executed using the *OpenSees* interpreter and software framework (McKenna et al. 2010). Development of the model and verification that the program can perform accurate moment-curvature analysis of reinforced-concrete sections by comparison of results to other commercially available structural analysis software are presented in this section. *OpenSees* is an open-source finite-element analysis platform for performing structural and geotechnical analysis. Besides being free, the primary advantage of *OpenSees* over commercially available software is that every aspect of the analysis is directly controlled by the user, giving unparalleled ability to model irregular and unique systems.

For this verification, results generated using the authors' program are compared to results from the computer programs *XSECTION*, developed and used by Caltrans, and *CONSEC*, a commercial program developed by the company StructSource that is used in industry and by other transportation agencies to perform reinforced-concrete section analysis. The example problem used for comparison is documented on the website http://structsource.com/pdf/Momcurv_web.pdf (Mathews 2001). All three programs analyze a so-called "fiber model" in which the section is discretized into separate zones (fibers) characterized by unique uniaxial stress-strain behavior representative of reinforcing steel, confined concrete, unconfined concrete, and/or defective concrete. Finite-element analysis of a fiber model is a more robust approach for defining moment-curvature relationships than conventional "method of slices" approaches implemented by hand calculations or in a spreadsheet solution because the complex nonlinear stress-strain behavior of the materials can be handled independently and exactly. Furthermore, fiber models can exactly capture circular cross sections by using radial discretization rather than a series of linear slices which approximate the section geometry.

Verification Problem Definition

Moment-curvature analysis is performed for a 36-inch diameter circular reinforced concrete section representative of a column or drilled shaft foundation. Reinforcement consists of longitudinal bars and spiral transverse bars. The effects of confinement provided by the transverse steel is considered explicitly according to the recommendations of Mander et al. (1988). The confined concrete core exhibits increased strength and ductility in comparison to unconfined concrete, and consideration of these effects is not only more accurate but also beneficial from a design point of view. The confined concrete properties are estimated based on the unconfined concrete properties and the transverse reinforcement details (*e.g.*, transverse bar size, spiral pitch, yield stress, etc.). The Mander et al. (1988) equations for computing the confined concrete stress-strain relationship are not replicated here but can be found for the specific design values of this example in the Mathews (2001) reference. The steel stress-strain relationship considers an initial linear range of behavior up to the yield stress followed by a perfectly-plastic plateau to the strain hardening strain, followed by strain hardening to the ultimate stress. The initial tangent of the strain hardening range is taken as 1/30 of the initial elastic modulus. The section is shown in Fig. 1 and material properties are given in Tables 1 and 2, below.

© 2016 Deep Foundations Institute

Table 1: Concrete material properties. After Mathews (2001) example.

Parameter	Value	
	Unconfined Concrete[a]	Confined Concrete[a]
Maximum Stress	5,200 psi	6,900 psi
Strain at Maximum Stress	0.002	0.00527
Ultimate Stress	2,500 psi	3,300 psi
Ultimate Strain	0.005	0.01432[b]
Initial Modulus of Elasticity	4,110,328 psi	4,110,328 psi

Notes:
[a] Using Mander et al. (1988) equations.
[b] Using formula by Priestley et al. (1996)

Table 2: Steel material properties. After Mathews (2001) example.

Parameter	Value
Yield Stress	68,000 psi
Yield Strain	0.0023
Initial Modulus of Elasticity	29,000 ksi
Hardening Strain	0.0125
Ultimate Stress	95,000 psi
Ultimate Strain	0.09

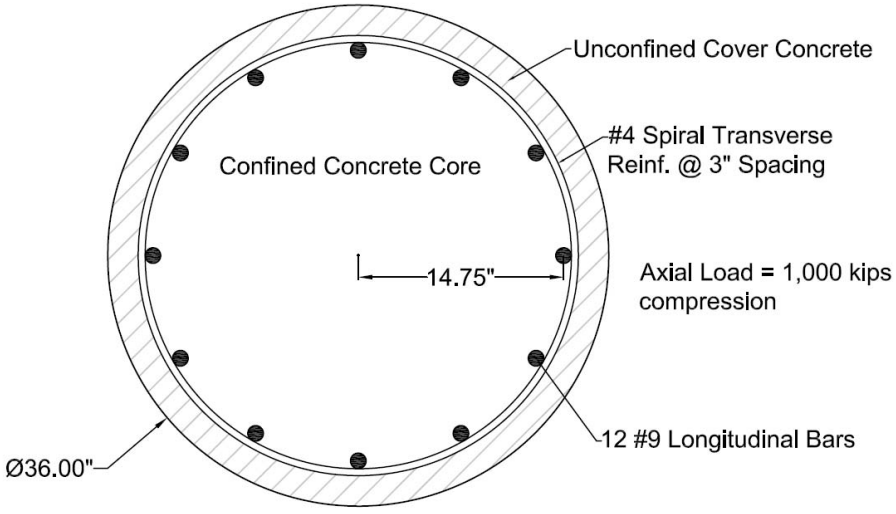


Fig. 1: Example section for moment-curvature analysis.

© 2016 Deep Foundations Institute

OpenSees *Modeling Parameters*

The *OpenSees* software framework includes several uniaxial material models for concrete and steel to capture various aspects of cyclic and monotonic behavior. For this exercise, the *UniaxialMaterial Concrete02* and *UniaxialMaterial ReinforcingSteel* material models were used with the parameters defined in Tables 1 and 2. These material models were chosen because they are based on the same theoretical stress-strain relationships for concrete (Mander et al. 1988) and steel (Chang and Mander 1994 family of models) as the models utilized by *XTRACT* and *CONSEC*. More information about these material models can be viewed at: http://opensees.berkeley.edu/wiki/index.php/UniaxialMaterial_Command .

The moment-curvature relationship is determined by imposing incrementally larger values of curvature to the section and using a finite-element solution approach to solve for the corresponding moment. The following assumptions are used for the moment-curvature analysis:

- Plane sections remain plane during bending (Euler-Bernoulli beam theory),
- Strain compatibility between the concrete and longitudinal steel reinforcement,
- Concrete strength in tension is neglected to account for the potential of cracking prior to extreme event loading, and
- Constant axial load with zero eccentricity at all levels of curvature.

Verification Problem Results

The moment-curvature results are shown in Fig. 2. The results from the authors' program are in excellent agreement with the results from *XSECTION* and *CONSEC* in terms of initial flexural rigidity (*EI;* which is the slope of the moment-curvature plot), prediction of cracking moment, post-yield stiffness, and ultimate moment strength. The slight deviation between the *OpenSees* results and the other results observable in Fig. 2 in the range immediately following yielding is due in part to the assumption made by *XSECTION* and *CONSEC* that the confined concrete core extends to the centerline of the transverse reinforcement spiral. While this is true at the level of the transverse steel, the theoretical and experimental observations of Mander and his colleagues clearly showed that in the region between the spiral reinforcement bars, the zone of effective confinement does not extend all the way to the radius defined by the spiral (15.75 inches in this case). A more appropriate average radius of the confined zone is defined to the center of the longitudinal bars (14.75 inches in this case), which is the assumption implemented in the authors' results shown in Fig. 2. The remaining deviations between the different software results arise because of slight variations in the shape of the stress strain curve between the peak stress and ultimate stress (or between peak and strain hardening for the steel).

When moment-curvature analysis is performed to define specific properties such as the nominal moment, ultimate moment, effective *EI* before and after yielding, *etc.*, for simple limit state designs, the slight variation between the software results is negligible. For more sophisticated nonlinear modeling of structures in which the moment-curvature relationship will be used directly in subsequent finite element analyses, the subtle differences may become more important and the analyst should use the most accurate approximations such as described herein for the *OpenSees* analysis. These results demonstrate that the authors' program, executed in *OpenSees*, is capable of performing accurate moment-curvature analysis for reinforced concrete sections, and furthermore provides more advanced and more realistic user control over material stress-strain properties than other commercially-available software.

© 2016 Deep Foundations Institute

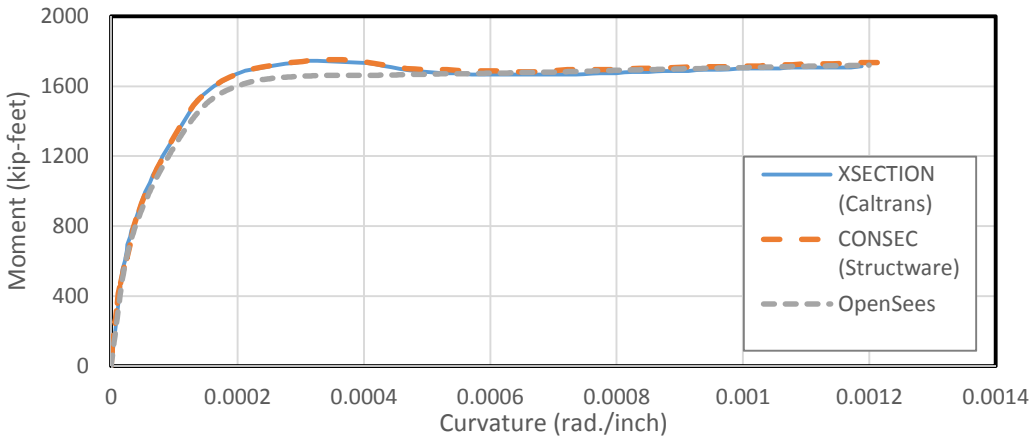


Fig. 2: Moment-curvature analysis results for 36-inch diameter R.C. section with twelve No. 9 longitudinal bars and axial load *P* = 1,000 kips compression.

CASE STUDY: MOMENT-CURVATURE ANALYSIS FOR DRILLED SHAFT FOUNDATIONS WITH DEFECTIVE COVER CONCRETE

During inspection, several drilled shaft foundations supporting a major structure were found to have defective concrete at the foundation-superstructure joint location. As a remedial measure, the defective concrete was removed via hydro-jetting through drilled access tubes and replaced with high-strength grout. However, post-jetting inspection with video cameras showed that the jets were unable to remove the defective concrete from a "shadow" zone located behind each of the longitudinal reinforcement bars. Because the defective concrete remains in these zones, the nominal moment capacity of the section is different than for the case where all of the defective concrete had been replaced. The tool developed by the authors and verified in the preceding section was used to calculate the nominal moment capacity through a moment-curvature analysis that made explicit consideration of the remaining defective concrete. The results show that despite the slight decrease in structural resistance attributable to the remaining voids, the section was still capable of resisting the factored demands of the project. The as-designed section is depicted in Fig. 3.

© 2016 Deep Foundations Institute

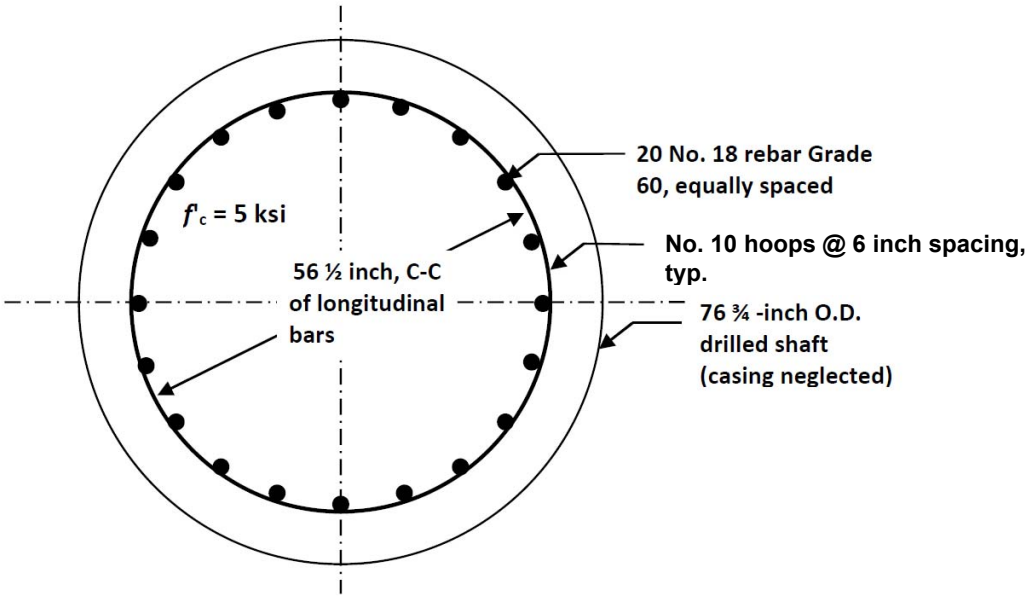


Fig. 3: As-designed drilled shaft foundation section for analytical purposes.

Analysis Approach

The flexibility of the authors' program makes it ideally suited to performing the analysis for this case because the defective concrete zones can be modeled exactly as they are believed to exist in the drilled shafts through the fiber-modeling approach. In addition to the assumptions stated in the verification problem section, the following assumptions were used in the analysis based on project-specific requirements and the results of post-jetting inspection:

- Grout used to replace the defective concrete has a compressive strength of at least that specified for the original concrete (6 ksi),
- Although the as-designed case includes two bundled No. 18 bars at each of the locations that a single bar is shown in Fig. 3, only one bar is considered because the other bars are assumed to lack sufficient development length (project requirement),
- Nominal material properties are assumed without overstrength factors (*e.g.*, yield strength of 60 ksi for Grade 60 steel),
- The defective concrete extends behind the longitudinal bars in a concentric wedge shape to the perimeter of the section (depicted below), and
- The defective concrete has zero strength.

Material Properties

The material properties for confined and unconfined concrete and reinforcing steel are given in Tables 3 and 4. The defective concrete is assumed to have zero strength and is effectively modeled as a void. Stress-strain plots for each material are shown in Figs. 4 and 5.

Confined concrete exhibits greater strength and ductility than unconfined concrete. For this project, the relationships developed by Mander et al. (1988) and Saatcioglu and Razvi [1992, with Razvi and Saatcioglu (1999) updates] based on theoretical derivations and experimental observations are used to estimate the

© 2016 Deep Foundations Institute

confined concrete properties as a function of the nominal unconfined concrete properties and the transverse reinforcement steel details. For analysis of the section described subsequently, the Saatcioglu and Razvi (1992) method is used because it resulted in a smaller increase in confined concrete strength relative to the unconfined strength. Because of the relatively small clear spacing between adjacent transverse ties (4.75 inches) and the large area of the confined core, the confined concrete exhibits a peak compressive strength increase of about 40 percent relative to the unconfined cover concrete.

Table 3: Concrete material properties.

Parameter	Value	
	Unconfined Concrete[a]	Confined Concrete[a]
Maximum Stress	6,000 psi	8,360 psi
Strain at Maximum Stress	0.002	0.0059
Ultimate Stress	0 psi	0 psi
Ultimate Strain	0.011	0.064
Initial Modulus of Elasticity	4,030 ksi	4,030 ksi

Notes:
[a] Using Saatcioglu and Razvi (1992) equations

Table 4: Grade 60 steel material properties.

Parameter	Value
Yield Stress	60,000 psi
Yield Strain	0.0021
Initial Modulus of Elasticity	29,000 ksi
Hardening Strain	0.0125
Ultimate Stress	90,000 psi
Ultimate Strain	0.09

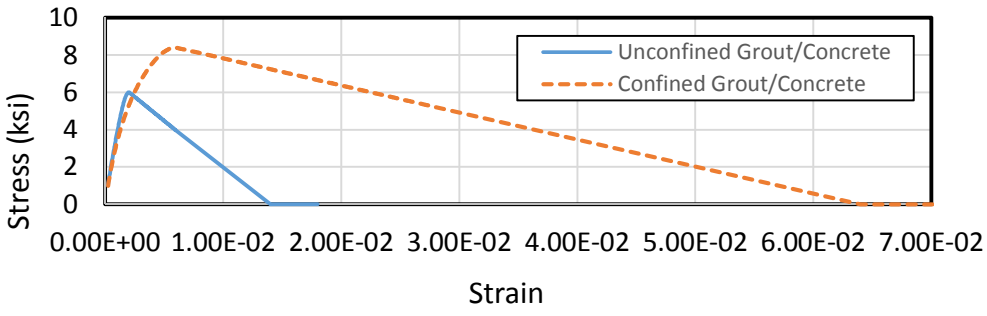


Fig. 4: Stress-strain behavior for concrete. Confined concrete model after Saatcioglu and Razvi (1992).

© 2016 Deep Foundations Institute

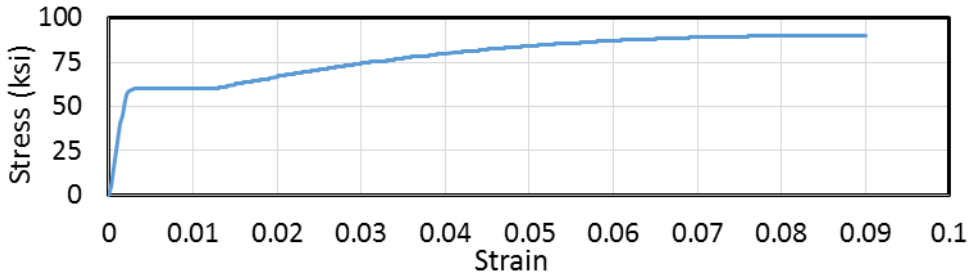


Fig. 5: Stress-strain behavior for Grade 60 reinforcing steel.

Fiber Discretization

The radial discretization is shown qualitatively in Fig. 6. The actual number of radial and theta increments was adjusted in the analysis until a sufficient number of fibers resulted in stable analysis results; the final number of increments for each section are shown in Table 5. The longitudinal reinforcing bars are modelled as circular fibers matching the size and location of each bar in the real section. For the "as-designed" case, the defective concrete zones shown in Fig. 6 are assumed to have the unconfined concrete properties given in Table 1. For the "with defective concrete" case, the defective zones are modeled as voids. The as-designed case serves as a baseline for comparison to ensure that the moment-curvature analysis results are reasonable.

Table 5: Fiber discretization.

Zone	No. Radial Increments	No. Theta Increments
Confined Concrete Core	40	20
Unconfined Cover Concrete—between each shadow zone (13.4° angular width)	6	4
Defective Cover Concrete--shadow zone (4.6° angular width)	6	1

Finite-Element Analysis Parameters

The *OpenSees* analysis is performed with the following parameters:

- Curvature-controlled integration scheme with 1,000 increments,
- Energy increment convergence test with 1.0E-9 tolerance,
- Plain constraints handler, and
- Newton-Raphson solution algorithm.

© 2016 Deep Foundations Institute

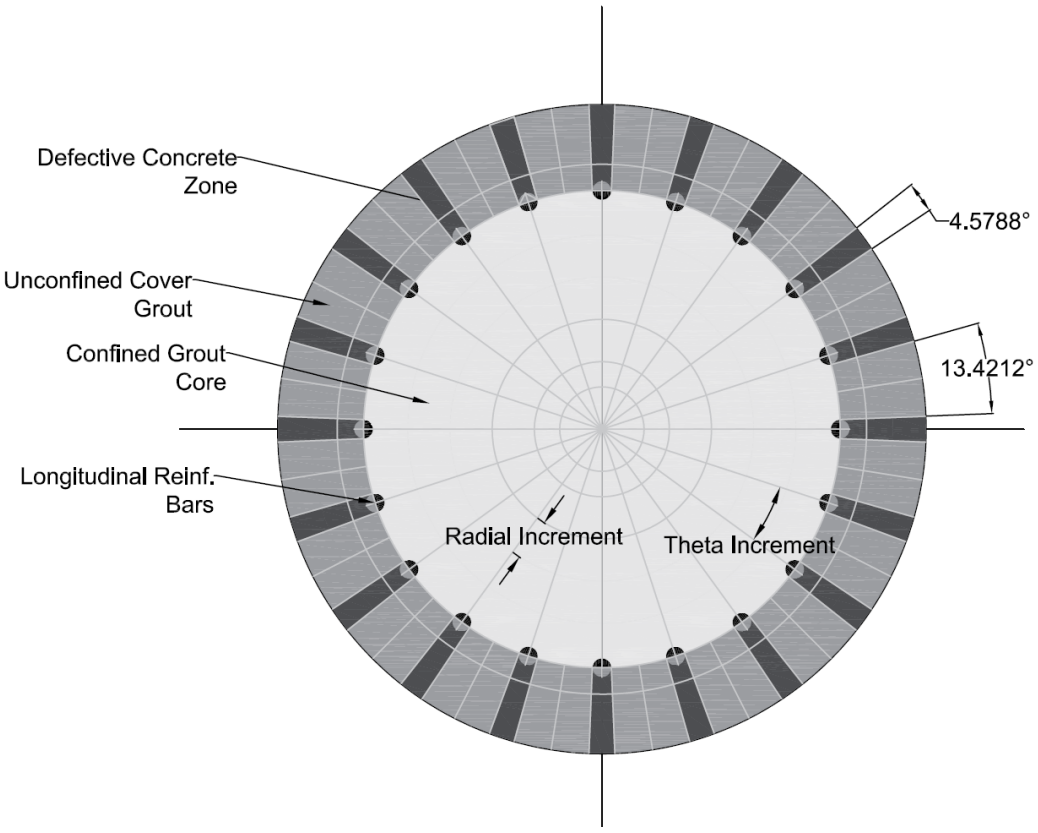


Fig. 6: Fiber model—see Table 5 for actual number of increments in each zone.

Results

Moment-curvature analysis results are shown in Fig. 7 for the factored axial design load of 4,760 kips (compression). The "as-designed" case (no defective concrete) is shown for reference, and it can be seen that including the defective concrete in the model only results in a small decrease in the section moment capacity—the peak moment is about 5-percent less for the defective concrete case. The relatively small difference is due to the fact that the defective concrete only makes up about 10-percent of the total section area, and it is situated outside of the confined core. The increased strength of the confined core relative to the unconfined cover concrete does not have a significant influence on the peak moment because the stress-strain response of the two materials is similar up to the unconfined concrete "strain at maximum stress" (see Fig. 4). Nonetheless, modeling the concrete core with consideration of confinement is more realistic and so is used here for accuracy.

Nominal Moment Capacity

Nominal moment capacity (M_n) of a reinforced concrete section is defined by ACI (2011) as the moment at which the strain in the concrete extreme compression fiber reaches the crushing strain, taken as 0.003. Moment capacity depends on axial load because the compressive stress applied to the section by a compressive axial load counterbalances tension in the section due to flexure and hence retards the onset of concrete cracking. Fig. 8 presents the relationship between nominal moment capacity and axial force P for the drilled shaft cross section under consideration.

© 2016 Deep Foundations Institute

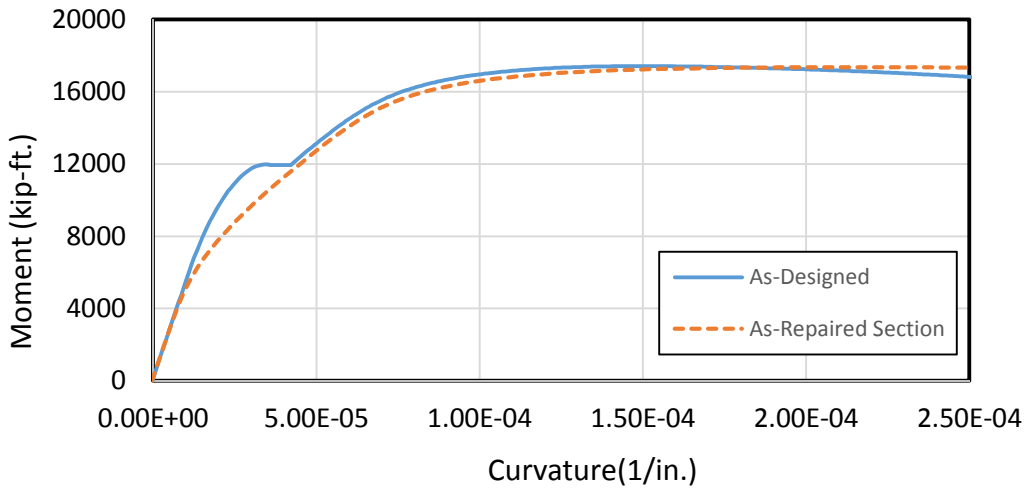


Fig. 7: Moment curvature analysis results for axial load P=4,760 kips (compression).

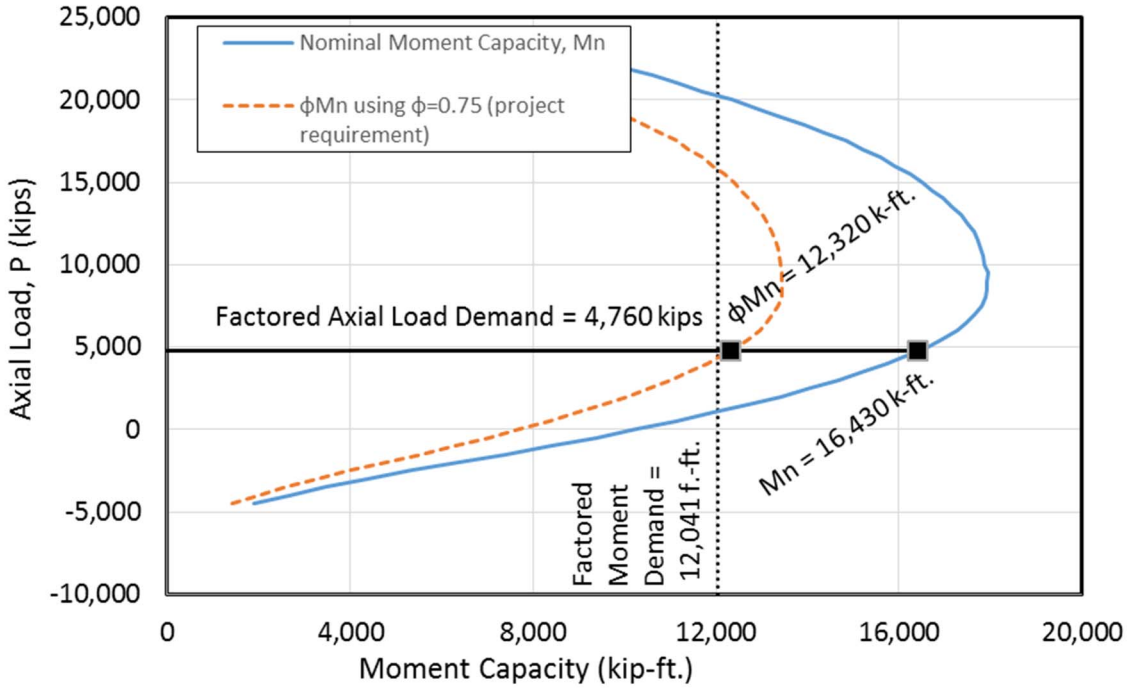


Fig. 8: *P-M* interaction diagram for drilled shaft foundation section including defective concrete. Positive axial load indicates compression.

Results: Flexural Strength

Explicit consideration of the defective concrete that remains on the outer perimeter of the longitudinal bars via a robust moment-curvature analysis has demonstrated that the defective concrete has a negligible effect of the moment capacity of the section. The factored moment capacity of the section, including the defective

© 2016 Deep Foundations Institute

concrete, is 12,320 kip-feet, which exceeds the factored moment demand of 12,041 kip-feet. For comparison, the as-designed section has an estimated factored moment capacity of 13,230 kip-feet.

CONCLUSIONS

A method for realistic analysis of drilled shafts with defective concrete is presented. By explicitly analyzing the structural behavior of the defective section, a rational decision can be made as to whether a shaft with defects can still meet the project requirements, or to guide repair schemes. The tool also provides a means to evaluate potential improvements in the moment-curvature response of drilled shafts for various repair schemes, for example the addition of high-strength bars or replacement of defective concrete with high-strength grout.

The analytical tool presented herein is simple, cost-effective, and flexible enough to handle a wide variety of construction defects in terms of material properties and geometry of the anomalies. Furthermore, it makes the best use of time, money, and effort spent on collecting data during integrity testing, since those results are directly incorporated into the analysis. Future projects could realize significant cost savings and avoid delays by utilizing this tool or a comparable approach.

REFERENCES

ACI (American Concrete Institute). ACI 318-11, Building Code Requirements for Structural Concrete and Commentary. American Concrete Institute, Farmington Hills, Michigan, 2011.

Chang, G. and Mander, J. (1994). "Seismic Energy Based Fatigue Damage Analysis of Bridge Columns: Part I – Evaluation of Seismic Capacity." *NCEER Technical Report 94-0006*.

Mander, J., Priestley, M., and Park, R. (1988). ”Theoretical Stress-Strain Model for Confined Concrete.*” J. Struct. Eng*., 114(8), 1804–1826.

Mathews, Robert (2001). Moment Curvature. http://structsource.com/pdf/Momcurv_web.pdf

McKenna F.T., Scott, M.H., and Fenves, G.L. (2010*)*. “Nonlinear Finite-Element Analysis Software Architecture Using Object Composition.” *Journal of Computing in Civil Engineering*, 10.1061/(ASCE)CP.1943-5487.0000002, 95-107.

O’Neill, M.W., and Sarahan, H.A. (2004). “Structural resistance factors for drilled shafts considering construction flaws.” *Proc. GeoTrans 2004*, J.A. DiMaggio and M.H. Hussein, eds., ASCE, p. 166-185.

Petek, K., Felice, C.W., and Holtz, R.D. (2002). “Capacity analysis of drilled shafts with defects.” *Proc. Deep Foundations 2002*, M.W. O’Neill and F.C. Townsend, eds., ASCE, p. 1120-1135.

Poulos, H.G. (2005). “Pile behavior—consequences of geological and construction imperfections.” *J. Geotechnical and Geoenvironmental Eng.*, 131(5), p. 538-563.

Priestley, M.J.N., Seible, F., and Calvi, G.M. (1996). *Seismic Design and Retrofit of Bridges,* John Wiley & Sons.

Razvi, S.R. and Saatcioglu, M. (1999). “Confinement Model for High-Strength Concrete.” *J. Struct. Eng.*, 125(3), 281–289.

Saatcioglu, M., and Razvi, S.R. (1992). “Strength and ductility of confined concrete.” J. *Struct. Engrg*. , ASCE, 118 (6), 1590–1607.

© 2016 Deep Foundations Institute

This page left intentionally blank

© 2016 Deep Foundations Institute

COMPARISON OF THE PRE-CONSTRUCTION AND PRODUCTION QC TEST RESULTS FOR THE SELA-22 ELLIPTICAL JET GROUTING PROJECT (NEW ORLEANS, LA)

Filippo Maria Leoni, TREVIICOS, Charlestown, MA 02129 fleoni@treviicos.com, 1-617-241-4800

Gianluca Pianezze, TREVIICOS, Charlestown, MA 02129 gpianezze@treviicos.com, 1-617-241-4800

Alessandro Bertero, TREVI GROUP, Cesena (Italy) abertero@trevispa.com, +39-0547-319100

ABSTRACT

As part of the Southeast Louisiana (SELA) drainage program, designed by the U.S. Army Corps of Engineers (USACE) to reduce flood damages in the City of New Orleans and surrounding parishes through the construction of new pumping stations and better drainage canals, the SELA-22 project entailed the installation of a concrete covered canal along Jefferson Ave. and Prytania Street, in a highly urbanized portion of Uptown New Orleans, LA. The scope of the required soil improvement was to replace the soil between two parallel lines of sheet piles with a soil-cement mass to eliminate under-seepage and provide structural support for the concrete culvert. The USACE selected the jet grouting (Jet Grout) technology for the construction of the bottom plug. The bottom plug is between 18 and 21.5 ft thick with a maximum depth of approximately 40 ft, for a total length of approximately one mile. The treated soil comprised soft clays and silts with occasional presence of sands. Project specifications required 100% area coverage, a 28-days unconfined compressive strength of 100 psi and hydraulic conductivity of 1x10-6 cm/s, to be verified by testing specimens from cored samples. The specialty geotechnical contractor proposed to accomplish the task utilizing their proprietary and innovative elliptical bi-fluid Jet Grout technology, and elected to perform a pre-construction bench scale laboratory mixing program to determine the most suitable grout mix features (i.e. binder type and proportions, binder content, etc.) to be applied in the subsequent field test and production stages. This paper will summarize and compare the results obtained from the different pre-construction and construction stages; interpretations of the data will be provided, along with general considerations regarding the effectiveness and significance of bench scale testing for jet grouting applications.

Keywords: jet grouting (elliptical), pre-construction tests, construction QC/QA

INTRODUCTION

In general, the effectiveness of the construction parameters in any ground improvement work depends largely on the physical and mechanical properties of the soil to be treated. Therefore, well designed laboratory and field test programs, aimed to disclose the interaction between the site-specific soils and the mixing parameters, are essential to achieve the desired end product.

To this extent, usually a pre-construction soil investigation campaign is performed to assess soil properties and to retrieve samples of different soil layers for the laboratory Bench-Scale Testing phase (Bench Test). The Bench Test is to be designed using various binder types, binder contents (or cement factors - CF), and grout water/cement ratios (W/C) in each of the soil types; the selection of the different combinations and dosages for the Bench Test is based on past experiences on similar materials.

Following the laboratory results, a full scale Field Test is designed and executed. The Field Test typically entails installing multiple features (i.e. columns, elements, panels, etc.) to verify the results of the Bench Test and fine tune the construction parameters, such as: binder type and dosage, grout mix proportions, equipment configuration, injection procedures, etc. For a Jet Grout treatment, specifically, the final target

© 2016 Deep Foundations Institute

of the pre-construction test section is to determine the most effective combination of pressures, flows, withdrawal times, and grout properties (altogether defined as specific energy) to achieve the required and/or designed geometries and dimensions capable to meet the specific project requirements.

PROJECT INFORMATION

Part of the Southeast Louisiana (SELA) drainage program, designed with the purpose of reducing flood damages in the City of New Orleans and surrounding parishes, the SELA-22 - Jefferson Ave. Canal II project is located in one of the most urbanized areas of those involved with the program. It stretches for approximately 0.7 miles along Jefferson Avenue in Uptown New Orleans, between Dryades St. (northern boundary) and Constance St. (southern boundary), and additional approximately 0.4 miles along Prytania St. between Nashville Ave. on the west and Jefferson Ave. itself on the east (Fig. 1).

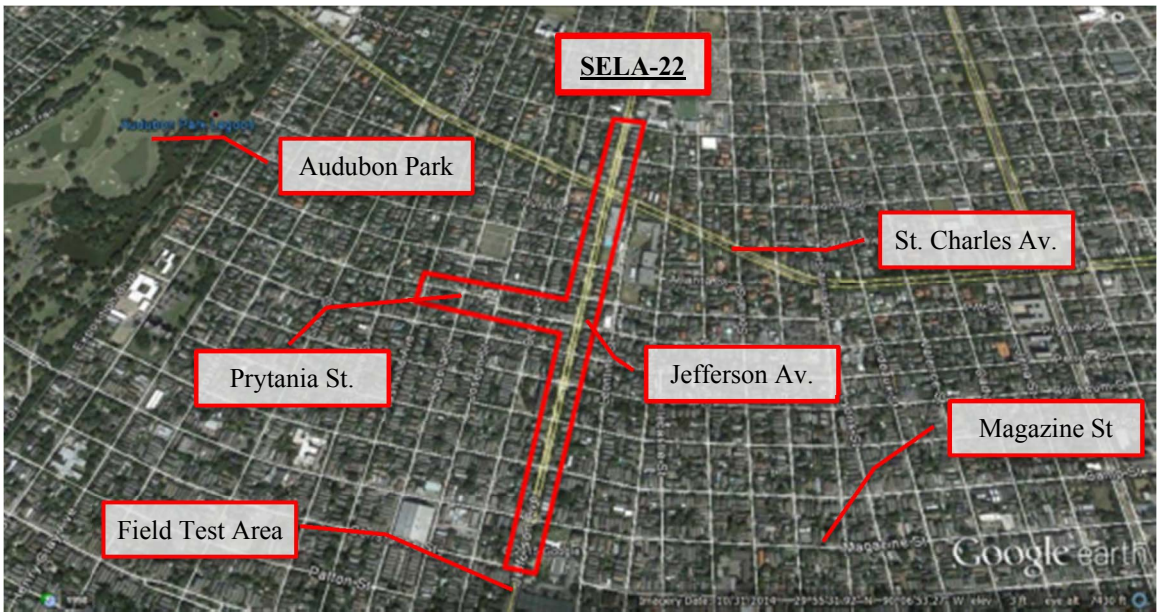


Fig. 1. SELA-22 project location

The Project entailed the construction of a concrete covered canal along these paths as part of the network that will enhance the drainage of the city of New Orleans. Soil improvement was required to replace the soil, characterized by poor geotechnical properties, between two parallel lines of sheet piles with a soil-cement mass to eliminate under-seepage, thus creating a so called bottom plug, and provide stability during construction and long term. In addition, the treatment greatly reduced constructability issues and allowed the General Contractor to work in a dry and stable environment for all their subsequent operations (excavation, cast-in-place, etc.), and eventually required installing only one level of struts, whereas at least two levels of bracing are generally required for similar excavation depths.

The USACE selected the bi-fluid jet grouting technology for the construction of the bottom plug. In particular, based on the different logistical conformation of the Project and the different design criteria, two distinct geometries of the improvement were required:

1) Along Jefferson Avenue (north-south alignment) the block of improved soils was designed to be 21.5 ft thick and 18.0 ft wide (within the outermost edges of the sheet pile wall), with a maximum bottom depth of approximately 38.0 ft from ground level;

© 2016 Deep Foundations Institute

2) Along Prytania Street (east-west alignment) the block of improved soil was designed to be 18.5 ft thick and 11.5 ft wide (within the outermost edges of the sheet pile wall), with a maximum bottom depth of approximately 32.0 ft from ground level.

The jet grout treatment was designed to cover 100% of the volume comprised between the two parallel lines of sheet piles, for a total horizontal length of over 5,000 ft and an overall net improvement volume of approximately 58,000 cy.

The quality of the work was to be checked by means of continuous coring to be executed on 5% of the installed columns. At intervals of 3.0 ft of vertical treatment, soil-cement mixture was to be tested for unconfined compressive strength (UCS) and hydraulic conductivity (HC) and the 28-days results needed to comply with the minimum requirement of 100 PSI and $1x10^{-6}$ cm/s, respectively.

Based on the requirements of the ground improvement, geometry and coverage above all, the specialty geotechnical contractor awarded the jet grout scope of work, proposed to accomplish the task utilizing their proprietary and innovative elliptical bi-fluid jet grout technology. The great benefit this technology offers is the possibility of significantly reducing the overlap between adjacent columns, and consequently decreasing the overall number of installations. The Specialty Contractor's past experiences using the elliptical geometry, in fact, had demonstrated a saving of approximately 40% on the number of columns and the production times. Conceptually similar to the traditional bi-fluid jet grout technology, where the dimensions of a cylindrical column are achieved by selecting the appropriate combination of fluid pressures and flow rates, step time and height, rotational speed, and withdrawal rates, this innovative technology relies on the alternation of slow and fast rotational speeds and on its computerized guidance (Fig. 2). Specifically, when the injection nozzles are oriented towards the designed longer axis of the ellipse, the computer reduces the rotational speed of the jet grout rods in order for the pressurized fluids (air and grout in this case) to act for a longer time onto the soils. The exact opposite is accomplished along the designed shorter axis of the ellipse.

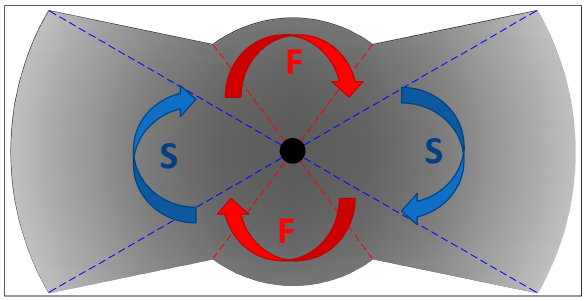


Fig. 2. Typical plan view of an elliptical ("bow-tie") jet grout column (F=fast; S=slow)

Due to the particular configuration of the SELA-22 project (Fig. 3), two different layouts and sets of construction parameters were selected.

SOIL CONDITIONS

The Project's subsurface was characterized by the presence of soft to very soft sensitive clays, and silty sands, which combined with the proximity of the Project location with the Mississippi River and a consequent shallow water table (Mississippi River stages typically vary between 0 and 14 ft above sea level with peaks during the spring and summer seasons, while the ground elevation at project location is between 4 and 8 ft above sea level) make the underground conditions unsuitable for the construction both under an engineering and constructability points of view.

© 2016 Deep Foundations Institute

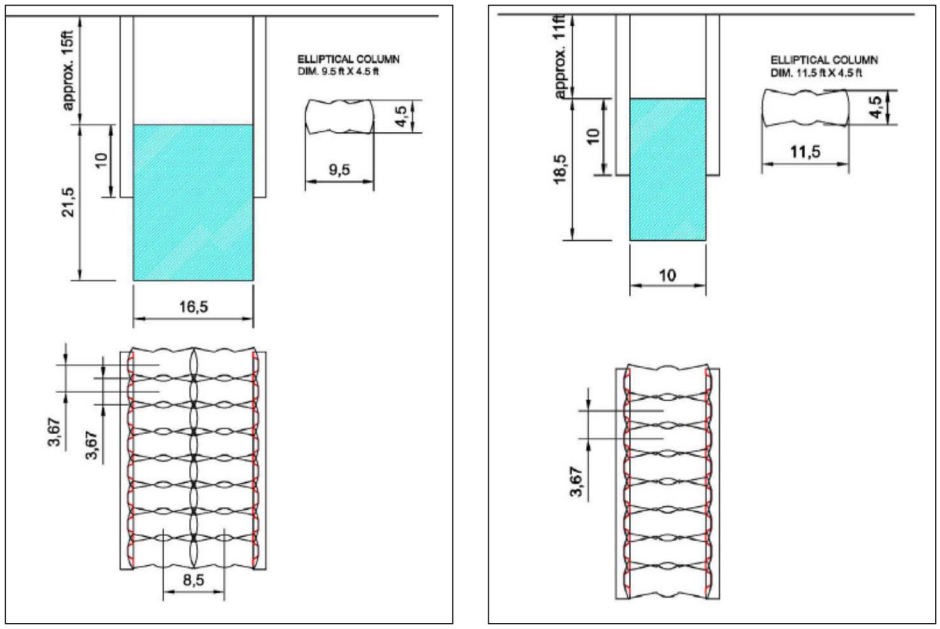


Fig. 3. Typical jet grout layouts for SELA22 (a) Jefferson Av.; (b) Prytania St.)

The simplified geological profile presented in Table 1 gives an approximate idea of the subsurface settings. The profile is inferred both from the geotechnical data available with the contract documents and post-award investigation performed to complement the existing data and to obtain soil samples for a bench test mixing program to be executed prior to the field test and the actual construction.

Table 1. Simplified soil profile (B.o.H = Bottom of Hole)

Depth [ft]	Soil type	General description
From 0 to max 8	Fill	Clay, organics and shell fragments
From min 2.5 to max 29	Lean Clay	Soft to very soft gray lean clay and silt, saturated
From min 9 to B.o.H (B-1)	Silt; silty and clayey sand	Soft gray silts and silty fine sands, saturated
From min 29 to B.o.H	Sand	Fine to poorly graded gray sands

It is to be noted that, given the geographical configuration of the Project, the sand layer tends to be higher towards the south portion of the alignment (i.e. towards the Mississippi River) while it tends to disappear northward at the depths involved in the ground improvement. It is also worth mentioning that the available SPT data show values between 0 and 10 in the large majority of the cases.

BENCH-SCALE TESTING

As above mentioned, in order to complement the geotechnical information provided with the contract documents and to obtain fresh soil samples, a soil exploration campaign was performed. During this stage, 6 additional borings were executed to approximately 40ft below ground elevation (i.e. beyond the foreseen maximum depth of the Jet Grout treatment). Recovered soil samples were taken to the laboratory facility, photographed and classified. Those representing the soils involved in the ground treatment underwent geotechnical assessments.

© 2016 Deep Foundations Institute

The laboratory tests performed on the soil samples included: moisture content, Atterberg limits (Liquid Limit, Plastic Limit, Plasticity Index), grain size analysis (Gravel, Sand, Fines), organic content, natural unit weight, and wet unit weight. Based on the results of these tests, the soils were sorted into three separate group characterized by similar geotechnical properties. The so identified soil type, along with their average indexes, are presented in the following Table 2.

Table 2– Average geotechnical properties of the soils

Soil Type	Dry density [g/cm³]	Natural density [g/cm³]	Water content [%]	Organic content [%]	Liquid limit	Plastic limit	Plasticity index
S1 - Sensitive Clay	1.158	1.679	29.8-56.5	2.60	33.7	19.3	14.3
S2 - Transition Layer	1.216	1.775	28.4-54.8	2.73	29.5	19.5	10.0
S3 - Sand	1.603	1.839	14.7-43.3	0.63			

Following the classification of the soil layers, the bench-scale testing proceeded according to a sequence of steps, such as:

Selection of the materials: as far as the soils were concerned, an appropriate amount of each identified type was scheduled to be blended with different combination of grout slurries. Two distinct types of binder were selected to prepare the grout slurry: a) type I/II Ordinary Portland cement (OPC) complying with ASTM C 150 andb) a blend of Portland and blast furnace slag cement (PBFC). City water was going to be used during the construction activities, thus the same was utilized in the preparation of the Bench Test batches.

Preparation of the soil samples: upon their classification, selected soil samples were pushed through a ¾" mesh in order to breakdown lumps and make their remolding easier. After the soil was molded together, a specimen was collected for assessment of moisture content and the molded soil was divided into the required portions for each batch. The remainder of material that was going to be used for subsequent batches was sealed and stored in a manner that would preserve its moisture content.
The moisture content measured after remolding was used to calculate the total water/cement ratio of the soil-cement mixture for more accurate analysis of the results.

Design of the mixing batches: in order to properly design the batches where the soil is mixed with a pre-determined amount of grout, the first step was to decide what types of grout were to be used and what ranges of cement factor were to be applied to the different soils. Based on previous experiences with similar materials, two different mix proportions were initially selected: 1) W/C 1.00 and 2) W/C 1.35. A third one (W/C 0.80) was added during the mixing operations on the basis of the observations carried out. At the same time, a maximum of three different values for each type of soil were chosen to test a specific soil/binder combination. Table 3 summarizes the batches that were completed for the Bench Test.

Table 3– Summary of Bench Test batches

Soil ID	No. of Batches	Cement Type	Grout W/C range	Binder Factor [kg/m³]	Total Water Content [kg/m³]	Total W/C
S1	4	PBFC	0.80-1.35	250-450	770-1,128	2.0-3.1
S1	4	OPC	1.00-1.35	250-450	770-1,128	2.2-3.1
S2	2	PBFC	1.00-1.35	250-450	708-1,065	2.0-2.8
S2	2	OPC	1.00-1.35	250-450	708-1,065	2.0-2.8
S3	4	PBFC	0.80-1.35	250-450	544-902	1.5-2.2
S3	4	OPC	1.00-1.35	250-450	544-902	1.7-2.2

© 2016 Deep Foundations Institute

Determination of the mixing procedures: the binder grout was prepared progressively adding the established amount of the dry binder to a known quantity of water, while stirring the compound by means of a mixing blade attached to a high-velocity hand drill. Once the powder had been entirely introduced, the mixing continued for 3 minutes.

In general accordance with the procedures proposed by the *Virginia Polytechnic Institute and State University – Center for Geotechnical Practice and Research*, once the grout had been prepared a known quantity of the slurry was gradually added to a known amount of soil in a pastry-mixer while the mixture was gently stirred. Once the full anticipated amount of grout had been added, the soil/grout mixture was thoroughly mixed for 10 more minutes, making sure to stop the mixing every 2-3 minutes to clean the stirrer and the side walls of the mixing bowl.

Mixing and casting of specimens: each resulting mixture was placed into 2"x4" PVC cylinders by filling in 5 lifts, each lift tamped 15 times with a ½" diameter rod. After casting, the cylinders were capped and stored in a temperature and moisture-controlled curing room.

Although the results of the mechanical mixing operated by the pastry mixer cannot be directly correlated with what is actually occurring during jet grouting improvements, where the disaggregation of the soil and blending with the grout is exclusively due to the hydraulic/kinetic energy of the jets, observations concerning the consistency of the blend, proneness to breakup, etc. were however carried out and recorded.

In particular, for all the types of soil, from the cohesive to the granular, it was observed the mechanical mixing blended the ingredients fairly easily with all the different combinations of CF, W/C and type of binder to create a homogeneous mixture. Moreover, due to the presence of fine sand, which reduced the cohesion of the fine-grained soil, the resulting mixtures had a "soupy" aspect and were almost pourable in the PVC cylinders.

Specimens curing, UCS and permeability testing, observations and results: the soil-cement specimens cast underwent unconfined compressive strength and hydraulic conductivity testing according to the following schedule: UCS: 7, 14, and 28 days; HC: 28 days. UCS testing was performed in general accordance with the applicable portions of ASTM D2166, D1633, D4832, while hydraulic conductivity testing was performed as per ASTM D5084.

In order to keep account of the anticipated differences between lab mixing and in situ mixing for the Jet Grout application, it was decided to slightly adjust the concept according to which the target UCS values for Bench Tests should be twice as much as those required by the ground improvement project specifications; thus, the following, arbitrary, correction factor was applied to the 28-days UCS results for the cohesive soils only:

- Estimated field UCS correction factor for cohesive soils (S1, S2) $= \frac{\text{Measured laboratory UCS}}{\text{Estimated field UCS}} = 2.5$

The distinction between material types was assumed in correlation with the typical reduced proneness of cohesive soils to be eroded and disaggregated than the granular soils. The correction factor was not used for the permeability data both because there is not enough bibliography regarding this matter, because it was considered pointless to divide it by a number on a logarithmic scale or too conservative to reduce its order of magnitude.

The corrected test results, where applicable, were then plotted against different indexes: curing time, initial (i.e. grout) and total (i.e. in situ) W/C ratios, binder factors, etc. to determine the most suitable sets

© 2016 Deep Foundations Institute

of material and quantities to be tested during the field section. The charts in Figures 4 and 5, as a matter of example, display the data sets for all soils at 28 days of age against the total W/C ratio.

The UCS chart (Fig. 4a) shows that out of the two compositions of binder tested, only the PBFC blend could safely ensure the compliance with the project strength requirements for all the soil layers. Thus, only this blend was selected for the field test. It is also to be noted that the UCS results decrease, as typically occurs for in situ mixing of soil and grout, as the values of total W/C ratio increase. In the specific, however, also considering the displayed values are "corrected", there is still a safe margin above the minimum strength requirement, which seemed to potentially allow the utilization of either lighter grout slurries or lower binder contents.

On the other hand, although showing less definite trends than the UCS, all the HC results ("not corrected" – Fig. 4b) were within the project requirements for all soil layers and grout designs; nonetheless, it is evident the different rate of performance between the PBFC and the OPC, with the latter much closer than the former to the project acceptance criterion.

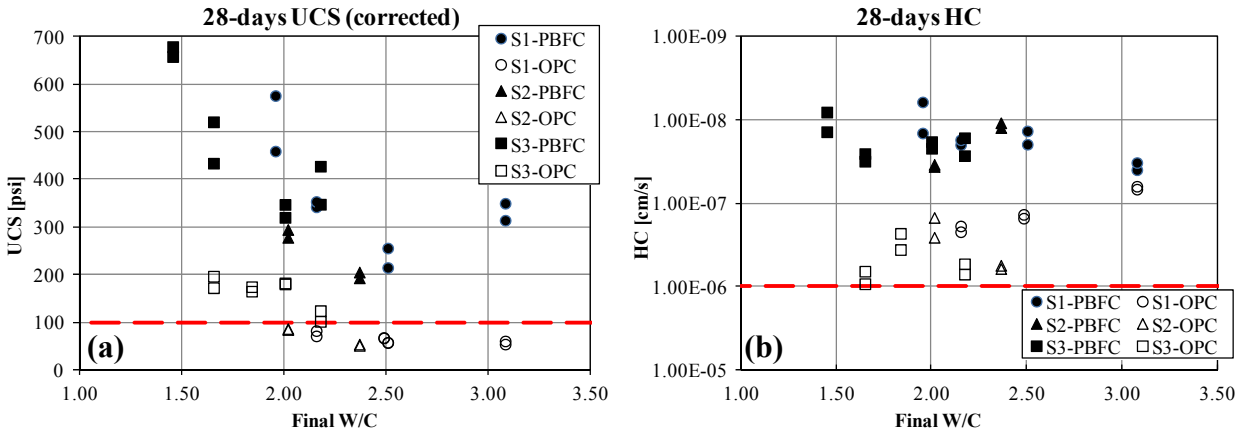


Fig. 4. 28-days UCS (a) and HC (b) results for the bench scale test

The selection of the PBFC binder blend for the following stages of the project is, therefore, further justified, since the outcomes of the Bench Test proved conservative enough to tolerate the potentially larger variations anticipated for the field QC results. The hydraulic conductivity of the treated mass, or at least that measured through testing of cored specimens as prescribed by the project specifications was, in fact, expected to be much more sensitive than the strength due to possible defects in the specimens, such as small soil inclusions, presence of roots and/or rootlets, porosity, microfactures, etc. either in the nature of the jet grouting application or caused by the coring operation itself.

FULL-SCALE FIELD TEST

Following the outcomes of the Bench Test, the geotechnical contractor, in accordance to the project reuirements, proceeded with the execution of a full-scale field test, which had the purposes of: 1) apply in the field the most suitable combination/s of binder proportions to achieve the required strength and permeability of the treated soils, and 2) determine the proper construction procedures (i.e. injection parameters) to ensure the anticipated geometry, dimensions, and overlap to ensure the specified 100% coverage. In order to explore different options, a few distinct clusters of elliptical Jet Grout columns were installed up to almost ground level. Table 4 summarizes the properties of the various installations.

Once cured (Approximately around 28 days upon completion), the columns were cored to verify continuity and homogeneity of the treatment, retrieve and test specimens according to the project

© 2016 Deep Foundations Institute

specifications. In addition, they were exposed for approximately the top 5 ft to observe the actual shape and dimensions (Fig. 5).

Table 4– Summary of Field Test columns

Target column dimension [ft]	11.5 x 4.5	9.5 x 4.5
No. of Clusters	4	2
No. of Columns	8	4
Binder type	PBFC	PBFC
W/C	0.80-1.35	0.80-1.35
Cement Factor [kg/m^3]	250-450	250-450
Energy [MJ/m^3]	10.0-20.0	10.0-20.0



Fig. 5. top of a Jet Grout cluster exposed during field test

At a minimum, coring was performed both towards the outer edge and at the center overlap of each cluster. Overall, 13 investigations were conducted, which led to a total of 25 UCS tests and 38 HC tests.

In order to narrow down the various sets of construction parameters used for the field test and consequently applying the most suitable set of parameters for the actual construction, the results of the lab tests on the cored specimens were weighed against the different indexes in order to gather as much information as possible and combine them with the field observations of the exposed columns.

With the purpose of obtaining a more representative comparison of the data, however, the binder factor was normalized with respect to the W/C ratio (i.e. CF/WC) to provide a common factor against which the test results could be more easily compared. As a matter of example, the UCS and HC records versus the CF/WC normalized values are presented in Fig. 6 (a) and (b), respectively. It is nonetheless to be noted that, while the target binder factor is function of the injection parameters (grout flow rate and withdrawal rate above all), the actual binder factor (i.e. the factor in place) is largely affected by the treated volume of the individual column, which for the Jet Grout technology greatly depends upon the local soil conditions, and amount of spoil return.

The corresponding strength (both recorded and "corrected") and permeability results obtained during the laboratory stage are also included in the graphs of Fig. 6 for comparison purposes.

© 2016 Deep Foundations Institute

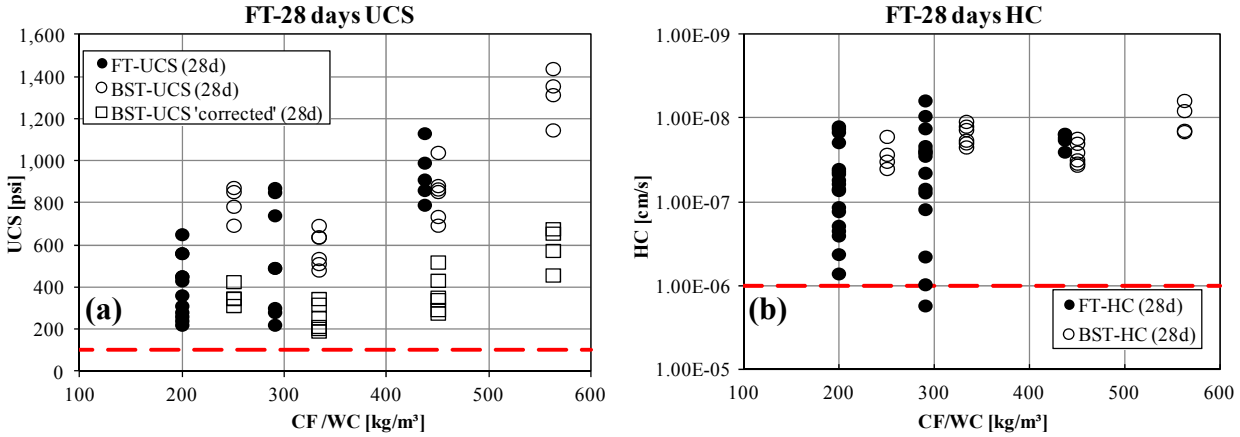


Fig. 6. UCS (a) and HC (b) results for the field test

The first remark that can be inferred from the charts concerns the more significant scatter recorded for the data from the field test. This is, as anticipated, a very likely consequence of the variability of the local properties of the soils and their rheology to the Jet Grout treatment, which, in fact, is not expected to be as accurate in field as it is in the lab. The comparison with the lab results also seems to show that the correction factors applied to the 28-day UCS data obtained during the Bench Test may have been slightly conservative for the lowest W/C ratio and the highest binder content (i.e. highest CF/WC), while they appear to be "on target" with the other grout/soil combinations, as far as the individual trends exhibit. Overall, in only one occurrence the in situ permeability resulted in not complying with the acceptance criteria of the SELA22 project. This occurrence is, however, part of a very limited set of data that shifts off the general trends, otherwise very neat and homogeneous.

PRODUCTION

The evidences described above ultimately allowed further tuning of the designed injection parameters for the actual construction of the Jet Grout bottom plug. In particular, a set of parameters was chosen for the Jet Grout treatment along Jefferson Ave, and a different one was selected for Prytania St., mostly in light of the different column layout (refer also to Fig. 3). Approximately 2,040 Jet Grout columns along Jefferson Ave and approximately 360 Jet Grout columns along Prytania St. were constructed; these quantities, per the project specifications, required QC investigations in the amounts displayed in Table 5, which also shows some of the relevant outcomes of the QC program.

Table 5– Summary of production QC results

Unconfined Compressive Strength

	Coring Performed [No]	Specimen Tested [No]	Average UCS [PSI]	Max UCS [PSI]	Min UCS [PSI]	St. Dev. [PSI]	UCS <100PSI [No]	UCS <100PSI [%]
Jefferson	102	694	361	1,150	20	148	3	0.43%
Prytania	18	120	321	560	100	106	0	0.00%
Total		814	355	1,150	20	143	3	0.37%

Hydraulic Conductivity

	Coring Performed [No]	Specimen Tested [N]	Average HC [cm/s]	Min HC [cm/s]	Max HC [cm/s]	St. Dev. [cm/s]	HC >1x10^{-6} cm/s [N]	HC >1x10^{-6} cm/s [%]
Jefferson	102	690	5.45E-07	1.52E-09	1.68E-04	6.58E-06	19	2.75%
Prytania	18	120	2.67E-07	1.29E-09	5.66E-06	5.70E-07	3	2.50%
Total		810	5.04E-07	1.52E-09	5.66E-06	6.07E-06	22	2.72%

© 2016 Deep Foundations Institute

The QC/QA tests performed for the actual ground improvement showed results that were very consistently meeting the acceptance criteria.

Considering, also, that for each stretch of the project the Jet Grout parameters were constant, the average UCS and HC results can be compared to corresponding outcomes for the similar binder/soil combinations utilized both for the Bench Test and the Field Test. The results of this analysis, which again uses the normalized CF/WC values, are presented in the charts of Fig. 7. These plots also include the records from the Bench Test and the Field Test for comparison purposes.

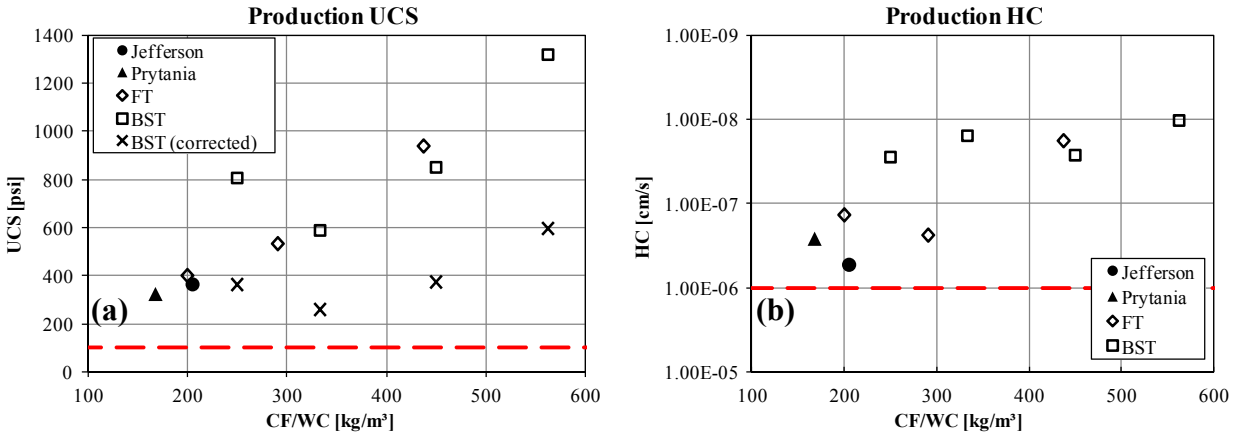


Fig.7. average UCS (a) and HC (b) results for production cored samples (all soil types)

Significantly, the average UCS for the production data sets aligns almost perfectly with those of the FT and the Bench Test "not corrected", exception made for the lowest range of normalized binder factor (i.e. low CF and high W/C), for which the application of the correction factor to the UCS measured during the Bench Test seems more appropriate.

In a similar way, the HC results from the production QC testing on the cored specimens, notwithstanding the anticipated more important scatter due to the different mixing conditions between lab and field, seem to align along the virtual trend line originated by the permeability results of the Field Test, whereas the HC results recorded during the Bench Test typically are one order of magnitude higher.

The interpretation that can be given to these evidences is that, while the actual strength values obtained during the pre-construction laboratory mixing test could have been reliably used without any correction to forecast the in situ resistance of the Jet Grout improvement, the HC values recorded during the Bench Test should have probably been reduced by an order of magnitude to better simulate the field performance.

If the average production QC data are plotted against the average retrieval depth of the specimens to attempt a better correlation with the local soil boundaries, and are compared to the average UCS and HC results of the corresponding soil types identified during the Bench Test (excluding the transition layer that, as such, is more a blend of S1 and S3 and cannot be easily located) and Field Test treated with similar parameters, the outcomes seem to tell a different story. In fact, the UCS chart in Fig. 8, even considering the different normalized binder factor, show that an adjustment to the strength values of the soil-cement mixtures obtained in the lab is at all necessary.

On the other hand, while the HC results from production cored samples display one order of magnitude less than the specimens prepared in the lab confirming what is described above (see also Fig. 7), it is to be

© 2016 Deep Foundations Institute

noted how the in situ permeability of specimens retrieved from the field test column shows higher values that the production one. However, this occurrence can be explained with the much larger variability associated with the greater number of specimens tested for the production phase as opposed to those tested for the field section, as well as the geographical extension of the work and the consequent likelihood of encountering largely variable soil conditions.

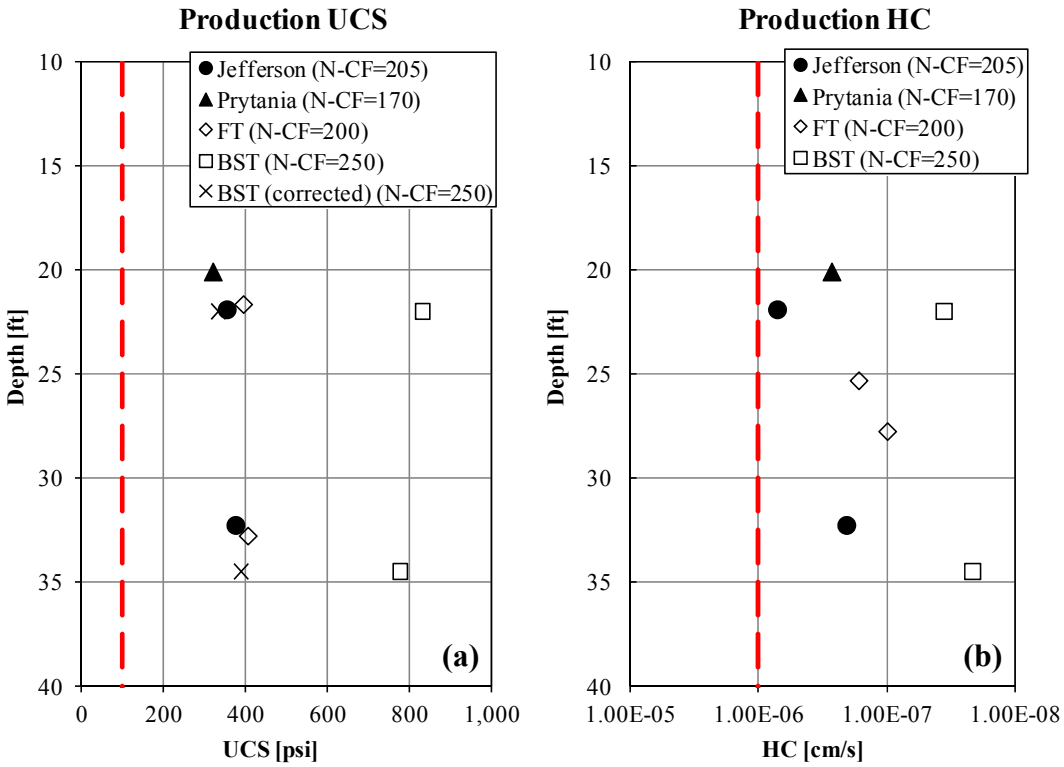


Fig.8. comparison of UCS (a) and HC (b) average results (S1 & S3 layers)

CONCLUSIONS

Without denying the importance of well-designed pre-construction laboratory programs for ground improvement projects, the analyses carried out and presented within this paper show that, for the subject jet grouting construction at the SELA22 project involving mostly cohesive soils, the outcomes of the bench-scale test could have been misinterpreted if not followed by a properly planned field test section.

The Field Test, in turn, other than verifying in situ the assumptions made upon the lab results, gives the opportunity to assess dimensions and geometries of the Jet Grout columns, even more importantly in this case due to the elliptical shape of the columns, in order to allow adjustments to the injection parameters either in a more conservative or aggressive way.

In any case, given the nature of the geotechnical engineering work, the only way to back-validate all the hypotheses made at the pre-construction stage is through the QC/QA investigation specified for the production; which at times might prove too late.

Ultimately, the interesting aspect of this study is that the interpretations herein presented could be used, and possibly ameliorated, in future similar ground improvement projects requiring the Jet Grout technology.

© 2016 Deep Foundations Institute

This page left intentionally blank

© 2016 Deep Foundations Institute

DESIGN, INSTALLATION, AND TESTING OF HOLLOW BAR TIEBACKS USED AS EXCAVATION SUPPORT

Marco D. Boscardin, Boscardin, PhD, PE, DGE, Boscardin Consulting Engineers, Inc., Amherst, MA, USA, 413-549-3804, marco@boscardinconsulting.com
Kenneth A. Pidgeon, PE, Engineers Construction, Inc., Williston, VT, USA, 802-863-6389, kpidgeon@ecivt.com
Adriane G. Boscardin, PhD, Boscardin Consulting Engineers, Inc., Amherst, MA, USA, 413-549-3804, adriane@boscardinconsulting.com

ABSTRACT

Hollow bar tiebacks can offer an economical alternative to conventional solid bar and strand tieback systems for use in temporary excavation support construction. However, the limitations associated with the installation of hollow bar tiebacks require special attention during design, construction and load testing to verify conformance with conventional performance and proof testing criteria (PTI, 2014). In particular, providing a reliable free length is complicated by the 10-foot (3-m) -long, segmental, coupling-to- coupling nature of the free length sheath in the hollow bar system, and addressing the fully grouted annulus of the bond zone and the free length zone at the end of installation are key concerns. In addition, it is often more convenient to install a greater number of more closely spaced, lower capacity tiebacks with the hollow bar system, compared to conventional tiebacks. This paper examines how these issues were addressed for a project involving a 60-foot (18-m) -deep sheet pile excavation through a highway embankment and a 70-foot-deep sheet pile and soldier pile and lagging excavation through a railroad embankment, both supported by a hybrid system of hollow bar tiebacks and hollow bar soil nails. The project involved approximately 300 tiebacks and 400 soil nails.

Keywords: hollow bar anchors, self-drilling, tiebacks, soil nails, design, installation, proof testing, performance testing, testing, free length, bond zone

INTRODUCTION

Engineers Construction, Inc. (ECI), constructed a pair of 32-foot (9.8-m) -wide (clear span), 30-foot (9-m) -high (21 feet (6.4 m) above the stream bed), cast-in-place concrete arch culverts as a design-build project for the Vermont Agency of Transportation (VTrans) in East Ryegate, Vermont. The new culverts replaced an existing 8-foot (2.4-m) -wide by 6-foot (1.8-m) -high cast-in-place concrete culvert under US Route 5 (RTE5), and twin, 2-foot (0.6-m) -wide by 5-foot (1.5-m) -high granite block culverts under the Washington County Railroad (WACR) alignment. The culverts convey Manchester Brook eastward, through the embankments for RTE5 and the WACR, on its way to the Connecticut River. The Connecticut River is located approximately 100 feet (30 m) east of the WACR embankment. The existing structures were undersized and backed up water behind the embankments during high flow events; and often trapped debris that flowed down the brook and became clogged. The existing culverts also had cracks and openings that have resulted in the loss of ground into the culverts and the formation of sinkholes in the sides of the embankments. Moreover, the reason for the large cross-sectional dimensions of the culverts was to make them of sufficient size and openness to encourage the migration of fish up the stream to spawn. The culvert through the RTE5 embankment is 144 feet (44 m) long, and the culvert through the WACR embankment is 128 feet (39 m) long, with a 57-foot (17.4-m) -long by 32–foot (9.8-m) -wide by 17-foot (5.2-m) -deep 10 feet (3 m) deep above the stream bed) open channel section between the two culverts. A plan view of the culvert alignment is presented in Figure 1.

© 2016 Deep Foundations Institute

A key aspect of the construction was to maintain both the railroad and highway traffic flows during construction. This was achieved by the design and installation of support of excavation (SOE), so that the excavations could be kept sufficiently narrow to permit construction of temporary bridges to carry the highway and railroad traffic safely and with minimal disruption. This resulted in the excavation and support of a 60-foot (18-m) - deep by 55 foot (16.8-m) -wide cut through the RTE5 embankment, and a 70-foot (21-m) -deep by 55-foot (16.8-m) -wide cut through the WACR embankment. These are among the deepest temporary excavations made in Vermont.

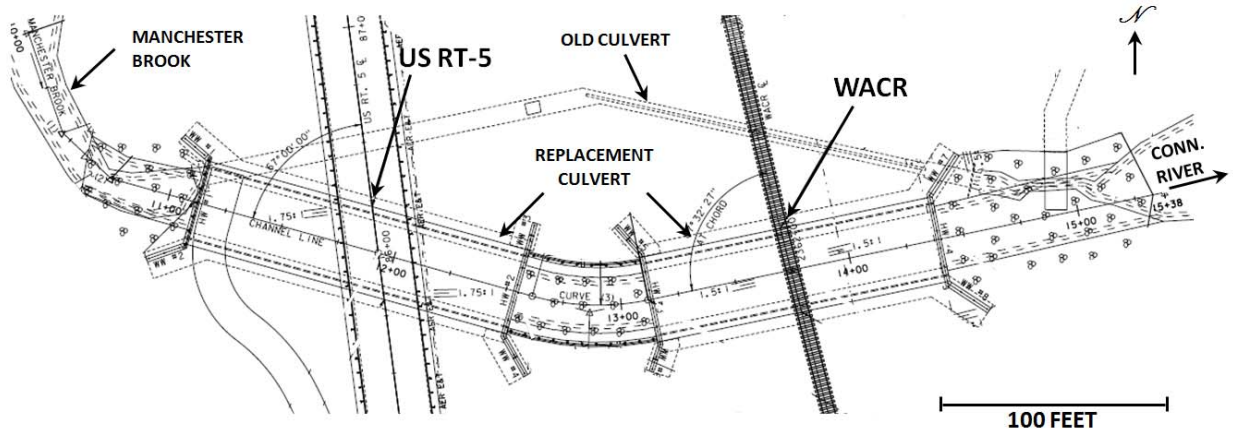


Fig. 1. Site Plan

GEOTECHNIOCAL CONDITIONS

A subsurface profile consisting of five general layers were identified for this project, as described below and shown in Figure 2. Unified System classifications are given for each layer. The layers are listed in order of increasing depth (decreasing elevation).

Embankment Fills - Very loose to loose, fine to coarse Sand to Silty Sand to Gravelly Silty Sand Fill (SW, SM, SP)

Sand and Gravel 1 - Medium dense, fine to coarse Sand and Gravel to Gravelly Silty Sand with Cobbles to Sand (SW, GW, GP, SM).

Sand and Gravel 2 - Medium dense to dense Sand and Gravel to Gravelly Silty Sand with Cobbles to Sand (SW, GW, GP, SM).

Sand and Gravel 3 - Dense to very dense Sand and Sand and Gravel (SW, GW).

Rock - Weathered Rock and Rock, moderately hard to very hard gray gneiss, rock core recoveries ranged from 60 to 100% and Rock Quality Designations (RQD) ranged from 50 to 100. Weathered rock was at the rock-soil interface in some borings and when present was relatively thin, about 6 inches (150 mm) to 1 foot (300 mm). The toe of the excavation support was at or near the rock soil interface along most of both culverts alignments.

© 2016 Deep Foundations Institute

Water – The non-flood water level was only a few feet above the stream bed, as a consequence only the lower 10 feet (3 m) of the SOE had to contend with ground water inflows. However the culvert excavations were in and near the old stream bed of the brook, so managing and controlling ground water inflows was an important consideration.

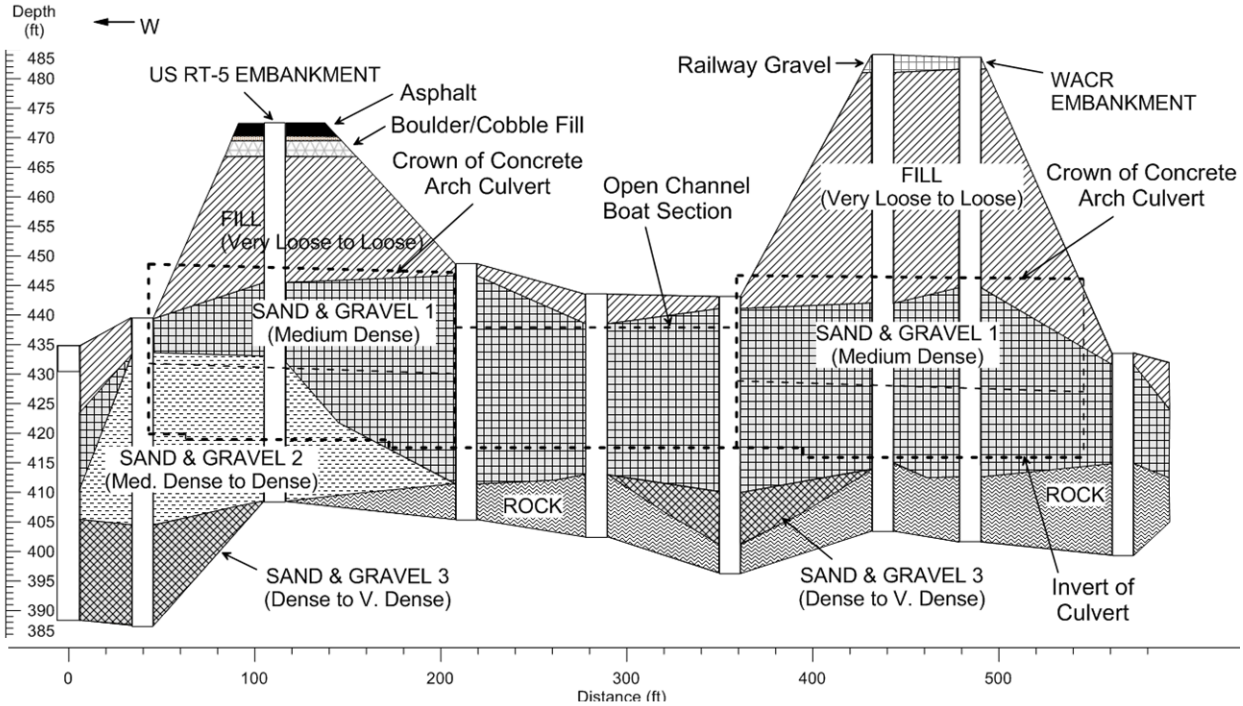


Fig. 2. Geologic Profile

SOE DESIGN

Given the loose to dense, granular nature of the site and embankment soils, and the likely need to cut off the ground water, an excavation wall comprised of interlocked steel sheet piles driven into place using a vibratory driver was selected. Provisions to install steel H-piles and use an impact hammer were also included in the event that locally more resistant ground conditions were encountered. Tiebacks and soil nails were selected to support the SOE wall due to the potential presence of rock near the invert elevations of the culvert excavations; and the advantages of maintaining a clear open area for the erection of the forms for casting the culvert arch structures and related headwalls. Tiebacks were selected for the upper sections of the SOE walls (generally the Embankment Fills), and soil nails were selected for the lower sections of the SOE walls (generally natural soils). The reason for the upper tiebacks was so that a tension could be induced in long tieback elements to control and limit movements in the looser upper soils that could affect the temporary bridge structures. The dense nature of the lower soils, and the close proximity of rock to the toe of the SOE walls meant that SOE deflections were a much lower concern at depths, so soil nails were selected for SOE wall support.

The initial stages of design included examination of the anticipated SOE needed for the maximum section of each embankment with the anchors perpendicular to the wall horizontally and having a 15° downward dip. The RTE5 design section incorporated HS20 surcharge loads. The WACR design section

© 2016 Deep Foundations Institute

incorporated Cooper E-80 and crane surcharge loads. Surcharge loadings due to the temporary bridges were not included because the bridge abutments were supported by H-piles driven to bedrock. The wall section and tieback/soil nail loadings, for each maximum section, were evaluated using three methods: WALLAP staged analyses; SNAILZ analyses; and apparent pressure diagrams based on the assumption that the vertical spacing of the wall support would be 7 feet (2.1 m). The design approach was to use the larger of the loadings from the three analyses. Based on these initial sections, MSZ 14-340 cold-formed steel sheet piles were selected for the SOE wall and 40/20, 40/16, and 52/26 steel (yield about 80 ksi (552 MPa)) hollow bar tiebacks and soil nails were selected for the wall support system. This resulted in a base design consisting of a tieback or soil nail in each belly of a pair of sheet piles for a horizontal spacing of 5.8 feet (1.8 m), except for the upper row of very lightly loaded tiebacks which were set at a horizontal spacing of 11.6 feet (3.5 m) with standard walers. The 5.8-foot (1.8-m) horizontal spacing allowed the use of small walers and bearing blocks thereby minimizing obstruction of the work area and simplifying waler fit-up.

Final design of the tiebacks and soil nails was based on the initial analyses adjusted for actual vertical and horizontal spacing based on tributary area, adjusted for actual dip and yaw required to accommodate changes in direction of the wall and to avoid known obstructions (e.g. existing culvert immediately north of the new culvert alignment and other soil anchors), and actual depth of cut and surcharge loadings at specific locations.

Design allowable soil to grout bond was 0.75 kips per foot (11 KN/m) of bond zone for the loose sand fills, 1.5 kips per foot (22 KN/m) of bond zone for the medium dense sands, 3.5 kips per foot (51 KN/m) for the dense sands and natural soils. An allowable ground to grout bond of 3.5 kips per foot (51 KN/m) was also used for the rock. Design allowable bond was based on an effective anchor zone diameter of 1.5 drill bit diameters, and a factor of safety of 2.

INSTALLATION

Reasons for using self-drilling, hollow bar anchors for this project were: cement grout could be used as a drilling fluid; and the self-drilling aspect avoided the need to remove drill steel and insert the anchor tendon element. This was important on this project due to the cohesionless, granular nature of the ground which was expected to have the tendency to collapse with thinner drilling fluids and during removal of the drill steel and insertion of the anchor tendon. The self-drilling feature reduced the potential for ground loss and settlement of the highway or railroad due to over excavation during the anchor drilling process.

However, creating a free length using the self-drilling process is very sensitive to drilling details. The bars used on this project were in 10-foot (3 m), fully threaded lengths and were coupled end to end as the drilling progressed. Bars that were intended to be in the bonded zone were installed bare, without any covering and bars that were intended to be in the free length were fitted with plastic sleeves that spanned from coupler to coupler. The role of the sleeve is to serve as a bond breaker so that the bar in the free length zone can elongate without interaction with the soil surrounding that portion of the tieback and the loads can make it to the bond zone near the end of the tieback. To do this, the sleeve must be smooth, sufficiently robust to resist the drilling forces and be sealed to the coupler at each end to limit penetration of the grout into the annulus between the sleeve and the bar. In addition, the exposed surfaces of the couplers will tend to bond with the grout, which in turn bonds to the ground resulting in a short bonded zone in the middle of the free length.

© 2016 Deep Foundations Institute

To address the free length, we found that a minimum of a schedule 40 PVC pipe that freely slides over the threaded hollow bar and is of similar outside diameter as the coupler is needed for the free length, see Figure 3. Prior to sliding the PVC over the bar, we coated the inside of the pipe with a debonding oil such as used for concrete formwork. Duct tape was used to seal the intersection of the couplers and the pipe sleeve at each end of the pipe sleeve. The duct tape was placed to form a thin layer with little or no ridges or bumps that could interlock and bond with the grout.



Fig. 3. PVC casing for free length portion of tieback

We gave consideration to drilling with a thinner cement grout and only using heavier, higher strength cement grout for the actual bond zone. However, upon considering the relatively small volumes of grout to be used during the drilling, the benefits of a heavier grout relative to maintaining drill hole stability, and the complications associated with switching back and forth between mixing partial batches of thin drilling grout and heavier bond zone grout led to the decision to drill with the bond zone grout.

A potential complication of drilling with a cement grout is that when installation of the tieback is done, there may be a continuous column of grout from the anchor zone up tight to the back of the SOE wall. If that is the case, testing of the tieback can yield to misleading results due to the so called "donut hole effect," (Cadden et al., 2010) This occurs when the testing load is transmitted to the bond zone by the steel hollow bar, but the grout column transmits part of the test load to the soil around the unbonded zone and up to the back of the wall and bypasses transmitting the full test load to the ground in the anchor zone. The result can be an overestimate of the grout-to-ground bond capacity and an underestimate of the tieback deformation under load. To avoid this in part, we flushed the grout out from along the 3 feet (0.9 m) of the tieback immediately behind the wall and filled that zone with loose soil to limit the annulus grout bearing on the back of the sheets during the tests. This did not completely eliminate the "donut hole effect" because the load path to the soil around the unbonded zone still existed, however this is now

© 2016 Deep Foundations Institute

similar to the conditions for a single stage grouted solid bar tie back with a debonding sheath to create the free length zone.

It also helps to pack some filter fabric, straw or similar material at the hole where the tieback passes through the wall to prevent piping and loss of ground from behind the wall.

The drilling and anchor grout was a neat cement grout with a water/cement ratio (w/c) of 0.45 ± 0.05. Daratard grout set retarding agent was to be used at the manufacturer's recommended dosage, if needed to delay grout set until after drilling of a tieback hole was completed. The grout mix was monitored using a mud balance. The target was a mud balance weight of at least 114 pcf (1.82 Mg/m^3) which corresponded to a w/c of 0.5. Mud balance weights measured ranged from 112 pcf (1.79 Mg/m^3) to 125 pcf (2.0 Mg/m^3), averaging 117 pcf (1.87 Mg/m^3). The corresponding 3-day unconfined strengths for tests on grout cubes were >2500 psi (17 MPa) and for 7- days >3500 psi (24 MPa). Testing of tiebacks occurred at least 36 hours after grouting or shorter if a grout strength of at least 1500 psi (10 MPa) was demonstrated.

When installing the anchors, the team worked in units of 10 feet (3 m), the lengths of individual hollow bar segments. The bond zones were generally rounded up to the next 10-foot (3-m) increment and similarly the free lengths were rounded up to the next 10-foot (3-m) increment. This led to greater conservatism than the base design, but it was judged to be more economical than cutting the hollow bar considering time to cut the bar and the wastage associated with small, unusable pieces of hollow bar.

TESTING

Tieback testing consisted of performing Performance and Proof tests. All tiebacks were proof tested to 120% of their design load (DL). Two of the first four tiebacks installed per embankment were performance tested to 133% DL. Thereafter, 2% of the tiebacks were performance tested. The maximum test load on a tieback was limited to be no greater than 80% of the guaranteed ultimate tensile strength (GUTS) or the yield strength of the bar. The testing procedures used were based on performance and proof testing procedures in PTI (2014) with some modifications. Modifications included:

- Using a load cell to monitor test loads, the pressure gauge on the pump served as a backup.
- If during a proof test, if the elongation does not reach 75% of the free length, cycle the load and repeat the proof test.
- At the start of a creep portion of a test, the time zero was started after the creep load was considered stable, dropping off less than 500 lbs (2.22 kN) over one minute.
- During creep tests, creep loads were maintained by adjusting if the load cell indicated a drop off of 500 lbs (2.22 kN).
- Apparent free length limit was not to be less than 75% of the design free length based upon the elastic movement from the initial alignment load to the maximum test load at the start of the creep test.

Early on we had difficulty testing the upper, shallow tiebacks because the surcharge portion of the design loads was very high due to the highway and railroad loads. These surcharge loads were not present during the tieback testing and the pressures exerted by jacking system on the steel sheet pile approached the passive resistance available for the loose upper soils behind the sheet pile. This resulted in the soils immediately behind SOE wall compressing due to creep and causing the loads in the jacking system to drop off. However, the creep measurements for the tieback indicated negative creep, meaning that the

© 2016 Deep Foundations Institute

anchor zone was not moving, but rather that the wall was pushing back into the soil. Once testing reached the third tier deep of tiebacks, this behavior largely disappeared.

Another early issue was the stick-slip nature of the load-deformation curve, see Figure 4. This occurred due to bonding of couplers in the free length zone and grouting of the annulus between the PVC sleeve (not coated with a debonding oil) and the hollow thread bar. This was mostly remedied by oiling the inside of the PVC and taking care during the taping of the joint between the PVC and the couplers to avoid ridges, rough areas and high spots. We found that relying on creating joints between the couplers and the PVC alone was not sufficient.

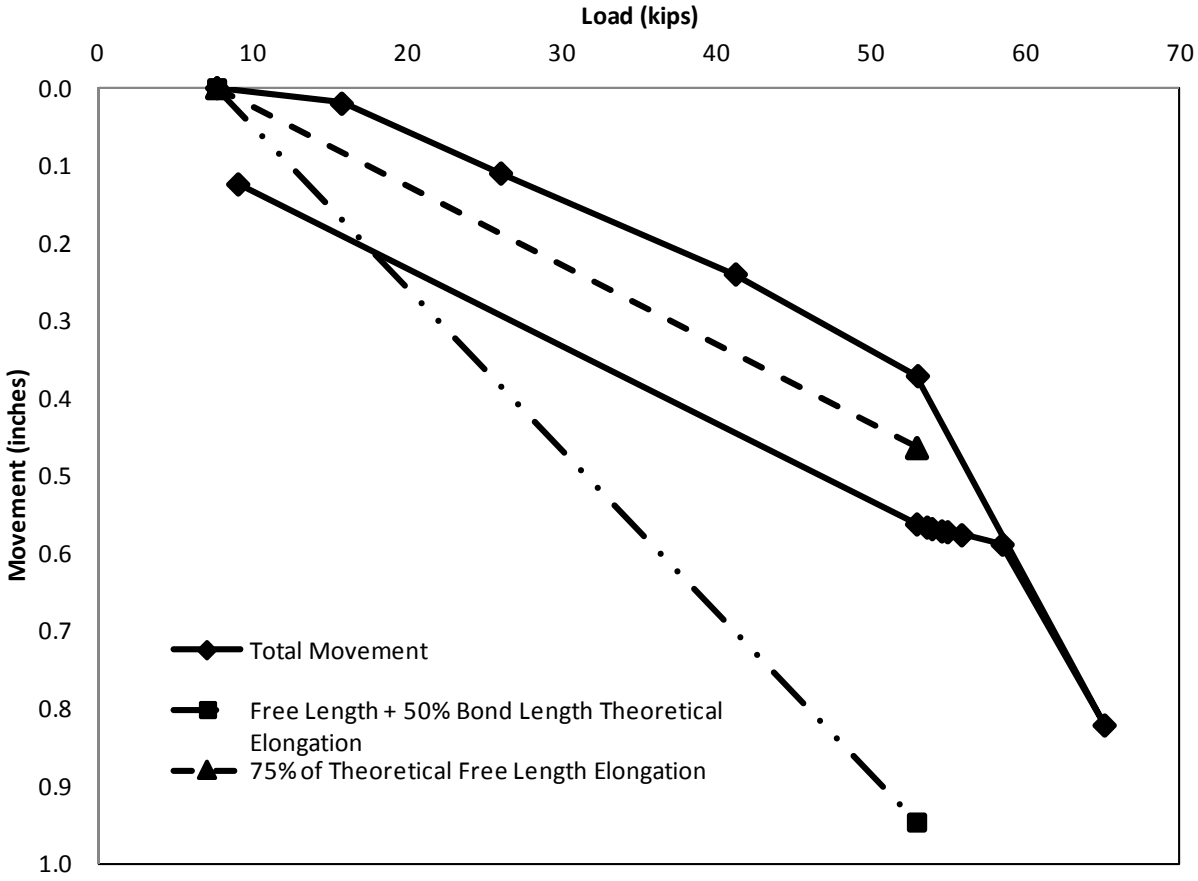


Fig. 4. Proof test on tieback DO-1 exhibiting stick-slip behavior

It also became apparent that the rebound displacements of a tieback could not consistently be relied upon to define the total elastic deformation of the tieback. The bonding of the couplers in the free length sometimes appeared to lock in residual load in the tiebacks that was never recovered. Apparent free length was determined using the loading data and checked relative to the 45°-ϕ/2 line up from the final subgrade elevation of the excavation to verify that sufficient load reached the anchor zone during load testing.

© 2016 Deep Foundations Institute

We also noticed that when testing in zones of very loose soils, it often took larger initial deformations to engage the full bond zone capacity of the anchor. In these cases, the creep deformations that accompanied the larger initial deformations were small and within the acceptance criteria, see Figure 5.

As installation occurred deeper within the excavations where the tiebacks were in medium dense to dense soils, the behavior of the tiebacks approached the more idealized behavior of conventional tieback installations, see Figure 6. This is most likely due to two factors. One, the installation team learned from the load tests that details of installation were key to achieving acceptable test results. Two, the denser material appeared to hold an open hole during drilling better and a straighter (less vertical arc) hole could be drilled. This led to less binding on the sides of the hole and less friction in the free length zone during the tests.

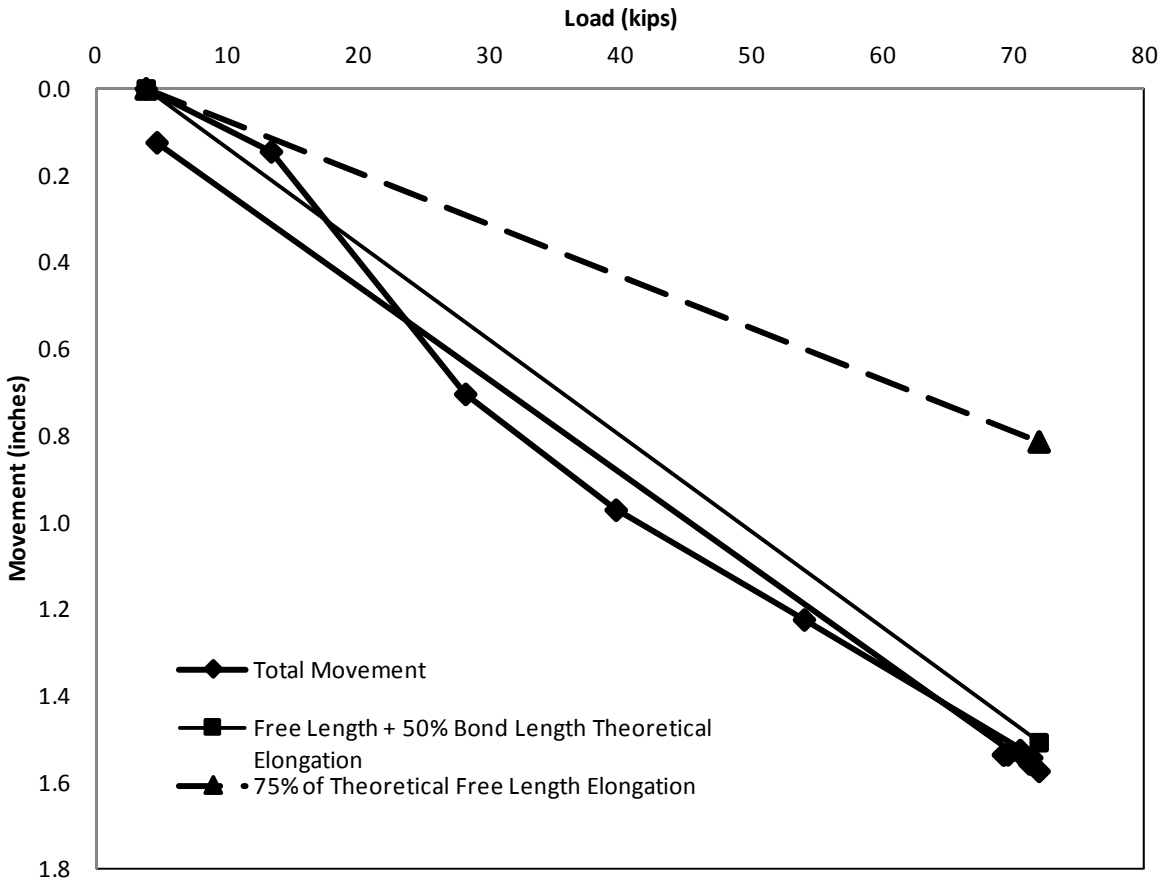


Fig. 5. Proof test on tieback EP-2 exhibiting last initial movement to fully mobilize bond zone

PERFORMANCE OF WALLS

Performance of the walls was monitored with prisms mounted on the walls and read both manually and with an automated motorized total station (AMTS). Prisms were mounted at the top, middle and bottom of the sheet piles as well as near the bottom of the sheet piles at 25-foot (7.5-m) -horizontal intervals in the deepest portions of north and south SOE walls in each embankment. Total maximum movement of the

© 2016 Deep Foundations Institute

SOE walls ranged from about 2 to 3 inches (50 to 75 mm) or about 0.3% of the height of the walls. This is consistent with typical performance of tied back sheet pile walls in sand data presented in Clough and O'Rourke (1990). Inclinometers located approximately 20 feet (6 m) behind the SOE walls of the WACR embankment show similar movements.

The lateral movement of the walls caused about 1 to 2 inches of settlement of the ground surface behind the walls. Provisions were in place to resurface the road surface during construction when settlements resulted in a dip of about 1 inch. Similarly, the line and grade of the railroad track was monitored with provisions to relevel, if necessary. The road surface was augmented with an inch of pavement once, and the railroad required minor regrading during construction, in part due to pile activities. In addition, when the SOE and temporary bridges were removed, ½-to-¾-inch gaps beneath the temporary bridge abutment pile caps were observed.

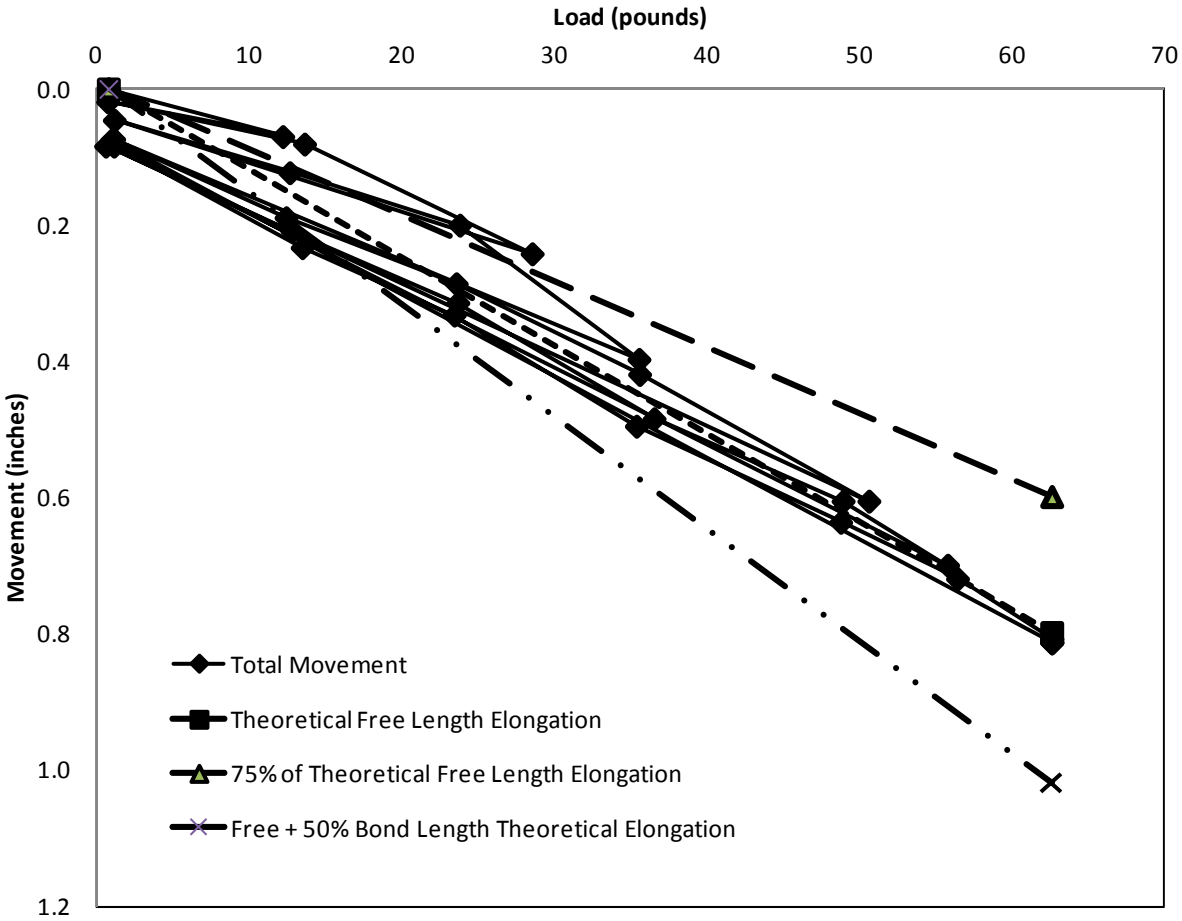


Fig. 6. Performance test on tieback T-1

SUMMARY AND CONCLUSIONS

This project demonstrated the efficiency and productivity of using self-drilling hollow bar anchors for temporary excavation support systems. Technical challenges specific to installing unbonded free lengths and adapting standard PTI testing protocols were addressed by the contractor and refined during the

© 2016 Deep Foundations Institute

project. Details of the construction and testing were key to the success of the tieback performance. They included:

- Using the anchor zone grout mix throughout the tieback drilling;
- Flushing the grout from behind the sheets to reduce the "donut hole effect" influencing the anchor testing;
- Using debonding form oil inside the PVC pipe sections of the free length zone and care with sealing the PVC to the hollow bar couplers;
- Testing generally followed PTI recommended procedures with modifications to deal with difficulties in achieving a free length zone;
- Noting apparent negative for shallow tiebacks where test loads were near the passive resistance of the soils behind the SOE wall, and relating it to displace displacement of the wall into the soil during the creep tests;
- Estimating elastic displacement during tieback loading and apparent free length of a tieback based on loading portion of the tests to avoid problems with residual loads present in the tiebacks upon unloading; and
- Modifying test loadings to accommodate the large displacements needed to fully develop bond zone adhesion during initial loading and to address "stick-slip" behavior due to local bonding of couplers in the free length zone.

Safety and maintenance of highway and railroad traffic adjacent to temporary excavations of significant depth were clearly dependent upon the successful performance of the anchors. The moderately small wall and ground movement measurements verified that the anchorage system performed as intended.

ACKNOWLEDGMENTS

The authors wish to acknowledge the project team that participated in the design, installation, testing and evaluation of the SOE systems for this project. They include: Nate Patenaude, Ben MacKinney, and Gene Trombly of ECI who led the installation and testing of the anchors; Mike Flynn and Mary Nodine of GEI Consultants, Inc., who performed initial base analyses and design; and Adriane Boscardin and Tristan Boscardin of BCE who assisted with developing test procedures, test data evaluation, and preparation of this manuscript. DuBois and King, Inc. is the design-build designer for the permanent culvert structures. Vermont Agency of Transportation is the project owner.

REFERENCES

Cadden, A., Gómez, J., Baxter, A., and Bird, T., 2010. Hollow Bar Soil Nails Pullout Test Program, Report No. FHWA-CFL/TD-10-001, Central Federal Lands Highway Division, Lakewood, CO, 48 p.

Clough, W.G. and O'Rourke, T.D., 1990. Construction Induced Movements of Insitu Walls. Design and Performance of Earth Retaining Structures, Geotechnical Special Publication No.25, ASCE. P.C. Lambe and L.A. Hansen, eds., pp.439 - 470.

Post Tensioning Institute, 2014. Recommendations for Prestressed Rock and Soil Anchors.. Post Tensioning Institute Publication No. PTI DC35.1-14, 110 p.

© 2016 Deep Foundations Institute

DRILLED SHAFT ACCEPTANCE CRITERIA BASED UPON THERMAL INTEGRITY PROFILING

George Piscsalko, Pile Dynamics, Inc., Solon, Ohio, USA, 216-831-6131, gpiscsalko@pile.com
Garland Likins, Pile Dynamics, Inc., Solon, Ohio, USA, 216-831-6131, glikins@pile.com
Gray Mullins, University of South Florida, Tampa, Ohio, USA, gmullins@foundation.cc

ABSTRACT

Quality control of drilled shafts is greatly dependent upon the practices of the site personnel. For drilled shafts cast under slurry, inspection of the hole prior to concreting is very difficult or impossible. There are numerous non-destructive test (NDT) methods currently available to assess the integrity of drilled shafts. This paper will discuss the theory and use of an emerging NDT technology known as Thermal Integrity Profiling (TIP). The Thermal Integrity Profiling method measures the elevated concrete temperatures that occur during the hydration process. These temperature measurements are made along the length of the pile and can determine the integrity over 100% of the pile cross section, both inside and outside the reinforcing cage. With the known shaft volume information, TIP can evaluate the effective shaft radius at each measurement location. With the increased use of TIP on highway projects, there is a need to have standard criteria for shaft acceptance. Shaft acceptance criteria can be based upon thermal measurements and subsequent analysis of the data to determine the average shaft radius, local concrete cover, and cage alignment. With this additional information obtained via the thermal testing method, acceptance methods based upon concrete cover can be developed. In this paper the Thermal Integrity Profiling method will be described, results from a case history will be discussed, and an acceptance criteria based upon concrete cover will be proposed.

INTRODUCTION

Drilled shafts are an attractive foundation element in many applications due to their large axial and lateral capacities. When drilled shafts are cast in a dry hole, it is possible to inspect the hole prior to casting, allowing for very basic level of quality control, although the shape of the completed element is still unknown without some form of post construction testing. When drilled shafts are installed where soil conditions are unstable, the shafts will often be cast under slurry to support the surrounding soils during the construction process. When casting a drilled shaft under slurry, it is very difficult to impossible to accurately and efficiently inspect the hole prior to casting concrete and it is equally difficult or impossible to inspect the shaft during the casting process.

There are several non-destructive testing methods available for testing the integrity of completed elements. Each of these methods has advantages and limitations with TIP being the only method able to test the entire element. Some test methods can test the integrity within a small proximity of an access tube while other methods will test the shaft core but cannot test the areas outside the reinforcing cage (concrete cover). The

© 2016 Deep Foundations Institute

TIP method involves measuring the temperature generated during the hydration process of the concrete both inside the cage as well as outside the cage.

This Thermal Integrity Profiling (TIP) method has the ability to evaluate the entire cross-section of the element under test, along the entire shaft length, allowing for verification of concrete quality or concrete cover while also evaluating the core of the shaft. Pile length to diameter ratios which can restrict some other integrity testing methods (such as low strain integrity testing) are not a restriction to the TIP method. Additionally, the TIP method is not limited by large non-uniform cross section changes that can occur by design or unintentionally during the construction process. As the TIP method determines the effective shaft radius and overall shape, designers now can better assess the usability of shafts where defects have been detected within the shafts. The inherent limitations with TIP testing are the time sensitive nature of the test, as the data must be collected during the hydration process as well as the need to cast sacrificial wires or access tubes into the shaft. This paper will discuss the TIP testing method in detail along with recommendations for acceptance criteria based upon reduction of both radius and concrete cover. An example will be included showing the TIP method in practice.

THERMAL INTEGRITY PROFILE BACKGROUND

The Thermal Integrity Profiling (TIP) method determines the integrity of a shaft both inside and outside the reinforcing cage by measuring the temperature of the hydrating concrete along the entire length of the shaft. The temperature measurements are made by either passing a thermal probe through a de-watered access tube (Mullins, 2004) or from embedding thermal cables (Piscsalko, 2011) within the shaft. At each depth all temperature readings are averaged together and, along with the total volume data, used to determine the overall shape of the shaft as a function of depth (Sellountou, 2013). The accuracy of the effective radius calculation is dependent upon the accuracy of the volume data.

Curing concrete exhibits a normal heat signature with shaft temperatures dependent upon the shaft diameter, concrete mix design, concrete quality, and (to a lesser extent) soil conditions. Insufficient cement content (defect) will cause a local reduction in temperature near the defect. For smaller diameter shafts, a defect may be detected on the opposite side of the shaft. Any temperature measurements which are cooler than the overall average are areas of reduced concrete volume (defect) or poor concrete quality and any area with a higher temperature than the average are areas of increased concrete volume (typically a bulge). The example shown in Figure 1 has temperature measurements for a small diameter shaft which would indicate a defect located closer to wires 3 and 4 at a depth of 5 feet below top of shaft (the normal temperature signature is reduced more at wire locations 3 and 4 as compared with wire locations 1 and 2).

In addition to determining concrete integrity, the TIP test will also reveal any potential issues with reinforcing cage alignment by comparing TIP measurements from radially opposite locations versus the average value. If a single measurement location is cooler or warmer than the average and the radially opposite location behaves in an opposite manner then the cage is not concentric within the shaft. For example, if a first measurement location is warmer than the average this indicates that this location is closer to the shaft center, and if a second diagonally opposite measurement location is cooler than the average this indicates that this location is closer to the surrounding soil, so thus the cage is not concentric with the hole.

© 2016 Deep Foundations Institute

In short, the average temperature profile (from all wires or tubes) defines the shape of the shaft and local variations from the average indicate cage offsets from center.

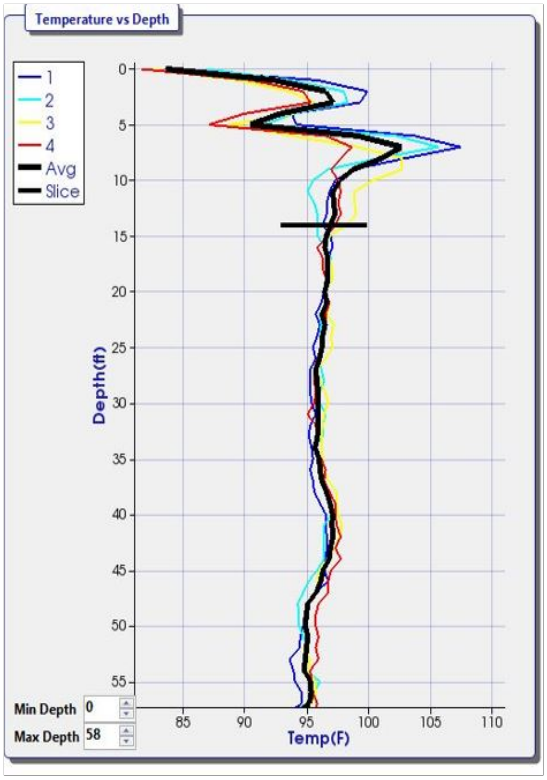


Figure 1

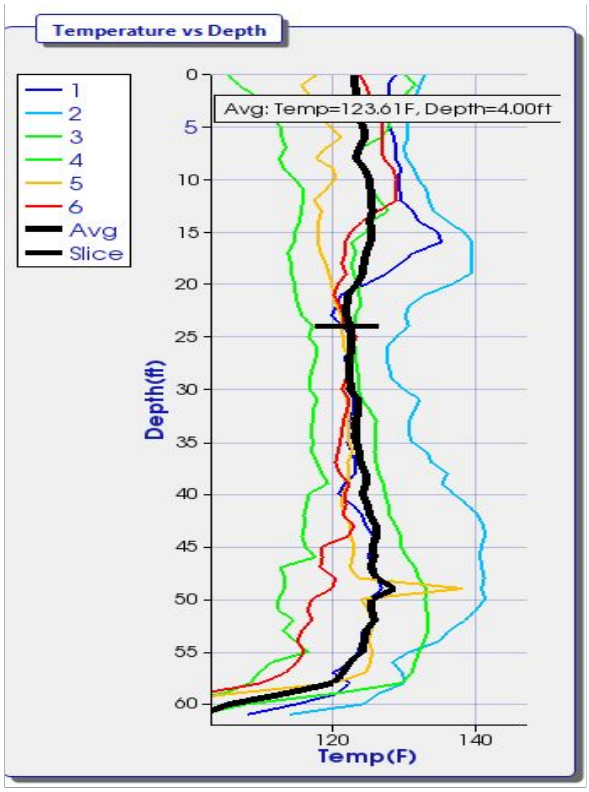


Figure 2

When considering both these measurements together, it can be determined that the cage has shifted such that location one is closer to the shaft center and location two is closer to the surrounding soil. Figure 2 shows wire 2 being consistently warmer than the average (wire 2 is closer to the warmer center of the shaft) while wire 4 is consistently cooler than average (wire 4 is closer to the cooler surrounding soils). This gives additional information on concrete cover. There is reduced concrete cover at wire location 4.

The recommended number of measuring locations (e.g. access tubes or thermal wires) per ASTM D7949 is one per foot of shaft diameter (e.g. 10 thermal cables installed for a 10 foot diameter shaft) and spaced approximately equally around the reinforcing cage perimeter. It is recommended that an even number of tubes or wires be installed, with pairs being placed diametrically opposite one another to enable lateral movement, if any, of the reinforcing cage to be easily determined. The TIP method will then easily determine the complete shaft cross-section and along with the volume data, can generate a three dimensional image of the shaft.

Generally heat transfer away from the shaft is only radial along the length of the shaft. However at the top and bottom of the shaft the heat transfer is both radial and longitudinal and thus the temperatures are typically reduced at the top and bottom ends of the shaft. This top and bottom of shaft temperature reduction (roll-off), typically seen in a thermal integrity profile, has a hyperbolic tangent shape. Knowing this

© 2016 Deep Foundations Institute

characteristic roll-off shape allows for an adjustment to be applied to the thermal measurements at the top and bottom of the shaft (Johnson, 2015). When the adjustment is applied to the shaft top and bottom, the roll off portions of the adjusted curve then match the theoretical interior measurements (curves generally flatten out). When end bearing is to be included in the shaft design, the values used for the roll-off correction at the shaft bottom should be carefully chosen such that the true shape of the shaft bottom and any anomalies are properly depicted. Once the top and bottom of the curves have been adjusted, the analysis in these areas is similar to the remainder of the measurements made along the length of the shaft.

The TIP measurements are obtained using Thermal Wire cables which are attached to the reinforcing cage prior to cage insertion into the shaft. The TIP wires are embedded directly into the concrete, placing one wire for each one foot of shaft diameter (6 foot diameter shaft will have 6 wires), equally spacing the wires around the shaft. These cables have temperature sensors placed every foot vertically along the length of the cable. Once the concrete has been placed in the shaft, the cables are connected to special purpose data loggers. The thermal measurements are taken automatically at regular time intervals (usually approximately every 15 minutes) at least until the shaft has reached its peak temperature.

Alternately, TIP measurements can be obtained using a thermal probe passed through de-watered access tubes installed in the shaft. These tubes can be steel or plastic. The test will be performed typically 12 to 48 hours after completion of the shaft. The optimum time is dependent upon the shaft diameter and mix design. Optimum results are obtained between a time when concrete temperature is one half peak temperature to a time shortly after peak temperature. The test is performed by lowering the probe into the access tube at a rate of no more than 0.3 ft/sec, recording and averaging all temperatures from four infra-red temperature sensors located at every 90^0 radially around the probe

Using the concrete volume installation records and the total measured concrete volume, the overall average temperature is correlated to the average radius. Once this average temperature to average radius correlation has been established, the effective radius at any point along the shaft can be directly calculated. The effective radius is considered to be the radius of intact good quality concrete that would have exhibited the measured temperature. This effective radius is computed directly from the relationship of shaft volume placed, shaft length, and the average overall shaft temperature measured from all locations and depths. The effective radius is best evaluated at approximately the time of peak temperature. The time of peak temperature is not known a priori, but may be estimated from the mix design. A search for local defects is best made at the time after casting is complete that is only halfway to the peak temperature; the temperature versus time history for the TIP wires can be searched.

EVALUATION OF THERMAL INTEGRITY PROFILING TEST RESULTS

Shaft acceptance criteria based on thermal integrity profiling extends current practices by now knowing the average shaft radius, local shaft cover, and cage alignment (eccentricity). Therefore acceptance can consider all aspects of load carrying capacity as well as durability afforded by the concrete cover thickness. To this end, a broad specification may cover a majority of probable conditions but more refined considerations may be more appropriate for a given project and are available for evaluation by the design team.

The load carrying requirements of drilled shafts can be controlled by geotechnical side shear (most common) or structural bending and/or compression. These are directly related to the circumference surface area of the shaft, the moment of inertia, and the cross sectional area, respectively. Using a percent radius

© 2016 Deep Foundations Institute

reduction approach means that each will be affected differently; circumference linearly related, moment of inertia effects based on reduction raised to the fourth power, and area effects related to the square of the reduction. Figure 3 shows these effects irrespective of shaft diameter but where the loss of section is assumed in the worst case position, outside the cage.

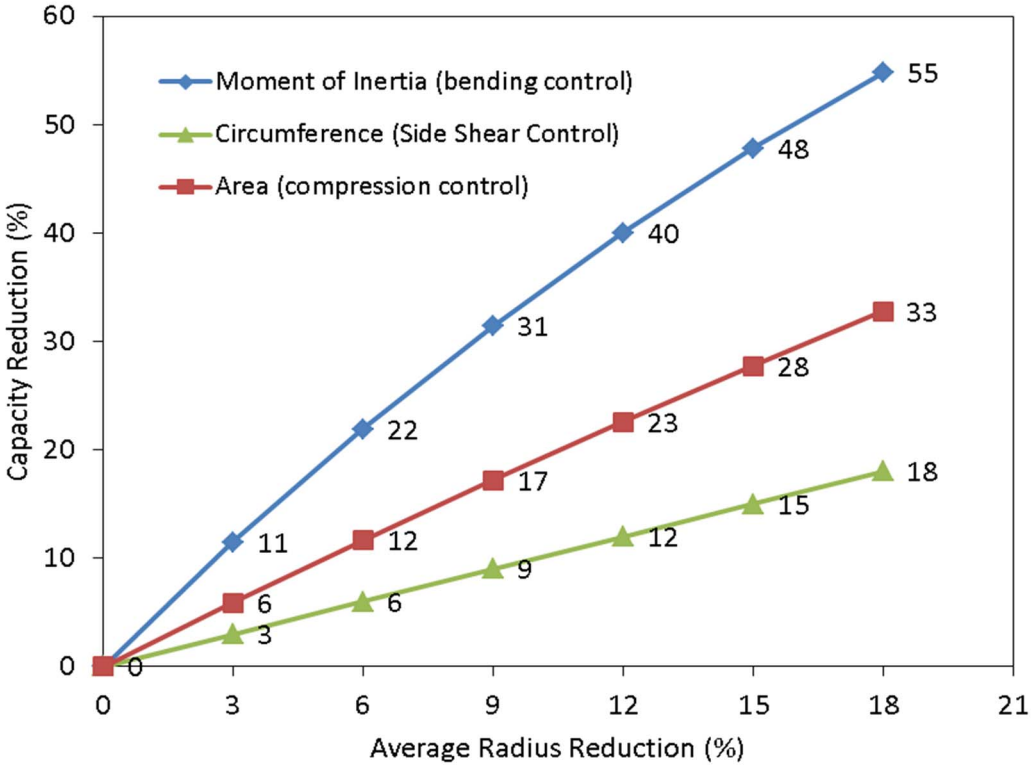


Figure 3

While the average radius is an indication of the cross sectional properties, the local radius is a better indication of the concrete cover and cage alignment/eccentricity. For highway bridges, the AASHTO recommended minimum cover of 4 inches is often used throughout the U.S.A., but individual states have adopted different acceptance criteria based on local needs or conditions.

However, private or commercial designers and some state agencies allow a design concrete cover of 3 inches, which is the ACI minimum cover for foundations cast-in-place. While this was intended for spread footings poured on-grade, many use this criterion for deep foundations as well. Figure 4 shows the effect of two cover loss considerations on the local radius reduction. If a 1.5 inch of remaining cover is acceptable, but with a design cover of 3, 4, or 6 inches, the permissible maximum local radius reduction is given. If 2 inches of remaining cover is the permissible criterion (ACI exterior concrete minimum for above ground applications), and an initial cover of 4 inches is assumed, then that effect is also shown.

© 2016 Deep Foundations Institute

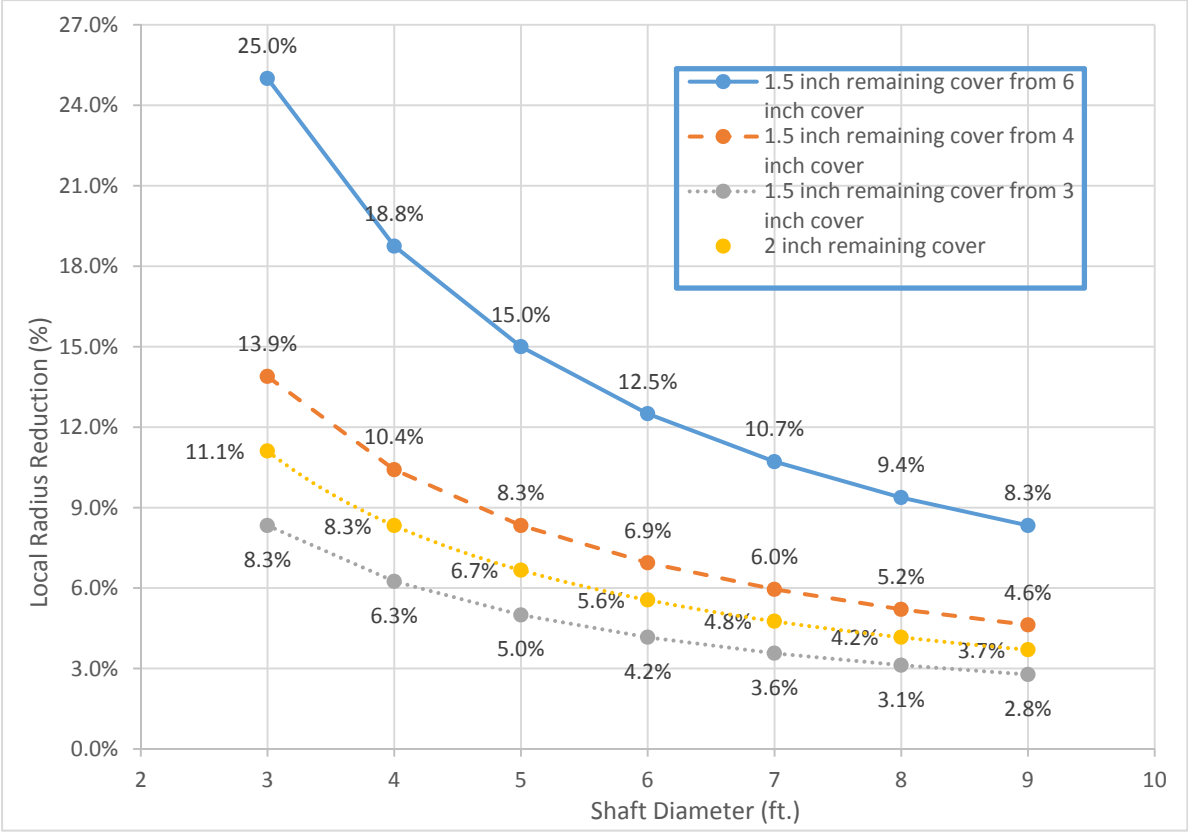


Figure 4

In reality, a 3 inch design cover provides no leeway for error as any cage movement in a perfectly-sized shaft impinges on the minimum cover for cast-in-place concrete and the 2 inch ACI minimum for above ground, exterior conditions is not applicable.

If a 0 to 6% and above 6% radius reduction criteria is applied to shafts as satisfactory and questionable respectively, the net effect on shaft properties can be summarized in Table 1.

Table 1. Effect of radius reduction on various shaft performance indicators.

Radius Reduction	Bending Capacity Loss	Compression Capacity Loss	Side Shear Reduction	Cover Loss (4 inch cover, 6ft dia. shaft)
3%	11%	6%	3%	1.08in
6%	22%	12%	6%	2.16in
>6%	>22%	>12%	>6%	>2.16in

© 2016 Deep Foundations Institute

Based on the above considerations acceptance criteria can be implemented as:

Satisfactory (S)

0 to 6% Radius Reduction and

Local Cover Criteria Met

Anomaly (A) Requiring further evaluation

Radius Reduction > 6% or

Local Cover Criteria Not Met

When a tested shaft is categorized as Anomaly (A), evaluation of a horizontal slice, estimated from the TIP measurements at the location in question should be required so that a structural evaluation of the shaft be performed prior to implementation of any corrective measurements. Once a shaft is categorized as having an anomaly, all other possible information on the shaft construction as well as soil boring logs should be fully vetted along with the TIP results to determine acceptance of the shaft.

TIP CASE HISTORY

TIP testing was performed on all production shafts for a project in Washington State. TIP was the only testing method used on this project. The 10 ft. diameter shaft was 125 ft. long. There were ten TIP wires installed in the shaft. The TIP testing began immediately upon completion of concreting the shaft and continued for 120 hours.

The TIP test results indicated a sharp temperature reduction (anomaly) approximately 90 feet below the pile top (Figure 5). Analysis was done approximately 40 hours after casting was completed. After inputting the volume data, the TIP temperature data was converted into effective radius (Figure 6).

© 2016 Deep Foundations Institute

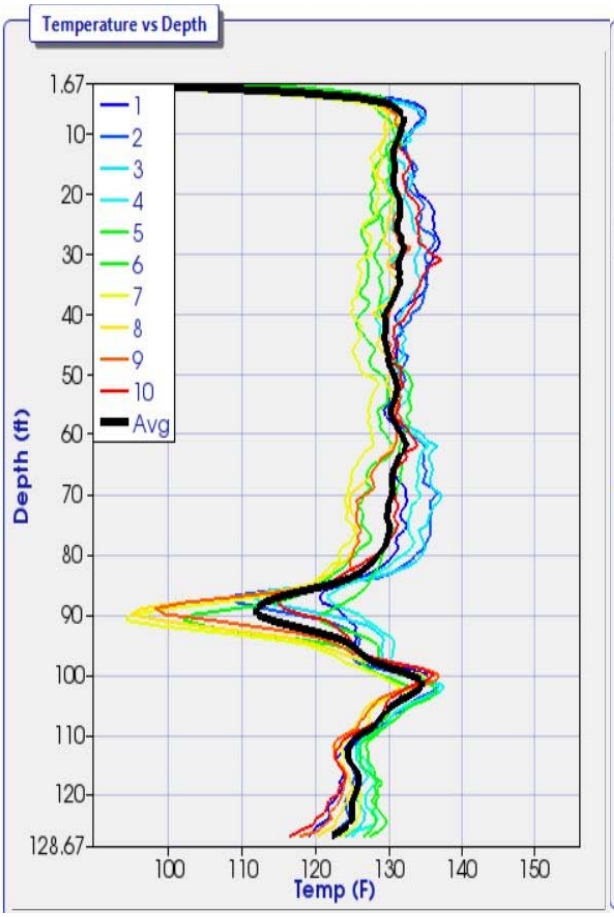


Figure 5

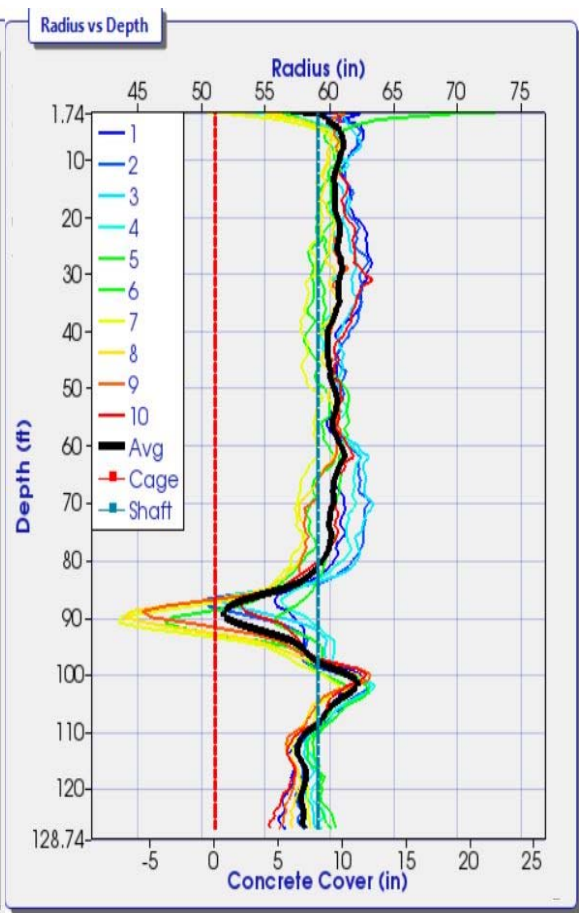


Figure 6

Figure 6 shows the effective radius and concrete cover as a function of depth. The concrete cover on one side of the shaft (wire locations 6 through 10) at a depth of 90 feet was less than the minimum allowable concrete cover (6in) and the total reduction in radius at this location is 14.2% and thus this shaft should be classified as Anomaly under either the radius reduction or minimum concrete cover criteria and warrants further evaluation in that zone. Some wire locations at that depth show the defect extended well inside the cage. The percent radius reduction in this region was 14.2%, resulting in a reduction of 26.3% in the cross-sectional area, which also triggered structural and geotechnical concerns along with the cover durability issue. Further evaluation included coring of the shaft which confirmed the defect present at this location identified by the TIP testing (Figure 7). The coring location was approximately 6 inches inside the reinforcing cage and located between TIP wires 7 and 8, which was the location the TIP testing revealed as having the greatest loss in effective radius. The defect was repaired using pressure grouting, saving the project from a potentially costly foundation failure.

© 2016 Deep Foundations Institute



Figure 7

CONCLUSIONS

The general trend in the deep foundation industry has been an increase in the use of drilled shafts. These shafts are often installed with little or no knowledge of the final shaft integrity, particularly when cast under a slurry, and to minimize concerns and reduce risk of failure, NDT methods are usually employed to investigate their structural integrity. Many common current NDT methods can each provide partial information as to shaft integrity, but each method also has limitations. The TIP method measures the shaft temperature during the hydration process to make an assessment of the shaft integrity. From these temperature measurements, the effective shaft radius can be estimated. The TIP method allows for assessment of 100% of the shaft cross-section, including concrete cover, which no other single current method can provide. Additionally, the cage alignment can be investigated and the concrete cover evaluated from the TIP data. Frequently the results of the TIP test are completed within 12 to 48 hours after the shaft has been cast, which is a major advantage over current methods as this can accelerate the construction process.

With the increased use of TIP on drilled shaft projects, there is a need to harmonize the acceptance criteria used. As shown from the included example, TIP can effectively locate defects within a shaft and can provide the designers with the radius reduction associated with these defects and allow for clear determination on when a shaft requires further analysis based on the acceptance criteria proposed in this paper.

© 2016 Deep Foundations Institute

REFERENCES

ASTM Standard D7949-14, "Standard Test Methods for Thermal Integrity Profiling of Concrete Deep Foundations," ASTM International, West Conshohocken, PA

Johnson, K. R. (2015). "Analyzing Thermal Integrity Profiling Data for Drilled Shaft Evaluation," Outstanding Student Paper, DFI National Convention, Oakland, CA.

Mullins, A.G., 2010. Thermal Integrity Profiling of Drilled Shafts, DFI Journal Volume 4 No.2, Hawthorne , NJ, pp. 54-64

Piscsalko, G. and Cotton, D., 2011. Non-Destructive Testing Methods for Drilled Shaft and ACIP Piles, Proceedings from Deep Foundation Institute 36th Annual Conference; pp. 525-532

Sellountou, A., Alvarez, C., Rausche, F., 2013. Thermal Integrity Profiling: A Recent Technological Advancement in Integrity Evaluation of Concrete Piles, Proceedings from the First International Conference, Seminar on Deep Foundations, Santa Cruz, Bolivia

© 2016 Deep Foundations Institute



Deep Foundations Institute
326 Lafayette Avenue
Hawthorne, NJ 07506
USA
Tel: 973-423-4030 | Fax: 973-423-4031
staff@dfi.org | www.dfi.org